Structural, Environmental, Coastal and Offshore Engineering

Edited by
Abd Nasir B Matori, Zubair Imam Syed,
Mohamed Hasnain Isa and Bashar S. Mohammed

TRANS TECH PUBLICATIONS

Structural, Environmental, Coastal and Offshore Engineering

Edited by
Abd Nasir B Matori
Zubair Imam Syed
Mohamed Hasnain Isa
Bashar S. Mohammed

Structural, Environmental, Coastal and Offshore Engineering

Selected, peer reviewed papers from the
2nd International Conference on
Civil, Offshore and Environmental Engineering
(ICCOEE 2014),
June 3-5, 2014, Kuala Lumpur, Malaysia

Edited by

**Abd Nasir B Matori, Zubair Imam Syed,
Mohamed Hasnain Isa and
Bashar S. Mohammed**



Copyright © 2014 Trans Tech Publications Ltd, Switzerland

All rights reserved. No part of the contents of this publication may be reproduced or transmitted in any form or by any means without the written permission of the publisher.

Trans Tech Publications Ltd
Kreuzstrasse 10
CH-8635 Durnten-Zurich
Switzerland
http://www.ttp.net

Volume 567 of
Applied Mechanics and Materials
ISSN print 1660-9336
ISSN cd 1660-9336
ISSN web 1662-7482

Full text available online at *http://www.scientific.net*

***Distributed** worldwide by*

Trans Tech Publications Ltd
Kreuzstrasse 10
CH-8635 Durnten-Zurich
Switzerland

Fax: +41 (44) 922 10 33
e-mail: sales@ttp.net

and in the Americas by

Trans Tech Publications Inc.
PO Box 699, May Street
Enfield, NH 03748
USA

Phone: +1 (603) 632-7377
Fax: +1 (603) 632-5611
e-mail: sales-usa@ttp.net



FOREWORD

ASSOC. PROF. IR. DR. MOHD SHAHIR LIEW

Head of Civil Engineering Department &
Chairman of ICCOEE2014
Universiti Teknologi PETRONAS

Dear Distinguished Delegates, Sponsors and Exhibitors,

Greetings and welcome to the 2nd International Conference on Civil, Offshore & Environmental Engineering 2014 (ICCOEE2014).

Universiti Teknologi PETRONAS warmly welcomes you to the 2nd International Conference on Civil, Offshore & Environmental Engineering 2014 (ICCOEE2014) in Kuala Lumpur, Malaysia. ICCOEE 2014 is an international forum of distinguished intellectuals engaged in scientific, engineering and technological research dedicated toward the sustainability of civil engineering knowledge and application.

The conference provides a venue for you to share and exchange the wealth of knowledge in the civil engineering fraternity with the delegates. ICCOEE2014 is part of the World Engineering, Science & Technology Congress (ESTCON2014), whereby 8 other conferences are being held simultaneously at the same venue. The potential collaboration is unlimited as participants can freely attend any of the other conferences. ICCOEE2014 will bring together colloquy and exchange of ideas of latest research and development in the main traditional areas of civil engineering, including coastal and offshore structures. It is our aspiration that this conference will nurture research in the areas of civil engineering, and amplify its positive impact to the mainstream built environment.

Malaysia is fast becoming a hub for knowledge and R&D for South East Asia. With PETRONAS' support, the University conducts extensive research activities in collaboration with PETRONAS and other institutions and industries locally and internationally.

It is my pleasure to personally invite you to participate in this conference for showcasing your latest academic achievements and for networking with key researchers from all over the world.

Come and join us in Kuala Lumpur Convention Centre on the 3rd-5th June 2014 at our once in two years Engineering Congress, ESTCON 2014, in particular the ICCOEE 2014.

Thank you.

Conference Organizing Committee

CONFERENCE CHAIR
Assoc. Prof. Ir. Dr. Mohd Shahir Liew

CO-CHAIR
Assoc. Prof. Dr. Shamsul Rahman Mohamed Kutty

SECRETARY
Dr. Teh Hee Min
Dr. Zubair Imam Syed

TREASURER
Ms. Niraku Rosmawati Ahmad
Dr. Nurul Izma Mohammed

TECHNICAL
Dr. Zahiraniza Mustaffa (L)
Assoc. Prof. Dr. Salah Elias Zoorob
Dr. Montasir Osman Ahmed Ali
Mr. Muhammad Hafiz Baharun

PUBLICATION
Assoc. Prof. Dr. Abd Nasir Matori (L)
Assoc. Prof. Dr. Bashar S Mohammed
Assoc. Prof. Dr. Mohamed Hasnain Isa

LOGISTICS
Dr. Syed Baharom Azahar Syed Osman
Ir. Idris Othman

PUBLICITY & PROTOCOL
Dr. Muhammad Raza Ul Mustafa
Assoc. Prof. Ahmad Mustafa Hashim

IT & MULTIMEDIA
Dr. Ibrisam Akbar

SPONSORSHIP
Dr. Noor Amila Wan Abdullah Zawawi
Assoc. Prof. Ir. Dr Mohd Shahir Liew

F & B
Mr Ahmad Zamdi Ab Hamid

EVENT MANAGEMENT
Assoc. Prof. Dr. Amirhossein Malakahmad
Assoc. Prof. Dr. Khamaruzaman Wan Yusof

REVIEWERS

Abdul Nasir Matori
Abdullah Zawawi Awang
Abu Bakar Hassan
Ahmad Al Yacouby
Ahmad Mustafa Hashim
Ahmad Khairi Abd Wahab
Amirhossein Malakahmad
Azam A Rahman
Bashar Mohammed
Chen J. Paul
Chimay Anumba
Fadzli M Nazri
Faridah Othman
Faridah Sedek
Fatimah De'nan
Hanaa Elsayad
Hasanuddin Zainal Abidin
Ramli Nazir
Husna Takaijudin
Idris Othman
Indra Sati H. Harahap
Kamal Nasharuddin Bin Mustapha
Khairunisa Muthusamy
Khamaruzaman Wan Yusof
Khandker M. Nurul Habib
Kousik Deb
Lam Wei Haur
M Nazmi M Ali
M Sapihie B. Ayob
Madzlan Napiah
Mastura Jaafar
Mehdi Setareh
Mohamad Khattak
Mohamed Mubarak Abdul Wahab
Mohamed Hasnain Isa
Mohammad Ismail
Mohd Azrai Azman
Mohd Sanusi S. Ahamad
Mohd Shahir Liew
Muhammad Joehan Rohani
Muhammad Raza Ul Mustafa
Muhd Fadhil Nuruddin
Muhd Zaimi Abd Majid
Narayanan Sambu Potty
Nasir Shafiq
Niraku Rosmawati Ahmad
Noor Amila Wan Abdullah Zawawi
Norhazilan Md Noor
Nur Izzi Md. Yusoff
Nurul Izma Mohammed
Othman Che Puan
Preben Pedersen
Raza Ali Khan
Roderick Jones
Saied Saiedi
Shaliza Binti Ibrahim
Shamsul Rahman Kutty
Sih Ying Kong
Sivadass Thiruchelvam
Syed Baharom Azahar Syed Osman
Teh Hee Min
Velluruzhathil John Kurian
Teo Wee
Yutaek Seo
Zafarullah Nizamani
Zahiraniza Mustaffa
Zubair Imam Syed



PLENARY SPEAKER 1

PROF. DR. IR. PIETER VAN GELDER

Professor of Safety Science,
Faculty of Technology, Policy and Management, Delft University of Technology,
The Netherlands.

Safety Matters in Civil Engineering - A Historical Overview and a Look into the Future

BIOGRAPHY

Prof. Dr. Ir. Pieter van Gelder is a full-time professor of safety science at the Faculty of Technology, Policy and Management of Delft University of Technology since 2013. Until then he was the associate professor of probabilistic design methods at the Faculty of Civil Engineering and Geosciences of Delft University of Technology. He has actively involved in research and education on safety and reliability since 1991. His research interests are in risk analysis and optimization of systems, processes and structures. He teaches 4^{th} and 5^{th} year courses at TU Delft and has supervised over 50 MSc students and 10 PhD students. He conducts research on new methods and techniques in risk analysis. van Gelder has authored and co-authored more than 290 journal papers, and several books in the field of risk and safety. He is the project leader in several ongoing national and EU research projects, namely iNteg-Risk (Large scale EU integrated project on integrated risk management in industrial systems), SMARTEST (Smart Resilience Technology, Systems and Tools) and MATRIX (New multi-hazard and multi-risk assessment methods for Europe). Van Gelder is a member of Technical Programme Boards and a scientific committee member of annual international conferences such as the ESREL and IPW (International Probabilistic Workshop) series. He is co-editor and reviewer of several journals, i.e. RESS (Reliability Engineering and System Safety) and AJSE (Arabian Journal of Science and Engineering). van Gelder is also a coordinator and member of the curriculum committee of the Technical Module of the post-academic course on public safety at Delft Toptech.

PLENARY SPEAKER 2



PROF. DR. PRIYAN MENDIS

Professor of Department of Infrastructure, Engineering
Member of the Melbourne Energy Institute (MEI),
Built Environment Research Group,
The University of Melbourne.

Engineering Challenges in Safe and Sustainable Tall Buildings

BIOGRAPHY

Prof. Dr. Priyan Mendis has a distinguished and internationally recognized track record for research in tall buildings, behaviour of concrete structures under extreme loading and sustainability aspects of build environment as evidenced by publishing several books and book chapters, more than 100 journal papers and 200 conference papers. He is a leading member of the Melbourne Energy Institute (MEI) Built Environment research group and currently leading the infrastructure node. He obtained his PhD from Monash University in 1987. He worked as a Structural Engineer at Connell Wagner Ltd in Melbourne before joining the University of Melbourne in 1991. He has been an expert consultant for design of high-rise structures in Australia and overseas (Malaysia, Dubai etc), including tallest buildings in the world. He is an expert in design of structures for dynamic effects such as wind and earthquakes and also other effects such as blast and fire. He has also led the CTBUH (World Council of Council on Tall Buildings and Urban Habitat) sub-committee of use of high-performance concrete in tall buildings and is a member of the Performance-based design and progressive collapse committees. Prof. Mendis has also served as the Chair of ACI International Sub-Committee on High-Strength Concrete between 1996 and 2001. He was the chairman of the working group nominated to revise the Australian Concrete Standard, AS3600 to include High-strength Concrete (HSC) up to 100 MPa and a key member of the AS3600 code committee for more than 20 years. His current research includes sustainable infrastructure, protective technology of structures as well as disaster mitigation and management.

Table of Contents

Foreword, Committee, Reviewers and Speakers

Chapter 1: Environmental and Water Resources Engineering

Air Quality Profile in an Enclosed Car Park
N.I. Mohammed, N. Othman and K.B. Baharuddin 3

Comparison of Soil Water Retention Functions for Humid Tropical Soils
N.M. Babangida, M. Askari, K.W. Yusof and R.U.M. Muhammad 8

Courtyard as a Microclimatic Modifier Experimental Study on Actual Site
A. Abdulbasit, I. Norhati, S.S. Ahmad and W.M.N.W. Salleh 14

Determination of Adsorption Capacity of Agricultural-Based Carbon for Ni (II) Adsorption from Aqueous Solution
T. Khan, M.H. Isa, M. Chaudhuri, R.U.M. Muhammad and M.O. Saeed 20

Effect of Low Pressure on Irrigation Uniformity of Solid Set Sprinkler Irrigation System
M. Osman, S. Bin Hassan and K.W. Yusof 26

Effect of Rainfall and Groundwater Level on Sandy Beach Profile
A.K.A. Wahab, N. Othman, M.H. Jamal and S.R. Samat 32

Effects of Groundwater Withdrawal on the Interaction of Ex-Mining Pond, River, and Aquifer
R. May, I. Yusoff and W. Tahir 38

Electrochemical Disintegration of Activated Sludge Using Ti/RuO_2 Anode
G.C. Heng and M.H. Isa 44

Environmental Screening Method for Dredging in Contaminated River
N. Manap and N. Voulvoulis 50

Experimental Investigation on the Performance of Four Types of Solar Stills in Malaysia
A. Riahi, K.W. Yusof, M.H. Isa, B.S.M. Singh, A. Malakahmad and N.B. Sapari 56

Feasibility of Alum Sludge as Phosphate Removal
M.Z. Nazirul, C.K. Hua and L.M. Sidek 62

Floating Treatment Wetland as an Alternative for Water Quality Improvement: A Preliminary Study
M.N. Nur Asmaliza, M.S. Lariyah, K.H. Kok, H.S. Humaira and B. Hidayah 68

Investigation of Modified Mangrove Bark on the Sorption of Oil in Water
A. Robabeh, N.B. Sapari, M.H. Isa and K.U. Orji 74

Kinetic Study of PAHs Degradation in Produced Water Using Ti/RuO_2 Anode
A. Yaqub, M.H. Isa, S.R.b.M. Kutty and H. Ajab 80

Langat River Basin Hydrologic Model Using Integrated GIS and ArcSWAT Interface
M.F. Ali, N.F.A. Rahman, K. Khalid and N.D. Liem 86

Modeling of Contaminant Transport and Groundwater Flow of Tamangapa Landfill in Makassar Indonesia
Hajrah, A. Arsyad and A. Zubair 92

Optimization of Activated Sludge Physical Properties by Magnetic Field via Response Surface Modeling
Z. Nur Syamimi, K. Muda, J. Sohaili and M. Sillanpää 98

POME Treatment Efficacy as Affected by Carrier Material Size in Micro-Bioreactor System
W.L. Liew, K. Muda, M.A. Kassim, K.Y. Lai, Z.Y. Si, Y.H. Thong and S.K. Loh 104

Possible Stabilization of Sludge from Groundwater Treatment Plant Using Electrokinetic Method
S.B.S. Osman and F. Iqbal 110

Post-Treatment of Anaerobically Digested Palm Oil Mill Effluent by Polymeric Flocculant-Assisted Coagulation
A. Malakahmad, S.Y. Chuan and M. Eisakhani 116

Prediction of Suspended Sediments in a Hyper – Concentrated River Using Neural Networks
R.U.M. Muhammad, A.S.A. Bakar, M.H. Isa and K.W. Yusof 122

Preliminary Investigation and Design Considerations for the Rehabilitation of Trash Screen at Jor Reservoir Low Level Outlet
L. Jansen, L.M. Sidek and P.Y. Julien 128

Response of Partially Covered Road Embankments and its Environmental Impact
K.W. Yusof, S.M.H. Shah, M.B. Zahiraniza and A.M. Hashim 133

Survival of *Pseudomonas putida* for Biodiesel Blend (B5) in Soil Bioremediation
N.M. Sunar, Q.A. Emparan, A.T.A. Karim, S.F.M. Noor and M. Maslan 139

The Art of Integrated GIS/AHP for Siting Landfill: A Review
M.O. Saeed, H.A. Aziz and K.A.M. Azizli 144

The Effects of Feedstock Sources and Pyrolytic Temperature on Biochars Sorptive Characteristics
S. Yavari, A. Malakahmad and N.B. Sapari 150

The Impact of Stormwater Runoff on Nutrient Removal in Sand Columns
T. Husna, A.G. Aminuddin and Z. Nor Azazi 155

The Performance of Trapezoidal Glass Cover Solar still during Monsoon Period of Tropical Environment
N.B. Sapari, N.A. Mohd Ahmadan, A. Riahi and K.U. Orji 161

Treatment of Wastewater Using an Integrated Submerged Attached Growth System
E.H. Ezechi, S.R.b.M. Kutty, M.H. Isa and A.F.A. Rahim 167

Volatile Fatty Acids Production through Degradation of Biomass by Anaerobic Digestion (Mesophilic and Thermophilic)
A.F.A. Rahim, S.R.M. Kutty and E.H. Ezechi 172

Water Quality Assessment of Ex-Mining Lakes in Perak, Malaysia as Alternative Source of Water Supply
K.U. Orji, N.B. Sapari, K.W. Yusof, A. Robabeh and E. Olisa 177

Determination of Soil Polluted with Kerosene Using Electromagnetic Cell
H. Al-Mattarneh, M. Dahim, R. Ismail and M.F. Nurudinn 183

Chapter 2: Coastal and Offshore Engineering

A Study on the Structural Failure Mechanism and Reserve Strength Ratio of Tarpon Monopods
L.H. Eik and M.S. Liew 191

A Study on Mooring Systems of an Offshore Floating Platform for Different Configurations
A. Yenduri, M.O. Ahmed and J.V. Kurian 197

Behaviour of Mooring Systems for Different Line Pretensions
M.O. Ahmed, A. Yenduri and J.V. Kurian 204

Broadside Vessel Collision Forces for Conventional Riser-Guard
D.K. Palaniandy, Z.I. Syed, M.S. Liew and S. Karuppanan 210

Computational Aspects of Submarine Slide Generated Tsunami
V.N.P. Huan and I.S.H. Harahap 216

Development of Platform Selection Tool for Offshore Decommissioning in Malaysia
N.A.W.A. Zawawi, N.K. Lun and M.S. Liew 222

Dynamic Response of Free-Span Sub-Sea Pipelines under Vortex Induced Vibrations
S. Charanvarma and A.P. Shashikala 228

Dynamic Responses of Classic Spar Platform: Short Crested Waves vs. Long Crested Waves
C.Y. Ng, J.V. Kurian and M.S. Liew 235

Effect of Anodes on Hydrodynamic Coefficients of Tubular Cylinders - Model Tests
J.V. Kurian, A.M. Al-Yacouby, A.A. Sebastian, M.S. Liew and V.G. Idichandy 241

Effects of Marine Growth on Hydrodynamic Coefficients of Rigid Tubular Cylinders
A.M. Al-Yacouby, J.V. Kurian, A.A. Sebastian, M.S. Liew and V.G. Idichandy 247

Finite Element Assessment of Difficult Pipelines at Bends
Z. Mustaffa, T.M.B. Albarody and A.M. Roshdi 253

Hydrodynamic Forces on Linear and Multi-Dimensional Arrays of Circular Cylinders
A.A. Sebastian, J.V. Kurian, A.M. Al-Yacouby, M.S. Liew and V.G. Idichandy 259

Investigation of Vortex Induced Vibration of Offshore Pipelines near Seabed
F. Namazi-Saleh, J.V. Kurian and M.B. Zahiraniza 265

Multivariate Regression Analysis for Screening Process of Reliability Assessment
J.V. Kurian, M.C. Voon, M.M.A. Wahab, N.A. Iskandar and M.S. Liew 271

Performance of Mangrove Forests in Coastal Protection
A.M. Hashim and N. Khairuddin 277

Reliability Assessment Model for Aging Jacket Structures in Malaysian Waters
J.V. Kurian, S.S. Goh, M.M.A. Wahab and M.S. Liew 283

Resonant Motion of Liquid Confined between Floating Structures
N.V. Nasma Noor and A.P. Shashikala 289

Response of Monopod Platform under Extreme Wave in Malaysian Water
M.A.B. Jamaluddin, M.S. Liew and J.V. Kurian 295

Seabed Condition from Single Beam Echo Sounder from Penang Port, Malaysia
W.T. Yew, W.H. Lam, C. Soon and R. Aziz 301

System Reliability of Existing Jacket Platform in Malaysian Water (Failure Path and System Reliability Index)
J.V. Kurian, M.M.A. Wahab, T.S. Kheang and M.S. Liew 307

Wave Attenuation of Interlocking Concrete Unit - V (ICU-V)
A.M. Hashim, N.D.M. Noor and S.N.H. Abdullah 313

Wave Transmission over a Submerged Porous Breakwater an Experimental Study
H.M. Teh 319

Deformation Monitoring of Offshore Platform Using the Persistent Scatterer Interferometry Technique
A.N. Matori, A.S. Ab Latip, I.S.H. Harahap and D. Perissin 325

Chapter 3: Structures and Materials

A Novel Method for Monitoring Hydration Process of Cement Paste Material
H. Al-Mattarneh, A. Alwadie, A. Malkawi and M.F. Nurudinn 333

An Experimental Study on the Effects of Biaxial Bending due to Eccentric Load on RC Beam
N. Shafiq, M. Imran and I. Akbar 339

Analytical Prediction of the Mechanical Properties of High Performance PVA Fiber Reinforced Concrete
T. Ayub, N. Shafiq and M.F. Nurudinn 345

Behaviour of Oil Palm Shell Reinforced Concrete Beams Added with Kenaf Fibres
S.M. Syed Mohsin, S.J. Azimi and A. Namdar 351

Characterization of Stand Chopped Basalt Fiber Self – Compacting Reinforced Concrete (SCB-SCC)
N. Shafiq, M.F. Nuruddin, A.F.M. Salih and A.E.A. Elshekh 356

Drying Shrinkage of Fly Ash-Based Self-Compacting Geopolymer Concrete
M.F. Nuruddin, F.A. Memon, N. Shafiq and S. Demie 362

Durability of Sugar Cane Bagasse Ash (SCBA) Concrete towards Chloride Ion Penetration
N. Shafiq, A.A. Elhsameed and M.F. Nurudinn 369

Effect of Calcined Kaolin on the Mechanical Properties of High-Strength Concrete as Cement Replacing Material
M.F. Nurudinn, S.U. Khan and N. Shafiq 375

Effect of Chopped Basalt Fiber on the Fresh and Hardened Properties of Fly Ash High Strength Concrete
N. Shafiq, M.F. Nuruddin, A.E.A. Elshekh and A.F.M. Salih 381

Effect of Flexural Static Load on the Strength of GFRP Gratings
A. Izzuddin and I. Akbar 387

Effect of MIRHA and Fly Ash in Ductile Self-Compacting Concrete on Abrasion and Impact Performance
M.F. Nuruddin, N.M. Azmee and K.Y. Chang 393

Effective Method of Repairing RC Beam Using Externally Bonded Steel Plate
M.A. Alam, A.S.A. Jabbar, M.Z. Jumaat and K.N. Mustapha 399

Effects of Geopolymer Concrete Fly Ash Based on Alkali Silica Reaction (ASR)
M.F. Nurudinn and A.R. Siti Nooriza 405

Flexural Behaviour of Concrete Beams Bonded with Wire Mesh-Epoxy Composite
I.M.I. Qeshta, P. Shafigh, M.Z. Jumaat, A.I. Abdulla, U.J. Alengaram and Z. Ibrahim 411

Interrelationship Analysis of Geopolymer Components Using Pearson Correlation Technique
A. Kusbiantoro, N. Rahman and N.F. Shahedan 417

Low Energy Compaction of Aggregate Packing Mechanism
Y.G. Suliman, N. Madzlan, I. Kamaruddin and J.A. Olufemi 422

Mechanical Properties of Engineered Cementitious Composites Mixture
B.S. Mohammed, M.H. Baharun, M.F. Nurudinn, O.P.D. Erikol and N.A. Murshed 428

Microwave Incinerated Rice Husk Ash (MIRHA) and Used Engine Oil (UEO): Towards Sustainable Concrete Production
N.L. Mohd Kamal, S. Beddu, M.F. Nurudinn, N. Shafiq and Z.C. Muda 434

Numerical Investigation of the Response of Protective Barrier under Blast Loading
K.S. Ying, A.M. Remennikov and B. Uy 440

POFA: A Potential Partial Cement Replacement Material in Oil Palm Shell Lightweight Aggregate Concrete
K. Muthusamy and Z. Nur Azzimah 446

Precast Concrete Sheetpile for the Stabilization of Road Embankment on Soft Ground Adjacent to River
N. Fadilah, C.Y. Ong and K.K. Choong 451

Precast Concrete Soldier Pile System with Corrugated Section Post for Riverbank Protection
N. Akmilah, C.Y. Ong and C.K. Keong 457

Prediction of Failure Loads of RC Dapped-End Beams
M. Aswin, Z.I. Syed, T. Wee and M.S. Liew 463

Prediction the Shear Strength for FRP Shear Strengthened RC Beams Based on Optimised Truss Models
H. Yin and T. Wee 469

Predictive Stress-Strain Models for High Strength Concrete Subjected to Uniaxial Compression
N. Shafiq, T. Ayub and M.F. Nurudinn 476

Prospect of Adopting Kapok Fibre as Roof Insulation
M.F. Nurudinn, N.H.A. Puad, K.A.M. Azizli, S.A. Farhan and A. Zainal 482

Rehabilitation of RC Structures Exposed to Salinity and Moisture Using CFRP
H. Fazli and T. Wee 488

Shear Capacity of RC Beams with Web Openings Strengthened with Multi Layers of CFRP
B.S. Mohammed and O. Alanni 494

Single-Degree-of-Freedom Based Pressure-Impulse Diagrams for Blast Damage Assessment
Z.I. Syed, M.S. Liew, M.H. Hasan and S. Venkatesan 499

Strength Development of Concrete Incorporating Metakaolin and PVA Fibres
S.U. Khan, M.F. Nurudinn and N. Shafiq 505

Strengthening Schemes for Flexure and Torsion Using FRP Laminates: A State of Art Review
M. Imran, N. Shafiq and I. Akbar 511

Tension Stiffening Analysis for Cyclically Loaded RC Beams
A.A. Bin Shukri and M.Z. Jumaat 517

The Effect of MIRHA and Fly Ash on Mechanical Strength and Chloride Penetration Depth of DSCC
M.F. Nurudinn, K.Y. Chang and N.M. Azmee 522

The Effect of Palm Oil Fuel Ash as a Cementreplacement Material on Self-Compacting Concrete
B. Alsubari, P. Shafigh, M.Z. Jumaat and U.J. Alengaram 529

The Laminated Composite Thermosetting Pipe
T.M.B. Albarody and M.B. Zahiraniza 535

The Utilization of Rice Husks Powder as an Antioxidant in Asphalt Binder
M.H. Nahi, I.B. Kamaruddin and N. Madzlan 539

Unconfined Compressive Strength Performance of Cement Stabilized Peat with Rice Husk Ash as a Pozzolan
L.S. Wong 545

Chapter 4: Construction and Project Management

A Field Study of Mould Growth for Institute Higher Education Library Buildings in Malaysia
N.A.W. Suriani, N.I. Mohammed, M.K. Faris and N. Jamaludin 553

Challenges for Implementation of Building Information Modeling (BIM) in Malaysian Construction Industry
S.S.S. Gardezi, N. Shafiq, M.F. Nurudinn, S.A. Farhan and U.A. Umar 559

Embodied Carbon of Buildings: Tools, Methods and Strategies
S.A. Farhan, N. Shafiq, K.A.M. Azizli, U.A. Umar and S.S.S. Gardezi 565

Evaluation of Multi Storey Structures in Malaysia
N.S. Potty and M.R.A. Hamid 571

Evaluation of Roofing Systems in Malaysia Based on MS 1553 BS 6399, EC1-1-4 and IS 875 Wind Codes
K. Seavhai and S.P. Narayanan 577

Implementation of Dam Safety Management Program in Malaysia: From Theory to Practice
M.S. Lariyah, B. Hidayah, S. Thiruchelvam, S.M. Rahsidi, A.R. Azwin Zailti and A. Zuraidah 583

Major Challenges to the Sustainable Operations of Construction Equipment in Malaysia
M. Waris, M.S. Liew, M.K. Faris and I. Arazi 589

Number of Bidders in Small and Medium Public Construction Procurement in Malaysia
M.A. Azman 595

Private Finance Initiatives (PFI): Getting it Right
A.A. Umar, N.A.W.A. Zawawi, A.G. Otairu and I. Othman 601

Resource Management in Construction Project
I. Othman, M. Napiah and N.S. Potty 607

Risk Ranking of Malaysian Public Private Partnership Projects
H. Sarvari, A. Valipour, N. Yahaya and M.N. Norhazilan 613

Service and Construction Sector of Malaysia: Causality Link (1991-2013)
R.A. Khan, M.S. Liew and Z. Bin Ghazali 619

The Development of Building Information Modeling (BIM) Definition
A.L. Aryani, J. Brahim and M.S. Fathi 625

The Effects of Orientations on the Room's Thermal Performance in the Tropics
L.P. Chung, M.H. Ahmad, D.R. Ossen, M.B. Hamid and M. Baharvand 631

The Importance of Lightweight Concrete Technology Development for IBS Industry in Malaysia Based on Cost Comparison between Concrete Slab and Hollow Core Slab: A Case Study of LRT Car Park Project
M.Z. Ramli, H.M. Mahayudin, G. Hayder, Z.M. Hafiz, M. Daud and A.M. Salleh 637

The Performance Measurement of Supply Chain Management (SCM) in Malaysian Infrastructure Project
M.R.A. Wahab and H. Ahmad 642

Research on HGV Collisions with Concrete Bridge Piers
T. Wee, H. Yin, M. Maharun, K. Saravanan, M.S. Liew, A.R. Salleh and T.C. Wong 648

Analytic Network Process Approach to Risk Allocation of EPC Projects Case Study: Gas Refinery EPC Projects in Iran
A. Valipour, H. Sarvari, N. Yahaya, M.N. Norhazilan and S.M. Khoshnava 654

Chapter 5: Building, Highway, Geotechnical, Transportation Engineering and Geoinformatics

A Review on the Factors Influencing the Park-and-Ride Traffic Management Method
I.A. Memon, N. Madzlan, M.A.H. Talpur, M.R. Hakro and I.A. Chandio 663

Assessing UAV Landslide Mapping Using Unmanned Aerial Vehicle (UAV) for Landslide Mapping Activity
M.R.M. Mokhtar, A.N. Matori, K.W. Yusof, A.M. Embong and M.I. Jamaludin 669

Assessment on Bearing Capacity of Two Clay Layers Soil Using COMSOL
M. Md Nujid and M.R. Taha 675

Bearing Capacity of Shallow Foundation's Prediction through Hybrid Artificial Neural Networks
A. Marto, M. Hajihassani and E. Momeni 681

Comparison of Seismic Performance between Single and Double Unit Tunnel Form Building under In-Plane Lateral Cyclic Loading
S.A. Anuar and N.H.A. Hamid 687

Development Spectral Library of Vegetation Stress for Hydrocarbon Seepage
M.I. Jamaludin, A.N. Matori, M.F. Kholik and M.M. Mokhtar 693

Distribution of Stress on Stone Column-Reinforced Soft Soil under Cylindrical Storage Tank
K. Deb and A.K. Das 699

Effect of Soil Depth on the Quantification of Soil Moisture Content Value Estimated from NOAA Satellite Images
A.A. Hassaballa, A.N. Matori and H.Z.M. Shafri 705

Erosion Assessment of Slope Failure Tragedies; A Case Study in Malaysia
M.F. Ali, M.A. Makatar, K. Khalid and N.F.A. Rahman 711

Flood Disaster Forecasting: A GIS-Based Group Analytic Hierarchy Process Approach
A.N. Matori and D.U. Lawal 717

Generation, Propagation, Run-Up and Impact of Landslide Triggered Tsunami: A Literature Review
I.S.H. Harahap and V.N.P. Huan 724

Human Error Causes in Slope Engineering Practices
S. Qasim, I.S.H. Harahap, S. Baharom and M. Imran 730

Measuring Driver's Percent-Time-Spent-Following Using a Moving Video Recording Technique
N.I. Muttaka and O. Bin Chepuan 736

Modeling Pedestrian Behavior in Rail Transit Terminal
A.R. Zanariah, M. Mustafa, Y. Ashaari and A.F.M. Sadullah 742

Statistical Analysis of Dynamic Bearing Capacity of Driven Pile
A. Arsyad, Suyadi and L. Samang 749

The Use of Bitumen Linear Viscoelastic Properties to Assess Rutting Sensitivity
S.E. Zoorob, I.B. Kamaruddin and N. Madzlan 755

Time-Space Geography: A Creditable Transport Accessibility Measure for Rural Dwellers
M.A.H. Talpur, N. Madzlan, A. Irfan, I.A. Chandio and S. Hussain 763

Application of Geographic Information System (GIS) and Analytic Network Process (ANP) for Sustainable Tourism Planning in Cameron Highlands, Malaysia
M. Aminu, A.N. Matori, K.W. Yusof and R.B. Zainol 769

CHAPTER 1:

Environmental and Water Resources Engineering

Applied Mechanics and Materials Vol. 567 (2014) pp 3-7
© (2014) Trans Tech Publications, Switzerland
doi:10.4028/www.scientific.net/AMM.567.3

AIR QUALITY PROFILE IN AN ENCLOSED CAR PARK

Nurul Izma Mohammed[a], Nurfadhilah Othman[b], Khairul Bariyah Baharuddin[c]

Department of Civil Engineering, Universiti Teknologi PETRONAS, Bandar Seri Iskandar, 31750 Tronoh, Perak, MALAYSIA.

[a]izma.mohammed@petronas.com.my, [b]fadh.othman@gmail.com, [c]bariyah.baha@gmail.com

Keywords: air pollution, emission, Kuala Lumpur, Malaysia, nitrogen dioxide, sulphur dioxide

Abstract

Complaints on poor air quality in an enclosed car park have been raised up among the public, which might cause serious health effects to the drivers, passengers, and labours who are working at the premises. Improper design of mechanical ventilation systems in a car park would result in a poor indoor environment. The exhaust emission of motor vehicle contains a variety of potentially harmful substances encompassing carbon monoxide, nitrogen oxides, sulphur dioxide, hydrocarbons, and fine particulates. In Kuala Lumpur, there is a great demand but a short supply of lands and building spaces. Thus, a large multi-storey underground car parks is a common solution for both, the government and developers. Although the health effects of the motor vehicle emissions and ambient air pollution are already known, but due to the nature of enclosed multi-storey car parks, these health risks are predicted to be intensified. Thus, it is crucial to investigate and evaluate the status of the air pollution in the enclosed car parks with emphasis on sulphur dioxide (SO_2) and nitrogen dioxides (NO_2). Samples were collected in one of the famous shopping malls in Kuala Lumpur using a GrayWolf Advanced Sense Direct Sense; Toxic Gas Test Meters from 8 am until 5 pm on weekdays and weekends. The results demonstrate that the concentrations of SO_2 and NO_2 on weekends is higher than weekdays. Besides, the concentrations for both weekdays and weekends have exceeded the standard limit set by the Malaysian Ambient Air Quality Guideline (MAAQG).

Introduction

In a metropolis such as Kuala Lumpur, there is a great demand but a short supply of lands and building spaces. This results in very high prices and expensive rents for commercial, industrial, and residential properties. Commercial and industrial buildings are almost invariably high-rise and densely populated. The trapping of an affluent and industrious society includes a relatively large vehicle population for the usable land area [1]. There is a huge demand for an off-street parking. A large multi-storey underground car parks is a common solution for both the government and developers [2]. However, a concern regarding the underground car parks is the health implications to thee users and personnels manning the car parks. Although the health effects of the motor vehicle emissions and ambient air pollution are already known, but due to the nature of enclosed multi-storey car parks, these health risks are predicted to be intensified [2]. This has becoming a main issue as there is a possibility of the augmented cumulitive effects and also due to the employees and subcontractors working in security, maintenance, and other various services may be subjected to work in these environments for a substantial period of time. The exhaust emission of the motor vehicle contains a variety of potentially harmful substances including carbon monoxide, oxides of nitrogen, sulphur dioxide, hydrocarbons, and fine particulates, which are discharged into the atmosphere [3, 4, 5, 6, 7]. Under poor ventilation conditions, the level of these contaminants will raise, posing hazards to human health.

The city of Kuala Lumpur has many underground car parks which are located in hotels, shopping complexes, and private residential buildings. Although many studies have been carried out to determine the state of the air pollution in the city, only a few have examined the level of air pollutants in an enclosed car park [8]. Kuala Lumpur city centre is one of the national vertexes, located in Kuala Lumpur. Every day, it caters high number of locals, tourists, and workers. As a capital city, it is imperative to have a good image of a sustainable management in all aspects, including the car parks. Emissions from mobile sources have been a major contributor of air pollution in Malaysia, contributing to at least 70 % to 75 % of total air pollution [9, 10]. Thus, it is crucial to investigate and evaluate the status of air pollution in enclosed car parks with emphasis on nitrogen dioxides (NO_2) and sulphur dioxide (SO_2).

Materials and Methods

Study area. Kuala Lumpur is a capital city of Malaysia, where the KLCC; the tallest twin tower in the world is located [11]. Every year, Kuala Lumpur is visited by thousands of visitors from all over the world. In order to accommodate the demand for car park, two types of parking; indoor and open parkings, have been built in many of the shopping malls in Kuala Lumpur. However, this research was focusing only on an enclosed car park, in one of the famous shopping malls in Kuala Lumpur.

Air pollutants. The air pollutants that were considered in this research were nitrogen dioxide and sulphur dioxide. The samples of the air pollution were collected for every one (1) minute interval from 0800 hour to 1700 hour. The data collected was tabulated for an hourly average by using Microsoft Excel. The sampling took place in the same location everyday so that the pattern of the air pollutants concentration is comparable. The sampling result is focusing on weekdays and weekends.

Measurement Methods of Air Pollutants. The air pollutants sample were collected by using a GrayWolf Advanced Sense Direct Sense; Toxic Gas Test Meters, as shown in Fig. 1. It provides a descriptive name for every files using a virtual keyboard. The air pollutants samples were recorded as a snap-shot data captures, or as trend logs over time. It can also be documented by using a Data Analysis and Generation software provided by GrayWolf.



Fig 1: GrayWolf Advanced Sense Direct Sense; Toxic Gas Test Meters

Data analysis. The samples of the air pollutants were analysed by using a time series model. Time series is a sequence of data points, measured typically at successive points in time spaced at uniform time intervals. By using the time series model, the trend of NO_2 and SO_2 concentrations at the site with the variation of time can be observed.

Results and Discussions

Concentration of SO_2. Fig. 2 represents the trend of SO_2 concentration on weekday and weekend.

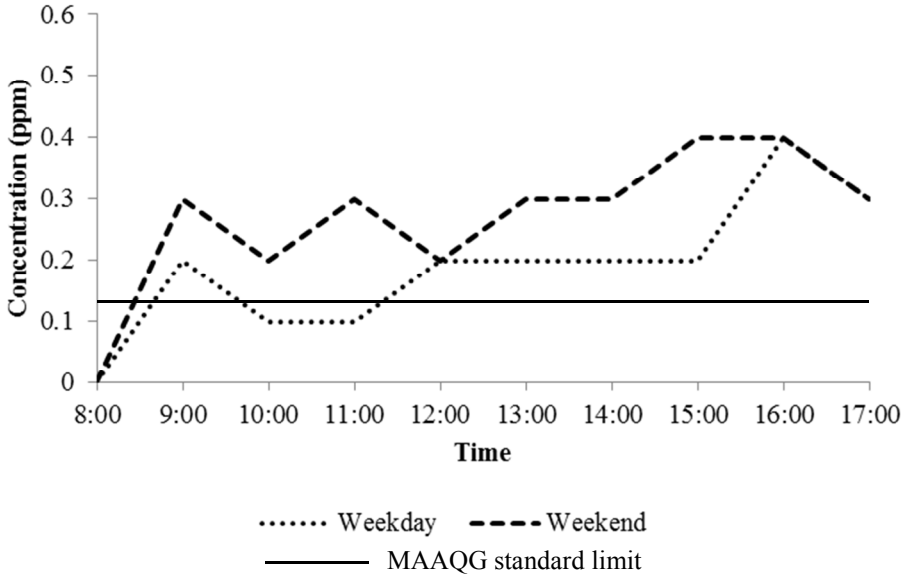


Fig. 2: SO_2 Concentrations on Weekdays and Weekends

Fig. 2 demonstrates that SO_2 concentration was higher during weekends than weekdays for the entire day. SO_2 concentration was recorded highest in the evening with 0.4 ppm for both times of sampling. It also illustrates that the fluctuation pattern of SO_2 among weekdays and weekends are different. The lowest fluctuation concentration for weekdays was 0.1 ppm while for weekend it was 0.2 ppm. Based on Fig. 2, most of the SO_2 concentrations for both sampling days exceeded the standard limit of Malaysian Ambient Air Quality Guideline (MAAQG), which is 0.13 ppm (an average time of 1 hour) and 0.04 ppm (an average time of 24 hour).

From Fig. 2, the fluctuation peak of SO_2 concentrations during weekdays were recorded at 0900, 1200, and 1600. In Malaysia, most companies begin work and have lunch between 0800 to 0900 and 1200 to 1300, respectively. The end of working time varies but normally, it was implemented at 1600 to 1700 every day. Thus, the daily routines of workers are parallel with the findings in Fig. 2. SO_2 is a highly reactive gas and is produced from the combustion of high sulfur containing fuels [7]. Therefore, SO_2 concentrations will be higher during the peak time where there are a lot of vehicles movements.

During weekends, the peak fluctuation of SO_2 concentration was recorded at 0900, 1100, 1300, 1400, 1500, and 1600 (Fig. 2) and the trend was different from the weekdays sampling period. According to Fig. 2, SO_2 concentration increased from 0800 to 1600 and began to decrease after that. Based on the SO_2 concentration in Fig. 2, it represents the trend of people coming to the shopping mall.

Concentration of NO_2. Fig. 3 represents the trend of NO_2 concentration on weekdays and weekends.

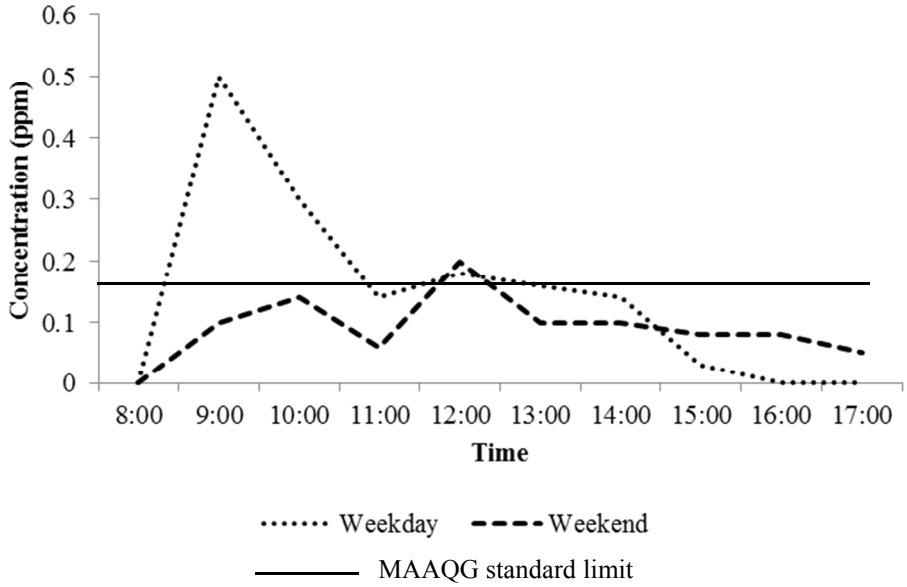


Fig. 3: NO_2 Concentration on Weekdays and Weekends

In Fig. 3, the concentration of NO_2 was recored highest in the morning and started to decrease until it reached 0 ppm at 1600 hour for weekdays sampling day. The highest reading of NO_2 recorded was 0.38 ppm. This value has exceeded the standard limit of Malaysian Ambient Air Quality Guideline (MAAQG), which is 0.17 ppm (an average time of 1 hour) and 0.04 ppm (an average time of 8 hour). Based on the study, a huge amount of vehicles were passing through the road that is connected to the highway during the weekdays. This might be a factor for the high NO_2 concentration documented.

During weekdays, the numbers of vehicles are higher during the peak hours (0800 to 0900, 1200 to 1300, and 1600 to 1700). However, the results in Fig. 3 illustrate that the highest concentration was recorded in the morning despite of other peak hour times. This was most probably due to the reaction of the NO_2 and the UV light in the car park that produced secondary pollutants, ozone, for the whole sampling day [12]. This result followed the trends of NO_2 reported by Ghazali et al., (2009).

On weekends, the recorded NO_2 concentration showed a different pattern when compared to the weekdays [Fig. 3]. The number of vehicles entering the car parks on weekends was not relying on the peak time, which were high for most of the time and increasing since morning. These results agree with the finding in Fig. 2. Due to the continuous emission of NO_2 from vehicles, the photochemical reaction of NO_2 cannot be seen clearly. Thus, a study on the relationship between NO_2 and ozone in an enclosed area needs to be conducted in the future for a better understanding.

Conclusions

The results conclude that the concentration of NO_2 and SO_2 exceeded the standard limit set by MAAQGS. The concentrations of SO_2 were higher at the peak times (morning, lunch hour, evening) on weekdays and this is parallel with the workers daily routines. On weekends, the concentration of SO_2 represents the trend of people coming to the shopping mall. NO_2 concentration was recorded higher in the morning on weekdays and decreased through out the day due to the photochemical reaction. However, due to the continuous emission of NO_2 from vehicles on weekends, the photochemical reaction of NO_2 cannot be seen clearly. Thus, a study on the relationship between NO_2 and ozone in enclosed area needs to be conducted in the future for a better understanding.

References

[1] Department of Statistics, Malaysia. (2010). *Basic Population Characteristic by Administrative Districts*.

[2] Burnett, J. & Chan, M.Y. (1997). Criteria for Air Quality in Enclosed Car Parks*, Proc. Instn Civ. Engrs, Transp*., 123, 102- 110.

[3] Hough, A. M., & Derwent, R. G. (1990). Changes in the global concentration of tropospheric ozone due to human activities. *Nature, 344*(6267), 645-648.

[4] Pani, B. (2007). *Textbook of environmental chemistry*. India. IK International Pvt Ltd.

[5] Ramli, N. A., Ghazali, N. A., & Yahaya, A. S. (2010). Diurnal fluctuations of ozone concentrations and its precursors and prediction of ozone using multiple linear regressions. *Malaysian Journal of Environmental Management, 11*(2), 57-69.

[6] USEPA (United States Environmental Protection Agency), (2013). [Online], [Accessed on 5 June 2013].

[7] USEPA (United States Environmental Protection Agency), (2006). *Air quality criteria for ozone and other photochemical oxidants*, Vol. I. EPA-600/R-05/004bF, U. S. Environmental Protection Agency, U. S. Environmental Criteria and Assessment Office, Research Triangle Park, N. C.

[8] Yaziz, M.I. & Yen, A.W.P. (1986). A Study of the Air Quality in Underground Car Parks with Emphasis on Carbon Monoxide and Airborne Lead. *Pertanika*, 9(2), 193 -199

[9] Afroz, R., Hassan, M. N., & Ibrahim, N. A. (2003). Review of air pollution and health impacts in Malaysia. *Environmental Research, 92*(2), 71-77.

[10] Yahaya, N., Ali, A. and Ishak, F. (2006). *Air Pollution Index (API) and the Effects on Human Health: Case Study in Terengganu City, Terengganu, Malaysia*. International Association for People-Environmental Studies (IAPS) Conference, September 2006, Alexandria, Egypt.

[11] Tourism Malaysia portal. (2013). [Online], [Accessed on 5 June 2013].

[12] Ghazali, N. A., Ramli, N. A., Yahaya, A. S., Yusof, N. F., Sansuddin, N., & Madhoun, W. A. (2009). Transformation of nitrogen dioxide into ozone and prediction of ozone concentrations using multiple linear regression techniques. *Environmental Monitoring and Assessment*, *165*, 475- 489.

[13] Bernstein, J. A., Alexis, N., Bacchus, H., Bernstein, I. L., Fritz, P., Horner, E. (2008). The health effects of nonindustrial indoor air pollution. *American Academy of Allergy, Asthma & Immunology* , 4.

Applied Mechanics and Materials Vol. 567 (2014) pp 8-13
© (2014) Trans Tech Publications, Switzerland
doi:10.4028/www.scientific.net/AMM.567.8

Comparison of Soil Water Retention Functions for Humid Tropical Soils

Nuraddeen Muhammad Babangida[1,a], Muhammad Askari[2,b,*],

Khamaruzaman Wan Yusof[1,c] and Muhammad Raza-ul Mustafa[1,d]

[1]Department of Civil Engineering, University Teknologi Petronas (UTP), Malaysia.

[2]Institute of Environmental and Water Resources Management, University Teknologi Malaysia (UTM).

[a]nuraddeenb@gmail.com, [b]muhaskari@utm.my, [c]khamaruzaman.yusof@petronas.com.my, [d]raza.mustafa@petronas.com.my
*Corresponding Author. Tel.: 07-5531536

Keywords: Soil water retention functions; Soil water retention curve; Humid tropical soils.

Abstract. The determination of soil hydraulic properties is of paramount importance as they are needed in many models of water and solute transport in soils, however conventional methods are quite difficult, expensive and sometimes cumbersome to use. Most studies of soil water retention functions are for temperate soils and their soil water retention curve (SWRC) cannot be extrapolated to tropical region, as such this study focused solemnly on SWRC of soils of tropical region (Malaysia and Indonesia to be specific). The analytical models of Brooks & Corey, van Genuchten and Kosugi were applied to model the SWRC for humid tropical soils, parameters of the three models were optimised by fitting them to 191 soil samples, of 10 different classes (International society of soil science classification) using VBA & MS excel solver add in. A comparison of the fitting capabilities and model quality was made using the sum of square of errors (SSQE) between observed and modelled values and, Akaike information criterion (AIC) respectively. The Kosugi model was found to describe the SWRC of the tropical soil samples better than the other models, as it has the lowest SSQE and AIC values.

Introduction

The numerical modelling of water and solute transport through the unsaturated (vadose) zone is of significant importance at present, especially due to the growing number of pollutants percolating through the vadose zone and ultimately ending up in the groundwater. While several laboratory and field methods exist for measurement of hydraulic properties of soils (which are needed for studies of groundwater movement), they mostly require precise, cumbersome and time consuming procedures. In any numerical model that simulates transport in the vadose zone two important properties have been identified, viz the soil water retention curve (SWRC) and unsaturated hydraulic conductivity [1- 4].

The soil water retention curve is a hydraulic property of a given soil; it describes the relationship between the soil's matric potential (the words pore-water pressure, suction and matric potential are interchangeably used throughout this study) and its moisture content. Probably the easiest way to determine this property is by the use of either pedotransfer functions (PTF); which use soils readily measurable hydraulic properties to predict the moisture content at any given suction, or by the use of closed form analytical expressions. There are a number of analytical expressions used for unimodal soils, these include those of Brooks and Corey [5] , van Genuchten [6] and Kosugi [7] referred here in as B&C, VG and KG model respectively, and they are the subject of study.

Soils of the humid tropical region are known to exhibit different water characteristics from those of temperate regions. Humid tropical soils are highly weathered, due to the high amounts of rainfall

which essentially leaches out the nutrients out of the soils, thus it lacks the amount of organic matter and mineral riches that may be found in soils of other regions with lower amount of rainfall. An analysis of databases of soils of temperate region and that of soils of the tropics reveals significant differences in clay content, moisture content at the same pore water pressure, bulk density and cation exchange capacity [8]. Significant differences between PTF developed for tropical and that of the temperate soils have been reported [8-11]. It is thus apparent that fitting an analytical SWRC function to certain soil will give a local result, just like conventional measurement techniques, only that the function may be applicable to wider area depending on the range of soil data used for developing the function. Consequently functions developed for soil of one region are not applicable outside the location from which they were developed from [1, 8]. comparative study of performance of 10 SWRC analytical functions applied to temperate soils reveals the van Genuchten (1980) as the best model [12].

There is little study that uses tropical humid soils to determine their SWRC. Van den Berg [13] was the first to predict a PTF for ferrasols and similar related soils using exclusively soil from the tropical regions of South America, Africa and South East Asia, other studies like [9], [14] and [15] followed suit. [8] Highlighted that there's a large insufficient measurement of soil properties in the topics. It is thus apparent that the study is lacking. Therefore the main objective of this study is to develop and compare some analytical soil water retention functions for soils of the humid tropical region.

Theory

The empirically derived, four parameter power function of B&C (Eq. 1) even though old, still remains one of the most widely used expression in the field of unsaturated soil hydrology.

$$\theta = \theta_r + (\theta_s - \theta_r)\left(\frac{h_B}{h}\right)^{-\lambda}. \quad (1)$$

θ is volumetric water content, θ_s is saturated water content, also referred as porosity in some cases, but in truth this is generally known to be less than porosity due to entrapped air in the voids. It is typically between 5%-10% less than porosity [16]. θ_r is residual water content, h_B is a dimensionless number that represents the air entry value, $\boldsymbol{\lambda}$ is the pore-size distribution index, and, h is suction.

Van Genuchten [6] proposes another empirically driven closed form equation (refer Eq.2) with four independent parameters θ_s, θ_r, α and n. In van Genuchten equation, m may be taken as equal to 1-1/n (as the VG retention model was a combination of an empirical power law and the Mualem model) or as a free independent parameter.

$$\theta = \theta_r + (\theta_s - \theta_r)\,[1 + |\alpha h|^n]^{-m}. \quad (2)$$

α is the inverse of the air-entry value, parameter n is dimensionless parameter indicating the pore size distribution index, m is dimensionless curve-shape parameter and as independent parameter, it yields better results; this is well documented by [17]. However with limited data it is recommended to use m as dependent variable [16].

Kosugi [7] came up with a theoretically derived model by assuming that the soil pore radius are log-normally distributed, and is given by Eq. 3.

$$\theta = \theta_r + (\theta_s - \theta_r).\,Q\left[\frac{\ln\left(\frac{h}{h_m}\right)}{\sigma}\right] \quad . \quad (3)$$

Where σ is a dimensionless parameter which decides the effective saturation at the point of inflection and h_m is related to the capillary pressure at the inflection point.

Q is a complementary normal distribution function given by Eq.4

$$\mathrm{Q(x)} = \frac{1}{\sqrt{2\pi}} \int_{-\infty}^{\mathrm{x}} \mathrm{e}^{-\frac{\mathrm{t}^2}{2}}\ \mathrm{dt}\ . \tag{4}$$

Methods

Data. The data for this study was obtained from two different studies. The first dataset was data from Indonesia (Flores, Kotawaringan Barat, Samarinda, Katai and Dan Gorontalo regions) extracted from [18] and constitutes the bulk of the data used in the study; totally there were 165 data samples. The second set of the data, was extracted from analytical results of a detailed survey (of Puchong farm of Universiti Pertanian Malaysia) in Selangor conducted by [19]. The extracted data consist of 26 data sets, making a total of 191 data sets. All the data consist of soil moisture content, measured at suction of approximately pF 0, pF 1, pF 2, pF 2.52 and pF 4.2 (pF is the 10-logarithmic value of the water column in cm). The data was then classified into 10 different soil textures according to the international society of soil science classification (ISSS).

Parameter Optimisation. The fitting parameters of the retention function were optimised using visual basic application (VBA) for excel and solver add-in function. The excel solver add-in uses the generalised reduced gradient method (GRGM) for solving non-linear problems. The method has a reputation for robustness compared with other non-linear optimisation methods [20].

Variety of error functions are available for use in optimisation problems (as to define agreement between the model and the observed value) a study of six error functions showed that the sum of square of errors (SSQR) given by eq.5 provide better fit for most soil textural classes [21].

$$SSQE = \sum_{i=1}^{N} (\theta_{io} - \vartheta_{im})^2\ . \tag{5}$$

Where N is number of observations; θ_o is observed value and θ_m is model value.

To evaluate the three models, the sum of square of errors (SSQE) (since it is to be used for model evaluation in the optimisation stage) and the Akaike information criterion (AIC) given by eq.6 for each model were computed. The AIC, is an index used to determine the most competitive model amongst several others, lower values indicate better competency or rather, better model quality [22].

$$\mathrm{AIC} = \mathrm{M}\left[\log(2\pi) + \log\left(\frac{\mathrm{SSQE}}{\mathrm{M-P}}\right) + 1\right] + \mathrm{P} \tag{6}$$

M is number of data points and, P is number of parameters to be optimised for the model in question.

For any particular retention function the parameters were fitted against the five retention data points. To prevent convergence to local minima, the parameters were initialised based on literature, where satisfactory results were not obtained a trial and error was used for the range of the parameter values until satisfactory result were obtained.

Results and Discussion

To clearly identify the model behaviour, a plot of SWRC (using average values of optimised model parameters) for randomly selected samples is shown in Fig.1. Generally all the models showed good fitting except at residual moisture content, this clearly indicates some of the limitations of these models. For clayey soils the KG model shows good fit everywhere including residual moisture content, the B&C and VG functions give fairly good fit too, except at high suction where they tend to overestimate the moisture content.

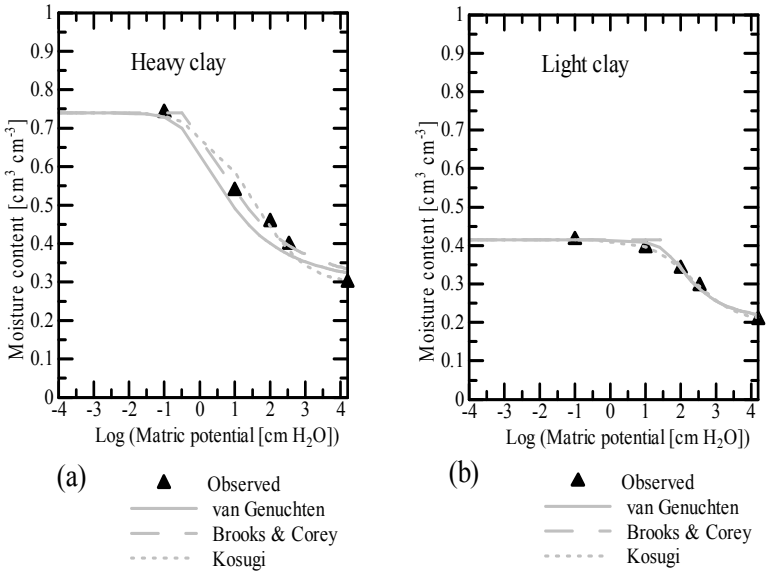


Figure 1. Observed and model fitted SWRC of some randomly selected samples: (a; Puchong sample and b; Indonesian sample)

In silty soils similar observation was made, only the KG function fits well at high suction. For Sands however all three models seem to overestimate the residual moisture content. The KG also underestimates the moisture content near inflexion for some soils in all the classes; this seems to be the case mostly for samples having high moisture content at saturation level. The B&C indicated better fitting around the inflexion point, since the B&C can describe very well, soils with distinct air entry values probably due to the air entry value description parameter incorporated in the model

Base on average values of the fitting (with SSQE as measure of goodness of fit), the KG indicates better fit among the models, as it recorded lowest values of SSQE, (see Table 1). In fact the SSQE was nil (correct to 4 decimals) for over 60 % of the datasets, with highest value of only 0.0006 cm^3 cm^{-3} for silty clay loam. The KG model also has the lowest AIC values indicating best model quality or suitability (as far the given data is concerned) amongst the three models.

Table 1. Average value of SSQE and AIC for the different soil samples

		Clay loam	Heavy clay	Light clay	Loam	Sand	Sandy clay	Sandy clay loam	Sandy loam	Silty clay	Silty clay loam
VG	***SSQE***	0.0005	0.0005	0.0005	0.0007	0.0005	0.0003	0.0004	0.0006	0.0006	0.0014
	AIC	-5.85	-6.16	-5.87	-5.29	-5.84	-7.05	-6.46	-5.62	-5.67	-3.85
B&C	***SSQE***	0.0006	0.0006	0.0008	0.0011	0.0012	0.0006	0.0006	0.0010	0.0008	0.0013
	AIC	-7.42	-7.40	-6.98	-6.10	-6.04	-7.51	-7.64	-6.48	-6.98	-5.76
KG	***SSQE***	0.0002	0.0002	0.0002	0.0004	0.0004	0.0002	0.0002	0.0003	0.0002	0.0006
	AIC	-9.46	-9.61	-9.68	-8.52	-8.55	-10.48	-10.31	-8.91	-9.89	-7.50

The theoretically derived log normal KG function describes well, the soil pore structure as many porous media are log normally distributed, in the case of humid tropical soils they have been quite leached out by relatively excessive rainfall thus, have increased pores, this is why the KG function gives better fitting.

Conclusion

The parameters of water retention models of B&C, VG and KG models have been obtained for soil of tropical region. With only five data points (residual and saturated moisture contents inclusive) the functions have proved to be very handy, successfully fitting the water retention curve of the soils with some good results. Good plots of SWRC were obtained using average values of the optimised parameters of each soil class, however the models were not so good in fitting the SWRC to moisture content levels at very high suction. A comparison of the three models showed the KG model as a better descriptor of SWRC of tropical soils.

It is again worth noting that the samples used are those of tropical region and that the superiority of the lognormal distribution model of KG as demonstrated with tropical samples, may not be better than the other models when used for temperate soils.

Acknowledgements

The First author gracefully acknowledges the financial support from UTP for Postgraduate sponsorship. This study was partially supported by the Ministry of Higher Education, Malaysia through UTM Research University Grant (vot number: R.J130000.7722.4D049 & R.J130000.7322.4B076).

References

[1] A. Mermoud and D. Xu, "Comparative analysis of three methods to generate soil hydraulic functions," *Soil Tillage Res.*, vol. 87, no. 1, pp. 89–100, May 2006.

[2] H. Vereecken, "Estimating the unsaturated hydraulic conductivity from theoretical models using simple soil properties," *Geoderma*, vol. 65, no. 1–2, pp. 81–92, Feb. 1995.

[3] R. Haverkamp, F. Bouraoui, C. Zammit, and R. A. Jarumillo, "Soil Properties and Moisture Movement in the Unsaturated Zone," in *The handbook of ground water engineering*, J. W. Delleur, Ed. Boca Raton: CRC Press, 1999, pp. 170–219.

[4] W. Durner and H. Fluhler, "Soil Hydraulic Properties," *Encyclopaedia of hydrological sciences*. John Wiley & sons, pp. 1103–1119, 2005.

[5] R. H. Brooks and A. T. Corey, "Hydraulic properties of porous media," *Hydrology Paper 3*, vol. 196. Fort Collins, 1964.

[6] M. T. van Genuchten, "A closed form equation for predicting the hydraulic conductivity of unsaturated soils," *Soil Sci. Soc. Am. J.*, vol. 44, no. 5, pp. 892–898, 1980.

[7] K. Kosugi, "Lognormal distribution model for unsaturated soil hydraulic properties," *Water Resour. Res.*, vol. 32, no. 9, pp. 2697–2703, 1996.

[8] B. Minasny and D. E. Hartemink, "Predicting soil properties in the tropics," *Earth Sci. Rev.*, vol. 106, pp. 56–62, 2011.

[9] J. Tomasella, Y. Pachepsky, S. Crestana, and W. J. Rawls, "Comparison of Two Techniques to Develop Pedotransfer Functions for Water Retention," *Soil Sci. Soc. Am. J.*, vol. 67, no. 4, p. 1085, Jul. 2003.

[10] M. G. Hodnett and J. Tomasella, "Marked differences between van Genuchten soil water-retention parameters for temperate and tropical soils: a new water-retention pedo-transfer functions developed for tropical soils," *Geoderma*, vol. 108, no. 3–4, pp. 155–180, Aug. 2002.

[11] P. P. Adhikary, D. Chakraborty, N. Kalra, C. B. Sachdev, A. K. Patra, S. Kumar, R. K. Tomar, P. Chandna, D. Raghav, K. Agrawal, and M. Sehgal, "Pedotransfer functions for predicting the hydraulic properties of Indian soils," *Aust. J. Soil Res.*, vol. 46, no. 5, p. 476, Aug. 2008.

[12] W. M. Cornelis, M. Khlosi, R. Hartmann, M. Van Meirvenne, and B. De Vos, "Comparison of Unimodal Analytical Expressions for the Soil-Water Retention Curve," *Soil Sci. Soc. Am. J.*, vol. 69, no. 6, p. 1902, 2005.

[13] M. van den Berg, E. Klamt, L. P. van Reeuwijk, and W. G. Sombroek, "Pedotransfer functions for the estimation of moisture retention characteristics of Ferralsols and related soils," *Geoderma*, vol. 78, no. 3–4, pp. 161–180, Aug. 1997.

[14] J. Tomasella and M. G. Hodnett, "Estimating soil water retention characteristics from limited data in Brazilian Amazonia," *Soil Sci.*, vol. 163, pp. 190–202, Mar. 1998.

[15] J. Tomasella, M. G. Hodnett, and L. Rossato, "Pedotransfer Functions for the Estimation of Soil Water Retention in Brazilian Soils," *Soil Sci. Soc. Am. J.*, vol. 64, pp. 327–338, 2000.

[16] M. T. van Genuchten, F. J. Leij, and S. R. Yates, "The RETC Code for Quantifying the Hydraulic Functions of Unsaturated Soils," , U.S. Salinity Laboratory. Report EPA/600/2/2–91/065. USDA, Agricultural Research Service, Riverside, CA., Riverside, CA., 1991.

[17] H. Vereecken, M. Weynants, M. Javaux, Y. Pachepsky, M. G. Schaap, and M. T. Van Genuchten, "Using Pedotransfer Functions to Estimate the van Genuchten–Mualem Soil Hydraulic Properties: A Review," *Vadose Zo. J.*, vol. 9, no. 4, p. 795, 2010.

[18] M. Askari, T. Tanaka, B. I. Setiawan, and S. K. Sapto, "Infiltration Characteristics of Tropical Soil Based on Water Retention Data," *J. Japan Soc. Hydrol. Water Resour. Japan Soc. Hydrol. Water Resour.*, vol. 21, pp. 215–227, 2010.

[19] Tessen and Yusop, "Detailed soil survey of UPM farm, Puchong," Universiti Pertainyan Malaysia, Selangor, 1979.

[20] L. Leon, W. Allan, D. Fylstra, L. Lasdon, J. Watson, and A. Warren, "Design and use of the microsoft excel solver," *Interfaces (Providence).*, vol. 28, no. October, pp. 29–55, 1998.

[21] L. R. Chevalier and J. N. Yesuf, "Spreadsheet Optimization for Parameter Estimation of Pressure–Saturation Equations Used for Two-Phase Groundwater Flow," *Water. Air. Soil Pollut.*, vol. 179, no. 1–4, pp. 57–65, Aug. 2006.

[22] H. Aike, "A New Look at the Statistical Model Identification," *IEEE Trans. Automat. Contr.*, vol. 19, no. 6, pp. 716–723, 1974.

Applied Mechanics and Materials Vol. 567 (2014) pp 14-19
© (2014) Trans Tech Publications, Switzerland
doi:10.4028/www.scientific.net/AMM.567.14

Courtyard As a Microclimatic Modifier
Experimental Study on Actual Site

Abdulbasit Almhafdy[1,a] , Norhati Ibrahim[2,b], Sabarinah Sh Ahmad[3,c],
Wan Mohd. Naim Wan Salleh[4,d]

[1,2,3,4] Faculty of Architecture, Planning and Surveying, University Teknologi MARA
Shah Alam 40450, Selangor, Malaysia

[a]mhf2000@msn.com, [b]norhati@salam.uitm.edu.my, [c]sabar643@salam.uitm.edu.my,
[d]mnaim1960@yahoo.com

Keywords: Experimental study, courtyard, design variants, microclimate performance

Abstract. An experimental study of two different forms of courtyards has been conducted in an existing hospital building, in the tropics. The experiments involved three design variants, namely form, size, and orientation. Three weather stations were used in three different courtyards, O- and U-forms and the third one was located in the outdoor area as benchmark. The courtyard, as a microclimatic modifier, has the ability to improve the thermal and the visual condition within the semi-outdoor area. Therefore, four physical environments variables, namely air temperature, humidity, solar intensity and wind were investigated and analyzed as these variables have not previously been studied in a single experiment of courtyard. The aim of this paper is to measure and examine the differences of thermal and visual performance in the courtyards during daytime. The results showed that form, wind orientation and number of floors had a significant effect on the microclimate and visual performance of the courtyard. Forms, orientation and number of floors are the key design variants that show a significant effect in the U-form courtyard.

Introduction

Courtyard is often an enclosed area surrounded by a building or wall and open to the sky [1]. It was originated from the ancient architecture of the Arabs and early Europe as well as other ancient civilizations. The history of good courtyard design renders it difficult for the generation of new ideas for courtyard design [2, 3].

Through the ages, this basic form of the courtyard has been modified to fulfill various environmental aspects such as geography, site restriction, building orientation and function to create new formal and modern form of courtyard such as U, L, T or Y [4]. Hence, courtyards can be semi-closed (three or two sided), and the orientation of the semi-closed courtyard is crucial as it could have significant effects as a microclimate modifier in some climate [5, 6].

Many studies have proven that courtyards are climate responsive [7]. Courtyard can be affected by form [8], size[9] and orientation[10]. Thus, this experiment attempts to study the thermal and visual performance of selected courtyards. The study was carried out through a comparative analysis of thermal and visual performance in two types of the courtyard through on-site measurements of the microclimate with varied parameters such as form, size and orientation,

Selection of courtyards

Malaysia has a tropical hot and humid climate. Serdang Hospital is a government-funded multi-specialty hospital located in the district of Sepang in the state of Selangor, Malaysia. It is situated in 101° 43' 12.07"E longitude and 2° 58' 37.38"N latitude. Out of 7 courtyards in Serdang hospital, 2 different forms are selected and investigated simultaneously during daytime along with another outdoor area as benchmark. The selection of the case study building was based on the following criteria:

Courtyards Configuration. Among all government hospitals in Malaysia, Serdang hospital is the only one that has many different types of courtyards. (Fig. 1, and Table 1). However, in this experiment, two different forms of courtyards were selected for this investigation.

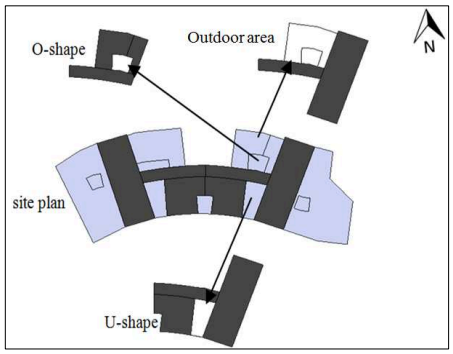


Fig. 1. The O and U-forms of courtyards and the outdoor area in Serdang Hospital

Table 1 : Courtyard forms and design variants

Form	Area (m^2)	Configuration	No. of floors	Opening side
O-form	381	Fully closed and has a square form	North : 3 South : 7 East : 5 West : 3	-
U-form	893	Three sided and has a rectangular form	North : 5 South : 0 East : 4 West : 3	South

Orientation and exposure. The following are further details of the fully enclosed and semi enclosed courtyards:

The O-form courtyard: Fig. 2, is a square shape and fully closed by walls. In this case, the significance will be on the size as well as the exposure rather than the orientation. As seen in Table 1, the courtyard is sided by 3 levels of floors from North & South, 5 levels from E and 7 levels from the South.



Fig. 2. The O-form courtyard



Fig. 3. The U-form courtyard

U-form courtyard: Fig. 3, is three sided, and the opening side is oriented to the South. The courtyard is a rectangle and has a different number of floors in the three sides as shown in Table 1.

The third weather station is located in the outdoor area (roof garden) within the hospital. This weather station is used as a benchmark.

Accessibility and cooperation. The hospital management has allowed the data collection during working hours between 10.00h and 18.00h. AutoCAD drawings of the hospital were provided by the Engineering department.

Data collection

This experimental study was carried out to investigate the existing conditions of microclimate performance of various forms of courtyards by analysing the effects of form, size and orientation on the microclimate. Three sets of weather stations have been used in this experiment. These weather stations were calibrated one day before the actual experiment in order to ensure the accuracy of data.

A continuous measurement was undertaken at the three locations. A weather station is located in the O-form and U-form of courtyards each. The benchmark weather station was located in the outdoor area (roof garden) within the hospital, during working hours between 10:30h and 17.30h on Tuesday, 23rd October 2012. The data logger weather station named PortLog (Fig. 4) was placed within the central part of each courtyard. The parameters were measured at 15 minutes intervals and recorded continuously at 1.1m above the ground corresponding to the average height of the centre of gravity for adults. At the end of the measurement period, the logged data was exported to Microsoft Excel 2010 spreadsheet for analysis.



Fig. 4. Weather Station

Moreover, a visual observation was also conducted, by the experiment team and hospital staff, during data collection as they could be used in the data analysis stage.

Findings

As mentioned before, two configurations of courtyards in term of form, size and orientation have been taken into consideration in order to observe the microclimate performance. Four physical factors are discussed in the following sections in order to analyze the most and least effected among the courtyards based in the actual condition. The net effect of the courtyard configuration design on thermal and visual performance would depend on the courtyard form, exposure and orientation.

Air temperature and humidity. The O-form is fully closed and has no natural ventilation at all while the U-form is surrounded by 3 walls and opened to the south side that allowed more natural ventilation. The results in Fig. 5 show that the O-form courtyard has more obvious effect on increasing air temperature than the U-form.

In addition, the highest difference of temperature between O-form courtyard and U-form courtyard was 1.7Cº, recorded at 14:15h. While, the lowest difference of temperature was 0.1Cº, recorded at 3pm.

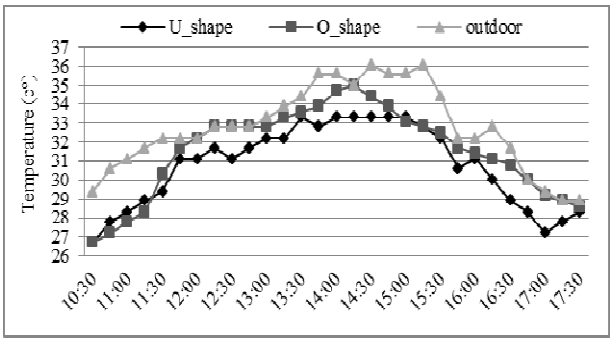


Fig. 5. Air temperature

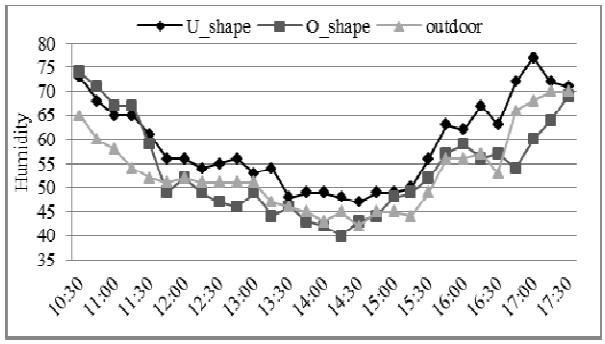


Fig. 6. Relative Humidity

However, the outdoor area (roof garden) performed the worst as it was considered as an open enclosure area that gained more solar intensity during the daytime. The highest temperature was 37Cº recorded at 15:15h.

On the other hand, relative humidity had an inverse relationship with temperature. As shown in Fig. 6, the relative humidity was higher in the U-form of the courtyard than the O-form of the courtyard.

Solar intensity. Solar radiation essentially provides information on how much solar energy hits a surface at a location on the earth during a particular time. As shown in Fig. 7, the O-form courtyard has the minimum amount of solar intensity. This due to the form as well as the size when compared with the U-form courtyard. In contrast, the outdoor area has the maximum amount of solar intensity. This is due to the open exposure of the outdoor area.

Although the U-form courtyard is considered bigger than the O-form, the results in the U-form were close to the O-form in terms of solar intensity. The number of floors and orientation were key variants that have been used in U-form. The U-form courtyard is rectangular and has 4 floors form the east and north sides and 3 floors from the west side (Table 1). This kind of treatment with such a design variants allowed for more shaded area and produced more comfortable ambiance.

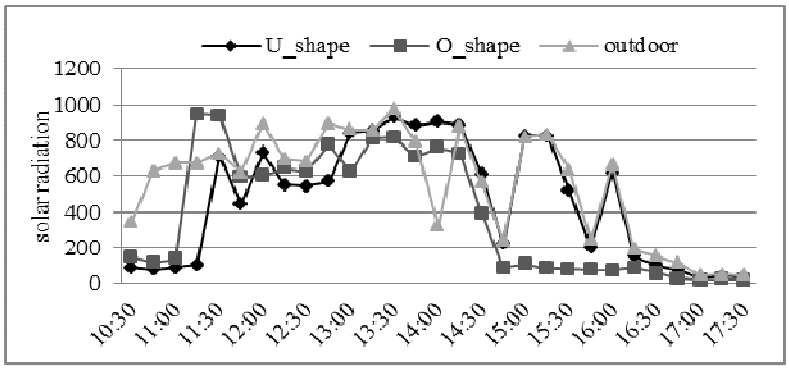


Fig. 7. Solar Intensity

Wind speed and direction. The results on wind speed showed better microclimate performance in the U-form than the O-form courtyard (Fig. 8). During the data collection, it was clear that the natural ventilation had key effect within the courtyard. The U form courtyard has an E-W orientation which opened to the south side, which allowed better ventilation during the daytime. The highest wind speed in the courtyard was between 13.00h and 16:30h, which fluctuated between 1.4

and 2.7m/s. The wind speed was recorded at 0mps in the O-form courtyard as it is fully enclosed on all sides.

On the other hand, Fig. 9 shows that the most frequent wind direction in the U-form varied from south direction (150) to west direction (250).

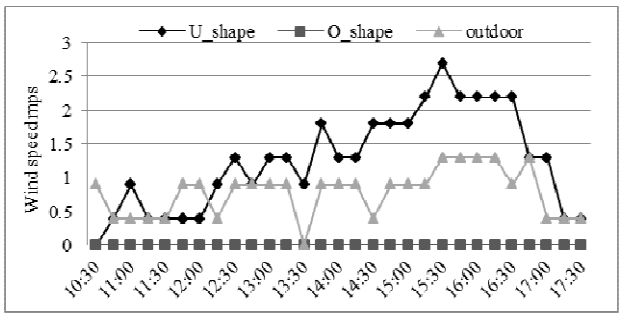


Fig. 8. Wind Speed

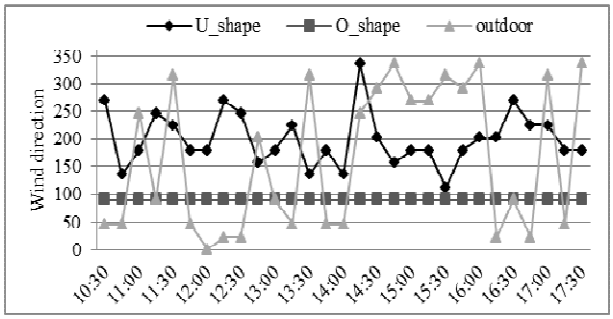


Fig. 9. Wind Direction

It is clear that the reason for that is the opening side of the U-form courtyard facing the south. The wind direction changed at 14:15h from north as the wind bounced from the south wall of the courtyard.

Analysis and discussion

This experiment aims to investigate the microclimate performance of two types of courtyard. This is to compare and analyze the treatments and methods of design variants of the courtyard that could be taken into consideration in future design for better thermal and visual comfort.

The U-form courtyard obviously played a distinct role in the microclimate performance compared with the O-form. In fact, orientation and number of floor were the key variants that affected in the U-form courtyard.

The orientation and number of floors could have a significant effect on the solar intensity by increasing the shading area, which affected the thermal and visual performance.

On the other hand, the form as a design variant could have a significant effect as well, depending on the orientation and number of floors (exposure).

The U-form courtyard as a rectangular courtyard with east-west orientation and opened towards the south provided greater opportunity for natural ventilation and shaded area. It provided more connection to outdoor and natural environment as well as produced better microclimate, considering the design variants of size and orientation.

Based on the visual observation, the O-form performed slightly better than the U-form in terms of minimising glare.

Conclusion

All in all, forms, orientation and number of floors were the key design variants that showed a significant effect in the U-form courtyard. The U-form courtyard provided more connection to outdoor and natural environment as well as produced better microclimate performance when the design variants of size and orientation were considered.

Although the U-form courtyard provided more connection to the natural environment as the open enclosure allowed for more solar intensity and glare as well as thermal discomfort. Shading media analysis could be future work using simulation techniques.

Future work

The study was done only in two courtyards, therefore, it could be difficult to draw generalised relations or trendlines. However, simulation studies are encouraged to be applied using the data collected for calibration and validation.

Acknowledgment

This research is made possible with the financial support provided by the Research Management Institute (RMI), Universiti Teknologi MARA, Malaysia under its Research Intensive Faculty (RIF) funding programme. We, therefore, thank RMI as well as the Faculty of Architecture, Planning and Surveying for this research opportunity.

References

[1] B. Edwards, M. Sibley, M. Hakmi, and p. Land, Courtyard housing: past, present and future: Spon Press, 2006.

[2] J. Reynolds, Courtyards: aesthetic, social, and thermal delight: Wiley, 2002.

[3] T. A. Saeed, "Studies on the geometrical properties of courtyard house form considering natural ventilation in hot-dry regions," 3492493 Ph.D., Illinois Institute of Technology, Ann Arbor, 2007.

[4] N. Das, "Courtyards houses of Kolkata: Bioclimatic, typological and socio-cultural study," Msc, Department of Architecture, College of Architecture, Planning and Design, Kansas State University, 2006.

[5] I. A. Meir, D. Pearlmutter, and Y. Etzion, "On the microclimatic behavior of two semi-enclosed attached courtyards in a hot dry region," Building and Environment, vol. 30, pp. 563-572, 1995.

[6] H. Safarzadeh and M. N. Bahadori, "Passive cooling effects of courtyards," Building and Environment, vol. 40, pp. 89-104, 2005.

[7] A. Aldawoud, "Thermal performance of courtyard buildings," Energy and Buildings, vol. 40, pp. 906-910, 2008.

[8] A. S. Muhaisen and M. B Gadi, "Shading performance of polygonal courtyard forms," Building and Environment, vol. 41, pp. 1050-1059, 2006.

[9] P. Moonen, V. Dorer, and J. Carmeliet, "Evaluation of the ventilation potential of courtyards and urban street canyons using RANS and LES," Journal of Wind Engineering and Industrial Aerodynamics, vol. 99, pp. 414-423, 4// 2011.

[10] S. Berkovic, A. Yezioro, and A. Bitan, "Study of thermal comfort in courtyards in a hot arid climate," Solar Energy, vol. 86, pp. 1173-1186, 5// 2012.

Applied Mechanics and Materials Vol. 567 (2014) pp 20-25
© (2014) Trans Tech Publications, Switzerland
doi:10.4028/www.scientific.net/AMM.567.20

Determination of Adsorption Capacity of Agricultural-Based Carbon for Ni (II) Adsorption from Aqueous Solution

Taimur Khan[a], Mohamed Hasnain Isa[b], Malay Chaudhuri[c],
Muhammad Raza Ul Mustafa[d] and Mohamed Osman Saeed[e]

Civil Engineering Department, Universiti Teknologi PETRONAS, 31750 Tronoh, Perak, Malaysia

[a]taimurkhan7@gmail.com, [b]hasnain_isa@petronas.com.my, [c]malaychaudhuri@yahoo.com,
[d]raza.mustafa@petronas.com.my, [e]osman.saeed@petronas.com.my

Keywords: Adsorption, rice husk carbon, Ni (II), isotherm, kinetics

Abstract. The aim of the study was to prepare potentially cheaper carbon for the adsorptive removal of Nickle [Ni (II)] from aqueous solution. The adsorption capacity of the prepared carbon to remove Ni (II) from aqueous solution was determined and adsorption mechanism was investigated. Rice husk carbon was prepared by incineration in a muffle furnace. The incinerated rice husk carbon (IRHC) was characterised in terms of surface area, micropore area, micropore volume, average pore diameter and surface morphology. Adsorption of Ni (II) by IRHC was examined. The influence of operating parameters, namely, pH, initial concentration and contact time on adsorption of Ni (II) by IRHC was evaluated. Batch adsorption tests showed that extent of Ni (II) adsorption depended on initial concentration, contact time and pH. Equilibrium adsorption was achieved in 120 min, while maximum Ni (II) adsorption occurred at pH 4. Langmuir and Freundlich isotherms were studied and the equilibrium adsorption data was found to fit well with the Langmuir isotherm model. Langmuir constants Q° and b were 14.45 and 0.10, and Freundlich constants K_f and $1/n$ were 4.0 and 0.26, respectively. Adsorption of Ni (II) by IRHC followed pseudo-second-order kinetics. Being a low-cost carbon, IRHC has potential to be used for the adsorption of Ni (II) from aqueous solution and wastewater in developing countries.

Introduction

In recent decades, the discharge of heavy metals to the aquatic environment has posed a challenging problem for environmentalists due to their non-biodegradability and toxic nature. Heavy metals can also enter food cycle and cause a major problem to human health. Nickle is a heavy metal. It is the fifth most naturally occurring abundant element in the earth. It is present in large concentrations in the discharged wastewater of many industries such as batteries manufacturing, motor vehicle, electroplating and aircraft, and causes toxic effects even at low concentrations. High concentration of Ni (II) causes cancer of lungs, nose and bone [1]. Though the World Health Organization, (WHO) has recommended that the maximum concentration of nickel in drinking water should not exceed 0.1 mg/L, but in wastewater generated from many electroplating industries, it is as high as 50 mg/L [2,3]. The protective and efficient removal of Ni (II) contaminated wastewater is a challenging issue that needs to be addressed because alternative low-cost removal techniques are not readily available. The main objective today is to implement suitable methods and to develop appropriate techniques either to prevent metal contamination or to reduce it to acceptable levels [2]. Several techniques have been suggested for treatment of Ni (II) in wastewater. These include membrane filtration, chemical precipitation, electrochemical reduction, ion exchange, adsorption [4] and phytoextraction [5]. These techniques are generally inefficient and/or expensive especially when practiced for the removal of heavy metal ions to low concentrations [6] and these techniques also produce sludge. Compared with other treatment techniques, adsorption technology has gained much attention because it is simple in design, economical for reducing trace quantities of heavy metals and it also does not produce sludge [7,8]. Many researchers suggest that active carbon

is very effective for the treatment of Ni (II) [9]. Commercial activated carbons are most commonly used by industries for heavy metals and other contaminants removal. The high price of commercial activated carbon limits its use in developing countries. Hence, there is a need to produce low-cost adsorbent alternative to commercial activated carbon for the effective and safe removal of heavy metals.

In the present investigation, rice husk was incinerated in order to develop a low cost carbon by a simple method for the removal of Ni (II) from aqueous solution. Adsorption isotherms and kinetics models have been tested for their usefulness in correlating the experimental data for the adsorption of Ni (II) by the incinerated rice husk carbon (IRHC).

Meterials and Methods

Preparation of IRHC. Raw rice husk was collected from a rice mill located in Perak (Malaysia). The collected raw rice husk was washed with tap water followed by washing with distilled water several times in order to remove dust. The washed rice husk was dried in an oven at 105℃ for 24 h. The washed and dried rice husk was then incinerated in a muffle furnace at 300°C for 4 h. The resulting IRHC was ground to a finer size of 212- 500 μm and used in various batch adsorption tests.

Adsorption Tests. Unless specified, batch adsorption tests were conducted by shaking 100 mL of Ni (II) solution of desired concentration with 0.2 g of IRHC in a conical flask at room temperature (22 °C), using an orbital shaker at 150 rpm. After a predetermined contact time, the flask was removed from the orbital shaker and the supernatant was filtered through 0.45 μm membrane filter and analysed for remaining Ni (II) concentration using a spectrophotometer. The effects of pH (2-7), contact time (5-180 min) and Ni (II) concentration (20-80 mg/L) were also determined. The pH of the solution was adjusted by 0.1 N NaOH or 0.1 N HCl. Adsorption isotherms and kinetics were studied based on batch equilibrium test using optimum contact time and pH.

Results and Discussion

Characterisation of IRHC. The BET surface area, micropore area, micropore volume and average pore diameter of IRHC are 76.47 m^2/g, 14.29 m^2/g, 0.006967 mL/g, and 40.20 Å, respectively. Scanning electron micrograph of incinerated rice husk (Fig. 1) shows presence of macro- and micro-pores.

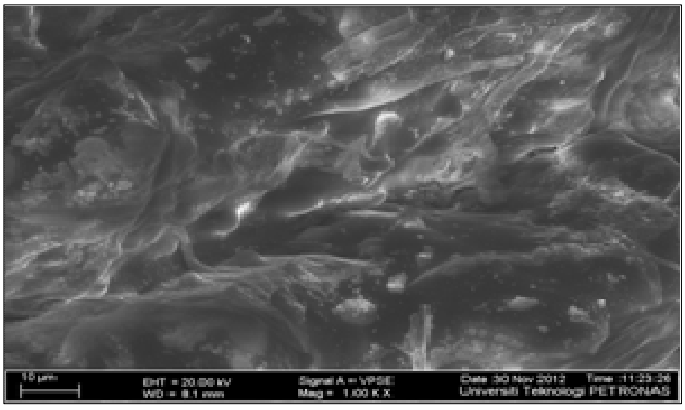


Fig. 1 Scanning electron micrograph of IRHC

Effect of Initial pH. The pH of an aqueous solution is one of the most important variables affecting both the solution chemistry of the metals ion and the surface charge of the adsorbent. This assumption is due to the fact that hydrogen ions themselves are strong competing ions and that the

solution pH affects the chemical speciation of the metal ions as well as the ionization of the functional groups on the surface of adsorbent [2,10]. The initial pH was varied in the range of 2-7 for a 20 mg/L Ni (II) solution. The results are shown in Fig. 2. It is noticed that the adsorption of Ni (II) was very little when pH of the solution was highly acidic (pH ≈ 2), while the adsorption increased with increase in pH. Maximum adsorption of 56.25% occurred at pH 4. The lower adsorption capacity at low pH is because of the presence of higher H^+ concentration in aqueous solution which compete with Ni(II) ions for the adsorption sites of the IRHC. When pH of the aqueous solution increases, the H^+ concentration decreases leading to high Ni(II) adsorption. Similar observation has been found by Reddy et al. [6] for biosorption of Ni (II) by *Moringa oleifera* bark. Rest of the batch adsorption testes were conducted at pH 4.

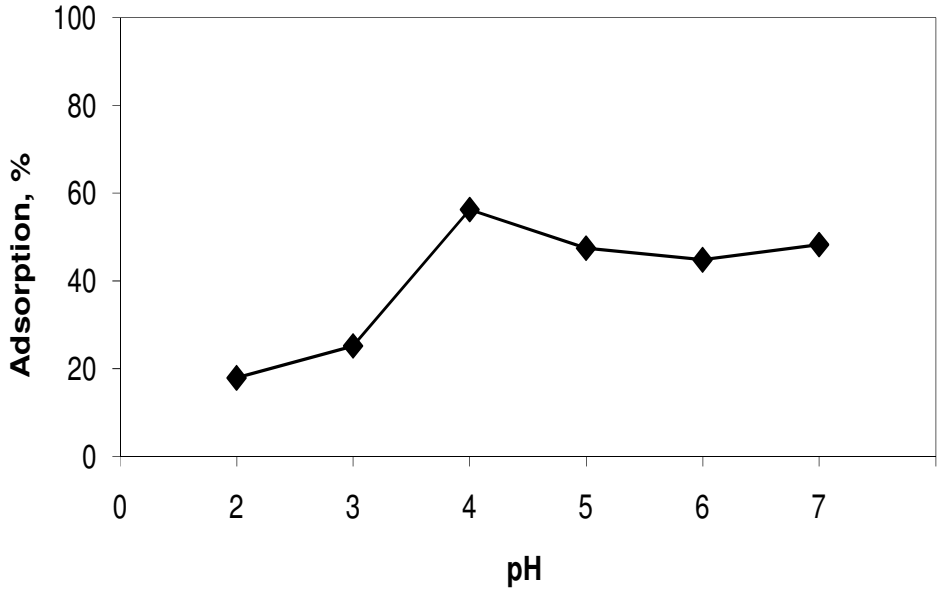


Fig. 2: Effect of pH on adsorption of Ni (II) by IRHC

Effect of Contact Time and Initial Ni (II) Concentration. To investigate equilibrium adsorption time, Ni (II) adsorption by IRHC at four different initial concentrations was calculated as a function of contact time. The effect of contact time on Ni (II) adsorption is shown in Fig. 3. The extent of Ni (II) adsorption increased as the initial Ni (II) concentration decreased and as the contact time increased. The adsorption rate of Ni (II) was rapid in the first 5 min. Equilibrium was achieved at 120 min and thereafter remained constant. Based on these results, a contact time of 120 min was taken as optimal contact time for all the following tests.

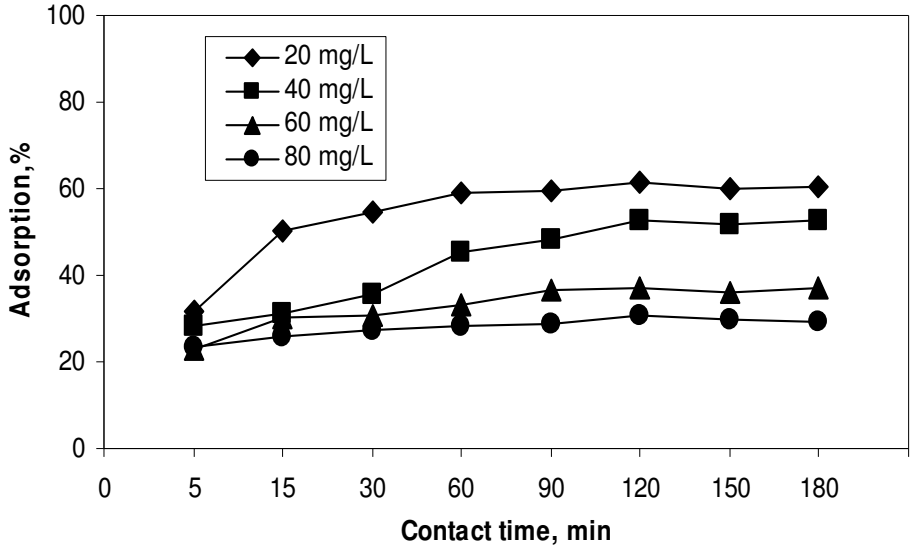


Fig. 3 Effect of contact time on adsorption of Ni (II) by IRHC

Adsorption Kinetics. Two kinetic models, pseudo-first-order and pseudo-second-order were applied to examine adsorption kinetics at different initial Ni (II) concentrations to describe the mechanism of the adsorption process [11,12]. The linear form of the pseudo-first-order model is written as in Eq. (1),

$$\log(q_e - q_t) = \log q_e - \frac{k_1 t}{2.303} \tag{1}$$

and the linear form of the pseudo-second-order model is in Eq. (2),

$$\frac{t}{q_t} = \left(\frac{1}{k_2 q_e^{\,2}}\right) + \left(\frac{t}{q_e}\right) \tag{2}$$

where, q_e and q_t are the amounts of metal ion adsorbed (mg/g) at equilibrium and any time t, respectively, k_1 is the equilibrium rate constant for pseudo-first-order kinetics (min^{-1}) and k_2 is the equilibrium rate constant for pseudo-second-order kinetics [g/(mg.min)]. Plots of log ($q_e - q_t$) versus t and of t/q_t versus t were plotted (graphs not shown). The experimental data fitted better to pseudo-second-order kinetic model than pseudo-first-order kinetic model, based on high R^2 for pseudo-second-order kinetic model. Hence, it is concluded that the adsorption of Ni (II) by IRHC is chemisorption. A similar trend of observation was reported for adsorption of Ni (II) by activated carbon derived from lotus stalks [10].

Adsorption Isotherms. In a solid-liquid system during adsorption, the distribution ratio of the solute between the solid and the liquid phase is a measure of the position of equilibrium. The preferred form of representing this distribution is to express the solute adsorbed per unit weight of the solid (q_e) as a function of equilibrium concentration (C_e) at a fixed temperature. This type of expression is known as an adsorption isotherm [13]. The Langmuir and Freundlich adsorption isotherms are represented in Eq. (3) and Eq. (4) respectively,

$$q_e = \frac{Q^{\circ} b C_e}{1 + b C_e} \tag{3}$$

$$q_e = K_f C_e^{\,1/n} \tag{4}$$

where, $Q°$ is the amount of solute adsorbed per unit weight of adsorbent in forming a monolayer on the surface (monolayer adsorption capacity), b is a constant related to the energy of adsorption, K_f is the Freundlich constant and $1/n$ represents the adsorption intensity of Ni (II) by adsorbent or surface heterogeneity.

Linear forms of the Langmuir isotherm ($C_e/q_e = 1/(bQ°) + C_e/Q°$) and the Freundlich isotherm ($\log q_e = \log K_f + (1/n) \log C_e$) were fitted to the adsorption data; shown in Fig. 4 and Fig. 5, respectively. Langmuir constants $Q°$ and b were 14.45 and 0.10, and Freundlich constants K_f and $1/n$ were 4.0 and 0.26, respectively. The Langmuir isotherm model gave better fit to the experimental data than Freundlich isotherm model.

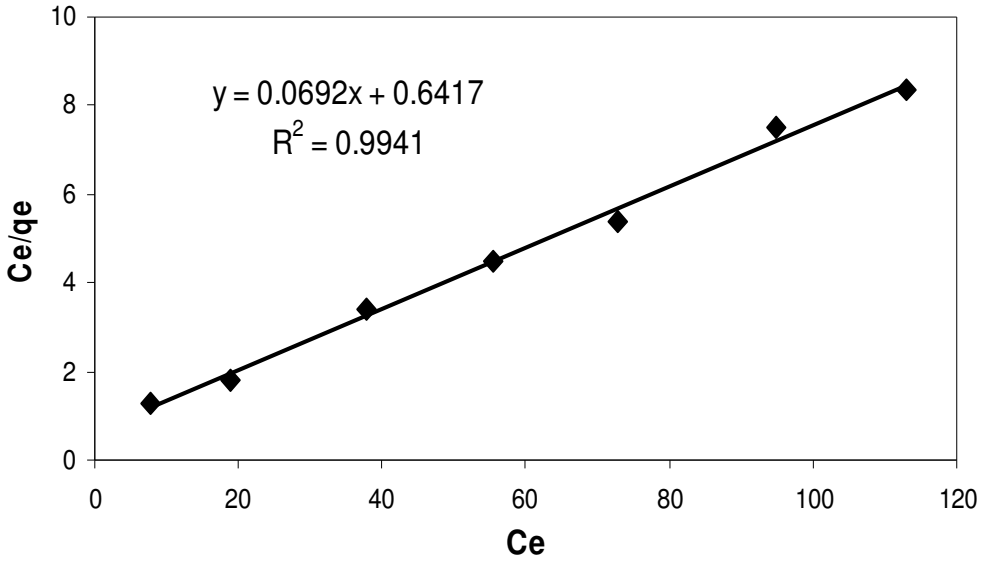


Fig. 4 Langmuir isotherm for Ni (II) adsorption by IRHC

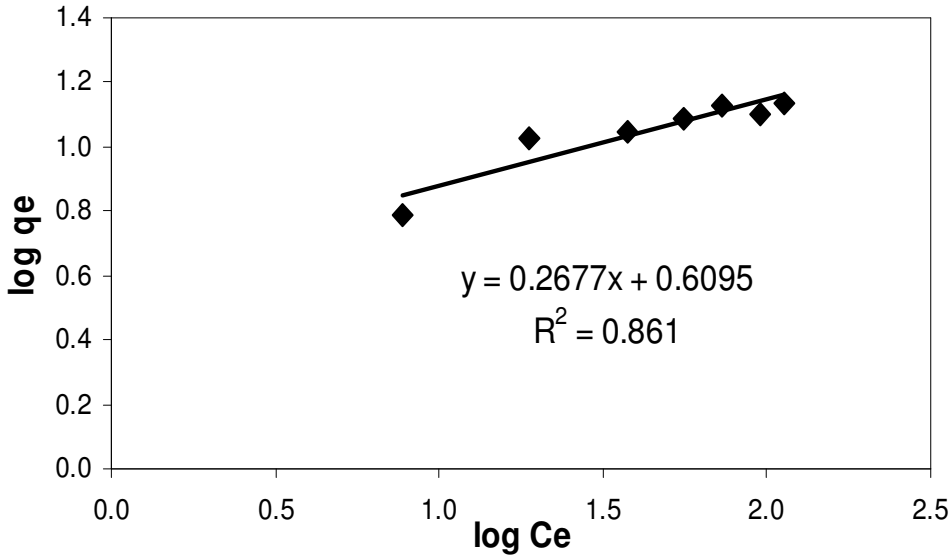


Fig.5 Freundlich isotherm for Ni (II) adsorption by IRHC

Conclusions

Incinerated rice husk carbon was found effective in the adsorption of Ni (II) from aqueous solution and maximum adsorption occurred in 120 min at pH 4. Langmuir isotherm model fitted the experimental data better than Freundlich isotherm model. Langmuir constants $Q°$ and b were 14.45

and 0.10, and Freundlich constants K_f and *1/n* were 4.0 and 0.26, respectively. The pseudo-second-order kinetic model fitted the experimental data well, indicating chemical adsorption of Ni(II). Being a low-cost agricultural by-product, rice husk is a good source for the preparation of rice husk carbon that can be employed as an effective adsorbent for the removal of Ni (II) and potentially for other heavy metals from aqueous solution and wastewater in developing countries.

ACKNOWLEDGEMENT

The authors are thankful to Universiti Teknologi PETRONAS (UTP) for providing facilities for this research and Graduate Assistantship to the first author.

References

[1] H. Hasar. Adsorption of nickel(II) from aqueous solution onto activated carbon prepared from almond husk, J. Hazrd. Materi. B97 (2003) 49–57.

[2] K. Totlani, R. Mehta, S.A. Mandavgane. Comparative study of adsorption of Ni (II) on RHA and carbon embedded silica obtained from RHA, Chem. Eng. J. 181-182 (2012) 376-386.

[3] World Health Organization, Applications of Guidelines for Drinking Water Quality, Document EHE/EHC/81.27, WHO, 1982.

[4] M.C. Basso, E.G. Cerrella, A.L. Cukierman, Activated carbons developed from a rapidly renewable biosource for removal of Cadmium(II) and Nickel(II) ions from dilute aqueous solutions, Ind. Eng. Chem. Res. 41 (2002) 180–189.

[5] M. Sprynskyy, B. Buszewski, A.P. Terzyk, J. Namie'snik, Study of the selection mechanism of heavy metal (Pb2+, Cu2+, Ni2+, and Cd2+) adsorption on clinoptilolite, J. Colloid Interface Sci. 304 (2006) 21–28.

[6] D.H.K. Reddy, D.K.V. Ramana, K. Seshaiah, A.V.R. Reddy, Biosorption of Ni(II) from aqueous phase by Moringa oleifera bark, a low cost biosorbent, Desalination 268 (2011) 150–157.

[7] U. Yetis, A. Dolek, F.B. Dilek, G. Ozcengizet, The removal of Pb (II) by Phanerochaete chrysosporium, Water Res. 34 (2000) 4090–4100.

[8] T. Khan, S.R.M. Kutty, M. Chaudhuri, Adsorptive removal of reactive yellow 15 from aqueous solution by coconut coir activated carbon, Adsorpt. Sci. Technol. 28 (2010) 657-667.

[9] E. Demirbaş, M. Kobya, S. Öncel, S. Şencan, Removal of Ni (II) from aqueous solution by adsorption onto hazelnut shell activated carbon: equilibrium studies, Bioresour. Technol. 84 (2002) 291–293.

[10] L.H. Huang, Y.Y. Sun, T. Yang, L. Li. Adsorption behavior of Ni (II) on lotus stalks derived active carbon by phosphoric acid activation, Desalination 268 (2011) 12–19.

[11] Y.S. Ho, G. McKay, Sorption of dye from aqueous solution by peat, Chem. Eng. J. 70 (1998) 115–124.

[12] M.H. Isa, N. Ibrahim, H.A. Aziz, M.N. Adlan, N.H.M. Sabiani, A.A.L. Zinatizadeh, S.R.M. Kutty. Removal of chromium (VI) from aqueous solution using treated oil palm fibre. J. Hazard. Mater. 152 (2008) 662-668.

[13] Weber, Jr., W.J., 1972. Adsorption: physiochemical processes for water quality control (ed.), Wiley-Interscience, New York, pp. 199-259.

Applied Mechanics and Materials Vol. 567 (2014) pp 26-31
© (2014) Trans Tech Publications, Switzerland
doi:10.4028/www.scientific.net/AMM.567.26

Effect of low pressure on irrigation uniformity of solid set sprinkler irrigation system

Manal Osman[1, a*], Suhaimi B. Hassan[2,b] Khamaruzaman B. Wan Yusof[3,c]

[1]Universiti Technologi PETRONAS/ Civil Engineering, Perak, Malaysia.

[2]Universiti Technologi PETRONAS/ Mechanical Engineering, Perak, Malaysia.

[3]Universiti Technologi PETRONAS/ Civil Engineering, Perak, Malaysia.

[a*]manal.osman96@yahoo.com, [b]suhaimiha@petronas.com.my,
[c]khamaruzaman.yusof@petronas.com.my

Keywords: Keywords: irrigation uniformity, uniformity coefficients, distribution characteristics, sprinkler irrigation.

Abstract. The irrigation requires an efficient and effective method of water application to realize maximum return and conserve water resources. The low pressure sprinkler irrigation system is the most commonly used due to: its low energy cost, but the irrigation uniformity of this system is not constantly good because it is affecting by the design factors such as: nozzle type, nozzle diameter, operating pressure and spacing layout. But the most important factors are the operating pressure and nozzle diameter. In this study the effect of low pressure on the irrigation uniformity of the solid set sprinkler irrigation system was studied. Different low operating pressures (62, 82, 102 and122 kPa) were selected and different nozzle diameters (4, 5 and 7 mm) were used. The solid set layout was square (12 m between the sprinklers along the line and 12 m among the line). The catch-cans test was used to determine the uniformity coefficients such as: Christiansen's coefficient of uniformity (CU), coefficient of variation (CV), distribution uniformity of low quarter (DU_{lq}) and distribution uniformity of low half (DU_{lh}). The distribution characteristics such as: throw radius and rotation speed were monitored. A comparison was made between the results obtained from different combination of operating pressures and nozzle diameters. The results of this study showed that, CU, DU_{lq} and DU_{lh} were increased when the pressure increased for all the nozzles. The greater values of CU, DU_{lq} and DU_{lh} were found with the combination of 7 mm nozzle diameter and 122 kPa. The coefficient of variation was increased when the pressure decreased for all the nozzles. The throw radius and rotation speed were increased gradually when the pressure increased. The throw radius was not significantly affected by the nozzle diameter while the rotation speed was more affected by the nozzle diameter.

Introduction

The efficient use of water and energy in agriculture became more relevance due to decreasing water resources and increasing energy cost in the world [1]. In many countries the open channel irrigation systems replaced by pressurized irrigation systems such as: sprinkler, trickle and drip irrigation which have high irrigation efficiencies and yields at same time save water [2]. Sprinkler irrigation is one of the most effective methods of irrigation due to many advantages including: the adaptation of the sprinkler with: different soil types, crop, and topography. In addition to the high irrigation efficiency and yield with low requirement of water and labors. Sprinkler irrigation systems characterized by more favorable operational conditions compare with surface irrigation systems because the discharge, the duration and the frequency of water application can be controlled [3-5].

Most of research interest focuses on sprinkler irrigation system because it produce 18% more yield, reduce consumption of water by 35% and increase the water efficiency by 30% of that used in the traditional irrigation system such as: surface irrigation. With the use of sprinkler irrigation system the major factor influencing its performance is the irrigation uniformity. The irrigation

uniformity is the ability of sprinkler to apply water evenly and uniformly over all the area, it used for the evaluation of sprinkler irrigation system performance. So it must be consider during design and installation of the system [6-7]. Sprinkler irrigation system requires a minimum value of 80% DU and 85% CU to obtain good irrigation uniformity. High irrigation uniformity can be achieved with a well system design, by applying the water to the soil without exceed the soil infiltration capacity that will avoid runoff [8-10].

The effect of the design factors in the irrigation uniformity of sprinkler irrigation system was studied by different researchers. Montero et al. [11] investigated the factors that affected on the uniformity of water distribution of the solid set sprinkler irrigation system such as: nozzle types and operating pressures. They concluded that, the sprinkler with double nozzle gave higher uniformity of water distribution, compared with single nozzle for all the pressures. Clark et al. [12] studied the CU of the solid set sprinkler irrigation system for multiple nozzle diameters and operating pressures using catch- cans method. Their results indicated that, CU values were ranged between 70% to 90% but those values were low with the low operating pressure and wider sprinkler nozzle. Tarjuelo et al. [13] Used different high pressures (300, 350 and 400 kPa) with different nozzle diameters (3.6, 4.4, 4.8 and 5.2 mm) using square and rectangular spacings (12 m x12 m) and (12 m x 15 m) to investigate CU of the solid set sprinkler irrigation system. They noticed that, the higher value of CU was 97% with 400 kPa pressure and 5.2 mm nozzle diameter. Also the results showed that, the CU decreased when the sprinkler spacing increased. But the main disadvantage of this system was the high energy cost. Montero et al. [14] studied the droplets distribution of the medium-size impact sprinkler using different nozzle diameters (2.4, 3.6 and 4.8 mm) and pressures (200, 350 kPa). They reported that, the working pressure was the main factor that influenced droplets distribution. Thus, as the pressure increased, drops increased that produced a uniform water jet. It was also noticed that, the droplets with a larger diameter fall farther away from the sprinkler. Gilley et al. [15] presented study in suitability of reduces operating pressure of center pivot sprinkler. Their study revealed that, any center pivot sprinkler system can be gave high irrigation uniformity with low operating pressure by using appropriate nozzle diameter. Tarjuelo et al. [16] compared between CU resulted from high and medium operating pressure of the sprinkler irrigation. They revealed that, the CU values were higher under the high pressures but more stable under the medium pressures.

From previous studies the irrigation uniformity of sprinkler irrigation system affected by many factors such as: nozzle type, nozzle diameter, operating pressure and spacing layout. But the most important factors affected in the irrigation uniformity are the operating pressure and the nozzle diameter. High operating pressure has been conducted by many researchers. Actually, high operating pressure requires high pressure pump associated with the high energy cost. From this point of view, a low pressure is considered to be the best option due to low energy cost. This study was investigated the effect of low pressure in the irrigation uniformity of the solid set sprinkler irrigation system using different nozzle diameters. The uniformity coefficients and distribution characteristics of the system were studied for all the combination of operating pressures and nozzle diameter.

Materials and methods

Site description. This study was conducted at University Technology PETRONAS in Perak state (4° 25′16.5936″N, 100° 59′26.5056″E) turfgrass area. The soil at the research site was classified as loamy soil.

Experimental layout. In this study a double nozzle impact sprinkler of full circle rotation was used. The square system (12 x12 m) was designed. This system was consisted of a low pressure centrifugal pump, PVC pipe, control valve, pressure gauge, flow rate meter and sprinklers. The main line system had 2 laterals with 40 mm diameter, 4 risers with 20 mm diameter and 1m height. The schematic diagram of the experimental setup is shown in Fig 1. Different low operating pressures (62, 82, 102, and 122 kPa) were selected and different nozzles diameters (4, 5 and 7 mm) with 2.4 mm auxiliary nozzle were used.

Single sprinkler test. The outdoor test was conducted using catch-cans method. 32 graduated catch-cans with 95 mm diameter and 108 mm height were used. The area around the sprinkler divided into radial lines according to the throw radius. The radial lines were divided into 4 equal parts. Then the catch-cans were arranged along the radial line. The sprinkler was located at the center of the radial lines. The sprinkler was run for one hour, then, the caught volumes were measured. The catch-cans data was used to determine uniformity coefficients.

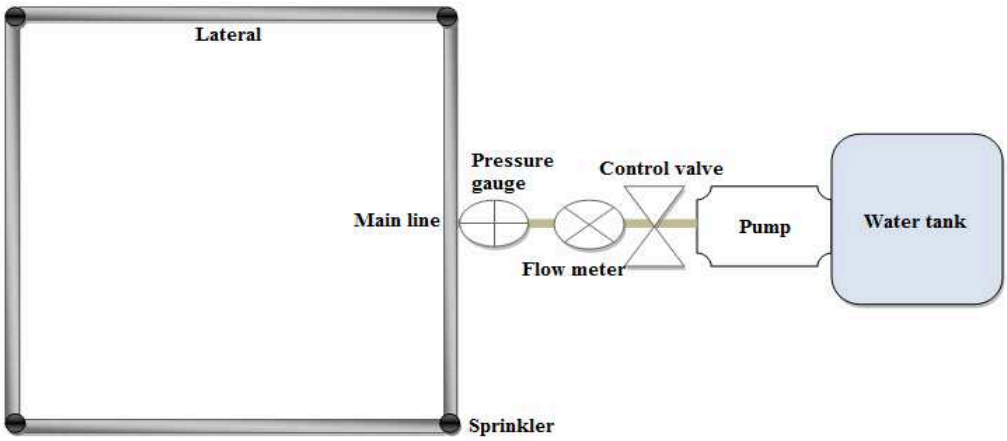


Fig. 1 Schematic diagram of the experimental setup.

Results and discussion

Irrigation uniformity coefficients. The uniformity coefficients (CU, CV, DU_{lq} and DU_{lh}) were determined based on catch-cans data. The relationships between the pressure and uniformity coefficients are presented in Figs. 2, 3, 4 and 5 using different nozzle diameters. As we can see in Fig.2, CU was increased when the pressure increased for all the nozzles. Also CU was increased rapidly when the nozzle diameter increased for all pressures. The average values of CU ranged between 26.7, 45.3 and 84.2% for the nozzles 4, 5 and 7 mm respectively. The highest value of CU was 95.8% that achieved with the combination of 7 mm nozzle diameter and 122 kPa pressure. Fig.3. shows the relationship between the pressure and the coefficient of variation (CV) using different nozzles size. As we can see in this Fig, CV was decreased when the pressure and nozzles sizes increased. The average values of CV were 23.43, 17.62 and 20.29 for nozzles 4, 5 and 7 mm respectively. The lowest value of CV was 1.35 that achieved with the combination of 7 mm nozzle diameter and 122 kPa.

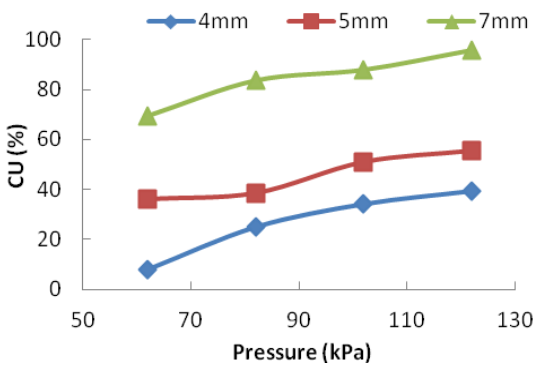


Figure. 2 The relationship between CU and pressure.

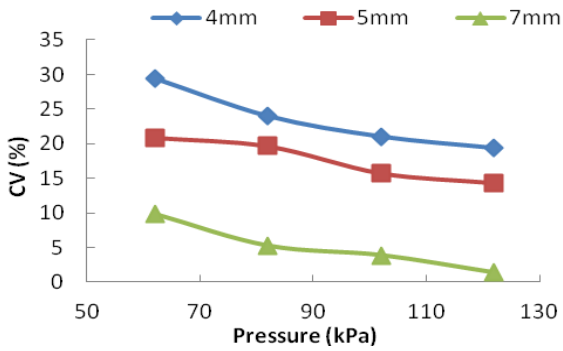


Figure. 3 The relationship between CV and pressure.

As shown in Fig.4, DU_{lq} was increased when the pressure and nozzle diameter increased due to uniform water distribution along the throw distance that produced less under irrigated areas. The average values of DU_{lq} ranged between 22.2, 39.2 and 76.2% for the nozzles 4, 5 and 7 mm

respectively. The highest value of DU_{lq} was 91.5% that achieved with the combination of 7 mm nozzle diameter and 122 kPa pressure due to even water distribution at all points of the wetted radius. DU_{lh} was increased when the pressure and nozzle diameter increased as shown in Fig.5. The average values of DU_{lh} ranged between 34.8, 47.7 and 86.6% for the nozzles 4, 5 and 7 mm respectively. The highest value of DU_{lh} was 97.1% hat achieved with the combination of 7 mm nozzle diameter and 122 kPa. CU values were greater than DU_{lq} values because CU considered both over and under irrigated areas, so that some balance occurred unlike DU_{lq} considered only the under irrigated areas. The DU_{lh} values were greater than CU and DU_{lq} values because DU_{lh} indicated the comparison between the caught volumes of low half that is greater than the caught volume of low quarter in the DU_{lq}. Although the comparison in CU was between the overall caught volumes but in DU_{lh} the comparison was between the half caught volumes.

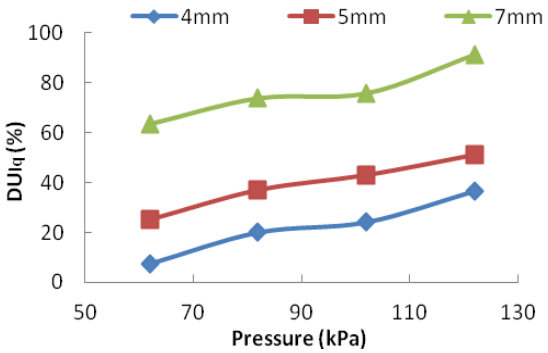


Figure. 4 The relationship between DU_{lq} and pressure.

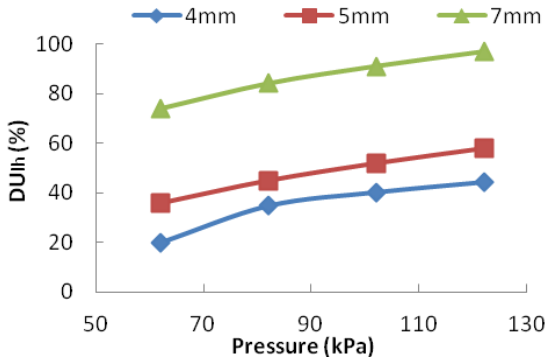


Figure. 5 The relationship between DU_{lh} and pressure.

Distribution characteristics. The distribution characteristics of the single sprinkler such as: throw radius and rotation speed were monitored. Fig.6. shows the relationship between the throw radius and pressure. The throw radius was increased when the pressure increased for all the nozzles. The higher values of throw radius were achieved with 5 mm nozzle diameter. The throw radius obtained with the nozzle 7 mm was smaller than that obtained with 5 mm this is referred to the high rotation speed with the nozzle 7 mm that led to reduce the throw radius due to high resistance between the droplets and air that resulted air shortening of the throw distance [17-18]. The greatest throw radius was 8.63 m that achieved with the combination of 5 mm nozzle diameter and 122 kPa pressure. There were small difference between the throw radiuses produced by the nozzle diameters 4 and 7 mm for the pressures 82 and 102 kPa. The rotation speed increased when the pressure and nozzle diameter increased as shown in Fig 7. But these increases were higher with the nozzle diameter 7 mm and more stable with the nozzle diameters 4 and 5 mm. There were small significant differences between the rotation speeds produced by the nozzle diameter 4 and 5 mm.

According to previous studies [10-11]. the irrigation uniformity of this system can be classified as poor with the nozzle diameter 4 mm for all the pressures and the nozzle diameter 5 mm for the pressures 62 and 82 kPa. This system can be classified as fair with the nozzle diameter 5 mm for the pressures 102 and 122 kPa. Also this system can be classified as good with the nozzle diameter 7 mm for the pressure 62 kPa and very good with the nozzle diameter 7 mm for the pressures 82 and 102 kPa. The optimum irrigation uniformity was achieved with the combination of 7 mm nozzle diameter and 122 kPa pressure with CU and DU_{lq} 95.8 and 91.5% respectively. From these results, the best irrigation uniformity was achieved with the combination of 7 mm nozzle diameter and 122 kPa pressure. So we can deduce that, the irrigation uniformity of sprinkler irrigation system was more affected by the combination of operating pressure and nozzle diameter, when the pressure and nozzle diameter increased the irrigation uniformity increased. When the pressure and nozzle diameter decreased the irrigation uniformity dropped.

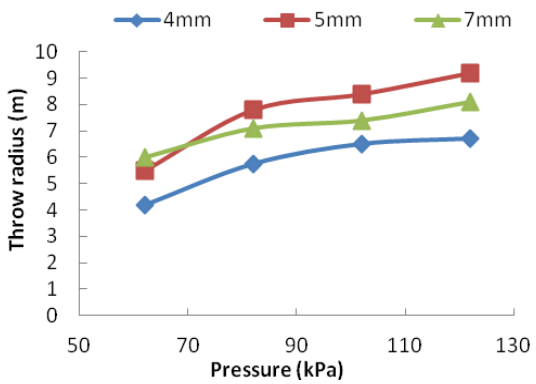


Figure. 6 The relationship between throw radius and pressure.

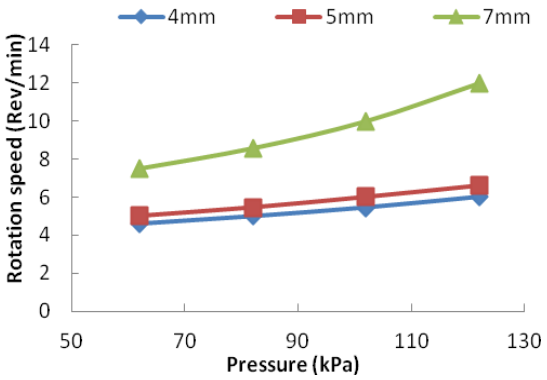


Figure. 7 The relationship between rotation speed and pressure.

Conclusions

In this study the effect of low pressure in the irrigation uniformity of the solid set sprinkler irrigation system was presented for different nozzle diameter. It was found that, the irrigation uniformity became lower with the combination of low pressure and small nozzle diameter and higher with the combination of high pressure and big nozzle diameter. All uniformity coefficients (CU, CV, DUlq and DUlh) were more affected by the operating pressure. When the pressure increased the uniformity coefficients increased for all nozzles. Furthermore they were affected by the nozzle size, when the nozzle increased the uniformity coefficients increased for all the pressures. Also the distribution characteristics such as: throw radius and rotation speed were monitored. The throw radius and rotation speed were affected by the pressure. When the pressure increased the throw radius and rotation speed increased for all the nozzles. The throw radius was not significantly affected by the nozzle diameter while, the rotation speed was more affected by the nozzle diameter. The higher rotation speeds were produced with the bigger nozzle diameter. So we concluded that, the irrigation uniformity of the low pressure is not constantly low, it can be modified by using appropriate combination of operating pressures and nozzle diameters.

References

[1] J. N. Ortíz, J. a. de Juan, and J. M. Tarjuelo, “Analysis of water application uniformity from a centre pivot irrigator and its effect on sugar beet (Beta vulgaris L.) yield,” Biosystems Engineering, vol. 105, no. 3, pp. 367–379, Mar. 2010.

[2] H. Liu, Y. Kang, S. Yao, Z. Sun, S. Liu, and Q. Wang, “Field evaluation on water productivity of winter wheat under sprinkler or surface irrigation in the north China plain O,” Journal of

Irrigation and Drainage Engineering, vol. 49, no. January, pp. 37–49, 2013.

[3] L. S. Pereira, “Higher performance through combined improvements in irrigation methods and scheduling: a discussion,” Journal of Agricultural Water Management, vol. 40, pp. 153–169, 1999.

[4] J. Li, “Effect of Pressure and Nozzle Shape on the Characteristics of Sprinkler Droplet Spectra,” Journal of Agriculture Engineering Research, pp. 15–21, 1997.

[5] J. Montero Martnez, R. S. Martnez, and J. M. Tarjuelo Martn-Benito, “Analysis of water application cost with permanent set sprinkler irrigation systems,” Journal of Irrigation Science, vol. 23, no. 3, pp. 103–110, Jul. 2004.

[6] M. Z. Muhammad Akram, Abdur Raoof, "Water use efficiency and economic feasibility of growing rice and wheat with sprinkler irrigation in the Indus Basin of Pakistan," Journal of Agriculture Water Management, vol. 87, pp. 292–298, 2007.

[7] F. Length, "Evaluation model development for sprinkler irrigation uniformity based on catch-can data," African Journal of Biotechnology, vol. 10, no. 66, pp. 14796–14802, 2011.

[8] M. Salmerón, Y. F. Urrego, R. Isla, and J. Cavero, "Effect of non-uniform sprinkler irrigation and plant density on simulated maize yield," Journal of Agricultural Water Management, vol. 113, pp. 1–9, 2012.

[9] M. Siosemarde and M. Byzedi, "Studding of Sprinkler Irrigation Uniformity," World academy of Science, Engineering and Technology, pp. 574–575, 2012.

[10] B. Nazari, A. Liaghat, and M. Parsinejad, "Development and Analysis of Irrigation Efficiency and Water," International Journal of Agronomy and Plant Production, vol. 4, no. 3, pp. 515–523, 2013.

[11] J. Montero, "Heterogeneity Analysis of the Irrigation in Fields with Medium Size Sprinklers," p. 11, 1999.

[12] D. H. R. G. A. Clark, K.Srinivas, "Measured and Simulated Uniformity of Low Drift Nozzle Sprinkler," American Society of Agricultural Engineers, vol. 46, no. 2, pp. 321–330, 2003.

[13] M. G. Jose Tarjuelo, "Working conditions of sprinkler to optimize application of water," Journal of Irrigation and Drainage Engineering, vol. 118, no. 6, pp. 895–913, 1993.

[14] J. Montero, "Sprinkler droplet size distribution measured with an optical spectropluviometer," Journal of Irrigation Science, pp. 47–56, 2003.

[15] J. R. Gilley, "Suitability of Reduced Pressure Center pivots," Journal of Irrigation and Drainage Engineering, vol. 110, no. 1, pp. 22–34, Mar. 1984.

[16] J. M. Tarjuelo, J. Montero, F. T. Honrubia, J. J. Ortiz, and J. F. Ortega, "Analysis of uniformity of sprinkle irrigation in a semi-arid area," Journal of Agricultural Water Management, vol. 40, 1999.

[17] N. K. Anumala, M. K. Ghosal, N. Sahoo, and P. L. Pradhan, "Uniform Water Distribution From Low Pressure Rotating Sprinklers," CIGRE J., vol. X, pp. 1–10, 2008.

[18] M. D. Dukes and Æ. C. Perry, "Uniformity testing of variable-rate center pivot irrigation control systems," Precis. Agric Precis. Agric, pp. 205–218, 2006.

Applied Mechanics and Materials Vol. 567 (2014) pp 32-37
© (2014) Trans Tech Publications, Switzerland
doi:10.4028/www.scientific.net/AMM.567.32

Effect of Rainfall and Groundwater Level on Sandy Beach Profile

Ahmad Khairi Abd. Wahab[1,2,a], Norasman Othman[2,3,b], Mohamad Hidayat Jamal[1,2,c] and Shairul Rohaziawati Samat[3,d]

[1]Faculty of Civil Engineering, Universiti Teknologi Malaysia,

81310 UTM Johor Bahru, Johor, Malaysia

[2]Coastal and Offshore Engineering Institute (COEI), Universiti Teknologi Malaysia

Kuala Lumpur, Jalan Semarak, 54100 Kuala Lumpur, Malaysia

[3]Faculty of Civil Engineering & Earth Resources, Universiti Malaysia Pahang,

Lebuhraya Tun Razak, 26300 Gambang, Kuantan, Pahang, Malaysia

[a]akhairi@utm.my, [b]norasman@ump.edu.my, [c]mhidayat@utm.my, [d]shairul@ump.edu.my

Keywords: swash zone, rainfall, groundwater, beach profile change, field experiment

Abstract. In Malaysia, rainfall distribution patterns are normally influenced by seasonal wind flow patterns coupled with local topographic features. Heavy rain spells and storms during the Northeast Monsoon will affect groundwater table elevation and the beach profile. The aim of this paper is to investigate the relationship between rainfall and groundwater elevation and their effect to beach profile change. This work was undertaken at the Desaru Beach, Johor. The rainfall, groundwater table, tides and beach profiles data were measured at the site. As a result, the findings revealed that the groundwater table is affected by rainfall intensity; higher during wet season and lower during dry season. Groundwater table near the coastline is also affected by the tides. However, the data showed that there is a lag time between rising and falling of groundwater table and tides. Finally, the beach profile was found to be eroded as the groundwater elevation increased on the beach.

Introduction

The swash zone is the part of the beach or nearshore which is alternatively covered and exposed by wave up-rush and backwash. Hydrodynamic processes in the swash zone are very complicated and challenging for researchers and engineers to understand and model. The area is characterised by strong and unsteady flows, high turbulence levels, large sediment transport rates and rapid morphological changes [1]. The characteristics of shallow, aerated, turbulent and rapidly varying swash flow certainly provide difficulties for even the most advanced and robust field hydrodynamic equipment during monitoring works. Processes like wave up-rush and backwash in the swash zone can contribute significantly to onshore and offshore sediment transport which is the dominant factor for beach accretion and erosion. The up-rush motion moves sand on to the shore while the backwash transports sediment offshore.

An understanding of the interaction between the water and the groundwater flow within the beach is necessary to be able to make a good prediction of beach evolution, especially in the swash zone. The groundwater level can be assumed as a continuation of the mean surface water into the beach, and therefore to have the same elevation as the tide [2]. However, decoupling might occur between the tidal elevation and the groundwater level due to the elevated groundwater exit point and the shoreline (Fig. 1). This occurs due to the rapid drop of tidal elevation compared to the gravity influenced drop of the groundwater level [2]. Water seepage will develop below the exit point at the beach face and can be identified by visual observation of a glassy surface. The groundwater elevation within the beach is affected by the tidal, waves, and to an extent the rainfall and also sediment properties such as size, shape, sorting, porosity and permeability [3]. Water infiltrates or exfiltrates from the beach surface during up-rush or backwash, depending on the beach material, permeability and the degree of soil saturation [4]. The up-rush and the backwash on the

swash will affect the groundwater table by altering the degree of saturation on the beach face [5]. The relationship between beach groundwater and swash hydrodynamics provide an important control for swash zone sediment transport, which affects the morphology of the coastline especially by controlling the potential for offshore or onshore sediment transport. The position of beach groundwater table will affect the swash zone saturation degree and infiltration/exfiltration flow velocity on the bed.

Most of beach groundwater studies for swash zone sediment transport processes have found that beaches with a low groundwater table are likely to accrete and beaches with a high groundwater table tend to erode. However, the beach groundwater table cannot respond with the rapid swash up-rush and backwash especially for finer sandy beaches due to the low value of hydraulic conductivity. In all beach groundwater table elevations, the differences of water level between coarse and fine sands reduce towards the sea. The results of the model simulations from the 'BeachWin' which is a process-based model have been developed for studying swash sediment transport and beach profile changes under influence of infiltration/exfiltration. It shows that the model is capable of simulating accretion effects of low beach groundwater tables on beach profile changes [6]. Based on the results of laboratory experiment [7], onshore sediment transport was enhanced when the groundwater level was lowered under both accretionary and erosive wave conditions, whereas higher groundwater level promoted offshore sediment transport.

The significance of this paper is to present the first research of field observation on hydrological effects like rainfall and groundwater level to sediment transport in the swash zone under Malaysia seasonal variation. The aim of this paper is to investigate the relationship between rainfall and groundwater elevation and their effect to beach profile change.

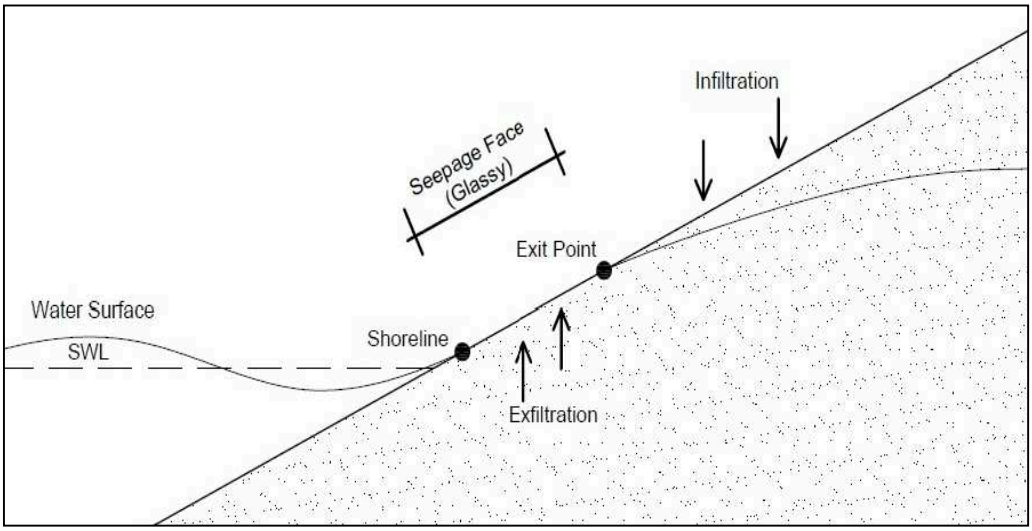


Figure 1. Groundwater and surface water on beaches (Source: [8])

Methodology

The field experiment was conducted at Desaru beach in Johor, Peninsular Malaysia, which is located about 400 km by road from Kuala Lumpur facing the South China Sea (Fig. 2). The beach is composed of fine sand with a median diameter, D_{50} of 0.2 – 0.4 mm. The beach experiences semidiurnal tide, with tide ranges of approximately 1.2 m. The upper beach is quite steep ($\tan\beta \approx 0.11$) and the lower beach is gentle ($\tan\beta \approx 0.03$).

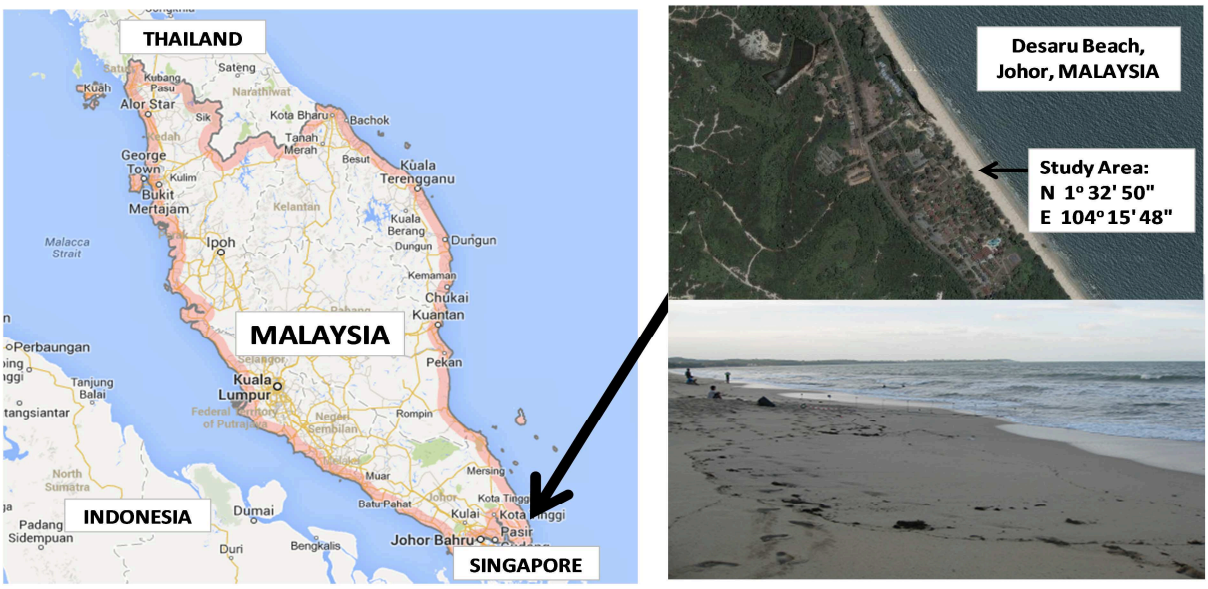


Figure 2. Location of Desaru beach

Steel rods with a spacing of 1 m were placed in a cross-shore transect. The beach level at the rods was measured monthly using a total station at low tides during spring tidal condition. For the effect of seasonal variation (dry season and wet season), one rain gauge station was installed within the field study to collect data of rainfall depth (every 10 minutes). For the beach groundwater table data, 2 monitoring wells were constructed and monitored during field data collection. The water tables were recorded using water level logger (also every 10 minutes). All equipment will be installed for 12 months starting from June 2013 until May 2014. For this paper, the results from the first six months (June – December 2013) of field data monitoring work will be presented and discussed. All the elevation data of beach profiles and groundwater were referred to the Land Survey Datum (LSD). The schematic diagram of the layout of the equipment installations is shown in Fig. 3.

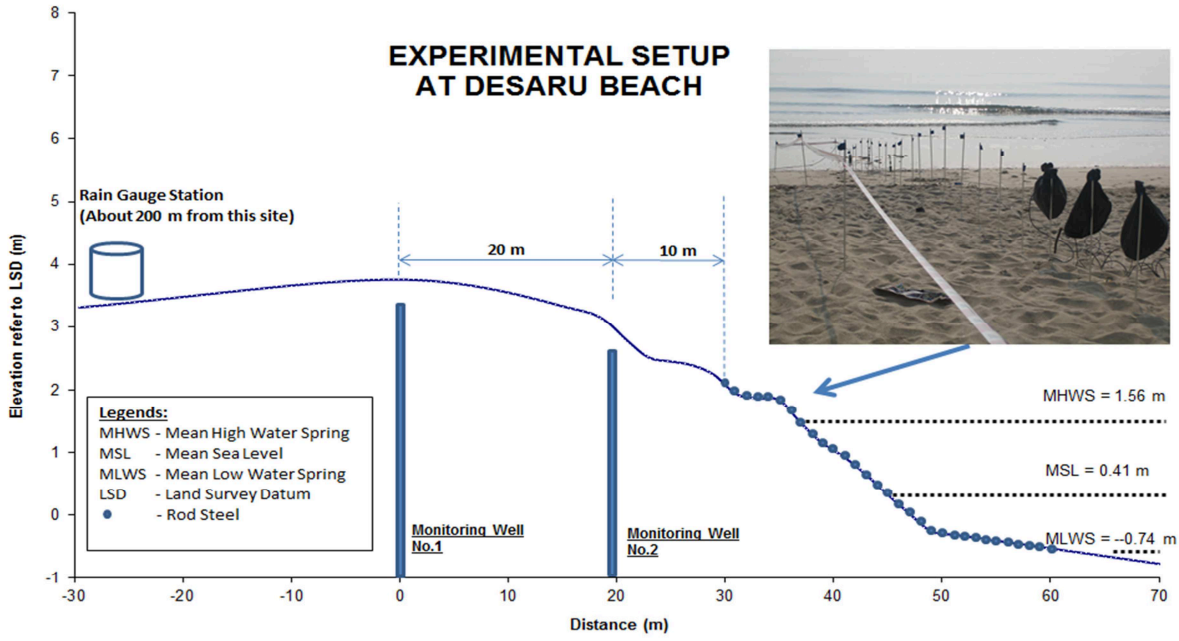


Figure 3. Profile of Desaru beach and the location of instruments

Results & Discussion

Fig. 4 and Fig. 5 show a relationship between the recorded data for daily rainfall depth and groundwater table for two monitoring wells in two periods of monitoring (July-August 2013 & November-December 2013). These two wells were located close to the shoreline. From these figures, both groundwater tables have been highly affected by the rainfall distribution especially during frequent and heavy rainfall events as shown in Fig. 5. The groundwater tables slightly dropped when there was no rain. The groundwater table monitoring well no. 2 is more fluctuated as this well is only about 15 m to the shoreline and the influence of tides may cause this fluctuation. The monitoring well no. 1 is located about 35 m from the shoreline which is further than well no. 2 and the pattern of this water table was less influenced by tides fluctuation. Also the pattern of groundwater table in well no. 1 shows that the rainfall distribution effect have played a major role for the fluctuation of water table readings which were considerably higher during heavy rainfall event (early December 2013) and slightly lower during no rainfall event. This higher water table has significantly made the swash zone more saturated and reduced the infiltration. This situation led the offshore sediment transport and erosive profile especially in the swash zone to be enhanced.

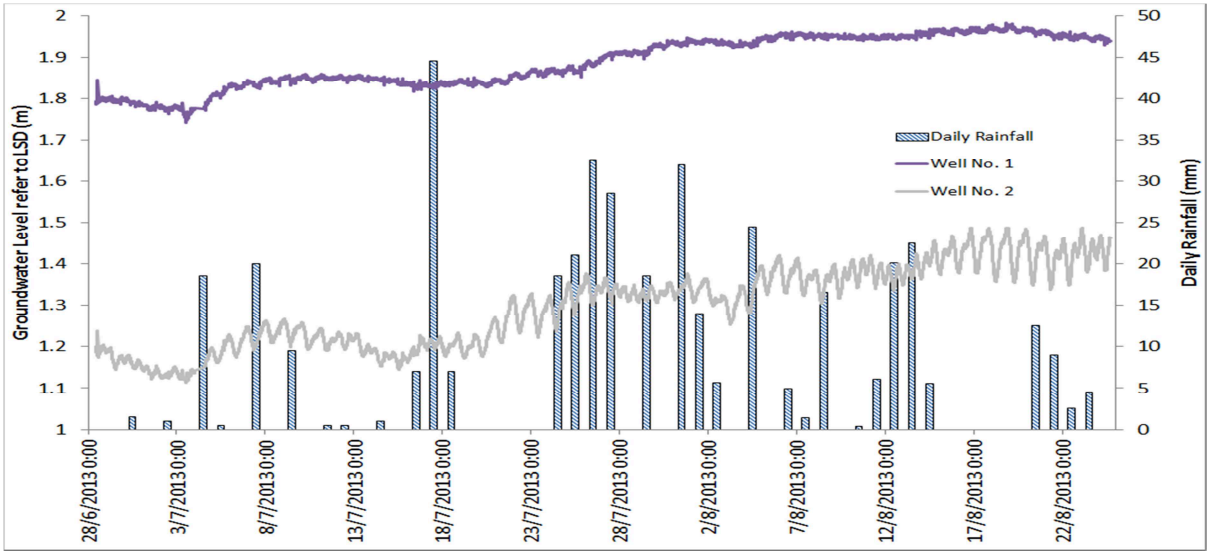


Figure 4. Daily rainfall & groundwater level from July to August 2013

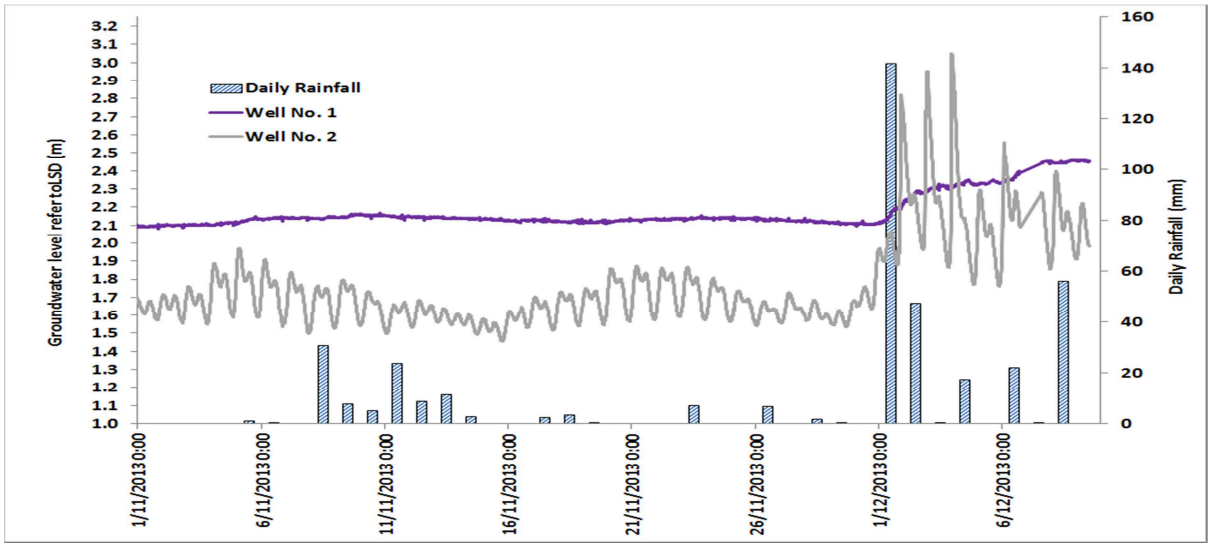


Figure 5. Daily rainfall & groundwater level from November to December 2013

Fig. 6 shows a relationship between tides and groundwater level on monitoring well no. 2 for the selected 4 days of monitoring. It was found that the lowest groundwater table is on flood and the highest groundwater table is on ebb. This lag time of about 6 hours could be due to the location of the well which was far from the shoreline and the minimum of up-rush effects at this point during the high tides. This situation was also largely contributed by the material of the beach (fine sand) and significantly decreased the groundwater flow in the beach due to lower hydraulic conductivity value. Therefore, rising or falling tides may not directly affect the groundwater table as the infiltrated water need time to fill and leave the soil.

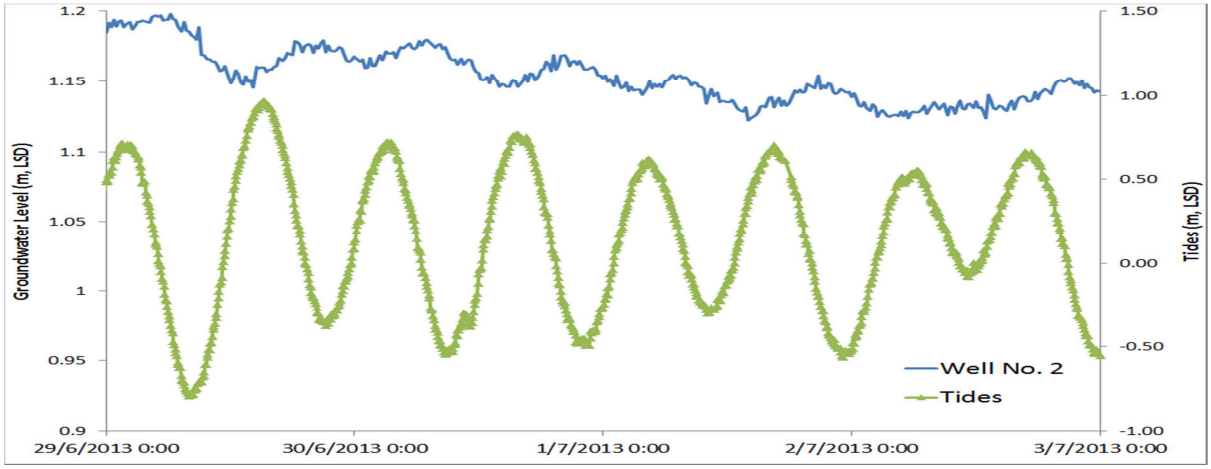


Figure 6. Groundwater table and tides

Fig. 7 shows the groundwater level and measured profiles of Desaru beach on 27th June 2013, 24th August 2013 and 9th December 2013. The increase of groundwater level is due to the increase of rainfall depths during the corresponding months. This situation resulted in the beach to be more saturated due to rainfall effect and enhanced the offshore sediment transport as the profile was eroded especially above the MSL. The beach was mainly eroded on the upper part and accreted on the lower part especially below the MSL. The highest erosion rate occurred in December due to the heavy rainfall depth with recorded data about 300 mm for 8 days in that month and this condition significantly increased the beach groundwater level. This time also shows the effect for length of up-rush flow further to the upper part of the beach due to decrease of infiltration flow on the saturated swash zone area.

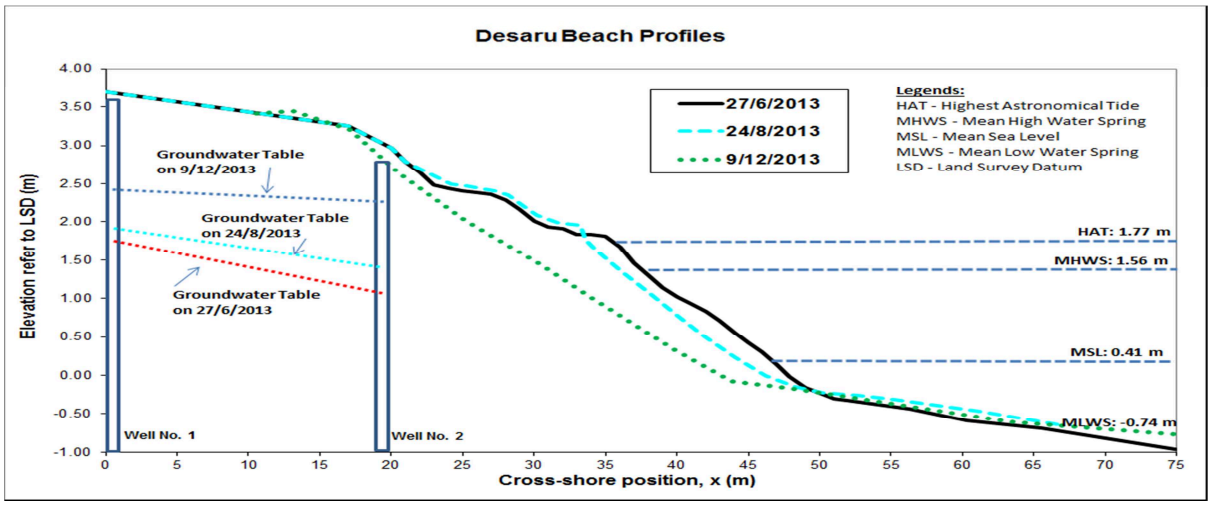


Figure 7. Relationship of groundwater and beach morphology

Conclusions and Recommendation

Conclusions that can be drawn from this study are as follows:

- Beach groundwater table was highly affected by the patterns of rainfall distribution (increase on wet period and decrease on dry period).
- Near to the shoreline, groundwater level is affected by tidal fluctuations.
- Higher groundwater level caused the beach to be eroded.

Field studies or research in the swash zone have been relatively few in numbers (none in Malaysia) and there is a clear need to improve current available field equipment in order to get high quality data for better understanding of this complex process. Current work will continue the field observation and monitoring for dry season in order to get a clear view of beach accretion process due to the lower groundwater table.

Acknowledgements

This research was funded by Universiti Teknologi Malaysia through Research University Grant No. 02H58 (Title: Modelling of Longshore Sediment Transport in Swash Zone) & 07J10 (Title: Erosion and Accretion in the Swash Zone). We also would like to express our appreciation to Desaru Development One Holding Sdn. Bhd. for the permission to use part of the beach for the study site and for the support in the field during monitoring works.

References

[1] Puleo, J.A., Beach, R.A., Holman, R.A., Allen, J.S., 2000. Swash zone sediment suspension and transport and the importance of bore-generated turbulence. Journal of Geophysical Research, Vol. 105, 17021-17044.

[2] Horn, D.P., 2006. Measurements and modelling of beach groundwater flow in the swash-zone: a review. Continental Shelf Research 26, 622–652.

[3] Foote, M., Horn, D., Li, L., 2002. Measuring swash zone hydrodynamics and morphodynamic change – a high-resolution laboratory system using digital video. Journal of Coastal Research SI 36, 300-316.

[4] Elfrink, B., Baldock, T.E., 2002. Hydrodynamic sand sediment transport in the swash zone: a review and perspectives. Coastal Engineering 45, 149–167.

[5] Butt, T., Russell, P., 2000. Hydrodynamics and cross-shore sediment transport in the swash-zone of natural beaches: A review. Journal of Coastal Research 16 (2), 255-268.

[6] Li, L., Barry, D.A., Pattiaratchi, C.B. Masselink, G. (2002). BeachWin: modelling groundwater effects on swash sediment transport and beach profile changes. Environmental Modelling & Software 17, 313-320.

[7] Horn, D.P., Baldock, T.E., Li, L., 2007. The influence of groundwater on profile evolution of fine and coarse sand beaches. Proceeding of Coastal Sediments ’07, New Orleans, ASCE, pp. 506-519.

[8] Jamal, M.H. 2011. Modelling coarse-grained beach profile evolution. PhD Thesis, University of Plymouth, UK.

Applied Mechanics and Materials Vol. 567 (2014) pp 38-43
© (2014) Trans Tech Publications, Switzerland
doi:10.4028/www.scientific.net/AMM.567.38

Effects of Groundwater Withdrawal on the Interaction of Ex-mining Pond, River, and Aquifer

[1, a] Raksmey May, [2]Ismail Yusoff and [1]Wardah Tahir

[1]Faculty of Civil Engineering, Universiti Teknologi MARA, 40450, Shah Alam, Selangor, Malaysia

[2]Department of Geology, Faculty of Science Building, University of Malaya, 50603 Kuala Lumpur, Malaysia

[a]may_raksmey@salam.uitm.edu.my

Keywords: groundwater and surface water interaction, pond-aquifer interaction, groundwater modeling, Visual MODFLOW, artificial recharge pond, ex-mining site

Abstract. The paper aims at evaluating the effects of groundwater abstraction on the interaction of an ex-mining pond, river, and aquifer system of the Langat Basin in Malaysia through a 3D numerical modeling. Many mining sites have been left behind from the massive mining exploitation in Malaysia. In the current study, an artificial recharge from an ex-mining pond in the Langat Basin was proposed due to its capacity to store >30 million m³ of water. The 3D numerical model was developed using the Visual MODFLOW to simulate the effects of these activities. The calibrated model was utilized to simulate two cases. The ex-mining pond was without and with pumping in Case 1 and 2, respectively. Both results showed that the pond and aquifer were in influent condition. In Case 1, the total inflow to the aquifer system were approximately 15,819 m^3/d of water from the constant heads, 1,202 m^3/d from the Langat River, and 66,951 m^3/d from the direct recharge of precipitation. In Case 2, due to the abstraction of groundwater, it caused a steep depression around the pumping well, river, and pond. The result of the water budget showed an increase rate of the inflow to the pumping zone from the pond and river around 6,945 m^3/d compared to Case 1. The outcome of the current study provides the useful information of the interactions between the river, pond, and aquifer system as regards the groundwater abstraction in the Langat Basin.

Introduction

Mining industry in Malaysia is now on the path to full recovery after this sector, once the world's most successful, collapsed almost entirely in the 1980s due to the price manipulation, increased production costs, and tough conditions [1,2]. The effects of unmanaged mining activities in Peninsular Malaysia during the late 19th and early 20th century have led two problems such as the dereliction of mining land and the continuous deterioration in the quality of river systems draining the mining effluents. At the same time, many mining sites have been left behind from the massive mining exploitations. These sites are able to accommodate more than a million cubic meters of water from precipitation, runoff, groundwater, and river. Most of the time, the mining sites are turned into ponds for recreational activities.

The use of artificial recharge becomes increasingly important to store surplus water underground for sustainable water resource development. The artificial recharge may be used to store treated wastewater and excess runoff for later utilization. Groundwater recharge may also be used to control a land subsidence, groundwater enhancement at pumping sites, and saltwater intrusion [3,4].

It is necessary to consider the effects of the artificial recharge and groundwater abstraction on the aquifer systems. The groundwater is considered to be a potential alternative water resource in Malaysia, and some industries have altered their surface water utilization to groundwater [5,6]. One of them was permitted to abstract >22,000 m^3/d of groundwater for its company's production in the Langat Basin. Therefore, the artificial recharge is essential for the sustainable groundwater development.

This paper focuses on the effects of the groundwater abstraction on the interaction between the seepage from the ex-mining pond and river with the aquifer system through the 3D numerical simulation in Visual MODFLOW.

Study Area

The central Langat Basin was selected to be the study area where it is located about 30 km from the Kuala Lumpur City Center (KLCC). The area is the alluvium floodplain; the average elevation of the ground surface is about 15 m above sea level (a.s.l.). The perimeter and area of the research vicinity area are approximated 65 km and 244 km^2, respectively. Fig. 1(a) shows the landuse types in the study area such as the gas station, pond, housing, forest, factory, plantation, workshop, and hotel. The ex-mining pond proposed as the artificial recharge pond is presented in Fig. 1(b). The area and perimeter of the pond are approximately 903,268 m^2 and 4,291 m, respectively. The normal water stage of the pond is at 2 m a.s.l. A pumping well has been operated in the study area with the pumping rate approximately 788 m^3/h.

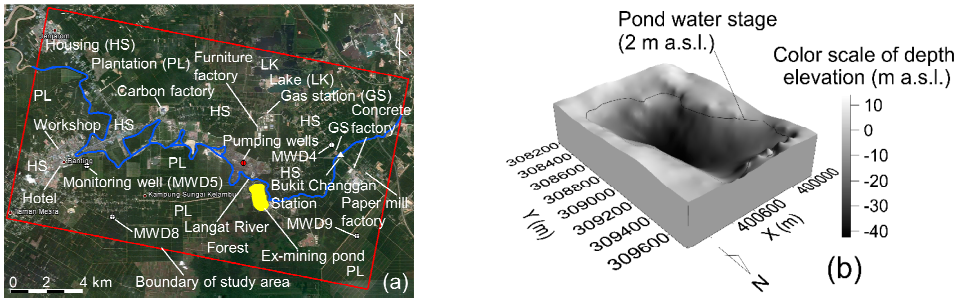


Figure 1. (a) Landuse distribution, monitoring wells, and hydrological station in the study area (b) 3D view of the ex-mining pond

The hydrological condition of the study area is characterized by the Langat River, evaporation, and precipitation. A segment of approximately 40 km of the Langat River is considered in the current study. The river width in the target area is approximately 60 m and 150 m upstream and downstream, respectively. At Bukit Changgan Station (Fig. 1(a)), the riverbed elevation and variations of the river stages and rainfalls in 2012 and 2010, respectively are shown in Fig. 2. The annual average rainfall and evaporation in the area are around 2,246 mm and 1,604 mm, respectively.

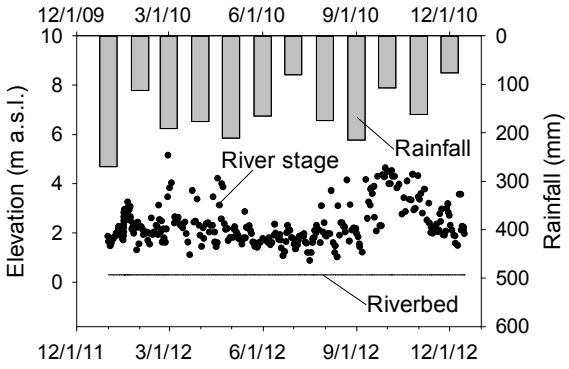


Figure 2. Riverbed elevation, river stage in 2012, and rainfall in 2010 at Bukit Changgan Station

Aquifer Characteristics

The stratigraphy of aquifer in the modeled area can be classified into two different layers. The maximum elevation of the first aquifer bottom is at -5 m a.s.l. and the minimum reaches at -25 m a.s.l. The horizontal hydraulic conductivity is approximately 5.8×10^{-5} m/s, while the vertical

hydraulic conductivity around 5.8×10^{-4} m/s [6]. The sand and gravel were dominantly found in the second aquifer layer. The horizontal hydraulic conductivity was approximately 2.9×10^{-4} m/s and the vertical hydraulic conductivity is about 9.7×10^{-6} m/s [6]. The average depth of the second aquifer was 90 m. The aquifer bottom is limited by the bedrock of sandstone, quartzite, and granite. The 3D conceptual model in Fig. 3(a) illustrated the aquifer system in the study area. The average recharge rate of 100 mm/y estimated by tank model [7] is assigned in the numerical simulation. This rate is comparable to the results computed by [6].

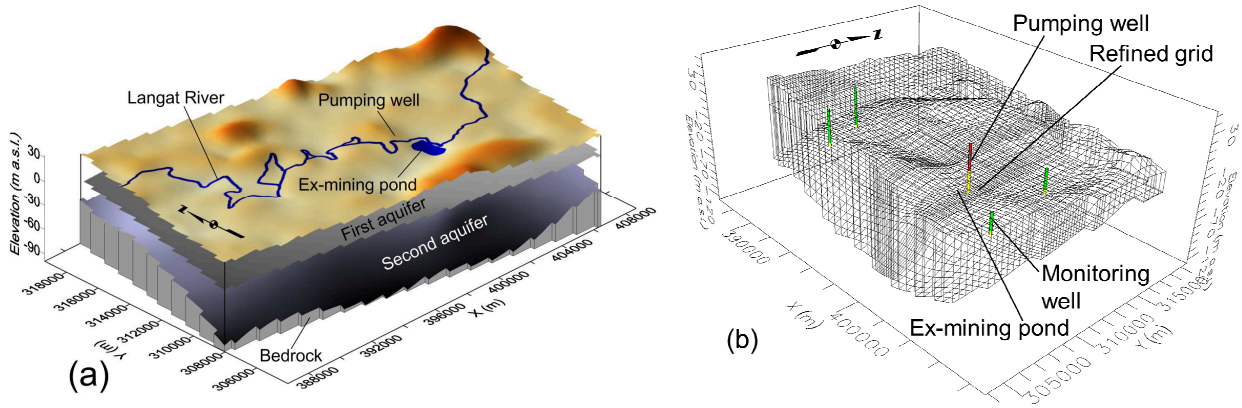


Figure 3(a). 3D conceptual model of the aquifer system (b) Variable-spacing finite-difference grid of the modeled area

Model Development

The numerical simulation of the groundwater flow was developed in Visual MODFLOW 2011.1 Build 4.6.0.159 from the Schlumberger Water Services. The modular finite-difference flow model (MODFLOW) established by the United States Geological Survey (USGS) is one of the components of the software. MODFLOW was developed based on the principle equations of Darcy's Law, conservation mass equation, and finite difference method. The study is heterogeneously discretized around the pumping well and ex-mining pond (Fig. 3(b)). The maximum grid sizes are 570 m × 390 m and minimum 140 m × 185 m.

Groundwater Flow and River-Pond-Aquifer Interaction Equations

The model is based on Darcy's Law and the equation of conservation of mass. The combination of both results in a partial differential equation for groundwater flow is given by [8,9] as follows.

$$S_s \frac{\partial h}{\partial t} = \frac{\partial}{\partial x}\left(K_{xx}\frac{\partial h}{\partial x}\right) + \frac{\partial}{\partial y}\left(K_{yy}\frac{\partial h}{\partial y}\right) + \frac{\partial}{\partial x}\left(K_{zz}\frac{\partial h}{\partial z}\right) - w \quad (1)$$

where K_{xx}, K_{yy}, and K_{zz} are values of hydraulic conductivity along the x, y, and z coordinate axes, which are assumed to be parallel to the major axes of hydraulic conductivity (L/T); h is the potentiometric head (L); w is a volumetric flux per unit volume and represents sources and/or sinks of water, with $w<0$ for the outflow of water from the aquifer system, and $w>0$ for the inflow in (L/T); S_s is the specific storage of the porous material (1/L); and t is time (T).

The interactions between the river and pond with aquifer are assigned as boundary conditions requiring the conductance parameters. The conductances of both bodies are defined as follows [9,10].

$$C_{riv} = \frac{K_{riv}}{B_{riv}} W \quad (2)$$

where K_{riv} is the hydraulic conductivity of the river bottom sediment (L/T), B_{riv} is the length of flow (thickness of river bed sediment) (L), and W is the width of river (L).

$$C_{pond} = \frac{K_{pond}}{B_{pond}} \tag{3}$$

where K_{pond} represents the hydraulic conductivity of the pond bottom sediment (L/T) and B_{pond} represents the thickness of the sediment (L).

Input Data

Aquifer parameters. They include the aquifer thickness, horizontal hydraulic conductivity, vertical anisotropy hydraulic conductivity, and recharge rate. These parameters are found in the sections "Study area" and "Aquifer characteristics".

River. The river stages and riverbed elevations are interpolated linearly from one location to another. Fig. 4(a) and Table 1 show the known locations along the river reaches. These data were derived from [6] and DID's online hydrological website [11].

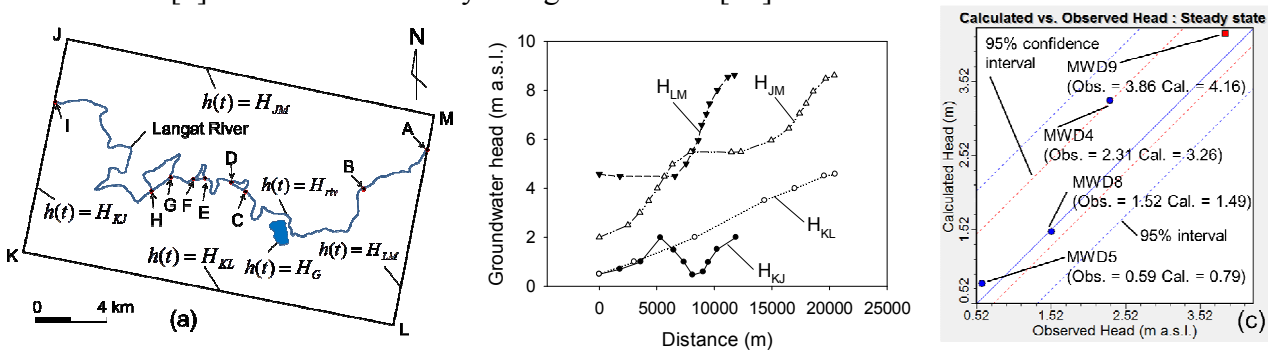


Figure 4(a). Boundary conditions and locations along the river where the river stages and riverbed elevations are known (b) Groundwater heads assigned as the constant head boundary conditions along the boundaries of the study area (c) Comparison between calculated and observed heads

Table 1. River stages and riverbed elevations input in the simulation

Location	A	B	C	D	E	F	G	H	I
River stage (m a.s.l.)	7.9	1.83	0.84	0.78	0.69	0.61	0.56	0.5	0
Riverbed elevation (m a.s.l.)	2.91	0.32	-6.03	-6.41	-7.13	-7.62	-7.98	-8.01	-8.94

Pond. In the current simulation, the ex-mining pond is proposed to be one of the artificial recharge sources for the Langat Basin. The hydraulic conductance of the pond bottom and horizon is estimated approximately 51.84/d. The general pond water stage is constantly set at 2 m a.s.l. (Fig. 1(b)).

Boundary Condition. In simulating groundwater model, the boundary condition is very important, especially for a simulation in a steady-state condition. The boundaries of the study area are assigned to be the constant head boundary conditions. The linear interpolation method based on the digitized results in Fig. 4(b) is adopted to assign the constant heads along the grid points in the simulation model.

Initial Condition. The initial condition expresses the specified value for the potentiometric head at the beginning of the simulation. The ground elevations are utilized to be the initial condition in the current simulation.

Results and Discussion

Model Calibration. Four monitoring wells (Fig. 1(a)) were prepared for the calibration processes. The comparison between calculated and observed potentiometric heads was presented in Fig. 4(c). The root mean square error was approximately 0.5 m. Therefore, the simulation was successfully achieved to demonstrate the aquifer behavior in the study area.

Discussion.

Case 1: Ex-mining Pond without Pumping. The pumping activity was excluded from the simulation for Case 1. The results of the potentiometric head distribution were plotted in Fig. 5(a). The Langat River was a gaining stream. The groundwater was supplied to the river from the northeast where the potentiometric heads gradually varied from 8.3 to 0.5 m a.s.l. The groundwater flow influenced all the river reaches from the direction of the southwest and southeast. Fig. 5(b) illustrated the equipotential lines of potentiometric head and velocity vectors and magnitudes from the groundwater, pond, and river. The water supply from the pond and aquifer discharged into the river. The maximum velocity in the illustration was about 2.2×10^{-6} m/s. The water budget in the aquifer was summarized in Fig. 5(e). For the total inflow, the constant head contributed approximately 15,819 m^3/d. The pond seepage, river leakage, and recharge supplied around 3,177 m^3/d, 1,202 m^3/d, and 66,951m^3/d, respectively. The total outflow was contributed from the constant head (about 22,018 m^3/d), pond seepage (around 1,122 m^3/d), and river leakage (around 64,008 m^3/d).

Case 2: Artificial Recharge Pond with Pumping. The pumping activity was included in this case. The change of the aquifer behavior was observed. The pumping well was operated at the rate of 18,900 m^3/d. The patterns of groundwater were altered around the pumping well [Fig. 5(c)]. The lowest drawdown elevation reached around -9 m a.s.l. In general, the groundwater and pond influenced all river reaches. The water supply to the pumping well was from the pond, river, and aquifer. Fig. 5(d) illustrated the equipotential lines of potentiometric head, drawdown, and velocity vector. The maximum velocity was around 3.4×10^{-5} m/s. The water budget in the aquifer was summarized in Fig. 5(f). The total inflow consisted of the fluxes from constant head (16,006 m^3/d), pond seepage (5,060 m^3/d), river leakage (6,077 m^3/d), and recharge (66,951 m^3/d). The total outflow was from the constant head about 20,981 m^3/d, pumping well around 18,900 m^3/d, pond seepage approximately 1,066 m^3/d, and river leakage about 53,145 m^3/d.

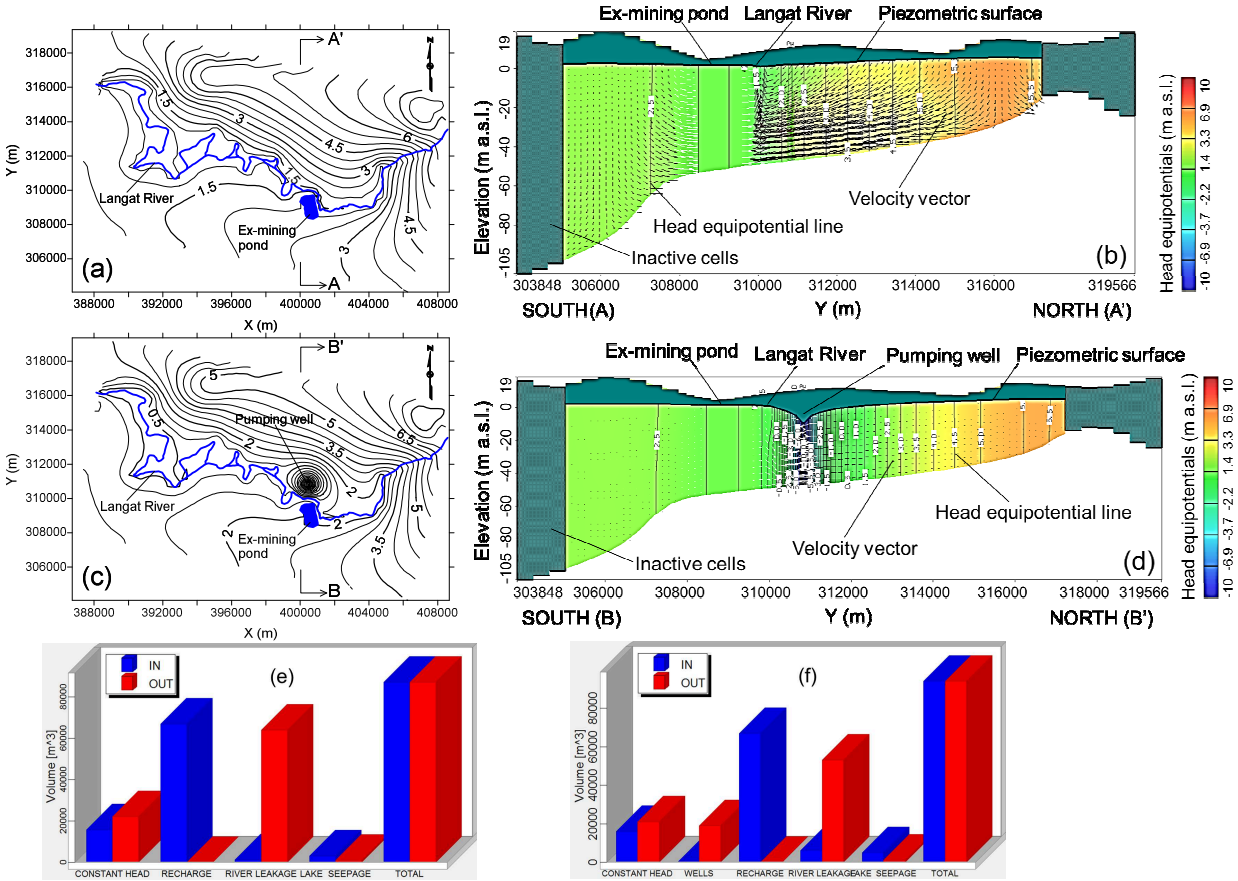


Figure 5. Contour maps (unit in m a.s.l. and 0.5 m interval) and Cross sections of the potentiometric heads (a) and (b) for Case 1 and (c) and (d) for Case 2 and Daily water budget in the aquifer system (e) Case 1 and (f) Case 2

Conclusion

The numerical model successfully simulated the effects of groundwater withdrawal on the aquifer system, especially the interaction with pond and river. The model results were calibrated by using four observation wells, and the error about 0.5 m was achieved. The selected study area at the central part of Langat Basin had the particular groundwater flow pattern where the Langat River was influenced by the groundwater flow and seepage from ex-mining pond in the case of no pumping. When the pumping well was operated, the seepage from the pond was increased. At the same time, the leakage from the river to the pumping well was observed. The modeling results provided the total inflow and outflow of both cases. The differences of water balance between pumping and no pumping were about 6,945 m^3/d. The simulation results could be an important tool to prepare for the future groundwater management projects within the study area.

Acknowledgements

The authors gratefully acknowledge the financial support of the Fundamental Research Grant Scheme [600-RMI/FRGS 5/3 (32/2012)] of the Ministry of Education (MOE), Malaysia. The Department of Minerals and Geoscience (JMG), Selangor, Malaysia is acknowledged for the secondary data and assistance during the site investigations. The Department of Irrigation and Drainage (DID) Malaysia is acknowledged for the hydrological data. Last but not least, the environmental laboratory assistants at the Faculty of Civil Engineering, Universiti Teknologi MARA (UiTM), are also thanked for their valuable assistance.

References

[1] BorneoPost Online (BPO), Malaysia's mining industry on way to full recovery. http://www.theborneopost.com/2012/08/07/malaysias-mining-industry-on-way-to-full-recovery-new/. Accessed 20 December 2012

[2] G. Balamurugan, Tin mining and sediment supply in peninsular Malaysia with special reference to the Kelang River Basin, Environmentalist 11(4):281-29, DOI: 10.1007/BF01266561 (1991)

[3] H. Bouwer, Artificial recharge of groundwater: hydrogeology and engineering, Hydrogeology Journal 10:121-142, DOI: 10.1007/s10040-001-0182-4 (2002)

[4] Organization of American States (OAS), Artificial recharge of aquifers. http://www.oas.org/dsd/publications/Unit/oea59e/ch18.htm. Accessed 20 November 2012

[5] Department of Environment (DOE), Environmental quality report. Ministry of Natural Resources and Environment, Malaysia (2006)

[6] Japan International Cooperation Agency (JICA) and Minerals and Geoscience Department Malaysia (MGDM), The study on the sustainable groundwater resources and environmental management for the Langat Basin in Malaysia. Vol. 1-5 (2002)

[7] A. Tsutsumi, K. Jinno, R. Berndtsson, Surface and subsurface water balance estimation by the groundwater recharge model and a 3-D two-phase flow model, Hydrol Sci 49(2):205-226 (2004)

[8] C.W. Fetter, Applied Hydrogeology, fourth ed., Prentice Hall, New Jersey, 2001, pp139

[9] M.G. McDonald, A.W. Harbaugh, A modular three-dimensional finite-difference ground-water flow model: Techniques of Water-Resources Investigations of the United States Geological Survey. US Geological Survey, Book 6, Chapter A1, Chapter 2, pp2-2 (1988)

[10] AQUAVEO, Groundwater Modeling System: GMS User Manual 8.3. Chapter 6, pp.314 (2012)

[11] Department of Irrigation and Drainage (DID), Online hydrological data. http://infobanjir.water.gov.my/ve/vmapsel.cfm. Accessed 24 April 2012

Applied Mechanics and Materials Vol. 567 (2014) pp 44-49
© (2014) Trans Tech Publications, Switzerland
doi:10.4028/www.scientific.net/AMM.567.44

Electrochemical Disintegration of Activated Sludge Using Ti/RuO_2 Anode

Gan Chin Heng[1, a] and Mohamed Hasnain Isa[1,b]

[1,2]Dept. of Civil Engineering, Universiti Teknologi PETRONAS, Bandar Seri Iskandar, 31750 Tronoh, Perak, Malaysia

[a]chgan26@gmail.com, [b]hasnain_isa@petronas.com.my

Keywords: Activated sludge, electrochemical, Pechini's method, Ti/RuO_2 anode.

Abstract. Electrochemical process is one of the most effective methods to enhance sludge disintegration. In this study, Ti/RuO_2 anodes were prepared by Pechini's method and the electrode surface morphology was characterized by FESEM and EDAX. The effects of various operating conditions were investigated including initial pH value of sludge, sludge concentration, electrolysis time and current density. The study showed that the removal efficiencies of TS, VS, TSS and VSS increased with the increase of pH in the alkaline range, electrolysis time and current density but decreased with the increase of initial sludge concentration. The application of electrochemical process using Ti/RuO_2 electrodes enhanced the sludge disintegration for possible subsequent biological treatment.

Introduction

Municipal and industrial wastewater treatment plants produce large amounts of excess sludge that requires proper management. Various methods have been proposed to enhance the sludge disintegration including salt content modification [1-3], acid or alkaline treatment [4-8], chemical oxidation [9-11], sonication [8], thermal treatment [8,12] and electrical treatment [13].

Electrochemical process has shown potential for elimination of organic pollutants from industrial wastewater. The reaction can occur directly at anodes and has a primary advantage of no addition of chemicals into wastewater and thus avoiding the risk of producing secondary pollution. Several electrode materials (Ti/RuO_2, Ti/IrO_2, Ti/PbO_2 and Ti/SnO_2-Sb) have been used for the electrolytic treatment of effluents containing organic compounds [14-17]. It is noted from the literature that a considerable number of studies have been carried out to explore electrochemical process using different types of anode for activated sludge treatment. Electrochemical process has a great potential in enhancing sludge disintegration according to the previous studies [13,18].

A number of process for manufacturing dimensionally stable anodes (DSA) have been reported in the literature such as sol-gel [19,20], spray pyrolysis [21], electrodeposition [22], thermal decomposition [23-25] and precursor solution, known as the Pechini method [26]. The last one is useful to prepare electrode films with controlled stoichiometry due to the formation of hydroxicarboxylic acids allied to their ability to form chelates with many cations. When these acids are heated in the presence of polyhydroxylic alcohols, an esterification reaction takes place and the cations are incorporated in the polymeric net, avoiding metal losses by volatilization during film calcination [27].

It was reported that Ti/RuO_2 anode can effectively convert high molecular weight biopolymer substances to low molecular weight products that can be easily removed by the subsequent biological treatment [28]. Therefore, the objective of this paper was investigating the effectiveness of Ti/RuO_2 electrodes coating by Pechini's method in terms of sludge reduction.

Materials and methods

Titanium plate electrodes (15 mm × 150 mm × 3 mm), with a working area of 43.65 cm^2 were coated with ruthenium oxide (RuO_2) by Pechini's method [27]. The electrodes surface was clean with sand paper prior to soaking them in a hydrochloric acid at 80 ^oC for 20 min. Then the plates were washed and dried with hot air blown at 105 ^oC for about 30 min before being coated with the ruthenium oxide. The precursor solutions were obtained from analytical grade reagents: citric acid, propanol and ruthenium (III) chloride hydrate. The anhydrocitric acid:propanol:ruthenium molar ratio for the electrode coating was 3:10:1. The solution was put in the water bath at 60 ^oC for 1h. The electrodes are coated with the solution and oven dried at 105^oC for 15-20 minutes followed by 550 ^oC for 10 minutes. Coating and drying was repeated 20 times for each electrode to a degreased and etched Ti plate. Finally, the electrodes were calcinated at 550 ^oC for 2 h.

In this study, waste activated sludge (WAS) was obtain from the return pipe from secondary clarifier sludge hopper of the municipal wastewater treatment plant in Universiti Teknologi PETRONAS. The sludge samples were thickened to the required solids concentration and stored in the cold room prior to use. The characteristics (range from triplicate samples) of the raw samples are presented in Table 1.

Table 1. The characteristics of raw activated sludge samples.

Parameter	Unit	Raw
pH	-	6.84-6.92
Total solids (TS)	mg/L	9062-13700
Volatile solids (VS)	mg/L	5674-9018
Total suspended solids (TSS)	mg/L	8727-12620
Volatile suspended solids (VSS)	mg/L	5655-8390
sCOD	mg/L	148-327

Analysis

pH measurement was performed using a pH meter (Hach sension 4) and a pH probe (Hach platinum series pH electrode model 51910, Hach Company). Solids (TS, VS, TSS and VSS) were measured according to the Standard Methods [29]. Soluble chemical oxygen demand (sCOD) was measured by the Reactor Digestion Hach method No. 8000 [30] and the sample was filtered through 0.45 μm membrane filter before measurement.

Field Emission Scanning Electron Microscopy (FESEM) (model Zeiss Supra 55 VP) was used for surface morphology recognition and Energy Dispersive Analysis of X-ray (EDAX) of coating material.

Results and discussion

Effect of anode and structure of coated Ti/RuO_2

Fig. 1 shows nano-scale particles on the coated surface of Ti/RuO_2 electrodes. The particles were uniformly distributed and could provide more active sites for electrochemical oxidation of organic matter. EDAX of electrode surface confirms the presence of ruthenium and oxygen at weight percentage of 36.85 and 32.15, respectively in Fig. 2.

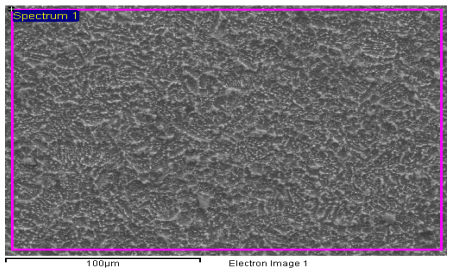


Figure 1. FESEM surface image of the Ti/RuO_2 electrode.

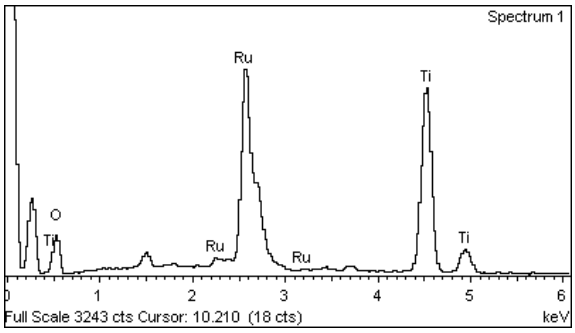


Figure 2. EDAX of the Ti/ RuO_2 electrode.

Effect of initial pH of sludge

The initial pH of the sludge sample was adjusted to 2-13 using sulphuric acid and sodium hydroxide. The operating conditions were as follows: sludge concentration 11.8 g/L, constant voltage of 20 V and electrolysis time 1h. The removal of the organic solids at each pH is shown in Fig. 3. Generally, the removal efficiencies of TS, VS, TSS and VSS were decreased with the increasing of pH in acid range, and increased with increasing pH in alkaline range, and similar trend was observed for sCOD. The highest removal of TS, VS, TSS and VSS were 18.8%, 16.6%, 19.8% and 17.6%, respectively achieved at pH 12. According to Neyens et al. [31], after the destruction of extracellular polymer substances by electrochemical process, the cell walls being exposed to a higher pH could not withstand the appropriate turgor pressure resulting in the disruption of cells and release of intracellular substances and hence contributed to the sludge reduction.

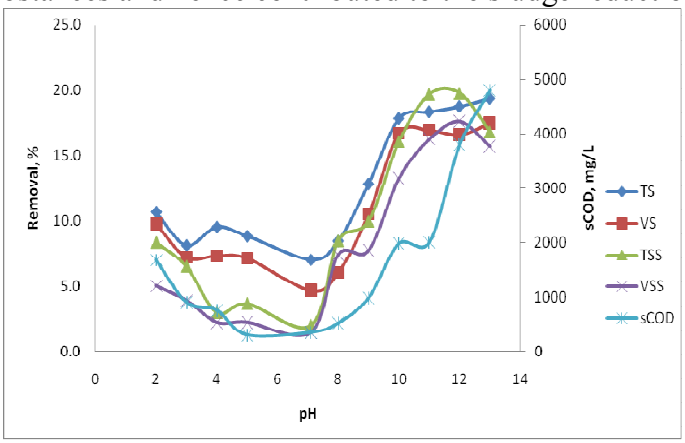


Figure 3. Effect of initial sludge pH on the removals of TS, VS, TSS and VSS.

Effect of sludge concentration

The initial sludge concentration (VSS) was adjusted to 2000-12000 mg/L. The operating conditions were as follows: pH of sludge 7, constant voltage of 20 V and electrolysis time 1h. The removal of the VSS is shown in Fig. 4. The graph indicated that the removal efficiency of VSS decreased with increasing sludge concentration and sCOD increased with increasing sludge

concentration. The mass transfer limitation may inhibit the rate of electrochemical process due to higher organic solid concentrations.

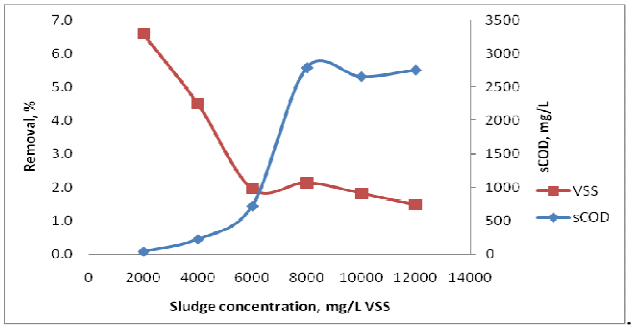


Figure 4. Effect of initial sludge concentration on the removal VSS.

Effect of electrolysis time

The effect of electrolysis time was studied with sludge pH of 7, constant voltage of 20 V and initial sludge concentration of 8900 mg/L. As shown in Fig. 5, the removal efficiencies of TS, VS, TSS and VSS increased with the time. Highest sCOD was achieved at 60 min and started to decrease after 60 min. It was noted that the removal efficiencies increased rapidly within 40 min and then increased gradually until 240 min. The removal efficiencies of TS, VS, TSS and VSS at 40 min were 5.5%, 7.9%, 5.5% and 6.4%, respectively, whereas the removal efficiencies of TS, VS, TSS and VSS increased to 15.4%, 15.8%, 11.7% and 11.2%, respectively at 240 min.

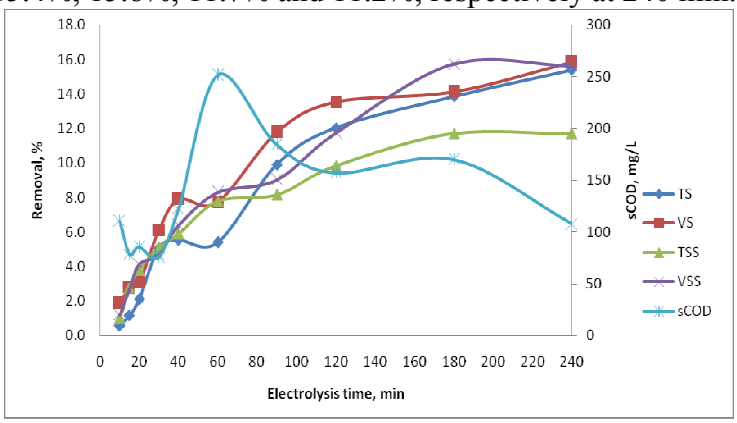


Figure 5. Effect of electrolysis time on the removals of TS, VS, TSS and VSS.

Effect of current density

The effect of current density was studied with pH of sludge 7.1, electrolysis time 1h and initial sludge concentration of 8900 mg/L. As shown in Fig. 6, the removal efficiencies of TS, VS, TSS and VSS increased with the current density, and similar trend was observed for sCOD. Higher current density could lead to more organic matters decomposed and solubilized. The removal efficiencies of TS, VS, TSS and VSS increased significantly from 7.5 mA/cm^2 to 10 mA/cm^2, from 13%, 20.2%, 15.1%, 22.4% to 41%, 37.1%, 42.6% and 38.9%, respectively. When the current density was greater than 10 mA/cm^2, the sludge sample was overheated indicating electric energy converted to heat during the electrolysis. Therefore, it is not advisable to apply such high current density due to power cost.

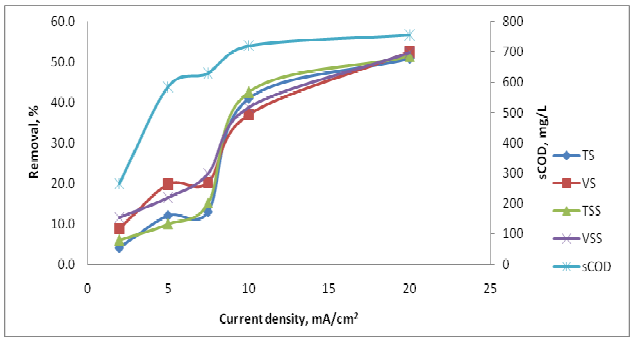


Figure 6. Effect of current density on the removals of TS, VS, TSS and VSS.

Conclusions

FESEM surface image and the EDAX of the Ti/RuO_2 electrodes indicated that preparation by Pechini's method can produce a uniform and homogeneous coating throughout the titanium plate. Subsequently, it gives promising result in electrochemical treatment for sludge disintegration.

Ti/RuO_2 electrode could improve the sludge disintegration and the removals of TS, VS, TSS and VSS by the electrochemical process were satisfactory. The removals efficiencies increased with the increase of pH value in the alkaline range, electrolysis time and current density but decreased with the increase of initial sludge concentration. The optimum removals were achieved when the pH value of the sludge was 12, sludge concentration 2000 mg/L, electrolysis time 40 min and current density 10 mA/cm^2. The application of electrochemical process using Ti/RuO_2 electrodes enhanced the sludge disintegration for possible subsequent biological treatment.

Acknowledgement

The authors are thankful to the Management and authorities of the Universiti Teknologi PETRONAS (UTP) and the Civil Engineering Department, UTP for providing facilities for the study.

References

[1] J.H. Bruus, P.H. Nielsen and K. Keiding, "On the stability of activated sludge flocs with implications to dewatering", Wat. Res., 26, pp. 1597-1604, 1992.

[2] D.C. Sobeck and M.J. Higgins, "Examination of three theories for mechanisms of cation induced bioflocculation", Wat. Res., 36, pp. 527-538, 2002.

[3] B. Jin, B.M. Wilen and P. Lant, "Impacts of morphological, physical and chemical properties of sludge flocs on dewaterability of activated sludge", Chem. Eng., 98, pp. 115-126, 2004.

[4] P.R. Karr and T.M. Keinath, "Influence of particle size on sludge dewatering", J. Wat. Pollut. Control Federation, 50, pp. 1911-1930, 1978.

[5] G. Surucu and F.D Cetin, "Effect of temperature, pH and DO concentration on filterability and compressibility of activated sludge", Wat. Res., 23, pp. 1389-1395, 1989.

[6] B.Q. Liao, D.G. Allen, G.G. Leppard, I.G. Droppo and S.N. Liss, "Interparticle interactions affecting the stability of sludge flocs", J. Colloid and Interface Sci., 249, pp. 372-380, 2002.

[7] Y. Chen, H. Yang and G. Gu, "Effect of acid surfactant treatment on activated sludge dewatering and settling", Wat. Res., 35, 2615-2620, 2001.

[8] O.G. Apul, I. Atalar, G.T. Zorba and F.D. Sanin, "The dewaterability of disintegrated sludge samples before and after anaerobic digestion", Drying Technol., 28, pp. 901-909, 2010.

[9] J. Pere, R. Alen, L. Viikari and L. Eriksson, "Characterisation and dewatering of activated sludge from pulp and paper industry", Wat. Sci. Technol., 28, pp. 193-201, 1993.

[10] J.H. Kwon, S.H. Ryu, K.Y. Park, I.T. Yeom and K.H. Ahn, "Enhancement of sludge dewaterability by ozone treatment", J. Chin. Ins. Chem. Eng., 32, pp. 555-558, 2001.

[11] E. Neyens, J. Baeyens, R. Dewil and B. De heyder, "Advanced sludge treatment affects extracellular polymeric substances to improve activated sludge dewatering", J. Hazard. Mat. 106B, pp. 83–92, 2004.
[12] E. Neyens and J. Bayeyens, "A review of thermal sludge pretreatment processes to improve dewaterability", J. Hazard. Mat., 98, pp. 51-67, 2003.
[13] H. Yuan, N. Zhu and F. Song, "Dewaterability characteristics of sludge conditioned with surfactants pretreatment by electrolysis", Bioresource Technol., 102, pp. 2308-2315, 2011.
[14] A.R. Andrade, P.D.P. Alves, C.H.V. Fidellis, P.M. Donate and J.F.C. Boodts, "Ethanol electrooxidation in ruthenium-oxide-coated titanium electrodes", J. Electrochem. Society, 145, pp. 3839-3843, 1998.
[15] G. Chen, X. Chen and P.L. Yue, "Electrochemical behavior of novel Ti/IrOx-Sb2O5-SnO2 anodes", J. Phys. Chem. B., 106, pp. 4364-4369, 2002.
[16] H. Li, Y. Chen, Y. Zhang, W. Han, X. Sun, J. Li and L. Wang, "Preparation of Ti/PbO2–Sn anodes for electrochemical degradation of phenol", J. Electroanalytical Chem., 689, pp. 193-200, 2013.
[17] H. Ding, Y. Feng and J. Liu, "Preparation and properties of Ti/SnO2-Sb2O5 electrodes by electrodeposition", Mat. Letters, 61, pp. 4920-4923, 2007.
[18] L.J. Song, N.W. Zhu, H.P. Yuan, Y. Hong, J. Ding, "Enhancement of waste activated sludge aerobic digestion by electrochemical pre-treatment", Water Res. 44 (2010) 4371–4378.
[19] C. Comninellis and G.P. Vercesi "Characterization of DSA®-type oxygen evolving electrodes: choice of a coating", J. Appl. Electrochem., 21, pp. 335-345, 1991.
[20] C.R. Costa, C.M.R. Botta, E.L.G. Espindola and P. Olivi, "Eletrochemical treatment of tannery wastewater using DSA® electrodes", J. Hazard. Mat., 153, pp. 616-624, 2008.
[21] R.D. Coteiro and A.R. De Andrade, "Electrochemical oxidation of 4-chlorophenol and its by-products using $Ti/Ru_{0.3}M_{0.7}O_2$ (M = Ti or Sn) anodes: preparation route versus degradation efficiency", J. Appl. Electrochem., 37, pp. 691-698, 2007.
[22] Y.J. Feng, Y. Cui, B. Logan and Z. Liu, "Perfomance of Gd-doped Ti-based Sb-SnO_2 anodes for electrochemical destruction of phenol", Chemosphere, 70, pp. 1629-1639, 2008.
[23] Y. Feng and X. Li, "Electro-catalytic oxidation of phenol on several metal-oxide electrodes in aqueous solution", Wat. Res., 37, pp. 2399-2407, 2003.
[24] M. Ferreira, H. Varela, R.M. Torresi and G. Tremiliosi-Filho, "Electrodes passivation caused by polymerization of different phenolic compounds", Electrochimica A-cta, 52, pp. 434-442, 2006.
[25] J.C. Forti, P. Olivi and A.R. De Andrade, "Characterization of DSA®-type coatings with nominal composition $Ti/Ru_{0.3}Ti_{(0.7-x)}Sn_xO_2$ prepared via a polymeric precursor", Electrochimica Acta., 47, pp. 913-920, 2001.
[26] R.G. Freitas, R.T.S. Oliveira, M.C. Santos, L.O.S. Bulhões and E.C. Pereira, "Preparation of Pt thin film electrodes using the Pechini method", Mat. Letters, 60, pp. 1906-1910, 2006.
[27] E.C.P.E. Rodrigues and P. Olivi, "Preparation and characterization of Sb-doped SnO_2 films with controlled stoichiometry from polymeric precursors", J. Phys. and Chem. of solids, 64, pp. 1105-1112, 2003.
[28] R.A. Torresa, V. Sarria, W. Torres, P. Peringera and C. Pulgarina, "Electrochemical treatment of industrial wastewater containing 5-amino-6-methyl-2-benzimidazolone: toward an electrochemical-biological coupling", Wat. Res., 37, pp. 3118-3124, 2003.
[29] APHA . 2005. Standard Methods for the Examination of Water and Wastewater. 21st ed. American Public Health Association, Washington D. C., USA.
[30] Hach. 2003. Water Analysis Handbook. 4th ed. Loveland, CO, USA: Hach Company.
[31] E. Neyens, J. Baeyens, R. Dewil, B. De heyder, "Advanced sludge treatment affects extracellular polymeric substances to improve activated sludge dewatering", J. Hazard. Mat., 106B, pp. 83–92, 2004.

Applied Mechanics and Materials Vol. 567 (2014) pp 50-55
© (2014) Trans Tech Publications, Switzerland
doi:10.4028/www.scientific.net/AMM.567.50

Environmental Screening Method for Dredging in Contaminated River

MANAP, Norpadzlihatun[1,a] and VOULVOULIS, Nikolaos[2,b]

[1]Department of Construction Management, Faculty of Technology and Business, 86400 Parit Raja, BatuPahat, Johor, Malaysia

[2]Centre for Environmental Policy, 1515, 15 Prince's Gardens, Imperial College London, South Kensington Campus, London SW7 2AZ, United Kingdom

[a]padzliha@uthm.edu.my, [b]n.voulvoulis@imperial.ac.uk

Keywords: Dredging, Risk management, Environmental screening, Contaminated sediments, Ecological Risk Assessment

Abstract. Dredging in a contaminated river has been widely accepted to have an impact on the environment; however environmental risk assessment analysis could be costly, time-consuming and difficult to perform. Therefore, a screening method acting as a preliminary risk assessment analysis to screen potential contaminated areas is necessary. The aim of this study is to demonstrate a new screening method for risk assessment analysis in a scenario where economy, time and simplicity factors had been a concern. The development of this method is based on a variation of standard Ecological Risk Assessment. An analysis will be performed on two elements. Firstly, the level of contaminants in the water, groundwater and air (known as the media) and, secondly the behavior of environmental indicators during monitoring of historical dredging. This analysis is performed in order to establish the degree of contamination in an area that is about to be dredged, in where the publicly accessible contamination level in the media and the historical dredging monitoring data will be utilized. Eight dredged sites in Peninsular Malaysia are selected as the case studies of this research. This research showed that Sungai Perlis has a very high total risk value, which could have a fatal impact on its biodiversity if dredging is performed with negligence at this location. This research could provide an opportunity for Malaysia to increase its efforts to avoid dredging impacts without being constrained on time, cost and simplicity factors.

Introduction

Dredging, which is performed in a highly contaminated site but has not been identified as a risk, could prove fatal for biological resources. Such cases have been observed in the developing country of Malaysia [1-4]. This could be due to current understanding of low number of contaminated sites owing to its slower development rate in comparison to countries like the US and the UK, in that their contaminated land requires strict environmental rules and regulations [4]. Moreover, it has been generally accepted that assessing environmental risks and providing mitigation measures is costly [5-7], which is a discouraging factor for many developing countries to use the already developed tools and assessments. In fact, a research which explored dredging issues in the developing country of Malaysia, confirmed that it lacks efficient tools and practices to assess the environmental risks of dredging [8]. Therefore, the need remains for an efficient tool or assessment, which takes into account a country's economic capability, to be developed in order to identify possible risks of dredging.

Ecological Risk Assessment (ERA) has been widely used to assess impacts of chemical exposure on endangered biological resources [9-11]. This analysis involves simplistic phases of risk assessment and three phases of ERA have been suggested by the United States Environmental Protection Agency (US EPA) (1998) namely: problem formulation, extent of impacts from exposure to chemicals over toxicity levels, and characterization of risk [10, 12].

The ecological impacts caused by exposure to contaminated sediments have generated considerable research interest in the US and the UK and many frameworks have been developed in order to characterize the risks of the presence of contaminated sediments for biological resources.

This includes assessment of ecotoxicological risks related to the depositing of dredged materials on soil and assessment of ecological risks of sediments dredged from ports and estuarine zones [7, 13]. Unfortunately, these frameworks can be time-consuming and are often difficult to perform, which is unfavourable to middle income countries, which are currently in the state of rapid development [7]. Therefore, an alternative approach that is easy to perform and not time-consuming is a necessity.

This paper introduces a new screening method and demonstrates its application to identify dredging-related risks in an area by using a simplified variation of ERA framework. This method utilizes the publicly accessible data and the historical monitoring of dredging data by using Malaysia as its case studies. As a result, this research will determine a location that is having a very high degree of contamination level.

Methodology

1st step. The objective of this first step of the screening method is to identify historical dredging risk values through three distinct stages; assessment of exposure level (namely; concentration level of mercury, cadmium, arsenic, lead, copper, zinc, dissolved oxygen, biochemical oxygen demand, total suspended solids, and chemical oxygen demand) from historical dredging activities, assessment of toxicity level associated with exposed substances, and characterization of the risks found. The execution of this step can circumvent the unnecessary sediment analysis, which can often be costly.

Eight maintenance dredging projects performed between 2006 and 2011 in Peninsular Malaysia were selected as the case studies for this paper. The reason for using historical dredging data lays in the fact that previous research indicates that concentration levels of metals in sediments increased after dredging. This means that contaminants dispersed by dredging are deposited back onto the new layer of sediments, exposed after excavation [14-16]. This creates a potential for future dredging to disperse the contaminants that have been re-deposited. Additionally, critical changes in indicators, monitored after historical dredging in an area, indicated its high contamination levels, which could have been initially caused by contaminants inputs from neighbouring land. Therefore, it is vital to analyse the behaviour of contaminants and the risk of re-contamination from adjacent land and therefore utilized in this step.

2nd step.The objective of this second step is to assess and quantify contamination level in media (the water, groundwater and air) as a total risk value using three types of data, namely number of rivers with polluted and slightly polluted status of Water Quality Index, number of days with very unhealthy and unhealthy status of Air Pollution Index and number of sampling points exceeding the standards of groundwater levels.

The reason behind the selection of this data to screen for ecological risks lays within the contaminants pathways. The contaminant originates from point and diffuse sources and penetrates sediments, which are about to be dredged, through precipitation, emission and dissipation from various media, including air, groundwater, and surface and marine water [17-19]. Therefore, it is necessary to assess these media (air, groundwater, and surface and marine water) to indicate its quality that determines the degree of contamination in an area.

The Water Quality Index, Air Pollution Index and groundwater level that have been monitored annually on a national level, can be good indicators of the quality of media [20-23]. Moreover, the utilization of this publicly accessible data can save cost and time to screen the dredging risks for the environment. Quantification of these indicators can be used in accordance to their indexes, however it should be noted that the lower the Water Quality Index becomes, the worse the water quality is. This is in contrast to the Air Pollution Index, which denotes that the risk increases, as the index itself increases. A stable quantification of risk is required to relate these indexes, which can signify the environmental risks. Therefore, it is suggested that the number of rivers in the river basin of the area to be dredged, that have a polluted and slightly polluted status of Water Quality Index, the number of days in the area, which have a very unhealthy and unhealthy status of Air Pollution Index and the number of sampling points, which exceed standards of groundwater levels in the area,

should be used for this step of the screening. It should be noted that the duration of data monitoring depends on data availability; however a similar the monitoring should have a similar duration in each location in order to ensure a fair comparison between areas.

3td step. The final step of this screening stage is to combine risk values found in previous steps for a total risk value and to determine the degree of contamination of an area. The terminology for the degree of contamination can be found in Table 1 [11].

Table1. Degree of contamination

Total risk ratio (Y)	Degree of contamination
Y<7	Low
7<Y<14	Moderate
14<Y<28	Considerable
Y>28	Very high

Result

1st step results. Sungai Perlis has been found to have the highest average total risk value of historical dredging, compared to other locations Fig 1.

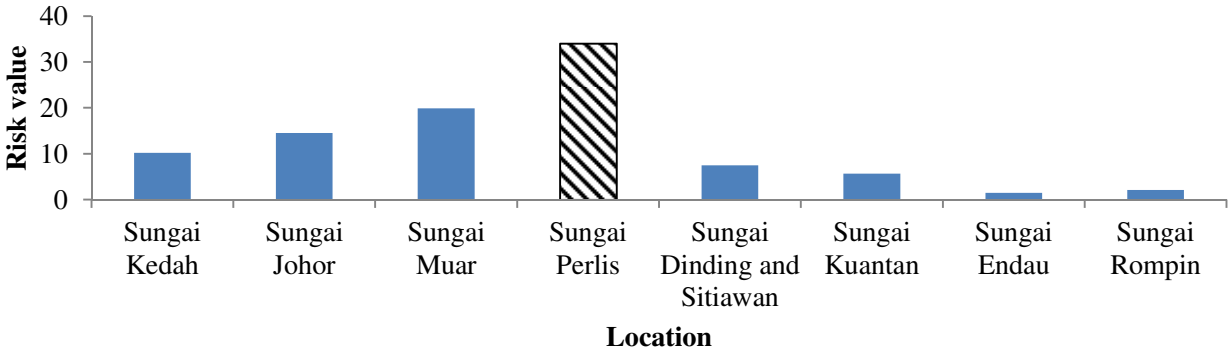


Figure 1. Average of total historical dredging risk value at location of case studies

2nd step results. The results for the second step in the screening stage can be found in Fig 2 which shows media risk values for each case study location. Sungai Muar has the highest average total of contamination level in media.

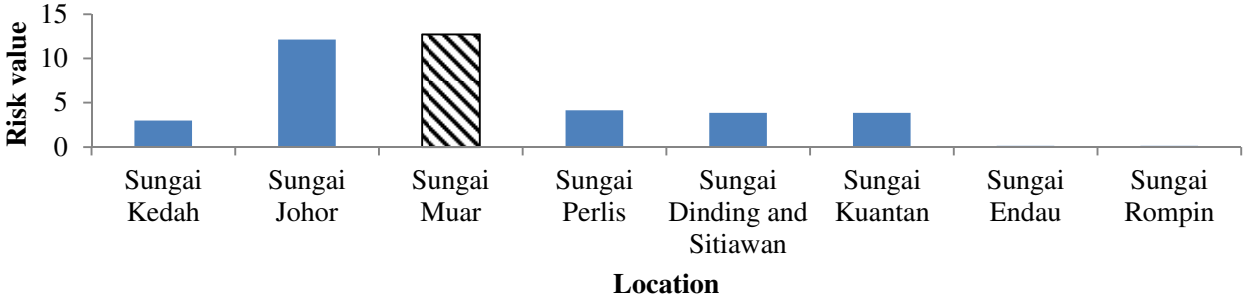


Figure 2. Average of total media risk value at the location of case studies

3td step results. The results have been illustrated in Fig 3. It was found that the river, which has a very high degree of contamination, was Sungai Perlis.

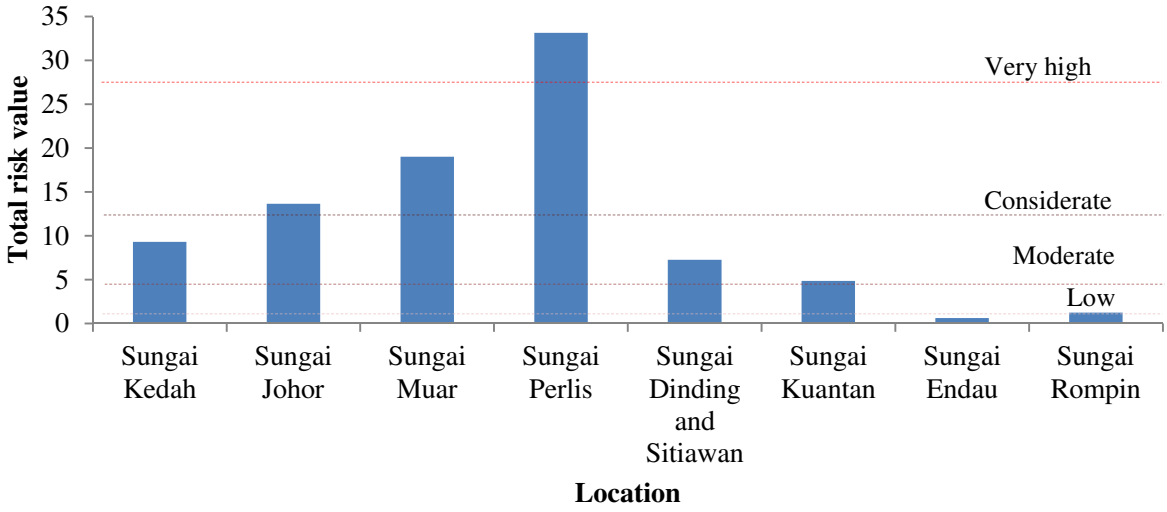


Figure3. Results of total risk value at the location of case studies

Discussion

Prior work highlighted the environmental impacts of dredging and many tools and assessments to identify dredging risks have been developed, but remain difficult to utilise, costly and time-consuming. This becomes the discouraging factor to use them by party that seeks for economic, simplicity and time benefits. In this paper, a newly developed method that utilizes free publicly accessible data and already available data in order to initially identify risks of dredging has been demonstrated in the scenario of a developing nation. This method corroborated the ERA phases suggested by US EPA (1998), well matched to the behavior of indicators, when being dredged by utilizing historical dredging monitoring data, and well suited to the contamination level in media into sediments, when using media contamination level data.

This method was demonstrated in Malaysia using eight case studies. It has been found that Sungai Perlis has the highest value of total historical dredging risk, whereas Sungai Muar is the location with the highest value of total media risk. The analysis of total risk value (addition of total historical risk value and total media risk value) found that Sungai Perlis has a very high degree of total risk value. This indicates that the contamination level at Sungai Perlis is categorized as very high.

However, it should be noted that this result is arguable due to the fact that it was not possible to retrieve groundwater data prior the execution of this study. Nevertheless, the research highlights the insufficiency of monitoring of this vital environmental indicator (groundwater data) on a national level in this country. At the same time, this becomes a good indicator to demonstrate how this country deals with the issue of contaminated land. It should be stressed that contamination from point and diffuse sources can dissipate into groundwater and be transferred from one area to another. Therefore, the lack of monitoring on a national level for this vital pathway shows that the issue of contaminated land has not been recognized in Malaysia.

It should be highlighted that ERA was initially suggested to protect endangered species and there can be tolerance for its risk values, only if they do not affect the entirety of populations and communities [30]. For example, Sungai Perlis has been characterized as having a very high degree of contamination, but if its biodiversity is not endangered and is highly mobile, the very high degree of contamination of this area can be tolerated with caution.

As countries like Malaysia are well-known for their biodiversity, which has become one of its sources of income, proactive action towards protecting them from the harmful effects of dredging is strongly needed. The results from this study should be looked upon as an opportunity for countries like Malaysia to improve their efforts to protect their environment from harmful dredging impacts. Thus, a detailed analysis on biodiversity composition and mobility should be further analyzed.

This screening method enables the accurate initial prediction of environmental dredging risks and it is straightforward and efficient in terms of time and cost. This could encourage parties that stress upon benefits in cost, simplicity and time, like Malaysia, to take proactive actions toward protecting their environment, whilst increasing their economic strength.

Conclusion

Dredging has been proven to have an impact on the environment and many tools and assessments have been developed. However these are difficult to perform, costly and time-consuming. This study demonstrated a newly developed screening method for the environmental risks of dredging, using publicly accessible data and available historical dredging monitoring data in its variation of ERA phases suggested by US EPA (1998). This method was demonstrated in a scenario of a developing country, Malaysia, where economic impact has always been a concern. It has been found that Sungai Perlis has the highest value of total historical dredging risk, whereas Sungai Muar is the location with the highest value of total media risk. The analysis of total risk value (addition of total historical risk value and total media risk value) found that Sungai Perlis has a very high degree of total risk value. This indicates that the level of contamination at Sungai Perlis is categorized as very high. However, this result is arguable due to the fact that it was not possible to retrieve groundwater data prior the execution of this study. Nevertheless, this research highlighted the many insufficiencies of environmental monitoring in this country, where this method could provide an opportunity to improve current efforts to prevent environmental damage due to dredging. This improvement should be reflected in future dredging projects, when this method is used, in order to benefit from its low cost, time efficiency and straightforwardness.

Acknowledgment

This research performed to fulfill the requirement of Short Term Research grant and acknowledgments are given to the Office for Research, Innovation, Commercialization and Consultancy Management (ORICC), Universiti Tun Hussein Onn Malaysia for all their support during the publication of this paper.

References

[1] S. Su, *Potential Long-Term Ecological Impacts Caused by Disturbance of Contaminated Sediments:A Case Study*, Environ.Manage. 29 (2002), pp. 234-249.
[2] R. Guerra, A. Pasteris and M. Ponti, *Impacts of Maintenance Channel Dredging in a Northern Adriatic Coastal Lagoon. I: Effects on Sediment Properties, Contamination and Toxicity*, Estuar.Coast.Shelf Sci. 85 (2009), pp. 134-142.
[3] A. Toes, *Effects of Deposition of Heavy-Metal-Polluted Harbor Mud on Microbial Diversity and Metal Resistance in Sandy Marine Sediments*, Arch.Environ.Contam.Toxicol. 55 (2008), pp. 372-385.
[4] C.Y. Yi and A.S. Talib, *Overview of Brownfields in Malaysia*, Jurutera. April (2006), pp. 16-23.
[5] D.J. Morrisey, *Environmental Impact assessment—A Review of its Aims and Recent Developments*, Mar.Pollut.Bull. 26 (1993), pp. 540-545.
[6] J. Burton G.Allen, *Sediment Quality Criteria in use Around the World*, Limnology. 3 (2002), pp. 65-76.
[7] R.B. Choueri, A. Cesar, D.M.S. Abessa, R.J. Torres, I. Riba, R.D. Morais, A.A. Mozeto and T.A. DelValls, *Harmonised Framework for Ecological Risk Assessment of Sediments from Ports and Estuarine Zones of North and South Atlantic.*, Ecotoxicology. 19 (2010), pp. 678-696.
[8] N. Manap, N. Voulvoulis and N. Zulkifli, *The Application of Driving Force-Pressure-State-Impact-Response (DPSIR) in Malaysia's Dredging Industry*, Journal of food, agriculture and environment. 3 & 4 (2012).

[9] H. Pekey, D. Karakaş, S. Ayberk, L. Tolun and M. Bakoğlu, *Ecological Risk Assessment using Trace Elements from Surface Sediments of Izmit Bay (Northeastern Marmara Sea) Turkey*, Mar.Pollut.Bull. 48 (2004), pp. 946-953.
[10] U.S. Environmental Protection Agency, *Guidelines for Ecological Risk Assessment* (1998).
[11] H. Pekey, D. Karakaş, S. Ayberk, L. Tolun and M. Bakoğlu, *Ecological Risk Assessment using Trace Elements from Surface Sediments of Izmit Bay (Northeastern Marmara Sea) Turkey*, Mar.Pollut.Bull. 48 (2004), pp. 946-953.
[12] National Research Council, *Risk Assessment in the Federal Government: Managing the Process*, National Academy Press, Washington, D.C., 1983.
[13] Y. Perrodin, M. Babut, J. Bedell, M. Bray, B. Clement, C. Delolme, A. Devaux, C. Durrieu, J. Garric and B. Montuelle, *Assessment of Ecotoxicological Risks Related to Depositing Dredged Materials from Canals in Northern France on Soil*, Environ.Int. 32 (2006), pp. 804-814.
[14] S. Ware, S.G. Bolam and H.L. Rees, *Impact and Recovery Associated with the Deposition of Capital Dredgings at UK Disposal Sites: Lessons for Future Licensing and Monitoring*, Mar.Pollut.Bull. 60 (2010), pp. 79-90.
[15] S. Piou, *Changes in the Geochemistry and Ecotoxicity of a Zn and Cd Contaminated Dredged Sediment Over Time After Land Disposal*, Environ.Res. 109 (2009), pp. 712-720.
[16] M. Munawar, *In Situ Bioassessment of Dredging and Disposal Activities in a Contaminated Ecosystem: Toronto Harbour*, Hydrobiologia. 188-189 (1989), pp. 601-618.
[17] B. Moss, J. Madgwick and G. Phillips, *A Guide to the Restoration of Nutrient-Enriched Shallow Lakes*, W W Hawes, United Kingdom, 1996.
[18] C.K. Jain and D. Ram, *Adsorption of Metal Ions on Bed Sediments / Adsorption d'Ions Métalliques Sur Les Sédiments De Fond*, Hydrological Sciences Journal. 42 (1997), pp. 713.
[19] M. De Nobili, R. Francaviglia and P. Sequi, *Retention and Mobility of Chemicals in Soil*, in *Developments in Soil Science* Vol. Volume 28, Part 1, A. Violante, P.M. Huang,J.-M.Bollag and L.Gianfreda, ed., Elsevier, 2002, pp. 171-196.
[20] M. Department of Environment, *Environmental Quality Report 2006 - 2011*, Annual Environmental Quality Report of Malaysia (2006), pp. 1-78.
[21] M. Department of Environment, *Environmental Quality Report 2007*, Annual Environmental Quality Report of Malaysia (2007), pp. 1-78.
[22] M. Department of Environment, *Environmental Quality Report 2008-2011*, Annual Environmental Quality Report of Malaysia (2008), pp. 1-78.

Applied Mechanics and Materials Vol. 567 (2014) pp 56-61
© (2014) Trans Tech Publications, Switzerland
doi:10.4028/www.scientific.net/AMM.567.56

Experimental investigation on the performance of four types of solar stills in Malaysia

Ali Riahi[1,a,*], Khamaruzaman Wan Yusof[1,b], Mohamed Hasnain Isa[1,c], Balbir Singh Mahinder Singh[2,d], Amirhossein Malakahmad[1,e] and Nasiman Sapari[1,f]

[1]Department of Civil Engineering, Universiti Teknologi PETRONAS, 31750 Tronoh, Perak, Malaysia.

[2]Department of Fundamental and Applied Sciences, Universiti Teknologi PETRONAS, 31750 Tronoh, Perak, Malaysia.

[a]ali_riahiupm@yahoo.com, [b]khamaruzaman.yusof@petronas.com.my, [c]hasnain_isa@petronas.com.my, [d]balbir@petronas.com.my, [e]amirhossein@petronas.com.my, [f]nasiman@petronas.com.my

Keywords: Solar distillation system, sand, black paint, PV-DC heater, potable water.

Abstract. This study aims at improving a solar distillation still by comparing the performance of four types of double slope single basin solar stills to produce adequate amount of potable water in the areas with confined fresh water. These solar stills fabricated with similar shapes. In each solar still a stainless steel basin with the length of 50 cm, width of 30 cm and depth of 8 cm was utilized. The still configurations differed based on inclusion of 2 cm depth of sea sand layer in the basin, a layer of black paint in the basin and use of a 50 W PV-DC heater. The study was conducted to increase the potable water production under Malaysia tropical condition. A comparative research of cumulative water production among these solar stills showed that solar still with black painted basin was the more efficient; producing 234 %, 190% and 148% the potable water produced by a conventional solar still, solar still with sand layer in basin and solar still connected to a PV-DC heater, respectively.

Introduction

Malaysia is aspiring to become a developed nation by the year 2020. One of the challenges in this journey is to supply clean fresh water to everyone. Some of the States in Malaysia are already facing difficulties in supplying fresh water that complies with Malaysian Department of Environment (DOE) as well as World Health Organization (WHO) standards. These standards for drinking water supply require removal of chemicals and heavy metals from natural water resources [1]. One of the reasons for water supply shortages in Malaysia is the pollution of rivers by toxic and chemical discharges. The use of brackish and saline water as feed water to water treatment plants requires application of expensive desalination processes such as reverse osmosis and distillation. As Malaysia receives enough sunshine throughout the year, solar energy can be tapped to provide an economical means of treating water for potable use [2,3]. The principle of conventional solar distillation system operation is based on the fact that transparent cover materials have the property of transmitting solar radiation. Thus this visible radiation passes through the cover into the still and heats the water for natural evaporation, therefore cooling of vapors can be occurred due to environmental conditions for condensation and collection of the condensed water. During the last decade, some researchers have conducted studies on different configurations of solar stills such as a solar still equipped with one flat plate collector [4], the usage of two flat plate collectors combined with a single sloped solar still [5], a solar still modified with 5 steps as absorber plates [6], a solar still with a pyramid shape using PV- solar fan for circulating air inside the solar still [7] and a double slope solar still using two AC heaters for increasing the evaporation [8].

The aim of this study is to develop the solar distillation technology by fabricating four types of solar stills: conventional solar still, solar still with sand layer in basin, solar still equipped with (PV-DC heater) and solar still with black painted basin and to compare their outputs to enhance the quantity of potable water production.

Nomenclature

T_w	temperature of water (˚C)
T_a	temperature of ambient air (˚C)
T_{ic}	temperature of inner cover (˚C)
I_s	solar radiation intensity (W/m²)
W_h	hourly water production (L/m²)
W_c	cumulative water production (L/m²)

Methodology

Fig. 1 (a) and (b) show the schematic diagram and photograph of the experimental set up of these solar stills, respectively. Four types of single basin double slope solar stills were constructed with similar shapes. Each of them had one stainless steel trough as a basin with a length of 50 cm, a width of 30 cm and a depth of 8 cm (volume 12 L). The double slope frame, cover and trough (basin) of all solar stills were made of PVC pipe, transparent polythene film and stainless steel, respectively. The solar stills were light and hence, portable. The PVC pipes and polythene film have three to five years durability [9]. The four types of solar stills studied are:
Solar still 1 (S1) - Conventional solar still
Solar still 2 (S2) - Conventional solar still with sand layer in basin
Solar still 3 (S3) - Conventional solar still connected to PV-DC heater
Solar still 4 (S4) - Conventional solar still with black painted stainless steel basin.
A 2 cm sea sand layer was included in the solar still basins as indicated above. The Photovoltaic-DC heater used had ratings of 50 W and 12 V- DC. One experiment was conducted to study the performance of the four solar stills in Universiti Teknologi PETRONAS campus in Malaysia:
Solar stills 1, 2, 3 and 4 were exposed to similar solar radiation in an open field (Fig. 1).
A digital thermometer was used to measure temperatures of water, inner cover of solar stills and ambient air. A solarimeter (SL200) was used to measure the solar radiation intensity. Each solar still basin was filled with 4.5 L of lake water (3 cm depth) for the experiments. Water vapor was condensed on the transparent cover and naturally collected as shown in Fig. 1.

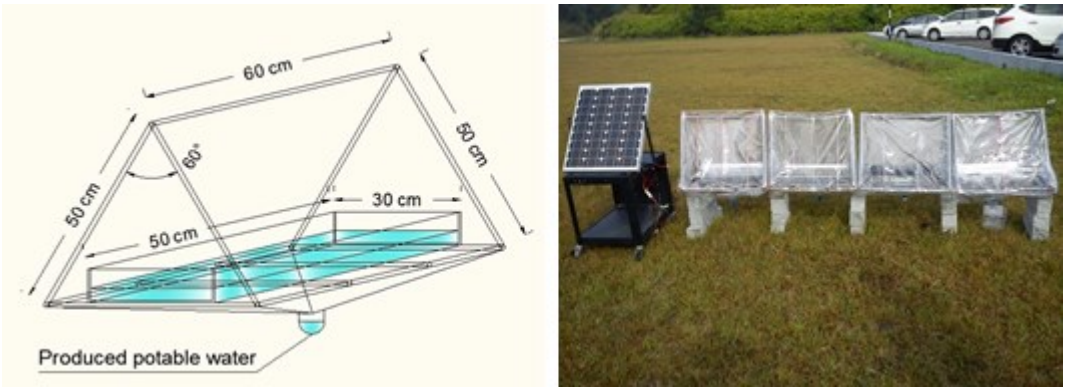


Figure. 1 a) Schematic diagram of solar still and b) Photograph of experimental set-up.

3. Results and discussion

Effect of solar radiation on water, inner cover and ambient air temperatures. Fig. 2 shows the diurnal variation of temperatures of water and inner cover for four solar stills, temperatures of ambient air and solar radiation intensity during experiment on 11 July 2013. The temperature increase corresponded to the increase in solar radiation intensity. It is revealed that when solar radiation intensity reached a maximum value from 559 W/m² at 9:00 am to 1110 W/m² at 1:00 pm, the highest T_{W1}, T_{W2}, T_{W3}, T_{W4} and T_a were observed with the values of 46, 47, 49 and 52 ˚C respectively; the corresponding maximum inner cover temperatures T_{ic1}, T_{ic2}, T_{ic3}, T_{ic4} were 39, 40, 41 and 41 ˚C. T_{W4} was generally higher than T_{W1}, T_{W2}, T_{W3} and T_a throughout the day. A sharp fluctuation in solar radiation intensity were observed with a decrease from 1110 W/m² at 1:00 pm to 678 W/m² at 2:00 pm and an increase to 901 W/m² at 3:00 pm which caused a mild fluctuations of temperatures of water and inner cover for four solar stills.

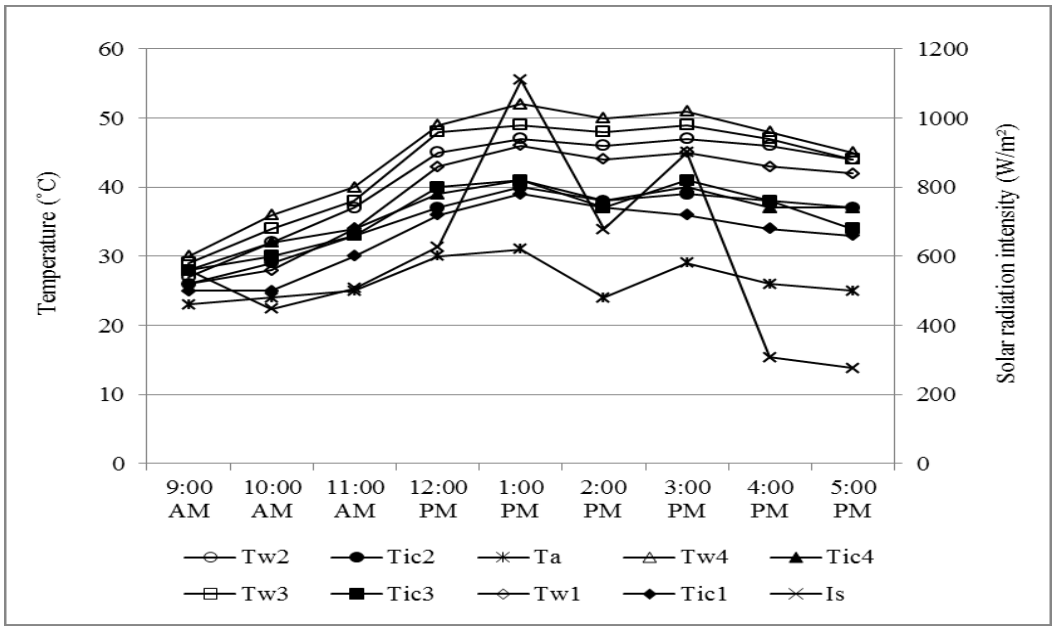


Figure. 2 Diurnal variations of solar radiation intensity and temperatures of water, inner cover of solar stills and ambient air on 11 July 2013.

Effects of solar radiation and water temperature on hourly water production. Fig. 3 shows the hourly water production for four solar stills corresponding to solar radiation intensities and water temperatures showed in Fig. 2. It is observed that with increase in solar radiation intensity and water temperature, the hourly water production also increased during experiment. The highest hourly water production for stills S1, S2, S3 and S4 was 0.199, 0.206, 0.344 and 0.495 L/m² respectively, obtained at 1 pm corresponding to respective solar radiation intensity and water temperature (Fig. 2). It can be concluded that the modifications to the conventional solar still i.e. use of PV-DC heater or use of black paint in basin were instrumented in producing more water from the stills. The effect of black paint in basin was clearly higher due to higher heat absorption for water evaporation. The strategy of including black paint in the solar still basin yielded the maximum amount of water among all configurations studied.

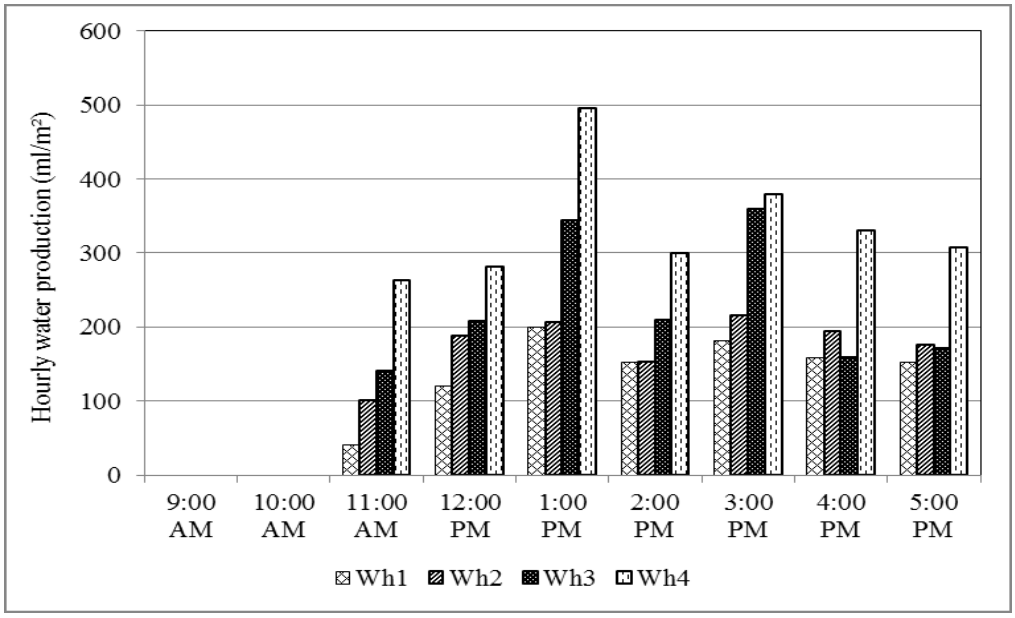


Figure. 3 Hourly water production of solar stills 1, 2, 3 and 4 on 11 July 2013.

Cumulative water production. Fig. 4 shows the cumulative water production from S1, S2, S3 and S4 on 11 July 2013. Water produced from S1 was the least throughout the day. At the end of the experiment, the total amount of water produced from S1, S2, S3 and S4 was 1.01, 1.24 and 1.60 and 2.36 L/m² respectively. W_{C4} being the highest amount of water produced from all solar stills, confirms that the configuration adopted in S4 was the most effective.

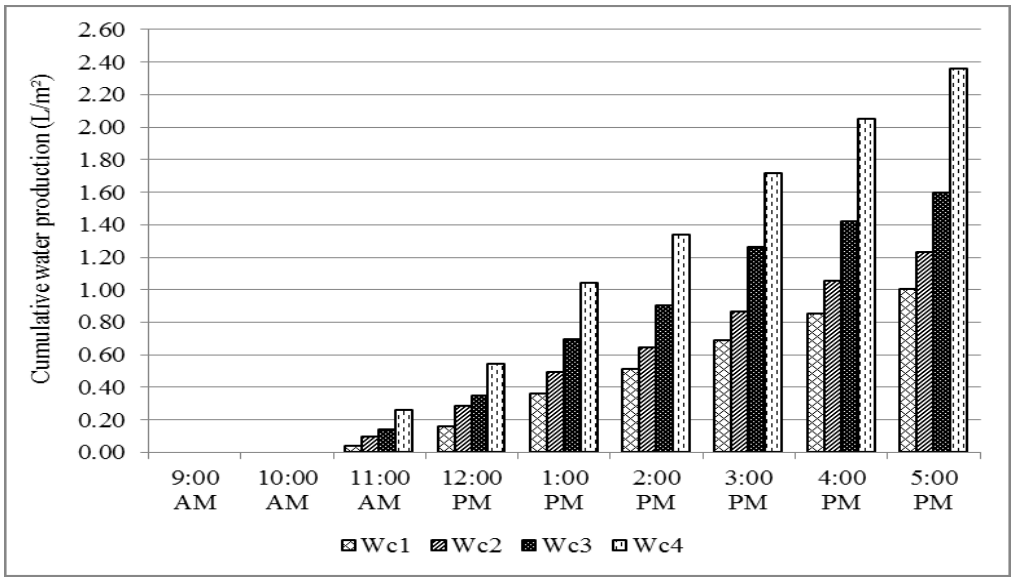


Figure. 4 Cumulative water production of solar stills 1, 2, 3 and 4 on 11 July

In this study, S4 yielded a cumulative water production of 2.36 L/m² using black paint in stainless steel basin, while a modified solar distillation system in India [10] produced 1.8 L/m² using stepped solar still with fin, pebble and sponge together with solar pond. This research also shows higher water productivity compared to solar still studies in India [11-13], Turkey [14] and Jordan [15].

Conclusions

Despite daily fluctuations due to cloud coverage, solar energy can be effectively harnessed and converted to thermal energy for potable water production using solar still with black paint in stainless steel basin. The conventional solar still using direct sun radiation only produced 1.01 L/m² of potable water, while the solar distillation system with added sand layer produced 1.24 L/m² and that equipped with a 50 W PV-DC heater produced 1.60 L/m² under Malaysia's meteorological conditions. Water production can be enhanced to 2.36 L/m² by using black painted basin into the conventional type solar still. A comparative research of cumulative water production among these solar stills showed that solar still with black painted basin was the more efficient; producing 234 %, 190% and 148% the potable water produced by a conventional solar still, solar still with sand layer in basin and solar still connected to a PV-DC heater, respectively. The solar still with black painted basin in this study produced more than twice as much water as the conventional still.

Acknowledgement

The authors are thankful to Universiti Teknologi PETRONAS research and innovation office to provide grant (STIRF NO. 0153AA-C55) for this research.

References

[1] S. Jasrotia, A. Kansal, V. V. N. Kishore, Application of solar energy for water supply and sanitation in Arsenic affected rural areas: A study for Kaudikasa village, India, Journal of Cleaner Production. 37 (2012) 389-393.
[2] A. Riahi, K. Wan Yusof, N. Sapari, B. S. M. Singh and A. Mustafa Hashim, Novel configurations of solar distillation system for potable water production, IOP Conference Series: Earth and Environmental Science. 16 (2013) 012135.
[3] N. Syuhada, A. Ahsan, U.A. Thomas, M. Imteaz, A.H. Ghazali, A low cost solar still for pure water production, Journal of Food, Agriculture and Environment. 11 (2013) 990-994.
[4] Ali A. Badran, Ahmad A. A1-Hallaq, Imad A. Eyal Salman, Mohammad Z. Odat. A solar still augmented with a flat-plate collector, Desalination. 172 (2005) 227-234.
[5] Shiv Kumar, G.N. Tiwari, M.K. Gaur. Development of empirical relation to evaluate the heat transfer coefficients andfractional energy in basin type hybrid (PV/T) active solar still. Desalination. 250 (2010) 214–221.
[6] Kabeel A.E., Khalil A., Omara Z.M., Younes M.M.Theoretical and experimental parametric study of modified stepped solar still. Desalination. 289 (2012) 12–20.
[7] Taamneh Yazan, Taamneh Madhar M. Performance of pyramid-shaped solar still: Experimental study. Desalination. 291 (2012) 65–68.
[8] Ahmed Z. Al-Garni, Productivity Enhancement of Solar Still Using Water Heater and Cooling Fan, Journal of Solar Energy Engineering. 134 (2012) 031006.
[9] A. Ahsan, A. Rahman, A. Shanableh, NN Nik Daud, TA Mohammed, ANA Mabrouk, Life cycle cost analysis of a sustainable solar water distillation technique, Desalination and Water Treatment. 51 (2013) 1-8.
[10] V. Velmurugan, J. Mandlin, B. Stalin, K. Srithar. Augmentation of saline streams in solar stills integrating with a mini solar pond. Desalination. 249 (2009) 143–149.
[11] K. Vinoth Kumar and R. Kasturi Bai. Performance study on solar still with enhanced condensation. Desalination. 230 (2008) 51–61.

[12] M.K. Phadatare and S.K. Verma, Influence of water depth on internal heat and mass transfer in a plastic solar still. Desalination. 217 (2007) 267–275.
[13] K. V. Kumar and R. K. Bai, Performance study on solar still with enhanced condensation, Desalination. 230 (2008) 51-61.
[14] HS Aybar and H Assefi, Simulation of a solar still to investigate water depth and glass angle, Desalination and Water Treatment. 7 (2009) 35-40.
[15] MSK Tarawneh, Effect of water depth on the performance evaluation of solar still, Jordan J. Mech. Ind. Eng. 1 (2007) 23-29.

Applied Mechanics and Materials Vol. 567 (2014) pp 62-67
© (2014) Trans Tech Publications, Switzerland
doi:10.4028/www.scientific.net/AMM.567.62

Feasibility of Alum Sludge as Phosphate Removal

Nazirul Mubin Zahari[1,a], Chua Kok Hua[2,b] and Lariyah Mohd Sidek[3,c]

[1,2,3] Centre for Sustainable Technology and Environment (CSTEN)
Universiti Tenaga Nasional (UNITEN)
Putrajaya, Malaysia

[a] mubinzahari@gmail.com (corresponding author), [b]ckh@uniten.edu.my, [c]lariyah@uniten.edu.my

Keywords: phosphate; phosphorus removal; alum sludge; wastewater treatment

Abstract. Alum sludge contained a large portion amount of the aluminum derived from the coagulation process in secondary stage water treatment**.** Alum sludge is discharge to the landfill and it can affect on disposal management. This study investigates the treatment of wastewater using the low-cost adsorption material and also an innovation in green technology for the preservation of the environment. This finding attempts to determine the effectiveness of dewatered water treatment alum sludge as media to remove pollutant (phosphate) from wastewater. The continuous flow test approach with constant speed allocate is being used in this study. Alum sludge was prepared in 2.36 mm sieve size in dry condition and the initial synthetic water concentration (phosphate solution) was set in increasing order 2.6 mg/L to 30.5 mg/L. The test was monitored over 30 days with constant flow rate. The results indicated removal phosphate in beginning of contact time at 30% - 90%. The maximum percentage removal is 91% - 98% in various condition. The dewatered alum sludge from water treatment plant has great potential as phosphate removal.

Introduction

In year 2010, 1,055 water quality monitoring station located at 570 Malaysian rivers. From this assessment, that found 527 (50%) are clean, 417 (40%) slightly polluted and 111 (10%) polluted [5]. Instead of that, the polluted source mainly from agricultural activities and sewage treatment plant. Generally in Malaysia, main factors influenced the water pollution are domestic waste, surface runoff, industrial waste, and livestock [6]. One of the element donating water pollution come from phosphorus. This inorganic contaminant can harmful human health and environment [10]. Excessive phosphorus in agricultural and industrial area possibility can causes land and water pollution. Phosphorus also can be found in natural source such as rocks, soils and organic material. Phosphorus in wastewater may exist in different type, i.e. organic phosphate, inorganic phosphate and other ionic forms [9]. Excessive phosphorus may increase the growth of algae and aquatic plant in a pond that leads to eutrophication phenomena [9,10].

Aluminum sulphate $AL^2(SO_4)_3$ commonly used in Malaysian water treatment plant as their coagulants mediator. Aluminum salt is added in the coagulation process succeeding flocculation process before settling mass appear in the tank. The settle mass as known as alum sludge form in a semi-solid condition before transfer to the drying bed. Alum sludge contained a large portion amount of the aluminum (Al) derived from the coagulation process in secondary water treatment [2,10,12]. Succeeding, alum sludge is discharged to landfill and it reduces the landfill lifespan. Besides that, inappropriate management of alum sludge can contaminate the land with the presence of the heavy metal (aluminum) and generate the enormous disposal cost [2]. Alum sludge can be transformed into a solid waste substance to useful recycle product in wastewater treatment facilities.

Potential of heavy metal removal using alum sludge also has been carried out in research [3]. Previous research regarding on usage of alum sludge as phosphate (PO_4) adsorbent has been proved. Babatunde (2009) archive in a study on removal based on a specific area of alum sludge and pH effect. Mortula (2007) discover that dewatered alum sludge can be used on agriculture activities in order to remove phosphorus. The past literature review shows that the alum sludge has a high potential as agent for removal of phosphorus [8,14].

In Ireland, most of the studies are conducted a research study using local alum sludge [1,2,8,13,14,15]. However, diminutive study was conducted using dewatered alum sludge from

Malaysian water treatment plants. This study investigates the behavior of removal of PO_4 with a different capacity of synthetic water using Malaysian water treatment alum sludge. It also monitors the pH effect after using the Malaysian alum sludge. This study renders an idea for creating the low cost removal and convert into beneficial reuses-able material [1,2].

Methodology

Preparation of Material. Raw dewatered alum sludge was collected from the local water treatment plant and desiccated at 105ºC for 24 hours. Dried alum sludge is sieved to particle size of 2.36 mm. The dried alum sludge was prepared at 500 g each test. Potassium Dihydrogen Phosphate (KH_2PO_4) is used to make up the synthetic water (PO_4 solution). The variances of initial PO_4 concentration were set in increase order, i.e. 2.6 mg/L, 10.2 mg/L, 19.74 mg/L, 30.5 mg/L. Orthophosphate is being selected because it is one of most important species inside phosphorus element [8].

Measurement. Spectrophotometer (HACH DR-2800) was used to analyze the sample according to the total phosphate HACH 8190 standard methods. The sample was monitored intimated in the first three hours and after that every two or three days. The pH probe is used to measure the pH level during the monitoring process until the end of the experiment. The result is presented as PO_4 percentage removal against contact time and pH against contact time.

Continuous Flow Test. The transparent acrylic column was used to run the test with the diameter of 7.4 cm and 100 cm long. The support gravel was placed at the base of the tube to prevent the losses of the dried alum sludge. The water sample will pass through the system by gravitational flow. The sample is being collected at the bottom of the acrylic column. A submersible pump is used to recycle the effluent for continuous flow until 30 days. This test is run with the constant flow rate, the constant high hydraulic loading, but with variable initial PO_4 loading. This test operates at constant speed of 5.16 $x10^{-4}$ m^3/d and was monitored every two or three days. Fig. 1, shows the fundamental diagram of the continuous flow test system.

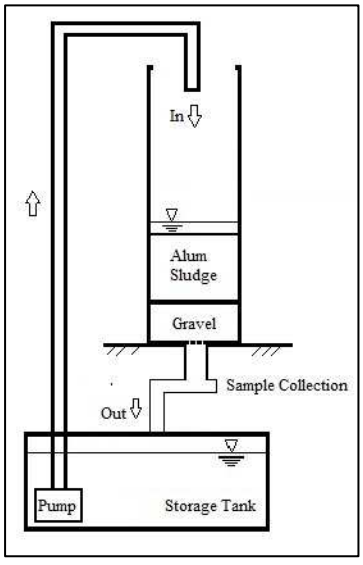


Fig. 1. Continuous flow test diagram

Result and Discussion

Efficiency removal of PO_4 in early stage operation hours. Fig. 2 shows the graph in early stage(first three hours) in percentage of PO_4 removal. The graph represents the percentage removal at different initial PO_4 concentration. The lowest initial PO_4 concentration was 2.6 mg/L and increased with concentration of 30.5 mg/L. This various of initial PO_4 concentration is to study the influence of initial PO_4 concentration will affect the removal rate. The graph shows that PO_4 removal starts at one hour contact time and proceeded at a reducing rate. The graph shows excellent PO_4 removal on first three hours.

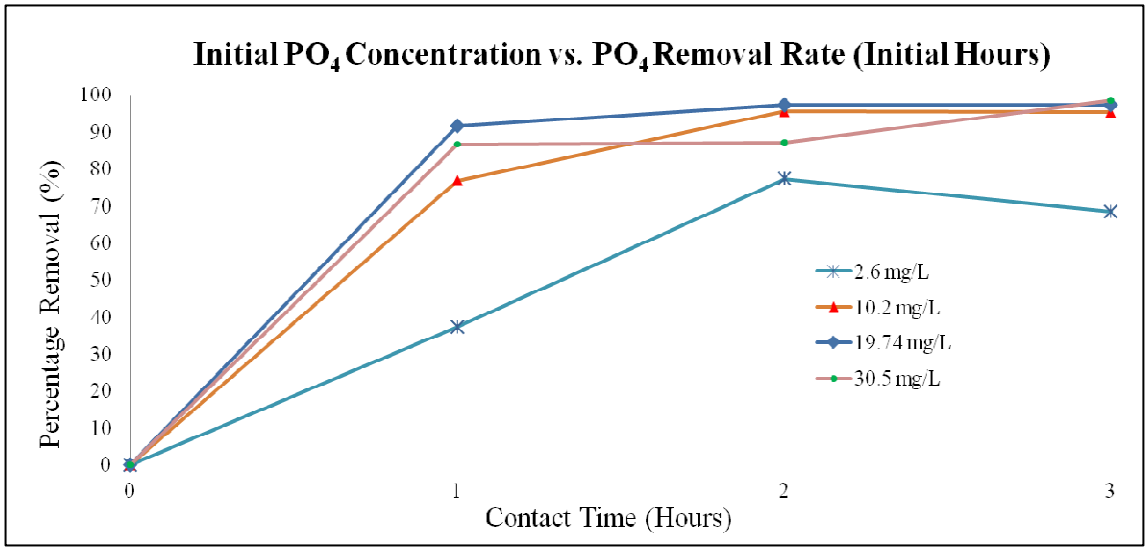


Fig. 2. PO_4 removal rate in early stage experiment

Efficiency removal of PO_4 in long-term operation hours. Fig. 3 shows the experiment result over 720 hours (30 days). It showed that removal effectiveness of 90% at end of test. The initial PO_4 concentration of 2.6 mg/L has a lowest removal rate, but still its affected removal rate of 85% which is relatively high. But has lowest percentage removal according to the initial PO_4 concentration because percentage based on *Ce/Co* (current reading divide by initial). It shows that highest percentage PO_4 removal at highest initial PO_4 concentration. The maximum removal rate is 91.0%, 97.5%, 97.82%, and 98.69% respectively for initial PO_4 concentration of 2.6 mg/L, 10.2 mg/L, 19.74 mg/L and 30.5 mg/L.

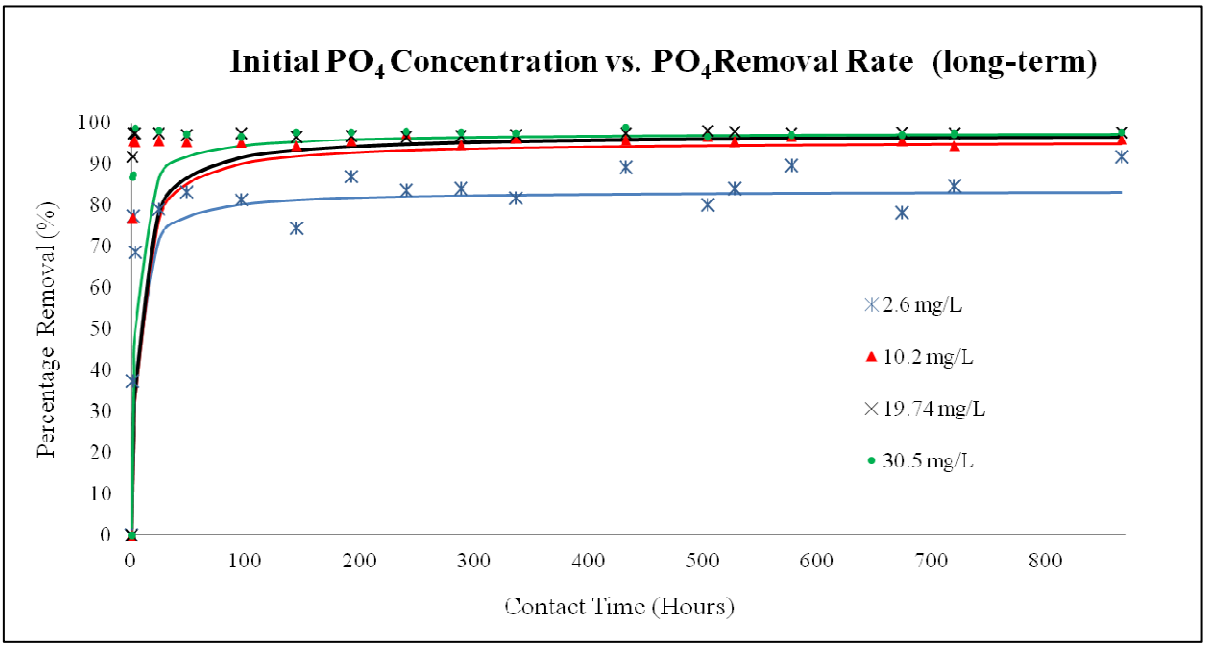


Fig. 3. PO_4 removal rate in long term operating hours

Percentage removal in this study shows the result in agreement with the other researchers. Similar test was conducted by Razali (2007) using Ireland local alum sludge shows that the efficiency removal of 80% for 28 days. Another experiment conducted by Mohammed (2012) that the percentage removal can reach 85% by increasing of contact time. The removal pattern shows that rate removal increase rapidly during the initial contact time. Then it gradually reduces and reach a plateau after 24 hours. This could due to all PO_4 molecules start instantaneously to migrate into an alum sludge adsorption site.

The PO_4 solution flow non-stop until reach 30 days. After 24 hour contact time, the increasing of the removal reaches to plateau stage where all the alum sludge particle has adsorbed the entire P molecules. It indicates that entire PO_4 molecules in the column has been adsorbed into the alum sludge and it has no more space available to adsorb the PO_4 molecules. The residual PO_4 molecules still remain in the PO_4 solution and maintain the concentration inside the storage tank until end of test. Alum sludge in that system are fully utilized and no more space to adsorb the remaining PO_4 inside the synthetic water [7,11,14].

The pH monitoring on experiment (early stage). Fig. 4 show the pH result in early stage experiment. The sample is being monitored for the pH during the experiment. Initial pH is recorded to be at pH 7.96, 7.12, 7.16, 7.41 for 2.6 mg/L, 10.2 mg/L, 19.74 mg/L and 30.5 mg/L respectively. At first hour contact time, pH reading of 2.6 mg/L, 10.2 mg/L, 19.74 mg/L and 30.5 mg/L is 7.5, 7.04, 7.1, and 6.87 respectively. The result indicates there is minor changes in pH after the PO_4 solution pass through the alum sludge median.

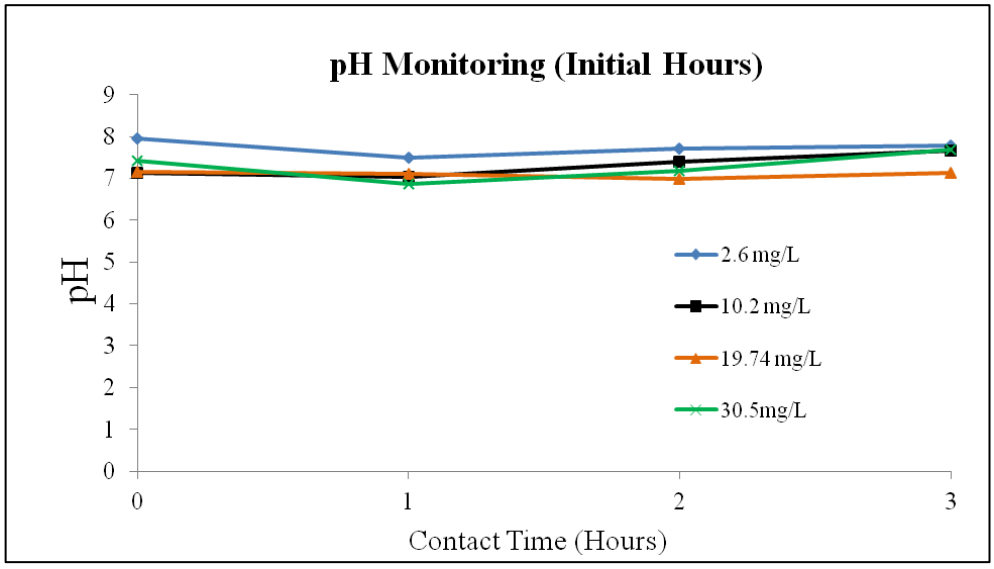


Fig. 4. The pH monitoring in early stage experiment

The pH monitoring on experiment (long-term). Fig. 5 shows the pH result in long-term operation. The pH reading is continuously monitored over 720 hours. The maximum pH for 2.6 mg/L, 10.2 mg/L, 19.74 mg/L, 30.5 mg/L is pH 7.96, 7.89, 7.76, 7.92 respectively. An average pH ranges from 6.5 to 7.5 between various PO_4 solutions. The objective of pH measurement is to investigate the changes on the pH after penetration of PO_4 solution into alum sludge medium whether it becomes more acidic or otherwise. Furthermore, pH monitoring is to show the Malaysia alum sludge workability of removal rate in pH neutral condition. Reported by Yang (2006) adsorption workabiltiy PO_4 removal between range pH 4.3 to 8 and greater than pH 8 will reduce workability of PO_4 removal. Meanwhile, the different of pH between variable initial PO_4 concentrations slightly change in small percentage. No further study in pH test is carried out on PO_4 solution in acidic or alkaline condition.

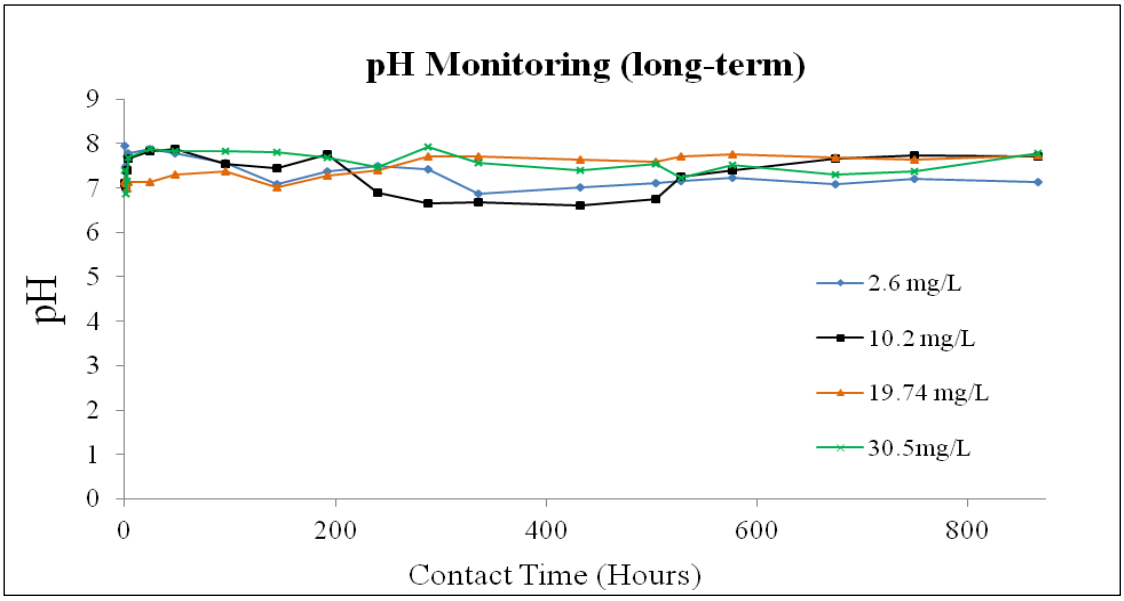


Fig. 5. The pH monitoring in long term operating hours

Conclusion

Alum sludge residual was dried and sieved accordingly. Orthophosphate is used to make-up the PO_4 solution and represent the high portion percentage in phosphorus species. The study shows that the alum sludge has high potential for removing the phosphorus from wastewater. The result indicates that the maximum PO_4 removal rate of 2.6 mg/L, 10.2 mg/L, 19.74 mg/L and 30.5 mg/L are 91.0%, 97.5%, 97.82%, and 98.69% respectively. Also, there are no major changes in pH after the PO_4 being absorbed by the alum sludge filter media. From the result, alum sludge from Malaysian water treatment plant can remove the PO_4 in various of initial concentration. It shows that, this study is important in the development of green material in Malaysia for water treatment process by using the low-cost adsorption material.

Acknowledgement

The authors acknowledge the scholarship provided by Yayasan Tenaga Nasional (YTN).

References

[1] Babatunde, A.O, Y.Q. Zhao, A.M. Burke, M.A Morris, and J.P. Hanrahan. "Characterization of aluminium-based water treatment residual for potential phosphorus removal in engineered wetlands." *Envinronmental Pollution*, 2009: 2830-2836.

[2] Babatunde, A.O., and Y.Q Zhao. "Equilibrium and kinetics analysis of phosphorus adsorption from aqueous solution using waste alum sludge." *Journal Hazardous Materials* 148 (2010): 746-752.

[3] Babatunde, A.O., Y.Q. Zhao, Y. Yang, and P. Kearney. "Re-use of dewatered alumunium-coagulated water treatment residual to immobilize phosphorus : batch and column trials using a condensed phosphate." *Chemical Engineering Journal*, 2007: 108-115.

[4] Chu, Wei. "Lead Metal Removal By Recycle Alum Sludge." *Wat. Res.*, 1999: 3019-3025.

[5] Department of Environment (DOE). "Malaysia Environmental Quality Report 2010." 2010.

[6] Ishak Bin Haji Omar, F.A., and W.M. Soffie. "National Report of Malaysia on the Formulation of a Transboundary Diagnostic Analysis and Preliminary Framework of a Strategic Action Programme for the Bay of Bengal. United Nations Environment Programme East Asian Regional Coordinating Unit." 2003.

[7] Mohammed, W.T, and S.A Rashid. "Phosphorus removal from wastewater using oven-dried sludge." *International Journal of Chemical*, 2012: 1-11.

[8] Mortula, M.M., and G.A. Gagnon. "Alum residuals as a low technology for phosphorus removal from aquaculture processing water." *Aquacultural Engineering*, no. 36 (2007): 233-238.

[9] Murphy, Sheila. *General Information of phosphorus.* April 23, 2007. http://bcn.boulder.co.us/basin/data/NEW/info/index.html (accessed June 15, 2012).

[10] Peavy, Howard S., Donald R. Rowe, and George Tchobanoglous. *Environmental Engineering.* International Edition. New York, USA: McGraw-Hill Book Company, 1985.

[11] Razali, M., Y.Q. Zhao, and M. Bruen. "Effectiveness of a drinking-water treatment sludge in removing different phosphorus species from aqueous solution." *Separation and Purification Technology*, 2007: 300-306.

[12] Wagner, E. G., and R.G. Pinheiro. *Upgrading Water Treatment Plants.* New York, USA: Spon Press, 2001.

[13] Yang, Y., D. Tomlinson, S. Kennedy, and Y.Q. Zhao. "Dewatered Alum Sludge: a potential adsorbent for phosphorus removal." *Water Science & Technology*, 2006: 207-213.

[14] Yang, Y., Y.Q Zhao, A.O. Babatunde, L. Wang, Y.X. Ren, and Y. Han. "Characteristic and mechanisms of phosphate adsorption on dewatered alum sludge." *Separation and Purification Technology*, 2006: 193-200.

[15] Zhao, Y.Q., A.O. Babatunde, Y.S.Hu, J.L.G Kumar, and X.H. Zhao. "Pilot field-scale demonstration of a novel alum sludge-based constructed wetland system for enhanced wastewater treatment." *Process Biochemistry*, 2011: 278-283.

Applied Mechanics and Materials Vol. 567 (2014) pp 68-73
© (2014) Trans Tech Publications, Switzerland
doi:10.4028/www.scientific.net/AMM.567.68

Floating Treatment Wetland as an Alternative for Water Quality Improvement: A Preliminary Study

Mohd. Noor Nur Asmaliza[1,a], Mohd. Sidek Lariyah[1,b], Kah Hoong Kok[1,c], Haron Siti Humaira[1,d], Basri Hidayah[1,e]

[1]Center for Sustainable Technology and Environment (CSTEN), College of Engineering, Universiti Tenaga Nasional, Jalan IKRAM-UNITEN, 43000, Kajang Selangor, Malaysia.

[a]asmalizamn@gmail.com,[b]lariyah@uniten.edu.my,[c]kahhoong_kok@yahoo.com, [d]sthumaira10@gmail.com, [e]BHidayah@uniten.edu.my

Keywords: Floating wetland; Removal efficiency; water quality; Hydraulic retention time

Abstract. Floating treatment wetland (FTW) is one of green innovation in order to enhance water quality as an alternative treatment for water quality improvement. The aim of this study is to identify the capability of floating wetland to remove stormwater pollutant in the river. The lab scale floating treatment wetlands were set up using three different sizes of the floating system with floating mat that made from plastics. Water quality samplings had been conducted starting from 4 December 2012 until 14 December 2012 to evaluate the performance for floating treatment wetland. The results indicate the removal efficiency gradually increased with the hydraulic retention time for water quality parameters such as Total Suspended Solid (TSS), Biochemical Oxygen Demand (BOD), Chemical Oxygen Demand (COD), Total Phosphorus (TP) and Total Nitrogen (TN) with a range of removal efficiency from 70% to 100%, -5.55% to 88.9%, 9.1% to 68.2%, -8.3% to 63% and 31.4% to 70.3% respectively.

Introduction

Evolution in water quality treatments rapidly occurred where in last two decades, wetlands are accepted as stormwater treatment devices but presently being integrated into water sensitivity urban design practices [1]. Free water surface wetland is most commonly used as stormwater treatment either in temperate or tropical climate and it had been showed the successful capability to enhance water quality of stormwater [2];[3];[4]. However, there is a problem in handling free water surface wetland such as the rooted vegetation used can only tolerate relatively shallow water depths and short periods of total submergence therefore the depths (and residence times per unit area) of the wetlands are generally less than stormwater retention ponds.

Floating Treatment Wetland (FTW) is an alternative to solve that problem. It can be defined as a modified of constructed wetland technology which consist of emergent wetland plants growing hydroponically on floating structures which located on the surface of a pond-like basin [1]. Fig. 1 shows the cross section of FTW in treatment system. FTW has a potential to improve the treatment performance through the integration with emergent macrophytes without having any constrains of shallow water depth. The FTW emergent plants growths in a floating matrix and do not affected by variable of water depth changes. However to the date, the information related to the design, construction and performance of FTWs are very little. The successful application of FTW has been proven in New Zealand, India, China, United Kingdom, Belgium and Singapore. The study

conducted in Belgium indicated the removal efficiency of 33%-68% for COD, 66%-95% for SS, and 24%-61% for TP but variable for TN removal [5]. The findings based on conducted study at Heathrow Airport in the United Kingdom indicated the removal efficiency for 20-30% for cuprum [6]; [7].

Nevertheless, there is no study conducted to evaluate the capability of Floating Treatment Wetland in order to remove the stormwater pollutant in the river under tropical climate. Therefore the objective of this study is to identify the capability of Floating Treatment Wetland to remove stormwater pollutant in the river.

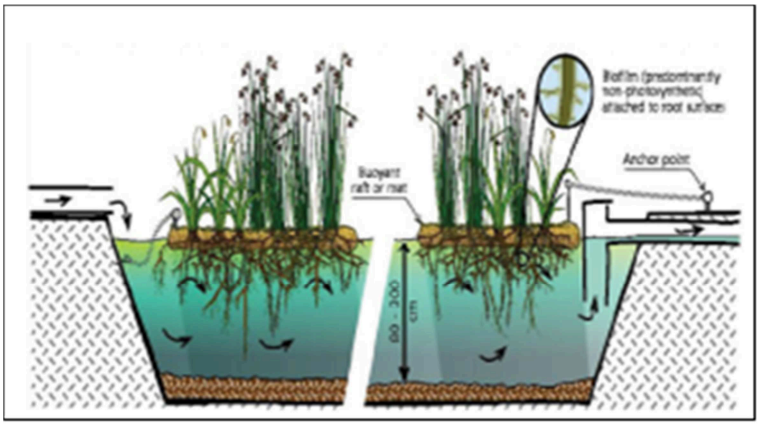


Fig.1: Cross section of FTW in Treatment system (Healey and Tanner, 2000)

Methodology

The experiments are conducted using three tanks with the volume of $0.2m^3$ at Civil Engineering Laboratory, Universiti Tenaga Nasional starting from 4 December 2012 until 14 December 2012. The tanks were supplied with the lake water from nearby lake at College of Engineering, Universiti Tenaga Nasional in order to have the actual characteristics of pollutants. There are three different sizes for floating mat area with various sizes where Set 1 consist of 30 Eichhornia crassipes plants, Set 2 consist of 20 Eichhornia crassipes plants and Set 3 consist of 10 Eichhornia crassipes plants. Fig.2 shows the example of Eichhornia crassipes plants. Water quality sampling and testing are conducted in accordance to Standard Method for Examination of Water and Wastewater 18^{th} Edition for Day 0, 1,3,8 and 10 in order to evaluate the performance of Floating Treatment Wetland.



Fig. 2: Eichhornia crassipes plant

Result and Discussion

Percentage of pollutant removal for TSS, BOD, COD, TP and TN based on hydraulic residence time are performed as in Fig. 3, Fig. 4, Fig. 5, Fig.6 and Fig. 7 respectively. Fig. 3 shows the percentage removal of TSS with hydraulic residence time. The results indicate the percentage for Set 1 around 80% on Day 1 and decreased to 70% on the Day 3 but on Day 8 and 10 increased to 100%. While for Set 2, the results indicated the 80% of removal for Day 1 and increased to 100% on Day 3 then maintained at 100% in Day 8 and Day 10. For Set 3 the 70% of removal recorded for Day 1 and increased to 100% in Day 3 and 8. However, in Day 10, the percentage of removal was decreased to 70%. The higher percentage of removal for TSS was affected by long term trapping of suspended solids and settlement at the bottom of the box which mean the longer detention time will lead to the higher of percentage of removal. Moreover the numbers of plant also play an important role in TSS removal as the suitable numbers of plant was set in Set 2. As a result, the combination between longer detention time and the numbers of plants indicate the optimum removal efficiency of TSS.

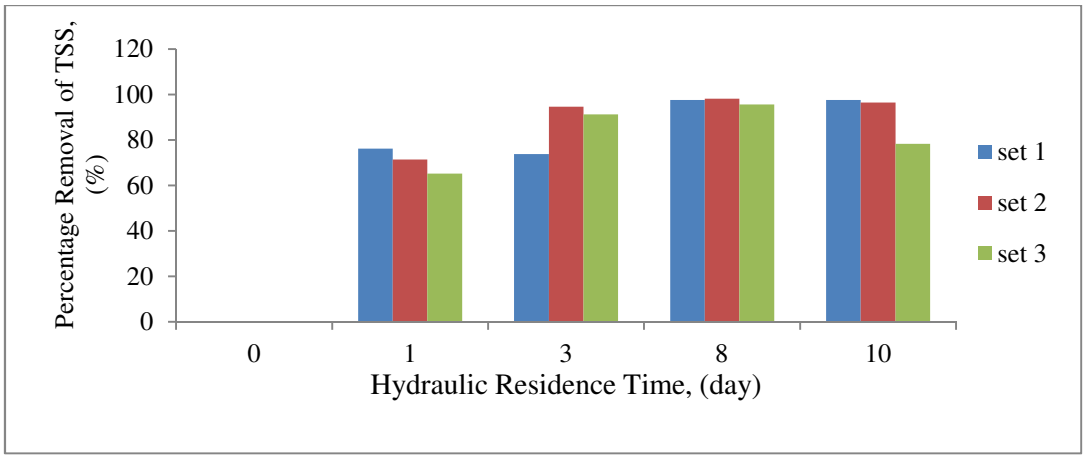


Fig. 3: Percentage removal of TSS with hydraulic residence time

Fig. 4 shows the percentage removal of BOD with the hydraulic residence time. Set 1 indicated the fluctuate values of percentage of removal starting from Day 1, Day 3, Day 8 and Day 10 with the value of 65%, 52%, 65% and 91% respectively. While in Set 2, the percentage of removal started at 20% at Day 1 but decreased to 0% at Day 3 before increased to 55% and 85% at Day 8 and Day 10 respectively. Set 3 shows the same pattern with Set 1 with fluctuate values of percentage of removal starting with -5.5% at Day 1, 55.6% at Day 3, 33.3% at 8 and 88.9% at Day 10. The results indicate the optimum removal efficiency is recorded by Set 1 with the numbers of plants around 30 plants. Active microorganisms are usually associated with the solid surface such as litter, sediments and submerged plants. In floating treatment wetland systems, BOD is principally removed by microbiological activity with plants and litter providing surfaces for biofilm growth [9]. Therefore the bigger amount of plants will help to accelerate the BOD removal process as these plants will provide the surface for biofilm growth. The study conducted at Heathrow Airport by [6] has been indicated that the floating wetland gave the poor removal of BOD compared to the nutrients.

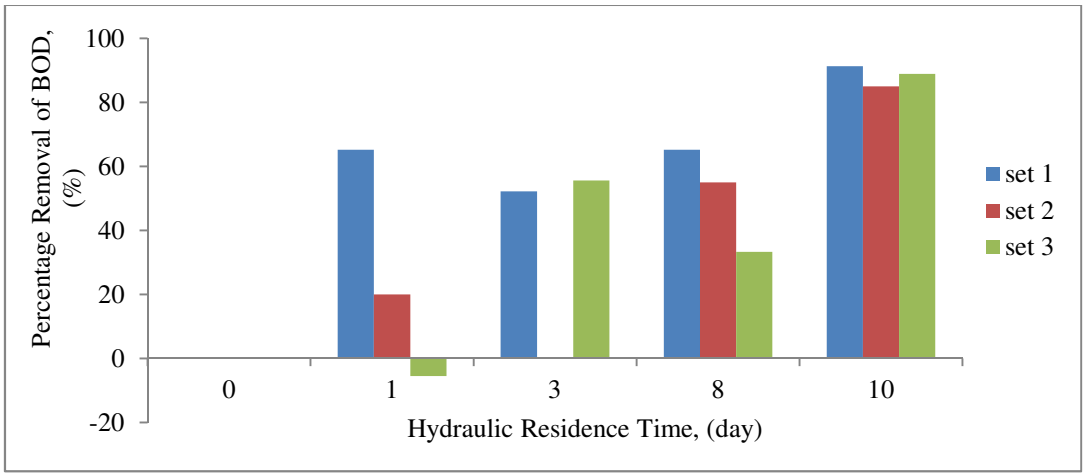


Fig. 4: Percentage removal of BOD with Hydraulic Residence Time

The results for removal percentage of COD with different residence time are showed in Fig.5. Three sets with the same values of hydraulic residence time; Day 1, Day 3, Day 8 and Day 10 were compared and indicated the highest values of removal percentage was shown by Set 2 with the removal percentage of 59.1%, 45.5%, 63.6% and 68.2%. The other two sets show the fluctuate values of removal percentage. Set 1 indicated the removal percentage of 27.3%, 9.1%, 27.2% and 36.4% while Set 3 indicted the removal percentage of 21.4%, 14.3%, 42.7% and 28.6%.The highest COD removal performance might be due to good growth of vegetation resulting in a high concentration of dissolved oxygen which can be seen as the electron acceptor for heterotrophs attached to the rhizomes [10].

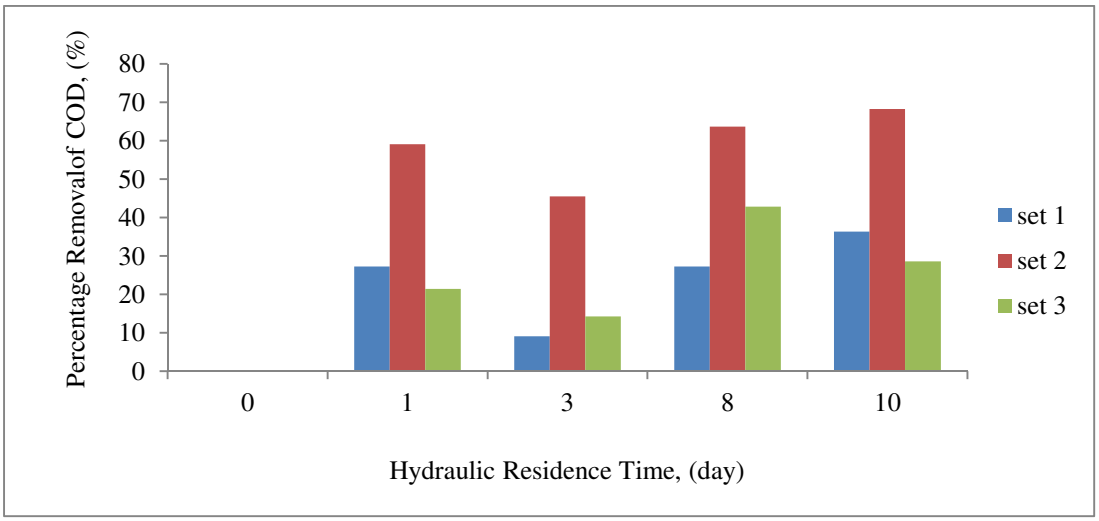


Fig.5: Percentage removal of COD with Hydraulic Residence Time

Fig.6 shows the removal percentage for TP with hydraulic residence time. Set 1 indicate the values of percentage removal fluctuate with 29.6%, 37.0%, 63.0% and 59.3% while Set 2 indicated the gradually increased with the removal percentage values of 25%, 41.7%, 54.2% and 58.3%. The similar pattern had been observed in Set 3 with the percentage of removal of 33.3%, 25.0%, 41.7% and -8.3%. The short water residence time may reduce the settling of particles with attached phosphorus and may lead to the resuspension of previously settled particles [11].

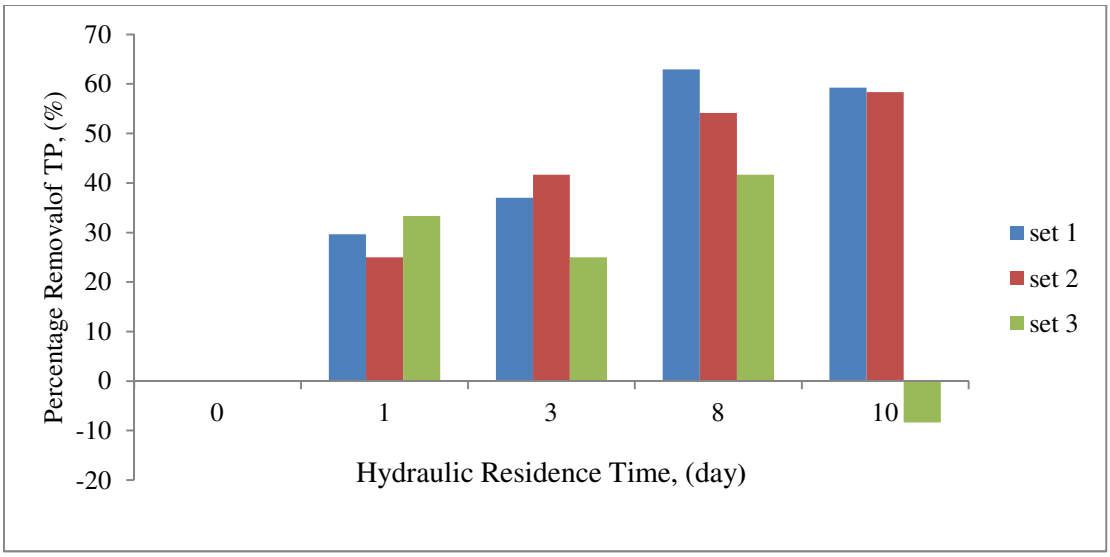


Fig.6: Percentage removal of TP with Hydraulic Residence Time

TN is one of elements that being considered in order to evaluate the performance of floating wetland as water quality improvement. Fig. 7 shows the percentage removal of TN with hydraulic residence time. Based on this preliminary study, the results indicated that the Set 1 gave the highest removal efficiency with the percentages range from 56.1% to 70.3% for hydraulic retention time Day 1, 3, 8 and 10 respectively. While Set 2 depicted the percentage of removal ranges from 31.4% to 64.1% and Set 3 indicated the percentage of removal ranges from 31.9% to 37.3%. Plants were important for the wetlands as plants provided good growth condition for microbes which removed the majority of N from constructed wetlands through the investigation in the nitrogen distribution pathway and removal efficiency [12].

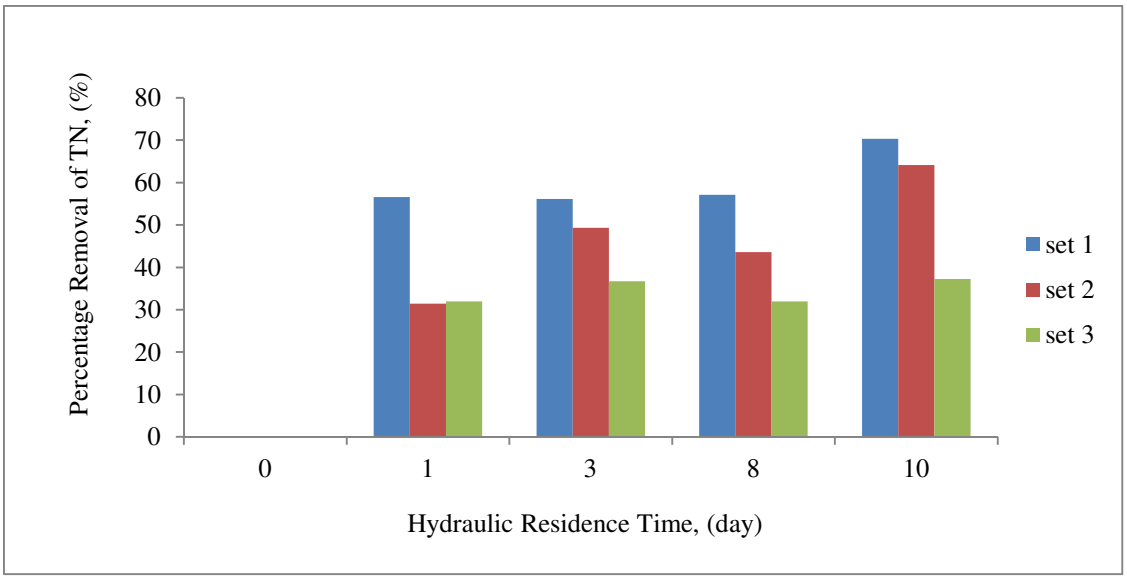


Fig.7: Percentage removal of TN towards Hydraulic Residence Time

Conclusion

In conclusion, the Floating Treatment Wetland is capable to remove nutrients such as TP and TN compared to BOD and COD. The results indicated the Set 2 with 20 Eichhornia crassipes plants gave the better removal efficiency compared to Set 1 with 30 Eichhornia crassipes plants and Set 3 with 10 Eichhornia crassipes plants. However, plants species also play the important element in order to provide the optimum removal efficiency for Floating Wetland. Further research and study

need to be carried out to investigate the suitable plants species in order to produce the optimum removal efficiency of pollutant.

Acknowledgment

This work was supported by Ministry of Higher Education (MOHE) under Long Research Grant Scheme (LRGS) Project entitled "Urban Water Cycle Processes, Management and Societal Interaction: Crossing from crisis to sustainability" with Grant Number 203/PKT/672000.

References

[1] T. Headley and C.C. Tanner, "Floating Treatment wetlands: An Innovative Option for Stormwater Quality Application", 11th International Conference on Wetland Systems for Water Pollution Control, November 1-7, Indore, India 2008.

[2] N.A. Mohd Noor, L. Mohd Sidek, R. Abdullah and A.Ab Ghani, "Performance of Artificial Wetland in Removing Contaminants from Stormwater under Tropical Climate", IAHS Publication 357, (2013), 1-9

[3] A.O. Babatunde, Y.Q. Zhoa, M.O. Neill and B.O. Sullivan, "Artificial Wetland for Environment Pollutant Control: A Review of Development, Research and Practice in Ireland. Environment International 34, (2008), 116-126

[4] D. Zhang, M.G. Richard and S.K. Tan, "Constructed Wetland in China". Ecological Engineering 35 (2009), 1367- 1378.

[5] J. Van Acker, L. Buts, C. Thoeye and G. De Gueldre, "Floating Plants Beds: BAT for CSO Treatment?" In Book of Abstract From International Sysmposium on Wetland Pollutant Dynamics and Control, September 4-8, Ghent Belgium (2005), 185-187.

[6] D.M. Revitt, R.B.E. Shutes, N.R.Llewellyn and P. Worrall, "Experimental Reed Bed Systems for the Treatment of Airport Runoff", Water Science and Technology, 36 (8-9), (1997) 385-390.

[7] T.R. Headley and C.C. Tanner, "Application of Floating Wetlands for Enhance Stormwater Treatment: A Review", NIWA Client Report: HAM2006-123, (2006).

[8] American Public Health Association, "American Water Works Association and Water Environment Federal, Standard Methods for the Examination of Water and Wastewater 18th Edition", APHA, Washington DC (1995).

[9] M. Greenway, and A, Woolley, "Construction Wetland In Queensland: Performance Efficiency And Nutrient Bioaccumulation". Ecological Engineering 12, (1999), 39-55.

[10] Y. Dong, P.R. Wilinski, M. Dzakpasu, M, Scholz "Impact of hydraulic loading rate and season on water contaminant reductions within integrated constructed wetlands". Wetlands 31(3): (2011) 499-509

[11] D.A. Kovacic, R.M. Twait, M.P. Wallace, and J.M. Bowling, "Use of created wetland to improve Water Quality at the Midwest- Lake Blooming case study". Ecological Engineering 28, (2006), 258–270.

[12] J. Vymazal, "Constructed wetlands with emergent macrophytes:From experiments to a high quality treatment technology". Dias V., Vymazal J. (eds.) Proceedings of the 10th International Conference on Wetland Systems for Water Pollution Control, 23–29 September , (2006), 3–27.

Applied Mechanics and Materials Vol. 567 (2014) pp 74-79
© (2014) Trans Tech Publications, Switzerland
doi:10.4028/www.scientific.net/AMM.567.74

Investigation of Modified Mangrove Bark on the sorption of oil in water

Robabeh Asadpour[a]*, Nasiman Bin Sapari[b], Mohamed Hasnain Isa[c], Kalu. U. Orji

[a]Geosciences & Petroleum Engineering Department, UniversitiTeknologi PETRONAS, 31750 Tronoh, Perak, Malaysia.

[b,c,d]Civil Engineering Department, UniversitiTeknologi PETRONAS, 31750 Tronoh, Perak, Malaysia.

email:[a]asadpour1981@gmail.com, [b]nasiman@petronas.com.my, [c]hasnain_isa@petronas.com.my, [d]suunyboy2008@yahoo.com

Keywords: Mangrove bark; Fatty acid; oil spill; sorption capacity

Abstract. Today oil spills generally cause worldwide worry due to their damaging effects on environment. Use of agricultural wastes such as raw and modified mangrove barks (*RhizophoraApiculata*), as an abundant and low cost adsorbent for oil-products spill cleanup in aquatic systems, has been developed to control these spills. Sorption capacity can improve by modification of adsorbent. The modification significantly increased the hydrophobicity of the adsorbent. The raw mangrove bark was modified using fatty acid (Palmitic acid) to improve its adsorption capacity. Oil sorption capacity of the modified bark was studied and compared with the raw bark. Kinetic tests were conducted with a series of contact time. The kinetic studies show good correlation coefficients for a pseudo-first-order kinetic model. A correlation between surface functional groups of the adsorbent was studied by FTIR spectrum. The results gave the maximum adsorption capacity of 2640.00 ± 2.00 mg/g for Palmitic acid treated bark (PTB). The prepared adsorbent revealed the potential to use as a low-cost adsorbent in oil-spill clean-up.

1. Introduction

Today fossil oil is a most important raw material and energy source in the world.The risk of water contamination by petroleum products has been increased due to their exploration, transportation, and refining process. Every year the totalinflow of petroleum into water is about 10 million metric tons [1].It takes a very long time to bring the environment back to its original state. Thus it is essential to find a rapid, efficient and effective method to eliminate the potential oil pollution hazard and recover the spilled oil concurrently .Several methodsare currently used for the removal of spilled oil on the sea surface it suffers various processes such asbooms, skimmers, dispersant, in-situ burning, bioremediation, chemical agents such as dispersants. These methods is still a major challenge due to the limitations and highcost of current cleanup practices [2-6]. Sorbents are preferable in small scale applications due to their ability to change oil from liquid phase to semi solid or solid phase[4]. Sorbents can be classified in to three classes: natural organic sorbent, inorganic sorbent and synthetic sorbent. Effective oil sorbents have properties such as highoil uptake rate, oleophilicity-hydrophobicity, lowcost, reusability, and biodegradability.Among these natural sorbent, organic fibers such as cotton, milkweed, kenaf, and wool have been reported to be the best natural sorbent due to sorption capacity and availability.Thus natural materialssuch as agricultural products are sorbents of choicedue to their low cost, easy availability, environmental friendliness and biodegradability[7].

Limitations of agriculture sorbents aretheir proportionately lower sorption capacity. To overcome this limitation chemical modification of agricultural by-product has been tried by a number of researchers to increasethesorption capacity of the materials. These include barley strawmodifiedby surfactant, sawdust grafted with fatty acid, banana trunk fibers modified by Fatty Acid, wheat straw modified by acid hydrolysis, Jute fiber, sugarcane bagasse and rice straw modified by acetylation[8-14].Mangrove bark peel is an abundant byproduct of charcoal industry that produces cooking fuel

particularly for recreational activities. It is easily available in the charcoal factory as a waste material. Mangrove bark peel consists of cellulose, hemicelluloses and lignin. The first two constituents are hydrophilic, and the lignin is hydrophobic. These properties can be changed by chemical modification or surface modification of its components.Thisworkconcentrateson the potential of modified mangrove bark peel to recover spilled oil in aqueous system and compare with the unmodified bark. Surfacemodification was applied to increaseoil sorption capacity and improved its hydrophobicproperties. Esterification reaction by using fatty acidwas introduced to increase the hydrophobicity of the bark peel.Kinetics study was evaluated using pseudo-first-order, pseudo-second-order to fit the experimental data.

2. Materials and Methods

2.1 Materials

The mangrove barks used in this study was obtainedfrom a localcharcoal factory.A mechanical debarkerwas used to take barks peel. The collected peels were washed and dried in an oven at 105°Cover night. A mechanical grinder was used to grind the bark into a fineground. The groundbark peel was sieved to a constant size using the U.S.A Standard Testing Sieve A.S.T.M. No. 300 microns. Crude oil samples used in this study wereTapis Malaysian crude oil obtained from Petronas Refinery in Melaka, Malaysia,Density measurement of crude oil was carried out using density Meter (Anton Paar, Austria). Viscosity of crude oil was measured using EV1000 ViscometerPhysical properties of Tapiscrude oilis shown in Table 1.Fourier Transform Infrared (FTIR) spectrum was used to find chemical structure of adsorbent and its functional groups. It was scanned over the range of 400 cm^{-1} until 4000 cm^{-1} wavelength.

Table 1: Crude oil quality specifications

Tapis Crude oil 25 -30° C	
Density (g/cm^3)	0.80
Viscosity (cP)	2.32

2.2 Preparation of Mangrove Bark

Two grams of sieved untreated bark (300 μm) wastreated with 1.2 g of palmitic acid in 200 ml of n-hexanein the presence of one to three drops of concentrated sulfuric acid (99%) as catalyst. The mixture was refluxed at 60°C ± 5°C for 6 hours. The mixturewere then extensively washed with n-hexane and dried in an oven at 105°C for 24 [10]. The raw and treated barks are denoted as UTB (untreated bark), and PTB (Palmitic acid treated bark).

2.3Adsorption experiments

40 ml of crude oilwas mixed with 250 ml artificial sea water (3.5%NaCl) inside a 500-ml beaker for 5 min by constantlystirring at room temperature. Afterstirring, the oil willform a layer at the surface of the water. 1 g of sorbent (UTB and PTB) was added to the beaker and the mixture was agitated forvarious times (5 to 50 min) on an orbital shaker (150 rpm/min). The sorbent and liquid was then separated by filter and the residue was dried in an oven at 70°C for 20 min to reach a constant weight. The amount of crude oil sorbed by sorbent was calculated by subtracting the weight of sorbent before sorption from that after sorption[11]. All tests were conducted in triplicate.

3. Results and discussion

3.1 Fourier Transform Infrared (FTIR) Analysis of Sorbent

The FTIR spectrum of UTB, PTB, and OPTB (oil absorbed palmitic acid treated bark) are shown in Fig. 1 The band that fall in the range of 3403 cm^{-1}shows the results of hydrogen-bond (O-H) present in cellulose, hemicellulose, and lignin. The two peaks between 2919 and 2850 cm^{-1}indicate the presence of C-H asymmetric stretching of CH_3 and CH_2 groups[11, 15]. The bands present at 1440 and 1374 cm^{-1}may represent C-Hbending vibration and OH bending, respectively[16].The band observed at 1604 cm^{-1}corresponds to the benzene ring stretching vibrationsof lignin[17]. It can be seen from the FTIR spectrum of untreated and treated samples,a weak band was created at 1,735 cm^{-1}, related to the stretching vibration of the ester linkages between 1,725 and1,750 cm^{-1}[18]whichshows thatthe fibers had been esterified.The bands at 2919, 2850, 1440 cm^{-1} and 1374cm^{-1}had considerablydecreaseddue to the breaking of C-H band. These results show that the treatment by palmiticacid removes some C-H band and creates some active sites for interaction with C-H groups from crude oil. This phenomenon can be seen from the FTIR spectrum of crude oil attached onto the surface ofPTBwhich demonstrate the peaks atbands of 2850, 2919 and 1440 cm^{-1}become more prominentafter the adsorption process.

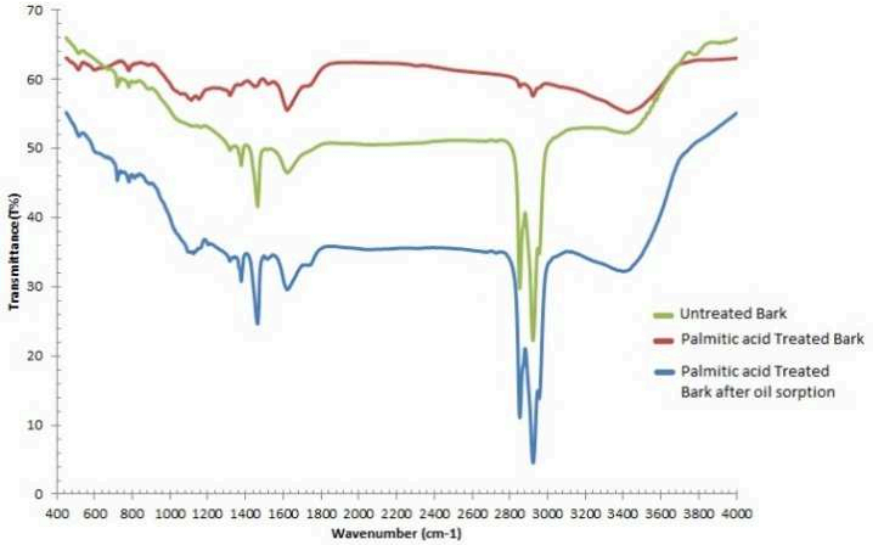


Fig.1. FTIR spectra of Untreated bark,Palmitic acid treated bark andPalmitic acid treated bark after oil adsorption

3.2 Effect of Modification on Sorption Capacity

Tests were conducted using UTB and PTB as adsorbents to remove crude oil from artificial sea water. However, the UTB was found to show low efficiency for crude oil removal with the adsorption uptake of 1120 ± 2.00 mg/g. This low sorption capacity is probably becauseof the existence of hydroxyl groups on its surface. These groups are mainly hydrophilic; theyforce back the crude oil molecules and thuslower the oil adsorption uptake. Treated mangrove bark shows higher affinity to oil.The adsorption of oil by PTB was up to 2640.00± 2.00 mg/g. This indicates that fatty acid treatment is effective in increasing the oleophilicity of UTB. These results reveal that removal of hydroxyl groups from cellulose, hemicelluloses and lignin by esterification process could improve the sorption capacity of the bark by more than two times.

3.3 Effect of Contact Time on Sorption Capacity

The effect of contact time on the uptake of oil by UTB and PTB is shown in Fig.4. There was increase in the sorption capacity as the contact time increased from first time to 30 min This initial increase was due to the condensation of oil molecules with surface of sorbent and then reach to

equilibrium The results also show that after 30 min, no significant adsorption was taking place;indicating that the sorbents were almost saturated with oil.

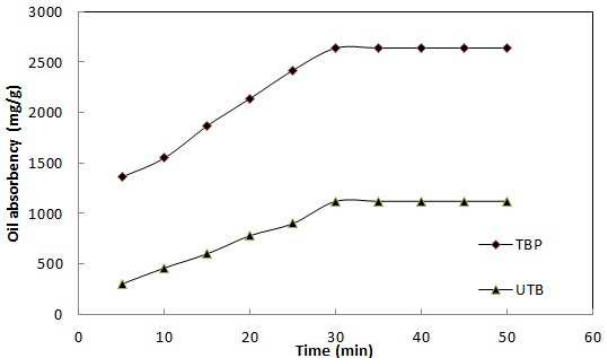


Fig. 4.Effect of sorption time on oil sorption capacity

3.4 Kinetics Study

In order to experimental data, adsorption mechanism was analyzed using the kinetic models. Pseudo-first-order and Pseudo-second-order adsorption kinetic modelswere used to determine the sorption kinetics of crude oil on raw mangrove bark and treated mangrove bark. The first-order kinetic model equation is given as[19]:

$$log(q_e - q_t) = log\ q_e - \frac{k_1\, t}{2.303} \quad (1)$$

The amounts of the oil sorbed (milligrams per gram) onto sorbent at equilibrium and at time t is q_1 and q_t, respectively. k_1 (per minute) is the rate constant of first order adsorption. Fig5 shows the plots of log (q_e−q_t) versus time.

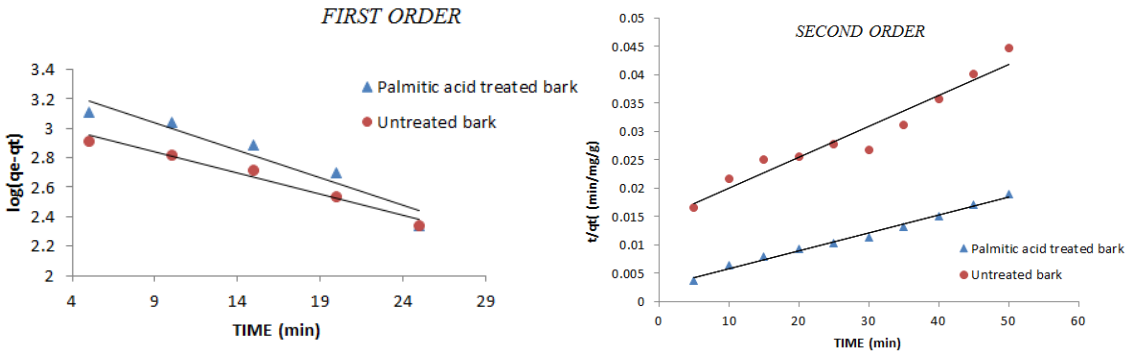


Fig. 5. Pseudo-first-order and Pseudo-second-order for crude oil sorption onto Untreated bark and palmitic acid treated bark

The pseudo-second-order kinetic equation is followed as[20]:

$$\frac{t}{q_t} = \frac{1}{k_2 q_e^2} + \frac{1}{q_e t} \quad (2)$$

Here k_2(g/mg min) is the rate constant and $q_e$and q_t(mg/g) are the amount of crude oil adsorbed on the sorbents at equilibrium and at time *t* (min). The correlation coefficients, expected q_e values, and the calculated q_e values are for the first and second-order kinetic model were for the sorbents as indicated in Table 2.The results of the pseudo first- and second-order for the adsorption of crude oil shows that the first-order kinetic model is best described based on the correlation coefficient and $q_e$value. The calculated q_e values for sorbents were close the expected $q_e$values in pseudo first-order.

Table 2: Comparison of thepseudo-first-order and pseudosecond-order kinetic model

sorbent	q_e (exp)	Pseudo-first-order kinetic model			second-order kinetic model		
		k_1	q_e	R^2	k_2	q_e	R^2
UTB	1120	0.0658	1241	0.97	$1.72*10^{-5}$	2000	0.94
PTB	2640	0.0861	2370	0.93	$3.33*10^{-5}$	3333	0.98

4. Conclusions

The present work shows oil sorption capacity of raw and treated mangrove bark. The results of this study indicate that the sorption capacity of mangrove bark can be improved by palmitic acidtreatment. The treated barks aremore hydrophobic than the raw bark and have less affinity for water. Contact time was a factor to control the sorption capacity. The optimum contact timewas 30 min.The sorption of crude oil by sorbents fits best in the pseudo first-order kinetic models.The correlation coefficients, R^2, and expected $q_e$are acceptable for the application of the pseudo-first-order model.The study shows the potential of a waste material vizmangrove bark to be used as sorbent for oil spillage cleanup

Acknowledgements

The authors would like to thank Universiti Teknologi PETRONAS for providing facilities and funding through the University Internal Research Funding (URIFGrant No: 0153AA-B18) and Ministry of Higher Education(FRGS Grant No: 0153AB-I09) for the financial support.

References

[1.] M. Hussein, A. Amer, and I. I. Sawsan, Oil spill sorption using carbonized pith bagasse. Application of carbonized pith bagasse as loose fiber. Global Nest Journal, 2009. 11(4): p. 440-448.

[2.] R. Z. Hoff, Bioremediation: an overview of its development and use for oil spill cleanup. Marine pollution bulletin, 1993. 26(9): p. 476-481.

[3.] M. A. Zahed, et al., Optimal conditions for bioremediation of oily seawater. Bioresource technology, 2010. 101(24): p. 9455-9460.

[4.] M. Abdullah, A. U. Rahmah, and Z. Man, Physicochemical and sorption characteristics of Malaysian Ceiba pentandra (L.) Gaertn. as a natural oil sorbent. Journal of hazardous materials, 2010. 177(1-3): p. 683-691.

[5.] D. Angelova, et al., Kinetics of oil and oil products adsorption by carbonized rice husks. Chemical Engineering Journal 172, 2011: p. 306-311.

[6.] R. Asadpour, et al., Application of Sorbent materials in Oil Spill management: A review. Caspian Journal of Applied Sciences Research, 2013. 2(2): p. 46-57.

[7.] T. T. Lim and X. Huang, Evaluation of hydrophobicity/oleophilicity of kapok and its performance in oily water filtration: Comparison of raw and solvent-treated fibers. Industrial Crops and Products, 2007. 26(2): p. 125-134.

[8.] X.-F. Sun, R. Sun, and J.-X. Sun, Acetylation of rice straw with or without catalysts and its characterization as a natural sorbent in oil spill cleanup. Journal of agricultural and food chemistry, 2002. 50(22): p. 6428-6433.

[9.] S. Ibrahim, H.-M. Ang, and S. Wang, Removal of emulsified food and mineral oils from wastewater using surfactant modified barley straw. Bioresource technology, 2009. 100(23): p. 5744-5749.

[10.] S. S. Banerjee, M. V. Joshi, and R. V. Jayaram, Treatment of oil spill by sorption technique using fatty acid grafted sawdust. Chemosphere, 2006. 64(6): p. 1026-1031.

[11.] K. Sathasivam and M. R. H. M. Haris, Adsorption kinetics and capacity of fatty acid-modified banana trunk fibers for oil in water. Water, Air, & Soil Pollution, 2010. 213(1-4): p. 413-423.

[12.] D. SIDIRAS and I. KONSTANTINOU, A New Oil Spill Adsorbent from Sulfuric Acid Modified Wheat Straw.
[13.] M. Teli and S. P. Valia, Acetylation of Jute fiber to improve oil absorbency. Fibers and Polymers, 2013. 14(6): p. 915-919.
[14.] X. Sun, R. Sun, and J. Sun, Acetylation of sugarcane bagasse using NBS as a catalyst under mild reaction conditions for the production of oil sorption-active materials. Bioresource technology, 2004. 95(3): p. 343-350.
[15.] J. Wang, Y. Z. , and A. W. , Investigation of acetylated kapok fibers on the sorption of oil in water. Journal of environmental sciences, 2013. 25(2): p. 246–253.
[16.] H. Yang, et al., Characteristics of hemicellulose, cellulose and lignin pyrolysis. Fuel, 2007. 86(12): p. 1781-1788.
[17.] M. Haussard, et al., Use of treated bark for the removal of lipids from water. Journal of the Air & Waste Management Association, 2002. 52(1): p. 76-83.
[18.] P. Lodha and A. N. Netravali, Characterization of stearic acid modified soy protein isolate resin and ramie fiber reinforced 'green'composites. Composites Science and Technology, 2005. 65(7): p. 1211-1225.
[19.] B. Hameed, D. Mahmoud, and A. Ahmad, Sorption equilibrium and kinetics of basic dye from aqueous solution using banana stalk waste. Journal of Hazardous Materials, 2008. 158(2): p. 499-506.
[20.] Y. Ho and G. McKay, A kinetic study of dye sorption by biosorbent waste product pith. Resources, conservation and recycling, 1999. 25(3): p. 171-193.

Applied Mechanics and Materials Vol. 567 (2014) pp 80-85
© (2014) Trans Tech Publications, Switzerland
doi:10.4028/www.scientific.net/AMM.567.80

Kinetic Study of PAHs Degradation in Produced Water using Ti/RuO_2 Anode

Asim Yaqub[1, a], MohamedHasnain Isa[1,b], SRM Kutty[1,c] and Huma Ajab[2,d]

[1] Civil Engineering Department, UniversitiTeknologi PETRONAS, Bandar Seri Iskandar 31750 Tronoh, Perak, Malaysia.

[2] Chemical Engineering Department, UniversitiTeknologi PETRONAS, Bandar Seri Iskandar 31750 Tronoh, Perak, Malaysia.

[a]environment_green@yahoo.com, [b]hasnain_isa@yahoo.co.uk, [c]shamsulrahman@petronas.com.my,[d]humaajab@hotmail.com

Keywords: Produce water, PAHs, Electrochemical, Degradation and Kinetics.

Abstract. Oil production offshore and onshore results in production of huge amount of water, called produced water (PW). PW is one of source of polycyclic aromatic hydrocarbons PAHs to the aquatic environment. Degradation kinetics of 16 priority PAHs were studied in PW treatment using Ti/RuO_2 anode in a batch setupat three different current densities 3.33, 6.67 and 10 mA/cm^2. GC-MS was used for quantification of each PAH. Kinetics study confirmed that electrochemical degradation of all PAHs had follow first-order kinetic using Ti/ RuO_2. Results showed that values of rate constant *k* were increase by increasing current density.

Introduction

Produced water (PW) has characterized by presence of toxic organics (phenols, aromatics and polycyclic aromatic hydrocarbons), inorganic (sulfides) and heavy metals (lead, chromium, cadmium, etc) which need to be removed before discharge. Among these, polycyclic aromatic hydrocarbons (PAHs) are quite stable and they are most likelyimportant analytesbecause many of these compounds are potential or proven carcinogens [1].The watewater containing refractory organic pollutants haschallenged the conventional biological treatment.

In advanced oxidation processes,electrochemical oxidation have drawn considerable attention in industrial wastewater treatment research because of its compatiblity, small space requirement, and effectiveoxidation ability [2-4]. Electrochemical processrecommendsvarious oxidation pathways like direct electrolysis, electrochemical oxygen transfer reaction and indirect mediated oxidation processes through formation of oxidants [5, 6]. The electrode material plays vital role durring electrochemical oxidation of organics to CO_2 and H_2O [7]. In recent years, transition metals oxides such as IrO_2 [8], RuO_2 [9, 10] and Ti/Pt [11] have shown good efficiency in electrochemical oxidation of organic pollutants.RuO_2 and IrO_2 coated titanium anodes considered as active anodes due to their good catalytic activity towards oxygen evolution reactions and only permit the partial oxidation of organic compounds [12].

PAHs are oftenrefractory to the conventional biological wastewater treatment.The objective of this study was to investigate the degradation kinetics of priority PAHs inPW using Ti/RuO_2 anode.

Materials and Methods

Electrochemical reactor. Laboratory scale electrochemical batch reactor was used for electrochemical oxidation experiments for degradation of PAHs from PW. The electrochemical reactor of volume 100ml consisted of an anode (Ti/RuO_2) and a cathode (Ti plate) connected to DC power supply. Electrodes distance was 2cm remains same in all experiments. All experiments were performed under galvanostatic conditions. Dimensions of electrodes used in this study were 8cm × 10cm × 0.2 cm. Real PW samples were used for all electrochemical experiments. Ti/$RuO_2$was prepared in the lab by thermal decomposition process [13, 14].

Sampling. Produced water samples were collected from local offshore crude oil terminal. Characteristics of produced water are given in Table 1.

Table 1. Characteristics of produced water

Parameters	Values
pH	7.8
Conductivity	30,000 mS/cm
Turbidity	72 NTU
TDS	16105 mg/l
TSS	250 mg/l
BOD	590mg/l
COD	1347mg/l
TOC	1022mg/l
Phenol	13.8mg/l
NH3-N	8.5mg/l
Chlorides	> 10,000mg/l
Sulfates	156mg/l

Analytical techniques.PAHs were extracted by Liquid-Liquid Extraction GC-MS Method [15]. Dichloromethane DCM was used as solvent for the extraction of PAHs from water samples. GC-MS was used for the detection of each PAH. Each PAH was separately quantified using a five-point calibration of mixed standard solutions.

Results and Discussion

Following first order kinetic model was atempted to determine the rate constant *k* for the experimental kinetic data of each PAHs degradation (Eq. 1).

$$\frac{d[\mathrm{PAH}]_t}{dt} = -k\,[\mathrm{PAH}]_o \qquad \text{Equation 1.}$$

After integration, the above equation becomes (Eq. 2):

$$\ln\left(\frac{[\mathrm{PAH}]_t}{[\mathrm{PAH}]_o}\right) = -kt \qquad \text{Equation 2.}$$

where *k* is the rate constant, and $[\mathrm{PAHs}]_o$ (generally, C_o) correspond to the initial concentration of each PAH and $[\mathrm{PAHs}]_t$ (generally, C) correspond to concentration of each PAH after a period of time *t*.

Fig. 1 and Fig. 2, a plot of $\ln(C/C_0)$ versus time shows linear relationship in 4 h of electrolysis time confirming that the oxidation of each PAHs using Ti/RuO_2 displays first-order kinetic behavior. The apparent kinetic rate constants *k* were determined from the magnitude of the slopes of the straight lines for each current density shown in Table 2. Rate constant was positively affected by increase in current density in all experimental. The rate constant *k* values were increase with current density. Acenaphthene shows higher rate constant of 0.0357 min^{-1}among all the PAHs. In one study shows second order reaction kinetics for naphthalene using Ti/Pt_{90}-Ir_{10} anode in presence of Na_2SO_4 while fluoranthene and pyrene showed the common first order behavior [16]. PAHs with 3 bezene rings werehigher *k* values,probably due to its higher solubility compared to 4-6 benzene rings PAHs and thus higher affinity toparticipate in the indirect homogenous chemical oxidation reaction. Ti/RuO_2 falls in active anodes type, in literature the active anodes are typically denoted low oxidation power anode towards organic compounds. The presence of chloride ions was proposed to inhibit the oxygen evolution reaction causing an increase in anode potential and, therefore, a higher reactivity of adsorbed oxidised chloride species[16]. Contribution of chloride ions and $OH^{\bullet}$ radical's is imperative for total removal of PAHs. The presence of chloride ions in PW significantly enhanced the PAHoxidation rates due to indirect oxidation pathways. PAHs were effectively

degrade by indirect oxidation pathways due to electro-generated hypochlorite radicalsandhypochlorous acid.

Table 2. Valuse of rate constant *k* at different current densities and electrolysis time.

PAHs	Initial concen. (µg/l)	Current Density (mA/cm^2) 3.33	6.67	10
Naphthalene	58.06	0.0036	0.0046	0.0067
Acenaphthylene	13.66	0.0127	0.0202	0.0331
Acenaphthene	6.42	0.0142	0.0225	0.0357
Fluorene	14.43	0.0116	0.0149	0.0200
Phenanthrene	2.29	0.0226	-	-
Anthracene	15.44	0.0093	0.0144	0.0193
Fluoranthene	12.77	0.0087	0.0171	0.0202
Pyrene	12.44	0.0079	0.0172	0.0188
Benz(a)anthracene	6.87	0.0139	0.0231	0.0224
Chrysene	2.82	0.0091	0.0171	0.0212
Benzo(b)fluoranthene	4.59	0.0115	0.0177	0.0212
Benzo(k)fluoranthene	2.24	0.0091	0.0179	0.0225
Benzo(a)pyrene	3.61	0.0087	0.0173	0.0288
Indeno(1,2,3-cd) pyrene	2.28	0.0130	0.0173	0.0245
Dibenz (a,h) anthracene	1.75	0.0159	0.0189	0.0238
Benzo (g,h,i) perylene	1.19	0.0108	0.0121	0.0144

Following reaction scheme was proposed for chlorine evolution and indirect oxidation of organic compounds.

$$Ti/RuO_2 + Cl^- \rightarrow Ti/RuO_2—Cl^- + e- \quad (1)$$

$$Cl^- + Ti/RuO_2—Cl^- \rightarrow Ti/RuO_2 + Cl_2 + e- \quad (2)$$

$$Ti/RuO_2–2Cl^- \rightarrow Ti/RuO_2 + Cl_2^{\uparrow} + 2e- \quad (3)$$

$$Cl_2 + 2OH^{\bullet} \rightarrow Cl^- + OCl^- + H_2O \quad (4)$$

$$Cl_2 + H_2O \rightarrow HOCl + H^+ + Cl^- \quad (5)$$

$$HOCl \rightarrow H^+ + OCl^- \quad (6)$$

Conclusion

Ti/RuO_2 anode showed sound electrocatalytic performance during electrochemical degradation of PAHs in produced water. Experimental results showed first-order kinetic for electrochemical degradation of all PAHs had follow using Ti/ RuO_2 and rate constant *k* increased by increasing current density.

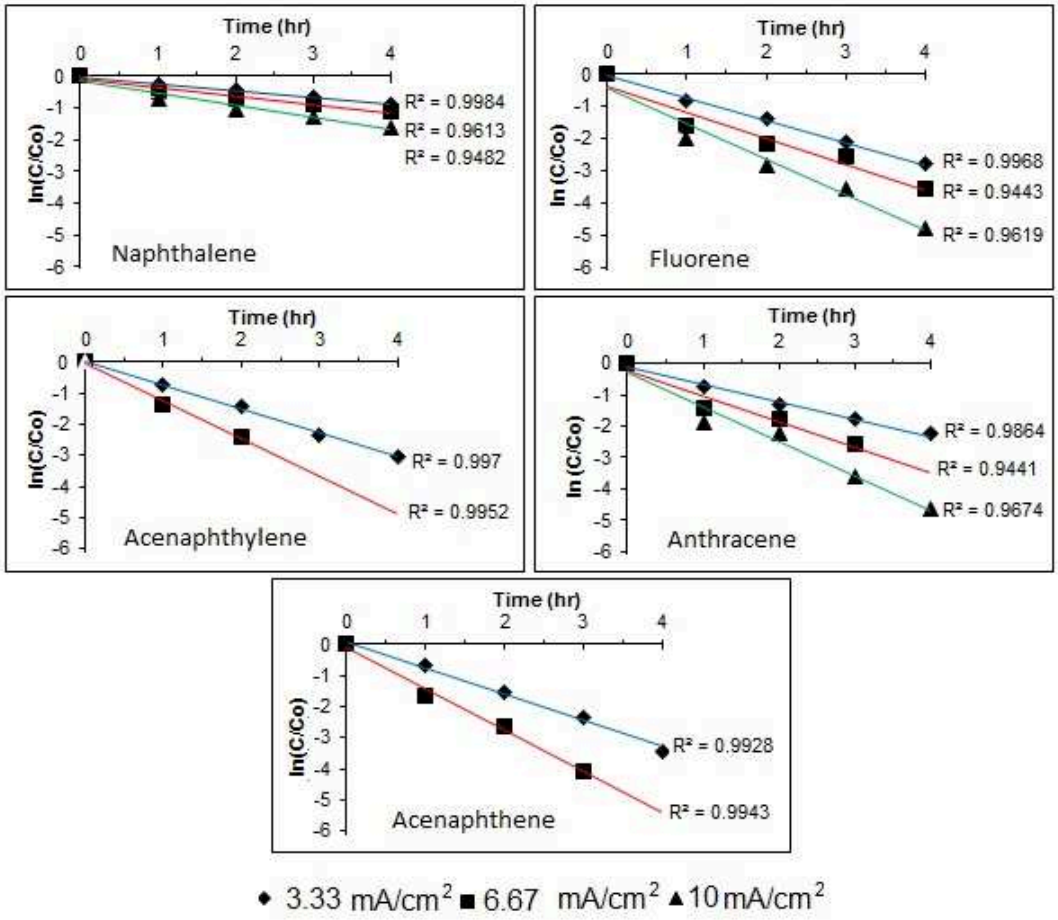


Figure 1. Plots of $\ln(C/C_o)$ vs. time for the degaradation of PAHs having bezene rings (2 and 3) at 3.33, 6.67 and 10 mA/cm^2.

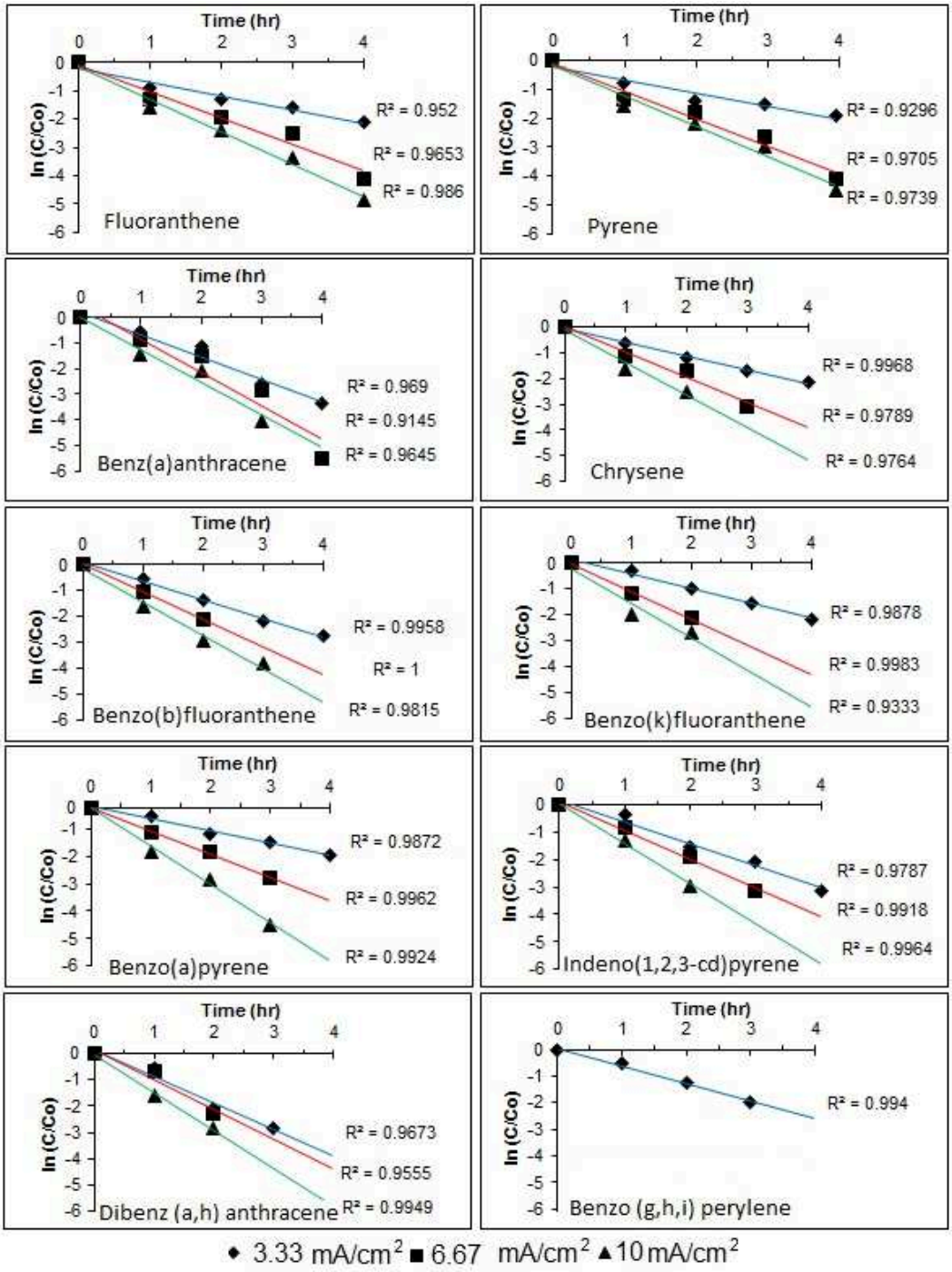


Figure 2: Plots of $\ln(C/C_o)$ vs. time for the degaradation of PAHs having bezene rings (4, 5 and 6) at 3.33, 6.67 and 10 mA/cm^2.

References

[1] A. Pavlova, R. Ivanova, Determination of petroleum hydrocarbons and polycyclic aromatic hydrocarbons in sludge from wastewater treatment basins, J. Environ. Monit. 5 (2003) 319–323.

[2] Y. H. Cui, X. Y. Li, G. Chen, Electrochemical degradation of bisphenol A on different anodes, Water Res. 43 (7) (2009) 1968–1976.

[3] C. A. Martinez-Huitle, A. De Battisti, S. Ferro, S. Reyna, M. Cerro-Lopez, and M. A. Quiro, "Removal of the pesticide methamidophos from aqueous solutions by electrooxidation using Pb/PbO_2, Ti/SnO_2, and Si/BDD electrodes, Environ. Sci. Tech. 42 (18) (2008) 6929–6935.

[4] A. Yaqub, H. Ajab, M.H. Isa, H. Jusoh, M. Junaid, R. Farooq,Effect of ultrasound and electrode material on electrochemical treatment of industrial wastewater.J New Mater. Electrochem. Systems, 15, 289 (2012).
[5] C. A. Martinez-Huitle, S. Ferro, Electrochemical oxidation of organic pollutants for the wastewater treatment: direct and indirect processes. Chem. Soc. Rev.35(12) (2006)1324-1340.
[6] A.Yaqub, H. Ajab, Applications of sonoelectrochemistry in wastewater treatment system. Rev. Chem. Eng.29(2) (2013) 123-130.
[7] F. Montilla, E. Morallon, J. L. Vazquez, Evaluation of the electrocatalytic activity of antimony-doped tin dioxide anodes toward the oxidation of phenol in aqueous solutions, J.Electrochem.Soc. 152 (10) (2005) B421–B427.
[8] R. Tolba, M. Tian, J. Wen, Z.-H. Jiang, A. Chen, Electrochemical oxidation of lignin at IrO_2-based oxide electrodes, J. Electroanal. Chem. (2010),
[9] J. Gaudet, A.C. Tavares, S. Trasatti, D. Guay, Physicochemical characterization of mixed RuO_2–SnO_2 solid solutions, Chem. Mater. 17 (2005) 1570–1579.
[10] R.F.Yunus, Yu-Ming Zheng, K.G.N. Nanayakkara, J.P. Chen, Electrochemical Removal of Rhodamine 6G by Using RuO_2 Coated Ti DSA. Ind. Eng. Chem. Res.48 (2009), 7466–7473.
[11] M. Panizza, C. Bocca and G. Cerisola, Electrochemical Treatment of Wastewater Containing Polyaromatic Organic Pollutants, Water Res. 34 (9) (2000) 2601-2605.
[12] M. Panizza. Chapter. Importance of Electrode Material in the Electrochemical Treatment of Wastewater Containing Organic Pollutants. In (Editor Ch. Comninellis, G. Chen), Electrochemistry for the Environment.Springer Science. 2010.
[13] A.Yaqub, M. H. Isa, S. R. M. Kutty, H.Ajab. Surface Characteristics of Ti/IrO_2 Anode Material and its Electrocatalytic Properties for Polycyclic Aromatic Hydrocarbons (PAHs) Degradation in Aqueous Solution. J. New Mater. Electrochem. Sys. (2014) (In press).
[14] A.Yaqub, M. H. Isa, S. R. M. Kutty."Electrochemical Oxidation of PAHs in Aqueous Solution." in Developments in Sustainable Chemical and Bioprocess Technology, pp. 89-96. Springer US, (2013).
[15] Y.AlSalka, F.Karabet, M. S. Hashem, Removal Efficiency of Polycyclic Aromatic Hydrocarbons from Synthetic Water Samples by Electrocoagulation Processes. Damascus Uni. J. for BASIC SCIENCES.27 (2011) 65-80.
[16] J.Muff, E. G. Søgaard.Electrochemical degradation of PAH compounds in process water: a kinetic study on model solutions and a proof of concept study on runoff water from harbour sediment purification. Water Sci. Technol., 61(8)(2010).

Applied Mechanics and Materials Vol. 567 (2014) pp 86-91
© (2014) Trans Tech Publications, Switzerland
doi:10.4028/www.scientific.net/AMM.567.86

Langat River Basin Hydrologic Model Using Integrated GIS and ArcSWAT interface.

Mohd Fozi Ali[1, a], Nor Faiza Abd Rahman[1,b] , Khairi Khalid[1,c] and Nguyen Duy Liem[2,d]

[1] Faculty of Civil Engineering

Universiti Teknologi MARA,Malaysia

[2] Department of Applied Geomatics

Nong Lam University- Ho Chi Minh City

Vietnam

[a] mohdfozi@salam.uitm.edu.my, [b] norfaiza128@gmail.com, [c] khairikh@pahang.uitm.edu.my, [d]nguyenduyliem@hcmuaf.edu.vn

Keywords: ArcSWAT;Langat River; Stream flow and Hydrologic Modeling.

Abstract. Increase of socio-economic activities in the urban area has led to many water scarcity problems. Thus, the need to investigate the current state of Langat river is increasing. An integrative computational model, ArcSWAT with GIS interface was being used to predict daily stream flow of the study area. Historical data from years 1999 to 2010 was used for modeling purposes. The results reviewed that the calibrated model is able to simulate the flow for the river basin successfully with the R2 = 0.64 and Nash-Sutcliffe Index, NSI= 0.64. The results proved that GIS technology and ArcSWAT model is capable for simulating the stream flow in the Langat river basin and can be applied for other river basins. This shows that SWAT can be a tool for a hydrologic modeling in Malaysia in the future.

Introduction

Malaysia consists of 150 rivers in Peninsular Malaysia and another 50 rivers in Sabah and Sarawak. However, some of the rivers are receiving the impact of rapid growth through land development, urbanization and industrialization. Serious environmental problems have slowly crept into many river basins of Malaysia with the attendant problems such as flooding, water pollution, and sedimentation [1]. It is critically vital to develop the knowledge and skills that are necessary to safeguard our catchments and river basins without altering the socioeconomic development, in order to manage the water resources available in a sustainable way [2].

High annual rainfall does not solve water scarcity problem and may contribute to storm water runoff in the river. Conducting field experiments and collection of long term data can be very expensive. This is where the utilization of water quality modeling becomes crucial. Modeling approaches are well known in helping relevant authorities, researchers, engineers and policy makers in Malaysia to predict the future impacts of the urban development to the river water quality in the specific basin.

Considering all the above issues, this study utilizes the integrated hydrology model, Soil and Water Assessment Tool (SWAT) to investigate the rainfall relationship to stream flow particularly within Langat catchment. The goals of the study are (1) to establish the hydrologic database for Langat's river (2) to predict stream flow using ArcSWAT , and (3) to evaluate the effectiveness of a GIS interface physically based hydrologic model in predicting daily stream flow from study catchment.

Materials and method

Study Area. The Langat river basin has a total catchment area of approximately of 1,815km2. The length of the main river is 141 km and mostly situated 40 km east of Kuala Lumpur. The catchment is drained by three major tributaries; Langat River, Semenyih River and Labu

River[3]. However, the research undertaken the upper part of the Langat catchment. The main tributary, Langat River flows about 182 km from the main range (Banjaran Titiwangsa) at the Northeast of Hulu Langat District in south-southwest direction, and draining into the Straits of Malacca. The main reach of Semenyih River is flowing south-southwest direction through the town of Semenyih, Bangi Lama and finally merges with Langat River at about 4 km to the east of Bangi Lama town. There are two reservoirs in the study area including Langat dam and Semenyih dam. Currently about eight water treatment plants are operating in the Langat basin [4].

Input Data and Model Setup. Data sets of 12 years were used for this study. For model set up, data from 1999 to 2002 were used for model warm up. Data from 2003 to 2004 were used for model calibration and data from 2005 to 2006 were used for model validation. Those are the period which naturalized flow data are available. Data of meteorological and hydrological such as rainfall, humidity, wind and solar gained from the Department of Irrigation and Drainage Malaysia (DID) and Malaysian Meteorological Department which are the stations are scattered in the upper part of the catchment area. The Federal Department of Town and Country Planning supplied Land use map for Peninsular Malaysia and the population data were obtained from local authorities. Catchment map and survey map were attained from Department of Survey and mapping Malaysia (JUPEM).

Building the model. The project model was developed in GIS interface with input from Digital elevation model (DEM) map with 30 m x 30 m resolution. Once the model was able to generate the DEM, the process of delineating the watershed was carried out. Input of monitoring points precipitation gage, temperature, humidity gage, solar and wind gage and outlet were added inside the GIS window by giving the coordinates of the gages in terms of X and Y. River path is drawn in SWAT by adding to the main river shape file in the Element window. The direction of the flowing river is built from the headwaters (upper stream) of the main river. The whole process is continued by building the entire network of the Upper Langat Catchment. The watershed delineation of the Langat Catchment is shown in Figure 1.

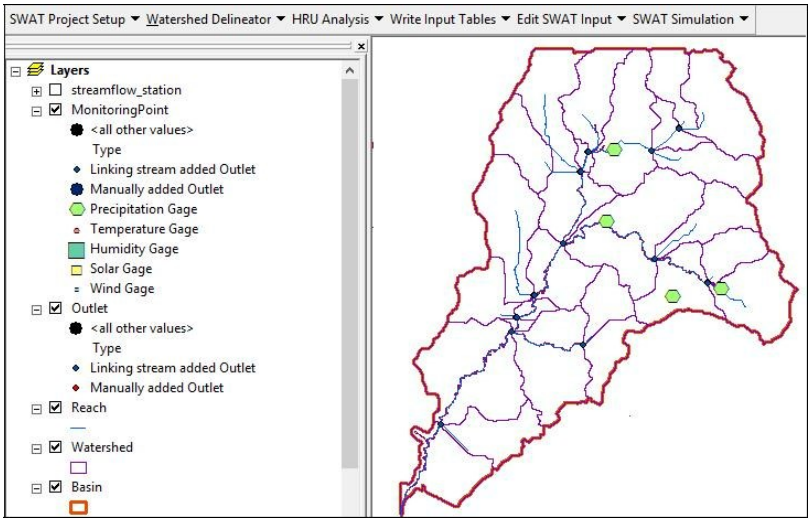


Fig. 1. Watershed Delineation of the Langat Catchment.

The SWAT model approach, flowchart of hydrologic modeling in Langat River applied to the case study area of the Langat river basin is shown in Figure 2. The steps are including watershed delineation and map overlay.

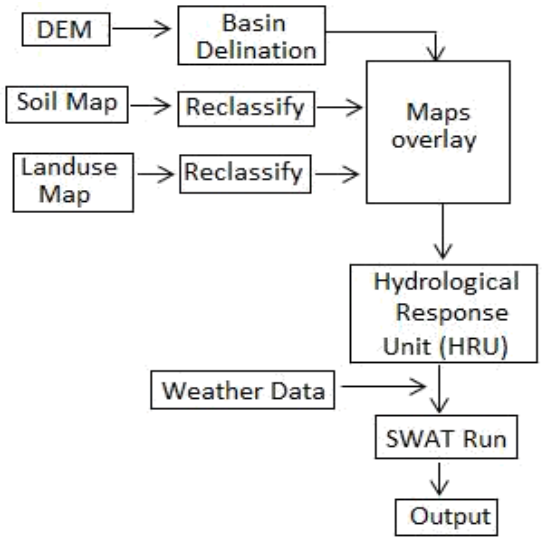


Fig. 2. Flowchart of hydrologic modeling in Langat River

Model Calibration and Validation. Hydrological processes occurring in the catchment were modelled, on a monthly time-step. It is known that gist of an accurate hydrological modelling is stream flow, it was calibrated based on 2001 to 2003 weather data. Simulated monthly flows were compared with observed monthly stream flow from the Department of Irrigation, Selangor. Model calibration was carried out on adjusting relevant parameters which control the peak flow and base flow and also lag time for surface flow. Table 1 shows the adjusted parameters in the calibration process and its values. In validation process, different data set of weather was used from year 2004 to 2006 and using the same parameters for the calibration process.

Table 1. Adjusted parameters in calibration process

No.	Function	Parameter	Calibrated value
1	Initial SCS runoff curve number	CN2	0.0575
2	Subsurface water response	ALPHA_BF	0.235
3	Subsurface water response	GW_DELAY	53.0
4	Threshold depth of water	GWQMN	2.0
5	Subsurface water response	RCHRG_DP	1.0

SWAT Overview. The Soil and Water Assessment Tool (SWAT) model was developed by the US Department of Agriculture – Agriculture Research Service (USDA-ARS). It is a conceptual model that functions on a continuous time step. Model components include weather, hydrology, erosion/sedimentation, plant growth, nutrients, pesticides, agricultural management, channel routing, and pond/reservoir routing. SWAT is a theoretical model that operates on a daily time step. In order to adequately simulate hydrologic processes in a basin, the basin is divided into subbasins through which streams are routed. The subunits of the subbasins are referred to as hydrologic response units (HRU's) which are the unique combination of soil and land use characteristics and are considered to be hydrologically homogeneous. The model calculation was performed on HRU basis and flow and water quality variables are routed from HRU to subbasin and subsequently to the watershed outlet [5,6].

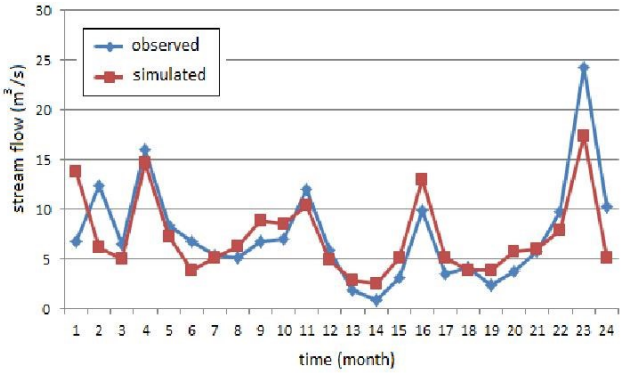
Results and Discussion

Model calibration is the initial testing of a model and tuning it to reflect a set of field data. For this project, calibration results were considered moderately strong. The simulated stream flow was significantly fit with the observed flow data pattern. The model was run for 100 times simulation with 5 adjusted parameters and the result of coefficient of determination is $R^2 = 0.63$ and the Nash-Sutcliffe Index, NSI = 0.64. Validation is concerned with building the right model. It is utilized to determine that a model is an accurate representation of the real system. Validation is usually achieved through the calibration of the model, an iterative process of comparing the model to actual system behavior and using the discrepancies between the two, and the insights gained, to improve the model. This process is repeated until model accuracy is judged acceptable. Table 2 shows the model performance evaluation on calibration and validation values.

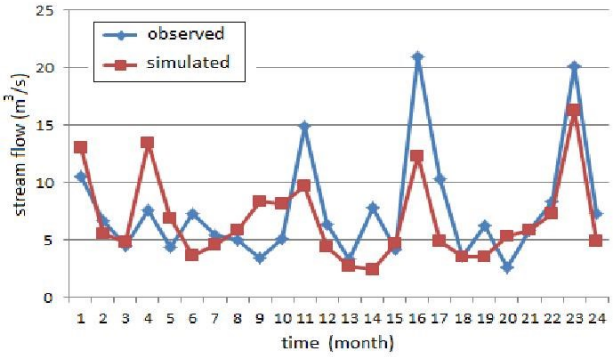
Table 2. Calibration and validation value

Model Performance Evaluation for Stream Flow [m^3/sec]	Calibration	Validation
coefficient of determination (R^2)	0.64	0.64
Nash–Sutcliffe Index (NSI)	0.48	0.45

Based on the results, calibration and validation were generally acceptable. The flow were considerably fit with the observed data as shown in Figure 3(a) and Figure 3(b). In this study, the calibration results are higher compared to the validation results but still both were acceptable. The trends of observed and simulated values were promising.



(a)



(b)

Fig. 3(a). Simulated and observed flow for calibration period Simulated and
Fig. 3(b). observed flow for validation period

After identification of sensitive parameters in calibration, the model was used to predict simulation of stream flow on 2010. Figure 4 shows the cumulative predicted and observed values for simulation Year 2010 to see the trends of prediction. The results of the stream flow simulation after model calibration and validation for the year 2010 was slightly different. The observed stream flow values seem higher compared to the simulated values. This may due to additional reservoir and dam nearby Langat basin area that were installed after the year 2006 (validation period). To increase the accuracy of the result, data on dam and subbasin shall be included in the model in future simulation. Thus, simulation will be carried out again after input on reservoirs and dams nearby Langat River basin.

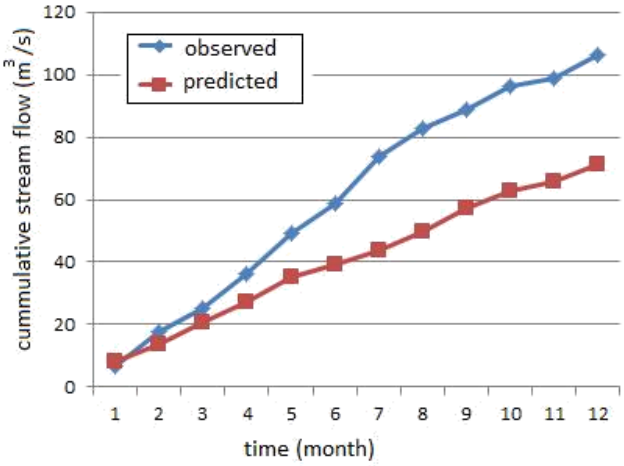


Fig. 4. Cumulative predicted and observed flow for the year 2010

Conclusion

In this research, stream flow of the upper part of Langat Catchment was modeled by the version of Soil and Water Assessment Tool (SWAT), ArcSWAT2009.93.b embedded in ArcGis 10. Based on this research, ArcSWAT2009 model was found prominent as ArcGis interface physically based model. The model can be used for long term and short-term simulation and application in different areas of study. The capability of the model in predicting the stream flow using different data sets was proven.

From this study, the results obtained in calibration and validation is generally acceptable which R^2 values range from 0.48 to 0.64 for flow parameters. This model was able to simulate the predicted stream flow for the year 2010 successfully but needed further adjustment on input data to increase its accuracy. Thus, in all conscience the ARCSWAT2009 is capable as one of the reliable tools for hydrologic modeling. A further direction of this study is to re-calibrate and re-validate the model by testing different parameters for hydrologic model, which can predict accurately changes of water quality in the basin.

Acknowledgment

This project was funded by Ministry of Higher Education under the Fundamental Research Grant Scheme (FRGS) 600-RMI/FRGS/ 5/3 (78/2013) and Research Management Institute (RMI) of Universiti Teknologi MARA (UiTM), Malaysia.

References

[1] K.R. Ayub, L.S. Hin, & Hamidi Abd Aziz, “SWAT application for hydrologic and water quality modeling for suspended sediments:A case study of Sungai Langat’s Catchment in Selangor”, International Conference on Water Resource, May 2009.

[2] A.G. Bobba, T.D. Prowse, J.Y. Diiwu and D. Milburn. “Sensitivity of hydrological variables in the arctic watershed, Coppermine River, NWT, Canada due to hypothetical climate change,” in Journal of Environmental Hydrology, vol.13,22,2005.

[3] M. F. Ali., M.H. Ahmad, K. Khalid & N.F. Abd Rahman, “Water quality measures using QUAL2E; A study on RoL project at Upper Klang River”, International Civil and Infrastructure Engineering Conference 2014, Kuching 22-24 Sept, 2013.

[4] M. F. Ali., A. Saadon, N.F Abd Rahman and K. Khalid, "An Assessment of Water Demand in Malaysia Using Water Evaluation and Planning (WEAP) System", International Civil and Infrastructure Engineering Conference 2014, Kuching 22-24 Sept, 2013.

[5] Susan L. Neitsch et al., 2009. Overview of Soil and Water Assessment Tool (SWAT) Model. In: Soil and Water Assessment Tool (SWAT): Global Applications. Special Publication No. 4.,3-23. Arnold, J et al.: Funny Publishing.

[6] N.D. Liem & N.K.Loi, "Assessing water discharge in BE river, Vietnam using SWAT model", International Symposium on Geoinformatics for Spatial Infrastructure Development in Earth and Allied Sciences,pp. 230-235,2012

Applied Mechanics and Materials Vol. 567 (2014) pp 92-97
© (2014) Trans Tech Publications, Switzerland
doi:10.4028/www.scientific.net/AMM.567.92

Modeling of Contaminant Transport and Groundwater Flow of Tamangapa Landfill in Makassar Indonesia

Hajrah[1], Ardy Arsyad[1], Achmad Zubair[1]

[1]Department of Civil Engineering, Faculty of Engineering, Hasanuddin University, Makassar Indonesia

hajrah_bulan@yahoo.com

Keywords: Landfill, modflow, groundwater, leachate, contaminant.

Abstract. This paper aims to analyze the groundwater flow direction of Tamangapa landfill and to predict the contaminant in the groundwater over the period of 20 years, accounted for the year of 2000 until 2020. To understand the natural condition of the landfill, geological and hydrogeological survey were undertaken, consisting of geological survey, geomorphology and geo-resistivity surveys. Hydrogeological survey comprises groundwater level measurement, chemical analysis of leachate and groundwater samples which were later used as input data for numerical model. Based on the result of groundwater flow models, the direction of groundwater is found to be flowing from the north to the south. The minimum concentration for manganese (Mn) is 1.519 mg/l and 2.701 mg/l for iron (Fe). Over the period of 2020, Fe concentration increases significantly, reaching the level of 56.427 mg/l, Mn concentration for 299.5594 mg/l. It can be suggested that the groundwater quality of Tamangapa landfill has already exceeded the standard for water quality, leading to potential severe impact to local people around the landfill.

Introduction

Tamangapa landfill is the only one landfill in Makassar, the capital of Province of South Sulawesi Indonesia. The landfill is assigned to cover all garbage in the city, containing organic and inorganic waste from markets, households, and offices. The waste, in particular for organic waste, disposed on the landfill will be decomposed, resulting in leachate which contains chemicals, both organic and inorganic, some of pathogenic bacteria parasites, so it is dangerous to human health (Health Ministry, 2002). As rainwater passes through a pile of garbage, leachate will seep into the soil and contaminate the groundwater.



Figure1. Aerial View of Tamangapa Landfill.

The Interesting phenomenon in this study is the vulnerability of groundwater quality problems in Tamangapa landfill as a result of leachate contamination in the groundwater. The purpose of this study is to analyze the flow of groundwater in Tamangapa landfill area and modeling the contaminant transport and its influence on the groundwater system.

Study Area

Study area is Tamangapa landfill located in the Tamangapa village, District of Manggala, 9.80 km south eastern from the downtown of Makassar, South Sulawesi Province in Indonesia. The landfill area covers 4.2 hectares and started operation in 1993 with open dumping processing system (Figure 1). The landfill stands on the ground with about 24 meters above sea level, where the highest level is located at the northeast of the area, and the lowest level is about 6 meters located at the southeast of the area (Figure 2). This study undertook the measurement of topography of the landfill including the stratigraphy of landfill subsurface by using geo-resistivity test. There are four lines of geo-resistivity tests as shown Figure 2. The test resulted in four geo-resistivity profiles, showing the stratigraphy of landfill subsurface. The indication of what kind of rock or soil layers in the subsurface can be generated by using correlation between geo-resistivity values and type of rock or soil (Telford, et al., 1990), including the hydraulic conductivity (Bouwer, 2002). The stratigraphy of the subsurface is shown in Table 1.

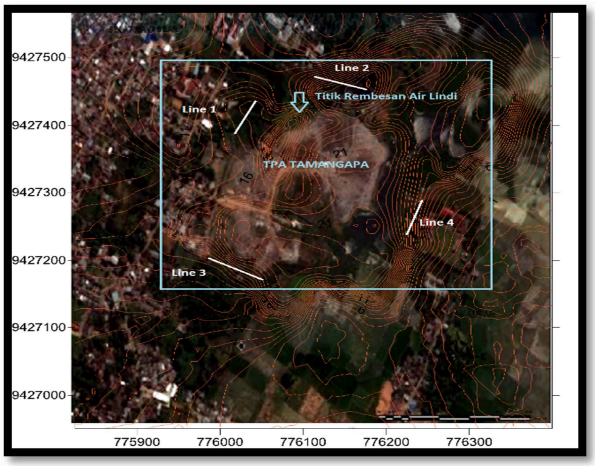


Figure 2. Topography map and geoelectric test map on the landfill.

Table 1.Stratigraphy of landfill subsurface.

Line	Resistivity (Ωm)	Layer	Depth (m)	Hydraulic conductivity (m/day)
1	0,5-300	Aquifer	2,5-14,5	10^{-8}
	1-1000	Clay sand		0,0001
2	0,5-300	Aquifer	2,5-14,5	10^{-8}
	1-1000	Clay sand		0,0001
3	0,5-300	Aquifer	7,5-12,8	10^{-8}
	1-1000	Clay sand		0,0001
4	0,5-300	Aquifer	7,5-19	10^{-8}
	1-1000	Clay sand		0,0001

Method

The data collections consist of geo-resistivity and topography survey, leachate quality, water quality, soil characteristics, and rainfall data. Analytical methods were undertaken by utilizing a numerical modeling. Geo-resistivity and topography data were processed with Res2dinv and software surfer in order to determine the groundwater level and the groundwater flow direction. The analysis of leachate concentration is Manganese (Mn) and Iron (Fe), determined by using a modern Atomic Absorption Spectrophotometer (AAS). The data was used as the input data in VISUAL MODFLOW software to obtain the model of leachate contaminant transport.

Results

In the simulation of groundwater flow steady state MODFLOW model, the groundwater level was obtained. The model as shown in Figure 3 reveals that the groundwater flows from the northern side to southern side of the landfill. The result was validated with lithology data where the depth of aquifer is 2.5 meters in the northern region, while the depth of aquifer is 7.5 meters on the southern depth areas.

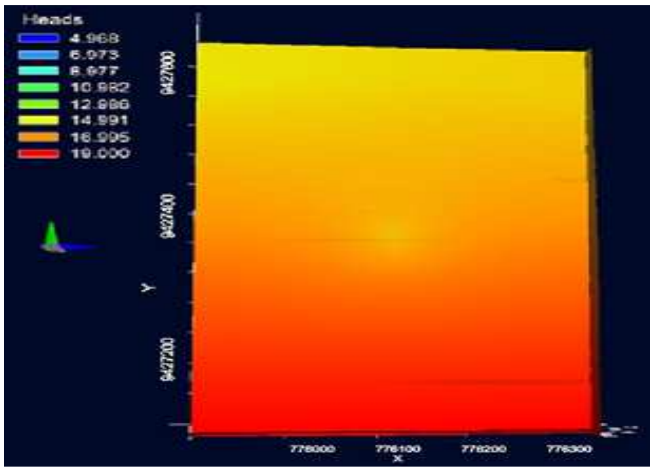


Figure.3. Elevation of Groundwater

Conditions of leachate treatment plant in the landfill is no longer function due to damage in the pipes used to drain water from the impermeable layer to the leachate treatment ponds. At this point, seepage modeling was defined as a contaminant source area. Modeling of the leachate spread focused on the leachate concentrations of inorganic chemical constituents, Manganese (Mn) and Iron (Fe). Although Manganese and Iron are an essential element required for humans, but chronic exposure in high concentrations are able to generate health problems. One of the effect irons is damage on the health of the intestinal wall and manganese can cause the neurological disorder, which can result in death.

From the simulation results using model MT3DMS leachate contamination, it can be seen that the concentration of manganese (Mn) and Iron (Fe) move from north to the south of the landfill, concomitant of the groundwater flow simulation. The migration of contaminants corresponds to the spread of groundwater flow in the landfill. The spreading pattern of Mn and Fe shows such south oval migration. Concentrations of manganese (Mn) obtained from the data quality test results is 1.519 mg/l and Iron (Fe) for 2.701 mg/l. Meanwhile, according to the quality standards of Health Minister Regulation No.492 of 2010 on Drinking Water Quality Requirements is 0.4 mg/l for Mn and 0.3 mg/l for Fe. The infiltration of leachate into groundwater can be categorized as groundwater contamination because the concentration goes far beyond a predetermined threshold. This would be very detrimental to the people living near landfill area since they still rely on groundwater for their water supply.

The model was simulated over a span of 20 years starting in 2000 until 2020. Day period used is 1 days, 730 days, 1460 days, 2190 days, 2920 days, 3650 days, 5475 days, and 7300 days. Leachate contaminant simulation results with MT3DMS models for 7300 day get the lowest concentrations of Manganese (Mn) at 1.519mg/l (Figure 4) and the highest concentration at 299.5594 mg/l (Figure 6). While the iron (Fe) lowest concentration at 2,701 mg/l (Figure 7) and the highest concentration at 356.427 mg/l (Figure 10). The modeling results obtained contaminant transport saturation point is above 2920 days caused by the nature of the study area of clay soil (Figures 5 and 9). The accumulation of modeling results is described in Table.2.

Conclussions

1. Groundwater direction moves from the north to the south.
2. The contaminant follows groundwater flow direction with minimum concentration for manganese (Mn) is 1.519 mg/l and 2.701 mg/l for iron (Fe). As a prediction in 2020, iron (Fe) concentration in aquifer is high as 356.427 mg/l and 299.5594 mg/l for the manganese (Mn).
3. It can be suggested that groundwater quality of Tamangapa area has already exceeded the water quality standard and it leading to severe impact to people living near the landfill.

Table.2. Recapitulation Time, Concentration, and wide Distribution of Contaminants Table

Contaminant	Time (Day)	Concentration (mg/l)	wide distribution (m^2)
Manganese (Mn)	1	1,519-3,276	662
	730	0,015-285,560	8468
	1460	0,0074-296,529	12216,5
	2190	0,0041-298,237	12492,5
	2920	0,0024-298,831	13725
	3650	0,0014-299,115	14001
	5475	0,0005-299,499	14136
	7300	0,0002-299,559	14201
Iron (Fe)	1	2,701-4,620	729
	730	0,027-337,846	6825
	1460	0,013-352,588	7738
	2190	0,0073-354,807	7986
	2920	0,0042-355,504	8688
	3650	0,0026-355,889	8765
	5475	0,0010-356,349	8873
	7300	0,0003-356,427	8964

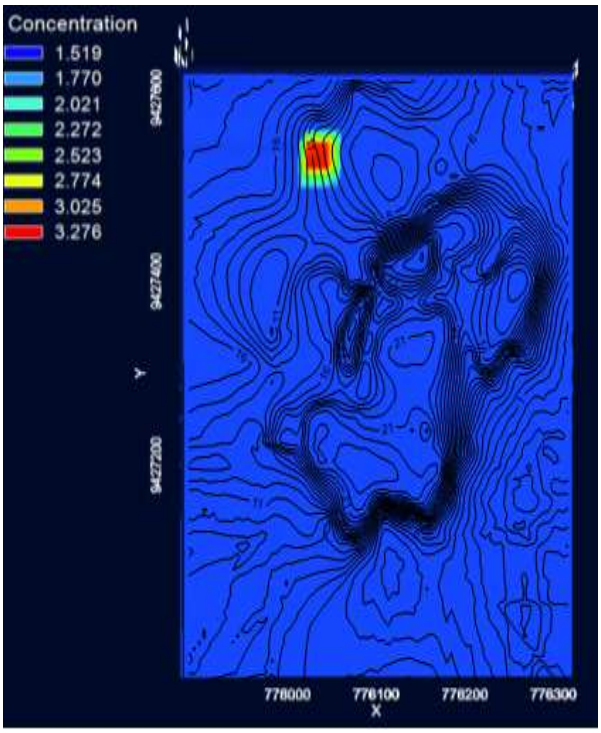


Figure.4.Modeling results for1 Day Contaminants Mn (Lowest Concentration)

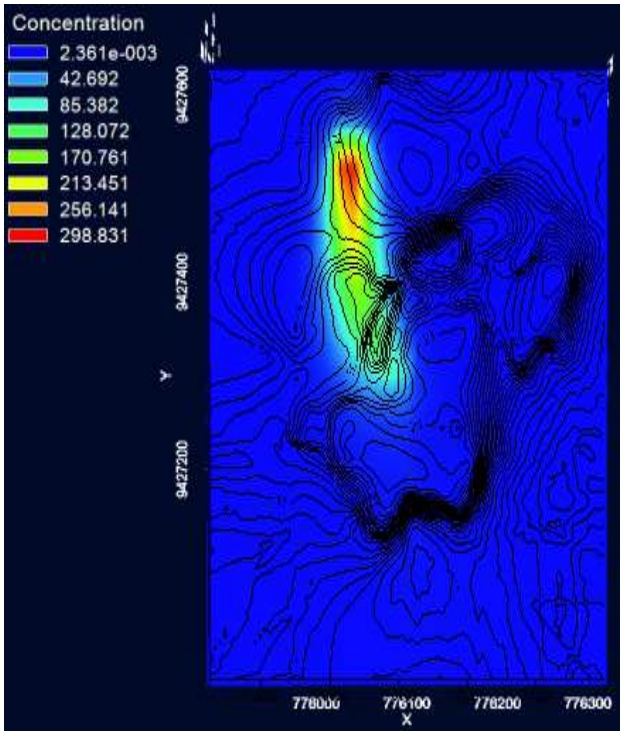


Figure.5.Modeling results for 2920 Days Contaminants Mn (Saturation Point)

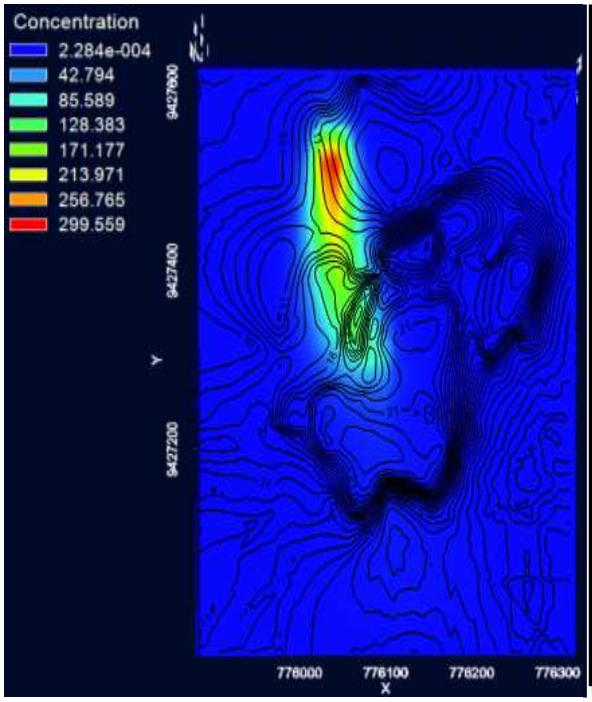


Figure.6. Modeling Results for 7300 Days Contaminants (Highest Concentration) Mn

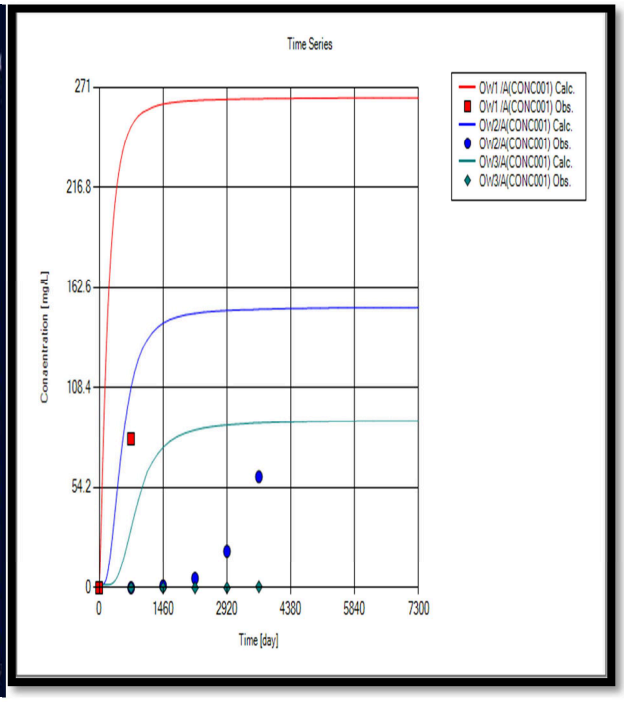


Figure.7.Relationship Charts Feconcentration against Pollution Time Period

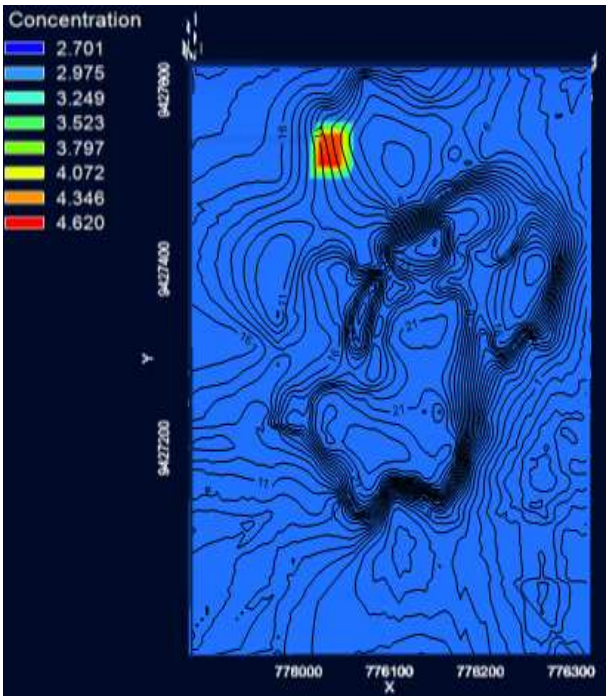


Figure.8.Modeling resultsfor1 Day Contaminants Fe (Lowest Concentration)

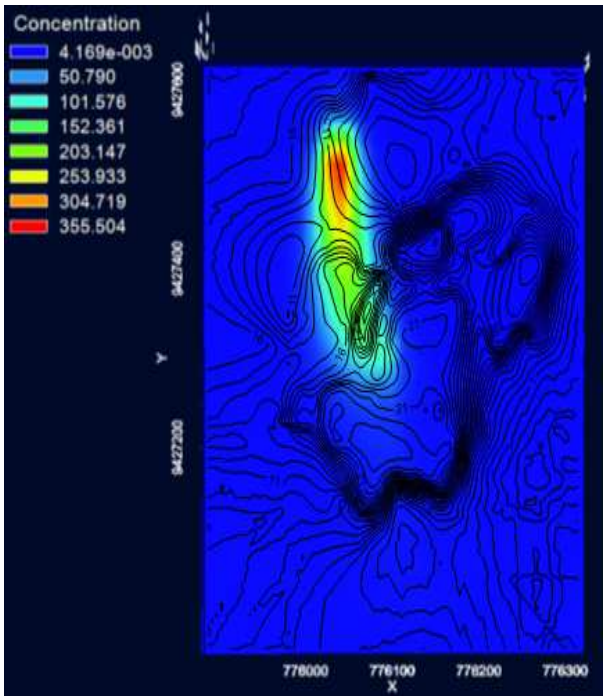


Figure.9.Modeling results for 2920 Days Contaminants Fe (Saturation Point)

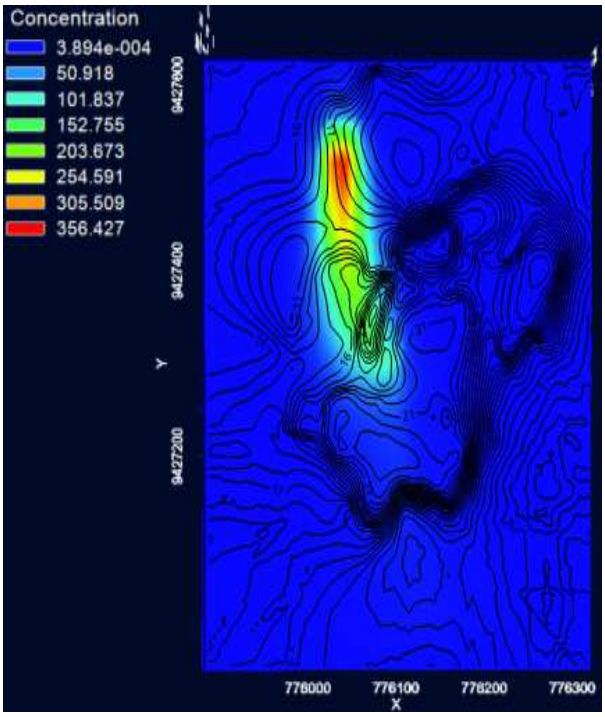


Figure.10.Modeling Results for7300 Days Contaminants (Highest Concentration) Mn

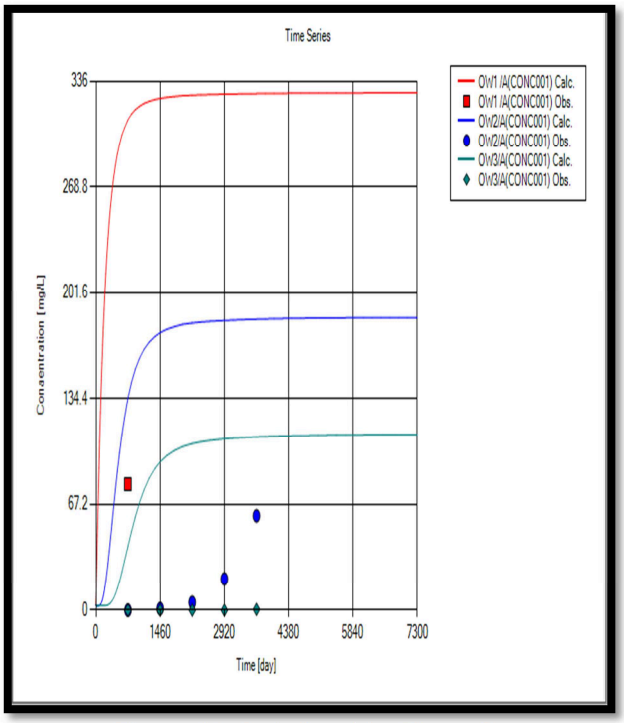


Figure.11. Relationship Charts Fe concentration against Pollution Time Period

References

[1] Bouwer., H. 2002. Artificial recharge of groundwater: hydrogeology and engineering. Hydrogeology Journal 10, 121-142

[2] Health Ministery of Republic Indonesia, 2010.Government Code of Drinking Water Quality, PP. No. 492.

[3] Telford, W.M., Geldart, L.P., Sheriff, R.E., 1990. Applied Geophysics, 2nd ed. Cambridge University Press, Cambridge, UK.

Applied Mechanics and Materials Vol. 567 (2014) pp 98-103
© (2014) Trans Tech Publications, Switzerland
doi:10.4028/www.scientific.net/AMM.567.98

Optimization of Activated Sludge Physical Properties by Magnetic Field via Response Surface Modeling

NUR SYAMIMI ZAIDI[1, a], KHALIDA MUDA[1, b], JOHAN SOHAILI[1, c] and MIKA SILLANPÄÄ[2, d]

[1]Faculty of Civil Engineering, Universiti Teknologi Malaysia (UTM), 81310 Johor Bahru, Johor, MALAYSIA
[2]Laboratory of Green Chemistry, Lappeenranta University of Technology, Patteristonkatu 1, 50100 Mikkeli, FINLAND

[a]nursyamimi@utm.my, [b]khalida@utm.my, [c]johansohaili@utm.my, [d]Mika.Sillanpaa@lut.fi

Keywords: Activated sludge; Wastewater treatment; Magnetic field; RSM; Physical properties

Abstract
In this study, activated sludge was exposed by magnetic field exhibited from NdFeB – type of permanent magnets. The exposure was aimed to improve the physical properties of the activated sludge used in treating wastewater. Hence, it was hypothesized that the magnetically-exposed activated sludge is potential in enhancing the efficiency of removal performances of the wastewater treatment processes. The influence of magnetic field, exposure time, biomass concentration and mixing intensity on turbidity reduction, aggregation and settling velocity was thoroughly investigated. Response surface methodology (RSM) was applied for experimental design, analysis and optimization. Based on the results, magnetically-exposed activated sludge displayed certain trends showing that its properties were positively affected by magnetic field. At the optimum conditions of magnetic field of 88.0 mT, exposure time of 38.5 hrs, biomass concentration of 3380 mg/L and mixing intensity of 345 rpm achieved 68.3%, 60.1% and 0.0104 cm/s of turbidity reduction, aggregation and settling velocity, respectively.

Introduction

Magnetic field has been successfully applied for separation purposes [1,2]. Magnetism is a unique physical property that independently facilitates applications such as water purification by affecting the physical properties of contaminants in water. In combination with other processes, it can improve the efficiency of purification technology [3]. The principle for the magnetic technology in such applications is that by treating fluids through a magnetic field of specific intensity that later caused the fluid particle of positive and negative charges become perpendicularly aligned with the direction of the magnetic field. With the resulting alignment, the fluid particles become more stable, thus inducing the process of coagulation and aggregation to occur.

Until recent, magnetic field has been implemented for several common wastewater treatment processes. For instance, magnetic field were applied for the removal of heavy metals [4], turbidity and suspended solids [4,5,6], organic compounds [7,8,9], nutrients consisting of nitrogen and phosphorus compounds [10,11] and toxic chemicals [12]. Generally, most of the treatment processes shown improvement in their performances under specific magnetic conditions.

According to Tomska and Wolny [11], activity of the activated sludge was proven to be improved, thus enhanced as well the pollutant treatments in the wastewater under the appropriate magnetic field intensity. Mostly, high strength in magnetic field intensity exhibited negative impact to the activated sludge. Studies by [7] and [8] showed the same conclusion that the removal efficiency of organic matter was initially increased by strengthening the magnetic field intensity, reaching a maximum value, but decreased with a further increase of the intensity. Weak static magnetic field of 7 mT was also reported to significantly influence the formaldehyde (FA) biodegradation in synthetic wastewater. Decreases in FA concentration and COD were greater, by 30% and 26% respectively [9]. A mixed effect of the magnetic field on biodegradation of organic

pollutants indicates that different bacteria which responsible in degradation process may have their unique level of magnetic susceptibility. These bacteria may act differently, either being inhibited or enhanced, therefore similarly reflected to the wastewater treatment performances.

Therefore, the aim of this study is to investigate the influence of magnetic field, exposure time, biomass concentration and mixing intensity on the separation and settling property of activated sludge in terms of turbidity reduction, aggregation and settling velocity. The central composite design (CCD) approach was employed to quantitatively analyze the effects of those factors, the interactions between them and to indicate any correlation between the factors and the responses.

Materials and Methods

Experimental Design

The magnetic field, exposure time, biomass concentration and mixing intensity were identified as the set of four independent process variables that been investigated due to the influence on the responses, viz. turbidity reduction and settling velocity of activated sludge. The CCD method was adopted to decide the number of batch test experiments to be performed for optimization of the process variables. As the range of process variables are defined, the limits are coded as ± 1 for factorial points, 0 for centre point and ± α for axial points. In this study, α for axial points was set to 1.0 (also known as face-centered) based on consideration that the region of interest is approximately same as the region of operatibility [13]. Thus, the limit for axial points were eventually same as the factorial points. The selected process variables with their limits are given in Table 1.

Table 1 Process control variables and their limits

Variables	Factorial		Star points*		Centre point
	-1	+1	-1	+1	0
A: Magnetic field (mT)	15.0	88.0	15.0	88.0	51.5
B: Exposure time (hours)	0.5	48.0	0.5	48.0	24.25
C: Biomass concentration (mg/L)	2000	4000	2000	4000	3000
D: Mixing intensity (rpm)	200	400	200	400	300

* Limit for star points is the same as factorial due to the consideration taken of α = 1.0 (face-centered)

Experimental Procedures

A total volume of 500 mL containing mixture of measured wet volume activated sludge biomass (2000 – 4000 mg/L) and raw wastewater was mixed in a glass flask that placed in a shaker. The shaker was fabricated to allow an installation of the permanent magnets of sizes 100 x 50 x 5 mm, arranged at both side surfaces of the flask in an alternate order. The stationary magnetic field was generated by permanent magnets (NdFeB – N42) manufactured by Ningbo Newland International Trade Co., Ltd, China. The permanent magnets are sintered NdFeB with the effective magnetic flux area is 100 x 50 mm. The variation of magnetic field applied ranges from 15.0 to 88.0 (±10%) mT. The mixture of the activated sludge was exposed within exposure time of 0.5 to 48.0 hours. The initial values of the responses were first measured before the batch tests started. Throughout the experiments, the mixture was mixed under a specified mixing intensity (200 to 400 rpm). After the exposure to magnetic field, the mixture was allowed to idle for 10 min before 10 mL of the liquid samples were collected and analyzed for final turbidity. The magnetically-exposed sludge was then taken in order to measure for the final settling velocity.

Analytical Methods

All tests were conducted based on the Standard Methods for the Examination of Water and Wastewater [14] – MLSS with method 2540B and settling velocity with method 2710E. A spectrophotometer (DR5000 HACH) was used for measuring COD (mg/L).YSI 556 MPS (YSI incorporated, USA) was used for recording the values of pH, temperature (°C) and dissolved oxygen (mg/L) for BOD purposes. Turbidity parameter (FNU) was measured using Milwaukee Turbiditimeter. As for aggregation, the parameter was measured in terms of turbidity.

Results and Discussions

Response Surface Analysis on Turbidity Reduction, Aggregation and Settling Velocity of Activated Sludge

The results of analysis of variance (ANOVA) for the three responses are summarised in Table 2. There were statistically analysed using full quadratic terms, which include linear, square and interactional terms with the aid of Design-Expert® (version 6.0.4).

Table 2 *P*-values of response surface modeling analysis for turbidity reduction, aggregation and settling velocity of activated sludge

	***P*-values**		
Term	**Turbidity reduction**	**Aggregation**	**Settling velocity**
A: Magnetic field	0.0087	0.0027	<0.0001
B: Exposure time	0.0168	0.0342	0.1022
C: Biomass concentration	0.4773	0.0086	0.0002
D: Mixing intensity	0.4235	0.0051	0.0110
A^2	0.0002	0.0414	0.9864
B^2	-[a]	-[a]	0.0012
C^2	-[a]	0.0874	0.0013
D^2	-[a]	0.0106	0.3459
AB	-[a]	-[a]	0.7625
AC	-[a]	0.3516	0.5475
AD	-[a]	-[a]	0.5475
BC	-[a]	-[a]	1.0000
BD	-[a]	0.0054	1.0000
CD	0.1678	0.0344	0.7625
R-squared value	61.8%	88.7%	89.6%

[a]Eliminated values resulted from the improved model

For the response of turbidity reduction, *P*-values of the model terms that been listed in Table 2 are the terms that obtained after the statistical model been improved. The purpose of the improvement is because the initial model was insignificant. Therefore, several model terms that have *P*-values of greater than 0.1 were eliminated. As a result, the *P*-value was improved from 0.0882 to 0.0006. The best statistical model for the turbidity reduction is given in Eq. (1).

$$\text{Turbidity reduction (\%)} = + 74.17 + 7.25 *A + 6.51 *B + 1.82 *C - 2.06 *D - 17.44 *A^2 + 3.82 *C *D \quad (1)$$

Based on Table 2, the only interaction left was between biomass concentration and mixing intensity. Although the interaction between those variables is insignificant (*P*-values of 0.1678), but their existance as the only interaction model term on the turbidity reduction makes it allowable to be further discussed. Fig. 1 illustrate the relationship between the biomass concentration and mixing intensity. The figure suggested that at high mixing intensity, an increase in biomass concentration resulted in increased of the turbidity reduction from about 68% to 76%. Contrary, under low biomass concentration, an increase in mixing intensity from 200 to 400 rpm resulted in reverse effect to the turbidity reduction. Such trend was indicated due to the lack of adaptation of the activated sludge towards the magnetic effect as the mixing intensity reached 400 rpm. The rapid mixing could cause minor failure to the activated sludge to form flocs. They might probably be sheared into smaller, tiny and weak flocs, thus caused difficulty to coagulate.

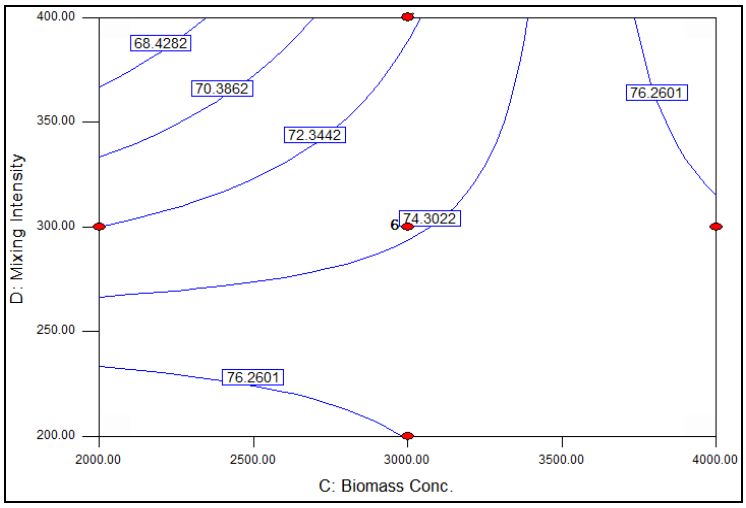


Fig. 1 Contour plot representing the relationship between the biomass concentration and mixing intensity on turbidity reduction

Statistical model as shown in Eq. (2) was also developed to relate the magnetic field, exposure time, biomass concentration and mixing intensity to aggregation. Similar to the turbidity reduction, ANOVA for aggregation was also improved.

$$\text{Aggregation} = +43.31 + 4.44*A + 2.94*B + 3.77*C - 4.08*D + 7.09*A^2 + 5.84*C^2 + 9.19*D^2 - 1.30*A*C + 4.28*B*D + 3.11*C*D \quad (2)$$

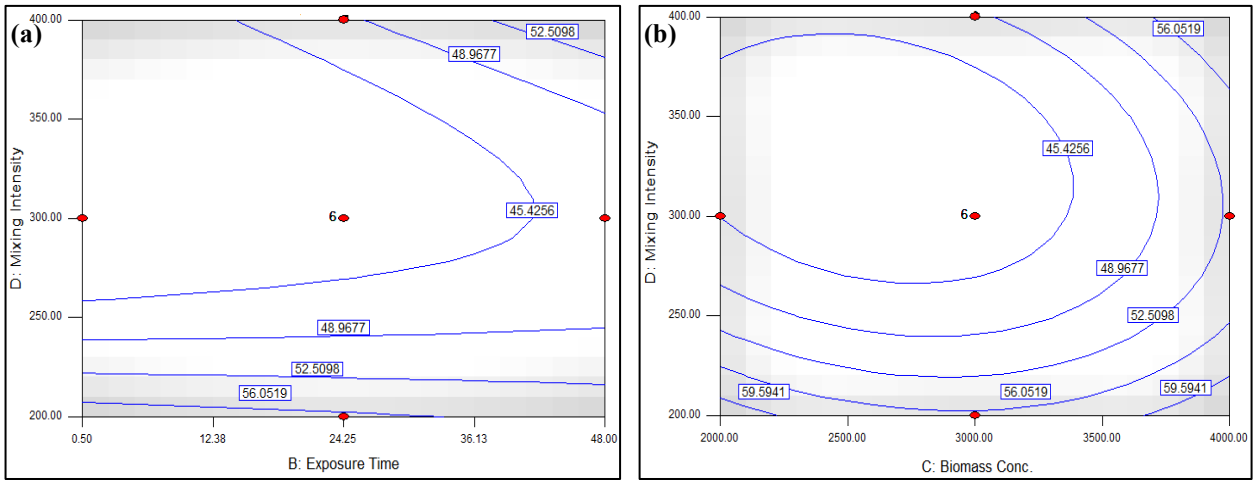


Fig. 2 (a) Contour plot representing the relationship between the exposure time and mixing intensity; **(b)** Contour plot representing the relationship between the biomass concentration and mixing intensity on aggregation

As shown in Table 2, linear terms of magnetic field, exposure time, biomass concentration and mixing intensity, square terms of magnetic field and mixing intensity, interactional terms between exposure time and mixing intensity, as well as biomass concentration and mixing intensity are significant. Fig. 2 particularly illustrate the relationship between the interactional terms on the aggregation of activated sludge. Based on Fig. 2 (a), it is clearly shows that as the exposure time increase, the aggregation also increase. However, due to the interaction with the mixing intensity, as such parameter increase from 200 to 400 rpm, it caused decrease in aggregation even though under an increase in exposure time. The similar trend is also indicated in Fig. 2 (b)**.** The increase in aggregation became reversed as the mixing intensity increase regardless when the biomass concentration is as well increased. However, there are points at exposure time and biomass concentration that had eventually sufficient to slightly increase the aggregation despite the further

reduction. For example, between the interaction of exposure time and mixing intensity, the aggregation reached the minimum value about 45% somewhere at exposure time of 36.0 hrs, but began to slightly increase as the exposure time increase greater than 36.0 hrs.

For the response of settling velocity, the results in Table 2 show that the linear terms of magnetic field, biomass concentration and mixing intensity as well as square terms of exposure time and biomass concentration are significant. The analysed R-squared value of 89.6% indicates the acceptability of the model. The best statistical model that describes the relationship between settling velocity and the variables is given in Eq. (3).

$$\text{Settling velocity} = +0.010 + (1.556 \times 10^{-4})*A + (3.333 \times 10^{-5})*B + (9.444 \times 10^{-5})*C + (5.556 \times 10^{-5})*D + (8.772 \times 10^{-7})*A^2 + (2.009 \times 10^{-4})*B^2 - (1.991 \times 10^{-4})*C^2 - (4.912 \times 10^{-5})*D^2 - (6.250 \times 10^{-6})*A*B - (1.250 \times 10^{-5})*A*C - (1.250 \times 10^{-5})*A*D - (6.250 \times 10^{-6})*C*D \quad (3)$$

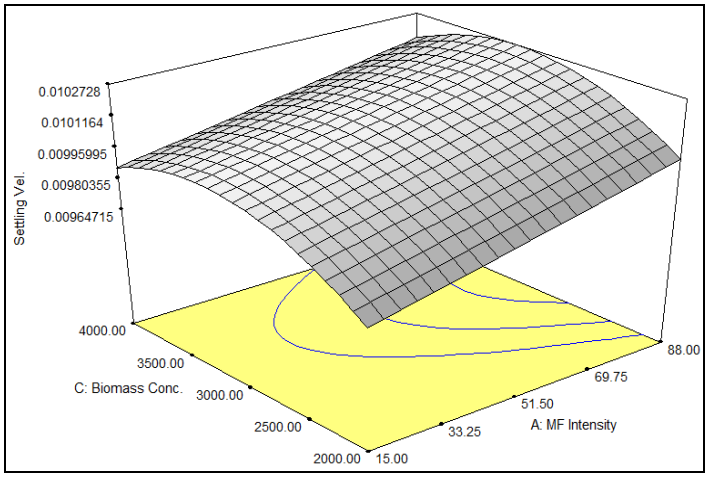


Fig. 3 Three-dimensional response surface plot of the magnetic field and biomass concentration on settling velocity of activated sludge

Fig. 3 illustrate the relationship between magnetic field and biomass concentration. In the figure, the concave shape of the surface plot explained that the maximum settling velocity was achieved between the low and high range of the variables. The maximum response obtained was about 0.0102 cm/s which seems to occur at the intermediate value of the low and high range of the magnetic field and biomass concentration. This trend could be reasoned due to the fact that greater intensity of magnetic field could be harmful to the microorganisms in the activated sludge, thus cause them to exhibit adverse effect in the settling process [7,15]. As for the effect influenced by biomass concentration, minimum improvement of settling velocity could be reasoned in terms of relationship of the available food (substrate) and microorganisms (biomass). Although the biomass concentration is increased from 2000 mg/L to 4000 mg/L, but the substrate could be the limiting factor as it was degraded throughout the experiment period. As a result, microorganisms may reached its starvation state thus caused reduction in their activity.

Experimental Condition Optimization

The optimization of experimental conditions was identified by considering whether the turbidity reduction, aggregation and settling velocity were higher than the arbitrarily chosen constraint values. According to the model, the predicted optimized conditions occurred at magnetic field of 88.0 mT, 38.5 hrs exposure time, 3380 mg/L of biomass concentration and at mixing intensity of 345 rpm. These conditions resulted in 68.3% of turbidity reduction, 60.1% of aggregation and 0.0104 cm/s of activated sludge settling velocity. In order to verify the optimization results obtained from Design-Expert, a batch test experiment was carried out in triplicate using the obtained optimum conditions. Average turbidity reduction of 70.0%, aggregation of 59.3% and settling velocity of 0.0104 cm/s were recorded against the predicted optimum responses.

Conclusions

Overall, the element analysis suggested that the applied magnetic field could enhance the settling property of the activated sludge through the improvement on its aggregation capability. These imply that the magnetic field is reliable for accelerating the activated sludge settleability, thus potential to enhance the performance efficiency of the wastewater treatment systems. Under the optimal condition of 88.0 mT magnetic field, 38.5 hrs exposure time, 3380 mg/L biomass concentration and 345 rpm mixing intensity, the maximum turbidity reduction, aggregation and settling velocity of 70.0%, 59.3% and 0.0104 cm/s, respectively, were then obtained.

Acknowledgement

We would like to thank Universiti Teknologi Malaysia (UTM) and Ministry of Science, Technology and Innovation (MOSTI) for the financial support (Vote No: 4S032).

References

[1] P.A. Augusto, T. Castelo-Grande, and P. Augusto, Magnetic classification in health sciences and in chemical engineering, Chem. Eng. J., 111 (2005) 85-90.
[2] P. Ali-Zade, O. Ustun, F. Vardarli, and K. Sobolev, Development of an electromagnetic hydrocyclone separator for purification of wastewater, Water Environ. J., 22 (2008) 11-16.
[3] R.D. Ambashta, and M. Sillanpää, Water purification using magnetic assistance: A review, J. Hazard. Mater, 180 (2010) 38-49.
[4] M.S. Kamariah, Subsurface flow and free water surface flow constructed wetland with magnetic field for leachate treatment, Thesis of Master of Engineering (Civil-Wastewater), Universiti Teknologi Malaysia, 2006.
[5] C.-J.M. Chin, P.-W. Chen, and L.-J. Wang, Removal of nanoparticles from CMP wastewater by magnetic seeding aggregation, Chemosphere, 63 (2006) 1809-1813.
[6] Q. Xie, X. Liu, C. Wu, Y. Wang, and G. Zhu, Design and simulation of flow field for magnetic flocculation reactor, J Jiangsu Uni. (Nat. Sci. Edi.), 31 (2010) 473-477.
[7] H. Yavuz and S.S. Çelebi, Effect of magnetic field on activity of activated sludge in wastewater treatment, Enzyme Microb. Technol., 26 (2000) 22 – 27.
[8] Y. Ji, Y. Wang, J. Sun, T. Yan, J. Li, T. Zhao, X. Yin, and C. Sun, Enhancement of biological treatment of wastewater by magnetic field, Bioresour. Technol., 101 (2010) 8535 – 8540.
[9] M. Łebkowska, A. Rutkowska-Narożniak, E. Pajor, and Z. Pochanke, Effect of a static magnetic field on formaldehyde biodegradation in wastewater by activated sludge, Bioresource Technol., 102 (2011) 8777 – 8782.
[10] S. Liu, F. Yang, F. Meng, H. Chen, and Z. Gong, Enhanced anammox consortium activity for nitrogen removal: Impacts of static magnetic field, J. Biotechnol., 138 (2008) 96 – 102.
[11] A. Tomska and L. Wolny, Enhancement of biological wastewater treatment by magnetic field exposure, Desalination, 222 (2008) 368 – 373.
[12] J. Jung, B. Sanji, S. Godbole, and S. Sofer, Biodegradation of phenol: A comparative study with and without applying magnetic fields, J. Chem. Technol. Biotechnol., 556 (1993) 73 – 76.
[13] S. Kraber, Handbook for experimenters. Stat-Ease Inc., Minneapolis, USA, 2002.
[14] American Public Health Association, Standard Methods for the Examination of Water and Wastewater (APHA), 21th ed. Washington DC, USA, 2005.
[15] N.S. Zaidi, J. Sohaili, K. Muda, and M. Sillanpää, Magnetic field application and its potential in water and wastewater treatment systems: A review, Sep. Pur. Rev., 43 (2014) 206 – 240.

Applied Mechanics and Materials Vol. 567 (2014) pp 104-109
© (2014) Trans Tech Publications, Switzerland
doi:10.4028/www.scientific.net/AMM.567.104

POME Treatment Efficacy as Affected by Carrier Material Size in Micro-Bioreactor System

Wai Loan LIEW[1, a], Khalida MUDA[1, b], Mohd. Azraai KASSIM[1,c], Kok Yan LAI[1, d], Zi Yang SI[1, e], Yeap Hong THONG[1, f] and Soh Kheang LOH[2,g]

[1]Water Research Alliance, Level 2, Block C07, Faculty of Civil Engineering, Universiti Teknologi Malaysia, 81310 Skudai, Johor, Malaysia

[2]Malaysian Palm Oil Board, P.O.Box 10620, 50720 Kuala Lumpur, Malaysia

[a]wailoan_liew@yahoo.com, [b]khalida@utm.my, [c]azraai@utm.my, [d]mystery_event90@hotmail.com, [e]yang_89@live.com, [f]yhong26@hotmail.com, [g]lohsk@mpob.gov.my

Keywords: Attached-growth; Biodegradation; Material size; Removal performance; Wastewater treatment.

Abstract. This paper presents the effect of different sizes of palm kernel shell (PKS) activated carbon as the carrier material in a micro-bioreactor system to treat the palm oil mill effluent (POME). Three different sizes of PKS activated carbon were used as the carrier material, i.e. 4.750 – 2.360 mm (large), 1.180 – 0.710 mm (average) and 0.425 – 0.300 mm (small). The systems were run for a total of 29 days under hydraulic retention time (HRT) of 24 hours. The performances of several effluent quality parameters of POME regarding the use of PKS activated carbon of different sizes were studied. PKS activated carbon with size 1.180 – 0.710 mm showed the highest removal performances for chemical oxygen demand (COD), ammoniacal-nitrogen (AN), and solids, with 41 %, 84.6 %, and 88 % of removal respectively. The system with PKS activated carbon of size 4.750 - 2.360 mm showed the highest performance in removing TP (45 %), while 1.180 – 0.710 mm size of PKS activated carbon showed the highest performance in removing TN (53 %). The system was also found to effectively reduce the effluent colour. In overall, the PKS activated carbon of size 1.180 – 0.710 mm showed the best results as a carrier material to be used in the micro-bioreactor system in treating POME compared to the other two sizes.

Introduction

Palm oil which is a form of edible vegetable oil, is reddish brown in color due to its high content of beta-carotene. It is semi-solid under room temperature and it does not contain cholesterol [1]. Palm oil is widely used as food ingredients and is the most common cooking oil in the Southeast Asia and the Africa. During the 15th century, the usage of palm oil was introduced in the South East Asia and the Latin America [2]. According to the Malaysian Palm Oil Council (MPOC), the first commercial planting in Malaysia took place in Selangor in 1917. A total of 4.49 million hectares of land in Malaysia is under oil palm cultivation; which could produce 17.73 million tons of palm oil and 2.13 tons of palm kernel oil. Nowadays, Malaysia is one of the largest producers and exporters of palm oil in the world, accounting for 11 % of the world's oils and fats production and 27 % of export trade of oils and fats [3].

Although the widespread of palm oil industry brought great benefits to Malaysia, it is also associated with environmental impacts. Palm oil mills produce three types of by-products, i.e. liquid effluent, solid waste and gaseous emission, which are harmful to the environment if they are not properly treated. The main focus of the current study is on the liquid effluent, which is also identified as the palm oil mill effluent (POME). The process of crude palm oil from the fresh fruit bunches (FFB) require large quantities of water. About 50 % of the water results in POME and 50 % being lost as steam, mainly through sterilizer exhaust, piping leakages as well as wash water. Thirty six percent of POME is generated from the sterilization process and 60 % of POME is

generated from the clarification process while the hydrocyclone process generated about 4 % of the total POME [4].

In 2005, Malaysia had discharged 53 million m^3 of POME from 14.8 million tonnes of palm oil production [5]. POME shows very high water pollution level which was determined from environmental parameters such as the oil and grease (OG) and the biochemical oxygen demand (BOD). Thus, POME has to be effectively treated in order to comply with the Malaysian effluent discharge standard set in the Environmental Quality Act 1974 [6]. Nowadays, there are a lot of systems that can be used to treat the POME. Conventional ponding treatment system is widely practiced in most of the palm oil mills in treating POME [7]. Two types of treatment systems are categorized under conventional ponding treatment system, i.e. ordinary ponding system and open digesting tank. This low cost system consist of the de-oiling tank, the acidification ponds, the anaerobic ponds and the facultative or aerobic ponds [8]. Open digesting tank is applied when there are limited spaces for treatment plant construction.

Carrier material were widely used in wastewater treatment by acting as a media for biomass attachment and hence influence the removal performance of the wastewater treatment system. Since biomass is very light and can be easily washed out from the reactor, a longer hydraulic retention time (HRT) is required to let the biomass to settle down. Hence, reducing the efficiency of the system applied. Generally, the carrier material allows the biomass to grow on it. Thus, the quality of the effluent can be improved with good application of carrier material. Good carrier material should have several criteria such as insoluble, not biodegradable, high mechanical stability, high diffusivity, simple immobilization procedure, high biomass retention, minimal attachment of other organisms and preferably a low cost price in the treatment of wastewater [9].

One of the critical issues encountered in the palm oil mill wastewater treatment system is sludge washout problem, which will negatively affect the system performance. Carrier material has been used in reactor system in order to retain high volume of biomass, reduce settling time and increase the effectiveness of the system. On the other hand, exploitation of milling by-product as carrier material could benefit the palm oil industry due to its low cost, high availability, and non-complicated regeneration process. Palm kernel shell (PKS) for example, is a waste from the palm oil extraction and would be developed into a good carrier material in treating the POME. The use of PKS activated carbon to treat the POME has been studied by several researchers [10, 11, 12]. Nevertheless, not much study had been conducted in investigating the performance of PKS activated carbon as a carrier material as well as in different sizes in treating the POME. Suitable size of carrier material can result in the optimization of the reactor's performance.

Therefore, the study is aimed to investigate the best size carrier material in the treatment of the POME. Activated carbon produced from a kind of by-product (the PKS) was attempted to treat another by-product of the palm oil industry (the POME). Besides, its effectiveness in the removal of colour from the effluent was investigated.

Materials and Methods

Wastewater Sample and the Seeding Sludge. The sample for anaerobically-treated POME and seeding sludge were collected from the Bukit Besar Palm Oil Mill, located in Kulai, Johore. The POME sample was obtained from the discharge point of the anaerobic pond. Leaving the anaerobic pond, the effluent will be further treated in the facultative ponds, algae ponds, and a tertiary treatment system. The samples were collected into wide-mouth plastic bottles and were then kept at 4°C until further analyze in the laboratory. The seeding sludge was collected from the facultative pond of the same palm oil mill.

Carrier Material Preparation. PKS activated carbon was obtained from a previous study conducted here in UTM. They were crashed and sieved to three group of sizes: 4.750 – 2.360 mm (large size), 1.180 – 0.710 mm (average size), and 0.425 – 0.300 mm (small size). The PKS

activated carbon was then washed with distilled water, dried at 104^{o}C for 24 hours and kept in air-tight containers until use.

System Set-up. Six micro-bioreactor systems were fabricated in UTM using borosilicate glasses. Each micro-bioreactor contained 50 mL of sludge, 50 mL of carrier material and 500 mL of the POME. Total working volume of the system was 600 mL. The micro-bioreactor was connected to an aeration pump to simulate an aerobic condition. An outlet was design to regulate the pressure of the system. All the micro-bioreactor systems were subjected to a HRT of 24 hours.

Table 1. The parameters for treatment efficiency evaluation and their respective methods.

Parameters	Methods
Chemical Oxygen Demand (COD) [mg/L]	HACH Method 8000
Mixed Liquor Suspended Solids (MLSS) [mg/L]	APHA 2540D
Mixed Liquor Volatile Suspended Solids (MLVSS) [mg/L]	APHA 2540E
Ammoniacal-Nitrogen (AN) [mg/L]	HACH Method 8038
Total Phosphorus (TP) [mg/L]	HACH Method 10127
Total Nitrogen (TN) [mg/L]	HACH Method 10072
Colour [ADMI]	HACH Method 10048
Colour [Pt/Co]	HACH Method 8025

Method of Analysis. For every treatment cycle, the influent and effluent from the micro-bioreactor systems were kept for quality analysis. Samples stored in the cold room should be well shake and filtered before entering the systems for treatment. After a 24 hours reaction time, the systems were shut down to allow settling of the effluent before subsequent discharging and replacing the effluent. Analysis of the wastewater were conducted in accordance to the Standard Methods [13] and the HACH Water Analysis Handbook [14]. They are listed as in Table 1.

Results and Discussion

The use of PKS activated carbon as biomass-coated carrier material generally produces good removal performance of selected parameters in the POME. Fig. 1(a) showed the COD profile for the micro-bioreactor systems applying difference sizes of PKS activated carbon. Based on the figure, the removal performances increased against time. At the initial stage of the experiment, the graph showed negative profile, which may due to inadequate settling time given to the micro-bioreactor systems. The biomass was not completely settled, and washed out during the replacement of wastewater. This caused the values of parameters tested to be higher than the influent, therefore an increase in COD concentration was obtained. However, the removal performances improved and stabilized on the 11th day of the experiment for all sizes of the PKS activated carbon. At this stage, more bacteria have been able to attach to carrier material and able to retain in the system, improving the removal performances. The removal performances for PKS activated carbon of sizes 4.750 – 2.360 mm and 1.180 – 0.710 mm reached their peaks on the 29th day of the experiment with 38.3 % and 41.0 % of removal respectively. While PKS activated carbon of size 0.425 – 0.300 mm showed highest removal performance at the 22nd day with 36.0 % of removal.

Fig. 1(b) shows the profile of MLSS and MLVSS concentrations against time. From day 4 and onwards, the concentrations of MLSS and MLVSS started to drop from the high initial concentrations and remained low but fluctuating towards the end of the experiment. At day 15, a sudden increased in the concentrations of MLSS and MLVSS can be seen, especially for PKS activated carbon size 0.425 – 0.300 mm. PKS activated carbon size 1.180 – 0.710 mm showed the lowest concentrations for both MLSS and MLVSS in the final reading when compared to the other two sizes. As the experiment continues, the microbes within the micro-bioreactor systems had attached and grew on the carrier material. Since the biomass-coated carrier material has good settling properties, the suspended sludge could be retained in the micro-bioreactor column. This resulted in almost consistent concentration of sludge biomass in the micro-bioreactor column on day 8 to day 29. On the 15th day of the experiment, the profile of MLSS and MLVSS showed an

increasing peak, this was because the POME influent very saturated due to the factory undergoes heavy duty of extraction of palm oil.

Based on Fig. 1(c), increasing AN concentrations were observed on the first two readings (day 1 and day 4) of the experiment. At the 8th day of the experiment, removal performances of AN jumped dramatically and showed the highest values for PKS activated carbon of sizes 4.750 – 2.360 mm, 1.180 – 0.710 mm and 0.425 – 0.300 mm, with 70.0 %, 84.6 % and 75.0 % of removal respectively. The removal performances stabilized on the 11th day and remained on positive profile from that day onwards.

The removal performance of TP is shown in Fig. 1(d). All micro-bioreactor systems were operated with HRT in 24 hours. From Fig. 1(d), as the time increases, the removal performance becomes stable. The highest removal was on the 25th day of the experiment with 45 % removal performance. The data showed that the larger size (4.750 - 2.360 mm) of carrier material gave better TP removal performance as compared to the other sizes of carrier materials. The system with larger size of carrier material gave better TP removal profile compared to intermediate size and smaller size. Although the larger size of carrier material has smaller surface area as compared to the smaller size, but it was the heaviest among the three sizes of the carrier materials causing the larger size of carrier material could settled within a short period of settling time and remained in the micro-bioreactor systems. The figure showed that the system still has not able to achieve its stable performance. It is suggested that the experiments should be conducted with a longer period to achieve stable performance. Fig. 1(d) also shows the removal performance of TN increased with time for three different sizes of carrier materials. From the removal profile, the 1.180 - 0.710 mm size of PKS activated carbon gave highest removal performance which was 53 %. However, the 0.425 – 0.300 mm size of carrier material showed a smooth profile.

Quantification of the colour content in the POME was conducted in the study in both ADMI and Pt/Co units. Apparently, the colour removal performances using different sizes gave different outcome. Fig. 1(e) shows the profile of colour removal performance in ADMI unit against time. The study was conducted for a period of 29 days. At the early stage of the experiment, the result showed increased in colour concentrations. However, the removal performances improved and resulted in stable removal performances since the 11th day of the experiment. PKS activated carbon with size 0.425 – 0.300 mm showed the highest removal performance (42.4 %) followed by size 1.180 – 0.710 mm (40.0 %) and size 4.750 – 2.360 mm (34.9 %). Fig. 1(e) also shows the profile of removal performance of colour in the ADMI unit (pH adjusted) against time. The results reached the peak on the second readings (day 4). The removal performances resulted in stable removal performances on the fourth readings (day 11) onwards. The micro-bioreactor systems were found to have continuous colour removal, suggesting that a longer experimental period is required to achieve the steady state. PKS activated carbon of size 1.180 – 0.710 mm (36.1 %) gave highest removal performance, followed by 0.425 – 0.300 mm (32.8 %) and 4.750 – 2.360 mm (31.2 %). In general, the colour removal performances of POME using original sample are higher compared to sample with pH adjustment.

Fig. 1(f) shows the profile of removal performance of colour (Pt/Co unit) against time. The graph presents increasing removal performance over time. Nevertheless, the micro-bioreactor system have not reached their stable states due to insufficient period of study. PKS activated carbon of size 1.180 – 0.710 mm gives highest removal performance (40.0 %), followed by size 0.425 – 0.300 mm (39.6 %) and size 4.750 – 2.360 mm (38.1 %).

The concentrations of solids, total nitrogen and AN are regulated in the Environmental Quality (Prescribed Premises) (Crude Palm Oil) Regulations, 1977 and the limits are 400 mg/L (suspended solids), 200 mg/L (value of filtered sample), and 150 mg/L (value of filtered sample) respectively [6]. The effluent resulted from the micro-bioreactor system in this study were within the parameter limits and hence the application is capable of handling the anaerobically-treated POME to comply with the watercourse discharge regulation.

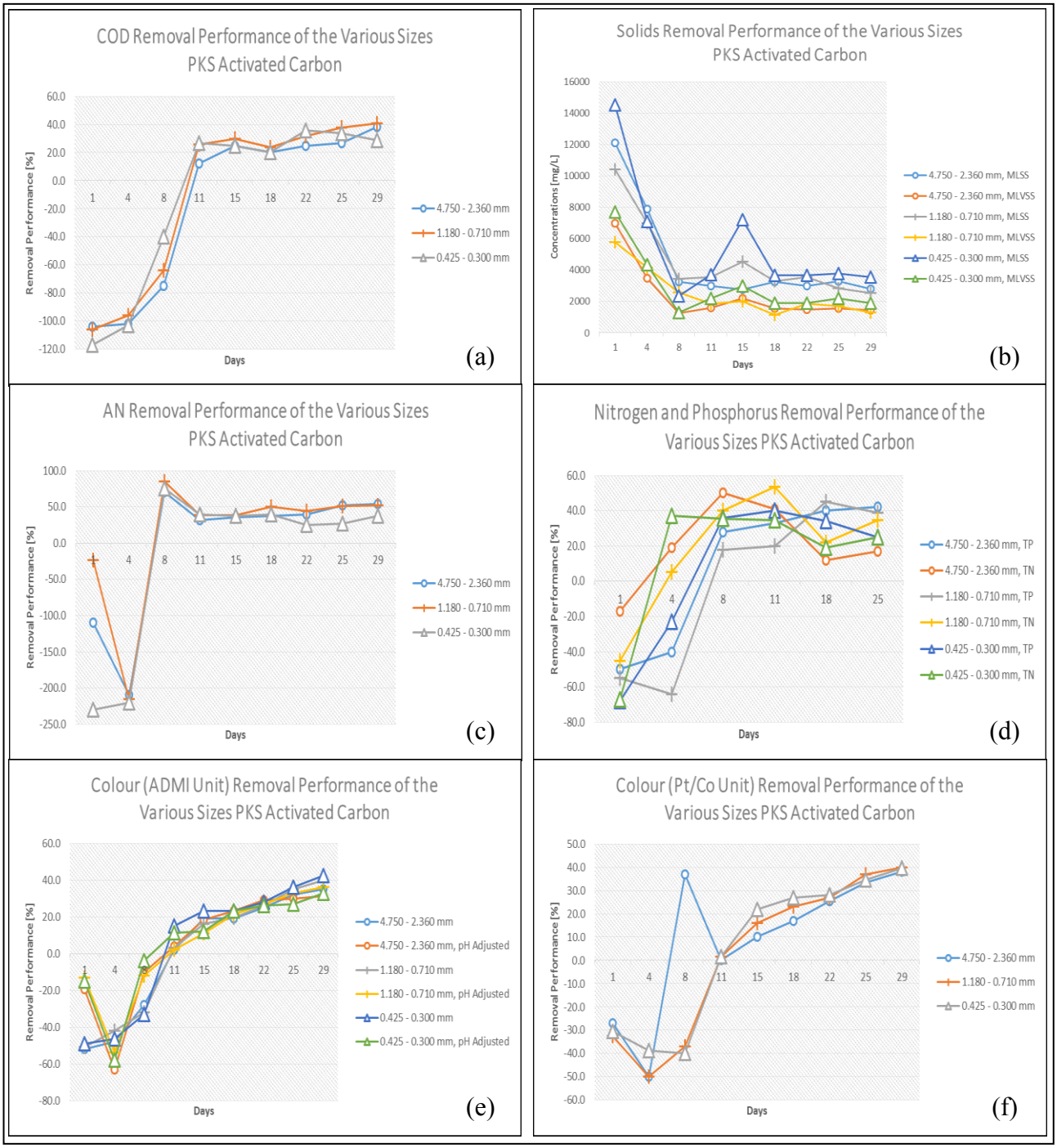


Fig 1. Performances of the various sizes PKS activated carbons used as biomass-coated carrier materials in the micro-bioreactors treating POME: (a) COD, (b) solids, (c) AN, (d) nitrogen and phosphorus, (e) colour as in the ADMI unit, and (f) colour as in the Pt/Co unit.

Summary

PKS activated carbon as biomass-coated carrier material is effective in treating POME. Several water quality parameters were tested and the results showed increasing removal performances over time. This reflects that PKS activated carbon (derived from oil palm waste itself) is suitable to be applied as the carrier material in the treatment of POME. The study also concluded that PKS activated carbon is effective in the decolourization of POME. Both the colour tests (in ADMI and Pt/Co unit) gave increasing removal performances over time. Most importantly, the study demonstrated the result of different removal performances by using different sizes of carrier

materials. In overall, PKS activated carbon of size 1.180 – 0.710 mm (average size) showed the best results in the removal of COD, solids, AN, TN, colour in both ADMI (pH adjusted) and Pt/Co units. The size 4.750 – 2.360 mm (large size) was effective in TP removal while the size 0.425 – 0.300 mm (small size) was found to successfully remove the effluent's colour as measured in ADMI unit.

Acknowledgement

The authors wish to thank Universiti Teknologi Malaysia (UTM) and Ministry of Education for funding the study through Research University Grant (GUP) under cost center number Q.J130000.2509.05H28.

References

[1] R.C. Cottrell, Introduction: nutritional aspects of palm oil, The American Journal of Clinical Nutrition. 53 (1991) 989-1009.

[2] K.F. Kiple, K. Conee Ornelas, The Cambridge World History of Food, Cambridge University Press, United Kingdom, 2000.

[3] Information on http://www.americanpalmoil.com/pdf/USITCpre-PublicHearing-V2.pdf

[4] M.I.R.H. Thani, W.W.R. Ibrahim, M.S. Sulaiman, Industrial Processes and the Environment: Crude Palm Oil Industry, handbook 3, Department of Environment, Malaysia, 1999.

[5] A.A.Z. Lorestani, Biological Treatment of Palm Oil Mill Effluent (POME) using an Up-Flow Anaerobic Sludge Fixed Film (UASFF) Bioreactor, Thesis of Doctor of Philosophy, Universiti Sains Malaysia, Malaysia, 2006.

[6] Legal Research Board, Environmental Quality Act 1974 (Act 127) & Subsidiary Legislation, Petaling Jaya, Malaysia, 2008.

[7] A.O. Alade, A.T. Jameel, S.A. Muyibi, M.I.A. Karim, Z. Alam, Application of semifluidized bed bioreactor as novel bioreactor system for the treatment of palm oil mill effluent (POME), African Journal of Biotechnology. 10 (2011) 18642-18648.

[8] K.S. Chan, C.F. Chooi, Ponding system for palm oil mill effluent treatment, Proceedings of the Regional Workshop on Palm Oil Mill Technology & Effluent Treatment. (1984) 185-192.

[9] E.J.T.M. Leenen, A.P.D.S. Vitor, C.F.G. Katja, J. Tramper, R.H. Wijffels, Characteristics of an selection criteria for support materials for cell immobilization in wastewater treatment, Water Research. 30 (1996) 1985-2996.

[10] R.R. Mohammed, Decolorisation of biologically treated palm oil mill effluent (pome) using adsorption technique, International Refereed Journal of Engineering and Science. 2 (2013) 1-11.

[11] A.K. Che Ibrahim, Kinetic Parameter Studies of Activated Sludge Process for Anaerobic Pre-Treated Palm Oil Mill Effluent, Thesis of Doctor of Philosophy, Universiti Sains Malaysia, Malaysia, 2007.

[12] L.C. Lau, N.M. Nor, A.R. Mohamed, K.T. Lee, Adsorption of hydrogen sulfide using palm shell activated carbon: an optimization study statistical analysis, International Journal of Research in Engineering and Technology. 2 (2013) 302-311.

[13] APHA, Standards Methods for the Examination of Water and Wastewater, centennial ed., American Public Health Association, Washington, American Water Work Association, Water Environment Federation, 2005.

[14] HACH, Water Analysis Handbook, seventh ed., Hach Company, Colorado, 2013.

Applied Mechanics and Materials Vol. 567 (2014) pp 110-115
© (2014) Trans Tech Publications, Switzerland
doi:10.4028/www.scientific.net/AMM.567.110

Possible Stabilization of Sludge from Groundwater Treatment Plant Using Electrokinetic Method.

Syed Baharom Syed Osman[1,a], Farhan Iqbal[2]

[1]Civil Engineering Department, University Technology Petronas, Perak, Malaysia

[2]Petroleum Management Unit, Petronas, Kuala Lumpur, Malaysia

[a]sybaharom@petronas.com.my

Key words: Electroosmotic stabilization, electrokinetic, consolidation, underground water sludge.

Abstract. Among the available methods of disposing sludge from water treatment is to dispose them in landfills or to deposit them at a certain location to form lagoons. Once fully deposited, the landfills or lagoons can be converted into a recreational area or even housing area depending upon the final strength of the sludge. An attempt to look into the possibility to stabilize and strengthen sludge from underground water source using electroosmotic method was carried out in a laboratory environment. Several samples of sludge containing predominantly ferrous oxide were placed in specially fabricated electro-osmotic cells. Direct current was then applied through the samples via copper electrodes at the two ends of the samples. All the samples were subjected to seven days of treatment with variation in the surcharge/load imposed and voltage applied on the samples. Results from the tests demonstrated positive effects on the treated sludge samples. There were significant increase in the shear strength and reduction of moisture content which could be an early indication that sludge which predominantly contains ferric oxide could be strengthen by means of electroosmotic stabilization.

Introduction

One of the available methods of disposing sludge from either water or wastewater treatment is by disposing the sludge in landfills or lagoons. Among the reasons for this approach is the availability of space and alternative methods are considered to be expensive. These landfills and lagoons if properly engineered and treated could eventually be converted into recreational areas or even residentials depending upon the final strength of sludge. In this paper, research was conducted on a lagooned groundwater sludge located in the Kelantan state where sludge production of approximately 5 tons daily was deposited. The sludge being a by-product of groundwater treatment contains minerals with high moisture content causing it to have extremely low shear strength. Generally, current treatment method includes wetting the sludge until it can be pumped elsewhere; addition of dry material to permit it to be shoveled; or avoiding stabilization completely by capping or encapsulating the lagoon [1]. This research however, concentrates on stabilizing and strengthening of the groundwater sludge which predominantly contains ferric oxide using electroosmotic method of treatment.

Literature Review

Electroosmosis which is a part of electrokinetic has been utilized as a soil improvement and dewatering methods in projects such as stabilization of earth dams, embankments and slopes. Electroosmotic method has been proven to be effective in stabilizing and consolidating soils both in the laboratory and in the field [2, 3], where it was observed that electroosmotic consolidation induced the reduction of moisture content and increase in shear strength [4-6]. Besides soils, electroosmosis is also utilized in dewatering and stabilizing mine tailings, water and wastewater sludge. Other fields of application of electroosmotic and electrokinetic methods include the treatment and removal of contaminants in soil especially in industrial lands and landfills.

Historically, in 1809, Reuss was probably the first man to observe when a direct current was applied to a clay-water mixture using two electrodes, the pore water in the soil flows from anode to cathode. When the electric potential was removed, the flow of water immediately stopped. This phenomenon is termed electroosmosis. Hence, electroosmosis is a process of transferring free water in the capillaries of the soil under the influence of electrical potential. Cassagrande in 1951 was credited to be the pioneer in the practical application of electroosmosis in soil and its usage as a stabilizing method was increased ever since then.

The movement of pore water in the soil is generated in the diffuse double layer or soil moisture film. Helmholtz-Smoluchowski's theory describes that the basis of electroosmotic theory lies in the fact that when a direct current is applied, the mobile positive ions will be attracted towards the cathode, dragging with them the free water molecules causing a general movement of water from anode to cathode as shown in Fig. 1.

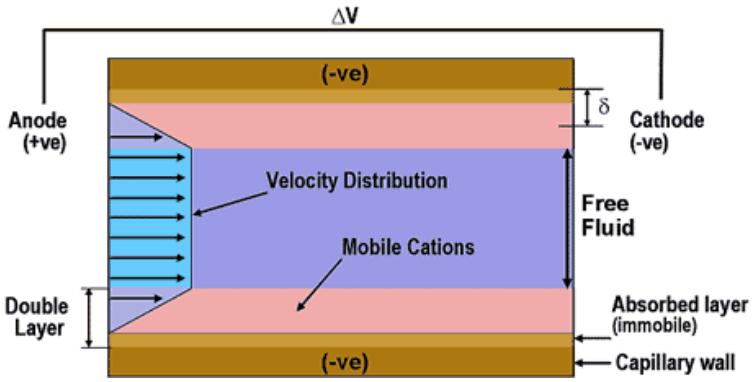


Figure 1. Helmholtz-Smoluchowski model for electroosmosis flow [7]

The overriding benefit of electroosmosis, contrary to the case of hydraulic permeability, k_h, is that the electroosmotic permeability, k_e is shown to be independent to the pore size or the presence of macropores [8]. This is in contrast to the hydraulic permeability k_h, which decreases markedly with the pore size. In fact, it was found that electroosmotic treatment can be up to 10^4 times faster than the conventional hydraulic treatment method and is particularly relevant to materials such as slurries and sludges [1]. In addition to this, some researchers [9] have noted a k_e value for sewage sludge of about 5 times that of many soils. Electroosmosis may be combined with conventional surcharging where electroosmosis is used to induce an additional effective consolidation pressure to accelerate the dissipation of positive pore water pressure.

Materials and Methods

Sludge. Underground water sludge was obtained from a groundwater treatment plant located in the state of Kelantan. Basic testing of the sludge was conducted and it was found that the average initial moisture content of the raw sludge coming directly from the drying filters in the treatment plant was very high. The pH value indicates that the sludge was a weak base which was due to the influence of lime inside the sludge. The lime was used to promote the precipitation of colloidal solid inside the groundwater. The specific gravity of the sludge was within the average value of specific gravity for common clay minerals. Results from XRF analysis shows that the main constituent of the sludge was ferric oxide (Fe_2O_3) along with other compounds such as calcium oxide etc. The summarize results are given in Table 1.

Table 1. Basic properties of sludge

Properties	
Initial moisture content, %	383.7
Specific gravity	2.56
pH	8.22
Electrical conductivity, μS	310
Fe_2O_3, %	76.7
CaO,%	11.2

Electroosmotic tests. The electroosmotic test set-up is shown in Fig. 2. It should be noted that the power supply was set in such a way that the copper electrode on top of the Perspex cell is the positive end while the one at the bottom is the negative end.

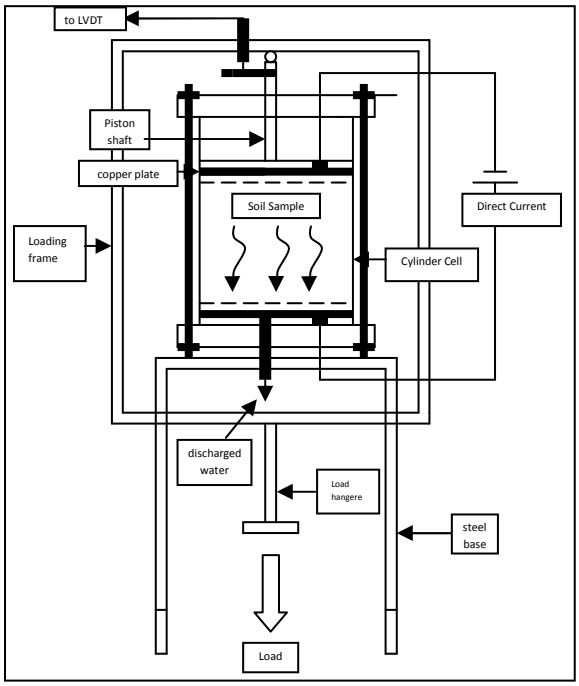


Figure 2. Diagram of the electroosmotic test set-up

After putting together the Perspex cell apparatus, a layer of silicon grease was applied on the interior wall of the cell before the placement of the sludge. The grease was applied to prevent formation of film of water at the interface between the soil sample and the cylinder. Formation of the film of water would short circuit the system rendering the electroosmotic process ineffective. A previously weighted 1 kg raw sludge was then placed in the cell in layers of about 25 mm thick and rodded to remove entrapped air. The procedure was repeated until all the sludge was placed. The cell was then tightly closed with the top cover by tightening the three tie rods at both ends with wing nuts.

Once all the equipment and instrumentations were set up, electroosmotic stabilization tests began by applying the electrical current concurrently with the application of surcharge and opening of the drainage outlet. Simultaneously, logging of the vertical settlement measured using vertical distance transducer (LVDT) was automatically done using the data acquisition unit (ADU) and the current was recorded using logging multi-meter. Both the readings for settlement and current were logged throughout the test for 7 days for all the samples. Once completed, the treated soil was immediately subjected to vane shear test after which the same specimen was cut into 4 equal slices of about 25 mm each where tests on moisture content, pH and conductivity were carried out. The final length of the specimen was approximately 100 mm.

The same procedure was applied for all the test specimens with variations in surcharge and voltage applied. The combinations of surcharges and voltages were 10kPa-0V, 10kPa-10V, 10kPa-30V, 20kPa-0V and 20kPa-10V.

Results and Discussion

Settlement. Fig. 3 shows much of the settlement for all the tests with or without voltage took place within 2000 minutes (33 hours). It could be observed that the final settlement for 10kPa-30V test increased more than 12 mm than the 10kPa-0V test indicating the effectiveness of the electroosmotic treatment. Maximum settlement of about 30 mm however was achieved through the 20kPa-10V test signifying the important effect of surcharge in the settlement process.

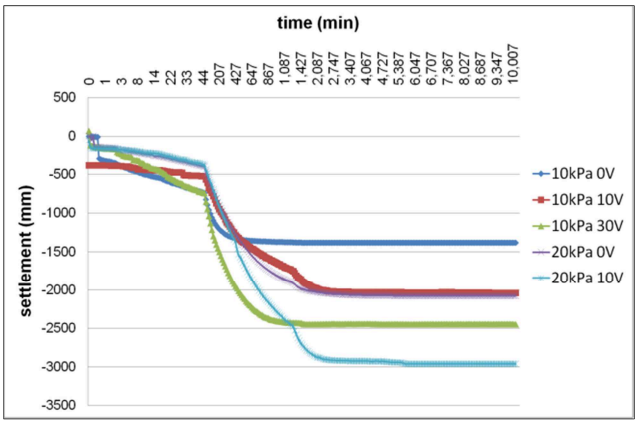


Figure 3. Settlement versus time

It could also be seen that the rate of settlement (slope of settlement against time) was about the same for all tests with the major difference being the variation of the magnitude of settlement that occurred within the same period. This is in agreement with observations from previous researchers who found that electroosmotic permeability does not influence the rate of consolidation but only influence the magnitude of consolidation [10]. It is interesting to note here that the period of major reduction in the magnitude of the current for the tests seems to tally with the period of major settlement for the same test which was within the 2000 min (33 hours) period.

Shear strength. It was also interesting to note that from Fig. 4, the tests for 10kPa-10V produced the highest shear strength of 23.8 kPa as oppose to the 20kPa-10V test which produced a shear strength of approximately the same in spite of having a higher surcharge.

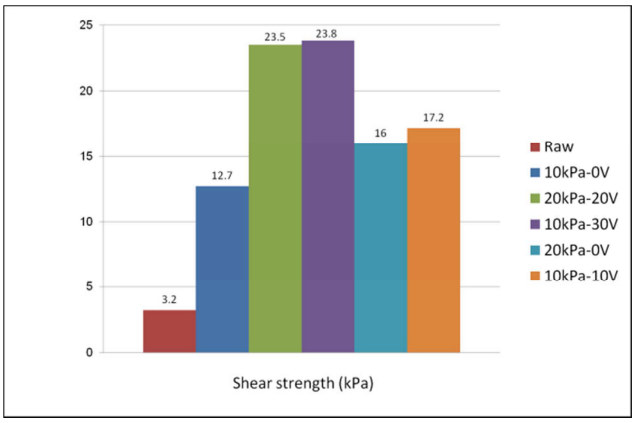


Figure 4. Shear strength

Although the consolidation for the 20kPa-10V was higher, the factors contributing to the strength of the 10kPa-10V sample must have also come from other strengthening mechanism besides

consolidation. Both the tests without voltage gave lower values than those with voltage but were still significant compare to the untreated raw sludge with shear strength of only 3.2 kPa.

Moisture content. It could be observed from Fig. 5 that for the non-electroosmotic test (10kPa-0V and 20kPa-0V), the amount of moisture content was about the same throughout the whole distance from anode. The electroosmotic tests on the other hand exhibits significant reduction and variations of moisture content especially for the 10kPa-30V test which contains 525% moisture at location close the cathode. This is even higher than the original moisture content which was 368% and this phenomenon was due to the fact that the rate of drawing out excess pore water from the upper part was relatively too rapid resulting in the pooling of moisture at the bottom part near the cathode.

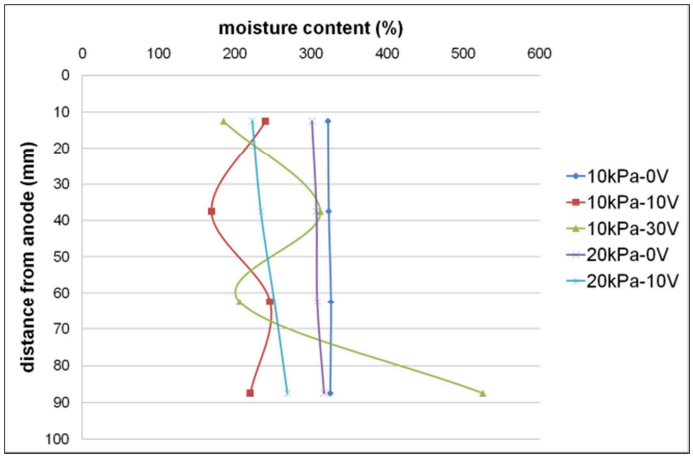


Figure 5. Variation of moisture content from anode

pH. The role of pH or changes of pH in electroosmotic treatment is perhaps the governing factor in the effectiveness of the stabilization process especially stabilization through cementation or mineralization. In Fig. 6, it could be seen that again, the variation of pH values for the electroosmotic tests indicate rigorous ionic activities throughout the sludge samples. The high pH value towards the cathode was resulted from the release of hydroxide (OH^-) ions from the cathode. Barker [11] pointed out that the dissolution of alumina starts to increase significantly at pH>8. It is therefore suspected that the high pH value for the 10kPa-30V test led to the dissolution of alumina and silica ions from the aluminium oxide and silica dioxide in the sludge and reacted with the calcium ions present. This reaction produced armorphous calcium aluminate hydrate (CAH) and calcium silicate hydrate (CSH) gels, which thereafter crystallized with time to form strong cementitious material.

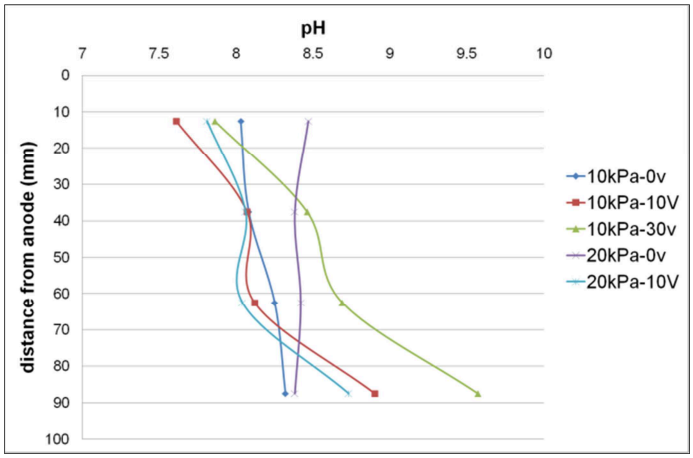


Figure 6. Variation of pH from anode

Conclusion

The electroosmotic tests conducted proved the positive effects of electrical current on the treated groundwater sludge. The samples were treated for only 7 days and yet there were at least two major improvements noted:

i. Higher consolidation, meaning higher reduction of moisture content. The 10kPa-0V test resulted in a total settlement of only 14 mm while the 10kPa-10V test produced a settlement of 25 mm; an increase of approximately 78 percent (11 mm). It was observed that the bulk of the settlement occurred within 33 hours of the test.

ii. Increase in shear strength especially for the higher voltage test which in the case of the 10kPa-30V test resulted in the increase of approximately 87 percent (11.1 kPa) more than the 10kPa-0V test. The increase of shear strength was contributed by the reduction of moisture content coupled with the probable formation of cementitious material. This formation need to be confirmed with further test especially using XRF equipment.

As a concluding remark, the overall experiment on the effect of electroosmotic treatment on the groundwater sludge strongly indicates the possibility of stabilizing the sludge using electrical current. However, further testing is required in order to ascertain the best combination of variables such voltage, time of treatment, type of electrodes and so forth.

Acknowlegement

The assistance and help from the geotechnical laboratory technologies; Mr. Zaini and Miss Imma are highly appreciated. Special thanks also goes to Mr. Faisal from the mechanical department for the XRF test.

References

[1] Jones, C.J.F.P., Glendinning, S., Huntley, D.T. and Lamont-Black, J., Geosynthetics, J. Kuwano & J. Kosegi (eds), 539 (2006)

[2] Chappel, B.A. and Burton, P.L., Journal of the Geotechnical Engineering Division, ASCE, 101 (GT8), 733 (1975)

[3] Mitchell, J.K. and Wan, T.Y., Proceedings of 9th International Conference on Soil Mechanics and Foundation Engineering, Tokyo, 219 (1977)

[4] Bjerrum, L., Moum, J. and Eide, O., Geotechnique, 17, 214 (1967)

[5] Lo, K.Y. and Ho, K.S., Canadian Geotechnical Journal, 28, 763 (1991)

[6] Shang, J.Q. and Dunlap, W.A., Journal of Geotechnical Engineering Division, ASCE, (122), 274 (1996)

[7] Mitchell, J.K., Fundamental of Soil Behavior, John Wiley & Sons Inc., New York (1993)

[8] Acar,Y.B. and Alshawabkeh, A.N., Environmental Science and Technology, 27 (13), 2638 (1993)

[9] Glendinning, S., Jones, C.J.F.P., Huntley, D.T., and Lamont-Black, J., Geosynthetics, J. Kuwano & J. Koseki (eds), 527 (2006)

[10] Esrig, M.I., Journal of Soil Mechanics and Foundation Division, ASCE, 93, 109 (1968)

[11] Barker, J.E. and Rogers, C.D.F., Ground Improvement, Vol. 8, No. 2, 47-58 (2004)

Applied Mechanics and Materials Vol. 567 (2014) pp 116-121
© (2014) Trans Tech Publications, Switzerland
doi:10.4028/www.scientific.net/AMM.567.116

Post-treatment of Anaerobically Digested Palm Oil Mill Effluent by Polymeric Flocculant-Assisted Coagulation

Amirhossein Malakahmad[1, a], Sim Yeong Chuan[1,b] and Mahdieh Eisakhani[2,c]

[1]Civil Engineering Department, Universiti Teknologi PETRONAS (UTP), 31750 Tronoh, Malaysia

[2]Social, Development and Environmental Studies Centre, Universiti Kebangsaan Malaysia (UKM), Malaysia

[a]amirhossein@petronas.com.my, [b]911syc@gmail.com, [c]mahdieh_eisakhani@yahoo.com

Keywords: Alum, Industrial discharge, Physico-chemical treatment

Abstract. Typically, palm oil mill industries use conventional anaerobic ponds for treatment of palm oil mill effluent (POME). But, this method alone cannot produce effluent discharge to an allowable limits set by the authorities. This study aimed to investigate further treatment of anaerobically digested POME (COD = 682±14 mgL^{-1}, TSS = 29±7 mgL^{-1} and turbidity = 106±3 NTU) by coagulation-flocculation process. Alum, an industrial-accepted coagulant and OC 100 and PC 100W as two industrial-based polymeric flocculants were used in coagulation-flocculation process. Results indicate coagulation process in its optimum conditions (pH = 6, alum dosage = 1800 mgL^{-1}, rapid mixing = 5 min, and slow mixing = 20 min) reduces the COD, TSS and turbidity by 59%, 80% and 86%, respectively. Flocculants OC 100 and PC 100W caused further reduction of TSS (85–88%) and turbidity (97–98%). By application of post treatment, the POME characteristics reached to an acceptable discharge level enforced by Malaysian department of environment (DOE).

Introduction

Statistical information shows, Malaysia produces 51% of world palm oil and its world export reaches to 62% [1]. Simultaneous to this considerable production, huge volume of highly polluted wastewater referred as palm oil mill effluent (POME) is produced. Palm oil mill plants are located near the rivers from which water is utilized for their milling operations. Prior to the initiation of stringent environmental control, some palm oil mills discharge their effluents into the rivers in an untreated or partially treated conditions. Consequently, the POME discharge with high BOD and COD contributed to the rise of oxygen demand in the river, causing lack of oxygen supply and eventually death of aquatic life [2].

Therefore, a wide range of methods such as biological treatment [3, 4], sedimentation and centrifugation [5, 6], adsorption [7, 8] and membrane technologies [9, 10] have been used for treatment of POME to lessen its pollution problems. The most frequently used method is biological treatment, which consist of anaerobic and facultative pond systems. But, unaided anaerobic treatment could hardly produce effluents to a level complying with the department of environment (DOE) discharge limits. The reported results in Table 1 show the anaerobically treated POME contains high COD, BOD and solids concentrations. Environmental Quality Act (EQA) 1974, Act 127, Part IV, section 30A stated that for palm oil industries near catchment areas and municipalities, enhanced wastewater treatment facility is needed to prevent river pollution. According to the DOE Malaysia, the COD of effluent from crude palm oil mills should not be above 400 mgL^{-1} before it is being discharged to rivers [11]. Therefore, a post-treatment technique which could be economical for the industries and effective to meet the standard limits requirements is desirable.

Table 1. Characteristic of typical anaerobically digested POME

Parameter [a]	Chan et al. (2010) [4]	Ho and Tan (1989) [2]	Phang and Ong (1988) [12]	Vijayaraghavan (2007) [3]
pH	7.4	7.1	7.24	7.8
BOD	1355	655	1938	-
COD	13,650	5430	20,314	1372
TS	19,370	8300	20,889	-
TSS	12,750	3100	14,686	512
TN	320	-	-	134

[a] All parameters in mgL^{-1} except pH

Application of coagulation-flocculation process is reported broadly for treatment of different wastewaters, as it is cost effective, energy-saving, convenient and efficient alternative. Coagulation-flocculation process is mainly used for the removal of colloidal materials, which cause colour and turbidity. Successful applications of coagulation-flocculation process have been reported for treatment of different discharges such as abattoir wastewater [13], pulp and paper mill wastewater [14], olive mill effluents [15] as well as landfill leachate [16]. In coagulation-flocculation process, many factors can influence the efficiency of the process. The aim of this study was to investigate the treatability of anaerobically digested POME using alum and two industrial-based polymeric flocculants (OC 100 and PC 100W) by optimizing pH, rapid and slow mixing durations and coagulant and flocculants dosages.

Materials and Methods

Anaerobically Treated POME Preparation and Characterization. POME was collected from the anaerobic pond system of a local palm oil milling plant. After collection, the samples were transported to the laboratory and kept in a cool storage at 4°C to stop any microbiological activities and to avoid composition changes. The pH was not adjusted and no chemicals were added to the wastewater. The required volume was thawed to room temperature (28 ± 2ºC) before performing coagulation-flocculation experiment.

pH, total suspended solid (TSS), turbidity, biochemical oxygen demand (BOD), chemical oxygen demand (COD), total kjeldahl nitrogen (TKN), and total organic carbon (TOC) were measured. pH of the samples were determined using HACH pH meter (Sension 4, USA). TSS was determined by filtering the wastewater samples through a 47 mm filter disc. Turbidity was determined in NTU (Nephelometric Turbidity Unit) using a HACH portable turbidimeter (2100P, USA). BOD_3 was analysed on samples incubated for 3 days at 27ºC. The initial and final dissolved oxygen (DO) were measured using a DO meter (YSI 5000, USA). COD was measured using HACH spectrophotometer (DR 2800, USA). TKN was measured through colorimetric method (DR 2000, USA). TOC of the wastewater was analysed using a total organic carbon analyser (1020A, USA) in accordance with the Standard Methods [17]. Table 2 contains characteristics of the anaerobically treated POME.

Experiments. Coagulation is not an exact process and therefore, selection of coagulant dosage is determined experimentally by the jar test instead of quantitatively by formula. The jar test simulates the coagulation/flocculation process in a batch mode. A series of batch tests were run in which pH, coagulant and flocculants dosages and mixing time were varied to get the optimal dosage (lowest residual turbidity).

Table 2. Characteristics of anaerobically treated POME

Parameter	Temperature [°C]	pH	COD [mgL^{-1}]	BOD_3 [mgL^{-1}]	TKN [mg NL^{-1}]	TSS [mgL^{-1}]	TOC [mgL^{-1}]	Turbidity [NTU]
value[a]	29 ± 4	8.63 ± 0.008	682 ± 14	367 ± 15	186 ± 44	29 ± 7	282 ± 13	106 ± 3

[a] The values are average of three measurements. The differences between the measurements for each parameter were < 1%.

Table 3. Descriptions of flocculants

Flocculant	Chemical name	Charge	Dosage [mgL^{-1}]	pH	Hazard	Biodegradability
PC 100W	Cationic Acrylamide Copolymer	Medium Cationic	20-200	4-7	No	Yes
OC 100FC	Organic Coagulant	Cationic	20-200	5-8	No	N/A

The experiments were carried out in a Phipps & Bird jar-test apparatus (USA) equipped with six 6 one-liter beakers. Coagulation of alum releases hydrogen ions as well as coagulant species. These hydrogen ions neutralize alkalinity. Since optimum pH values must be maintained for best coagulation and since alkalinity must be presented for hydroxide floc formation, the pH value of each jar was adjusted to the desired value using 0.1 M HCl. Then, the coagulant was added with a dosage varying from nil to 3000 mgL^{-1}. The alum used in this study was in powder form with the formula $Al_2(SO_4)_3 \cdot 18H_2O$ (M = 666.42 $gmol^{-1}$, 51 - 59% $Al_2(SO_4)_3$, pH 2.5 - 4). Immediately after the coagulant was added the samples were flash-mixed at a constant speed of 150 rpm for 5 to 30 minutes to ensure complete dispersion of the chemicals. This was followed by slow mixing for 10 to 60 minutes at 30 rpm to aid the formation of flocs and simulation of flocculation basin. Two types of cationic flocculants were used in this study; PC 100W and OC 100 (Table 3). At the end of the flocculation period the stirrers were turned off and the floc was allowed to settle for one hour. flocculants were added prior to slow mixing to facilitate floc agglomeration. After this settling period supernatant samples were drawn off from each sample and analyzed for COD, TSS and turbidity.

Results and Discussion

Effect of pH. pH of the samples were varied in range of 4 to 8 and other characteristics were fixed at 1800 mgL^{-1} of alum dosage and 30 minutes of rapid and slow mixing times. Fig. 1(a) shows the COD, TSS and turbidity removal efficiencies at different pH of the wastewater.

The removal efficiencies in terms of COD, TSS and turbidity were increased gradually from 28.4%, 33.9% and 60.3% at pH 4 to 57.5%, 76.0% and 86.5% at pH 6. The low alkalinity of solution at pH 4 and possibly pH 5 affected the hydroxide flocs formation. The highest removal efficiencies obtained at pH 6 which indicates the appropriate buffering capacity of the solution [18]. The removal efficiencies then dropped gradually for COD and turbidity and rapidly for TSS from pH 6 to pH 8. At pH 8, removal efficiencies of 46.8%, 15.9% and 66.8% were achieved for COD, TSS and turbidity, respectively which shows increasing of pH from 6 to 8 destroys the buffering capacity in the samples and interferes with formation of flocs.

Effect of Coagulant Dose. The dosage of alum was varied from 600 to 3000 mgL^{-1}. The pH was maintained at 6 and the rapid and slow mixing time remained unchanged at 30 minutes. COD, TSS and turbidity removal efficiencies at different alum dosages are shown in Fig. 1(b). The best result was achieved at alum dosage of 1800 mgL^{-1} whit COD, TSS and turbidity removal efficiencies of 56.1%, 79.0% and 83.5%, respectively. Optimum dosage of alum is a critical factor in coagulation process since excessive usage of coagulant results in less vacant sites and consequently restabilising the particles. Overdosing with coagulants can result in restabilising the suspension. If enough aquometallic ions (such as $AlOH^{2+}$, $Al(OH_2)^{+}$ and $Al_7(OH)_{17}{}^{4+}$) are formed and adsorbed, the charges on the particles become reversed and the ionic clouds reform, with negative ions being the counter ions [19].

Effect of Contact Time. After determination of optimum values of pH and coagulant dosage, the rapid mixing was varied for 5 to 30 minutes at 150 rpm [20, 21]. The slow mixing time remained constant at 30 minutes. Fig. 1(c) illustrates COD, TSS and turbidity removal efficiencies at rapid mixing time ranged from 5 to 30 min. The results indicate that increment in rapid mixing duration did not produce any significant improvement on the COD and turbidity removal efficiencies. The

highest removal efficiency was identified to be 58.3% of COD and 75.9% of turbidity at 15 and 5 minutes, respectively. TSS removal however, dropped with increase of rapid mixing time. This can be explained by the rupture of floc caused by prolonged agitation which results in high TSS and turbidity. The highest TSS removal efficiency was 76.0% at 5 minutes rapid mixing time. It can be deduced that a rapid mixing time of 5 minutes gave the most desirable outcome. The slow mixing time was varied from 10 to 60 minutes at 30 rpm [21]. The pH, alum dosage and rapid mixing time were fixed at 6, 1800 mgL^{-1} and 5 minutes, respectively. Fig. 1(d) shows the removal efficiencies of COD, TSS and turbidity at different slow mixing time. The profile of COD shown in Fig. 1(d) indicates that the slow mixing time rise did not cause any major effect on removal efficiencies. The highest COD removal efficiency was found to be 57.3% at 30 minutes of slow mixing time. The TSS and turbidity removal generally exhibited the same pattern of curve as the time increased. The maximum removal efficiency for turbidity (79.5%) and TSS (82.0%) were observed at 10 minutes.

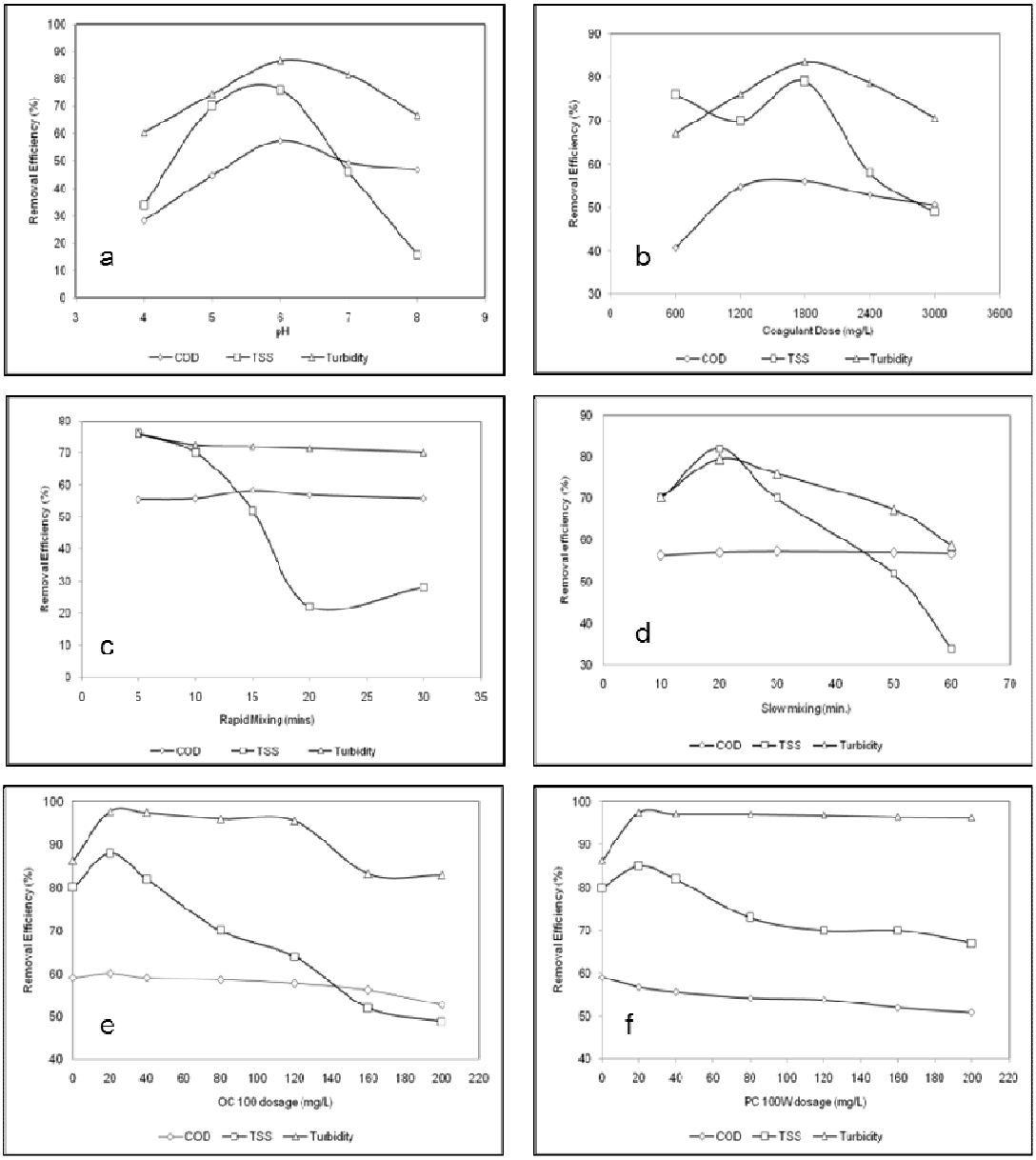


Figure 1. (a) Effect of pH on COD, TSS and Turbidity removal efficiencies, (b) effect of coagulant dosage on COD, TSS and Turbidity removal efficiencies, (c) effect of rapid initial mixing on COD, TSS and Turbidity removal efficiencies, (d) effect of slow mixing on COD, TSS and Turbidity removal efficiencies, (e) COD, TSS and Turbidity removal efficiency with addition of PC 100W flocculant, (f) COD, TSS and Turbidity removal efficiency with addition of OC 100 flocculant.

The drastic drop after 30 minutes is best explained by the agitation which caused the rupture of floc fragments, resulting in high TSS and turbidity.

Flocculation. With the confirmed optimum conditions, the jar tests were repeated with the addition of flocculants (PC 100W and OC 100) with a range of 20 - 200 mgL^{-1}. Fig. 1(e) and (f) illustrate the COD, TSS and turbidity removal efficiencies using PC 100W and OC 100. COD removal efficiency decreased by addition of PC 100W and the highest removal efficiency was obtained at 20 mgL^{-1} flocculant dose (56.8%). This was lower than the removal efficiency achieved without addition of flocculant (59.0%). As shown in Fig. 1(f) the TSS and turbidity removal efficiency was decreased with increasing of flocculant dosage in range of 20 - 200 mgL^{-1}. This may be due to re-suspension of the particles at higher dosage of flocculant. TSS and turbidity removal efficiencies of 85.0% and 97.5% was achieved using 20 mgL^{-1} of OC 100 flocculant. This result indicates same condition as the one was discussed where flocculant PC 100W was added. The COD removal efficiency was not improved significantly by addition of flocculants. The TSS and turbidity removal efficiency however, initially were boosted with addition of flocculant dose. At 20 mgL^{-1}, TSS removal efficiency of 88.0% was observed and turbidity was removed almost completely. Nonetheless, it was found that the removal efficiencies reduced with increase of OC 100 dosage. Reduction of the removal efficiencies was obviously obtained with any further addition of flocculant. Consequently, TSS and turbidity removal efficiencies were improved by addition of flocculants but not practically for COD. OC 100 proved to be more capable flocculant compared to PC 100W in improving the quality of anaerobically treated POME.

Conclusion

The coagulation-flocculation process has shown to be an efficient process for further treatment of anaerobically digested POME. The study reveals that COD, TSS and turbidity removal efficiencies of up to 59%, 80% and 86% , respectively during coagulation process by optimization of the experiment procedures at pH of 6, 1800 mgL^{-1} of alum dosage and 5 and 20 min of rapid and slow mixing duration. Addition of flocculants OC 100 and PC 100W with fixed alum dosage of 1800 mgL^{-1} enhanced the removal efficiency of TSS (85–88%) and turbidity (97–98%), respectively. The COD removal efficiency however, was not sensibly improved during flocculation. Coagulation-flocculation process in this research could produce the effluent with the pollution levels less than the amount set by Malaysian department of environment (DOE).

The obtained results in this study are useful in suggesting coagulation process using alum to palm oil mill industries to be applied as polishing for anaerobically treated POME since it is energy and cost efficient, controllable and has short duration.

Acknowledgements

The authors gratefully acknowledge Nasaruddin Palm Oil Mill for allowing the collection of anaerobically treated POME as well as KenEp Resources (Asia) Sdn. Bhd. for providing the chemicals in flocculation process.

References

[1] Malaysian Palm Oil Council, Malaysian Palm Oil Council Annual Report, (2011).

[2] A. Malakahmad, Y. C. Sim, Application of response surface methodology to optimize coagulation–flocculation treatment of anaerobically digested palm oil mill effluent using alum, Desalin. Water Treat. 51 (2013) 6729-6735.

[3] K. Vijayaraghavan, D. Ahmad, M. Ezani Bin Abdul Aziz, Aerobic treatment of palm oil mill effluent, J. Environ. Manage. 82 (2007) 24-31.

[4] Y.J. Chan, M.F. Chong, C.L. Law, Biological treatment of anaerobically digested palm oil mill effluent (POME) using Lab-Scale Sequencing Batch Reactor (SBR), J. Environ, Manage. 91 (2010) 1738-1746.

[5] M.D. Mashitah, H. Masitah, M.Y. Kamaruddin, Palm oil mill effluent: A potential substrate for cellulase production. In: The Proceedings of RSCE and 16th SOMChE, Malaysia, (2002) 209–216.

[6] P.W. Wong, N.M. Sulaiman, M. Nachiappan, B. Varadaraj, Pre-treatment and membrane ultrafiltration using treated palm oil mill effluent (POME), Songklanakarin J. Sci. Technol. **24 (2002)** 891–898.

[7] A.L. Ahmad, S. Sumathi, B.H. Hameed, Residual oil and suspended solid removal using natural adsorbents chitosan, bentonite and activated carbon: a comparative study, Chem. Eng. J. **108 (2005)** 179–185.

[8] A. Ariffin, S.A. Shatat, A.R. Nik Norulaini, A.K. Mohd Omar, Synthetic polyelectrolytes of varying charge densities but similar molar mass based on acrylamide and their applications on palm oil mill effluent treatment, Desalination. 173 (2005) 201-208.

[9] A.L. Ahmad, S. Ismail, S., Bhatia, Water recycling from palm oil effluent (POME) using membrane technology, Desalination. 157 (2003) 87 – 95.

[10] T.Y. Wu, A.W. Mohammad, J.Md. Jahim, N. Annuar, Palm oil mill effluent (POME) treatment and bioresources recovery using ultrafiltration membrance: Effect of pressure on membrane fouling, Biochem. Eng. J. 35 (2007) 309-317.

[11] Laws of Malaysia Reprint Act 127 Environmental Quality Act 1974, The Commissioner of law revision, Malaysia under the authority of the revision of laws act 1968 in collaboration with percetakan nasional Malaysia, (2006).

[12] S.M. Phang, K.C. Ong, Algal biomass production in digested palm oil mill effluent, Biol. Waste. 25 (1988) 177–191.

[13] O.S. Amuda, A. Alade, Coagulation/flocculation process in treatment of abattoir wastewater, Desalination. 196 (2006) 22-31.

[14] J.P. Wang, Y.Z. Chen, X.W. Ge, H.Q. Yu, Optimization of coagulant-flocculant process for a paper-recycling wastewater treatment using response surface methodology, Physicochem. Eng. Aspects. 302 (2007) 204-210.

[15] G. Andreas, M. Thrassyvoulos, M. Dionissios, Treatment of olive mill effluents by coagulation-flocculation-hydrogen peroxide oxidation and effect on phytotoxicity, J. Hazard. Mater. 133 (2006) 135-142.

[16] L. Castrillón, Y. Fernández-Nava, M. Ulmanu, I. Anger, E. Marañón, Physico-chemical and biological treatment of MSW landfill leachate, Waste Manage. 30 (2010) 228-235.

[17] APHA, Standard Methods for the Examination of Water and Wastewater, American Public Health Association, Washington, DC, NW. 1992.

[18] L. Metcalf, H.P. Eddy, Wastewater Engineering Treatment and Reuse, Fourth ed., McGraw Hill, 2003.

[19] H.S. Peavy, D.R. Rowe, G. Tchobanoglous, Environmental Engineering, McGraw-Hill, New York, 1985.

[20] A.L. Ahmad, S. Sumathi, B.H. Hameed, Coagulation of residue oil and suspended solid in palm oil mill effluent by chitosan, alum and PAC, Chem. Eng. J. 118 (2006) 99-105.

[21] S. Bhatia, Z. Othman, A.L. Ahmad, Coagulation-flocculation process for POME treatment using *Moringa oleifera* seeds extract: Optimization studies, Chem. Eng. J. 133 (2007) 205-212.

Applied Mechanics and Materials Vol. 567 (2014) pp 122-127
© (2014) Trans Tech Publications, Switzerland
doi:10.4028/www.scientific.net/AMM.567.122

Prediction of Suspended Sediments in a Hyper – Concentrated River Using Neural Networks

Muhammad Raza Ul Mustafa[1, a], Ahmad Safwan Abu Bakar[1,b] ,
Mohamed Hasnain Isa[1,c], Khamaruzaman B Wan Yusof[1,d]

[1]Department of Civil Engineering, Universiti Teknologi PETRONAS, Tronoh 31750, Perak, Malaysia

[a]raza.mustafa@petronas.com.my, [b]ahmadsafwanabubakar@gmail.com,
[c]hasnain_isa@petronas.com.my, [d]khamaruzaman.yusof@petronas.com.my

Keywords: Prediction; Sediment; River; Radial Basis Function; Neural Network

Abstract. Prediction of suspended sediment concentration in hyper-concentrated rivers is a crucial task in modeling and designing of hydraulic structures such as dams, reservoirs, barrages and water intake inlets. In this study, suspended sediment concentration in Kinta River has been predicted using radial basis function (RBF) neural network modeling technique. Time series of suspended sediments and stream discharge data from 1992 to 1995 are used in the training and testing stages of the model. The data were divided into two sections based on the model stages as training and testing. The Thin Plate Spline (TPS) basis function was used to establish TPS - RBF prediction model. The input neurons were selected based on previous studies about the suspended sediment prediction models. The number of hidden neurons was determined by trial and error method. The spread of the basis function was determined by normalization method. The performance of the prediction model was evaluated using three statistical performance measures namely root mean square error (RMSE), coefficient of efficiency (CE) and coefficient of determination (R^2). The results showed that the TPS – RBF model predicted the suspended sediment values close to the observed data. The statistics of the model showed that the prediction model performed very well and produced R^2 values close to one in both training and testing stages.

Introduction

Estimation of suspended sediment is vital in water resources engineering as the design of hydraulic structures relies on suspended sediment. Additionally, suspended sediments also induce pollution in rivers. Therefore, it is important to quantify the suspended sediment in order to mitigate any problems related to sediments, such as pollution and structural concerns. The common method of estimation is by establishing sediment rating curves to describe the relationship between discharge and sediment concentration. However, sediment rating curves method is found to be less accurate and often displays errors due to the non-linear behavior of suspended sediment. Therefore, nonlinear soft computing techniques are more suitable in order to solve nonlinear problem hence accurately estimate and predict the suspended sediment concentration of a river.

In the prediction of suspended sediment concentration, various soft computing techniques such as support vector machine, multiple linear regression, genetic algorithm, neural networks and neuro-fuzzy have been used in previous studies [1-8]. These studies showed that different types and training algorithms of artificial neural network modeling techniques are capable to capture the nonlinear behavior of suspended sediment data [5]. Though, it was observed that while predicting the suspended sediment using radial basis function (RBF) neural networks, the researchers mostly used the Gaussian basis function merely [1, 2]. However, thin plate spline basis function could also be one of the competent tools to predict the suspended sediments in hyper-concentrated rivers. Therefore, this study is intended to predict the suspended sediment behavior in Kinta River using thin plate spline (TPS) basis function neural network and to evaluate the performance of the TPS - RBF model using several statistical measures.

Study Area and Data Source

The research data are obtained from the Department of Irrigation and Drainage (DID) for the river of Sungai Kinta. Sungai Kinta is located in the state of Perak. Kinta River is the second important water resource in Perak. This River has prime importance due to its pivotal source of water supply for drinking as well as irrigation purposes in Ipoh and surrounding areas. Kinta River has the catchment area of 2540 and the major contributors for Kinta River are Pari River, Raia River and Kampar River. The measuring station "Station 431" is located nearby Tanjung Tualang. The geography of the Kinta River catchment in the north and east side comprises high degree of steepness mountains that are covered with forest. The Kinta Valley lies in the southern part of the Ipoh, where mainly the land is used for human activities. Earlier, the Kinta Valley was famous for its tin mining activities which resulted to formation of ponds and lakes around the area. Since 1992 to todate, many development activities were carried out in the catchment as well as on nearby regions of Kinta River [9].

Data of suspended sediment concentration and stream discharge of Kinta River are from the year of 1992-1995. The data were chosen based on the availability of most recent and complete dataset from the DID. Having a complete data is essential in establishing a pattern to be identified by RBF model, in order to produce a highly accurate estimation. Loopholes or missing data will resulted to high skewness and scattered data, which consequently increasing the complexity of the learning process of RBF model. The average value of suspended sediment during training and testing stages are 3322 tons/d and 3860 tons/d respectively.

Development of TPS – RBF Model

The typical architecture of RBF mainly consists of three layers namely input layer, hidden layer and output layer [10-13]. Apart from that, the spread coefficient of the RBF model needs to be determined as well. Prior to the development of RBF model, the data need to be properly selected, partitioned and normalized to reduce the complexity of the learning process of RBF model, hence providing prediction with high accuracy. The schematic architecture of TPS – RBF model is shown in Fig. 1. Where, Qt, Q(t-1) and Q(t-2) are the current, first antecedent and second antecedent values of river discharge respectively. St is the current suspended sediment value [5].

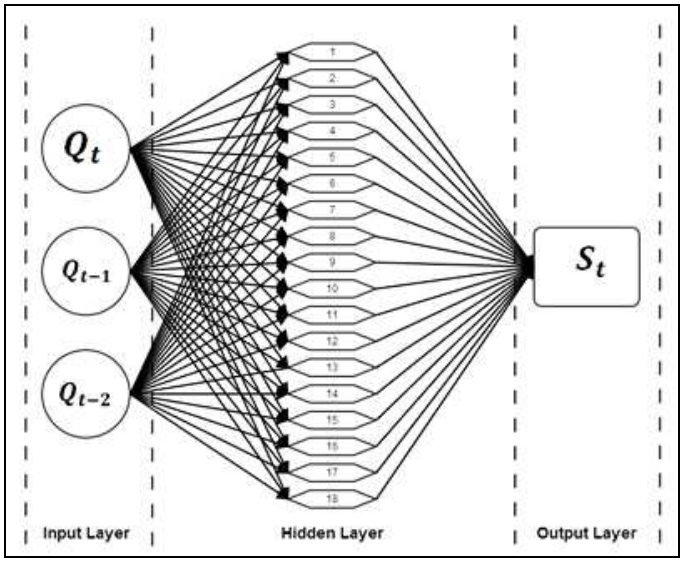


Figure1. Schematic respresentation of TPS – RBF model architecture.

The network consists on three layers viz input, hidden and output layers. Current discharge with two antecedent discharge values are appropriate to predict the current suspended sediment value in the river [5]. Therefore, the input layer contains three input variables, Qt, Qt-1 and Qt-2, which are connected to each of the neurons in the hidden layer. The number of hidden neurons were acheived using trial and error procedure. Since the exteceted output is only the current suspended sediment value, therefore the output neuron is limited to St. The spread of the basis function were determined as normalization method and its value is 0.8077.

Summary of TPS – RBF Model Development

Spread, σ	= 0.8077
Basis Function	= Thin plate spline
Input Variables	= 3 (Q_t,Q_{t-1}, Q_{t-2})
Hidden Layer	= 18 neurons
Output Neuron	= 1(S_t)

Results and Discussion

Time series of suspended sediment data at Kinta River was successfully predicted using thin plate spline basis function neural network. The comparison between time series of observed and predicted suspended sediment concentration during training stage is shown in Fig. 2. It can be observed that the RBF model sucessfully learned the exact pattern of the data and produced predicted values close to the observed ones. This showed that the model is trained well and could be able to capture nonlinear behavior of suspended sedimen data during the testing stage. The comparison between the observed and predicted value during testing stage is shown in Fig. 3. Similar to the training stage, the predicted and observed data are close to each other verifying that the good performance of the model at the testing stage. The predicted values at testing stage followed the exact pattern of the observed data.

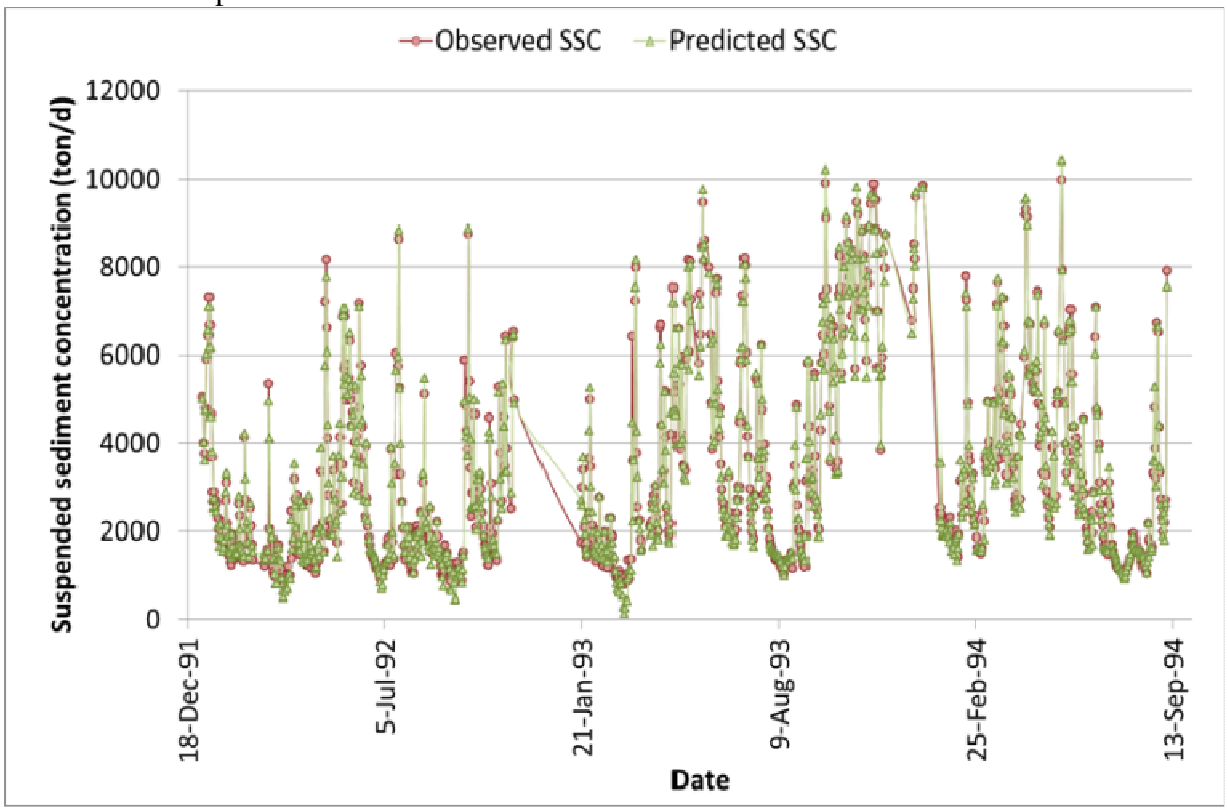


Figure 2. Comparison of time series of observed and predicted suspended sediment concentration during training stage.

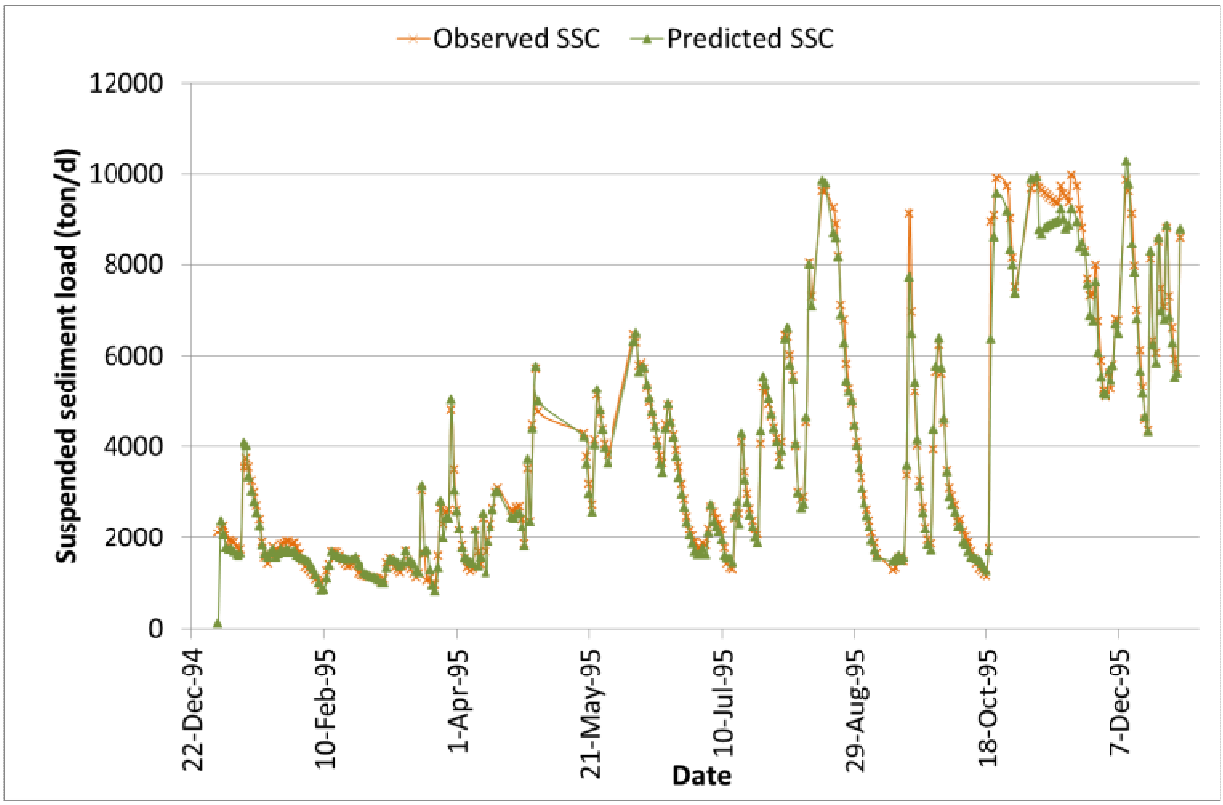


Figure 3. Comparison of time series of observed and predicted suspended sediment concentration during testing stage.

A statistical analysis was performed to evaluate the performance of the RBF model. The results were analyzed using three different statistical analysis measures root mean square error (RMSE), coefficient of efficiency (CE) and coefficient of determination (R2). A summary of perforamnce statistics of the model is shown in the following Table 1.

Table 1. Statistical Analysis of Prediction Performance

Data Set	*RMSE*	*CE*	R^2
Training	267	0.9852	0.9856
Testing	319	0.9845	0.9884

The performance statistics of the model shows that the RMSE produced during training and testing stages are 267 and 319 respectively. The RMSE value during training and testing stages are 1/12 of the average value of the suspended sediment data (i.e. 3322 & 3860 tons/d) during the training and testing stages respectively. This indicates that the model performed very well and produced very less error with respect to the mean values of the datasets. Another most important statistical measure used is Nash- Sutcliffe efficiency coefficient (CE). Predictive performance in term of efficiency of hydrological models is gauge by CE [14]. Both datasets of training (CE = 0.9852) and testing (CE = 0.9845) stages produced significantly high value of efficiency, which are close to 1. These high values of CE validate that the TPS - RBF model developed in this study is able to predict suspended sediments in hyper-concentrated Kinta River with high efficiency. Coefficient of determination (R2) equal to one is considered as ideal case. Table 1 shows that the TPS – RBF model produced coefficient of determination close to one in both training (R2 = 0.9856) and testing (R2 = 0.9884) stages. This shows that the model predicted the sediment values very close to the predicted ones.

Conclusions

Time series of suspended sediment concentration at Kinta River, Perak, Malaysia was successfully predicted using thin plate spline basis function neural network. The study showed that the thin plate spline basis function is able to capture the nonlinear behavior of suspended sediment with three numbers of inputs, eighteen numbers of hidden neurons and with spread value of 0.8077. Furthermore, the statistical analysis for performance evaluation of the model recommended that thin plate spline basis function is competent with other basis functions and training algorithms for prediction of suspended sediments in hyper-concentrated rivers. Therefore, thin plate spline basis function can be used as an alternative of the typical soft computing techniques.

Acknowledgment

The authors are thankful to the Department of Irrigation and Drainage (DID) Malaysia for providing hydrological data required to achieve the objectives of this research.

References

[1] M. R. Mustafa, M. H. Isa, and R. B. Rezaur, "A comparison of artificial neural networks for prediction of suspended sediment discharge in river-a case study in Malaysia," World Academy of Science, Engineering and Technology, vol. 81, pp. 372-376, 2011.

[2] M. R. U. Mustafa, M. H. Isa, and R. R. Bhuiyan, "Prediction of river suspended sediment load using radial basis function neural network-a case study in Malaysia," in National Postgraduate Conference (NPC), 2011, 2011, pp. 1-4.

[3] H. Azamathulla, Y. Cuan, A. Ghani, and C. Chang, "Suspended sediment load prediction of river systems: GEP approach," Arabian Journal of Geosciences, pp. 1-12, 2012.

[4] O. Kisi, A. H. Dailr, M. Cimen, and J. Shiri, "Suspended sediment modeling using genetic programming and soft computing techniques," Journal of Hydrology, vol. 450–451, pp. 48-58, 2012.

[5] M. R. Mustafa, R. B. Rezaur, S. Saiedi, and M. H. Isa, "River Suspended Sediment Prediction Using Various Multilayer Perceptron Neural Network Training Algorithms - A Case Study in Malaysia," Water Resources Management, vol. 26, pp. 1879-1897, 2012.

[6] E. Kakaei Lafdani, A. Moghaddam Nia, and A. Ahmadi, "Daily suspended sediment load prediction using artificial neural networks and support vector machines," Journal of Hydrology, vol. 478, pp. 50-62, 1/25/ 2013.

[7] Q.-J. Liu, Z.-H. Shi, N.-F. Fang, H.-D. Zhu, and L. Ai, "Modeling the daily suspended sediment concentration in a hyperconcentrated river on the Loess Plateau, China, using the Wavelet–ANN approach," Geomorphology, vol. 186, pp. 181-190, 2013.

[8] M. R. Mustafa, M. H. Isa, and R. B. Rezaur, "Artificial Neural Networks Modeling in Water Resources Engineering: Infrastructure and Applications International," World Academy of Science, Engineering and Technology, vol. 62, pp. 341-349, 2012.

[9] M. K. Y. Nabeel M. Gazzaz, Ahmad Zaharin Aris, Hafizan Jauhir and a. M. F. Ramli, "Kinta River Water Quality and Land Use Patternrecognition and Modeling Using Artificial Neural Network (ANN)," Proceedings of Postgraduate Qolloquium Semester 1 2009/2010, pp. 169 - 177, 2010.

[10] M. R. Mustafa, R. B. Rezaur, H. Rahardjo, and M. H. Isa, "Prediction of pore-water pressure using radial basis function neural network," Engineering Geology, vol. 135–136, pp. 40-47, 2012.

[11] A. W. Jayawardena, Pengcheng Xu, and W. K. Li, "Radial basis function network for prediction of hydrological time series," Water Resources Systems-Water Availability and Global Change (Proceedings of symposium US02a held during 1UGG2003 at Sapporo. July 2003). IAHS Publ. no. 280. 2003., pp. 260-266, 2003.

[12] M. Alp and H. K. Cigizoglu, "Suspended sediment load simulation by two artificial neural network methods using hydrometeorological data," Environmental Modelling & Software, vol. 22, pp. 2-13, 2007.

[13] D. A. K. Fernando and A. Y. Shamseldin, "Investigation of Internal Functioning of the Radial-Basis-Function Neural Network River Flow Forecasting Models," Journal of Hydrologic Engineering, vol. 14, pp. 286-292, 2009.

[14] J. E. Nash and J. V. Sutcliffe, "River flow forecasting through conceptual models part I - A discussion of principles," Journal of Hydrology, vol. 10, pp. 282-290, 1970.

Applied Mechanics and Materials Vol. 567 (2014) pp 128-132
© (2014) Trans Tech Publications, Switzerland
doi:10.4028/www.scientific.net/AMM.567.128

PRELIMINARY INVESTIGATION AND DESIGN CONSIDERATIONS FOR THE REHABILITATION OF TRASH SCREEN AT JOR RESERVOIR LOW LEVEL OUTLET

Jansen Luis[1], Lariyah Mohd Sidek[2], Pierre Y. Julien[3]

[1]Post Graduate Student, UNITEN; [2],UNITEN, Jalan IKRAM-UNITEN, 43000 Kajang, Selangor;
[3]Department of Civil Engineering, Colorado State University, Fort Collins
[1]jansenla@tnb.com.my; [2]lariyah@uniten.edu.my; [3]pierre@engr.colostate.edu

Keywords: Reservoir drawdown, reservoir sedimentation, rehabilitation of low level outlet.

Abstract. Jor reservoir was constructed to assure flow regulation for the Woh hydroelectric power station, as well as to provide storage for flood control. The reservoir outlet is frequently operated once every three months to flush the deposited sediments accumulated within the reservoir. Preliminary testing and inspection on the reservoir outlet revealed that the trash screen located at upstream of reservoir outlet had been damaged and dislodged creating a large opening at the trash screen thus permitting entry of larger logs which blocks the passage of water through the reservoir outlet. Bathymetric survey showed the total height of sediment deposition above the reservoir outlet covering the trash screen was estimated at approximately 13 m. The sediment volume estimated to be cleared from above the reservoir outlet area is 15,000 m^3. Soil investigation conducted shows that the sediments deposited within the reservoir exhibits various different profile and characteristics. The average sediment distribution at deeper depths closer to the trash screen was found to be of 27% clay, 26% silt, 43% sand and 4% gravel. The rehabilitation works on structure as the low level outlet serves as an important feature for reservoir sedimentation management as well as for safe flood discharge release as designed for the dam. It is important that the function of the reservoir outlet structure is maintained in accordance to the International Dam Safety Standards.

1. Description of Jor Reservoir

Jor reservoir was constructed to assure flow regulation for the Woh hydroelectric power station, as well as to provide storage for flood control [1]. The reservoir is confined by two earthfill dams namely Jor Dam and Jor Saddle Dam which forms part of the Batang Padang Hydroelectric Scheme. Jor Dam is situated in a narrow section of the valley of the Sungai Batang Padang, together with the saddle dam on the low ridge on the right bank of the river. Jor reservoir covers a total area of 80 acres (350,000 m^2) and has an approximate total storage volume of 3.8 million m^3 with approximately 3.0 million m^3 as live storage for hydropower power generation. During the preliminary stage of construction, a 14 ft (4.3 m) diameter concrete lined diversion was driven from the outlet structure to connect with the spillway tunnel. The Batang Padang River was diverted through the diversion tunnel and spillway tunnel on October 1965 and the diversion tunnel was closed on July 1967 when the impounding of the reservoir commenced.

2. Description of Jor reservoir outlet

The Jor reservoir low-level outlet is equipped with a hollow jet valve of 72 in diameter [1]. The sill level of the outlet intake is 463.30 m (1520 ft). The hydraulic capacity of the valve is 1100 ft³/s (31 m³/s) when the reservoir is draw down just below the sill level of Menglang tunnel intake that is 468.78 m (1538.5 ft). This flow of 31 m³/s corresponds to the average natural inflows to Jor

reservoir of 10 m^3/s plus the peak discharge from Jor power station of 21 m^3/s [2]. In normal hydrologic conditions the low-level outlet has sufficient capacity to evacuate the entire flow entering Jor reservoir. Apart from discharging flood waters and to provide control during reservoir draw down and flood release [3], the reservoir outlet is frequently operated once every three months to flush the deposited sediments accumulated within the reservoir. Above the low level outlet, is the trash screen constructed from pre-cast concrete Class ¾.

3. Problem Statement

The reservoir outlet is an important structure to control the release of flood discharge downstream. This control enable the operator to adhere to the strict restriction imposed by the local authorities to reduce downstream flooding as well to maintain the acceptable water quality during the release. The reservoir outlet began experiencing blockage since 2007 where the guard valve could not be closed completely during regular reservoir drawdown.

Investigation revealed that the trash screen above the reservoir outlet failed to sieve off the large in-coming logs from the upstream end. It was suspected that the trash rack bars of the screen might have been damaged and dislodged creating a large opening at the trash screen thus permitting larger logs to enter the reservoir outlet.

4. Objectives

The rehabilitation Works on the trash screen was immediately recommended to be carried out urgently to enable the continuous use of the outlet valves without further blockages. The objectives of the paper are to:

i. Discuss the findings of the preliminary investigation during project planning;
ii. Discuss the scope of work adopted to execute the underwater rehabilitation work;
iii. Present the basic design parameters for the project.

5. Rehabilitation investigation

Given the complex nature of the project, each component for the project was required to be investigated in detail and custom designed to suit the site condition as well as to maintain an economical cost for the rehabilitation works. Among the field investigation carried out prior to the rehabilitation works includes:

- Bathymetric survey and estimation of sediment depth and volume above reservoir outlet;
- Soil investigation for sediment characteristic profiling;
- Physical dam safety inspection to determine and further signs of damages;
- Reservoir outlet testing to confirm discharge capabilities;
- Dam instrumentation monitoring and interpretation.

5.1 Bathymetric Survey

From the survey, the cross section of the reservoir bed was plotted which shows an average existing bed elevation of 476 m. The reservoir outlet is located at an elevation of 463 m. From the data analyzed, the total height of sediment deposition above the reservoir outlet covering the trash screen was estimated at approximately 13 m. The final sediment volume estimated to be cleared from above the reservoir outlet area was 15,000 m^3.

5.2 Soil Investigation

Soil investigation was carried out in accordance with the requirements of BS 5930. The soil investigation report is included in the reference. Samples were extracted at two specific locations namely BH 14 and BH 15. The soil investigation showed that the sediments deposited within the reservoir exhibits various different profile and characteristics. The average observed sediment types at deeper depths closer to the trash screen location have sediment distribution of 27% clay, 26% silt, 43% sand and 4% gravel. As results of the soil investigation, it is concluded that the design of de-sludging mechanism must be of portable heavy – duty submersible pump type with capacity of de-sludging rate ranging between 200 - 300 m^3/hr and capable of de-sludging / dredging a wide range of sediments types and to be fitted with two agitators to stir or churn heavily cemented or compacted type of sludge conditions.

6. Scope of rehabilitation works

The implementation of the entire rehabilitation works includes:-

- To carry out Pre, Interim & Post Hydrographic Survey to continuously monitor the sediment build up at the excavated area;
- To design and construct a complete set of dredger pontoon equipped with the working platform, lifting equipment, mechanical pump, agitators/cutters;
- To carry out de-sludging/dredging Works to clear the sediments, trash, debris, tree branches, etc. deposited on top of the existing trash screen;
- To carry out underwater physical inspection;
- To design, fabricate and install a new high tensile trash screen above the reservoir outlet area;
- To design and fabricate a complete set of turbidity/silt curtains as a separator and as sediment control system;

7. Rehabilitation works design considerations

7.1 Design for dredger and working pontoon

A customized pontoon design was proposed for the project to include all dead and live loading and working platform for all other associated equipments including cutters and compressors, pump handling equipment, air conditioning or heating, anchor booms, production measuring equipment, and pipeline components, power pack, operators, etc. and for the installation of the trash screen, platform launching for divers and stationing of divers equipments (facilities), connecting of the cables with mounted pumps and agitators, etc. The main design parameter considered for the pontoon design is as shown in Table 1.

Table 1: Basic design parameters for dredger and working pontoon

Dredger Pontoon		
Proposed Width, W	15	m
Proposed Length, L	15	m
Proposed Depth, d	1.6	m
Working Pontoon		
Proposed Width, W	6	m
Proposed Length, L	6	m
Proposed Depth, d	1.5	m

7.2 Design selection for dredger pump

The de-sludging pumps was designed to be a complete set of diesel driven de-sludging equipments which includes Portable Heavy-Duty Submersible de-sludging pumps (Dragflow) and fit for deep water dredging / de-sludging activities with capacity range between 200 - 300 m^3/hr, and with compressors or agitators to stir or churn heavily cemented or compacted type of sludge conditions. The pumps, compressors, agitators, etc shall have readily available complete set of locally available spare parts, maintenance. The main design parameter considered for the dredging pump design is as shown in Table 2.

Table 2. Basic design parameters for dredger pump selection

De-sludging Pump Selection		
Sediment Quantity	40,000	tons
Rate Per Hour of Sand	133	tons
Dredging Rate	m3/hr	200 - 300
Specific Gravity of Slurry	2.65	-
Average Particle Size	0.6	mm
Concentration of Solids	30	%
Static Discharge Head, Zd	3	m
Submerged Working Depth, Zm	28	m
Suction Head, Zs	0	m
Total Length of Pipeline	278	m

7.3 Design selection for sediment control system

During the lowering of the reservoir it is highly anticipated that high sediment volumes will convey to the downstream area towards the working or dredged area. Therefore the silt curtain was proposed to be installed at selected locations to reduce the inflow and as containment for the dredged sediments to be pumped into. The technical requirement was designed for moderate current conditions. The silt curtain has the following properties:

- Fabric - Polyester reinforced vinyl high visibility yellow 18 oz/yd^2 weight.
- Connector - Shackled and bolted load lines.
- Flotation - 8" expanded polystyrene over 19 lbs/ft buoyancy.
- Ballast Line/Ballast - 5/16" galvanized chain (1.1 lbs/ft).
- Top Load Line - 5/16" galvanized wire rope enclosed in heavy tubing.

7.4 Design of New Trash Screen

The design of the trash screen includes the provision for overburden loads and pressure from the deposition of sediments, trash, logs, debris, etc. in design for the trash screen. The loads were calculated based on the characteristics of the sediments depths and volume deposited above the reservoir outlet. The new trash screen was designed to be fabricated at factory and install underwater directly on top of the existing trash screen. Suitable factors of safety were adopted in order to determine the most practical depth of sediment deposition expected for a period of 50 years. The metal works installation includes:

- High tensile, hot – dipped steel trash screen including all necessary fittings to be installed above the existing trash screen at the reservoir outlet.

- The new trash screen were to be fully assembled at factory and be installed directly on top of the existing trash screen by drilling;
- The new trash screen mobilization and installation works was designed to be carried out entirely underwater.

During the design of the trash screen, provision is included for over design estimation due to unavailability of as-built drawings, overburden loads and pressure from the deposition of sediments, trash, logs, debris, etc. in design for the trash screen. The basic design values are shown in Table 3.

Table 3. Basic design parameters for steel trash screen

Highest Possible Water Level	1623	ft
Base Level of Screen	1519	ft
Maximum Sediment Deposition (70% of Depth)	64	ft
Sediment Density Characteristics (Saturated and dense sand, silt and clay)	16.5	kN/m^3
Water Density	10	kN/m^3
Density of Submerged Logs	12	kN/m^3

8. Summary

The operation of reservoir outlet is frequently impeded due to the increase in annual sediment deposition in the reservoir. As this sediment deposits further at deeper depths within the reservoir it undergoes rapid consolidation due to the overburden pressure and making the sediment flushing less efficient. Another challenge faced in operation of reservoir outlet is the strict restrictions on discharge regulations imposed by the local authorities. The restriction is normally imposed to reduce flooding to downstream populations as well to control the environmental concerns on water quality during release. The sediment flushing structure such as the low level outlet serves as an important control structure for hydropower plant operators for reservoir sedimentation management as well as for safe flood discharge release as designed for the dam. It is important that the function of the reservoir outlet structure is maintained in accordance to the International Dam Safety Standards.

Acknowledgment

All view expressed are the writers and do not necessarily reflect those of the Tenaga Nasional Berhad.

Reference

[1] Batang Padang Hydro-Electric Scheme, Operating And Maintenance Recommendations, Civil Engineering Structures, Preece, Cardew and Rider, (1968).
[2] Cameron Highlands and Batang Padang Hydro-Electric Rehabilitation Project – Flood Study for Ringlet Reservoir, SNC-Lavalin Power, April (2002).
[3] Jansen, L. Jor reservoir drawdown, safety measures, procedures and challenges, Cameron Highlands and Batang Padang Hydroelectric Scheme, *International Conference on Construction and Building Technology*, ICCBT (2008).
[4] Cameron Highlands And Batang Padang Hydro-Electric Rehabilitation Project – Hydraulic Impact of Shutdown of Sultan Idris II Woh Power Station on Batang Padang River, Safety Measures and Flow Regulation Procedures SNC-Lavalin Power. (2006).

Applied Mechanics and Materials Vol. 567 (2014) pp 133-138
© (2014) Trans Tech Publications, Switzerland
doi:10.4028/www.scientific.net/AMM.567.133

Response of Partially Covered Road Embankments and its Environmental Impact

Khamaruzaman Wan Yusof[1], Syed Muzzamil Hussain Shah[2], Zahiraniza Mustaffa[3], and Ahmad Mustafa Hashim[4]

[1, 2, 3, and 4]Civil Engineering Department, Universiti Teknologi PETRONAS, Malaysia

[1]khamaruzaman.yusof@petronas.com.my

Keywords: Road Embankments, Surface Cover, Tropical Rainfall, Turbidity, Total Suspended Solids

Abstract. Tropical regions have always suffered soil loss by water which deteriorates the surrounding environment in several ways. This paper focuses on one of an issue that under the tropical rainfall event how the newly constructed bare highway affects the water turbidity and total suspended solids in a water channel. The study was based on a pilot scale field test which was constructed in compliance with the real field conditions. The study was limited to the tropical rainfall event of 40 mm/hr, native grass cover, sandy loam, and for the road side slope of 1V:1.5H (~ 30°). To determine the turbidity and total suspended solids (TSS), three plots were observed with the different percentage of covers namely, no cover (plot A-control plot), 50% of the grass covered surface (plot B), and 30% of the grass covered surface (plot C). The purpose of the study was to observe the influence of these three plots on the dependent variables that is turbidity and TSS. The study summarizes that the presence of cover is adequate enough to cope with this issue to an extent. The results obtained showed that the bare soil surface performed worst under the rainfall intensity of 40 mm/hr for both the dependent variables. The maximum turbidity values observed from plot B and plot C were 30% and 90.25% respectively of the maximum turbidity value obtained from plot A. Similarly, the maximum TSS values observed from plot B and plot C were 35.21% and 63.76% respectively of the maximum TSS value observed from plot A.

Introduction

In spite of its limited periphery roads cannot be disregarded while comparing the soil loss with the agricultural activities [1]. The soil loss observed from the exposed embankments is similar to that of observed from the parched lands [2]. By the year 2050, the urban community is expected to reach the globe by 9.5 billion and most of the increment is anticipated in the developing regions like Asia and Africa which are susceptible to water contamination. Roads construction is among the vital source of soil loss which aids the sedimentation process by flowing towards the water channel in the form of surface runoff [3]. Not only the construction activities but the public works, logging activities and agricultural activities are considered equally responsible for the occurrence of soil loss [4]. Road construction induces higher erosion rates as it usually remains bare and uncovered which makes it exposed to the rain drop impact [5] that ultimately influences the natural surrounding [6]. On the contrary, the need of roads is necessary for the economic development of the country [7]. Therefore, to lessen the soil loss phenomenon, immediate surface cover is required to protect the exposed soil surface once the road construction phase is completed [8]. Fig. 1 shows the view of newly constructed bare road embankment affected by the rain drop impact.



Figure 1. Newly constructed embankment [2].

Intimately, 50 to 80 percent of the sediment load which contribute to the stream channels is mainly by soil erosion from the road surfaces [9] that not only aggravate the water carrying capacity of the channel but also affects the aquatic life [10]. A study reported that the construction spoils observed from a newly constructed highway in China were found to be 2-5 million m^3 per 100 km [7]. In the last few tenners the rapid development activities are held accountable for the worsening of the water bodies [11, 12] therefore, this issue has been much prioritized due to its influence to the water channels which deteriorate the channel capacity of the streams and worsen the water quality in the sense of severe turbidity and the presence of suspended particles [13].

There are two tracts through which the sediments reaches the water body that is either by mass failure or by surface erosion. Mass failure occurs in the areas having sharp inclinations and slopes whereas; surface erosion is very common in the areas of stable slopes which usually occur from roads, filled slopes, and cut slopes [14]. The impact of surface erosion allows the extraneous sediments to deposit in the water body [15] which affects the survival of aquatic habitats [16].

With the passage of time surface erosion reduces from the roads compared to its time of construction, as the top soil surface gradually erodes away which exposes the soil beneath that erodes at slow tempo may be due to its different properties [17]. Unpaved roads are the major source of surface runoff which does not allow water to infiltrate and leads to the land degradation by detaching the individual soil particle that flows with the generated runoff [1]. Moreover, the logging roads are considerd responsible both for the sediments deposition in the water body and for the influx of the toxic contaminants to the water channel through road vehicles [18]. Specifically, to mitigate this problematic issue from the exposed road side slope areas immediate soil protection is required.

Research Method

The study was conducted at Universiti Teknologi PETRONAS (UTP), Malaysia. A side slope with the gradient of ~ 30° was observed under the simulated rainfall conditions with the different percentage of land covers. The rainfall intensity opted for the experimental run was 40 mm/hr (the average rainfall event) for which the rainfall data of Perak, Malaysia (2005-2011) was attained and analyzed. Each plot (2 meters length x 6 meters width) was served under the similar simulated rainfall conditions, soil type, and slope inclination for estimating the water turbidity and TSS values from the bare soil surface, 50% of the grass covered surface, and 30% of the grass covered surface. The study area was sheltered by a roof and covered with the plastic so that the plots can be protected in case if the natural rainfall occurs as shown in Fig. 2. The rainfall intensity was adjusted to 40 mm/hr on the flow meter which was kept noticed so that it assures that the rainfall conditions remained constant throughout the experimental phase. A container was placed at the bottom of each plot so that the water samples can be collected after every 15 min for a period two hours. The water samples were collected in the labeled plastic bottles from all the plots so that the samples cannot be

mixed with each other. The individual sample collected was used both for determining the turbidity and TSS values. The samples were then taken to the lab for further processing.

The water samples collected were quite turbid however to compute the turbidity values the dilution of 1 in 50 was used. From the each diluted sample, three samples were collected to determine the water turbidity by using the turbidity meter as shown in Fig. 3 (a & b). For estimating the TSS values, the filter papers were first washed and cleaned which were then placed in the oven at 105° for 24 hours. The dried filter papers were then weighed and labelled. The water samples collected during the experimental runs were then diluted (the dilution used was 1 in 10). Three samples were then taken from the each diluted sample. The filter papers containing suspended particles were dried again for 1 hour and placed in the desiccators for 20 min. The dried filter papers were then weighed and the difference was observed. This gave the average TSS value, obtained at different time intervals as shown in Fig. 3 (c & d).

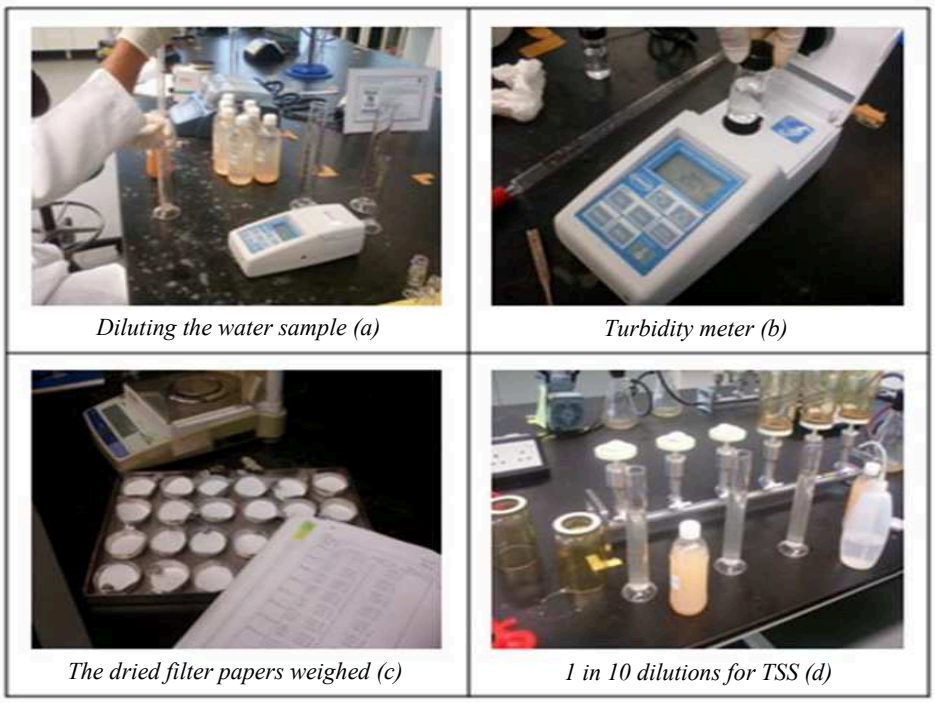


Plot A – Bare soil surface (Control plot)

Plot B – 50% of the grass covered surface

Plot C – 30% of the grass covered surface

Figure 2. Bare soil surface, 50% of the covered surface, and 30% of the covered surface.



Diluting the water sample (a)

Turbidity meter (b)

The dried filter papers weighed (c)

1 in 10 dilutions for TSS (d)

Figure 3. Estimation of turbidity and total suspended solids.

Results and Discussions

The results obtained from plot A were drastic for both the dependent values. The impact of moderate rainfall event of 40 mm/hr dislodged the soil particles, which were carried away by the surface runoff to the bottom channel under the force of gravity. Both the turbidity and TSS values were exceptional when compared with plot B, the reason for which is suggested that there was not provided any surface cover to protect the exposed soil and to distract the generated runoff which raised the turbidity values and the amount of suspended solids in the water channel. However, the maximum turbidity and TSS values obtained from plot A were found to be 1631.5 (NTU) and 69 (mg/L) respectively.

The results obtained from plot B were quite low both for the turbidity and TSS values when compared with the bare soil scenario. The maximum turbidity and TSS values obtained from plot B were 490 (NTU) and 24.3 (mg/L), respectively, which were only 30% and 35% of the maximum turbidity and TSS values obtained from plot A. This shows that even the partially covered soil surface is adequate enough to cope with the moderate rainfall event in reducing the soil loss which in turn reduced the turbidity and TSS.

The results attained from plot C were ineffective. 30% of the ground cover surface did not perform well in mitigating the turbidity and TSS values. However, the maximum turbidity and TSS values obtained from plot C were 1472.5 (NTU) and 44 (NTU) respectively which were quite near to the results obtained from plot A.

The turbidity values obtained from plot A and plot C nearly equated. The maximum turbidity value observed from plot C was found to be 1472.5 NTU which was only 1.10 times lower than the maximum turbidity value obtained from the bare soil surface. The reason for the proximity in the results is suggested that plot C was 70% exposed and only 30% covered. Moreover, the largely spaced grass patches allowed the detached fine soil particles to flow with the generated runoff which raised the turbidity values. Although, the soil loss was also observed from plot B but the closely spaced grass patches retained the soil particles from flowing away which acted as a filter and reduced the turbidity values.

The concentration of TSS attained from plot A and plot C followed the similar scenario as observed for the turbidity for which the similar reason is suggested. However, the graph attained for TSS showed variations at different time intervals for which several reasons are suggested. Firstly, this could have happened as the soil loss occurred at different rates at different time intervals. Secondly, the settled particles could have settled in the bottom container depending on the particle density while collecting the water samples. Lastly, the surface water discharge received in the bottom container could have disturbed the particles in suspension during samples collection.

Fig. 4 shows the graph for turbidity incurred from all the plots under the moderate rainfall event of 40 mm/hr whereas; Fig. 5 shows the result obtained for TSS from all the plots under the same rainfall event.

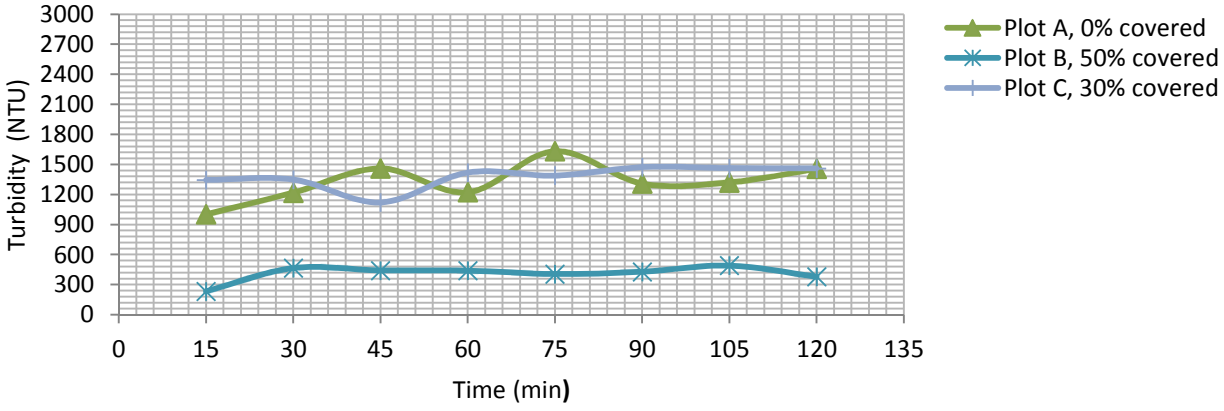


Figure 4. Turbidity values incurred from all the plots under the moderate rainfall event.

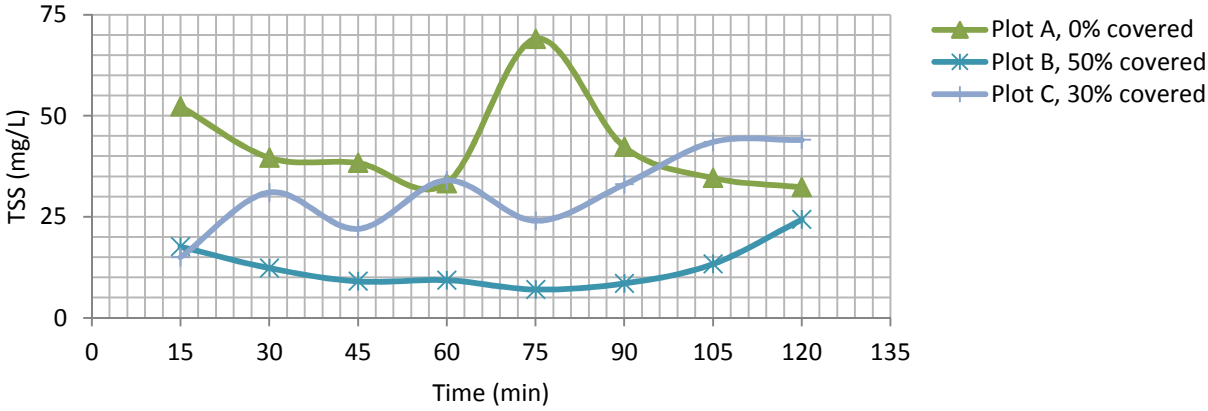


Figure 5. TSS values obtained from all the plots under the moderate rainfall event.

Summary and Concluding Remarks

Based on the results obtained from all the plots this study recommends that the areas where the average rainfall remains moderate must cover the newly constructed bare embankments with at least 50% of the grass covered surface so that it assures immediate protection to the soil loss and reduces the water turbidity and the presence of suspended solids to the water body. Moreover, 30% of the grass covered surface was just examined to notice its efficiency against the moderate rainfall event which did not work. Moreover, the grass growth rate was also observed for plot B, and Plot C. The observation made for plot B showed that the plot area was covered up to 80% within a period of 2 months only after commencing the study whereas; for plot C it hardly reached up to 40% and majority of the grass was observed to be dying.

Acknowledgement

The author earnestly acknowledges University Research Incentive Funds (URIF, code # 22/12) for funding this research. The author would also like thank Universiti Teknologi PETRONAS for the provision of assistantship through the graduate assistantship (GA) scheme and for providing the platform to conduct the study.

References

[1] Ziegler, A.D. and T.W. Giambelluca, Importance of rural roads as source areas for runoff in mountainous areas of northern Thailand. Journal of hydrology, 1997. 196(1-4): p. 204-229.

[2] Cerdà, A., Soil water erosion on road embankments in eastern Spain. Science of the total environment, 2007. 378(1): p. 151-155.

[3] Chow, M., Z. Yusop, and M. Mohamed, Quality and first flush analysis of stormwater runoff from a tropical commercial catchment. Water Science & Technology, 2011. 63(6): p. 1211-1216.

[4] Wycherley, P.R., Conservation in Malaysia1969: Internat. Union for Conservation of Nature and Natural Resources.

[5] De Oña, J., F. Osorio, and P. Garcia, Assessing the effects of using compost–sludge mixtures to reduce erosion in road embankments. Journal of hazardous materials, 2009. 164(2): p. 1257-1265.

[6] Shah, S.M.H., Yusof, K.W., Mustaffa, Z., Hashim, A.M., Mitigation of soil erosion using sludge on road embankments—A conceptual study. in Humanities, Science and Engineering (CHUSER), 2012 IEEE Colloquium on. 2012. IEEE.

[7] Dong, J., K. Zhang, and Z. Guo, Runoff and soil erosion from highway construction spoil deposits: A rainfall simulation study. Transportation Research Part D: Transport and Environment, 2012. 17(1): p. 8-14.

[8] De Oña, J., A. Ferrer, and F. Osorio, Erosion and vegetation cover in road slopes hydroseeded with sewage sludge. Transportation Research Part D: Transport and Environment, 2011. 16(6): p. 465-468.

[9] Hogans, D.K., W.E. Weaver, and M.A. Madej. Long-term on-site and off-site effects of logging and erosion in the Redwood Creek Basin, northern California. in American Geophysical Union meeting on cumulative effects. Technical bulletin. 1986.

[10] Yahyapour, S. and A. Golshan, Removal of Total Suspended Solids and Turbidity within Experimental Vegetated Channel: Optimization through Response Surface Methodology. Journal of Hydro-environment Research, 2013.

[11] Fatt, C.S., Sediment problems and their management in Peninsular Malaysia. Water international, 1985. 10(1): p. 3-6.

[12] Lai, F., J. Ahmad, and A.M. Zaki, Sediment yields from selected catchments in Peninsular Malaysia. IAHS Publications-Series of Proceedings and Reports-Intern Assoc Hydrological Sciences, 1996. 236: p. 223-232.

[13] Gregersen, B., Aalbæk, J., Lauridsen, P., Kaas, M., Lopdrup, U., Veihe, A., & van der Keur, P., Land use and soil erosion in Tikolod, Sabah, Malaysia. ASEAN Review of Biodiversity and Environmental conservation (ARBEC), Jan-Mac, 2003.

[14] Bilby, R.E., Sullivan, Kathleen, Duncan, Stanley H., The generation and fate of road-surface sediment in forested watersheds in southwestern Washington. . Forest Science, 1989. 33((2)): p. 453-468.

[15] Brooks, K.N., P.F. Ffolliott, H.M. Gregersen, and J.L. Thames., Hydrology and the management of watersheds. University of Iowa Press, Ames, IA. 1991.

[16] Moyle, P.B., Leidy R. A., Loss of biodiversity in aquatic ecosystems: evidence from fish faunas. in P.L. Fiedler and S.K. Jains (eds.). Conservation biology: the theory and practice of nature conservation, preservation, and management. Chapman and Hall, New York., 1992.

[17] Lal, R., and Elliot, W., Erodibility and erosivity. Soil Erosion Research Methods. St. Lucie Press, Delray Beach, FL, 1994.

[18] Coffin, A.W., From roadkill to road ecology: a review of the ecological effects of roads. Journal of Transport Geography, 2007. 15(5): p. 396-406.

Applied Mechanics and Materials Vol. 567 (2014) pp 139-143
© (2014) Trans Tech Publications, Switzerland
doi:10.4028/www.scientific.net/AMM.567.139

Survival of *Pseudomonas putida* for Biodiesel Blend (B5) in Soil Bioremediation

N. M. Sunar [a,1], Q. Emparan[b,2], A. T. A. Karim[c,3], S.F.M. Noor[d,4], M. Maslan[e,5]

[a,e]Department of Chemical Engineering Technology, Faculty of Engineering Technology (FTK), Universiti Tun Hussein Onn Malaysia (UTHM), 86400, Parit Raja, Batu Pahat, Johor, 86400, Parit Raja, Batu Pahat, Johor, Malaysia

[b,c] Department of Water And Environmental Engineering, Faculty of Civil And Environmental Engineering (FKAAS), University Tun Hussein Onn Malaysia (UTHM) 86400, Parit Raja, Batu Pahat, Johor, Malaysia

[d]Department of Science and Mathematics, Centre for Diploma Studies, University Tun Hussein Onn Malaysia (UTHM) 86400, Parit Raja, Batu Pahat, Johor, Malaysia

[1]shuhaila@uthm.edu.my,[2]quinston89@gmail.com,[3]tarmizi@uthm.edu.my,[4]fatimah@uthm.edu.my, [5] masayu@uthm.edu.my

Keywords: Bioremediation, Biodiesel Blend (B5), *P.putida*

Abstract. The soil-contaminated areas can be cleaned-up by the emerging science and technology of bioremediation. This study aims to investigate the survival of *Pseudomonas putida* (*P. putida*) as biodegradable agent in soil contaminated with biodiesel/diesel blends (B5). The spillage simulation of B5 was conducted at laboratory scale for 24 days of treatment. The results show that contamination of biodiesel/diesel blends in soil induced a reduction growth of *P. putida*. The growth of *P. putida* was measured high in control compared to B5 sample proved the inhibitory effect has occurred. Nevertheless, the *P. putida* colonies counts for sample B5 were persisted high until the end of treatment period at 5.0 x10^6 CFU/ml. *P. putida* is very sensitive to any ecosystem perturbation therefore this study notably serves as necessary information and potentially exploits as a useful oil-soil biodegradable agent in soil bioremediation.

Introduction

Diesel-soil contamination has become an attractive topic of scientific research in the 20th century. Major contamination pathways include leakage from underground storage tank or pipelines, tank truck or rail accidents [1]. Based on 'Eurostat' data there were 484.8 million tons of oil products used in the European Union (EU) in 2003, which was by 2% higher than in 2002 [2]. The increase for diesel demand and consumption will make petroleum reserves decrease day by day. Therefore, the scarcity of known petroleum reserves will make several renewable energy sources more attractive. In order to meet the requirements of the Kyoto protocol (1997) and Madrid declaration (1994), several alternatives source of energy especially biodiesel are extensively used as an alternative to diesel fuel. Recently, biodiesel fuels have attracted increasing attention worldwide as blending components or direct replacements for diesel fuel in conventional diesel engines. It can be legally blended and used in many different proportions such as B2 (blend 2% biodiesel + 98% diesel), B5 (blend 5% biodiesel + 95% diesel), B20 (blend 20% biodiesel + 80% diesel) and B100 (100% biodiesel). The most common biodiesel blend is B20, which qualifies for fleet compliance under the Energy Policy Act of 1992 [3]. Since the early 21th century onwards, other states such as Australia, Brazil, Canada, Germany, China, South Korea and also Malaysia are also beginning to mandate that all diesel fuel sold at the petrol stations should at least contain 2% of biodiesel [4]. This indicates that pure biodiesel and their diesel blends will be used in the energy sector attending

to transport vehicles driven by conventional diesel engines in the near future; however this means new threats to the environment.

The commercialization of pure biodiesel and their diesel blends on market can cause environmental damage due to spills. The long term effects of genotoxic compound in contaminated soil can adversely affects the live or well being of many living organisms including human beings, by exposing them through diverse pathways, such as ingestion of plants that uptake soil pollutants and also leaching of compound from contaminated soil to ground and surface water used as drinking water [5]. The contaminated areas can be cleaned-up by a highly promising approach known as bioremediation. It is a technique based on the action of microorganisms, in which hazardous contaminants will be turned into non toxic substances such as carbon dioxide (CO_2), water (H_2O) and biomass [6]. Potentially, bioremediation technology is cost-effective and environmentally friendly compared with conventional physical-chemical treatments.

Increasing attention has been paid to bacteria, which act as efficient tools in the bioaugmentation process. For biological treatment of soil-contaminated, bacteria belonging to the genera *Pseudomonas*, *Acinetobact*or, *Coryneform, Flavobacterium*, and *Burkholderia* were often used [7, 8, 9]. Even though natural soil bacteria such as *Pseudomonas* can present in dormant or slow-growing state, but when stimulated by optimum environmental conditions, they multiply rapidly and then adapt to new environment. The microbial growth is one of the consequences of the biodegradability of biodiesel/diesel blends [4]. Therefore, this study aims to evaluate the survival of *P. putida* as biodegradable agent focusing on sample of (B5) biodiesel/diesel blend. The growth rate of *P. putida* on contaminated soil with biodiesel/diesel blend were tested and evaluated accordingly.

Materials and Methods

Biodiesel

The biodiesel is palm-based biodiesel which was produced by transesterification with methanol and obtained from Biodiesel Pilot Plant, Faculty of Engineering Technology, Universiti Tun Hussein Onn Malaysia (UTHM). Petroleum diesel oil (EN 590:2004) was purchased from commercial diesel pump station at Parit Raja, Batu Pahat, Johor.

Soil

The soil samples (soil sandy gravel) were taken from campus area. The soil samples were collected in the range of 7-8 kg from the surface of 5-10 cm deep layer of soil.

Pseudomonas Putida Broth Culture

Pure *Pseudomonas putida* ATCC 49128 samples were purchased from United States of America (USA) in dry culti-loop form. They were stored in chiller at temperature of 4 ºC prior to cultivation procedure. Approximately 16g of medium (nutrient broth) was filled into 2000 mL Erlenmeyer flask containing 2000 mL of distilled water. The mixtures were stirred gently and then dissolved by heating on hot plate at temperature of 100 ºC for about 2 hours until complete dissolution. After that, the medium was sterilized in autoclave at temperature of 121 ºC for about 15 minutes. It was then allowed to cool down for a few minutes until its temperature drop in between 35 ºC to 37 ºC. One loops shaft was removed from the handle straight into the medium according to the manufacturer's instruction. The mixtures were then stirred until homogeneous and keep in the chiller at 4 ºC for 48 hours prior to further inoculation procedures.

Soil-Biodiesel/Diesel and *Pseudomonas Putida* Mixture

Spill simulations with biodiesel/diesel blends in soil were carried out in accordance with Taylor [10], with modification. A 5% of biodiesel (20 mL) and 95% of diesel (480 mL) was added into container containing 1000 g of soil for sample B5. The contaminated soil samples were inoculated with approximately 200 mL of *P. putida* broth culture and placed in dark condition. As a control sample another soil was prepared and then inoculated with *P. putida* without addition of both biodiesel and diesel. The day when the soil was mixed with biodiesel, diesel and their blends as well as *P. putida* was considered as Day 0. The measurement of all testing parameters was conducted at interval of three day for up to Day 24 of bioremediation period (Day 0, 3, 6, 9, 12, 15, 18, 21 and 24). After inoculation of *P. putida* into the contaminated soil samples, all testing parameters were subsequently carried out accordance with standard method. All measurements were made in three replications.

Enumeration of *Pseudomonas Putida*

Approximately 25 g of inoculated soil samples were dissolved in 250 mL Erlenmeyer flask containing 225 mL of sterilized distilled water. The flask was shaken on orbital digital shaker with shaking speed of 200 rpm for approximately 30 minutes. After leave for sedimentation time approximately for 2 hours, then 1 mL of supernatant from the flask was placed into seven sterile dilution bottles each containing 9 mL of sterile distilled water in triplicate. Approximately 1 mL of the previous dilution was added into 9 mL of sterile water in other dilution bottles. Next, each sample volume from dilution bottles was passed through a membrane filter under partial vacuum. The filter papers were placed onto warm Chromagar *Pseudomonas* media agar. The Chromagar *Pseudomonas* media agar was prepared according to manufacturer's instruction. Inoculated media agar has been incubated at temperature of 37 ºC in incubator. After 24 hours of incubation the colonies of *P. putida* were counted.

Results and Discussion

Fig. 1 shows the *P. putida* colonies has slightly increased from Day 0 (1.2×10^7 CFU/ml) to Day 9 (5.0×10^7 CFU/ml) for sample B5. The addition of carbon source offered from biodiesel/diesel blends may lead to increase of *P. putida* growth. The hydrocarbons support the survival of microorganisms [11], in this case for *P. putida* as it act as a valuable source of carbon and energy or induce inhibition of *P. putida* colonies and activity.

However, after Day 9, the amount of colony *P. putida* starts to deplete up to 1 Log until Day 24 (5.0×10^6 CFU/ml). The depletion colony *P. putida* might be due to the availability of nutrient in the sample has become low once the bacteria has used them as source of carbon and energy [4]. The same pattern of *P. putida* growth was in line with Schleicher [12] who verified that microbial will be rose up from the beginning but will decreased throughout bioremediation period; however it also depends on fuel composition in samples. The presence of B5 biodiesel/diesel blends into soil was induced a reduction in growth of *P. putida* started at Day 9.

It can be concluded that prolonged bioremediation period reduced the *P. putida* viability. Nevertheless, the amount of *P. putida* is still high which is at 10^6 CFU/ml until up to Day 24 (Table 1). This result indicated that the *P. putida* survival is high. The growth of *P. putida* was elevated high in control sample compared to B5. This indicated that the fuels in sample B5 inhibited the growth of *P. putida* in the soil.

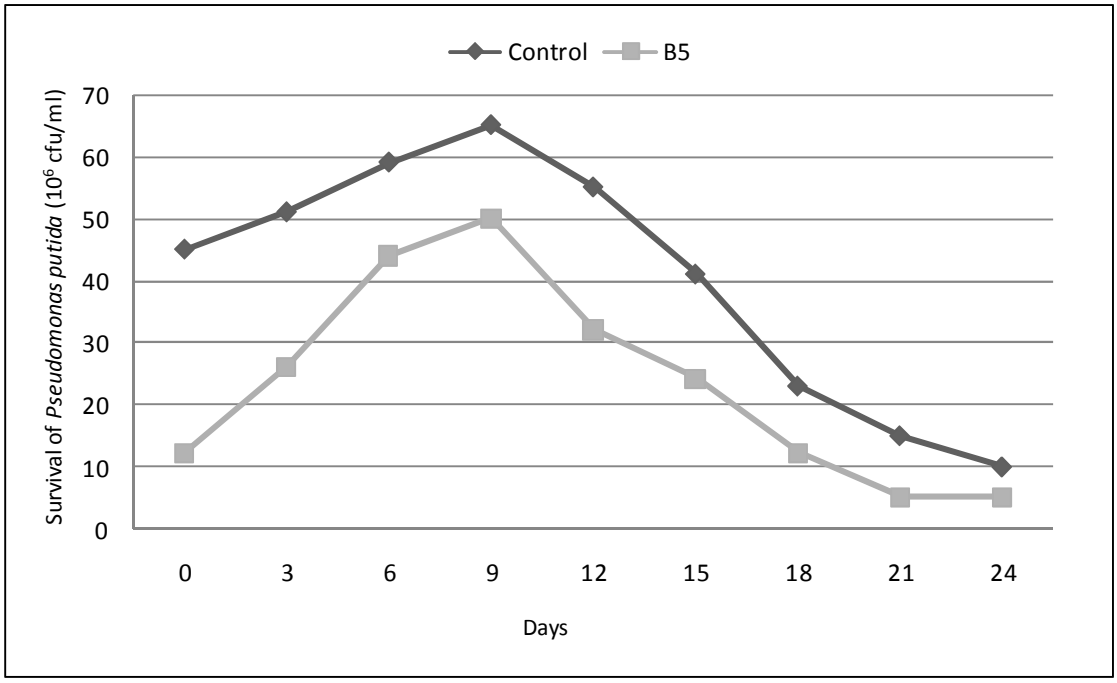


Fig. 1 The survival *of Pseudomonas putida* (10^6 CFU/mL) for sample of B5 and control.

Table: 1 The summary of *P. putida* colonies measured in contaminated soil with B5 biodiesel/diesel blend.

Sample	Bioremediation period (Day); *P. putida* growth (CFU/ml) (n=3)								
	0	3	6	9	12	15	18	21	24
B5	$1.2x10^7$	$2.6x10^7$	$4.4x10^7$	$5.0x10^7$	$3.2x10^7$	$2.4x10^7$	$1.2x10^7$	$5.0x10^6$	$5.0x10^6$
Control	$4.5x10^7$	$5.1x10^7$	$5.9x10^7$	$6.5x10^7$	$5.5x10^7$	$4.1x10^7$	$2.3x10^7$	$1.5x10^7$	$1.0x10^7$

Conclusion

Based on the obtained data it is concluded that the contamination of soil with biodiesel/diesel blends influenced the survival of *P. putida*. This study demonstrated the inhibitory effect on growth of *P. putida* in sample B5; however the *P. putida* colonies counts was persisted high until the end of treatment period. The observation on the growth of *P. putida* in the samples gives good indication the bioremediation process occurred in soil biodiesel/diesel contamination. Future study was recommended by prolonged time length of bioremediation for optimum survival rate of *P. putida* in biodiesel-soil contamination.

Acknowledgement

We are grateful to the Incentive Research Grant (Vote 1192), Research Acculturation Grant Scheme (Vote R002) and Multidiscipline Research Grant Scheme (Vote1104) from Research & Innovation Centre UTHM for financial supports of this work.

References

[1] M. Farhadian, C. Vachelord, D. Duchez, C. Larrochec, In situ bioremediation of monoaromatic pollutants in groundwater : a review, Bioresource Techn. 99 (2008) 5296-5308.

[2] Information on http://epp.eurostat.cec.eu.int/.

[3] Information on http://www.biodiesel.org/docs/ffs-basics/clean-cities-fact-sheet-biodiesel-blends-april.pdf?sfvrsn=4

[4] N. M. Sunar, Q. Emparan, A. T. A. Karim, S. F. M. Noor, M. Maslan, F. Mustafa, N. Khaled, The effectiveness of *Pseudomonas putida* 49128 as biodegradable agent in biodiesel soil contamination in *Proc*. INCIEC, Springer Singapore, (Part VIII), (2014) 817- 823.

[5] T. Watanabe, T. Hiramaya, Genotoxicty of Soil, J.Health Sci. 47 (2001) 433-438.

[6] A.P. Mariano, R.C. Tomasella, D.L.M. Oliveira, J.C., D. Angelis, Biodegradability of diesel and biodiesel blends, African Journal of Biotechnology, 7 (2008) 1323-1328.

[7] S.Y. Wang, C.Vipulanandan, Biodegradation of naphthalene contaminated soils in slurry bioreactor, J. Environ. Eng. 127 (2001) 748-754.

[8] N. M. Sunar, Q. Emparan, A. T. A. Karim, S. F. M. Noor, M. Maslan, F. Mustafa, N. Khaled, The effectiveness of bioremediation treatment for diesel-soil contamination, Advanced Materials Research, 845 (2014) 817-823.

[9] N. M. Sunar, Q. Emparan, A. T. A. Karim, S. F. M. Noor, M. Maslan, F. Mustafa, N. Khaled, Bioremediation of bio-fuel-soil contamination by using *Pseudomonas putida*, Advanced Materials Research, 845 (2014) 138-145.

[10] L.T, Taylor, and D.M. Jones, Bioremediation of coal tar PAH in soil using biodiesel, Chemosphere. 44 (2001) 1131-1136.

[11] A. Mrozik, B. Piotrowska-Seget, S. Labuzek, Bacterial degradation and bioremediation of polycyclic aromatic hydrocarbons, Polish J. Environ. Stud. 12 (2003) 15-25.

[12] T. Schleicher, R. Werkmeister, W. Russ, R. M. Piroff, Microbiological stability of biodiesel-diesel mixture, Bioresour. Technol. 100 (2009) 724-730.

Applied Mechanics and Materials Vol. 567 (2014) pp 144-149
© (2014) Trans Tech Publications, Switzerland
doi:10.4028/www.scientific.net/AMM.567.144

The art of integrated GIS/AHP for siting landfill: A review

Mohamed Osman Saeed[1]*, Hamidi Abdul Aziz[2], Khairun Azizi Mohd Azizli[1,3]

Sustainable Resource Mission Oriented Research (SUREMOR)[1], UTP
[3]Chemical Engineering Department,
Universiti Teknologi PETRONAS[1,3], Bandar Seri Iskandar 31750, Tronoh, Perak, Malaysia

School of Civil Engineering[2], Universiti Sains Malaysia,
14300 Nibong Tebal, Penang, Malaysia

*osman.saeed@petronas.com.my, cehamidi@usm,edu.my
kharun_azizli@petronas.com.my,

Keywords. Geographic information system software; hierarchy process; multi-criteria decision analysis/aid or multi-criteria decision makers; landfill; planning.

Abstract. This article reviewed selected works on how decision makers (DMs) utilize integrated geographic information system (GIS)/analytical hierarchy process (AHP) tools to analyze land suitability for sanitary landfill sites as part of regional planning. We analyzed the hierarchy process of certain pervious works to facilitate better understanding. The innovative work of Siddiqi et al. in 1996 highlighted the advantages of integrating AHP in GIS software and reviewed some limitations. The present paper explained the background study on multi-criteria decision analysis/aid (MCDA) so-called multi-criteria decision makers (MCDM) in conjunction with the advantages of GIS as a new remedy for utilizing the AHP weights of the decision makers. For this study we often use the term MCDA and MCDM.

1. Introduction

A sanitary landfill is a hygienic facility area for dumping of municipal solid waste (MSW) to reduce public and environmental risk (Tchobanoglous et al., 1993). The application of the 3R (reuse, recycle, and reduce) policy significantly minimizes the risk of MSW on the environment (Saeed et al., 2009). Dumping is preferred for MSW over incineration because of the former's lower operational costs and normal employee skills requirement. However, dumping site requires a vertically large land size. Developed nations consider widely recognized parameters to select a new landfill, including 'environmental', 'economical', 'social', 'engineering', and 'political'. Some scholars (Tchobanoglous et al., 1993, Bolton, 1995, Agamuthu, 2003) categorize landfill sites into anaerobic, aerobic, and semi-aerobic based on whether fresh air (including oxygen) is allowed to feed the site or not. The semi-aerobic landfill site of Fukuoka is totally dependent on the pumping and re-pumping of leachate to and from the same landfill site (Theng et al., 2005). This type of cycling purifies and improves the property of leachate and facilitates the settlement of heavy metals inside the landfill. Leachate and gases are products of micro organic activities within the site. This phenomenon requires biodegradation of organic wastes in both aerobic and anaerobic conditions hence, proper management of leachates and gases. Failure to implement these measures will lead to serious groundwater problem, air pollution, and soil damage (over-fertilization). Leachate is a result of the interaction of domestic organic waste with water that percolates through the landfill layer, an interaction that produces highly polluted wastewater (Umar et al., 2010). The complex composition of leachate is highly dependent on the property of domestic waste and the degree of separation and segregation of waste prior to disposal. Less complex leachate results indicate an efficient level of MSW separation. Various technologies and methods are used to clean, purify, and treat leachate to meet the standard guidelines of local authorities before it is discharged to nearby water bodies (Abu Amr et al., 2013; Umar et al., 2010). These methods include physicochemical methods such as coagulation, flocculation, and adsorption (Aziz et al., 2005) of finely dispersed and suspended solid particles (Aziz et al., 2011); adsorption of dissolved impurities such as heavy metals (Igwe and Abia, 2003; Saifuddin and Kunaran, 2005); selective crystallization; reverse osmosis (Ahmad et al.,

2003); and ion-exchange procedure (Bashir et al., 2010). Secondary biological process is performed subsequent to the primary treatment stage.

2. Application of AHP

The first innovation of AHP was completely intended for business orientation. Saaty (1980) was the first to apply this method in a study that minimized the distance between customers and a desirable facility (i.e., a shopping mall). Ho (2007) extensively reviewed the integration of AHP technique with five operational research-based approaches. These approaches include mathematical programming, quality function deployment, meta-heuristics, Strengths Weaknesses, Opportunities and Threats (SWOT) analysis, and data envelopment analysis. AHP has been adopted in education, industry, management, manufacturing, personal engineering, government, etc. as well as in social and political issue (Vaidya and Kumar, 2006; Ho, 2007, 2012). Integrated AHP is robust and enables more realistic decision making compared with AHP alone. The reviewed results show that scholars focus on two problematic areas, namely, transportation route and product design. The first area is close to the application of AHP with GIS theory. Hussein et al. (1987) utilized the AHP model to select a nuclear power plant site for power production and water desalination in Saudi Arabia. They compared four candidate sites that applied AHP with 54 attributes. However, several of these attributes, such as security, cooling water characteristics, fuel shipment considerations, and seawater purity for desalination, were problem-specific. Kathawala and Gholamnezhad (1987) designed a general AHP framework description of siting facility position for theoretical problems. The first hierarchy level included initial operating costs, transportation and labor availability, community acceptability, climate, and governmental power. The AHP model was applied in Japan to find a location for an integrated circuit factory (Tone and Yanagisawa, 1989). The authors selected three sites for further consideration. The second hierarchy level decomposition frame consisted of three factors, namely, technological, economical, and social. Erkut and Neuman (1989) applied the AHP method to locate undesirable facilities through a distributed survey. Researchers studied appropriate methods to locate landfill sites because of the dramatic increase in domestic solid waste. AHP (without GIS) is often used for siting and ranking landfill facilities. Erkut and Moran (1991) is a revolutionary work in this field. They articulated the basic AHP procedure to locate an obnoxious or undesirable facility location in Edmonton City, Alberta, Canada for the first time. They also identified and ranked several landfill sites, as well as demonstrated the effective modeling of landfill siting through AHP. Their study constructed decision hierarchy, established weightings for the decision process, identified and ranked candidate sites, and provided information regarding the robustness of the overall results. Several studies in the critical area of landfill selection were conducted using various applications of AHP following this study (Kontos et al, 2005, Wang et al., 2009, Saeed et al., 2012). The hierarchy model of Erkut and Moran (1991) consisted of a preferred landfill site at the first level followed by three primary decision factors, namely, environmental, social and economic at the second level. Environmental factors at the third level included hydrology, which was further divided into surface water and sub-surface water conditions, drainage, and ecology. Social factors included population, community structure (amenities and land-use condition), social acceptability, traffic, and property value (actual and perceived). Economic factor at the second level had no sub criteria. Environmental and social factors at the third level were subdivided into three and six sub factors respectively. Environmental factor was subdivided into drainage, ecology, and hydrology. Social factors included property value, traffic, community structure, social acceptability, and population. Economic factor remained undivided.

6. AHP application in GIS software for landfill

This section highlights and reviews the structure of the level of decomposition hierarchy process in pioneer and previous studies. Level 1 was dominated by the aim of the study, which is the siting of new sanitary landfill sites. Level 2 was dominated by factors (or named: criteria). Level 3 was dominated by sub-factors and/or sub-criteria. Level 2 (objectives) highlights the concept of

hierarchy decomposition process as a general approach, as reported in literature. Erkut and Moran (1991) selected three factors i.e. environmental, socio-cultural and engineering-economical at level 2 for Edmonton City, Alberta, Canada. Siddiqui et al. (1996) used hydrogeology/geology, land use, and proximity as major factors at Level 2 for Cleveland County, Oklahoma. Charnpratheep et al. (1997) later applied three main factors, namely, human settlement, natural resources, and roads and topography, to site a landfill in Thailand. Kontos et al. (2005) designed the study area of Lemnos Island, North Aegean Sea, Greece through decomposition hierarchy. They considered three main factors: environmental, social, and economic. However, Kontos et al. (2003) adopted a slightly different hierarchy model in Lesovs, Greece. Saeed et al. (2012) designed a hierarchy composed of proximity and engineering at Level 2 of the hierarchy. Siddiqui et al. (1996) divided hydrogeology/geology into depth of bedrock, depth of water table, permeability, slope, and texture at Level 3 (sub-objectives) of the study area to avoid contamination. Similarly, they considered three cities (Moore, Morman, and Noble) and their distances under the proximity factor. No sub-criteria were found for land use. Human settlement factor at Level 3 comprises six sub-criteria, namely, groundwater level, school, village, temple, urban built-up, and archaeology (Charnpratheep et al., 1997). Factors such as surface water, forest, and agricultural land were added under the natural resources criteria. In their study, topography comprised slope, lineament, elevation, cravel, and stoney. Kontos et al. (2005) merged and simplified Levels 2 and 3, of the previous work, into Level 2. For example, hydrology/hydrogeology factor contained water permeability and distance from water resources. Environmental factor was divided into three sub-criteria, namely, surface water, sensitivity ecosystem, and land cover. However, social factor included four sub-criteria, namely, urban areas, cultural areas, visibility, and land use. Technical/economic factors only contained morphology and wind orientation. Proximity at Level 2 was decomposed into four sub-factors, and engineering factor contained two sub-factors (Saeed et al., 2012). Their study decomposed proximity into forest, rivers, electricity power line, and access road. Engineering factor included soil and drainage system. Previous studies show that the hierarchy model at Level 4 is dependent on the decision making and understanding of how this level is derived and constructed.

7. Results and discussions of previous works

Erkut and Moran (1991) found that social factor scored 0.714, which they considered an important factor in their study. Environmental and economic factors had an equal score of 0.143. Population and traffic, which were categorized under social factor in the hierarchy, dominated the highest weight scores in Level 3 at 0.314 and 0.202 respectively. However, social acceptability scored 0.069, the only sub-criteria that accounted for more than 5% of the decision. This result indicates that the contribution and public awareness of Edmonton City, Alberta toward site planning, operation, costs, and subsequent impact are very high. The remaining 10 elements accounted for 19.4% of the decision. The largest single factor represented only 4%. Surface condition under the hydro-geological sub-criterion scored a weight of 0.078, which accounted for more than half of the total weight of environmental factor. Four out of nine sites were considered as candidate sites. Site 4 obtained a score of 0.365, followed by Site 49 with a score of 0.269. The characteristics of these sites were similar to the final preferences of the council. However, they preferred Site 4 because of the small population and short traffic access. Siddiqui et al. (1996) developed spatial AHP for the selection criteria and area attributes. Potential landfill area could be identified and ranked from the data recorded on GIS-based maps. Three scenarios were considered to derive the weights of soil based on relative importance weights, namely, land use and proximity. The suitability map of the best landfill areas were clustered around Norman, the most populated city of the study area. This finding was obtained from scenario two, where proximity was high, followed by soil and land use. Results from scenario three, where land use was high, followed by proximity and soil, shows that the best site was located in the agricultural area. This finding confirmed the result of the weights obtained in scenario one, where soil was ranked high followed by land use and proximity. Sensitivity analysis was conducted, which showed that the areas with the best attributes obtained a higher rank regardless of the weighting scheme. Charnpratheep et al. (1997) showed that the

Boolean model, which recognized 99.8% of the study area, was unsuitable for landfill sites. Fuzzy sets, which differentiated the membership and non-membership grades of potential landfills, were 0.2% and 64.2% respectively. However, the weights derived by AHP yielded satisfactory results over the fuzzy logic applied. According to Ohman et al. (2007), expert responses from developed and developing countries were different. For example, legislation in the USA scored a higher priority rating because of landfill operation by the private sector. Health and safety and environment were rated first for landfills that reached their closing phase. However, these same factors were less prioritized in the earlier planning stage when the distance was more than 1 km from the nearest residential area. Health and safety obtained a slightly higher score and priority in the dry climate region, whereas experts were less concerned about environment and public perception. Saeed et al. (2012) used the hierarchy model from the previous studies to select a study area in Pulau Pinang, Malaysia.

9. Improvements and limitations

The inclusion of a minimum 8 DMs to 12 DMs is recommended in policy studies such as finding a landfill location (Balana et al., 2010). An expert who served as DM evaluated four final landfill sites in Edmonton, Alberta, Canada (Erkut and Moran, 1991). Siddiqui et al. (1996) ignored groundwater and flood plain factors, but emphasized the Cleveland County environment. Charnpratheep et al. (1997) claimed that the AHP model works no better than fuzzy logic in their Thailand study, a finding that was a disadvantage to their research. Although the present application of the AHP method has been successful, both methods have advantages and disadvantages. Ohman et al. (2007) performed an international survey called Dolphin. This method abets the challenges of the applied methodology and assesses the sufficiency of the length of interview by phone and/or by fax. Obtaining the accurate evaluation of the rate or rank of factors provided by outside experts was difficult. Choosing respondents who are knowledgeable and familiar with the study area and who possess similar backgrounds such as language and homogenous environment is recommended in the survey technique. The statistical overview indicates the difficulty of obtaining a conclusion regarding the final rating of factors in Level 2 of the hierarchy based on the geometric mean. Charnpratheep et al. (1997), Kontos et al. (2005), and Saeed et al. (2012) did not conduct a sensitivity analysis in the final research findings, which was considered a disadvantage.

10. Conclusion

This study reviewed landfill technology and its related publications. GIS can store, analyze, and display spatial data. We highlighted the application of AHP, GIS, and GIS/AHP over the last 20 years in selecting sanitary landfills, with particular focus on the application of integrated GIS/AHP. Several GIS studies on landfill selection were also performed. However, GIS/AHP is flexible in applications that provide accurate and informative results when inconsistency ratios and sensitivity analysis are applied. Most of the authors agreed that this approach is utilized to identify and rank a number of landfills. However, the sites were not exact or specific because of the sensitivity of the public and the potential political issues.

Acknowledgment

We take this opportunity to express great thank to Research and Innovation Office (RIO), UTP for the financial support under STIRF Grant No.0153AA-C25/2013. Special thanks extend to all those who assisted one day to finalize this project successfully.

References

[1] Abu Amr SS, Aziz, HA, Adlan MN (2013) Optimization of stabilized leachate treatment using ozone/persulfate in the advanced oxidation process, Waste Management, 33, (6), pp 1434-1441.
[2] Agamuthu, P (2003) Solid waste: Principals and management with Malaysian case studies. Universiti Malaya press, Kuala Lumpur, Malaysia.
[3] Ahmad A, Ismail S, Bhatia S (2003) Water recycling from palm oil mill effluent (POME) using membrane technology. Desalination 157 (1-3): pp 87-95.
[4] Aziz SQ, Aziz HA, Yusoff MS, Bashir MJK (2011) Landfill leachate treatment using powdered activated carbon augmented sequencing batch reactor (SBR) process: Optimization by response surface methodology, Journal of Hazardous Materials, 189, (1–2), pp 404-413
[4] Aziz HA, Yusoff AS, Adlan MN, Zahari MSM, Alias S (2005) Physico-chemical removal of iron from semi-aerobic landfill leachate by limestone filter, Waste Management 24: pp 353-358.
[5] Balana BB, Mathijs E, Muys B (2010) Assessing the sustainability of forest management: An application of multi-criteria decision analysis to community forests in northern Ethiopia. Journal of Environmental Management 91, (6): pp 1294-1304.
[6] Bolton, N, (1995) The Handbook of Landfill Operations, Blue Ridge Solid Waste Consulting, Bozeman, Montana.
[7] Bashir JK, Aziz HA, Yusoff MS, Adlan MN (2010) Application of response surface methodology (RSM) for optimization of ammoniacal nitrogen removal from semi-aerobic landfill leachate using ion exchange resin Desalination, 254, (1–3), pp 154-161.
[9] Charnpratheep K, Zhou Q, Garner B (1997) Preliminary landfill site screening using fuzzy geographical information systems. Waste Management & Research 15: pp 197-215.
[10] Erkut E, Neuman S (1989) Analytical models for locating undesirable facilities. European Journal of Operational Research 40: pp 275-291.
[11] Erkut E, Moran RS (1991) Locating Obnoxious Facilities in the Public Sector: An application of the analytic hierarchy process to municipal landfill sitting decisions. Socioeconomic Planning Science 45(2): pp 89-102.
[12] Ho W, (2007) Integrated analytical hierarchy process and its application-A literature review, European Journal of Operational Research, 186: pp 211-228.
[13] Hussein FM, Obcid MA, El-Malahy KS (1987) Site selection of a dual purpose nuclear power plant in Saudi Arabia. Nuclear Technology Journal, 79: pp 311-321.
[14] Igwe JC, Abia AA (2003) Maize Cob and Husk mill wastes water pollution. as adsorbents for removal of Cd, Pb and Zn ions from waste water. The Physical Scientist 2: pp 83-92.
[15] Ohman KVH, Hettiaratchi JPA, Ruwanpura J, Balakrishnan J, Achari G (2007) Development of a landfill model to prioritize design and operating objectives. Environmental Monitoring and Assessment 135: pp 85-97.
[16] Kontos TD, Komilis DP, Halvadakis CP (2003) Sitting MSW landfills in Lesvos Island with a GIS-based methodology. Waste Management & Research 21, (3): pp 262-327.
[17] Kontos TD, Komilis DP, Halvadakis CP (2005) Sitting MSW landfills with a spatial multiple criteria analysis methodology. Waste Management 25: pp 818-832.
[18] Kathawala Y, Gholamnezhad H (1987) New approach to facility locations decisions, In International Journal System Science 18: pp 389-402.
[19] Saaty TL (1980) The analytical hierarchy process, McGraw-Hill. New York.
[20] Saaty TL (1982) Decision making for leaders. Belmont, Calif: Lifetime Learning Publications.
[21] Saifuddin MN, Kunaran P (2005) Removal of heavy metal from industrial waste water using Chitosan Coated Oil Shell Charcoal. Electronic Journal Biotechnology, 8: pp 1-7.
[22] Saeed OM, Ahamad MS, Aziz HA, Ahmad S (2012) An integrated AHP-GIS technique for landfill siting: A case study in Malaysia, Kuwait Journal of Science and Engineering 39(2B), pp 23-46.
[23] Saeed OM, Hassan NM, Mujeebu MA (2009) Assessment of municipal solid waste generation and recyclable materials potential in Kuala Lumpur, Malaysia. Waste Management 29(7): pp 2209-2213.

[24] Siddiqui MZ, Everett JW, Vieux BE (1996) Landfill sitting using geographic information systems: A Demonstration. Journal of Environmental Engineering 122: pp 515-523.
[25] Tchobanoglous G, Theisen H, Vigil SA (1993) Integrated Solid Waste Managem-ent: Engineering Principles and Management Issues. McGraw-Hill, New York, USA.
[26] Theng LC, Matsufuji Y, Hassan MN (2005) Implementation of the semi-aerobic landfill system (Fukuoka method) in developing countries: A Malaysia cost analysis. Waste Management 25(7) 702–711.
[27] Tone K, Yanagisawa S (1989) Site selection for a large scale integrated circuit factory. In the Analytic Hierarchy Process: Applications and Studies (Golden B, Wasil E, Harker P (Eds.)), in Springer-Verlag, Berlin, pp 242-250.
[28] Umar M, Aziz HA, Yusoff MS (2010) Trends in the use of Fenton, electro-Fenton and photo-Fenton for the treatment of landfill leachate. Waste Management 30 (11): pp 2113-2121.
[29] Vaidya O, Kumar S (2006) Analytic hierarchy process: An overview of applications, European Journal of Operational Research, 169,(1), pp 1-29.
[30] Wang W, Li Q, Guoxue L, Lijun C (2009) Landfill site selection using spatial information technologies and AHP: A case study in Beijing, China. Journal of Environmental Management 90(8): pp 2414-2421.

Applied Mechanics and Materials Vol. 567 (2014) pp 150-154
© (2014) Trans Tech Publications, Switzerland
doi:10.4028/www.scientific.net/AMM.567.150

The Effects of Feedstock Sources and Pyrolytic Temperature on Biochars Sorptive Characteristics

Saba Yavari[1, a], Amirhossein Malakahmad[1, b] and Nasiman B Sapari[1, c]

[1]Civil Engineering Department, Universiti Teknologi PETRONAS, Bandar Seri Iskandar, 31750 Tronoh, Perak, Malaysia

[a]sabayavari2005@yahoo.com, [b] amirhossein@petronas.com.my, [c] nasiman@petronas.com.my

Keywords: rice husk, empty fruit bunches, functionality, elemental composition, surface area, sorption.

Abstract. Biochar addition to soil and water environments has been shown to be effective in sequestering contaminants. This study evaluated the effects of biomass type and the preparation temperatures of biochars on their properties as a sorbent. Rice husk and empty fruit bunches of oil palm were used as the source of biomass for the production of biochars by heating at 300, 500 and 700°C. The biochars properties including functional sites, elemental components and BET surface area were determined to assess the biochars sorption mechanisms. The biochars produced in low temperature were found to have more polar functional groups effective in sorption of polar molecules while the highest temperature increased biochars surface area which is effective in non-selective sorption of contaminations.

Introduction

The biomass-derived char, biochar, is a carbon-rich black substance manufactured as a by-product of energy generation during pyrolysis that is a thermo-chemical conversion of biomass such as plant residues, manure and sludge, under the absence or limited supply of oxygen and at relatively low temperatures of less than 700°C [1]. The pyrolysis technology has high energy recovery, so it is self-sufficient in energy usage. Moreover, it produces less contamination than other conversion processes, e.g. incineration [2].

The biochars effectiveness for specific function is determined by the characteristics of the biochars. The biochars with high surface area can be considered as efficient sorbents to reduce environmental pollutions [3]. Biochar is the precursor for producing activated carbon (AC). Although AC has superior adsorptive properties (high surface area and porosity) but the costly commercial production, presence in toxic form after sorption, the need for regeneration and the loss of sorption efficiency after regeneration make limitations for its ample applications [4]. Biochar is cheap and more sustainable as it does not require chemical reagents and can be made from waste materials [5]. It is possible to improve the sorption properties of biochars to comparable capacities with AC through optimizing the production procedures. The properties of biochar are dependent on the original material and the pyrolysis conditions under which the biochar is made, especially the highest treatment temperatures (HTT) [1,3]. Many research have been conducted to optimize the production conditions to enhance sorption capacity of biochars [3,6,7]. Although the exact mechanism of sorption process has not been confirmed, a number of studies clearly have shown that to optimize the sorption of contaminants it is necessary to increase the biochar surface area through increasing the pyrolytic temperature [8,9]. Based on Yu et al. the biochar made at 850°C rather than 450°C showed greater affinity for sorption of organic materials because of its higher surface area and nano-porosity [7]. A study conducted by Chen et al. showed that with increasing pyrolysis temperature from 100°C to 700°C the surface area of pine needle biochars increased from 0.6 to 490.8 $m^2.g^{-1}$. According to their results, the adsorption shows a transition from a polarity-selective in biochars produced in low temperatures (200-400°C), which promotes specific interactions for polar organic materials, to a porosity-selective process in biochars produced between 500 and 600°C, hindering the sorption of large molecules, and displays no selectivity with biochars

produced in temperature 700°C, suggesting that the pores are all accessible to different molecules [6].

The type of biomass has also effects on the sorption capacity of biochars [1]. Agricultural wastes are among the initial feedstock used in biochar making. Over the recent decades, the total amount of the wastes has been increasing in the world (220 billion tons annually) [10]. Managing the wastes and recycling processes pose a significant environmental burden that leads to environmental pollution [11]. Diverting the wastes into biochar has the potential to reduce anthropogenic emissions from these activities. The volume and weight of the wastes is also reduced through biochar making [12]. Biochar has many potential applications including affinity for sorption of toxic substances, so it is beneficial to make good use of biochar as an added value as its resource is cheap and renewable [13]. In Malaysia, agricultural wastes including rice husk (RH) and oil palm processing wastes are increasing each year leading to disposal problems. It has been estimated that the total amount of produced rice husk is about 350,000 tons.yr^{-1} [14]. RH is a low-priced organic waste, ecologically sound and without environmental pollution which can be found easily in many parts of the world. Empty fruit bunches (EFB) of oil palm are also of the agricultural residuals found in large volumes in Malaysia, as the palm oil sector is the biggest agricultural producer in this country [15]. Considering that Malaysia produces about 18.5 million tons of EFB annually [16], determining environmentally friendly ways to reuse the waste seems vital. RH and EFB can be considered as good source biomass for pyrolysis with their huge production that makes them inexpensive and sustainable. Sorption capacity of RH and EFB biochars are high and they have the potential to be used as sorbent [13,17,18], however, there are limited reports on these wastes as biomass for biochar making. In this study an attempt was done to show the relative importance of the biomass and HTT parameters on the sorptive properties of biochar, which is an important step towards production of designed biochar that fulfils the needed and favorite sorptive properties. So the objective of the study is to determine the quality variations of RH and EFB biochars generated at different pyrolysis temperatures in terms of their sorption capacity.

Methodology

Collection of RH and EFB and Preparation of Samples. The rice husk was obtained from Bernas rice mill in Perak state. Prior to biochar production, the biomass was oven-dried for 12 h at 80°C. EFB was collected from an oil palm mill located in Perak state. The EFB was kept in cold room immediately after collection, and then samples were oven-dried for 12 h at 80°C. Before pyrolysis, the bunches of EFB were chopped into small pieces.

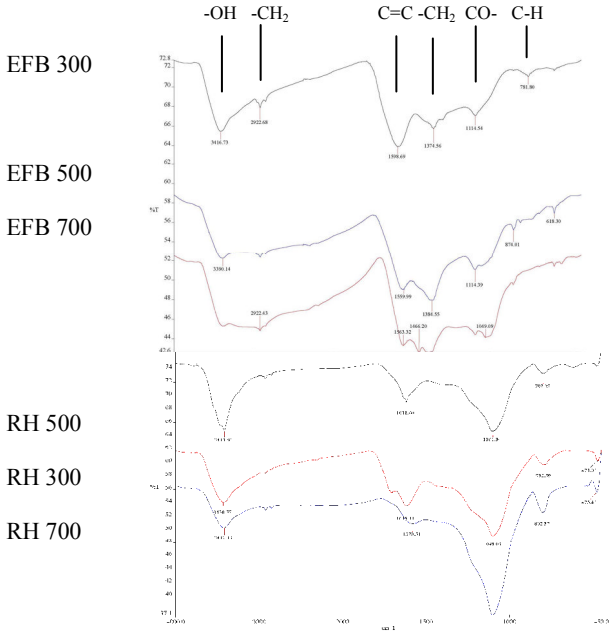
Pyrolysis. The RH and EFB biochars were produced at three different temperatures (300, 500 and 700°C) under limited supply of oxygen in ceramic crucibles covered with fitting lids using a furnace. These temperatures were selected to investigate the effects of different temperatures on sorptive properties of biochars as described by Chen et al. [6]. The produced biochar were ground and passed through a 200 μm sieve.

Determination of Biochars Properties. The characteristics of the produced biochars were analyzed to determine the carbon, hydrogen, nitrogen, sulfur, and oxygen contents by CHNS elemental analyzer (CHNS 932, Leco-US), surface morphology using field emission scanning electron microscope (FE-SEM, Supra 55 VP, Carl Zeiss-Germany), surface area by using Brunauer, Emmet and Teller method (BET, TriStar II 3020, micromeritics-UK) and functional groups by fourier transform infrared spectroscopy (FTIR, Spectrum one, Perkim Elmer-US).

Results and Discussion

The FTIR spectra of the six produced biochars are presented in Fig. 1. The peaks, representing various chemical bonds in the biochars, experienced different changes as the temperature increased in all samples. The intensities of the band at 3650-3200 cm^{-1} (assigned to –OH polar group) showed a decreasing trend with increasing the temperature as a result of dehydration of cellulosic and ligneous components [3]. The bands at 2922 cm^{-1} and 1466-1374 cm^{-1} (assigned to aliphatic -CH_2

units) were detected only in EFB biochars. The sorption peaks at 1619-1559 cm^{-1} are assigned to aromatic C=C vibration and decreased with temperature rise, similar in both samples. The same results were obtained by Chen and Chen in their study on orange peels biochars [19]. Based on their results, with increasing the temperature the aromatic C=C and C=O presented a decreasing tendency, however these peaks were the only bands observed in the highest temperatures, indicating only hard-carbon components remain. A wide absorption peak at 1250-1050 cm^{-1} is attributed to CO- bond which exhibited a growing trend as the temperature increased. The aromatic C-H bond (874-792 cm^{-1}) also showed the same changes suggesting a change from aliphatic to aromatic carbon structures. These changes were more significant in RH biochars.



Figures 1. FTIR spectra of the biochar samples

The data related to elemental compositions, surface area and total pore volume of the biochars samples are shown in Table 1 confirming the FTIR results. Based on the data, with increasing pyrolytic temperature in both RH and EFB biochars the carbon content increased, whereas hydrogen and oxygen contents decreased. Increase in temperature caused the decrease of molar H/C ratio (aromaticity index) which indicates that the high temperature biochars are highly carbonized and exhibit a highly aromatic structure [20]. The decrease in (O+N)/C ratios (polarity index) and O/C ratio (hydrophilicity index) represent that with increasing the temperature the polar functional groups on the surfaces of the biochars decreased and the hydrophilicity increased. Similar pattern were detected from the pyrolysis of pine needles into biochar by Chen et al. [6].

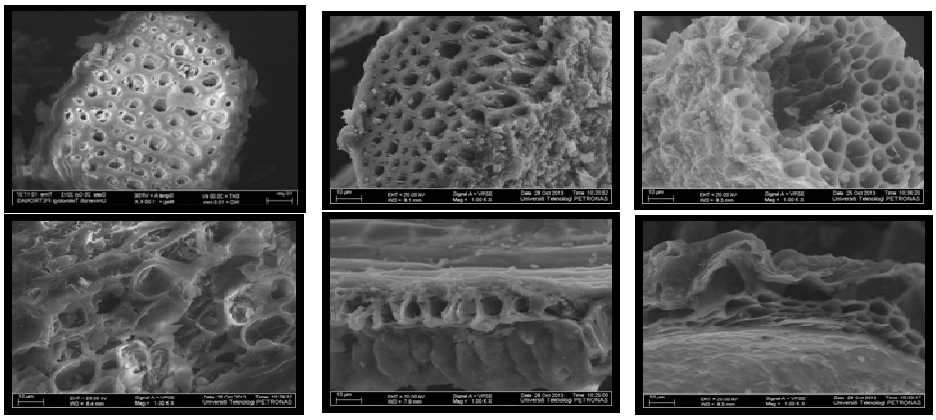
Based on the results indicated in Table 1, the BET surface area of the produced biochars expanded with increasing pyrolytic temperature and reached to 71.428 $m^2.g^{-1}$ in EFB biochars produced at 700°C. This increase was more significant in RH biochars. So that the biochars produced at 700°C represented the surface area of 400.761 $m^2.g^{-1}$ which is quiet large when is compared with AC having 1036 $m^2.g^{-1}$ surface area [6]. Total pore volume also exhibited an increasing trend as the temperature increased in both EFB and RH biochars. According to Chen and Chen the removal of carbon mass as volatile matters from the structure of biomass creates pores in the biochars that result in enlargement of surface area [19].

Table 1. Elemental compositions and atomic ratios, specific surface area (SA), and total pores volume (TPV) of the biohars produced at different temperatures.

Sample	C%	H%	N%	O%	(O+N)/C	O/C	H/C	SA [$m^2.g^{-1}$]	TPV [$mL.g^{-1}$]
EFB 300	**48**	**3.71**	**2.61**	**45.45**	**0.756**	**0.710**	**0.928**	**1.354**	**0.003044**
EFB 500	**49.65**	**1.44**	**3.47**	**45.30**	**0.744**	**0.684**	**0.349**	**-**	**-**
EFB 700	**50.13**	**1.51**	**5.69**	**42.47**	**0.732**	**0.635**	**0.363**	**71.428**	**0.037196**
RH 300	**40**	**2.13**	**0.756**	**55.50**	**1.089**	**1.040**	**0.639**	**12.909**	**0.014599**
RH 500	**39.73**	**1.41**	**0.744**	**54.80**	**1.120**	**1.034**	**0.427**	**-**	**-**
RH 700	**44.31**	**1.15**	**0.732**	**48.10**	**0.937**	**0.814**	**0.312**	**400.761**	**0.09125**

(O+N)/C: Polarity index, O/C: Hydrophilicity index, H/C: Aromaticity index.

The images of SEM analysis are presented in Figures 2 which indicates the presence of honey comb-shaped structure in both RH and EFB biochars. In biochars produced in low temperature the pores were small and blocked. With increasing the temperature they started to get opened, merged and bigger and the walls between the pores became thinner as a result of biomass chemical decomposition effecting on the physical nature of the biochars. It has been shown that thermal degradation of organic compounds starts at temperatures above 120°C losing chemically bound moisture. Hemicelluloses, cellulose and lignin -the major compositions of biomass- are degraded as the pyrolysis temperatures increases from 200 to 500°C [12].



Figures 2: SEM images of produced biochars in 300, 500 and 700°C from left to right (above are EFB biochars and below are RH biochars) in 1000X magnification.

Conclusion

Major changes in biochars, regulated by the pyrolytic temperature, would have huge impacts on their sorptive properties through the changes in chemical compositions, functional groups, surface area and pores size. Biochars produced in high temperature would have high surface area and large pore size that are applicable for sorption of substances including heavy metals and organic materials. The low pyrolysis temperature provides biochars with polar functional sites effective in sorption of polar organic contaminants. The sorptive properties of biochars produced in different conditions can further be investigated for potential removal of different contaminations from the polluted soil and water bodies.

Acknowledgments

We are highly grateful to University Technology PETRONAS (UTP) for the financial supports and Bernas rice mill in Perak state for providing with the rice husk samples.

References

[1] W. Song, M. Guo, Quality variations of poultry litter biochar generated at different pyrolysis temperatures, J. Anal. Appl. Pyrolysis. 94 (2012) 138–145.
[2] Y. Fernández, J. Menéndez, Influence of feed characteristics on the microwave-assisted pyrolysis used to produce syngas from biomass wastes, J. Anal. Appl. Pyrolysis. 91 (2011) 316–322.
[3] L. Zhao, X. Cao, O. Mašek, A. Zimmerman, Heterogeneity of biochar properties as a function of feedstock sources and production temperatures, J. Hazard. Mater. 256 (2013) 1–9.
[4] V.C. Srivastava, I.D. Mall, I.M. Mishra, Adsorption thermodynamics and isosteric heat of adsorption of toxic metal ions onto bagasse fly ash (BFA) and rice husk ash (RHA), Chem. Eng. J. 132 (2007) 267–278.
[5] A. Bridgwater, Renewable fuels and chemicals by thermal processing of biomass, Chem. Eng. J. 91 (2003) 87–102.
[6] B. Chen, D. Zhou, L. Zhu, Transitional adsorption and partition of nonpolar and polar aromatic contaminants by biochars of pine needles with different pyrolytic temperatures, Environ. Sci. Technol. 42 (2008) 5137–5143.
[7] X.Y. Yu, G.G. Ying, R.S. Kookana, Reduced plant uptake of pesticides with biochar additions to soil, Chemosphere. 76 (2009) 665–671.
[8] T.T. Wang, J. Cheng, X.J. Liu, W. Jiang, C.L. Zhang, X.Y. Yu, Effect of biochar amendment on the bioavailability of pesticide chlorantraniliprole in soil to earthworm, Ecotox. Environ. Safe. 83 (2012) 96–101.
[9] H. Zhang, K. Lin, H. Wang, J. Gan, Effect of Pinus radiata derived biochars on soil sorption and desorption of phenanthrene, Environ. Pollut. 158 (2010) 2821–2825.
[10] P. Sugumaran, S. Seshadri, Evaluation of selected biomass for charcoal production, J. Sci. Ind. Res. 68 (2009) 719–723.
[11] G.C. Matteson, B.M. Jenkins, Food and processing residues in California: Resource assessment and potential for power generation, Bioresour. Technol. 98 (2007) 3098–3105.
[12] J. Lehmann, S. Joseph, (Eds), Biochar for environmental management: Science and technology, first edi., Earthscan, Lodon, 2009.
[13] N.Z. Rebitanim, W.A. Wan Ab Karim Ghani, D. Khalid Mahmoud, N.A. Rebitanim, M.A. Mohd Salleh, Adsorption of methylene blue by agricultural solid waste of pyrolyzed EFB biochar, Journal of Purity, Utility Reaction and Environment. 1 (2012) 376-390.
[14] Information on http://www.bernas.com.my/c/ document_library/, 2011.
[15] W. Azlina, D. Wan Ab Karim Ghani, K. Amin, D. Matori, G. da Silva, Physical and thermochemical characterisation of malaysian biomass ashes, The Journal of the Institution of Engineers. 71 (2010) 9-18.
[16] Information on http://www.mardi.gov.my/c/ document_library/, 2011.
[17] A. Masulili, W.H. Utomo, M.S. Syechfani, Rice husk biochar for rice based cropping system in acid soil 1. The characteristics of rice husk biochar and its influence on the properties of acid sulfate soils and rice growth in West Kalimantan, Indonesia, J. Agric. Sci. 2 (2010) 39-47.
[18] S.T. Shafie, M.A. Mohd Salleh, L. Lek Hang, M.M. Rahman, W.A. Wan Abdul Karim Ghani, Effect of pyrolysis temperature on the biochar nutrient and water retention capacity, Journal of Purity, Utility Reaction and Environment, 1 (2012) 323-337.
[19] B. Chen, Z. Chen, Sorption of naphthalene and 1-naphthol by biochars of orange peels with different pyrolytic temperatures, Chemosphere, 76 (2009) 127-133.
[20] Y. Chun, G.Y. Sheng, C.T. Chiou, B.S. Xing, Compositions and sorptive properties of crop residue-derived chars, Environ. Sci. Technol. 38 (2004) 4649–4655.

Applied Mechanics and Materials Vol. 567 (2014) pp 155-160
© (2014) Trans Tech Publications, Switzerland
doi:10.4028/www.scientific.net/AMM.567.155

The Impact of Stormwater Runoff on Nutrient Removal in Sand Columns

HUSNA Takaijudin[1,2 a], AMINUDDIN Ab. Ghani[2,b] and NOR AZAZI Zakaria[2,c]

[1]Department of Civil Engineering, Faculty of Engineering, Universiti Teknologi PETRONAS, 31750, Tronoh, Perak, Malaysia

[2]River Engineering and Urban Drainage Centre, Engineering Campus, Universiti Sains Malaysia, Seri Ampangan, 14300 Nibong Tebal, Penang, Malaysia.

[a]husna_takaijudin@petronas.com.my, [b]redac02@eng.usm.my, [c]redac01@eng.usm.my

Keywords: bioretention; mulch materials; column study; nutrient pollutants; stormwater runoff; treatment efficiency

Abstract. Mulch layer also assists filtration of pollutants mainly larger sediment particles in bioretention. The objective is to evaluate the efficiency of bioretention facilities in removing nitrogen and phosphorus by varying the types of mulch layers through sand column. 200 mm filter media cells consisted of river sand with composited fine and coarse sand. Three types of mulch layer wood chip, tea waste and coconut husk were applied at the top of the sand layer at 50 mm depth. Runoff was monitored and analyzed to measure nutrient concentration within six hours. Woodchip showed the highest capability in removing phosphorus by 60.3% as compared to tea wastes and coconut husk. Lower removal efficiency was seen for nitrogen for all mulch materials. Tea waste provides additional nitrogen in effluent concentration. Coconut husk has a potential to be applied as mulch materials based on its capability even wood chip was seen to be favorably materials.

Introduction

Urban stormwater runoff that flows through road surfaces, parking areas, vehicle and buildings carries a broad range of pollutants that are transported to rivers and other water bodies which affects the environment and ecology negatively. Effects on receiving waters include oxygen depletion, eutrophication, species stress, and toxicity [1]. Bioretention systems are designed to remove both dissolved pollutants and particulate matter from stormwater runoff [2]. Another advantage of bioretention systems is their ability to significantly reduce stormwater volumes through infiltration and evapotranspiration [3]. Bioretention has been demonstrated to be promisingly efficient in the removal of phosphorus and organic nitrogen from infiltrating runoff [4]. A 5 to 8 cm shredded hardwood mulch layer was added to the surface to maintain soil moisture and filter incoming sediment [4]. In a typical configuration; bioretention includes a layer of approximately 75 to 100 cm of an engineered soil/sand/organic media, supporting a mixed vegetated layer [5].

Nitrogen and phosphorus, the primary nutrients implicated in eutrophication, enter water bodies via a variety of pathways [4]. Eutrophication causes algae growth on water surfaces which leads to oxygen depletion and high turbidity levels in aquatic ecosystems. The presence of nitrogen in stormwater runoff may come from fertilizers, atmospheric deposition and nutrient cycling while the presence of phosphorus may also come from fertilizers, atmospheric deposition and other sources such as soil erosion, animal waste and detergents.

Bioretention have shown impressive pollutant removal through laboratory studies where the reduction in concentration of phosphorus (70 to 85%) and ammonium (60 to 80%) [4]. Another study also showed that the selection of filter media plays an important role in removing pollutants especially nitrogen and phosphorus [6,7]. From a study conducted by Hsieh and Davis (2005) on phosphorus removal, the column media with high hydraulic conductivity overlying one with low hydraulic conductivity was more efficient in total phosphorus removal that ranged from 67% to >98% compared to the column media with low hydraulic conductivity overlying high hydraulic conductivity as less permeable soil layer at the bottom of the column increases the retention time between dissolved phosphorus and media [6]. Another study on nitrogen removal whereby two

different columns with different filtration media configuration gave different removal rate where the first column was designed for high-rate infiltration and second column was designed for runoff retention [8]. The second column proved greater net mineral nitrogen removal efficiency compared to the first column as the water was held longer time in the filter media to allow nitrification and denitrification to occur.

Mulch layer is one of the components in bioretention as it has its own functions which lead to it being evaluated in this project. Mulch layer acts as a medium to promote plant growth, maintain the infiltration rate into the soil layer and reduce pollutant concentration [7]. In addition, a thin layer of wood mulch in the bioretention can help to avert erosion from occurring, avoid the soil layer from extreme drying and contribute to the stormwater treatment process [4]. Other than that, Hsieh and Davis (2005) found that the mulch layer acts as a filter for the incoming TSS, prevents underlying media from clogging, maintains the soil during dry weather and provides nutrients for future vegetation [6]. Pine bark, tree fern, rice husk and wood fibers are a number of natural materials that is used to remove dissolved pollutants from aqueous media as they are inexpensive compared to activated carbon and synthetic resin [9]. They also highlighted the common garden store variety hardwood mulch can be used to remove water soluble pollutants such as heavy metals and toxic organic compounds that are normally found in stormwater runoff. Hence, this research was carried out to examine and evaluate the capabilities of different types of mulch materials in removing nitrogen and phosphorus through a sand column and further select the best performance which can be applied for the design and construction purposes.

Material and methods

Sand Preparation. Construction sand was used in this experiment with approximately 80% of coarse sand and 20% fine sand. The combination of sand to make sure it can be distributed uniformly in the column. In order to determine of the particle size distribution of the coarse sand and fine sand, a standard procedure of sieve analysis was conducted using BS 1377: Part 2: 1990 as references. The test was used to determine the sediment grain size distribution as well as the D_{10} sediment size diameter which 10% of the materials are smaller in size and the mean sediment grain size which represented as D_{50} [10].

Column. Three (3) sand columns were designated to the scale of 1:53 with the design and specifications as listed in Table 1. Three (3) layers were set up based on MSMA requirements which representing an impermeable system of bioretention as illustrated in Fig. 1 [11]. These three (3) layers were provided their own functions. Mulch layer can retain moisture for plants to grow and act as a filter for TSS. The thickness of 50 mm was recommended in providing some filtration process of pollutants such as Total Suspended Solids (TSS). Filter layer which consisted of the mixture of sand was functioning to allow the water to seep through and some of the larger particles will be trapped in this layer. It also was used to prevent the migration of mulch particles to the outlet.

Table 1: Design and specification of column setup

Design characteristics	Specification
No. of columns monitored	3
Drainage area	0.04ha
Actual Peak Discharge	8.487L/s
Column diameter	46 mm
Column height	400 mm
Inflow	25 mL/min
Filter media depth	200 mm
Fill media specifications	80% Fine sand and 20% Coarse sand
Mulch layer depth	50 mm
Mulch layer types	Woodchip, coconut fiber tea waste
Gravel	30 mm

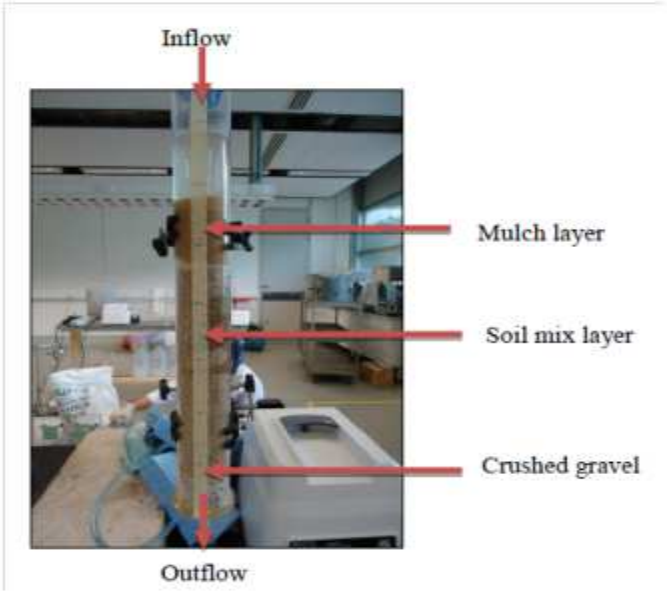


Fig. 1: Filter media configuration.

Selection and Preparation of Mulch Layer. There were three (3) materials was used as mulch which were wood chips, tea leaf waste, and coconut husk. These selections were based on their characteristics and availability. Many researches in the United States and Australia used woodchip as the main material of mulch layer. This material is good in remaining moisture content of topsoil as well as for vegetation survival.

As the main focus will be on the efficiency of the mulch layer in removing the concentration of nitrogen and phosphorus, there will be three different types of mulch that will be used which are:

(1) Tea waste was an organic waste from the restaurant or kitchen waste. However, it is quite limited to use for a larger scale of bioretention.
(2) Wood chip was commonly used in rain garden based on previous studies. However, limited use in Malaysia due to it has been used for another purpose such as furniture and others.
(3) Coconut husk was also organic materials which can easily obtain in large amount from coconut plantation or rural areas. It has potential for mulch purposes.

These materials are commonly used as organic mulch in landscaping, inexpensive and easily available. Organic mulch is preferred over inorganic mulch as it adds nutrients to the soil as it decomposes. Before putting the mulch layer in the sand column, all of the materials were soaked in distilled water and air dried in an oven for 12 hours to remove any contaminants that may have been present. After drying and placed inside the sand column, it was once again flushed with 1 liter of distilled water to cleanse and ensure that water was able to transmit through the mulch layer and down into the underlying soil layer. The sand column was left for 24 hours before the laboratory experiment begins to allow water dried out from the filter media.

Experimental Procedures. An analog pump with a maximum capacity of 100rpm was used to supply the stormwater runoff into the sand columns. An early run was conducted to test the maximum flow rate of the pump which was 42mL/min at 100rpm. The experiment was run in a 6 hour period where a volume of 9 litres stormwater runoff was pumped through the sand column. Therefore, a constant flow rate of 25mL/min was kept throughout the whole experiment. To determine the nutrient content from stormwater**,** stormwater influent and effluent was collected for each sand column (i.e. two (2) samples obtained from each sand column). Each sample was tested and analyzed for nitrogen and phosphorus concentration. Three (3) runs were conducted for each sand column. The stormwater sample collected was from a drain outlet between a parking lot and an open field. The nitrogen concentration was tested using the Nessler Method where the unit is in mg/L NH_3-N. Phosphorus concentration was tested using the Acid Per sulfate Digestion Method where the unit is in mg/L PO_4^{3-}.

Result and Discussion

Particle Size Distribution (PSD). Although particle size distribution of the sand is not the main focus of the project, however, it is important in terms of the hydraulic performance of the sand column. Therefore, sieve analysis was conducted to determine the particle size distribution of the selected coarse and fine sand. The ratio of the soil mix was 80% fine sand and 20% coarse sand. Fig. 2 shows the sieve analysis result of the soil mixture that was used in the sand column. According to Biofiltration Filter Media Guidelines by the Facility of Advancing Water Biofiltration [12] the particle size distribution of the soil mixture should range between 0.075mm to 4.75mm sieve for it to be a well-graded filter media. Based on Fig. 2, the particle distribution of the soil mix was within the range thus, where D_{10} is 0.7 mm, D_{30} is 1.3 mm, D_{50} 1.5 mm and D_{60} is 1.6mm which acceptable to be used in the sand column. Thus, the Coefficient of Uniformity (C_u) is 2.29 and Coefficient of Curvature (C_c) is 1.51 which indicated that the sand sample is classified as uniformly graded.

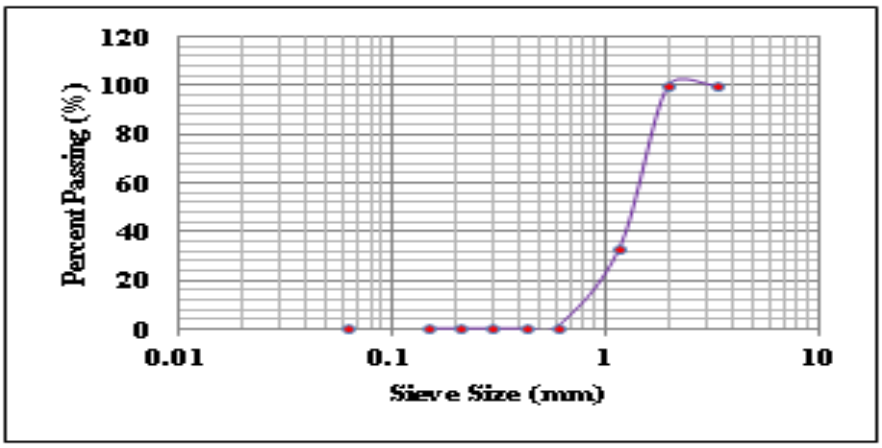


Fig.2: Particle size distribution of river sand composition

Nutrient Removal Efficiency. Fig. 3 illustrates the capability of each mulch material in removing nitrogen pollutants. The effluent concentration of each selected material is constant. Woodchip showed the highest performance in removing nitrogen up to 24% compared to tea leaves and coconut husk. Besides, coconut husk also has a potential in minimizing the nitrogen concentration even though it was only 4.6 % removal. It was suggested to provide a carbon source layer to enhance the capability of this material [13]. However, the effluent concentration of storm water samples was greater once it passes through the column which has tea waste as mulch layer. The rest provide the significant reduction of the effluent concentration.

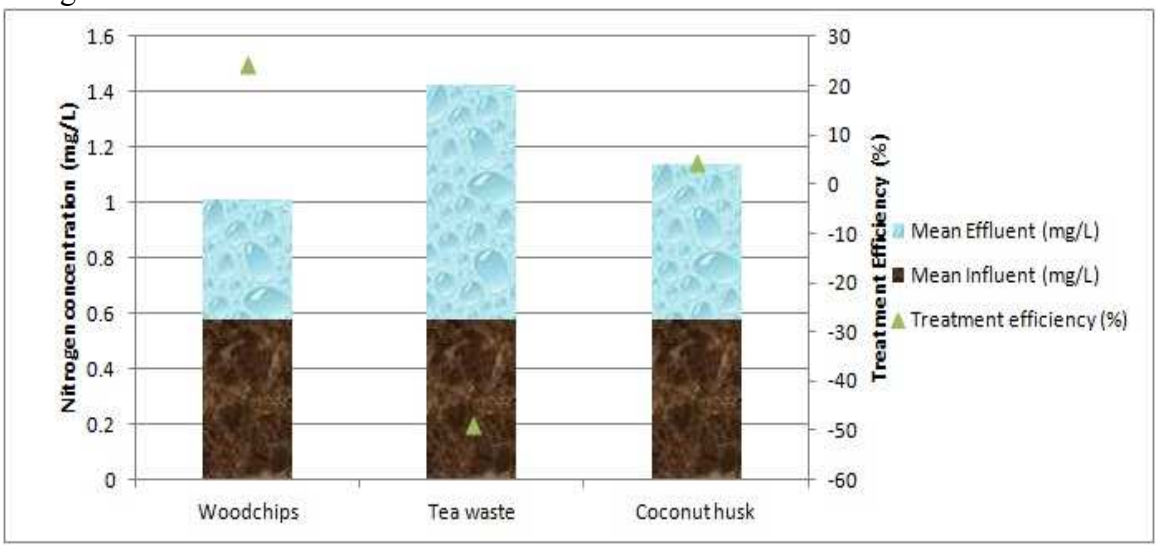


Fig.3: Nitrogen treatment efficiency of selected mulch materials

Thus, the result reflecting treatment efficiency whereby the negative value of treatment performance indicates the additional nitrogen was existed in the effluent which seeps through the tea waste. It showed that tea wastes were unable to show any capability in reducing the nitrogen concentration from the stormwater runoff. The concentration was getting higher in the effluent might be due high production of NO_x. This might happened by the occurrence of nitrification and there was little denitrification was taking place due to limited carbon source [14,15]. Instead, the effluent increased from an average of 0.58mg/LNH_3-N from influent to 0.84mg/LNH_3-N, a 44.8% increment of nitrogen concentration in the sand column. However, it was mentioned that tea leaves is a good compost material as it is high in nitrogen content of 4.15 %, which acts as a natural fertilizer to the plant [16].Besides, all of the mulch materials were able to reduce the phosphorus concentration from the stormwater runoff as shown in Fig. 4. The sand column with woodchip as the mulch layer reduce an average of 1.34mg/L $PPO_4^{3-}$of effluent to 0.35mg/L$PO_4^{3-}$of influent, a reduction of 73.9% of phosphorus concentration. From Fig.4, mulch layer that uses tea leaves reduces the phosphorus concentration an average of 22.8%. For the bioretention that uses the coconut husk, the phosphorus was reduced by an average of 50% treatment efficiency.

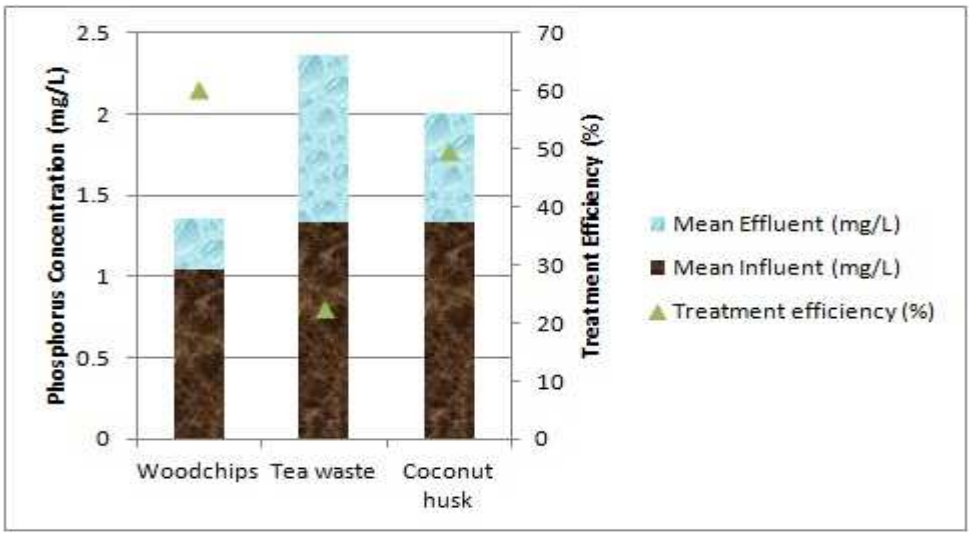


Fig.4: Phosphorus treatment efficiency of selected mulch materials

Comparing the three (3) different mulch layers for nitrogen and phosphorus removal from Fig. 3 and Fig. 4, the woodchip has the best capability with an average efficiency of 24.4% for nitrogen and 60.3% for phosphorus. One main factor is the surface area of the woodchip is larger compared to tea leaves and coconut husk which enables it to adsorb better from the stormwater runoff. Larger surface area allows higher adsorption from the stormwater runoff and water retention. As the surface area gets smaller, in this case tea wastes and coconut husk, the capability to adsorb water decreases which causes the pollutant from incoming stormwater runoff to immediately infiltrate the underlying soil. Although coconut husk has an irregular pore matrix due to the uneven particle size where it is more porous and less permeable compared to the tea leaves, it performed better in removing nitrogen and phosphorus than the tea leaves with an average removal efficiency of 4.6% for nitrogen and 50% for phosphorus. As mentioned earlier, tea leaves were stated as good compost in most landscaping articles. However, it was inefficient in removing the nutrient concentration especially nitrogen.

Conclusion

Bioretention is seen as an attractive stormwater management practice that can be implemented in Malaysia as it shows the ability of removing pollutant from the stormwater runoff. Out of the three organic mulch layer, woodchip has the highest nitrogen and phosphorus removal efficiency with an average removal efficiency of 24.4% for nitrogen removal and 73.2% for phosphorus removal.

From an economical point of view, although the wood chip shows favorable results, the coconut husk would be the possible alternative implemented for rain gardens mainly in tropical countries.

This is because coconut plantation produces higher amounts of this type of waste materials. Coconut husk is a more feasible option to be implemented in a large scale field as it can be obtained easily as coconut husk is thrown out and the hard shells which contain the water and flesh is kept to be sold commercially. Thus, it is one alternative that can be considered to replace woodchip as mulch purposes. Besides, woodchip is quite expensive for landscaping material in Malaysia as it has other uses in the manufacturing and furniture industry.

Further studies will be focused on the actual view of bioretention column which consist of engineered soil in filter media. By having different composition in the filter media, the adsorption rate and water retention capacity would be greater which can promote a higher removal rate. Thus, a future study of correlation between the permeability coefficient and pollutant removal can be conducted to further investigate the efficiency of bioretention in removing pollutants. As the nitrogen removal rate was very low, further research work will be continued by applying a different thickness of the mulch layer in the bioretention column. Then, it will integrate will the full specification of bioretention by adding a vegetation layer can further enhance the adsorption, especially of nitrogen from the stormwater runoff as it is used for plant growth.

References

[1] A. P.Davis, M.Shokouhian, H.Sharma, & C.Minami, Laboratory Study of Biological Retention for Urban Stormwater Management. Water Environment Research, 78(1) (2001) 5-14.
[2] J.Read, T.Wevill, T. Fletcher, & A.Deletic. Variation among plant species in pollutant removal from stormwater in biofiltration systems. Water Research, 42 2008 893-902.
[3] A.Roy-Poirier & Y.Filion. Review of bioretention system research and design: past, present and future. Journal of Environmental Engineering, 136(9) (2010) 878-889.
[4] A.P. Davis, M.Shokouhian, H.Sharma, & C.Minami,. Water quality improvement through bioretention media: nitrogen and phosphorus removal. Water Environment Research, 78(3) (2006) 284-293.
[5] C.Hsieh, A. P.Davis, & B.A. Needelman, Bioretention column studies of phosphorus removal from urban stormwater runoff. Water Environment Research. 79(2), (2007a) 177-184.
[6] C.Hsieh, & A.P.Davis,. Evaluation and optimization of bioretention media for treatment of urban storm water runoff. Journal of Environmental Engineering. 131(11) (2005) 1521-1531.
[7] K.M. DeBusk & T.M. Wynn, Stormwater bioretention for runoff quality and quantity mitigation. Journal of Environmental Engineering, 137(9) (2011) 800-808.
[8] C.Hsieh, A. P. Davis & B.A. Needelman. Nitrogen removal from urban stormwater runoff through layered bioretention columns. Water Environment Research, 79(12), (2007b) 2404-2411.
[9] A.B. Ray, A.Selvakumar & A.N.Tafuri, Removal of selected pollutants from aqueous media by hardwood mulch. Journal of Hazardous Materials, B136 (2006) 213-218.
[10] D.Carpenter & L. Hallam, Influence of planting soil mix characteristics on bioretention cell design and performance. Journal of Hydrologic Engineering, 15(6) (2010) 404-416.
[11] Department of Irrigation and Drainage of Malaysia (DID). Stormwater Management Manual for Malaysia (MSMA): Bioretention Systems. Kuala Lumpur, 2012.
[12] Facility of Advancing Water Biofiltration (FAWB), Stormwater Biofiltration System: Adoption Guidelines. Monash University. Monash: Monash University, Australia. 2009.
[13] H.Yang, D.C.Florence, E.L.Mc Coy, W. A.Dick,& P.S.Grewal, Design and hydraulic characteristics of a field-scale biphasic bioretention rain garden system for stormwater management. Water Science and Technology, 59 (2009) 1863-1872.
[14] H.Kim, E.A.Seagren, & A.P. Davis, Engineered bioretention for removal of nitrate from stormwater runoff. Water Environ. Res., (2003) 355-367.
[15] G.T. Blecken, Y. Zinger, T. M. Muthanna, A.Deletic, T.D. Fletcher,& M. Viklander,. The Influence of temperature on nutrient treatment efficiency in stormwater biofilters systems. Water Science and Technology, 56(10) (2007) 83-91.
[16] D.L. Martin & G. Gershuny, The Rodale of Book Composting:Easy Methods for Every Gardener. USA: Rodale Press, Inc. 1992.

Applied Mechanics and Materials Vol. 567 (2014) pp 161-166
© (2014) Trans Tech Publications, Switzerland
doi:10.4028/www.scientific.net/AMM.567.161

The performance of trapezoidal glass cover solar still during monsoon period of tropical environment

Nasiman Sapari[1,a], Nor Asyidah Mohd Ahmadan[1,b], Ali Riahi[1,c], Orji Kalu Uka[1,d]

[1]Department of Civil Engineering, UniversitiTeknologi PETRONAS, Bandar Seri Iskandar, 31750 Tronoh, Perak, Malaysia

[a]nasiman@petronas.com.my, [b]idah491@gmail.com, [c]ali_riahiupm@yahoo.com, [d]suunyboy2008@yahoo.com

Keywords: Solar Still; Seawater; Brackish Water; Distillation; Solar Energy; Solar Intensity; monsoon; tropical.

Abstract. Seawater or brackish water desalination process using Reverse Osmosis as one of the current treatment technologies is expensive. A cheaper alternative is by using solar still. The paper presented the performance of solar still under tropical environment during monsoon period. The solar still was constructed using black stainless steel basin. Measurement of temperatures, solar intensities and distillate produce were recorded in the month of November and December, 2013, between 8 am and 6 pm. It was found that the distillate production rates obtained varied from 1.88 kg/m^2/d to 2.26 kg/m^2/d with efficiency of 37.7 %.

Introduction

United Nation found that 1.2 billion people at present do not have access to clean drinking water and by the year 2050, between 2 and 7 billion people will face acute water shortage [1]. Rapidly development of a country has caused many environmental problems. Particularly the aquatic environment is suffering from municipal wastewater and industrial effluent from cities and industries. River water quality is currently degraded by sediments from land clearance and solid wastes [2]. According to the World Watch Institute, it has been predicted that in 2025 two third of world population will be facing shortage of drinking water due to water pollution and poor quality of fresh water. This situation will cause water treatment to become expensive. Another problem is the effect of changes of water distribution due to global warming where certain part of the world receives excessive water and floods while other suffers from too little rainfall [3]. In this situation, supply of drinking water can be affected because of serious contamination of water due to flooding or lack of water due to dry condition. During monsoon periods many part of the affected country become flooded and experiencing shortage of water because of operational problems. This paper aims to examine the performance of solar distillation for water supply from brackish or saline water. To overcome this problem, seawater or brackish water is used as the source of fresh water through desalination process but the current technology of desalination is relatively expensive particularly to low income countries. Water desalination using solar still is a cheaper method of getting drinking water by optimizing solar energy to distill seawater or brackish water without chemical or electrical energy.

Solar desalination can be either direct or indirect. Direct solar desalination uses solar energy to produce distillate directly in the solar collector whereas indirect solar desalination combines external energy source with the conventional techniques [13].The efficiency of the basic type solar still with direct solar radiation ranges from 19 % to 39% [22]. External solar energy collector for solar still has been studied. The efficiency of the system in producing water has not been clearly presented although higher rate of production were achieved [22]. Research findings indicate that the efficiency of solar still production is between 1.3 kg/m^2/d to 5.5 kg/m^2/d as presented in Table 1.

Table 1. Yield and Efficiency of different types of solar still

Author	Year	Configuration	Yield kg/m^2/d	Solar intensity (MJ/m^2/d)	Efficiency (%)
Tiwari and Tiwari[13]	2006	Basin solar still	1.3	14.6	22%
Velmurugan et al.[14]	2008	Basin solar still	1.6	16.2	39%
Badran et al.[15]	2005	Solar still with flat plate collector	2.3	23.3	22%
Velmurugan et.al[14]	2008	A fin type solar still	2.5	16.2	60%
Sadineni et al.[16]	2008	A weir type inclined solar still	5.5	26	-
Ward[17]	2003	Plastic solar water purifier	1.41	28	30%

The factors affecting the productivity of solar still are inlet flow rates, water thickness over the absorber plate, solar radiation intensity, ambient temperature and water temperature [19]. To maintain high water temperature, a high incoming radiation must be absorbed by the water in the basin. Efficient solar still require low absorption glazing and a good radiation absorbing surface [19]. The production rate is also affected by the temperature difference between feed water and condensing surface. Large temperature difference will produce more water droplets [20]. Measuring cylinder is used to measure the condensate water. The efficiency of solar still is measured in terms of distilled water output and by comparing the results with previous research result.

The objective of this study is to produce fresh water using trapezoidal glass cover solar still with black stainless steel basin for drinking purpose during periods when water supply is interrupted or very limited.

Materials and Methods

A solar still of 0.1749 m^2 (0.33m x 0.53m) was fabricated and used in this experiment. The still was made from stainless steel with the whole basin surfaces were coated with black paint to increase absorptivity. The bottom and side of the basin were insulated with polystyrene board to prevent heat loss. To collect distillate output, a trough was provided at the lower part of the basin cover. Plastic pipes were connected to the troughs to drain the fresh water to a measuring cylinder. The basin was covered with a commercial clear glass sheet inclined at approximately 35°. The solar still was kept in open area for exposure of direct sunlight. The experimental setup was provided facilities to measure the temperatures at different points of the still (temperatures of water, inner cover and ambient).Water droplets that were formed at the surface of glass cover were collected through inclined water channel located around the base of the solar still trough and finally flows into collection cylinder.

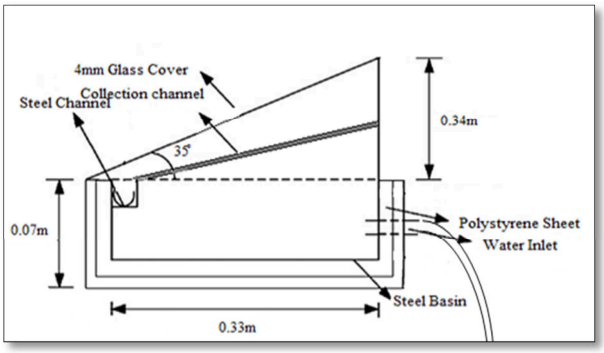


Fig 1. Schematic diagram of solar still connected to steel tubes system



Fig 2. Experimental Setup of Solar Still

The experiment was conducted from 8.00 am to 6.00 pm during the period of November and December 2013 for five sunny days. Solar radiation, production of fresh water, water and glass temperature are monitored and measured for every 2 hours. The parameters are shown in Table 2. The efficiency of a solar still can be calculated using the following formula [22].

$$n_d = \frac{\sum m_{ew} x h_{fg}}{\sum AxI(t)} \quad [1]$$

Where,
m_{ew} = Mass of water production
h_{fg} = Latent heat of vaporization
I(t) = Daily solar radiation
A = Whole area of solar collector

Table 2. Measured parameters

Monitoring Parameters	
$\mathbf{I_s}$	Hourly solar radiation
$\mathbf{T_w}$	Temperature of water in solar still
$\mathbf{T_{ic}}$	Temperature of inner glass of solar still
$\mathbf{T_{oc}}$	Temperature of outer glass of solar still
$\mathbf{T_a}$	Ambient temperature
$\mathbf{W_{hexp}}$	Hourly water production of solar still
$\mathbf{W_{dexp}}$	Daily water production of solar still

Results and Discussions

Results of the hourly monitoring of temperatures and solar radiation are presented in Figure 5. The days of 25th November 2013 was sunny, windy with a clear sky and reach a maximal ambient temperature of 26℃. The maximum water temperature was recorded between 12.00 to 2.00 p.m. It ranges between 55℃ to 60℃. The distillate production increases when the difference between water and glass temperature increases. A maximum temperature difference of 9℃ was observed at 2pm. This corresponds to the peak distillate production rate of 697.54ml/m^2/h.

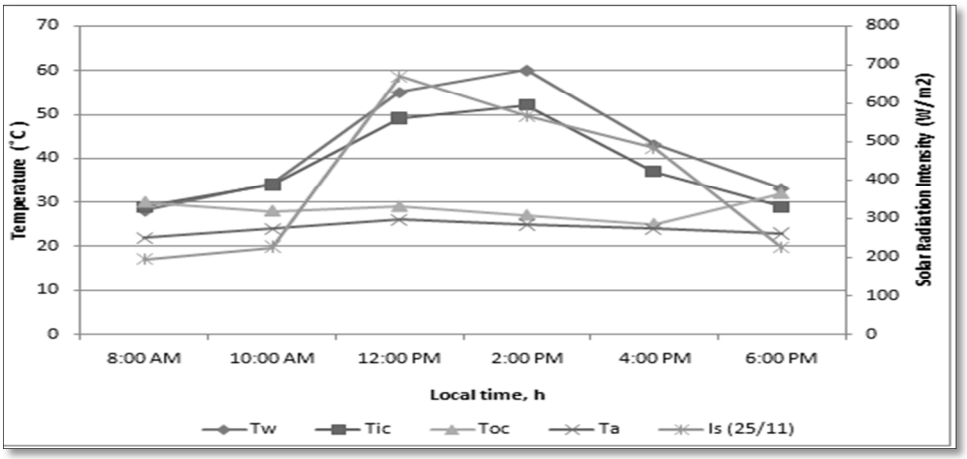


Figure 5. Variation of temperature and solar radiation

Figure 6 shows the production of solar still on 25th November 2013.The production of distillate increases as the solar intensity increases. The solar still production increase gradually until it reaches the peak rate at 12.00 pm and 2.00 pm. The maximum hourly production was 714 ml/m^2/h under solar radiation intensity of 670 W/m^2.The average solar radiation intensity of the day was 395 W/m^2 approximately 14.19 MJ/m^2.The cumulative production is 2.26 kg/m^2/d. According to World Health Organization (WHO), a person needs 2-3 Liter per day for survival [21].Thus, the application of solar still can support the water need for a person during the same period.

Malaysia is a tropical climate country which has a monsoon and sunny seasons. This study was conducted during the monsoon month of November and December 2013. The temperature and solar radiation varies significantly during monsoon season. The range of productivity and solar radiation intensity is shown in Figure 7 and Figure 8. The average solar radiations vary from 395 W/m^2 to 217 W/m^{2}during sunny days whereas the daily productivity ranges from 1.88 kg/m^2/d to

2.26 kg/m^2/d during sunny days. During peak hours the solar radiation is between 445 W/m^2 to 670 W/m^2 and corresponds with productivity rate of 97.2 ml/m^2/h to 714 ml/m^2/h.

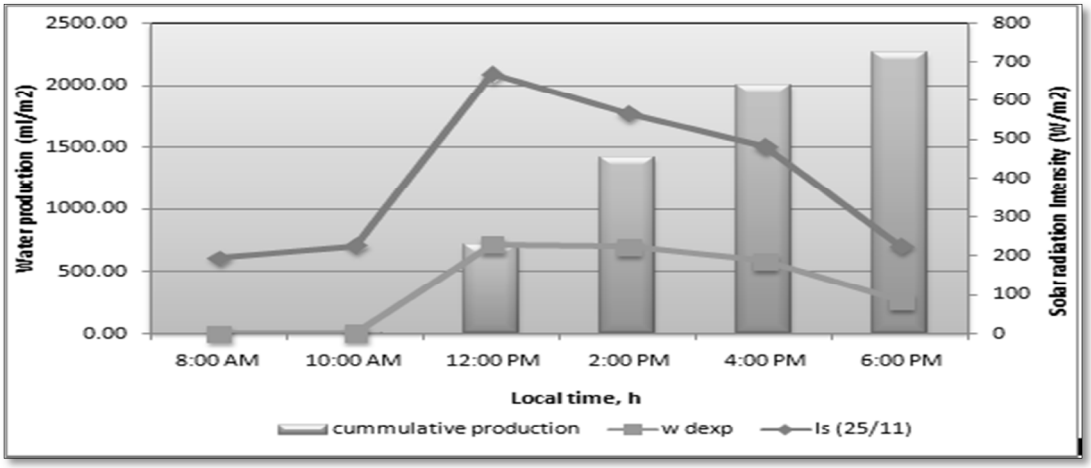


Figure 6. Cumulative and daily production of solar still for 5 sunny days

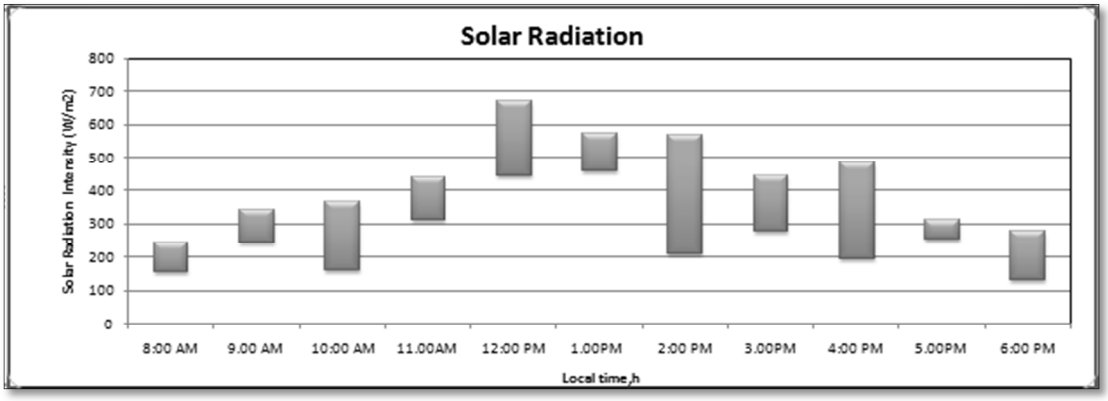


Figure 7. Maximum and minimum solar radiation for 5 sunny and cloudy days

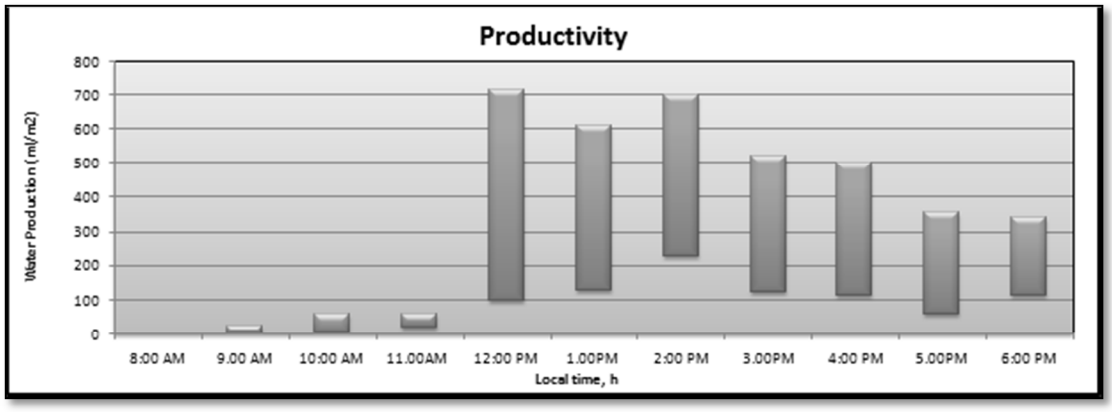


Figure 8. Maximum and minimum hourly productivity of five sunny and cloudy days

The efficiency,η_d in this study was found to be 37.7 %. The average efficiency of basic solar still is between 19% and 39 % [22]. The solar still used in this study can be considered as efficient considering the weather during the study was mostly cloudy.

4. Conclusions

Desalination using solar still is a good alternative for producing drinking water even during monsoon period with many intermittent and sunny days. During the sunny days of monsoon period, the daily production rate varies from 1.88kg/m^2/d to 2.26 kg/m^2/d under monsoon season. The productivity is expected to increase during dry season due to high solar intensity. This kind of water production may be applicable to individual house by collecting sun energy from roof area for remote communities or during severe weather conditions. Distilled water from solar still is lacking of minerals. Mineralization process is recommended to balance up the need for minerals.

References

[1] World Health Organization. (2006). Meeting the MDG drinking water and sanitation target: the urban and rural challenge of the decade. Retrieved from http://www.who.int/water_sanitation_ *health/monitoring/jmpfinal.pdf*

[2]Borhan,H. ,&Ahmed,E.M. (2012). Green Environment: Assessment of Income and Water Pollution in Malaysia. *Procedia – Social and Behavioral Sciences, 42,166-174.*

[3] Piduirny,M. (2012, October 12). The encyclopedia of Earth.*Global distribution of precipitation.*Retrieved December 31, 2013, from http://www.eoearth.org/view/article/153027.

[4] Saidur, R., Elcevvadi, E.T, Mekhilef, S., Safari, A., & Mohammed, H.A.(2011). An overview of different distillation methods for small scale application.*Renewable and sustainable energy reviews ,15, 4756- 4764.*

[5]Rodriguez, L.G.andCamacho,C.G. (2001). Perspective of solar assisted seawater distillation, *Desalination 136, 213-218.*

[6]Velmurugan,V. ,&Srithar, K.(2011). Performance analysis of solar stills based on various factors affecting the productivity- A review. *Renewable and sustainable energy reviews 15, 1294-1304.*

[7]Qiblawey,H.M., &Banat,F. (2008). Solar thermal desalination technologies.*Desalination, 220,633-644.*

[8] Wan Nik, W.B, Ibrahim, M.Z, Samo,K.B., &Muzathik, A.M. (2012), Monthly mean hourly global solar radiation estimation. *Solar Energy ,86 , 379-387.*

[9]Muzathik, A.M., Wan Nik, W.B., Samo, K.B., Ibrahim, M.Z., 2010.Reference solar radiation year and some climatology aspects of East Coast of West Malaysia. *American Journal of Engineering andApplied Sciences 3, 293–299.*

[10]Jamaludin, A.F.B. (2009), Energy mix and alternative energy for sustainable development in Malaysia, *University Putra Malaysia.*

[11]Mekhilef , S., Safari, A., Mustaffa,W.E.S., Saidur, R.,Omar, R., &Younis,M.A.A.(2012). Solar energy in Malaysia: Current state and prospects. *Renewable and sustainable energy reviews, 16, 386-396.*

[12]Fotso, J., Ezeh, A.C., Madise, N.J., &Ciera, J. (2007). Progress towards the child mortality millennium development goal in urban sub-Saharan Africa: they dynamics of population growth, immunization, and access to clean water. *BMC Public Health, 7*, 218.

[13] Qiblawey,H.M., &Banat,F. (2008). Solar thermal desalination technologies.*Desalination, 220,633-644.*

[14]Tiwari, A.K., Tiwari, G.N. Effect of water depths on heat and mass transfer in a passive solar still: in summer climatic condition. Desalination 2006; 195:78–94.

[15] Badran, A.A, Al-Hallaq, A.A., Eyal Salman,.IA.,Odat, M.Z. A solar still augmentedwith a flat-plate collector. *Desalination 2005; 172:227–34.*

[16] Sadineni SB, Hurt R, Halford CK, Boehm RF. Theory and experimental investigation of a weir-type inclined solar still. *Energy 2008;33:71–80.*

[17] Ward John. A plastic solar water purifier with high output.*Solar Energy.2003; 75:433–7.*

[18] Abdullah, A.S.(2013). Improving the performance of stepped solar still. *Desalination 319, 60-65.*

[19]Zoori, H.A,.Tabrizi, F.F., Sarhaddi, F. &Heshmatnezhad. Comparison between energy and exergy efficiencies in a weir type cascade solar still. Desalination 2013: 325: 113-121.

[20]Yousef H Zurigat, Mousa K Abu Arabi. Modelling and performance analysis of a regenerative solar desalination unit.*Applied Thermal Engineering 2004; 24:1061–72.*

[21]Reed,B., Reed,B. (2011). World Health Organization.How much water needed in emergencies.

[22] Xiao, G., Wang, X., Ni, M., Wang, F., Zhu, W., Luo, Z.,& Cen, K.(2013). A review on solar still for brine desalination.*Applied Energy, 103, 642-652.*

Applied Mechanics and Materials Vol. 567 (2014) pp 167-171
© (2014) Trans Tech Publications, Switzerland
doi:10.4028/www.scientific.net/AMM.567.167

Treatment of wastewater using an integrated submerged attached growth system

Ezerie Henry Ezechi[1,a], Shamsul Rahman Bin Mohamed Kutty[1,b], Mohamed Hasnain Isa[1,c], Ahmad Fitri Abd Rahim[1,d]

[1]Department of Civil Engineering, Universiti Teknologi PETRONAS, 31750 Bandar Seri Iskandar, Perak, Malaysia.

[a]honhenry2k5@yahoo.com, [b]shamsulrahman@petronas.com.my, [c]hasnain_isa@petronas.com.my, [d]fitryshah@gmail.com

Keywords: Aero-packer, Bio-balls, Attached growth, Integrated, Single sludge.

Abstract. The performance of a single sludge integrated attached growth system comprising of an aerobic and anoxic tanks in biological nutrient removal was evaluated in treating synthetic wastewater simulating medium strength domestic wastewater. An aero-packer and bio-balls were installed in the aeration and anoxic tank occupying about 40% and 25% of both tanks respectively. The efficiency of the integrated attached growth system was evaluated on the removal of chemical oxygen demand (COD), ammonia removal (NH_3), nitrate removal (NO^3), total suspended solids removal (TSS) and biochemical oxygen demand removal (BOD_5). Effluent results show that the integrated attached growth system had a removal efficiency of 97.8% (COD), 97.5% (NH_3), 87.5% (NO3), 97% (TSS) and 97.1% (BOD). These results support the viability of an integrated system in mitigating the enormous challenges of a conventional wastewater treatment.

Introduction

The entrance into waterways of both organic and inorganic compounds from various wastewater sources can result to undesirable effect due to pollution. These pollutants can originate from different categories of wastewater sources such as urban and agricultural run-offs, industrial run-offs, domestic run-offs and sewage effluents [1]. Wastewater discharged from these sources contains nitrogenous compounds (ammonia, nitrite and nitrate). These nutrients constitute a high percentage of global water body pollution. About 25% of all water body impairments are attributed to nutrients [2]. Excessive enrichment of water body by nutrients results to eutrophication [3]. Nitrate can also be toxic to aquatic animals when it reacts with hemoglobin causing shortage of oxygen in their body (methaemoglobin) and finally death [1]. In human intestines, nitrate is converted to nitrite under anaerobic conditions and this could lead to methaemoglobinaemia in infants [4]. In addition, formation of nitrosoamines from nitrite can result to cancers of the digestive tract since nitrosamines are the most efficacious carcinogens in mammals [5].

Biological wastewater treatment has been widely investigated and used in the removal of nutrients from wastewater due to its efficiency and reduced cost. However, different configuration of biological treatment abound based on purpose and objective of such investigation. Several literature has reported different biological treatment system which include the use of MBR systems in treating high strength synthetic wastewater [6], aerobic treatment of palm oil mill effluent [7], domestic wastewater treatment using a UASB reactor [8], sewage treatment using the combination UASB-SBR activated sludge [9].

Attached growth system of activated sludge is a process used to improve the growth of biomass within the reactor. Due to immobilization of microorganism, attached growth processes can have a high concentration of biomass. Its advantages include higher biomass concentrations in the reactor tank, consortia of aerobic and anoxic metabolic activities within the same biomass ecosystem and lower sensitivity to toxicity effects [10].

Normally, the various chambers of a conventional wastewater treatment plant are segregated. This has the capacity to occupy a large array of land. In order to overcome this problem, an integrated reactor is introduced where all components are assembled in an integrated arrangement. The advantages of this reactor include high sludge age and low food-microorganisms (F/M) ratio which enhance the growth of slow growing nitrifying bacteria as well as improved nitrification due to smaller floc size which allows higher mass transport of nutrients and oxygen into sludge flocs.

With the recent revision of the *Environmental Quality (Sewage) Regulations (2009)* for ammonia-nitrogen from 50 mg/L to 5 mg/L by the Department of Environment (D.O.E) Malaysia [11], cost effective techniques are required to meet this stringent regulation.

The objective of this study is to investigate the performance of a single sludge integrated attached growth process in meeting the new discharge limit of the (D.O.E) Malaysia.

Methodology

Synthetic wastewater preparation. Synthetic wastewater was prepared with Purino Alpo high protein dog food to simulate a medium strength domestic wastewater. The synthetic wastewater constituted COD (400 mg/L), BOD (208 mg/L), phosphorus (9 mg/L), ammonia was supplemented with ammonia chloride (40 mg/L) as primary nutrients while $CaCl_2$ (1.2 mg/L), $MgSO_4.7H_2O$ (0.8 mg/L), potassium (1.2 mg/L) and sodium (0.9 mg/L) as trace nutrients. $NaHCO_3$ (280 mg/L) was added to maintain pH between 7 and 8.

Reactor set-up. The reactor set up consists of an aeration tank with volume (0.01 m^3), anoxic tank with volume (0.02 m^3) and a clarifier with volume (0.15 m^3). The reactor configuration is post-anoxic with the aeration tank receiving the influent. The aeration tank is integrated into the anoxic tank and the anoxic tank integrated into the clarifier. The aeration tank is internally demarcated from the anoxic tank with a baffle to push samples from the aeration tank into the anoxic tank. The submerged attached growth media was inserted into the aeration tank while bio-balls were attached in the anoxic tank. Oxygen was supplied in the aeration tank using an air pump. Influent sample was pumped into the aeration tank using masterflex precision pump at a flowrate of 15 L/d. The mixed liquor recirculation (MLR) is recirculated for 60 seconds at every 90 minutes from the clarifier to the aeration tank. The reactor design was based on the assumed daily mixed-liquor temperature of 25°C to compensate for the changes in Malaysian weather.

Reactor operating conditions and sampling. The hydraulic retention time for the aeration and anoxic tanks are 8 h and 16 h respectively. The solid retention time (SRT) was maintained at 30 days. An MLSS concentration of 3000 mg/L was used in the aeration tank. The DO concentration ranges between 3-5 mg/L. The biomass acclimatization period was 10 days. Samples were collected for analysis at the bottom of the influent tank, aeration tank, anoxic tank and effluent using a 25 mL glass pipette at regular intervals of 2 days.

Attached growth media. Two different attached growth media was used in this study. In the aeration tank, an aero-packer designed with Perspex having a new geometry and good surface area with thickness of 1cm was used. In the anoxic tank, bio-balls was held firm using a tiny fish net.

Analytical methods. Chemical oxygen demand (COD), total suspended solids (TSS), mixed liquor suspended solids (MLSS) and mixed liquor volatile suspended solids (MLVSS) were analyzed according to the 21st edition of standard methods for the examination of water and wastewater. Ammonia-nitrogen (NH_3-N), and Nitrate (NO_3-N) were determined using spectrophotometric method with DR 2000. Biochemical oxygen demand (BOD_5) was determined by standard method number 5210.

Results and discussion

Organic matter removal (COD and BOD) and Total suspended solids (TSS). The average COD removal efficiency in the aeration tank, anoxic tank and effluent is depicted in Fig. 1a. The influent COD maintained a downward trend in removal efficiency for all the chambers. A COD removal

efficiency of 89%, 87% and 98% was observed for the aeration tank, anoxic tank and effluent sample respectively. This suggests that there was effective biodegradation of substrate within the reactor. Similar trend was observed for BOD removal within all chambers. A BOD removal efficiency of 95%, 93% and 96% was observed for the aeration tank, anoxic tank and effluent sample respectively as depicted in Fig. 1b. Total suspended solids (TSS) as depicted in Figure 1c for the influent and effluent showed high removal efficiency. TSS is an important physical characteristic of wastewater and its high removal indicates adequate biodegradation. The result obtained from the analysis so far indicate that the reactor configuration has met the D.O.E Malaysia discharge limit for COD, BOD and TSS.

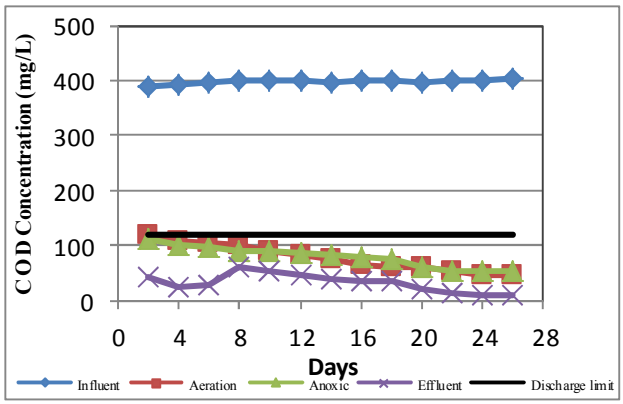


Figure 1(a) COD removal efficiency

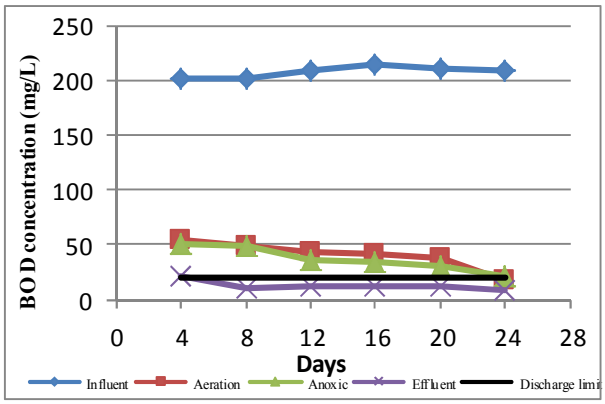


Figure 1(b) BOD removal efficiency

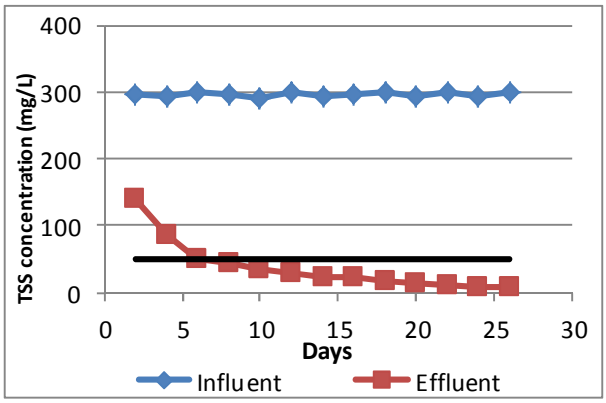


Figure 1(c) TSS removal efficiency

Removal of Ammonia-Nitrogen and Nitrate. Ammonia nitrogen is an important parameter of concern in this study. In wastewater treatment processes, nitrogen could be removed either through assimilation into biomass or by biological nitrification under aerobic conditions and denitrification process under anoxic conditions [6]. In this study, extended aeration was employed to provide the biomass sufficient oxygen for nitrification. Ammonia was oxidized to nitrate in the aeration tank and nitrate was subsequently fed to the anoxic tank for denitrification process. The nitrification removal efficiency of ammonia in the aeration tank, anoxic tank and effluent sample are 97%, 94% and 98% respectively as shown in Figure 2a. This result indicates effective and adequate nitrification within the reactor. Nitrate produced during nitrification was subsequently used up in the anoxic tank resulting to nitrate removal efficiency of 91%, 90% and 88% for aeration tank, anoxic tank and effluent respectively as shown in Figure 2b. The result for both ammonia-nitrogen and nitrate meets the D.O.E Malaysia regulation.

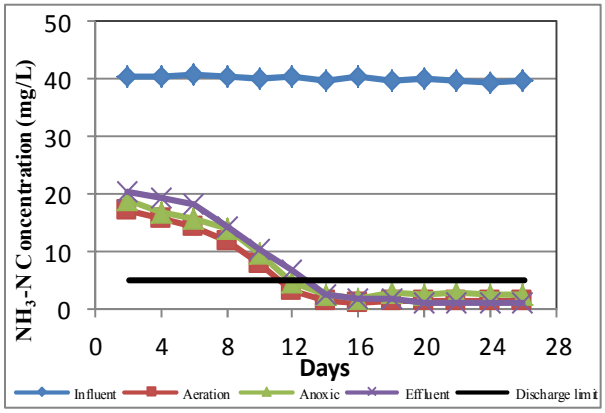


Figure 2(a) Ammonia removal efficiency

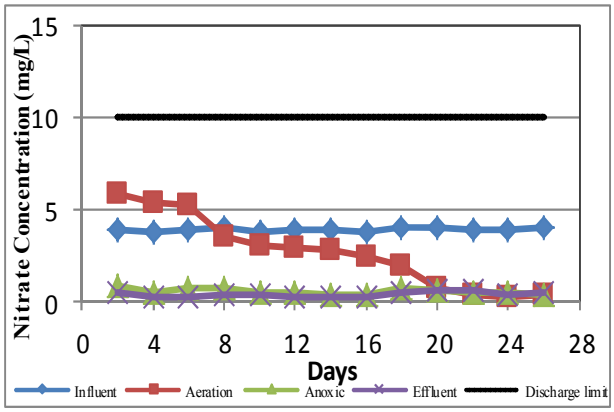


Figure 2(b) Nitrate removal efficiency

MLVSS, pH and Temperature evaluation. Table 1 shows the values for the measured parameters at steady state. Steady state of the biomass was maintained by periodic withdrawal of sludge from the reactor. The average pH of the influent sample was maintained between 7.4-7.6 and the pH of the effluent was about 7.8-7.9. Influent temperature was observed to be about 25°C due to the weather; however the effluent temperature was about 20-22°C due to aeration process.

Table 1: Average value of measured parameter at steady state

parameter	Influent	Aeration	Anoxic	Effluent
MLSS (mg/L)	-	4200	4089	-
MLVSS (mg/L)	-	2832	2669	-
pH	7.5	7.7	7.6	7.8
Temperature (°C)	25.8	24	23	22

Conclusion

Single sludge integrated attached growth reactor showed tremendous capacity to meet the revised D.O.E stipulation for ammonia nitrogen. The removal efficiency for COD, BOD, TSS, NH_3-N and NO_3-N in this study met the D.O.E standard. This reactor is cost effective because it does not occupy a large array of land due to its integrated nature, easy to operate, more accessible and can also be commercialized as an alternative in domestic sewage treatment plants.

Acknowledgment

The authors would like to acknowledge the project Supervisors and Universiti Teknologi PETRONAS (UTP) for supporting this research.

References

[1] J.A. Camargo, A. Alonso, A. Salamanca, Nitrate toxicity to aquatic animals: A review with new data for freshwater invertebrates. Chemosphere, 58 (9), (2005) 1255-1267.

[2] U.S. EPA. 2007. National Section 303(d) List Fact Sheet. (2007). Information Online at www.iaspub.epa.gov/waters/national_rept.control.

[3] S. Ghafari, M. Hasan, M.K. Aroua, Bio-electrochemical removal of nitrate from water and wastewater—a review. Bioresource Technology, 99 (10) (2008) 3965-3974.

[4] A.Nora'ainia, A.W. Mohammad, A. Jusoh, M.R. Hasana, N. Ghazalia, K. Kamaruzamana, Treatment of aquaculture wastewater using ultra-low pressure asymmetric polyethersulfone (PES) membrane. Desalination, 185 (1) (2005) 317-326.

[5] M. Zhou, W. Wang, M. Chi, Enhancement on the simultaneous removal of nitrate and organic pollutants from groundwater by a three-dimensional bio-electrochemical reactor. Bioresource Technology,. 100 (20) (2009) 4662-4668.

[6] S. J. Khana, S. Ilyasa, S. Javida, C. Visvanathanb, V. Jegatheesanc , Performance of suspended and attached growth MBR systems in treating high strength synthetic wastewater. Bioresource Technology,. 102 (9) (2011) 5331-5336.

[7] K.Vijayaraghavan, D. Ahmad, M. Ezani Bin Abdul Aziz, Aerobic treatment of palm oil mill effluent. Journal of Environmental Management, 82 (1) (2007) 24-31.

[8] E. Behlinga, A. Diaza, G. Colinaa, M. Herreraa, E. Gutierreza, E. Chacina, N. Fernandeza, C.F. Forster, Domestic wastewater treatment using a UASB reactor. Bioresource Technology,. 61 (3) (1997) 239-245.

[9] P. Guimaraes, H.N. Melo, P.F. Cavalcanti, A.C. Van Haandel, Anaerobic–aerobic sewage treatment using the combination UASB-SBR activated sludge. Journal of Environmental Science and Health, Part A,. 38 (11): (2003) 2633-2641.

[10] C. Chang, J. Chang, C. Chen, C. Chiemchaisri, S. Vigneswaran., An innovative attached-growth biological system for purification of pond water. Bioresource Technology, , 101(5), (2010) 1506-1510.

[11] S. M. Kutty, M.H. Isa., L.C. Leong, Removal of Ammonia-Nitrogen (NH_3-N) and Nitrate (NO_{-3}) by Modified conventional activated sludge system to meet new D.O.E regulations, in International conference on Environment and Industrial Innovation (IPCBEE) (2011), IACSIT Press, Singapore, 103-107.

Applied Mechanics and Materials Vol. 567 (2014) pp 172-176
© (2014) Trans Tech Publications, Switzerland
doi:10.4028/www.scientific.net/AMM.567.172

Volatile Fatty Acids Production through Degradation of Biomass by Anaerobic Digestion (Mesophilic and Thermophilic)

Ahmad Fitri Abd Rahim[1,a], Shamsul Rahman Mohamed Kutty[1,b] and Ezerie Henry Ezechi[1,c]

[1]Civil Engineering Department, Universiti Teknologi PETRONAS, 31750, Tronoh, Perak Darul Ridzuan, Malaysia

[a]fitryshah@gmail.com, [b]shamsulrahman@petronas.com.my, [c]honhenry2k5@yahoo.com

Keywords: Volatile fatty acids, anaerobic digestion, biomass

Abstract. Volatile fatty acids (VFAs) are fatty acids with a carbon chain of six carbons or fewer and usually referred to as short-chain fatty acids (SCFA). Degradation of biomass through anaerobic digestion will produce volatile fatty acid (VFAs) through anaerobic digestion process. The volatile fatty acids obtained can be recovered and used to produce methyl or ethyl esters which, could be advantageously used as additive for biodiesel [1]. Anaerobic digestion is a biological process that can degrade waste organic material by concerted action of a wide range of microorganisms in the absence of oxygen. The objective of this study is to degrade the biomass through anaerobic digestion for the production of volatile fatty acids by two different temperatures condition which are mesophilic and thermophilic; 35°C and 55°C respectively. The production of volatile fatty acids was optimized by varying the cycle period of the digestion process with the concentration of Mixed Liquor Suspended Solid (MLSS) maintained at 8000 mg/L for each cycle. The degradation of biomass was carried out using anaerobic sludge digester which 2L of biomass was digested from day 1 until day 24 (cycle period). The tests of MLSS and Mixed Liquor Volatile Suspended Solid (MLVSS) was conducted by Standard Method 2540-D while test for VFAs was conducted through Standard Method 8196. The highest production of volatile fatty acids was obtained in day 5 of cycle period where the concentration is 441 mg/L as acetic acid (HOAC).

Introduction

Due to the unpredictable price of the fuel in the world market, world is searching for alternative cheap and renewable energy resources that promises no environmentally impact like biodiesel, bioethanol and biogas derived from renewable biomass. There are some advantages of biodiesel compared to conventional diesel such as renewable, less toxic, biodegradable, low emission, excellent lubricity and could provide similar energy density to diesel [2]. Application of sludge digestion methods to intensify production of volatile fatty is the predominating tendency in the anaerobic digestion development. The technology that can stimulate higher hydrolysis rate can also intensify volatile fatty acids production. In order to degrade the biomass through anaerobic digestion, closed tank, heating and mixing was used. In anaerobic digestion, waste organic material is digested by concerted action of a wide range of microorganisms in the absence of oxygen. It has also been used for the treatment of waste activated sludge prior to final disposal and has been employed worldwide [3] where 20%-30% of the sludge Total Solid (TS) is mineralized [4]. At lower costs and the high destruction rate of pathogens, the stabilization of large volumes of organic sludge is obtained [5]. In term of efficiency, thermophilic conditions gives more advantages such as higher convention rate, better pathogen reduction effect and shorter retention time than mesophilic digestion [6]. The objective of this study is to degrade the biomass through anaerobic digestion for the production of volatile fatty acids by two different temperatures condition which are mesophilic and thermophilic; 35°C and 55°C respectively.

Methodology

For this study, the sample of sludge was taken from wastewater treatment plant at Universiti Teknologi PETRONAS (UTP). The sludge was collected in secondary clarifier that promises high amount of MLSS.

Digestion of primary sludge. Two liters of primary sludge were digested in a 2 L reactor (anaerobic sludge digester) for different batches with varying digestion cycle periods (1 to 24 days); at two different temperatures; mesophilic (35°C) and thermophilic (55°C). In order to maintain the biomass constant for each reactor, the MLSS of the sludge was determined and each reactor received only 8000 mg/L concentration of biomass. The sludge was mechanically mixed at a constant speed of 125 rpm by reactor stirrers. Anaerobic conditions were assured by keeping the digester reactor sealed. When the cycle period finished, 200 mL of sludge were sampled and analyzed for VFAs, mixed liquor suspended solids (MLSS) and mixed liquor volatile suspended solids (MLVSS).

Analytical Method. The samples were centrifuged at 8500 rpm for 15 min and the supernatant was filtered through a 47 mm filter paper disc prior to analyses. MLSS and MLVSS test was performed according to Standard Methods 2540-D. For VFAs determination, 0.5 ml of the filtrate supernatant was used for the test. The sample was tested according to Esterification method (Standard Method 8196) using spectrophotometer. The results of the VFAs were read in mg/L HOAC.

Results and Discussions

MLSS Concentration. The result below (Fig. 1) indicated that the initial MLSS concentration of 8000 mg/L decreased to 5200 mg/L and 6433 mg/L, for mesophilic and thermophilic conditions, respectively. This may be due to the acclimatization of the biomass to the new environment. However, it can be observed from Figure 1 that as the digestion period was increased, the MLSS concentration increased gradually for both temperature conditions until day 5. From day 6 until day 24, the digestion process under thermophilic phase seems to be stabilized. For mesophilic phase, the degradation pattern almost the same with the thermophilic phase but at day 20, the MLSS concentration slightly dropped. The increase of MLSS concentration in the thermophilic phase was found to be slightly higher than the mesophilic phase.

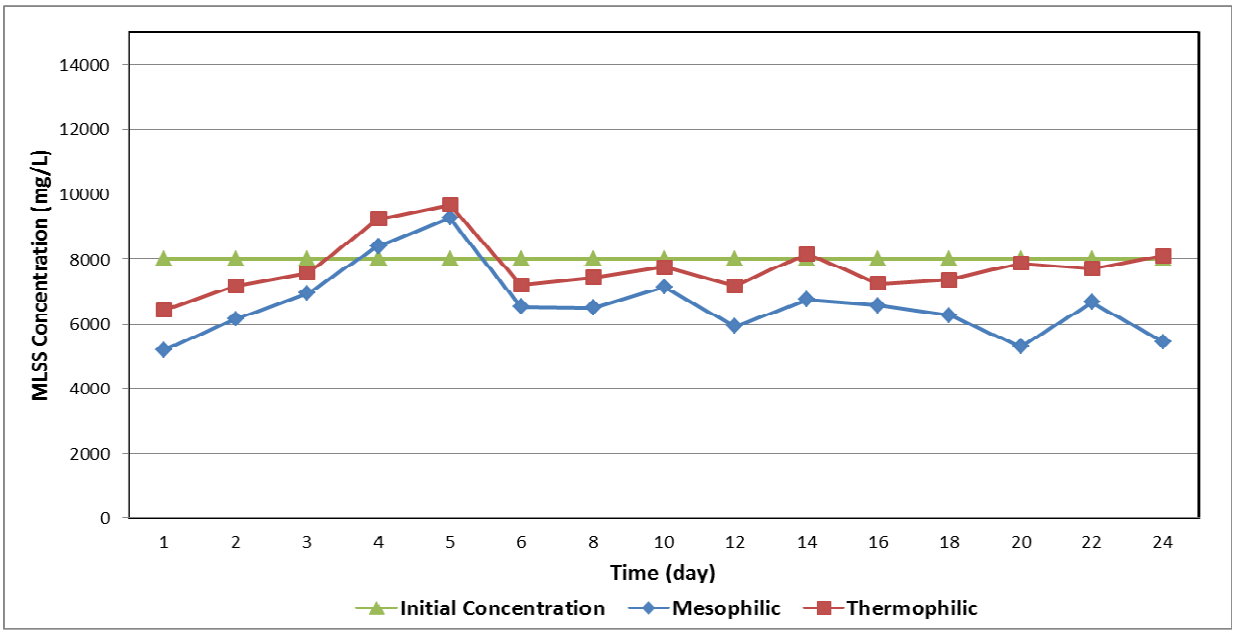


Figure 1: Graph of MLSS concentration vs time

MLVSS Concentration. The TSS and VSS concentration in the primary sludge composition were important parameters that influenced the production of VFAs. In order to predict VFAs production, sufficient TSS and VSS must be present [7] with high solids content promoting higher VFAs production [8]. From the result shown in Fig. 2 below, the growth of MLVSS was found to be similar as MLSS in Figure 1. When the digestion period was less than 4 days, it can be observed that initial MLVSS decreased at the end of each cycle period. After day 5 of digestion, the MLVSS was dropped drastically and starting on day 8, the MLVSS concentration tend to stabilized until day 24. At a digestion period of 5 days, highest production of MLVSS was achieved which promises the production of VFAs.

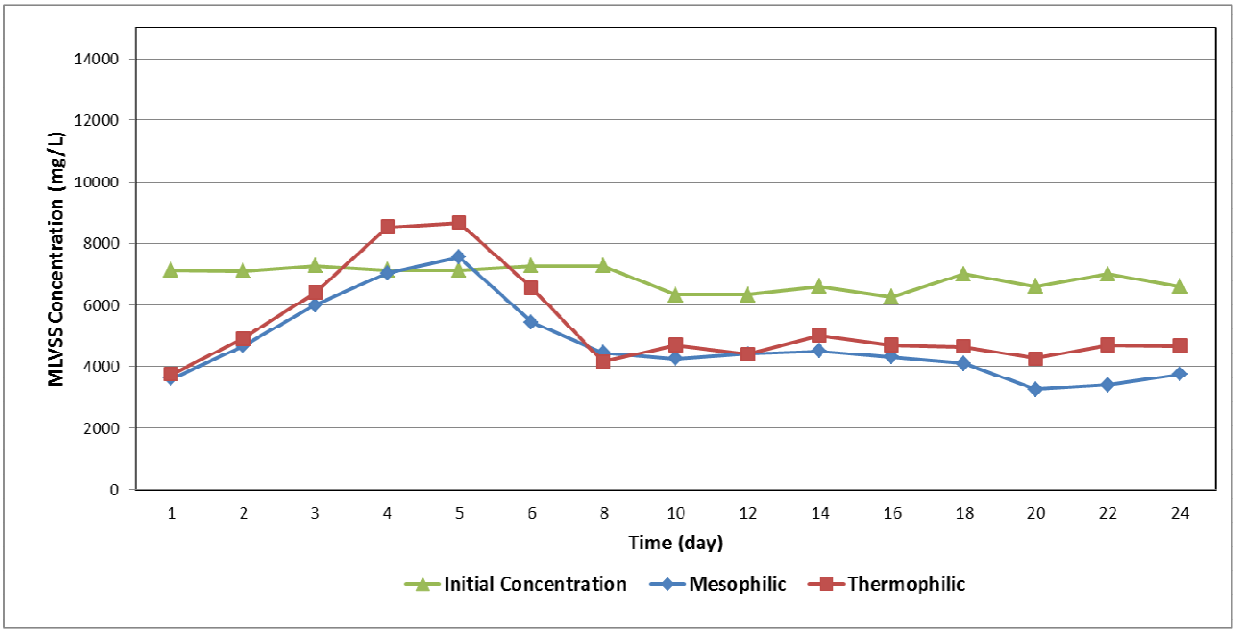


Figure 2: Graph of MLVSS concentration vs time

Volatile Fatty Acids (VFAs). In Figure 3, it can also be observed that for mesophilic digestion, the production of VFAs was much slower compared to the thermophilic digestion whereby VFAs rapidly increased starting for reactors operating at day 1 to day 5 digestion periods. The thermophilic digestion operated for 5 days achieved the highest production of VFAs compared to the mesophilic digestion which, the concentration is 441 mg/L. Comparing to other researchers result, [9] has shown that the production of VFAs was up to 2154 mg/l after 6 days of digestion under mesophilic condition with the initial TSS of 9730 mg/l. In another experiment, [10] has shown that the VFAs production was 2500 mg/L and 1200 mg/L for mesophilic and thermophilic condition; respectively, with the initial TSS of 10000 mg/L. These other researchers result shows that the mesophilic condition gives higher VFAs production meanwhile the result of author's experiment shows that the thermophilic condition contributes higher VFAs production. The differences of VFAs production may due to the sludge characteristics and technology used.

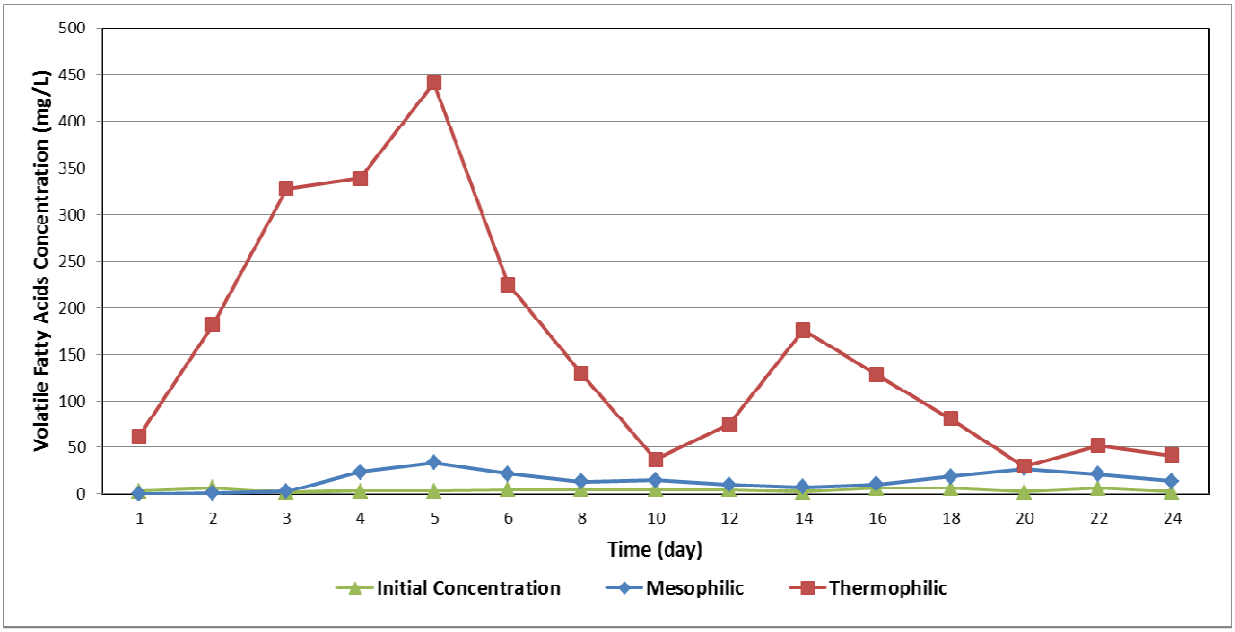


Figure 3: Graph of Volatile fatty acids vs time

Summary

As conclusion, the degradation of biomass through thermophilic condition gives better result in volatile fatty acids production compared with mesophilic condition. With an initial MLSS of 8000 mg/L at the beginning of the digestion, the highest production of VFAs was achieved after five days of digestion which are 441 mg/L HOAC and 33.7 mg/L HOAC under thermophilic and mesophilic conditions respectively.

Acknowledgment

Financial support was provided by Exploratory Research Grant Scheme (ERGS) by Ministry of Higher Education of Malaysia. The authors would also like to thank the Environmental Laboratory staff, Civil Engineering Department of Universiti Teknologi PETRONAS for their support in this research.

References

[1] D'Addario, E., Pappa, R., Pientrangeli, B., Valdiserri, M. (1992). "The acidogenic digestion of the organic fraction of municipal solid waste for the production of liquid fuels"

[2] Siddiquee MN, Rohani S. (2011). Lipid extraction and biodiesel production from municipal sewage sludge: A review. Renewable and Sustainable Energy Reviews , 15:1067-1073

[3] M. Dohanyos, J. Zabranska. (2001). Sludge into biosolids: processing, disposal and utilization. IWA , 13: 223-241.

[4] W. Rulkens. (2008). Sewage sludge as a biomass resource for the production of energy: overview and assessment of the various options. Energy Fuel , 22: 9-15.

[5] T. Liu. (1998). Anaerobic digestion of solid substrates in an innovative Two-Phase Plug-Flow Reactor (TPPFR) and a conventional single-phase continuously stirred tank reactor. Water Sci. Technol., 38 (8–9), 453–461.

[6] Ahring, B.K., Ibrahim, A.A., Mladenovska, Z. (2001). Effect of temperature increase from 55 to 65°C on performance and microbial population dynamics of an anaerobic reactor treating cattle manure. Water Resource, Vol. 35, No. 10. 2446-2452.

[7] S.S.Banister and W. Pretorius (1998). Optimization of primary sludge acidogenic fermentation for biological nutrient removal. Water SA. 24(1), 35-41.

[8] Zeng R. J., Yuan Z. and Keller J. (2006). Effects of solids concentration, pH and carbon addition on the production rate and composition of volatile fatty acids in prefermenters using primary sewage sludge.

[9] Q. Yuan, R. Sparling, J.A. Oleszkiewicz (2010). VFA generation from waste activated sludge: Effect of temperature and mixing. Chemosphere 82. 603–607.

[10] G. Hui Yu, P. Jing He, L. Ming Shoa, P. Pei He. (2008). Toward understanding the mechanism of improving the production of volatile fatty acids from activated sludge at pH 10.0. Water Research. 4637-4644

Applied Mechanics and Materials Vol. 567 (2014) pp 177-182
© (2014) Trans Tech Publications, Switzerland
doi:10.4028/www.scientific.net/AMM.567.177

Water Quality Assessment of Ex-mining Lakes in Perak, Malaysia as Alternative Source of Water Supply

Kalu Uka Orji[1,a], Nasiman Sapari[1,b], Khamaruzaman Wan Yusof[1,c], Robabeh Asadpour[1,d], and Emmanuel Olisa[1,e]

[1]Department of Civil Engineering, Universiti Teknologi PETRONAS, Bandar Seri Iskandar, 31750 Tronoh, Perak, Malaysia

[a]suunyboy2008@yahoo.com, [b]nasiman@petronas.com.my, [c]khamaruzaman.yusof@petronas.com.my, [d]asadpour1981@gmail.com, [e]emidear2003@yahoo.com

Keyword: Ex-mining lakes, Perak, rivers, water quality, heavy metals, physico-chemical properties

Abstract

This study investigated the water quality of some of the ex-mining lakes in Perak State of Malaysia for possible use as alternative to water supply and compared them to water quality of some of the rivers used for intake of water treatment. A total of twelve (12) water samples were collected for analyses from selected sampling sites. These samples were analyzed for physico-chemical properties, heavy metals concentrations, and organic pollutants concentrations. The analyzed results indicated that average temperature varied from 28.1 ^{o}C to 34.1 ^{o}C, pH 6.2 to 9.0, EC 55 to 400 µs/cm ,turbidity 5.6 to 74.2 NTU, DO 3.21 to 9.56 mg/l, TDS 36.8 to 268 mg/l, F^- 0.017 to 0.182 mg/l, Cl^- 0.483 to 3.339 mg/l, Br^- 0 to 0.392 mg/l, SO_4^{2-} 0.051 to 15.307 mg/l, Mg 0.833 to 1.466 mg/l, Na 0.669 to 3.668 mg/l, and Ca 2.85 to 26.77 mg/l. Heavy metals concentrations (mg/l) were: Zn 0.04 to 0.057, Pb 0.019 to 0.075, Cd not detected, Ni 0.013 to 0.105, As not detected to 0.004, and Cu not detected while COD 4 to 51 mg/l. Analyses revealed that all the water samples were turbid and containing slightly high concentration of Pb. Generally, they had common water quality problem. Further work should carry out more tests on other water quality parameters particularly on heavy metals, chemical and biological pollutants at different seasons.

1 Introduction

Owing to the increase in river pollution in Malaysia, it becomes relevant that the other water sources be explored in order to either augment the existing ones or serve as alternative sources of water supply. Shah Alam and Sandakan in Selangor State have introduced rainwater harvesting in order to augment the rivers within the area [1]. Kelatan, Perlis, Pahang, Selangor, and Terengganu State have also been combining surface water with groundwater [2].

Ex-mining pools have primarily been used for irrigation and sewage disposals but not for drinking due to the view that they are polluted with heavy metals and other contaminants. Study has shown that ex-tin mining pools located in Bestari Jaya area, Selangor contained heavy metals [3 & 4]. More research has to be conducted in other parts of Malaysia in order to ascertain the quality of these ex-mining pools for public water supply. The objectives of this research were to characterize the water quality of some of these abandoned mining lakes water in Perak; and to make comparison with the water qualities of the rivers used for water treatment in Perak water supply.

2 Materials and methods

2.1 Sample locations

A total of 12 water samples were collected for analyses from selected sampling locations. Four (4) samples were obtained from ex-tin mining lakes in Tronoh. Six (6) samples were collected from different ex-mining lakes in Batu Gajah. Two (2) samples were collected from Kinta River and Perak River in Batu Gajah and Bota. Information about the sampling sites are given in Table1. The sample collections were carried on the 29th of July to 2nd of August, 2012. The above rivers are actively used by the Metropolitan Utilities Corporation Sdn Bhd (MUC) as intake points for water supply to the State of Perak.

2.2 Methods

All the water samples were collected using water sampler. The samples were collected within the range of 2 – 5m deep from the surface of the sources. The physico-chemical properties of the water samples such as the temperature, pH, Electrical Conductivity (EC), and turbidity were directly measured in the field at each sampling point. The Total Dissolved Solids (TDS) was calculated by multiplying the EC value by a conversion factor of 0.67. The other parameters were measured in the laboratory. The pH and temperature were measured with pH meter (HACH – Sension 4, USA), Turbidity with turbidimeter 2100P (HACH, USA), Dissolved Oxygen with DO Meter (YSI 5000), and Electrical Conductivity with EP meter (MYRON, USA). Details of the water quality parameters measured are shown in Figure 1-16. The samples were measured in triplicates and the average values were used. The samples were initially filtered with Whatman® No.1filter paper. Some portion were directly stored in the cold room without acidification for anion measurement and the rest of the samples were preserved with acidified HNO_3. The samples were later digested using the standard methods and preserved in polyethylene bottles [5]. These plastic bottles were previously soaked with 10% HNO_3 and rinsed with deionized water. They were then stored in the dark cold room of the laboratory at 4 ^{o}C for analyses.

All chemicals used were of analytical grades. Fluoride, chloride, bromide, and sulphate in the samples were measured using Ion Chromatography (Metrohm) whereas Ca, Na, Mg, Cu, As, Ni, Pb, Zn, Cd, etc were measured using air-acetylene Atomic Absorption Spectrophotometer (AA-6800, SHIMADZU, Japan). The Chemical Oxygen Demand (COD) was determined using Spectrophotometer DR 2800 and DRB 200 (HACH, USA) after digestion with the appropriate reagents [5]. The quality of the water samples were compared with the National Water Quality Standard for Malaysia (NWQSM) and its classification.

3 Results and Discussion

3.1 Physico-Chemical Parameters

Results of the analyses of Physico-chemical parameters from the 12 sampling stations indicated the overall temperatures of the sampling sites fell within the range of 27.8 – 35.3^{o}C, similar to a report obtained by Yap et al for Rivers and Drainages of Peninsular Malaysia (RDWPM) [6]

The highest range of TDS was found in Kampung Bemban G. G. 2 mining lake (S8). This could be as a result of the runoff of agricultural activities and soil erosion from the surrounding area. The

TDS in all the locations were found to be below 500mg/l limits as stipulated by the WHO and NWQSM for domestic water use (Figure 1).

The pH level was still within the range (4.96-9.81), which was also reported by Yap et al in 2009 [6]. Figure 2 has shown that Perak River (Sungai Perak – S10) was more acidic than the others while Tronoh Jaya (S1) had the highest alkalinity level.

The results in Figure 2 showed that the water from source S4, S5, and S12 met up with the DO prescribed standard; whereas, S1, S2, S7, S9 and S11 fell in the category of class II of NWQSM

The turbidity values of the water samples ranged from 5.6 to 85 NTU (Figure 3). The turbidity values of location S2 to S12 fell in class II while location S1 fell in class III.

The EC in the water sources ranged from 55 to 400 μS/cm and as shown in Figure 4. Perak River (S10) had the lowest EC while and Kampung Bemban G. G. 2 mining lake (S8) had the highest EC. The results also showed that the EC of all the water samples met up with the WHO standard [7] and the NWQSM [5] for drinking water.

All the concentrations of Ions (Cations and Anions) tested in the water samples fall within the prescribed limit. Details of these are shown in figure 5 – 12.

3.2 Heavy Metals Concentrations

Details of the heavy metals concentrations are found in Figure 12-15. As, Zn, Cd, and Cu fall within the prescribed limit. The concentrations of Pb in all the samples except S8 and S9 are slightly above the maximum contaminant level and fell in class II and III of the NWQSM. This result was similar to the ones obtained by Yap et al 2009 (0.001-1.523mg/l) for RDWPM and Yap et al 2011 (0.018-0.377mg/l) but wider than the one reported by Shuhaimi et al (1.4mg/l) for Sungai Sedii Kecil [6, 8, & 9]. For Ni, sample S1, S4, S5, S7 and S9 have slightly higher Ni concentration than the maximum permissible limit of the WHO and NWQSM.

3.3 Organic Pollutant

COD was found within the range of 4 to 51mg/l (Figure 16). The results of the water samples from river sources - S10 and S11 (35 and 40 mg/l) were almost similar to the ones reported by Malakahmad and Eisakhani in 2009 during high water flow for Jasar river, Ulung river, Bertam river, and Burong river [10]. Water sample S6 had the highest COD value of 51 mg/l.

4 Conclusions

Both the rivers and the ex-mining lakes are generally turbid and contain slightly high concentrations of Pb. This suggested that both of them have common water quality problem.

However, future work should carry out more tests on other water quality parameters particularly on heavy metals, chemical and biological pollutants at different seasons. The future research should also determine the sources of water recharge. These would assist in determining the seepage velocity of the recharged water of the lakes.

5 Acknowledgements

The authors would like to thank the Universiti Teknologi PETRONAS, especially the Department of Civil Engineering for the facilities provided for this research.

Table 1: Sampling sites descriptions.

Sample *No*	Date /Time	Site/Source	Site Description	Coordinates	Elevation *m*
S1	29/7/12 11:30am	Laluan Tronoh Jaya 4, Tronoh Mines/Ex – Mining Pool	It is an inactive mining site that is partly surrounded by residential buildings and forests. The vicinity of the other part is used for cattle grazing.	4°25'47.4"N 100°58'53"E	30.79
S2	29/7/12 12:01pm	Cooperate Sec. of State land, Tronoh Mines/ Ex – Mining Pool	Same future as in S1.	4°25'05.9"N 101°00'59"E	27.13
S3	29/7/12 6:31pm	Bemban 1, Jalan Changkat, Batu Gajah/ Ex – Mining Pool	A lake with muddy shore. It is surrounded by forests. It is located near the roadside and a construction site.	4°28'05.9"N 101°00'59"E	42.07
S4	30/7/12 4:16pm	Bemban 2, Jalan Changkat, Batu Gajah/ Ex – Mining Pool	A mangrove area. Sewage is discharge into it through a drainage busy road. Some restaurants and stores in the vicinity.	4°28'08.4"N 101°01'31"E	40.85
S5	31/7/12 4:31pm	Train Station, Batu Gajah/ Ex – Mining Pool	It is located adjacent to a busy road and train station. It is almost fully surrounded by forests and used for fishing by the villagers.	4°27'44.7"N 101°03'04"E	20.12
S6	30/7/12 6:17pm	Taman Permai, Bemban, Batu Gajah/ Ex – Mining Pool	It lies by the side of a busy road, agricultural area and residential buildings. Wreckages of renovated building deposited close to shoreline of the lake.	4°27'57.0"N 101°00'56"E	42.38
S7	31/7/12 7:05pm	Kampung Bemban G.G.1, Batu Gajah/ Ex – Mining Pool	It lies by the side of forests, agricultural area and residential buildings. It is basically used as irrigation water.	4°27'52.0"N 101°00'54"E	42.99
S8	31/7/12 6:10pm	Kampung Bemban G.G.2, Batu Gajah/ Ex – Mining Pool	It has the same future as in S7.	4°27'48.2"N 101°00'53"E	41.46
S9	02/8/12 7:05pm	Taman Tasik Putra, Opp. ESSO Mobil/ Ex – Mining Pool	It is located opposite a filling station and surrounded by forests.	4°23'56.9"N 100°59'09"E	18.90
S10	31/7/12 5:34pm	Kepayan Bay, Bota/Sungai Perak	A river with fishing site. Turtle breeding center, market, restaurants and abattoir are also located within the vicinity.	4°21'18.1N 100°52'25"E	18.29
S11	02/8/12 6:00pm	Batu Gajah/ Sungai Kinta	The river cuts across residential area. The bank faces erosion. Malls, restaurants, and busy rods are within its vicinity.	4°28'25.9"N 101°03'08"E	25.00
S12	02/8/12 6:30pm	Universiti Teknologi Petronas, Tronoh/ Ex – Mining Pool	This is an open mining lake that is surrounded by few trees, and close to a filling station and hostels.	4°23'04.0"N 100°58'43"E	18.60

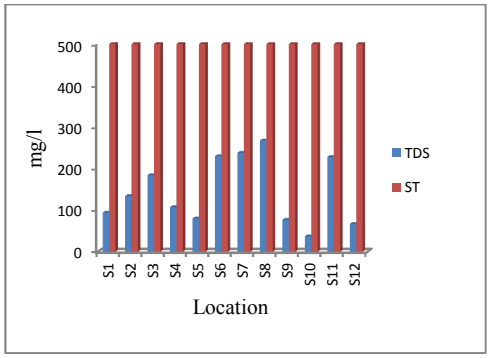


Figure 1: Concentration of TDS in water samples

ST = WHO Standard

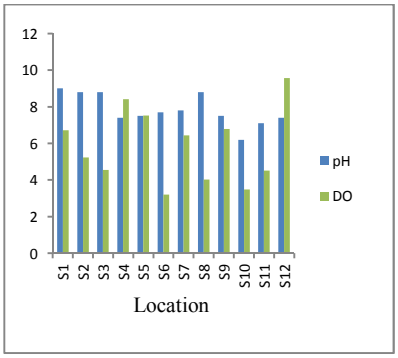


Figure 2: Concentration of pH & DO in water samples

ST = WHO Standard

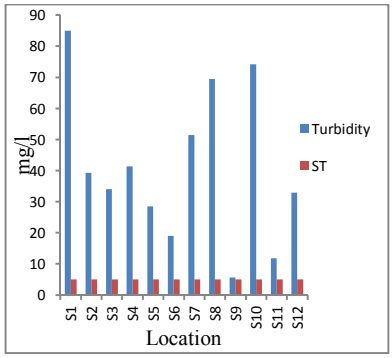


Figure 3: Concentration of Turbidity in water samples

ST = WHO Standard

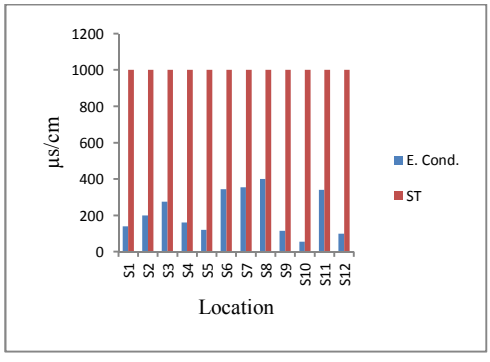


Figure 4: Concentration of EC in water samples

ST = WHO Standard

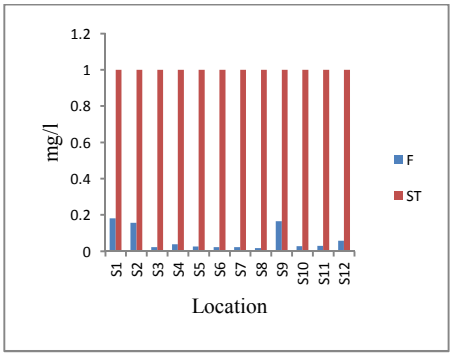


Figure 5: Concentration of Fluoride in water samples

ST = WHO Standard

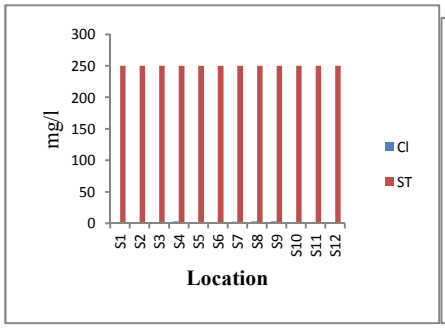


Figure 6: Concentration of Cl in water samples

ST = WHO Standard

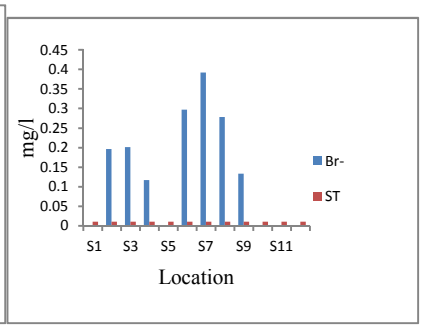


Figure 7: Concentration of Bromide in water samples

ST = WHO Standard

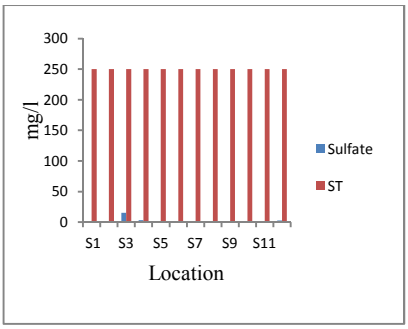


Figure 8: Concentration of Sulfate in water samples

ST = WHO Standard

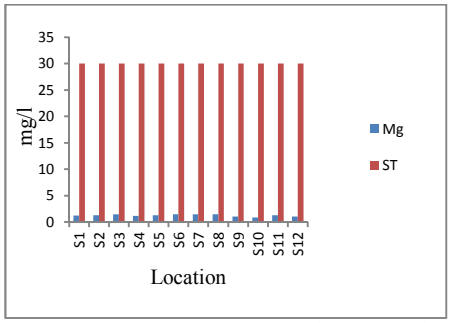


Figure 9: Concentration of Magnesium in water samples

ST = WHO Standard

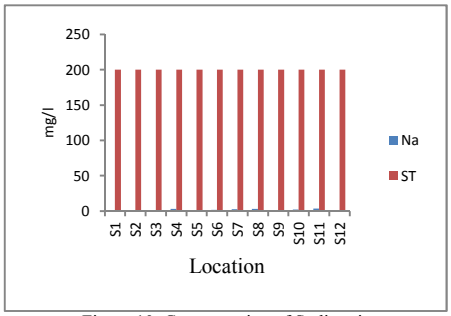


Figure 10: Concentration of Sodium in water samples

ST = WHO Standard

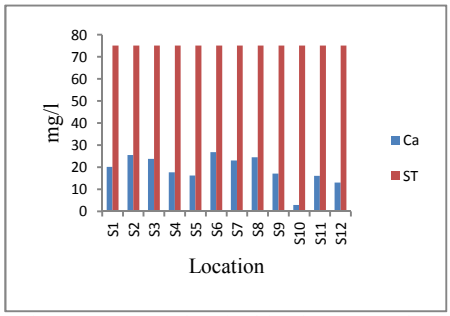


Figure 11: Concentration of Calcium in water samples

ST = WHO Standard

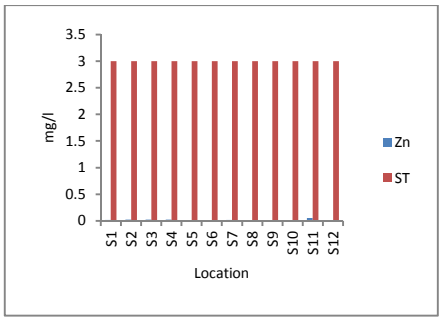


Figure 12: Concentration of Zinc in water samples

ST = WHO Standard

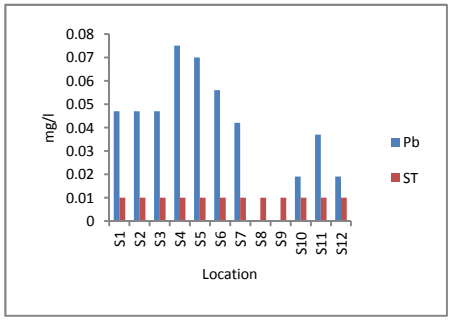


Figure 13: Concentration of Lead in water samples

ST = WHO Standard

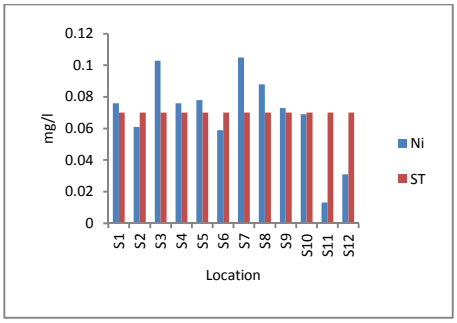


Figure 14: Concentration of Nickel in water samples

ST = WHO Standard

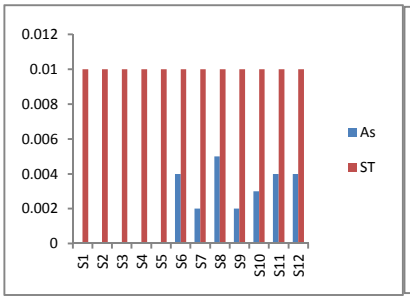


Figure 15: Concentration of Arsenic in water samples

ST = WHO Standard

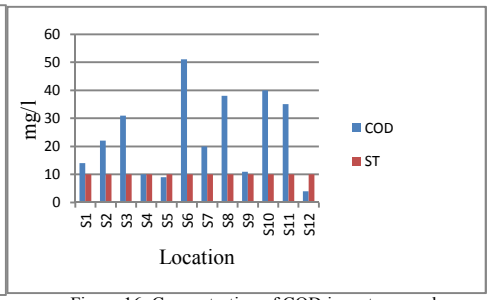


Figure 16: Concentration of COD in water samples

ST = WHO Standard

References

[1] Mohd-Shawahid, H. O., Suhaimi, A. R., Rasyikah, M. K., Jamaluddin, S. A., Huang, Y. F., Farah, M. S. (2007). Policies and Incentives for Rainwater Harvesting in Malaysia, Paper Presented at Rainwater Utilization Colloquium on 19 and 20 April 2007 at NAHRIM Mini Auditorium.

[2] Azuhan, M., (2012). Utilization of Groundwater Resources in Peninsular Malaysia, J. of Groundwater and Geoscience.

[3] Muhammad, A. A., Mohd, J. M., Ismail, Y. (2010). Study of water Quality and Heavy Metals in Soils and Water of Ex – Mining Area Bestari Jaya, Peninsular Malaysia, Int. Journal of Basic and Applied Sci., Vol. 10, No. 3

[4] Department of Environment [DOE], (2010). Malaysia Environmental Quality Report, Ministry of Natural Resources and Environment Malaysia.

[5] APHA – AWWA (2005). Standard Methods for Examination of Water and Wastewater, 21st sd., American Public Health Association/American Water Works Association.

[6] Yap, C. K., Fairuz, M. S., Yeow, K. L., Hatta, M. Y., Ismail, A., Ismail, A. R., and Tan, S. G. (2009). Dissolved Heavy Metals and Water Quality in the Surface Waters of Rivers and Drainages of West Peninsular Malaysia, Asian Journal of Water, Environment and Pollution 6(3): 51 – 59

[7] World Health Organization (WHO) (2011). Guidelines for Drinking-Water Quality: 4th Edition, WHO Press, Geneva, Switzerland

[8] Yap, C. K., Chee, M. W., Shamrina, S., Edward, F. B., Chiew, W., and Tan, S. G. (2011). Assessment of Surface Water Quality in the Malaysian Coastal Waters by Using Multivariate Analyses, Journal of Sains Malaysiana 40(10), pp. 1053-1064.

[9] Shuhaimi-Othman, M., Nadzifah, Y. and Azmah, M. (2012). Metal Concentrations in Sungai Sedii Kecil, Johor, Peninsular Malaysia, Journal of Tropical Marine Ecosystem, Vol. 1, pp. 15-23.

[10] Malakahmad, E. and Eisakhani, M. (2009). Water Quality Assessment of Bertam River and its Tributaries in Cameron Highlands, Malaysia, World Applied Sciences Journal 7(6): 769 – 776.

Applied Mechanics and Materials Vol. 567 (2014) pp 183-188
© (2014) Trans Tech Publications, Switzerland
doi:10.4028/www.scientific.net/AMM.567.183

Determination of Soil Polluted with Kerosene Using Electromagnetic Cell

Hashem Al-Mattarneh[1,a], Mohamad Dahim[2,b] , Rabah Ismail[3,c] and Muhd Fadhil Nuruddin[4,d]

[1,2,3]Civil Engineering Department, College of Engineering, Najran University, Saudi Arabia

[4]Civil engineering department, University Technology Petronas, Malaysia

[a]hmalmattarneh@nu.edu.sa, [b]madahim@yahoo.com, [c]rmaiw2002@yahoo.com, [d]fadhilnuruddin@petronas.com.my

Keywords: Soil pollution; Kerosene and Electromagnetic.

Abstract. Soil contamination with petroleum hydrocarbons has become one of the most serious problems due to its negative repercussion on ecosystems. For this reason, different analytical techniques have been developed to evaluate the quantity and the quality of organic pollutants using electrochemical techniques, and a geophysical methods have been developed which utilizes the contrast caused by the contaminant on physical properties of the soil dielectric methods shows high potential for characterization kerosene contaminated soil and determination of the level of contaminant. The potential of dielectric measuring techniques for soil characterization has not been fully explored. For this purpose, dielectric measurements, in the frequency range from 100 kHz to1000 kHz, were carried out in sandy soil samples, contaminated with solutions of kerosene, at different concentrations. The differences of the dielectric behavior with contaminant content suggest that the monitoring of complex dielectric constant has the potential to quantify contaminants.

Introduction

The oil industry has had a negative impact on the environment due to flights or spills caused by flaws in its infrastructure, either inside or outside its facilities. However previously, there were not appropriate disposal means for these pollutants, hence, contaminated areas where oil was confined caused soil pollution [1,2]. And these pollutants has caused critical environmental and health defects for short and long term.

Soil is a multi-functional medium. It is a vital for life and provides a wide range of services, which are mostly taken for granted. Its quality is defined as the capacity of a soil to function within ecosystem boundaries to sustain biological productivity, maintain environmental quality, and promote plant and animal health [3]. Last decade a constantly growing interest is discerned in the development of effective methods for the detection of subsurface contamination and monitoring environmental pollution [4].

To characterize subsurface contamination the most commonly used methods involve collecting representative samples of soil and pore fluid and analyzing them for targeted species in the laboratory. In general, this way of characterizing the contamination of a soil-fluid system is the only one acceptable to regulatory agencies [5]. However, sample collection and analysis in the laboratory pose significant problems: (1) sampling of the soils is extremely time consuming and expensive; (2) sampling is destructive in the case of removing the soil samples; (3) the sampling is not continuous with time; and (4) samples can be contaminated during sampling, transportation, and analysis in the laboratory.

Thus several geophysical methods have been developed which utilizes the contrast caused by the contaminant on physical properties of the soil [6,7]. Electromagnetic and dielectric methods shows high potential for characterization hydrocarbon contaminated soil and determination of the level of

contaminant. In additional use of this method; rely upon the availability of information about the dielectric properties of the contaminated soil. Development of such information has formed a focus of research by many authors around the world over several years [7,8]. Abidin investigated the feasibility of using dielectric measurement of soil materials to determine the soil porosity [9]. In the first stage of his study, the dielectric constants of a natural sand and glass bead in two sizes at various porosities were determined at 13 MHz. A linear relationship between the dielectric constant and porosity of soil-water mixtures was observed for both cases with coefficient of correlation values over 0.97.

In this study, electromagnetic measurements have been directed towards the development of reliable quality assurance tests for soil. The particular areas of interest are detection of hydrocarbon in soil material and determination of the contents of this contaminates. It is hoped to produce equipment, which will provide assistance to the practicing civil engineer. The current work is directed towards achieving the understanding for electromagnetic mechanisms involved in such a complex material.

Dielectric Properties of Soil

Soil as a dielectric material can be characterized by its complex permittivity. Complex permittivity of soil material is a complex parameter represents the interaction between electromagnetic signal and soil. It is also control the propagation of the signal in soil. Complex permittivity of soil is composed of real and imaginary parts. The real part results from the polarization of material, while the imaginary part is due to ohmic and polarization losses. The Complex permittivity of soil material can be given by:

$$\varepsilon^* = \varepsilon^{'} - j\varepsilon^{''} . \tag{1}$$

Where ε^* is the complex permittivity. $\varepsilon^{'}$ is the real part (dielectric constant) and it represents the amount of energy stored in soil from the applied electric field. $\varepsilon^{''}$ is the imaginary part (loss factor) and it represents the energy loss as conductive current. By dividing Eq. (1) by the permittivity of a vacuum (ε_0), the complex permittivity of soil become unitless representing the dielectric constant and loss factor of soil with respect to air.

Experimental Program

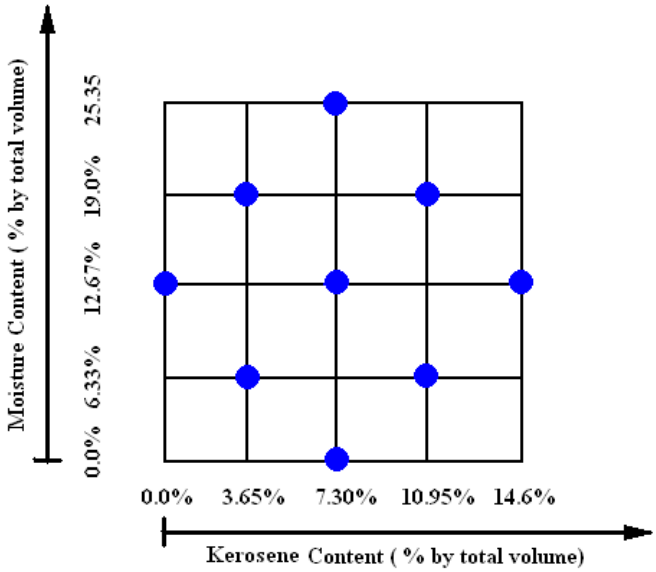
Materials and Sample Preparation

In this research a quartz sand with porosity (N= 0.4, according to the procedure described in AASHTO manual. 1974) was dried. Fourteen sany soil samples of 500 g each were prepared from the dried sample at constant deionized water content and at five different concentrations of kerosene (supplied by PETRONAS (M) Sdm. Bhd. with density 0.89). By adding the required concentration of water and kerosene to the dry sample. Therefore, five soil sample sets were taken and recognized for the kerosene concentration level. The soil samples were shacked for 15 minute then kept for three hours in sealed plastic container to avoid any evaporation. Three impedance measurements were obtained at each frequency and the average value was determined.

To evaluate the effect of kerosene contamination on sandy soil, five samples were prepared. The total liquid (water and kerosene) was 40% by volume in order to saturate the sand soil with porosity 0.4. Five different kerosene contents were used in order to contaminate the sand soil. The details of these five samples are shown in Table 1. Using the central composite design to prepare nine soil samples with nine different combinations of moisture and kerosene content Fig. 1.

Table 1. Samples of Kerosene Contaminated Soil

Sample Code	Weight (gram)				Volume Fraction			
	Soil	Water	Kerosene	Air	Soil	Water	Kerosene	Air
K0W2	500	40.0	0.00	00.0	0.600	0.1267	0.0000	0.273
K1W1	500	20.0	9.23	00.0	0.600	0.0633	0.0365	0.300
K1W3	500	60.0	9.23	00.0	0.600	0.1900	0.0365	0.174
K2W0	500	0.00	18.46	00.0	0.600	0.0000	0.0730	0.327
K2W2	500	40.0	18.46	00.0	0.600	0.1267	0.0730	0.200
K2W4	500	80.0	18.46	00.0	0.600	0.2535	0.0730	0.074
K3W1	500	20.0	27.696	00.0	0.600	0.0633	0.1095	0.227
K3W3	500	60.0	27.696	00.0	0.600	0.1900	0.1095	0.101
K4W2	500	40.0	36.93	00.0	0.600	0.1267	0.1460	0.127

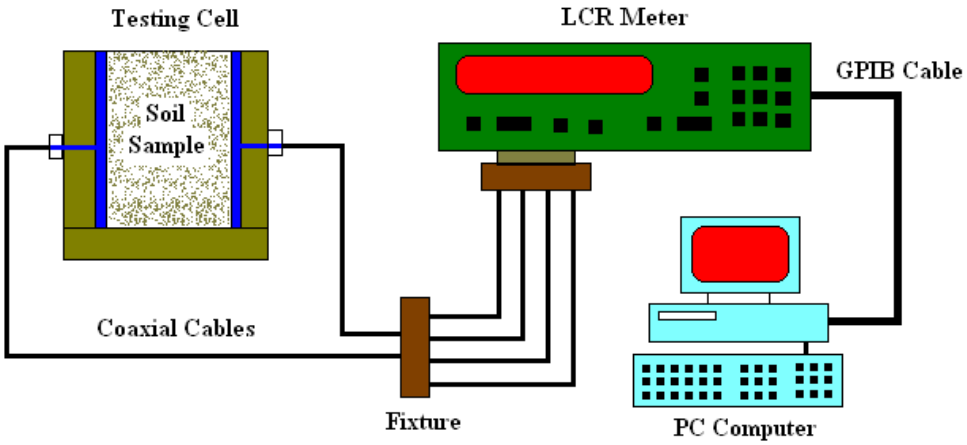


Figures 1. Combination of Moisture and Kerosene Content Using ICC Design

Electromagnetic Measurements and Test Cells

The test cells were of internal dimensions 80×80×40mm. Copper electrodes with dimensions of 80×80×2 mm were attached to two opposite faces of the cell. Copper connections were passed through the cell walls and connected to the electrodes. All impedance measurements were acquired using the LCR meter, operating in voltage-drive mode, with the signal voltage being 1000 mV. A linear sweep over the frequency range of 1 kHz to 1000 kHz was used with the data, recorded at 21 frequency points within this range.

The connection to the LCR meter was by means of short, individually screened coaxial cables to the voltage (V), high/low and current (I) output/input terminals. Cable impedance, plate impedance and fringing impedance were determined using an appropriate model circuits. From the measurements, the impedances of soil sample were calculated and all data is logged by a PC. The complex permittivities (real part dielectric constant and imaginary part loss factor) of soil samples were deduced from the impedance of the soil. The setup of the system is shown in Fig. 2.

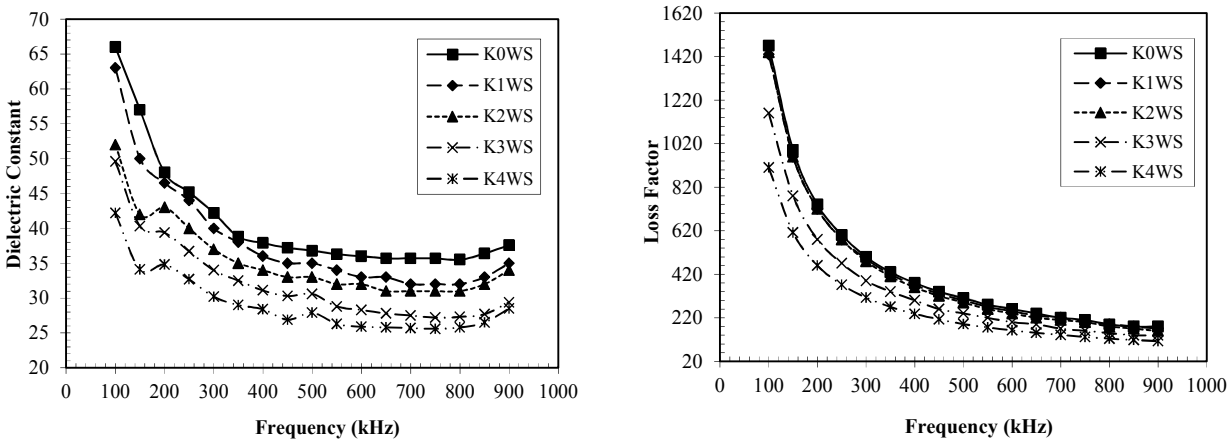


Figures 2. Schematic diagram of the dielectric measurement system

Results and Discussion

The effect of kerosene content on the measured electromagnetic properties of contaminated soil has been evaluated. Five levels of kerosene content were used to contaminate the soil samples. These five levels of kerosene were evaluated at frequency range of 100 to 1000 kHz.

The results of dielectric constant and loss factor of soil contaminated with deferent level of kerosene versus frequency are shown in Fig. 3, while the relations between the dielectric properties and loss factor of soil with kerosene content are shown in Fig. 4.



Figures 3. Dielectric constant and loss factor of sandy soil contaminated with kerosene at various frequency.

The dielectric constants and loss factors decrease by increasing the frequency at all kerosene content as shown in Fig. 3, at low frequency it clears that has a rapid decreasing in dielectric constant, and the most appropriate frequency should be higher than 600 kHz.

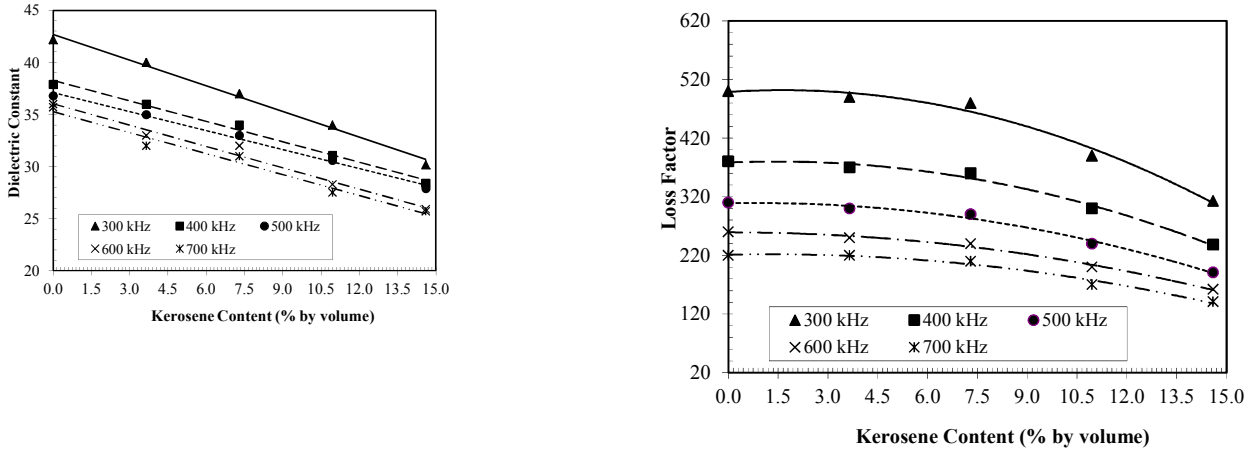


Figure 4. Effect of kerosene concentration on dielectric constant and loss factor of sandy contaminated soil.

It is clear from the Fig. 4 for kerosene-contaminated soil at saturation condition that both dielectric constant and loss factors of soil are decreased with increasing kerosene content. The dielectric constant shows linear decrease with increasing kerosene content while loss factor shows high rate of decrease with increasing kerosene content.

Conclusions

This study was conducted to develop an electromagnetic measurement method for electromagnetic characterization of petroleum and hydrocarbon contaminated soil.The dielectric constant (real part of permeativitty) and loss factor (imaginary part of permeativitty) were studied in the frequency range of 100 to 1000 kHz for kerosene contaminated soil. And the experiments confirmed both dielectric constant and loss factors of soil samples decrease with increasing frequency. Complex impedance of contaminated soil shows change in trends at different frequency. A cut off frequency change with liquid content in soil, therefore the results indicate that single frequency is not recommended for characterization of contaminated soil and the most appropriate frequency should be higher than 600 kHz. In contaminated soil with kerosene and over all frequency range of 100 to 1000kHz both dielectric constant and Loss factors of soil samples decrease with increasing kerosene-contaminated content. This can be attributing to the decrease of conductivity of the soil when the high conducting water is replaced by very low conductivity kerosene.

Acknowledgements

This work was supported by a grant “No. NU064/12 Petroleum Soil Contamination” from Deanship of Scientific Research, Najran University, Kingdom of Saudi Arabia. The authors would like to acknowledge the help of staff members in the faculty of engineering for help and providing access to the testing facilities.

References

[1] M. Juárez, J. Sánchez and A. Sánchez, Química del Sueloy Medio Ambiente, Universidad de Alicante, San Vicente (2006).

[2] Dickerson, United States Patent. Process and Material for Bioremediation of Hydrocarbon Contaminated Soils. Patent Number 5,609,667 (1997).

[3] SSSA., Internet Glossary of Soil Science Terms, Soil Science Society of America. UN-CSD. 1996. Indicators for sustainable development: Framework and Methodologies. United Nation, New York (1998).

[4] V. Saltasetal, F. Vallianatos, P. Soupios, J.P. Makris and D. Triantis., Dielectric and conductivity measurements as proxy method to monitor contamination in sandstone,

Journal of Hazardous Materials, doi:10.1016/j.jhazmat.2006.08.051 (2006).

[5] C. N. Okoye, R. R. Cotton, and O'Meara, D. "Application of resistivity cone penetration testing for qualitative delineation of creosote contamination in saturated soils." Geoenvironment 2000, ASCE, New York, N. Y., 151-160. (1995).

[6] G. R. Olheft, Direct detection of hydrocarbon and organic chemicals with ground penetrating radar and complex resistivity, Proceedings of the NWWA/API Conference on Petroleum Hydrocarbons and Organic Chemicals in Ground Water-Prevention, Detection, and Restoration, Houston, November 12-14, 284-305 (1986).

[7] D. Chenaf, & N. Amara, Time domain reflectometry for the characterization of diesel contaminated soils, Proceedings of the second international symposium and workshop on time domain reflectometry for innovative geotechnical applications, Northwestern University (2001).

[8] J. M. Arocena, & P. M. Rutherford, Properties of hydrocarbon-and salt-contaminated flare pit soils in northeastern British Columbia (Canada), Chemosphere 60:567 .575 (2005).

[9] K. Abidin, Evaluation of Soil Porosity Using a Low MHz Rang., Properties of hydrocarbon-and salt-contaminated flare pit soils in northeastern British Columbia (Canada), rsistivity, Proceedings of the NWWA/API Conference on Petroleum Hydrocarbons and Organic Chemicals in Ground Water-Prevention, Detection, and Restoration, Houston, November 12-14, 284-305 (2005).

CHAPTER 2:

Coastal and Offshore Engineering

Applied Mechanics and Materials Vol. 567 (2014) pp 191-196
© (2014) Trans Tech Publications, Switzerland
doi:10.4028/www.scientific.net/AMM.567.191

A Study on the Structural Failure Mechanism and Reserve Strength Ratio of Tarpon Monopods

Lee Hsiu Eik[1, a], Mohd Shahir Liew[2,b]

[1]Universiti Teknologi PETRONAS, 31750 Tronoh, Perak, Malaysia

[2] Universiti Teknologi PETRONAS, 31750 Tronoh, Perak, Malaysia

[a] aaronlhe@gmail.com, [b] shahir_liew@petronas.com.my

Keywords: Tarpon monopod, PETRONAS, platform, SACS v5.3, in place, collapse, ultimate strength, failure mechanism, Reserve Strength Ratio, guying system, intact, damaged, anchor piles, plasticity

Abstract. This paper addresses the structural response and characteristics of a Tarpon platform, presented as an in depth sensitivity study of its structural system from the perspective of its reserve strength ratio and mode of failure. The Tarpon platform is one of many marginal field minimal platform concepts in use worldwide. PETRONAS currently owns and operates several Tarpons in Malaysian waters. A single platform of which its data is most complete and available is chosen to represent the fleet of Tarpon Monopods in Malaysian waters. The platform, heretofore named Platform A, situated offshore Terengganu, is modeled and simulated in SACS v5.3 to reflect it's as built condition. The SACS Collapse module was utilized to simulate the Tarpon's ultimate strength which serves as a benchmark for the comparison of the static in place analysis to obtain the Reserve Strength Ratio (RSR). The initiating mode of failure was determined to be at the anchor piles. The results point out that the Tarpon Monopod has a low structural redundancy, especially where there is a loss of wire rope.

Introduction

As Malaysia's conventional offshore oil and gas reserves continue to deplete, attention in the country is shifting to the harder to tap deep water reserves and the once un-economical marginal fields. To address the latter, new minimal, low cost platform concepts are coming onto the mainstream which renders the marginal fields economical. The Tarpon Monopod is an example of such minimal platforms. With several Tarpons operating in Malaysian waters, there is a pressing need for a better understanding of their behavior in terms of structural response, characteristics and sensitivity to the forces exerted on it by the environment it is placed in. In particular, this study addresses this need from the standpoints of ultimate strength, reserve strength and initiating mode of failure.

A single platform has been chosen to represent the entire fleet of Tarpon monopods owned by PETRONAS in Malaysian waters. The platform, coined Platform A is situated in approximately 76m water depth, offshore Terengganu. It was chosen for this study due to complete documentation and key data. The Tarpon Monopod is a highly standardized minimal platform design, hence justifies the use of a single platform to represent, for this study, in general any Tarpons situated in water depths ranging from 70 – 80m, subjected to approximately equivalent metocean conditions.

Specific studies relating to the structural behavior and limitations of the Tarpon monopod in the open literature is very limited. Hence despite benefits like that of short fabrication time, little is known about the Tarpon's structural characteristics. More knowledge on its ultimate strength, reserve strength ratio and failure mode is a pre-requisite in order to effectively gauge the risks involved intrinsic in deploying Tarpon platforms and to contribute to further improvement in its design via optimization and the like.

The Tarpon Monopod

The Tarpon Monopod is also known as a cable guyed caisson. As of the year 1999, there were 37 of such platforms operating in the Gulf of Mexico, West Aftica and Indonesia. It was first used back in 1987 with Stolt Comex Seaway as the initial owner of the patents for the system. [4]

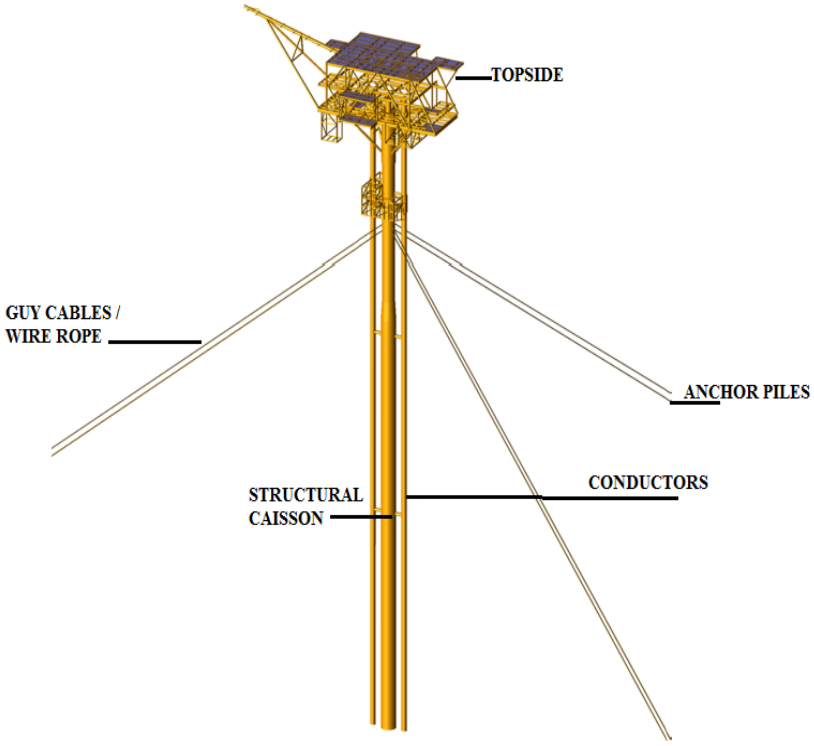


Figure 1 Components of the Tarpon Monopod

Today, there are more than 56 installations worldwide installed in water depths in water depths ranging from 60 ft to 350 ft. [6]

Table 1 showcases the main Tarpon platform elements and their primary functions [3] while a 3-dimensional graphical illustration is portrayed in Figure 1.

Table 1 Tarpon components and functions

Component	Function
Main caisson	To anchor / fix the guy wires to the mudline/seabed
Anchor piles	A steel caisson with a diameter typically larger than the conductors which acts as the platform's leg, bracing points for the conductors via clamps, and in some cases, can be used to house several internal wells.
Conductor	A steel caisson or riser used to protect the well and production tubing.
Conductor clamps	To vertically fix the conductor casings to the caisson
Guy cables	To provide lateral resistance and stability for the platform.
Topside	The superstructure located above the reach of waves, equipped with facilities such as production equipment, jib crane, boat landing, helideck and a flare boom.

The representative Tarpon model will heretofore be referred to as Platform A. The general design data for Platform A platform as modelled in SACS 5.3 is as shown in Table 2.

Table 2 Generic model details [3]

Platform details	Platform A
Platform type	Monopod
Accommodation	Unmanned, no quarters
Year installed	2006
Water depth	76.2m
Jacket height	82.2m
Water Depth	76.2m
Deck weight	184.8 MT
Jacket weight	800 MT
Pile weight	150.34 MT

Reserve Strength Ratio

The Reserve Strength Ratio (RSR) in a common form known to both industry practitioners and researchers is depicted in Equation 1 [1];

$$\text{RSR} = \frac{\text{Ultimate platform resistance}}{\text{Design Load}} \tag{1}$$

A closely related parameter to the RSR can be interestingly defined by the terminology of the Residual Resistance Factor (RIF) as in Equation 2 [1].

$$\text{RIF} = \frac{\text{Damaged structural capacity}}{\text{Ultimate capacity}} \tag{2}$$

The definitions for RSR in the open literature vary from author to author, and also from different contexts. For the purpose of this study, the author has opted to define a measurement the Tarpon's structural RSR to be defined herein as the ratio of the ultimate structural caisson mud line moment generated via pushover analysis and the maximum design mud line moment taken from the in place static analysis.

$$\text{RSR} = \frac{\text{Ultimate platform resistance}}{\text{Design Reactions}} \tag{3}$$

Simulated Scenarios

The static in place analysis was performed via modelling in SACS Precede module and simulation in SACS IV. The pushover analysis for the modelled guyed caisson monopod was performed in SACS via the Collapse module and interpreted using the corresponding results output file and the graphical results interpreter, Colvue.

Table 3, showcases the four different sets of storm metocean criteria and the design water depth respectively used in the study. Table 3 metocean data does not apply to pushover analysis, as the initial load is arbitrarily defined by the author which is then incremented until structural failure.

Table 3 Design Data

Data	100 year return period		
	PTS [5]	*Joint Density*	*As Designed [2]*
Wave Height [m]	5.77 (H_s)	5.7 (H_s)	11.3 (H_{max})
Wave Period [s]	8.06	Assume 6 and 8 seconds	9.3
Current [m/s]	1.67 @ surface 1.33 @ mid 0.36 @ seabed	0.69 @ -3m	1.3 @ surface 0.7 @ seabed
Wind (1 hour mean) [m/s]	23.2	13.2	36.4
Design Water Level [m]	78		

Pushover Analysis and Mode of Failure

Failure of the structure was initiated at the anchor piles, where for most instances, pile plasticity occurred and in some scenarios, SACS recorded pile pullout events in the degraded soil models. Pile failure / plasticity for both instances are equal and this enforces the notion that the integrity of the Tarpon structure is controlled primarily by the anchor piles. Table 4 showcases the summary of the ultimate strength prior to complete structural failure of the Tarpon Platform A. Another key result that can be extracted is the maximum Tarpon deflection prior to initiation of failure. This value , taken at 130 cm as seen from the rounded –pre failure value in Table 5 provides an insight into the amount of displacement that can be experienced by the Tarpon before failure is initiated at the piles.

Table 4 Maximum results prior to structural failure

Storm direction	Soil condition	Max displacement (cm)	Base Shear (kN)	Max base moment (kN.m)
NE	Intact	189.5	4329	17830
SW	Intact	373.6	6493	23090
NE	Degraded	115.8	1883	10518
SW	Degraded	253.1	4936	15169

Pile failure / plasticity for both instances are equal and this enforces the notion that the integrity of the Tarpon structure is controlled primarily by the anchor piles. A snippet of the anchor pile failure during the pushover analysis is given in Table 5.

Table 5 Collapse for a fully guyed Tarpon (North East Storm Approach)

Increment	Load factor	Caisson deflection (cm)
11	6.88	76.9
12	7.68	93.6
13	8.84	111.0
14	9.82	129.8
15	10.80	152.6 -PILE PLASTIC
16	11.78	196.6 – PILE PLASTIC

Ultimate Load in the Guying System

An important assumption regarding the ultimate strength of guy cables is the nominal breaking strength of the wire ropes which is taken to be 713 tons [2]. Taking g = 9.80665 m/s2, that equates to 6992 kN. Each of the guy wires are analyzed to act in set of pairs and in the condition that one of the wire in the pair snaps. Table 6 showcase the guy cable tension summary for a signature in place condition at the structural failure at pushover. The factor of safety (FOS) for the guy wires are computed for each predominant monsoon season direction when failure is first initiated in the pushover analysis. The FOS is defined by Equation 4;

FOS = 6992/ axial load (4)

Table 6 Guy Wire strength check at pile plasticity

	NE load (kN)	SW Load (kN)	NE FOS	SW FOS
Simulated (fully guyed)	2580.1	2685.5	2.7 (pair) 1.4 (single)	2.6 (pair) 1.3 (single)

It is clear from Table 6 that the guy cables will not fail in axial tension. Even with the pushover analysis, the guy cables still possess relatively large reserve strengths. Hence, should any set of guy cables be observed to have failed attention should be given to its connections at the terminator clamps and anchor piles while investigating the potential role of corrosion , creep and fatigue in its failure.

Reserve Strength Ratio

Table 7 showcases the RSR values for various Tarpon conditions subjected to metocean conditions as recommended for PMO operations by PTS 2010.

The instinctive hypothesis one would infer from a first look at a Tarpon monopod is confirmed here, that the platform is highly dependent on its guying system which plays a crucial role in maintaining lateral stability. By inspection of table 7 this becomes clear as the RSR of the Tarpon is seen to be more than adequate in its fully guyed condition (intact) but is drastically reduced as the guy wires fail in function or physically. Notice that the dually guyed Tarpon will have an RSR value approximately equal to its fully guyed condition if and only if the storm direction acts against the tension pulling capabilities of both guy wires.

Table 7 Summary of Tarpon A Reserve Strength Ratio

	Condition	RSR
PTS 2010 Metocean approaching from North East (Monsoon)	Freestanding	0.41
	Singly guyed	1.05
	Two guys	6.72
	Fully guyed	6.10
PTS 2010 Metocean approaching from South West (Monsoon)	Freestanding	0.46
	Singly guyed	0.53
	Two guys	9.57
	Fully guyed	8.55

Summary

The Tarpon Monopod utilized for this study is situated in a water depth of approximately 76 meters. It is anticipated that this study can be applied for any generic Tarpon structure worldwide situated in similar metocean conditions and within the water depth range of 70 – 80 meters.
The main take away from this study is as summarized below;

- The Tarpon Monopod is a sound structure if and only if its guying system is intact.
- The wire ropes will not fail in axial tension even in the event of structural failure. Hence, should the wire ropes be observed to have snapped or failed, attention should be given to its connections at the anchor piles and terminator clamp, or even consider dynamic failure modes through vortex induced vibration or excessive fatigue. This can be taken up as future research.
- The initiating mode of failure is through the anchor piles, by which they turn plastic or experience pile pull out in weak soil. Once the lateral holding capabilities of the guying system has been diminished by such an event, the Tarpon will face a high risk of failure.
- A way forward would be to increase the structural redundancy of the Tarpon and to increase the anchor pile holding capacities.

References

[1] Bolt H M , C J Bilington & J K Ward (1996). OTH 92 365: A Review of the Ultimate Strength of Tubular Framed Structures. Health and Safety Executive.

[2] ECL (2008). Development Project – Detailed Engineering Design of Substructure for LEDP-A Guyed Caisson (Ledang LEDP-A Substructure Design Manual). ECL Project No. 709605.

[3] Mohamed Syamsul Faiz Bin Samsudin (2012). Structural Sensitivity and Parameter of Tarpon Platform (Unpublished dissertation). Universiti Teknologi PETRONAS, Perak, Malaysia.

[4] Oil and Gas Journal (1999). Tarpon monotower develops further from 37 field applications. Retrieved from http://www.offshore-mag.com/articles/print/volume-59/issue4/news/generalinterest/tarpon-monotower-develops-further-from-37-field-applications.html

[5] PETRONAS (2010). PETRONAS Technical Standards – PTS 34. 19.10.30 – Design of Fixed Offshore Structures.

[6] Tarpon Systems LLC (2012). Tarpon System – Making Marginal Field Production More Profitable than Ever. Retrieved from http://tarponsystems.com/pdf/Tarpon2page2NoAdd.pdf

Applied Mechanics and Materials Vol. 567 (2014) pp 197-203
© (2014) Trans Tech Publications, Switzerland
doi:10.4028/www.scientific.net/AMM.567.197

A Studyon Mooring Systemsof an Offshore Floating Platform for Different Configurations

Anurag Yenduri[1, a], Montasir Osman Ahmed[2, b], V. J. Kurian[3, c]

[1, 2, 3]Dept. of Civil Engineering, Universiti Teknologi PETRONAS, Tronoh, Perak, Malaysia – 31750

[a]yendurianurag@gmail.com, [b]montasir.ahmedali, [c]kurian_john@petronas.com.my

Keywords: Configuration; Station-keeping systems; Mooring line; Quasi-static analysis

Abstract. Moored systemsof floating platforms typically have mooring lines in groups,attached to hull of the platform in different configurations.Study on therestoring behaviour of these systemsfor variousparameters of mooring lines gives an insight to decide on the preliminary design of platforms.This paper includesparametric study on the behaviour of mooring systems for various symmetric, asymmetric configurations of the lines. To compute the restoring forces of the mooring system,quasi-static analysis has been adopted and a MATLAB code named *QSAML* has been developed, validated with experimental tests and used for the parametric study.It has been observed that, the restoring capability of mooring system reduces whenthe lines are placed away from the wave heading.For any wave heading, the variation in restoring behaviour of mooring system with symmetric configurations is insignificant up to relatively small excursions of the platform.

Introduction

Mooring systems are widely used in station-keeping of floating systems. In the recent years, the operational scope of the oil companies started shiftingto deep and ultra-deep waters in order to meet the oil demand-supply equity.Hence, the initiative to exploit the reserves in deeper waters has led the researchers to extend the limits of station-keeping systems for the offshore floating platforms.Till date, several mooring systems have been designed for floating platforms. Among the different types present, the spread moorings typically consisting of mooring lines spread around the platformare preferred as they have long service life and can be used for all sizes of the platform at any water depths.

Placement of several mooring lines around the platform provides the principal resistance to displacements in the horizontal plane induced by the environmental loading [7].There is a need to incorporate the dynamic considerations in the analysis/design procedure for the deep-water mooring systems but the Quasi-static approach which has been proven to be a proper design tool for the mooring systems is considered a better choice in the first approach as it is almost certain to achieve convergence and if desired, further analysis may then be carried out using the output of the static analysis as initial conditions for the dynamic analysis [5, 6,7, 8].

This paper involves developing a numerical code for the analysis of multi-component catenary mooring lines using Quasi-static approach, which after validation with the experimental results is used to conduct the parametric study. The motivation for this work lies with investigating the behaviour of mooring systems for various configurations of the lines which can givean insight to the design engineers in selecting mooring line configurations for the platforms.

Governing Equations for the Mooring Line Analysis

The nonlinear relationship between the restoring force and horizontal excursion of a mooring line usually requires an iterative solution. The key assumptions made for the analysis of mooring lines are – (a) components of the mooring line move very slowly so that the drag forces on the line can be treated as negligible; (b) change in the line geometry is insignificant and thereby, in the line force due to direct fluid loading caused from the waves; (c) the clump weight segment is inextensible; and (d) only horizontal excursion of the line is considered.

Using equation of a catenary for the evaluation of force-excursion relationship of the mooring line, the vertical and horizontal projection of any segment hanging freely under its own weight *w* per unit length, is as given in Eq. 1, Eq. 2.

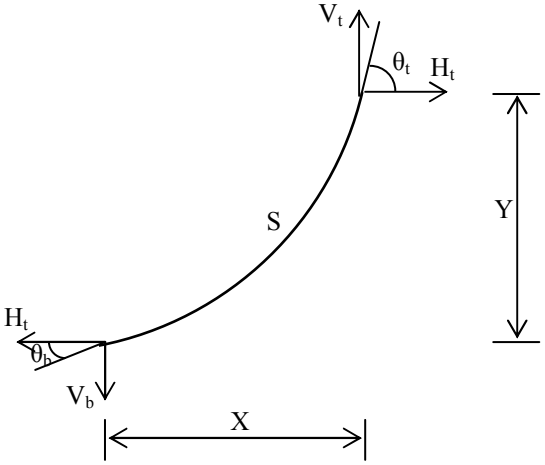


Fig. 1 Free body diagram of a freely suspended mooring line

$$Y = \frac{H_t}{w}[\cosh\{\sinh^{-1}(\tan(\theta_t))\} - \cosh\{\sinh^{-1}(\tan(\theta_b))\}] \quad (1)$$

$$X = \frac{H_t}{w}[\sinh^{-1}(\tan(\theta_t)) - \sinh^{-1}(\tan(\theta_b))] \quad (2)$$

The extension of any segment under increased line tension can be evaluated using Eq. 3.

$$S = S_0\left(1 + \frac{T - T_0}{EA}\right) \quad (3)$$

where T_0 – Initial line tension when the segment length is S_0, T – Increased average line tension.

The analysis has been carried out for the mooring line with disturbed clump weight by referring to the procedure steps mentioned in [1]; incorporating the two conditions stated for lifting-off of the clump weight. The behaviour of the mooring system i.e. the resultant horizontal force *H*, for an excursion δ can be computed using the Eq. 4.

$$H(\delta) = \sum_{j=1,p} H_j(\delta_j)\cos(\pi - \theta_j) \quad (4)$$

where p – Total number of mooring lines; θ_j – Angle between the j^{th} mooring line and the direction of excursion; δ_j – Excursion for the j^{th} mooring line; $H_j(\delta_j)$ – Associated horizontal force with $\delta_j = \delta\cos(\pi - \theta_j)$.

Numerical Modelling of the Mooring Lines

The motions offloating platform depend on the restoring performance of mooring lines attached to it at the hull. Hence, mooring lines configurations greatly affect the design of the platform.Therefore, it is essential to study their effect on the behaviour of mooring systems and opt for the best suitable.

For the parametric study, a floating platform having the fairleads at a height of 941.832m from the sea bed is considered.Various symmetric and asymmetric configurations are studied fortwo mooring line arrangements: 3×3 and 4×4(*Note:* I×J - 'I' denotes number of mooring line groups & 'J' denotes number of lines in each group).These two arrangements are chosen in regards to the present scenario of floating platforms containing mooring lines more commonly in three or four groups with three to four lines in each group.

To ease the analysis procedure, each I^{th}mooring line group is considered as one line representing the total restoring behaviour of 'J' mooring lines in each group as shown in Fig. 2.

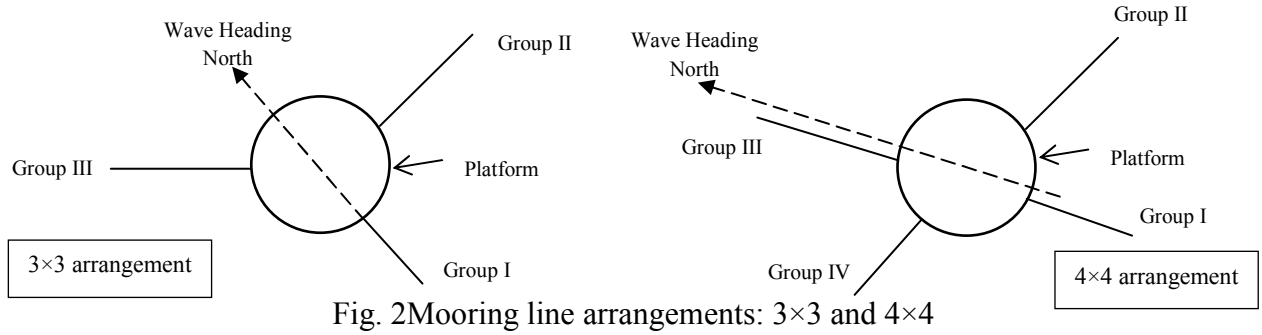


Fig. 2Mooring line arrangements: 3×3 and 4×4

Symmetric. The mooring lines are placed symmetrical to each other and various configurations have been generated by changing the wave headingwith respect to one mooring line, from 0^0 to 60^0 for 3×3 arrangement and 0^0 to 45^0 for 4×4 arrangement, as depicted in Table 1.

Asymmetric. For 3×3 arrangement, these configurations are generated by changing only one mooring line (with other lines retained as in symmetric configurations) with respect to the wave heading from 0^0 to 60^0. Similarly, for 4×4 arrangement these configurations are generated for two cases: (1) Only one mooring line is changed; and (2) Two mooring lines are changed simultaneously; from 0^0 to 45^0 with respect to the wave heading, as depicted in Table 1.

Table 1 Configurations of mooring lines considered for the parametric study
(Azimuth angles are mentioned with respect to *wave heading south*)

Legend	Nomenclature	Mooring Line Arrangement	Mooring Line Configurations	Remarks
Symmetric	Study-1	3×3	a) 0^0, 120^0, 240^0 b) 15^0, 135^0, 255^0 c) 30^0, 150^0, 270^0 d) 45^0, 165^0, 285^0 e) 60^0, 180^0, 300^0	All the three lines are placed at 120^0 to each other
	Study-2	4×4	a) 0^0, 90^0, 180^0, 270^0 b) 15^0, 105^0, 195^0, 285^0 c) 30^0, 120^0, 210^0, 300^0 d) 45^0, 135^0, 225^0, 315^0	All the four lines are placed at 90^0 to each other
Asymmetric	Study-3	3×3	a) 15^0, 120^0, 240^0 b) 30^0, 120^0, 240^0 c) 45^0, 120^0, 240^0 d) 60^0, 120^0, 240^0	–
	Study-4	4×4	a) 15^0, 90^0, 180^0, 270^0 b) 30^0, 90^0, 180^0, 270^0 c) 45^0, 90^0, 180^0, 270^0	Case 1
	Study-5		a) 15^0, 105^0, 180^0, 270^0 b) 30^0, 120^0, 180^0, 270^0 c) 45^0, 135^0, 180^0, 270^0	Case 2

To compute restoring forces in mooring lines, Quasi-static approach is adopted for the analysis and a MATLAB code named *QSAML* has been developed. The numerical code is validated with experiment tests by comparing the mooring stiffness curve obtained for the MARLIN truss spar mooring configuration given in Table 3, Fig. 3.

The material properties – wet weight, effective modulus, breaking loads and lengths of the various components of mooring linesused for MARLIN truss spar platform are as given in Table 4.

Table 3 MARLIN truss spar mooringconfiguration
(Azimuth angles are mentioned with respect to *wave heading south*)

Group	Configuration
I	0^0, 5^0, 5^0
II	115^0, 120^0, 125^0
III	235^0, 240^0, 245^0

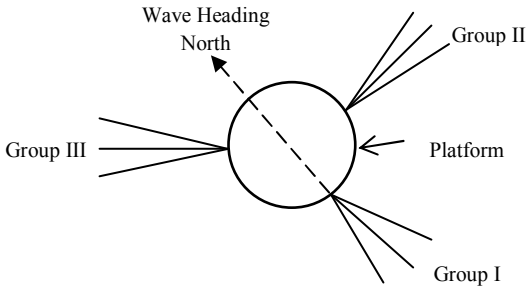


Fig. 3 Mooring arrangement of the platform used for validation

Table 4Characteristics of the MARLIN truss spar mooring lines

Legend	Top Component	Middle Component	Lower Component
Type	Chain cable	Spiral strand cable	Chain cable
Length (m)	76.2	1828.7	45.7
Wet weight (kN/m)	2.73	0.636	2.73
Effective Modulus (kN)	665852	1338848	858882
Breaking load (kN)	13188	12454	13188

Results and Discussion

The results obtained from numerical code, *QSAML* and experiments tests for mooring configuration-I are as shown in Fig 4. The experimental tests were performed on a 1:61 scale truss spar model by Amooc in Offshore Technology Research Centre (OTRC) wave tank at Texas A&M University [9].

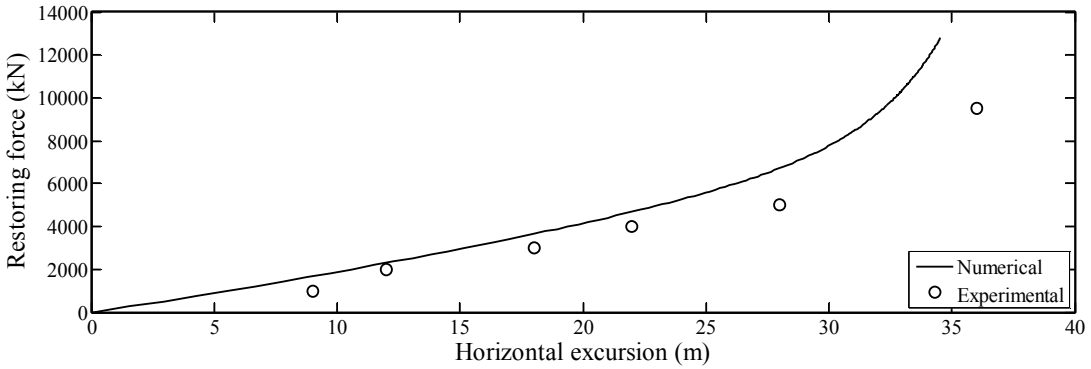


Fig. 4 Validation of numerical predictions with experimental measurements

The difference in the results can be attributed to change in the mooring line set up between the prototype and experimental model i.e. the prototype is considered with nine mooring lines whereas

experimental model with only five mooring lines (one line from group: I, III and three lines from group-II); which otherwise can be concluded that there is a good agreement between the numerical and experimental results.

Symmetric Configurations. The restoring behaviour of mooring system for different configurations is as shown in Figs. 5 and 6. It can be inferred that restoring force of the two mooring line arrangements: 3×3, 4×4 decreases as the lines are shifted away from wave heading.

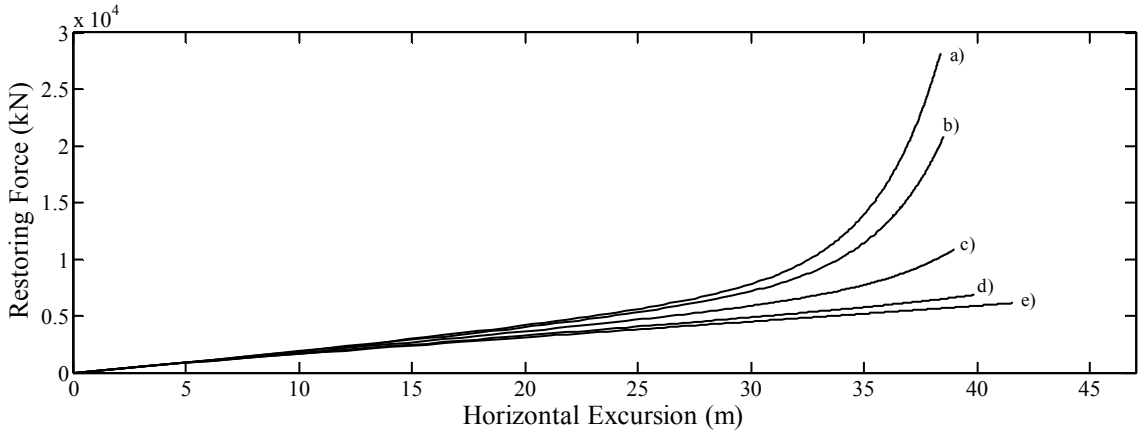


Fig. 5Mooring restoring force in 3×3 arrangement for symmetric configurations (Study-1)

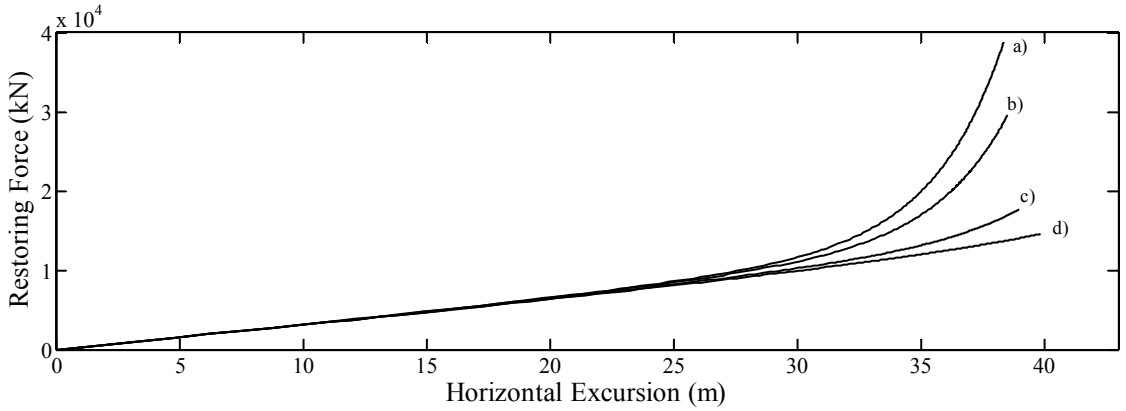


Fig. 5Mooring restoring force in 4×4 arrangement for symmetric configurations (Study-2)

The variation in restoring behaviour of mooring system is found to be insignificant for all the wave headings. For 3×3 arrangement, the restoring behaviour of mooring system does not show significant difference until 20m of excursion and for 4×4 arrangement, until 30m of excursion and thereafter a significant variation is observed.It also implies that as the number of mooring line groups are increased, variation in the restoring behaviour of mooring system remains insignificant up to relatively large excursions of the platform.

Asymmetric Configurations. Similar to the symmetric configurations study; from Figs. 7 and 8, it can be observed that the restoring capability of the mooring system decreases for both the arrangements: 3×3, 4×4 as the lines are placed away from the wave heading.

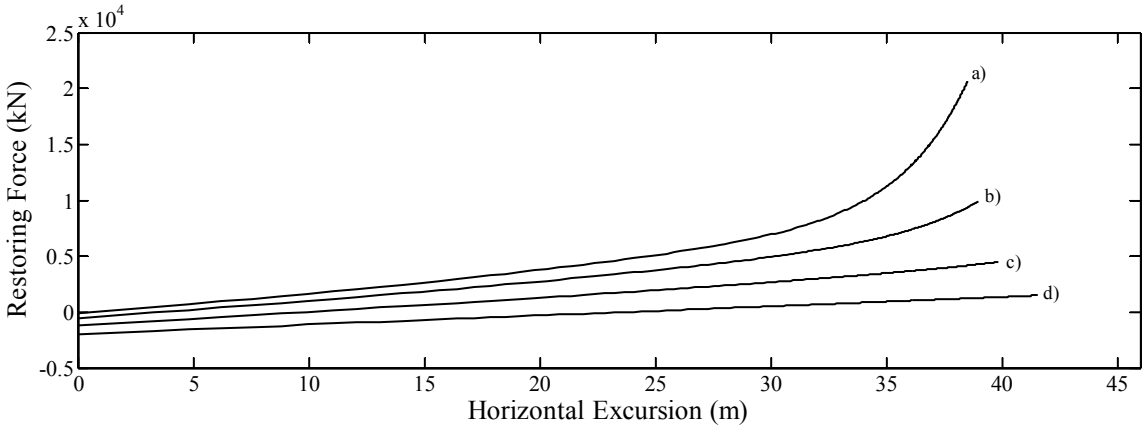


Fig. 7Mooring restoring force in 3×3 arrangement for asymmetric configurations (Study-3)

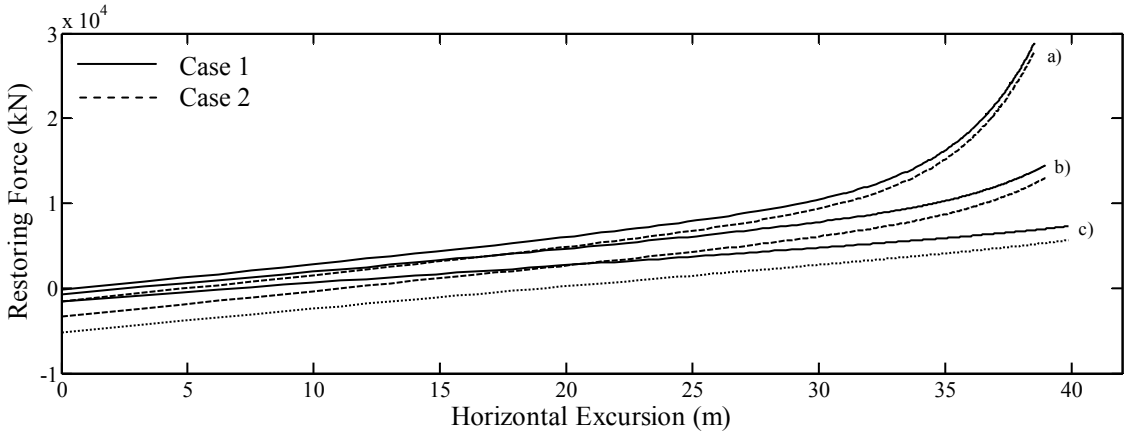


Fig. 8Mooring restoring force in 4×4 arrangement for asymmetric configurations (Study-4, 5)

From Fig. 8,it can be observed that the difference in restoring behaviour between cases: 1 and 2 for line configurations: (a),(b) and (c) is less with difference for(a) being the least.

Conclusions

Based on the numerical study conducted, following conclusions can be drawn:

1) In general, the restoring capability of any mooring system with symmetric or asymmetric configuration decreases as the line group is shifted away from wave heading.
2) For relatively small horizontal excursions, mooring systems with symmetric configurations show insignificant difference in their restoring behaviour for any wave heading.
3) In conjunction withconclusion-2; when the number of mooring line groups is increased, the differencecan be insignificant even up to relatively large excursions.
4) Study conducted on asymmetric configurations (for 4×4 mooring arrangement)obtained by varying one and two mooring linesconclude that there is no significant difference betweenrestoring behaviour of the two mooring configurations i.e. respective case: 1 and 2.

References

[1] A. K. Agarwal, A. K. Jain, Dynamic behaviour of offshore spar platforms under regular sea waves, Journal of Ocean Engineering 30 (2003) 487-516.
[2] Jason I. Gobat, Mark A. Grosenbaugh, A simple model for heave-induce dynamic tension in catenary moorings, Journal of Applied Ocean Research 23 (2001) 159-174.
[3] M. B. Rosales, C. P. Filipich, Full modelling of the mooring non-linearity in a two-dimensional floating structure, International Journal of Non-Linear Mechanics 41 (2006) 1-17.
[4] M. J. Downie, J. M. R. Graham, C. Hall, A. Incecik, I. Nygaard, An experimental investigation of motion control devices for truss spars, Journal of Marine Structures 13 (2000) 75-90.

[5] R. Pascoal, S. Huang, N. Barltrop, C. GuedesSoares, Assessment of the effect of mooring systems on the horizontal motions with an equivalent force to model, Journal of Ocean Engineering 33 (2006) 1644-1668.
[6] R. Pascoal, S. Huang, N. Barltrop, C. GuedesSoares, Equivalent force model for the effect of mooring systems on the horizontal motions, Journal of Applied Ocean Research 27 (2005) 165-172.
[7] Russel J. Smith, Colin J. MacFarlane, Statics of a three component mooring line, Journal of Ocean Engineering 28 (2001) 899-914.
[8] S. A. Mavrakos, V. J. Papazoglou, M. S. Trintafyllou, J. Hatjigeorgiou, Deep water mooring dynamics, Journal of Marine Structures 9 (1996) 181-209.
[9] ZhihuangRan, Coupled dynamic analysis of floating structures in waves and currents, Ph.D Thesis, Texas A&M University, Texas, 2000.

Applied Mechanics and Materials Vol. 567 (2014) pp 204-209
© (2014) Trans Tech Publications, Switzerland
doi:10.4028/www.scientific.net/AMM.567.204

Behaviour of Mooring Systems for Different Line Pretensions

Montasir Osman Ahmed[1, a], Anurag Yenduri[2, b], V. J. Kurian[3, c]

[1, 2, 3]Dept. of Civil Engineering, Universiti Teknologi PETRONAS, Tronoh, Perak, Malaysia – 31750

[a]montasir.ahmedali, [c]kurian_john}@petronas.com.my, [b]yendurianurag@gmail.com

Keywords: Pretension; Station-keeping systems; Mooring line; Quasi-static analysis

Abstract. Mooring lines are the most commonly used station-keeping systems for floating platforms as they are easy to install and relocate. The mooring lines are usually pre-tensioned so as to use their energy absorption to reduce the platform motions and thereby, to lower the forces in the lines. To decide on the preliminary design of the platforms, it is necessary to investigate the restoring behaviour of the mooring systems for various parameters. In this study, two different mooring configurations with and without mooring line in wave heading direction are considered for determining its behaviour for various pretensions in the lines. A MATLAB code named *QSAML* has been developed using quasi-static approach to compute the restoring forces of the mooring system. The code is validated with experimental tests and used in this study. It has been observed that with increase in pretension of the mooring line, restoring performance of the mooring system can be improved. The maximum permissible excursions by mooring system in the wave heading direction are found to be more for relatively lower pretension values.

Introduction

In recent years, the oil exploration and production companies have started increasing their operational scope from shallow waters to deep and ultra-deep waters in order to meet the oil demand-supply equity. Hence, the initiative to exploit reserves in deep-waters has led the researchers to extend the limits of station-keeping systems for the offshore floating platforms. Among the different types of mooring systems, the spread moorings are preferred as they have long service life and can be used for all sizes of the platform at any water depths.

The mooring lines are usually multi-component catenary anchor lines, attached to the hull of the platform near its centre of pitch for low dynamic loading [1]. These catenary mooring lines are pre-tensioned and typically subjected to the loads caused by the wave frequencies and vessel motions [9]. Hence, there is a need to incorporate the dynamic considerations in the analysis/design procedure of the deep-water mooring systems. The quasi-static approach which has been proven to be a proper design tool for the mooring systems is considered in the first approach. Quasi-static analysis is almost certain to achieve convergence and if desired, further analysis may then be carried out using the output of this analysis as initial conditions for the dynamic analysis [5, 6, 7, and 8].

The study in this paper includes developing a numerical code for the analysis of multi-component catenary mooring lines using quasi-static approach, which after validation with the experimental results, is used to conduct a parametric study on the behaviour of the mooring systems for various line pretensions.

Governing Equations for the Mooring Line Analysis

The relationship between the restoring force and horizontal excursion of a mooring line is nonlinear and requires an iterative solution. The key assumptions made for the analysis of mooring lines are – (a) components of the mooring line move very slowly so that the drag forces on the line can be treated as negligible; (b) change in the line geometry is insignificant and thereby the in-line force due to direct fluid loading caused from the waves is also insignificant; (c) the clump weight segment is inextensible; and (d) only horizontal excursion of the line is considered.

Using equation of a catenary for the evaluation of force-excursion relationship of the mooring line, the vertical and horizontal projection of any segment hanging freely under its own weight w per unit length, is as given in Eq. 1, Eq. 2.

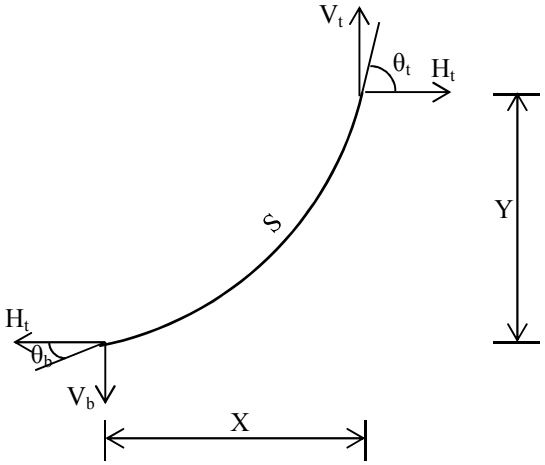


Fig. 1 Free body diagram of a freely suspended mooring line

$$Y=\frac{H_t}{w}[\cosh\left\{\sinh^{-1}(\tan(\theta_t))\right\}-\cosh\left\{\sinh^{-1}(\tan(\theta_b))\right\}\} \quad (1)$$

$$X=\frac{H_t}{w}[\sinh^{-1}(\tan(\theta_t))-\sinh^{-1}(\tan(\theta_b))] \quad (2)$$

The extension of any segment under increased line tension can be evaluated using Eq. 3. Let the initial average line tension be T_0 when the segment length is S_0 and for increased average line tension T, the stretched length becomes:

$$S=S_0\left(1+\frac{T-T_0}{EA}\right) \quad (3)$$

The analysis has been carried out for the mooring line with disturbed clump weight by referring to the procedure steps mentioned in [1]; incorporating the two conditions stated for lifting-off of the clump weight. The behaviour of the mooring system i.e. the resultant horizontal force H, for an excursion δ can be computed using the Eq. 4.

$$H(\delta)=\sum_{j=1,p} H_j(\delta_j)\cos(\pi-\theta_j) \quad (4)$$

where p is the total number of mooring lines; θ_j is the angle between the j^{th} mooring line and the direction of excursion; δ_j is the excursion for the j^{th} mooring line; $H_j(\delta_j)$ is the associated horizontal force with $\delta_j=\delta\cos(\pi-\theta_j)$.

Numerical Modelling of the Mooring Lines

Pretension installed in the mooring lines has an appreciable impact on the design of the floating structure as this tension at the fairleads shall be incorporated in the platform structure design. Hence, it is very essential to study the effect of pretension on the performance of mooring systems and install optimum pretension in the mooring lines.

To compute the restoring forces in mooring lines for various pretension values, quasi-static approach is adopted for the analysis and a MATLAB code named *QSAML* has been developed. The numerical code is validated with experiment tests by comparing the mooring stiffness curve obtained for the mooring configuration-I (MARLIN truss spar) given in Table 1.

For the parametric study, a floating platform having the fairleads at a height of 988m from the sea bed is considered. Two mooring configurations as shown in Fig. 2: I) nine lines arranged in

three groups with one line group in wave heading; and II) ten lines arranged in four groups with no line group in wave heading, are chosen. To study the effect of pretension, configurations: I and II as given in Table 1, are investigated for pretension values ranging from 1.8×10^3 to 6.5×10^3kN. The material properties – wet weight, effective modulus, breaking loads and lengths of the various components of the mooring line are as given in Table 2.

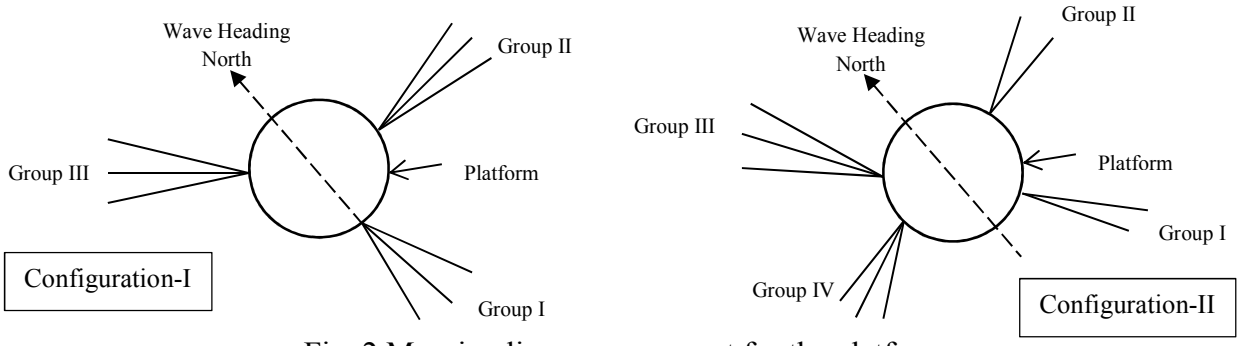


Fig. 2 Mooring lines arrangement for the platform

Table 1 Mooring line configurations
(Azimuth angles are mentioned with respect to *wave heading south*)

Group	Configuration-I	Configuration-II
I	0^0, 5^0, 5^0	45^0, 50^0
II	115^0, 120^0, 125^0	125^0, 132.5^0
III	235^0, 240^0, 245^0	222.3^0, 229.7^0, 235^0
IV	–	308.5^0, 314.1^0, 320.3^0

Table 2 Characteristics of the mooring line

Legend	Top Component	Middle Component	Lower Component
Type	Chain cable	Steel strand cable	Chain cable
Length (m)	76.2	1828.7	45.7
Wet weight (kN/m)	2.73	0.636	2.73
Effective Modulus (kN)	665852	1338848	858882
Breaking load (kN)	13188	12454	13188

Results and Discussion

The results obtained from numerical code, *QSAML* and experiments tests for mooring configuration-I are as shown in Fig 3. The experimental tests were performed on a 1:61 scale truss spar model by Amooc in Offshore Technology Research Centre (OTRC) wave tank at Texas A&M University [10]. The difference in the results can be attributed to change in the mooring line set up between the prototype and experimental model i.e. the prototype is considered with nine mooring lines whereas experimental model with only five mooring lines (one line from group: I, III and three lines from group-II); which otherwise can be concluded that there is a good agreement between the numerical and experimental results.

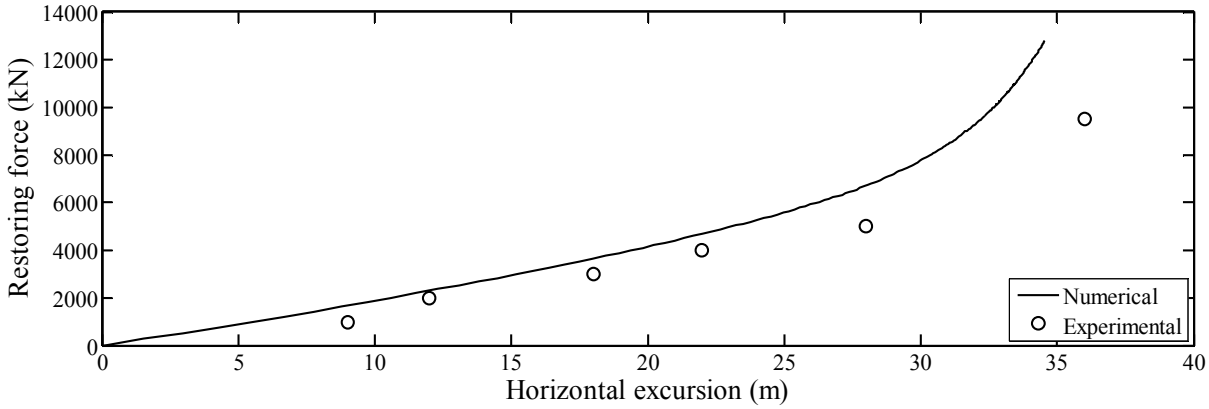


Fig. 3 Validation of numerical predictions with experimental measurements

From Figs. 4 and 5, it can be inferred that for any excursion of the platform, mooring system restoring force increases with increase in the line pretension for both configurations. For example, considering the mooring configuration-I at an excursion of 10m, the lines when installed with pretension 1.8×10^3kN offered lowest restoring force of 0.04×10^4kN whereas when installed with pretension 2.5×10^3kN offered higher restoring force of 0.28×10^4kN and so on.

Maximum permissible excursions of the two mooring systems for various line pretensions are as given in Fig. 6. It can be inferred that the maximum permissible excursion by the two mooring system configurations decreases as the line pretension is increased. These maximum excursions are found to be more for relatively lower line pretensions. For pretensions 1.8×10^3kN to 2.0×10^3kN, the mooring systems can permit excursions ranging from 52m to 114m to the platform in wave heading and for pretensions 2.1×10^3kN to 6.5×10^3kN, the maximum permissible excursions of the mooring systems range from 6m to 38m.

The reduction in maximum permissible excursions is more for relatively lower line pretensions and is less for relatively higher line pretensions. For pretensions 1.8×10^3kN to 2.1×10^3kN, the reduction ranges from 13m to 30m and for pretensions 2.1×10^3kN to 6.5×10^3kN, the reduction ranges from 0.3m to 8m.

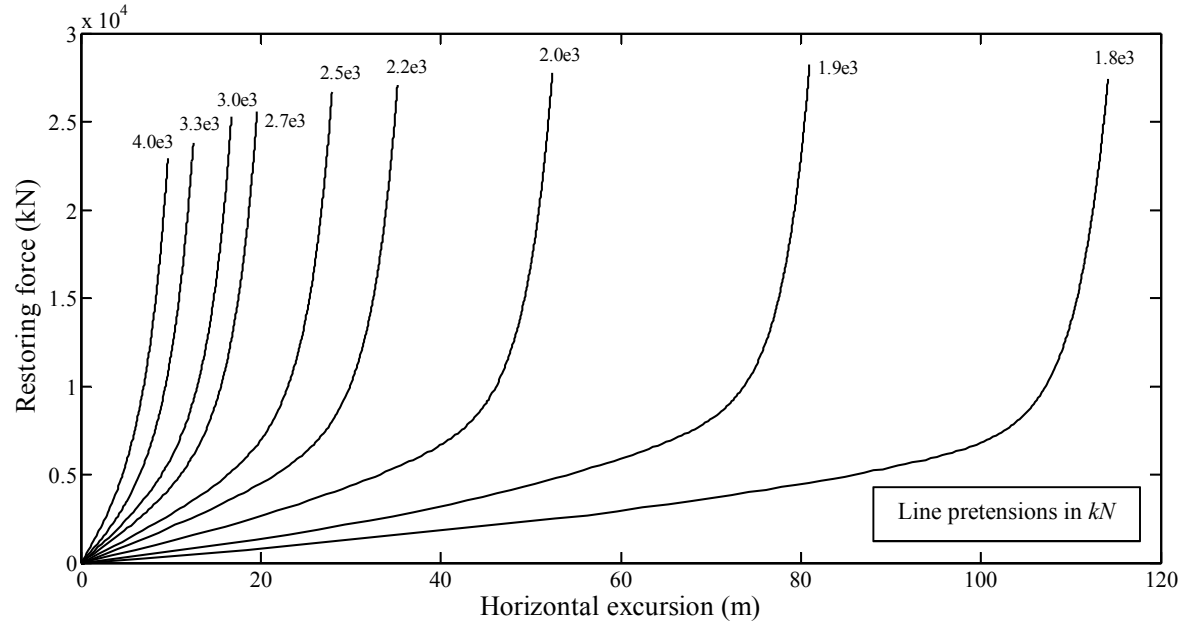


Fig. 4 Variation of the restoring force in configuration-I for different line pretensions

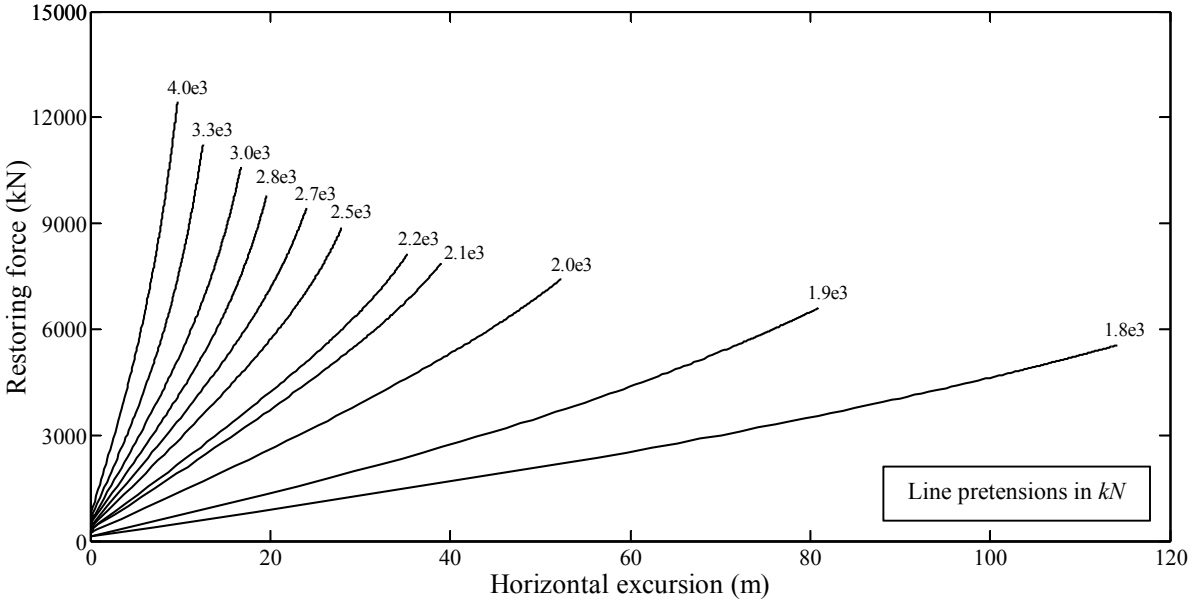


Fig. 5 Variation of the restoring force in configuration-II for different line pretensions

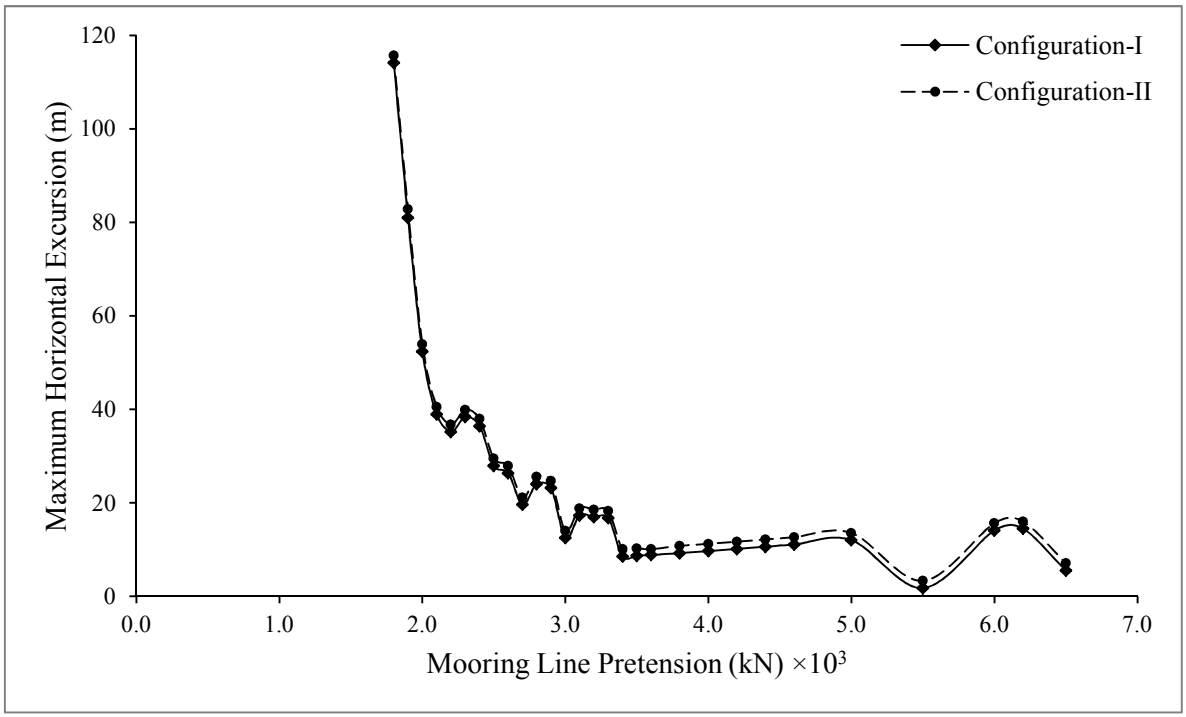


Fig. 6 Maximum permissible horizontal excursions by the mooring system in the wave heading

Conclusions

Based on the numerical study conducted, following conclusions can be drawn:

1. For any mooring line configuration, restoring performance of the mooring system can be enhanced with increase in the line pretensions.
2. The maximum permissible excursion by the mooring system decreases as the line pretension is increased.
3. The reduction in the maximum permissible excursions of the mooring system is significant for relatively lower line pretensions.
4. Though increase in line pretension improves the restoring behaviour of mooring system, decrease in maximum permissible excursions shall be taken into consideration while designing the mooring system of any floating platform.

References

[1] A. K. Agarwal, A. K. Jain, Dynamic behaviour of offshore spar platforms under regular sea waves, Journal of Ocean Engineering 30 (2003) 487-516.
[2] Jason I. Gobat, Mark A. Grosenbaugh, A simple model for heave-induce dynamic tension in catenary moorings, Journal of Applied Ocean Research 23 (2001) 159-174.
[3] M. B. Rosales, C. P. Filipich, Full modelling of the mooring non-linearity in a two-dimensional floating structure, International Journal of Non-Linear Mechanics 41 (2006) 1-17.
[4] M. J. Downie, J. M. R. Graham, C. Hall, A. Incecik, I. Nygaard, An experimental investigation of motion control devices for truss spars, Journal of Marine Structures 13 (2000) 75-90.
[5] R. Pascoal, S. Huang, N. Barltrop, C. Guedes Soares, Assessment of the effect of mooring systems on the horizontal motions with an equivalent force to model, Journal of Ocean Engineering 33 (2006) 1644-1668.
[6] R. Pascoal, S. Huang, N. Barltrop, C. Guedes Soares, Equivalent force model for the effect of mooring systems on the horizontal motions, Journal of Applied Ocean Research 27 (2005) 165-172.
[7] Russel J. Smith, Colin J. MacFarlane, Statics of a three component mooring line, Journal of Ocean Engineering 28 (2001) 899-914.
[8] S. A. Mavrakos, V. J. Papazoglou, M. S. Trintafyllou, J. Hatjigeorgiou, Deep water mooring dynamics, Journal of Marine Structures 9 (1996) 181-209.
[9] Zhen Gao, Torgeir Moan, Fatigue damaged induced by non-Gaussian bimodal wave loading in mooring lines, Journal of Applied Ocean Research 29 (2007) 45-54.
[10] Zhihuang Ran, Coupled dynamic analysis of floating structures in waves and currents, Ph.D Thesis, Texas A&M University, Texas, 2000.

Applied Mechanics and Materials Vol. 567 (2014) pp 210-215
© (2014) Trans Tech Publications, Switzerland
doi:10.4028/www.scientific.net/AMM.567.210

Broadside Vessel Collision Forces for Conventional Riser-Guard

Dinesh Kumaran Palaniandy[1,a], Zubair Imam Syed[1,b] , Mohd. Shahir Liew[1,c] and Saravanan Karuppanan[1,d]

[1]Universiti Teknologi PETRONAS, Bandar Seri Iskandar, 31750, Tronoh, Perak, Malaysia

[a]nesharan@gmail.com, [b]imam.syed@petronas.com.my, [c]shahir_liew@petronas.com.my, [d]saravanan_karuppanan@petronas.com.my

Keywords: Vessel collision, equivalent impulse load, conventional riser-guard.

Abstract. Oil and gas operators have taken considerable amount of measures to prevent offshore service vessel collision with risers, especially in the wake of the Mumbai High North disaster. One of the measures taken is the installation of steel riser-guards on fixed offshore jacket platforms. The conventional riser-guard however, has been associated with several design related issues, which provide room for further design optimisation, or even a potential replacement with other alternatives. Quantification and selection of appropriate design load for riser-guard system is highly desirable for design improvement and optimization. This study attempts to investigate and establish the impulse loads equivalent to the broadside collision of a 2500 tonne displacement vessel with the conventional riser-guard. Parametric study was performed to investigate the effects of varying width to the resulting impulse load equivalent to vessel collision forces. General purpose finite element modelling software was used to perform dynamic analysis and establish the equivalent impact loads.

Introduction

In offshore oil and gas operation, risers are defined as large-diameter pipes which facilitate the transfer of reservoir contents to the processing facilities on surface. The reservoir contents can be in the form of crude oil, gas, or drilling mud for the case of drilling risers. Risers are in some cases attached to the jacket bracing for additional support to cope with the harsh sea conditions. This method of providing additional support to risers may enhance unintended threat to the platform operation, which comes in the form of accidental vessel collision. Between the years of 1975 to 2001, statistics published by the HSE Department of U.K [1] shows that collision incidents involving supply vessels constitute the highest percentage in terms occurrence. Table 1 presents the collision statistics published in the UK HSE collision database.

Table 1. Reported Collision Incidents in the UK Continental Shelf from the years of 1975 to 2001 [1]

Vessel type	Supply Vessels	Stand-by vessels	Attendant vessels	Passing Vessels	Unspecified vessels
Number of Incidents	353	87	74	8	35
Percentage of occurrence	63.4%	15.6%	13.3%	1.4%	6.3%

Responding to this indication of threat from supply vessels, oil and gas operators in Malaysian waters opted to use the conventional riser-guards as a riser-protection system. The conventional riser-guard consists of steel space frames made of hollow tubular members which are designed to resist static forces equivalent to a collision [3]. To serve the purpose of protecting the risers from vessel impact, tubular members made from mild steel became the primary choice of material for its ability to deform well upon collision and dissipate the kinetic energy of the colliding vessel. Removal and replacement of tubular members will be necessary in the event of a vessel collision,

which is very likely to induce permanent deformation on the tubular members. However, being made of steel, the conventional riser-guards installed on fixed jacket platforms have caused major concerns to oil and gas operators and the root causes of this situation are excessive weight, high cost during installation and maintenance difficulties.

In light of the design issues raised by operators, there is a high level of desire for a new system which can substitute the conventional riser-guard and provide adequate protection while being light in weight, easily attachable and detachable for ease of maintenance and possess high energy dissipation capability. However, there is a clear gap in existing knowledge regarding the structural response and performance of riser-guards due to accidental vessel impact. The amount and mechanism of load transfer during vessel collision needs to be established to explore the possibilities of improvement of conventional riser-guard design or to find a better alternative. This study involves the dynamic assessment of conventional riser-guard to establish impulse loads equivalent to a 2500 tonne displacement vessel collision with a conventional riser-guard. Once established, these forces can be used as a baseline for assessment and design evaluation of any potential new system.

Collision Mechanics

Design for vessel impact on offshore structures has been highlighted in the design manuals and standards for offshore structural design [4-6]. Figure 1 shows the recommended deformation curve by DnV [1] for the case of a vessel with displacement of 5000 tonnes. The deformation curve was intended for the use in the design of jacket legs against bow, stern and broadside impacts [4]. The development of this relationship is based on the penetration of an infinitely rigid cylinder with diameter of 1.5 meters, representing jacket leg and 10 meters for large diameter columns.

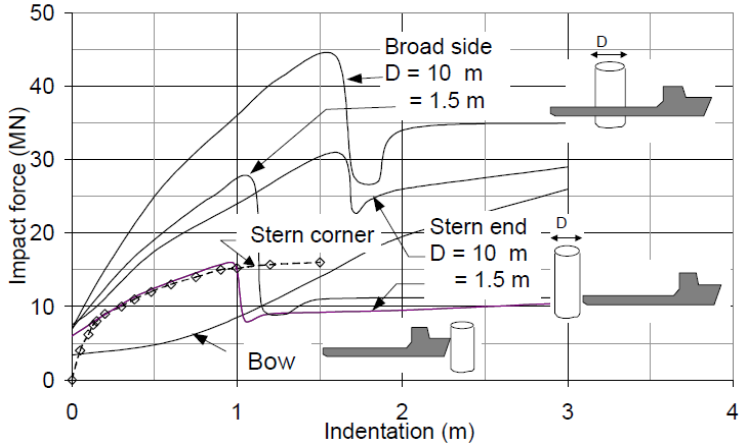


Figure 1. Recommended deformation curve by DnV RP-C204 [4]

Impulse load or impact force due to a colliding body can be defined using Equation 1. The impulse force largely depends on the mass of the impacting body, velocity at the point of impact, and the time taken for the change in momentum to occur. For vessel collision against bridge piers, the change in ship momentum during collision is taken as the impulse force acting on the vessel [7]. This approach can be expressed in the form of Equation 1,

$$F_p = \text{Rate of change in vessel momentum} = m\,(v_i - v_f)/\Delta t \quad (1)$$

where m is the total mass of the vessel (kg), v_i and v_f are the initial and final vessel velocity (m/s), respectively, and Δt is the time taken for the change in momentum to occur completely. Similarly, the US Army Corps of Engineers employed the same approach to determine the impact forces of wooden debris on floodplain structures [8]. The dissipation of kinetic energy from impacting vessel

is dictated by the type and purpose of an installation. During collision between vessel and riser-guard, the vessel kinetic energy will be dissipated as strain energy in the form of elastic and plastic deformation. The design impact energy for offshore platforms varies between regions of operation. The Recommended Practice by DnV for design against accidental loads [4] specifies that an offshore structure should be capable of withstanding an impact equivalent to 5000 tonne supply vessel at a velocity of 2.0 m/s or more [9], which generates about 20 MJ of impact energy. However, for operations in Malaysian waters, the PETRONAS Technical Standards [10] specifies lower requirement for design impact energy for a range of vessel displacement, which is available in Table 2.

Table 2. Design Impact Energy of Conventional Riser- Guard System by PTS [10]

Vessel displacement (Tonnes)	Energy (MJ)
1000	1.00
1500	1.25
2000	1.80
2500	2.25

Finite Element Modelling

Finite Element Modelling (FEM) was performed using the general purpose FEM software package, ANSYS [11]. The CAD model of a conventional riser-guard was constructed using ANSYS Design Modeller while the dynamic analysis was performed using Transient Dynamic Analysis module. Four CAD models with dimension provided in Table 3 was constructed to study the effect of varying width to the resulting equivalent impulse loads. The height of the model was fixed at 10 meters to comply with typical range of a splash zone where vessel impact is imminent. The material properties of typical mild steel [11] used in this analysis is presented in Table 4.

Table 3. Dimensions of conventional riser-guard CAD models.

Model Number	**Dimension (Width X Height)**
1	8.0 m X 10.0 m
2	10.0 m X 10.0 m
3	12.0 m X 10.0 m
4	14.0 m X 10.0 m

Table 4. Properties of a typically used mild steel [11].

Mild Steel Properties	
Yield Strength, F_y	240 MPa
Ultimate Strength, F_u	434 MPa
Modulus of Elasticity, E	200 GPa
Density of Steel, ρ	7850 kg/m^3
Elastic Strain Limit, ϵ_{pl}	0.0012
Ultimate Strain, ϵ_u	0.38

The broadside collision between a vessel and the conventional riser-guard is graphically illustrated in Figure 2. The impact load is assumed to be acting uniformly across the tubular members in contact with the vessel. The problem can then be simplified further by applying symmetric boundary condition and only considering half of the conventional riser-guard model due to its symmetric property. Figure 3 shows half of the model of 14 meter wide conventional riser-guard with tubular members highlighted in red which are in contact with vessel during broadside impact. Using the bearing load option in ANSYS Pre-processing interface, triangular impulse load was applied to simulate the action of collision forces of a colliding vessel. The triangular impulse load is applied in the form shown in Figure 4. F_p is the peak value of impulse load which can be calculated using Equation 1. The value of F_p is directly dependent on the value of Δt which is the time taken for the change in vessel momentum to occur, where vessel velocity gradually approaches 0 m/s and comes to a complete halt.

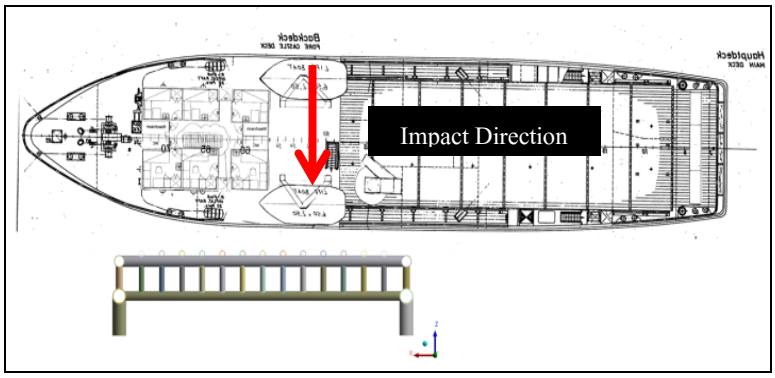


Figure 2. Illustration of a broadside impact scenario

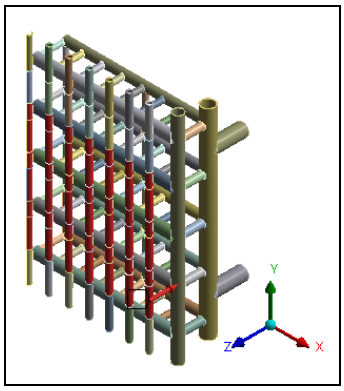


Figure 3. 14 meter wide conventional riser-guard model with symmetric boundary condition

Using trial and error method, a series of Δt values were assumed, the corresponding F_p values were then computed and applied onto the CAD model. The resulting strain energy from the applied load is then compared to the values of design impact energy requirements for 2500 tonnes displacement vessel. The F_p value which results in strain energy closest to the energy values presented in Table 2 will be taken as the equivalent force to a vessel collision. This process can be summarised in to the flow chart presented as Figure 5.

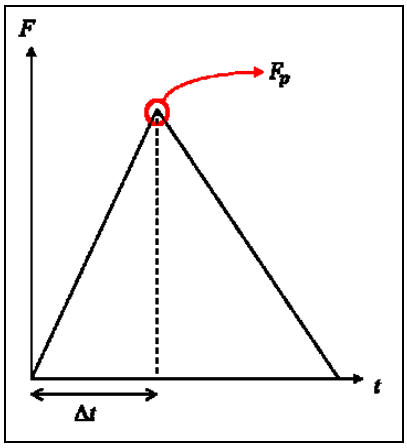


Figure 4. Triangular impulse load representing vessel collision force

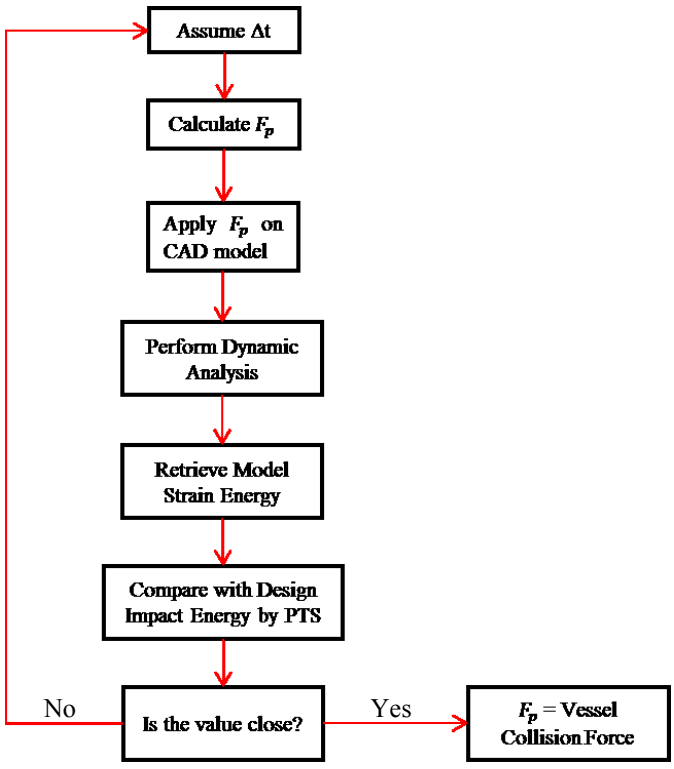


Figure 5. Flow-chart of analysis approach

Results and Discussion

A. Impulse load

In this study, the equivalent impact forces were established by trial and error method using four models of conventional riser-guard with varying width. The resulting strain energy is then compared with the design impact energy for the specific vessel. The effect of change in model width to impulse forces equivalent to a 2500 tonne displacement vessel collision is presented in Table 5.

Table 5. Impulse loads equivalent to the collision forces of a 2500 tonnes vessel.

Model Number	Model Width, m	F_P,(10^6 N)
1	8	14.6
2	10	14.1
3	12	13.6
4	14	13.3

Figure 6 provides a range of equivalent collision forces which would result in strain energy close to the design impact energy for 2500 tonne displacement vessel, which is 2.25 MJ. The broadside collision force of a vessel is assumed to be translated as a uniformly distributed impulse load across the vertical tubular members of conventional riser-guard model. When the model width is reduced, the structural stiffness increases and its effectiveness in dissipating the vessel kinetic energy during collision will decrease. This reduction in structural stiffness eventually increases the impulse force during a vessel collision.

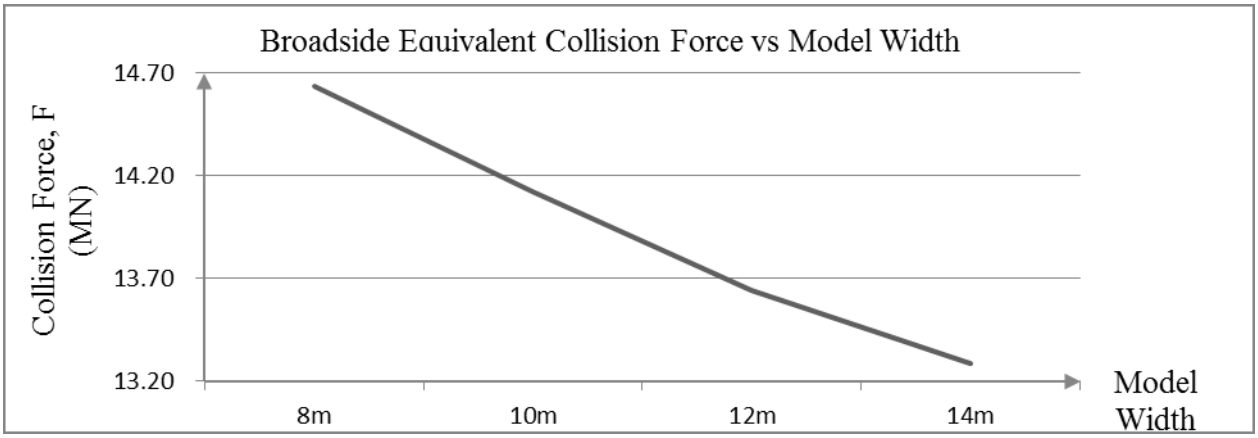


Figure 6. Change in equivalent impulse force equivalent to a broadside collision of 2500 tonne displacement vessel with respect to varying width of conventional riser-guard model.

B. Damage Assessment

Plastic strain is used as the parameter to perform damage assessment on the models. The maximum values of strain occurring at critical the critical joint for each model are presented in Table 6.

Table 6. Values of maximum strain as a result of collision force application.

Model Number	Model Width, m	Maximum Strain, ϵ
1	8	0.12
2	10	0.11
3	12	0.10
4	14	0.09

The strain values presented in Table 6 shows strain values beyond the elastic strain limit of 0.0012. This indicates that permanent deformation has occurred on the conventional riser-guard. The location of this permanent damage for model number 1 is presented in Figure 7. This location was identified to be the critical joint, whereby a significant damage at this location could result in severe loss in structural stiffness. Since the strain values are still lower than the ultimate strain, complete failure is yet to occur and the damaged members still possess some capacity in resisting further impact. This capacity may be minimal but due to the large residual strain in the global structure, total riser-guard replacement will be necessary in the event of a vessel collision.

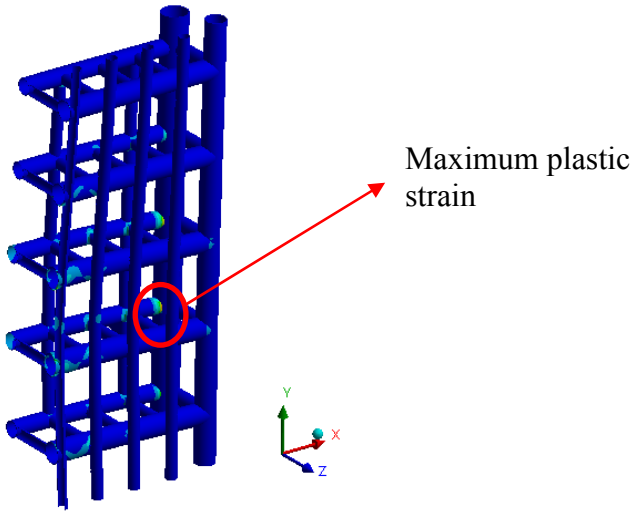


Figure 7. Location of maximum plastic strain during collision on 8 meter wide conventional riser-guard.

Conclusion

Recommended vessel collision forces for offshore structures which are currently available in the recommended practice and design codes for fixed offshore platforms provide references on the required design capacity of jacket legs and brace members against vessel collision. Figure 6 provides a range of collision forces which can now be used as a basis for comparison when design modifications are performed on the conventional riser-guard, which was previously unavailable. This range can also be used as a benchmarking when a new riser-guard system is to be developed and introduced for platforms in Malaysian waters.

References

[1] J. K. Robson, "Ship/platform Collision Incident Database," HSE Books, Norwich, 2003.
[2] N. K. Mitra, P. K. Dileep and A. Kumar, "Revival of Mumbai High North-A Case Study," Mumbai, 2008.
[3] M. A. El-Reedy, "Riser Guard," in Offshore Structures Design, Construction and Maintenance, 1 ed., C. I. diacriTech, Ed., Oxford, Gulf Professional Publishing, 2012, p. 192.
[4] Det Norske Veritas, Design Against Accidental Loads, Oslo: Det Norske Veritas, 2010.
[5] International Standard (ISO: 19902), Petroleum and Natural Gas Industries- Fixed Offshore Steel Structures, vol. Edition 1, Switzerland: ISO, 2007.
[6] American Petroleum Institute, Recommended Practice for Planning, Designing and Constructing Fixed Offshore Platforms - Working Stress Design, Washington: American Petroleum Institute, 2007.
[7] A. A. Sayed and W. A. Attia, "Finite Elements Analysis Techniques of Vessel Collision with Cable-Stayed Bridge," Life Science Journal, vol. 9, no. 2, pp. 1179-1190, 2012.
[8] R. B. Haehnel and S. F. Daly, "Maximum Impact Force of Woody Debris on Floodplain Structures," Virginia, 2002.
[9] R. Nataraja and K. Pemsing, "Impact Energy due to Supply Vessel Collision," in 3rd International Conference on Integrity of Offshore Structures, Glasgow, 1987.
[10] W. B. Shiiun, "Design of Fixed Offshore Structures," PETRONAS, Kuala Lumpur, 2012.
[11] ANSYS Inc, "Ansys Mechanical," 2013. [Online]. Available: http://www.ansys.com/Products/Simulation+Technology/Structural+Analysis/ANSYS+Mechanical. [Accessed 26 December 2013].
[12] R. C. Hibbeler, Mechanics of Materials, Singapore: Prentice Hall, 2008.

Applied Mechanics and Materials Vol. 567 (2014) pp 216-221
© (2014) Trans Tech Publications, Switzerland
doi:10.4028/www.scientific.net/AMM.567.216

Computational Aspects of Submarine Slide Generated Tsunami

Vo Nguyen Phu Huan[1, a], Indra Sati H. Harahap[2, b]

[1]Civil Department, Universiti Teknologi Petronas, Perak, Malaysia

[2]Civil Department, Universiti Teknologi Petronas, Perak, Malaysia

[a]phuhuan129@yahoo.com, [b]indrasati@petronas.com.my

Keywords: tsunami, landslide, parallelization, simulation

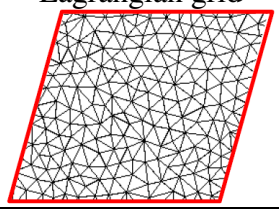
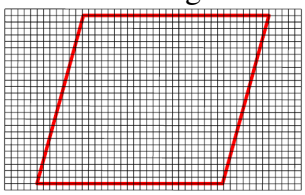
Abstract. Submarine landslide is the most serious threat on both local and regional scales. Tsunami phenomenon induced by submarine slide has put us on the challenge in understanding from generation mechanism to propagation and coastal inundation and mitigating the risk from submarine slide generated tsunami. This research presents the numerical simulation methodology by Smooth Particle Hydrodynamics (SPH) to investigate the impact forces of tsunami waves with the aid of physical modeling. By using parallelSPHysics, it is a source code based on the SPH method to model nearly-incompressible flows, including various physical processes. The conclusions may potentially be taken as guideline of mitigate the risk from tsunami wave.

Introduction

Tsunami can be generated by the energy transfer from submarine slide motion to water motion. The characteristics of a tsunami generated by a submarine landslide are mainly determined by the volume, the initial acceleration, the maximum velocity. Tsunami need to be carefully evaluated before field development can start, as they present threat to human life, environment, seabed installation and drilling operation. However, the tsunami and their impact are not well known.

So far Computational Fluid Dynamics (CFD) has focused on grid-based methods, where two different frames are usually considered for describing the physical governing equations, namely: the Eulerian and the Lagrangian description (Table 1). The grid based numerical methods have achieved remarkably, and they are currently the dominant methods in numerical simulations for solving practical problems in engineering and science.

Table 1. Summary of grid-based method

Lagrangian grid	Eulerian grid
	
✓ Attached on the material ✓ Does not deal with large deformations (remesh) ✓ History of all the variables can be easily obtained ✓ Used by FEM	✓ Fixed in space and with time ✓ Not easy to treat the irregular or complicated geometries ✓ Difficult to tract moving boundary and interface ✓ Used by FDM, FVM

However, the major difficulties are resulted from the use of grid/mesh, which can lead to various difficulties in dealing with problems with free surface, deformable boundary, moving interface, and extremely large deformation and crack propagation. Moreover, for problems with complicated geometry, the generation of a quality mesh has become a difficult, time-consuming and costly process.

Alternative to grid-based methods is a meshfree approach. The development of mesh free methods offers a reliable approach to tackle the simulation of such difficult problems.

Mesh free method

Provide accurate and stable numerical solutions for governing equations with a set of arbitrarily distributed nodes without using any mesh. There are 3 types mesh free method:

- Strong form formulation (simple to implement but instable in some cases).
- Weak form formulation (excellent accuracy but required a background mesh).
- Particle methods.

The state of the system is represented by a set of particles, which possess individual material properties and move according to the governing equations. Smooth Particle Hydrodynamics (SPH) invented by Lucy, Gingold and Monaghan, has been the most popular and successful when applied to coastal hydrodynamic and offshore engineering in general and to free-surface hydrodynamics in particular. It is a mesh free Lagrangian particle method which models fluid flow.

To approximate the values of functions, derivatives at a particle using the information at all the neighboring particles. SPH approximation consists of kernel approximation and particle approximation.

- Kernel approximation: field functions approximated by integral representation method (smoothing effect like weak form)

$$f(x)=\int_{\Omega} f(x_j)W(x-x_j,h)dx_j \tag{1}$$

- Particle approximation: replacing integrations with summations at the neighboring particles in a local domain so-called support domain (sparse matrices).

$$f(x)\approx\sum_{j=1}^{N} m_j \frac{f_j}{\rho_j} W(x-x_j,h) \tag{2}$$

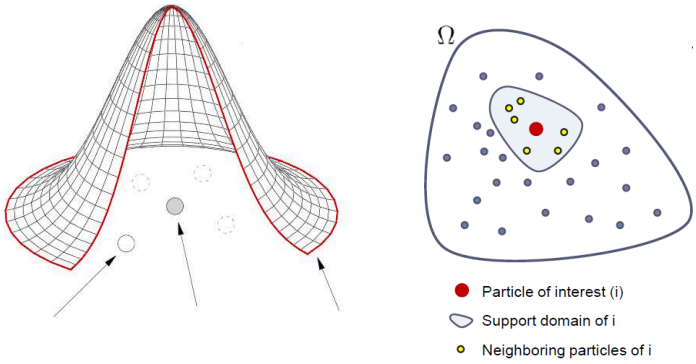


Fig. 1. Particle approximation diagram (Shao, 2009)

By deploying particles at specific positions at the initial stage before the analysis, the free surfaces, material interfaces, and moving boundaries can all be traced naturally in the process of simulation regardless the complicity of the movement of the particles. SPH does not use a grid/mesh. This allows a straight forward handling of very large deformations, since the connectivity between particles are generated as part of the computation and can change with time

Parallelization

❖ Definition of parallelization

Parallel computing is the simultaneous execution of the same task on multiple processors in order to obtain faster results. It is widely accepted that parallel computing is a branch of distributed computing, and puts the emphasis on generating large computing power by employing multiple processing entities simultaneously for a single computation task. These multiple processing entities

can be a multiprocessor system, which consists of multiple processors in a single machine connected by bus or switch networks, or a multicomputer system, which consists of several independent computers interconnected by telecommunication networks or computer networks.

❖ Motivation of parallel computing

The main purpose of doing parallel computing is to solve problems faster or to solve larger problems.

Parallel computing is widely used to reduce the computation time for complex tasks. Many industrial and scientific research and practice involve complex large-scale computation, which without parallel computers would take years and even tens of years to compute. It is more than desirable to have the results available as soon as possible, and for many applications, late results often imply useless results.

While a serial computer can work on one unit area, a parallel computer with N processors can work on N units of area, or to achieve N times of resolution on the same unit area. In numeric simulation, larger resolution will help reduce errors, which are inevitable in floating point calculation; larger problem domain often means more analogy with realistic experiment and better simulation result.

❖ Theoretical model of parallel computing

The widely-used theoretic model of parallel computers is Parallel Random Access Machine (PRAM). A simple PRAM capable of doing add and subtract operation is described in Fortune's paper. A PRAM is an extension to traditional Random Access Machine (RAM) model used to serial computation. It includes a set of processors, each with its own PC counter and a local memory and can perform computation independently. All processors communicate via a shared global memory and processor activation mechanism similar to UNIX process forking. Initially only one processor is active, which will activate other processors; and these new processors will further activate more processors. The execution finishes when the root processor executes a HALT instruction. Readers are advised to read the original paper for a detailed description.

❖ Architectural models of parallel computer

Despite a single standard theoretical model, there exist a number of architectures for parallel computer. Diversity of models is partially shown in Fig 2. This subsection will briefly cover the classification of parallel computers based on their hardware architectures.

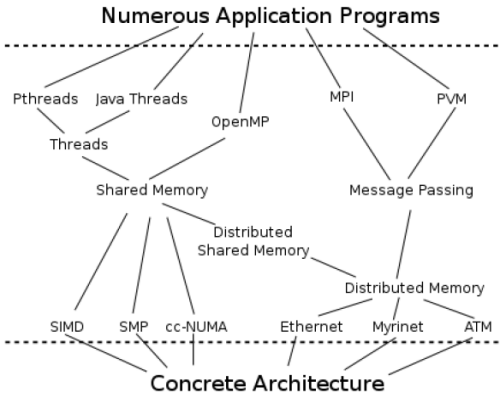


Figure. 2. Diversity of models is partially (Mahantia, 2004)

❖ Hardware and software environments in parallel computing

In this part, we will focus on hardware and software platforms we use in our research.

✓ **Hardware:**

- With the hardware, we have 4 types: Computer Cluster, Computational Grid, Network of Workstations, Vector processing in commodity CPU and GPU. And we propose to use Computational Grid to integrate our system into other components of whole system.
- Computational Gird is designed to integrate distributed computing power to form a single supercomputer, which would be a rather powerful hypercomputer to tackle large-scale computation problems. When message passing programming is to be considered, the

mainstream Message Passing Interface (MPI) implementation, MPICH, has support for Grid-based communication. Unfortunately, in practice there are a lot of problems to be circumvented. For example, for many computer clusters, only the head node has the public Internet Protocol (IP) address, which makes the direct Grid-based communication between 2 client nodes residing in different computer clusters impossible. When our research is to be considered, the heterogeneous nature and hierarchical structure of Gird are further barriers to efficient deployment of our flat-structured MPI program.

✓ **Software:**

- Parallel programming is a complex task. In order to reduce this complexity, different programming models are abstracted, with each providing tools such as special-purpose compilers, libraries and frameworks to simplify programming task. These tools hide many details about parallel execution, such as message transfer and routing, task allocation and migration, and platform differences. Our research is based on message passing programming model and specifically on Message Passing Interface (MPI) standards and MPICH library.
- Message Passing Interface, or MPI, is the most widely-used message passing standard. The basic functions are defined by the MPI standard, and with many implementations targeting almost all distributed memory architectures, it is the industrial standard for message passing programming.
- Basically, MPI provides two types of communication operations. Point-to-point operations allow any two processes to exchange information via MPI_Send (for sending), MPI_Recv (for receiving) and their variants. Collective operations are provided so that a set of processes, known as a communicator, can share and dispatch data through broadcast and reduction operations.
- When an MPI program runs, the user will explicitly specify the number of parallel processes and how the processes are mapped to physical processors. On startup, each processor starts one or more processes to execute the same program body. Each parallel process will be assigned a rank, which serves as the identity of the process, and which will also cause processes to carry out different computation despite their common program body. During the execution, processes carry their own computation, without synchronization with other processes unless they encounter an explicit synchronization command. Processes communicate with each other using point-to-point or collective communication primitives, using process rank to address the recipient or sender if it is required. The whole parallel program exits when all the parallel processes have finished.

Parallel SPHysics

This part shows how to apply parallel computing in SPHYSICS code.

Launching the parallelSPHysics code will depend heavily on the architecture using. The code is parallelized using MPI formalism and thus require MPICH or OpenMPI to be installed on your parallel machine. The code has been developed with the assumption that most parallel environments are using on Linux not on Windows.

❖ SPHYSICSgen: creates the initial conditions and files for a given case.

✓ **Creating compiling options**: The compilation of SPHysics code depends on nature of the problem under consideration and on the particular features of the run. Thus, the user can choose the options that are better suited to any particular problem and only those options will be included in the executable versions of SPHysics. There are only two new options to choose the MPI FORTRAN compiler and whether to activate optimization of the MPI partitioning (i.e. load balancing).

- ✓ **Compiling and Running the executable:** The SPHysics code has been developed on machine that use the LSF (Load Sharing Facility) and the SGE Submission systems. With the code the script file: script_bsub.bsub and script_qsub.qsub have been provide for the LSF and SGE Submission systems. The parallel SPHysics code has been designed to perform simulations of million of particles by using Load Sharing Facility (LSE) and SGE Submission systems.

❖ SPHYSICS: Run the selected case with the initial condition created by SPHYSICgen code.

- ✓ A number of subroutines are necessary to deal with transfer of particles and their information between adjacent processors. The MPI topology must be accessible by each subroutine (i.e. rank, east & west neighbors, MPI communicator, etc.).
- ✓ Grid sweep:
  - Around each cell, the E, N, NW & NE neighboring boxes are checked to minimize repeating the particle interactions. This process is shown schematically in Fig 3.

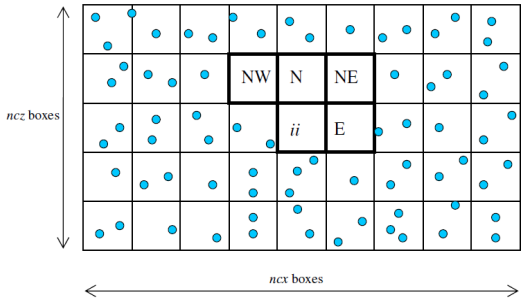


Figure. 3. Grid sweep (SPHysics guide, 2011)

  - This provides an efficient method of identifying the connectivity of the particles with each other. To parallelize the code, the workload needs to be distributed amongst the available processors. Fig 4 displays a typical situation where the domain has been split amongst three different processors.

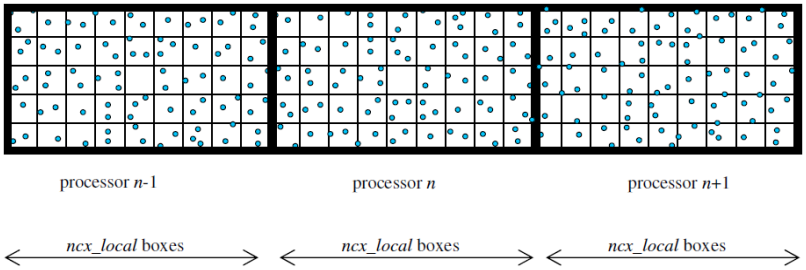


Figure. 4. Domain decomposition in parallel SPHysics (SPHysics guide, 2011)

  - However, when the domain is split up amongst several processors and box ii is located on the boundary of the processor, the code needs to know the contents of box-position ii+1, i.e. E & NE which lie on a different processor. The easiest method to accomplish the necessary transfer of information is to use a column of ghost cells of width 2h as shown in Fig 5.

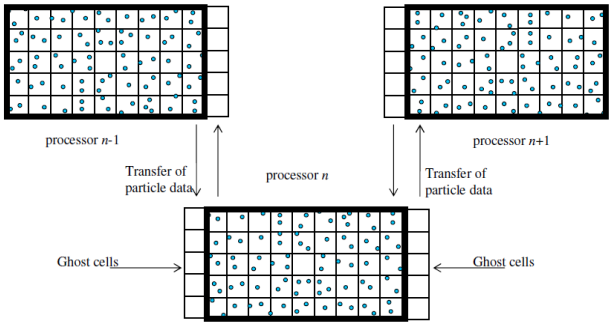


Figure. 5. Importing particle information into ghost cells from neighboring processor (SPHysics guide, 2011)

❖ Some results from parallelSPHysics

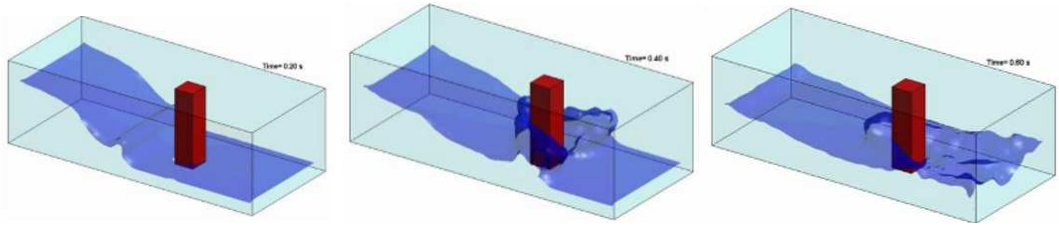


Figure. 6: Tsunami wave hitting a structure (SPHysics test, 2012)

Conclusion

Now, physical understanding of slide tsunami hazards is poor. We must understand substance of tsunami clearly and how to find methods to reduce damage from tsunami wave. This is not simple task because of the complexity and multi scale of process. For this reason, numerical simulation about tsunami wave from submarine slide are very necessary.

To simulating tsunami wave is not simple, because we have some problem with free surface, deformable boundary, moving interface, and extremely large deformation and crack propagation. Moreover, for the problems with complicated geometry, the generation of a quality mesh has become a difficult, time-consuming and costly process.

Alternative to grid-based methods is a mesh free approach. The development of mesh free methods offers a reliable approach to tackle the simulation of such difficult problems. Of the mesh free techniques developed over past decade, Smooth Particle Hydrodynamics (SPH) invented by Lucy, Gingold and Monaghan, has been the most popular and successful when applied to coastal hydrodynamic and offshore engineering in general and to free-surface hydrodynamics in particular. That approach still remains limitations need to be improved related to accuracy and stability, inconsistency problem, or non-conservation of linear and angular momentum. Therefore, the need for comprehensive model base on mesh free method that could cover all aspects of tsunami phenomena and provide real-time modeling of the event would be one of good future research direction.

The conclusions may potentially be taken as guideline of mitigate the risk from tsunami wave.

References

[1] B. Ataie-Ashtiani, G.Shobeyri, “Numerical simulation of landslide impulsive waves by incompressible smoothed particle hydrodynamics”, Int. J. Numer. Meth. Fluids 56:209–232, 2008.

[2] S. Shao, D. I. Graham, C. Ji, D. E. Reeve, P. W. James, and A. J. Chadwick, “Simulation of wave overtopping by an incompressible SPH model”, Coastal Engineering, Vol. 53, No. 9, pp. 723-735, 2009.

[3] J.M. Cherfils, G. Pinona, E. Rivoalena, “A parallel SPH code for free-surface flows”, Computer Physics Communications 183 1468–1480, 2012.

[4] A. Mahantia, D.L. Eagerb, “Adaptive data parallel computing on workstation clusters”, Journal of parallel and distributed computing 64, 1241 – 1255, 2004.

[5] A. Migdalas, G. Toraldo, V. Kumar, “Nonlinear optimization and parallel computing”, Parallel Computing 29,375–391, 2003.

[6] N. Tremblay, M. Florian, “Temporal shortest paths: parallel computing implementations”, Parallel computing 27, 1569 – 1609, 2001.

[7] M. Cannataro, D. Talia, P.K. Srimani, “Parallel data intensive computing in scientific and commercial applications”, parallel Computing 28, 673–704, 2002.

Applied Mechanics and Materials Vol. 567 (2014) pp 222-227
© (2014) Trans Tech Publications, Switzerland
doi:10.4028/www.scientific.net/AMM.567.222

Development of Platform Selection Tool for Offshore Decommissioning in Malaysia

Noor Amila W.A. Zawawi[1, a], Na Kai Lun [1, b] and M.S. Liew[1, c]

[1]Civil Engineering Department, Universiti Teknologi PETRONAS, Bandar Seri Iskandar, 31750 Tronoh, Perak, Malaysia

[a]amilawa@petronas.com.my, [b] nakailun@gmail.com, [c]shahir_liew@petronas.com.my

Keywords: Decommissioning; criteria; decision making tool; Relative Importance Index.

Abstract. Decommissioning of offshore structures is not a novel issue in the oil and gas industry. Malaysia is now dealing with a fleet of ageing platforms slated to be decommissioned. There are several alternatives of decommissioning such as "complete removal" and conversion to artificial reefs; "partial removal", "remote reefing" and "topple in-situ". Given the list of options, the decision to undertake the best option is challenging as the current method of comparative Best Practicable Environmental Option (BPEO) assessment is only implemented at the end of platform's life. Therefore, the main goal is to develop a management decision making tool which is incorporated throughout the life cycle of an oil field. Expert elicitation is conducted to verify the relevant decommissioning criteria. The criteria were then ranked accordingly through calculation of Relative Importance Index (RII), and a conceptual system is established to complement the existing asset management system. In summary, this study could benefit the knowledge of offshore decommissioning planning through prioritization of decommissioning criteria**.**

Introduction

Since the first oil discovery in 1910, Malaysia has progressively developed into the second largest oil and natural gas producer in South East Asia and the second largest exporter of liquefied gas in the world. The industry makes up about 20 percent of the nation's total gross domestic product (GDP) in 2012 [1]. Unfortunately, many of the existing platforms are approaching their design life. Conventionally, the platforms are typically designed for a service life of 25-30 years. Among 249 offshore structures scattered in Malaysian water, 48% of the platforms already reached their design life of 25 years [2]. With this, decommissioning activities are expected to increase significantly in the near future. Identified platforms which are no longer economic feasible required to be decommissioned without instigating any environmental complications. Malaysia is still green in the area of decommissioning with only a few of executed offshore decommissioning projects. In 2004, the conversion of a platform into artificial reef through decommissioning of BARAM 8 platform off the coast of Miri, Sarawak, marks the first of its kind in the country. Recently in 2012, PETRONAS successfully facilitated the removal of two shallow water platforms, SM4 and SMVA [3]. In decommissioning, the main options include either removal or leave in place [4]. Each alternative incurs considerably large amount of money with certain extent of complexity. As such, the decommissioning decisions are never easy to make. Hence, this paper presents a conceptual decision making selection tool which aids decommissioning planning decisions. The proposed selection tool recommends the 'most feasible' decommissioning alternative with regards to its existing structural characteristics. Prevailing local decommissioning practices involve detailed planning of individual decommissioning exercise, as per needs basis. Only when a platform is approved for removal, pre-decommissioning planning commences. Decommissioning decisions are made based on unique comparative assessment. The Best Practicable Environmental Option (BPEO) assessment practiced locally evaluates the relative performance of each option at the end of a platform's life and is often subjected to subjective and unaided ranking of the proposed

alternatives. With the increasing number of platforms approaching their design life, the effective management of obsolete platforms could amount to immense cost savings and organization productivity. The proposed toolkit with weighted decommissioning criteria could provide a baseline for selection process which takes into account the characteristics of structures, on top of the BPEO practice. Apart from that, the research is relevant to the body of knowledge as it provides the ranking of pre-decommissioning criteria based on expert group elicitation.

Decommissioning

Fundamentally, all options include removal of deck and production facilities to the shore for storage, reuse or disposal while the only difference between the options is the handling of disused jackets [5]. The jacket and deck structures are subjected to removal and onshore disposal, reuse or conversion to artificial reefs. Nevertheless, the feasibility of each decommissioning method depends on several factors such as water depth, location, feasibility of technology and condition of structures to be decommissioned [6]. Complete removal involves the severance of conductors and removal of jacket structure and platform materials to shore for disposal, reuse or recycling purposes. Complete removal is enforced through a guideline set by International Maritime Organization (IMO), where a platform structure of jacket weight less than 4,000 tonnes and located in water depth shallower than 100m needs to be completely removed [7]. Another type of removal is partial removal. Conductor and jacket are severed to at least 55m subsurface as to allow clearance for safe navigation [8]. The severed parts are sent to shore for disposal, reuse or recycling purposes. Hence, selecting optimum location for jacket cut points is substantial in minimizing the diver's and cutting tool's onsite duration [9]. Over the years of platform's production, the structure becomes a habitat for sea creatures hence building up a new ecosystem. Therefore, by partially removing the structures, the habitat of ocean life could be conserved apart from improving the biodiversity thus leading to better fishery exploitations [10]. At present, the trend of converting the decommissioned platform to artificial reefs is rising up especially in Gulf of Mexico. Conversion of platform structures to an artificial reef has been found to be appropriate for implementation in Malaysia due to its naturally shallow water depths, similar to that of the Gulf's [11]. Reuse is an option that lengthens the life of the decommissioned structures by upgrading them to fit the new capacity [12]. It has been recognized to be a cost and time effective solution for steel fabrication as it eliminates the need to fabricate a new one. Reuse option could reduce up to 40-50% of the lead time-saving costs, based on current steel prices and fabrication charges of a new platform [13]. It still retains the original state of material and helps to reduce the capital cost while shortening the time of construction and installation from years to several months [8]. In order to reuse any platform facilities, it requires additional considerations with respect to fatigue, material, inspection, removal and reinstallation [14]. According to API RP 2A-WSD, when structures are considered for reuse, inspection should be executed to verify suitability for the intended application and establish the condition of the structures. For example, structural connections having fatigue damage ratios of equal or more than 30% would impair the intended service of the platform hence should be upgraded or removed [14]. In short, reuse option comes with detailed consideration to ensure that the refurbished platform could perform under its extended service. Recycle will feasibly come into consideration when the structures did not pass the inspection or reuse option is found to be uneconomical. To date, there are less than 10 handling facilities that can cope with jacket recycling in the region [13]. Throughout the decommissioning stages, four criteria have been listed as the main criteria which will structurally affect the course of decommissioning, namely: platform integrity, platform type, resources and lifting management. In platform integrity, the existing platforms may be removed and relocated for continued use at a new site. The structures have to be reanalyzed and reevaluated for the use, conditions and loadings anticipated during operations or at the new site. Hence, the analysis of existing structures requires additional considerations with respect to fatigue, reserve strength ratio and structural integrity of connection and corrosion protection system. Platform type focuses on the

features of platform such as the platform location, water depth and number of piles. The environmental condition surrounding the platform location such as wave climate, determine the complexity of decommissioning execution process. Hence, this proves that water depth and platform location is an essentially important in decommissioning planning. Besides, if the option of reuse were to be considered, it is important to look into platform characteristic so it will match the new proposed facilities. In terms of resources, the fundamental considerations in pre-decommissioning planning is the availability of resources for project execution. In practice, removal operation will require extensive use of vessels and cranes. Nonetheless, the availability of those vessels are limited and requires advanced booking [15]. In addition vessel transportation contributes as the highest factor in decommissioning cost estimation. For lifting management, the process requires utilization of crane vessels in which the capacity of vessel is determined by jacket weight, topside weight and pile weight. Lifting management plays a significant role during the mobilization and demobilization process. The structures may be lifted in one piece, modular section, or in small pieces, depending on the capacity of barges and cutting management of structures [15].

This study proposes a selection system aiming at optimization of costs and improved productivity, proposed based on a multi-criteria decision framework, based on ranking of scores. The scores reflect the significance of each criterion to decommissioning activities, ranked by the experts in decommissioning field. Relative Importance Index (RII) made it possible to cross compare the relative importance of the factors as perceived by the three groups of respondents [16]. This method has been widely used in researches to determine the RII of factors. Gunduz, Nielsen, and Ozdemir used RII to quantify and rank the delay factors for construction projects in Turkey [17]. It is similar to this research as it also solicit expert's evaluation to verify the pre-identified delay factors in construction, in which the factors are extracted from literature research and studies. The same method was adapted to this study for the analysis of data collected from the questionnaire survey, within various groups as classified according to the role of respondents in decommissioning activities. As a result, a rapid and transparent outcome could be produced in which different stakeholders will have their say in the decision making process. A set of questionnaire is distributed to the appointed expert groups in decommissioning planning, which are project manager, contractor and consultant. The respondents are chosen based on their involvement in decommissioning and expertise in structural integrity. RII is then used to rank the criteria. RII are calculated for each criteria as in Eq. (1):

$$RII = \frac{\Sigma W}{(A*N)} \tag{1}$$

Whereby; W= weighting given to each criteria by respondents (ranging from 1 to 5), A= highest weight (ie: 5 in this case) and N= total number of respondents. The RII value had a range of 0 to 1, with 0 not inclusive. Higher value of RII indicates higher criteria importance.

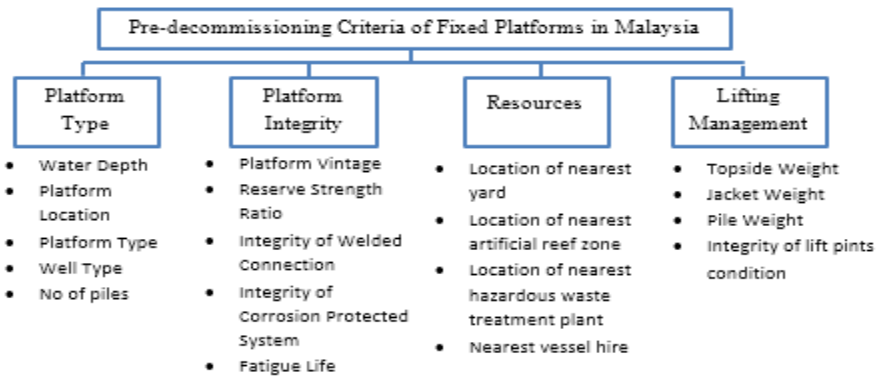


Figure 1. Proposed pre-decommissioning criteria of fixed platforms in Malaysia

Results and Discussion

The survey comes in as the validation of those identified criteria through expert group elicitation. Fig. 1 outlines the listed criteria in a form of decision framework. The main goal is to prioritize the pre-decommissioning criteria of fixed platforms in Malaysia. The ranking is established by using the method of Relative Importance Index (RII). Listed below is the rank of sub-criteria in accordance to their importance level. From the results in Table 1, vessel hire (RII=0.029) ranked as the most important criteria of pre-decommissioning. This is indeed relevant considering that transportation is the biggest factor in cost estimation of decommissioning.

Table 1. Rank Of Pre-Decommissioning Criteria

Sub-criteria	RII	Rank	Sub-criteria	RII	Rank
Nearest vessel hire	0.029	1	Platform Vintage	0.567	10
Topside Weight	0.267	2	Platform Location	0.600	11
Jacket Weight	0.333	3	Reserve Strength Ratio	0.600	12
Platform Characteristics	0.343	4	Well Type	0.629	13
Location of Nearest Yard	0.371	5	Location of Nearest Waste Hazardous Treatment Plant	0.629	13
Integrity of Welded Connection	0.433	6	Fatigue Life	0.633	15
Water Depth	0.457	7	Integrity of lift point	0.633	15
Pile Weight	0.500	8	Integrity of Corrosion Protection System	0.733	17
Location of Nearest Artificial Reef Zone	0.543	9	No of Piles	0.800	18

Hence, in decision to decommission, vessel hire needs to be prioritized above other criteria, as the availability of vessel is limited and the booking will take years in advance [15]. Then, the rank followed by topside and jacket weight. The rank is found to be appropriate since the size and weight of structures is closely related to the required capacity of vessels or barges for transportation and lifting purposes. The average RIIs is then calculated for each group in order to evaluate the ranking of mean criteria, as listed in Table 2.

Table 2. Rank of Main Criteria From Mean RIIs

Main Criteria	Sub-Criteria	RII	Mean RII	Main Criteria	Sub-Criteria	RII	Mean RII
Resources	Nearest vessel hire	0.029	0.393	**Lifting Management**	Topside Weight	0.267	0.433
	Loc. Nearest yard	0.371			Jacket Weight	0.333	
	Loc. AR zone	0.543			Pile Weight	0.500	
	Loc. Hazard TP	0.629			Integrity of lift point	0.633	
Platform Type	Platform Characteristic	0.343	0.566	**Platform Integrity**	Integrity Welded	0.433	0.593
	Water Depth	0.457			Platform Vintage	0.567	
	Platform Location	0.600			RSR	0.600	
	Well Type	0.629			Fatigue Life	0.633	
	No of Piles	0.800			Integrity Corrosion	0.733	

Table 2 describes the cluster of sub-criteria according to their respective group and the ranking of main criteria. In summary, Resources is the most significant main criteria of pre-decommissioning. This ranking correlates with the ranking of sub-criteria as previously discussed. It is a good practice to evaluate the ranking based on the group's preference, done according to the group of main criteria. From the results, it is observed that vessel hires and structures weight scored the top five ranks even from different background of experts. According to the calculated RII, consultant and project manager tends to give out many tied ranks due to similar RII value. This is due to limited number of respondents from both groups. On the contrary, RIIs for contractor is more varied, resulting in a more proper ranking of criteria. Therefore, it is recommended to have larger number of respondents from each identified groups to have a better consensus on the ranking. There is slight variance for the lowest five ranks observed from the three groups of experts. Integrity of corrosion protection system, platform vintage and fatigue life scored the lowest five from contractor and consultant's preferences. However, those three criteria were given a better rank by project manager group. The difference in correlation between groups of experts is determined using Spearman's

Correlation Test [18], to measure the agreement between contractor, consultant and project manager. From Table 3 it can be concluded that contractor and consultant have almost similar view in ranking the criteria i.e. the correlation is strong (0.823). This is probably due to their technical expertise in structural aspects of offshore structures.

Table 3. Spearman's ρ (or rs) coefficient between groups of experts

	Contractor vs Consultant	Contractor vs Project Managers	Consultant vs Project Managers
Main Criteria	1.000	0.949	0.949
Platform Type	0.351	0.000	0.821
Platform Integrity	0.866	-0.500	-0.866
Resources	0.949	0.949	1.000
Lifting Management	0.949	1.000	0.949
Average	**0.823**	**0.479**	**0.570**
Strength of correlation	**strong**	**moderate to low**	**moderate**

The reliability of the results is verified using Cronbach's alpha to check for internal inconsistency estimate of test scores reliability. The result yields value of 0.57, indicating poor internal consistency among the 22 criteria. This reflects lack of consistency while giving judgment resulting in a poor reliability score. The greater the consistency in responses among items, the higher coefficient alpha will be. Besides, the poor consistency is verified by moderately low correlation between expert groups. This may be is due to different interests in decommissioning activities, hence the importance of criteria is reflected by the poor Spearman's correlation. In order to solve the inconsistency in the survey, it is recommended for second survey to be followed up in future research. Regardless of the slight inconsistency, this approach could directly involve the stakeholders in the decision process hence optimizing complex trade-offs through voting theory from the stakeholders. As the outcomes, a relatively transparent and understandable result could be obtained to reach the consensus among stakeholders. Several additional criteria have also been addressed by the experts: field economics, legislation requirements, feasibility of decommissioning technology and environmental impact. For improvement of this research, these criteria could be included in future survey.

Conclusion and Recommendation

Decommissioning revolves around a complex framework with several alternatives available hence the decision making to choose the best option is often tricky. This research aims to develop a tool to assist in identifying and prioritizing the pre-decommissioning criteria of fixed offshore structures during the lifecycle of a platform. From the finding, the feasibility of equipment and facilities are highlighted as the most important criteria. The correlation between groups of respondents has been found to be moderately low, verified by the poor internal consistency in judgment, which could be improved through implementation of second survey. The involvement from the related parties such as the environmentalist, legal bodies and technical team could give a better consensus on decommissioning decision making.

References

[1] History of Oil and Gas in Malaysia, 2013. [Online]. Available: http://www.mprc.gov.my/industry/history-of-oil-gas-in-malaysia. [Accessed June 2013].

[2] B. Twomey, Study Assesses Asia-Pacific Offshore Decommissioning Costs, 15 March 2010.

[3] PETRONAS Research & Scientific Services Sdn. Bhd, Best Practicable Environmental Option (BPEO) for SM-4, SMV-A and EMV-A Decommissioning Study, Kuala Lumpur, 2006.

[4] Booth, D., Fowler, A., & Macreadie, P. (2013). How do you determine when rigs to reefs is a suitable decommissioning option? University of Technology Sydney.

[5] K. V. John, Decommissioning of Offshore Platforms, in 2nd Construction Industry Research Achievement International Conference (CIRAIC), Kuala Lumpur, 2009.

[6] Department of Resources, Energy and Tourism of Australia, Decommissioning Australia's Offshore Oil and Gas Facilities, Department of Resources, Energy and Tourism, Canberra, 2008.

[7] "International Maritime Organization (IMO)," 19 October 1989. [Online]. Available: http://www.imo.org/blast/mainframe.asp?topic_id=1026. [Accessed June 2013].

[8] S. M. Wiegand, An Analysis to the Main Economic Drivers for Offshore Wells Abandonment and Facilities Decommissioning, University of Texas, Austin, 2011.

[9] Proserv Offshore, Review of the State of the Art for Removal of GoM US OCS Oil & Gas Facilities in Greater than 400' Water Depth. U.S Department of the Interior, Minerals Management Service, Houston, Texas, 2009.

[10] M.K. Kaiser. The Louisiana Artificial Reef. Marine Policy, 30,(6),2006, pp 605-623

[11] N. A. W. A. Zawawi, M. S. Liew and K. L. Na, Decommissioning of Offshore Platform: A Sustainable Framework, in IEEE Colloquium on Humanities, Science & Engineering Research (CHUSER), Sabah, Malaysia, 2012.

[12] Oil & Gas UK, 2012 Decommissioning Insight, London: The United Kingdom Offshore Oil and Gas Industry, 2012.

[13] "Industry weighs reuse of platform," 10 January 2002. [Online]. Available: http://www.offshore-mag.com/articles/print/volume-62/issue-10/news/industry-weighs-reuse-of-platforms.html

[14] American Petroleum Institute, API RP 2A-WSD Recommended Practice for Planning, Designing, and Constructing Fixed Offshore Platforms-Working Stress Design, Washington, 2000.

[15] "How Does Decommissioning Work?", 2012. [Online]. Available: http://www.rigzone.com/training/insight.asp?i_id=354.

[16] D. W. M. Chan and M. M. Kumaraswamy, A Comparative Study of Causes of Time Overruns in Hong Kong Construction Projects, International Journal of Project Management, pp. 55-63, 1997.

[17] M. Gunduz, Y. Nielsen and M. Ozdemir, Quantification of Delay Factors Using Relative Importance Index Method for Construction Projects in Turkey, American Society of Civil Engineers, 2013.

[18] A. A. Umar, N. A. Wan Abdullah Zawawi, M. F. Khamidi and A. Idrus, Stakeholder Perceptions on Achieved Benefits of PFI Procurement Strategy, Modern Applied Science, pp. 31-39, 2013.

Applied Mechanics and Materials Vol. 567 (2014) pp 228-234
© (2014) Trans Tech Publications, Switzerland
doi:10.4028/www.scientific.net/AMM.567.228

Dynamic Response of Free-span Sub-sea Pipelines under Vortex Induced Vibrations

Charanvarma.S[1,a] , A.P.Shashikala[2,b]

[1]M.Tech, Civil Engineering Department NIT Calicut, India

[2]Professor, Civil Engineering Department NIT Calicut, India

[a]charan.2340@gmail.com,[b]apska@nitc.ac.in

Keywords: Free span pipelines, Vortex-induced vibrations, Van Der Pol model, Duffing model.

Abstract: Study of dynamic behavior of pipeline is required to access fatigue life of pipeline welds. Semi-empirical mathematical model is thus proposed to calculate responses of free-span pipelines under vortex induced vibrations. A two equation model interacted through velocity coupling with a non-linear stiffness term for pipeline model and a non-linear damping term for wake is considered. The proposed model is found to represent the real situation of responses to a greater extent.

1. Introduction: Sub-sea pipelines are subjected to various environmental loads due to waves, currents and other installation loads. A special class of pipelines arises due to uneven sea-bed in deep sea susceptible to vortex induced loads called Free-span pipelines. The Free-span pipelines have their ends lying on sea-bed and span freely suspended. As the span length increases, the structural behavior turns out to be more slender, thus inhibits the vortices to shed around the pipelines. Vortices are shed due to both waves and currents. But at bottom sea bed conditions, as the effects due to waves are negligibly small, the effects due to currents are alone considered.

Vortex-induced vibrations on free-span pipelines are a potential reason for fatigue failures. A study of dynamic behavior of pipelines is thus required to access the fatigue life. Earlier studies had focused on studying the response of such pipelines considering behavior of Vortex- induced vibrations through a Van Der Pol oscillator model and a linear model for pipeline. Choi [1] showed axial load effect on the natural frequencies and allowable free span lengths of the pipeline for various boundary conditions. Facchinetti *et al* [2] proposed a model to investigate the behavior of structure under vortex induced vibrations. The appropriate coupling of structure with wake is investigated and concluded that acceleration coupling succeeds in modeling features of vortex induced vibrations. Gautam Chaudhury [3] proposed a model by replacing damping term with drag term. Reduced lift and hydrodynamic damping methods were proposed for determination of drag and lift coefficients. Farshidianfar *et al* [4] proposed a two oscillator model unlike classical model. It was studied that velocity coupling represent the phenomenon qualitatively. Narokorn Srinil [5] proposed two equations each representing a degree of freedom. The model included a geometric cubic term and quadratic non-linear term to represent responses of structure-fluid interaction.

In this paper, a non-linear oscillator for structural model is considered to account for the geometric nonlinearity that is arising due to installation and initial configuration of Free-span pipelines. A Duffing oscillator model is proposedto study the non-linearity of structure and Van Der Pol model is considered to represent the vortex induced vibrations. Both these non-linear models are coupled using velocity coupling. A non-dimensional semi-empirical coupled model is thus proposed to study the dynamic response of pipelines.

2. Theoretical Formulation

2.1. Duffing model: Structural behavior of pipe should be represented by a non linear stiffness unlike linear models as proposed earlier [3] [4]. This non linearity arises due to installation forces, and initial curvature of free span pipelines. Physical behavior of pipeline using Duffing oscillator is described in Fig. 1. A Duffing model is thus proposed to represent its properties in the form as shown here,

$$m\ddot{x} + c\dot{x} + k(x^3 - x) = f(t) \tag{1}$$

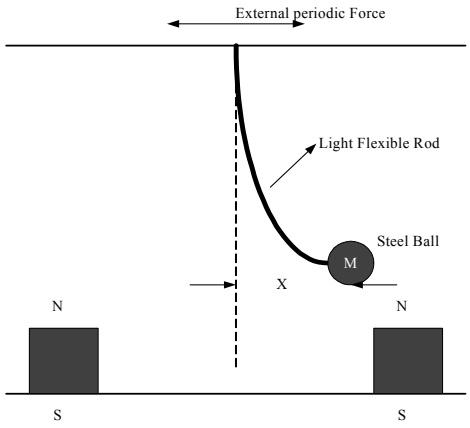


Figure1: Description of Duffing model

$$m = m_s + m_f = m_s + c_m \rho \frac{\pi}{4} D^2 \tag{2}$$

$$c = c_s + c_f = 2m\omega\xi + \gamma\rho D^2 \omega_f \tag{3}$$

$$k = m\omega^2 \tag{4}$$

m =total mass, m_s =structural mass, m_f =fluid mass, c_m =coefficient of added mass, c =total damping, c_s =structural damping, c_f =fluid damping, γ= stall parameter, ρ =density of sea water, D =diameter of pipeline, k =stiffness of pipeline, ω=natural frequency of pipeline, ω_f =frequency of vortex shedding, $f(t)$=forcing function.

Using the above Duffing model, we see that the pipeline does not oscillate about its position but instead exhibits a non linear behavior as shown in Fig. 2 and Fig. 3 for free vibration. Fig. 4 and Fig.5 represent the behavior of Duffing oscillator for forced vibration. Dynamic behavior for both free vibration and forced vibrations allows us to apply this model for pipelines influenced under vortices.

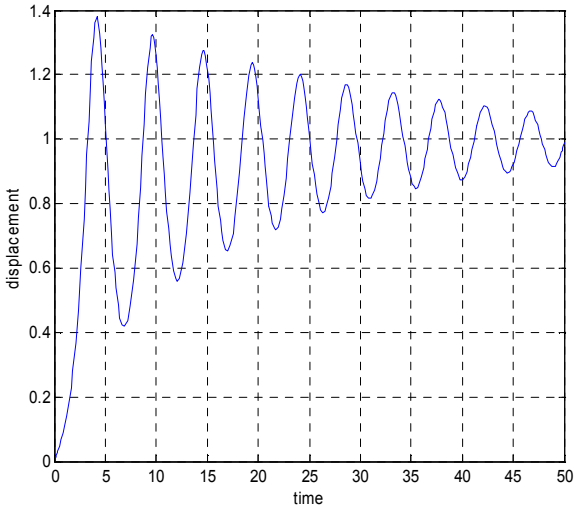


Fig. 2: Displacement Vs Time for $f(t)$=0

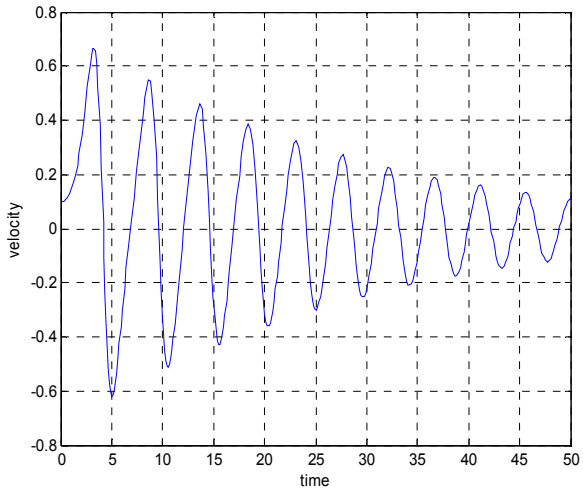


Fig. 3: Velocity Vs Time for $f(t)$=0

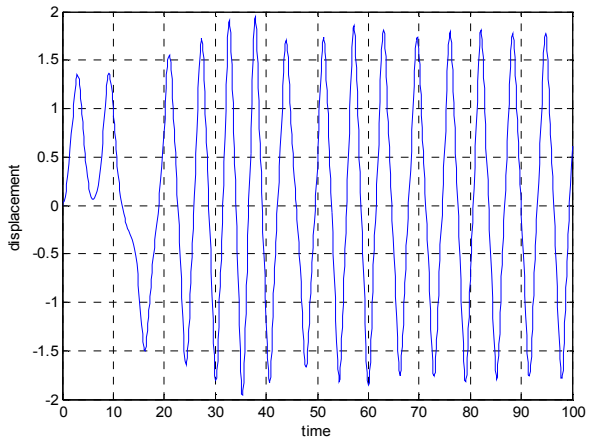


Fig. 4: Displacement Vs Time $f(t)=\cos wt$

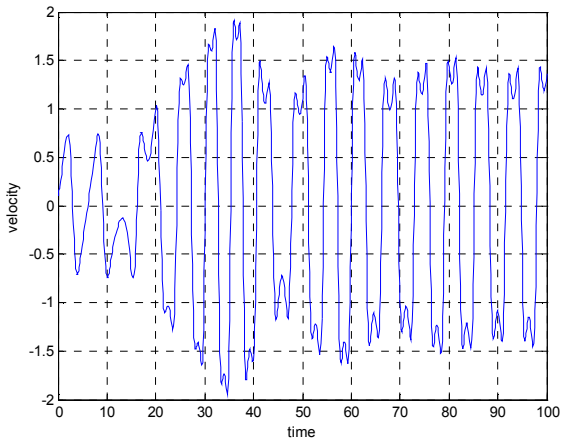


Fig. 5: Velocity Vs Time $f(t)=\cos wt$

2.2. Van Der Pol model: The response of wake is represented by self-regulating equation as used by most of the earlier literature [3] [4]. This equation is as follows:

$$m_f\ddot{c}_L + Ac_f(c_L^{\,2}-1)\dot{c}_L + kc_L = g(t) \tag{5}$$

A=parameter, $g(t)$=forcing function.

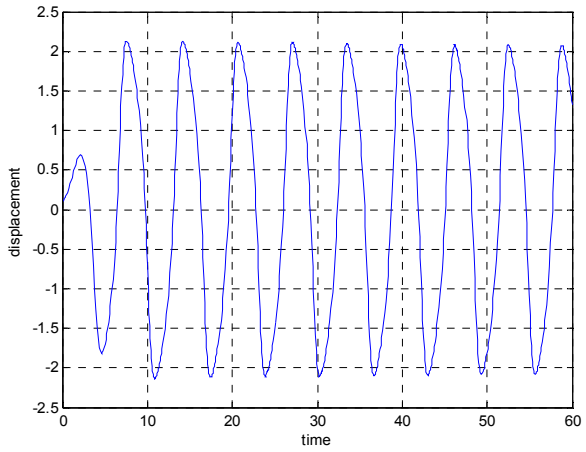


Fig. 6: Displacement Vs Time for ε=1

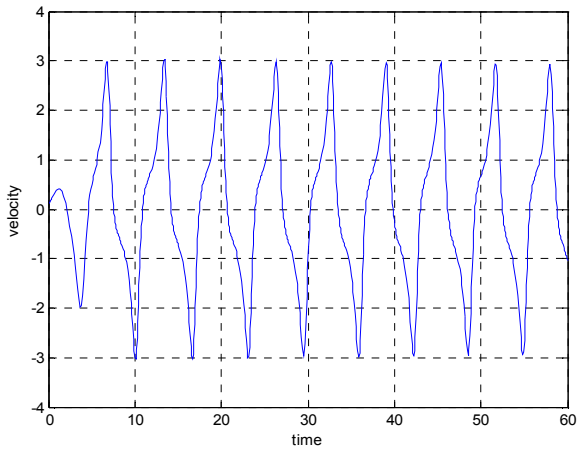


Fig. 7: Velocity Vs Time for ε=1

The non-linear damping term represents the Vortex-induced phenomenon with a negative damping at low amplitude and a positive damping at high amplitude. The dynamic characteristics are studied as in Fig. 6 and Fig. 7. This response of self-limiting nature for high amplitude ratios and self-exciting nature at low-amplitude ratios makes it strongly recommended for wake representation.

3. Non-dimensional coupling

The two individual equations (1) and (5) are coupled with each other to represent fluid-structure interaction. This interaction is done by velocity coupling and the two equations are converted to non-dimensional form.

$$X = \frac{x}{D}\ ;\ Q = \frac{C_L}{C_{L0}}\ ;\ \delta = \frac{\omega_s}{\omega_f};\ \mu = \frac{m}{\rho D^2};\ s_t = \frac{\omega_f D}{2\pi U}\ ;\ T = tD \tag{6}$$

C_{L0} = lift coefficient for fixed pipeline.

Using all the above non-dimensional quantities equations (1) and (4) converts to

$$\ddot{X} + \left(2\zeta\delta + \frac{\gamma}{\mu}\right)\dot{X} + \delta^2(D^2X^3 - X) = f(t) \quad (7a)$$

$$m_f\ddot{Q} + \varepsilon c_f(Q^2 - 1)\dot{Q} + kQ = g(t) \quad (7b)$$

Now these two equations are coupled using velocity coupling of forcing terms to represent pipe-wake interaction.

$$f(t) = \frac{B}{16\pi^2\mu s_t{}^2}\dot{Q}; \quad \text{B=parameter} \quad (8a)$$

$$g(t) = C_{L0}\dot{X} \quad (8b)$$

On substituting equation (8a) and (8b) in equation (7a) and (7b) and solved using Range-kutta fourth order method will result in a coupling responses of Free-span pipelines in a perpendicular direction to wave motion. The same equations can also be applied to in-line Vortex-induced vibrations by considering drag coefficients in place of lift coefficients for above equations. Parameters A and B are to be adjusted according to experimental or CFD results which are different for in-line and cross-flow responses.

4. Results and discussions

The range of applicability can be extended depending on structure and environment conditions. Free-span pipeline subjected to current in deep sea conditions are studied here. All the non-dimensional constants mentioned in the mathematical model with velocity coupling are calculated depending on the values in real situations. Pipeline and flow situation details in practical scenario are considered below in Table 1

Table 1: Range of values considered for model

Property	Practical Range
Diameter of pipe	0.6-1.5 m
Current velocities	0.5-1 m/s
Density of steel	7850 kg/m^3
Density of sea water	1025 kg/m^3
Reynolds number	$5\times 10^5 - 1.5\times 10^6$
Strouhal number	0.212

The study on frequencies for pipeline is included in fig 8 to explain the significance of frequency ratio in the model representation. Thus with increase in length the wake response is further increased due to reduction in frequency for a similar current velocity. This will also depends on soil properties at the supporting ends of free-span pipelines as explained in fig 8.

Fig. 9a, Fig. 9b represents the displacement and velocity profiles of pipeline under velocity coupling. The response indicates that there is a transient state at the beginning and attains a steady-state gradually with time. The model is also capable of representing non-linearity that exists in real case situation of free-span pipelines. Similar trend is observed for wake responses as shown in Fig. 10a, Fig. 10b the response of wake adjusts itself within a certain range and repeated loading is applied on pipe. Fig. 9c, Fig. 10c are state-space representation of responses to study the future states of response at a given initial conditions. Also the natural frequency variation with length of pipeline and end conditions is shown in Fig.8 which signifies that frequency ratio is not a value but a range and the response over the entire range need to be considered to further take into account of stress range and fatigue life due to vortex induced vibrations.

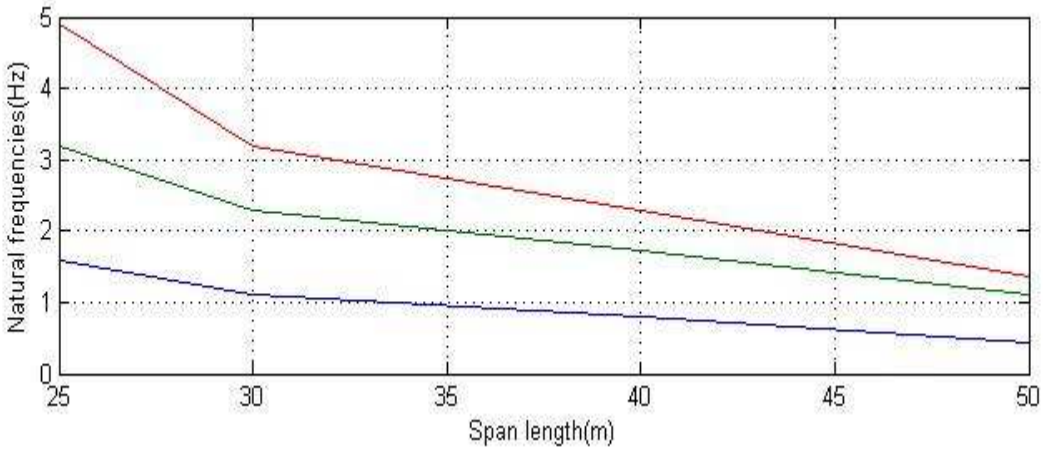


Fig. 8: Variation of natural frequencies with span-length and end conditions.

The response of pipeline observed in Fig. 9a is of major significance in calculating fatigue life at critical joints. The displacement patterns observed is extended to stress history for calculating fatigue life. The state-space representation of pipeline represents a stable chaotic behavior about equilibrium points. Similar to pipelines behavior the wake behavior is also represented in fig 10a, Fig 10b and Fig 10c. The chaotic nature of wake is well represented and its effect on pipeline is included through velocity coupling for every time step. Thus velocity coupling proposed here represents the fluid-structure interaction to a greater extent in cross flow situations.

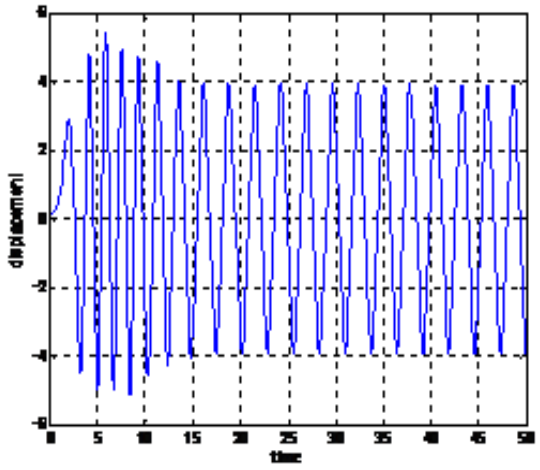


Fig. 9a: Displacement Vs Time of pipeline

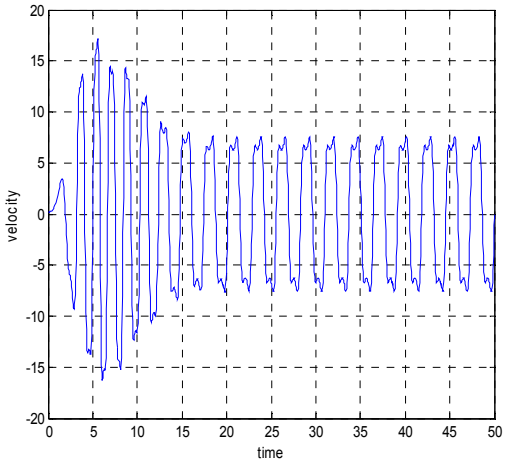


Fig. 9b: Velocity Vs Time of pipeline

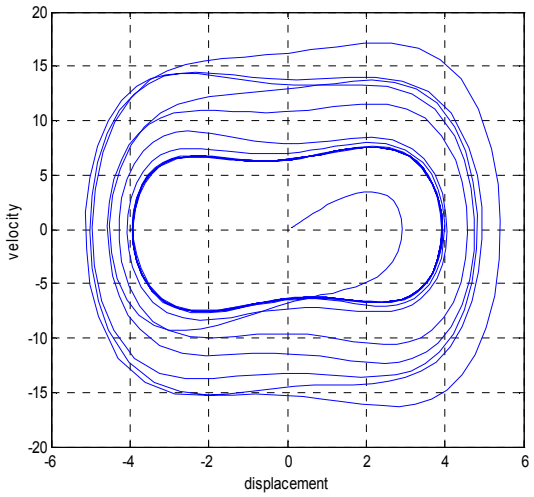


Fig. 9c: State-Space representation of pipeline

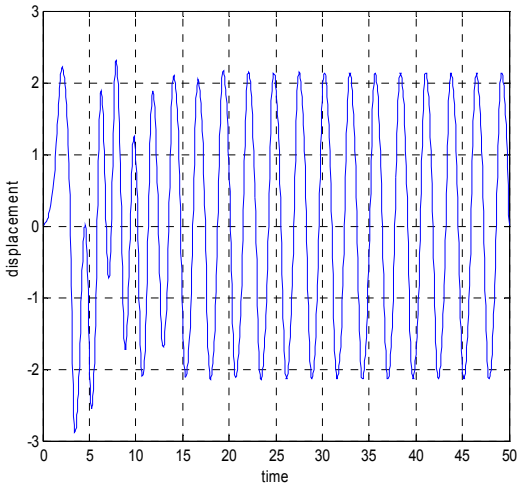


Fig. 10a: Displacement Vs Time of wake

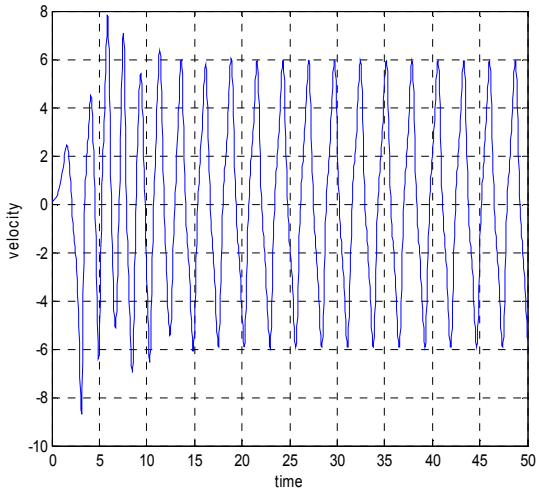


Fig. 10b: Velocity Vs Time of wake

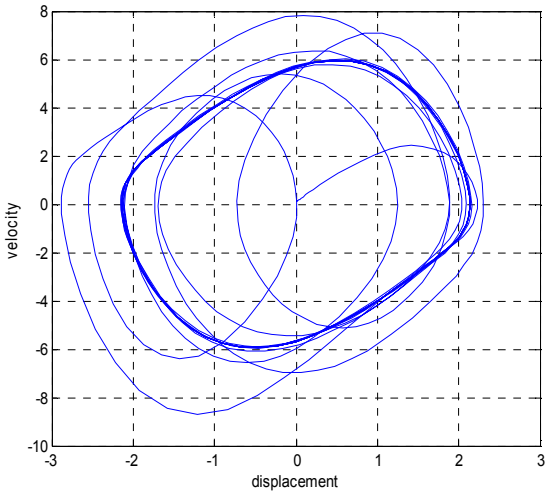


Fig. 10c: State-Space representation of wake

5. Conclusions

The fatigue life estimation of sub-sea pipelines under vortex induced vibrations is of major importance in the model representation using a velocity coupled Van Der Pol –Duffing representation. The present model represents the real situations of free-span pipelines by adjusting the non-dimensional variables and also the additional parameters included in model to match with experimental results of vortex induced vibrations. The model can be extended to various structures with different non-dimensional parameters and checked for validity of model over a wide range of applications. The proposed model is capable of representing response of sub-sea pipelines under vortex-induced vibrations for cross-flow situations and can be extended to in-flow response

References

[1] Choi.H.S.,2001 ,"Free Spanning Analysis of Offshore Pipelines," Journal of Ocean Engineering, vol.28, pp.1325-1338.

[2] Fachinetti, *et al*., 2004,"Coupling Of Structure And Wake Oscillators In Vortex -Induced Vibrations,"Journal of Fluids and Structures, vol.19, pp.123-140.

[3] Gautam Chaudhury., 2011,"An Engineering SDOF Model for Transverse VIV Response of a Cylinder In Uniform Steady Flow," Journal of Offshore Mechanics and Arctic Engineering, vol.133, pp.031106-1-6.

[4] Farshidianfar.A,Zanganeh.H.,2010,"A Modified Wake Oscillator Model For Vortex-Induced Vibration Of Circular Cylinders For A Wide Range Of Mass-Damping Ratio, "Journal of Fluids and Structures,vol.26,pp.430-441.

[5] Srinil.N., Zanganeh.H., 2012," Modelling of coupled cross-flow/in-line VIV using double Duffing & van der Pol oscillators," Journal of Ocean Engineering vol.53, pp.83-97.

[6] Det Norske Veritas (DNV), 2006. Free span Pipelines.

Applied Mechanics and Materials Vol. 567 (2014) pp 235-240
© (2014) Trans Tech Publications, Switzerland
doi:10.4028/www.scientific.net/AMM.567.235

Dynamic Responses of Classic Spar Platform: Short Crested Waves vs. Long Crested Waves

C.Y. Ng[1], V.J. Kurian[2], M.S. Liew[3]

NG Cheng Yee[1, a], VELLURUZHATHIL John Kurian[2, b]

and MOHD. Shahir Liew[3, c]

[1, 2, 3] Civil Engineering Dept., Universiti Teknologi PETRONAS, Tronoh, Perak, Malaysia

[a] carrol.ng82@gmail.com, [b] kurian_john@petronas.com.my, [c] shahir_liew@petronas.com.my

Keywords: classic spar; RAO; short-crested waves; long-crested waves; wave tank test.

Abstract. The long-crested wave properties have been widely implemented in the design of offshore structures. However, long-crested waves are seldom found in the real sea condition. Many research papers have also stated that wave forces obtained by the waves would be overestimated. Indeed, the real sea conditions are better represented by the short-crested waves. Hence, in order to obtain an optimum design for the offshore structures with cost and time effective, consideration of the short-crested nature of waves is necessary. In this paper, a study comparing the responses of the classic spar due to short-crested waves and long-crested waves obtained experimentally has been performed. The model tests have been carried out in the wave tank of Offshore Laboratory for Universiti Teknologi PETRONAS. In the model tests, short-crested waves and long-crested waves were generated. Responses of the classic spar model were recorded by the Optical Tracking System (OptiTrack). The responses of the classic spar due to short-crested waves and long-crested waves were compared among. From the comparisons, the responses for short-crested waves in all the three degree of freedom (DOF) were found to be about 35% less than the responses for long-crested waves. Thus, it could be concluded that optimized and economical designs can be arrived at by considering the short-crestedness of the waves for classic spar structures.

Introduction

In the design of offshore structures, environmental condition is one of the important aspects that shall be considered. Wind, wave, current and iceberg are some of the common types of environmental force considered in the design. Wave forces are the dominating force among the total environmental forces. Wave forces are categorized as long-crested and short-crested based on the direction of the wave propagated. Long-crested waves (LCW) are defined as waves that propagate to only one direction. Short-crested waves (SCW) are defined as groups of LCW that propagate to various directions and the waves are randomly varying in the magnitude and direction. For the real sea conditions, waves would be better represented by SCW, whereby many aspects of the SCW shall not be ignored and could not be simulated by LCW [1]. The appearance of the SCW was found to be three dimensional, complex and short-crested [2]. By the wave properties of SCW in the design of offshore structures, optimum design of the structures with cost and time effectiveness could be arrived at.

Even though researches focused on wave forces have been widely performed, however the documents are concentrated mainly on LCW. Colby et al [3] performed a study focused on coupled and decoupled analysis of a deepwater spar in varying water depth subjected to LCW. Ran et al [4] performed a study focused on regular, bi-chromatic and long-crested irregular waves incorporated with and without currents to investigate the response characteristics of a spar by experimental and numerical method. A numerical simulation to investigate the coupled analysis of floaters subjected to LCW with current was developed by Ran [5]. In the simulation, tethered spar, classic spar, truss spar and tension leg platform were considered, where the results of coupled time domain analysis were systematically compared with the model test results of uncoupled analysis and frequency domain analysis. A relationship between the components, system performance of the offshore

foundation and its mooring system of a spar was investigated by Young [6]. In this study, the reliability assessment of the platform under extreme environment for LCW was focused on the investigation. Sun [7] performed a study to analyze the force acting on a 3D cylinder with arbitrary cross section subjected to LCW. In his analysis, viscous effects such as viscous damping and viscous exciting force were considered. Experimental and theoretical study of wave forces and overturning moment acting on two geometrically similar concrete oil production platform subjected to LCW was performed by Garrison et al [8]. Pijfers and Brink [9] presented a method to obtain the mean and slowly varying drift force on a semi-submersible due to hydrodynamic loading in regular and irregular waves. From the survey, it was found that LCW were widely adopted in the study for offshore platforms, coastal platforms and so on, it is more precise to consider SCW wave properties in simulation of real sea condition. Researches on SCW were found since 1970s, which mainly focused on directional wave force, directional wave spectrum, wave kinematics and vertical circular cylinder. Zhu [10] developed a solution for diffraction of SCW incident on a bottom-seated circular cylinder. From this study, the wave loading from plane incident waves was found overestimated when incident waves were short-crested. Another solution in closed form for the velocity of the nonlinear diffracted SCW subjected to vertical cylinder was presented by Zhu and Satravaha [11]. The theory presented by Zhu was extended by Jian et al [12] to include the effect of a uniform current for different incident angles. An analytical solution for diffraction of short-crested incident wave along positive x-axis direction on a large circular cylinder with current was developed. The Zhu's theory again extended by Zhu and Moule [13] to incorporate the effect of wave induced forces due to SCW subjected to vertical cylinders with circular, elliptical and square cross section. Scaled Boundary Finite Element Method (SBFEM) was proposed by Tao et al [14] to solve the boundary value problem composed of short-crested incident wave diffraction on vertical circular cylinder. The method was presented as a novel semi-analytical method developed in elasto-statics and elasto-dynamic areas which used the advantages of both the finite element method and boundary element method. The method was extended by Song and Tao [15] to investigate the wave interactions of two cylinder systems with partially solid wall or opening subjected to 3D short-crested incident waves. Liu and Lin [16] [17] again extended the method to investigate the wave-platform interaction of the concentric platform with double layer arc-shaped perforated cylinders in SCW.

From the literature, very few numerical and experimental studies were found reported about the dynamic responses of spar platforms subjected to short-crested waves. In this paper, a study comparing the responses of the classic spar due to short-crested waves and long-crested waves that obtained experimentally is reported. The results have been compared and discussed.

Methodology

Wave tank tests were performed on the classic spar platform models to investigate the dynamic responses of the model subjected to both long-crested and short-crested waves in all the three DOF. The tests were conducted in the wave tank in the Offshore Engineering Laboratory of Universiti Teknologi PETRONAS. Details of the tests are illustrated as follow.

Laboratory facilities and instrumentations. The model tests were conducted in the wave tank measured approximately 22m total length, 10m width and 1.5m water depth as illustrated in Fig. 1 The wave maker is a multi-element wave maker that the paddles move individually forward and backward to generate various waves. Waves can be simulated to propagate in various angles such as bi-directional and multi-directional waves instead of uni-directional wave.

Model description. Classic spar model were fabricated by using steel plates with scaling factor 1:100 as shown in Fig. 2. Table 1 summarized the general structural data for the classic spar model.

Long-crested waves. Table 2 shows the random wave series considered for the wave spectrum method, where the JONSWAP spectrum with peak enhancement factor 3.3 was adopted. Data obtained from OptiTrack were analyzed and post-processed by Discrete Fast Fourier Transformation (DFFT) method to determine the response spectra. In this study, response in term of response amplitude operator (RAO) was considered, where RAO is given as

$$RAO = \sqrt{\frac{S_R(f)}{S(f)}} \quad (1)$$

Where S_R *(f)* is the motion response spectrum for the model, *S(f)* is the wave spectrum and *f* is the wave frequency.



Figure 1. Wave tank in Offshore Laboratory of UTP

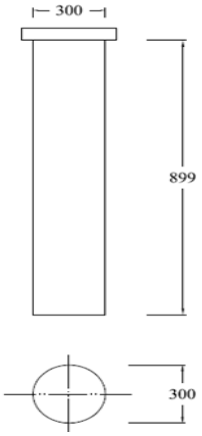


Figure 2. Drawing of classic spar model

Table 1. Structural data of classic spar model

Description	*Model (m)*	*Prototype (m)*
Diameter	0.300	30.00
Overall Length	0.899	89.90
Draft	0.699	69.90
Vertical CG from keel	0.31	31
Vertical CB from keel	0.40	40
Total mass, kg	13.302	13.302 x10^6

Table 2. Long-crested wave series

Wave series	*Wave Frequency, Hz*	*Wave Period, sec*	*Targeted Wave Height, m*
RD1	0.83	1.20	0.06
RD2	0.77	1.30	0.08
RD3	0.71	1.40	0.09
RD4	0.61	1.63	0.10

Short-crested waves. Spreading function technique is implemented with the method of modes to produce the short-crested waves. For each frequency in turn, the spreading function is integrated over the angular range corresponding to each mode, to obtain a series of factors. In the study, build in spreading function, $cos^2\theta$ was used. In this case, the formula is factored so that during the integration over the possible range of direction ($\pm\pi/2$), the result is 1.0 for the spreading function. Table 3 tabulated the short-crested wave series generated.

Table 3. Short-crested wave series

Wave series	*Directional Spreading Function*		*Spectrum*
MC2	Cos^2 Spread		JONSWAP
Wave series	*Wave Freq, Hz*	*Wave Period, sec*	*Targeted Wave Height, m*
A	0.50	2.00	0.08
B	0.63	1.60	0.08
C	0.71	1.40	0.08
D	0.83	1.20	0.08
E	1.00	1.00	0.08
F	1.25	0.80	0.08
G	0.71	1.40	0.07
H	0.83	1.20	0.07
I	1.00	1.00	0.06
J	1.25	0.80	0.06

Experimental set-up. The tests were intended to study the dynamic responses of the models subjected to long-crested and short-crested waves. The displacements and rotations of the models were recorded by the OptiTrack system. The system recorded the motion in surge, sway, heave; roll, pitch and yaw thru reflective markers installed on top of the models with varied additional heights to provide randomness. The arrangement of the model setup in plan view is shown in Fig. 3.

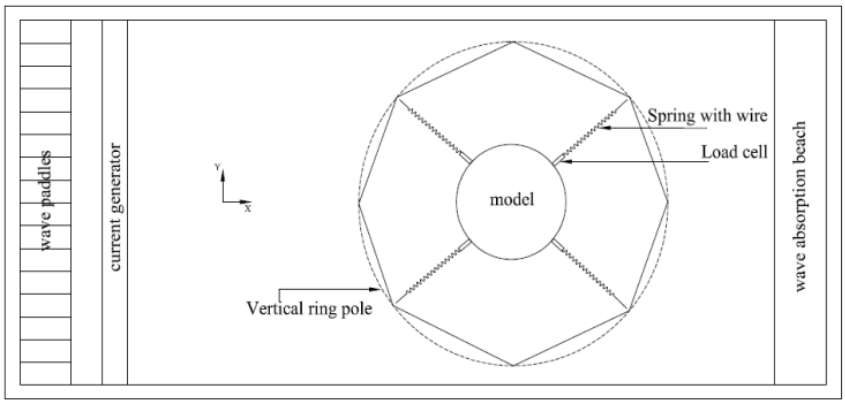


Figure 3. Model setup – Plan view

Results and discussion

The responses in surge, heave and pitch motion of the classic spar estimated by the numerical simulations for long-crested and short-crested waves are shown in Figs. 4 ~ 6. It could be observed from the figures that the trends of the responses agreed fairly well. Smaller responses by short-crested waves are observed in the comparison with the results by long-crested waves. The short-crested waves were found smaller than the responses due to long-crested waves for the surge, heave and pitch motions. Fig. 4 shows the surge RAO comparison due to long-crested and short-crested waves for classic spar. From the figure, it could be observed that the responses due to short-crested waves generally yield about 35% smaller compared to long-crested waves. It could be seen that similar trend generally yield, and the time phase different was found to be the reason that cause the peak occurred at f=0.05Hz. Fig. 5 shows the heave RAO comparison due to long-crested waves and short-crested waves for classic spar. The trend of the responses agreed quite well, where the responses decreased substantially from 0.06Hz to 0.07Hz, and slightly reduced to almost nil at high frequencies range. From the comparison, it could be summarized that the responses due to short-crested waves yield smaller responses compared to long-crested waves at the low frequency range. It can be understood that short-crested wave forces act horizontally to the structure; the vertical heave motion might not experience significant changes due to the wave directionality effects. Fig. 6 shows the pitch RAO comparison due to long-crested and short-crested waves for classic spar. From the figure it could be observed again that the responses due to short-crested waves yield about 38% smaller compared to long-crested waves.

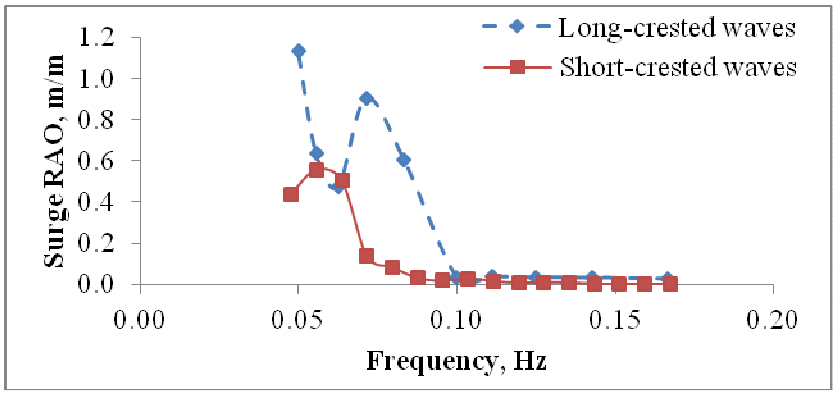


Figure 4. Surge RAO comparison for classic spar

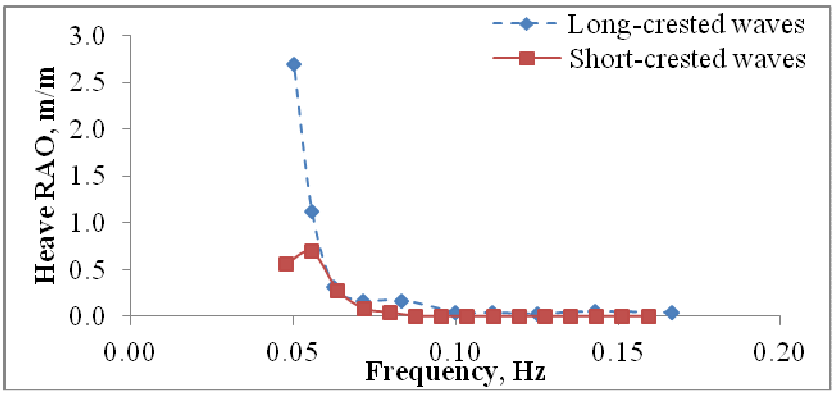


Figure 5. Heave RAO comparison for classic spar

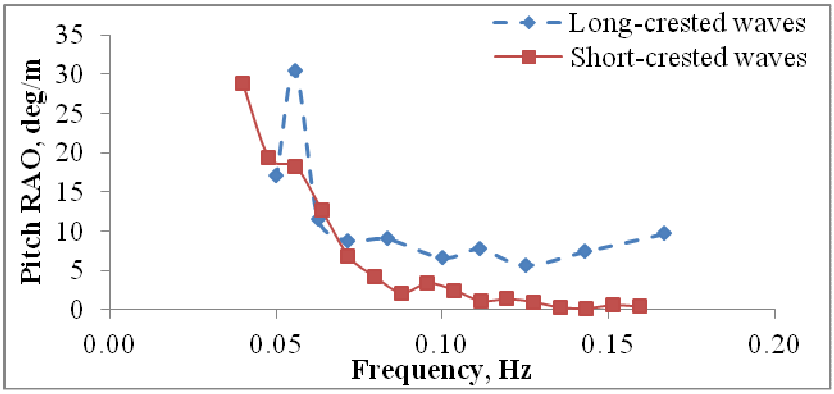


Figure 6. Pitch RAO comparison for classic spar

Conclusion

In this paper, a series of wave tank tests that have been carried out in order to study the dynamic responses of classic spar model due to long-crested and short-crested wave actions was presented. The results measured from the tests were compared and presented. From the results obtained the following conclusions were drawn. It could be observed that the results obtained from short-crested waves are about 35% smaller than that by long-crested waves for surge and pitch RAOs. This is mainly due to the assumption of large offshore platform stretch acted up on by long-crested waves. In this case, design considering the long-crested waves would be overestimated. On the other hand, in the real state, various short-crested waves will be hitting the stretch length in different angles and the net effect will be quite likely to be less. Hence, from the results obtained it could be concluded that the responses of the classic spar model that subjected to short-crested waves on the stretch length in different angle are expected to be less. It is important to highlight that this study only limited to uni-directional regular wave environment and classic spar platform.

References

[1] H. Mitwally and M. Novak, “Wave forces on fixed offshore structures in short-crested seas”, J. Eng. Mech, 115, (1989) 636-655.

[2] S.K.Chakrabarti, “Hydrodynamic of Offshore Structures.”, WIT Press, 2001

[3] C. Colby, N. Sodahl, E. Katla and S. Okkenhaug, "Coupling effects for a deepwater spar", OTC, (2000) 1-7.

[4] Z. Ran, M.H. Kim, J.M. Niedzwecki, R.P. Johnson, “Responses of a Spar Platform In Random Waves And Currents (Experiment Vs. Theory)”, International Journal of Offshore and Polar Engineering, 6, 1, (1996) 27-34.

[5] Z.H. Ran, "Coupled dynamic analysis of floating platforms in waves and currents", PhD Dissertation, Texas A&M University, 2000.

[6] J.C. Young, “Reliability assessment of foundations for offshore mooring systems under extreme environments”, PhD Dissertation, The University of Texas at Austin, 2007.
[7] F.Z. Sun, "Analysis of motions of semi-submersible in sea waves", Offshore Technology Conference, (1980) 429-442.
[8] C.J. Garrison, A. Torum, C. Iversen, S. Leivseth and C.C. Ebbesmeyer, "Wave forces on large volume platforms - A comparison between theory and model tests", Offshore Technology Conference, (1974) 1061-1070.
[9] J.G.L. Pijfers and A.W. Brink, "Calculate drift forces of two semi-submersible platform types in regular and irregular waves", Offshore Technology Conference, (1977) 155-165.
[10] S. Zhu, “Diffraction of short-crested waves around a circular cylinder”, Ocean Engineering, Vol. 20. No. 4, (1993) 389-407.
[11] S. Zhu and P. Satravaha, “Second-order wave diffraction forces on a vertical circular cylinder due to short-crested waves”, Ocean engineering, Vol. 22, No. 2, (1995) 135-189.
[12] Y.J. Jian, J.M. Zhan and Q.Y. Zhu, “Short-crested wave-current forces around a large vertical circular cylinder”, European Journal of Mechanics B/Fluids, Vol 27, (2008) 346-360.
[13] S. Zhu and G. Moule, “Numerical calculation of forces induced by short crested waves on a vertical cylinder with arbitrary cross section”, Ocean Engineering, Vol. 21, No.7, (1994) 645-662.
[14] L. Tao, H. Song and S. Chakrabarti, “ Scaled boundary FEM solution of short-crested wave diffraction by a vertical cylinder”, in Computer Methods in Applied Mechanics and Engineering, Vol. 197, Issues 1–4, Pages 232–242, 1 December 2007.
[15] H. Song and L. Tao, “Short-crested wave interaction with a concentric porous cylindrical platform”, Applied Ocean Research, Vol. 29, No. 4, pp. 199–209, November 2007.
[16] J. Liu and G. Lin, “Scaled boundary FEM solution of short-crested wave interaction with a concentric platform with double-layer arc-shaped perforated cylinders “, Computers &Fluids, Vol. 79, (2013). 82–104.
[17] J. Liu and G. Lin, “Numerical modeling of wave interaction with a concentric cylindrical system with an arc-shaped porous outer cylinder”, European Journal of Mechanics / B Fluids, Vol. 37, (2013) 59-71.

Applied Mechanics and Materials Vol. 567 (2014) pp 241-246
© (2014) Trans Tech Publications, Switzerland
doi:10.4028/www.scientific.net/AMM.567.241

Effect of Anodes on Hydrodynamic Coefficients of Tubular Cylinders - Model Tests

V. J. Kurian[1, a], A. M. Al-Yacouby[2], A. A. Sebastian[3], M. S. Liew[4] and V. G. Idichandy[5]

[1,2,3,4]Department of Civil Engineering, Universiti Teknologi PETRONAS, 31750 Tronoh, PERAK, Malaysia

[5]Department of Ocean Engineering, IIT Madras, INDIA

[a]kurian_john@petronas.com.my

Keywords: Anodes, Cathodic protection, Drag coefficient, Hydrodynamic forces, Inertia coefficient, Malaysian offshore locations, Morison equation, Tubular cylinders.

Abstract. This paper examines the hydrodynamic behavior of a tubular vertical cylinder with anode fittings subjected to regular waves. The model experiments were carried out in the wave basin of Universiti Teknologi PETRONAS. The model was made from galvanized steel, with outer diameter D_o= 0.034 m and total length l = 1.23 m, fixed vertically to the soffit of the wave tank bridge, and the free end was immersed in the wave tank to form a cantilevered beam with wetted length of 0.85 m. Overall, seven anodes were welded to the wetted length of the tubular cylinder, at a center to center spacing of 0.12 m. The model was subjected to regular wave with H_{max} varying from 0.1 m to 0.2 m, with wave height increment of 0.05 m, and the time period varying from T = 1 s to 3 s. The tests were conducted for Keulegan-Carpenter number ranging from 3.9 to 23.3. The hydrodynamic forces and the corresponding hydrodynamic coefficients of the smooth cylinder were compared with the force responses of a tubular cylinder with the same outer diameter, fitted with anodes. A scale factor of 1:55 was adopted in this experimental study based on the limitations of the maximum water depth in the wave tank, and the scaled up force responses of the full scale prototype were analyzed and discussed. The results show that, installation of anodes has increased the drag coefficients by up to 20% depending on the wave frequencies at which the model was tested.

Introduction

Anodes are part of cathodic protection system used in offshore engineering to mitigate corrosions. The cathodic protection is the most cost effective and technically appropriate method adopted for controlling corrosion of offshore platforms [1]. This technique is utilized either alone or in conjunction with protective coatings which is mainly limited to splash zones. The CP system consists of sacrificial anodes, with a design life equal to the expected life of the platform i.e. 20 -30 years. These types of anode are maintenance-free, and positioned in primary bracing and on primary horizontal bracing of offshore platforms. The CP system is capable of polarizing all submerged steel to a potential between -800 mV and -1100 mV [2]. For instance, in Malaysian offshore locations, anodes with 350 mm stand-doff type, made of aluminum, with minimum alloy weight of 350 kg, and approximate anode weight of 440 kg are recommended by PTS [3]. From the structural view point, anodes increase the projected areas of tubular cylinders, and consequently, increase the added mass and the hydrodynamic loadings. Hence, a good understanding of the effect of anodes on hydrodynamic responses of tubular cylinders is important for accurate estimation of hydrodynamic loading on these structures. To accommodate the effects of anodes during the estimation of hydrodynamic forces, the codes of practice normally specify modified coefficients. For tubular smooth cylinders Cm = 1.60 and Cd = 0.65 [4], while the specified values for inertia and drag coefficient for tubular cylinders with anodes are Cm = Cd =2 [3]. The pioneering study on estimation of hydrodynamic coefficient experimentally was conducted by Morison et al.[5]. Much later, Sarpkaya [6] correlated the hydrodynamic coefficients of smooth cylinder with Reynolds

number and Keulegan-Carpenter number. In addition, another study was conducted by Chakrabarti [7] to determine the hydrodynamic coefficients of a vertical cylinder in the wave tank, and the findings were compared with those presented by Sarpkaya [6]. Additional materials in this topic can be found in [8-14] where the authors provided comprehensive experimental investigations on hydrodynamic forces and hydrodynamic coefficients of slender cylinders. However, to the author's knowledge, literature that addresses the effect of anodes on hydrodynamic coefficients for Malaysian offshore locations are not available.

Theoretical Background

Estimation of Wave Forces: Morison equation is generally used for estimating the external viscous hydrodynamic forces on tubular cylinders subjected to wave loadings [5]. This equation assumes that the total in-line hydrodynamic force on a tubular cylinder consists of inertia and drag forces added linearly. The total wave force due to drag and inertia can be estimated using Equation 1.

$$F = \rho g V (\frac{H}{2d}) \tanh kd \times [C_m \sin\theta + C_d (\frac{H}{4\pi D}) \frac{2kd + \sin sh2kd}{\sin sh2kd} |\cos\theta| \cos\theta] \quad (1)$$

where ρ is the water density , V is the volume of displaced water $= \pi D^2 d / 4$, H is the wave height, C_m and C_d are the hydrodynamic inertia and drag coefficients respectively and D is the pipe diameter.

Determination of Hydrodynamic Coefficients: The values of drag and inertia coefficients can be determined by substituting the measured hydrodynamic forces in Equation 1, and estimating the wave kinematics using airy waves theory. However, as the values of *Cm* and *Cd* are functions of the phase angle θ, the best combination of *Cm* and *Cd* and the corresponding phase angles that satisfy Equation 1 have been selected as the optimum drag and inertia coefficients for each loading case.

Experimental Details

Wave Tank Details: The model experiments were carried out in the wave basin of Universiti Teknologi PETRONAS (UTP). The wave tank dimensions are 20 m by 10 m with a maximum water depth of 1 m. Regular waves were generated with wave heights ranging from 0.02 m to 0.2 m, for model periods varying from 0.6 s to 3.25 s. The wave-maker was controlled through an integrated remote control software package capable of generating regular, irregular and multidirectional waves, while the wave profiles were recorded using four wave probes placed around the model. Two wave probes were placed before the model, whilst the remaining two were placed after the model at a center to center spacing of 1.8 m.

Experimental Set up and Procedure: As shown in Figure 1, two vertical rigid cylinders were used in this experimental investigation. The first cylinder is smooth, while the second cylinder was fitted with anodes. Each cylinder was vertically mounted to form a cantilevered beam. One end was fixed to the wave tank bridge to form a rigid cantilevered beam, while the free ends were submerged in the wave tank. The model pipes were made of galvanized steel, with outer diameter D_o= 34 mm and wall thickness t = 2.5 mm. The wave forces were measured using wave force sensors, specially designed and fabricated by the research group in UTP. Detail of the load sensor used in this study was published earlier by Idichandy [15]. The physical properties of the model and the scaled up prototype details are shown in Table 1. The counter balancing moment is eliminated by placing the strain gauges at the locations where the moment is almost negligible.

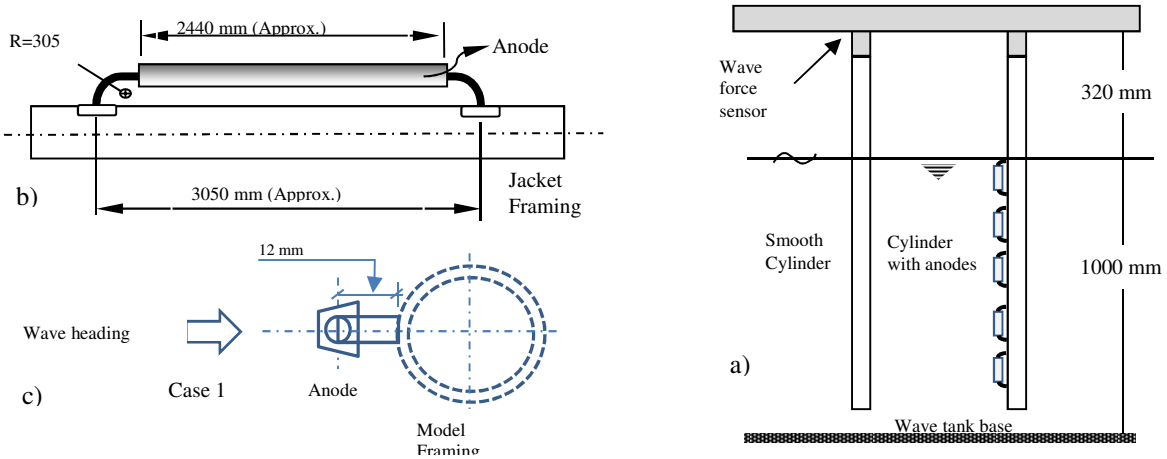


Figure 1: Test models' details: (a) Model set-up in wave tank, (b) Typical anode fixing details, and (c) anode orientation with respect to wave heading

Table 1: Properties of the Model and the Prototype

Model			Prototype		
Pipe Diameter (m)	Pipe Length (m)	Wall Thickness (m)	Pipe Diameter (m)	Pipe Length (m)	Wall Thickness (m)
0.034	1.23	0.0032	1.87	67.65	0.176

Experimental Programme: In order to investigate the effects of anodes on drag and inertia coefficients, an extensive experimental investigation was conducted in the wave tank at UTP. Table 2 depicts the different wave periods and the associated wave frequencies generated in the wave tank during the model test. These wave periods were generated using modal wave heights of 0.2 m, 0.15 m and 0.1 m. as shown in Table 3. The corresponding prototype wave heights are 11 m, 8.25 m and 5.5 m respectively. The hydrodynamic forces and the associated hydrodynamic coefficients for the prototype resulting from these loading conditions were scaled up using a scale factor of 1:55 and the findings are discussed in the following sections.

Table 2: Details of Wave Characteristics Generated in the Wave Tank

Model	Prototye		
Wave Periods (s)	Frequency (Hz)	Wave Period (s)	Frequeny (Hz)
1	1	7.416	0.135
1.5	0.667	11.124	0.090
2	0.500	14.83	0.067
2.5	0.400	18.540	0.054
3	0.333	22.249	0.045

Table 3: Details of Wave Heights Generated in the Wave Tank

Model	Prototype
Wave Height (m)	Wave Height (m)
0.2	11
0.15	8.25
0.1	5.5

Experimental Results and Discussion

Hydrodynamic Forces: Figure 2 depicts the hydrodynamic forces for a smooth rigid cylinder with outer diameter of 2.31 m, compared with the force responses of a similar cylinder with the same physical properties, fitted with anodes. The results show that, when the smooth cylinder was

subjected to regular wave with H_{max} = 11 m, and wave period T = 14.83 s, the hydrodynamic force was 331.49 kN. However, when anodes were fitted to the smooth cylinder as shown in Figure1, and the test was repeated with the same wave characteristics, the results show that the average hydrodynamic force on the cylinder with anode fittings was 434.92 kN, an increase of 31% on the total hydrodynamic force. This clearly shows that anodes can significantly affect the hydrodynamic performance of tubular cylinders. In addition, while keeping the wave height constant at 11 m, the wave period was increased from T = 14.83 s to 18.54 s, and the forces were measured. As shown in Figure 3, the average hydrodynamic force on the smooth cylinder was 222.42 kN, whilst the corresponding response of the cylinder fitted with anodes was 273.09 kN, an overall increase of 22 % on the total hydrodynamic forces as a result of anode fittings. Here, it can also be observed that although in both the above cases, the number of anodes and wave headings were the same, changing the wave frequencies has considerably influenced the magnitudes of hydrodynamic responses of the prototype.

Similarly, as presented in Figure 4, the wave period was decreased to 11.12 s while the wave height was 11 m, and the hydrodynamic forces were measured. Here, it can be observed that the force reposes of the smooth cylinder was 469.81 kN, while the corresponding hydrodynamic forces on the cylinder fitted with anodes was 398.63 kN, a reduction of 15% on the overall hydrodynamic forces. The reason behind this reduction in the force responses can be associated with the frequency of applied wave at this particular case. However; further investigations need to be conducted in order to explain this phenomenon experimentally.

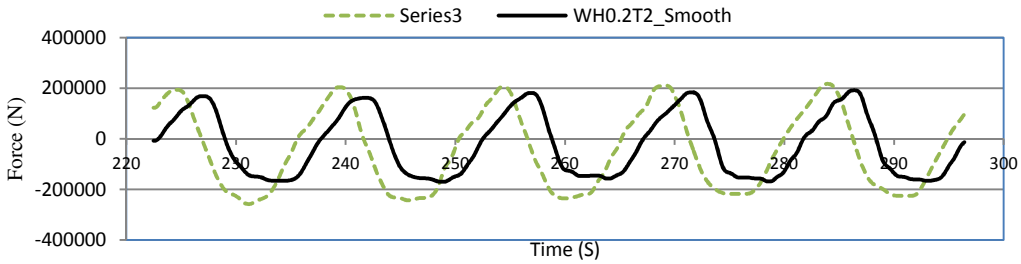


Figure 2: Hydrodynamic Forces for 2.31 m Diameter, Smooth, and Anodes Fitted Cylinders Subjected to Regular Waves with H_{max} = 11 m and T = 14.83 s

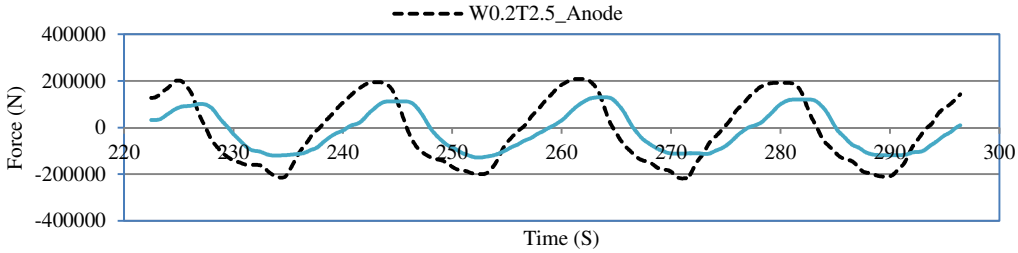


Figure 3: Hydrodynamic Forces for 2.31m Diameter, Smooth, and Anodes Fitted Cylinders Subjected to Regular Waves with H_{max} = 11 m and T = 18.54 s

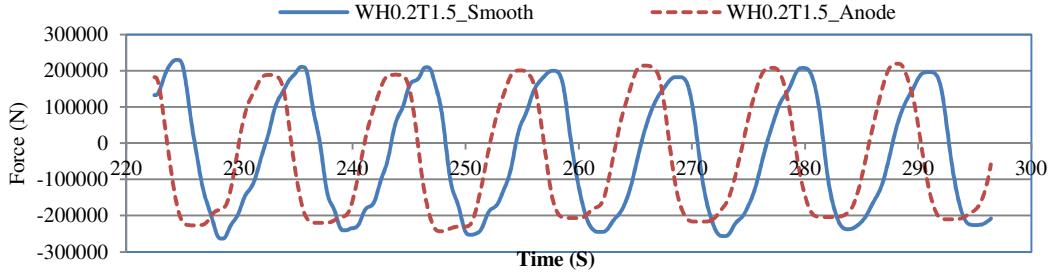


Figure 4: Hydrodynamic Forces for 2.31 m Diameter, Smooth, and Anodes Fitted Cylinders Subjected to Regular Waves with H_{max} = 11 m and T = 11.12 s

Estimation of Hydrodynamic Coefficients: In this section, drag and inertia coefficients for a smooth cylinder, and a similar cylinder fitted with anodes, subjected to regular waves are discussed. The hydrodynamic forces were determined using Morison equation, and *Cm* and *Cd* were determined by equating the measured forces to the theoretical values estimated using the wave kinematics. The hydrodynamic coefficients were determined for different loading conditions as discussed in the following paragraphs.

Figure 5 shows the scaled up inertia coefficients for the full scale prototype smooth cylinder compared with those of a similar cylinder fitted with anodes. Both the cylinders have an outer diameter D_o = 2.31 m, subjected to regular waves with H_{max} =11, 8.25 and 5.5 m, and wave periods varying from T = 11.12 s to 24.1 s. The results show that the minimum inertia coefficient for the smooth cylinder, *Cm* = 1, recorded for H_{max}= 5.5 m and *T* = 18.54 s, while the maximum *Cm* = 2.79 recorded at H_{max}= 11m and *T* = 22.25. The corresponding minimum and maximum *Cm* values for the cylinder fitted with anodes are 0.85 and 2.1 recorded at H_{max} = 8.25 m, *T* = 22.248, and H_{max} =11 m, *T* = 22.24 s respectively.

Similarly, as shown in Figure 6, the drag coefficient for the smooth cylinder was varied from *Cd* = 0.4 to 1.5, with the minimum value observed at H_{max} = 5.5 m and *T* = 14.83 s, the maximum drag coefficient was recorded at H_{max}= 5.5 m and *T* =22.24 s, while the maximum drag coefficient for the cylinder fitted with anodes was *Cd* = 0.6 recorded at H_{max}= 8.25 m and *T* =22.24 s, while the maximum drag coefficient was determined as *Cd* = 1.8 for wave with H_{max}= 11 m and *T* = 22.24 s. Here, it can be observed that anode fittings have increased the drag coefficients up to 20% depending on the wave heights and the frequencies at which the model was tested. The inertia coefficients also have shown some changes due to anode fittings, but these changes remain small as compared to drag coefficients.

Generally, drag and inertia coefficients determined experimentally in this study are in good agreement with the specified ranges in PTS [3] and API [4] as *Cm* = 1.60 and *Cd* = 0.65. The large part of the findings are comparatively smaller than the specified ones, which is encouraging for design of more sustainable and cost effective platforms for Malaysian offshore locations. This indicates that the specified values are more conservative.

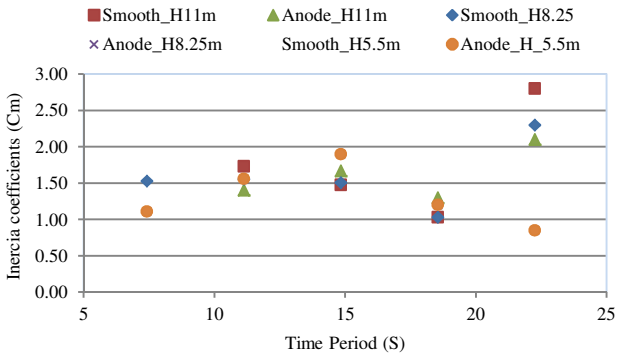


Figure 5: Inertia coefficients for 2.31 m Diameter, Anodes fitted and Smooth Cylinders Subjected to Regular Waves with H_{max} = 11 m

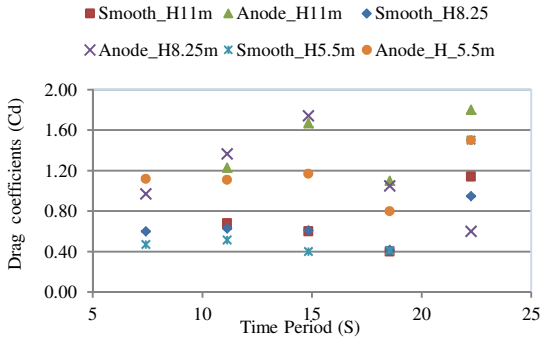


Figure 6: Drag coefficients for 2.31 m Diameter, Anodes fitted and Smooth Cylinders Subjected to Regular Waves with H_{max} = 8.25 m

Conclusions

From the extensive model tests on the effects of anodes on the hydrodynamic forces and on the hydrodynamic coefficients, the following conclusions can be drawn for the scaled up prototype:

1. The experimental results show that installation of anode fittings to a smooth tubular cylinder with outer diameter of 2.31 m has increased its hydrodynamic forces. The influence of

anodes on hydrodynamic forces depending on the wave heights and the wave frequencies at which the model was tested.

2. Generally, anode fittings have modified the geometry of the tubular cylinder, and as a result, the drag coefficients were increased significantly. The effects of anode fittings on inertia coefficients were generally small as compared to drag coefficients. The findings also suggest that drag and inertia coefficients are highly dependent on the wave frequency as well as on the wave heights at which the cylinder was tested.

3. Drag and inertia coefficients determined experimentally in this study are in good agreement with *Cm* and *Cd* values specified by PTS and API. The large part of the findings are comparatively smaller than the specified values, which is encouraging for design of more sustainable and cost effective platforms for Malaysian offshore locations.

Acknowledgment

The authors would like to gratefully acknowledge their gratitude to Universiti Teknologi PETRONAS for support and encouragement.

References

[1] Lemieux, E. and W. Hartt, *Galvanic anode current and structure current demand determination methods for offshore structures.* Corrosion, 2006. 62(2): p. 162-173.
[2] Norsok, *Actions and action effects*, in *Standards Norway, N-003, Edition*. 2007.
[3] PTS, *Petronas Technical Standards*, in *Design of Fixed Offshore Structures*. 2012.
[4] API, R., *RP 2A-WSD,(2007). Recommended Practice for Planning, Designing and Constructing Fixed Offshore Platform-Working Stress Design*. 2007, API Publishing Services, Washington, DC.
[5] Morison, J., J. Johnson, and S. Schaaf, *The force exerted by surface waves on piles.* Journal of Petroleum Technology, 1950. 2(5): p. 149-154.
[6] Sarpkaya, T. *Hydrodynamic forces on various multiple-tube riser configurations*. in *Offshore Technology Conference*. 1979.
[7] Chakrabarti, S.K., *Hydrodynamic coefficients for a vertical tube in an array.* Applied Ocean Research, 1981. 3(1): p. 2-12.
[8] Sarpkaya, T. *In-Line and Transverse Forces, On Cylinders in Oscillatory Flow at High Reynolds Numbers*. in *Offshore Technology Conference*. 1976.
[9] Sarpkaya, T., *Forces on a circular cylinder in viscous oscillatory flow at low Keulegan-Carpenter numbers.* Journal of Fluid Mechanics, 1986. 165(61-71): p. 11-15.
[10] Justesen, P., *Hydrodynamic forces on large cylinders in oscillatory flow.* Journal of Waterway, Port, Coastal, and Ocean Engineering, 1989. 115(4): p. 497-514.
[11] Chakrabarti, S.K., *Wave Force Coefficients for Rough Vertical Cylinder.* Journal of Waterway, Port, Coastal, and Ocean Engineering 1984. Vol. 110(No. 1): p. 101-104.
[12] Bryndum, M., V. Jacobsen, and D. Tsahalis, *Hydrodynamic forces on pipelines: Model tests.* Journal of Offshore Mechanics and Arctic Engineering, 1992. 114: p. 231.
[13] Sumer, B. and J. Fredsoe, *Hydrodynamics around Cylindrical Structures,(1997).* World Scientific, Singapore.
[14] Arndt, H., S. Uwe, and O. Hocine, *Wave Forces on Groups of Slender Cylinders In Comparison to an Isolated Cylinder due to Nonbreaking Waves.* Coastal Engineering Proceedings, 2008.
[15] Idichandy, V. *Strain-gauge-based force transducers in hydrodynamic research*. in *Second International Conference on Experimental Mechanics*. 2001. International Society for Optics and Photonics.

Applied Mechanics and Materials Vol. 567 (2014) pp 247-252
© (2014) Trans Tech Publications, Switzerland
doi:10.4028/www.scientific.net/AMM.567.247

Effects of Marine Growth on Hydrodynamic Coefficients of Rigid Tubular Cylinders

A. M. Al-Yacouby[1], V. J. Kurian[2, a], A. A. Sebastian[3], M. S. Liew[4], V. G. Idichandy[5]

[1,2,3,4] Department of Civil Engineering, Universiti Teknologi PETRONAS, 31750 Tronoh, Perak, Malaysia

[5] Department of Ocean Engineering, IIT Madras, INDIA

[a]kurian_john@petronas.com.my

Keywords: Drag coefficient, Hydrodynamic forces, Inertia coefficient, Marine growth, Morison equation, Tubular cylinders.

Abstract. In this paper the wave induced hydrodynamic forces and the corresponding hydrodynamic coefficients for a 42 mm diameter model pipe subjected to regular waves was investigated experimentally and the results were compared with the responses of a similar rigid cylinder fitted with marine growth. The main objective of this study was to quantify the effects of marine growth on the hydrodynamic forces experimentally and determine the associated hydrodynamic coefficients. The experimental data were generated from a set of wave tank model tests and the results were scaled up using a scale factor of 1:55. The thickness of marine growth applied on the model pipe was varied with respect to the water depth in the ratio of 3:2:1. Regular waves were generated with wave heights ranging from 0.02 m to 0. 2 m for modal period varying from 0.6 s to 3.25 s. The tests were conducted for Keulegan-Carpenter number ranging from 3.9 to 23.3. The findings of the experimental results revealed that increasing the thickness of the full scale prototype cylinder by 110 mm due to marine growth fittings, has increased the overall wave hydrodynamic forces by 16 to 90% depending on the wave heights and the wave frequencies at which the model was tested, proving that the drag coefficients have considerably increased.

Introduction

Marine growth is commonly defined as unwanted surface coat caused by marine organisms such as plants, animals, micro-organisms, bacteria and algae, on underwater surfaces of marine structures, ships, buoys, offshore platforms, etc.[1]. From the structural view point, knowledge on the effects of marine fouling on offshore structures is important for accurate estimation of hydrodynamic loading on these structures [2] as marine growth can increase the tubular pipe diameters and consequently, the added mass and the hydrodynamic loading increase. This phenomenon can result in hydrodynamic instability, as a result of vortex shedding and possible corrosion effects [1]. According to the existing literature, marine growth varies based on the geographical location, as well as with respect to water depth. For instance, in Malaysian offshore locations, marine growth thickness of up to 127 mm is to be considered in wave force computations, with dry unit weight of marine growth to be taken as 10 kN/m^3 [3] Designers normally use Morison equation to estimate the hydrodynamic forces on rough and smooth slender tubular members. To accommodate the effects of surface roughness during the estimation of hydrodynamic forces, the codes of practice specify modified coefficients. For tubular smooth cylinders Cm = 1.60 and Cd = 0.65, while the specified values for inertia and drag coefficient for rough tubular cylinders are 1.2 and 1.05 respectively [3], [4]. However, drag and inertia coefficients are not constant; they are functions of Keulegan-Carpenter number and Reynolds number [5]. Hence, several successful research studies have been conducted to determine the hydrodynamic coefficients of tubular cylinders experimentally. For instance, the pioneering study was conducted by Morison et al.[6]. Much later, extensive laboratory research was conducted by Sarpkaya [7]. In this study, the author correlated

the hydrodynamic coefficients of smooth cylinder with Reynolds number and Keulegan-Carpenter number. In addition, Chakrabarti [8] conducted another study in the wave to determine the hydrodynamic coefficients of a vertical cylinder and the results were compared with those presented by Sarpkaya [7]. Additional materials in this topic can be found in [9], [10], [11], [12], [13] and [14]. Further, several research have also been conducted to estimate the effects of marine growths on hydrodynamic coefficients. Detailed study in this topic was presented by [12], [2] and [15]. However, to the author's knowledge, literature that addresses the effects of marine growth on hydrodynamic coefficients for Malaysian waters are not available. The Malaysia offshore locations are generally situated in the monsoon regime.

Theoretical Formulations

Calculation of Hydrodynamic Forces. In offshore engineering, the determination of accurate wave forces exerted on structures is very complex and cumbersome task. Morison equation is generally used for estimating the external viscous hydrodynamic forces on tubular cylinders subjected to wave loadings [6]. Morison equation assumes that the total in-line hydrodynamic force on a tubular cylinder consists of inertia and drag forces added linearly. The total hydrodynamic forces over the full water depth due to drag and inertia can be estimated using Equation 1.

$$F = \int_0^d f ds = \int_0^d [C_m \frac{\rho \pi D^2}{4} \frac{du}{dt} + C_d \frac{\rho D}{2} |u + U_c| (u + U_c)\,] ds \quad (1)$$

where d is the water depth, D is the pipe diameter, u is the horizontal water particle's velocity, U_c is the current velocity, du/dt is the water particle's acceleration, C_m and C_d are the hydrodynamic inertia and drag coefficients respectively and ρ is the water density, and ds indicates the length of integration which is done over the wetted length of the cylinder. The linear airy wave theory, which is applicable when the amplitude is small compared to the wave length and the water depth, gives the horizontal water particles velocity and accelerations as:

$$U_{ix} = \frac{\partial \Phi_i}{\partial x} = \frac{\pi H \cosh ks}{T \sinh kd} \cos\theta \quad (2)$$

and

$$\dot{U}_{ix} = \frac{\partial U_{ix}}{\partial t} = \frac{2\pi^2 H \cosh ks}{T^2 \sinh kd} \sin\theta \quad (3)$$

Determination of Hydrodynamic Coefficients. The values of drag and inertia coefficients can be determined by substituting the measured hydrodynamic forces in Equation 1, and estimating the wave kinematics using airy waves theory,. As the values of *Cm* and *Cd* are functions of the phase angle θ , the best combination of *Cm* and *Cd* and the corresponding phase angles that satisfy Equation 1 have been selected as the optimum drag and inertia coefficients for each loading case.

Experimental Details

Wave Tank Details. The model experiments were carried out in the wave basin of Universiti Teknologi PETRONAS (UTP). The wave tank dimensions are 20 m by 10 m with a maximum water depth of 1 m. Regular waves were generated with wave heights ranging from 0.02 m to 0.2 m, for modal periods varying from 0.6 s to 3.25 s. The wave-maker was controlled through an integrated remote control software package capable of generating regular, irregular and multidirectional waves, while the wave profiles were recorded using four wave probes placed around the model. Two wave probes were placed before the model, whilst the remaining two were placed after the model at a center to center spacing of 1.8 m.

Experimental Set up and Procedures. As depicted in Fig. 1, two vertical rigid cylinders were subjected to regular waves. The first cylinder was smooth, while the second was covered with marine growth. The two models were vertically mounted on the overhead bridge to form a rigid connection at one end, while the other end of each cylinder was immersed in the wave tank to form a cantilevered beam. The model pipes were made of galvanized steel. The outer diameter of the smooth pipe was D_{os}= 42 mm and its wall thickness t_1= 2.5 mm, while the second model with marine growth has an average outer diameter D_{or}= 45 mm. The wave forces were measured using wave force sensors designed and fabricated by the research group in UTP. Details of the wave load sensor used in this study was published earlier by Idichandy [16]. The physical properties of the model and the scaled up full scale prototype details are shown in Table 1 and 2.

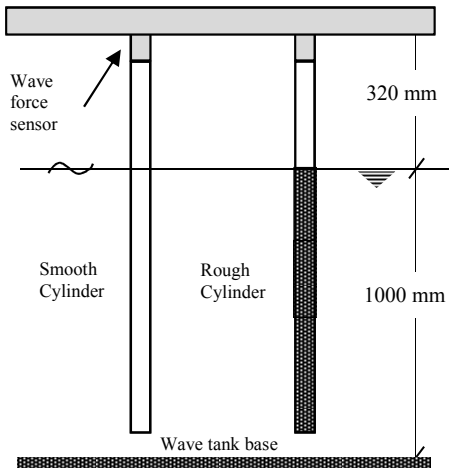


Figure 1. : Fixing details of the model in the wave tank

Table 1: Properties of the model and the prototype

Model			Prototype		
Pipe Diameter (m)	Pipe Length (m)	Wall Thickness (m)	Pipe Diameter (m)	Pipe Length (m)	Wall Thickness (m)
0.042	1.23	0.0032	2.31	68.75	0.176

Table 2: Details of marine growths with respect to water depth [3]

Model			Prototype		
Water Depth (m)	Pipe Outer Diameter (mm)	Marine Growth Thickness (mm)	Water Depth (m)	Pipe Outer Diameter (mm)	Marine Growth Thickness (mm)
MSL - 0.2	47	2.5	MSL - 12	2585	137.5
-0.2 - 0.40	46	2	12 - 21	2530	110
-0.40 - Seabed	45	1.5	-21- Seabed	2475	82.5

Wave Tank Loading Conditions. Table 3 depicts the different wave periods and the associated wave frequencies generated in the wave tank during the model test. These wave periods were generated using modal wave heights of 0.2 m, 0.15 m and 0.1 m as shown in Table 4. The corresponding prototype wave heights are 11 m, 8.25 m and 5.5 m respectively. The hydrodynamic forces and the associated hydrodynamic coefficients for the prototype resulting from these loading conditions were scaled up using a scale factor of 1:55 and the findings are discussed in the following sections. The Reynolds number and Kuleugan-Carpenter number for the prototype can estimated using the scaled up parameters in accordance with the well-known similitude theory.

Table 3: Details of wave characteristics generated in the wave tank

Model		Prototye	
Wave Periods (*s*)	Frequency (*Hz*)	Wave Period (*s*)	Frequeny (*Hz*)
1	1	7.416	0.135
1.5	0.667	11.124	0.090
2	0.500	14.83	0.067
2.5	0.400	18.540	0.054
3	0.333	22.249	0.045

Table 4: Details of wave heights generated in the wave tank

Model	Prototype
Wave Height (m)	Wave Height (m)
0.2	11
0.15	8.25
0.1	5.5

Results and Discussions

Hydrodynamic Forces. Fig. 2 shows the hydrodynamic forces for a smooth rigid cylinder with outer diameter of 2.31 m, compared with the responses of a similar cylinder with the same physical properties, fitted with marine growth to increase its surface roughness which can be defined as a measure of the texture of a given surface. The surface roughness was achieved using sand paper type SDP34. The results show that, when the smooth pipe was subjected to regular wave with H_{max} = 11 m, and wave period T = 11.13 s, the hydrodynamic force was 690.6 kN. However, when marine growth was applied to the same pipe and the test was repeated with the same loading condition, the results show that the average hydrodynamic force on the cylinder was 803.6 kN, an increase of 16 % on the total hydrodynamic force. This clearly shows the effects of marine growths on the hydrodynamic forces of tubular cylinders. In addition, while keeping the wave height constant at 11 m, due to space limitations, the wave period was increased from T = 11.13 s to 14.8 s and the forces were measured. As shown in Fig. 3, the average hydrodynamic force on the smooth cylinder was 473.6 kN, whilst the corresponding response of the rough cylinder was 780.8 kN, an overall increase of 65% on the hydrodynamic forces due to marine growths effects. Moreover, it can also be observed that although in both the above cases, the marine growth thickness was the same, changing the wave period has considerably influenced the hydrodynamic responses of the prototype. The average force is estimated by taking the average of the force height from the graphs.

Similarly, the wave period was increased from 14.83 s to 18.54 s, then to 22.24 s and the hydrodynamic forces were investigated. As shown in Fig. 4, the marine growth fittings have increased the responses of the full scale prototype from 262.2 kN to 505.5 kN, an increase of 90%. However, when the wave period was increased to 22.24 s, the response of the pipe fitted with marine growth has comparatively produced smaller hydrodynamic forces as depicted in Fig 5. The hydrodynamic force decreased by 20% i.e. from 682.1 kN to 542.8 kN. The reason can be associated with the wave frequency generated for this particular loading case; however, in-depth further investigations need to be conducted to prove this experimentally.

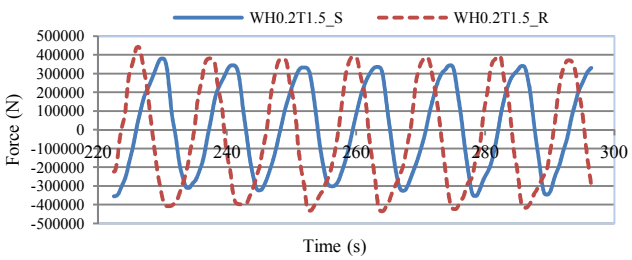


Figure 2: Hydrodynamic forces for 2.31 m diameter, rough (R) and smooth (S) cylinders subjected to regular waves with H_{max} = 11 m and T = 11.12 s

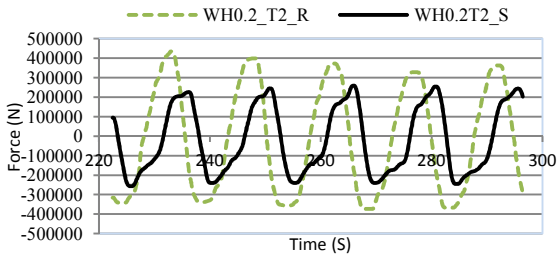


Figure 3: Hydrodynamic forces for 2.31 m diameter, rough (R) and smooth (S) cylinders subjected to regular waves with H_{max} = 11 m and T = 14.83 s

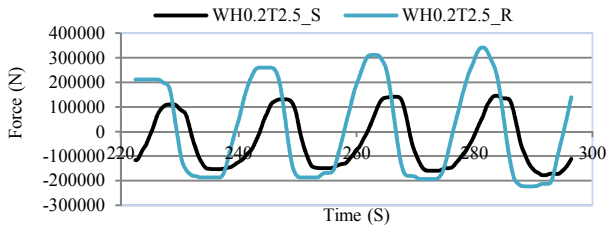


Figure 4: Hydrodynamic forces for 2.31m diameter, rough (R) and smooth (S) cylinders subjected to regular waves with H_{max} = 11 m and T = 18.54 s

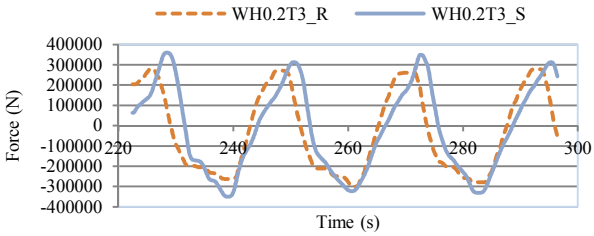


Figure 5: Hydrodynamic forces for 2.31m diameter, rough (R) and smooth (S) cylinders subjected to regular waves with H_{max} = 11 m and T = 22.25 s

Estimation of Hydrodynamic Coefficients. In this section, drag and inertia coefficients for smooth and rough tubular cylinders, subjected to regular waves are discussed. The hydrodynamic forces were determined using the well-known Morison equation and *Cm* and *Cd* were determined by equating the measured forces to the theoretical values estimated using the wave kinematics. The hydrodynamic coefficients are determined for different loading conditions as discussed in the following paragraphs.

Fig. 6 shows the scaled up drag and inertia coefficients for the full scale prototype cylinder with outer diameter D_o = 2.31 m subjected to regular waves with H_{max} =11 m, and wave periods varying from T =11.12 s to 24.1 s. The results show that the minimum drag coefficient, *Cd* = 0.4, while the maximum *Cd* = 1.14 recorded at T = 18.50 s and T = 22.25 s respectively. The corresponding minimum and maximum *Cd* values for the rough cylinder are 1.05 and 1.77 recorded at T = 22.25 s and 14.83 s respectively. In addition, the inertia coefficients for the smooth cylinder varied from *Cm* = 1.03 to 2.8. Similarly, the inertia coefficient *Cm* for the cylinder with marine growth fittings varied from *Cm* =1.3 to 2.03, with the minimum and maximum values observed at T = 22.25 s and T = 14.83 s respectively. Further, as depicted in Fig. 7, the prototype was subjected to regular waves with H_{max}= 8.25 m and the corresponding hydrodynamic coefficients were determined. The values of *Cd* corresponding to rough cylinder were higher than that of smooth pipe. The *Cm* values also showed slight increment due to marine growth fittings. Generally, the analysis of the results show that some of drag and inertia coefficients determined experimentally in this study are in good agreement with the limits of *Cm=1.60* and *Cd* =0.65 specified in PTS [3] and API [4], while the large part of the findings are comparatively smaller than the specified values, which is encouraging for design of more economical offshore platforms for Malaysian waters.

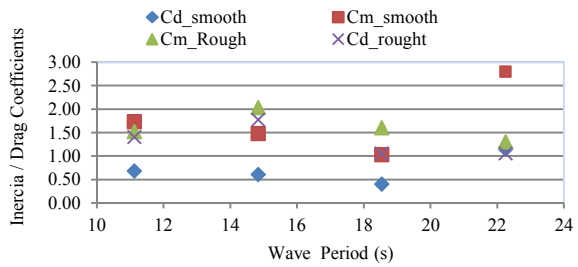


Figure 6: Hydrodynamic coefficients for 2.31 m diameter, rough and smooth cylinders subjected to regular waves with H_{max} = 11 m

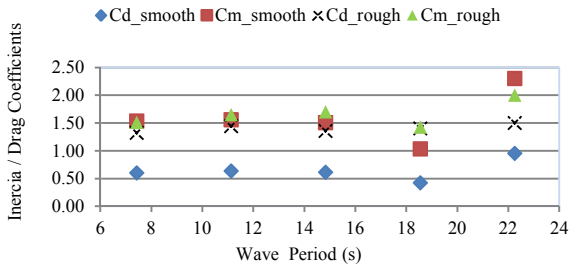


Figure 7: Hydrodynamic coefficients for 2.31 m diameter, rough and smooth cylinders subjected to regular waves with H_{max} = 8.25 m

Concluding Remarks

From the model tests on the effects of marine growths on drag and inertia coefficients, the flowing conclusions can be drawn for the prototype:

1. Applying average marine growth thickness of 110 mm to a tubular cylinder with outer diameter of 2.31 m has increased its hydrodynamic forces by 16 to 90% depending on the wave heights and the wave frequencies of the loading condition.

2. Generally, increasing the surface roughness of the tubular cylinder has increased the drag coefficients significantly. The effects of marine growth fittings on inertia coefficients were generally small as compared to drag coefficients.

3. Drag and inertia coefficients determined experimentally in this study are in good agreement with *Cm* and *Cd* values specified by the design code of practices. The large part of the findings are comparatively smaller than the specified values, which is encouraging for design of more economical offshore platforms for Malaysian offshore locations.

Acknowledgment

The authors would like to gratefully acknowledge their gratitude to Universiti Teknologi PETRONAS for support and encouragement.

References

[1] Norsok, Actions and action effects, in Standards Norway, N-003, Edition. 2007.
[2] Wolfram, J. and A. Theophanatos. The effects of marine fouling on the fluid loading of cylinders: some experimental results. in Offshore technology conference. 1985.
[3] PTS, Petronas Technical Standards, in Design of Fixed Offshore Structures. 2012.
[4] API, R., RP 2A-WSD,(2007). Recommended Practice for Planning, Designing and Constructing Fixed Offshore Platform-Working Stress Design. 2007, API Publishing Services, Washington, DC.
[5] Chakrabarti, S.K., Hydrodynamics of offshore structures: Mathematical theory and its applications in structures. 1987.
[6] Morison, J., J. Johnson, and S. Schaaf, The force exerted by surface waves on piles. Journal of Petroleum Technology, 1950. 2(5): p. 149-154.
[7] Sarpkaya, T. Hydrodynamic forces on various multiple-tube riser configurations. in Offshore Technology Conference. 1979.
[8] Chakrabarti, S.K., Hydrodynamic coefficients for a vertical tube in an array. Applied Ocean Research, 1981. 3(1): p. 2-12.
[9] Sarpkaya, T. In-Line and Transverse Forces, On Cylinders in Oscillatory Flow at High Reynolds Numbers. in Offshore Technology Conference. 1976.
[10] Sarpkaya, T., Forces on a circular cylinder in viscous oscillatory flow at low Keulegan-Carpenter numbers. Journal of Fluid Mechanics, 1986. 165(61-71): p. 11-15.
[11] Justesen, P., Hydrodynamic forces on large cylinders in oscillatory flow. Journal of Waterway, Port, Coastal, and Ocean Engineering, 1989. 115(4): p. 497-514.
[12] Chakrabarti, S.K., Wave Force Coefficients for Rough Vertical Cylinder. Journal of Waterway, Port, Coastal, and Ocean Engineering 1984. Vol. 110(No. 1): p. 101-104.
[13] Bryndum, M., V. Jacobsen, and D. Tsahalis, Hydrodynamic forces on pipelines: Model tests. Journal of Offshore Mechanics and Arctic Engineering, 1992. 114: p. 231.
[14] Sumer, B. and J. Fredsoe, Hydrodynamics around Cylindrical Structures,(1997). World Scientific, Singapore.
[15] Sarpkaya, T. Hydrodynamic Lift and Drag on Rough Circular Cylinders. in Offshore Technology Conference. 1991.
[16] Idichandy, V. (2001). *Strain-gauge-based force transducers in hydrodynamic research.* Paper presented at the Second International Conference on Experimental Mechanics.

Applied Mechanics and Materials Vol. 567 (2014) pp 253-258
© (2014) Trans Tech Publications, Switzerland
doi:10.4028/www.scientific.net/AMM.567.253

Finite Element Assessment of Difficult Pipelines at Bends

Zahiraniza Mustaffa[1, a], Thar M. Badri Albarody[1, b]
and Azrulfirdaus Muhamad Roshdi[1]

[1]Civil Engineering Department, Universiti Teknologi PETRONAS, Bandar Seri Iskandar, 31750
Tronoh, Perak, Malaysia

[a]zahiraniza@petronas.com.my, [b]t.albarody@ymail.com

Keywords: Structural response; pipelines; unpiggable; bends; finite element method (FEM); ANSYS.

Abstract. This paper presents numerical assessment of difficult pipelines at bends using the finite element method (FEM). Difficult pipelines are those that are unable to be inspected using a pig inspection tool. These unpiggable pipes, especially at the bend sections, exhibit difficulties to be piggable for several reasons, thus they are exposed to hazards that can neither be inspected nor controlled. The structural response of the bends is then required to be investigated. This paper aims at simulating the structural response of bends caused by internal corrosions using the ANSYS FEM software. Circular pitting corrosion at different depths and diameters were applied to simulate the stress distribution for three pipe models, namely standard 90° pipe bend, miter bend and unbarred full-bore tees pipe bend near dead end. The results of different corrosion equivalent stress distribution were compared and the most reliable type of bend was reported.

Introduction

A typical pipeline system comprises different components and fittings, namely, the pipe itself, valve, bend, elbow, transitions (contraction, expansion) etc. The use of pipe bend, for instance, is important to cross obstacle and directional change of the flow. For a pipeline system used in the oil and gas industry, the pipe is required to be inspected and cleaned at certain interval period of time in order to ensure smooth operation of the whole system. The so called *pigging* (*pig*) is a common tool used in the maintenance of pipelines which functions to remove deposits which could obstruct or retard flow through a pipeline. The pigs are inserted into and travel throughout the length of a pipeline driven by a product flow. Their occurrence usually does not interrupt production.

Although an oil and gas pipeline is proposed to be designed with the consideration of a pig system with it, it is quite unlikely to be the case at all time, especially for old pipelines developed in the 1980s. This pipeline system is then classified as *unpiggable*.

One of the major threats for an unpiggable pipeline system is corrosion. The World Corrosion Organisation (2010) for example, highlighted an estimated $2.2 trillion annual cost of corrosion worldwide (3 to 4 % of gross domestic product (GDP) of industrialized countries). Leakage from corrosion failures lead to oil spill in the sea water and this is something intolerable and has become one of the greatest public attentions and concerns.

For a bend placed in an unpiggable pipeline system that is prone to corrosion problem, the possibility for it to be cleaned and inspected will become a major concern. This is an example of a case of a *difficult pipeline*. The reliability and integrity of such pipe cannot be easily determined using any empirical or mathematical equations. Numerical analysis is believed to provide better solution to such problem.

This paper aims at analysing the structural response of difficult pipelines towards corrosion effect by means of numerical modeling. The effect of corrosion to three different pipe models, namely *standard 90° pipe bend*, *miter bend* and *unbarred full-bore tees pipe bend near dead end* was analysed using ANSYS finite element method (FEM). The unbarred full-bore pipe bend near dead end in particular, was chosen because of its uniqueness in design, sample of which is shown in the

Methodology section of this paper. The structural response is reported by means of stress distributions resulted from the simulation. Internal corrosions of various sizes were simulated for comparison.

Theories on Corrosions in Difficult Pipelines

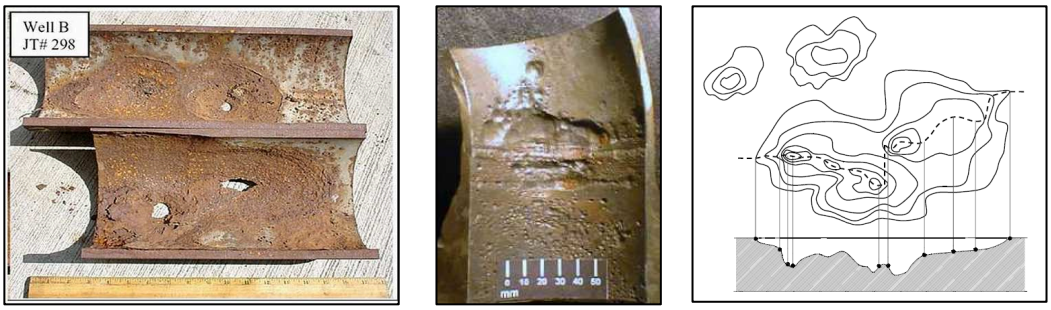
Pigging. *Pigging* in the maintenance of pipelines refers to the practice of using pipeline inspection gauges or *pigs* to perform various operations without stopping the flow of the product in the pipeline. Pipeline pigs are inserted into and travel throughout the length of a pipeline driven by a product flow. They were originally developed to remove deposits which could obstruct or retard flow through a pipeline. Their occurrence usually does not interrupt production. Physically, the pig can be spherical, elongated or composed of several parts.

Corrosion maintenance using the IP has received numerous attentions in the present world because of enhancement in technology. Different types of pigs have been developed and extended, a summary of which has been reported in [1]. The *in line inspection* (ILI) tool or *smart*/*intelligent pigs* (IP) are used to provide an overview (mapping) of the condition of a corroded pipe. The tool is extensively used to carry out inspection and maintenance works on corroded pipelines.

Difficult Pipelines. Difficult pipelines are pipelines that cannot be inspected by a standard pig. They exist due to some limitations in a pipeline system, such as

- No access, in case where the launcher and receiver are not equipped to the system.
- Existing piping component, such as 90° miter bends, dead ends, off-takes, reduction, dead end, one-cut bend, unbarred full bore T and valve.

Corrosions. Corrosion is the chemical or electrochemical reaction between a material, usually a metal, and its environment that produces deterioration of the material and its properties. They deteriorate the structural strength and integrity of a pipeline. In general, corrosions can be observed either at the *internal* or *external* side of the pipeline wall. The shape of corrosion pit is governed by several *length scale* parameters, namely the *depth* (*d*), *longitudinal length* (*l*) and *circumferential width* (*w*). The shapes of corrosion, however, may be difficult to characterize, as shown in Figure 1.



(a) (b) (c)

Figure 1. Examples and skectch of pipeline failures due to internal corrosions

Finite Element Method Analysis at Pipe Bends

Pipe bends are critical components in a piping system. Pipe bends are curved bar with annular cross section whose reaction to external loading is complex. Several numerical studies involving pipe bends with the use of finite element methods have been carried out previously, part of which will be briefly summarized in Table 1.

Table 1. Summary of Research Works on Pipe Bends

Authors	Concern	Outcomes
Prasad and Rao, 2013 [2]	Effect of applying internal pressure to the ovality of the **bends**.	Considering the total deflection and stresses.
Bhattacharya and Long, 2010 [3]	Pipe **bend** for the stress intensification factor and flexibility factor.	Analyse assumptions made within and outside the of ASME B31 piping codes.
Swart et al., 2010 [4]	Pipe **bends**, in general.	Gurson plasticity model simulated pipe behaviour due to the longitudinal deformation, ovalization and warping. To compare with integrated Heterosis elements results.
Kim et al., 2009 [5]	Corrosion defect for hot **bend** pipe. Hot bend pipe is used for route change that is more than 16°.	Prediction of burst pressure using a pre-assumed value of bend coefficient and average thickness to the corroded.
Eckart, 1996 [6]	Pipe **bends**, in general.	To determine bend loading capacity and fatigue strength.

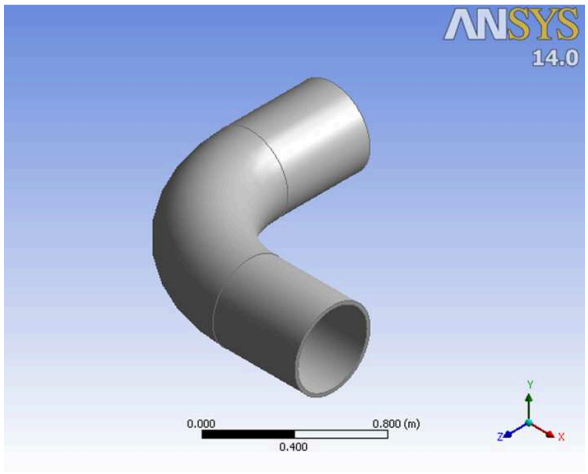
It can be seen from Table 1 that most works on pipe bends were based on understanding the impact of the structure towards different assumptions and concerns. Only the typical types of bends were selected in their studies. Not much work has been given to unique bend such as the *unbarred full-bore pipe bend near dead end*, which is considered to be unpiggable. Thus this is a gap that will be further investigated in this study. The outcomes from this will be later compared with the common *standard 90° pipe bend* and *miter bend.*

Methodology

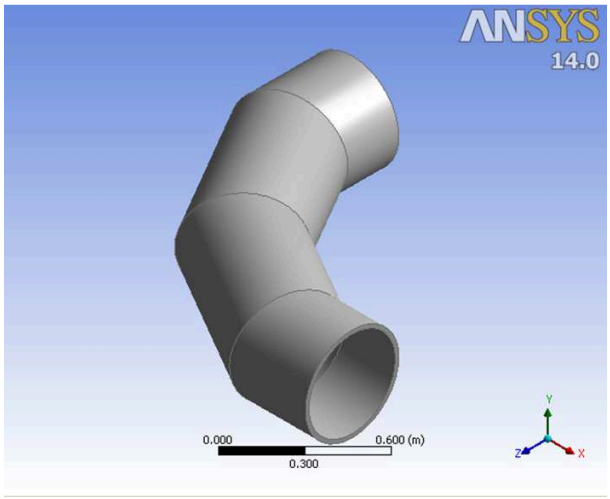
Pipe Bend Model. Three different pipe models, *i.e.* standard 90° pipe bend (Model 1), miter bend (Model 2) and unbarred full-bore tees pipe bend near dead end (Model 3) have a constant nominal diameter of 450 mm and wall thickness of 17.45 mm. The 3D models of the bends were constructed using ANSYS Workbench version 14.0, as shown in Figure 2.

Corroded Pipe Bend. Pitting corrosion defect is defined as circular shape. In ANSYS, its volume was taken out from the internal wall of the pipe [Fig. 3(a)]. In this paper, the modelling of pitting was controlled by two dimensions, namely (i) area and (ii) depth of corrosions. Model 3 in particular, was simulated with two corrosion pits (Model 4), as shown in Fig. 3(b). The value of corrosion pit depths were set to 2.0 mm, 4.0 mm, 6.0 mm, 8.0 mm, 10.0 mm and 12.0 mm. The areas of corrosion pit were varied by means of setting different diameter of pit, ranging from 0 to 80 mm. With this variations, a total of 80 cases were analysed in this study.

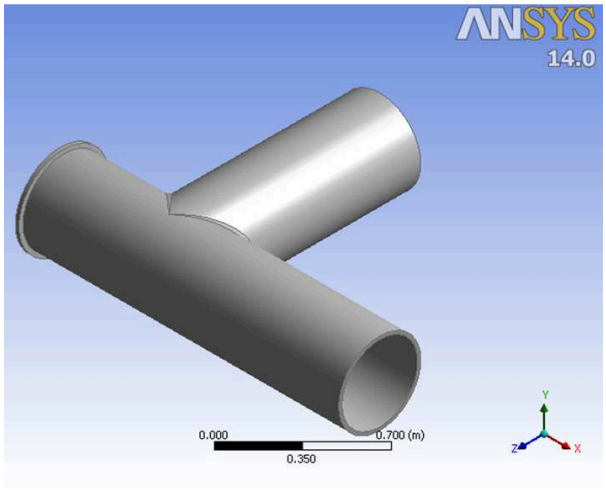
Loading. The loadings applied to the FEM pipe models were tested under the *standard earth gravity load* of 9.8066 m/s² and *internal pressure* of 250 bar.



(a) Standard 90° pipe bend (Model 1)

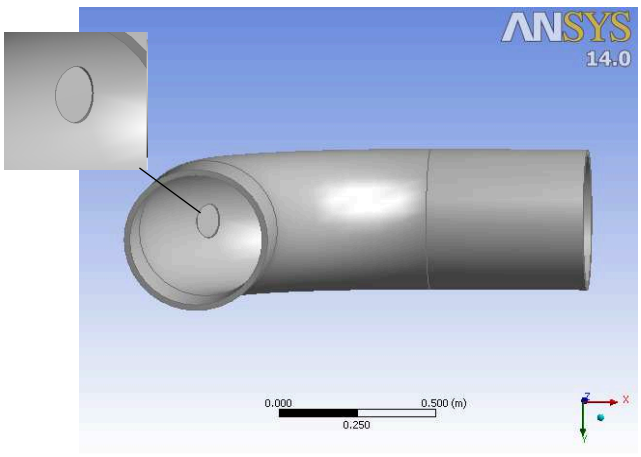


(b) Miter bend (Model 2)

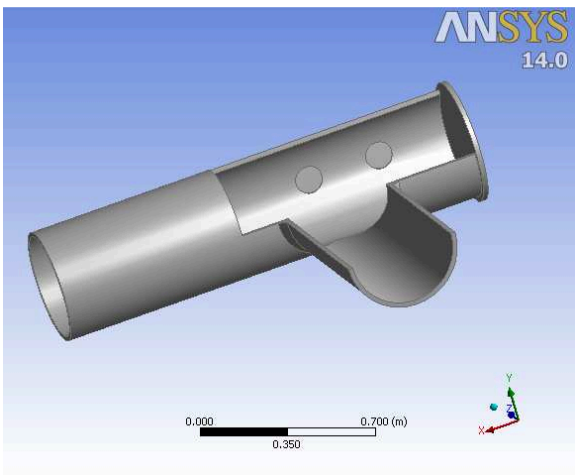


(c) Unbarred full-bored pipe bend near dead end (Model 3)

Figure 2. Three pipe bend models constructed using the ANSYS FEM



(a) Pit corrosion in Models 1 and 2



(b) Two corrosion pits in Model 4

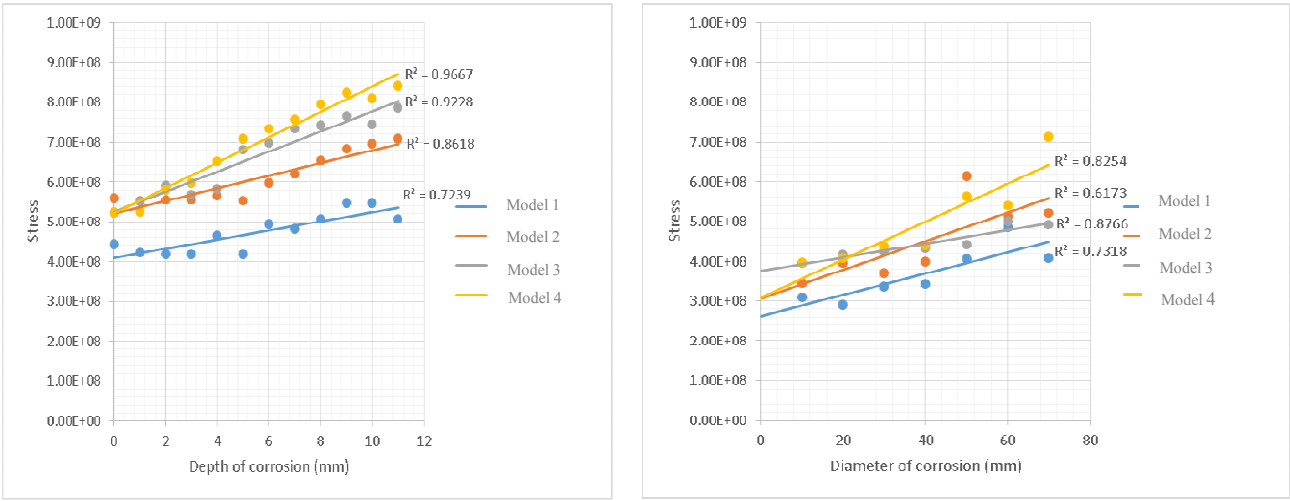
Figure 3. Sample of pitting corrosions at pipe bend models constructed using the ANSYS FEM

Results and Discussion

Stress Definition. Equivalent stress or sometimes referred to as the *Von Mises Stress* (σ_e) is related to principle stress by the equation,

$$\sigma_e = \left\{ \frac{1}{2} \left[(\sigma_1 - \sigma_2)^2 + (\sigma_2 - \sigma_3)^2 + (\sigma_3 - \sigma_1)^2 \right] \right\}^{1/2} \quad (1)$$

with σ_1, σ_2, and σ_3 represent stresses exerted on different surfaces of a 3D body. The structural performance of the corroded pipe bends was described using Equation (1) and the results are presented in Figure 4 (a) and (b).



(a) Corrosion pit with varying depths

(b) Corrosion pit with varying areas (by varying diameter)

Figure 4. Stress distributions obtained for different corrosion scenarios

In general, results from all pipe bends showed an increment in stresses when the corrosion pit was made deeper (through its depth) or larger (through its diameter). Higher stress responds to greater danger to a structure.

A miter bend (Model 2) exhibited higher stresses than a normal standard bend. This is true because such bend comprises several joints made by beveling each of two surfaces, usually at a 45° angle, to form a corner, usually a 90° angle. Thus such design creates more frictions to the structure. Frictions can be considered as obstacles to a structure. Therefore a mitered bend design tends to produce more stresses compared to a frictionless bend (Model 1).

Results for the difficult pipe bend (Model 3) were compared with those from Models 1 and 2. It can be seen that the unique design of Model 3 produced higher stresses as compared to the common bend shapes of the two models. Such bend design coupled with its limitation to be inspected and cleaned (piggable) will then raise a concern to pipeline operators on the potential hazards that it is exposed to.

The impact of corrosion density at difficult pipe bend could be illustrated by comparing results from Models 3 and 4. As expected, the stresses of Model 4 which has more corrosion pits were higher to the one with less corrosion pits (Model 3). This supports the fact that corrosion at a difficult area will influence the integrity of a pipeline.

Summary

Extensive finite element method (FEM) ANSYS simulations were presented in this paper for different pipe bend models by means of varying the size (depth or area) of the corrosion pits. Difficult pipe bend of type unbarred full bore pipe bend near dead end produced highest stress due to its unique design, followed by the mitered bend and the standard 90° bend. As expected, difficult pipe bend with more corrosion pits will provide more hazards to the structure. Therefore, an unpiggable pipe bend of such type should be properly monitored and inspection to avoid corrosion damage to the pipeline system. It has been shown that the FEM is well suited for the prediction of pipe bends failure with respect to maximum stress distribution of a pipe bend.

References

[1] A. M. Roshdi, Structural Assessment of Difficult Pipeline at Bends, Universiti Teknologi PETRONAS (2013).

[2] K. R. Prasad and T. B. Rao, Ovality in Pipe Bends by Finite Element Analysis. International Journal of Engineering Research and Development, (2013) pp. 91-97.

[3] A. Bhattacharya and D. Long, A Finite Element-Based Investigation on Stress Intensification and Flexibility Factors for Pipe Bend, Oxford, (2010).

[4] A. Swart, S. Karamanos, A. Scarpas and J. Blaauwendraad, Finite element analysis of damage in pipeline bends, Heron Journal, Vol. 55, No. 1, (2010), pp. 33-50.

[5] W. Kim, J. Baek, and Y. Kim, Integrity Assessment For Corrosion Defect in Hot Bend Pipe of Natural Gas Pipeline, the 24th World Gas Conference (2009).

[6] W. Eckart, A. Lietzmann, and J. Rudolp, Linear and nonlinear finite-element analyses of pipe bends, International Journal of Pressure Vessels and Piping, (1996) pp. 211-217.

Applied Mechanics and Materials Vol. 567 (2014) pp 259-264
© (2014) Trans Tech Publications, Switzerland
doi:10.4028/www.scientific.net/AMM.567.259

Hydrodynamic Forces on Linear and Multi-Dimensional Arrays of Circular Cylinders

A.A.Sebastian[1], V.J.Kurian[1,a], A.M.Al-Yacouby[1], M.S.Liew[1] and V.G.Idichandy[2]

[1]Department of Civil Engineering, Universiti Teknologi PETRONAS, 31750 Tronoh, Perak, Malaysia

[2]Department of Ocean Engineering, IIT Madras, Chennai, India

[a]kurian_john@petronas.com.my

Keywords: Wave forces, Linear array, Two dimensional array, Transverse spacing, In-line spacing, Force coefficients, Morison equation.

Abstract. In this paper, major focus is given for determining the accurate wave forces recorded on circular cylinders present in different array configurations. Investigation is made to establish any trend in variation of these forces, when the wave time periods, location of the cylinders in the array and the spacing between cylinders are varied. Wave tank model tests were conducted in regular waves. Tandem cylinder configurations involving a maximum of four cylinders were considered for the present study. In addition to this, two linear arrays of four cylinders each, were installed side by side in the waves and the forces on each of the cylinders were determined. The spacing between the cylinders in this two dimensional array was varied and the trend in the variation of forces are presented. Change of transverse spacing between the cylinders was found to have more effect on the forces on cylinders, than the change in in-line spacing. The wave forces acting on singly existing cylinders were found to be less than that acting on individual cylinders present in the different array configurations considered. The variation of force coefficients with respect to the time periods was found to be of random nature. Morison equation is made use in the determination of these coefficients.

Introduction

The increasing oil and gas demand and the decommissioning of the aged platforms have led to an increase in the offshore platform constructions. On these platforms, many of the members are present in the neighborhood of similar members. To achieve safe and economic design of the offshore platforms, the accurate estimation of the forces on all these members is very essential. The riser tubes are an essential part of offshore platforms and are usually present in groups. Recent investigations on the hydrodynamics of riser interference have been presented in [1,2]. Flow interference between these cylindrical tubes has significant effects on the hydrodynamics of the cylinders [3]. A common practice in the force estimation on the offshore platform members, is to ignore the effect of flow interference on the platform members [4]. Thus the members present in groups are idealized to be isolated members and the isolated member force estimation is done for these kinds of members as well.

The present study is aimed at estimating the wave forces and hydrodynamic force coefficients acting on circular cylinders present in arrays, subjected to regular waves. The influence of various parameters like time period of the waves, position of cylinders in the array, spacing between cylinders, on the wave forces are investigated. Many previous works, including [5,6], presented the relation between the hydrodynamic force coefficients and the Keulegan-Carpenter (KC) number. Since KC number is a function of water depth, it could be inferred that, in the design of cylindrical members to be installed in waves, the designer should consider different coefficient values at different depths of the member considered. Since that is a very tedious and time consuming practice, normally the designers are adopting a conservative value for the force coefficients, that would result in the overdesign of the platform and considering the huge number of members in a

platform, this would also badly affect the economy of the high budget platform design and fabrication. In this project, attempt has been made to estimate the hydrodynamic force coefficients, in relation to the wave time periods, rather than the KC number.

Theoretical Formulations

Estimation of Hydrodynamic Forces: The wave forces acting on circular cylindrical members are estimated using the well known Morison equation [7]. The Morison equation which gives the force on a unit length of a vertical cylinder is given in Eq. 1

$$F = C_M \frac{\rho \pi D*D}{4} \dot{U} + C_D \frac{\rho D}{2} U |U|. \quad (1)$$

Assuming that the cylinder extends from the ocean floor to the still water level, the total force on the cylinder is obtained by integrating Eq. 1 between the water depth limits and making necessary substitutions for the terms. The resulting equation is Eq. 2.

$$F = \rho g V \frac{H}{2d} \tanh kd \left[C_M \sin\phi + C_D \frac{H}{4 \pi D} \frac{2kd+\sinh 2kd}{\sinh kd*\sinh kd} \cos\phi |\cos \phi| \right]. \quad (2)$$

where ρ is the water density, g is acceleration due to gravity, V is the volume of cylinder under water, H is wave height, d is water depth, k is wave number, C_M and C_D are inertia and drag coefficients, D is cylinder diameter and ϕ is the phase angle.

Experimentation and Methodology

Model Tests: The experiments were carried out in a 22m long, 10m wide and 1.5m deep wave tank at Universiti Teknologi PETRONAS (UTP), Perak, Malaysia. Unidirectional, regular waves with prototype wave height and maximum prototype time period of 4.125m and 22.25s respectively are studied.

Cylindrical test specimens of model diameter 0.034m were made out of galvanized iron material and were of wet length 0.95m. Each of these cylinders was fitted at its top, with special wave force sensors of dimensions 0.10m x 0.05m x 0.03m, which were capable of measuring wave forces acting on the entire length of the test cylinders, irrespective of the bending moments. Design details of the load cell were published in an earlier paper [8].

These cylinders fitted with the sensors, were installed in the waves as a vertical cantilever fixed at the top. The cylinders were tested in waves with wave height 4.125m and at different time periods as given in Table 1. All the model parameters and forces were scaled up to the corresponding prototype values by making use of Froude's scaling law [9].

Table 1. Time periods and Frequiencies of the waves studied

Model T (S)	Model Frequency (Hz)	Prototype T (S)	Prototype Frequency (Hz)
1.0	1.000	7.42	0.135
1.5	0.667	11.12	0.090
2.0	0.500	14.83	0.067
2.5	0.400	18.54	0.054
3.0	0.333	22.25	0.045

Three different linear array configurations of cylinders, involving two, three and four cylinders respectively, were considered in the present study. In all these configurations, the cylinders were arranged in tandem along the direction of the wave propagation; with the in-line cylinder spacing (IS) and transverse spacing (TS) being integral multiples of cylinder diameter (D). Fig.1 shows

these three configurations along with a single cylinder configuration. Two linear array configuration involving four cylinders each, were installed side by side in the waves to obtain a two dimensional array with eight cylinders as shown in Fig.2.

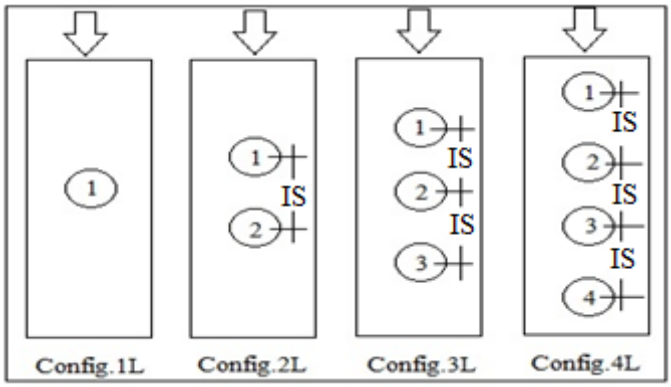


Fig. 1: Linear array configurations

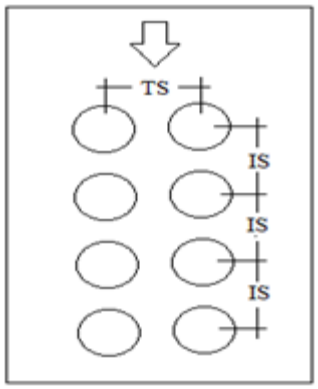


Fig. 2: 2-D array configuration

Methodology: In all the linear array configurations considered (Fig.1), the forces acting on each of the cylinders were plotted against the time period of the waves. Observation is made to find any trend in the variation of wave forces with respect to the position of the cylinder in the array considered. To find the effect of the introduction of a neighboring linear array of four cylinders on the forces acting on an existing similar array, a configuration shown in Fig.2 is made. To study the effect of transverse spacing (TS) between the two linear arrays, on the wave forces acting on each of the cylinders, TS was varied as integral multiples of the cylinder diameter, from 3D through 5D (Config.1TS, 2TS, 3TS), while IS was kept a constant at 3D. In another set of experiments, TS was kept a constant at 3D and IS was varied from 3D through 5D (Config.1IS, 2IS, 3IS). This was to find the effect of the variation of in-line spacing on the wave forces. In addition to all these, forces acting on a single cylinder were also measured for comparison purposes. It is to be noted that Config.1TS and Config.1IS are one and the same with TS and IS both equal to 3D.

The hydrodynamic force coefficients were estimated using numerical computation by adopting the most suitable combination of drag and inertia coefficient and phase angle, such that the deviation of the numerically computed wave forces at the peaks and the zero-crossing points, from the experimental forces, were minimal simultaneously. Eq. 2 was made use for estimating the force coefficients.

In many researches till date [5,6], only a small section of the cylinder will be instrumented and the wave forces acting on this section only will be recorded. The section would normally be near to the water surface where the effect of wave would be felt significantly. The recorded wave forces on the instrumented small portion were used to calculate the hydrodynamic force coefficients. In the present work, wave forces on the entire depth of the cylinders were measured using specially designed wave force sensors and this total wave forces were used for the estimation of force coefficients. Since the KC number is varying with water depth, the presently obtained force coefficients could not be related to a particular KC value. Thus the estimated coefficients were plotted against time periods of the waves.

Results and Discussion

Forces on linear array of cylinders: For all the cylinders in different configurations considered, a decreasing trend, in the wave force, is generally observed when the time periods were increased at the particular wave height considered. Fig.3 shows this decreasing trend recorded for cylinders in different configurations.

The forces on cylinder in Config.1L is found to be less than that acting on cylinders in all the three linear cylinder configurations considered, as can be seen from Fig.3. The dotted line shows the force variation on Config.1L cylinder. This shows that, when the cylinders are present in waves

as a linear array, the forces on them are generally hiked when compared with the forces acting on a singly existing cylinder.

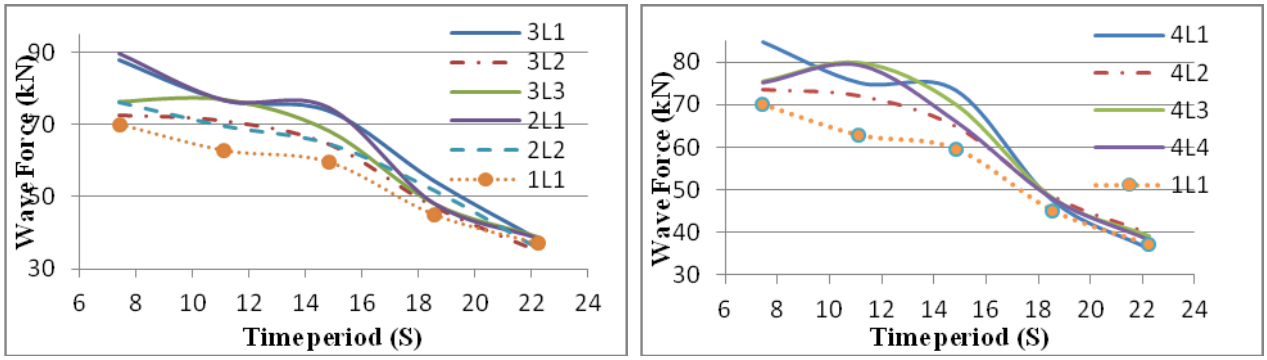


Fig. 3: Variation of wave forces with time periods in linear array configurations

The dashed line in both these figures shows the force variation on the second cylinder in the corresponding configuration indicating that this cylinder is bearing the lowest wave force in the configuration for lower time periods. When time period was increased beyond 14.83s, it was observed that the forces acting on all the cylinders were becoming closer to each other.

Influence of neighbouring cylinders on the wave forces: To study the effect of introduction of leading and trailing cylinders, on the wave forces acting on an existing cylinder, the wave forces acting on first and last cylinders in each of the cylinder configuration is studied. When an individual pipe was tested (Config.1L in Fig. 2), the maximum force observed was 70 kN at T = 7.4s as can be seen from Fig.3 plot 1L1.

Introduction of leading cylinders: In this section, the cylinder under consideration is referred to as the active cylinder (the last cylinder along the wave direction in every configuration). When a leading cylinder was introduced, as in Config. 2L, the maximum force on the active cylinder was found to be hiked by 8.8%. As can be seen in Config. 3L, when two leading cylinders were introduced, the maximum force recorded on the active cylinder was found to have an increase of 9.3% when compared to the individual cylinder tested in Config. 1L. When three cylinders were introduced in front of the active cylinder as in Config. 4L, the maximum force on active cylinder was raised by 7.5%. All these maximum forces were recorded at a T = 7.4s.

Introduction of trailing cylinders: In this section, the cylinder under consideration is referred to as the active cylinder (cylinder 1 in every configuration). When a trailing cylinder was introduced, as in Config. 2L, the maximum force on the active cylinder was found to be hiked by 27.9%. Another trailing cylinder was introduced and the maximum force recorded on the active cylinder was found to have an increase of 25.4% when compared to the individual cylinder tested in Config. 1L. When three cylinders were introduced behind the active cylinder as in Config. 4L, the maximum force on active cylinder was raised by 20.8%. Here also, these maximum forces were recorded at a T = 7.4s. The above results show the significant modifications on the wave forces acting on the cylinders when existing in the vicinity of other cylinders.

Forces on multi-dimensional array of cylinders: To find the effect of the variation of in-line spacing (IS) between the cylinders in configurations involving eight cylinders, the transverse spacing (TS) was kept constant at 3D and the IS was varied as 3D, 4D and 5D and the corresponding three configurations were named as Config.1IS, 2IS and 3IS. The average wave forces acting on the two 1st and two 3rd cylinders, in all these three cylinder configurations are presented in Fig.4.

It was observed that, the forces acting on all the cylinders were found to be close to each other at all the time periods. This shows that the introduction of a new linear array beside an existing array at a distance of 3D between them, doesn't modify the forces on the existing array to a significant extent. It was also noted that the variation of IS had a very minor effect on the wave forces,

because for all the configurations with different IS, the forces on the array were observed very close to that acting on a linear array having four cylinders (Config. 4L), as can be seen in Fig.4.

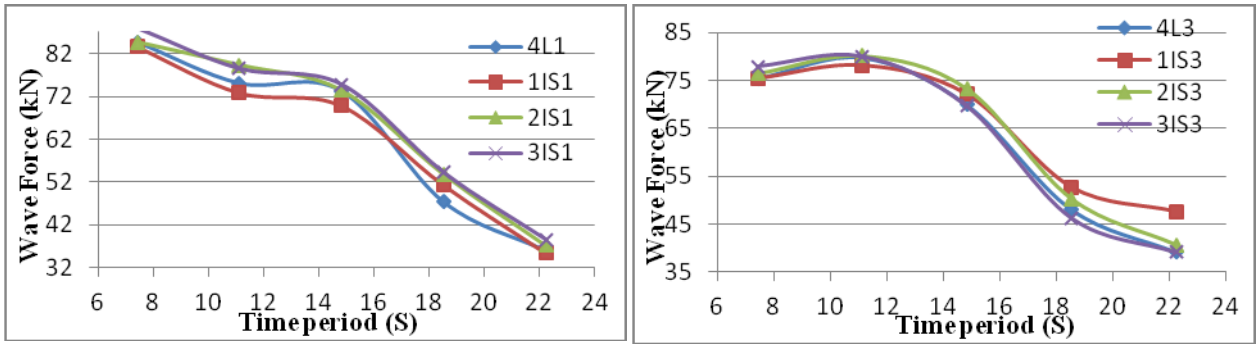


Fig. 4: Variation of wave forces with time periods in 2-D array configurations, showing the effect of variation of in-line spacing

When the TS between the two linear arrays were increased as 3D, 4D and 5D, while keeping IS a constant at 3D, it was observed that for time periods beyond 14.83s, the forces recorded on the cylinders in Config.2TS and Config.3TS are showing a deviation towards the higher side. This is shown in Fig.5.

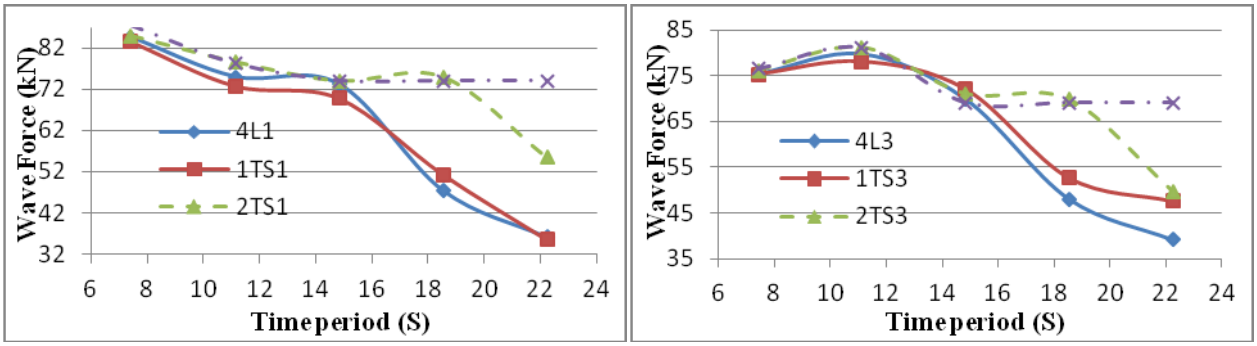


Fig. 5: Variation of wave forces with time periods in 2-D array configurations, showing the effect of variation of transverse spacing

All the above shown force variation recorded on the cylinders when existing in groups calls for some refinements to be made in the force coefficients to be used in the Morison equation for the estimation of wave forces for the purpose of design of jacket platforms. One of the major aims of the ongoing project is to develop a semi-empirical model to predict the hydrodynamic coefficients for group of tubular cylinders. As an initial step towards this the variation of drag and inertia coefficients for the linear arrays studied, are presented here.

Fig.6 shows the scatter of the drag and inertia coefficients acting on cylinders in all the linear array configurations, for the wave height and time periods considered.

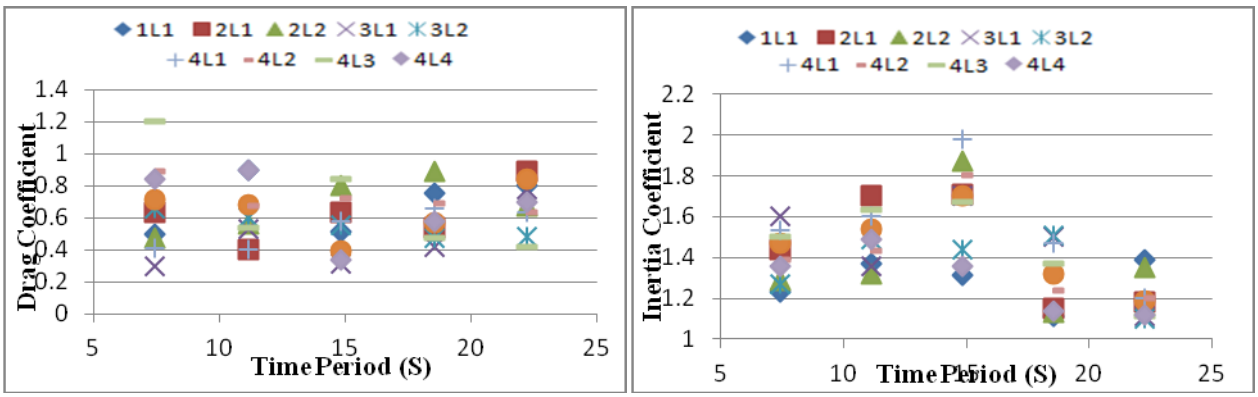


Fig. 6: Variation of drag and inertia coefficients with time periods for cylinders in linear array configurations

The wave forces acting on all these cylinders, as shown in Fig.3, are close to each other and the force variation on each cylinder is similar to one another. Unlike this trend, the drag and inertia coefficients are showing a very random variation with respect to the time periods considered.

Conclusions

The major conclusions emerging out of the present study are listed here:

1. When the cylinders are present in waves as a linear or multi-dimensional array, the forces on them are generally hiked when compared with the forces acting on a singly existing cylinder.
2. In a two dimensional array,
    a. when the in-line spacing between the cylinders are increased keeping the transverse spacing as a constant, the force acting on the cylinders remain close to that acting on the corresponding cylinders in a single linear array.
    b. when the transverse spacing between the cylinders are increased keeping the in-line spacing as a constant, the forces acting on the cylinders remain close to that acting on the corresponding cylinders in a single linear array, except for high time periods.
3. Variation of force coefficients with time periods, for cylinders in all the linear array configurations is random in nature.

References

[1] R.D. Blevins, Model for forces on and stability of a cylinder in a wake, J.Offshore Mech. Arct. Eng., 2004, 127(1), pp: 39-45.

[2] W. Wu, S. Huang and N. Barltrop, Multiple static solutions and stability of a vertical riser in the wake of an upstream vertical riser, 2001, Proceedings of the 12th International Offshore and Polar Engineering Conference, 2002, pp: 171-178.

[3] D. Zeki, H. Tore, Force measurements on production risers interacting with waves and currents, Report of joint industry riser test program, 1984.

[4] J. C. Heideman, and T. Sarpkaya, Hydrodynamic forces on dense arrays of cylinders, Proceedings of the 17th Anuual Offshore Technology Conference, 1985, pp: 425-429.

[5] S. K. Chakrabarti, Wave force on small structures, in Hydrodynamics of offshore structures, Computational Mechanics Publications, Southampton, 1987, pp. 168–170.

[6] S. Kato, S. Ohmatsu, K. Sekita and M. Yamaguchi, Wave loading on a prototype cylinder, Proceedings of the 2nd International Offshore and Polar Engineering Conference, 1992, pp: 406-416.

[7] J. Morison, J. Johnson, and S. Schaaf, The force exerted by surface waves on piles, Journal of Petroleum Technology, 1950, 2(5): pp: 149-154.

[8] V.G. Idichandy, Strain gauge based force transducers in hydrodynamic research, Proceedings of the 2nd International Conference on Experimental Mechanics, 2001, pp: 357-362.

[9] S.K. Chakrabarti, Modeling laws, in Offshore structure modeling, Advanced Series on Ocean Engineering, World Scientific, 1994, pp: 12-37.

Applied Mechanics and Materials Vol. 567 (2014) pp 265-270
© (2014) Trans Tech Publications, Switzerland
doi:10.4028/www.scientific.net/AMM.567.265

Investigation of Vortex Induced Vibration of Offshore Pipelines near Seabed

F. Namazi-Saleh[1, a], V.J. Kurian[1, b], Z. Mustaffa[1, c]

[1]Department of Civil Engineering, Universiti Teknologi PETRONAS, Bandar Seri Iskandar, 31750 Tronoh, Perak, Malaysia

[a] fa_namazi@yahoo.com, [b] kurian_john@petronas.com.my, [c] zahiraniza@petronas.com.my

Keywords: Offshore Pipelines, Vortex Induced Vibration, Navier-Stokes equations, Artificial Dissipation Method.

Abstract: Recently, dynamic interaction between pipelines, seabed and the ocean currents has received wide concern from marine pipeline designers and researchers. The analysis of dynamic responses of subsea pipeline, in vicinity of the seabed in severe ocean environments, is very important. In this regard, this study reviews and sums up recent researches and investigations performed on vortex induced vibration of pipelines near seabed for analysis and design. In addition, the preliminary results of a developed model around a pipe subjected to steady current have been presented. Future trends and challenges in this research are also identified.

Introduction

In oil and gas industry, owing to the highly increasing activity, submarine pipelines become basic arteries of fluid and energy transportation. These pipelines are laid on different soils and are exposed to different hydrodynamic conditions. In this regard, considerable research effort has been devoted in the recent years for the installation and operation of pipelines in deep water [1, 2].

When a submarine pipeline laid on an erodible seabed is subjected to ocean currents, complex interactions between pipeline, soil and current are developed. Pipeline may become free spanning in some locations as a result of the scour around the pipeline and/or unevenness of the seabed. As discussed by [3], the hydrodynamic forces caused by the flow action, acting on marine pipeline spans are represented by two components; one the drag force (in-line with the flow) and the other is the lift force (perpendicular to the flow). In vibrating pipes with two degrees of freedom, experimental results demonstrate that the amplitudes of in-line vibration are typically much less than those in cross-stream vibration. Hence, many researchers focus their attentions on the cross stream vibrations of cylinders [4]. At the downstream part of the marine pipe, due to the incidence of vortex shedding, oscillation and unsteady nature in pipe vibration are inevitable. According to [5], vortex shedding leads to Vortex-Induced-Vibration (VIV), which has been extensively known as one of the main reasons of the fatigue damage in pipelines. Therefore, forecasting behavior of vortex-induced-vibration in the proximity of seafloor is a major factor for pipeline design.

Vortex Induced Vibration

Generally, when a pipeline is placed in a flow path, the flow structures are changed by this obstacle close to the seabed. In the disturbed flow field around a cylinder, four typical regions are distinguished. As depicted in Fig.1, (a) the upstream postponed flow region; (b) the boundary layers that develop at upstream side of the cylinder; (c) the accelerated, curvilinear sidewise flow region; and (d) the downstream flow region named ‘‘the wake’’, are these four regions. This downstream flow region is the most complex part of the flow around a cylinder exposed to current. The interaction between the body and the fluid flow can cause vortices behind the body [6]. According to [7], vortex shedding is caused as a result of instability existing between two shear layers released from the separation points at top and bottom of cylinder toward the downstream flow (Fig. 2).

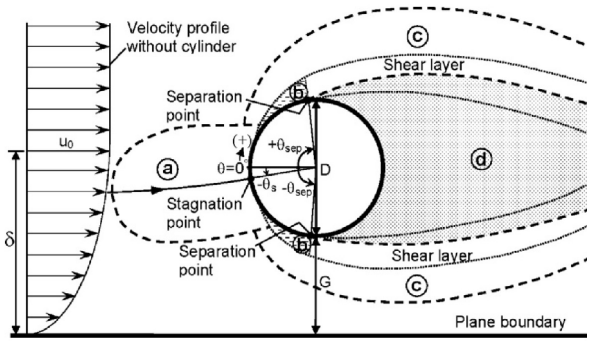


Figure.1 Four typical regions around a circular cylinder in steady flow

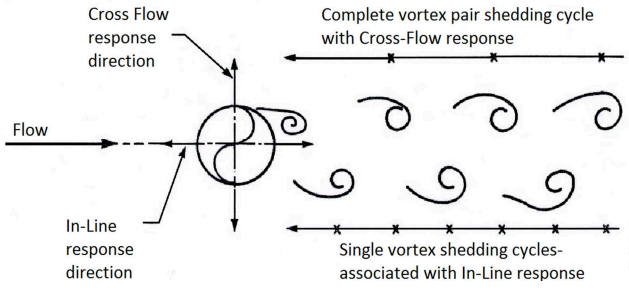


Figure. 2 Staggered alternate vortex shedding cross-flow and in-line response

Experimental Studies on Vortex Induced Vibration

As a result of vortices produced by the flow passing through a bluff body, vibration may occur due to several factors. The hydrodynamic force, material damping, Reynolds number, shedding frequency, added mass effects, and the structural stiffness of the bluff body are just a few of these factors.

By considering the mechanism of vortex shedding phenomenon behind a fixed bluff body, Bearman [8] concluded that the primarily reason for creation of vortex shedding is existence of two shear layers. Existence of bluff body, instead of directly causing the vortex shedding, improve the vortex shedding by giving feedback between the shedding of circulation and the wakes at two separation points of the body surface. Also the span-wise which is coupled between two shear layers, leads to generation of vortex shedding but it is usually weak. This shows that unsteady quantities which lead to vortex shedding (e.g., pressure of body surface) in the span of the body are not constant. Moreover Bearman manifest the frequency of the vortex shedding by the natural frequency of the body in the range of reduced velocity is inevitable. The length of vortex shedding is considerably increased when the vortex shedding frequency is near to the body fluctuations frequency. Drag and lift forces on a surface of cylinder have a beating motions because of following reasons: (1) decrease in the mean drag coefficient; (2) raising up in the root mean square of fluctuating drag coefficient; (3) increase in the primary excitation zones. Similarly the time-averaged of drag coefficient value is consistently higher when the cylinder is held fixed and this result is basically self-dependent on Reynolds number [8]. As investigated by Sumer and Fredsoe [9], for a tubular body exposed to a current flow, vortex shedding will happen if the Reynolds number is larger than about 40. As mentioned before, the vortex shedding results in periodical changes in the quantity of hydrodynamic force on the surface of cylinder. The lift force fluctuates at the frequency of vortex shedding, whereas the drag force fluctuates at twice the frequency of vortex shedding. If the pipeline is flexibly built, these forces may cause the pipe to vibrate. When the reduced velocity reach in the range of $5 < V_r < 7$ ($V_r = U/f_n D$), the frequency of vortex shedding locks into natural frequency of pipe. This means that the Strouhal law is not valid to control the vortex shedding, but the pipe vibration has significant influence on vortex shedding. The separation vortices enforced to cooperate with the body vibration, caused to vortex shedding at a same frequency of body vibration. Then the body fluctuation and the vortex shedding frequency overtake to a single frequency near to the natural frequency of the oscillated body which is identified as lock-in phenomenon [3, 9].

VIV can be categorized into three main types; (i) wake–body, wherein the wake fluctuations and the body are coupled over common phase; (ii) single degree-of-freedom, a single dynamic equation with interaction of inertial, elastic and aerodynamic forcing terms; (iii) force–decomposition, based on measurement of particular factors of the forces on the surface of body [8]. Physics behind pipelines near a boundary are quite different from free cylinder. For a free cylinder placed in steady

flow, the vibrations are caused by regular vortex shedding, and frequency is determined by the Strouhal number. In the case of presence of a boundary near pipe, this vortex shedding takes place even if the distance between the wall and cylinder is larger than about 0.3d (d being the pipe diameter). Closer to the wall, regular vortex shedding does not take place. However, vibrations still take place [9]. The comparison of cross-stream vibration and in-line vibration shows that the amplitudes of in-line vibration are usually much less than cross-stream vibration [10].

Numerical Studies on Vortex Induced Vibration

The calculation of hydrodynamic forces on pipe, vortex induced vibration and local scour often need proper simulation of the flow near and around the pipe. Some recent studies on numerical modeling proved that, using different models to calculate flow equations, affects on result. Most of the previous researches like Li and Cheng [11], Liang and Cheng [12, 13], Smith and Foster [14] used numerical modeling to simulate fluid flow around pipe. They observed the k-ω and k-ε turbulence models that under-predicted the fluctuation vortices as well as the mean drag coefficient. Besides, 2D Smagorinsky's model (SGS) at all times calculates stronger vortex shedding than that observed in experiments. The model is also affected by the computational mesh, the change in grid size affecting the frequency and magnitude of the shedding [12, 14]. It has been understood that the mild slope of the scour hole is mainly due to the vortex shedding. Likewise, simulation of the scour dose not much depend on the mass of computational mesh [13]. Liang and Cheng asserted that in the 2D scour modeling, the standard k-ε turbulence modeling is much preferred than the SGS [13]. And also it is capable to model the velocity profile near an offshore pipeline [14]. Smith mentioned that as the grid size decreased, LES model accurately estimated the mean velocity profiles, but overestimated the size of eddies and it was unable to reproduce the length of the wake [14].

In the work by Zhao, sediment transport and pipeline response were coupled in the numerical model, the vibrating forces to be shed from the bottom side of pipeline which is closer to the seabed. According to the results, three vortex shedding modes were identified: (i) When the reduced velocity is very small, the vortex shedding is in the single-vortex mode only, and shed from the top of the cylinder; (ii) vortex shedding after bounce-back mode, occurs when the VIV amplitude increases with increasing reduced velocity; (iii) vortex shedding before bounce-back mode, occurs in the resonance range of reduced velocity [15].

Simulation of steady flow over a pipeline by using Reynolds-Averaged-Navier-Stokes equation with k-ε turbulence closure model was also done by Kazeminezhad and Yeganeh-Bakhtiary [16]. They proved that by analyzing the power spectrum of the momentary lift force the Strouhal number can be calculated. Main finding shows that the Strouhal number is slightly affected by the gap to diameter ratio while the root mean square of lift coefficient and the mean force coefficients are involved by the gap ratio. Yeganeh-Bakhtiary [17], evolved a numerical model using an Euler–Lagrange coupling two-phase flow model to explore the current-induced live-bed scour. Finally they agreed on a general trend of scour depth formation at the whole scour processing.

Mathematical Model

In this area for modeling the flow field around a subsea pipeline, the incompressible two-dimensional Reynolds averaged Navier Stokes (RANS) equations are used:

$$\frac{\partial \mathrm{u_i}}{\partial \mathrm{x_i}} = 0 \tag{1}$$

$$\frac{\partial \mathrm{u_i}}{\partial \mathrm{t}} + \mathrm{u_j}\frac{\partial \mathrm{u_i}}{\partial \mathrm{x_j}} = -\frac{1}{\rho}\frac{\partial \mathrm{p}}{\partial \mathrm{x_i}} + \vartheta\frac{\partial}{\partial \mathrm{x_j}}\left(\frac{\partial \mathrm{u_i}}{\partial \mathrm{x_j}} + \frac{\partial \mathrm{u_j}}{\partial \mathrm{x_i}}\right) - \frac{\partial \overline{\acute{u}_i \acute{u}_j}}{\partial \mathrm{x_j}} \tag{2}$$

While $x_i\ (i = 1, 2)$ indicates the Cartesian coordinate system, the x_1 is referred to the horizontal *(x)* and x_2 is referred to the vertical *(z)* direction, respectively. In the cited equations u_j and p implies the x_j components of pressure and velocities in x and z direction, t implies time marching, $\overline{\acute{u}_i \acute{u}_j}$ implies Reynolds stress tensor and υ implies kinematics viscosity. Boussinesq assumption is

used to model the Reynolds stress tensor. By introducing ϑ_t as a eddy viscosity, following formulation is reached:

$$-\overline{\acute{u}_\iota \acute{u}_j} = \vartheta_t \left(\frac{\partial u_i}{\partial x_j} + \frac{\partial u_j}{\partial x_i}\right) - \frac{2}{3} k \delta_{ij} \quad (3)$$

In which k is dimensionless turbulent kinetic energy and δ_{ij} is the Kronecker delta. The variables of mentioned equations need to be converted to non-dimensional form by dividing x and y by L, a reference length u and v by $U0$, upstream wind velocity, and $p$by ρU_0^2.

Liang and Cheng [13] Smith and Foster [14] and Kazeminezhad and Yeganeh-Bakhtiary [16] illustrated that the $k-\varepsilon$ turbulence model is more adequate to simulate the streamlines of flow around a circular cylinder. Therefore, the $k-\varepsilon$ model is employed to compute turbulent schemes.

$$\frac{\partial \mathrm{k}}{\partial \mathrm{t}} + \mathrm{u_j} \frac{\partial \mathrm{k}}{\partial \mathrm{x_j}} = \frac{\partial}{\partial \mathrm{x_j}} \left[\left(\vartheta + \frac{\vartheta_\mathrm{t}}{\sigma_\mathrm{k}}\right) \frac{\partial \mathrm{k}}{\partial \mathrm{x_j}}\right] + \mathrm{p_k} - \varepsilon \quad (4)$$

$$\frac{\partial \varepsilon}{\partial \mathrm{t}} + \mathrm{u_j} \frac{\partial \varepsilon}{\partial \mathrm{x_j}} = \frac{\partial}{\partial \mathrm{x_j}} \left[\left(\vartheta + \frac{\vartheta_\mathrm{t}}{\sigma_\varepsilon}\right) \frac{\partial \varepsilon}{\partial \mathrm{x_j}}\right] + [\mathrm{c_{\varepsilon 1}} \mathrm{p_k} - \mathrm{c_{\varepsilon 2}} \varepsilon] \frac{\varepsilon}{\mathrm{k}} \quad (5)$$

$$\mathrm{p_k} = \vartheta_\mathrm{t} \frac{\partial \mathrm{u_i}}{\partial \mathrm{x_j}} \left(\frac{\partial \mathrm{u_i}}{\partial \mathrm{x_j}} + \frac{\partial \mathrm{u_j}}{\partial \mathrm{x_i}}\right) \quad (6)$$

Where ε and p_k are show dissipation rate of turbulences and produce k. The eddy viscosity is distinguished by using k and ε value as well:

$$\vartheta_\mathrm{t} = \mathrm{c_\mu} \frac{\mathrm{k}^2}{\varepsilon} \quad (7)$$

The standard $k-\varepsilon$ model coefficients are consider as bellow value [16]:

$$c_{\varepsilon 1} = 1.44, \quad c_{\varepsilon 2} = 1.92, \quad c_\mu = 0.09, \quad \sigma_k = 1.00, \quad \sigma_\varepsilon = 1.30 \quad (8)$$

The scour profile under the pipe due to crossing flow will forcefully rely on shear stress which acts on the sandy soil of seabed. To find out the scour profile, calculation of the shear stress acting on sandy soil under the pipe is very important. So in this research, shear stress has been derived by the flow field acquired through the Navier-Stokes equations.

Numerical Method and Preliminary Result

In this research, the discretization process is based on "Galerkin Finite Volume Method" to derive the discrete formulas of the governing equations on triangular meshes. The main problem is increasing numerical errors, which usually disturbs the explicit solution of the formulations. This was overcome by adding artificial dissipation terms, suitable for the triangular meshes. These extra terms are used to reduce the unwanted errors and stabilize the procedure of numerical solution while conserving the accuracy of the results. In order to develop the computational efficiency, various numerical techniques such like Runge-Kutta multi-stage time stepping, edge-base algorithm and the residual smoothing have been applied. Free stream velocity imposed at inflow unit as boundary conditions and pressure is imposed at outflow boundaries unit as well. At every computational node, the free stream flow factors such as inflow velocity and outflow pressure, are set as initial conditions.

The test case consider as cylindrical body facing an incompressible viscid flow. The flow field around this object is modeled in a discrete form using 2529 grid points and 7191 unstructured triangular elements (Fig.3). The effect of artificial compressibility coefficient on converge behavior was examined by [18], and the in this test case convergence behavior was satisfied (Fig.4.). As well, Fig.5 indicates the computed results on the cylinder wall at supercritical Reynolds number ($\mathrm{Re} = 4.5 \times 10^5$) plotted in terms of colored stream line with velocity value.

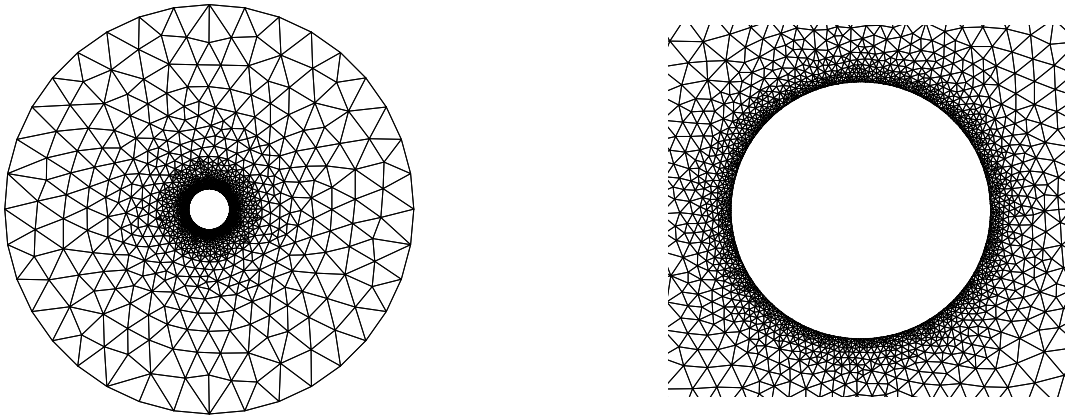


Figure. 3 Unstructured triangular mesh for a circular cylinder general view and closed view

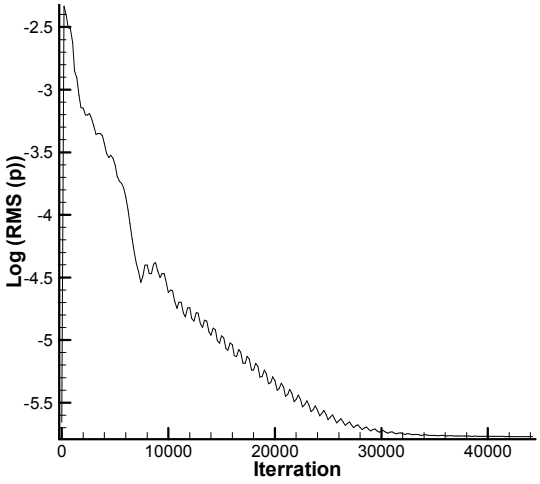


Figure. 4 Converge Error behavior

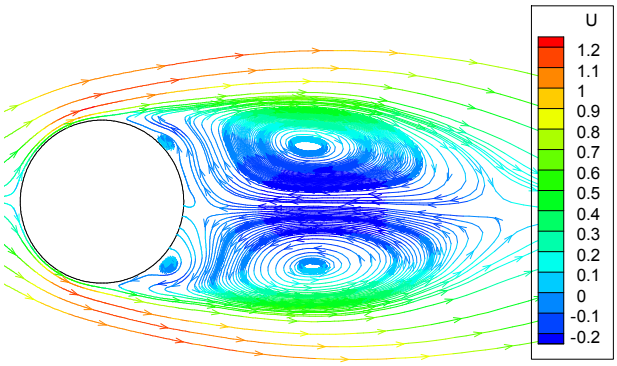


Figure. 5 Stream line colored with velocity at supercritical Reynolds number

Concluding Remarks

Significant research has been conducted to study vortex induced vibrations of a pipelines close to a solid boundary, and extensive findings have been reached during the last three decades. Recent evidences have proven that physical modeling is a useful method to understand the mechanisms of the phenomenon. However, numerical models can enable engineers to understand and appraise the process and developing phases of local scour under marine pipelines. Consequently it is essential to develop suitable numerical modeling to investigate the coupling effects between seabed, ocean currents and the pipelines. Finding from literature shows (1) VIV is naturally self-regulated, nonlinear and multi-degree of freedom fact; (2) Vortex shedding is caused by complex forces; (3) For pipes which are laid on seabed, three vortex shedding modes may take place; (4) Till the scour depth under the pipe becomes large enough, the VIV does not happen.

A preliminary mathematical model has been developed to numerically simulate a fluid flow around circular cylinder to model submarine pipelines. The results show that in computational modeling to solve the equations, the artificial dissipation method is well adapted to limit unwanted errors.

Outlook on Future Challenge

The overview of the references and preliminary results show clearly that Galerkin finite volume method has the potential to play an effective role in the analysis and design of pipelines for the calculation of dynamic interaction between pipe, current and seabed. Although there are proofs for

the existence of rapid development in recent years, some of the main challenges may stimulate thinking for the next research in this area, mainly including:

- Improve the model to calculate hydrodynamic forces that result from the flow action.
- Effective method to determine frequency of pipeline motions due to vorticity around pipe.
- Numerical approach which considers interaction of vortex induced vibration and scour beneath pipe lying on seabed.

Acknowledgements

The authors are grateful for the funding and facilities support by Universiti Teknologi PETRONAS.

References

[1]. Sumer, B.M., R.J. Whitehouse, and A. Tørum, *Scour around coastal structures: a summary of recent research.* Coastal Engineering, 2001. 44(2): p. 153-190.

[2]. Gao, F., X. Gu, D.S. Jeng, and H. Teo, *An experimental study for wave-induced instability of pipelines: the breakout of pipelines.* Applied ocean research, 2002. 24(2): p. 83-90.

[3]. Yang, B., F.-P. Gao, D.-S. Jeng, and Y.-X. Wu, *Experimental study of vortex-induced vibrations of a pipeline near an erodible sandy seabed.* Ocean engineering, 2008. 35(3): p. 301-309.

[4]. Khalak, A. and C. Williamson, *Motions, forces and mode transitions in vortex-induced vibrations at low mass-damping.* Journal of Fluids and Structures, 1999. 13(7): p. 813-851.

[5]. Gao, F.-P., B. Yang, Y.-X. Wu, and S.-M. Yan, *Steady current induced seabed scour around a vibrating pipeline.* Applied Ocean Research, 2006. 28(5): p. 291-298.

[6]. Oner, A.A., M. Salih Kirkgoz, and M. Sami Akoz, *Interaction of a current with a circular cylinder near a rigid bed.* Ocean Engineering, 2008. 35(14): p. 1492-1504.

[7]. Koushan, K., *Vortex induced vibrations of free span pipelines*, in *Ph.D. thesis in Norwegian University of Science and Technology*. 2009, Linköping.

[8]. Gabbai, R. and H. Benaroya, *An overview of modeling and experiments of vortex-induced vibration of circular cylinders.* Journal of Sound and Vibration, 2005. 282(3): p. 575-616.

[9]. Sumer, B. and J.F.M. FREDSØE, *A review on vibrations of marine pipelines.* International Journal of Offshore and Polar Engineering, 1995. 5(2).

[10]. Yang, B., et al, *Experimental study on vortex-induced vibrations of submarine pipeline near seabed boundary in ocean currents.* 2006.

[11]. Li, F. and L. Cheng, *Prediction of lee-wake scouring of pipelines in currents.* Journal of waterway, port, coastal, and ocean engineering, 2001. 127(2): p. 106-112.

[12]. Liang, D. and L. Cheng, *Numerical modeling of flow and scour below a pipeline in currents: Part I. Flow simulation.* Coastal Engineering, 2005. 52(1): p. 25-42.

[13]. Liang, D., L. Cheng, and F. Li, *Numerical modeling of flow and scour below a pipeline in currents: Part II. Scour simulation.* Coastal engineering, 2005. 52(1): p. 43-62.

[14]. Smith, H.D. and D.L. Foster, *Modeling of flow around a cylinder over a scoured bed.* Journal of waterway, port, coastal, and ocean engineering, 2005. 131(1): p. 14-24.

[15]. Zhao, M. and L. Cheng, *Numerical investigation of local scour below a vibrating pipeline under steady currents.* Coastal Engineering, 2010. 57(4): p. 397-406.

[16]. Kazeminezhad, M., A. Yeganeh-Bakhtiary, and A. Etemad-Shahidi, *Numerical investigation of boundary layer effects on vortex shedding frequency and forces acting upon marine pipeline.* Applied Ocean Research, 2010. 32(4): p. 460-470.

[17]. Yeganeh-Bakhtiary, A., M. Zanganeh, E. Kazemi, L. Cheng, and A.A. Wahab, *Euler–Lagrange Two-Phase Model for Simulating Live-Bed Scour Beneath Marine Pipelines.* Journal of Offshore Mechanics and Arctic Engineering, 2013. 135: p. 031705-1.

[18]. Sabbagh-Yazd, R., N. Mastorakis, F. Meysami, and F. Namazi-Saleh, *2D Galerkin Finite Volume Solution of Steady Inviscid/Viscous/Turbulent Artificial Compressible Flow on Triangular Meshes.* International Journal of Computers, 2008. 2(1): p. 39-46.

Applied Mechanics and Materials Vol. 567 (2014) pp 271-276
© (2014) Trans Tech Publications, Switzerland
doi:10.4028/www.scientific.net/AMM.567.271

Multivariate Regression Analysis For Screening Process of Reliability Assessment

V.J. Kurian [1,a], M.C. Voon [2,b], M.M.A. Wahab[3,c], N.A. Iskandar[4,d], M.S. Liew[5,e]

[1,2,3,4,5]Civil Engineering Department, Universiti Teknologi PETRONAS, Tronoh, Malaysia

[a]kurian_john@petronas.com.my, voonminchin@gmail.com[b],

[c]mubarakwahab@petronas.com.my, [d]nabilaiskandar@gmail.com, [e]shahir_liew@petronas.com.my

Keywords: Regression, Reserve Strength Ratio, Reliability.

Abstract

Reliability is one major concern in the Oil and Gas industry to date. Reliability issues due to aging and increasing environmental loading are common for jacket platforms in Malaysia. Authors have studied system reliability assessment on existing jacket platforms in Malaysian waters and concluded that the current reliability assessment in the industry practice is tedious. The scope of the study includes regression analysis using three different methods to generate regression equation which could serve as a simplified reliability prediction model. Regression equations generated in this study seek to improve the current reliability assessment of jacket platforms in Malaysia by providing means for screening process before proceeding to tedious reliability analysis.

Introduction

Life extension of offshore platforms has become one major concern in the Malaysian Oil and Gas industry because majority of the jacket platforms are operating beyond their design life. The marginal oil field or oil field that seems impossible to harvest ten years back, is now harvested with advancement in technology via the enhanced oil recovery method. Thus, there are increasing demands to extend the life of these platforms. Modifications or upgrading result in platforms being subjected to higher loading for which they may not been originally designed for [1]. An existing platform should undergo assessment process if there is addition of personnel, increased loading on structure, and damage found during inspection [2]. Pushover Analysis is incorporated in Risk Based Inspection (RBI) to provide Reserve Strength Ratio (RSR) value to proceed to Simplified System Reliability Analysis (SSRA) to obtain the probability of failure and reliability index of an assessed platform [3, 4]. RBI will categories platform based on probability of failure and recommends corrective plan accordingly. Instead of Pushover Analysis which requires a lot of technical competency and time, authors formulated a relationship between RSR and other variables to produce a simplified prediction model using regression analysis.

Regression Analysis

The regression analysis analyzes several variables to formulate relationship between a dependant variable and one or more independent variable(s) to arrive at a function that fits the data and returns an array of values that describes the function. The purpose of regression analysis to establish a formulation between the variables to produce an equation in which the parameters such as wave heights, initial air gap, water depth, and number of years after installation can be input to obtain the RSR value. The method using this simplified prediction model will be very useful to eliminate the lengthy process and costly work of conducting conventional reliability analysis [5]. Linear Regression has a curve fitting protocol carried out in a way that the data will be represented by a linear function. By utilizing the Regression Analysis provided in the Microsoft Excel's Data Analysis Tool, Linear Regression equation obtained from the regression analysis returns the best fit for linear function to represent the variables. The linear regression equation generated is in the form

shown in Equation 1, where y is the 'dependant' variable, RSR value and x is the ' independent' variable, input parameters [6]. Non Linear Regression could be implemented to fit a non linear function to the data for the data which are not described by the linear function. There are two Non Linear Regression approach that will be discussed in this paper, namely LOGEST and log. LOGEST is one of the regression analysis functions in Microsoft Excel to generate an exponential curve that fits the data [5]. The log approach is similar to LOGEST approach which generates an exponential curve with slight difference [7]. The LOGEST and log regression equation generated are as in the form shown in Equation 2 and 3, respectively;

$$y=\beta_0+\beta_1x_1+\beta_2x_2+\beta_3x_3+\beta_4x_4 \quad (1)$$

$$y= \beta_0*m_1^{x1}*m_2^{x2}*m_3^{x3}*m_4^{x4} \quad (2)$$

$$y= \beta_0*x_1^{m1}*x_2^{m2}*x_3^{m3}\ x_4^{m4} \quad (3)$$

Methodology

Prior to the regression analysis, the data ought to be sorted according to categories. 102 sets of RSR values accompanied by various other variable data such as numbers of years after installation, water depth, initial air gap, and wave height were obtained from the operating platforms. Since the data set is huge and varies from platform to platform, one regression equation generated is not possible to represent the whole set of data. Hence, the data was divided to 5 categories according to wave height. 92 data set was used for regression analysis while the 10 data set was used for sample testing. Hence, there were 2 testing samples for each category [8]. The methodology flow chart of the regression analysis is shown in figure 1.

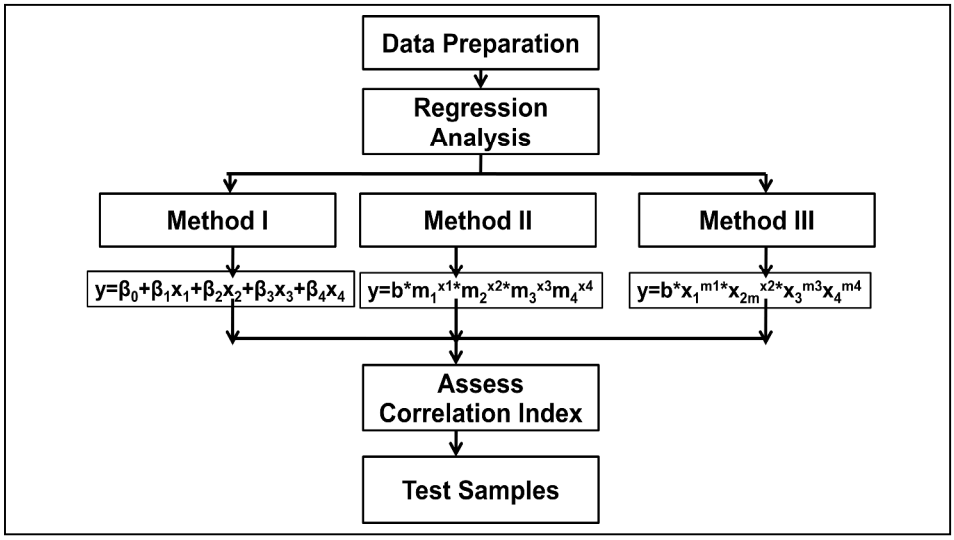


Fig. 1. The flowchart of the regression analysis methodology

Regression Analysis aims to generate formulae that will predict the RSR value based on the variable parameters. Linear and Non Linear Regression Analysis were used to generate the formulae representative of all jacket platforms in Malaysia. Correlation analysis was performed on 102 data sets and Table 1 shows the correlation coefficients for each input variable. Initial air gap and wave height are positively correlated with RSR, and have correlation coefficients of 0.139 and 0.295, respectively. The number of years installed and water depth are negatively correlated with RSR with correlation coefficients of -0.332 and -0.153, respectively. Generally, each variable contributes towards the predicting power of the regression equation generated and elimination of any variable results in lower predicting power. No matter how insignificant the correlation coefficient of each

variable, the inclusion of more variable to regression produces regression equation of higher predicting power, as long as the variables are correlated.

Table 1. Correlation Coefficients for Each Variables

CORRELATION ANALYSIS FOR 102 DATA SETS					
VARIABLES	No. of Years Installed	Water Depth	Initial Air Gap	Wave Height	RSR
No. of Years Installed	1.000				
Water Depth	-0.279	1.000			
Initial Air Gap	-0.412	0.182	1.000		
Wave Height	-0.414	0.409	0.539	1.000	
RSR	-0.332	-0.153	0.139	0.295	1.000

The correlation index or also known as r^2 value expresses the proportion of variance in the dependant variable explained by the independent variables. Increasing r^2 value towards 1 shows that the functions fit the data more accurate and decreasing r^2 value towards 0 means that the function is less accurate in representing the data [6]. Microsoft Excel 2007 was used to assess three different methods of performing regression in Excel. Method I was the Linear Regression data analysis package in Excel which produces a best fit linear function to represent the variables. Method II was the LOGEST function, also available in Excel, which could calculate an exponential curve to fit the data. The equation formulated was in a form of exponential function. Method III was the log approach where the regression analysis was performed using the logarithms of parameters as shown in Equation 5 and then transformed to format of Equation 6 [7].

$$logR = logA + x\log B + ylogC + zlogD \quad (4)$$

$$R = AB^xC^yD^z \quad (5)$$

The data was broken down into groups according to the wave heights as analysis conducted on full set of data may returned regression equation which has low prediction power. At the end of the analysis, formulae to predict the RSR value by input varying the independent variable such as number of years after installation, wave height, water depth and initial air gap is generated. The symbols representing of each variable in the formulae are shown in Table 2.

Table 2. Parameters for Method I, II, and III

Symbol		Remarks
1	y	RSR
2	β_0, β_1, β_2, β_3, β_4 ,b, m_1, m_2, m_3, m_4	Constants/coefficients
3	X_1	Numbers of year after installation
4	X_2	Water Depth
5	X_3	Initial Air Gap
6	X_3	Wave Height

Result

The formulae generated by the regression analysis are shown in Table 3. Variables can be input to obtain the RSR value straightaway from the formulae. The function generated using method I is linear fit function and the function generated using method II and III are exponential fit functions. Correlation index among all the methods are compared to each other as in Table 4 to observe the method which best describes the relationship between the independent variables with the dependant variable.

Table 3. Formulas Derived (Method I, II, and III)

Method I	**Method II**	**Method III**
Wave Height < 8m	**Wave Height < 8m**	**Wave Height < 8m**
$y = 4.2626 - 0.1844X_1 - 0.02035X_2 + 0.02118X_3 + 0.8625X_4$	$y = 3.7657 * 0.9321^{x1} * 0.9935^{x2} * 1.01619^{x3} * 1.4048^{x4}$	$y = 516.02 * X_1^{-2.0822} * X_2^{-0.2168} * X_3^{0.0387} * X_4^{1.467}$
8m ≤ Wave Height < 10m	**8m ≤ Wave Height < 10m**	**8m ≤ Wave Height < 10m**
$y = 0.9857 - 0.1290X_1 - 0.01892X_2 - 0.1017X_3 + 0.7862X_4$	$y = 0.9909 * 0.9631^{x1} * 0.9928^{x2} * 0.9560^{x3} * 1.3233^{x4}$	$y = 56.17 * X_1^{-1.1449} * X_2^{-0.0861} * X_3^{-1.1164} * X_4^{0.4894}$
10m ≤ Wave Height < 12m	**10m ≤ Wave Height < 12m**	**10m ≤ Wave Height < 12m**
$y = -3.207 - 0.08005X_1 - 0.02193X_2 + 0.05564X_3 + 0.8343X_4$	$y = 0.4082 * 0.9726^{x1} * 0.9917^{x2} * 1.02093^{x3} * 1.3089^{x4}$	$y = 0.03956 * X_1^{-0.5061} * X_2^{-0.3257} * X_3^{0.1395} * X_4^{2.8603}$
12m ≤ Wave Height < 14m	**12m ≤ Wave Height < 14m**	**12m ≤ Wave Height < 14m**
$y = 2.7850 - 0.01571X_1 - 0.03179X_2 - 0.07725X_3 + 0.2044X_4$	$y = 3.3389 * 0.9954^{x1} * 0.9878^{x2} * 0.9722^{x3} * 1.0572^{x4}$	$y = 0.8983 * X_1^{-0.1171} * X_2^{-0.3585} * X_3^{-0.3348} * X_4^{1.3684}$
14m ≤ Wave Height	**14m ≤ Wave Height**	**14m ≤ Wave Height**
$y = -3.6447 + 0.01861X_1 - 0.01880X_2 - 0.01872X_3 + 0.4294X_4$	$y = 0.5458 * 1.0012^{x1} * 0.9956^{x2} * 0.9770^{x3} * 1.1261^{x4}$	$y = 0.02103 * X_1^{0.01932} * X_2^{-0.2107} * X_3^{-0.3549} * X_4^{2.2621}$

Table 4. Comparison Table for Correlation Index, r^2 for Two Methods

Regression Analysis			
Group	Method I	Method II	Method III
H < 8m	0.5166	0.4704	0.4923
8m ≤ H < 10m	0.3822	0.4291	0.3695
10m ≤ H < 12m	0.7777	0.7323	0.6965
12m ≤ H < 14m	0.4842	0.4926	0.3890
14m ≤ H	0.6198	0.5650	0.5751

Ten set of data samples were used to conduct a validation test using the regression equation generated by the three approaches. There were 2 test samples in each category. Table 5 shows the comparison of percentage of sample testing for all three methods studied. The results show that method III has the least percentage error compared to method I and II. Figure 2 shows the comparison of validated RSR with the estimated RSR of all three methods from the training data sets. Figure 3 shows the comparison of validated RSR with the estimated RSR of all three methods from the testing data sets. It can be observed that the regression equation predicts RSR towards the correct convergence of the RSR value.

Table 5. Comparison of Percentage Error for All Three Methods

Validated RSR	**METHOD I**		**METHOD II**		**METHOD III**	
	RSR	**% error**	**RSR**	**% error**	**RSR**	**% error**
1.61	0.86	46.74	1.19	25.81	1.35	16.01
3.09	3.85	24.70	3.92	26.84	3.35	8.53
2.06	3.45	17.65	2.87	2.11	2.72	7.33
2.93	2.49	20.68	1.99	3.46	2.10	2.12
1.96	2.27	15.68	2.14	9.23	2.20	12.25

2.40	2.43	1.22	2.24	6.80	2.26	5.65
3.15	3.37	6.85	3.34	6.05	3.08	2.23
2.73	3.75	37.27	3.76	37.68	3.41	24.82
1.99	1.63	17.85	2.01	1.14	1.97	1.11
3.37	3.32	1.45	3.13	7.15	3.16	6.08
Average % error		**19.01**		**12.63**		**8.61**

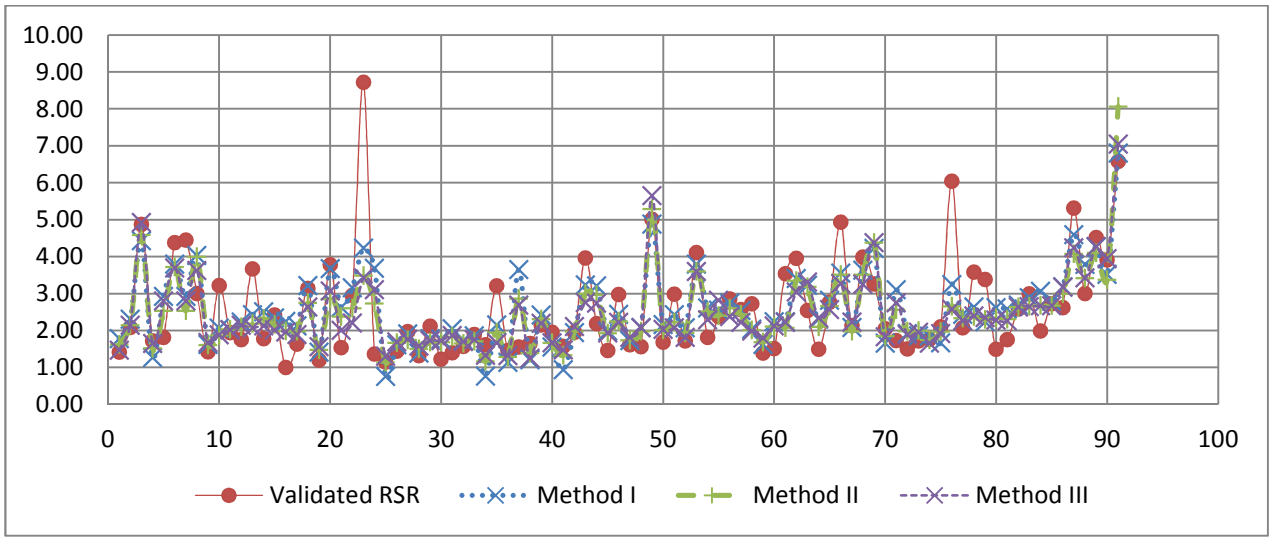


Fig. 2. The comparison graph between Validated RSR and Estimated RSR of training data set

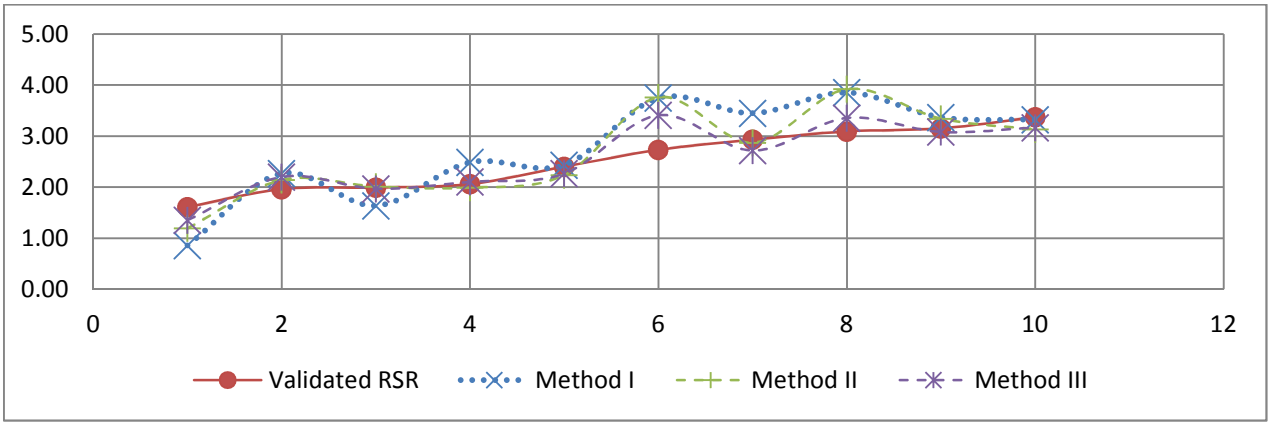


Fig. 3. The comparison graph between Validated RSR and Estimated RSR of testing data

Discussion

Table 4 shows the correlation indexes for the 3 methods studied. It was observed that the correlation index is not near to 1.0. This may due to a lot of uncertainties contributing to a platform's RSR, instead of just the four variables which are number of years after installation, water depth, initial air gap, and wave height. However, the regression equations obtained show promising predicting power as seen in Figure 3 and Table 5 where the predicted RSR do not differ much from the actual validated RSR value. This means that by utilizing the four variables, reliability engineers can use the regression equations provided to estimate the RSR value. This however does not confirm reliability of a jacket. If the RSR estimated shows value within the range of 1.0-2.0, reliability engineers can go ahead and conduct pushover analysis to determine accurate RSR values. It is noted that the data used for regression consists of 102 validated RSR results and available parameters from platforms in Malaysian waters. The regression equation generated displays significant prediction power, especially method III which gives percentage error at 8.61%. It is recommended that for further

study, more numbers of platforms and other parameters such as current velocity, wind speed, deck loading, and etc can be considered. More numbers of platform considered will improve on the data size hence it can represent the Malaysian jacket platform more in general. Besides, inclusion of more parameters may increase the prediction power of the regression equation produced as well.

Conclusion

The following conclusion can be made using the results provided from above:

1. Regression equation generated shows significant prediction power for preliminary reliability screening process.
2. Regression equation produced using method III which is a Non Linear regression produces the best result among the three methods used.

References

[1] N.W. Nichols, Petronas Carigali Sdn Bhd; T.K.Goh, Petronas Research & Scientific Services Sdn Bhd; H. Bahar, Petronas Carigali Sdn Bhd, "Managing Structural Integrity for Aging Platform", Proceedings, SPE Asia Pacific Oil and Gas Conference and Exhibition, Adelaide, Australia, No SPE101000, September 2006

[2] S. A. Kheiri and M.R. Bahaari, "Evaluation of Ultimate Strength of Jacket Type Structures under Marine Loading", Proceedings, 7th International Conference on Coasts, Ports and Marine Structures

[3] Narayanan S.P. and M. Kabir B.M.A, "Structural Integrity Management for Fixed Offshore Platforms in Malaysia", World Academy of Science , Engineering and technology 58 2009

[4] Group Technical Soulution (GTS) (2011), "Global Ultimate Strength Analysis for SBO Platform: SMJT-E", Report ID: RD-PLE-CSP-RBI-S309

[5] Pattaradanai Pueksap-anan, "Sensitivity Analysis for RSR Offshore Steel Type Platforms", M. Sc. Thesis, Asian Institute of Technology, School of Engineering and Technology, Thailand, August 2010.

[6] A.M. Brown, "A Step-by-step Guide to Non-linear Regression Analysis of Experimental Data Using a Microsoft Excel Spreadsheet",Computer Methods and Programs in Biomedicine 65 (2001) 191-200

[7] C.Y. Ng, V.J. Kurian, and M.A. Yassir, " Regression Analysis for the Dynamic Responses of Semi-Submersible Platform ", 7th International Conference on Steel & Aluminium Structures, Kuching, Sarawak, Malaysia July 13-15, 2011.

[8] J.C. Lui, M.L. Sue, and C.H. Kou, " Estimating the Strength of Concrete Using Surface Rebound Value and Design Parameters of Concrete Material ", Tamkang Journal of Science and Engineering, Vol. 12, No.1, pp.1-7 (2009).

Applied Mechanics and Materials Vol. 567 (2014) pp 277-282
© (2014) Trans Tech Publications, Switzerland
doi:10.4028/www.scientific.net/AMM.567.277

Performance of Mangrove Forests in Coastal Protection

Ahmad Mustafa Hashim[1, a] and Noraini Khairuddin[2, b]

[1,2]Universiti Teknologi PETRONAS, Bandar Seri Iskandar, 31750 Tronoh, Ipoh, Perak, MALAYSIA

[a]mustafa_hashim@petronas.com.my, [b]hannie1990@gmail.com

Keywords: Mangrove, Laboratory Experiment, Wave Dissipation

Abstract. The importance of mangrove forest as a natural protection system has been a focused interest especially after the 2004 tsunami. It was reported that human deaths and property losses were reduced in areas of dense mangrove forests. Devastating incidents in recent years due to extreme environmental and catastrophic conditions that lead to various degrees of damages in the coastal areas have significantly increased awareness on the role of mangrove forests as eco-engineering approach to coastal stability and defense. With the recent urge for mangroves protection and replanting, a sound basis for a more optimum strategy in maintaining mangroves as coastal protection buffer is inevitably required. Hence, this study is aimed to quantify the reduction of wave height by 10 years old mangroves with various densities and tree arrangements. The laboratory experiments were conducted in a narrow wave flume using artificial mangrove models. The results showed that wave height reduction in areas of 100 m width of 10 years old mangroves was 2.5 times more effective as compared to areas without mangroves. Earlier investigation revealed that for areas with 20 years old mangroves was able to dissipate waves four times greater compared to areas without mangroves. For areas with 200 m width of 10 years old mangroves, a density of 0.11 trees/m² is sufficient to reduce wave height over 77 %. With a difference of less than 3%, the investigation also revealed no significant difference of wave reduction between tandem and staggered arrangements when the mangroves are of 10 years old.

Introduction

Mangroves ecosystems provide an important service in providing protection to the coastal areas from various natural hazards. Mangroves have been well acknowledged as natural barriers and important protection buffer for the coastal area [1]. Although more quantifiable evidence is required, mangrove forests are still considered to be one of the most valued ecosystem that offers significant ability to lessen the impact caused by tsunamis and tropical storms [2]. December 26, 2004 marked a historical event when the Acheh tsunami in the Indian Ocean caused economic and ecological disasters in a total of 13 Asian and African countries [3]. The disastrous waves had killed more than 0.2 million people, caused about two million people homeless with a loss of US$ 6 billion in 13 countries. It seems however, that the coastal communities that lived beyond the mangrove forests essentially escaped from the impactful force of the tsunami [3]. Areas with coastal tree vegetation were noticeably less devastated than areas without any vegetation [4]. Coastal vegetation can remarkably reduce the severity of tsunami waves and dissipating the calamitous amount of energy associated with them [5][3][6][7].

Factors affecting rate of wave dissipation by mangrove forests. Various modeling and mathematical studies revealed that mangrove forests can attenuate waves energy which is a function of the forest density, diameter of stems and roots, forest floor slope, bathymetry, the spectral characteristics (height, period, etc.) of the incident waves, and the tidal stage at which the wave enters the forest [8][9][10][11].

Density. The density of mangroves vegetation and the diameter of aerial roots and stems are expected to affect the ability of mangroves to reduce storm surged water levels [12]. High density forest composed of species with aerial roots and dense canopies are consequently expected to reduce waves and wave set-up more effectively. However, few data are yet available to support this assumption. Wave reduction is expected to be reliant on the density of vegetation and the surge water level. When the waves encounter the densest vegetation, the largest rates of wave reduction occur [13][11]. These showed that mangroves may have the ability to perform significantly in reducing wave set-up and run-up during storm surges, thereby reducing impacts on local infrastructures. In addition, it was explained that high density mangrove forest with above ground roots provide a much greater drag force to incoming waves than does by bare sandy or mudflat [14].

Mangrove Width. Earlier study stated that depending on the mangrove species, stem density and area characteristics, the optimum mangrove forests width ranges from 100 m to 1500 m [15]. According to [13], across a 500 m width of mangrove forest, attenuation rates suggest that wave height would be reduced by 50 % to 99 %. It was previously noticed that villages having wider area of mangrove belts between them and the coast had significantly fewer deaths toll than villages with narrower mangrove belts or with no mangroves [2]. Furthermore, the same observation deduced that in the absence of mangroves there would have been 1.72 additional deaths per village within 10 km of the coast [2].

Mangrove Forest Structures. Another important factor affecting the rate of wave attenuation is the structure and characteristics of the mangroves vegetation [13]. The stem configurations, roots and branches diameter together with the submerged part of the vegetation plays important role in the magnitude of energy dissipation [12][16][8][11]. These physical characteristics also directly related to the age of the mangroves. Collectively, these parameters determine the nature of obstacles encountered by waves as they passed through the mangrove forests [13]. Greater obstacles will result in higher resistance which eventually gives significant impact on wave attenuation.

Methodology of the Study

Experimental Setup. The laboratory experiments were conducted in a narrow wave flume in the Offshore Laboratory of Universiti Teknologi PETRONAS. The wave flume was 23 m long, 1.5 m wide and 1.2 m high. The setting up of the experiments is as shown in Fig. 1. One wave gauge was placed before the slope and nine wave gauges with gaps of 0.5 m placed above the flat platform to measure the wave heights in the purlieu of the mangrove field. The investigation was carried out simulating a 10 years old *Rhizophora* trees that were scaled down from the actual tree geometry by a factor of 10. Typical 10 years old *Rhizophora* in the field that were used as reference were having average trunk diameter of about 15 cm, root height of up to 1.12 m and root diameters in the range of 3 to 6 cm.

Test Conditions

Test for tandem and staggered arrangements of trees. The mangrove models were arranged in tandem and staggered order. For tandem arrangement, the trees were arranged with specified spacing between rows of trees. Alternative staggered arrangement was set-up in such a way that the gaps between the trees were blocked by the trees behind them (Fig. 2). The water depth specified for both arrangements was 0.15 m deep and wave height was 0.05 m high.

Test for trees densities. For the testing of trees densities, the trees were categorized into two different groups, namely, for natural grown mangrove forests and the other for replanted mangrove forests. Four densities were being tested. The density of 11 trees/m² (sparse) represented for natural grown mangrove forests. Whereas, density of 16 trees/m² (median), 22 trees/m² (dense) and 36 trees/m² (super dense) represented for the category of replanted mangrove forests (Fig. 3). For all

the four densities tested, water depth and wave height conditions were specified to 0.15 m and 0.07 m, respectively in the experiment set up.

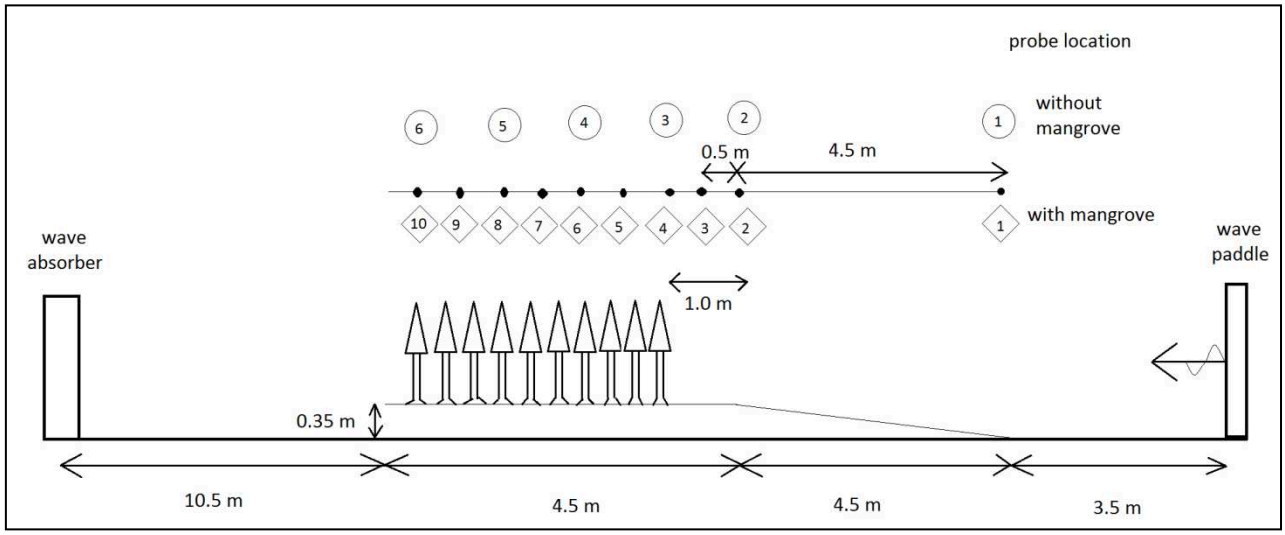


Fig. 1 Schematic diagram of narrow wave flume set up

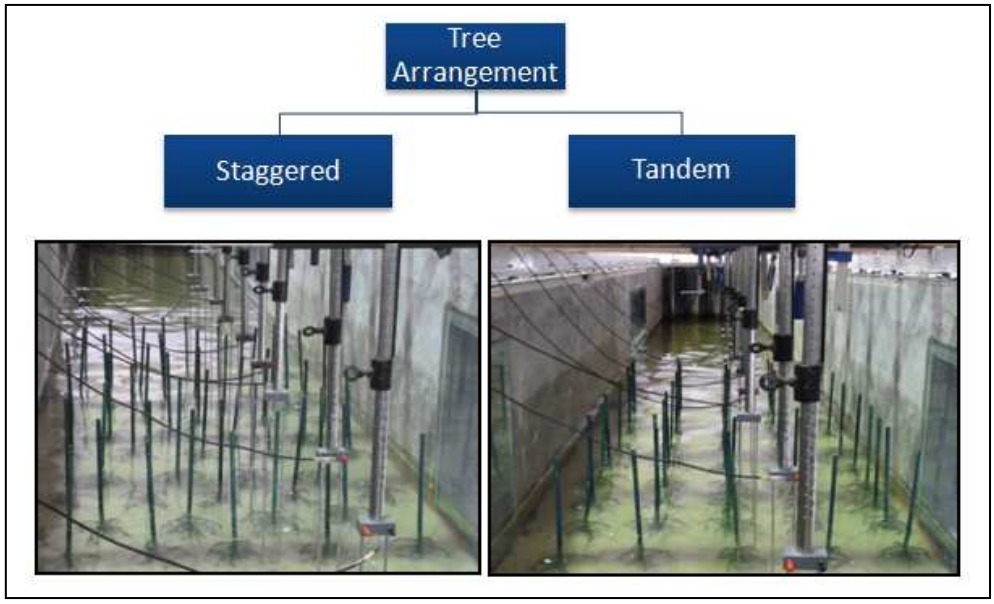


Fig. 2 Test for tree arrangements

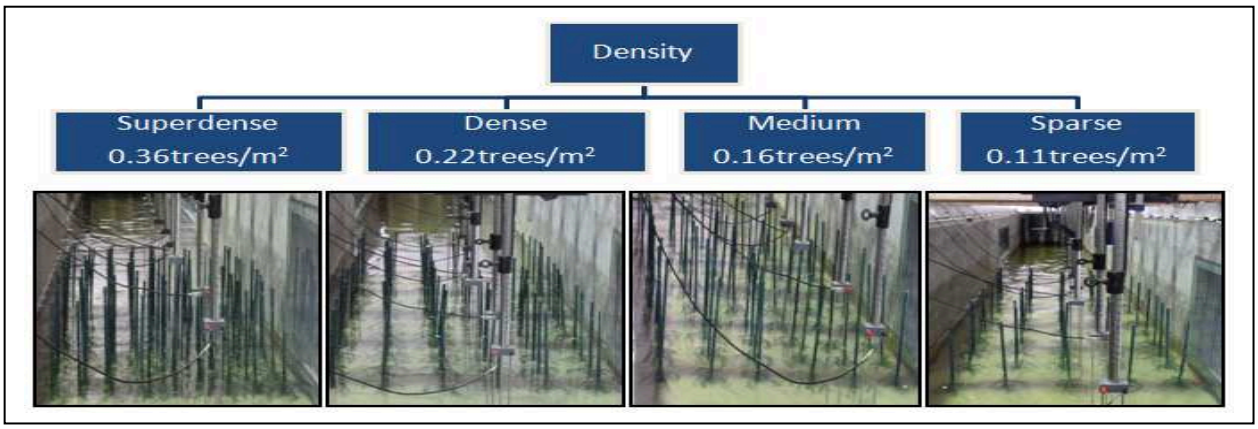


Fig. 3 Test for tree densities

Results and Discussion

It was estimated in this study that for a 100 m wide 10 years old *Rhizophora* with density of 0.11 trees/m^2, the wave reduction was over 51.1 % compared to 20.7 % in the case of bare land, about 2.5 times larger. The experimental results clearly showed that the wave heights reduced when the waves travelled further into the mangrove field. Whereas in the area without mangroves, there was only a slight reduction in the wave heights, mainly caused by the bottom friction due to the sandy bed surface. The wave reduction was significantly higher in area with mangroves due to the additional friction contributed by the trunks and root system. Recent physical model investigation found that waves height reduction by 20 years old mangrove trees attenuate 80 % (Fig. 4) of total wave reduction for a 100 m wide mangrove forest which is four times greater compared to bare land [17]. This suggested that resistance exerted by mangroves also significantly depending on the mangrove age due to their different structures and sizes of trunk and root system. Earlier field measurement in 2007 found that the waves height reduction by a 31.8 m wide mangrove forest dominated by *Kandelia candel* was 5 to 7.5 times larger compared to bare land [11]. The wave height reduction through mangroves was larger than just by bottom friction only, indicating the significant role of mangrove forests in surface wave attenuation.

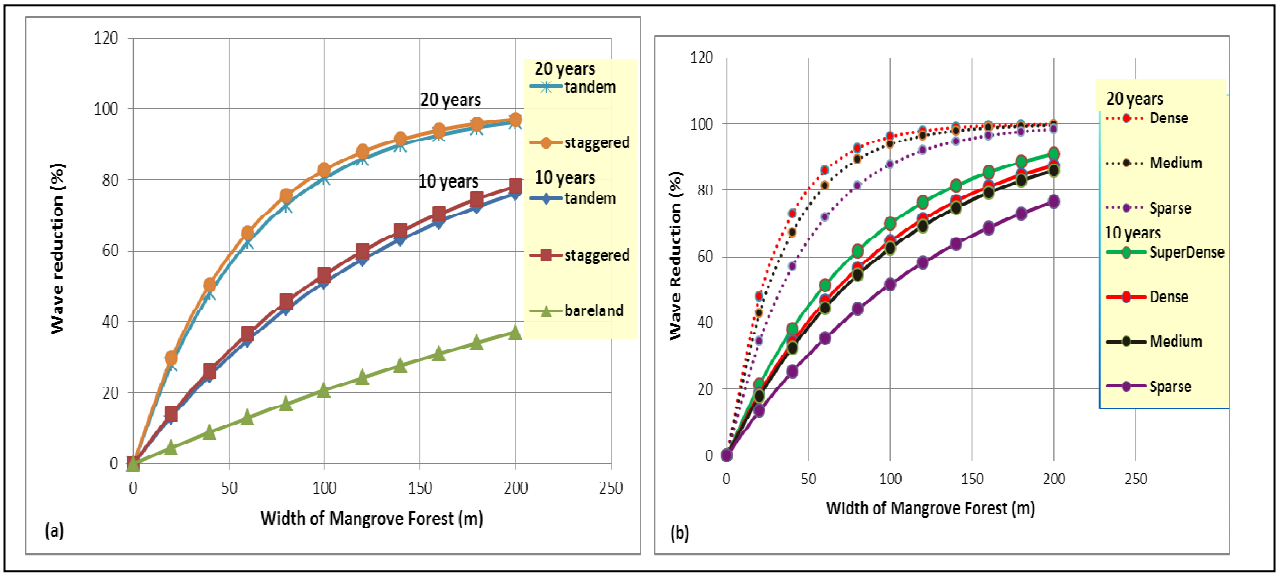


Fig. 4 Wave reduction (%) with respect to age group on different (a) tree arrangement and (b) forest densities (Also incorporating results from [17])

The wave reduction was greater by 3% when the mangrove models of 10 years were arranged in staggered order compared to tandem arrangement (Fig. 4). This slight improvement in wave dissipation was due to the alternate tree arrangement which reduces the free gaps in between the mangrove trees and thus provides additional obstruction to the propagating wave flow. This difference in total wave reduction for both arrangements for 20 years mangroves was also less than 3 %, which can be considered as not significant (Figure 4(a)) [17]. The above findings strengthen the suggestions by [17] that the performance of a band of matured mangrove has no critical reliance to the arrangement of mangrove seedlings during mangroves replanting project. As the group of *Rhizophora* gets older, their root structure spread widely and in most cases overlap with adjacent trees. As most of the waves were dissipated by the roots system, the wave reduction through matured mangroves was still considerably high and less dependent to the initial trees arrangement, either tandem or staggered order.

It is clearly observed that dense mangrove forests attenuated waves more effectively (Fig. 4). The spacing between mangrove trees is smaller in denser forest as they are closer to each other. This poses greater resistance and creates more obstruction to the incoming waves due to larger quantity of trunks and roots available per m² area. The density of 0.36 trees/m² represented a spacing of

1.7 m between trees in real mangroves site. In real condition, naturally grown matured forests, the distance between *Rhizophora* trees are seldom less than 3.0 m because the prop roots spread wide enough and take up lots of space [17]. At Kuala Sepetang Mangrove Park, *Rhizophora apiculata* and *Rhizophora mucronata* were planted at the spacing of 1.2 m and 1.8 m, respectively. As noted during the site visits to the mangrove forest, the spacing of naturally-grown mangrove trees was about 3.0 m, equivalent to 0.11 trees/m² and this density was also being tested in the laboratory. For a 100 m wide 10 years *Rhizophora* forest, the total wave reduction estimated for super dense, dense, medium and sparse forest were 70.0 %, 64.7 %, 62.6 %, and 51.7%, respectively. Currently, the Malaysian's guideline has specified 200 m mangroves buffer zone along the coast for coastal protection. The experimental investigations found that a 10 years old *Rhizophora* forest of similar width with a density of 0.36 trees/m² is able to reduce wave height about 91 %. Whereas a 20 years *Rhizophora* forest can offer up to 98 % wave reduction.

Conclusion

The study found that a 100 m wide 10 years old *Rhizophora* has the potential to dissipate waves 2.5 times larger than area without mangroves. Whereas a similar width of 20 years old mangroves was earlier found to be able to attenuate waves four times more than area in the absence of mangroves. In the area with the presence of mangrove forests, the wave impact on shore is reduced. The study showed that the arrangements of the mangrove trees did not reflect significant effect on waves reduction with differences of less than 3 % over 200 m width. This indicated that if the full grown mangroves are used as performance benchmark, then arrangement of mangrove seedlings is not of great concern during mangroves replanting project. A 10 years mangrove of 200 m width, with density of 0.11 trees/m² is able to dissipate wave height over 77 %. Whereas the 20 years old mangroves of same width and density are able to dissipates waves as high as 98 %. Apparently age plays an important role in determining the effectiveness of the mangrove forests in attenuating surface wave. When the age of mangroves increases, the trees grow bigger and the root system becoming more developed and denser, resulting in greater resistance to the incoming waves. During replanting project, the seed can be planted at a closer distance with higher density and later thinning process could be carried out. The findings further emphasize the significant role of mangrove forest as the natural protection buffer for the coastal area. It is inevitable that mangroves re-planting effort along the coast should continue, but in a more structured way especially in the areas that are susceptible to the impact of waves [17]. The knowledge and understanding of wave attenuation capability of mangroves trees especially few years after re-planting will provide better estimation of the performance of each stage of mangrove forests in attenuating surface wave. This is eminent for better planning and management of mangrove forest as a sustainable natural coastal protection.

Acknowledgments

The authors would like to express gratitude to Universiti Teknologi PETRONAS for providing the facility and funding to conduct this research.

Literature References

[1] UNEP-WCMC. (2006). In the frontline: shoreline protection and other ecosystem services from mangroves and coral reefs. UNEP-WCMC, Cambridge, UK

[2] Das, S., and J. R. Vincent. 2009. Mangroves protected villages and reduced death toll during Indian super cyclone. Proceedings of the National Academy of Sciences USA 106:7357–7360

[3] Kandasamy, K., & Narayanasamy, R. (2005). Coastal mangrove forests mitigated tsunami. Estuarine, Coastal and Shelf Science 65, 601-606

[4] Danielsen, F., Sorensen, M.K., Olwig, M.F., Selvam, V., Parish, F., Burgess, N.D., Hiraishi, T., Karunagaran, V.M., Rasmussen, M.S., Hansen, L.B., Quarto, A., & Suryadiputra, N. (2005). The Asian tsunami: a protective role for coastal vegetation. Science 310, p. 643

[5] Dahdouh-Guebas, F., Jayatissa, L.P., Di Nitto, D., Bosire, J.O., Lo Seen, D., & Koedam, N. (2005). How effective were mangroves as a defense against the recent tsunami? Curr. Biol. 15, 443-447

[6] Tanaka, N., Sasaki, Y., Mowjood, M.I.M., Jinadasa, K.B.S.N., Homchuen, S. (2007). Coastal vegetation structures and their functions in tsunami protection: experience of the recent Indian Ocean tsunami. Landsc. Ecol. Eng. 3, 33-45

[7] Shuto, N. (1987). The effectiveness and limit of tsunami control forests. Coast Eng Jpn 30, 143–153

[8] Massel, S.R., Furukawa, K., & Brinkman, R.M. (1999). Surface wave propagation in mangrove forests. Fluid Dynamics Research 24, 219-249

[9] Mazda, Y., Magi, M., Kogo, M., & Hong, P.N. (1997a). Mangrove as a coastal protection from waves in the Tong King delta, Vietnam. Mangroves and Salt Marshes 1, 127-135

[10] Vo-Luong, H.P., & Massel, S.R. (2008). Energy dissipation in non-uniform mangrove forests of arbitrary depth. J. Mar. Syst. 74, 603 – 622

[11] Quartel, S., Kroon, A., Augustinus, P.G.E.F., Santen, P.V., Tri, N.H. (2007). Wave attenuation in coastal mangroves in the Red River delta, Vietnam. J. Asian Earth Sci. 29(4), 576 – 584

[12] Alongi, D.M. (2008). Mangrove forests: resilience, protection from tsunamis, and responses to global climate change. Estuarine, Coastal and Shelf Science 76, 1-13

[13] McIvor, A.L., I. Möller, T. Spencer and M. Spalding. (2012). Storm Surge Reduction by Mangroves, Cambridge Coastal Research Unit, Cambridge, 27 pp

[14] Bao, T.Q. (2011). Effect of mangrove forest structures on wave attenuation in coastal Vietnam. Oceanologia 53(3), 807 – 818

[15] Lacambra, C., Spencer, T., & Moeller, I. (2008). Tropical coastal ecosystem as coastal defences. Report on The Role of Environmental Management and Eco-Engineering in Disaster Risk Reduction and Climate Change Adaptation. Cambridge Coastal Research Unit, Department of Geography, University of Cambridge, United Kingdom

[16] Hashim, A.M., Catherine, S.M.P., & Takaijuddin. H. (2013). Effectiveness of Mangrove Forests in Surface Wave Attenuation: A Review. Research Journal of Applied Sciences, Engineering and Technology 5(18): 4483-4488, 2013

[17] Hashim, A.M., & Catherine, S.M.P. (2013). A Laboratory Study on Wave Reduction by Mangrove Forests. APCBEE Procedia 5(2013) 27–32.

Applied Mechanics and Materials Vol. 567 (2014) pp 283-288
© (2014) Trans Tech Publications, Switzerland
doi:10.4028/www.scientific.net/AMM.567.283

Reliability Assessment Model for Aging Jacket Structures in Malaysian Waters

V. J. Kurian[1,a], S. S. Goh[1,b], M. M. A. Wahab[1,c] and M. S. Liew[1,d]

[1]Civil Engineering Department, Universiti Teknologi PETRONAS, Tronoh, Malaysia

[a]kurian_john@petronas.com.my, [b]gohshuenshyan@gmail.com,
[c]mubarakwahab@petronas.com.my, [d]shahir_liew@petronas.com.my

Keywords: Reserve Strength Ratio (RSR), probability of failure, reliability index, reliability assessment model.

Abstract. As the world is progressing towards deeper water technology, jacket platform still remains as an important production structure for oil and gas in Malaysian shallow water regions. Besides the discovery of new oil and gas, enhanced oil recovery (EOR) allows more oil to be extracted from the old fields. As a result, service life of existing fixed jacket platforms need to be extended. The overall reliability of aged platform has to be reevaluated in order to monitor the integrity of the structure, and to prevent unexpected failures. Reserve Strength Ratio (RSR) is a widely adopted measure to quantify the ultimate strength of a structure. However, structural strength alone is inadequate to express a structure's reliability. Reliability is best defined as the probability that the extreme load will not exceed the ultimate strength of a structure. It can be expressed either in probability of failure or reliability index, which is the inverse normalized form of probability of failure. This paper presents the study of existing jacket platforms in Malaysia's three oil and gas operating regions. Relationship between probability of failure, reliability index and RSR has been formed to provide a simple reliability assessment model of jacket structure in Malaysia water regions.

Introduction

Fixed jacket platform is among the very first structure to be introduced in the offshore industry. The design of jacket structure is based on the response of components to the applied loads, where the ultimate goal is to ensure the level of safety is above the minimum requirements of relevant design codes. If a platform is put in service beyond its initial design life, a requalification process has to be conducted to check the safety of the platform. Among the many offshore jacket platforms being installed in Malaysia, more than half of them have already exceeded their design life.

Being introduced to the offshore field in 1980s, reliability assessment has become an increasingly popular tool for analyzing structural safety. A structure's reliability is usually measured as probability of failure and/or reliability index. Load and resistance are the two core variables that form the failure function in reliability analysis. If the maximum load exceeds the minimum capacity of the structure, load and resistance distributions will overlap and a nonzero probability failure will be formed. The overlap between the two curves provides a qualitative measure of the probability of failure.

Load as the name suggests, consist of gravity load (dead load, live load) and environmental load. On the other hand, resistance has to do with the reserve strength of a structure. RSR as the outcome of non-linear collapse (push-over) analysis is the indicator of the system strength for offshore jacket structure. The concept of reserve strength was first being introduced in Blume's 'Reserve Energy Technique'. [1] It is commonly defined as the ability of a structure to sustain loads in excess of the design value. In literature, RSR is measured in a variety of ways. One of such is the ratio of the ultimate platform resistance to the design load. RSR is also quoted as ratios of platform base shear or overturning moment. For different load case or load combination, various RSR will be

generated. Besides, load case which produce the highest component utilization ratio does not necessary produces the lowest RSR.

After obtaining the basic variables, reliability analysis can be carried out. Reliability of a jacket platform is governed by the structural system and this system is the combination of series and parallel subsystems. For instance, jacket legs illustrate series or chain reliability system. When a member fails, the entire system fails. On the other hand, structural bracings are an example for parallel system. One bracing member failure does not cause immediate failure to the structure. Instead, the load carried by the failed member will be transferred to the other intact members in the group. [2]

There are two types of reliability analysis methods: approximate analytical methods such as first and second order reliability methods (FORM & SORM), and simulation method such as the Monte Carlo simulation (MCS). MCS is easy to use but requires great number of analysis to achieve good approximation of probability of failure. When the probability of failure is small (i.e., 10E-5), this method requires long computation time and takes up too much RAM. [3] Thus, FORM has been widely adopted by many researchers. [4] [5] [6] The FORM solution provides geometrical interpretation of reliability index as the distance between origin and design point in standard normal space. Anyhow, study conducted by Haldar and Mahadevan [6] has shown that if the number of simulation cycles is relatively large, results generated by Monte Carlo simulation would be similar to the FORM method.

Methodology

This paper mainly discusses the relationship between three important reliability parameters: RSR, reliability index and probability of failure, specifically for Malaysia water regions.

Three platforms located at the three oil and gas operating regions in Malaysia are studied. They are Platform A in Peninsular Malaysia Operations (PMO), Platform B in Sarawak Operations (SKO) and Platform C in Sabah Operations (SBO).

Met-ocean data at specific locations are obtained from the design report and recorded in Table 1. Only wave and current loadings are considered in this analysis.

Table 1: Location Specific Met-Ocean Data (Omni-Directional)

Platform	Wave Parameters		Current Speed [cm/s]		
	H [m]	***T [s]***	***1.0*D***	***0.5*D***	***0.01*D***
A	10.9	9.5	147	117	32
B	11.7	10.9	120	95	55
C	7.7	9.6	94	86	44

Pushover or collapse analyses are conducted to obtain the ultimate strength of each platform, which is recorded as Reserve Strength Ratio (RSR). Fixing gravity load acting on the structure, environmental load is gradually increased until the structure collapse or fail. Design base shear is acquired at load factor one while the base shear at structure's collapse is the ultimate strength. Calculation of RSR is given in Equation 1.

$$\text{RSR} = \text{Collapse Base Shear (Ultimate Strength)} / \text{Design Base Shear.} \quad (1)$$

Next, by adopting First Order Reliability Method (FORM) for reliability analysis, structure's reliability is determined in the form of probability of failure and reliability index. Curve Fitting Tool (CFTOOL) in MATLAB is used to perform regression analysis so that relationships between RSR, probability of failure and reliability index can be generated.

Results

Results from the analyses are recorded in the following sections:

Resistance

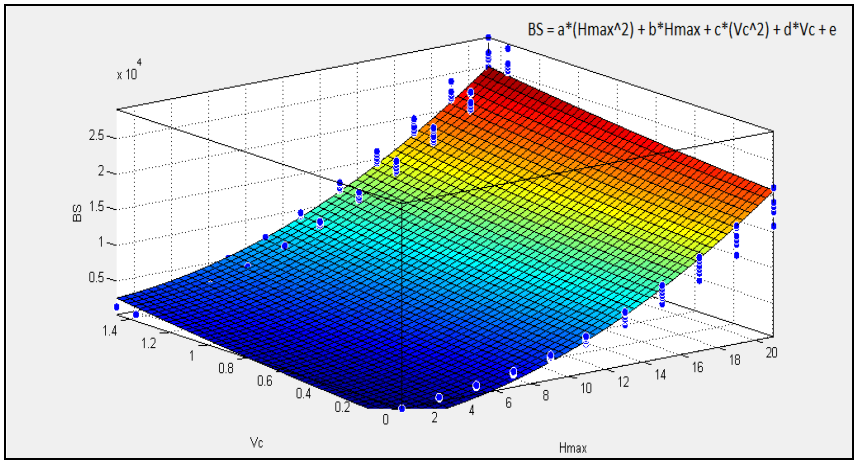
Resistance of a platform can be represented by the reserve strength of the structure, which is usually measured as Reserve Strength Ratio (RSR). In this study, RSR are obtained using collapse analysis and the results for the three platforms are recorded in Table 2.

Table 2: RSR at Different Direction

Dir [deg]	RSR Platform A	RSR Platform B	RSR Platform C
000	1.087	3.120	3.940
045	1.360	3.758	4.660
090	1.782	3.530	5.710
135	2.820	4.619	4.740
180	2.963	3.671	4.870
225	1.485	4.192	7.760
270	1.139	3.020	7.350
315	1.220	4.650	5.409

Load

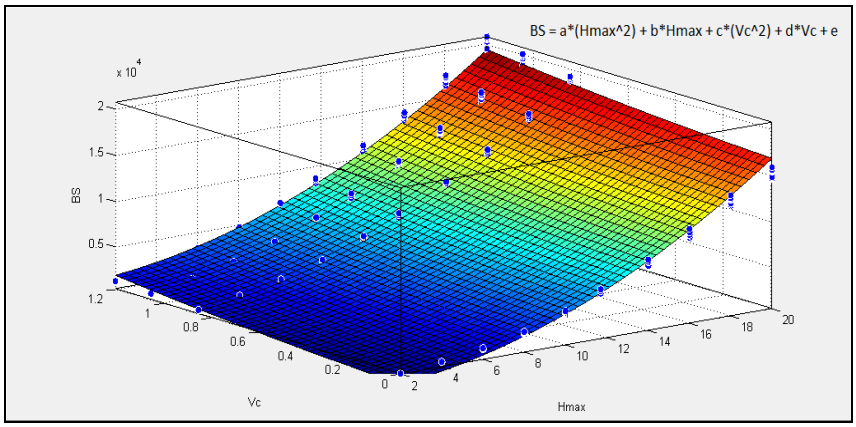
Response surface functions illustrating the effect of environmental loadings (wave and current) on the base shear (BS) of the structure are recorded in Figures 1, 2 and 3. Two-degree polynomial equation is selected to be the most suitable function describing the two parameters, which is given in the figure. Coefficients of each polynominal equation are tabulated as a – e, while BS, Hmax and Vc represent base shear, maximum wave height and current respectively. From the obtained R-square value for each function, it can be observed that all functions have confidence level more than 90%.



a	47.12
b	77.40
c	680.90
d	1837.00
e	-1708.00
R^2	0.97

$BS = 47.12*(Hmax^2) + 77.40*Hmax + 680.9*(Vc^2) + 1837*Vc - 1708$

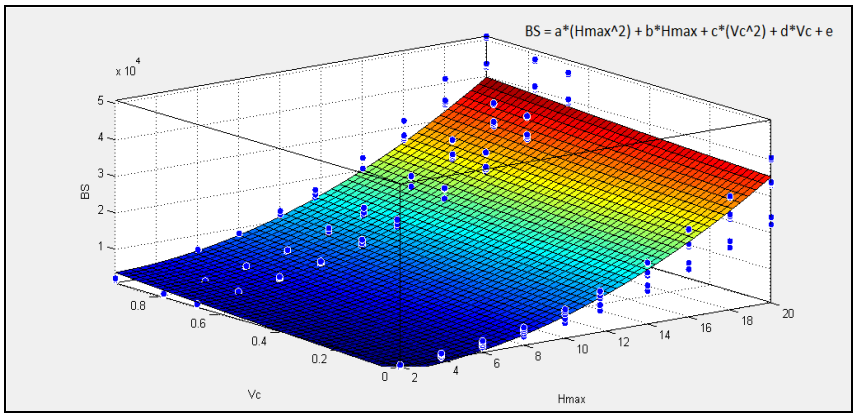
Figure 1: Response surface for Platform A



a	40.88
b	64.52
c	756.60
d	1199.00
e	-932.90
R^2	0.99

$BS = 40.88*(Hmax^2) + 64.52*Hmax + 756.60*(Vc^2) +$

Figure 2: Response surface for Platform B



a	105.20
b	-318.10
c	1259.00
d	3473.00
e	-653.90
R^2	0.93

$BS = 105.20*(Hmax^2) - 318.10*Hmax + 1259.00*(Vc^2) +$

Figure 3: Response surface for Platform C

Reliability Analysis

Reliability analysis is an analysis that link resistance and load to the safety of a structure. By adopting the resistance and load variables in reliability analysis, the reliability of the structure can be found as reliability index and probability of failure. Reliability index (RI) and probability of failure (Pf) for the three platforms are tabulated in Table 3. Although environmental load acting on each direction is similar, the reliability varies due to the different resistance provided by each direction.

Table 3: Reliability Index & Probability of Failure

Dir [deg]	Platform A		Platform B		Platform C	
	β	Pf	β	Pf	β	Pf
000	1.09	2.36E-01	3.12	6.61E-06	3.94	1.22E-06
045	1.36	6.20E-02	3.76	8.51E-07	4.66	2.04E-07
090	1.78	6.09E-03	3.53	1.66E-06	5.71	3.04E-08
135	2.82	3.59E-05	4.62	1.13E-07	4.74	1.72E-07
180	2.96	2.01E-05	3.67	1.09E-06	4.87	1.31E-07
225	1.48	3.17E-02	4.19	2.81E-07	7.76	3.17E-09
270	1.14	1.87E-01	3.02	9.61E-06	7.35	5.92E-09
315	1.22	1.27E-01	4.65	1.06E-07	5.41	4.89E-08

Best fits describing connections between RSR, reliability index and probability of failure are plotted in Figure 4. 5% of upper and lower boundaries are outlined in the graphs as well. Exponential functions are found to be the most suitable equation for all the three relationships. The functions are given in the figure.

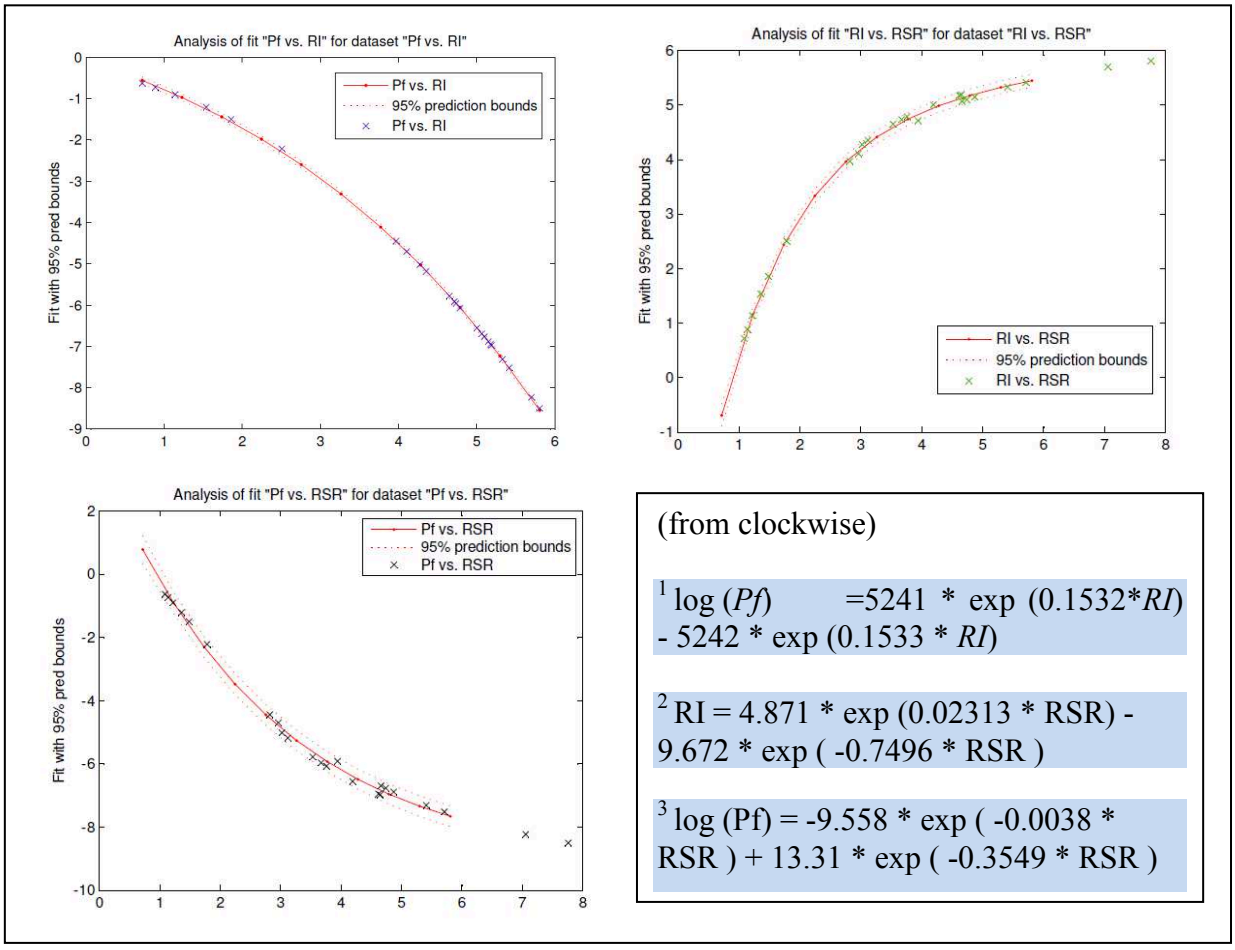


Figure 4: Relationship of probability of failure, reliability index and RSR at 95% confidence level check

Discussion

The met-ocean loadings at Platform C is the lowest as compared to Platform A and B. It can be predicted that the platform is safer than the other two. According to the results of the analyses, Platform C has the highest reserve strength ratio and reliability index (or lowest probability of failure). Environmental loadings do have distinctive effect to the reliability of a platform.

Besides, the RSR value for different platform direction varies. Platform A which is located at PMO has the lowest RSR value of 1.087 at 0° while Platform B (SKO) has its lowest RSR value, 3.020 at 270°. For Platform C (SBO), the lowest RSR value is 3.940 from 0°. There is a certain distribution of RSR values at different directions, differs for each platform. RSR distribution describes the strength distribution of the platform. The directions mentioned earlier are the weakest points for Platform A, B and C, and the RSR values at those directions have been used in reliability analysis.

Much as the RSR value presenting the strength of a structure, the reliability of a structure is affected by the loadings acting on the structure. Response surface analyses are performed to generate global response functions for the environmental load acting on the three structures. Polynomial functions are developed to link base shear and the incoming wave and current loadings.

Additional analyses have been performed to calculate the reliability of the structure as reliability index and/or probability of failure, using resistance and load failure function. The trend of reliability index comparison graph is similar to the one in RSR comparison. However, the reliability indexes for Platform B and C seem to be more even in the eight directions, generally because of the configuration of the structures. Platform A is rectangular shaped while Platform B and C are squared. Anyhow, it is observed that certain relationships can be developed for the three parameters, namely RSR, reliability index and probability of failure.

Three exponential fits plotted using MATLAB's Surface Fitting Tool include 'probability of failure versus reliability index', 'reliability index versus RSR' and 'probability of failure versus RSR'. All data used for the three graphs fulfills the 95% confidence level, which indicates that the generated equations are able to describe the relationship precisely. The first fit conveys a message that as the probability of failure gets higher, the reliability index becomes lower. Similar relation is found in the third fit that plots probability of failure versus RSR whereas the second fit has the opposite relationship. If the RSR value is high, the reliability index will be high too. RSR has an inverse relationship with probability of failure and a direct relationship with reliability index. The exponential equations generated enable simplified reliability assessment to be carried out. Without having to run complicated reliability analysis, the reliability of jacket platforms in Malaysia waters can be determined easily.

Conclusion

In this paper, the following conclusions are made from the results discussed above:

1. Met-ocean loadings affect the strength and reliability of a platform.
2. The RSR values of a platform vary with the direction of action of environmental load with respect to the orientation of the platform.
3. The RSR value has an exponential relationship with both the reliability parameters, namely reliability index and probability of failure.

References

[1] J.A. Blume, "A Reserve Energy Technique for The Earthquake Design And Rating of Structures in The Inelastic Range," Proceedings 2nd World Conference on Earthquake Engineering, Tokyo, 1960.

[2] E.S. Gharaibeh, D.M. Frangopol, and T. Onoufriou, "Reliability-based importance assessment of structural members with applications to complex structures," In Computers and Structures 80, 2002, pp. 1113-1131.

[3] University of Surrey, "A Review of Reliability Considerations for Fixed Offshore Platforms," HSE, Offshore Technology Report – OTO 2000 037.

[4] F. Moses and B. Stahl, "Calibration Issues in Development of ISO Standards for Fixed Steel Offshore Structures," Transactions of the ASME, Vol. 122, Feb 2000.

[5] Z. Hassan, "Calibration of Deterministic Parameters for Reassessment of Offshore Platforms in The Arabian Gulf using Reliability Based Method," PhD, Mechanical Engineering, University of Western Australia, 2008.

[6] N.J. Cossa, "Environmental Load Factor for ISO Design of Tubular Joints of A Malaysia Fixed Offshore Steel Jacket Platform," MSc. Dissertation, Universiti Teknologi PETRONAS, Perak, Malaysia, 2012.

[7] R.G. Bea, "Reliability Based Requalification Criteria for Offshore Platforms," Proc. 12th International Conference on OMAE, Glasgow, 1993.

[8] A. Haldar and S. Mahadevan, "Reliability Assessment Using Stochastic Finite Element Analysis," John Wiley and Sons, United State of America, 2000.

Applied Mechanics and Materials Vol. 567 (2014) pp 289-294
© (2014) Trans Tech Publications, Switzerland
doi:10.4028/www.scientific.net/AMM.567.289

RESONANT MOTION OF LIQUID CONFINED BETWEEN FLOATING STRUCTURES

Nasma Noor N.V[1,a] , A.P Shashikala[1,b]

Department of Civil Engineering, NIT Calicut, Kerala, India.

[a]nasmanoornv@gmail.com, [b]apska@nitc.ac.in

Key words: Resonant motion, Multi body interaction, Wave profile within the gap, Frequency domain

Abstract. Many applications occur in the field of marine hydrodynamics where two or more vessels are in sufficiently close proximity to experience significant wave action. The motion of such floating bodies in waves is frequency dependent. In the case of multiple floating bodies, when resonance occurs, the effect of confined liquid between the bodies has some serious implications on the safety and operation of the offloading system. The main objective of the work is to determine the hydrodynamic behaviour of two bodies freely floating in water. A frequency domain method is adopted for the prediction of the resonant frequency. 3D linear diffraction radiation analysis is used to solve the problem. Structures are modelled in ANSYS AQWA and analysed in selected range of frequency with different spacing. As the spacing increases the resonant frequency in roll is found to be decreasing for both ship and tugboat and the frequency shift between the two is increasing. The wave elevation pattern within the spacing has been observed and the result has been shown for different spacings.

Introduction

In cases of multi body interactions, such as marine operations involving multiple vessels and platforms or replenishment operations of two ships, the proximity is temporary but nevertheless important. Hydrodynamic interactions related to wave effects are particularly significant, due to the oscillatory phase of the waves in relation to the spacing, and the large horizontal scale of the wave influence. There has been extensive research in the area of multi body interactions considering different configurations of the structures in time domain [1] and frequency domain method [2, 3]. This problem is more complex than that of a single floating structure. Most of the authors concentrated on finding the hydrodynamic coefficients, forces and responses [4, 5]. A very few works are seen in determining wave elevation within the gap and the resonant frequency for a particular spacing [6].

The present study focuses on the frequency domain analysis of two floating structures and the resonant behaviour of water confined between two structures which are free to move. The effect of one structure on the response of other is also included in the present study.

Formulation and Solution of the Problem

To describe the motion responses between two bodies in waves, consider three sets of right handed orthogonal coordinate systems as shown in Fig.1. O-XYZ is the space fixed coordinate system, O_A-$X_AY_AZ_A$ and O_B-$X_BY_BZ_B$ are the oscillatory coordinate systems fixed with respect to ship A and B, respectively. The O-XY plane coincides with the undisturbed free surface, the X-axis in the direction of the body's forward and the Z-axis vertically upward. Oscillatory coordinate systems O_A-$X_AY_AZ_A$ and O_B-$X_BY_BZ_B$ are used to describe the body motion in six degrees of freedom with complex amplitudes ξ_i (i=1,2,… *12*). Here *i=1...6* and *i=7....12* represent surge, sway, heave, roll, pitch and yaw for ship A and for ship B, respectively.

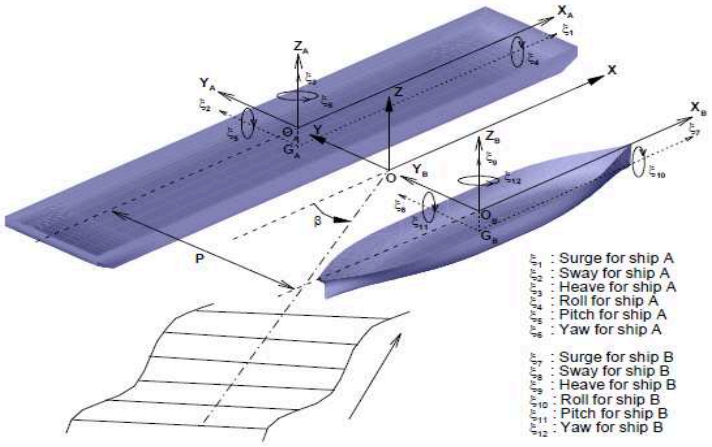


Fig.1. Definition sketch of co-ordinates

The state of fluid can be completely described by the velocity potential, ∅(x,y,z,t) satisfying the Laplace equation

$$\nabla^2\phi = 0. \quad \text{in the fluid domain} \tag{Eq.1}$$

The total unsteady potential for a sinusoidal wave excitation with encounter frequency, ω_e, can be expressed as

$$\Phi(x,y,z,t) = [\Phi_I(x,y,z) + \Phi_D(x,y,z) + \sum_{i=1}^{12} \xi_i \Phi_i]e^{-i\omega_e t}. \tag{Eq.2}$$

where $\Phi_I(x,y,z)$ is the incident wave potential representing the incident waves; $\Phi_D(x,y,z)$ is the diffraction potential representing the disturbance of the incident waves diffracted from the body; Φ_i(i=1,2,… ,12) are the radiation potentials due to oscillations of the two bodies in calm water with unit amplitude.
The incident wave potential is expressed as

$$\Phi_I = -\frac{ig\xi_a}{\omega_0} e^{kz} e^{i(kx\cos\beta + ky\sin\beta)} e^{-i\omega_e t}. \tag{Eq.3}$$

Where ω_0 is the wave frequency, ξ_a is the wave amplitude, k is incident wave number, $k = {\omega_0}^2/g$ β is an arbitrary heading angles.

The individual potentials have to satisfy in the fluid domain, on the free surface, the submerged body surface, the sea bed and a suitable far field radiation condition at infinity.
Linear free surface condition

$$-{\omega_e}^2 \Phi + g \frac{\partial}{\partial z}\Phi = 0. \text{ on z=0} \tag{Eq.4}$$

Body boundary condition for diffraction potentials

$$\frac{\partial}{\partial n}(\Phi_I + \Phi_D) = 0. \text{ on ship A and ship B} \tag{Eq.5}$$

Body boundary condition for radiation potentials

$$\frac{\partial}{\partial n}\Phi_i = -i\omega_e n_i. \text{ (i=1,2,...6) on Ship A} \tag{Eq.6}$$

$\frac{\partial}{\partial n}\phi_i = 0.$ (i=7,8,...12) on Ship B (Eq.7)

$\frac{\partial}{\partial n}\phi_i = 0.$ (i=1,2,...6) on Ship A (Eq.8)

$\frac{\partial}{\partial n}\phi_i = -i\omega_e n_i.$ (i=7,8,...12) on Ship B (Eq.9)

Where,

$(n_1, n_2, n_3) = \vec{n}$. on ship A
$(n_4, n_5, n_6) = \vec{r} \times \vec{n}$. on ship A
$(n_7, n_8, n_9) = \vec{n}$. on ship B
$(n_{10}, n_{11}, n_{12}) = \vec{r} \times \vec{n}.$ on ship B (Eq.10)

With $\vec{n}$ is the outward unit normal vector on ship A and ship B and $\vec{r}$ is the position vector with respect to the origin of the reference frame on ship A and ship B.

Sea bed condition

$\frac{\partial}{\partial n}\phi = 0.$ for z=-h (Eq.11)

Radiation condition at infinity

$\lim_{kr\to\infty} \sqrt{kr}\left(\frac{\partial \phi}{\partial n} - ik\phi\right) = 0.$ (Eq.12)

The wave exciting force F_i can be divided into the incident wave part, F_i^I, and the diffraction part, F_i^D.

$F_i = F_i^I + F_i^D = -i\rho\omega_e \iint_{S_A+S_B} (\phi_I + \phi_D)\, n_i ds.$ (Eq.13)

The motion induced force is

$E_i = -i\rho\omega_e \iint_{S_A+S_B} \sum_{j=1}^{12} \xi_j \phi_j n_j ds = \sum_{j=1}^{12} T_{ij}\xi_j.$ (Eq.14)

where, $T_{ij} = \omega_e{}^2 A_{ij} - i\omega_e B_{ij}.$ (Eq.15)

The terms A_{ij} and B_{ij} are added mass and damping coefficients, respectively.

$A_{ij} = \frac{\rho}{\omega_e} Im\left[\iint_{S_A+S_B} \phi_j n_j ds\right].$ (Eq.16)

$B_{ij} = -\rho\, Re\left[\iint_{S_A+S_B} \phi_j n_j ds\right].$ (Eq.17)

Under the assumption that the responses are linear and harmonic, the twelve linear coupled differential equations of motion for two floating bodies can be written in the following form

$\sum_{j=1}^{12}\left[-\omega_e{}^2(M_{ij} + A_{ij}) - i\omega_e B_{ij} + C_{ij}\right]\{\xi_j\} = F_i.$ for (i=1,2,....12) (Eq.18)

Where M_{ij} is the generalised mass matrix for the ship A and ship B, C_{ij} is the restoring force matrix for ship A and Ship B respectively, ξ_j is the complex amplitude of the response motion in each six degree of freedom for each body, and F_i is the complex amplitude of the wave exciting force for ship A and ship B. The diffraction and radiation potential can be represented by the distribution with the density on the surface S_A and S_B.

$$\iint_{S_A+S_B} \sigma(Q)G(P,Q)ds\,(Q) = 4\pi\varphi(P). \quad \text{for inside fluid} \qquad \text{(Eq.19)}$$

The unknown source density σ can be found by imposing the body boundary conditions and it gives

$$\frac{1}{2}\sigma(P) + \frac{1}{4\pi}\iint_{S_A+S_B} \sigma(Q)\frac{G(P,Q)}{\partial n} ds\,(Q) = V_n \text{ . for body surface} \qquad \text{(Eq.20)}$$

Wave Elevation within the Gap

The wave elevation between two ships is affected by several factors, such as ship motions, the incident wave, diffraction wave, and radiation wave etc. Hence the formula of linear wave elevation at any point 'o' between two ships can be expressed as follows,

$$\frac{\eta}{a} = \frac{i\omega\rho(\phi_{I0}+\phi_{Da0}+\phi_{Db0}+\sum_{j=1}^{6}\phi_{jRao}\zeta_{ja}+\sum_{j}^{6}\phi_{jRb0}\zeta_{jb}}{\rho g a}. \qquad \text{(Eq.21)}$$

Where

ϕ_{jRao}: radiation potential per unit displacement on the free surface point o due to the jth mode motion of ship A while ship B is fixed

ϕ_{jRb0}: radiation potential per unit displacement on the free surface point o due to the jth mode motion of ship B while ship A is fixed

ϕ_{Da0}, ϕ_{Db0}: diffraction potential on the free surface point o due to oscillation of ship A or ship B respectively

ϕ_{I0}: incident wave potential on the free surface point o.

Description of the Model

Two structures, a ship and tug boat are modelled for six different separation distances between them. The body is modelled as quadrilateral elements with four nodes. Each element generates pressure and hydrostatic forces. The structures are modelled in ANSYS for the details given in Table 1. The ship and tug boat are arranged side by side as shown in Fig. 2. Distance between the COG of structures varies from 0.2B, 0.4B, 0.6B, 0.8B, 1.0B and 1.2B, where B is the breadth of ship. The far field is fixed so as to avoid the effect of reflecting waves and depth is chosen to account for deep water case.

Table. 1 Details of the model

Items	Ship	Tugboat
Length [m]	65.42	38.25
Breadth [m]	14.6	11.05
Depth [m]	6	5.8
Draft [m]	4.2	3.5
Displacement [m^3]	2388.22	674.738
KG [m]	4.54	3.6
K_{xx} [m]	3.878	2.988
K_{yy} [m]	14.395	7.889
K_{zz} [m]	14.833	8.28

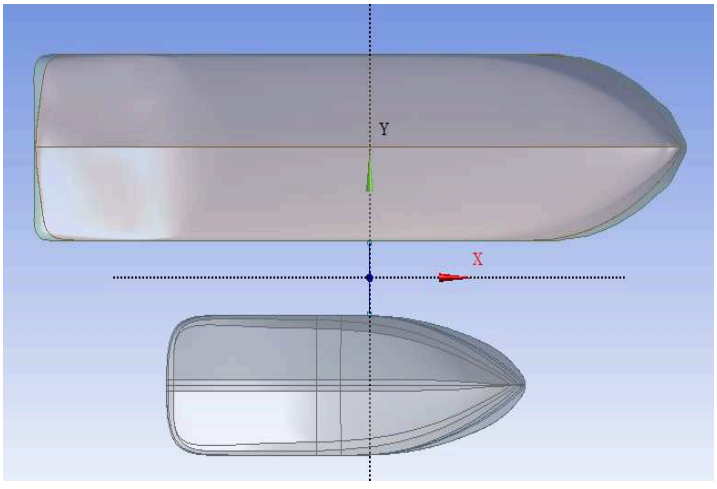


Figure. 2. Ship and tugboat in side by side arrangement

Resonant Frequencies

The ship- tugboat system is analysed and the natural frequencies in heave, roll and pitch motions of both structures are found for all spacings. The natural frequency of the system in different modes is compared with wave frequencies to obtain the resonant frequencies. The resonant frequency of the tug boat is shown in Table 2. It was observed that as the spacing increases, the roll resonant frequency decreases whereas the heave and pitch frequencies are negligible. The resonant frequency of ship is higher than tugboat and the difference between the resonant frequency of ship and tugboat increases as the spacing increases.

Table. 2 Resonant frequency of Ship and Tugboat

RESONANT FREQUENCIES [rad/s]				
Spacing	**Structure**	**Heave**	**Roll**	**Pitch**
0.2B	Ship	1.137	0.675	1.285
	Tugboat	1.318	0.653	1.346
0.4B	Ship	1.137	0.606	1.285
	Tugboat	1.318	0.568	1.421
0.6B	Ship	1.137	0.549	1.285
	Tugboat	1.318	0.499	1.421
0.8B	Ship	1.137	0.499	1.285
	Tugboat	1.318	0.444	1.428
1.0B	Ship	1.137	0.457	1.285
	Tugboat	1.318	0.400	1.421
1.2B	Ship	1.137	0.421	1.285
	Tugboat	1.318	0.363	1.418

Wave Elevation within the Spacing for 0^0 Wave Heading

The gap between the two bodies is modelled as an abstract geometry and the wave heights at field points are obtained. Free surface elevation within the gap show large variation at each point within the gap. Wave surface profile is plotted at three locations namely near ship, near tugboat and centre of the system as shown in Fig.3. Fig.4 shows the wave elevation at the centre of gap for different spacing. It is observed that the wave elevation remains same for lower range of frequencies and varies as the frequency increases. All the spacing show same trend with increase in amplitudes as the spacing increases. An increase in water surface elevation was observed at spacing 0.4B when compared to 0.6B.

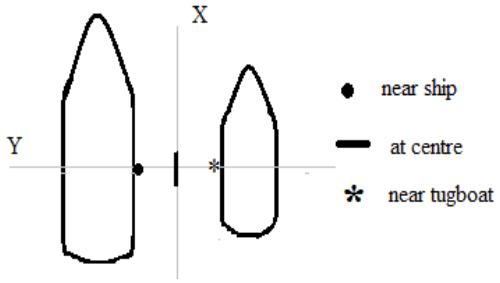


Figure. 3. Sketch showing location of points for

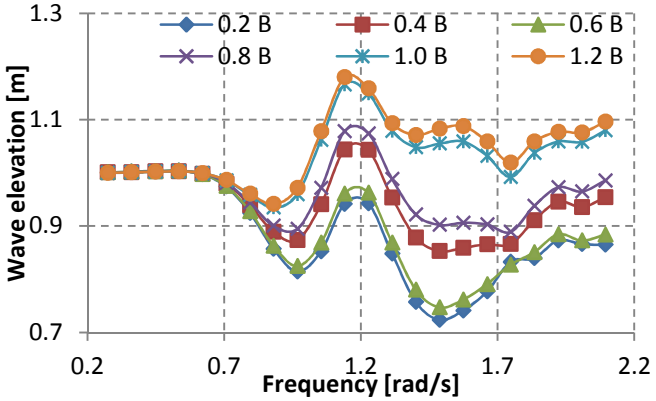


Figure. 4. Wave elevation at the centre of gap for different spacing

Fig. 5 and 6 show the wave surface elevation at the locations on the ship, tugboat and centre of the system for spacing 0.6B and 1.2B. It is observed that for spacing up to 0.6B, surface elevation on the tug boat is more as shown in Fig.5. As the spacing increases, wave surface elevation increases and increased amplitude is seen at the centre of the system from spacing 0.8B to 1.2B.

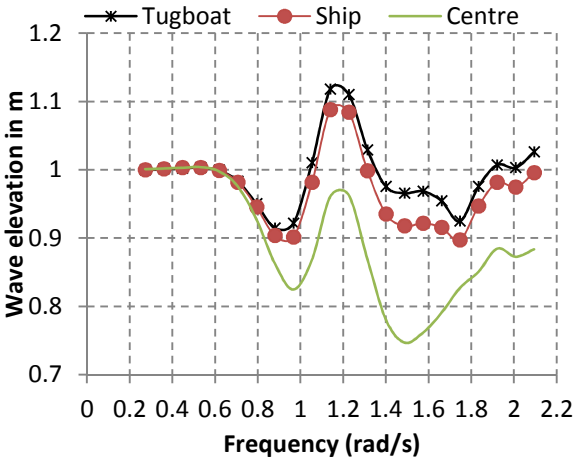


Figure. 5. Wave elevation within the gap 0.6B spacing

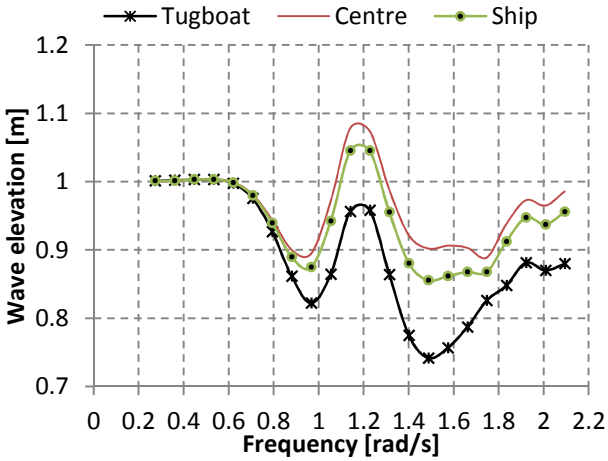


Figure. 6. Wave elevation within the gap for for 1.2B spacing

Conclusions

The resonant frequency in heave and pitch is observed independent of spacing and is significant in the case of roll resonant frequency which decreases as the spacing increases. Wave elevation at three different points is calculated for all the spacing for different wave heading angles. The wave elevations within the gap at three different points are plotted which show large variation for all the cases and which is same in low frequency range for a particular spacing. The maximum amplitude of elevation is showing a wide scatter with spacing and location. The wave elevation of ship is lying in between the other two points and the same at the centre is high for 1.2B. Hopefully this method can be used to study the wave surface profile within the gap between two floating structures in waves. Since the behaviour varies from case to case, a careful understanding of the motion of water waves within the gap is necessary for the safety of the adjoining structures.

References

[1]ZHU Hai-rong, ZHURen-chuan and MIAO Guo-ping., A Time Domain Investigation On The Hydrodynamic Resonance Phenomena Of 3-D Multiple Floating Structures , Journal of Hydrodynamics, 20(5), (2008), 611-616.

[2]Mun-Sung Kim and Mun-Keun Ha., Prediction Of Motion Responses Between Two Offshore Floating Structures In Waves, Journal of Ship and Ocean Technology, 6(3), (2002), pp.13-25.

[3]Koo, B.J. and Kim, M.H., Hydrodynamic Interactions And Relative Motions of Two Floating Platforms With Mooring Lines In Side-By-Side Offloading Operation, Applied Ocean Research, 27, (2005), pp. 292–310.

[4]Wang, C.Z. and Wu, G.X., Analysis Of Second-Order Resonance In Wave Interactions With Floating Bodies Through A Finite-Element Method, Ocean Engineering, 35, (2008), pp. 717–726,

[5]Sun, L., Eatock Taylor, R. and Taylor P. H., First And Second Order Analysis Of Resonant Waves Between Adjacent Barges, Journal of Fluids and Structures, 26, (2010),954–978.

[6]Ming-Chung Fang and Gung-Rong Chen., The Relative Motion and Wave Elevation Between Two Floating Structures in Waves, The International Society of Offshore and Polar Engineers , ISBN 1-880653-51-6, (2001), pp. 361-368

Applied Mechanics and Materials Vol. 567 (2014) pp 295-300
© (2014) Trans Tech Publications, Switzerland
doi:10.4028/www.scientific.net/AMM.567.295

RESPONSE OF MONOPOD PLATFORM UNDER EXTREME WAVE IN MALAYSIAN WATER

MOHD Affiq Bin Jamaluddin[1, a], MOHD Shahir Liew[2, b],
VELLURUZHATHIL John Kurian[3, c]

[1, 2, 3] Civil Engineering Dept., UniversitiTeknologi PETRONAS, Tronoh, Perak, Malaysia

[a]maffiq.jamaluddin@gmail.com, [b] shahir_liew@petronas.com.my,
[c]kurian_john@petronas.com.my

Keywords: monopod platform, response, displacement, environmental loads

Abstract. This paper investigated the structural response of an existing monopod platform under extreme wave condition in Malaysian water. The estimation of the response plays an important role in the design of offshore structure. In this investigation, in-place analysis is performed to measure the reliability of monopod structure owing to the extreme environmental load condition in Malaysian water.The response of the structure to the varying conditions of the structure and varying environmental loads directions are analysed using well defined in-place analysis method [1]. In the present analysis, the deflection of the structure is studied for the number of guyed wires supporting the structure and multi-direction of environmental loads applied onto the structure.

Introduction

The basic information underlying in this monopod platform is a small deck sustained by a single caisson, which contains the wells, or by a braced sub-structure. Monopod platform implement tarpon system which consists of a central caisson stabilized by three cable guys located about 120 degree apart, composed of two cables each, pinned to an anchor pile at or below the mudline and pinned to the central caisson below the water level as shown in Fig. 1.

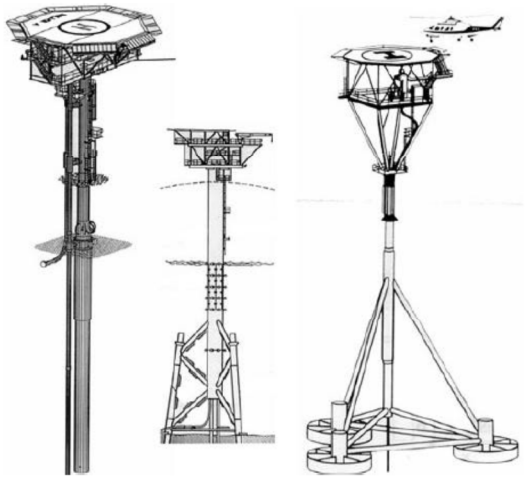


Figure 1. Typical monopod platforms used in shallow water

The first monopods were installed on the North West Shelf (NWS) in 1986, just 2 years after offshore production commenced in the region. Monopods have since become the dominant NWS platform selection, as they have cost advantages for exploiting small, shallow water fields and can be fabricated in Western Australia [2]. The tarpon system has been existence for almost 30 years but the system was widely used in the North Sea by oil major players with over 20 installations to-date. However in Malaysia, this system is still new. The system was first installed at

Semarang Kecil oil field in year 200 and was later applied at the North Lukut and Penara oilfields in 2002 and LedangAnoain 2006.

Structural behaviour of monopod platforms designs under wave loading platform quite complex due to several factors. Firstly, monopods are installed in shallow water, where non-linear wave kinematics is important especially in harsh environments. Secondly, unlike the larger platforms, the platform's configuration is such that the fundamental dynamic bending behaviour is concentrated in the wave zone, rather than throughout the water column. Studies have proved that the wave zone is the most sensitive region in which the failure of a braced monopod on the North West Shelf during a tropical cyclone was localized in the wave zone [3, 6].

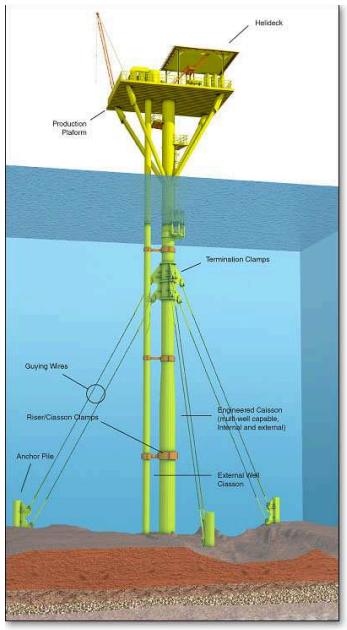


Figure 2. Typical designs for Tarpon system

Platform Configurations

A specific configuration of minimum monopod platforms is used as a reference to study its reliability under harsh environmental loads condition in Malaysian water. The platform is located on the South China Sea, namely Peninsular Malaysia Ocean (PMO) in water depth of 60 meter. The self-weight of the topsides is to be approximated of 200 tonnes. All other external loads such as secondary structures, appurtenances and live load are defined as individual load in the analysis. The central caisson's outer diameter is 2.13 meter (84 inches) with varying thickness throughout the caisson. Each guying wire fixed to the caisson which has a pretension of 355.86 kN (80 kips) to provide external support to the platform.

The computer 3-D model of monopod platform is shown in Fig. 3. As per requirement of inputs to SACS, the structural members and environmental loads are defined. All the designs of its members and materials properties are based on PETRONAS Technical Standard (PTS). All loads required for the analysis are included in the program.

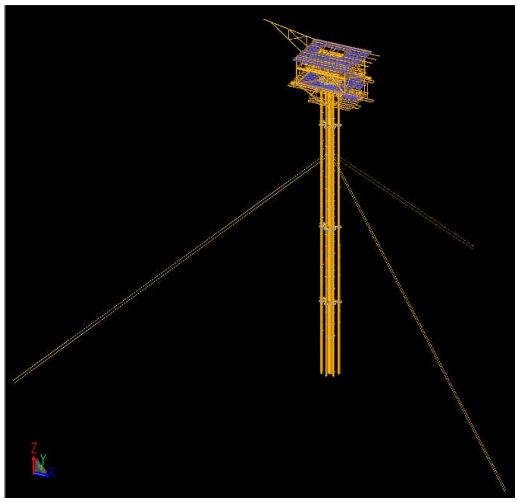


Figure 3. Computer 3-D Modelling for Monopod Platform Model

Loads Configuration

For the present analysis, wind speed that will be used is 39.97 m/s. The determination of wave forces exerted on offshore platform is very complex. Wave theory can be divided into three categories which are sinusoidal waves, cnoidal waves and solitary waves. Wave theory should be understood before one can properly calculate the wave forces [4]. In this analysis, Stokes theory is used to perform the analysis.

Pierson-Moskowitz Spectrum was proposed in 1964 for new formula for an energy spectrum distribution of a wind generated sea state [5]. PM Spectrum describes a fully-developed sea determined by one parameter, namely, wind speed and is widely accepted in the whole world. PM Spectrum can be describes as:

$$S(\omega) = (A/\omega^5)*e^{(-B/\omega 4)} \quad (2)$$

Where,

$A = 0.0082g^2$

$B = 0.74(g/u)^4$

$\omega = 2\pi f$

Where,

u = wind speed (m/s)

g = gravitational acceleration (m/s)

f = frequency (Hz)

The statistical parameters were evaluated using the spectral moments as follows:

Significant wave height, $H_s = 4\sqrt{m_0}$ (3)

Zero crossing wave period, $T_z = \sqrt{\frac{m_0}{m_2}}$ (4)

For this present analysis, the value for wind speed, wave height and wave period is 39.97 m/s (77.7 knots), 13.29 m and 11.10 s respectively.

Result and Discussion

The static analysis of Monopod Platform is carried out for 60 m water depth with different several conditions. The overall topside member's weight is designed for 200 tonnes. The topsides design is as illustrated in Fig. 3.

The platform will be analysed for load combination of dead load, live load and environmental loads to provide real life situations. The platform will be firstly analysed for eight different directions (omni-direction) of environmental loads with the three wired guys are attached to the caisson. The platform then will be analysed for free standing platform where all the wired guys are removed to compare the deflection between these two conditions.

The caisson displacements to the combined load cases and number of wired guys attached to the platform are studied.

Displacement of the Platform

Figure below illustrated one of the directions of the wind force, wave force and current when subjected to the platform.

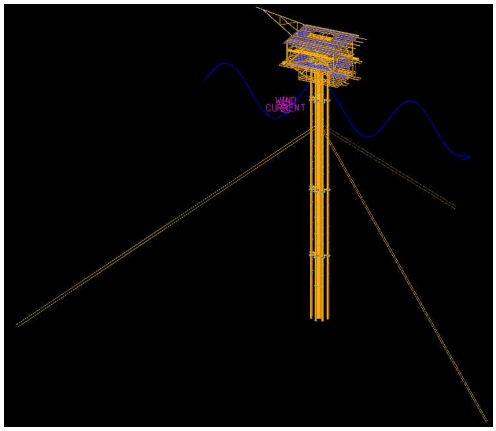


Figure 4. Environmental Loads from 0º

It should be noted that deflections are considered in the total of global X-direction and global Y-direction. The deflections observed are based on the deflections of the caisson of the platform from the mudline level to the top of the caisson excluding the topside.

Fig. 4 illustrated the environmental loads when subjected from 0º direction of the platform. The estimated deflection due to the environmental loads from each direction is illustrated in the Fig. 5-12 below.

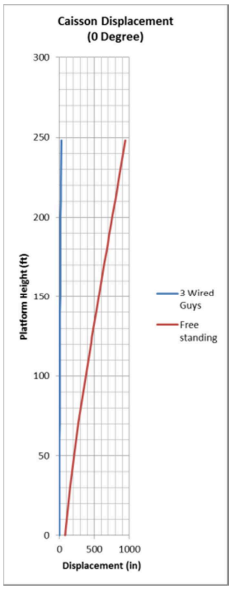


Figure 5. Caisson Displacement at 0º Direction

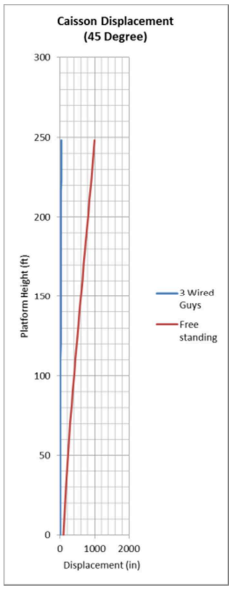


Figure 6. Caisson Displacement at 45º Direction

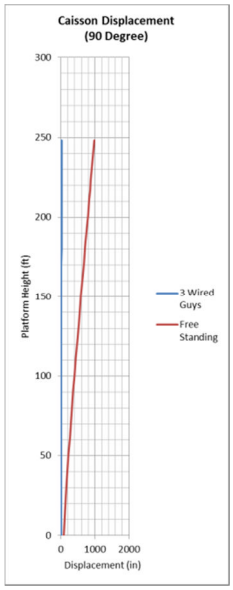


Figure 7. Caisson Displacement at 90º Direction

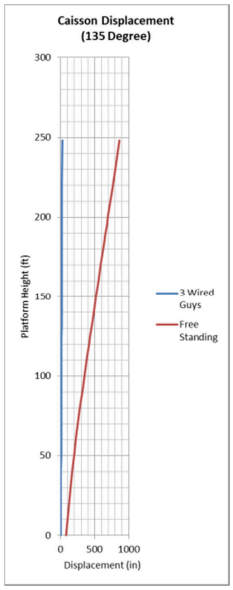


Figure 8. Caisson Displacement at 135º Direction

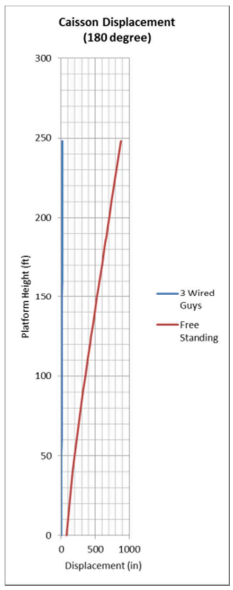


Figure 9. Caisson Displacement at 180º Direction

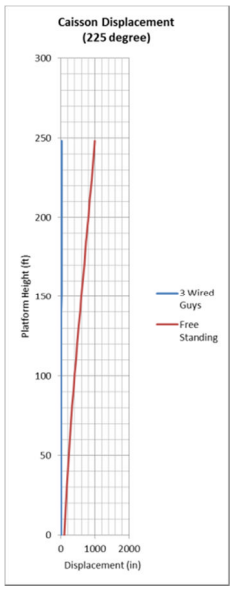


Figure 10. Caisson Displacement at 225º Direction

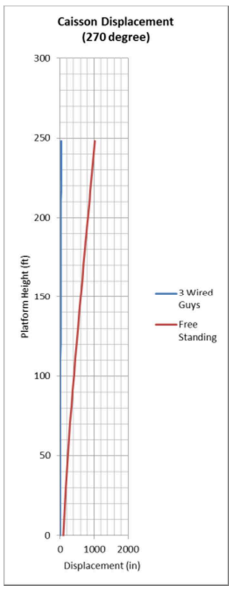


Figure 11. Caisson Displacement at 270º Direction

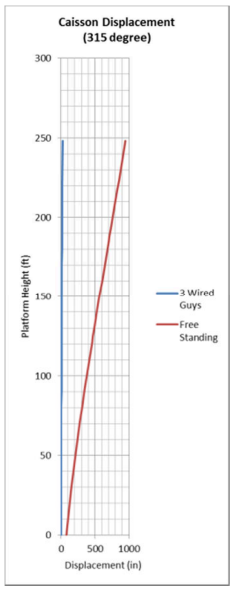


Figure 12. Caisson Displacement at 315º Direction

From the figures above, we observed that the pattern for caisson displacement is alike for all environmental loads directions. When the wired guys are removed from the caisson, the deflection of the caisson is much greater than the deflection of the caisson when supported by wired guys. In the design, the platform will be considered as collapsed when the deflection of the members of the caisson is greater than 1 meter. In this analysis, we can observe that the platform is collapsing in all environmental loads direction during free standing condition.

The maximum displacement of the caisson when supported by 3 wired guys is 89.53 cm (35.25 in) when subjected to environmental loads from 270º direction. Meanwhile, the maximum displacement of the caisson during free standing condition is 2598.12 cm (1022.88 in) when subjected to the environmental loads from the same direction.

From the analysis, we observed that displacement of the caisson also occurred at the mudline level. The maximum caisson displacement is 4.45 cm when subjected from 135º direction environmental loads for 3 wired guys condition. The displacement of the caisson during free standing condition is 224.78 cm when subject to the environmental loads from 270º direction. The displacement occurrence is based on the strength of the soil during the analysis which will not be discussed in this present analysis.

Conclusions

In this present analysis, the deflection of the caisson is studied for omni-direction when subjected to environmental loads. From the analysis, the maximum displacement of the caisson is 89.53 cm and 2598.12 cm for 3 wired guys and free standing condition, respectively. Additionally, we can observe that the critical condition is when the environmental loads are coming from 270º for both conditions.

The platform is considered as collapsed when the caisson has a displacement more than 1 m. In this case, it is noted that the platform is collapsing when the wired guys are removed from the platform. We can conclude that the importance of the wired guys to the monopod platform in structural reliability which provides the stability of the platform during extreme conditions.

References

[1] E. Fakas, S. Tuty, B.F. Ronalds, R. Pinna, Case Study: Effects of Wind Loading on Structural Reliability, Proceedings of the Eleventh (2001) International Offshore and Polar Engineering Conference (2001)

[2] M. Pilotto, B.F. Ronalds, R. Stocker, Dynamic Response of Shallow Water Monopod Platforms, Proceeding of OMAE'02 21st International Conference on Offshore Mechanics and Artic Engineering (2002).

[3] N. H.,S. Mandal, S. B., S. Rao, Analysis of Offshore Jacket Platform, Natl. Conf. on Sustainable Water Resources Management (2010).

[4] Chakrabarti, S. K., Hydrodynamics of Offshore Structures, Eastbourne, (2001).

[5] M. Pilotto, B.F. Ronalds, R.Sticker, The Dynamic Sensitivity in Monopod Platforms in the Wave Zone, AIOM.

[6] B. F. Ronalds, D. G. Cosson, R. Pinna, G. K. Cole, Towards Monopod Design Criteria for Uniform Reliability, Journal of Petroleum Science and Engineering (2007).

Applied Mechanics and Materials Vol. 567 (2014) pp 301-306
© (2014) Trans Tech Publications, Switzerland
doi:10.4028/www.scientific.net/AMM.567.301

Seabed Condition from Single Beam Echo Sounder from Penang Port, Malaysia

Wan-Tian Yew[1,a], Wei-Haur Lam[1,b], Cindy Soon[1,c] and Ruslan Aziz[2]

[1] Department of Civil Engineering, Faculty of Engineering, University of Malaya, 50603, Kuala Lumpur, Malaysia
[2]Marine Operations & Hydro, SBU Marine, Penang Port Sdn. Bhd., North Butterworth Container Terminal, 12000 Butterworth, Penang, Malaysia

yew_wantian@hotmail.com[a], wlam@um.edu.my[b], cindysoon87@gmail.com[c]

Keywords: Seabed Condition, Single Beam Echo Sounder, Penang Port

Abstract. Ship's propeller wash induced scour is a well-known engineering problem for port structures along the shoreline. However, insufficient recorded data makes it difficult to justify that ship's propeller wash induced scour is taking place in Malaysia's major ports. This study reported the seabed condition of the two wharves in Penang Port using Single Beam Echo Sounder (SBES) data. The presence of seabed scour due to ship manoeuvring is investigated based on seabed data. The results showed that Penang Port is experiencing a severe siltation problem instead of ship's propeller wash induced scour impacts.

Introduction

Increasing shipping activities will always lead to the need of using larger ship's propeller to improve its ships' speed and manoeuvrability. An obvious consequence of using large ship's propeller is the increase of interaction between vessel flow and seabed and causes seabed scour which will eventually exposes coastal structure foundations to saline water. The potential damage by propeller jet to the harbour's structures has been described by Whitehouse[1], Sumer and Fredsøe[2] and Gaythwaite[3]. These authors investigated the action of the propeller jet to the seabed scouring. Hamill and Johnston[4], Hamill et al. [5] and Lam et al [6,7,8,9,10,11,12] described the propeller jet flow characteristics on how the flow is interacts with the sea floor.

The study of ocean floor topography is important as the initial step to determine the influence of ship propeller wash. Sediment transport undersea is the primary source that affects the seabed topography. Changes in seabed morphological can be loosely classified into two groups which are seabed scouring and seabed sedimentation. These changes will affect the seabed topography. Therefore, in order to detect the changes on seabed level and to uphold the application of seabed, hydrographic surveys play an important role to define this. Hydrographic surveys are important to tabulate bathymetry grids along coasts, ports and harbours. In common practice, there are different methods used to tabulate seabed level which are Echo Sounder Light Detection & Ranging (LIDAR), Ray (Theodolite), Sonar System, and GPS satellite as discussed in Sciortino [13].

Peninsular Malaysia has a total coastal line of 2,068 kilometres which plays important roles on fisheries, rearing natural habitats and maritime activities. Therefore, monitoring the morphological changes on seabed level is important in managing the coastal activities and maintaining the infrastructures along the coastal line. Numerous factors affects the changes in seabed morphological such as a ship's propeller induced scour, coastal erosion, siltation, hydrodynamic forces and biological activities.

The current study focused on the northern port in Malaysia which is Penang Port. Two wharves were selected from the Penang port which are the North Butterworth Container Terminal (NBCT) and Dermaga wharf (also known as Swettenham Pier). These two berths actively serve as the northern region container and cruise ship destination in Malaysia. The geographical map of Penang Port in the Straits of Malacca is shown in Figure 1. Soon and Lam[14] stated that the increasing shipping activities in Penang Port increase the potential of scouring effects from the ship's propeller

wash. Therefore, this paper will provide an overview of seabed morphological changes on seabed level along the coastal line in Penang port to observe the presence of ship's propeller scour wash in the north region of Malaysia.

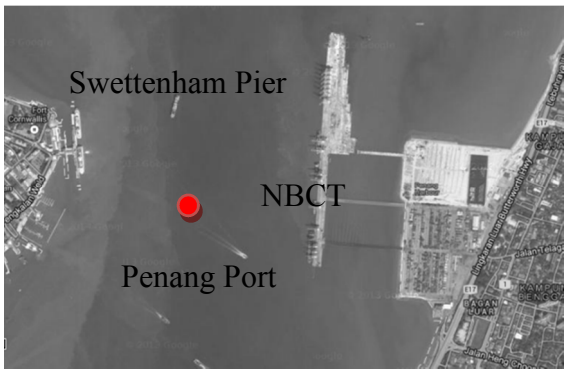


Figure 1: Location of Penang Port, Malaysia

Methodology

The data collection was done by Marine Department of Penang port in the year 2011 to 2013. For each survey, one month duration is taken to run the hydrographic survey with data acquisition and analysis.

Measurement system and procedure. The seabed level measurement was taken with various hardware and software which are Single Beam Echo Sounder (SBES), Differential Global Positioning System (DGPS), Sound Velocity Probe (SVP), Tide Guage, Trimble HydroPro software, HydroPro Navedit software, Trimble Terramodel software and AutoCAD software. The functions of the both hardware and software used are listed in table 1.

Table 1: Summary of functions of hardware and software used in hydrographic survey

Equipments/Software	*Functions*
Hardware	
Single Beam Echo Sounder (SBES)	To tabulate ocean topography
Differential Global Positioning System (DGPS)	Fix the vessel position during hydrographic survey
Sound Velocity Probe (SVP)	Measure the sound velocity
Tide Gauge	To measure height and time of tide
Software	
Trimble HydroPro	To process hydrographic data
HydroPro Navedit	To edit depth related data
Trimble Terramodel	To process hydrographic data
AutoCAD	To present processed hydrographic data

Hydrographic survey procedures can be generalised into five stages which are preparation before survey, data collection, data processing, data analysis and data rendering as mentioned by Maritime Safety Authority of New Zealand [15]. The preparation consists of equipment calibration, correct draught setting to ensure that the measurement is taken at the depth below sea surface but not the depth below the transducer. Data collection focuses on verify and log the collected data into accurate parameters so that the data can further be processed. Data processing consists of selecting the appropriate data and to ensure the data is in appropriate formats. Then, data analysis and rendering is the quality checking of the entire work and the conversion into user friendly formats such as reports and study records for further use.

Single beam echo sounder (SBES). SBES has been being practicing since the 1990's, and it is still the most economical method to be used to tabulate the ocean topography. SBES method only requires a transducer for both transmission and receptions when compares to other methods. However, with the advancement of the technology, the SBES method now incorporates with motion sensors such as DGPS to improve the results. The accuracy of SBES method can achieve sub-decimal in the shallow water analysis which generally less than 200m depth as studied by the International Hydrographic Oraganisation (IHO) [16, 17]. In addition, data acquisition software such as Trimble HydroPro, HydroPro Navedit and Trimble Terramodel are also used along with SBES to maximise the data presentation and the accuracy when tabulating the echogram. The typical SBES schematic diagram is showed in figure 2.

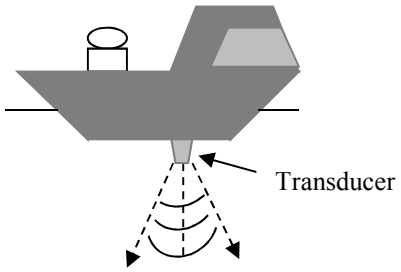


Figure 2: Typical single beam echo sounder (SBES)

Geographical characteristic. Malaysia is well known with their soft compressible alluvial deposits on the mainland and so the soil along the shoreline. According to Paramananthan and Zauyah [18, 19] areas along the peninsular Malaysia especially marine and estuarine area, are widely filled with clay and silt layer of soil. Clay soil has different arrangement when they are in different state. According to Das [20], clay soil has van der Waals forces act as the attractive forces and their spacing between the particles is very small and causes the attractive force is greater than the repulsive force. Thus, clay and silt soil has a sticky behaviour compared to sandstone.

Results and Discussions

From the given hydrographical data, sediment transport of the soil that alters the seabed level is able to observe through analysis. With these results, engineers are able to determine the occurrences of ship's propeller scour or sedimentation effects along the Penang Port shoreline.

Seabed level of Penang port. The seabed level data of Penang Port are taken from two wharves which are North Butterworth Container Terminal (NBCT) and Swettenham Pier from year 2011 to 2013 by using SBES method incorporated with aforementioned hardware and software. The areas of study for both wharves namely A1 and A2s are shown in figures 3 and 5. The contour maps of the area of study for both wharves are tabulated using Golden Surfer, a contour map plotting software.

NBCT. According to Penang Port [21], NBCT contains a total of six berths which measured in length of 1500m. NBCT has a design depth of 12.3m for the maritime activities. The area of study, A1 and contour plot of NBCT is shown in figures 3 and 4. From the contour plot, it was found that

the seabed level increased from year 2011 to 2012 and then decreased in year 2013. However, in overall, there is no obvious propeller scour effects were observed.

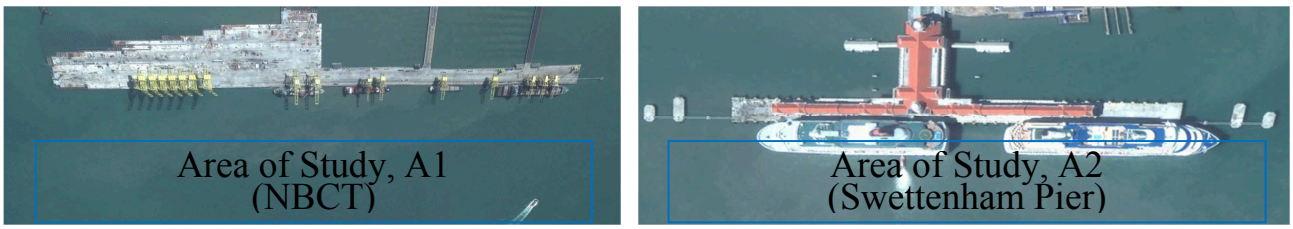


Figure 3: NBCT and Swettenham Pier, Penang

Swettenham Pier. The area of study, A2 and of Swettenham Pier is shown in figure 5. Swettenham Pier has design depth in a range of 9.3m to 11.3m and is shorter in length when compared with NBCT which only 366 metres. It shows minor siltation effects from year 2011 to year 2012, then a decrease on seabed level depth in year 2013. As same with NBCT, no significant scour impact contributed by the ship's propeller is reported.

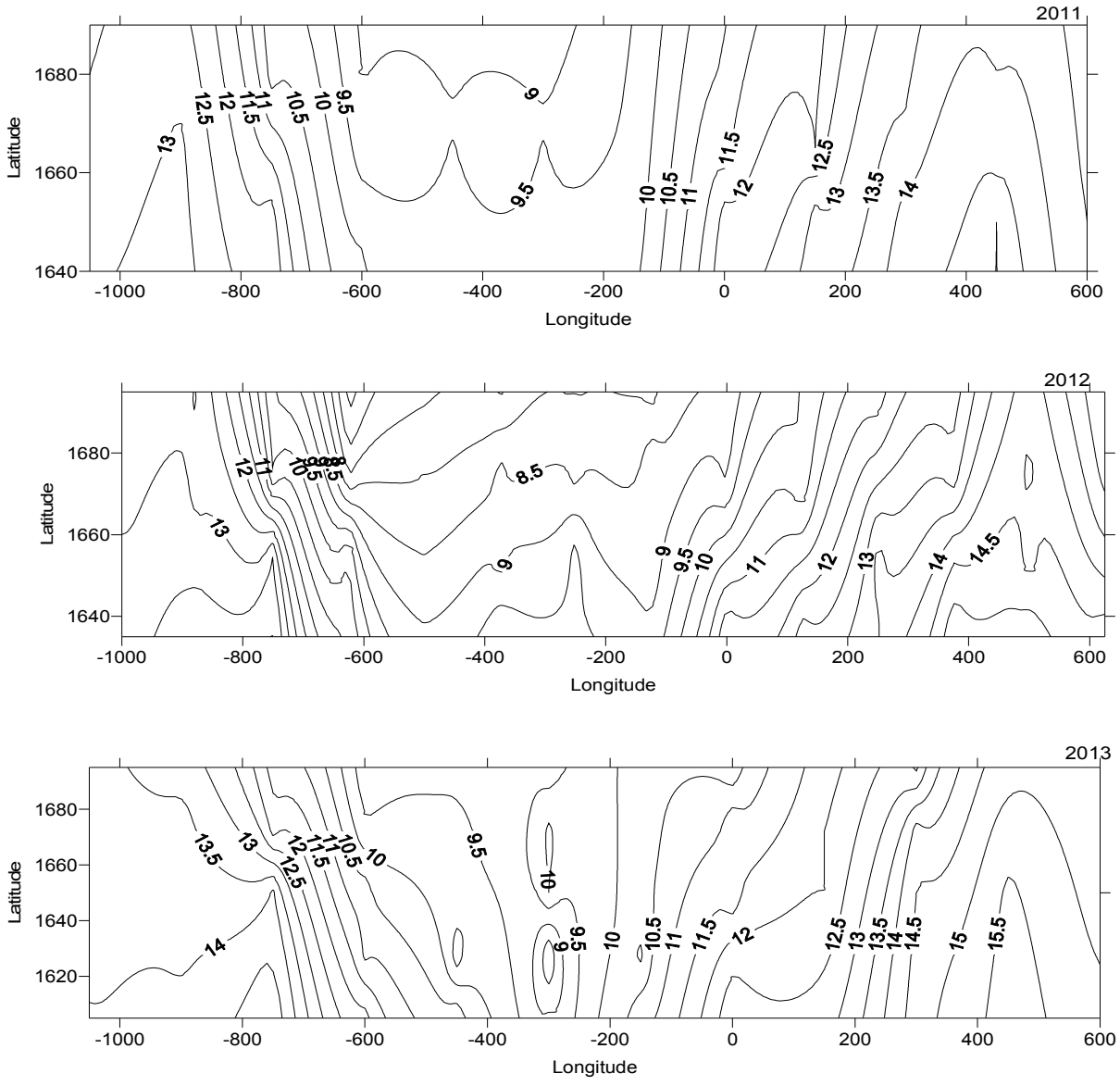


Figure 4: Contour plots for NBCT for year 2011-2013

Sediment transport. In overview, sediment transport especially sedimentation does occur along the both wharves at Penang Port. According to Penang Port Sdn. Bhd. [22], the increase of seabed level is due to the net southward littoral drift contributes approximately 200,000 m^3 volume of soil yearly. Secondly, the siltation problem is also due to the natural behaviour of clay and silt soil type. According to Sutherland et al. [23], due to the flocculation behaviour of clay in saline water, clay materials will promote settling behaviour than transported away. Thirdly, the shipping activities at Penang Port as mentioned in Soon and Lam [14] is far lesser than those major ports that experiencing ship propeller scour problem in the United Kingdom and Europe. The descending of seabed level in year 2013 is due to the agitation dredging done by the port authority to maintain the seabed level for the maritime activities. The continuously increase of sediments along the shoreline of Penang Port has caused the port management to increase the frequency of their dredging maintenance. This directly increases the total cost on managing the port. Therefore, further research is required to study the remedies to overcome this problem.

Conclusion

The analysis of seabed condition along the Penang Port shoreline is presented. The overview of seabed morphological changes along the coastal line of Penang Port is also discussed. Based on analysis, there are no significant ship's propeller scour impacts along the Penang Port. Instead of scouring problem, Penang Port is exhibiting siltation problem. Further research on the remedies to overcome the siltation problem will be carried out to ensure the continuous improvement of this field.

Acknowledgement

The authors wish to extend their gratitude to the Ministry of Higher Education for the financial support under the UM/MOHE High Impact Research Grant (H-1600-00-D000047) and technical discussion with Penang Port Sdn. Bhd.

References

[1] Whitehouse, R., 1998. Scour at Marine Structures: A Manual for Practical Applications. Thomas Telford Publisher, ISBN: 0727726552.

[2] Sumer, B.M., Fredsøe, J., 2002. The Mechanics of Scour in the Marine Environment. World Scientific Publisher, ISBN: 9810249306, 552p.

[3] Gaythwaite, J., 2004. Design of Marine Facilities for the Berthing, Mooring, and Repair of Vessels. ASCE Publications, ISBN: 0784407266 531 pages.

[4] Hamill, G.A., Johnston, H.T., 1993. The decay of maximum velocity within the initial stages of a propeller wash. J. Hydraul. Res. 31 (5), 605–613.

[5] Hamill, G.A., Stewart, D.P.J., Johnston, H.T., 1999. Propeller wash scour near to quay structures Journal of Waterway, Port, Coastal and Ocean Engineering. Am. Soc. Civ. Eng. 125 (4), 170–175, Jul/ Aug 1999.

[6] Lam, W., Hamill, G.A., Robinson, D.J., Raghunathan, S., 2010. Observations of the initial 3D flow from a ships propeller. Ocean Eng. 37, 1380–1388.

[7] Lam, W., Hamill, G.A., Song, Y.C., Robinson, D.J., Raghunathan, S., 2011a. A review of the equations used to predict the velocity distribution within a ship's propeller jet. Ocean Eng. 38 (1), 1–10.

[8] Lam, W., Song, Y.C., Raghunathan, S., Hamill, G.A., Robinson, D.J., 2011b. Investigation of a ship's propeller jet using momentum decay and energy decay. Can. J. Civ. Eng. 38, 605–615.

[9] Lam, W., Hamill, G.A., Song, Y.C., Robinson, D.J., Raghunathan, S., 2011c. Experimental investigation of the decay from a ship s propeller. Chin. Oceanic Eng. 25, 265–284.

[10] Lam, W.H., Hamill, G.A., Robinson, D.J., Raghunathan, S., 2012a. Semi-empirical methods for determining the efflux velocity from a ship's propeller. Appl. Ocean Res. 35, 14–24.

[11] Lam, W.H., Hamill, G.A., Robinson, D.J., Raghunathan, S., Song, Y.C., 2012b. Analysis of the 3D zone of flow establishment from a ship's propeller. KSCE J. Civil Eng. 16 (4), 465–477.

[12] Lam, W.H., Robinson, D.J., Hamill, G.A., Zhao, J.F., Jia, M., 2012c. Time-averaged velocity and turbulence intensity at the initial downstream flow from a six bladed ship propeller. Ocean Eng. 51, 85–93.

[13] Sciortino, J.A., 2010. Fishing harbour planning, construction and management. FAO Fisheries and Aquaculture Technical Paper. No. 539. Rome, FAO. 2010. 337p.

[14] Soon, C., Lam, W.H., 2013. The growth of seaports in Peninsular Malaysia and East Malaysia. Ocean and Coastal Management 78, 70-76.

[15] Maritime Safety Authority of New Zealand, 2004. Final guidelines of good practice for hydrographic surveys in New Zealand ports and harbours. Retrieved on 12.06.13, from, http://www.maritimenz.govt.nz/Publications-and-forms/Commercial-operations/Ports-and harbours/Hydrographic-surveys-guidelines.pdf

[16]International Hydrographic Oraganisation, 2005. Manual on Hydrography, 1st Edition May 2005. Retrieved 01.06.14, from http://www.fig.net/commission4/iho/M-13_Chapter_3.pdf

[17] International Hydrographic Organisation, 2008. IHO standards for hydrographic survey special publication N°44, 5th Edition February 2008. Retrieved on 12.06.13, from. http://www.iho.int/iho_pubs/standard/S-44_5E.pdf

[18] Paramananthan, S., Zauyah, S., 1986. Soil landscape in Peninsular Malaysia. GEOSEA V Proceeding vol 1., Geol. Soc. Malaysia, Bulletin 19, April 1986, pp565-583.

[19] Paramananthan, S., 2012. Keys to the identification of Malaysian soils using parent material. Second edition, March 2012. Published by Param Agricultural Soil Survey (M) Sdn. Bhd.

[20] Das, B.M., 2010. Principles of Geotechnical Engineering. 7th Edition (SI Edition). Published by United States of America: Cengage Learing.

[21] Penang Port, 2013. Retrived on 14.01.14. From, http://www.penangport.com.my/

[22]Penang Port Sdn. Bhd., 2004. Penang harbour siltation study volume 1 draft final report, 2004. Seberang Perai Utara, Penang. Penang Port Sdn. Bhd.

[23]Sutherland, B.R., Barrett K.J., Gingras, M.K., 2013. Clay settling in fresh and salt water. Retrieved from: http://www.ualberta.ca/~bsuther/papers/claysettle/preprint.pdf

Applied Mechanics and Materials Vol. 567 (2014) pp 307-312
© (2014) Trans Tech Publications, Switzerland
doi:10.4028/www.scientific.net/AMM.567.307

System Reliability of Existing Jacket Platform in Malaysian Water (Failure Path and System Reliability Index)

V. J. Kurian[1,a], M. M. A. Wahab[2,b], T. S. Kheang[3,c], M. S. Liew[4,d]

[1,2,3,4]Civil Engineering Department, UniversitiTeknologi PETRONAS, Tronoh, Malaysia

[a]kurian_john@petronas.com.my, [b]mubarakwahab@petronas.com.my, [c]kheang@outlook.com, [d]shahir_liew@petronas.com.my

Keywords: System Reliability Index, System Probability of Failure, Failure Paths, Reliability Assessment Model.

Abstract. The objective of this work is to determine the structural reliability of an existing jacket platform in Malaysia, by determining the system probability of failure and its corresponding reliability index. These two parameters are important indicators for assessing the integrity and reliability of the platform, and will point out whether the platform is suitable for continued operation. In this study, pushover analysis is used to determine possible failure paths of the structure, while First Order Reliability Method (FORM) and Simple Bound Formula are used to determine the failure probability and reliability index. Three failure paths of the platform are established. The reliability index of these paths is found with the highest Reliability Indexto be 18.82 from the 315-degree path, while the system reliability index is 9.23. This illustrates that the platform is robust and the chances of collapse is very small.

Introduction

In Malaysia, there are approximately over 200 oil and gas platforms to support the industry[1]. Majority of them are fixed offshore platforms which are located in the shallow waters. The design life for fixed offshore platforms, according to PETRONAS Technical Standards is 30 years. Nonetheless, some of the platforms have exceeded the design life and are still in operation. Thus, there has been lot of effort recently to assess the safety and integrity of those structures.

Among the popular methods to determine the excess strength of a platform is Reserved Strength Ratio (RSR) method. It is the ratio of platform ultimate strength over the platform design strength, which illustrates the excess load that a platform can take. However, it does not decisively show how reliable the platform is and its corresponding probability of failure.

Reliability analysis can be done either on component level or system level. At component level, the analysis measures only the strength ratio or the failure probability of the component, and thus it does not show the integrity of the system as a whole. At system level, the integrity and safety of the system are considered. The system reliability analysis is employed to determine dominant failure paths, the failure probability of each failure paths, and the combined probability of failures of those failure paths. The reliability index can then be obtained from the system probability of failures.

This study aims to determine the system reliability index and its corresponding probability of failure of an existing jacket platform in Sarawak Operation region with a water depth of 94.6m. Aging parameters of the platform was assumed insignificant for the purpose of this initial study.

Methodology

System Reliability analysis is a relatively new area with extensive ongoing researches in the field. For statistically determinate structures, in some instances the reliability of individual members is sufficient since the failure of one member will lead to the whole structure failure. However, this is not the case for highly redundant structures. The failure of one or few members does not necessarily result in the collapse of the system. In that sense, the system will contain numerous failure paths. A failure path is defined as the failure sequence of members in the structure until it totally collapses. Based on the random nature of load and resistance distributions, some failure

paths are more likely to occur than other. The probability of those failure paths and the method of determinations are the basis of system reliability analysis.

A structure especially for complex one can contain a large number of possible failure paths. Including all the possible failure paths in the analysis is infeasible and inefficient, since many of the failure paths have a very low probability of occurrence. A variety of methods to determine dominant failure modes are discussed in[2].The methods are divided into three approaches: "Enumeration Approach", "Plasticity Based Approach" and "Simulation Based Approach". In "Enumeration Approach", failure trees are generated by extending the sequence of element failures step by step until the system collapses. Some examples of the approaches are incremental loading method (pushover analysis) and branch-and-bound method. In incremental loading method, the failure modes are generated by incrementally factoring the load to cause sequence of member failures. The method is deterministic, and can obtain crucial failure paths with few repetitions of structural analysis. However, with this method not all dominant failure paths can be determined. The branch-and-bound method, on the other hand, employs probabilistic search algorithm, which searches possible failures mode by considering their probabilities of occurrences. Though the branch and bound method is theoretically rigorous, the required computing power can be very high.

In this study, pushover analysis is used to determine most probable failure paths. The environmental load was applied from three critical directions namely 270^o, 315^o and 360^o relative to platform North.

Limit State Function and Probability of Failure. In this study, the limit state functionas in Eq. 1 is derived from utilization ratio for cylindrical members subjected to combined compression and bending.The adopted utilization ratio formula is according to API-RP2A WSD[3].

$$g(\cdot) = 1.0 - \left(\frac{f_a}{F_a} + \frac{f_b}{F_b} \right). \qquad \text{(Equation 1.)}$$

Where:

- f_a and f_b are axial stress and bending stress respectively, obtained from structural analysis.
- $F_a$and F_b are the resistance parameters determined from API RP 2A-WSD code equations.

The limit state function divides the surface into two different regions which are safe region, where $g(\cdot) \geq 0$ and unsafe region, where $g(\cdot) < 0$. The probability of failure, P_f, can be determined from Eq. 2 with X as random variables.

$$P_f = P[g(X) < 0]. \qquad \text{(Equation 2.)}$$

When X is normally distributed and uncorrelated, the reliability index is determined from Eq. 3.

$$\beta = -\phi^{-1}(P_f). \qquad \text{(Equation 3.)}$$

Similarly, P_f can be calculated from Eq. 4.

$$P_f = 1 - \phi(\beta) = \phi(-\beta) \qquad \text{(Equation 4.)}$$

Where $\phi(\cdot)$ is the standard normal distribution.

In general, the probability of failure P_f,is given by the integral as in Eq. 5.

$$P_f = \int \ldots \int_{g(\cdot)<0} f_x(x_1, x_2, \ldots, x_n)\, dx_1 dx_2 \ldots dx_n \qquad \text{(Equation 5.)}$$

where f_x $(x_1,x_2,....,x_n)$ is the joint probability density function for the basic random variables, $X_1,X_2,\ldots,X_n$ and the integration is conducted over the failure region, $g(\cdot)<0$.

Since the direct integration of Eq. 6 is extremely complicated, methods such as FORM (First-Order Reliability Method) is used to evaluate when the limit state function is a linear function or uncorrelated normal variables or when the non-linear limit state function is represented by a first order (linear) approximation with equivalent normal variables. In this study, FORM will be employed to determine the probability of failures of the component.

Load and Resistance Parameter

Wave: Two-parameter Weibull distribution is used to fit the significant wave height data,*Hs* for the platform. From that, shape and scale parameter for the distribution is obtained and used to generate random loads.

Current: Similarly, Weibull parameters for current speed at water surface are derived.The current velocity is independently generated from the wave height as wave height and current velocity is not always correlated due tothe random nature of the sea.

Wind: Wind is determined as static point load and applied on the topsides. Wind is assumed to be deterministic and not a random parameter for this study purpose.

Resistance Variables: The resistance parameters used in this study is based on the study in[4].The axial resistance,F_a,and bending resistance, F_b, of the tubular components are given in API RP 2A-WSD code.The random parameters (diameter, wall thickness and yield strength) are used to determine both $F_a$and $F_b$which will be the inputs of the limit state functions.

Analysis Method

Structural Idealization:A structural system usually can be modelled as a series system, parallel system or combination of both[5].A series system is a system in which failure in a structural element will lead the whole system collapse. For parallel system failure in a member does not usually lead to total system collapse. For complex structures it is assumed that the structural system is a series of parallel systems, in which each parallel system represent a failure path.In this study, the structure is regarded as a hybrid system in which each failure path is a parallel system.

Reliability Bound. In order to determine the probability of failure of the system, approximate techniques or bounding techniques were used. Simple Bounds is described below.

Simple Bound. For convenience, Boolean variables are used. Let S be a system with n failure elements $E_1,\ldots,E_i,E_{i+1},\ E_n$. For each failure element$E_i,i=1,\ldots,n,$a Boolean variable $e_i$is defined by:

$$e_i=\begin{cases} 1, \text{ if the failure element is in a nonfailure state.} \\ 0, \text{ if the failure element is in a failure state.} \end{cases}$$

For series system, the simple bound is given by:

$$\max_{i=1,\ldots,n} P(e_i=0) \le P_{fs} \le 1-\prod_{i=1,\ldots,n}\left(1-P(e_i=0)\right). \qquad \text{(Equation 6.)}$$

The lower bound in Eq. 6 is equal to the exact value of P_{fs} if there is full dependence between all elements and the upper bound correspond to no dependence between any pair of elements. When the probability of failure of one element is predominant in relation to the other failure elements then the probability of failure of series system is approximately equal to the predominant probability of failure and the gap between the upper bound and lower bound is narrow. However, when the probabilities of failure are in the same order the simple bounds are wide.

For parallel system, the simple bound formula is given by:

$$\prod_{i=i,\ldots,n} P(e_i=0) \le P_{fp} \le \min_{i=1,\ldots,n} P(e_i=0). \qquad \text{(Equation 7.)}$$

The lower bound in Eq. 7 is equal to the exact value of P_{fp} if there is no dependence between any pair elements and the upper bound corresponds to full dependence between all elements.

Component Post-Failure Behavior: In order to accurately determine failure paths, post-failure behavior of the component needs to be modelled correctly. The failure element can be regarded as perfectly brittle element or perfectly ductile element. For brittle element, it will become ineffective after failure. However, if the element is ductile, it still effective and is able to carry some load.

In this study, a semi-brittle model is used as shown in Fig. 1. The member force increases elastically to the member capacity or resistance. After failure, that is, if the axial deformation in the element is increased beyond its failure value, the element force abruptly drops to a fraction, φ, of its unfailed capacity. For this application a deterministic value of φ = 0.4 was used for members failing in compression and φ= 1.0 for tension failure. In other words we assumed ductile tension failure behavior, maintaining the failure load and an abrupt drop to 40 % capacity when failing in compression.

Response Surfaces: Response Surfaces method will be employed to perform the reliability analysis. This approach can reduce the number of structural analysis required for probabilistic analysis. It is divided into two stages which are "Global Response Surfaces" and "Local Response Surfaces."

Global Response Surface: The global response surfaces relate the environmental load to the global response of the structure. The environmental load considered for the global response surfaces in this study is, maximum wave height, $H_{max,}$and current velocity, V_c, while the global response of the structure is the base shear. The wind speed is not taken as one of the variable as its contribution to the load is insignificant. The G function is taken as the global response as in Eq. 8.

$$BS = aH_{max}^2 + bH_{max} + cV_c^2 + dV_c + e\,. \qquad \text{(Equation 8.)}$$

In order to determine the response of the structure, 20 sets of environmental loads (H_s and V_c) were generated based on Weibull distribution.Structural analysis is then carried out. From the analysis, 20 sets of base shears are obtained. The coefficients *a,b,c,d and e* in Eq. 8are determined using Matlab Curve Fitting Tool.

Local Response Surface: The local response surface, which are $f_a$andf_b, relate the global response of the structure to the local response of each member. Second-degree polynomial equation is used as in Eq. 9 and 10 respectively.

$$f_a = aBS^2 + bBS + c\,. \qquad \text{(Equation 9.)}$$

$$f_b = aBS^2 + bBS + c\,. \qquad \text{(Equation 10.)}$$

The local response surface was used in the Limit State Function to determine the probability of failure of the component.

Failure Tree Generation and Reliability: From non-linear collapse analysis, the structure and members are incrementally loaded beyond its yielding capacity. At the point where a member will be no longer able to sustain the load, it will buckle or fracture. The first member that fails in that way is recorded. In order to choose the second failure element, the first member needs to be removed and replaced with fictitious loads. If the first member failed in compression, a pair of load with the magnitude of $0.4xR_C$ will be applied at the joints. If it failed in tension, the load of $1.0xR_T$ will be used instead. Pushover analysis will be then carried out again with this new modified structure, and the first member that fails for this new matrix is the second failure element in the path. The same process is repeated until there are no longer members fail in either buckling or fracture, and the structure fails by collapsing or by having large deflection. In this way, for each direction a path is generated.

In the pushover analysis, before removing that failed element, the member reliability must be obtained. 20 random environmental loadsare generated to determine the global response of the platform. From that, local response is obtained. After that, it is used as the input in the limit state

function along with resistance variables. First Order Reliability Method (FORM) from FERUM 4.1 Program is used to determine the P_f, and reliability index from the limit state function.

After carrying out the analysis, failure tree is produced based on the sequence of the failures for each direction. The failure tree will consist of 3 paths. One failure path will be obtained from each direction, and the probability of failure of those three paths will be determined using the Simple Bound formula for parallel system. The system reliability of the structure is then determined from those three probability of failures using Simple Bound formula for seriessystems.

Results

Failure Tree. Fig. 2 shows the failure tree of the platform. Each branch represents a possible failure path, and each node is the failed member in the corresponding damaged structure. The number in the node is the failure element, identified by two joint numbers.

Probability of Failure and Reliability Index: The probability of failure for the first path, second path and third path are shown in Table 1, Table 2and Table 3 respectively.

The reliability bound for the failure paths determined using Simple Bound for parallel system formula. The lower and upper bound of the three failure paths is shown in Table 4.

Table andTable 6 show system reliability and probability of failure based on lower bound and upper bound respectively.Simple Bound for Series System is used to determine those parameters, which are based on the upper and lower bound of those failure paths.

The third path has the highest reliability index, β=18.82, and thus lowest probability of failure. This may be due to that the load of the path is applied at the corner of the structure, which contains more members. The system reliability index based on the upper bound is found out to be $\beta = 9.23$ with corresponding probability of failure of $P_f = 1.36\text{E} - 20$

β=9.23 is less than the reliability index determined on a platform in Sotong Field as in [6]. The author found that the β for the platform is 10.91. Nonetheless, it should be noted that in this study safety factor is employed in the limit state equation, while it was not in [6].

Conclusion

In this study, three failure paths of the platform are established. The reliability index of those paths are also found with the highest β of 18.82 from 315-degree path, while the system reliability index is β=9.23. This illustrates that the platform is robust and the chances of collapse is very small.

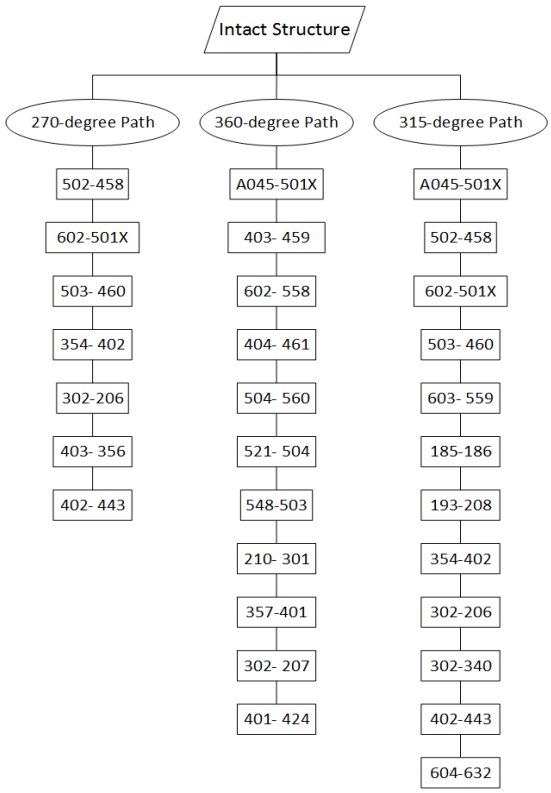


Figure 2. Failure Tree

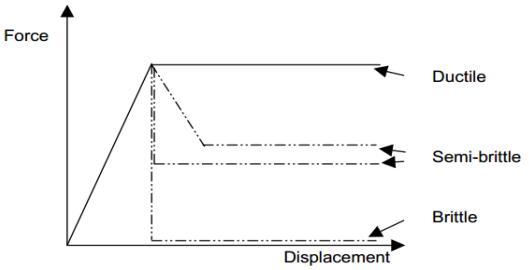


Figure 1. Element Failure Model

Table 1. First Failure Path

Sequence	Member	β	P_f
1	502-458	3.54	1.99E-04
2	602-501X	6.62	1.80E-11
3	503-460	6.70	1.03E-11
4	354-402	4.73	1.13E-06
5	302-206	4.18	1.47E-05
6	403-356	4.50	3.50E-06
7	402-443	9.23	1.36E-20

Table 2. Second Failure Path

Sequence	Member	β	P_f
1	A045-501X	6.29	1.62E-10
2	403- 459	11.98	2.29E-33
3	602- 558	13.50	8.60E-42
4	404- 461	12.21	1.39E-34
5	504- 560	11.90	6.51E-33
6	521- 504	10.06	4.03E-24
7	548-503	8.87	3.68E-19
8	210- 301	8.76	1.01E-18
9	357-401	12.66	5.18E-37
10	302- 207	6.07	6.54E-10
11	401- 424	5.36	4.07E-08

Table 3. Third Failure Path

Sequence	Member	β	P_f
1	A045-501X	7.00	1.26E-1
2	502-458	6.00	9.65E-10
3	602-501X	7.21	2.73E-13
4	503-460	10.02	6.23E-24
5	603-559	9.42	2.27E-21
6	185-186	13.02	4.83E-39
7	193-208	3.43	2.97E-04
8	354-402	18.82	2.79E-79
9	302-206	17.24	7.25E-67
10	302-340	2.20	1.38E-02
11	402-443	1.91	2.82E-02
12	604-632	8.56	5.76E-18

Table 4. Failure Probability and Reliability Index of Each Path

Path	Lower Bound		Upper Bound	
	P_f	β	P_f	β
1st Path	2.93E-62	16.6105	1.36E-20	9.23
2nd Path	5.95E-263	34.6217	8.60E-42	13.50
3rd Path	3.05E-285	36.0726	2.79E-79	18.82

Table 5. System Probability of Failure and Reliability Index Based on Lower Bound

Lower Bound		Upper Bound	
P_f	β	P_f	β
2.93E-62	16.61	0	inf

Table 6. System Probability of Failure and Reliability Index Based on Upper Bound

Lower Bound		Upper Bound	
P_f	β	P_f	β
1.36E-20	9.23	0	inf

References

[1] N. S. Potty and M. K. B. M. Akram, "Structural Integrity Management for Fixed Offshore Platforms in Malaysia," *World Academy of Science, Engineering and Technology,* 2009.

[2] S. Shao and Y. Murotsu, "Approach to Failure Mode Analysis of Large Structures," *Probabilistic Engineering Mechanics,* pp. 169-177, 1999.

[3] "Recommended Practices for Planning, Designing and Constructing Fixed Offshore Platforms-Working Stress Design," American Petroleum Institute, 2007.

[4] Z. Nizamani, "Environmental Load Factors and System Strenght Evaluation of Jacket Platforms in Offshore Malaysia," Univerisiti Teknologi PETRONAS, 2013.

[5] P. T. Christensen, "System Reliability," in *Engineering Design Reliability Handbook*, CRC Press LLC, 2005, pp. 15-1.

[6] C. C. D. CHIN, "A Reliability Analysis of a Malaysian Jacket Platform," UTM, 2005.

Applied Mechanics and Materials Vol. 567 (2014) pp 313-318
© (2014) Trans Tech Publications, Switzerland
doi:10.4028/www.scientific.net/AMM.567.313

Wave Attenuation of Interlocking Concrete Unit - V (ICU-V)

Ahmad Mustafa Hashim[1, a], Nur Diyana Md Noor[1, b],
Siti Nur Hanis Abdullah[1, c]

[1] Civil Engineering Department, Universiti Teknologi PETRONAS, Bandar Seri Iskandar, 31750 Tronoh, Perak, MALAYSIA.

[a]mustafa_hashim@petronas.com.my, [b]nurdiyana12@yahoo.com, [c]hanis90_11@yahoo.com

Keywords: Wave Transmission; Concrete Armor Unit; ICU-V; Crest Width; Crest Height

Abstract. Wave transmission is one of the components resulted from interaction between incident wave and coastal structure. Factors influencing wave transmission include structure height, crest width and wave condition. This paper presents the analysis of wave transmission and dissipation capability of Interlocking Concrete Unit-V (ICU-V) under different wave conditions and structural parameters based on a 2-D physical model testing. The transmitted wave was reduced more than half of the incident wave when the relative crest height is greater than zero. Structural irregularity of ICU-V promotes breaking of wave on the breakwater crest and the sloping surface. The crest is less effective when the submergence depth greater than -0.20 m or the relative freeboard is greater than -0.286. Overall, ICU-V offers good ability for wave dissipation, which leads to promising performance in sheltering coastal area.

Introduction

Coastal structure such as breakwater is aimed to minimize wave action and provide sheltering effect. Sheltering effect is important especially for navigation and berthing purpose in harbor as well as for other coastal protection measures. Incident wave energy might transform into reflected energy, dissipated by structure, generated into other types of energy and transmitted through and over the structure as shown in Eq. 1 [1] .Waves interact with structure in three different regions as illustrated in Fig. 1 [2] [3]. Ability of structure to attenuate wave is represented by transmission coefficient, K_t, which occurs through (Region R_1) and over the structure (Region R_2). Overtopping results from transmission over the structure in Region R_2. Wave transmission through structure contributed by permeability and run-up in Region R_1 allows a portion of wave energy transmitted behind the structure [3]. Structure configurations and wave climate are among factors governing transmission capability of a structure and control the wave condition in Region R_3.

$$E_i = \pm E_{ref} \pm E_{diss} \pm E_{gen} \pm E_t \tag{1}$$

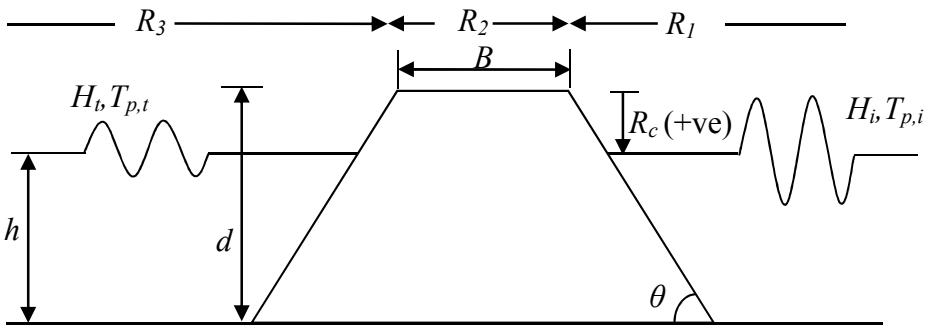


Figure 1: Factors affecting Wave Transmission

Studies have identified various parameters affecting wave transmission. K_t is sensitive to submergence depth, R_c, incident wave height, H_i, and crest width of structure, B [2]. Transmission

coefficient reduces when the ratio of wave height, H_i, over wave length, L increases [4]. Transmission coefficient also increases as the ratio of water depth, d, over wave length, L, decreases, as more waves able to pass over the structure causing turbulent flow in Region R_3 [5]. The crest width, B, can reduce K_t to 0.3 when B is half of the wavelength [6]. Most of the overtopping wave breaks at the crest and results in more energy dissipation in Region R_2 as referred to Fig. 1. In addition, the crest surface also provides additional friction to assist dissipation of wave. Eq. 2 summarizes dimensionless parameters affecting wave transmission [2]. Earlier study by Dick et al. [6] claimed that 36% and 64% of transmitted wave transforms into higher harmonic incident wave due to the limited depth above the structure [7]. Relative crest (R_c /H_s), wavelength and crest width are important factors influencing wave transmission [8] [9] [10]. Transmission over the structure mostly occurred in submerged condition, while transmission through the structure occurred when little or no allowance for overtopping due to high crest level. The transmission through structure is limited by the ratio of effective crest width over nominal material diameter, B/D_{eff} [11].

$$K_t = \frac{H_t}{H_i} = f\left(\frac{R_c}{H_i}, \frac{H_i}{L}, \frac{B_{eff}}{L_o}, \frac{H_i}{D_{eff}}, \frac{B_{eff}}{D_{eff}}, \frac{h_c}{h+H_i}\right) \tag{2}$$

Interlocking Concrete Unit-V (ICU-V). Conventional breakwater uses specific rock sizes for the primary layer of breakwater. Concrete armor unit is used to replace rock when the required rock size is unavailable or the ground could not sustain heavy weight due to geotechnical limitation [12]. Several features are introduced to increase the stability such as interlocking members, friction section, density and placement method [7]. Accropode and Core-Loc armor unit developed by SOGREAH are among the well-known concrete armor units used worldwide. Interlocking Concrete Unit-V (ICU-V) is an armor unit developed by Universiti Teknologi PETRONAS with the primary aim to reduce dependency on weight by incorporating interlocking and friction feature to enhance stability as shown in Fig. 2. ICU-V is designed using 40 MPa unreinforced concrete as suggested by Fleming et al. [13] and it consists of three elongated members with friction enhancer.

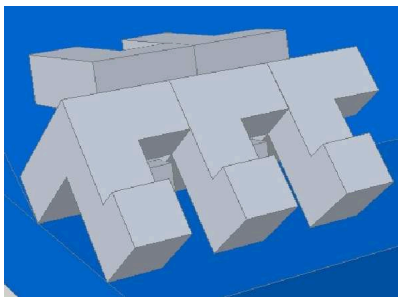


Figure 2: Illustration of ICU-V

Experimental Work

A 2-D physical model test was conducted to measure the dissipation capability of a breakwater armored with ICU-V. The objectives of the experimental work are to investigate the capability of ICU-V in dissipating the incident wave and to analyze the effect of crest level, crest width and wave condition on the wave transmission. The test was conducted in Universiti Teknologi PETRONAS wave flume by varying the significant incident wave height, H_s, peak wave period wave period, T_p and submergence depth, R_c. Individual wave profiles were captured by using wave gauges as indicated by G1 until G6 in Fig. 3. Reflection analysis was performed to separate the incident and reflected wave using method suggested by Masard et al. [14] [15]. The summary of test conditions is tabulated in Table I and equipment setup is shown in Fig. 3.

TABLE I
TEST CONDITION

Parameter	Test Range
Significant Incident Wave Height, H_s (m)	0.05 m - 0.30 m (Δ 0.025 m)
Peak Wave Period, T_p (s)	1.4 s, 1.6 s, 2.0 s
Submergence depth, R_c (m)	0.20 m, 0.10 m, 0 m, -0.10 m, -0.20 m
Crest Width, B (m)	0.30 m, 0.50 m, 0.80 m
Structure Slope	1:1.5
Nominal Diameter, D_{eff} (m)	0.10

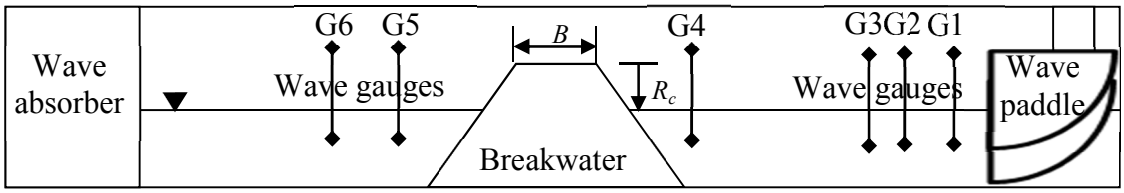


Figure 3: Equipment Setup in Wave Flume

Result and Discussion

Effect of Crest Level on Wave Transmission. High crest level gives a lower transmission as compared to low-crest level as shown in Fig. 4. Most of the wave interacts with sloping surface in Region R_1 and dissipated by permeability of the structure that contributes to K_t less than 0.20. Incident wave energy dissipated by transmission and reflection component when relative crest height, R_c /H_i, greater than 0. Obstruction by crest level and rough structural surface provides resistance to the wave motion and promotes wave breaking. Fig. 5 shows that the transmission coefficient do not differ significantly with varying incident wave condition in emerged condition, where most of the waves interact and feel the obstruction by the structure. Transmission coefficient increase when submergence depth increases due to the decreasing in effective structure height, D_e, in contact with the wave, where D_e is the ratio between crest level, d, and water level $(h+H_s)$. Higher transmission is expected when D_e is less than 1.0 as the wave easily propagate over the structure resulting in K_t higher than 0.30. Crest does not provide friction effect on the wave when the relative freeboard, R_c /d, is more than -0.286 which allows transmission more than 0.70 as shown in Fig. 6.

Application of ICU-V has shown wave reduction around 40% to 70% when the crest level at mean water level. This can potentially reduce the construction cost since the use of low crest level will require less material in reducing almost half of incident wave. High transmission when R_c /d= 0 is resulted from small wave, where H_s /D_{eff} less than 1.0 especially at submerged condition where transmission nearly 1.0 and most of the wave passed over the structure without feeling the crest surface. Reduction in transmission occurred when H_s /D_{eff} is greater than 1.0 because the crest starts to provide friction in overtopping condition for R_c /d= -0.286 and -0.167. Besides, the limited depth at the crest promotes wave breaking that reduces the transmitted wave. Meanwhile, K_t slightly increases when R_c /d is 0.167 and 0.40 which denotes emerged condition, where the wave able to overtop and causes more wave energy passes over the structure.

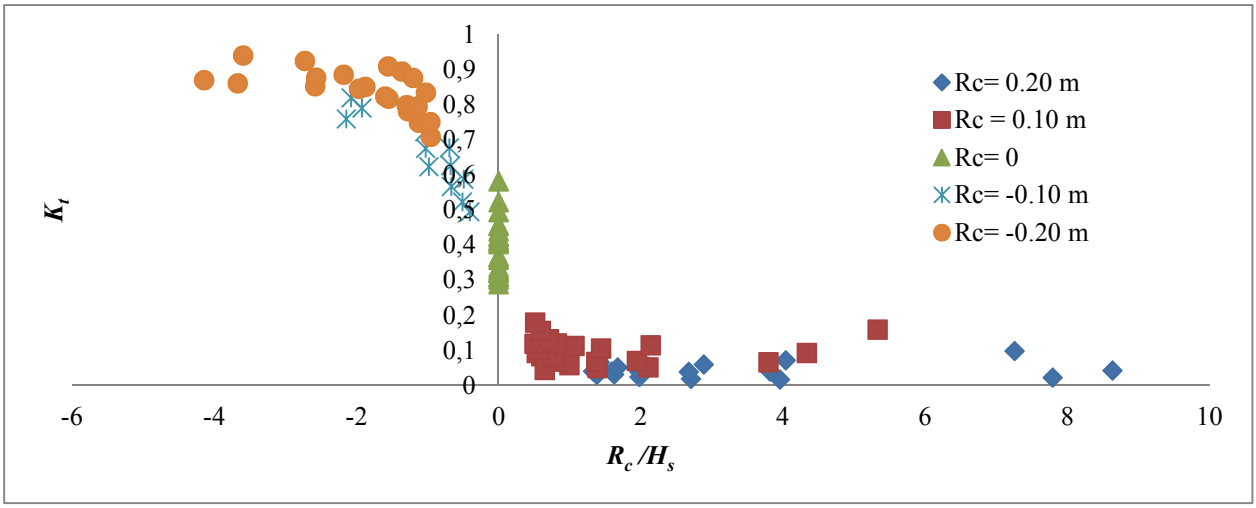


Figure 4: Effect of Submergence Depth in Transmission for T_p 1.4 s – 2 s

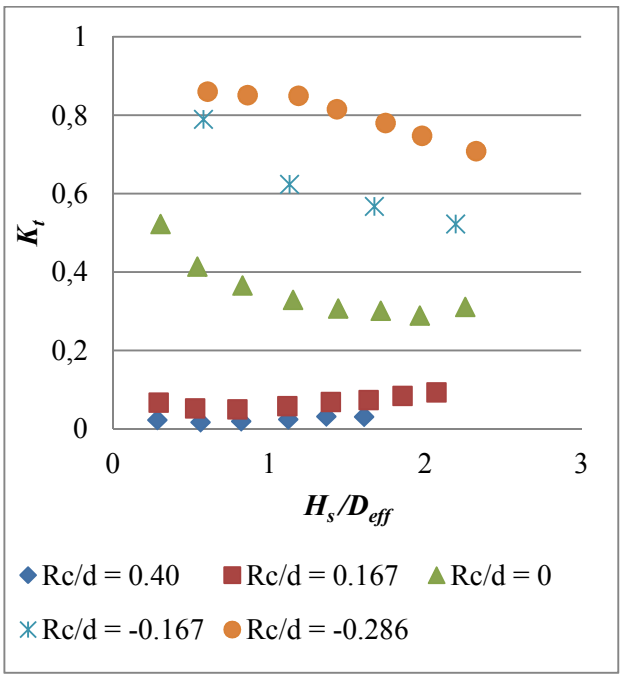


Figure 5: Effect of Wave under Different Crest Level for T_p 1.4 s

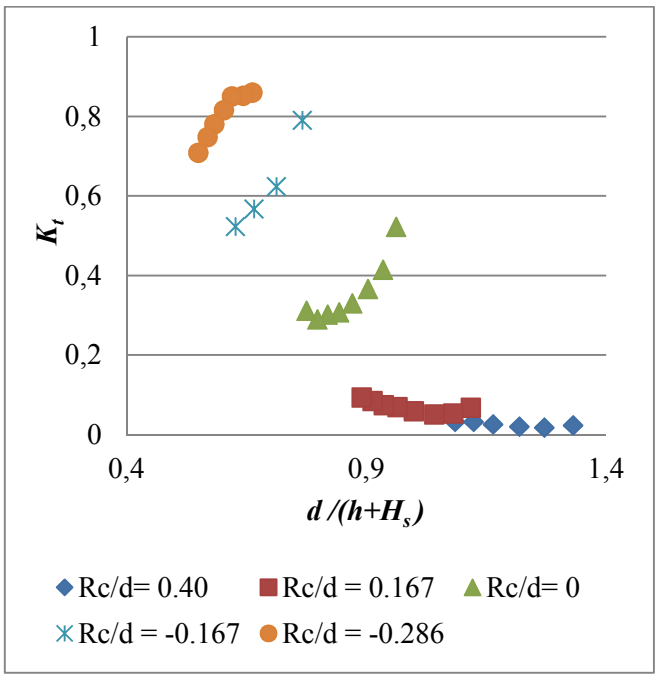


Figure 6: Effect of Effective Depth on Transmission

Effect of Crest Width on Wave Transmission. Crest provides surface roughness and promotes wave breaking. Wider crest gives more resistance and more contact surfaces to wave motion passing over the structure. This is illustrated in Fig. 7 and 8 where the transmission coefficient reduces when the crest width increases, especially when the relative crest is 0 because almost all the waves interact with the crest, and wave is dissipated in Region *R2* as referred to Fig. 1. Crest width of 0.80 m resulted into transmission lower than 0.20 when R_c/H_s is 0. As the crest width increases, the transmission reduces. Transmission of wave reduced to half when crest width increased from 0.30 m to 0.80 m. Effectiveness of crest on transmission is less when R_c/H_s is -4.0 because roughness provided by the crest is no longer obstructing the wave.

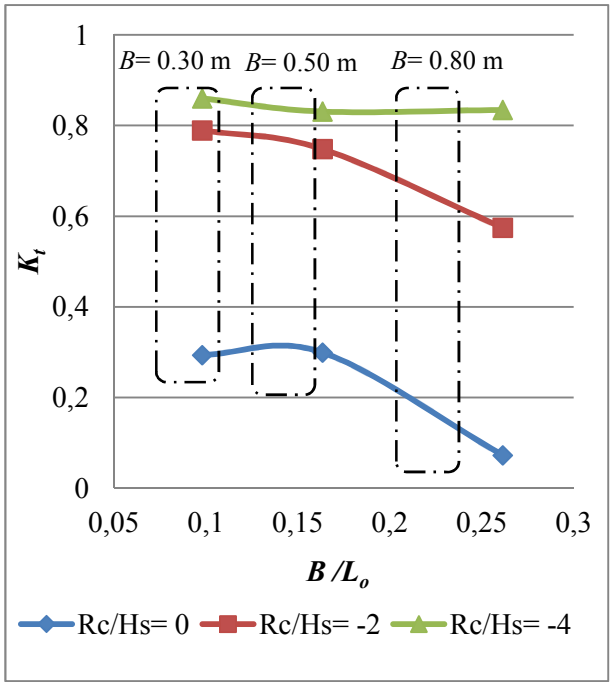


Figure 7: Effect of Crest Width on Transmission for T_p= 1.4 s

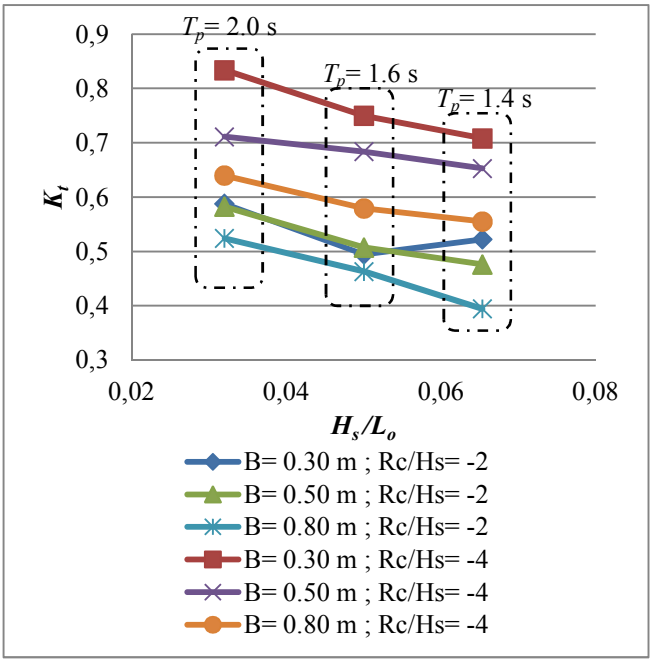


Figure 8: Effect of Wave Period on Transmission for H_s= 0.20 m

Effect of Wave Period on Wave Transmission. Wave transmission also affected by wave period that controls the wavelength and type of wave. The wave steepness (H_i/L_o) is generally used to describe the effect of the wave parameters on transmission. High wave period resulted into long wave length, which leads to higher transmission as indicated in Fig. 8, because longer wave has more potential in passing over the structure. The effect of the wave period is dominant when water depth is higher than crest level ($h>d$). Fig. 8 shows that wave dissipation increases more than 10% as the wave period increases from 1.4 s to 2.0 s. Besides, crest width has a greater effect in wave dissipation for shorter wavelength.

Conclusion

Interlocking Concrete Unit-V shows an initial promising performance in reducing wave transmission more than 40% when submergence depth is zero. The structural irregularity of ICU-V crest surface also plays an important role in dissipation capability of the structure that promotes wave breaking and friction to wave motion. In addition, increasing the crest width improves wave dissipation, especially when the relative freeboard (R_c/d) between -0.167 and 0 or the relative crest height (R_c/H_s) is between 0 and -2.0.

Acknowledgement

The authors would like to thank Universiti Teknologi PETRONAS and Centre of Graduate Studies in funding the study.

References

[1] K.W. Pilarczyk, and R.B. Zeidler, Offshore Breakwaters And Shore Evolution Control, Taylor & Francis, (1996)

[2] S. R. Seabrook, and K. R. Hall, Wave Transmission At Submerged Rubblemound Breakwaters, Coastal Engineering Proceedings 1(26), (1998).

[3] J. Van der Meer, R. Briganti, B. Zanuttigh, and B. Wang, Wave Transmission and Reflection at Low Crested Structures; Design Formulae, Oblique Wave Attack and Spectral Change, Coastal Engineering 52, (2005).

[4] C.K. Sollitt, and R. H. Cross, Wave Transmission through Permeable Breakwater, In Proc. 13th Coastal Engineering Conference, Vancouver, (1972), pp. 1827-1846, ASCE.

[5] A.M. Kamel, U.S. Army Eng. Waterways Exp. Sta. Res. Rep. H-69-1, (1969).

[6] T.M. Dick, and A. Brebner, Solid and permeable submerged breakwaters, Proceeding of 11th International Conference on Coastal Engineering, London, UK, 1968, pp.1141-1158.

[7] H.F. Burcharth, and Z. Liu, Design of DolosArmour Units, Coastal Engineering Conference, Vol.1, (1993) pp. 1053.

[8] J.W. Van der Meer, and K.W. Pilarczyk, Stability of Low Crested and Reef Breakwater, Proc. 22th ICCE, ASCE, New York, N.Y., 1990.

[9] J.W. Van der Meer, I.F.R. Daemen, Stability And Wave Transmission At Low Crested Rubble Mound Structures, Journal of Waterway, Port Coastal and Ocean Engineering 1, (1994) pp.1–19.

[10] K. d'Angremond, J.W. Van der Meer, and R.J. de Jong, Wave Transmission At Low Crested Structures, Proc. 25th Int. Conf. on Coastal Engineering, ASCE, (1996) pp. 3305–3318

[11] M. Buccino, and M. Calabrese, Conceptual Approach For Prediction Of Wave Transmission At Low-Crested Breakwaters, Journal Of Waterway, Port, Coastal, And Ocean Engineering, 133(3), (2007) pp. 213-224.

[12] U.S. Army Corps of Engineers, Coastal Engineering Manual, Washington D.C, USACE, (2003).

[13] C.A. Fleming, N.W.H. Allsop, M.B. Leeming, B.N. Sharp, D. Slater, A.J. Williams, P. Titman, and R.T.L. Allen, Concrete in Coastal Structure, Thomas Telford Ltd, London, 1998.

[14] E.P.D. Mansard, and E.R. Funke, The Measurement of Incident and Reflected Spectra Using a Least Squares Method, Coastal Engineering, Chapter 8, (1980) pp.154-172.

[15] S.A. Hughes, Physical Models and Laboratory Techniques in Coastal Engineering, World Scientific Publishing, Singapore, 1995.

Applied Mechanics and Materials Vol. 567 (2014) pp 319-324
© (2014) Trans Tech Publications, Switzerland
doi:10.4028/www.scientific.net/AMM.567.319

Wave Transmission over a Submerged Porous Breakwater: An Experimental Study

Hee Min Teh

Civil Engineering Department, Universiti Teknologi PETRONAS, Tronoh, Perak, Malaysia.

heemin.teh@petronas.com.my

Keywords: Submerged breakwater, wave transmission, porosity

Abstract. The present paper presents an experimental study of wave transmission for a trapezoidal submerged porous breakwater located in the nearshore region. Wave transmission characteristics of the breakwater subjected to unidirectional monochromatic waves have been ascertained via a systematic test program. A series of tests have been conducted to study the effect of porosity of the breakwater on wave transmission, and to assess wave attenuation performance of the breakwater in relation to wave steepness and the relative breakwater width. The test results have indicated that the breakwater of 20% porosity offers the highest hydraulic efficiency, and the breakwater provides higher wave suppression ability when exposed to shorter period waves particularly in shallow waters.

Introduction

Suppression of hydrodynamic loadings of waves on coastal facilities has long been a challenge to coastal engineers. Construction of breakwaters at coastal zone is one of the most prevalent practices adopted for reduction of hydraulic loadings on the shoreline at a desired level so as to sustain the dynamic equilibrium of the shoreline. Numerous studies have been undertaken to assess the shoreline response of the emergent offshore breakwaters via both physical and numerical modeling; nevertheless, the understanding of dynamic response of shoreline due to submerged porous breakwaters is rather insufficient and thus this aspect of the study worth further investigations.

Due to complexity of the wave and flow problems, understanding of behavior of the bottom mound submerged breakwaters exposed to various types of wave environments was mostly ascertained through physical modeling tests conducted by different researchers during the 70s. Based on the collective experimental results, some empirical formulae for optimum design of the submerged breakwaters have been developed for the use of the practicing engineers. The design formulas for wave transmission have been further improved by incorporating permeability, crest width, water depth in front of the barrier, angle of wave attack and some other important factors. Apart from single row breakwaters, hydrodynamic and morphodynamic response of multiple low crested breakwaters were also explored by researchers, *e.g.* Yoshida et al. [1] and Martinelli et al. [2].

Numerous numerical studies have been undertaken to study wave interaction with submerged rubble mound breakwaters and the hydrodynamic near-field processes. Garcia et al. [3] and Lara et al. [4] studied the near-field flow at low-crested permeable breakwaters using the COrnell Breaking waves And Structures (COBRAS) model, which was initially developed by Lin [5]. The COBRAS model solves the Reynolds Average Navier-Stokes (RANS) equations. The velocity and turbulence distribution around and inside the low-crested rubble-mound breakwaters was further explored by Losada et al. [6] using three-dimensional Large Eddy Simulation (LES) model. The nonlinear wave-structure-seabed interactions under varying wave conditions were studied under a laminar flow condition by Hur et al. [7].

Due to unavailability of the amour rocks near the construction sites, various innovative submerged breakwaters or artificial reefs that are made of reinforced concrete has been developed as replacements to the conventional rubble mound breakwaters. Sidek and Abdul Wahab [8] developed

a porous rectangular submerged breakwater of 40%-, 60%- and 80% porosities, and they found that influence of porosity on wave transmission, reflection and energy loss was relatively low. Semi-submersible semicircular porous breakwater is another innovative design that provides high stability against wave action. The semi-submersible semicircular breakwater that was first installed at the Yangtze River Estuary, China in year 2000 was proven to be effective in attenuating the wave energy [9]. The success of the Chinese submerged breakwaters in operation has inspired a number of research interests among the researchers. Sri Krina Priya et al. [10] experimentally explored the 'solid type' breakwater with different submergence ratios and they found that the breakwater offered higher wave attenuation ability when still water level was at the breakwater crest. Zhang et al. [11] and Teh et al.[12] investigated hydrodynamics behavior of the 'solid-type' semicircular breakwater seated at the bottom and located close to the surface of water, respectively. The hemispherical concrete units called Reef Balls are recently used to promote the growth of marine life. These balls are rested on the low crested rubble mound and are constantly immersed by water. The reef breakwaters have been installed at various sites at different parts of the world and the majority of them have been proven to be efficient in attenuating the wave energy. Further studies on reef breakwaters have been undertaken to develop a more precise engineering modeling of wave transmission for reef breakwaters [13,14].

In this study, a trapezoidal porous breakwater, as shown in Fig. 1, has been developed for investigation. The porosity of the breakwater is created by the means of 4 × 8-matrix circular pipes laterally connecting the seaward and shoreward of the structure. The primary aim of such design is to reduce wave reflection in front of the breakwater and to promote more frictional stress to the water that run through the connecting pipes embedded within the main structure. In this study, wave attenuation performance of the breakwater is evaluated via physical modeling. Extensive tests have been performed in a wave flume to determine (1) the optimum porosity of the breakwater; and (2) the wave transmission characteristics of the breakwater with respect to wave steepness and the relative breakwater width. More descriptions on the set-up of the experiment will be deliberated in the following section.

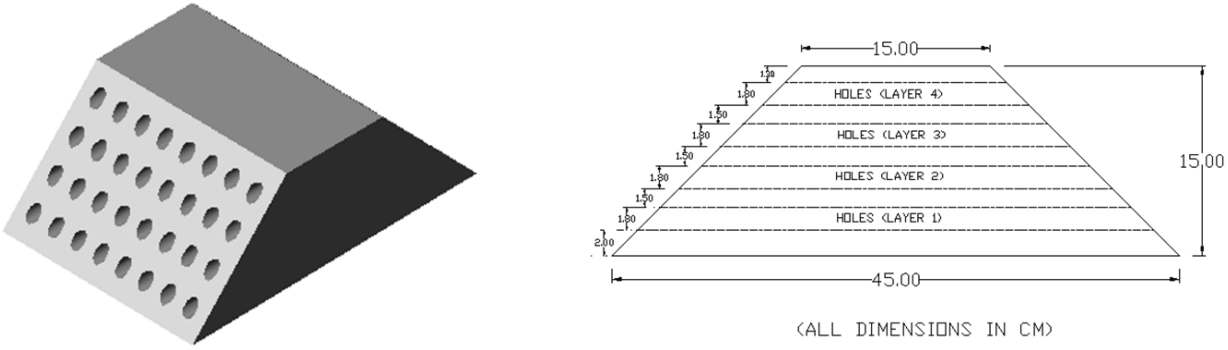


Figure. 1: Porous submerged breakwater: Isometric view (left) and side view (right)

Laboratory Set-up

Model Fabrication. The submerged breakwater was scaled down using Froude scaling of 1:20. The porous breakwater model was designed to be trapezoidal, in which the base width, crest width and height were 0.45 m, 0.15 m and 0.15 m, respectively. The main body of the breakwater was made of concrete and the porosity was controlled by the lateral placement of four rows of cylindrical PVC pipes as shown in Fig. 1. For each row, eight pipes of similar length were placed horizontally connecting the seaward and leeward of the breakwater model. The inner diameter of the pipes was 18 mm. The porosity of the breakwater ε was calculated based on $\varepsilon = (V_v/V_b) \times 100\%$ where V_v and V_b are void and bulk volumes of the breakwater. The porosity of the breakwater was adjusted by controlling the number of closures of the pipes using plasticine.

Test Facilities and Equipments. The experimental tests were conducted in a 10 m long, 0.3 m wide and 0.45 m high open channel flume at the Hydraulics Laboratory of Universiti Teknologi PETRONAS. The flume was raised from the ground level at about 1 m and the walls were built by using transparent tempered glass. The flume was equipped with a flap-type paddle at the end so as to operate as a fully-functioned wave flume. The paddle was capable of generating unidirectional monochromatic (regular) waves of varying wave period and height in a non-current condition. Reflection of wave energy from boundaries is one of the common laboratory effects that would deteriorate the quality of the physical tests. The reflected waves from the back wall of the flume were minimized by placement of an artificial beach covered by synthetic grass mats. The slope of the beach was adjustable so as to cater tests conducted in various water depths. The water level of the entire length of the flume was measured by a hook and point gauge. A wave probe was placed at the test section of the flume for measurement of the incident wave heights prior to the placement of the breakwater model. After the installation of the breakwater model in the flume, another wave probe was stationed at 1 m away from the lee of the model for the measurement of the transmitted wave heights. Prior to extensive experiment, both wave paddle and wave probes were carefully calibrated. The test parameters for this study are summarized in Table 1.

Table 1: Test parameter

Wave type	Monochromatic
Water depth, d (m)	0.15, 0.20, 0.25, 0.30
Wave period, T (s)	0.6, 0.8, 1.0, 1.2, 1.4, 1.6, 1.8, 2.0
Incident wave height, H_i (m)	0.026 – 0.126
Breakwater Porosity, ε (%)	0, 10, 20, 30

Results and Discussions

Wave transmission over the submerged breakwater is quantified by the wave transmission coefficient, $C_t = H_t/H_i$ where H_t and H_i are the transmitted and incident wave heights, respectively. The lower the C_t value, the lesser the wave energy is transmitted to the leeside of the breakwater. Note that the transmission coefficient can also be represented in teh form of energy whereby $C_t = (E_t/E_i)^{0.5}$ where E_t and E_i are the energies of transmitted and incident waves, respectively. Energy loss by the breakwater if often quantified by $C_L^2 = 1 - C_t^2 - C_R^2$ where C_R is the reflection coefficient.

Effect of Breakwater Porosity. The effect of breakwater porosity on wave transmission was assessed when the model was subjected to 1-s waves. Breakwater models of various porosities (*i.e.* 0%, 10%, 20% and 30%) were individually tested in water depths of 0.15, 0.20, 0.25 and 0.30 m. The wave transmission coefficients of the submerged porous breakwater for the tested water depths are presented with respect to porosity in Fig 2. It is clear from the graph that the C_t of d = 0.15, 0.20, 0.25 and 0.30 m gradually increases as porosity increases from 0% to 30%. The C_t of shallow waters tends to be suppressed further indicating that the breakwater is a better wave attenuator when adopted in shallow waters dominated by 1-s waves. This observation is sensible because the transmission of wave energy is restricted by the limited freeboard above the crest of the breakwater.

At d = 0.15 m (breakwater height-to-water depth ratio, h/d = 1), the still water level is located at the crest of the breakwater, in which the transmission of energy at the leeside of the breakwater is solely due to the overtopping waves. The C_t values remain at 0.3 as the breakwater porosity increases from 0% to 20%. For other water depths, the increments of C_t are considered marginal as the porosity is less than 20%. The solid submerged breakwater (porosity = 0%) tends to reflect more wave energy, which consequently results in confusing sea state in front of the structure. On the other hand, the porous breakwater minimizes wave reflection effect by inducing energy dissipation when water passes through the tubes embedded in the structure. Therefore, a porosity of 20% is regarded the most optimum to the submerged porous breakwater.

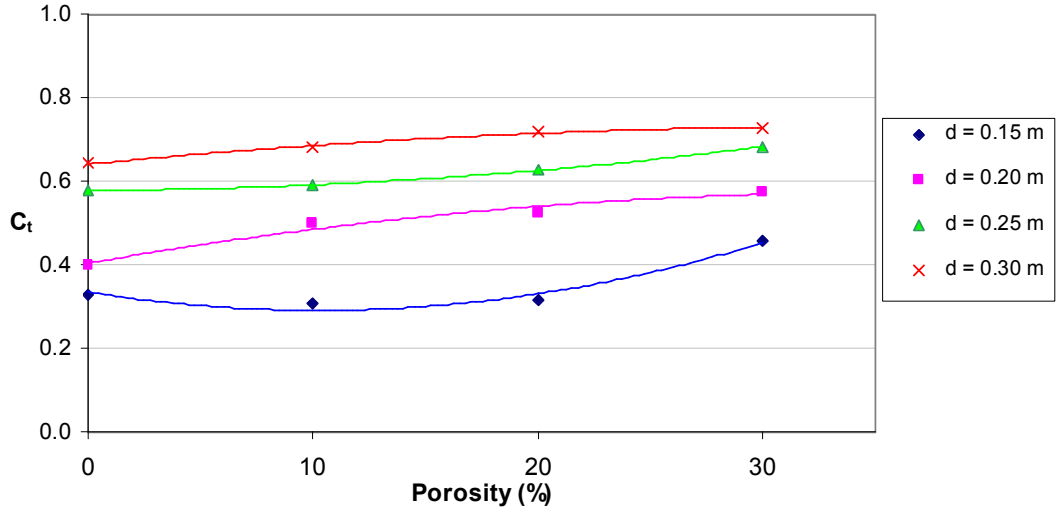


Figure. 2: Effect of the breakwater porosity on C_t when subjected to 1-s waves

Effect of Wave Steepness. Wave steepness is a dimensionless parameter, which gives representation of the wave size. In this study, the wave steepness parameter is presented as H_i/gT^2 where g and T are the gravitational acceleration and wave period, respectively. The higher the wave steepness parameter, the steeper will be the incident waves (due to increased wave height). For this study, the breakwater of the optimum porosity (*i.e.* 20%) was used to evaluate the wave attenuation performance with respect to a range of wave steepness parameter. Four water depths were considered in this study, namely d = 0.15, 0.20, 0.25 and 0.30 m, which are corresponding to the relative water depth h/d = 1.00, 0.75, 0.60 and 0.50. The correspondence of C_t with the wave steepness parameter is demonstrated in Fig. 3. It is seen that the C_t of the 20% porosity breakwater orderly decrease with an increase of h/d, again suggesting that the breakwater exhibits higher wave suppression ability when installed in shallow waters. It is also observed that the C_t of the respective h/d decrease with the increasing H_i/gT^2. Waves of mild steepness manage to transmit over the crest of the breakwater with less interaction with the structure due to their limited wave amplitudes. Nevertheless, as the wave amplitude increases, which in turn leads to higher H_i/gT^2, the wave tends to break on the seaward slope of the breakwater and to further dissipate its energy through frictional loss, heat and sound. As a result, lower C_t values will be anticipated when exposed to waves of higher steepness.

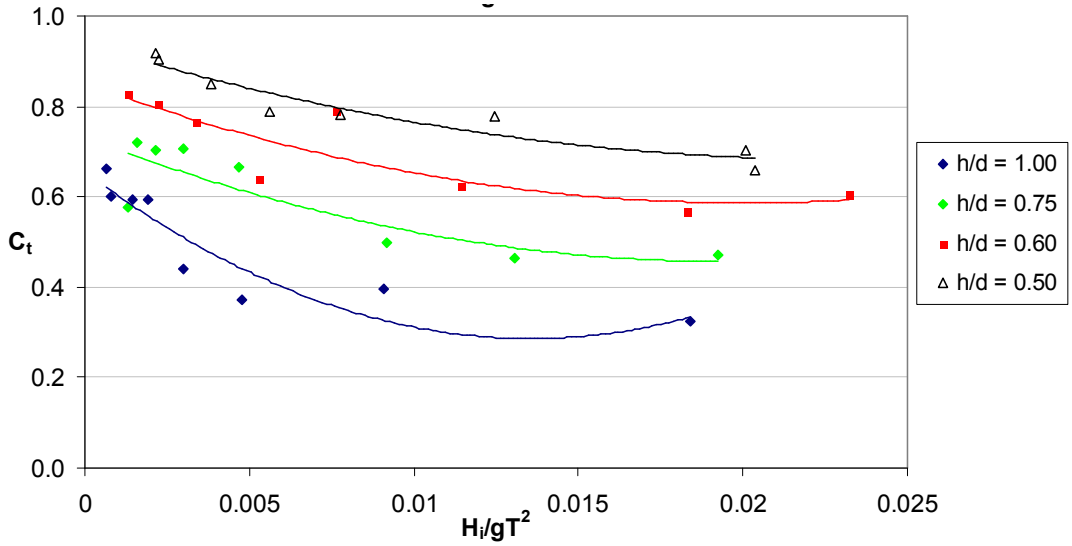


Figure. 3: Effect of wave steepness parameter on wave transmission coefficient

Effect of Relative Breakwater Width. The relative breakwater width is another preferred design parameter used by engineers in determining the most optimum size of the breakwater for a selected site. It is indeed a breakwater base width-to-wavelength ratio, B/L. Fig. 4 presents the relationship between C_t of the 20% porosity breakwater and B/L for h/d = 0.50, 0.60, 0.75 and 1.00. It is apparent that the C_t plots for the respective h/d are agreeable with each other by displaying a similar trend, whereby the C_t diminishes with the increasing B/L. This shows that the breakwater performs more efficiently in seas that are dominated by short period waves (with limited wavelength). Alternatively, lower wave transmission can also be attained by increasing the width (*i.e.* both crest and base) of the breakwater. The figure also verifies the efficiency of the porous breakwater when installed in shallow waters.

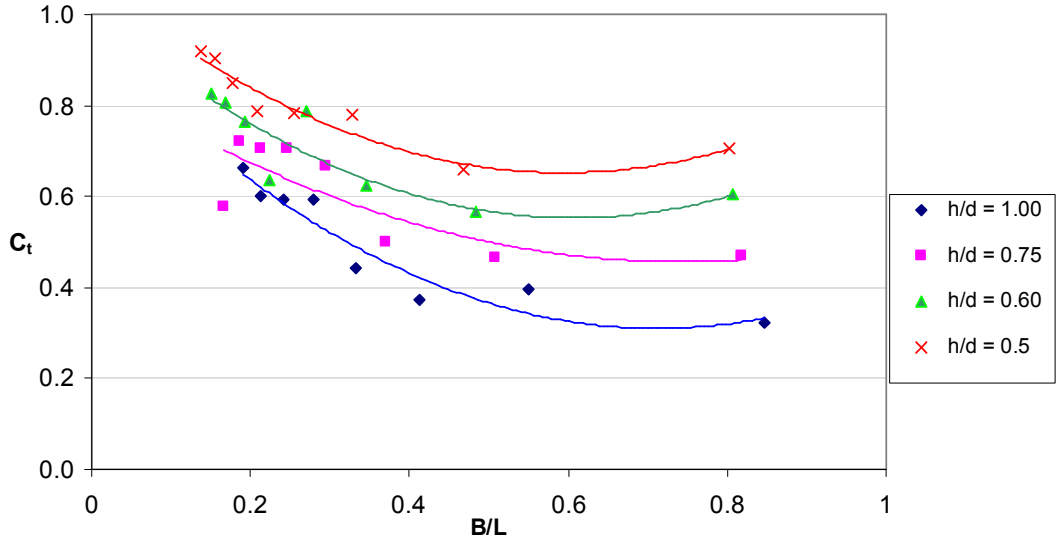


Figure. 4: Effect of the relative breakwater width on wave transmission coefficient

From the experimental results, wave attenuation performance of the trapezoidal submerged breakwater of 20% porosity is regarded reasonably good. Wave dampining rate of the breakwater with geometrical constraint of $0.5 \leq h/d \leq 1.0$ and $0.12 \leq B/L \leq 0.82$ varies from 20% to 70% when exposed to regular waves of $0.001 \leq H_i/gT^2 \leq 0.025$. It is anticipated that the breakwater in modular form may find its application at sandy-bed shallow waters where some level of wave tranquility is required.

Conclusions

This paper presents the wave transmission characteristics of a trapezoidal submerged porous breakwater in regular waves. The breakwater under different porosities, water depths, wave periods and wave heights were examined in a wave flume. The experimental results obtained in this study show that the breakwater of 20% porosity provided the highest hydraulic efficiency. Therefore, a porosity of 20% is considered as the optimum breakwater design. The breakwater of 20% porosity offered higher wave suppression ability when (i) installed in shallow waters, (ii) exposed to high steepness waves, (iii) subjected to waves of shorter period, and (iv) the width of the breakwater is expended sufficiently. It attenuated up to 70% of the incident wave height within the test limits of $0.5 \leq h/d \leq 1.0$, $0.12 \leq B/L \leq 0.82$ and $0.001 \leq H_i/gT^2 \leq 0.025$ in regular wave environment.

References

[1] A. Yoshida, S. Yan, M. Yamashiro and I. Irie, Experimental study on wave field behind a double-submerged breakwater, Proceedings of the International Conference of Coastal Engineering 2002, 1913-1922.
[2] L. Martinelli, B. Zanuttigh and A. Lamberti, Hydrodynamic and mophodynamic response of isolated and multiple low crested structures: Experiments and simulations, Coastal Engineering Journal 53 (2006), 363-379.
[3] N. Gracia, J.L. Lara and I.J. Losada, 2-D numerical analysis of near-field flow at low-crested permeable breakwaters, Coastal Engineering Journal 51 (2004), 991-1020.
[4] J.L. Lara, N. Gracia and I.J. Losada, RANS modeling applied to random wave interaction with submerged permeable structures, Coastal Engineering Journal 53 (2006), 395-417.
[5] P. Lin, Numerical modeling of breaking waves, PhD thesis, University of Cantabria (1998).
[6] I.J. Losada, J.L. Lara, E.D. Christensen, N. Garcia, Modelling of velocity and turbulence fields around and within low-crested rubble-mound breakwaters, Coastal Engineering Journal 52 (2005), 887-913.
[7] D.S. Hur, C.H. Kim, D.S. Kim and J.S. Yoon, Simulation of the nonlinear dynamic interactions between waves, a submerged breakwater and the seabed, Ocean Engineering Journal 35 (2008), 511-522.
[8] F.J. Sidek and M.A.J. Abdul Wahab, The effects of porosity of submerged breakwater structures on non-breaking wave transformations, Malaysian Journal of Civil Engineering 19(1) (2007), 17-25.
[9] S.L. Xie, Wave forces on submerged semi-circular breakwater and similar structures. China Ocean Engineering, 13 (1) (1999), 63–72.
[10] M. Sri Krishna Priya, K.A. Roop Sekhar, V. Sundar, R. Sundaravadivelu and K.U. Graw, Pressure exerted on submerged semicircular breakwaters. Leipzig Annual Civil Engineering Report 5 (2000), 551–560.
[11] N.C. Zhang, L.Q. Wang, and Y.X. Yu, Oblique irregular waves load on semicircular breakwater. Coastal Engineering Journal, 47 (4) (2005), 183–104.
[12] H.M. Teh, V. Venugopal and T. Bruce, Hydrodynamic characteristics of a free surface semicircular breakwater exposed to irregular waves. Journal of Waterway, Port, Coastal and Ocean Engineering, 138(2) (2012), 149-163.
[13] K. Nobuhisa, J. Pietropaolo and J.A. Melby, Deformation of reef breakwaters and wave transmission. Journal of Waterway, Port, Coastal and Ocean Engineering 139(4) (2013), 336-340.
[14] M. Buccino, I.D. Vita and M. Calabrese, Engineering modeling of wave transmission of reef balls. Journal of Waterway, Port, Coastal and Ocean Engineering (2014) [In press].

Applied Mechanics and Materials Vol. 567 (2014) pp 325-330
© (2014) Trans Tech Publications, Switzerland
doi:10.4028/www.scientific.net/AMM.567.325

Deformation Monitoring of Offshore Platform Using the Persistent Scatterer Interferometry Technique

Abd Nasir Matori[1,a], Amir Sharifuddin Ab Latip[1,b],
Indra Sati Hamonangan Harahap[1,c] and Daniele Perissin[2,d]

[1]Civil Engineering Department, Universiti Teknologi PETRONAS, Bandar Seri Iskandar, 31750 Tronoh, Perak, Malaysia

[2]Purdue University, School of Civil Engineering, USA.

[a]nasrat@petronas.com.my, [b]asharifuddin2@gmail.com, [c]indrasati@petronas.com.my, [d]tool.periz@gmail.com

Keywords: Offshore platform, deformation, PSI technique.

Abstract. One of the problems that occur during the exploitation of oil and gas is offshore platform deformation. It could occur due to the environments load as well as the extraction of oil and gas itself under the seabed that caused reservoir compaction. Offshore platform deformation may affect the platform structural integrity and cause loss of production, thus it is very important to monitor its occurrences. Offshore platform deformation monitoring has been carried out using the satellite-based Global Positioning System (GPS) technique until recently. Even though the technique has proven its worth for the job, it has however some limitations, the most prominent is it could only monitor selected portion of the offshore platform. Thus, this study presents an attempt of detecting and monitoring the deformation phenomenon of an offshore platform using the Persistent Scatterer Interferometry (PSI) technique. This technique would overcome some of the limitations of the previous (GPS) deformation monitoring technique. A total of 11 high resolution TerraSAR-X images (i.e., 3 m in StripMap mode) were acquired from Aug, 2012 to Apr, 2013 for this purpose, while one of the offshore platforms in South China Sea is being used as monitored platform. Preliminary results showed that detail and sensitive deformations could be detected by this technique. In addition, analysis results in the form of mean deformation velocity map and displacement time series would allow us to further understand the behaviour of offshore platform deformation.

Introduction

Offshore drilling platforms have become important assets due to the increasing demand for energy in our world (i.e., oil and gas production). One of the major problems that occur during the exploitation of oil and gas from an offshore platform is deformation. The deformation problem occurs due to the environments load as offshore platform is continuously exposed of extreme wind, wave, current, storm and seismic actions. Besides, the extraction of a large scale of oil and gas under the seabed caused instability of the structures. This instability phenomenon caused the offshore platform to undergo slow subsidence. Moreover, a shallow gas phenomenon in the vicinity of the platform can lead to the deformation of offshore platforms. Thus, monitoring the deformation of offshore platforms is significant to ensure that structural integrity is being maintained. Also, it can provide early detection of the possibility of platform damages and collapse. Any damage or collapse of offshore platforms can lead to loss of life, loss of oil and gas production, environmental pollution and severely affect industry reputation.

Interferometric Synthetic Aperture Radar (InSAR) is a radar imaging system that transmits signals of microwave through a SAR antenna on board of a satellite to illuminate targets in the surface. The InSAR is an effective way to measure vertical changes of the offshore platform by comparing the distance from a satellite to a ground point on the offshore platform taken at different times. When the ground point of the offshore platform moves away from (subsidence) or towards (uplift) the satellite, the distance between the satellite and the point has also changed. Moreover, the

InSAR can measure the surface deformation of offshore platform with higher densification of pixel-by-pixel basis and it provides a cost effective technique where it offers wide area coverage to comprehensively monitor multiple offshore platforms deformation on any single campaign. Recently, a new technique of InSAR which is called Persistent Scatterer Interferometry (PSI) was developed. This is an advanced technique to improve the ability of InSAR to detect deformation using a large number of Synthetic Aperture Radar (SAR) images over the same area [1]. The PSI technique selects the pixels that have stable amplitudes (i.e., those with the same backscattering amplitudes) from a large stack of interferograms to reduce the phase decorrelation and remove the atmospheric delay. This technique has the capabilities to achieve millimetre accuracy of the surface deformation estimations. A number of studies have demonstrated that the PSI technique have been successfully used for land deformation application such as landslide monitoring [2], volcano deformation [3] and urban deformation [4].

This study assessed the feasibility of the application of the PSI technique for monitoring the deformation of offshore platform using TerraSAR-X satellite images. The outcome of the study is presented in the form of mean deformation velocity maps and displacement time series of each measured Persistent Scatterer (PS) of the monitored platform.

Study Area and Data Availability

In this study, one of the PETRONAS offshore platforms (referred to P platform) in South China Sea is being used as monitored platform (refer with Fig. 1). The platform is located approximately 250 km off the east coast of Peninsular Malaysia. The platform is chosen as the first test site to apply the PSI processing technique due to previous study based on GPS has revealed the said platform has deformation history rate of 0.0094 m for the period of two months [5].



Figures 1: P platform

After deciding on the test site, the InSAR satellite data will be acquired. It was decided that the satellite data sets to be used is the TerraSAR-X. The TerraSAR-X satellite is a German Earth observation satellite launched in June 2007 at an altitude of 514 km. The TerraSAR-X satellite is chosen because this satellite has a better pixel resolution, short repeat orbit interval of 11 days with a shorter wavelength of X-band (3.1 cm). There are a total of 11 TerraSAR-X satellite images over the P platform from the descending track (North to South) were acquired in this study (refer with: Table 1). The images were acquired in the standard StripMap mode with 3 m pixel resolution. Each image has covered an area of 30 km (width) x 50 km (length), at an incidence angle range from 24.86 to 27.86 in HH polarization. The images were acquired every 11, 22 or 33-day repeat cycle, with a time span of 8 months from 25th August 2012 to 24thApril 2013. The image acquired on 04 January 2013 was selected as the master image because it has relatively short perpendicular and temporal baseline corresponding to other images. The maximum perpendicular and temporal baselines with respect to master image are 344.5 m and 132 days, respectively, while the minimum ones are 2.715 m and 11 days (refer with: Table 1).

Table 1: Date of acquisition, perpendicular and temporal baseline with respect to the master acquisition of the TerraSAR-X data used.

Image number	Date (dd/mm/yyyy)	Perpendicular baseline (B_{perp}) [meters]	Temporal baseline (B_{temp}) [days]
1	25.08.2012	167.8	132
2	27.09.2012	180	99
3	30.10.2012	344.5	66
4	21.11.2012	75.07	44
5	13.12.2012	180.2	22
6	24.12.2012	39.32	11
7	04.01.2013	0	0
8	26.01.2013	4.939	22
9	17.02.2013	2.715	44
10	22.03.2013	270.3	77
11	24.04.2013	63.7	110

PSI Processing

The Sarproz software was used in this study to perform the PSI processing. The procedures of data processing are described below:

Persistent Scatterer Candidate (PSC) Selection. The PSC is identified in a series of interferogram based on the pixels which have the phase stability characteristics in time. In this study, the phase stability of each pixel is determined by the amplitude dispersion index, since there is a statistical relationship between amplitude stability and phase stability. Ferretti et al. showed pixels with amplitude dispersion index less than 0.25 are expected to have small phase variants [6]. In this way pixels with a constant signal and high signal to noise ratio (SNR) are selected. The amplitude dispersion index is defined by Ferretti et al. as [6]:

$$D_A = \frac{\sigma_a}{\mu_a} \tag{1}$$

where D_A is the dispersion index, σ_a is the standard deviation of the amplitude return relative to each individual pixel and μ_a is the its average.

Network Construction and Estimation of the Model Parameters of Interest. After selection of all the PSC with D_A<0.25, they were connected to construct a network. The length of the arcs (i.e., the path of neighbouring PSC pairs) in the network is limited to a certain maximum length in order to minimize the effect of atmospheric and orbital errors. If there are N PSC phase observations, only N-1 couples of independent phase differences could be formed. The phase differences for a couple of PSC are influenced by several factors such as differential linear deformation, differential existing DEM inaccuracy, differential atmospheric phase screen (APS) and unmodelled deformation (nonlinear deformation and noise). After the calculation of the phase differences of the each couple of the PSC, the modelled parameters of interest (i.e., linear deformation difference and DEM error difference) can be estimated from them. Here, the deformation rate is in millimetres/year while the DEM error is in meters. Noted that the modelled parameters of interest are estimated from wrapped phase difference.

Spatial Integration and Integration Test. The ensemble phase coherence $\hat{\gamma}$ introduced by Ferretti et al. is used to evaluate how good the observed phase difference of each arc on fitting the modelled

parameters of interest [6]. The arcs with ensemble phase coherence $\hat{\gamma}$ lower than the threshold of 0.75 (i.e., with large residuals) are assumed to be unreliable and hence those arcs are removed [4]. The measure of the variation of the residual phase for a pixel (*x,y*) is defined as:

$$\hat{\gamma}_{x,y} = \frac{1}{N}\sum_{k=1}^{N} e^{(j.\phi\ error_{x,y})} \tag{2}$$

where N is the total amount of interferograms and j is the imaginary number. The residual phase $\phi_{error_{x,y}}$ is the difference between the modelled parameters and observed phase difference at location (*x, y*) in the interferogram. The parameters (linear deformation rate and DEM error) at each PCS pixel can then be obtained by spatial integration the modelled parameters of interest of each couple of PCS with respect to a stable reference point.

Atmospheric Error Estimation and Nonlinear Deformation Estimation. The residual phases at the PSC in each interferogram are calculated by removing the phase contribution by linear deformation difference and DEM error difference on arcs. Then, the residual phases can be unwrapped using the Integer Least Squares (ILS) approach [7]. The residual phases contain the phase contribution due to atmospheric effects and unmodelled deformation (nonlinear deformation and noise). Under the assumption that the atmospheric signal is strongly correlated in space and randomly in time, it can be subtracted from the other components of the residual phase (unmodelled deformation) using the low-pass filtering in the spatial domain and high-pass filtering in the temporal domain [4,6]. The atmospheric phase contribution for the pixels of each interferogram those are not included as the PSC in the network can be estimated by using a Kriging interpolation method. The result is known as APS. Finally, the nonlinear deformation component is estimated by using low pass filtering process in both time and space to the residual phase (i.e., after removal of the phase contribution due to the modelled parameters and atmospheric errors). It should be noted that this nonlinear deformation component will be added to the linear deformation estimates at the end of the processing.

Final Estimation of PS Points. From the differential interferograms without APS, the modelled parameters of interest (i.e., linear deformation difference and DEM error difference) can be estimated by the iteration process for all pixels or other PSC that have a lower amplitude dispersion index (i.e., D_A<0.40). In this way the number of detected PS points will be increased and significantly improved the PSI results. After estimation of the modelled parameters, the corresponding PSC is tested based on the ensemble phase coherence $\hat{\gamma}$ quality assessment (refer section 3.3) and the final set of PS points is selected. The estimated linear deformation is combined with the nonlinear deformation rate to derive the deformation time series.

Results and Analysis

Figure 2 shows a mean amplitude image corresponding to the study area. The mean amplitude image is generated from all the 11 SAR images. The high backscattering capability can be observed in the offshore platform while less backscattering in the ocean area. Hence bright region represents the offshore platform and offshore support vessel (OSV) while that dark region is the ocean. A total of 27 PS points is spread over the P platform (refer with: Fig. 2). However, there are no PS points are detected in the middle of P platform and on the OSV. This is due to displacements or movements of objects from their positions in the middle of P platform and the movement of the OSV. In other words, the middle portion of P platform and OSV are significantly influenced by temporal deccorelation effects, which lead to a loss of coherence.

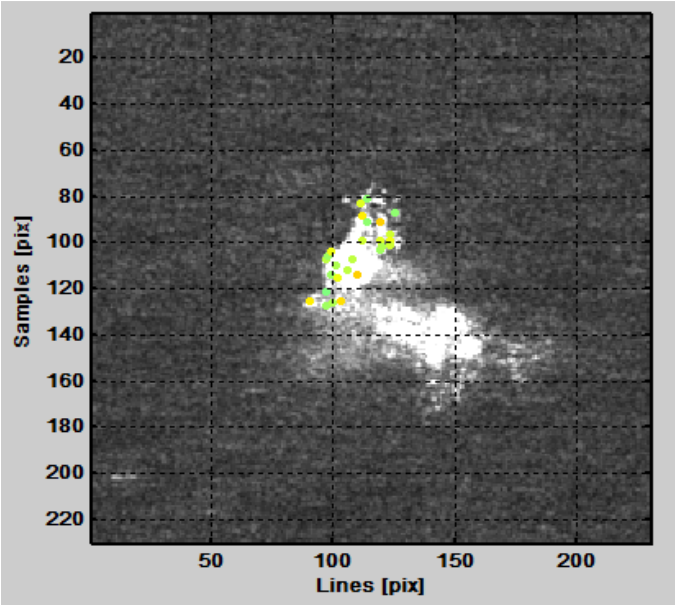
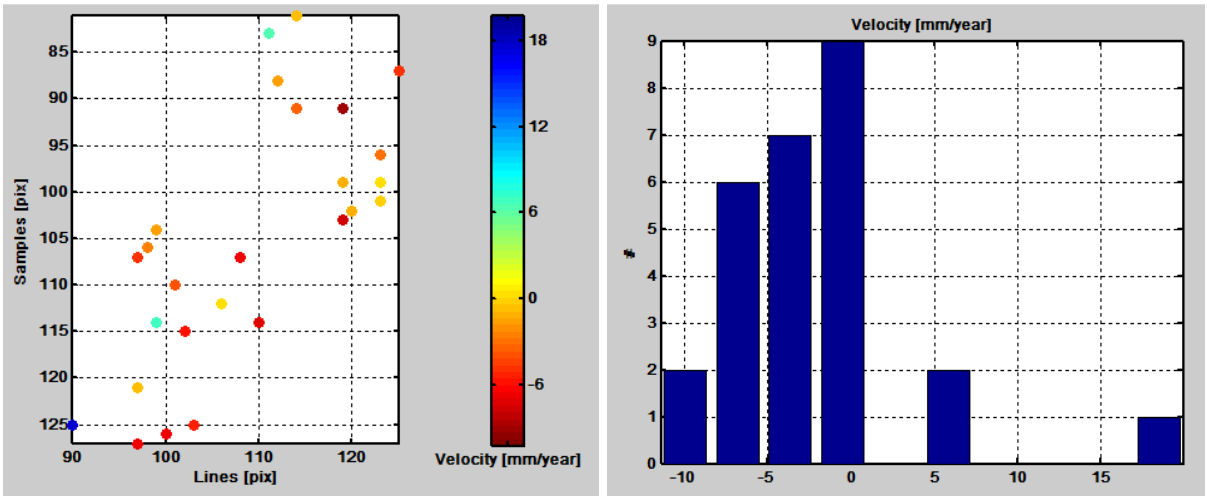


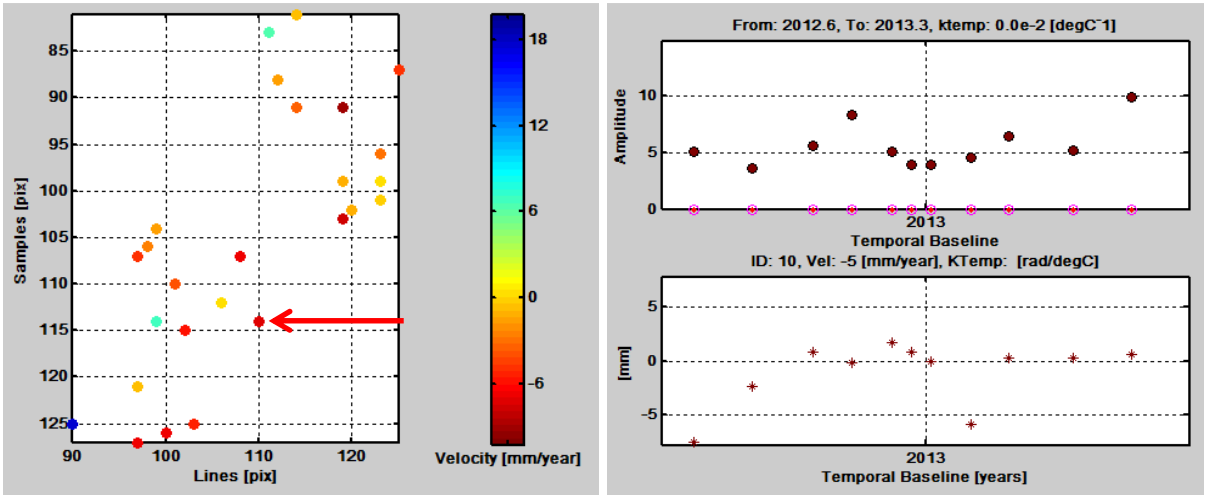
Figure 2: The distribution of 27 PS points, superimposed to the mean amplitude SAR image.

Figure 3 shows the colour variation of PS points corresponds to the variation in linear deformation rates, which is from -10 mm/year (red) to 20 mm/year (blue). The histogram shows that nine of the PS points were detected in the P platform have zero deformation rates which indicate the P platform is in a stable condition. On the contrary, 15 PS points demonstrate that subsidence have occurred on the P platform. The PS points have subsidence rates range of -1 mm/year to -10 mm/year. Also, three PS points show the P platform have uplift, two of them have uplift 5 mm/year, while one has uplift of 20 mm/year. Thus, the subsidence and uplift rate of the P platform indicates that the P platform has moderate movement.



Figures 3: Deformation rate estimation over the P platform. Deformation rates range from -10 mm/year to +20 mm/year.

Meanwhile, Figure 4 shows the deformation time series and amplitude variation of selected PS point which the PS point is located in the subsidence area. The position of the PS point is indicated by the red arrow. The results show that the deformation rates do not vary significantly over time.



Figures 4: Deformation time series and amplitude variation of PS point that identified in the subsidence area.

Concluding Remarks

The PSI technique has been utilized and tested to monitor the deformation of P platform. The moderate movement and minimum signal decorrelation make P platform very suitable for the application of PSI technique. This study has revealed that the P platform has experienced with some subsidence and uplift. In the next phase of this study, the accuracy of PSI results will be validated by comparing the observed deformation rates with GPS and levelling survey data. Once the PSI and GPS results are validated, it is proposed that PSI technique to be adopted for future offshore platform deformation measurements and monitoring.

6. References

[1] A. Ferretti, C. Prati and F. Rocca, Permanent Scatterers in SAR interferometry, Proceedings IGARSS 99, Hamburg, Germany, June 28-July 2 (1999).

[2] C. Colesanti, A. Ferretti, C. Prati and F. Rocca, Monitoring landslides and tectonic motions with the Permanent Scatterers technique, Engineering Geology. 68 (2003b) 3-14.

[3] A. Hooper, H. Zebker, P. Segall and B. Kampes, A new method for measuring deformation on volcanoes and other non-urban areas using InSAR persistent scatterers, Geophysical Research Letters. 31 (2004) L23611.

[4] A. Ferretti, C. Prati and F. Rocca, Nonlinear subsidence rate estimation using permanent scatterers in differential SAR interferometry, IEEE Transactions on Geoscience and Remote Sensing. 38(5) (2000) 2202–2212.

[5] N. Widjajanti and A.N. Matori, Evaluation of GPS data for offshore platform subsidence, 7th Asia Pacific Structural Eng. And Construction Conf. (APSEC 2009) & 2nd European Asian Civ. Eng. Forum (EACEF 2009), Langkawi, Malaysia (2009).

[6] A. Ferretti, C. Prati and F. Rocca, Permanent scatterers in SAR interferometry, IEEE Transactions on Geoscience and Remote Sensing. 39(1) (2001) 8–20.

[7] B.M. Kampes and R. F. Hanssen, Ambiguity resolution for permanent scatterer interferometry, IEEE Transactions on Geoscience and Remote Sensing. 42(11) (2004) 2446–2453.

CHAPTER 3:

Structures and Materials

Applied Mechanics and Materials Vol. 567 (2014) pp 333-338
© (2014) Trans Tech Publications, Switzerland
doi:10.4028/www.scientific.net/AMM.567.333

A Novel Method for Monitoring Hydration Process of Cement Paste Material

Hashem Almattarneh[1,a], Abdullah Alwadie[2,b], Ahmad Malkawi [3,c] and Muhd Fadhil Nuruddin[4,d]

[1,2,3]Faculty of Engineering, Najran University, Saudi Arabia

[4]Faculty of Engineering, University of Technology PETRONAS, Malaysia

[a]hmalmattarneh@nu.edu.sa, [b]asalwadie@nu.edu.sa, [c]abmalkawi@nu.edu.sa, [d]fadhilnuruddin@petronas.com.my

Keywords: Cement; Hydration; Dielectric.

Abstract. A new measurement system is developed to monitor the early hydration of cementitious materials based on measured dielectric properties of the material in low electromagnetic frequency range. The objectives of this paper were to evaluate the changes in the electromagnetic properties for samples with different fly ash content and to establish the reliability of the measurement technique by comparing with results obtained by traditional method such as thermal method that is either time consuming or impractical. The method adopted in the present experimental work is a parallel plate electrode system (PPES). The suggested monitoring device for concrete hydration and strength development is based on the relationship between the electromagnetic properties such as dielectric constant, loss factor and the strength development during hydration process and curing time. In this research the electromagnetic properties of concrete is found to be dependent on the hydration and strength of concrete. Therefore the development of microstructure and concrete compressive strength can be determined by monitoring its electromagnetic properties in the frequency range of 1 to 100 kHz.

Introduction

Hydration of cement based materials is an important process. The development of strength and low permeability is a result of hydration that involves a reaction between water and the anhydrous compounds present in the cement. Therefore, the degree of hydration can be monitored to identify the strength either it is higher or lower [1]. Corresponding to time, hydration will occur continuously and it will never cease. To what extent the hydration process has preceded is known as degree of hydration. These physical and chemical reactions are still very complicated to understand.

Such hydration process has attracted a considerable attention and has been studied by many methods, like the commonly used Vicat needle, universal testing machine, scanning electronic microscope (SEM), X-ray diffraction (XRD) and differential thermal analysis. However, most of these methods are conducted on small samples which needs special preparation process and considered to be cost and time consuming process. Moreover, the accuracy of these methods depends largely on the experience and skill of the person performing it, and such methods cannot provide a continuous information about hydration. Therefore, alternative techniques, which are accurate and non-destructive, are highly needed to monitor the hydration process of cement-based materials [2].

Non-destructive testing (NDT) techniques have attracted considerable attention for the concrete behavior characterization. Electromagnetic is one of the most important techniques. In most cases, electromagnetic techniques were used to monitor the hydration process of cement-based materials. [3,4,5,6]. It is easy to perform and provides correlation between electromagnetic and mechanical properties of dispersible systems such as rock, clays and other soils which have microstructures

similar to that of concrete. The hydration of various types of cement based materials have been characterized using electromagnetic technology by several researchers [7,8, 9, 10].

In this paper, electromagnetic system is developed for monitoring the evolution of materials properties in the early stage of hardening. The monitoring device for concrete hydration and strength development is based on the relationship between the electromagnetic properties such as dielectric constant, loss factor and the strength development during hydration process and curing time. The suggested system offers the following advantages: relatively simple technique, bridges the gap between sophisticated basic examination and traditional test, no time lost, non-destructive, the electromagnetic properties of concrete control by parameters which are impossible to measure in other ways and easy to adapt for use in the field. Preliminary results show good correlation between electromagnetic parameters and the best current knowledge concerning microstructure of concrete.

Experimental

To evaluate the hydration of cement paste, Portland cement paste was prepared using cements Type I and w/c ratio 0.5. The hydration of cement paste was monitored using three different methods. These methods are bound water, calorimeter and dielectric method using PPES. Another set of paste was prepared by partial replacement of Portland cement with fly ash. The replacement was of 20% by weight. The hydration processes were monitored using the dielectric method only.

The mixing of the cement pastes was complied with ASTM C305-91, in the room temperature and ambient humidity. The measurement was not conducted under isothermal conditions, and the samples were compacted into rigid Perspex molds for electrical measurements.

Measurement System and Testing Molds

The adopted device to monitor the hydration of cementitious material is known as parallel plate electrode system (PPES). This system involves sandwiching a thin sheet of material between two electrodes to form a capacitor. The device consists of a source of electromagnetic signal and a transmission line forming an electrical circuit. The cementitious material sample forms a component of this circuit. Then the setup device will measure the permittivity of the circuit. Using the Lump Model, the impedance of the cementitious material can be measured and the dielectric properties of cementitious material can be deduced.

All impedance measurements were acquired using the Hewlett Packard 4263B LCR meter. The measurements were conducted in frequency of 100 kHz. Calibration is an important technique to prepare the back ground reading of the LCR meter. There are two steps of calibration which are open and short calibration. Impedances of cable and plates, fringing and system without material (air-filled) were measured. The molds were made by Perspex and PVC pipes. Copper plates were used as electrodes. The diameter of the copper plates was 120mm, the model circuit of the PPES system and the testing molds are shown in Fig. 1



Figures 1. The model circuit of the PPES system and the testing molds.

Experimental Results

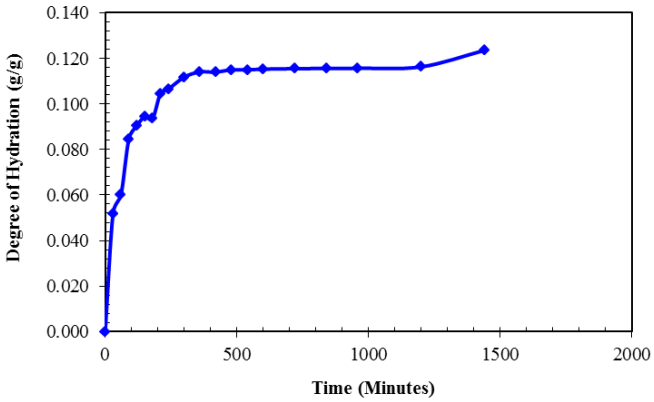
Hydration by Bound Water

The bound water of cement paste made with *w/c* of 0.5 was determined. The degree of hydration $\alpha(t)$ was calculated using Eq. 1. The results are shown in Fig. 2.

$$\alpha(t) = \frac{W(t)}{W_{pot}} \tag{1}$$

where *W(t)* is the bound water at time *t* and W_{pot} is the potential bound water liberated if all cement hydrated.

It is difficult to prevent water evaporation from cement paste during experiment; therefore the small change of bound water could not be measured for long period of time using gravimetric method. The degree of hydration using bound water showed higher values in the early age than expected. It was also time consuming, tedious, and costly.



Figures 2. Degree of hydration of cement paste measured during the first 24 hours using bound water method.

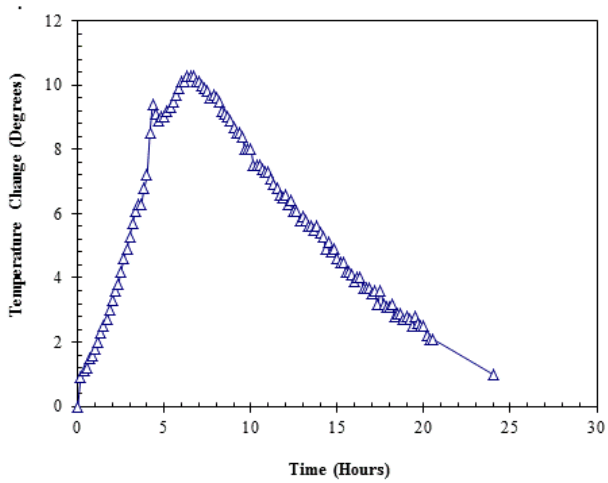
Hydration by Calorimetric Method

The temperature of cement paste was monitored and the results are shown in Fig. 3. The responses of heat evolution over curing time are shown in Fig. 4a. The degree of hydration of cement paste was calculated using Eq. 2. The degree of hydration is calculated using the model proposed by [11]. The results are shown in Fig. 4b the experimental results match the model. Since it is difficult to measure the temperature of specimens after one day of the experiment and almost three days in similar other studies reported by [11, 12].

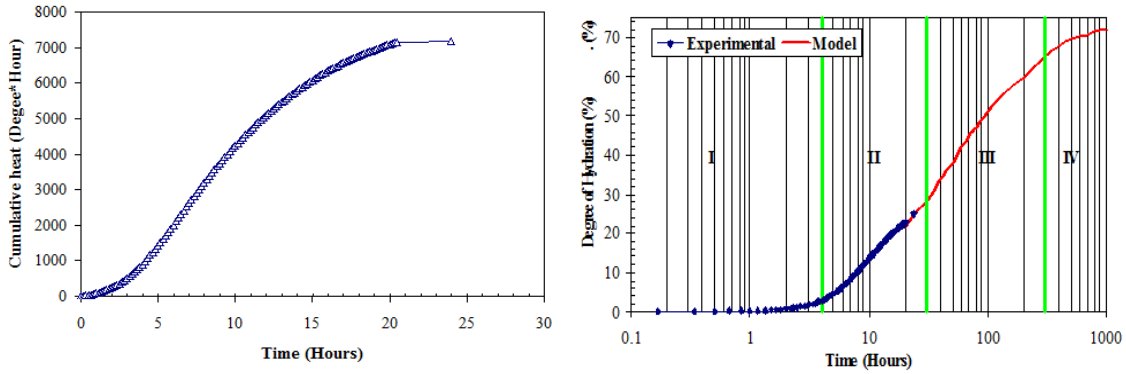
$$\alpha(t) = \frac{Q(t)}{Q_{pot}} \tag{2}$$

where *Q(t)* is the liberated heat at time *t* and Q_{pot} is the potential heat liberated if all cement hydrated.

Fig. 4 shows that calorimetric method indicates the foure different stages of hydration named as (I, II, III, and IV). These stages represent the different ammount of heat evolution and rate at each stage as a result of changing chemical reaction of cement paste.



Figures 3. Temperature released from cement paste measured during the first 24 hours.



(a) (b)

Figures 4. Monitor hydration process using heat evolution from cement paste measured during the first 24 hours, (a) cumulative temperature released, (b) degree of hydration

Hydration by Dielectric Properties

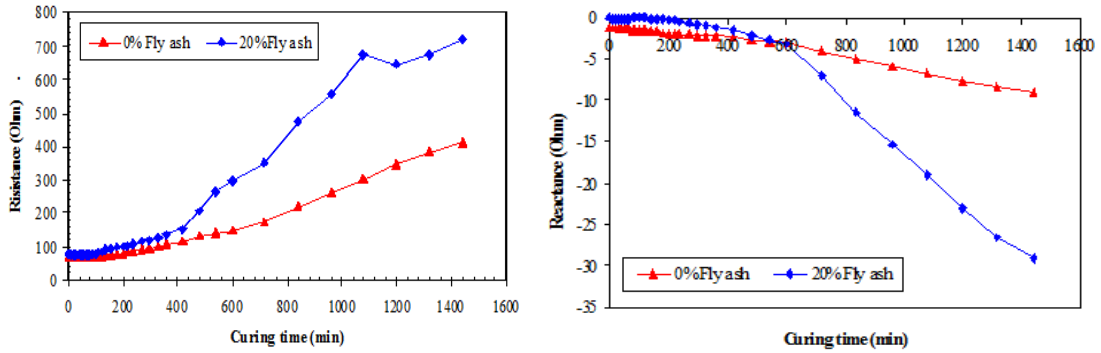
The complex impedances of the PPES containing Portland cement paste were measured during the first 24 hours. The results the real part of impedance (Resistance = R) and the imaginary part of the impedance (Reactance = X) are presented in Fig. 7. Continuous increasing of the resistance and decreasing of the conductance was noticed during the progress of the hydrations of cement paste. This could be as a result of reducing free water in the paste and bound the charges in the microstructures of cement paste. The calculated dielectric constant and loss factor of cement paste from the measured impedances are presented in Fig. 8. The results indicate that the dielectric properties could be used to monitor the hydration process and clearly explain the four different stages of hydration designated as I, II, III, and IV.

Two cement pastes of varying fly ash content were tested. When water was first added to cement, the dielectric constant of the paste was found to be as high as 4000 because of the release of a large amount of Ca^{++} and OH^{-} ions into the water. The presence of these ions resulted in the paste becoming highly polarizable and conductive. As expected, the resistivity at that point of time was very small (stage I). However, as hydration progressed the free water in the paste started changing to adsorbed water and bound water. Due to the increasing formation of the CSH gel, the polar molecules started getting bound and unable to polarize. Calcium hydroxide, the main source of ions,

started to crystallize. For these reasons, the dielectric constant showed a rapid decrease (stage II).The decrease in conductivity was also indicated by a tremendous increase in the resistivity.

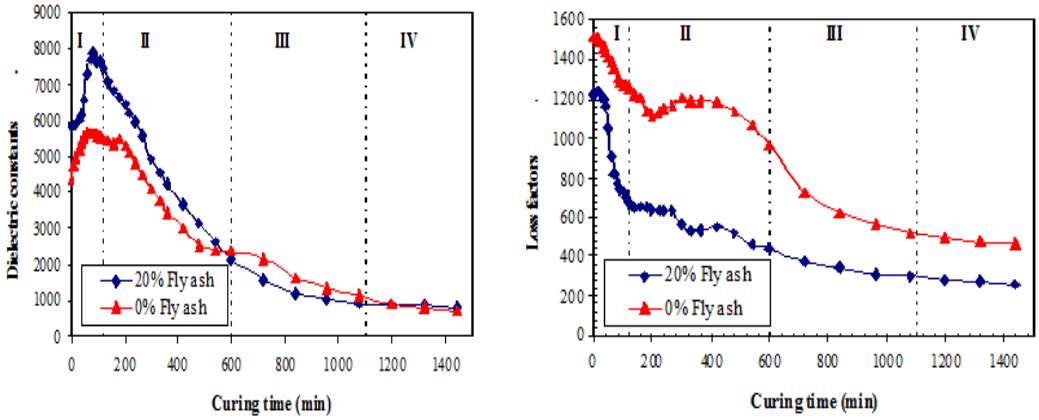
At about 5 hours after casting, there was an increase in the loss factor (stage III). At this point, there was a release of lime from the C_3S grains due to further hydration of the alite phase. The resulting increase of ions in the water increased the dielectric constant.

After this, the concrete hardened and the polar molecules found it difficult to move, resulting in less polarization and a decrease in the dielectric constant (stage IV). The dielectric constant has been observed to be higher for cement paste containing fly ash, as expected.



(a) (b)

Figures 7. The measured impedance (r) of cement paste measured during the first 24 hours, (a) real part, (b) imaginary part.



(a) (b)

Figure 8. Dielectric properties of cement paste measured during the first 24 hours, (a) dielectric constants, (b) loss factors.

Conclusions

Monitoring the hydration process by bound water and calorimetric methods is difficult to conduct and the results are sensitive to adiabatic and none adiabatic conditions and environmental changes. These methods also cannot be used to define the stages of hydration clearly. The measured impedances and the calculated dielectric constants and loss factors in the very early age of cement paste can be used to monitor the early hydration of cementitious material. In addition, the dielectric properties can be used to indicate the different stage of hydration of cement paste. Furthermore, the measured electromagnetic properties can be used to indicate the degree of hydration of Portland cement.

Acknowledgement

This work was supported by a grant "No. PCSED-015-12 Development near and far field electromagnetic sensors" from Deanship of Scientific Research and promising center of electronic sensors, Najran University, Kingdom of Saudi Arabia.

References

[1] K. van Bruegel, Hydration of Cement-Based Systems: Aspects of Hydration of Cement-based Systems and Possibilities to Quantify the Evolution of Hydration Processes, IPACS, Report BE 96-3843(2001):17-6, Sweden.

[2] J. Zhang, L. Qin, Z.J. Li, Hydration monitoring of cement-based materials with resistivity and ultrasonic methods, Mater. Structure and materials, 42 (1) (2009): 15–24.

[3] P. Antonaci, C.L.E. Bruno, A.S. Gliozzi, M. Scalerandi, Monitoring evolution of compressive damage in concrete with linear and nonlinear ultrasonic methods, Cement and Concrete Researches, 40 (7) (2010): 1106–1113.

[4] T. Gudra, B. Stawiski, Non-destructive strength characterization of concrete using surface waves, NDT&E International, 33 (1) (2000): 1–6.

[5] G. Trtnik, F. Kavcic, G. Turk, Prediction of concrete strength using ultrasonic pulse velocity and artificial neural networks, Ultrasonics, 49 (1) (2009): 53–60.

[6] T.T. Wu, J.S. Fang, G.Y. Liu, M.K. Kuo, Determination of elastic constants of a concrete specimen using transient elastic waves, Journal of Acoustic Society of America, 98 (4) (1995): 2142–2148.

[7] M. Kraus, K. Hariri, Determination of initial degree of hydration for improvement of early-age properties of concrete using ultrasonic wave propagation, Cement and Concrete Composites, 28 (4) (2006): 299–306.

[8] H.W. Reinhardt, C.U. Grosse, Continuous monitoring of setting and hardening of mortar and concrete, Construction and Buildimg Material, 18 (3) (2004): 145–154.

[9] S. Uchida, T. Kamada, K. Rokugo, Non-destructive testing for evaluation of physical properties in fresh cementitious materials using elastic-wave method, Advanced Testing of Fresh Cementitious Materials (Stuttgart) (Berlin:DGZfP), (2006) 131–138.

[10] J. Zhang, E.A. Weissinger, S. Peerhamparan, G.W. Scherer, Early hydration and setting of oil well cement, Cement and Concrete Researches, 40 (7) (2010): 1023–1033.

[11] K. V. Breugel, Hydration of cement based systems, Luleå University of Technology, Department of Civil and Mining Engineering, Division of Structural Engineering (2001), Sweden.

[12] J. H. Bungey, M. R. Shaw, M. N. Millard, B. A. Austin, The influence of concrete composition upon radar test results. Insight, 39(7) (1997): 474-8.

Applied Mechanics and Materials Vol. 567 (2014) pp 339-344
© (2014) Trans Tech Publications, Switzerland
doi:10.4028/www.scientific.net/AMM.567.339

An Experimental Study on the Effects of Biaxial Bending due to Eccentric Load on RC Beam

Nasir Shafiq[1, a], Muhammad Imran[1, b] and Ibrisam Akbar[1, c]

[1]Departmnet of Civil Engineering Universiti Teknologi PETRONAS, Tronoh 31750, Perak, Malaysia

[a]nasirshafiq@petronas.com.my, [b]engrimran_ce@hotmail.com, [c]ibrisam_akbar@petronas.com.my

Keywords: biaxial bending, eccentricity, flexure, reinforced concrete, torsion.

Abstract. Eccentric loads are very common in structures due to building configuration. Unequal slab length, circular ramp, large cantilevers are very common in modern architecture. The RC beams in previous studies were tested under the three and four point uniform loads. Therefore, a simple testing setup was arranged to understand the behaviour of RC beam under eccentric load applied at mid span. In this study the single point load applied eccentrically on RC beam. The beams were tested at different eccentricity and compared with control beam tested under the uniform load or zero eccentricity. Results have shown a drastically reduced crack load up to 54% compared to control beam as the eccentricity increased. However, small changed in ultimate load carrying capacity was observed up to 60mm eccentricity. Eccentric load caused biaxial bending due to high concentration of load on one side of beam, which change failure mode of RC beam from ductile to brittle.

Introduction

The reinforced concrete (RC) beam contain a variety of eccentric loads due to cantilever, uneven slab length, circular slab, supporting secondary beam, and restrained support eccentrically. Whereas, in bridges eccentric or unsymmetric loads on RC girder are due to non-uniform traffic movement, skewed girder, circular turning, centrifugal force, and uneven height of the column. This behaviour become sever during the event of seismic or wind when high eccentric loads become a major cause of inducing torsional moment together with normal bending and shear; which cause brittle failure of the structural member [1-4].

In many structures bending stresses are the major cause of deformation. However, shear stresses are complimentary with the flexure stresses. Similarly the torsion stresses induced, when the resultant force does not pass through the shear centre due to eccentric loads [5, 6]. Under symmetric loading the RC beam bends along its longitudinal plane and form a circular arc without distortion of the cross-section of RC beam. On the other hand, when the eccentric loads applied to the beam caused biaxial bending in longitudinal as well as transverse direction of the beam as shown in Fig. 1[7, 8].

Eccentric loads changed the structural response of RC beam. The behaviour of RC beam under three or four point loading is different, which cause uniform bending. Whereas, eccentric loads cause biaxial bending, which damage RC beam more rapidly compare to uniformly applied three or four point loading. These effects can cause significant reduction on first crack load, load-deflection response and failure mode of RC beam. Concrete has excellent strength against the compressive force, but the tensile strength is relatively low, usually the tensile strength ranges from 10% to 15% of the compressive strength, and in beams both act simultaneously and tensile stresses become severe under eccentric load [6].

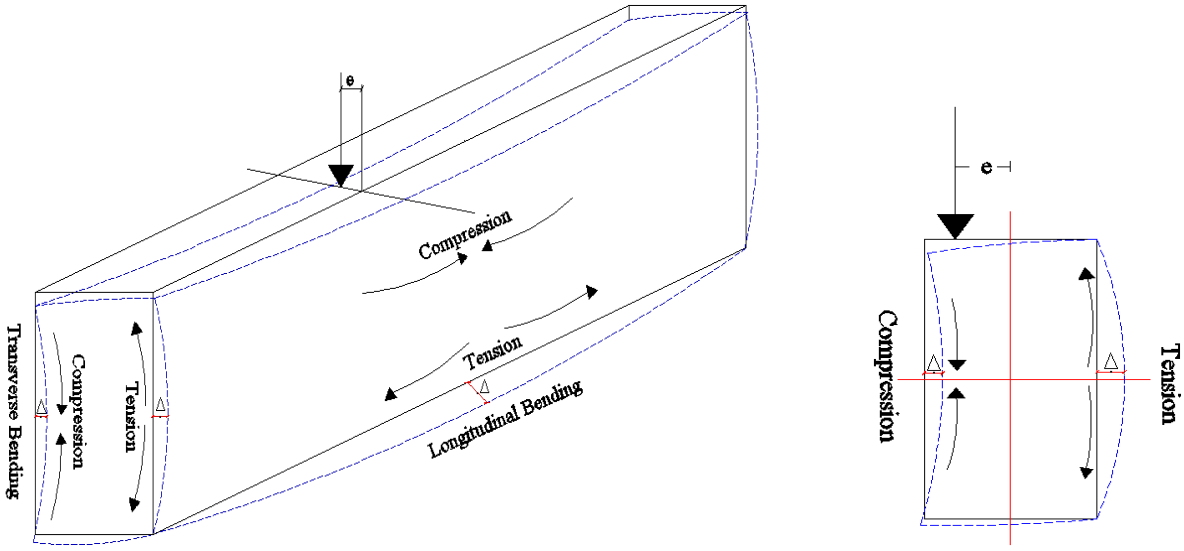


Figure 1: Biaxial bending due to eccentric load.

The flexure failure is occurred by gradual increments in deflection and cracks; these indicate the warning sign prior to failure. In contrast the shear and torsion failure is characterized by exhibiting small deflection with lack of ductility, and exhibiting no warning sign prior to failure [8, 9]. Therefore, building codes have design limitations for flexure reinforcement [10]. The compressive force is resisted by the concrete strength; whereas the tensile stresses are resisted by providing reinforcement bar in tension zone. The failure modes of RC beam depend on the properties of concrete and percentage of reinforcement used in the section [11]. However, these findings are based on uniformly applied three and four points loading on RC beam, therefore there was a need to study the effects of eccentric load that cause flexural and torsional stresses.

Research Significance

There are various types of loading act simultaneously on RC structure such as bridges and buildings Fig. 2. In modern construction the loads are not uniform due to structural configuration especially RC beams. RC beams/ girder contain non-uniform loads due to skewed girder, circular girder, uneven span length, non-uniform traffic, slab and circular ramp of parking etc. The need of understanding structure response of RC beam under eccentric loads is highly needed in modern era to maintain structure stability. The major reason behind lack of experimental investigation in this area includes difficulties in conducting experimental test and corresponding analysis due to complication. So far, there are limited experimental studies available which talk about the effect of eccentric load on RC beam. Therefore, a simple testing setup was developed in this study to investigate the effects of eccentric load on RC beam.



Figure 2: Non-uniform load on Structure [12-14].

Material Properties

The ready mixed concrete used to cast four RC beams with a cross section of 200 x 300 mm and the length of 2000 mm. The internal reinforcement of RC beam contained 2-16Ø mm at the bottom and 2-10Ø mm at the top respectively. All beams were transversely reinforced with 6Ø mm diameter mild bar, spaced at the 70 mm centre to centre throughout the length of the beam with the concrete cover of 25mm. The concrete compressive strength after 28 days of curing was 25 MPa. The RC beams were tested under three point loading with the eccentricity of 0 mm, 40 mm, 60 mm and 80 mm respectively using static actuator. The detail of loading and reinforcement arrangement of RC beam are presented in Fig. 3.

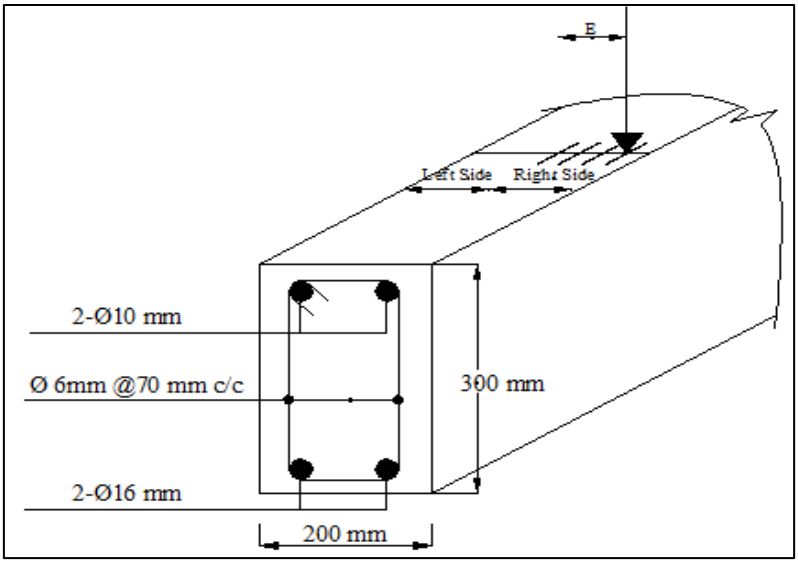


Figure 3: Reinforcement detail and eccentric loading arrangement of RC Beam with 40mm, 60mm & 80mm eccentricity respectively

Result and Discussion

The eccentric load on RC beam caused severe effects by reducing crack load capacity, crack pattern on face of RC beam, failure mode and strength loss due to eccentricity. These effects have discussed and highlighted on the basis of current experimental study. Four control RC beams tested CBE0, CBE40, CBE60 and CBE80 under the 0mm, 40mm, 60mm and 80mm eccentric load; to observe the effects of eccentric load on RC beam.

First Crack & Ultimate Load Carrying Capacity of RC Beams. The cracking load of RC beam initially higher due to uniformly distributed load as shown in Fig. 4. The bar chart represents the first crack load and ultimate load carrying capacity of normal RC beams under different eccentricity. As the load applied on the eccentricity of 40mm, 60mm and 80mm respectively, the initial crack load carrying capacity reduced significantly. The drop observed with respect to control RC beam from 50.01 KN to 34.07 KN, 30.09 KN and 25.02 KN respectively. However, the ultimate load carrying capacity remains stable for CBE0, CBE40 and CBE60 to 61.36 KN, 60.14 KN and 60.23 KN respectively.

On the other hand CBE80 exhibited highest ultimate load of 68.20 KN, this was because eccentric load induced couple moment due to high eccentricity and beam experienced torsional stresses that contribute in additional load carrying capacity, but sudden failure was observed due to rotation caused by eccentric load.

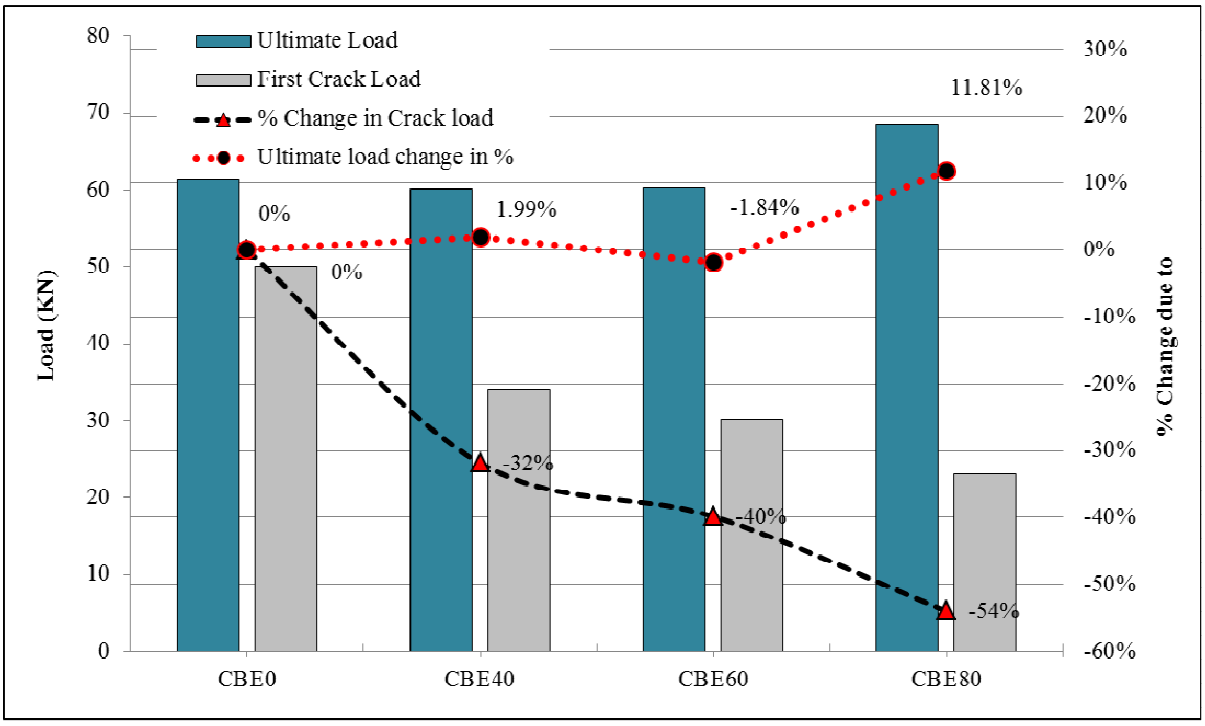


Figure 4. Percentage changed due to eccentric load

Effects of Eccentric Load on the First Crack on the Web of RC beam. Eccentric load induced biaxial bending on RC beam due to high concentration of load in one side; which caused compression on load face and tension on the face away from load as shown in Fig. 3. Therefore, tension face exhibits first cracking load on the other hand compression face reveal first crack after tension face as shown in Fig. 5. The obtained results were quite obvious due to properties of concrete; concrete is good compression and weak in tension.

Additionally, the reduction in the first crack load further decreased with the increment in eccentricity. The relation between the applied loads on the sides to the opposite side of RC beam was also highlighted as an important factor in the development of crack. The percentage decrease due to eccentric load at the load face of beam CBE40 only 32 % for first crack and 10% drop was observed on load side compared to CBE0. Whereas, CBE60 exhibited more quickly than CBE40 due to high eccentricity; the first cracking load strength of beam drop to 40% due to eccentric load, whereas 28% reduction was observed at load face.

Similarly, CBE80 reported its first crack earlier than all beams due to highest torsional moment compared to other beams, with the drop of 54% compared to CBE0. Similarly, second crack on load face appeared with the reduction of 34% compared to control beam CBE0 as present in Fig. 5. The behaviour of RC beam changed after 60 mm eccentricity the cracks appeared more quickly and torsional stresses start dominating together with normal bending. However, these effects are more severe in case of 80 mm eccentricity, which exhibited more cracks on smaller load value and caused premature failure due to eccentric load.

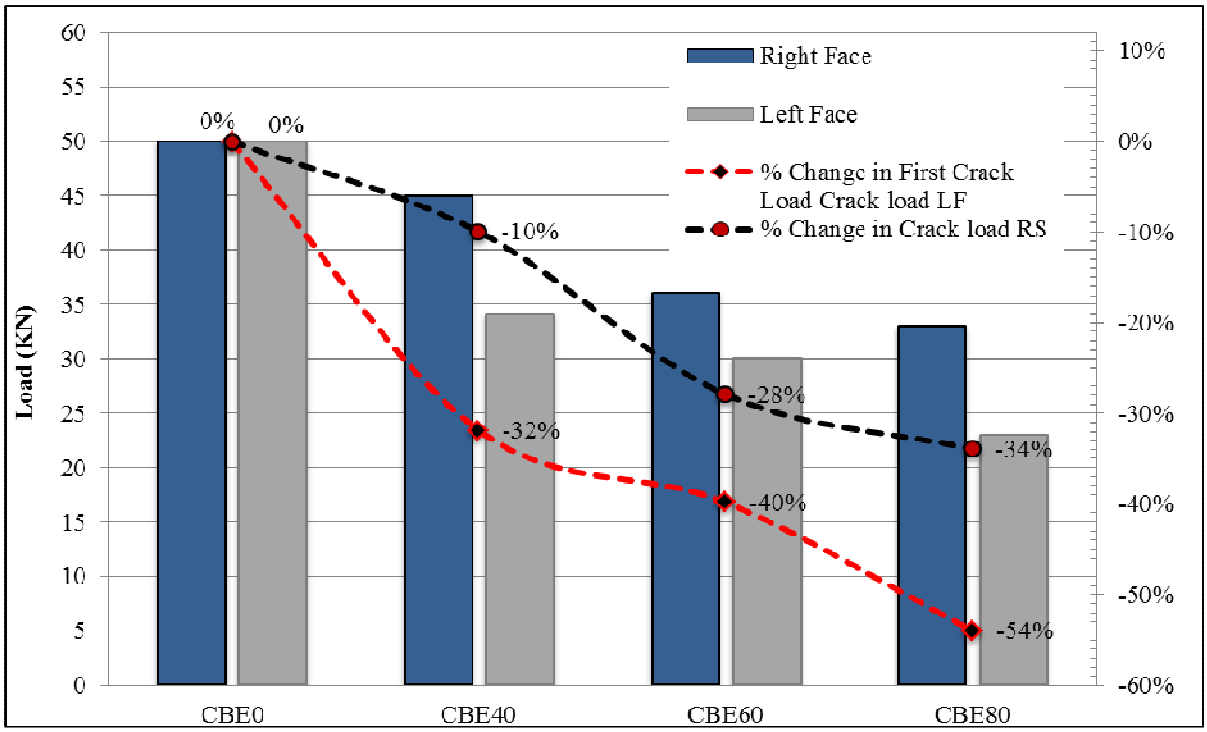


Figure 5. Percentage change in crack load due to eccentric load left face and right face.

Failure Mode. The failure mode changes from ductile to brittle as the eccentricity applied on RC beam. The failure mode of RC beams CBE0 and CBE40 was flexure failure. The failure mode of CBE60 due to eccentric load was accompanied by both flexure and torsion failure. The RC beam CBE80 failed suddenly by splitting edge of concrete cover due to applied loading near the edge of RC beam due to highest torsion moment. The summary of experimental study is summarized in Table 1.

Table 1: Summary of experimental study

Beam ID	Eccentricity (mm)	Ultimate load (KN)	First Crack Load (LS) (KN)	First Crack Load (RS) (KN)	Failure Mode
CBE0	0	61.358	50.01	50.01	Flexure
CBE40	40	60.137	34.073	45.02	Flexure
CBE60	60	60.231	30.093	36.047	Flexure & Torsional
CBE80	80	68.602	23.025	33.047	Torsion

LS: Left side or the side opposite to applied loading.
RS: Right side or the side where load applied.

Conclusion

The effect of eccentric load highly affects the behaviour of RC beam compared to the beam tested under three or four point loading. The study can be summarized as follow:

a) With simple experimental setup and small eccentricity the effects of biaxial bending can be clear found by exhibiting compression on applied load face and tension on opposite face.
b) The first crack load strength was decreased as the eccentricity increased due to biaxial bending.
c) The cracks appear more quickly at the opposite face than the load face, which was obvious due to concrete properties and the effect of biaxial bending.
d) The ultimate load carrying capacity to some extent not much effected due to eccentric load, however CBE80 exhibited slightly high load carrying capacity due to couple moment.
e) The failure mode of beams was flexure failure, flexure cum torsion with more cracks as the eccentricity increased except CBE80 which exhibited premature failure by splitting concrete cover due torsional moment.

Acknowledgement

The author would like to thanks Universiti Teknologi PETRONAS for the graduate assistantship (GA).

References

[1] A. Ghobarah, M. N. Ghorbel, and S. E. Chidiac, "Upgrading Torsional Resistance of Reinforced Concrete Beams Using Fiber-Reinforced Polymer," *Journal of Composites for Construction,* vol. 6, pp. 257-263, 2002.
[2] M. Ameli, H. R. Ronagh, and P. F. Dux, "Behavior of FRP strengthened reinforced concrete beams under torsion," *Journal of Composites for Construction,* vol. 11, pp. 192-200, 2007.
[3] M. Imran, N. Shafiq, I. Akbar, and T. Ayub, "A Review of RC Beams Strengthened for Flexure, Shear and Torsion Loading," presented at the ESTCON 2012, Kuala Lumpur, 2012.
[4] Muhammad Imran, Nasir Shafiq, and Ibrisam Akbar, "Strengthening Techniques & Failure Modes of RC Beam Strengthened Using Fiber Reinforced Polymer. A Review " *GSTF Journal of Engineering Technology,* vol. 2, August 2013 2013.
[5] A. S. Hall, *The Mechanics of Solids* SI Edition ed. Sydney John Wiley & Sons Australasia PTY LTD, 1973.
[6] E. G. Nawy, *Reinforced concrete*: Prentice-Hall Englewood Cliffs;, 1985.
[7] M. N. Hassoun and A. A. Al-Manaseer, *Structural concrete: theory and design*: J. Wiley, 2008.
[8] M. Imran, N. Shafiq, and I. Akbar, "Effects of Eccentric Load on Un-Strengthen and CFRP Strengthened RC Beams," in *The 3rd International Conference on Green Building Technologies and Materials*, Kuala Lumpur, Malaysia, 2013.
[9] S. H. Al-Tersawy, "Effect of fiber parameters and concrete strength on shear behavior of strengthened RC beams," *Construction and Building Materials,* vol. 44, pp. 15-24, 7// 2013.
[10] A. C. 318, *Building code requirements for structural concrete (ACI 318-05) and commentary (ACI 318R-05)*: American Concrete Institute, 2005.
[11] W. Radomski, *Bridge Rehabilitation*: Imperial College Press, 2002.
[12] M. M. Met, "Spectacular Bicycle Park Oasis," in *google image*, ed, 2012
[13] D. Battagello, "Windsor manufacturer stands behind its parkway girders," ed: The Windsor Star 2011.
[14] S. STATS, "Two directional car traffic on bridge in city, top view,"SHUTTERSTOCK STATS, 2013.

Applied Mechanics and Materials Vol. 567 (2014) pp 345-350
© (2014) Trans Tech Publications, Switzerland
doi:10.4028/www.scientific.net/AMM.567.345

Analytical prediction of the mechanical properties of high performance PVA fiber reinforced concrete

Tehmina Ayub[1,a], Nasir Shafiq[1,b] and M. Fadhil Nuruddin[1,c]

[1]Civil Engineering Department, Universiti Teknologi PETRONAS, Bandar Seri Iskandar, 31750 Tronoh, Perak, Malaysia

[a]tehmina@neduet.edu.pk, [b]nasirshafiq@petronas.com.my, [c]fadhilnuruddin@petronas.com.my

Keywords: High performance fiber reinforced concrete, PVA fibers, Compressive strength, Splitting tensile strength, Flexural strength, Analytical prediction.

Abstract. In this paper, mechanical properties of three series of high performance fiber reinforced concrete (HPFRC) containing 1, 2 and 3% of Polyvinyl Alcohol (PVA) fiber volume are presented. The first series of HPFRC was prepared by using 100% cement, whereas remaining two series were prepared by replacing 10% cement content with silica fume and locally produced metakaolin. All series were designed with water to binder ratio (w/b) of 0.4. The mechanical properties determined in this study include compressive strength, splitting tensile strength and flexural strength. Testing of the specimens was conducted at the 28 days of curing. Experimental results showed that the 3% PVA fiber is the optimum fiber volume to improve the mechanical properties of HPFRC. The variation in the mechanical properties due to the addition of PVA fibers was investigated and presented in the form of mathematical relationship. Further, interrelationship among the mechanical properties was also determined.

Introduction

In structural designing, knowledge of the mechanical properties of the construction materials is very important. For example, in column designing, compressive strength is very important, while for earthquake resistant structural design, tensile strength of the material is more important. On contrary, designing of concrete pavements and airport runways is based on the flexural strength and these structures are subjected to tensile stresses showing that the tensile strength is significant than compressive strength.

High performance fiber reinforced concrete (HPFRC) is a commonly used material in the construction of earthquake resistant structure as well as structures subjected to repetitive loadings such as airport runways, highway pavements and bridge decks, etc. The properties of the HPFRC are mainly influenced by the type of the fibers used. Upon reviewing the available literature, it has been found that the published work on HPFRC is mostly based on the steel fibers. Therefore, in this study, authors determined the mechanical properties of HPFRC containing PVA fibers and predicted the analytical dependency of the splitting tensile strength and flexural strength on the compressive strengthas well as on the PVA fiber volume. Beside this, relationship between the splitting tensile strength and flexural strength is also established. The reason for selecting PVA fiber is that this fiber, since 1990s, has been usedas a major constituent in Engineering Cementitious Composites (ECC) [1-3] due to its excellent properties such as toughness, high stability and durability, non-hazardous nature, high modulus of elasticity, high bonding strength with cement matrix and reasonable cost [4]. PVA fibers are organic manmade fibers from carbon, hydrogen, and oxygen [4] which are known as very high performance fiber reinforcement for concrete. Recently, Behrooyan and Ahmadian [5] investigated and compared the behavior of HPFRC reinforced with PVA and steel fibers and confirmed that PVA fibers, compared to the steel fibers, are better efficient to transfer tensile stresses in the concrete as well as to establish a bridging phenomenon prior to the failure of the fibers. They [5] associated the reason of such behavior of HPFRC to the better bond between cementitious matrix and the fibers which lead to the slow progressive post-peak slope of the load-displacement curve. On contrary, slipping of the steel fibers is reported due to the lack of bond between fibers and concrete. Moreover, they [5] mentioned that the use of PVA

fibers significantly improved the flexural stresses than compressive strength and the toughness of high strength concretes reinforced with PVA and steel fibers closed to each other. Therefore energy absorption of both concretes was almost in the same range and higher than plain HSC. Ayub et al. [6] recently investigated the behavior of HPFRC containing 1, 2 and 3% volume of the PVA fibers and reported the improvement in the mechanical properties, specially splitting tensile strength and flexural strength at higher fiber volume of 3%.

Experimental Materials, Concrete Mixes,Specimen Casting and Curing Details

HPFRC Concrete Mixes. Total three series of HPFRC were prepared and named as Series "PP", Series "SP" and Series "MP" (Refer Table 1). The materials and quantities used to prepare the matrix of HPFRC are also presented in Table 1.Silica fume and metakaolin were used to replace 10% cement content and the volume of the fibers was used as 1, 2 and 3% with respect to the volume of the concrete mix. The physical and chemical properties of cement, silica fume and metakaolin are given in Table 2. Straw type Kuraray RF 4000 PVA fibers were used with a diameter and cut length of 0.66 and 30mm. The tensile strength, flexural strength, specific gravity and the elongation were 900 MPa, 23 GPa, 1.3 and 7%, respectively.

Table 1. Mix quantities for HPFRC containing PVA fibers

Series Label	Mix designation	Mix quantity (kg/m^3)								Superplasticizer
		Cement	Silica fume	Metakaolin	Fine aggregate	Coarse aggregates		Water	PVA fibers	
						< 10mm	10-20mm			
"PP"*	PP-0	450	-	-	670	600	500	180	0	Variable, minimum slump 50 ± 10 mm
	PP-1	405	-	-	670	600	500	180	13	
	PP-2	405	-	-	670	600	500	180	26	
	PP-3	405	-	-	670	600	500	180	39	
"SP"	SP-0	450	45	-	670	600	500	180	0	
	SP-1	405	45	-	670	600	500	180	13	
	SP-2	405	45	-	670	600	500	180	26	
	SP-3	405	45	-	670	600	500	180	39	
"MP"	MP-0	450	-	45	670	600	500	180	0	
	MP-1	405	-	45	670	600	500	180	13	
	MP-2	405	-	45	670	600	500	180	26	
	MP-3	405	-	45	670	600	500	180	39	

* "PP" represents a plain concrete containing PVA fiber. The first letter in the series labels is representing the "Plain concrete", while second letter represents the "PVA". Similar notations were also followed in other series

Table 2. Physical and Chemical Composition of OPC, silica fume and metakaolin

Properties	OPC	Silica fume	Metakaolin
Specific gravity	3.05	2.2	--
BET Surface Area (m^2/g)	0.392	16.455	12.174
Loss on ignition (%)	--	2.0	11
Average particle size (μm)	--	--	2.5-4.5
SiO_2 (%)	20.44	91.40	53.87
Al_2O_3 (%)	2.84	0.09	38.57
CaO (%)	67.73	0.93	0.04
MgO (%)	1.43	0.78	0.96
SO_3 (%)	2.20	--	--
Na_2O (%)	0.02	0.39	0.04
K_2O (%)	0.26	2.41	2.68
TiO_2 (%)	0.17	--	--
MnO (%)	0.16	0.05	0.01
Fe_2O_3 (%)	4.64	--	1.40
TiO_2 (%)	--	0.04	0.95
P_2O_5 (%)	--	0.38	0.10

Note: Properties were determined by X-Ray Fluorescence (XRF) and Brunauer–Emmett–Teller (BET) Specific surface area analysis

Specimen Casting and Curing. For each series comprised of four mixes, total six cylinders (size: 100×200mmas per BS 1881-110:1983 standard), three cubes (size: 100×100×100mm as per BS 1881-108:1983 standard) and one beam (size: 100×100×500mm as per BS 1881 Part 118: 1983) were prepared. Out of the six, three cylinders were used for the compression test, while remaining

three cylinders were used to determine the splitting tensile strength. All ingredients of HPFRC were mixed in a pan mixer in compliance to BS 1881- 125: 1986 standard. For concrete mixes with fibers, extra time was given to ensure proper mixing and this duration was increased as the fiber volume increased. After mixing, slump of the concrete was first determined which was found in the range of 50±10mm. Concrete was then fully poured into the molds except cylinders where 3 mm to 6 mm space for the top surface of the molds was left unfilled. This space was then with the mortar, prepared with the cement content and water cement ratio similar to that used in the concrete, to provide capping as recommended in BS 1881-110:1983 standard. After 24 hours, specimens were taken out from the molds and soaked in the water tank for 28 days.

Specimens Testing Details and Results

Testing of all specimens was carried out at 28 days of wet curing and few hours of air-drying.

Compression Testing Detail and Results. Testing for the compressive strength of the three cubes of HPFRC was carried out as per BS 1881-111:1983, while testing of the three cylinders was performed in accordance with the ASTM C 39/ C 39 M: 2005. Compression testing machine of 3000 kN capacity was used to apply a compressive load with a loading pace of 3 kN/sec. Results of the average compressive strength of the three cubes and three cylinders are presented in Table 3.

Splitting Tensile Testing Detail and Results. Testing for the splitting tensile strength of HPFRC was carried out as per BS 1881-117:1973. Compression testing machine of 3000 kN capacity was used to apply a compressive load with a loading pace of 0.3 kN/sec. Results of average splitting tensile strength results of three cylinders are presented in Table 3.

Flexural Testing Details and Results. To test the three HPFRC beams; Universal Testing Machine (UTM) of 500 kN capacity was used. Two-point loading on the beams with a loading pace of 0.05 kN/sec as per BS 1881 Part 118: 1983.Flexural test results are shown in Table 3.

Table 3. Summary of the experimental results

Specimen labels	Compressive Test Results			Splitting Tensile Test Results		Flexural Test Results	
	Average cube strength (MPa)	Average cylindrical strength (MPa)	Cube Strength variation with respect to control	Splitting tensile strength (MPa)	Strength increase with respect to control	Flexural strength (MPa)	Ultimate* Moment (N-m)
Series "PP": Prepared by using 100% cement and 0, 1, 2 and 3% PVA fiber volume fractions							
PP-0	88.73	73.89	0.83	5.41	1	5.664	944
PP-1	94.43	73.97	0.78	5.524	1.02	6.36	1060
PP-2	96.2	74.81	0.78	6.51	1.20	6.52	1086.67
PP-3	95.08	75.38	0.79	7.04	1.30	5.75	958.33
Series "SP": Prepared by using 90% cement and 10% "Silica Fume" and 0, 1, 2 and 3% PVA fiber volume fractions							
SP-0	102.4	81.17	0.79	6.22	1.00	5.004	834
SP-1	102.8	82.17	0.80	6.65	1.07	6.20	1090
SP-2	104.8	83.39	0.80	7.684	1.24	6.21	1193.33
SP-3	104.2	84.54	0.81	7.992	1.28	6.38	1143
Series "MP": Prepared by using 90% cement and 10% "Metakaolin" and 0, 1, 2 and 3% PVA fiber volume fractions							
MP-0	101.27	84.85	0.84	6.27	1.00	5.91	984.8
MP-1	108.01	84.19	0.78	6.49	1.04	6.30	1050
MP-2	109.69	85.48	0.78	6.86	1.11	6.72	1120
MP-3	102.67	87.27	0.85	7.18	1.36	6.41	1068.33

Note: Each result presented in this table is an average of three specimens

Analysis of the Experimental Results

Compressive Behavior of High Performance Concrete with and without PVA fibers. With reference to the average compressive strength of the cubes and the cylinders shown in the Table 3, it was found that the use of mineral admixtures increased the compressive strength of the concretes. The use of silica fume increased the cube and cylindrical compressive strength as 15.37% and 9.85% compared to the plain concrete. However, the addition of metakaolin increased the cube and cylindrical compressive strength as 14.13% and 14.83%. This confirms the conclusion reported in [6] that the compressive strength increases with the use of silica fume and metakaolin.

For all series of HPFRC (Refer Table 2), Fig. 1 and Fig. 2 show the comparison of the average results of the cube and cylinder compressive strength ofHPFRC, which show the increase up to 3% PVA fiber volume. However, in plain series (Series "PP") and metakaolin series (Series "MP"), the cube compressive strength was found to be decreasing with 3% PVAfiber volume. The reason of the decrease in the compressive strength may be due to the smaller size of the molds which caused an improper compaction with 3% PVAfibers and finally resulted in the form of voids in the concrete mass. Presence of voids was confirmed by weighing the specimens after removal of the molds which showed that the density of all specimens i.e. cubes and cylinders was lowest among all the mixes. Compression test results of cylinders showed considerable less variation due to the capping which avoided the uneven loading surface of the cylinders.

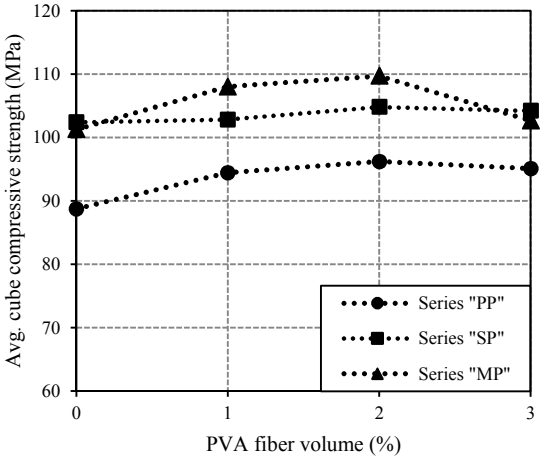


Fig. 1.Variation in cube compressive strength with respect to PVA fiber volume fraction

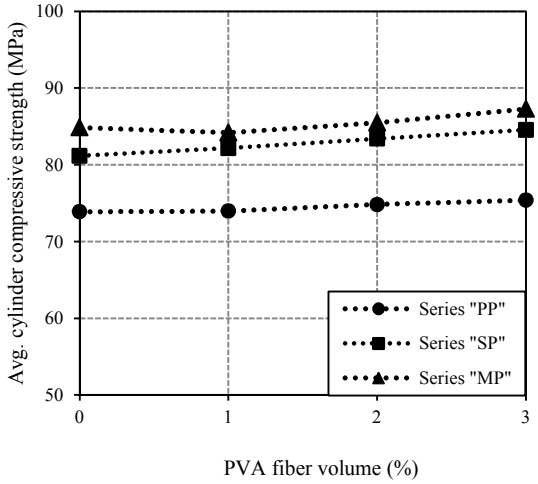


Fig. 2. Variation in cylinder compressive strength with respect to PVA fiber volume fraction

Across the groups, compressive strength results of Series "SP" and Series "MP" (for all fibers volumes) were found to be higher than the plain concrete (i.e. Series "PP"). As shown in Table 3, the cube and cylinder compressive strength results of Series "SP" and Series "MP" were close enough showing that the use of metakaolin can be a good alternative of silica fume to produce economical concrete. The relationship between the cylindrical compressive strength for all three series are developed based on the test data of current study and the fiber volume fraction used using square fitting approach. These relationships are shown in Eq. 1 (for Series "PP"), Eq. 2 (for Series "SP") and Eq. 3 (for Series "MP") as follows:

$$f_c = 0.1361(V_f)^2 + 0.1066\,(V_f) + 73.89 \qquad (R^2 = 0.9633) \qquad (1)$$

$$f_c = 0.0413(V_f)^2 + 1.0045\,(V_f) + 81.17 \qquad (R^2 = 0.9993) \qquad (2)$$

$$f_c = 0.6316(V_f)^2 - 1.0626\,(V_f) + 84.85 \qquad (R^2 = 0.979) \qquad (3)$$

Results of splitting tensile strength also confirm that addition of PVA fibers improved the tension behavior of concrete, especially with the increase of PVA fiber volume. The improvement in the splitting tensile strength with respect to control is plotted in the Fig. 3 which shows that the splitting tensile strength of the mixes containing 3% PVA fibers is highest. Against to this, the mixes containing 1% fiber volume exhibited the lowest splitting tensile strength as compared to those mixes which contained 2 and 3% PVA fiber content. This confirms that the effectiveness of the use of 3% PVA fibers in increasing the splitting tensile strength as an optimum fiber volume.

The dependence of splitting tensile strengthon compressive strength ($\sqrt{f_{c0}}$) is well known. Therefore, to predict the relationship of splitting tensile strength (f_{sp}) with the cylindrical compressive strength ($\sqrt{f_{c0}}$) and the fiber volume fraction (V_f), the data of all three series

presesented in Table 3 was used. These relationships are shown in Eq. 4 (for Series "PP"), Eq. 5 (for Series "SP") and Eq. 6 (for Series "MP") as follows:

$$f_{sp}= 0.514\ (V_f)+0.629\sqrt{f_{c0}} \qquad (R^2= 0.906) \qquad (4)$$

$$f_{sp}= 0.916\ (V_f)+0.69\sqrt{f_{c0}} \qquad (R^2= 0.995) \qquad (5)$$

$$f_{sp}= 0.295\ (V_f)+0.681\sqrt{f_{c0}} \qquad (R^2= 0.987) \qquad (6)$$

f_{c0} is the compressive strength of the respective control specimen of each series.

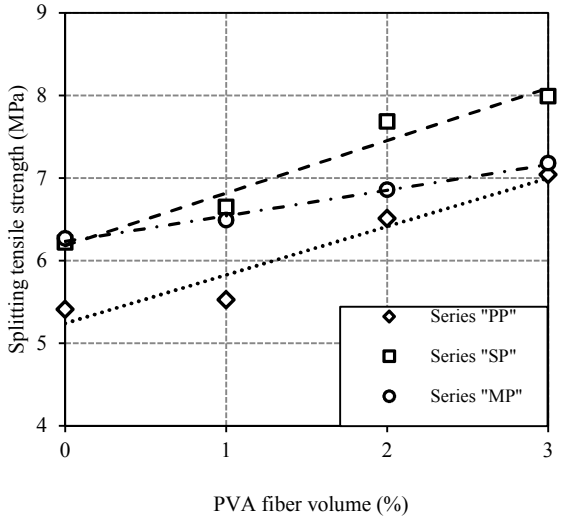


Fig. 3. Variation in the splitting tensile strength

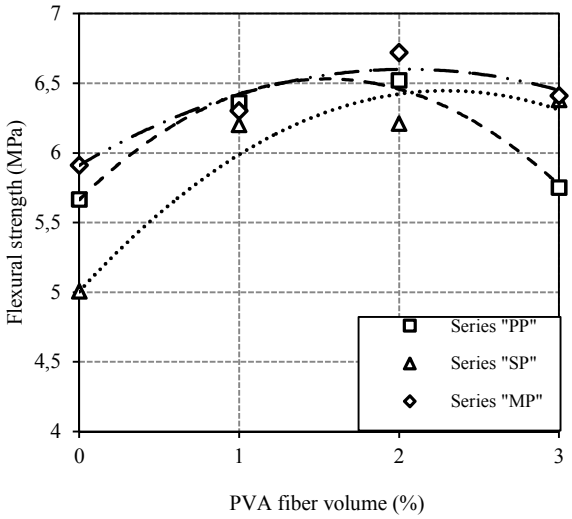


Fig. 4. Variation in the flexural strength

In case of flexure strength, the strength development of high performance concrete reinforced with PVA fibers is shown in Fig. 4 which shows the increase in the flexural strength with the increase in fiber volume fraction up to 2%, beyond which flexural strength observed to be decreasing. The dependence of flexural strength (f_{fl}) on the cylindrical compressive strength ($\sqrt{f_{c0}}$) of the control mix and the fiber volume fraction (V_f) is determined and given in Eq. 7 (for Series "PP"), Eq. 8 (for Series "SP") and Eq. 9 (for Series "MP") as follows:

$$f_{fl}=-0.3613(V_f)^2+ 1.1195\ (V_f)+0.659\sqrt{f_{c0}} \qquad (R^2= 0.9852) \qquad (7)$$

$$f_{fl}=-0.2742(V_f)^2+ 1.2577\ (V_f)+0.555\sqrt{f_{c0}} \qquad (R^2= 0.9212) \qquad (8)$$

$$f_{fl}=-0.165(V_f)^2+ 0.675\ (V_f)+0.642\sqrt{f_{c0}} \qquad (R^2= 0.9094) \qquad (9)$$

f_{c0} is the compressive strength of the respective control specimen of each series.

The dependency of splitting tensile strength (f_{sp}) and flexural strength (f_{fl}) on compressive strength ($\sqrt{f_{c0}}$) of the control concretes as well as the relationship between the splitting tensile strength (f_{sp}) and flexural strength (f_{fl}) is shown in Table 4.

Table 4. Interrelationship of the mechanical properties of HPFRC

Splitting tensile strength (f_{sp})	Flexural strength (f_{fl})	Splitting tensile strength (f_{sp}) and Flexural strength (f_{fl})	Remarks
$0.67\sqrt{f_{c0}}$	$0.62\sqrt{f_{c0}}$	$f_{fl} = 0.93 f_{sp}$	For no fiber
$0.69\sqrt{f_{c0}}$	$0.70\sqrt{f_{c0}}$	$f_{fl} = 1.01\ f_{sp}$	For 1% PVA fibers
$0.78\sqrt{f_{c0}}$	$0.72\sqrt{f_{c0}}$	$f_{fl} = 0.92 f_{sp}$	For 2% PVA fibers
$0.82\sqrt{f_{c0}}$	$0.68\sqrt{f_{c0}}$	$f_{fl} = 0.83 f_{sp}$	For 3% PVA fibers

Summary

Following conclusions are drawn from the current investigation:

1. In all of the three series of HPFRC, cylinder compressive strength with 3% PVAfiber volume was highest. At 3% fiber volume, results of cube compressive strength were observed to be lower than 1 and 2% fiber volumes due to the presence of void (confirmed by weighing the cube specimen). Across the groups, compressive strength results of Series "SP" and Series "MP" (for all fibers volumes) were found to be higher than the plain concrete (i.e. Series "PP"). Except 2% fiber volume, the compressive strength results of Series "SP" and Series "MP" were close enough showing that use of metakaolin can be a good alternative of silica fume.
2. In all of the three series of HPFRC, splitting tensile strength was found to be increasing with the increasing volume of PVA fibers. Moreover, use of mineral admixture (particularly silica fume) together with PVAfibers better improved the splitting tensile characteristics of HPFRC.
3. Similar to compressive strength results, the addition of 2% PVA significantly improved the flexural strength, while with 3% fiber volume, flexural strength was observed to be decreased.
4. Relationships were proposed to predict the dependency of the mechanical properties on the PVA fiber volume and the compressive strength of the plain concrete which can better correlates the experimental and predicted results.

Acknowledgment

Authors wish to acknowledge the financial support provided by the UniversitiTeknologi PETRONAS (UTP), Malaysia and the assistance from the lab technicians for their help during testing of the specimens and data acquisition.

References

[1] B. Suryanto, K.M.K. Nagai, V.C. Li, K. El-Kashif, K. Maekawa, B. Mobasher, S.-L. Gao, E. Mäder, Predicting the creep strain of PVA-ECC at high stress levels based on the evolution of plasticity and damage, J. Adv. Conc. Tech. 11 (2013) 35-48.

[2] V.C. Li, S. Wang, C. Wu, Tensile strain-hardening behavior of polyvinyl alcohol engineered cementitious composite (PVA-ECC), ACI Mater. J. 98 (2001) 483-492.

[3] V.C. Li, C. Wu, S. Wang, A. Ogawa, T. Saito, Interface tailoring for strain-hardening polyvinyl alcohol-engineered cementitious composite (PVA-ECC), ACI Mater. J. 99 (2002) 463-472.

[4] T. Horikoshi, A. Ogawa, T. Saito, H. Hoshiro, Properties of Polyvinylalcoholfiber as reinforcing materials for cementitious composites, in Int. RILEM workshop on HPFRCC in structural applications, (2006) 145-153.

[5] M.Behrooyan, H.R. Ahmadian, Effects of Polyvinyl Alcohol fibers on fracture energy of concrete, Int. Research J. Appl. Basic Sciences, 6 (2013) 484-491.

[6] T. Ayub, N. Shafiq, M.F. Nuruddin, S.U. Khan, Mechanical properties of high-strength concrete reinforced with PVA and Basalt fibres, in InCIEC 2013 Int. Civil and Infrastructure Engg., Kuching, Sarawak, Malaysia, 22-25th September 2013 pp. 286-289.

[7] T. Ayub, S.U. Khan, F.A. Memon, Mechanical characteristics of hardened concrete with different mineral admixtures: A review, The Scientific World J., 2014, Article ID 875082, p.15

Applied Mechanics and Materials Vol. 567 (2014) pp 351-355
© (2014) Trans Tech Publications, Switzerland
doi:10.4028/www.scientific.net/AMM.567.351

Behaviour of Oil Palm Shell Reinforced Concrete Beams Added With Kenaf Fibres

Sharifah Maszura Syed Mohsin[a], Sayid Javid Azimi[b] and Abdoullah Namdar[c,]

Faculty of Civil and Earth Resources, Universiti Malaysia Pahang, Malaysia

[a]maszura@ump.edu.my, [b]s.javidazimi@gmail.com, [c]anamdar@ump.edu.my

Keywords: Ductility, kenaf fibres, load carrying capacity, oil palm shell reinforced concrete

Abstract. The present article reports the findings of a study into the behaviour of oil palm shell reinforced concrete (OPSRC) beams with the addition of kenaf fibres. This work aims at examining the potential of kenaf fibres to improve the strength and ductility of the OPSRC beams as well as observing its potential in serving as part of shear reinforcement in the beams. Two different arrangements of the shear links in OPSRC beams with a selection of kenaf fibres content (10kg/m^3 and 20kg/m^3, respectively) were tested under monotonic loading. The results show that the addition of kenaf fibres enhances the load carrying capacity, ductility apart from altering the failure mode of the beams from brittle shear mode to flexural ductile mode. Furthermore, the study shows that kenaf fibres are compatible with OPSRC with desirable results.

Introduction

As one of the major oil palm producers in the world, Malaysia contributes to over 4 million tonnes oil palm shell (OPS) as agricultural waste [1,2]. Therefore, in order to preserve the environment, plenty work on using OPS as lightweight aggregate in lightweight concrete are carried out [1-4]. However, the performance of the OPS concrete with natural fibres has never been published. The current work incorporates the use of kenaf fibres in concrete as this type of fibre reinforced concrete was reported to be a potentially promising "green" construction material to be used in a number of different structural applications [5].

Therefore, the present work sets to investigate the potential advantages of adding kenaf fibres to oil palm shell concrete in order to enhance the structural response of the concrete structures. Furthermore, potential of kenaf fibres as part of shear reinforcement in oil palm shell (OPS) reinforced concrete beams were also observed by testing the beams with different amount of shear reinforcement.

Methodology

Preparation of the OPS concrete mixtures. Table 1 lists the properties of the OPS concrete mixtures. OPS kernels were taken from a local factory and was washed with soapy water before it was left for air dry. The OPS then was sieved and only those with size between 10 mm to 20 mm were used in the mixture.

On the other hand, the kenaf fibres included in the mixtures were 30 mm of length with a diameter between 0.1 mm to 2 mm. The amounts of fibres considered in this study were 10 kg/m^3 and 20 kg/m^3, respectively. The water/cement ratio of the mixture was set to 0.4. One mixture of the OPS concrete was used to cast the beam with full shear reinforcement, and this beam was taken as control beam.

Table 1 Properties of the OPS concrete mixtures

Content	Mix 1	Mix 2	Mix 3
Ordinary Portland Cement (kg/m^3)	510	510	510
Oil palm shell (kg/m^3)	848	848	848
Sand (kg/m^3)	308	308	308
Water (kg/m^3)	204	204	204
Superplasticizer (kg/m^3)	20.4	20.4	20.4
Kenaf fibres (kg/m^3)	0	10	20

Testing. The loading arrangement and reinforcement properties of the beam are illustrated in Fig. 1 and Fig. 2. The beams were initially designed with shear reinforcement less than that is required to cause shear failure. Two arrangements were considered (i) full shear reinforcement and (ii) reduced in shear reinforcement (this was carried out by increasing the spacing between the shear links by 50 %). Subsequently, two amounts of fibres contents were added into the OPS concrete mixture to examine the effect of kenaf fibres in OPS reinforced concrete beams. Therefore, five beams (three for full shear reinforcement and two for reduced in shear reinforcement) were tested under four-point bending test. The beam with full shear reinforcement without fibres was considered as the control beam. The test was carried out on the 56th day in order to ensure that the OPS reinforced concrete beams added with kenaf were fully hardened.

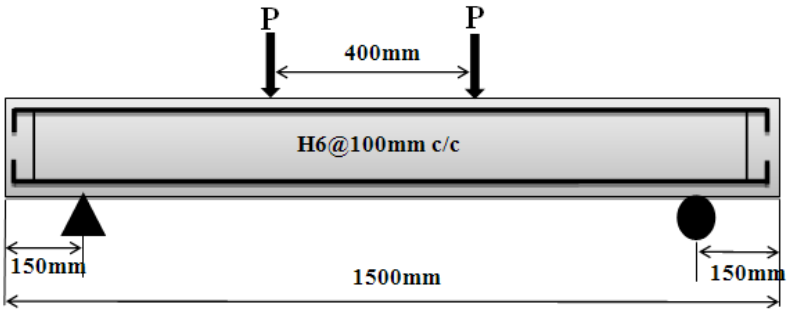


Figure 1 Loading arrangement and dimensions of the beam

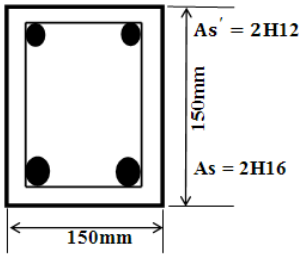


Figure 2 Main reinforcement arrangement and dimensions of the beam

Results

OPS Reinforced Concrete Beams With Full Shear Reinforcement. Fig. 3 illustrates the load-deflection curves of the experimental work obtained for OPS-kenaf fibre reinforced concrete (OPS_KFRC) beams for full shear reinforcement arrangement. It could be observed from the load-deflection curves, that the beam without fibres failed early at a deflection of 12 mm and at a load carrying capacity of 69.8 kN. However, the beams with the inclusion of fibres show an increase in the peak strength and ductility as the fibres content is increased.

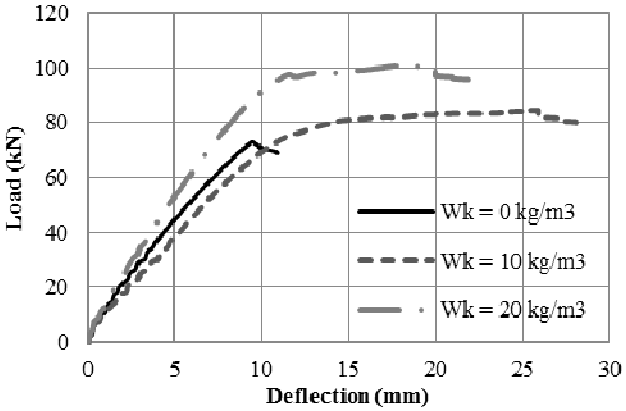


Figure 3 Load-deflection curves for OPS-KFRC beams with various fibres content

To study this further, the key results have been summarised in Table 2 below (where P_{max} represents the maximum strength, $P_{max,o}$ represents the maximum strength of the control beam, P_u the ultimate (i.e. residual) strength, δ_y the yield deflection, δ_u the ultimate deflection and μ the ductility). The table shows that the peak strength of the beam is increased to up to 22% with W_k = 20 kg/m^3. Notable increase in the stiffness can also be seen for beams with higher content of fibres. This suggests that there are clear benefits of adding fibres at the serviceability limit state. Furthermore, significant increase in the ductility to up to 67% may be observed from both Fig. 3 and Table 2. This demonstrates that with the inclusion of the fibres facilitates ductile mode of failure.

Table 2 Results for OPS-KFRC beams (* this ratio represents the change in maximum strength, † this ratio represents the change in residual strength, ‡ this ratio represents the change in ductility)

W_k (kg/m^3)	P_{max} (kN)	P_{max}/ P_{maxo}*	P_u (kN)	P_u/ P_{max}†	Δy (mm)	δu (mm)	$\mu=\delta u/\delta y$ ‡
0	73.4	1.00	69.8	0.95	10	12	1.20
10	78.0	1.06	82.0	1.05	12	24	2.00
20	89.4	1.22	90.8	1.02	12	20	1.67

Fig. 4, Fig. 5 and Fig. 6 show the cracking of the beams with W_k = 0 kg/m^3, W_k = 10 kg/m^3 and W_k = 20 kg/m^3, respectively at failure. The results obtained implies that the fibres acts appropriately in controlling the crack propagation of the beam. Hence, sufficient amount of fibres serve potential as part of shear reinforcement, which in turn changes the mode of failure from brittle (beam without fibres) to a more ductile manner (beam with fibres).



Figure 1 OPS reinforced concrete beam without fibres (Control beam)



Figure 2 OPS reinforced concrete beam added with 10 kg/m^3 kenaf fibres



Figure 3 OPS reinforced concrete beam added with 20 kg/m^3 kenaf fibres

OPS Reinforced Concrete Beams With Reduced Shear Reinforcement. A further investigation was carried out by reducing the shear reinforcement (this is carried out by increasing the spacing between the shear links by 50%), adding two amounts of kenaf fibres and testing under four-point bending test. The results obtained is depicted in Fig. 7 and are summarized in Table 3. In this shear links arrangement, only beams with inclusion of fibres were tested as the beam without fibres was believed to fail in more brittle manner compare to the control beam.

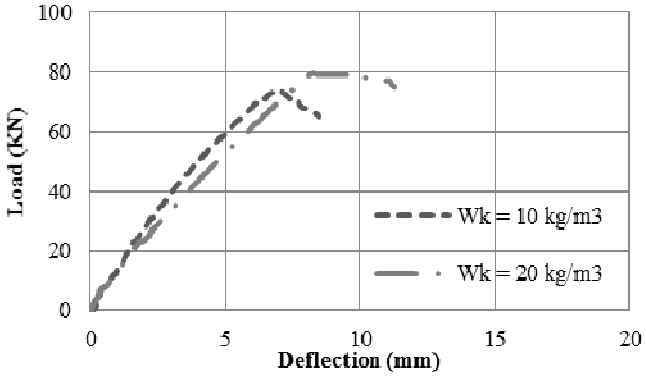


Figure 7 Load-deflection curves for OPS-KFRC beams with reduced in shear reinforcement

Table 2 Results for OPS-KFRC beams with reduced in shear reinforcement (* this ratio represents the change in maximum strength, † this ratio represents the change in residual strength, ‡ this ratio represents the change in ductility)

W_k (kg/m^3)	P_{max} (kN)	P_{max}/ P_{maxo}*	P_u (kN)	P_u/ P_{max}†	δy (mm)	δu (mm)	μ=δu/ δy ‡
10	74.2	1.01	65.0	0.88	8	9	1.10
20	80.0	1.09	78.8	0.88	8	12	1.46

The results show that the peak strength of the beams with reduced in shear reinforcement increased up to 10% in comparison to the control beam (with full shear reinforcement). Sufficient ductility is observed for both beams with 10% for W_k = 10 kg/m^3 and 46% for W_k = 20 kg/m^3. In comparison to the control beam, the ultimate deflection obtained for beam with W_k = 10 kg/m^3 is similar at 12 mm. This reflects the extremely brittle nature of the beams with reduced shear links and demonstrates the potential for fibres to enhance both peak strength and ductility.

Conclusion

A study on the behaviour of OPS reinforced concrete beams added with kenaf fibres was carried out. An enhancement in the load carrying capacity and ductility was observed with the presence of fibres. Similar results were observed on the study carried out for steel fibres [6]. This demonstrates that kenaf fibres serve good potential in restraining the crack propagation of the beam, hence contributing to higher strength and ductility. Furthermore, the mode of failure of the beams was observed to change into a ductile manner with the inclusion of fibres. Therefore, this result shows that kenaf fibres have potential to compensate for a reduction in shear links. This can be useful in

situations where the amount of shear reinforcement required can lead to congestion of the links and can also simply complex construction arrangements.

Acknowledgement

This project is supported by Universiti Malaysia Pahang, Malaysia, under internal research grant number RDU 1203108.

References

[1] U. J. Alengaram, B. G. Al Muhit, and M. Z. Jumaat, Utilization of oil palm kernel shell as lightweight aggregate in concrete – A review, Construction and Building Materials 38 (2013) 161–172.

[2] D. C. L. Teo, M. A. Mannan, V. J. Kurian, and C. Ganapathy, Lighweight concrete made from oil palm shell (OPS): Structural bond and durability properties, Building and Environment 42 (2007) 2614–2621.

[3] U. J. Alengaram, M. Z. Jumaat, H. Mahmud, and M. M. Fayyadh, Shear behaviour of reinforced palm kernel shell concrete beams, Construction and Building Materials 25 (2011) 2918–2927.

[4] M. A. Mannan, and C. Ganapathy, Concrete from agricultural waste-oil palm shell (OPS), Building and Environment 39 (2004) 441–448.

[5] A. Elsaid, M. Dawood, R. Seracino, and C. Bobko, Mechanical properties of kenaf fiber reinforced concrete, Construction and Building Materials 25 (2011) 1991–2001.

[6] S. Syed Mohsin, A. Abbas, and D. Cotsovos, Shear behaviour of steel-fibre-reinforced-concrete beams, 11th International Conference on Concrete Engineering and Technology 2012 (CONCET2012).

Applied Mechanics and Materials Vol. 567 (2014) pp 356-361
© (2014) Trans Tech Publications, Switzerland
doi:10.4028/www.scientific.net/AMM.567.356

Characterization of Stand Chopped Basalt Fiber Self – Compacting Reinforced Concrete (SCB-SCC)

Nasir Shafiq[1, b], Muhd Fadhil Nuruddin[1, c], Ahmed Fathi Mohamed Salih[1, a], Ali Elheber [1, d]

[1]Civil Engineering Department, Universiti Teknologi PETRONAS

Bandar, Seri Iskandar 31750 Tronoh, Perak Darul Ridzun, Malaysia

[a] alahmdy665@yahoo.com, [b] nasirshafiq@petronas.com.my, [c] fadhilnuruddin@petronas.com.my and [d] alielheber@yahoo.com

Keywords: Self-Compacting Concrete, Fly ash, MIRHA and Stand Chopped Basalt Fiber

Abstract. In the world today, producers of high performance concrete usually look for locally available material to provide low cost concrete. To reduce the total cost of concrete, it is recommended to use a mineral admixture by replacing the cement content while the improvement in the strength of concrete can be achieved by implementing the fibers as a discrete material in the concrete mix. Within this study, a attempt has been given to analyze the properties of self-compacting concrete (SCC) with microwave incinerated rice husk ash (MIRHA) and fly ash as a two types of filler. This was to enhance the properties of SCC with the Stand Chopped Basalt (SCB) fiber having been added to the concrete mix. The experimental work was a fresh and a hardened test with the trend of the result showing the possibility to increase the properties of SCC by using MIRHA and SCB fiber.

Introduction

The primary property that defines self-compacting concrete (SCC) is a high workability in getting compaction and the specified hardened characteristic. SCC not just flows under its very own weight but additionally fills the whole form and gets uniform consolidation without segregation. Hence, the technique for achieving self-compatibility involves not just the high deformability of the paste or mortar but additionally the capacity to avoid the segregation between the coarse aggregate and the mortar once the concrete flows with the limited zone of the reinforcing bars. However, because the concrete flowability increases, its stability decreases. This truly is due to the decrease in viscosity from the fresh concrete [1-4]. The phrase 'fiber reinforced concrete' is determined through the American Concrete Institute (ACI) within their ACI 116R Cement and Concrete Terminology document; it means a concrete that contains a spread of random oriented fibers. Naturally, concrete is brittle under tensile loading; it may be remembered that the brittleness refers to the inverse proportionality of the elongation at the break in the tensile testing [5-8]. Basalt fiber is totally new kind of fiber made out of basalt rocks through which possess better failure strain compared to carbon fibers, a greater possibility to resist the chemical attacks, higher impact load and fire with less poisonous fumes. From all of these advantages, the usefulness from the basalt fiber for any structural strengthening materials is highly expected. [9-11].Mineral admixtures, for example, fly ash, microwave incinerated rice husk ash (MIRHA), silica fume and ground granulated blast-furnace slag, enhance the engineering properties and performance of concrete whenever they are used as mineral additives or as partial cement replacements [12-14].The increase in cement content may lead to increase the all-inclusive costs; to avert this problem; the Cement Replacement Material (CRM) may be used. Plenty of reports have been performed to investigate the qualities of self-compacting concrete that contains a mineral admixture [15]. Fly ash may be the famous kind of CRM to switch the cement content within the concrete and could increase the workability qualities of the SCC mix [16]. Fly ash with various degrees of alternatives in the SCC mix has been analyzed to guarantee the effectiveness and the optimum amount of replacement that may be used in SCC

[17]. A microwave incinerated rice husk ash (MIRHA) had been discovered by M. F. Nuruddin, et al. Following the burning of the rice husk ash, which has been shown to have high silica content and be micro porous, the powerful utilization of MIRHA with SCC depends on its own amorphous silica content which may be removed by the proper burning of rice husk ash [18].The goal of this paper is to study the influence of Stand Chopped Basalt (SCB) fiber on the properties of SCC mixing with two types of CRM, such as fly ash and MIRHA.

Experimental Material

ASTM, type-1 ordinary Portland cement (OPC) had been utilized within the work. The fly ash used in this research was class F based on the BS EN 450:1995 and was actually obtained from the Manjung Power Station, Lumut, Perak, Malaysia. Microwave incinerated rice husk ash (MIRHA) was acquired through the burning the dried rice husk ash at 800 C^0 in the automatic microwave incinerator of Universiti Teknologi PETRONAS (UTP). The fine aggregate used within the test was in fact clean natural sand having a specific gravity of 2.61 and fineness modulus of 2.76 as well as the maximum size was just 3.35mm. Whilst, the coarse aggregate used was (10-5) mm crushed granite stone based on the BS: 812-103.2 1989 having a specific gravity of 2.66 in SSD. The RWR superplasticiser from SIKA-KIMIA, Malaysia, was applied to increase the workability of SCC according to the BS: 5075. A new type of natural fibers was used in the mixes. It was the Stand Chopped Basalt called SCB fiber acquired from China; its characteristics have been tabulated in Table 1.

Table 1: Physical Characteristics of the Stand Chopped Basalt (SCB) fiber

Physical Properties		Basalt Fiber
Length	(mm)	25.00
Diameter	(mm)	0.18
Density	(g/cm^3)	4100-4840
Tensile strength	(MPa)	2.65
Elastic modulus	(MPa)	100.110
Aspect ratio		138.89

Experimental Methodology

An experimental study has been conducted by the development of the SCB-SCC mix including fly ash and MIRHA. The actual blends were definitely checked with the fresh and hardened target; the fresh test was basically were slump flow, V-funnel and L-box tests in which have been controlled by the Specification of the European Federation of Producers and Applicators of Specialist Products for Structures- EFNARC. Whilst, the hardened characteristics were compressive and splitting tensile strength.There have been 12-mixes of SCB-SCC developed and divided mainly into three group based on the binder content as 100% OPC, 10% MIRHA and 30% fly ash, respectively. The SCB fibers were utilized as 1.0%, 1.5% and 2.0% per each group by weight of total binder. The cement content, super plasticizer fine and coarse aggregate were kept constant throughout the whole of the mixtures as 600kg/m^3, 12kg/m^3, 900kg/m^3 and 750kg/m^3, respectively. Table 2 shows details of the SCB-SCC mixtures.

Result and Discussion

1- Fresh Properties: The fresh properties have been evaluated by the slump flow, V-funnel and L-box test in order to characterize the SCB-SCC mixes regarding it is the flowability ,viscosity and passing ability as keys needed to insure the self-compatibility of the concrete according to the EFNARC standard , result has been tabulated and analyzed through the Table 3 and Fig.1(a), Fig.1(b) and Fig.1(c), respectively.

Table 2: Mixture Proportions

No	Mix Code	Binder			SCB Fiber	
		Type	%	Content Kg/m^3	%	Content Kg/m^3
1	G_1-SCB_1-0.0%	OPC	100%	600	0	0
2	G_1-SCB_2-1.0%	OPC	100%	600	1.0	6.0
3	G_1-SCB_3-1.5%	OPC	100%	600	1.5	9.0
4	G_1-SCB_4-2.0%	OPC	100%	600	2.0	12.0
5	G_2-SCB_1-0.0%	MIRHA	10 %	60	0	0
6	G_2-SCB_2-1.0%	MIRHA	10 %	60	1.0	6.0
7	G_2-SCB_3-1.5%	MIRHA	10 %	60	1.5	9.0
8	G_2-SCB_4-2.0%	MIRHA	10 %	60	2.0	12.0
9	G_3-SCB_1-0.0%	Fly ash	30 %	180	0	0
10	G_3-SCB_2-1.0%	Fly ash	30 %	180	1.0	6.0
11	G_3-SCB_3-1.5%	Fly ash	30 %	180	1.5	9.0
12	G_3-SCB_4-2.0%	Fly ash	30 %	180	2.0	12.0

Table 3: Slump Flow, V-Funnel and L-Box Results

Code Mix	M1	M2	M3	M4	M5	M6	M7	M8	M9	M10	M11	M12
Binder Type	100 % OPC				10% MIRHA				30% Fly ash			
Slump Flow (mm)	705	680	645	610	680	630	585	565	755	700	670	630
V-Funnel (second)	8	10	15	20	12	13	17	24	6	11	14	18
L-box (h_1/h_2)	0.82	0.85	0.92	1.2	0.93	1.0	1.2	1.4	0.80	0.86	0.97	1.0

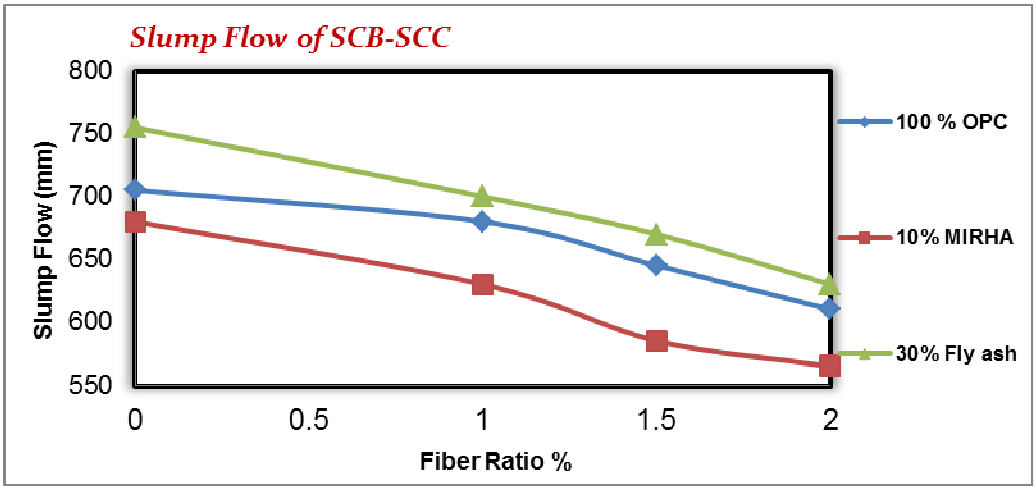


Figure 1 (a): Slump flow of SCB-SCC mixtures.

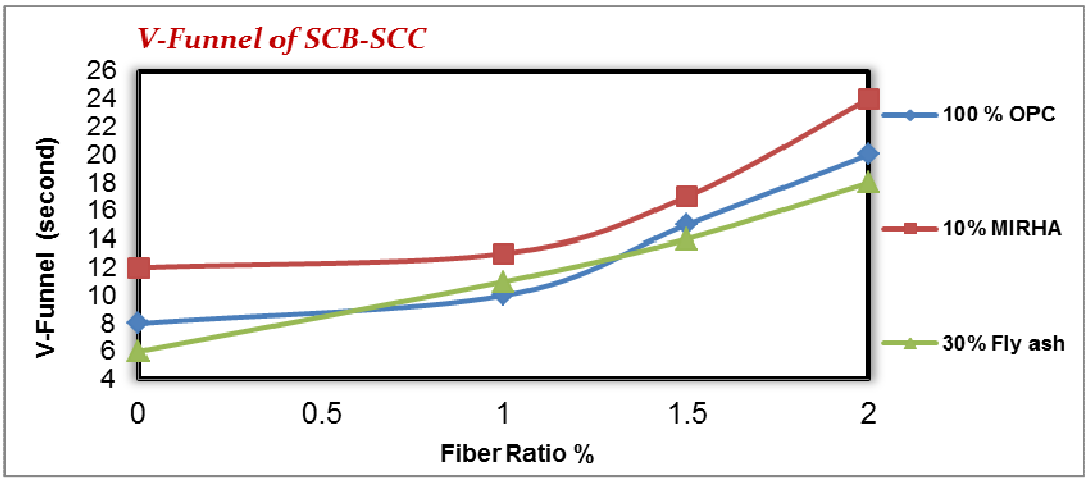


Figure 1 (b): V-Funnel of SCB-SCC mixtures.

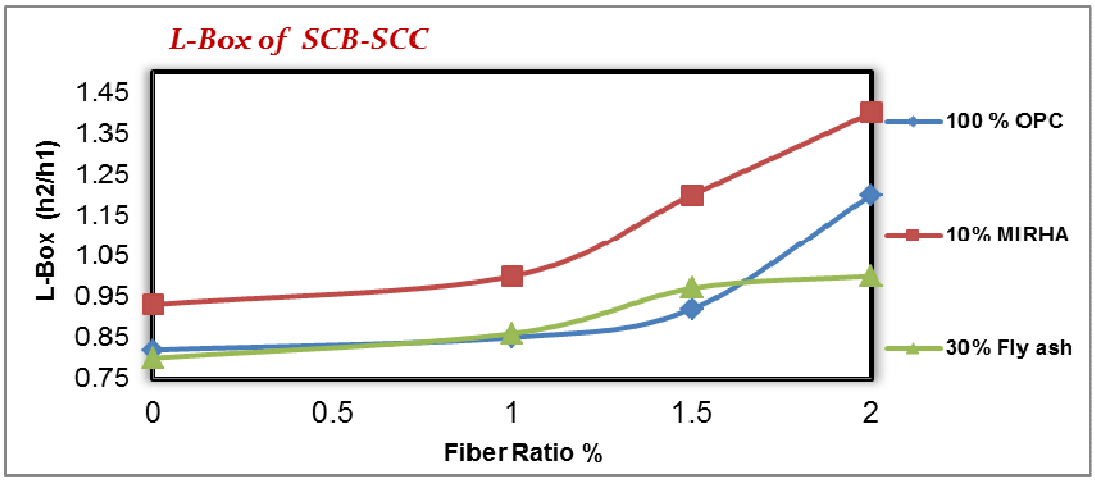


Figure 1 (c): L-Box of SCB-SCC mixtures.

2- Hardened Properties: The compressive strength at 7, 28 and 90 days and also the splitting tensile strength at 28 days have been carried out to be able to look at the hardened features of the whole mix based on the the BS 1881-part 116:1983 and BS 1881-part 117:1983. Fig. 2 and Fig. 3 show the results.

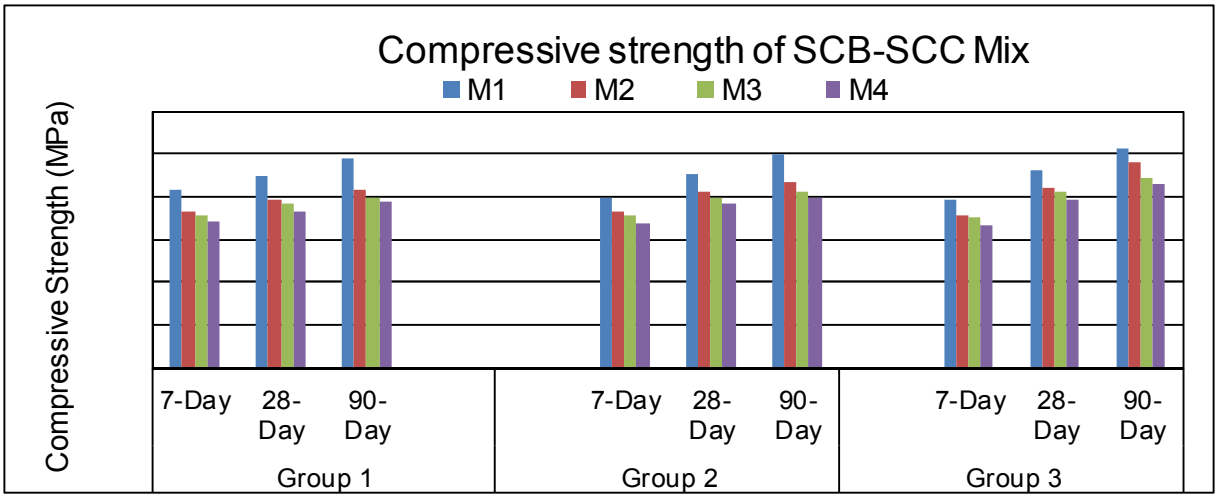
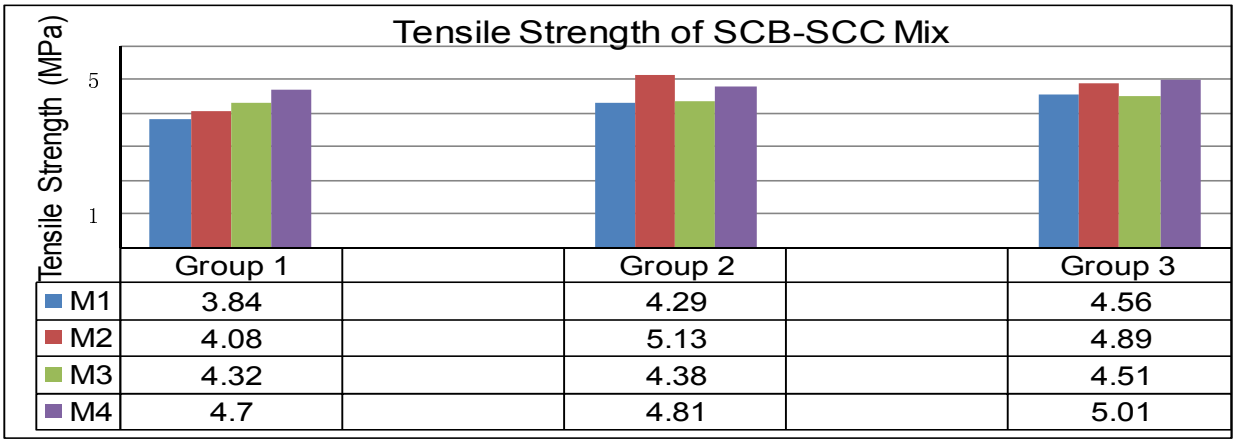


Figure 2: Compressive strength of SCB-SCC mix



	Group 1		Group 2		Group 3
M1	3.84		4.29		4.56
M2	4.08		5.13		4.89
M3	4.32		4.38		4.51
M4	4.7		4.81		5.01

Figure 3: Splitting Tensile Strength of SCB-SCC Mix

Conclusion

From the experimental study, the summary can be drawn as:

1- Slump flow result decreases with an increasing in the SCB-SCC fiber content because of the ability of the fibers to adsorb some of the water mixing. Hence; affect negatively on the flowability, according to EFNARC the whole mix shows self-compatibility.

2- V-funnel time results have been accepted according to the EFNARC except for those mixes that included 2.0% of the SCB fiber of groups 1 and 2. At 2.0%, the 100% OPC and 10% MIRHA showed the V-funnel time more than that of the EFNARC allowable range (6-12 seconds) but still, it can be considered as self-compacting concrete because there have been no bleeding or/and segregation found.

3- 30% of fly ash in group 3 possess lower ratio of L-box test compare with that of group 1 and 2; mix M4, M7 and M8 show ratios more than the EFNARC standard which means the negative effect of SCB fibers on the blocking ratio.

4- Compressive strength decreases with an increasing SCB fiber content; groups, two and three, show strength more than that of group one. The reduction in the compressive strength of groups two and three at the early age were already analyzed. The result shows that MIRHA reduces the compressive strength by 4.12% whilst the fly ash exhibits a reduction of 5.22%. Mainly, the SCB fiber did not increase the strength throughout the experiment because the fiber affects the area of the interfacial zone (ITZ) between the paste and the aggregate. Hence, the binder around the aggregate may face problems to get sufficient water for the hydration process.

5- Splitting tensile strength result proves that the two types of mineral admixtures have enhanced the splitting behavior significantly. 10% of MIRHA at 1.0% of the SCB-SCC fiber has been showed tensile strength more than that of 30% of the fly ash whilst at 2.0% of the SCB-SCC fiber the 30% fly ash was already split more than 10% of MIRHA. Besides that, the SCB fiber enhanced the splitting result for the whole mix; that may be due to the surface area of the fiber itself.

Acknowledgement

The authors are thankful and appreciate the Department of Civil Engineering at Universiti Teknologi PETRONAS (UTP) -Malaysia for their highly supported attitude to help finalize such experimental studies.

References

[1] P. Domone, "Self-compacting concrete: An analysis of 11 years of case studies," Cement and Concrete Composites, vol. 28, pp. 197-208, 2006.

[2] N. Su, K.-C. Hsu, and H.-W. Chai, "A simple mix design method for self-compacting concrete," Cement and Concrete Research, vol. 31, pp. 1799-1807, 2001.

[3] G. Sua-iam and N. Makul, "Utilization of limestone powder to improve the properties of self-compacting concrete incorporating high volumes of untreated rice husk ash as fine aggregate," Construction and Building Materials, vol. 38, pp. 455-464, 1// 2013.

[4] M. Mohamed, E. Ghorbel, and G. Wardeh, "Valorization of micro-cellulose fibers in self-compacting concrete," Construction and Building Materials, vol. 24, pp. 2473-2480, 2010.

[5] M. Sahmaran, A. Yurtseven, and I. Ozgur Yaman, "Workability of hybrid fiber reinforced self-compacting concrete," Building and Environment, vol. 40, pp. 1672-1677, 2005.

[6] W. Brostow and H. E. H. Lobland, "Brittleness of materials: implications for composites and a relation to impact strength," Journal of materials science, vol. 45, pp. 242-250, 2010.

[7] P. Hannant, "Fibre cements and fibre concretes," 1978.

[8] D. Hannant, J. Zonsveld, and D. Hughes, "Polypropylene film in cement based materials," Composites, vol. 9, pp. 83-88, 1978.

[9] M. Berozashvili, "Continuous reinforcing fibers are being offered for construction, civil engineering and other composites applications," Adv Mater Com News, Compos Worldwide, vol. 6, pp. 5-6, 2001.

[10] J. Sim, C. Park, and D. Y. Moon, "Characteristics of basalt fiber as a strengthening material for concrete structures," Composites Part B: Engineering, vol. 36, pp. 504-512, 2005.

[11] V. Brik, "Advanced concept concrete using basalt fiber composite reinforcement," Tech Res Report submitted to NCHRP-IDEA, Project, vol. 25, 1999.

[12] M. F. Nuruddin, N. M. Azmee, and C. K. Yung, "Effect of fire flame exposure on ductile self-compacting concrete (DSCC) blended with MIRHA and fly ash," Construction and Building Materials, vol. 50, pp. 388-393, 1/15/ 2014.

[13] N. Shafiq, M. Nuruddin, and I. Kamaruddin, "Comparison of engineering and durability properties of fly ash blended cement concrete made in UK and Malaysia," Advances in applied ceramics, vol. 106, pp. 314-318, 2007.

[14] A. Fathi, N. Shafiq, M. Nuruddin, and A. Elheber, "STUDY THE EFFECTIVENESS OF THE DIFFERENT POZZOLANIC MATERIAL ON SELF-COMPACTING CONCRETE," Journal of Engineering & Applied Sciences, vol. 8, 2013.

[15] R. Siddique, P. Aggarwal, and Y. Aggarwal, "Influence of water/powder ratio on strength properties of self-compacting concrete containing coal fly ash and bottom ash," Construction and Building Materials, vol. 29, pp. 73-81, 2012.

[16] N. Bouzoubaa and M. Lachemi, "Self-compacting concrete incorporating high volumes of class F fly ash: Preliminary results," Cement and Concrete Research, vol. 31, pp. 413-420, 2001.

[17] N. Shafiq and J. Cabrera, "Effects of initial curing condition on the fluid transport properties in OPC and fly ash blended cement concrete," Cement and Concrete Composites, vol. 26, pp. 381-387, 2004.

[18] M. Nuruddin, S. Quazi, N. Shafiq, and A. Kusbiantoro, "Compressive Strength & Microstructure of Polymeric Concrete Incorporating Fly Ash & Silica Fume," Canadian Journal of Civil Engineering, vol. 1, pp. 15-18, 2010.

Applied Mechanics and Materials Vol. 567 (2014) pp 362-368
© (2014) Trans Tech Publications, Switzerland
doi:10.4028/www.scientific.net/AMM.567.362

Drying Shrinkage of Fly Ash-Based Self-Compacting Geopolymer Concrete

M. F. Nuruddin, F. A. Memon, N. Shafiq, S. Demie*

Civil Engineering Department, Universiti Teknologi PETRONAS, Malaysia
*Civil and Urban Engineering Department, Institute of Technology, Haramaya University, Ethiopia

Keywords- Fly ash, Geopolymer concrete, Self-compacting Geopolymer concrete, Drying shrinkage

Abstract –The drying shrinkage behaviour of fly-ash-based self-compacting geopolymer concrete (SCGC) was studied for a period of one year. Two SCGC and One OPC-based conventional mixture were used in the present investigation. Drying shrinkage test commenced on the 7th day after casting the test specimens. Once the appropriate curing regime was completed, the specimens from each mix were placed in the laboratory room where the temperature was maintained at 23°C, however, the relative humidity of the room varied between 56 and 64 percent. Strain readings taken at specific intervals were analyzed to determine the time-dependent deformations of each mixture. Test results indicated that the heat-cured fly ash-based SCGC experienced very low drying shrinkage than that of water-cured OPC based concrete. After one year of exposure, in comparison to 466 με, the value experienced by OPC concrete, the drying shrinkage strains of SCGC mix specimens ranged between 141 and 159 με. These values were about 65-70% lower than that of OPC concrete. It is anticipated that the findings of this investigation would help in predicting the behaviour of SCGC.

I. INTRODUCTION

The use of Portland cement as a binder material in concrete production is often criticized by the circles concerned with environmental conservation. It is claimed that world's yearly cement production of 2 billion tons emits about 1.65 billion tons of CO_2, or about 7% of the total greenhouse gas emissions into the atmosphere [1, 2]. Due to the manufacture of Portland cement, it is estimated that by the year 2020, the CO_2 emissions will rise by about 50% from the current levels [3]. In view of such fact, concrete industry worldwide is under pressure to find the alternative binding materials, so the utilization of cement could be minimized.

Enormous efforts have been made throughout the world to reduce the use of Portland cement in concrete. These include the utilization of supplementary cementitious materials and the development of alternative binders to Portland cement [4]. An effort made in this regard is the development of geopolymer concrete. The geopolymer concrete is an innovative and alternative binding material that does not include Portland cement. Instead, utilizes waste materials that are rich in silica and alumina such as fly ash to produce the binder required to manufacture the concrete.

Concretes whether produced with Portland cement or geopolymer binder share the similar feature in that they are porous materials and can be expected to suffer an induced isotropic compressive stress within the rigid binder phase when the excess water begins to evaporate. This hydrostatic tension, commonly termed as shrinkage, causes capillary pressures leading to cracking in concrete [5]. It has been reported that the drying shrinkage of heat-cured geopolymer concrete is generally very low compared to that of OPC-based concrete. As displayed by Wallah and Rangan [6], in fly ash-based geopolymer concrete, most of the water released during the chemical reaction may evaporate during the curing process. As the remaining water contained in the micro-pores of the hardened concrete is small, the induced drying shrinkage is very low [6]. The statement is shared by Palomo et al. [7] who have reported that the engineering performance of geopolymer concrete synthesized from fly ash was excellent, and the drying shrinkage was significantly low. Other researchers [8] also noticed the same behaviour. However, Wang et al. [9] mentioned that due to the formation of silica-rich gel, GGBS-based concrete activated by water glass may experience higher shrinkage strains than in OPC-based concrete.

A research study on the development and mechanical behaviour of fly ash-based self-compacting geopolymer concrete (SCGC) was carried out. SCGC is relatively a new concept and latest advancement in the field of concrete technology. It is a novel material that involves innovation in the production and casting of concrete. SCGC is a type of concrete that does not require compaction for placing it and can be produced by complete elimination of OPC. It can be made using materials rich in silica and alumina such as fly ash and sodium hydroxide and sodium silicate as alkaline activator together with superplasticizer. SCGC represents an opportunity to simultaneously improve both environmental and engineering performance compared to traditional Portland cement concrete. This paper reports the results of the test carried out to assess the time-dependent deformations due to shrinkage of fly ash-based SCGC. It is hoped that findings of this study would help in predicting the behaviour of SCGC.

II. EXPERIMENTAL DETAILS

A. Materials for concrete mixtures

For making SCGC and OPC-based concrete mixes, the materials used were fly ash, silica fume, ordinary Portland cement, fine and coarse aggregate, sodium hydroxide and sodium silicate as alkaline activators, superplasticizer and water.

Fly ash

Fly ash, which contains high percentage of silica and alumina, is known to be a suitable source material for making geopolymeric concrete. Therefore, for the present work low-calcium fly ash classified as Class F by ASTM C 618 [10] was chosen as a source material for making SCGC mixes. Fly ash, complying with BS EN 450-1:2005 [11] was obtained from Manjung power station, Perak, Malaysia. The chemical composition of fly ash as determined by X-Ray Fluorescence (XRF) analysis is presented in Table 1.

Silica fume

Commercially available silica fume supplied by Elkem materials, complying with the mandatory requirements of BS EN 13263-1:2005+A1:2009 [12] was used as replacing part of the fly ash. The amount of silica fume was selected based on the results of previous research where the effect of silica fume on hardened properties of SCGC was studied [13]. The chemical composition of silica fume is presented in Table 1.

Ordinary Portland cement

Ordinary Portland cement (OPC), the principal ingredient in Portland cement concrete, is the most common type of cement extensively used around the world for general purpose. Commercially available Type I Portland cement supplied by Tasek Corporation Berhad (4698-W), Ipoh, Perak, was used in the preparation of OPC-based mix. The cement met the requirements of BS EN 197-1:2000 [14]. The chemical composition of the cement is given in Table 1.

Fine and Coarse aggregate

Locally available crushed granite of angular shape and of rough surface texture with 14 mm maximum size was used as coarse aggregate while natural quartzite sand, obtained from Tronoh, Perak, was used as fine aggregate in the preparation of all test specimens. The maximum size of coarse aggregate was selected as 14 mm in order to avoid any blocking effect of SCC. To remove fine silt particles, coarse aggregate was washed and used in saturated surface dry (SSD) condition.

Alkaline activators

Sodium hydroxide in pellet form with 99% purity, supplied by Quick Lab Sdn Bhd, Malaysia and Grade A53 sodium silicate in solution form with SiO_2-to-Na_2O ratio by mass of approximately

2, supplied by Malay-Sino Chemical Industries Sdn Bhd, Malaysia were used as alkaline activators. Concentration of sodium hydroxide was kept 10M and the sodium hydroxide solution was prepared by dissolving sodium hydroxide pellets in tap water. Sodium silicate and sodium hydroxide solutions were then mixed together and an alkaline solution was prepared.

Superplasticizer

To achieve superior workability and higher flowability in SCC, it is common practice to use superplasticizer. Commercially available high performance water reducing superplasticizer under the brand name of Sika Viscocrete-3430 was used in SCGC mixtures.

Water

Water that is fit for drinking is generally considered satisfactory for use in mixing concrete. In this research study, the tap water available in the concrete laboratory was used in the preparation of concrete mixes.

TABLE 1
CHEMICAL COMPOSITION OF FLY ASH, SILICA FUME AND OPC

Oxide	Fly ash	Silica fume	OPC
SiO_2	51.30	90.20	21.28
Al_2O_3	30.10	0.82	5.60
Fe_2O_3	4.57	1.67	3.36
CaO	6.73	1.24	64.14
MgO	0.89	0.31	2.06
K_2O	1.56	4.02	0.49
SO_3	1.40	1.40	2.14
Na_2O	0.26	0.10	0.05
P_2O_5	1.60	-	-
TiO_2	0.70	-	-
LOI	0.88	0.23	0.64

B. Mix proportions

For the present investigation, two fly ash-based SCGC and one OPC-based conventional mixture were formulated. All the three concrete mixes were designed to achieve targeted 28-days compressive strength of 45±5 MPa. The details of these mixtures are given in Table 2. The activator-to-fly ash and water-to-cement ratios were kept 0.5 while the total powder content was fixed at 400 kg/m^3. The coarse and fine aggregates constituted about 75 percent by mass in the mixes.

TABLE 2
MIX PROPORTIONS

Materials	SCGC-1 Mix	SCGC-2 Mix	OPC-based Mix
Fly ash (kg/m^3)	400	360	-
Portland Cement (kg/m^3)	-	-	400
Silica fume (kg/m^3)	0	40	-
Fine aggregate (kg/m^3)	850	850	850
Coarse aggregate (kg/m^3)	950	950	950
Sodium hydroxide (kg/m^3)	57	57	-
Sodium silicate (kg/m^3)	143	143	-
Activator/Fly ash ratio	0.5	0.5	-
Water/cement ratio	-	-	0.5
Water	48	48	200
Superplasticizer (%)	6	6	-
Curing time (hrs)	48	48	-
Curing temperature (°C)	70	70	-

C. Testing Procedure

Test Specimens

The drying shrinkage of concrete is generally measured following the procedure prescribed by ASTM C 157 [15]. In this method, concrete specimens are tested over a given period of time by

measuring the length change under a constant environment. For the present study, two rectangular concrete prisms measuring 76 x 76 x 285 mm were cast from each mix (Table 2). After casting, the SCGC mix specimens along with moulds were placed in the oven at 70°C for 48 hrs. After initial heat curing, the specimens were removed from the moulds and placed in room temperature for air curing until 7 days after casting. OPC mix specimens on the other hand were demoulded after 24 hrs of casting and cured in water at about 23°C until the age of 7 days. Prior to testing, steel studs were embedded at the ends of each prism as shown in Figure 1.

Test Procedure

Drying shrinkage test was performed in accordance with the specifications set forth by ASTM C 157 [15]. The drying shrinkage measurements started on the 7^{th} day after casting the concrete. After the appropriate curing regime, the test specimens were kept in a testing room under conditions of 23 ± 2°C and 60 ± 4 percent relative humidity. A mechanical dial gauge comparator was used to measure the shrinkage strains. Comparator readings for each specimen were carried out daily in the first week, followed by once a week until the fourth week, once in two weeks until the twelfth week, and then once in four weeks until one year. Figure 2 shows the shrinkage specimens kept in the testing room.



Figure 1 Specimens for Drying Shrinkage Test

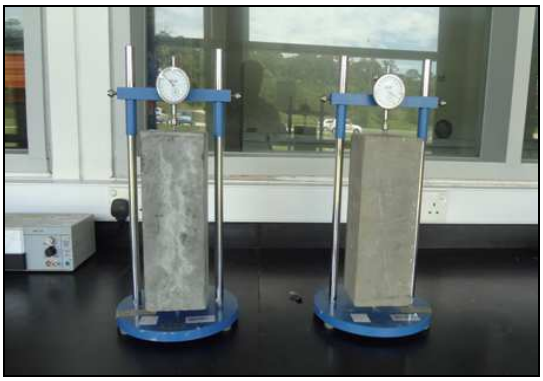


Figure 2 Drying Shrinkage Test Set up

III. RESULTS AND DISCUSSION

The drying shrinkage behaviour of fly ash-based SCGC was studied for one year. The strain developments versus time for the three concrete mixes (SCGC-1, SCGC-2 and OPC Mix) are presented in Figures 3 through 6. Test results indicate that heat-cured fly ash-based SCGC undergoes very low drying shrinkage compared to OPC-based concrete. It can be seen that the drying shrinkage strains of the OPC mix specimens cured in water are many folds larger than those experienced by the heat-cured SCGC mix specimens. As expected the shrinkage strain increased with the time of exposure. After one year of exposure, compared to the value of 466 microstrains,

experienced by OPC mix specimens, the drying shrinkage strains of fly ash-based SCGC mix specimens ranged between 141 and 159 microstrains. These values are about 65-70% lower than that of OPC concrete. This could be due to the less amount of water present in the micro-pores of the hardened SCGC. As, in heat-cured geopolymer concretes, most of the water is released during the geopolymerization process and evaporate during the curing process consequently reducing the drying shrinkage [1]. The lower drying shrinkage values obtained for SCGC mixes may also be partly due to a finer disconnected capillary network structure [16]. It is believed that the increased condensation processes occurring in heat-cured geopolymer-based concretes might have implications on the shrinkage process. Thus, when the condensation reaction of geopolymer concretes are accelerated by heat curing, the associated initial drying shrinkage is significantly reduced, signifying the completion of initial condensation reaction and the moisture loss from capillaries, as also verified by the associated rapid strength development [16].

The values of drying shrinkage strains for fly ash-based SCGC obtained in this study are in agreement with the results reported by other researchers [6, 16]. Wallah and Rangan [6] reported that after one year of exposure, the drying shrinkage strain values for heat-cured fly ash-based geopolymer concrete with compressive strengths of 41 to 65 MPa were around 100 microstrains. Similarly, Sagoe-Crentsil et al. [16] in their study on creep and drying shrinkage performance of geopolymer concrete reported that the shrinkage values of steam-cured fly ash-based geopolymer concrete fell well below the nominal 700 microstrain limit, with geopolymer concrete values typically less than 400 microstrain after one year.

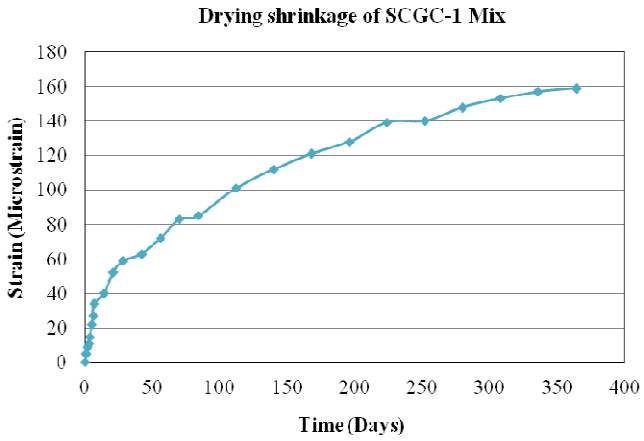


Figure 3 Drying shrinkage of SCGC-1 Mix

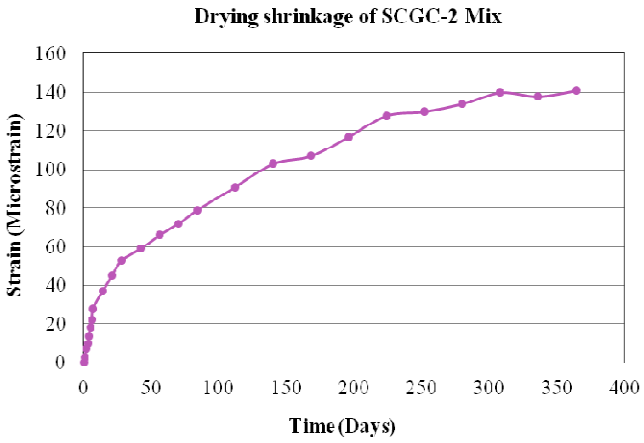


Figure 4 Drying shrinkage of SCGC-2 Mix

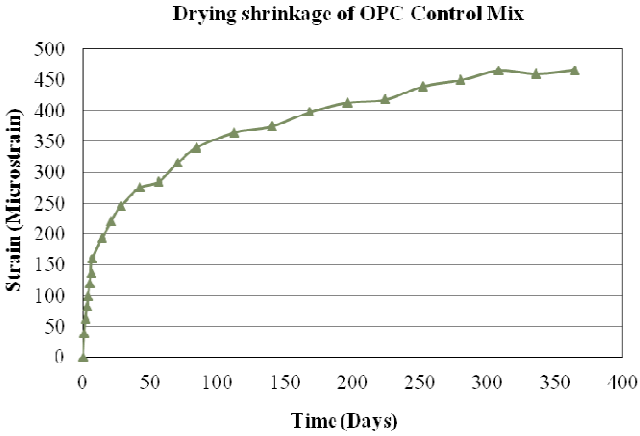


Figure 5 Drying shrinkage of OPC Mix

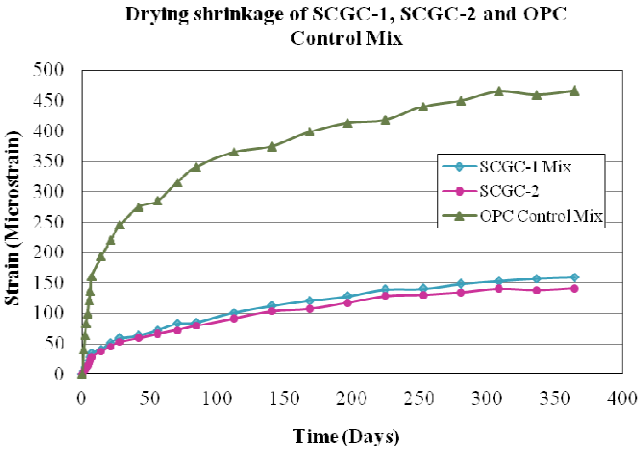


Figure 6 Drying shrinkage of SCGC and OPC Mixes

IV. CONCLUSION

This paper presents the study of drying shrinkage performance of SCGC manufactured using fly ash as its source material. Specimens were prepared to study the time-dependent deformation for the duration of test up to one year.

From test results, it is concluded that heat-cured fly ash-based SCGC undergoes very low drying shrinkage. The drying shrinkage strains of the SCGC mix concretes were about 65-70% lower than that of conventional OPC concrete. After one year of exposure, the drying shrinkage strains of fly ash-based SCGC ranged between 141 and 159 με in comparison to the value 466 με, experienced by Portland cement concrete. It is anticipated that the findings of this investigation would help in predicting the behaviour of SCGC.

ACKNOWLEDGMENT

The authors would like to acknowledge Universiti Teknologi PETRONAS, Malaysia for providing financial support and research facilities.

REFERENCES

[1] D. Hardjito, and B. V. Rangan, "Development and properties of low-calcium fly ash-based geopolymer concrete," *Research Report GC-1*, Faculty of Engineering, Curtin University of Technology, Perth, Australia, 2005.

[2] V. M. Malhotra, "Introduction: Sustainable development and concrete technology," *ACI Concrete International*, vol. 24, no. 7, pp. 22, 2002.

[3] T. R. Naik, "Sustainability of cement and concrete industries," in *International Conference on Global Construction: Ultimate Concrete Opportunities*, Dundee, Scotland, July 2005, pp. 141-150.

[4] B. V. Rangan, "Fly ash-based geopolymer concrete," *Research Report GC-4*, Faculty of Engineering, Curtin University of Technology, Perth, Australia, 2008.

[5] S. Mindess, F. J. Young, and D. Darwin, "Concrete," 2nd ed., Upper Saddle River: Prentice Hall, New Jersey, 2003.

[6] S. E. Wallah, and B. V. Rangan, "Low-calcium fly ash-based geopolymer concrete: Long-term properties," *Research Report GC-2*, Faculty of Engineering, Curtin University of Technology, Perth, Australia, 2006.

[7] A. Palomo, A. Fernandez-Jimenez, C. L. Hombrados, J. L. Lleyda, "Precast elements made of Alkali-activated fly ash concrete," in *Eighth CANMET/ ACI International Conference on Fly ash, Silica Fume, Slag adn Natural Pozzolans in concrete*, Los Vegas, USA, 2004.

[8] M. Olivia and H. Nikraz, "Properties of fly ash geopolymer concrete designed by Taguchi method," *Materials and Design*, vol. 36, pp. 191-198, 2012.

[9] S. D. Wang, X. C. Pu, K. L. Scrivener, P. L. Pratt, "Alkali-activated slag cement and concrete: a review of properties and problems," *Advance Cement Research*, vol. 7, no. 27, pp. 93– 102, 1995.

[10] ASTM C 618-05, "Standard Specification for Coal Fly ash and Raw or Calcined Natural Pozzolan for use as Mineral Admixture in Portland Cement Concrete," American Society for Testing and Materials, Annual Book of ASTM Standards, vol. 04, no. 02, 2005.

[11] BS EN 450-1:2005, "Fly ash for concrete - Part 1: Definition, specifications and conformity criteria," *British-Adopted European Standard*, 2005.

[12] BS EN 13263-1:2005+A1:2009, "Silica fume for concrete – Part 1: Definitions, requirements and conformity criteria," *British-Adopted European Standard*, 2009.

[13] Memon, F.A., Nuruddin, M.F., and Shafiq, N., Effect of Silica fume on Fresh and Hardened properties of Fly ash-based Self-Compacting Geopolymer Concrete*, International Journal of Minerals, Metallurgy and Materials,* Vol. 20, No. 2, 2013, pp. 205-213.

[14] BS EN 197-1:2000, "Cement – Part 1: Composition, specifications and conformity criteria for common cements," *British-Adopted European Standard*, 2000.

[15] ASTM C 157-08, "Standard Test Method for Length Change of Hardened Hydraulic-Cement Mortar and Concrete," *Annual Book of ASTM Standards*, 04.02 Concrete and Concrete Aggregates, American Society for Testing and Material, 2008.

[16] K. Sagoe-Crentsil , T. Brown and A. Taylor, "Drying shrinkage and creep performance of geopolymer concrete," *Journal of Sustainable Cement-Based Materials*, vol. 2, no.1, pp. 35-42, 2013.

Applied Mechanics and Materials Vol. 567 (2014) pp 369-374
© (2014) Trans Tech Publications, Switzerland
doi:10.4028/www.scientific.net/AMM.567.369

Durability of Sugar Cane Bagasse Ash (SCBA) Concrete towards Chloride Ion Penetration

Nasir Shafiq[1, a], Asma Abd Elhameed[1,b] and Muhd Fadhil Nuruddin[1,c]

[1, 2 and 3]Civil Engineering Department, Universiti Teknologi PETRONAS, 31750 Tronoh Perak, Malaysia

[a]nasirshafiq@petronas.com.my, [b]asmaa29705@yahoo.com, [c]fadhilnuruddin@petronas.com.my

Keywords: Sugar cane bagasse ash, durability, chloride penetration depth, weight loss, compressive strength loss, bond loss.

Abstract. In this study, the effect of sugar cane bagasse ash (SCBA) on chloride penetration resistance of concrete was investigated. 100-mm side cubes were cast and cured in water for 28 days followed by six months curing in 4% NaCl solution. The resistance to chloride penetration was assessed by measuring the chloride penetration depth, weight loss, compressive strength loss and bond strength loss. Chloride penetration depth was measured using $AgNO_3$–based method. It was obtained that inclusion of SCBA in concrete significantly reduced the chloride penetration depth, weight loss, compressive strength loss and bond loss that was attributed to the fine particles of SCBA that filled up the pores and prevented the chloride ingress in the concrete.

Introduction

Utilization of agricultural, industrial and agro- industrial wastes as cement replacement materials in concrete can reduce the cost of concrete and also reduce the negative environmental effects associated with the disposal of these wastes. Silica fume, rice husk ash, fly ash Metakaolin and ground granulated blast furnace slag are well established pozzolans because of high silica contents in their chemical composition. The calcium hydroxide (unfavorable product from the cement hydration) released during the hydration of Portland cement reacts with the silica content present in the pozzolans and water to form additional calcium silicate hydrate which is responsible for the compressive strength in concrete [1]. Since the last decade huge efforts have been made to encourage utilization of cement replacers in concrete due to the high energy consumption in cement production and the global warming which is caused by CO_2 emission[2].

Bagasse is an abundant waste produced in sugar factories after extraction of juice from sugar cane. The huge supply of bagasse needs meaningful disposal. In many countries this type of bulky waste usually used as the boiler fuel in the sugar mills. Increasing cost of natural gas and fuel oil resulting high prices of electricity, due to calorific properties of bagasse waste; since last decade it is being used as the principal fuel in cogeneration plants to produce electric power [3]. The burning of bagasse as fuel leaves bulk quantity of ash called sugar cane bagasse ash or SCBA. Sugar cane bagasse ash is recently accepted as a pozzolanic material; however, there is limited research data available on the effects of SCBA on the mechanical and durability properties of concrete.

A few studies have been conducted on the effect of SCBA on compressive strength by a few authors such as [4–8]; they obtained that the mechanical properties of concrete could be improved by incorporation of SCBA as CRM in concrete. The objective of this study is to determine the effect of SCBA on the concrete durability in terms of chloride penetration.

Experimental Program

Materials. The binder used in this study was type 1 ordinary Portland cement (OPC) in accordance with BS 12 (1996) [9] and MS 522 (1989) [10]. The chemical oxides of OPC are shown in Table 1. The coarse aggregates used through out the experimental program was crushed granite with a maximum particle size of 20 mm and fine aggregate was mining sand with a maximum particle size

of 4.75 mm according to BS 812-103.2 1989. The superplasticizer adopted in this study was a naphthalene formaldehyde sulphonate superplasticizer in a form of aqueous solution.

Sugar Cane Bagasse Ash (SCBA). The SCBA was obtained from Guneid Sugar factory, located in Gezira Province, Sudan. The obtained ash was further ground in a Los Angeles abrasion machine until the particles retained on 45 μm-sieve were less than 5%. The chemical composition of SCBA was determined using X-Ray fluorescence technique, XRF, the results are given in Table 1. The major oxide observed in SCBA is silica (SiO_2), weighs 77.25%. According to ASTM C 618: 2009 [11], the summation of SiO_2+ Al_2O_3+ Fe_2O_3 should be greater than 70%, the sum of these oxides in the Sudanese SCBA was 87.83% which is well above the ASTM requirements, therefore it can be classified as class F pozzolan.

Table 1. Chemical composition of OPC and SCBA

Oxide	Weight %	
	OPC	SCBA
SiO_2	20.44	77.25
Al_2O_3	2.84	6.37
Fe_2O_3	4.64	4.21
CaO	67.73	4.05
K_2O	0.26	2.34
MgO	1.43	2.61
Na_2O	0.02	1.38
P_2O_5	0.10	0.59
TiO_2	0.17	0.58
MnO	0.16	0.27
SO_3	2.20	0.11
LOI	-	1.4
SiO_2+Al_2O_3+ Fe_2O	-	87.83

Concrete Mixing and Casting. In this study 11 concrete mixes were prepared, one was chosen as the reference mix with 100% OPC (no SCBA replacement), coded by NC. The remaining 10 mixes were prepared by adding SCBA content as partial replacement to cement i.e. 5%, 10%, 15%;...up to 50%, these mixes are denoted by SCBA content, e.g. 5%SCBA. The mix proportions are shown in Table 2. The concrete mixing was done in accordance to with BS1881-125: 1986 [12], the superplasticizer dosage was kept constant for all mixes. The compression test was performed on 100 mm cubes and the compressive strength was measured according to BS 1881: Part 111: 1983 [13].

Table 2. Concrete mix proportions

Mix Code	OPC	SCBA	CA	FA	Water	SP
NC	500	0	945	745	190	3
5%SCBA	475	25	945	745	190	3
10%SCBA	450	50	945	745	190	3
15%SCBA	425	75	945	745	190	3
20%SCBA	400	100	945	745	190	3
25%SCBA	375	125	945	745	190	3
30%SCBA	350	150	945	745	190	3
35%SCBA	325	175	945	745	190	3
40%SCBA	300	200	945	745	190	3
45%SCBA	275	225	945	745	190	3
50%SCBA	250	250	945	745	190	3

$AgNO_3$ – Based Method. $AgNO_3$–based method is a very simple and fast method in measuring the chloride penetration depth in concrete in exposed to chloride environments, it was proposed since 1970s and it involves spraying only an $AgNO_3$ solution on a freshly fractured concrete cross section which leads to formation of white and brown zones in which the colour change boundary is very clear [14]. For the chloride penetration depth, 100 mm cubes were cast, after 24 hours the specimens were demoulded and cured for 28 days in water, after then they were immersed in 4% sodium chloride (NaCl) solution. After 180 days immersion the cubes were split into two halves by Diamond Trimmer and the freshly split surfaces were immediately sprayed with silver nitrate ($AgNO_3$) solution 0.1 M. The silver nitrate will react with the free chloride to form the silver chloride precipitate which is white in colour while at greater depth where there is no chloride present. The silver nitrate will react with the hydroxides to form the silver oxide (Ag_2O) precipitate which has a brown colour. The chloride penetration depth was measured from the face of the split surface up to the interface between the white and brown colour. The measurement was performed for the four sides of the split surface at 20 mm intervals. The test was performed according to [15] and the procedure is shown in Fig. 1. The chloride penetration resistance was also assessed by measuring the weight loss and compressive strength loss after 180 days immersion in 4% sodium chloride solution by measuring the weight and compressive strength of the cubes cured in tap water and NaCl solution at the same time.



Figure 1. Test procedure of Chloride penetration depth by $AgNO_3$

Results and Discussion

Chloride Penetration Depth. For normal concrete the average chloride penetration depth was found to be about 18 mm while it was about 8.95 mm for 5%SCBA which was about 50% lower than NC. From Fig. 2, it can be observed that the chloride depths were decreasing gradually with the increase of SCBA percentage until 6.2 mm at 25%SCBA level and started to increase slightly with the increase of SCBA percentage up to 50%SCBA which had a chloride depth of 11.16 mm. This increase might be associated with the decrease in the compressive strength which led to an increase in the porosity that allow the migration of chloride ion into the concrete, keep into consideration that 11.16 mm is 38% lower than NC, similar findings were reported by [16] Brazil, [8] Pakistan and [17] Thailand.

Ganesan et al., 2007 also used the Indian SCBA and observed that the chloride diffusion was dramatically reduced in SCBA concrete up to 25% replacement level while they observed a slight increase at 30% but the values were still less than the control concrete [5].

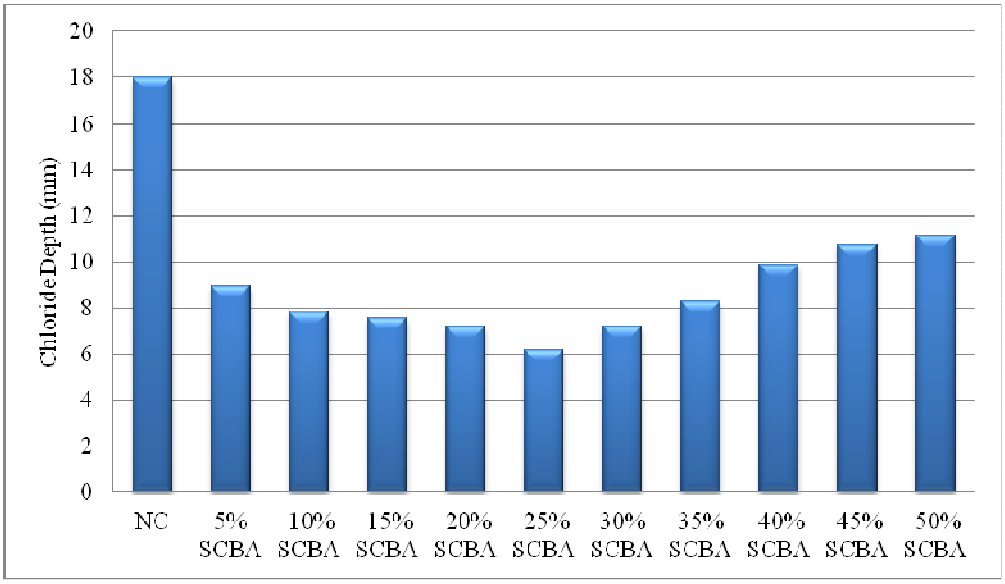


Figure 2. Chloride penetration depth of SCBA concrete

Change in Weight. The change in weight was determined as the relative weight by measuring the weight of the specimen cured in 4% NaCl solution for six months and dividing its weight by the weight of the specimen cured in tap water for six month at the same time and the weight loss was also calculated. The results of weight loss of SCBA concrete are presented in Fig. 3. The normal concrete, NC, experienced about 2.8% weight loss due to chloride penetration while all SCBA concrete mixes experienced weight loss in the range of 0.2% – 2.5%. It was observed that in the specimens 5%SCBA – 25%SCBA the weight losses were in the range of 0.2% – 0.4%, 30%SCBA and 35%SCBA exhibited weight loss of 0.6% and 0.84% respectively while mixes 40%SCBA – 50%SCBA experienced a weight loss in the range of 2% – 2.5%.

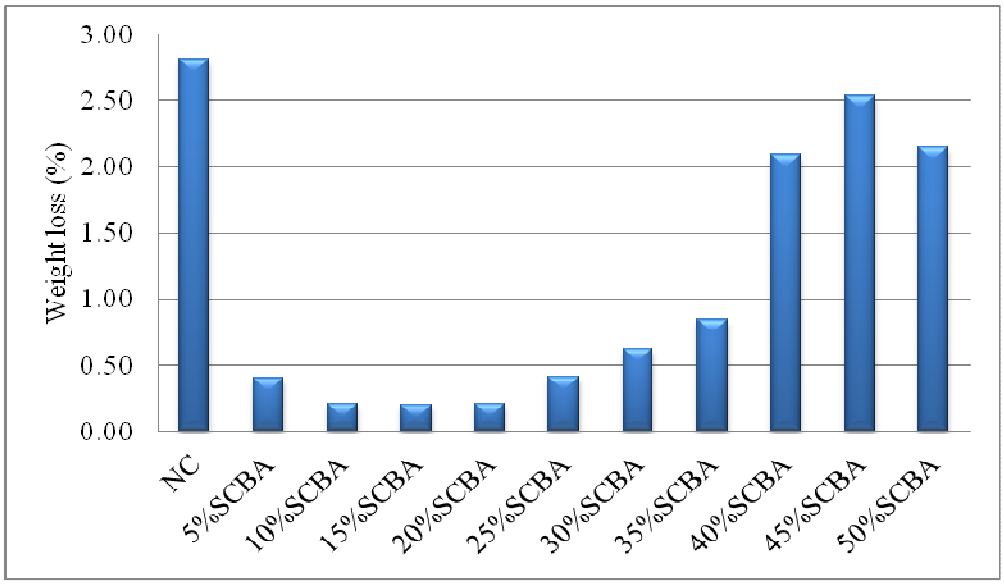


Figure 3. Change in weight of SCBA concrete

Change in Compressive Strength. In a similar way to the change in weight as described in the previous sub-subsection, the change in the compressive strength due to chloride penetration was also assessed by determination of the compressive strength loss the results are presented in Fig. 4; the normal concrete, NC, experienced a strength loss of about 2.6%, incorporation of SCBA in concrete greatly reduced the strength loss due to chloride penetration. 5%SCBA – 15%SCBA had a strength loss of 0.2%, from 20%SCBA – 30%SCBA experienced strength losses in the range of 0.7% – 0.9%, 35%SCBA and 40%SCBA showed similar strength loss of 1.2%. 45%SCBA and 50%SCBA experienced strength losses of 2.0% and 2.5% respectively.

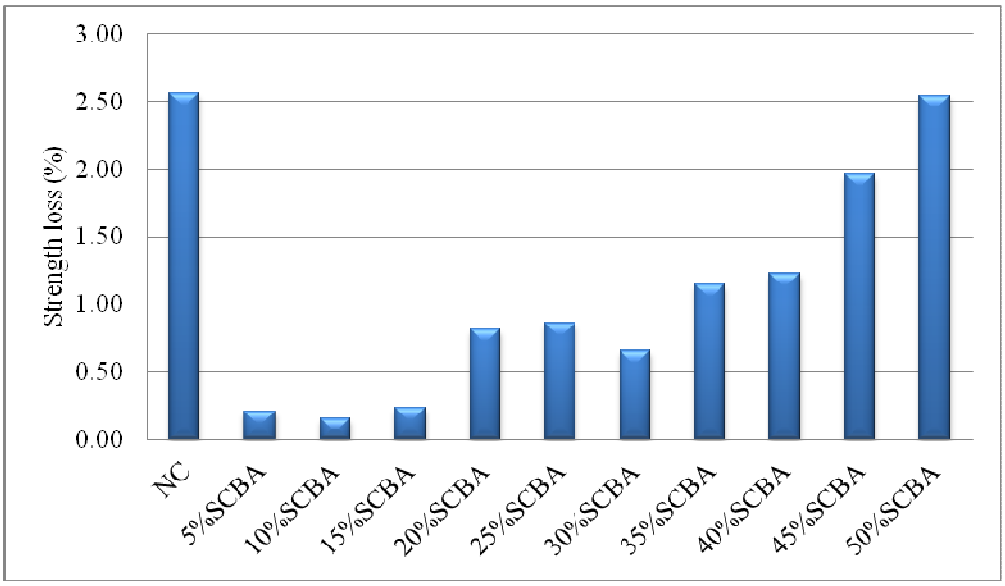


Figure 4. Change in compressive strength of SCBA concrete

Change in Bond Strength. The change in bond strength or was determined by pull out test as described earlier and the bond loss percentage was calculated from the failure load of the specimen cured in 4%NaCl solution compared to the failure load of the specimen cured in water. Fig. 5 illustrates the bond loss of SCBA concrete mixes compared to the normal concrete. The bond loss in the normal concrete NC was about 5.7% while it was less than 1% in SCBA mixes up to 15% replacement. At 20%SCBA and onwards the bond loss tended to increase gradually until it reached 4.3% at 50%SCBA.

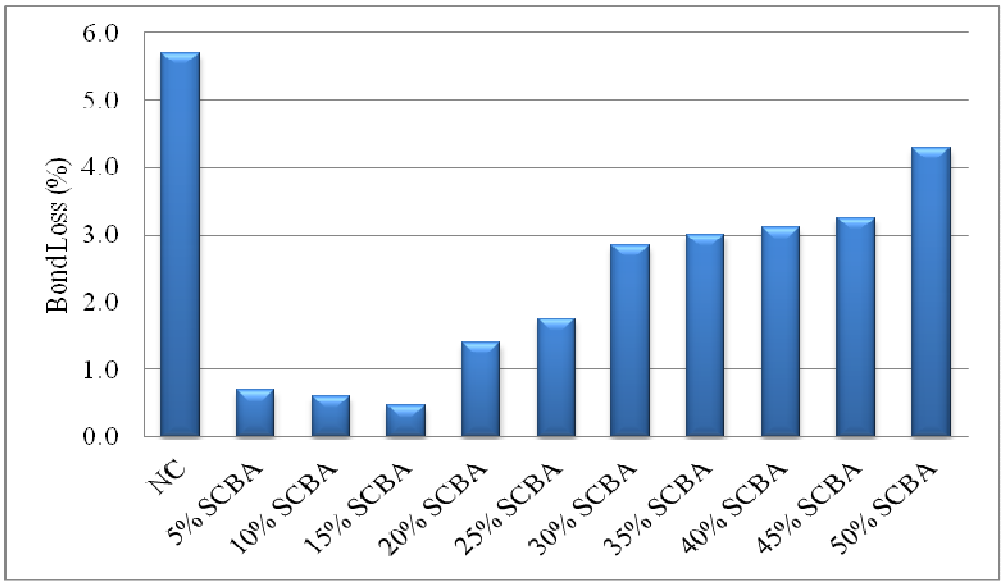


Figure 5. Bond loss of SCBA concrete

Summary. From the above mentioned observations it can be summarized that SCBA has a very high potential to be used effectively in structural concrete in chloride contaminated environments as it can offer an excellent resistance to chloride penetration and it can also reduce the weight loss, strength loss and bond loss. Keeping into consideration that more than 25%SCBA can lead to a slight increase in all the losses investigated in this study.

Acknowledgement. This work was supported by Universiti Teknologi PETRONAS graduate assistantship scheme (GA).

References

[1] S. J. S. Wansom, "Pozzolanic Activity of Industrial Sugar Cane," vol. 17, no. 4, pp. 349–357, 2010.

[2] E. M. R. Fairbairn, B. B. Americano, G. C. Cordeiro, T. P. Paula, R. D. Toledo Filho, and M. M. Silvoso, "Cement replacement by sugar cane bagasse ash: CO_2 emissions reduction and potential for carbon credits.," Journal of environmental management, vol. 91, no. 9, pp. 1864–71, Sep. 2010.

[3] M. Frías, E. Villar, and H. Savastano, "Brazilian sugar cane bagasse ashes from the cogeneration industry as active pozzolans for cement manufacture," Cement and Concrete Composites, vol. 33, no. 4, pp. 490–496, Apr. 2011.

[4] N. Chusilp, C. Jaturapitakkul, and K. Kiattikomol, "Utilization of bagasse ash as a pozzolanic material in concrete," Construction and Building Materials, vol. 23, no. 12, pp. 3523–3531, Dec. 2009.

[5] K. Ganesan, K. Rajagopal, and K. Thangavel, "Evaluation of bagasse ash as supplementary cementitious material," Cement and Concrete Composites, vol. 29, no. 6, pp. 515–524, Jul. 2007.

[6] S. Suvimol and C. Daungruedee, "Bagasse Ash : Effect Of Pozzolanic Activity And Application In Cement Use Aspect," 3rd ACF International Conference-ACF/VCA, pp. 165–173, 2008.

[7] R. and K. S. Srinivasan, "Experimental Study on Bagasse Ash in Concrete," International Journal for Service Learning in Engineering, vol. 5, no. 2, pp. 60–66, 2010.

[8] N. Amin, "Use of Bagasse Ash in Concrete and Its Impact on the Strength and Chloride Resistivity," no. May, pp. 717–720, 2011.

[9] "BS 12-Specifications for Portland Cement," British Standards Institute, London, 1996.

[10] "522: Part 4 Specification for Portland Cement (Ordinary and Rapid hardening)," Malaysian Standards, 1989.

[11] ASTM, "C 618-Standard specification for coal fly ash and raw or calcined natural pozzolan for use as a mineral admixture in concrete," Annual Book of ASTM Standards, 2009.

[12] "BS 1881-125 Testing Concrete: Methods of Mixing and Sampling Fresh Concrete in the Laboratory," British Standards Institute, London, 1986.

[13] "BS 1881: Part 111 Method for Determination of Compressive Strength of Concrete," British Standards Institute, London, 1983.

[14] F. He, C. Shi, Q. Yuan, C. Chen, and K. Zheng, "AgNO3-based colorimetric methods for measurement of chloride penetration in concrete," Construction and Building Materials, vol. 26, no. 1, pp. 1–8, Jan. 2012.

[15] E. Güneyisi, T. Özturan, and M. Gesog˘lu, "Effect of initial curing on chloride ingress and corrosion resistance characteristics of concretes made with plain and blended cements," Building and Environment, vol. 42, no. 7, pp. 2676–2685, Jul. 2007.

[16] G. C. Cordeiro, R. D. T. Filho, and E. M. R. Fairbairn, "Ultrafine sugar cane bagasse ash : high potential pozzolanic material for tropical countries Cinza ultrafina do bagaço de cana-de-açúcar : material," Ibracon Structures and materials journal, vol. 3, no. 1, pp. 50–58, 2010.

[17] S. Rukzon and P. Chindaprasirt, "Utilization of bagasse ash in high-strength concrete," Materials & Design, vol. 34, pp. 45–50, Feb. 2012.

Applied Mechanics and Materials Vol. 567 (2014) pp 375-380
© (2014) Trans Tech Publications, Switzerland
doi:10.4028/www.scientific.net/AMM.567.375

Effect of Calcined Kaolin on the Mechanical Properties of High-strength Concrete as Cement Replacing Material

M.F. Nuruddin[1, a], S.U.Khan[1, b] and N. Shafiq[1, c]

[1]Civil Engineering Department, Universiti Teknologi PETRONAS,

31750 Tronoh, Perak Darul Rizuan, Malaysia

[a]fadhilnuruddin@petronas.com.my, [b]sadaquat78@hotmail.com,
[c]nasirshafiq@petronas.com.my

Keywords: Calcined kaolin, Optimum Cement replacement, kaolin, Regression analysis, Mechanical properties

Abstract. Locally available kaolin has been calcined and used as cement replacing material (*CRM*) in High-strength concrete (*HSC*). Total five (05) mixes of concrete have been examined using calcined kaolin (*CK*) of 0, 5, 10, 15 and 20% by weight of cement. For each mix, compressive strength, splitting tensile strength and flexural strength have been determined by preparing three specimens. The effect of *CK* on the mechanical properties of HSC has been investigated at age of 7, 28, 56 and 90 days. Multiple linear regressions through least square error have been used to develop the expression and to predict the compressive, splitting tensile strengths and flexural strength of *HSC*. It has been found that *CK* as *CRM* increases the strength significantly. The models may predict the strengths closely match the measurements and optimum replacement of cement by *CK*.

Introduction

Calcination of kaolin is occurred at a temperature in the range of 600 to 850 °C (1112 to 1562 °F) [1]. Calcined kaolin or Metakaolin is a highly reactive pozzolan, but its physical and chemical characteristics greatly depend on the raw material used, the temperature during calcination and finishing process [2]. It has been identified as mineral admixture in 1990 [2] and since than it has been broadly studied as mineral admixture [3], highly reactive pozzolan [4] and to improve pore structure and transition zone (*ITZ*) [5]. Several strength models have been proposed mainly for steel fibre reinforced concrete (*SFRC*) [6-10]; however, all these models primarily are based on the corresponding cube strength of concrete without fibres and effect of addition of cement replacing material (*CRM*) has not been accounted in the strength contribution. The current investigation has been carried out to develop the pattern of strength development of High-strength concrete (*HSC*) incorporating calcined kaolin (*CK*). The basic focus of the current study is to capture the effect of *CK* on the strength of concrete. Cube compressive strength, splitting tensile strength and flexural strength of concrete has been observed to check the effect of *CK* of different replacement level. Multiple linear regressions through least square error have been used to develop the strength models and to predict the compressive, splitting tensile strength and flexural strength of *HSC*.

Experimental Investigations

Five (05) mix of concrete has been prepared. Nomenclature and mix proportion detail of the concrete has been mentioned in Table 1. Three specimens for all concrete mix have been prepared to determine average compressive strength (f_{cu}), splitting tensile strength (f_{sp}), and flexural strength (f_{fl}). Ordinary Portland cement (*OPC*) has been used. Sand passing through a 3.125 mm (1/8") opening sieve and retained on sieve # 200 has been used as fine aggregates in all concrete mix. 20 mm (3/4") opening sieve passing and 10 mm (3/8") opening sieve passing has been used as coarse aggregates. The water/binder ratio of 0.4 has been used in all mix. Locally available kaolin has been calcined to form *CK* and it has been used as *CRM*. *CK* has been used from 5 to 20% by weight of cement in concrete mixes. Superplasticizer of Type F or G of ASTM C 494 with a dosage 0.25 to

2% by weight of cement with a variation of 0.25% has been added in concrete mixes to achieve the slump of 100±10 mm in all concrete mix.

Table 1: Mix Design for Experimental Program and Mix Proportion

MIX	*CK*	*OPC*	Fine Aggregates	Coarse Aggregates	
				<10 (mm)	10-20 (mm)
	(kg/m^3)	(kg/m^3)	(kg/m^3)	(kg/m^3)	(kg/m^3)
00-0	0	450	670	600	500
00-5	22.5	427.5	670	600	500
00-10	45	405	670	600	500
00-15	67.5	382.5	670	600	500
00-20	90	360	670	600	500

Results and Discussion

In Table 2, the experimental results of *HSC* have been mentioned. These results have been used to develop the expressions for the mechanical properties of *HSC*. The spark line shows the effect of *CRM* with respect to control (00-0). Regression analysis has been used to understand the change in the value of the dependent variable (strength) when any one of the independent variables is varied, while the other independent variables are held fixed.

Table 2: Mechanical properties of *HSC*

Mix	Age	*CRM*	f_{sp}		f_{cu}		f_{fl}	
	(days)		(MPa)	Spark lines	(MPa)	Spark lines	(MPa)	Spark lines
00-0	7	0	3.6		67.43		5.88	
00-5	7	0.05	4.16		73.25		7.83	
00-10	7	0.1	4.98		78.43		7.21	
00-15	7	0.15	5.58		86.71		6.62	
00-20	7	0.2	4.39		84.78		7.63	
00-0	28	0	4.2		84.9		7.68	
00-5	28	0.05	4.89		89.06		7.96	
00-10	28	0.1	5.2		98.86		7.91	
00-15	28	0.15	5.42		99.74		7.16	
00-20	28	0.2	6.35		94.49		7.7	
00-0	56	0	4.39		91.16		8.15	
00-5	56	0.05	5.73		96.24		8.18	
00-10	56	0.1	5.78		100.6		8.45	
00-15	56	0.15	5.37		100.54		8.9	
00-20	56	0.2	5.64		96.84		8.17	
00-0	90	0	5.15		92.28		8.2	
00-5	90	0.05	5.66		97.13		8.19	
00-10	90	0.1	5.82		101.15		8.6	
00-15	90	0.15	5.62		103.67		8.85	
00-20	90	0.2	6.68		100.87		7.43	

Analytical Investigation

Before regression, dependent and independent variable has been correlated to verify whether these variables have significant effect on the corresponding dependent variable (strength) or not. The results have been mentioned in Table 3. As it is evident that $\sqrt{CRM}$ has the positive correlation with the cube compressive strength, splitting tensile strength and flexural strength. f_{cup} is strength of plain concrete without cement replacement and it has been correlated with the target strength. The total content of binder (*OPC*+*CK*) has been kept constant to get the effect of *CK* as *CRM* as shown in Table 1. This is the limitation of this study as all the results and expressions are valid for this fixed content of binder, however, expressions has been developed in such a way that the re-

analysis of the available experimental data with different content of binder will only need to change the corresponding coefficient and f_{cup}.

Table 3: Correlation between Dependent and Independent Variables

Variables for Cube strength	f_{cup}	$\sqrt{CRM}$	f_{CU}
f_{cup}	1		
$\sqrt{CRM}$	-	1	
f_{CU}	0.83927	0.504888	1
Variables for Splitting Tensile strength	$\sqrt{f_{cup}}$	$\sqrt{CRM}$	f_{sp}
f_{cup}	1		
$\sqrt{CRM}$	-	1	
f_{sp}	0.568772	0.659551	1
Variables for Flexural strength	$\sqrt{f_{cup}}$	$\sqrt{CRM}$	f_{fl}
f_{cup}	1		
$\sqrt{CRM}$	-	1	
f_{fl}	0.721845	0.165933	1

Following expressions have been proposed based on the correlation of variables for strength model of *HSC*:

$$f_{CU} = \propto f_{cup} + \beta\sqrt{CRM} \quad (1)$$

$$f_{sp} = \varphi\sqrt{f_{cup}} + \omega\sqrt{CRM} \quad (2)$$

$$f_{fl} = \Psi\sqrt{f_{cup}} + \Omega\sqrt{CRM} \quad (3)$$

Where,

$f_{CU} = Cube\ strength\ of\ concrete, (MPa)$
$f_{sp} = Splitting\ tensile\ strength\ of\ concrete, (MPa)$
$f_{fl} = Flexural\ strength\ of\ concrete, (MPa)$
$\alpha, \beta, \varphi, \omega, \Psi, \Omega = Coefficient\ of\ corresponding\ variables$
} Outputs

$f_{cup} = Cube\ strength\ of\ plain\ concretea\ without\ cement\ replacement, (MPa)$
$CRM = Fraction\ of\ cement\ replacing\ material\ (by\ weight) as\ shown\ in\ Table\ 2$
} Inputs

Multiple linear regressions through least square error have been used to determine the coefficients of independent variables. The significance level p-value 0.05 has been considered in this study that means there is a 5% probability or less that the predicted values will deviate from the true value due to unseen forces. The assumptions for linear regression are:

1. Each observation is independent of the others.
2. There is a linear relationship between the independent and dependent variables
3. Equal variance of the residuals, and
4. The residuals are normally distributed.

The first Assumption is already true as all the independent variables are not dependent to each other as shown in Table 3. The relationship between dependent (strength) variable and independent (CRM, f_{cup}) variables is not fundamentally linear (Refer Table 2); however, these terms have been used in the expression (by taking square root) so that their relation with dependent (strength) variable has been converted to linear. The third assumption has been verified by plotting the predicted strength against the standardized residuals. Similarly, the assumptions that the error (residuals) is normally distributed have been verified by plotting residuals of model against the residual under normality. Further details of the assumptions of linear regression models may be found elsewhere [11-13].

In Fig. 1 to Fig. 3, predicted and experimental strengths have been plotted. The predicted values have been calculated by Eq. 1 to Eq. 2 and the expressions have been developed through regression analysis. The equations with all known values of coefficients have been mentioned in Fig. 1 to Fig. 3. In Fig. 1, the value of R^2 is 0.998 which suggests that the equation is well fitted to the experimental value. The *p*-values of all the terms involved in Eq. 1 are less or equal to 0.001 which signifies that the expression fit the experimental data more than 99%. By comparing the coefficient of the term $f_{cup}$and $\sqrt{CRM}$, it is clear that *CK* as *CRM* has significant contribution in the gain of compressive strength and gradually increases with the increase in *CRM*.

In Fig. 2, the value of R^2 is 0.993 which shows that the equation is well fitted to the experimental value. The *p*-values are less than 0.001. The coefficient of the term $\sqrt{f_{cup}}$ and $\sqrt{CRM}$ suggest that *CK* as *CRM* has major contribution in the gain of splitting tensile strength as well and it gradually increases with the increase in *CRM* similar to compressive strength.

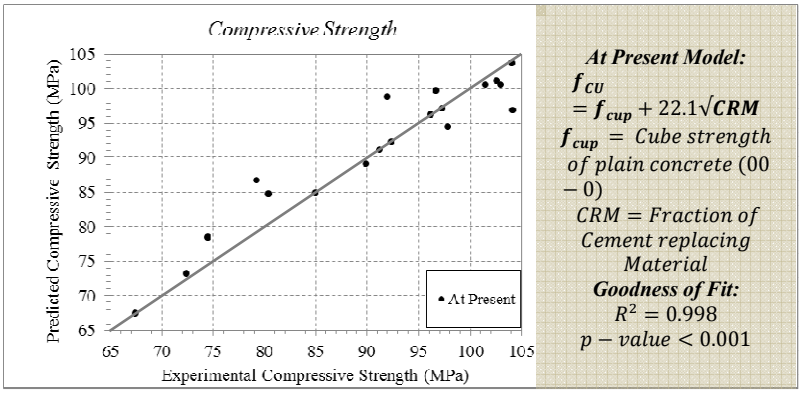


Fig. 1: Cube Compressive Strength Model of HSC

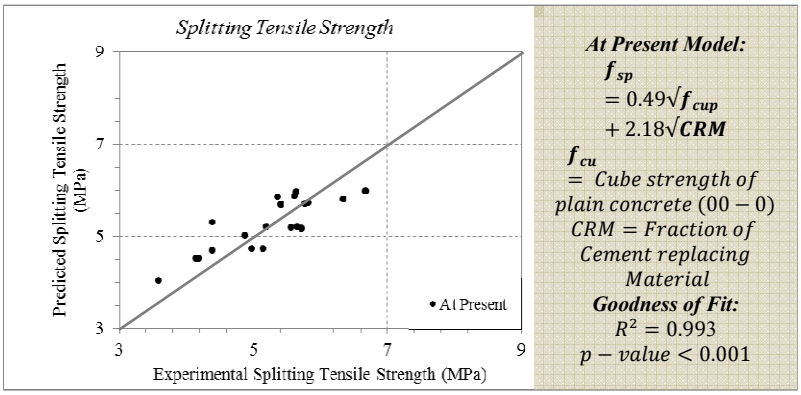


Fig. 2: Splitting Tensile Strength Model of HSC

In Fig. 3, the value of R^2 is 0.996 which indicates that the equation is well fitted to the experimental value. Most of the *p*-values are less or equal to 0.001; however, the *p*-value is relatively higher for the term$\sqrt{CRM}$. The higher *p*-value suggests that the term $\sqrt{CRM}$ is not as significant as in the case of cube compressive strength and splitting tensile strength. The coefficient of the term $\sqrt{CRM}$ suggests that *CK* as *CRM* has smaller contribution in the gain of flexural strength; however, the contribution of *CRM* increases with the increase in *CRM*.

In Fig. 4, the predicted strength and standardized residuals has been plotted for the observation of scatter plot. The assumption of equal variance over the values of the independent variable (homoscedasticity) is true as the scatter of points across the predicted values form a plot with no obvious decreasing or increasing pattern of residuals with increase in the predicted values. The sizes

of the residuals do not change as the values of the predicted outcomes changes, so the assumption of equal variance is true.

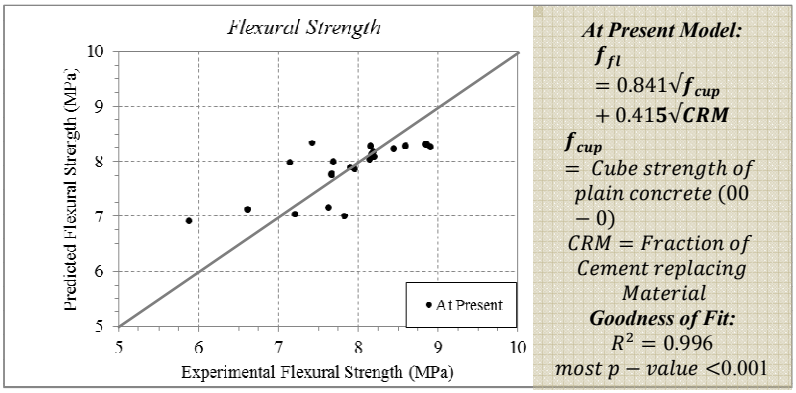


Fig. 3: Flexural Strength Model of HSC

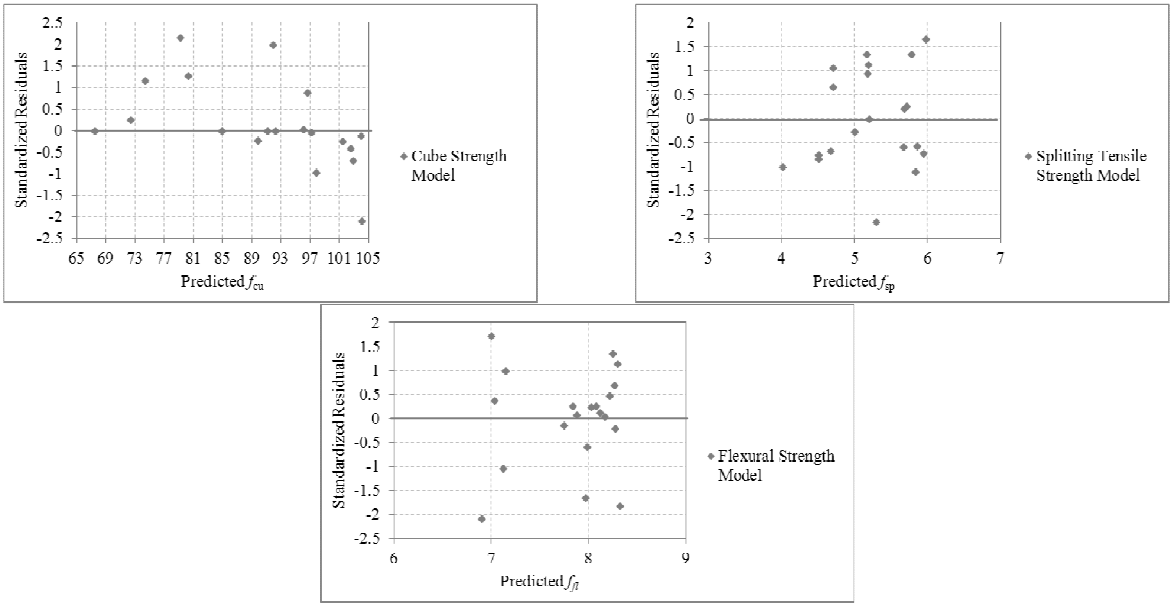


Fig. 4: Predicted vs. Standardized Residuals Plot

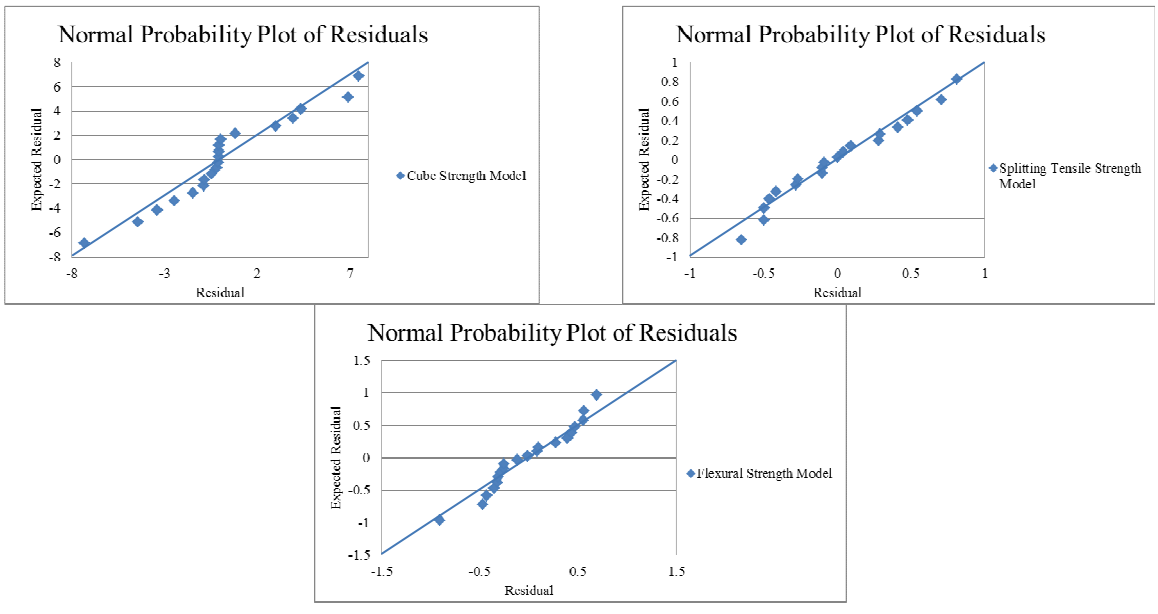


Fig. 5: Normal Probability Plot of Residuals

In Fig. 5, the normal probability of residuals has been plotted. The basic idea is that if the data follow a normal distribution with mean μ and variance σ^2, then a plot of the expected residual (normally distributed) versus the observed residual should be approximately linear. From Fig. 5, it is clear that there is a linear relation between the expected and observed residual. Hence, the errors (residuals) are normally distributed.

Conclusions and Recommendations

The mechanical properties of *HSC* with *CK* have been increased and reach to maximum at 10-15% replacement level; however, gain in compressive and splitting tensile strength is higher as compared to flexural strength. The spark lines suggest that the relationship between *CK* and strengths (f_{cu}, f_{sp}, f_{fl}) varies with the age and it is not a linear. The expressions developed for *HSC* predict values very close to the experimental showing effectiveness of the expressions. Also, expressions fulfil the assumptions of regression analysis.

References

[1] E. Güneyisi, M. Gesoğlu, T. Özturan and K. Mermerdaş, Microstructural properties and pozzolanic activity of calcined kaolins as supplementary cementing materials, Canadian Journal of Civil Engineering, 39(2012), 1274-1284.

[2] J. B. Newman, Advanced Concrete Technology:. Constituent Materials. Butterworth-Heinemann, 2003.

[3] Peter C. Hewlett, Ed., Lea's Chemistry of Cement and Concrete. Elsevier Science & Technology, 2004.

[4] S. J. Martin, The use of metakaolin in high strength concrete, RMC Ready mix Limited., Tech. Rep. Laboratory Report 78, 1995.

[5] P. Duan, Z. Shui, W. Chen and C. Shen, Effects of metakaolin, silica fume and slag on pore structure, interfacial transition zone and compressive strength of concrete, Construction and Building Material, 44(2013), 1-6.

[6] R. Agrawal, A. Singh and D. Singhal, Effect of fibre reinforcing index on compressive and bond strengths of steel fibre reinforced concrete, Journal of the Institution of Engineers, India, Civil Engineering Division, 77(1996), 37-40.

[7] S. Padmarajaiah and A. Ramaswamy, Flexural strength predictions of steel fiber reinforced high-strength concrete in fully/partially prestressed beam specimens, Cement and Concrete Composites, 26(2004), 275-290.

[8] S. Ghosh, C. Bhattacharya and S. Ray, Tensile strength of steel fibre reinforced concrete, Journal of the Institution of Engineers, India. Civil Engineering Division, 69(1989), 222-227.

[9] P. S. Song and S. Hwang, Mechanical properties of high-strength steel fiber-reinforced concrete, Construction and Building Material, 18(2004), 669-673.

[10] J. Thomas and A. Ramaswamy, Mechanical properties of steel fiber-reinforced concrete, Journal of Material and Civil Engineering, 19(2007), 385-392.

[11] I. R. Dohoo, W. Martin and H. Stryhn, Veterinary Epidemiologic Research. AVC Incorporated, 2003.

[12] S. Chatterjee and A. S. Hadi, Regression Analysis by Example. John Wiley & Sons, 2013.

[13] F. J. Anscombe, Graphs in statistical analysis, The American Statistician, 27(1973), 17-21.

Applied Mechanics and Materials Vol. 567 (2014) pp 381-386
© (2014) Trans Tech Publications, Switzerland
doi:10.4028/www.scientific.net/AMM.567.381

Effect of Chopped Basalt Fiber on the Fresh and Hardened Properties of Fly Ash High Strength Concrete

Nasir Shafiq[1,a], Muhd Fadhil Nuruddin[1,b], Ali Elheber Ahmed Elshekh[1,c] and Ahmed Fathi[1,d]

[1]Civil Engineering Department, Universiti Teknologi PETRONAS, Bandar Seri Iskandar, 31750, Tronoh, Perak Darul Ridzun, Malaysia

[a]nasirshafiq@petronas.com.my, [b]fadhilnuruddin@petronas.com.my, [c]alielheber@yahoo.com, [d]alahmdy665@yahoo.com

Keywords: Chopped Basalt Fiber stands, workability, mechanical properties, brittleness and toughness

Abstract. In order to improve the mechanical properties of high strength concrete, HSC, several studies have been conducted using fly ash, FA. Researchers have made it possible to achieve 100-150MPa high strength concrete. Despite the popularity of this FAHSC, there is a major shortcoming in that it becomes more brittle, resulting in less than 0.1% tensile strain. The main objective of this work was to evaluate the fresh and hardened properties of FAHSC utilizing chopped basalt fiber stands, CBFS, as an internal strengthening addition material. This was achieved through a series of experimental works using a 20% replacement of cement by FA together with various contents of CBFS. Test results of concrete mixes in the fresh state showed no segregation, homogeneousness during the mixing period and workability ranging from 60 to 110 mm. Early and long terms of compressive strength did not show any improvement by using CBFS; in fact, it decreased. This was partially substituted by the effect of FA. Whereas, the split and flexural strengths of FASHC were significantly improved with increasing the content of CBFS as well as the percentage of the split and flexural tensile strength to the compressive strength. Also, test results showed a progressive increase in the areas under the stress-strain curves of the FAHSC strains after the CBFS addition. Therefore, the brittleness and toughness of the FAHSC were enhanced and the pattern of failure moved from brittle failure to ductile collapse using CBFS. It can be considered that the CBFS is a suitable strengthening material to produce ductile FAHSC.

Introduction

HSC is being used widely in the developed construction industry; this is due to its mechanical and durability properties, and its effect on the overall cost of structures. Despite the popularity of this unique FAHSC, there are major shortcomings. The shortcomings of low tensile/low flexural strengths, rapid cracking and brittleness have limited the application of FAHSC. Concrete reinforced with steel reinforcement has drawbacks on the durability properties, such as corrosion and cracks. However, replacement of the steel reinforcement in structures has been required recently. A number of studies have successfully been carried out to cover the defect properties of traditional reinforced concrete using fiber reinforced as reported by [1, 2 and 3]. Carbon, Glass and Steel fibers have been used as the basic reinforcing elements of composite materials. With those kinds of fibers, their applications on real construction are very limited due to the unfriendliness character of steel to the environment and the high cost of glass fiber [1,4].

A few studies were conducted on developing new continuous basalt fibers. Basalt fiber is a common term used for a variety of volcanic rocks, which are gray and dark in colour, formed from molten material. There are large areas of this type in the world; especially here in Malaysia as it covers a very large area [5]. Continuous fibers have been classified as inert and natural, friendly to the environment, and nonhazardous materials. Basalt fibers are not only able to improve the mechanical properties of FAHSC, but they are also cheaper and chemically more stable than the E-

glass fiber composites. Moreover, they can be worked in a wide range of temperatures (-269 to 650^{o}C) [1, 6]. Investigation of basalt fibers on concrete as reinforced Polymer (FRP) external strengthening materials has been launched a few years ago by [1,6, and 7]. They pointed out that the properties of HSC, such as strength and durability, have been improved using FRP. External strengthening fiber materials have a good effect on the mechanical and durable properties but the bonding between the fiber and concrete become a problem for these systems [8, 9].

There is very little available literature on concrete strengthened by fiber as internal strengthening materials, or the addition inside materials especially on the HSC. Dias et al. [10] found that basalt fiber reinforcement geopolymeric concrete, BFRGC, has better fracture properties than basalt fiber reinforced OPC concrete. The dynamic compressive strength and energy absorption capacity of OPC concrete significantly improved by up to 26% and 14%, respectively, using 0.1% (volume fraction) of basalt fiber. Its effect on the strengthening and toughening of OPC concrete was higher than those of carbon fiber for OPC concrete reported by Li et al. [11, 12]. Conclusively, the use of basalt fiber as an internal fiber for normal HSC reduced the workability and compressive strength of FAHSC.

Using the FA with CBFS on HSC can partially substitute the reduction of the slump and compressive strength of HSC. FA as an addition or replacement material for cement is very well-known in available literature. It has several contributions on the properties of concrete, such as slump, long term compressive strength, durability and the cost of HSC [13, 14, 15, 16 and17]. These benefits depend on the type of FA, proportion used, mixing procedure and field conditions [18.19]

The main objective of this work was to assess the fresh and mechanical properties of FAHSC, such as tensile strength, brittleness and toughness, utilizing CBFS as the internal addition strengthening material.

Experimental details

Materials. Ordinary Portland cement type I and FA supplied from a local source (Mahjung, Panven ,Perak, Malaysia) were used as fine materials. Table 1 shows the chemical components of the cement and FA which were classified as class C. Crushed granite with well gradation, specific gravity of 2.68 and sizes ranging from 9 to 20 mm was used as a coarse aggregate. The fine aggregate used was a river sand with well gradation and finesse module F.M = 2.2. The proportion between the coarse aggregate and fine aggregate was found to be 1.32. Sika Viscorete 34-30 as a highly effective superplasticizer of 0.8% and drinkable water with a low content of 0.275% were used. CBFS manufactured in China from malting, natural rock with 25 mm length and 18 μmm diameter was used in different amounts of cement weight. The experiments have been conducted on the control mix mentioned earlier with 0.25%, 0.5%, 0.75%, 1%, 2% and 3% by weight of cement.

Proportion of materials and preparation of specimens. There is no guide line in the published literature to produce the HSC mix design; it is just the expert's basic steps. Many trial mixes have been prepared according to the basic steps of the HSC production to achieve the goals of this work. Among 10%, 20% and 30% replacements of cement by FA, the 20% was found to be the optimum according to their 28-day compressive strength [20]. Finally, the mix with 20% replacement of cement by FA (labelled as MF) was considered as the control mix for this study as shown in Table 2.

The slump test, in accordance to ASTM C 172, was conducted to check the workability of fresh concrete. For compressive strength, 100 mm cubes were cast according to ASTM C 39. 200 mm x 100 mm cylinders and 100 mm X 100 mm X 500 mm beams were cast according to ASTM C 466 and ASTM C 78 for split and flexural tensile strengths, respectively. All specimens were made dense by electrical vibrating hammer in three layers. After 24 hours of remaining in the moulds at room temperature, all of the specimens were demoulded and placed in the water tanks for curing till the test date.

Table 1
Chemical Components of Cement and Fly Ash

Chemical Composition	Binder	
	OPC	Fly Ash
SiO_2	20.3	56.39
Al_2O_3	4.2	17.57
Fe_2O_3	3	9.07
CaO	62	11.47
MgO	2.8	0.98
SO_3	3.5	0.55
K_2O	0.9	1.98
Na_2O	0.2	1.91

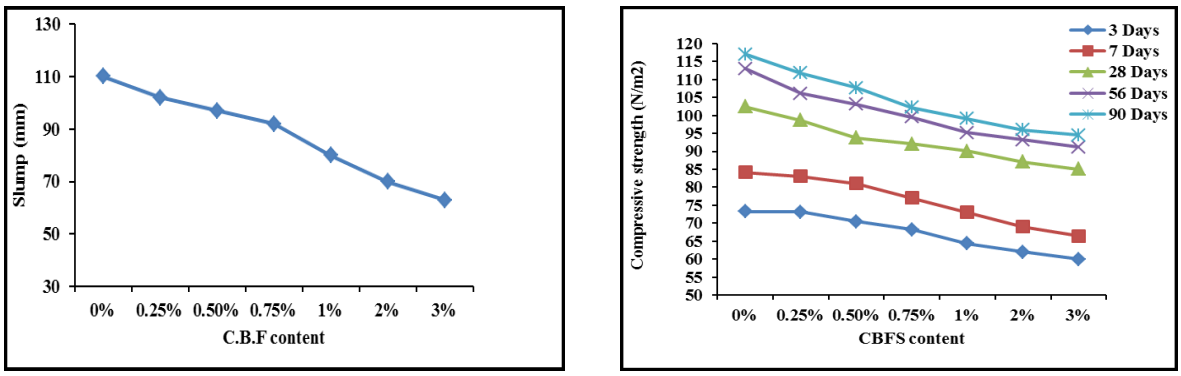
Table 2
Material Mix Proportions

No Mix	Cement [Kg/m^3]	F A [kg/m^3]	CBFS %	C. A [Kg/m^3]	F. A [Kg/m^3]	w/c ratio	S.P %
MF	440	110	0	975	740	0.275	0.8
MF_1	440	110	0.25	975	740	0.275	0.8
MF_2	440	110	0.5	975	740	0.275	0.8
MF_3	440	110	0.75	975	740	0.275	0.8
MF_4	440	110	1	975	740	0.275	0.8
MF_5	440	110	2	975	740	0.275	0.8
MF_6	440	110	3	975	740	0.275	0.8

Results and Discussion

Workability. The slump measurement of all samples made of fixed water to the cementitious material ratio of 0.275 and the dosage of the chemical admixture of 0.8% by weight of cement was investigated. Using CBFS up to 3% in HSC required a high effect of the chemical and mineral admixtures which were Sika Viscocrete 34-30 and FA. Concrete mixing with CBFS as addition internal materials required more time for mixing. This time increased as there was an increase in the dosage of CBFS to prevent the balling and provide the homogeneousness of the mix. The workability of FAHSC demands only a little amount of superplasticizer as compared to the normal HSC concretes. The reason here is that the small particle size and spherically shaped particles of FA decreased the resistance friction between the paste of the cement and the aggregates. Consequently, an improvement of the fresh properties of the concrete was observed as reported by Correlissen et al. [21] and Vanchai et al. [22]. Furthermore, addition of CBFS by this system increased the particle size, provided friction force between the paste of the cement and the aggregate, and absorbed some of the designed water from the mixing. Due to these reasons, the workability of the fresh concrete decreased with an increasing of the CBFS content as shown in Figure 1(a). However, the reduction of the workability of FAHSC by CBFS was partially substituted by utilizing the highly effective superplasticizer and FA. There was little effect of the 0.25, 0.5 and 0.75 on the workability of FASHC.

Compressive strength. Figure 1 (b) shows the compressive strengths of the CBFS series of 0.25, 0.5%, 0.75%, 1%, 2% and 3% by weight of cement as the addition material. The compressive strength of FAHSC after the addition of CBFS at the early age yielded lesser compressive strengths than that of the control mix. Due to the effect of CBFS, the compressive strength decreased as the age of the specimens increased. Using CBFS may make some porous areas in hardened concrete. First, collapse may happen through those void regions. The fibers, after mixing, had absorbed too much of the mixing designed water; therefore, the cement around them might not have gotten sufficient water for hydration. It can be seen that the reduction of the compressive strengths of the concrete mixtures containing CBFS was more negligible later than at the age of 56 days. Also, the results point out that 0.25%, 0.5% and 0.75% of CBFS showed little effect on the compressive strength of FAHSC.



(a) (b)

Figure 1 (a) Effect of CBFS on the fresh properties of fly ash HSC and (b) Effect of CBFS on the compressive strength of FAHSC

Split and flexural tensile strengths. Figure 2 (a) and (b) presents the split and flexural tensile strength test results conducted, respectively, which were measured through the indirect tensile test. It was observed that the split and flexural tensile strengths of FAHSC tended to improve slightly with the increasing of the CBFS content as well as the tensile strength to compressive strength ratio. Furthermore, the tensile strength of FAHSC was higher than that of the normal HSC; whereas, the grain and whole refinement of concretes resulted from the very high fineness of the particles and the FA reaction of the ashes. Moreover, CBFS helped to arrest the crack growth which appeared when the specimens were loaded, and it bridged the deformation cracks thus transferring the loads to the concrete.

Stress – strain relationship. The strain behaviour of the CBFS concrete cubes was observed through the stress-strain relationship curves for the control mix with and without a varied ratio of CBFS as mentioned previously. An electrical resistance strain control gauge was used to measure the strain of a plain concrete cube under the compressive strength test machine. The relationships were plotted as shown in Figure 3. From the test results, it can be seen that the ascending parts of the curves were linear consecutive parts having a non- linear shape up to the failure point. All the curve shapes changed with an increase in their strain by adding CBFS. The reason here is that CBFS enhances the interaction zone strength bond between the aggregate and cement paste. Depending on this result, we can say that the failure pattern of FAHSC moved from a brittleness collapse towards the ductile collapse. It can be seen that the effect of the 0.25%, 0.5% and 0.75% of the CBFS curves was very little compared with the 1%, 2% and 3%.

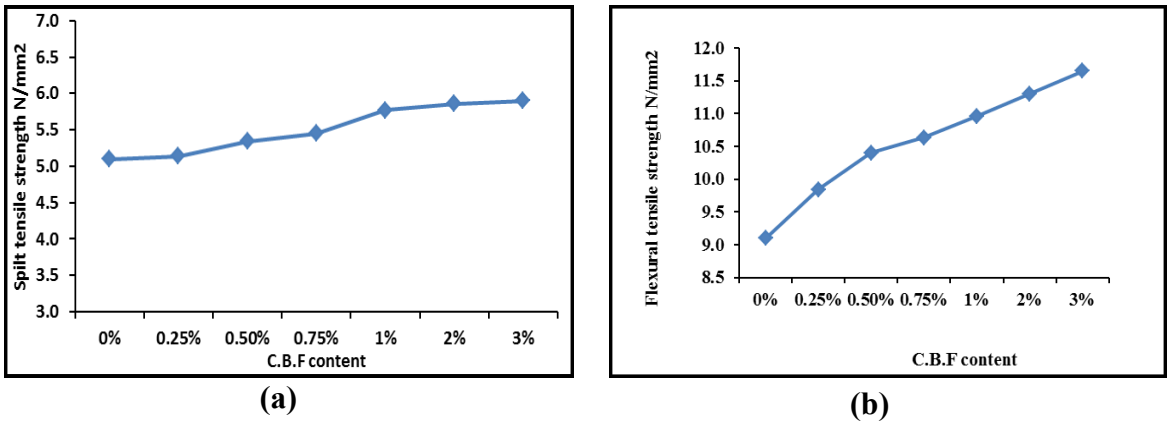


Figure 2: Effect of CBFS on the split (a) and flexural (b) tensile strengths of FAHSC

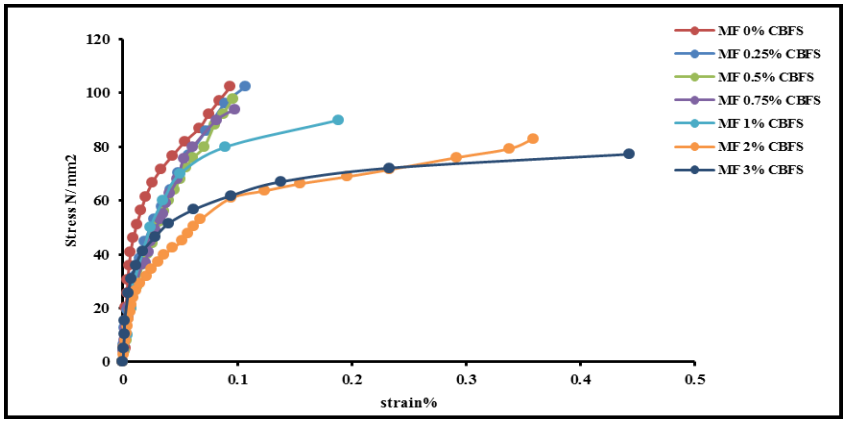


Figure 3: Effect of CBFS on the stress – strain relationship of FAHSC

Conclusion

The experimental application of the randomly distributed CBFS as an internal addition strengthening material was evaluated. During the mixing, it was observed that more time for mixing was needed during the process of adding CBFS, full homogeneousness was achieved, no balling of fibers was present and there was no aggregate segregation. Using a highly effective superplasticizer and fly ash as the chemical material controlled the reduction of the workability of HSC after CBFS addition. The results showed that the compressive strength of FASHC was not supported with CBFS. There was 11.21%, 12.49% and 17.65% reduction of 1%, 2% and 3% of CBFS, respectively.

Split and flexural strengths and the ratio to the compressive strengths of FAHSC steadily increased as there was an increasing of the CBFS content. Also, compressive stress-strain curves showed an increase in the areas under all of those curves. The toughness and ductility of FAHSC were remarkably improved using CBFS as an internal strengthening material. Finally, CBFS as internal strengthening materials can be considered as an alternative to other fiber reinforced plate strengthening systems.

Acknowledgment

The support received from Universiti Teknolgi PETRONS is sincerely acknowledged. This work could not have been completed without Mr Johan's and Mr Hafiz's help , lab technicians, and the authors would like to thank them for their help.

References

[1] KunalSingha ,."A Short Review on Basalt Fiber". International Journal of Textile Science 2012, 1(4): 19-28.
[2] A G Novitskii, V VSudakov; An unwoven basalt-fibre material for the encasing of fibrous insulation : an alternative to glass cloth; Refractories and Industrial Ceramics; vol 45, no 4, 2004, pp 234 - 241.
[3] Weimin Li a, JinyuXua,b" Mechanical properties of basalt fiber reinforced geopolymeric concrete under impact loading" Materials Science and Engineering A 505 (2009) 178–186.
[4] Gajanan Deshmukh; Basalt - The Technical Fibre; Man-made Textiles in India; July 2007; 258-261.
[5] Sahibin Abdu Rahim, Mohamad Md. Et al., "heavy metals compostion of some soils developed from basic and ultrabasic rocks in malaysia" Geological society of Malaysia, Annual Geological conference, 2001
[6] Weimin Li a, JinyuXua,b,. "Mechanical properties of basalt fiber reinforced geopolymeric concrete under impact loading". Materials Science and Engineering A 505 (2009) 178–186.
[7] D.P. Dias, C" Fracture toughness of geopolymeric concretes reinforced
[8] with basalt fibers". Cement & Concrete Composites 27 (2005) 49–54.
[9] W.M. Li, J.Y. Xu,." Impact characterization of basalt fiber reinforced geopolymeric concrete using a 100-mm-diameter split Hopkinson pressure bar " Material science and engineering A 513-514 (2009) 145-153.
[10] Lee YT, Lee JH, Hwang HS, Kim YD. Performance of concrete structures retrofitted with fiber reinforce polymers. Mag Korean ConcInst 2002;14(4):89–96.
[11] Mohmoud, L. Shafiq, N. Nureldin, M. F. Thanoon, A. M.W,. (2009). Fatigue behaviour of CFRP concrete joints under shear. Volume 162, Issue 5, , Pages 355-364
[12] Hong GH, Shin YS. Structural performance evaluation of reinforced concrete beams with externally bonded FRP sheets. J Korean ConcInst 2003;15(1):78–86.
[13] Mehta,P.K.,andR.W.Burrows, 2001, "Building Durable Structures in the 21st Century." Concrete International 23(3), pp. 57-63.
[14] Vengata G. K.B., 2009, 'High volume fly ash concrete for pavements', M.E. Dissertation, Department of Civil Engineering, Anna University, Chennai, India.
[15] Adams, T. H., 1988, "Marketing of fly ash concrete", MSU seminar: Fly ash applications to concrete (January), 1.10, 5.10, East Lansing: Michigan State University.
[16] Naik, T. R. and Ramme B.W. 1989, 'High Strength Concrete containing large quantity of fly ash', ACI Material Journal, Vol.86, No.2,pp.111-116.
[17] Raju, N. K., Ipe, T. V. and Srinath, N., 1994, 'mix Proportioning and strength characteristics of portland cement and pulverized fly ash concrete', ICI Bulletin No. 49, pp.27-32.
[18] American Coal Ash Association, 1995, 'Fly Ash Facts for Highway Engineers', Federal Highway Administration, Report No. FHWA-SA- 94-081, Washington, DC, December.
[19] VanitaAggarwal, S.M.Gupta, S.N.Sachdeva, "concrete durability through high volume fly ash concrete (hvfc) a literature review", International Journal of Engineering Science and Technology Vol. 2(9), 2010, 4473-4477.
[20] Ali. E. A. E, N.Sh, M. F. N, A. F," Mechanical properties of High Strength concrte using Fly Ash" 978-1-4673, 2013 IEEE.
[21] VanchaiSata a, Chai Jaturapitakkul b,*, KraiwoodKiattikomol b" Influence of pozzolan from various by-product materials onmechanical properties of high-strength concrete" Construction and Building Materials 21 (2007) 1589–1598.
[22] Cornelissen HAW, Hellewaard RE, Vissers JLJ. Processed fly ash for high performance concrete. In: The 5th international conference on fly ash. Silica fume, slag, and natural pozzolans in concrete.Wisconsin: American Concrete Institute; 1995. p. 67–79.

Applied Mechanics and Materials Vol. 567 (2014) pp 387-392
© (2014) Trans Tech Publications, Switzerland
doi:10.4028/www.scientific.net/AMM.567.387

Effect of Flexural Static Load on the strength of GFRP gratings

Amir Izzuddin [a] and Ibrisam Akbar [b]

Universiti Teknologi PETRONAS, Malaysia

[a]amerdeen89@gmail.com, [b]ibrisam_akbar@petronas.com.my

Keywords: Offshore, GFRP grating types, Pultruded, Moulded, Bonding matrix, Vinyl ester, Polyester, and Phenolic.

Abstract – The usage of steel in offshore deep water area contributes to the massive load of the offshore platform which will lead to the massive operational cost. Therefore, the reduction of weight of platform is the major issue that need to be tackled properly. The great improvement in strength to weight ratio compare to steel and high resistivity to corrosion makes Glass Fibre Reinforced Polymer (GFRP) grating preferable. GFRP gratings are normally made of two types of processes which are moulded and pultruded and it is usually consists of glass fibre and bonding matrixes of vinyl ester (VE), polyester (PE), or phenolic (PHE). However there is still doubt on GFRP grating application for offshore due to no consensus guidelines for the design of GFRP grating and there are many several types of GFRP grating available to be chosen. This paper presenting the study on two types of GFRP grating strength with variation of bonding matrixes under flexural static load. A total of six specimens of GFRP grating which consist of 1 each of molded vinyl ester, molded polyester, molded phenolic, pultruded vinyl ester, pultruded polyester and pultruded phenolic were tested to failure in flexure. The main parameters concerns in this study are 1) max load vs. mid-span deflection and 2) failure mode of the specimens.

Introduction

Fibre reinforced composites have been the alternatives of steel, metal and wood in many applications. The potential for using fibre reinforced composites for a wider range of applications is now being realized due to the need to repair and retrofit of rapidly deteriorating infrastructure in recent years. These materials offer excellent resistance to environmental agents and fatigue as well as the advantages of high stiffness-to weight and strength-to-weight ratios. In addition, the application of fibre reinforced composites has been driven by various attractive aspects like ease of handling, high adaptability, economy of fabrication, and damage tolerance. [1-3]. Weight reduction is a more immediate concern in the design stage of offshore structures especially floating platforms. This new interest in weight reduction that has increased awareness in all composites and has led to the first substantial use of composite grating. Shell Offshores Mars tension leg platform (TLP) marked the first use of phenolic grating to the tune of over 7440 m^2. The weight saving, compared with steel, was 70%. Shell stayed with the product on its next major called deep water venture Ram-Powell. On that project, purchases increased to nearly 9300 m^2 which clearly shows the satisfaction with the performance of the fibre grating. Continuing the trend, FRP grating was used on Shell's Ursa TLP which reported to be the largest platform structure in the Gulf of Mexico. In addition to a 13,020 m^2 of topside grating, Ursa has an additional 1,116 m^2 inside the hull for walkways, stairs, and landings. It now appears that composite grating is a serious player in the offshore market [4]. Even though GFRP has several benefits the growth rate is not as fast as it should be. Cost has been the major issue for the slow growth of GFRP grating application [5]. However, beyond the cost issues, the major obstacle that preventing the extended use of GFRP materials in civil engineering especially grating is lack of information and uncertainty associated with the due to no consensus guidelines for the design of GFRP grating comparable to the traditional construction materials. This study on the other hand focusing on the effect of GFRP grating's structural strength and performance under flexural static load.

Literature Review

Types of GFRP gratings. There are various technics for the manufacture of GFRP, which are hand lay-up, filament winding, press moulding, pultrusion, spray-up and auto-clave moulding. Among these processes, pultrusion and moulding techniques are normally used in manufacturing of GFRP gratings [6]. Pultruded grating is made from pultrusion process. It is a continuous, semi-automated process for manufacturing composite materials. The process involves continuous fibres of glass to be saturated with a thermo set resin mixture. The wetted fibre is then pulled through a preformer before entering a heated die to shape the composite and initiate curing of the resin mixture. The rigid composite is finally cut to the desired length with a cut-off saw [7, 8]. Pultruded grating is characterized by unidirectional mechanical properties and nominal corrosion resistance. Since pultruded bars are continuous and straight, the grating must be produced with the pultruded bars all aligned along a given axis. This results in relatively high strength and stiffness in the strong direction but zero strength and stiffness in the lateral direction. For simple structures without openings and rectangular or trapezoidal in shape, such type of grating will work fine in terms of structural design. However, platforms often require openings for piping, instruments, structural members and are often complex in shape. In these instances, the use of pultruded grating is problematic because every cut edge lateral to the strong axis must be fully supported. Pultruded grating has nominal corrosion resistance for two reasons. First, the pultrusion process inherently produces members with a relatively thin outer layer of resin. In other words, the glass reinforcement is close to the surfaces. Corrosion resistance in FRP is a function of many factors including the thickness of the resin rich surface and the chop strand reinforced liner. Both of these are quite thin in pultruded parts. On the other hand, the moulded GFRP grating is manufactured in a one piece construction process by interlacing pre-wetted glass reinforcing fibre strands in a liquid resin matrix within a given configuration. Once the resin matrix has cured, the moulded grid is removed from the mould. The one piece construction insures that all glass is impregnated with resin [7-9]. Moulded grating has biaxial strength and stiffness and has much more corrosion resistance than pultruded grating. For a given direction, the strength and stiffness of moulded grating will be significantly lower than the strong axis properties of pultruded grating because the percentage of fibres in moulded grating is lower. Biaxial properties are very helpful in many applications. For example, a simple rectangular platform can be decked with either pultruded or moulded grating. In cases the pultruded grating becomes problematic when cutting a hole in a pipe, the moulded grating, however, may be used with no difficulty.

Types of bonding matrix. Polymer matrix is the binder of GFRP and some of the roles include binding the fibres together, protecting the fibres from abrasion and environmental degradation, separating and dispersing the fibres within the composites and also providing shape to the GFRP component. Several different polymer matrixes have been used so far; however, one or two specific polymer types are typically used, depending on the intended purposes. Some of the polymer matrix that always been used is the industry is vinyl ester, polyester and phenolic. Vinyl ester has a high tensile strength, good chemical resistance, long term resistance to moisture, mechanical and temperature resistance combined with rapid curing and ease of processing. Vinyl ester also has low viscosity and short cure time, make it well suited for civil engineering application. Meanwhile, polyester has a good resistance to moisture attack, acid and alkaline, high flexural modules, low cost and relatively easy to process. However, polyester is prone to degradation by chloride solvent and fire. On the other hand, phenolic has a good fire resistance and can withstand temperature up to 200ºC with very low toxicity and low smoke emission. This property made phenolic to be a suitable matrix to be used in potentially fire-prone facilities as it can minimize the spread of fire. However, phenolic is brittle in nature.[5-7, 10-15]

Methodology

Grating specimen. The pultruded gratings were 760 mm long and 300 mm wide, with an I-section of load bearing bar with the depth of 38 mm and 15 mm width was used. The load bearing bars were spaced at 38 mm centre-to-centre distance. There are 5 cross ties placed in every 152.5 mm distance along the length of the bearing bar. The moulded gratings were 760 mm long, 300 mm wide and 38 mm depth, with the mesh of 38 mm x 38 mm. Figure 1 show the dimensions for both types the specimens.

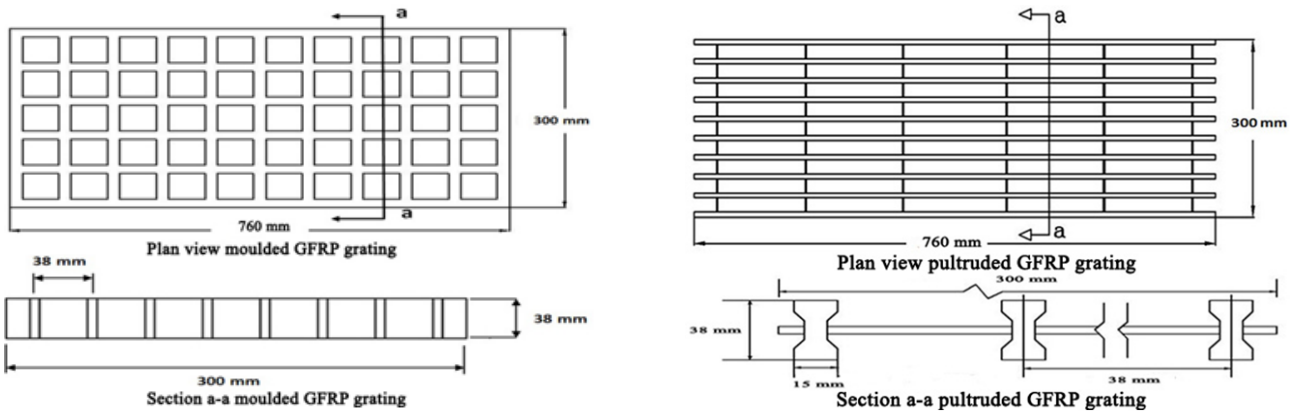


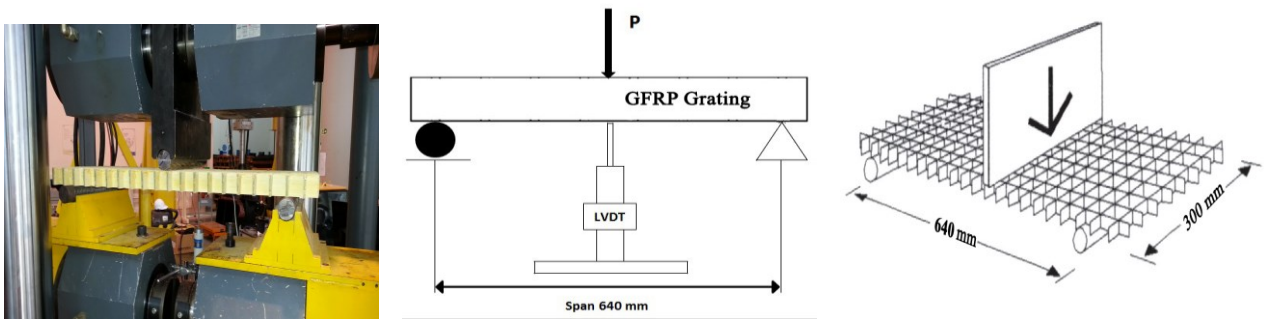
Figure 1: Dimensions of the specimen

Specimen Details. The specimen details and number of specimen tested is tabulated in Table 1.

Test setup. Universal Testing Machine (UTM) is used for the flexural static load test. The point load is located at the centre of the 640 mm span. The Linear Variable Differential Transformer (LVDT) was installed at the bottom of the specimen to measure the centre deflection. Figure 2 shows the view of the test setup.

Table 1 Tabulated the specimen's details

GFRP grating specimen name	Vinyl Ester Moulded (VEM)	Polyester Moulded (PEM)	Phenolic Moulded (VEM)	Vinyl Ester Pultruded (VEP)	Polyester Pultruded (PEP)	Phenolic Pultruded (PHEP)
No of specimen tested	1	1	1	1	1	1



a) Front View 1 b) Front View 2 c) Isometric View

Figure 2: Geometrical properties of the GFRP specimens

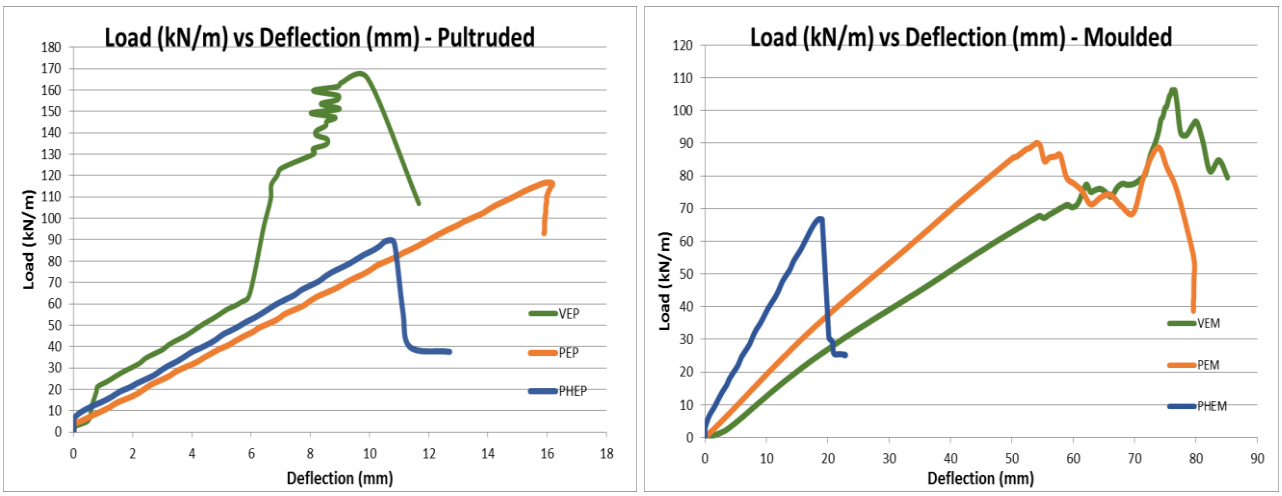
Result and findings

Maximum Load vs. mid-span deflection. The result shows that for the pultruded GFRP grating type, the grating with vinyl ester bonding matrix shows the highest maximum load can be sustained at 165.42 kN/m, followed by grating with polyester bonding matrix at 116.65 kN/m, and lastly grating with phenolic bonding matrix at 89.34 kN/m. Meanwhile for the moulded GFRP grating type, the grating with vinyl ester bonding matrix shows the highest maximum load can be sustained at 106.26 kN/m, followed by grating with polyester bonding matrix at 90.07 kN/m and lastly grating with phenolic bonding matrix 66.72 kN/m. The result is tabulated in the Table 2.

Table 2: Test Result from Flexural Static Load Test

GFRP grating types	Bonding matrix	Specimen's name	Maximum Load (kN/m)	Maximum mid-span deflection (mm)	Failure Mode
Pultruded	Vinyl Ester	VEP	165.42	9.94	Shear
	Polyester	PEP	116.65	16.15	Shear
	Phenolic	PHEP	89.34	10.56	Flexure
Moulded	Vinyl Ester	VEM	106.26	76.13	Flexure
	Polyester	PEM	90.07	54.07	Flexure
	Phenolic	PHEM	66.72	18.52	Flexure

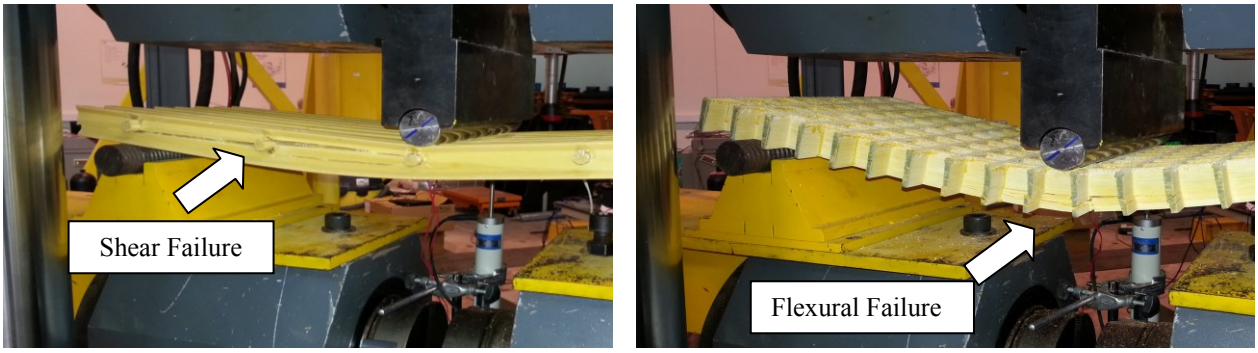
Figure 3a shows the graph of load vs. deflection of the pultruded specimens. The curves of all the specimens remain quite linear prior to failure except for VEP specimens, due its type of failure and high stiffness. The VEP specimens' mid-deflection is lower at maximum load than polyester and phenolic. Figure 3b shows the graph of load vs. deflection of the moulded specimens. The curves of all the specimens also remain quite linear prior to failure. The VEM specimens' mid-deflection is the highest at the highest maximum load as compared to polyester and phenolic. The overall observation based on all the figure; i) the pultruded specimen has higher strength and stiffness than the moulded specimen which lead to lower mid-span deflection at the maximum load, ii) the mid-span deflection of moulded specimen increase when the load increase while the pultruded specimen show different behaviour due to its stiffness.



a) Pultruded Specimens b) Moulded Specimens

Figure 3: Load vs. Deflection graph

Failure Mode of GFRP Grating. The GFRP grating is categorised as isotropic, homogeneous and brittle which will make it behave linear elastically under sustaining load. However, the types of GFRP grating tend to complicate the prediction of failure mode due to the grating types and variation of bonding matrixes. Based on the experiment, failure mode of all the specimens can be categorised into flexural failure and shear failure. The VEM, PEM, PHEM and PHEP specimens failed in flexure while VEP and PEP specimens failed in shear. The process of flexural failure under static load initiate with the development of parallel matrix cracks transverse to the longitudinal direction on the lower part of GFRP grating. On the other hand, the shear failures were initiated at one of the supports then propagates toward the middle span. This shear failure of pultruded composite (VEP and PEP) may be due to voids or micro-defect [16] or moderately high longitudinal-to-shear modulus ratio [17].



a) PEP Pultruded Specimens b) PEM Moulded Specimens

Figure 4: Failure mode of GFRP Grating specimens

Conclusions

This paper presents the findings of an experimental program that was conducted to investigate the effect of difference types of GFRP gratings and its bonding matrixes structure under static flexural static load test. Based on experiment it is observed that pultruded specimen is better in term of strength and stiffness as compared to moulded specimen. Meanwhile the grating of vinyl ester bonding matrix is better than polyester and phenolic bonding matrix. The failure mode of the specimens categorised into flexure and shear.

Acknowledgment

The authors would like to extend their acknowledgement to the Yayasan Universiti Teknologi PETRONAS (YUTP) for providing the funding and resources for the accomplishments of this research study

References

[1] Liao, K., Schultheisz, C.R., & Hunston, D.L., "Long-term environmental fatigue of pultruded glass-fiber-reinforced composites under flexural loading," International Journal of Fatigue, vol 21, pp. 485-495, 1999

[2] Gu H., "Behaviours of glass fibre/unsaturated polyester composites under seawater environment," Materials & Design, vol 30(4), pp. 1337-1340, 2009

[3] Buck, S.E., Lischer, D.W., & Nemat-Nasser, S., "Mechanical and microstructural properties of notched E-glass/vinyl ester composite materials subjected to the environment and a sustained load," material science and Engineering, vol. A317, pp. 128-134, 2001.

[4] Carlean, T., "Composite grating is right for today' offshore market," Reinforced plastics, vol. 40, pp. 38-44, 1996.

[5] Karbhari, V.M., Chin, J.W., Hunston, D., Benmokrane, B., Juska, T., & Morgan, R., "Durability gap analysis for fiber-reinforced composites in civil infrastructure," ASCE J Composite Construction, vol. 7, pp. 238-247, 2003.

[6] Hollaway, L., "Glass Reinforced plastics in construction: Engineering Aspects.," Bishopbriggs, Glassgow, Surrey University Press., 1978.

[7] AIMS. DeltaGrate TM HS High Strength Compression Moldedd Fiberglass Grating. Retrieved 2013 from www.aims-intl.com. AIMS Advanced Industrial & Marine Services,Inc

[8]CHINAGRATE. Fire strength Phenolic gratings guide. Retrieved 2013 from www.chinagrate.com

[9] Meng, X., & Tom, Lo., "Advances in FRP moulded grating in Asia," Reinforced plastics, vol. 44, pp. 46-47, 2000.

[10] Ceroni, F., Cosenza, E., Gaetano, M., & Pecce, M., "Durability issues of FRP rebars in reinforced concrete members," Cement and Concrete Composites, vol. 28, pp. 857-868, 2006.

[11] Mezghani, K., "Long term environmental effects on physical properties of vinylester composite pipes," Polymer Testing, vol. 31, pp. 76-82, 2012.

[12] Signor, A.W., VanLandingham, W., MarkR., & Chin, J. W., "Effects of ultraviolet radiation exposure on vinyl ester resins: characterization of chemical, physical and mechanical damage," Polymer Degradation and Stability, vol. 79, pp. 359–368, 2003.

[13] Mallick, P.K., Fibre reinforced composites; Materials, Manufacturing and design: 2ne ed. New York, Marcel Dekker, Inc., 1993.

[14] Benmokrane, B., Chaallal, O., & Masmoudi, R., "Glass fibre reinforced plastic (GFRP) rebars for concrete structures," Construction and Building Materials, vol. 9, pp. 353-364, 1995.

[15] Teng, J. G., Chen, J. F., Smith, S. T., & Lam, L., FRP strengthend RC structures: England, Jhon Wiley &Sons, Ltd., 2002.

[16] Paciornik, S.F.M.M., Martinho, F.M., De Mauricio, M.H.P., & d'Almeida, J.R.M., "Analysis of the mechanical behavior and characterization of pultruded glass fiber–resin matrix composites," Composites Science and Technology, vol. 63, pp. 295-304, 2003.

[17] Bank, L.C., Composites for construction: Structural design with FRP materials. New Jersey John Wiley and Sons Inc., 2006.

Applied Mechanics and Materials Vol. 567 (2014) pp 393-398
© (2014) Trans Tech Publications, Switzerland
doi:10.4028/www.scientific.net/AMM.567.393

Effect of MIRHA and Fly Ash in Ductile Self-Compacting Concrete on Abrasion and Impact Performance

Muhd Fadhil Nuruddin[1,a], Norzaireen Mohd Azmee[1,b] and Kok Yung Chang[1,c]

[1]Department Of Civil Engineering, Universiti Teknologi PETRONAS, Perak, Malaysia.

[a]fadhilnuruddin@petronas.com.my, [b]norzaireen@gmail.com, [c]kyung1987@gmail.com

Keywords: Abrasion Resistance, Impact Resistance, DSCC, MIRHA, Fly Ash

Abstract. The benefits of Microwave Incinerated Rice Husk Ash (MIRHA) as partial cement replacement materials in DSCC mixes has led to the research on the possibilities of combining both MIRHA and fly ash as an addition in DSCC replacing up to 20% of cement volume whilst maintaining satisfactory properties. The addition of both materials can improve concrete properties and reduce the cost of DSCC production. These supplementary cementitious materials are expected to give positive effects on the concrete abrasion and impact resistance. The incorporations of both MIRHA and fly ash in DSCC as cement replacement materials are considered as a new type of concrete. Therefore, it is important to have a complete knowledge on the behaviour of the composite material when being subjected to repetitive dynamic loading. The test results showed that MIRHA and fly ash combination in DSCC improved both abrasion and impact resistance of DSCC compared to reference specimens.

Introduction

Ductile self-compacting concrete (DSCC) combines both properties of self compacting concrete and high performance fiber reinforced concrete resulting to a composite material that can be used in several structural applications with technical and economic advantages [1,2]. DSCC can be considered as the most successful recent innovation in concrete construction that further extends the applications of self-compacting concrete (SCC). The concept of SCC was initially proposed in late 1980s in Japan with first significant applications in the 1990's [3]. The ordinary SCC however possesses low tensile strength, limited ductility and little resistance to cracking. Further enhancements were required to overcome these problems. In order to obtain the characteristics of DSCC, discrete and discontinuous steel fibers were randomly added into the concrete mix to ensure necessary ductility. Inclusion of fibers into concrete mixes is not new, the method has been around since 1960's to improve the concrete properties particularly tensile strength, abrasion resistance and energy absorbing capacity [4,5]. The presence of fiber helps to refrain crack growth or propagation and transer load to the unaffected area [6]. DSCC also require high usage of powder content. The positive benefits of MIRHA as partial cement replacement materials in concrete mixes reported by Nuruddin et al. [7,8] has led to the research on the possibilities of combining both MIRHA and fly ash as binary addition in DSCC.

When subjected to repetitive dynamic loading, the specimen with fibers possesses higher ductility than the specimen without fibers due to the effect of fiber bridging [9]. However the properties of fiber reinforced concrete would be affected by the type, volume fraction and aspect ratio of fiber [10]. Naaman [11] suggested 2% steel fiber volume fraction to achieve effectiveness in concrete composites. Several investigations have shown that the abrasion and impact resistance of fiber reinforced concrete has direct relationship with concrete strength [12-14]. Lin et al. [12] studied the effect of fibers and silica fume on abrasion and impact performance of concrete. The test results showed that the combination of 10% silica fume with 2% steel fibers gave highest value of abrasion resistance and impact energy absorbed as compared to others. The author also found that incorporation of silica fume helps fiber dispersion and significantly improves the bond between fiber and matrix. The incorporations of both MIRHA and fly ash as cement replacement material in

DSCC are considered as a new type of concrete, therefore, it is important to have a complete knowledge on the behaviour of the composite material when subjected to repetitive dynamic loading. The behaviour of DSCC with combined cement replacement materials subjected to abrasion and impact actions were studied in this paper.

Experimental Work

Work Programme. The specimens were divided into two group identified as group A and B. Mixes in group A refer to control mix (CM_A) and optimum mix (OM_A) without fiber inclusion whereas mixes in group B consist of mix CM_B and mix OM_B reinforced with volume fraction of 2% hybrid steel fibers. The standard cylinder specimens of 100mm diameter by 200mm from group B were used to evaluate the concrete abrasion performance using a Los Angeles (LA) Machine as suggested by Offenberg and Wang et al. [13,15]. Abrasion resistance testing procedure used conformed to ASTM C131: 2003 [16]. The specimens of 150mm diameter by 64mm height discs in both group A and B were used to inspect the impact resistance using drop weight test suggested by ACI 544 [17].

Material Properties. Both MIRHA and fly ash were used as cement replacement materials. MIRHA was produced from incineration of local rice husk using Microwave Incinerator. Images obtained from field emission scanning electron microscopy (FESEM) for both MIRHA and fly ash are presented in Figure 1 and 2 at magnification of 50x. FESEM image shows that MIRHA particles are angular and flaky and fly ash particles are composed of spherical shapes. The chemical oxide composition for OPC, MIRHA and fly ash are given in Table 1. River sand with a fineness modulus of 2.8 were used in all mixes. Polycarboxylic Ether (PCE) based superplasticizer was used to adjust the workability of DSCC. Two types of steel fibers namely straight fiber (SF) and end-hooked fiber (EH) having average aspect ratio of 100 and 84 respectively were employed in this study.

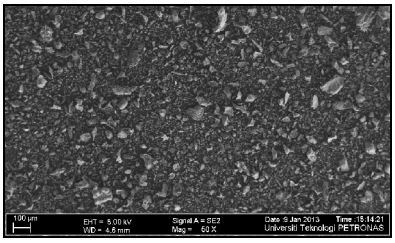


Fig. 1: FESEM image of MIRHA particles

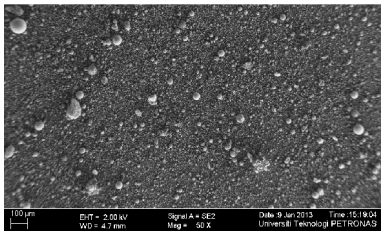


Fig. 2: FESEM image of fly ash particles

Table 1: Chemical oxide composition of OPC, fly ash and MIRHA

Oxide	Percentage (%)		
	OPC	Fly ash	MIRHA
Na_2O	0.20		0.12
MgO	2.42		0.49
Al_2O_3	4.45	29.1	0.45
SiO_2	21.45	51.7	89.34
P_2O_5	0.11	1.7	2.58
K_2O	0.83	1.6	4.98
CaO	63.81	8.84	0.76
TiO_2	0.22	0.7	0.02
Fe_2O_3	3.07	4.76	0.40
SO_3	2.46	1.5	0.90
MnO	0.20		0.08

Concrete Mix Proportions. Details of the mix proportions are given in Table 2. All DSCC mixes were selected based on the trial stage results of fresh and hardened testing done in earlier phase. All mixes fulfilled the SCC requirements.

Table 2: DSCC mixture proportion (parts by mass) and compressive strength

Group	Mix	OPC	MIRHA	FA	Sand	Steel Fibers	SP	Water	Compressive @ 28day (Mpa)
A	CM_A	1	-	-	1	-	0.025	0.17	120
	OM_A	0.8	0.1	0.1	1	-	0.025	0.18	122
B	CM_B	1	-	-	1	0.152	0.025	0.17	130
	OM_B	0.8	0.1	0.1	1	0.152	0.025	0.18	138

Experimental Programme. LA machine was used to evaluate the abrasion resistance and surface durability of concrete. Test was conducted following the specifications of ASTM C131-03 [16]. In this method single specimen was placed inside the rotating steel drum containing 12 numbers of steel balls with rotating speed of 30 rpm, the rotation of the drum was set to 100 and continued until 500 revolutions. Specimens were weighed before and after every 100 revolutions interval until it reached 500 revolutions. The impact test was carried out in accordance with ACI 544 [17]. The drop weight impact test was adopted to evaluate the impact resistance of the concrete specimens due to the simplicity of the testing method compared to other conventional tests. In this method, manually operated compaction hammer of 4.54kg was repeatedly dropped from a height of 457mm on a 63.5mm diameter steel ball, which was located at the center of the top surface of the specimen.

Results and Discussions

Abrasion Resistance Test. The abrasion coefficients for the different mixes of DSCC in group B were obtained by LA abrasion machine, the weight reduction of each specimen was recorded at every 100 revolutions until 500 revolutions were reached.



a) Before b) After a) Before b) After

Fig. 3: Group B Specimens Before and After 500 Cycles

Table 3: Results of abrasion test

Mix ID	Number of Cycle	Weight (g)	Weight Reduction (g)	Percentage Reduction (%)
CM	0	3898	-	0
	100	3801	97	2.49
	200	3743	155	3.98
	300	3684	214	5.49
	400	3594	304	7.80
	500	3483	415	10.65
OM	0	3865	-	0
	100	3777	88	2.28
	200	3716	149	3.86
	300	3661	204	5.28
	400	3585	280	7.24
	500	3499	366	9.47

The average weight reduction of concrete surface for each CM and OM mixes from group B were monitored and summarized in Table 3. Specimens' photos from both mix CM and mix OM subjected to 500 number of rotation are shown in Figure 3. It can be seen that the average weight reduction of the concrete specimens behaved as follows:

1- The reduction on weight of fibrous concrete specimens increases as the number of cycles increase and the edges of the cylindrical specimens for mix CM_B were more abraded compared to mix OM_B. Results similar to findings made by Wang et al. [15].
2- Weight reductions in mix CM_B are higher than the value in mix OM_B for all cases when subjected to abrasion due to rubbing, scraping, skidding or sliding of an object on the concrete surfaces. However, values of weight reduction for both mixes from both groups are small with highest values of less than 11%, these findings can be explained by study made by Lin et al. [14]. He found that the abrasion coeffecient of concrete remained steady with addition of steel fiber content that exceed 1% by volume.
3- From Table 3, it can be seen that the reductions by weight after 500 revolutions for mix CM_B and mix OM_B was 10.7% and 9.5% respectively. DSCC mix with incorporation of MIRHA and fly ash increased the abrasion resistance by 1.2%. The addition of these materials in concrete mix improved strength and porosity by strengthening the aggregate-cement paste and modify micropores structure. Modifications of micropores structure in concrete are done by filling up the empty spaces in concrete pore structures through pozzolanic reactions [8,18]. Incorporation of both MIRHA and fly ash in DSCC produces tougher and denser surface with higher surface durability compared to controlled DSCC, thus resulting in a higher resistance to wear for DSCC specimens.

Impact Resistance Test. Improved impact resistance such as improvement in dynamic energy absorption and strength is one of the important attributes in all fiber reinforced concrete. The number of impact blows at ultimate failure serves as a qualitative estimation of the energy being absorbed by the specimens. The average number of blows resulting to the first visible crack (N_1) and number of blows required for failure (N_2) were recorded and presented in Table 5. Table 5 also indicates the calculated ultimate impact energy (U) for all specimens in both groups. The ultimate impact energy can be calculated based on equation below:

$$U = (N_2)\, mgh \quad (1)$$

Where: U is the ultimate impact energy, m is the mass of the hammer, g is the acceleration due to gravity and h is the height of the fall.

Table 4: Results of impact test

Group	Mix	First crack resistance N_1	Ultimate resistance N_2	N_2-N_1	Percentage increase (%)	Ultimate impact energy, U (kN-m)
A	CM_A	329	335	6	1.8	6.8
	OM_A	380	390	10	2.6	7.9
B	CM_B	1588	6450	4862	306.2	131.3
	OM_B	1639	7074	5435	331.6	144



Fig. 4: Specimen failure in group A



Fig. 5: Specimen failure in group B

Figure 4 and 5 shows the image of broken specimens from group A and B. Results for non fibrous concrete in group A are used as references to study the effect of steel fibers on concrete impact performance. It can be seen that the impact resistance from group A and B of the concrete specimens behaved as stated below:

1- The increase in number of blows for first crack and at failure for mix CM and mix OM was significantly higher in group B compared to non fibrous specimens in group A with percentage increase in post crack resistance of 306.2 – 331.6% depending on the binder used. Incorporation of steel fibers in concrete exhibit ductile properties and higher energy absorption. Steel fibers added into the matrix will restrain the extension of crack and delay the crack growth rate. In the hardened state when fibers are properly bonded, they interact with the matrix at the level of micro-cracks and act as a bridge to delay the unstable growth of the micro-cracks [19]. Short stright fibers (SF) in concretes will act as a bridge to reduce the formation of micro-cracks however, due to the size; short fibers may be pulled out after the formation of macro-cracks. When micro-cracks turn into macro-cracks, the longer end hooked fibers (EH) will arrest the propogation of macro-cracks thus increases the concrete toughness.
2- The number of blows for first crack and at failure for mix CM_B is lower than mix OM_B. The differential of percentage increase in impact resistance for both mixes in group B is 25.4% that is around 573 number of blows. Incorporation of both MIRHA and fly ash in concrete matrix improved strength and reduced its porosity due to micropores structure modifications. Modifications of micropores structure in concrete are done by filling up the empty spaces in concrete pore structures through pozzolanic reactions. Incorporation of both MIRHA and fly ash in DSCC produces tougher and denser surface with higher surface durability compared to controlled DSCC, thus resulting in a higher impact resistance. Besides that, addition of both MIRHA and fly ash also improved fiber dispersion in concrete mix thus increases the bond between fiber and concrete matrix. Fly ash help fiber dispersion during mixing by having spherical shape, fly ash particles provide ball bearing effects and reduce internal friction in fresh concrete thus increase the flowability and compaction of the concrete [20]. Since fly ash and MIRHA provides the smallest particles of the matrix, it fills up the gaps resulting to an increased of fiber matrix adhesion.

Conclusion

Based on the results of this experiment the following conclusions can be made:

1- OM_B experienced higher abrasion resistance by 1.2% (49g) compared to CM_B when subjected to abrasion test at 500 revolutions. Incorporation of MIRHA and fly ash with steel fibers helped to improve the abrasion resistance of concrete.
2- Specimens from group A showed brittle behaviour and the ductility of specimens can be improved by the incorporation of steel fibers. Addition of MIRHA and fly ash by itself to the mixture in A improved the number of blows both at first crack and ultimate failure to 15.5% and 16.5%, respectively when compared to controlled specimens from the same group. Incorporation of MIRHA and fly ash with steel fibers as in mix OM_B improved the specimens' impact resistance by considerably more than inclusion of fiber alone (mix CM_B). The number of blows at first crack and ultimate failure rose to 3.2% and 9.7%, respectively. These results show that incorporation of MIRHA and fly ash as pozzolanic material replacing cement and steel fiber as crack arrestor improves the ability of concrete to absorb kinetic energy.

References

[1] A.E. Naaman, "High Performance Fiber Reinforced Cement Composites," Proceeding IABSE Symposium on Concrete Structures for the Future, Paris, France, pp. 371-376, September 1987.

[2] A.E. Naaman, and H.W. Reinhardt, "Characterization of High Performance Fiber Reinforced Cement Composites-HPFRCC," High Performance Fiber Reinforced Cement Composites 2, Proceedings of the Second International RILEM Workshop, France, pp. 1-24, 1996

[3] H. Okumura, and K. Ozawa, "Self-Compactable High Performance Concrete in Japan", ACI Special Publication No. 159, pp.31-44, 1996.

[4] R.M. Gutierrez, R, L.N. Diaz, and S. Delcasto, "Effect of the Pozzolans on the Performance of Fiber Reinforced Mortars", Cement and concrete composites, Vol.27, No.5, 2005.

[5] H. Li, M.H. Zhang, and J.P. Ou, "Abrasion Resistance of Concrete Containing Nano-Particles for Pavement", Wear Journal, Vol. 260, No.11, pp. 1262-1266, 2006.

[6] S. Swaddiwudhipong, and P.E.C. Seow, "Modelling of Steel Fiber Reinforced Concrete Under Multi-Axial Loads", Cement and Concrete Research, Vol.36, No. 7, pp. 1354-1361, 2006.

[7] N.L. Mohd Kamal, "Microwave Incinerated Rice Husk Ash (MIRHA) Concrete: A New Material In The Construction Industry", Masters Thesis, Universiti Teknologi PETRONAS, 2010.

[8] M.F. Nuruddin, N. Shafiq, and N.L. Mohd Kamal, "The Effect Of Types of Rice Husk Ash on The Porosity of Concrete", Joint Conferences APSEC – EACEF, 2009.

[9] K. Kesner, and S.L. Billington, "Investigation of Infill Panels Made From Engineered Cementatious Composites For Seismic Strengthening and Retrofit" Journal of Structural Engineering", Vol.131, No.11, pp. 1712-1720, 2005.

[10] P.W. Chen, and D.D.L. Chung, "Low-Drying-Shrinkage Concrete Containing Carbon Fibers", Composites Part B: Engineering, Vol. 27, No. 3, pp. 269-274, 1996.

[11] A.E. Naaman, "Engineered Steel Fibers With Optimal Properties for Reinforcement of Cement Composites", Journal of Advanced Concrete Technology, Vol. 1, No. 3, pp. 241-252, 2003.

[12] W.T. Lin, and D.C. Suen, "Experiment Study on The Abrasion and Impact Performance of Cement Based Composite Using Fiber and Silica Fume", Journal of the Chinese Institute of Engineers, 2008.

[13] M. Offenberg, "Proving Previous Concrete's Durability", ECON: The Concrete Producer, 2009.

[14] T. Rahmani, B. Kiani, M. Shekarchi, and A. Safari, "Statistical and Experimental Analysis on The Behaviour of Fiber Reinforced Concretes Subjected to Drop Weight Test", Construction and Building Materials, Vol. 37, pp. 360-369, 2012.

[15] Y.C. Wang, and M.G. Lee, "Ultra High Strength Steel Fiber Reinforced Concrete For Strengthening of RC Frames", Journal of Marine Science and Technology, Vol. 15, No. 3, pp. 210-218, 2007.

[16] ASTM C131-03, "Standard Test Method for Resistance to Degradation of Small-Size Coarse Aggregate by Abrasion and Impact in the Los Angeles Machine", 2003.

[17] ACI 544.2R-89, "Measurement of Properties of Fiber Reinforced Concrete", Reapproved 1999.

[18] M.R. Karim, M.F.M. Zain, M. Jamil, F.C. Lai, and M.N. Islam, "Strength Development of Mortar and Concrete Containing Fly Ash: A Review", International Journal of the Physical Sciences, Vol. 6, No. 17, pp. 4137-4153, 2011.

[19] N. Banthia, "Fiber Reinforced Concrete: Milestone in international Research and Development", Proceeding of FIBCON2012, Nagpur, India, pp. 48, February 13-14, 2012.

[20] S.F.U. Ahmed, M. Maalej, and P. Paramasivam, " Flexural responses of hybrid steel-polyethylene fiber reinforced cement composite containing high volume of fly ash, Construction building Material, No. 21, pp. 1088-1097, 2007

Applied Mechanics and Materials Vol. 567 (2014) pp 399-404
© (2014) Trans Tech Publications, Switzerland
doi:10.4028/www.scientific.net/AMM.567.399

Effective method of repairing RC beam using externally bonded steel plate

Md Ashraful Alam[1, a], Ali Sami Abdul jabbar[1,a] , Mohd Zamin Jumaat[2,c] and Kamal Nasharuddin Mustapha [1,d]

[1] Department of Civil Engineering, Universiti Tenaga Nasional, Malaysia

[2] Department of Civil Engineering, University of Malaya, Malaysia

[a]ashraful@unetin.edu.my, [b]alsami67@gmail.com,[c]zamin@um.edu.my, [d]kamal@uniten.edu.my

Keywords: steel plate, repair for shear, debonding, damaged beam, connectors.

Abstract. Repair of reinforced concrete beam with externally bonded steel plate or fibre reinforced polymer (FRP) laminate is becoming both environmentally and economically preferable rather than replacement of deficient beam. The well known advantages of external reinforcement over other methods include; low cost, ease of maintenance and the ability to strengthen part of the structure while it is still in use. The disadvantage of this method, however, is the premature debonding of the externally bonded strips which is brittle and undesired mode of failure. It is also known that debonding of the externally bonded steel plates prevents the reinforced concrete (RC) beam from reaching its full strengthening capacity. The aim of this study was to increase the scientific understanding on the behaviour of damaged reinforced concrete beams strengthened and/or retrofitted for shear using vertical steel plate fixed with adhesive and steel connectors to eliminate or delay debonding failure. Four reinforced concrete beam specimens were prepared to investigate the effects of connectors in preventing or delaying premature debonding of shear strips to restore the capacities of fully damaged beams. Three damaged beams have been repaired and strengthened with steel plates and loaded monotonically up to the maximum load capacities in order to define load–deflection relationship. It is concluded that the repairing of severely shear-damaged RC beams with steel plates by using steel and adhesive connectors can fully restore the original shear capacities of the beams.

Introduction

The use of externally bonded steel plates and fiber-reinforced polymer laminates are becoming a popular means of repair and rehabilitation to extend the service life of deficient structures. A large amount of the concrete infrastructure in the world is showing significant deterioration and distress. However, existing experimental research works show that the hypothetical high ultimate capacity of externally bonded strips used for strengthened RC beams often cannot be achieved because of the externally plate debonding or diagonal cracking [1]. The debonding of plates significantly reduces the strength enhancement provided by the externally bonded plate and can create brittle failures. As a result, elimination of premature debonding of shear strips is significant concern in terms of safety and effectiveness of the plate bonded strengthening systems.

Debonding failure of externally bonded strips of RC beams usually takes place in areas of high stress concentrations. The high concentrated interfacial stresses caused the cracks in the concrete subtrate which are usually associated with strips separation. The path of debonding propagation depends on properties of the substrate concrete, externally plated strip, and interface adhesive [2]. Steel plate debonding through the concrete substrate was identified as an important failure mode because it occurs at lighter load levels and the failure is very brittle. Although a lot of studies have been conducted on strengthening for flexural but till now there is no definitive guidance or solutions to eliminate the premature debonding of shear strips.

The most effective solution to prevent this early debonding was using mechanical anchorages. Defferent anchorage techniques had been used such as near surface mounted rods, mechanical fastening and bolts, to fix steel plates to the sides of reinforced concrete beams

for strengthening purposes [3]. Bolted steel plates was found to be as one of the most used solutions to prevent the debonding failure [4]. However, bolt anchorages may lead to initiate cracking in beams near the bolts holes or lead to a brittle rapture failure of the bonded strips or composed plates which is unwanted mode of failure. The aims of this study were to increase the scientific understanding on the behaviour of damaged reinforced concrete beams strengthened and/or retrofitted for shear by means of externally bonded steel plates with a new approach of adhesive and steel connectors. This experimental work concentrates on repairing and strengthening damaged beams by using vertical steel plates fixed with adhesive and steel connectors rather than the conventional anchoring systems i.e. bolts proposed by other researchers [5, 6 and 7].

Experimental program

In this research, four reinforced concrete beams with the dimensions of 150 mm x 300 mm x 2300 mm were prepared using 32 MPa concrete. The variations of beam specimens are shown in Table 1. At the first stage the beams had been damaged and loaded monotonically up to maximum load capacities in order to define the cracking load, the cracks width, the ultimate load capacity and the load deflection relationship. Then the damaged beams have been repaired and strengthened with the externally bonded steel plate for the second stage testing which aims to investigate the effectiveness of using the new proposed connectors to eliminate or delay the premature debonding failure of the steel plates to enhance the repair procedure or/and to increase the shear strengthening capacities.

Table 1. Dimensions of the shear connectors:

Beam ID.	Steel dimensions [mm]	Shear Connectors			
		Type of Connector.	Diameter of Connector. [mm]	Depth of Connector. [mm]	Number of Connectors
CB	-	-	-	-	-
RP1	2.7 X 40	Without connectors	-	-	-
RP2	2.7 X 40	Adhesive conn.	25	25	2
RP3	2.7 X 40	16 mm Steel conn.	25	25	2

The first beam RP1 repaired and strengthened with 40 mm width 2.7 mm thickness steel plates without connectors, the other two beams RP2, RP3 were repaired and strengthened with same steel plates but with two types of connectors, adhesive connector for RP2 and steel connectors for RP3 to investigate the efficiency of these connectors to eliminate the debonding failure and the enhance the shear capacities of the retrofitted beams. The details of connectors are shown in Table 1.

Materials and spacemen's preparation:

A concrete mix consisting of Portland Cement and maximum aggregate size of 20 mm in diameter had been used. Concrete strength was determined from standard cube samples taken for each mix. The concrete mix was designed for 30 MPa compreesive strength. The beam specimens were fabricated uisng 2-16 flexural reinforcement bars and 6 mm shear reinforcements with the spacing of 140 mm spacing. The shear reinforcements were used in 650 mm shear span of beam. The steel plates had been tested to establish their properties and obtained the yield strength and ultimate strength were 275 MPa and 420 MPa respectively. It was necessary to expouse the course aggregate at the bonding face of concrete surface to have strong bond behaviour between steel plate and concrete substrate of the damaged beams. To achieve this, a hand held grinder was used. The preparation was completed by blowing the specimen with compressed air to remove the remaining

excess particles before applying the adhesive to make sure that the bond surface is independent from all unwanted particles such as dust or lubricants and to get rid of other oxide layers. The steel plates also have been sandblasted previously to remove the oxide layer and roughen the surface for ensuring proper adhesion. Finally, acetone liquid was used to clean the surface of the steel plate and the interface bond area of concrete.

Repairing and strengthening the damaged beams

All the crack openings in the three beams (RP1, RP2 and RP3) were cleaned by water and acetone and then injected by Sika Dur-30 adhesive. These beams were strengthened with 2.7 mm x 40 mm width of steel plates at spacing of 110 mm. The plates of beam RP2 were bonded together with two 25 mm diameter adhesive connectors for each. This beam was repaired and strengthened by making double holes for each strip in the upper and lower part of the beam with clearance of 50 mm from the upper and lower edges. The last beam RP3 was repaired and strengthened by using the same steel plate's dimensions mentioned previously but with steel connectors, the same spacing of RP2 was used to drill the connector's holes then a steel bars of 25 mm were inserted in them. The details of connectors and the prepared surface of concrete beam are shown in Fig. 1.

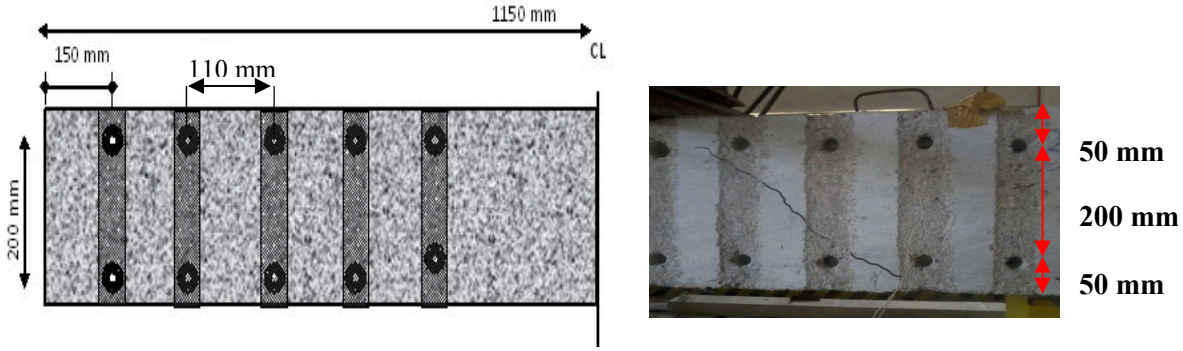


Fig. 1. Connector's holes 200 mm center to center and 50 mm clearness cover from upper and lower edges.

The epoxy adhesive Sika Dur-30 was mixed by a mechanical mixer as required by the manufacturing specification and then placed inside the connectors and the concrete surface by a steel knife. To simplify the repairing and fixing, the plates were attached to the beam with the beam lying on its side. Following thorough mixing, a 1–2 mm thick adhesive layer was applied to both the beam surface and the plate. The plate was gently pressed to remove the excess adhesive. The adhesive was allowed to cure for 7 days at room temperature, prior to testing. The details of strengthened beams are shown in Fig. 1.

Experimental results and discussions

The used shear strengthening and repair technique had enhanced the cracking and ultimate loads. As the load-carrying capacity increased, but the deflection capacity of the strengthened beam decreased for the same level of load. Considering the load carrying capacity, the repaired beams showed a sufficient strength enhancement comparing that of the corresponding post cracked reference beams. The level of enhancement had been affected by the variation of the type of connectors which were used to the externally bonded steel plates. Test results of retrofitted RC beams are summarized in Table 2. Beams RP2 and RP3 had shown 14% to 20% higher failure loads as compared to the control beam respectively. Beams RP2 and RP3 showed 10% and 12% higher failure loads as compared to beam RP1. Since connectors would delay the premature debonding, both beams had higher failure loads as compared to RP1.

Table 2. Test results of beam specimens

Beam ID.	Ultimate load before repairing [KN]	Ultimate load after repairing [KN]	Mode of failure before repairing	Mode of failure after repairing
CB	120	-	Shear failure	Shear failure
RP1	111	121	Shear failure	Debonding followed by shear failure
RP2	121	128.1	Shear failure	Cover peeling with spalling of concrete
RP3	122	148.3	Shear failure	Cover peeling with spalling of concrete

The experimental results showed that both steel and adhesive connectors delayed the premature debonding failure of steel plate as shown in Table 2 and Fig. 2 and 3 respectively. The strengthened beam RP1 without connectors failed by premature debonding followed by shear failure with lower load while beam RP2, RP3 failed by cover delamination with spalling of concrete. It was seen that the bottom connectors of strengthened beams failed due to spalling of concrete. Once the connectors failed the plate debonded. Since concrete spalled, connectors could not assist to prevent debonding of plates. However, results showed that the connectors played significant roles to delay debonding of plates.



Fig. 2. Failure mode of beam RP-2



Fig. 3 Failure mode of beam RP-3



Fig. 4 The shear crack inclination

The first cracks of RP2 and RP3 beams have been formed close to shear-span of the beams. Then, for RP1, those cracks have been extended to the neutral axis of beams with the effect of increasing load level and flexural cracks have been formed simultaneously. The crack, which is causing shear peeling of steel plate, has been formed at the end of bottom plate with the slope of approximately 33^{o}, as same as inclination of the original crack before repairing as shown in Fig. 4.

Fig. 5 shows the comparison of the load–deflection curves for test specimens with the control beam. The repaired beams have exhibited a moderate amount of reserve load-carrying capacity beyond the formation of cracking. The beams with steel connectors and without connectors had shown less dflections as compared to others. The deflections of repaired beams would depends on the degree of damage of the beams. Fig. 6 shows the plate strain behaviour of beam specimens. The plate strains of strengthened beams with connectors were found to be less as comapred to those of beam without connectors. Results also showed that the nature of plate strain curves for RP1, RP2 and RP3 had changed at around 90 kN, 115 kN and 120 kN loads respectively. It could be happened because of micro debonding of plates.

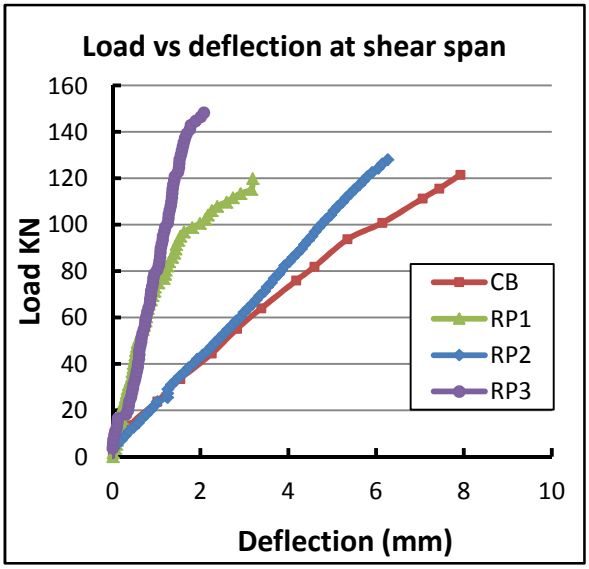


Fig. 5 The comparison of the load–deflection behaviour of beams

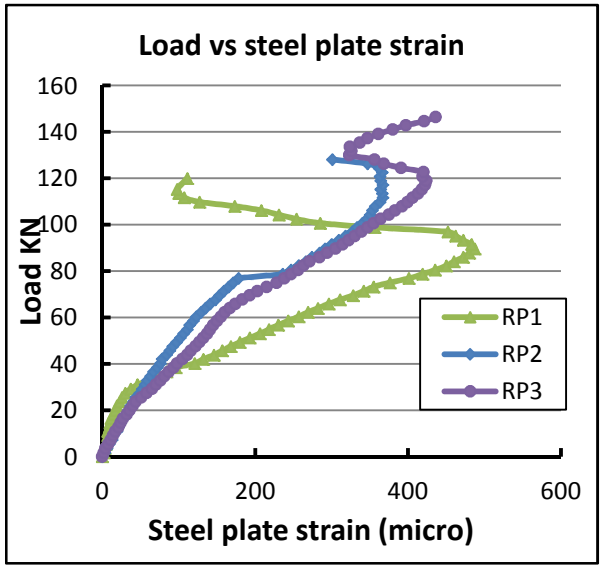


Fig. 6 The comparison of the load–plate strain behaviour of beams

Conclusions

The experimental study concluded that repairing of severely shear-damaged RC beams with (EB) steel plates by using steel and adhesive connectors can fully restore the original shear capacity of the beams. The capacities of repaired beams with steel and adhesive connectors were found to be 20% and 14% higher as compared to repaired beam without connectors respectively. The repaired damaged beams with connectors had shown higher shear capacities as compared with their original capacities. The connectors of repared damaged beams had failed due to spalling of concrete which caused the debonding of plate as well. The connectors delayed the debonding failure of steel plates.

Acknowledgement

The authors would like to express their gratitude to Ministry of Higher Education (MOHE) for providing the research grant under the grant number of 08012012ERGS to carry out this research. Thanks are also due to research management centre and Depratment of Civil Engineering, Universiti Tenaga Nasional for technical support.

Refrences:

[1] S. Altin, O. Anil and M. E. Kara, “Improving shear capacity of existing RC beams using external bonding of steel plates”, Engineering Structures, Vol. 27, 781–791, 2005.

[2] Oehlers, D. J., and Seracino, R. (2004). "Design of FRP and Steel Plated RC structures: Retrofitting Beams and Slabs for Strength, Stiffness and Ductility." Elsevier, UK.

[3] Hussain, Sharif, A., Basunbul, I. A., Baluch, M. H., and Al-Sulaimani, G.J., “Flexural Behavior of Precracked Concrete Beams Strengthened Externally by Steel Plates,” ACI Structural Journal, Vol. 92, No. 1, pp. 14-22, 1995.

[4] B. B. Adhikary and H. Mutsuyoshi, “Shear strengthening of reinforced concrete beams using various techniques”, Construction and Building Materials, Vol. 20, 366–373, 2006.
[5] R. A. Barnes and G. C. Mays, “Strengthening of reinforced concrete beams in shear by the use of externally bonded steel plates: Part 1 – Experimental programme”, Construction and Building Materials, Vol. 20, 396–402, 2006.
[6] Galal, K., and Mofidi, A. (2010). “Shear strengthening of RC T-beams using mechanically anchored unbonded dry carbon fiber sheets.” J. Perform. Constr. Facil., 24(1), 31–39.
[7] Garden, H. N., and Hollaway, L. C. (1998). “An experimental study of the influence of plate end anchorage of carbon fibre composite plates used to strengthen reinforced concrete beams.” Compos. Struct., 42(2), 175–188.

Applied Mechanics and Materials Vol. 567 (2014) pp 405-410
© (2014) Trans Tech Publications, Switzerland
doi:10.4028/www.scientific.net/AMM.567.405

Effects of Geopolymer Concrete Fly Ash Based on Alkali Silica Reaction (ASR)

Muhd.Fadhil Nuruddin[1,a] Siti Nooriza Abd. Razak[1,b]
[1]Universiti Teknologi PETRONAS, Bandar Seri Iskandar, 31750,Tronoh, Perak, Malaysia
[a]fadhilnuruddin@petronas.com.my, [b]ryuzakisi@gmail.com

Keywords: Alkali silica reaction, reactive silica, expansion.

Abstract. Alkali Silica Reaction (ASR) is a chemical reaction which affects both strength and durability of concrete. ASR occurs due to a chemical reaction between alkali oxides presents in the cement paste and reactive silica in aggregate. This reaction could lead to the volume expansion, cracking, loss of strength and potential failure of the concrete. This research aimed to investigate the potential alkali silica reactivity on geopolymer concrete. Specimens were prepared using Class F fly ash as binder while sodium hydroxide and sodium silicate as alkaline activators. ASTM C1260 was adopted to determine potential alkali silica reactivity by measuring the length change of mortar bar as well as the decrease in compressive strength test. Results show that fly ash based geopolymer concrete is less vulnerable to ASR as the expansion of mortar bar is below the threshold of ASTM standard limit which is 0.10% of expansion. In term of strength, the geopolymer concrete did not reduced instead it increased. From the results, it has indicated that both tests ensure that the durability of geopolymer concrete is excellent and can withstand a long life span.

Introduction

Over the past three decades, the search of alternative binder or cement replacement material in concrete technology had been done for the construction industry purposes. This research has been carried out in order to obtain good quality concrete materials that have the desired strength and durability. Even though Ordinary Portland Cement (OPC) possesses good strength, its durability performances have shown some concerns in some of the exposure conditions. For normal Portland cement, there is one problem that affects durability as well as strength which is Alkali Silica Reaction (ASR).

Alkali silica reaction (ASR) is a chemical reaction which occurs in concrete between alkali oxides in the cement and reactive silica in aggregate. This reaction could lead to volume expansion, cracking, loss of strength, and potential failure of the concrete structure. ASR commences the chemical reaction between alkaline solution hydroxyl ions and the aggregate at concrete interface. The hydroxyl ions react with the silanol groups (Si-OH) and the Si-O-Si (siloxane bonds). The second stage consists of the formation of expansion products. An internal pressure created within the cement matrix based on gel formation generated, hence triggering macroscopic expansion and degradation of the concrete matrix [1].

Three requirements must be met for ASR to occur which are 1) reactive forms of silica or silicate in the aggregate, 2) sufficient alkali (sodium or potassium) from cement and 3) sufficiently available moisture in the concrete. If these three requirements are not met, expansion due to ASR will not occur [2]. The reactive aggregates can be found in many common aggregate which contains reactive amorphous silica such as opal, tuff, cristobalite, quartz and etc. In alkaline environments, these forms of silica are susceptible to attack and greatly lead to the dissolution of the aggregate [3]. Low alkali cements used to prevent ASR often contain fly ash and granulated blast furnace slag (GGBFS). Class F and C fly ash pozzolan works effectively in mitigating or reducing expansive reaction resulting from ASR when 30% of Portland cement is replaced by mass. Silica fume were also found to beeffective in inhibiting ASR expansion.

In 1978, Joseph Davidovits, a French material scientist, had developed an amorphous three dimensional alumina-silicate materials, which he called ‘Geopolymer’. Geopolymer is a new kind of inorganic material as alternative binder for concrete which resulted from polymeric reaction of

alkaline liquid with silicon and aluminium in source materials [4]. The source materials can be of geological origin or by-product materials such as metakaolin, slag, fly ash and rice husk ash which is rich in silicon and aluminium content. Alkaline liquids used are sodium or potassium hydroxide in combination with sodium or potassium silicate. These materials are the most common used in the production of geopolymer concrete, where they also act as the primary binder to completely replace OPC [5, 6].

The present paper presents the results of research on expansion and compressive strength of the geopolymer mortar. Experimental studies show that geopolymer mortars which were activated with alkali solution expand less than 0.1% (ASTM threshold limit) after two weeks and ASR was not detected in these geopolymer mortar specimens.

Experimental Details

Material.

Fly Ash (FA)

The fly ash used is taken from Klang power station. This fly ash is categorized as Class F fly ash for having low calcium content. This fly ash was composed mostly of silica and a little alumina which makes it a good source material to make geopolymer concrete. The chemical composition of fly ash was given in Table 1.

Aggregate

Two types of aggregate such as natural sand and Arenite are used in the production of test specimens. Natural sand was chosen as control sand for non-reactive aggregate of ASR and Arenite as reactive aggregate for ASR which was obtained from Sarawak. The chemical composition of Arenite is given in Table 1.

Table 1: Chemical composition of fly ash and Arenite

Raw Material			
Fly Ash		*Arenite Rock*	
Components	*% by mass*	*Components*	*% by mass*
SiO_2	75.64	SiO_2	92.73
Al_2O_3	12.04	Al_2O_3	6.21
Fe_2O_3	3.36	Fe_2O_3	0.0388
CaO	2.35	K_2O	0.541
K_2O	2.02	TiO_2	0.050
TiO_2	1.20		

Alkaline Solution

To prepare the alkaline solution, sodium silicate solution and sodium hydroxide solutions (NaOH) are mixed together. In this project, the sodium silicate solution of grade A53 with SiO_2 to Na_2O ratio by mass value of 2.0 is used. For sodium hydroxide, the solution is prepared by dissolving NaOH pellets in potable water.

Mixture Proportion.

In this experimental study, a total of six mixtures are developed for each aggregate (natural sand and Arenite). The mixtures are varied in fly ash content ranging from 350 kg/m^3 to 450 kg/m^3 and sodium hydroxide concentration which is 8M and 12M. All the other materials are kept constant. Mixture proportion of the mortar specimens are shown in Table 3.

Table 3: Mixture proportionof mortar specimens for geopolymer

Mixture Code	Fly Ash (kg/m_3)	NaOH (kg/m_3)	NaSiO2 (kg/m_3)	Fine Agg (kg/m_3)	Water (kg/m_3)
8G1	**350**	41	103	700	35
8G2	**400**	41	103	700	40
8G3	**450**	41	103	700	45
12G1	**350**	41	103	700	35
12G2	**400**	41	103	700	40
12G3	**450**	41	103	700	45

Mixing, Casting and Curing.

The mixing process was carried out into two stages. First, the solid materials, such that Fly ash and aggregate (dry condition) are mixed together in a mortar mixer for about 1.5 minutes. After the dry mixing, a liquid mixture comprising of alkaline solution and extra water is added in the mixer and the wet mixing continued for another 3 minutes. The fresh mortar mix is then hand mixed for a further 2 to 3 minutes to ensure the mixture homogeneity. After that, the mortar mix is placed in 25 mm x 25 mm x 275 mm steel moulds as well as 50 mm x 50mm x 50mm steel moulds and was compacted using a tamping rod manually. Three specimens are cast for each test. After casting, the moulds were kept in the oven at a temperature of 60ºC for 24hrs . At the end of the oven curing period, the moulds are taken out from the oven and left undisturbed for about 15 mins in order to avoid a drastic change of environmental conditions. The specimens are then removed from the moulds and left to air dry at room temperature until the specified age of testing.

ASTM C1260 rapid mortar bar test and Compressive Strength test.

The rapid mortar bar test ASTM C1260 is conducted for every mortar specimen produced by measuring the length of the mortar bar specimen. For this test, all the specimens are cast in mortar bar mould of size 25mm x 25mm x 285mm. The specimens are immersed in 1M sodium hydroxide (NaOH) solution and placed in an oven at 80°C. The mortar bar specimens are tested at 3, 9, 14 and 21 days. According to ASTM C1260 expansion, 16 days after casting is classified as non-expansive if it is below 0.10%, potentially expansive if it is between 0.10% - 0.20% and expansive if it is over 0.20%. The 14^{th} day expansions are considered as the expansions for determining ASR resistance according to ASTM C1260 [9].Compressive strength test of similarly cured mortar cubes (50 x 50x 50 mm) is tested according to ASTM C109. An average of three measurements are used per each mixture for 7 days, 14 days and 28 days.

Results and Discussion.

The length change of mortar bars was measured after they have been conditioned in the sodium hydroxide solution at 80˚C as external alkali to assess the potential reactivity of an aggregate source or the ASR performance of combinations of SCMs and aggregates. Table 4 shows the results of expansion (%) of geopolymer mortar bar made with natural sand (NS) and Arenite (AR) for both 8M and 12M sodium hydroxide concentration. From this table, it also showed that as the concentration of the sodium hydroxide increases the expansion increases as well for both aggregate

The results of the mortar bar specimens tested as per ASTM C1260 for 8M and 12M NaOH concentration are shown in Figures 1 and 2.

Table 4: Expansion (%) of geopolymer mortar bars

Mixture Code	3 days	9 days	14 days	21 days	28 days	35 days	Mixture Code	3 days	9 days	14 days	21 days	28 days	35 days
8G1(350 NS)	0.053	0.070	0.078	0.083	0.084	0.084	12G1(350NS)	0.063	0.069	0.074	0.082	0.082	0.082
8G5(400NS)	0.066	0.069	0.076	0.085	0.085	0.085	12G5(400NS)	0.065	0.071	0.079	0.083	0.084	0.084
8G9(450NS)	0.070	0.074	0.087	0.089	0.089	0.089	12G9(450NS)	0.069	0.075	0.081	0.084	0.084	0.084
8G1(350AR)	0.054	0.067	0.070	0.075	0.076	0.076	12G1(350AR)	0.058	0.063	0.069	0.075	0.076	0.076
8G5(400AR)	0.069	0.072	0.076	0.079	0.08	0.079	12G5(400AR)	0.061	0.069	0.073	0.081	0.083	0.083
8G9(450AR)	0.070	0.075	0.082	0.086	0.088	0.088	12G9(450AR)	0.064	0.071	0.079	0.084	0.084	0.084

From Figure 1, the geopolymer specimens made with natural sand for 8M NaOH concentration showed expansion of 0.083%, 0.085% and 0.089% after 21 days as well as specimens made with Arenite of 8M NaOH concentration which showed expansion of 0.075%, 0.079% and 0.086% after 21 days when stored in sodium hydroxide solution. None of the geopolymer specimens exceeded the ASTM threshold as shown in the figure which is 0.10% of expansion. All the specimens appeared to be stable at the 35 day mark. The graph showed that the various content of fly ash used did not make any significant effects for this ASR expansion test even though the increment in fly ash content increase the expansion of mortar bar. These happened due to alkalis in geopolymer concrete are involved in the chemical reaction at the initial reaction and the remaining alkalis left will then attack the reactive aggregates. Alkalis in the fly ash and alkaline solution will be converted into cementitious binders and zeolyte crystals. Thus, with lack of calcium in the geopolymer matrix, the silica gel was found not expansive.

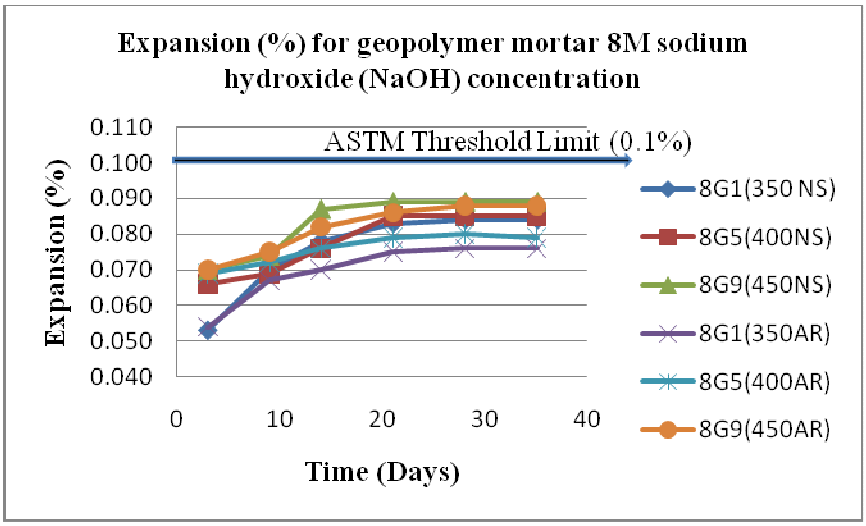


Fig.1: Expansion (%) for geopolymer mortar 8M sodium hydroxide (NaOH) concentration

From Figure 2, the geopolymer specimens made with natural sand for 12M NaOH concentration showed expansion of 0.082%, 0.083% and 0.084% after 21 days as well as specimens made with Arenite of 12M NaOH concentration which showed expansion of 0.075%, 0.081% and 0.084% after 21 days of being exposed to sodium hydroxide solution. None of the geopolymer specimens exceeded the ASTM threshold as shown in the figure which is 0.10% of expansion. All the specimens appeared to be stable at the 35 day mark The graph showed that the various content of fly ash used did not make any significant effect for this ASR expansion test even though the increment in fly ash content increases the expansion of mortar bar. These happened due to alkalis in geopolymer concrete are involved in the chemical reaction at the initial reaction and the remaining alkalis left will then attack the reactive aggregates. Alkalis in the fly ash and alkaline solution will be converted into cementitious binders and zeolyte crystals. Thus, with lack of calcium in the geopolymer matrix, the silica gel was found not expansive. Overall results showed that the geopolymer concrete made with 8M and 12M sodium hydroxide concentration does not exceed the

ASTM threshold limit and has excellent resistance against alkali silica reaction for both natural sand and arenite aggregate.

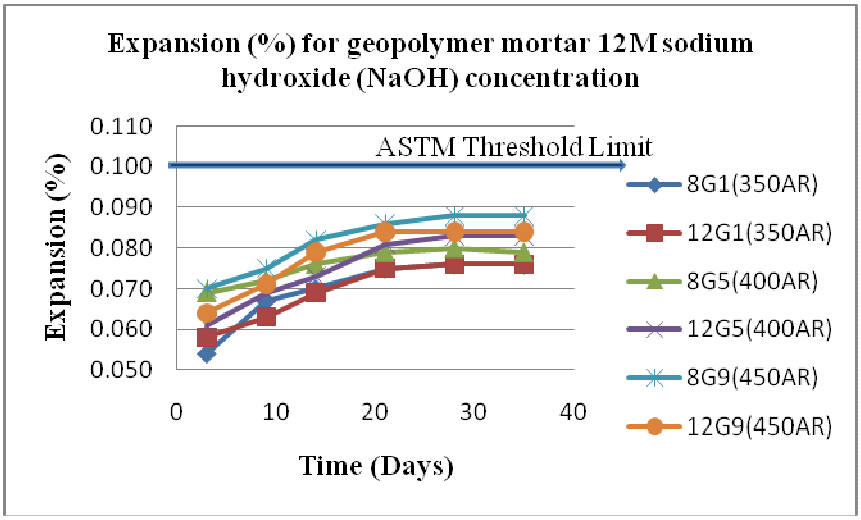


Fig.2: Expansion (%) for geopolymer mortar 12M sodium hydroxide (NaOH) concentration

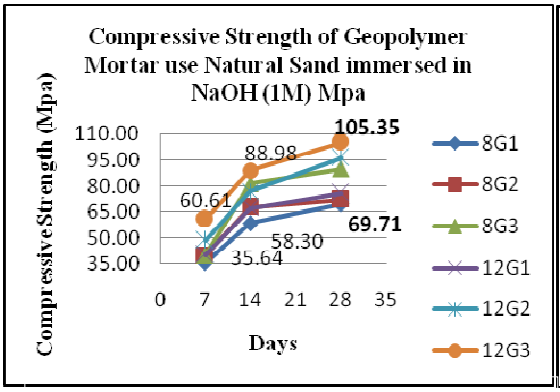


Fig.3: Strength of Geopolymer mortar NS immersed in NaOH (1M) in MPa

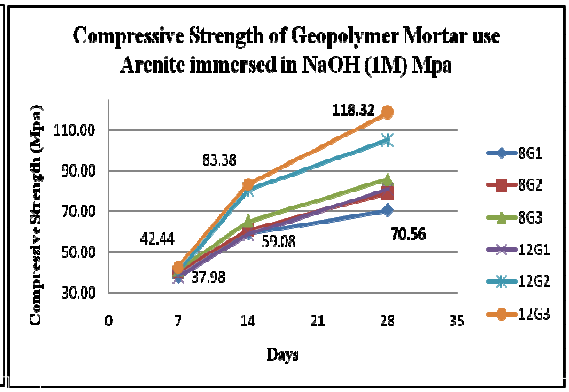


Fig.4: Strength of Geopolymer mortar AR immersed in NaOH (1M) in MPa

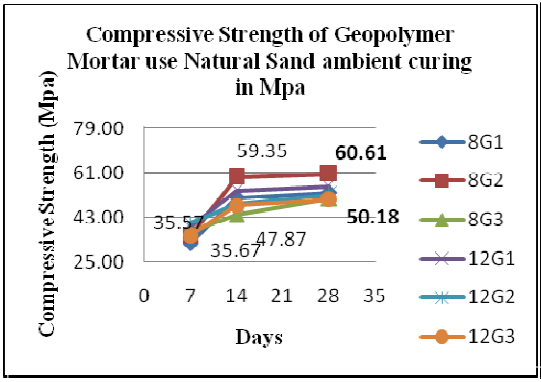


Fig.5: Strength of Geopolymer mortar NS at ambient curing in MPa

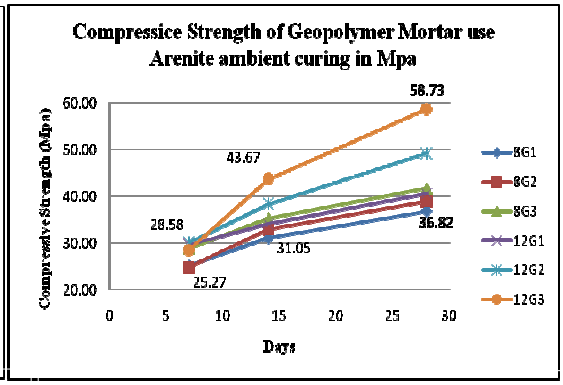


Fig.6: Strength of Geopolymer mortar AR at ambient curing in MPa

Figure 3 until Figure 6 showed results of compressive strengths for geopolymer mortar cube specimens in two conditions which are; immersed in NaOH (1M) solution and ambient curing. This is to check the reduction in the strength of geopolymer mortar if it is exposed to alkali silica reaction. This is because ASR can cause reduction in strength if the expansion of the specimens is greater that the threshold limit (0.10%). Figure 3 and Figure 4 showed the strength of specimens immersed in 1M NaOH solution while Figure 5 and Figure 6 showed the strength of specimens at ambient curing. It is apparent that the strength increased for specimens immersed in 1M NaOH

solution compared to specimens at ambient curing. Specimens which are immersed showed higher strength for both aggregates used. The strength recorded for specimens using natural sand was 105.35 MPa and specimens using Arenite was 118.32 MPa for specimens immersed in 1M NaOH. For specimens at ambient curing, the highest strength recorded was 60.61 MPa for specimens made with natural sand and 58.73 MPa for specimens using Arenite. The increased in strength for geopolymer mortar is due to the penetration of external NaOH solution in the geopolymer matrix which increases the rate of polymer formation and consequently, it develops more strength [1]. In the recent studies from Patil et.al showed that geopolymer specimen's compressive strength can reach up to higher than 100 MPa after 28 days being immersed in the NaOH solution [1]. The increment in strength is also related to the formation of Ca-based geopolymer network from the fly ash and alkaline solution.

An increase in strength of geopolymer specimens proves that geopolymer mortar effectively works in inhibiting the alkali silica reaction. These results showed that fly ash delays the reaction by mitigating the alkali transport and the formation of alkali silica gel. It also promotes the pozzolanic reaction of fly ash which resulted in higher strength.

Conclusion.

The results from the experiment showed that the ASR reactions due to the presence of reactive aggregate in fly ash based geopolymer concrete is non-expansive as the expansion did not exceed the threshold limit 0.10%. Although the increment in fly ash content and sodium hydroxide concentration do increase the expansion but it is still below the threshold limit of ASTM standard. It also showed that the strength of geopolymer specimens increased when exposed to 1M NaOH solution compared to specimens exposed at ambient curing. Hence, fly ash based geopolymer concrete is significantly less vulnerable to ASR.

References

[1] K.K. Patil, and E. Allouche, Impact of Alkali Silica Reaction on Fly Ash-Based Geopolymer Concrete, J. Mater. Civ. Eng. 25 (2013) 131–139.

[2] R. Helmut and D. Stark, Alkali silica reactivity mechanisms in: J.P.Skalny (Eds), Materials Science of Concrete 3, Westerville, American Ceramic Society, 1992, pp. 131-208.

[3] R.N. Swamy, The Alkali Silica Reaction in Concrete, New York, 1992

[4] J. Davidovits, Chemistry of Geopolymeric Systems: Terminology, Geopolymer International Conference, France, 1999

[5] F.A. Memon, M.F. Nuruddin, S. Demie, and N. Shafiq, Effect of Superplasticizer and Extra Water on Workability and Compressive Strength of Self-Compacting Geopolymer Concrete, R.J. Applied Sciences, Engineering and Technology. 4(2012) 407-414

[6] N. Lloyd and B. Rangan, Geopolymer Concrete with Fly Ash in: J. Zachar, P. Claisse, T. Naik, G. Ganjian (Eds), Second International Conference on Sustainable Construction Materials and Technologies, Italy, UMW Center for By-Products Utilization, 2010, pp. 1493-1501.

[7] B.V. Rangan, Low- Calcium Fly Ash Based Geopolymer Concrete, in: E.G. Nawy (Eds.), Concrete Construction Engineering Handbook, CRC Press, New York, 2008, pp. 26.1-26.20.

[8] ASTM C1260. Standard Test Method for Potential Reactivity of Aggregate (Mortar-Bar Method), ASTM International, 2008, pp. 677-681

Applied Mechanics and Materials Vol. 567 (2014) pp 411-416
© (2014) Trans Tech Publications, Switzerland
doi:10.4028/www.scientific.net/AMM.567.411

Flexural behaviour of concrete beams bonded with wire mesh-epoxy composite

Ismail M. I. Qeshta[1, a],PayamShafigh[2,b],Mohd Zamin Jumaat[3,c],
Aziz Ibrahim Abdulla [4,d],Ubagaram Johnson Alengaram[5,e],Zainah Ibrahim[6,f]

[1,2,3,5,6]Department of Civil Engineering, University of Malaya, 50603 Kuala Lumpur, Malaysia

[4]Civil Engineering Department, College of Engineering, Tikrit University, Iraq

[a]ismailqeshta@siswa.um.edu.my, [b] p_shafigh@yahoo.com, [c] zamin@um.edu.my,

[d] aziz_914@yahoo.com, [e] johnson@um.edu.my, [f]zainah@um.edu.my

Keywords: Flexural performance; concrete beam; welded wire mesh; composite

Abstract. This paper investigates the flexural performance of plain concrete beams bonded with wire mesh-epoxy composite. A total of four beam specimens were prepared and tested. Three specimens were bonded with same amount of wire mesh-epoxy composite with varying composite width and one plain concrete specimen was used as a control. The effect of wire mesh-epoxy composite on enhancing the flexural behaviour of concrete beams as well as the effect of different configurations of composite was studied. Test results showedthat the wire mesh-epoxy composite increased the flexural strength of concrete beams. The increase in energy absorption of bonded beams was remarkable. In addition, specimen with large composite width showed better behaviour with respect to energy absorption capability.

Introduction

Strengthening and retrofitting of reinforced concrete (RC) structures has become one of the most challenging tasks in the field of civil engineering. Bonding a steel plate tobeam tension face for the enhancement of its flexural capacity was first studied [1]. The main disadvantage of steel is its weak resistance to corrosion. Fibre reinforced polymer (FRP) has recently gained a large attention for strengthening of concrete structures [2]. However, the major drawback of beams strengthened with FRP is their significant decrease in ductility compared to the un-strengthened specimens [3,4]. Although the hybrid FRP composite was proposed to overcome the ductility problem in strengthened beams [5], the relatively high cost of different types of FRP materials and lack of reported information are still limiting its use. Moreover, the performance of RC beams can be enhanced by bonding ferrocement laminates to their soffit. The ferrocement laminate consists of wire mesh embedded in concrete mortar [6]. Because the flexural strength of mortar is considerably low, ferrocement laminate gains its flexural capacity mainly from the wire mesh. Basunbul et al. [7] tested RC beams bonded with ferrocement laminates. It was found that beams bonded with ferrocement exhibited increase in load carrying capacity, good cracking and ductility behaviour. In addition, Paramasivam et al. [8, 9] found that beams strengthened using ferrocement laminates showed enhancement in flexural stiffness and cracking behaviour. A steel wire mesh with relatively large wire diameter (3.2 mm) embedded in polymeric mortar was used by Xing et al. [10] for strengthening of RC beams. Test results showed that all strengthened beams had more stiffness and flexural capacity.

The flexural strength of plain concrete beam depicts its modulus of rupture value (f_r) which is very important for serviceability characteristics of concrete structures. A RC concrete beam starts to crack when the internal stresses reach the modulus of rupture value of concrete [11]. Therefore, it is important to improve the concrete modulus of rupture by adding external reinforcement. The main objective of this paper is to study the effectiveness of bonding welded wire mesh using the epoxy adhesive to plain concrete beamsoffit. Three plain concrete beam specimens bonded with different wire mesh-epoxy composite widths were prepared and tested. The amount of wire mesh

reinforcement and epoxy was kept the same for all specimens. It is important to study the effect of different widths on the performance of concrete beams. A study by Oh and Sim[12] showed that the beams with larger external bonded material width exhibit larger increase in load carrying capacity. In this paper, the effect of each configuration is studied with respect to ultimate load carrying capacity, deflection at failure, cracks propagation and energy absorption capability.

Experimental Program

Material properties

Concrete beam specimens with dimensions of 100 mm depth and width and 500 mm length were used in this study. The concrete 28 days cube compressive and flexural strengths were about 56 and 6.8 MPa, respectively. The 4×4 welded wire mesh with 0.64 mm wire diameter and 6.35 mm wire spacing was used. The wire mesh had an ultimate tensile strength, yield strength, elastic modulus and failure strain of 572 MPa, 440 MPa, 119.7 GPa and 1.5%, respectively. Fig. 1 shows a wire mesh roll used in this study. The 2-part epoxy resin usually used for bonding carbon fibre sheets was used. The tensile strength and elastic modulus of epoxy were 30 and 4500 MPa, respectively.

Specimen preparation and testing set-up

The composite material length in all specimens is 270 mm. The wire mesh layers were arranged such that all specimens are bonded with 32 wires. The testing matrix is shown in Table 1. It should be noted that the overall width of composite represents the width of wider layer in specimens A2 and A3. The wider layer had two more wires than the other wires in each specimen to maintain the same amount of reinforcement for all specimens. Before applying the wire mesh-epoxy composite, the concrete surface was abraded and followed by vacuum cleaning from the dust and other loose materials. A thin layer of epoxy was then applied by on the surface of concrete. The wire mesh layers were placed on concrete surface and the rest of epoxy was applied. An epoxy amount of 1.5 kg/m^2 per layer was calculated to ensure good bonding between the wire mesh and concrete surface. Fig. 2 shows the process of putting epoxy on wire mesh layers. Finally, the composite was covered by an acetate film and compressed by clamping in order to obtain smooth surface of the hardened composite. The composite was left for at least one week before testing the specimen. Fig. 3 shows the curing of composite after applying the acetate film and clamping. Four-point bending flexural test was performed for all specimens until failure at a span of 300 mm. The distance between the two point loads was 100 mm. The load was applied at a constant rate of 0.05 mm/min. Linear variable displacement transducer (LVDT) was used for measuring the mid-span deflection.

Table 1 .Testing matrix

Specimen	Bonded material overall width (mm)	Arrangement of wire mesh layers
Control	N/A	N/A
A1	95	Two layers (16 wires/layer)
A2	70	Two layers (10 wires/layer) + one layer (12 wires)
A3	45	Four layers (6 wires/layer) + one layer (8 wires)



Figures 1. Wire mesh roll



Figures. 2. Putting epoxy resin on wire mesh layers



Figures 3. Compressing of composite by clamping

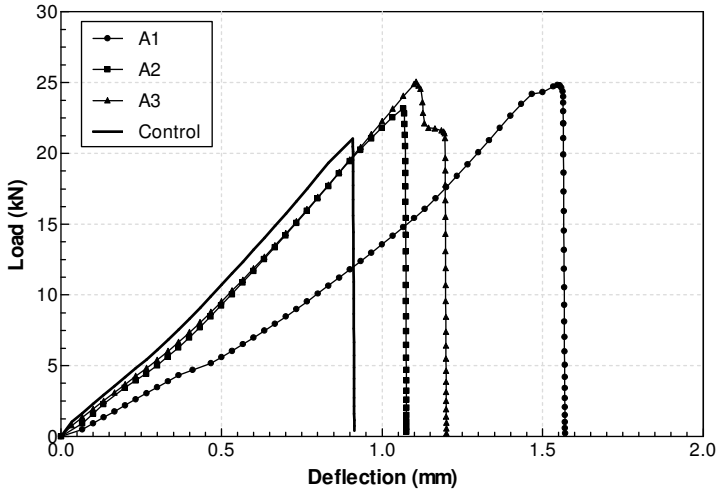
Results and Discussion

Flexural capacity and deflection at failure

The test results are summarized in Table 2. In addition, Fig. 4, presents the load-deflection relationships of all specimens. The load-deflection curves have two main stages. The first stage represents the linear increase in load with deflection. At this stage, the specimen maintains its full flexural rigidity. The second stage represents the reduction in slope and non-linear pattern of curve. This stage starts after the occurrence of first crack. All specimens bonded with wire mesh-epoxy composite exhibited increase in their load carrying capacity. This is due to the contribution of wire mesh-epoxy composite in the tension face of specimens. The plain concrete control specimen fails suddenly without showing any cracks. The failure took place immediately after the occurrence of first crack. Specimen A1 had increase in ultimate load of about 24.8 kN. A crack appeared in the specimen mid-span at load 24.0 kN. A small drop in the slope of load-deflection curve was observed at the occurrence of the first crack. The load then showed a small increase with the increase in deflection until the specimen failure. The increase in ultimate load value of specimen A2 was up to 23.2 kN. A crack was observed at load of 21.4 kN and propagated with the increase in load until the final failure. Fig. 6 shows the failure of specimen A2. Specimen A3 had a linear increase in load with deflection until 25.1 kN. A critical crack was observed at this load level. In addition, a large drop in load until 22.0 kN occurred. However, at this load level the specimen was able to carry load constantly until final failure. Fig. 7 shows the propagation of crack in specimen A3. In general, all bonded specimens had similar load carrying capacities. This is expected as the same amount of wire mesh was used for all specimens. In addition, it should be noted that the first crack load values of bonded specimens were higher than the failure load value of control specimen. The results reported in this study can be compared with the previous studies on the use of internal fibres for the improvement of concrete performance [13, 14]. The cracking behaviour of externally wire mesh-epoxy bonded concrete specimens is different from fibre-reinforced concrete. In the fibre-reinforced concrete, the first crack occurs at very early stage, whereas, in the wire mesh-epoxy bonded specimens the crack is delayed considerably. This is important for concrete under service load. The deflection at failure values of all specimens are shown in Table 2. All bonded specimens exhibited increase in deflection at failure compared to the plain concrete control specimen. Specimens A1, A2 and A3 had increase in deflection at failure of about 40%, 11% and 18% over the control specimen, respectively. Furthermore, the amount of epoxy used for bonding the wire mesh layers was found approximately 1.5 kg/m^2. The amount recommended by the manufacturer for bonding the carbon fibre using the same epoxy was in the range of 0.7~1.5 kg/m^2[15]. This shows the cost-effectiveness of using wire mesh-epoxy composite for enhancing the performance of concrete structures when considering the high cost of FRP material compared to wire mesh.

Table 2. Test results

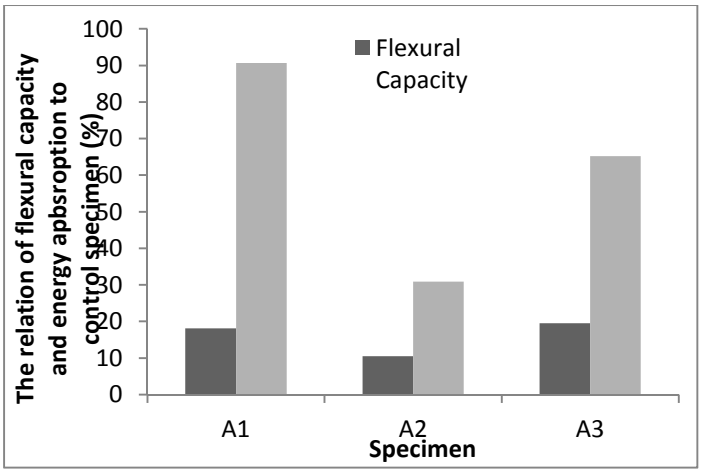
Specimen	Ultimate load (kN)	Deflection at failure (mm)	Energy absorption (N.m)
Control	21.0	0.91	8.85
A1	24.8	1.57	16.87
A2	23.2	1.08	11.58
A3	25.1	1.2	14.62



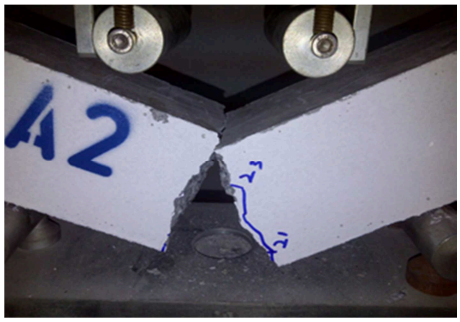
Figures 4. Load-deflection relationship of specimens

Energy absorption

Table 2, presents the energy absorption values of all specimens. The energy absorption value is obtained by calculating the area under the load-deflection curve. The plain concrete specimen had a sudden failure when the load exceeded its ultimate strength. The plain concrete normally has a number of micro cracks. These micro cracks propagate rapidly with the increasing stresses causing the fracture of specimen. Specimens A1, A2 and A3 could carry higher loads than the plain concrete specimen and deflected at higher values. Observations of specimens after failure revealed that the failure occurred after the rupture of wire mesh-epoxy composite. The percentage increase of energy absorption and flexural capacity of bonded specimens over the control specimen is shown in Fig. 5, Specimens with different wire mesh-epoxy composite widths had different amounts of energy absorption. Specimens A1 and A3 gained energy absorption of 91% and 65%, respectively, whereas, specimen A2 gained only 31% over the plain concrete specimen. From the results, it can be concluded that the specimen with the large wire mesh-epoxy composite width had the highest improvement in energy absorption. This is due to the fact that the wider composite had more contact area with the concrete surface. This provides more restraint to the micro cracks in the tension face of specimen and consequently prevents the rapid propagation of micro cracks which cause the specimen failure.In addition, it can be seen from Fig. 5, that the improvement in energy absorption capabilities of bonded specimens is large compared to the flexural capacity. The increase in flexural capacity and energy absorption of specimen A1, for example, was about 18% and 91% over the control specimen, respectively. This finding is similar to the reported studies for fibre-reinforced concrete [16] where the enhancement in energy absorption is much higher than ultimate load.



Figures 5. Percentage increase in flexural capacity and energy absorption of specimens



Figures 6. Failure of specimen A2



Figures 7. Propagation of crack in specimen A3 during test

Conclusions

This paper investigated the flexural performance of plain concrete beam specimens bonded with the same amount of wire mesh-epoxy in different configurations. The results showed that the use of wire mesh-epoxy composite is an effective method for enhancing the flexural performance of concrete beams. The enhancement in flexural capacity was up to 20% over the plain concrete specimens. The use of wire mesh-epoxy composite with larger width was found to improve the energy absorption capability better than smaller widths with an increase of up to 91% over the plain concrete specimen.

Acknowledgement

This research was funded by the University of Malaya, High Impact Research Grant (HIRG) No. UM.C/625/1/HIR/MOHE/ENG/36 (16001-00-D000036) -"Strengthening Structural Elements for Load and Fatigue".

References

[1] Swamy, R., R. Jones, and J. Bloxham, Structural behaviour of reinforced concrete beams strengthened by epoxy-bonded steel plates. Structural Engineer. Part A, 1987. **65**: p. 59-68.

[2] Bakis, C., et al., Fiber-reinforced polymer composites for construction-state-of-the-art review. Journal of Composites for Construction, 2002. **6**(2): p. 73-87.

[3] Grace, N.F., et al., Strengthening reinforced concrete beams using fiber reinforced polymer (FRP) laminates. ACI Structural Journal, 1999. **96**: p. 865-874.

[4] Ritchie, P.A., et al., External reinforcement of concrete beams using fiber reinforced plastics. ACI Structural Journal, 1991. **88**(4).

[5] Attari, N., S. Amziane, and M. Chemrouk, Flexural strengthening of concrete beams using CFRP, GFRP and hybrid FRP sheets. Construction and Building Materials, 2012. **37**: p. 746-757.

[6] 549, A.C., Guide for the Design, Construction, and Repair of Ferrocement. ACI Structural Journal, 1988. **85**(3): p. 325-351.
[7] Basunbul, I., et al., Repaired reinforced concrete beams. ACI Materials Journal, 1990. **87**(4).
[8] Paramasivam, P., C. Lim, and K. Ong, Strengthening of RC beams with ferrocement laminates. Cement and Concrete Composites, 1998. **20**(1): p. 53-65.
[9] Paramasivam, P., K. Ong, and C. Lim, Ferrocement laminates for strengthening RC T-beams. Cement and Concrete Composites, 1994. **16**(2): p. 143-152.
[10] Xing, G., et al., Experimental investigation of reinforced concrete T-beams strengthened with steel wire mesh embedded in polymer mortar overlay. Advances in Structural Engineering, 2010. **13**(1): p. 69-80.
[11] Nawy, E.G., Reinforced Concrete: A Fundamental Approach. 6th ed. 2005, New Jersey, United States: Prentice Hall.
[12] Oh, H.-S. and J. Sim, Interface debonding failure in beams strengthened with externally bonded GFRP. Composite Interfaces, 2004. **11**(1): p. 25-42.
[13] Padron, I. and R.F. Zollo, Effect of synthetic fibers on volume stability and cracking of portland cement concrete and mortar. ACI Materials Journal, 1990. **87**(4).
[14] Soulioti, D., et al., Effects of Fibre Geometry and Volume Fraction on the Flexural Behaviour of Steel-Fibre Reinforced Concrete. Strain, 2011. **47**(s1): p. e535-e541.
[15] Sikadur®-330, product data sheet, 2-part epoxy impregnation resin.<http://mys.sika.com/en/solutions_products-old/02/02a013/02a013sa06/02a013sa06100/02a013sa06105.html> [Edition 2012-05_1].
[16] Hassanpour, M., P. Shafigh, and H.B. Mahmud, Lightweight aggregate concrete fiber reinforcement–A review. Construction and Building Materials, 2012. **37**: p. 452-461.

Applied Mechanics and Materials Vol. 567 (2014) pp 417-421
© (2014) Trans Tech Publications, Switzerland
doi:10.4028/www.scientific.net/AMM.567.417

Interrelationship Analysis of Geopolymer Components Using Pearson Correlation Technique

Andri Kusbiantoro[1,a], Norbaizurah Rahman[1,b]

and Noor Fifinatasha Shahedan[1,c]

[1]Faculty of Civil Engineering and Earth Resources

University Malaysia Pahang, Tun Razak Highway, 26300 Kuantan, Pahang, MALAYSIA.

[a]andri@ump.edu.my,[b]norbaizurahrahman@yahoo.com,[c]noorfifinatasha@yahoo.com

Keywords: geopolymer; fly ash; setting time; strength; pearson correlation

Abstract. Performance of geopolymer based specimens is significantly affected by internal and external aspects. Curing temperature and air humidity are among the prominent external factors that contribute to the alteration of geopolymer properties. Nevertheless, internal component of geopolymer binder also carries essential effect to the hardened geopolymer binder produced. In this research, the study was concentrated on the elemental composition of source material components and their interrelation to the performance of geopolymer binder produced. Different types of fly ash were used as the source material in this research. Low calcium (class-F) fly ash was combined with high calcium (class-C) fly ash to determine the elemental composition effect, particularly SiO_2, Al_2O_3, and CaO to the geopolymer properties. Analysis using SYSTAT statistical software indicated the importance of oxide composition of source material to the geopolymer specimens produced. Initial setting time of geopolymer paste was also possibly important to the compressive strength of geopolymer specimens produced. Nevertheless, final setting time indicated less importance to the compressive strength development of geopolymer binder.

Introduction

Geopolymer binder is a remarkable material that substantially differs from Portland cement based binder, particularly in the material composition and particles reaction. Geopolymer binder is produced by reacting alumina-silica rich material (i.e. fly ash, kaolin, etc.) with alkaline solutions (sodium/potassium hydroxide, sodium/potassium silicate). Since geopolymer binder's framework is composed of various aluminium and silicon based bonds, different characteristic might occur in each geopolymer system could disturb the polymerization rate, generally class-F fly ash is preferred over class-C due to its low calcium content [1]. However the latest researches have revealed that development of geopolymer gels could possibly be assisted with the presence of Ca precursors, particularly in low temperature curing [2-4]. Fly ash with high calcium content was found to have more crystalline particles ranging from 25% to 45% of its total weight [5]. It was also observed that glassy phases in class C fly ash was usually more reactive due to the presence of high calcium content that makes the surface of glassy particles are highly strained [5]. In addition, when calcium reacted with aluminate and silicate monomers that dissolved from the source material, calcium silicate hydrates (C-S-H) and calcium aluminates (C-A-S-H) was formed. Therefore, geopolymerization process was enhanced and contributes to the mechanical strength [6].

Fresh geopolymer binder generally possesses higher fluidity yet shorter setting time than fresh Portland cement binder. Nevertheless, scarce amount of calcium in the source material is also affecting the polycondensation rate of aluminosilicate precursors, which consequently the performance of hardened geopolymer concrete as well. Hardened geopolymer concrete performance featured several characteristic based on the conducted test, i.e. compressive strength, flexural

strength, modulus of elasticity, porosity etc. Therefore Pearson correlation coefficient was adopted to provide an analysis in the correlation level between each geopolymer concrete feature with precursor. Correlation coefficient is mostly used in biomedical research to observe the strength of association between two variables, e.g. measurement of stress and personality characteristic by psychiatry, association between total serum cholesterol value and triglycerides by physician [7]. In the area of material characterisation, correlation coefficient is beneficial to support the development of causal models for further prediction of concrete quality [8]. The SYSTAT package of statistical programs was used to analyse the available data and measure the interrelationships between pairs of variables.

Methodology

Materials. Fly ashes were collected from two different sources, which represented Class-F and Class-C type of fly ash in this research. Class-C fly ash was obtained from Manjung Coal-Based Thermal Power Plant, Malaysia while Class-F fly ash was purchased from China. Chemical oxide content of fly ash is described in Table 1. As observed in Table 1, Class-F fly ash was dominantly comprised of SiO_2 (54.14%) and Al_2O_3 (37.82) oxides with every other minor oxide had its content not more than 3%. It is in contrast to class-C fly ash where SiO_2 (36.37%) and Al_2O_3 (17.57) oxides share their dominance with Fe_2O_3 (12.43%) and CaO (10.58%) content.

Table 1-Chemical oxide composition of class-C and class-F fly ash

Fly Ash	Oxide (%)									
	SiO_2	Al_2O_3	Fe_2O_3	CaO	MgO	K_2O	SO_3	TiO_2	Na_2O	LOI
Class-C fly ash	36.37	17.57	12.43	10.58	3.05	1.77	1.39	0.88	0.63	1.19
Class-F fly ash	54.16	37.82	2.92	2.4	0.87	0.97	0.41	1.28	0.15	1.69

These fly ashes were activated with a combination of sodium hydroxide and sodium silicate solution to produce binder paste specimens for subsequent characteristic tests. Sodium hydroxide solution used was 8 M solution, which was prepared by diluting 297 gram NaOH pellets (99% purities) with 703 gram water. Sodium silicate was a Na_2SiO_3 solution with Ms = 2.0 (Na_2O: 14.73%; SiO_2: 29.75%, and H_2O: 55.52%). These solutions were prepared 1 hour prior to the mixing process to prevent the excessive heat generated by sodium hydroxide dissolution from affecting the measurement of fresh geopolymer paste properties.

Specimen preparations. Geopolymer mixtures in this research were designed to accommodate the inclusion of class-F fly ash into class-C fly ash. Table 2 shows the detail of mix proportions used in this research. Since sole usage of class-F fly ash in this research produced unsuitable specimen for mechanical properties test, particularly under low temperature curing condition, the inclusion of class-F fly ash was designed with 10%, 20%, 30%, 40% and 50% replacement percentage of class-C fly ash. The amounts of NaOH solution and Na_2SiO_3 solution were kept constant in all mixtures at 41 kg/m^3 and 103 kg/m^3 respectively. In rheological properties analysis, fresh geopolymer paste was tested for its Vicat setting time and flow table workability. While for casting process, fresh geopolymer paste was poured into 50 mm steel cube moulds and kept in ambient temperature for 24 hours. After 24 hours, the hardened specimens were demoulded and kept in a room temperature ($\pm$ 30°C) until the testing days. Hardened geopolymer specimens were tested for it compressive strength at 1, 7, and 28 days. While elemental analysis on hardened geopolymer paste was extracted at 1 and 28 days using Hitachi S3400 SEM & Horiba EMAX EDX. Volume of permeable voids of hardened specimens was also measured after 28 days using saturation method as described in ASTM C 642. Results generated from the experiment were then analysed using SYSTAT statistical software to obtain proper interrelationship between source material components and geopolymer performances.

Table 2-Detail of mixture proportions

Mixture code	Class-C fly ash, (kg/m^3)	Class-F fly ash, (kg/m^3)	SiO_2/Al_2O_3 ratio	CaO (wt%)
Control	350	0	2.07	10.58
G1	315	35	1.95	9.76
G2	280	70	1.85	8.94
G3	245	105	1.76	8.13
G4	210	140	1.69	7.31
G5	175	175	1.63	6.49

Result and Discussion

Setting time and workability. Fig. 1(a) shows the result of Vicat setting Time test that consist of initial and final setting time combined with flow table workability. Initial setting time is the point where Vicat needle reach the penetration depth of 25 mm, while final setting time was recorded after no visible penetrations of Vicat needle were observed at the specimen. As presented in Fig.1(a), the inclusion of class-F fly ash into class-C fly ash extended the initial setting time up to 15 minutes longer and final setting time up to 405 minutes longer. Reduction of CaO content in the mixture and additional SiO_2 and Al_2O_3 from class-F fly ash has significantly affected the dissolution and polycondensation of geopolymer precursors. In addition, when the auxiliary of Si and Al source material such as class-F fly ash are necessary in sustaining VI-coordinated aluminium to meet effective SiO_2/Al_2O_3 ratio requirement and consequently gives better workability [9].

Compressive strength and porosity. Fig. 1(b) shows the correlation between compressive strength and porosity of geopolymer binder. It is interesting to note that the extended setting time provided by class-F fly ash was not followed by the enhancement in geopolymer framework performance.

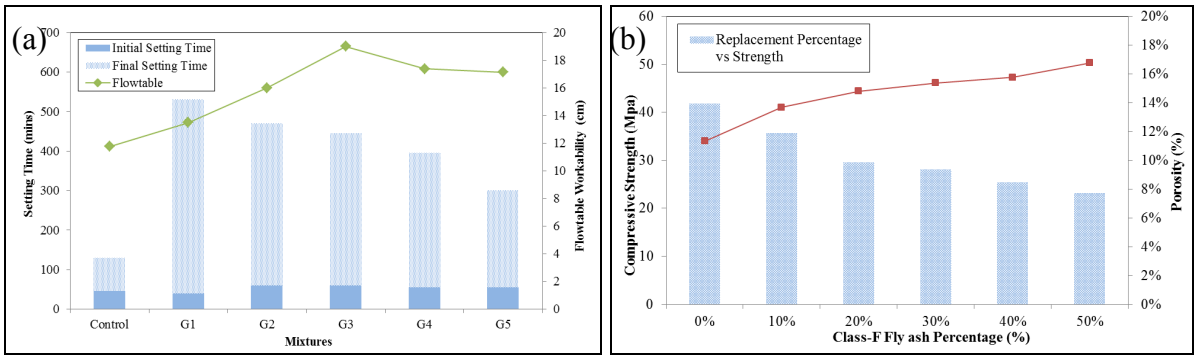


Figure 1-(a) Setting time and workability of fresh geopolymer paste; (b) Correlation between replacement percentage, compressive strength and porosity

Replacement of class-C fly ash with class-F has presented a strength degradation trend with an average of 10.99% for every 10% of class-F fly ash replacement. The increasing amount of permeable voids volume was also directly proportional to the increasing class-F fly ash percentage. The origin of porous framework was possibly generated by incomplete polycondensation of geopolymer precursors into solid geopolymer gels, The porous nature of cenosphere and plerosphere type of fly ash particle could also contribute to the increasing value of permeable voids in geopolymer specimen [10].

Energy dispersion x-ray analysis. Energy dispersive x-ray (EDX) analysis was conducted to obtain the elemental composition of ambient-cured geopolymer paste at one and 28 day of specimen age. Due to equipment limitation, analysis was conducted solely on control, G1, and G5 specimens. These specimens were preferred for the reason that analyses on setting time, compressive strength and porosity results have displayed consistent movements along with the replacement percentage of

source material, hence three data points between control and treated specimens would provide sufficient evidences for this analysis. As presented in Table 3, the escalating movement of Si/Al ratio from day 1 to 28 demonstrates continuous dissolution of Al and Si species from fly ash particles. This escalating ratio also occurs along with the increasing percentage of class-F fly ash used in the source material.

Table 3-Elemental composition ratio of geopolymer specimens (wt%)

Ratio	1-day			28-day		
	Control	G1	G5	Control	G1	G5
Si/Al	1.76	2.68	3.39	3.17	3.00	3.02
Ca/Si	0.21	0.29	0.22	0.32	0.70	0.20
Na/Si	0.72	1.33	1.73	1.24	1.46	1.15

Pearson correlation analysis. Table 4 shows Pearson Correlation matrix for fresh and hardened geopolymer properties in this research. Analysis on the result of fresh properties test (setting time, workability) and hardened properties test (density, compressive strength, porosity and elemental composition) exhibit various correlations that justify the effect of polymerization of geopolymer precursors to the geopolymer properties.

Table 4-Pearson correlation matrix of geopolymer properties

	Initial setting	Final setting	Workability	Density	Comp. Strength	Porosity
Initial setting	1	-	-	-	-	-
Final setting	0.113	1	-	-	-	-
Workability	0.831	0.373	1	-	-	-
Density	-0.536	0.020	-0.705	1	-	-
Comp. Strength	-0.482	-0.209	-0.581	0.856	1	-
Porosity	0.661	0.396	0.88	-0.821	-0.864	1

Table 5-Pearson correlation coefficient of geopolymer matrix elemental compositions to compressive strength

Coefficient	Independent Variable								
	C	O	Na	Mg	Al	Si	S	Ca	Fe
Day-1	0.986	-0.711	-0.957	0.523	0.858	-0.994	-0.906	-0.507	0.905
Day-28	0.486	-0.794	-0.831	0.932	-0.699	-0.602	0.027	0.454	0.387

Table 5 shows the Pearson correlation coefficient with compressive strength functioned as dependent variable, while elemental components acted as the independent variable. Based on the correlation coefficient data in Table 4 and 5, classification of these values is given as follows:

- Potentially important: Correlation coefficient between -1.0 and -0.8 or +0.8 and +1.0
- Possibly important: Correlation coefficient between -0.8 and -0.4 or +0.4 and +0.8
- Not important: Correlation coefficient between -0.4 and +0.4

It is apparent in here that role of carbon (C) in the early age development is potentially important to geopolymer system, since it is significantly affecting source material reactivity. It is followed by three elemental backbones of geopolymer system, which are Si, Al, and Na. An interesting feature of setting time is also observed in Table 4. Initial setting time displays a possibly important correlation with compressive strength performance, yet it shows higher coefficient to the porosity and workability characteristic. Meanwhile, final setting time indicates a non-important correlation to the geopolymer strength, porosity and workability. It appears that simultaneous dissolution and polycondensation process was rapidly occurred within initial setting time period, hence formation of geopolymer framework was significantly affected by the amount of reaction during phase.

Conclusions

Based on the result analysis, oxide compositions are potentially important to the initial setting time and workability of geopolymer paste. Rapid construction of geopolymer frameworks from dissolution and polycondensation of fly ash particles contributed to the enhancement of hardened geopolymer properties. However, geopolymer strength is possibly affected by initial setting time, yet less affected by final setting time of geopolymer paste.

Acknowledgement

The authors would like to thank Universiti Malaysia Pahang for the financial and instrument supports received under research grant RDU 120365 and GRS 120380.

References

[1] Gourley JT., Geopolymers: Opportunities for Environmentally Friendly Construction Materials, Material 2003 Conference: Adaptive Materials for A Modern Society.

[2] Temuujin J., Van Riessen A., Williams R., Influence of Calcium Compounds on The Mechanical Properties of Fly Ash Geopolymer Pastes, Journal of Hazardous Material, 167 (2009) 82-88.

[3] Puligilla S., Mondal P., Role of Slag in Microstructural Development and Hardening of Fly Ash-Slag Geopolymer, Cement and Concrete Research, 43 (2013) 70-80.

[4] Garcia-Lodeiro I., Paloma A., Fernandez-Jimenez A., Macphee DE., Compatibility Studies Between N-A-S-H and C-A-S-H Gels, Study in The Ternary Diagram Na2O-CaO-Al2O3-SiO2-H2O, Cement and Concrete Research, 41 (2011) 923-931.

[5] McCarthy GJ., Johansen DM., Steinwand SJ., X-Ray Diffration Analysis of Fly Ash, In:Advances in X-Ray Analysis, New York:Plenum Press, 31 (1988).

[6] Ivan Diaz-Loya E., Erez N. Allouche, Saiprasad Vaidya., Mechanical Properties of Fly-Ash-Based Geopolymer Concrete, ACI Material Journal, 108 (2011) 300-306.

[7] Chernick, MR., Friis, RH., Introductory Biostatistics for the Health Sciences, Wiley-Interscience (2003)

[8] Rose, K., Hope, BB., Ip, AKC., Strength and Durability of Concrete, Research and Development Branch, Ontario Ministry of Transportation (1988)

[9] Wu H.C, Sun.P, Effect of Mixture Compositions on Workability and Strength of Fly Ash-Based Inorganic Polymer Mortar, ACI Materials Journal, 107 (2010) 554-561.

[10] Kusbiantoro A., Nuruddin M.F, Shafiq N., Qazi S., The Effect of Microwave Incinerated Rice Husk Ash on The Compressive and Bond Strength of Fly Ash Based Geopolymer Concrete, Construction and Building Materials, 36 (2012) 695-703.

Applied Mechanics and Materials Vol. 567 (2014) pp 422-427
© (2014) Trans Tech Publications, Switzerland
doi:10.4028/www.scientific.net/AMM.567.422

Low Energy Compaction of Aggregate Packing Mechanism

Yasreen G. Suliman[1,a], Madzlan B. Napiah[2, b], Ibrahim Kamaruddin[3, c] and Johnson Olufemi A[4, d]

[1, 2, 3, 4] Civil Engineering Department, Universiti Teknologi PETRONAS, Tronoh, Perak, Malaysia

[a] neersay@yahoo.com, [b] madzlan_napiah@petronas.com.my, [c] ibrakam@petronas.com.my, [d] femfunk2005@yahoo.com

Keywords: Aggregate packing, Marshall Test, compaction energy, engineering properties, dynamic creep.

Abstract. Aggregate packing mechanism and its properties are always significant in the compaction, density and consequential strength and resistance of the bituminous mixture. Realizing that aggregate interlocking contributes to the strength, the packing of aggregate would increase the force of intact between aggregates. This work is focused on improving the compaction energy, engineering properties and rutting resistance of bituminous mixture by using the aggregate packing concept. After obtaining the optimum proportions for developed mixture via packing test, hot-mix asphalt samples are prepared and compacted with 50 and 75 blows, while well graded hot-mix asphalt samples are compacted with 75 blows. The Marshall Test result showed that developed mixture at lower compaction energy meets all the requirements of asphaltic concrete for heavy traffic and also exhibit higher density, stability, and lower air voids and voids in mineral aggregate compared to the well graded mixture. Developed mixture also demonstrated higher mixture stiffness and lower rut depth compared to the well graded one. This is due to the optimal distribution of the various aggregates sizes of developed mixture, which gives the interlocking necessary and stone to stone contact to improve the mixture density, stiffness and rutting resistance.

Introduction

In recognition of the importance of aggregate properties on pavement performance, the aggregate directly affects the mixture properties. The aggregate performance is characterized as a stone-on-stone skeleton; also known as interlocking. In previous study, the coarse aggregate contact of bituminous mix gradation dominated the interlocking performance of the pavement; therefore, a strong coarse aggregate skeleton is vital in bituminous mix. It is impossible, however, that each of the mix design would have the same resistance and performance since there is inconsistency between the aggregate types and its interlocking performances. The aggregate packing gradation comes up front as a way to ensure the consistency of the performance of the mix design. The idea is that it will reduce the inconsistency between aggregates since the gradation of coarse aggregate will be done by selection of percentage of different sizes of coarse aggregate which range from 5mm.

The packing density measured represents how well the aggregate would be packed together. It is impracticable to obtain a perfectly packed aggregate; since the finest aggregate size cannot be too fine and the largest aggregate size cannot be too large (there is a practical limit to the size range of the aggregate). Some voids will therefore remain unfilled. In addition to that, the shape of the aggregate particles has a limiting effect on the aggregate packing. What's more, the surface roughness of the aggregate particles would limit the effectiveness of the mixing and compacting process. High surface roughness means large inter-particle frictional forces which affect the mixing and compacting process. It will reduce the packing density of the aggregate. The wall effect and loose effect also contribute in reducing the effectiveness of process in approaching maximum packing density as shown in Figure 1.

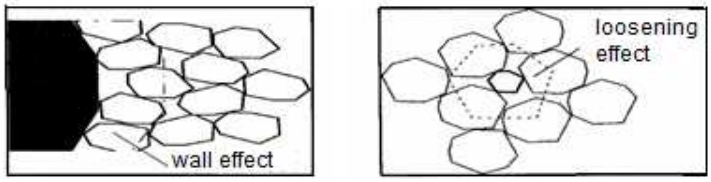


Figure 1: Condition which affects compacting and mixing process [1]

In bituminous mixture, poor interlock between the particles leads to permanent deformation. That's why, optimizing the particles packing whilst combining aggregate with binder could radically increase the strength and decrease the distress of the composite material [2]. Some researchers found that particles size distribution and grading zone affect the particles packing and consequently the performance of the pavement.

Shen et al. [3] studied the effect of particles size on permanent deformation. They concluded that rough textured, angular and large size of aggregate particles textured aggregates enhanced the rutting resistance and reduced the plastic flow of the bituminous mixture.

Airey et al. [4] investigated the effect of different packing characteristics on the aggregate degradation under compaction for continuously and gap-graded bituminous mixtures. Their results demonstrated that, gap-graded mixture experienced a greater amount of aggregate degradation compared to the continuously graded mixture. Shen et al. [3] found that aggregate gradation (distribution of particles sizes) also play significant effect in resisting the pavement distress. This is as well confirmed by Asi [5] when he studied the effect of aggregate interlocking on the fatigue life.

Theoretically, a better aggregate packing would reduce the permeability of the paste, asphalt cement and thus bleeding of the asphalt cement. It also would reduce the porosity of the pavement thus improved the pavement performance. It is obviously pointed out that aggregate properties have major effect on the asphalt mixture properties and its performance. Many studies have related the gradation, shape and texture of aggregate to the durability, workability, sheer resistance, tensile strength, stiffness, fatigue reaction, rutting susceptibility and optimum bitumen content. In the pursuance of maximizing the use of aggregate to improve the bituminous mix compaction, engineering properties, rutting resistance, this study is conducted to achieve that.

Methodology

Packing Test. Based on the Lees` rational method (as cited in [6]), different sizes; 20mm (A), 14mm (B), 10mm (C) and 5mm (D) are placed into metal mould of known volume and vibrated using the shaker machine. The aggregate particles in the container (mould) are then weighted. With the solid density of the aggregate particles known, the packing density of the aggregate (the volumetric ratio of the solid in the bulk volume) may be determined simply as ratio of bulk density of the aggregate to the solid density of the aggregate particles. The packing density thus measured represents how well the aggregate would be packed together.

Three kilograms from coarse aggregate A (100%) is measured and transferred into the mould. The surface of the aggregate in the mould is leveled using slit plate and the height and the gauge reading was recorded. Initially, the mould is vibrated by the shaker machine for 2.5 minutes and then the height and the gage reading are recorded very carefully. The vibration process was applied frequently every 2.5 minutes until constant height and gage reading are obtained. The vibration time that gave the constant height and constant gage reading is 35 minutes. All the previous steps are applied for 90% from A and 10% from B respectively until 0% from A mixed with 100% from B with vibration time 35 minutes.

All the preceding steps are applied again for coarse aggregate C, D and E. Taking into account that A and B are considered as one aggregate size (A+B) (after mixing optimum percentage of A with optimum percentage of B that gave the maximum density). The optimum percentage of (A+B) is mixed well with optimum percentage of C and considered as one aggregate (A+B+C). The

A+B+C are vibrated with D and the same previous steps for the percentages and vibrations are applied.

The optimum percentage of A+B+C is mixed well with optimum percentage of D and considered as one aggregate (A+B+C+D). The A+B+C+D is vibrated with E (sand that passed the 5mm sieve size and retained on 0.75 mm sieve size) and the same previous steps for the percentages and vibrations are applied to find out the optimum proportion for the A+B+C+D and for the E.

Sieve Analysis Test. Malaysian standard specification Jabatan Kerja Raya (JKR) [7] is used to conduct the sieve analysis test for well graded mixture aggregate. After obtaining the aggregate proportions of the well graded mixture, the packing density for both developed and well graded dry mixtures were determined.

Marshall Test. The aggregates and filler were heated to 160 ^{0}C and mixed with heated bitumen at the same temperature until all particles are coated with bitumen. Developed and well graded bituminous samples are compacted with 75 blows using Marshall Compactor. In addition developed mixture is also compacted with 50 blows compactive effort using Marshall Compactor. After that Marshall Test is conducted to measure the stability and flow of bituminous mixtures specimens [8].

Dynamic Creep Test. Three samples for each mixture are prepared at OBC using 50 blows compaction for developed mixture and 75 blows compaction for well grade mixture. Universal Testing Machine (UTM) is used to conduct dynamic creep test at 40^{0}C to assess the deformation. The resulting deformation on the same axis was measured using Linear Variable Displacement Transducers after repeated pulsed uniaxial stress was applied to a mixture specimen [9].

Results and Discussion

Packing Test Results. A total of 132 moulds are tested by the packing density test. The main concern of this test is to get the highest packing density that can be achieved with optimum combination of sample A, B, C, D and E. The results of the packing density test (Optimum percentages) for the different combinations of A with B are 40% for A, 60% for B, A+B with C are 60% for A+B, 40% for C, A+B+C with D are 60% for A+B+ C, 40% for D, and A+B+C+D with E are 65% for A+B+C+D, 35%for E.

Sieve Analysis Results. The total percentages passing of sieve analysis test for well graded mix are laid within the upper and lower limits of the JKR standard (1988). Since the result met the standard criteria of JKR, the percentages of 45%, 50% and 5% for coarse aggregate, fine aggregate, and filler are used for well graded mix design.

The developed mixture has higher packing density which is 2059.582 Kg/m^3 compared to the well graded one which has 2014.484 Kg/m^3 packing density. This is because the distribution of optimum percentages of the coarser and finer particles of developed mixture helps to formulate stone to stone contact to provide the necessary interlock. In addition, the proportions obtained for the finer particles are able to fill the voids between the big particles gradually until most of the voids of the coarse fraction are systematically filled with finer fractions. When the binder is added to the developed mixture the density is expected to increase. Excess of finer for well graded mixture leads to reduce the interlocking and this result in reduction in the packing density. This agrees with the conclusion specified by Satish and Thoma [10].

Marshall Results. The effects of optimizing the aggregate proportions and how this could improve the compaction energy and engineering properties of bituminous mixture are discussed in detail as follows:

Compaction Energy. According to the requirement of compaction for heavy traffic and as specified by Asphalt Institute Manual, 75 blows per face are required. Developed mixture showed better engineering properties at 50 blows compaction, and these engineering properties satisfied the requirements of the appropriate type of mix as given in Table 4.10 in JKR Manual (Test and Analysis Parameters for Asphaltic Concrete) [7]. This is because the aggregate proportioned in a way that allowed good packing, which brought the aggregate closer and with a little help of compaction the desired density and strength of the mixture is obtained.

Optimum Bitumen Content (OBC). The developed mixture has lower OBC (4.21%) compared to the well grade mixture (5.05%). This because the well graded mixture has a higher percentage of fine aggregate which is 50%. The finer or smaller particles mean a larger surface area which requires a larger amount of binder to cover the particles. Moreover the aggregate grading for developed mixture is much coarser and more continuous than for the well grade one. This is resulted in better aggregate interlocking mechanism, which decreases the voids between the particles. As the voids content in the mixture is reduced, the total amount of bitumen required for a given workability is decreased. Accordingly the volume of bitumen in the mixture is decreased and this will escort lower deformation, improved durability, and lower the cost [11]. The mixture properties for developed mixtures at two different levels of compactions and for well grade mixture at 75 blows are shown in Table I. it can be seen that all the engineering properties for developed mixture at 75 blows are within the standard limit except the air voids (2.7%), which is less than 3%. In addition to that developed mixture at 50 blows shows better density and stability compared to the developed mixture at 75 blows. Therefore developed mixture with 50 blows is better than 75 blows in term of satisfying the requirements, and then it can be compared with well grade mixture.

Table 1: The Engineering Properties for Developed and Well graded Mix at OBC

Engineering properties	Well graded at 75 blows	Developed at 75 blows	Developed at 50 blows
Density (Kg/cm^3)	2345	2426	2427
Stability (KN)	9.8	10.3	11.7
Flow (mm)	2.1	2.9	3
VMA (%)	15.85	12.1	12.8
VFA (%)	76	77.7	78.5
AV (%)	4.5	2.7	3.1

Density. As been expected and as shown in Table 1 and Fig. 2(a), density for developed mixture is very much higher (2427) than the well graded mixture (2345). This is due to the distribution of optimum percentages of large and finer particles for developing mixture, which make the mix more homogenous and helps to provide the necessary interlock and stone to stone contact. High density indicates that mixture has less volume and therefore less voids. High density signifies lower porosity, less binder use and therefore reduces in material cost.

Stability. As it can be seen from Table 1, and Fig. 2 (b), the developed mixture has got higher stability value (11.7KN) compared to the well graded mixture (9.8KN). Hence the interlocking properties of the coarse aggregate of the developed mixture filled voids, therefore more intact between aggregate particles that lead to higher interlocking force that identical to high stability.

Voids in Mineral Aggregate (VMA) and Air Voids (AV). The result for voids in mineral aggregate (VMA) and air voids (AV) for developed mixture is lower than well graded mixture as shown in Table 1 and Fig. 2 (c) and (d), respectively. When the packing density of aggregate is increased the VMA is reduced, this is attributed to the particles interlocking. It indicates the aggregate packing sample is less permeable and it would lead to high strength and durability. However, the porosity is still in the range of 3%-5%, where the mixture would not suffer bleeding.

Voids Filled with Asphalt (VFA) and Flow. The result for VFA at OBC as listed in Table 1, is a quite higher for developed mixture compared to the well graded one. From Table 1, it can also be seen that the flow for developed mixture is slightly higher than the well graded mixture. This result had not been expected since the high density mixture is expected to be stiff and less flexible. Checking with mixture stiffness at dynamic creep results, the developed mixture resulted in higher stiffness and it is lesser susceptible to deform compared to well grade mixture and this is crucial part of the result in terms of performance.

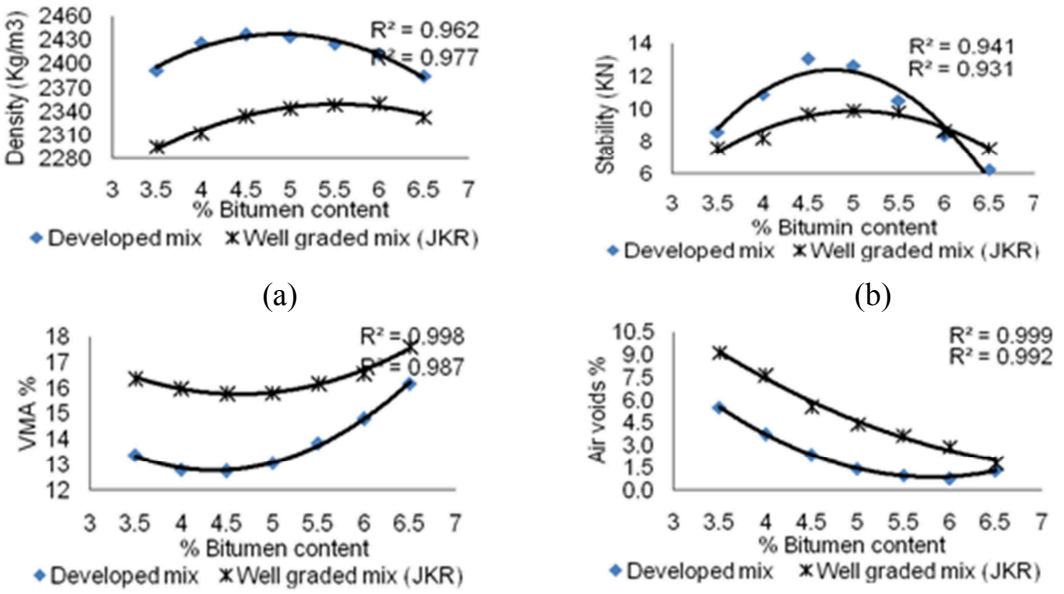


Figure 2: Marshall Test properties for developed (50 blows) and well graded mixtures (75 blows)

Dynamic Creep. The resistance to permanent deformation from the creep test was determined using the slope from log-log relationship of mixture stiffness (S_{mix}) versus binder stiffness (S_{bit}). S_{mix} was measured by universal testing machine at 40^0C for 1 hour loading time period, while the corresponding S_{bit} was calculated by using Van Der Poel's nomograph [12]. As can be noted from Fig. 3 (a), developed mixture showed a higher mix stiffness (lower slope) compared to the well graded one. The result pointed out that developed mixture is less susceptible to loading time in comparison to the well graded mixture. This is due to the fact that developed mixture grading is much coarser and more continuous grading resulted in better interlocking properties.

The results of rut depth estimation are shown in Fig. 3 (b), and are presented in relation to the number of standard axle repetitions. The result showed that estimated rut depth of developed mixture is lower than well grade mixture. Since the developed mixture has a higher resistance to rutting compared to the well graded one. The reason behind that can be attributed to the different particle sizes with optimum proportion which allows good interlocking. This results in continuous grading which increases the strength and stiffness for developed mixture to resist the rutting. This observation is in agreement with previous work (as cited in [2]).

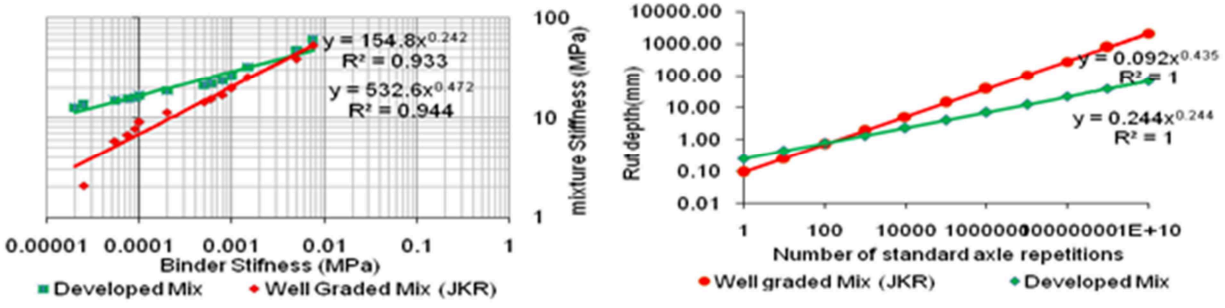


Figure 3: Mixture stiffness (S_{mix}) versus bitumen stiffness (S_{bit}) (a) and rut depth estimation related to the number of standard axle repetitions for developed and well graded mixtures (b)

Conclusions

According to the maximum density obtained from the packing test, the optimum proportions for the developed mixture is found to be 8.64% for coarse aggregate retain on 20mm, 12.96% for

coarse aggregate retain on 14mm, 14.4% for coarse aggregate retain on 10mm, 24% for coarse aggregate retain on 5mm, 32% for fine aggregate, and 8% filler. Developed mixture has a higher packing density compared to the well grade one.

The good interlocking behavior for developed mixture aggregate resulted in minimum voids within the aggregate. This indicates that the aggregate packing sample is less permeable and it would lead to high strength and durability. As a result developed mixture at lower compaction energy has presented a higher stability, density, stiffness, and rutting resistance and lower OBC, VMA and AV compared to the well graded one.

References

[1] F. D. Larrard, Concrete Mixture Proportioning: A Scientific Approach, E & FN Spon, London, 1999.

[2] Best Practices in Glass Recycling, Simple Particle Packing, Material Recycled Glass, CWC, Product Manufacturing Fusing, Nov 1996, pp. 1-2.

[3] H. D. Shen, F. M. Kuo and C. J. Du, Properties of Gap- Aggregate Gradation Asphalt Mixture and Permanent Deformation, Science Direct Journal of Construction and Building Materials, Vol. 19, 2005, pp. 147-153.

[4] G. D. Airey, A. E. Hunter and A.C. Collop, The Effect of Asphalt Mixture Gradation and Compaction Energy on Aggregate Degradation, Science Direct, Construction and Building Materials, Vol. 22, 2008, pp. 972-980.

[5] M. I. Asi, Performance Evaluation of Superpave and Marshall Asphalt Mix Designs to Suite Jordan Climatic and Traffic Conditions", Science Direct Journal of Construction and Building Materials, Vol. 21, 2007, pp. 1732-1740.

[6] Y. Abdel-Jawad, and S. W. Abdullah, Design of Maximum Density Aggregate Grading, Construction and Building Materials, Vol. 16, 2002, pp. 495-508.

[7] Flexible Pavement, Standard Specification for Road Works, Malaysia: Jabatan Kerja Raya, 1988, pp. 1-43.

[8] P. Ahmedzade, and M. Yilmaz, Effect of Polyester Resin Additive on the Properties of Asphalt Binders and Mixtures, Science Direct Journal of Construction and Building Materials, 2007.

[9] G. J. Cabrera and F. A. Nikolaides, Creep Performance of Cold Dense Bituminous Mixtures, Journal of the Institution of Highways and Transportation, Oct 1988, pp. 7–15.

[10] G. Satish and D. P. Thoma, Particle Packing, Encyclopedia of Soil Science, Copyright by Taylor and Francis, 2006, pp. 1245-1248.

[11] O. Karthik, K. Haejin, and L. Colin, Effect of Continuous (Well-Graded) Combined Aggregate Grading on Concrete Performance, Phase A: Aggregate Voids Content (Packing Density), Project D340 May 2007.

[12] S.P. Pell, The Analytical Design of Flexible Pavements, Lecture Notes, Department of Civil Engineering Symposium, University of Glasgow, Apr. 1979.

Applied Mechanics and Materials Vol. 567 (2014) pp 428-433
© (2014) Trans Tech Publications, Switzerland
doi:10.4028/www.scientific.net/AMM.567.428

Mechanical Properties of Engineered Cementitious Composites Mixture

Bashar S. Mohammed [1,a], Muhammad Hafiz Baharun [2,b],
Muhd Fadhil Nuruddin [3,c], Odu Paul Duku Erikole [4,d]
and Nadhir Abdulwahab Murshed [5,e]
[1,2,3,4,5]Department of Civil Engineering
[1,2,3,4,5]Universiti Teknologi PETRONAS,
[1,2,3,4,5]Bandar Seri Iskandar, 31750 Tronoh, Perak, Malaysia.
[a]bashar.mohammed@petronas.com.my, [b]mhafiz_baharun@petronas.com.my
[c]fadhilnuruddin@petronas.com.my

Keywords: Compressive Strength; Flexural Strength; and Tensile Strength; PVA fiber; Self-compacting concrete and Engineered Cementitious Composites.

Abstract. The aim of the research is to develop engineered cementitious composite mixtures satisfying the self-compacting concrete requirements and to evaluate the hardened properties of self-compacted ECC mixtures. To enhance the concrete performance, PVA is used. The PVA improved some characteristics and properties of the concrete. Ten mixes with different Polyvinyl Alcohol (PVA) fiber contents (0.0%, 1.0%, 1.5%, 2.0%, 2.5%, 3.0%, 3.5%, 4.0%, 4.5% and 5.0%) have been prepared. Three cubes (100mm x 100mm x 100mm), three beams (100mm x 100mm x 500mm) and three cylinders (150mm diameter and 300mm height) have been cast for each mix and tested at the age of 7 and 28 days for compressive strength and at age of 28 days for splitting and flexural strength. The V-funnel, L-box and slump test also have been conducted to access the fresh properties like workability and flowability of the concrete. The results indicated the increase in the strength of the concrete and the formulas for predicting the compressive, splitting and flexural strength from PVA (%) has been developed.

Introduction

The development of fiber-reinforced concrete (FRC) is to offset the problems associated with plain concrete such as very low tensile strength, low ductility and little resistance to drying shrinkage cracking and even improve the ductility [1]. The inclusion of PVA in ECC has improved the flexural strength, impact strength, toughness, fatigue strength and resistance to cracking [2]. ECC are a class of ultra-ductile fiber reinforced cementitious composites, characterized by high ductility and tight crack width control [3]. ECC exhibits tensile strain-hardening behavior through multiple micro-cracking with self-controlled crack width, leading to fracture toughness similar to aluminum alloys [4]. The objective of this project is mainly to develop a formula for predicting the compressive, splitting and flexural strength of ECC mixtures from PVA percentage.

Experimental program

Materials. The materials used in this project include an ordinary Portland cement (OPC) and Fly Ash (FA) with chemical compositions shown in Table 1, Sand passing 320 mm sieve, PVA fiber of length 12 mm and diameter, 39 micron, a Polycarboxylate based Superplasticizer with a solid content of 35.7% to improve flow ability and clean mixing water

Table 1. Chemical Compositions of OPC and FA

Chemical Composition	Percentage (%)	
	OPC	Fly Ash
SiO_2	20.3	43.25
Al_2O_3	4.2	20.59
Fe_2O_3	3	12.49
CaO	62	11.11
MgO	2.8	3.76
SO_3	3.5	1.45
K_2O	0.9	1.96
Na_2O	0.2	0.9

Mix proportions. Achieving ECC with better hardened properties such as high compressive, flexural and tensile strengths as well as improved ductility and tight crack control entirely depend on the mix compositions of ECC. The mix proportions of the matrices are shown in Table 2.

Table 2. Mix Compositions for Engineered Cementitious Composites

Mix ID	Water/ Cement ratio	OPC (kg/m^3)	Sand (kg/m^3)	Fly Ash (kg/m^3)	Water (kg/m^3)	PVA (kg/m^3)	Super-plasticizer
M_0	0.32	583	467	700	187	-	4.5
M_1	0.32	583	467	700	187	13 (1.0%)	4.5
M_2	0.32	583	467	700	187	19 (1.5%)	4.5
M_3	0.32	583	467	700	187	26 (2.0%)	9.5
M_4	0.32	583	467	700	187	32 (2.5%)	9.5
M_5	0.32	583	467	700	187	38 (3.0%)	9.5
M_6	0.32	583	467	700	187	45 (3.5%)	9.5
M_7	0.32	583	467	700	187	51 (4.0%)	9.5
M_8	0.32	583	467	700	187	58 (4.5%)	9.5
M_9	0.32	583	467	700	187	64 (5.0%)	9.5

Sample Preparation, Mixing/Casting and Curing. Quantities of each ingredient as shown in the mix proportions were measured and to ensure uniform fiber distribution, the constituents: sand, cement, fly ash and PVA fibers were mixed for 2 minutes in a Hobart mixer. Half of the Water and super plasticizers were then added and mixed for 3 more minutes. Finally, the remaining quantity of water and dosage of superplasticizers were added and the mixing was continued for 3 minutes. The total duration of mixing was therefore 8 minutes. Three 100mm x 100mm x 100mm cubes and three cylinders of 150 mm diameter and 300 mm height were cast for each mix. The samples were demoulded after 24 hours and then placed in curing tank at 20^0C. Curing was continued until the testing date at age of 28 days. On the test date, the samples were removed from the curing tank and their surfaces were dried before testing. Test for compressive strength was carried out in accordance with BS 1881-116 [5] and that for ME was conducted in accordance with ASTM C597 [6].

Results and Discussions

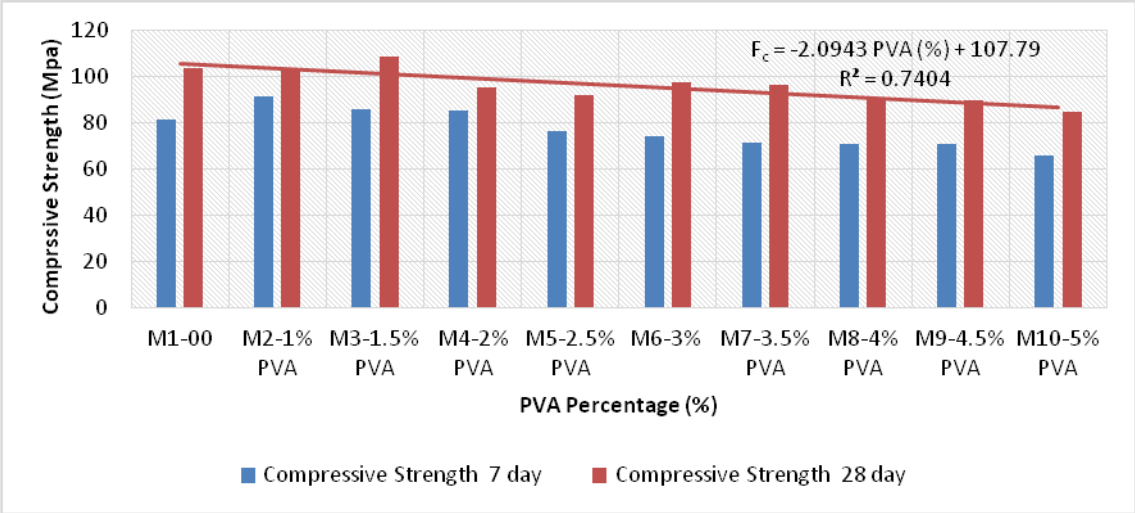
Fresh ECC Result. The fresh properties of PVA fiber-reinforced ECC are shown in Table 3. All the mixes satisfied the requirements for SCC established by EFNARC [7]. Slump flow fall within 650 mm and 800 mm except for mixes M_1 (830 mm) which exceeds the maximum requirement for SCC. The values of T_{50} obtained are all in the range of 2 – 5 seconds required for SCC. V-funnel flow times obtained were between 6 and 12 seconds and (h_2/h_1) for L-box were within the established range of 0.8 – 1.0. Visual Stability Index of zero (VSI = 0) has been assigned for all mixes based on ASTM C 1611 Ratings.

Table 3. Testing for ECC Requirements

Mix ID	Slump Flow				VSI	V - Funnel	L - Box		
	d_{max} (mm)	d_{perp} (mm)	S (mm)	T_{50}		t_v (sec.)	h_1 (mm)	h_2 (mm)	h2/h1
M_0	840	782	811	2	0	6	104	98	0.94
M_1	836	763	790	2	0	6	101	95	0.94
M_2	822	755	789	3	0	7	97	89	0.92
M_3	867	790	830	3	0	7	102	94	0.92
M_4	825	752	790	3	0	8	100	91	0.91
M_5	800	680	740	4	0	11	98	92	0.94
M_6	750	640	695	5	0	12	93	86	0.92
M_7	705	640	670	5	0	12	100	94	0.94
M_8	683	632	658	5	0	12	100	86	0.86
M_9	671	629	650	5	0	12	105	85	0.81
Note: The slump spread, $S = \frac{dmax + dperp}{2}$ to the nearest 5 mm									

Compressive Test for 7 and 28 Days. Fig. 3.1, showed the comparison for compressive test at 7 days and 28days, the compressive test at 28 days give higher results than 7days. Equations 1 for predicting the compressive strength of ECC with different percentages of PVA at 28 days. The Fig. 3.1, were obtained with coefficient of determination (R^2) 0.7404.

$$F_c = -2.0943\ PVA\ (\%) + 107.79, \quad \text{Where, } F_c = \text{compressive strength, MPa.} \tag{1}$$

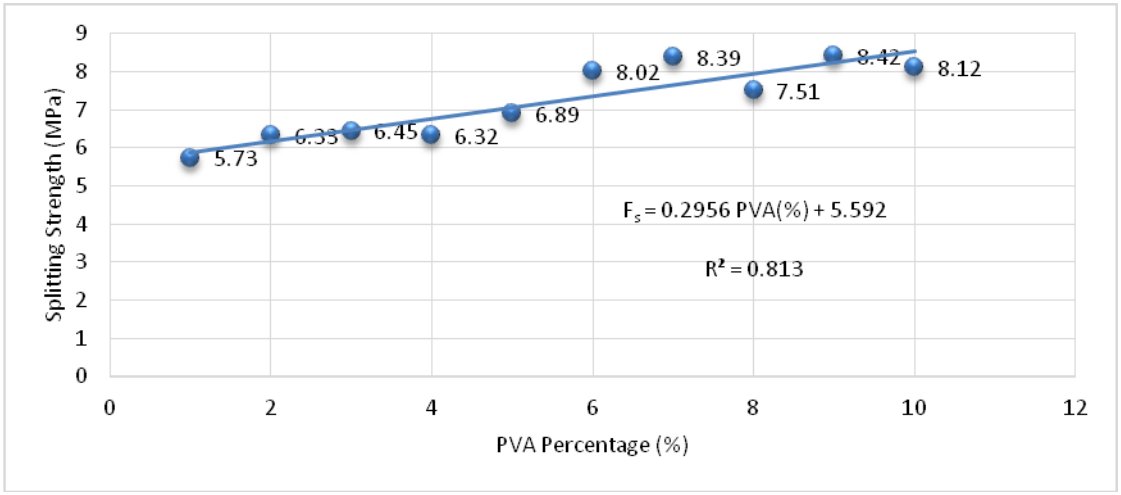


Figures 3.1. Compressive Strength Result

From the analysis, it can be seen that compressive strength of the concrete decrease with increasing of PVA percentage except for mixes M3 which the highest value compressive strength.

Splitting Test for 28 Days. Equations 2 for predicting the splitting strength of ECC with different percentages of PVA at 28 days. The Fig. 3.2, were obtained with coefficient of determination (R^2) 0.813.

$$F_s = 0.2956 \text{ PVA } (\%) + 5.592, \text{ Where, } F_s = \text{Splitting strength, MPa.} \quad (2)$$

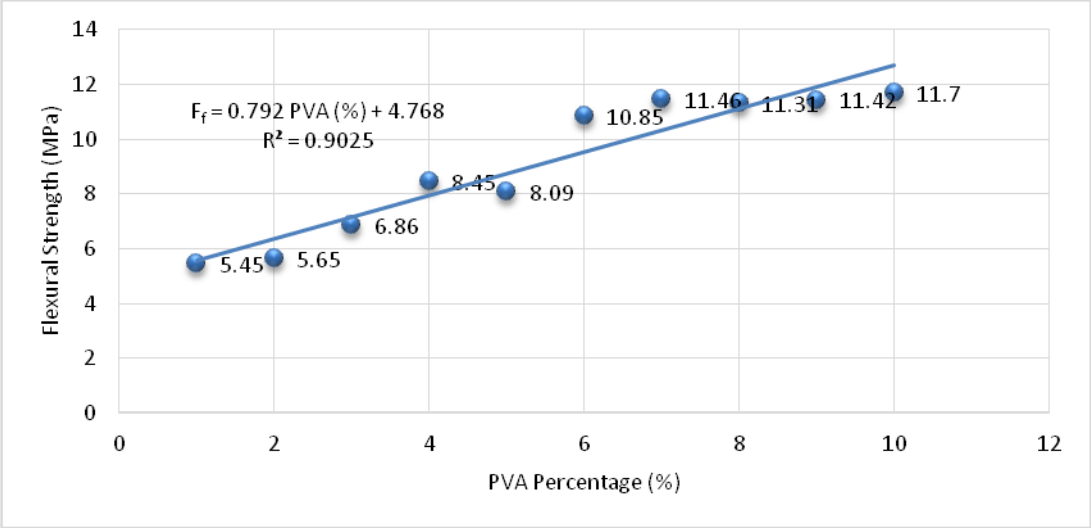


Figures 3.2. Splitting Strength Result

From the analysis, it can be seen that splitting tensile strength increased with increasing of PVA percentage.

Flexural Test for 28 Days. Equations 3 for predicting the flexural strength of ECC with different percentages of PVA at 28 days. The Fig. 3.3, were obtained with coefficient of determination (R^2) 0.9025.

$F_f = 0.792$ PVA (%) + 4.768, Where, F_f= Flexural strength, MPa (3)



Figures 3.3. Flexural Strength Result

From the analysis, it can be seen that the flexural strength increased with increasing of PVA percentage.

Conclusion

The following conclusions can be drawn from the experimental results of this study:

1) The slump spread or slump flow and the V-Funnel flow decrease with increase in the content of PVA fiber. This is because, as the PVA fiber content increases, the fibers tend to clump together. The workability of the ECC is therefore, reduced at high percentage of PVA due to lack of uniform distribution of the fibers.
2) The compressible strength of ECC decreases with increasing PVA fiber content. Splitting and flexural strength increases as the increasing PVA fiber content.
3) A new equations to predict the compressive, splitting and flexural strength of ECC F_c = -2.0943 PVA (%) + 107.79, F_s = 0.1759 PVA (%) + 5.6787 and F_f = 0.792 PVA (%) + 4.768 respectively has been developed in this study.
4) The coefficient of determination (R^2) for the compressive, splitting and flexural strength of ECC 0.7404, 0.31, and 0.9025 respectively has been obtained in this study.

References

[1] Mohammed B.S, Fang, O.C, Mechanical and durability properties of concretes containing paper-mill residuals and fly ash, Construction and Building Materials 25 (2011) PP. 717 - 725.

[2] S. H. Kosmatka, W. C. Panarese, Design and control of concrete mixtures. Third ed, Portland cement Association, 5420 Old Orchard Road, Skokie, Illinois 60077-1083 (1994)

[3] Z. Jian, Y. Guang, C. Oguzhan, B. Klaas, V.C. Li, Improved fiber distribution and mechanical properties of engineered cementitious composites by adjusting the mixing sequence, Cement & Concrete Composites. 32 (2012) 342-348.

[4] M. Maalej, T. Hashida, V.C. Li, Effect of fiber volume fraction on the off-crack plane energy in strain-hardening engineered cementitious composites. Journal of American Ceramic Society. 01 (1995) 78(12):3369–3375.
[5] BS 1881-116, Method for Determination of Compressive Strength of Concrete Cubes
[6] ASTM C597 – 09, Standard Test Method for Pulse Velocity Through Concrete
[7] Specification and Guidelines for Self-Compacting Concrete, EFNARC, Association House, 99 West Street, Farnham, Surrey GU9 7EN, UK, 2002

Applied Mechanics and Materials Vol. 567 (2014) pp 434-439
© (2014) Trans Tech Publications, Switzerland
doi:10.4028/www.scientific.net/AMM.567.434

Microwave Incinerated Rice Husk Ash (MIRHA) and Used Engine Oil (UEO): Towards Sustainable Concrete Production

NUR LIYANA MOHD KAMAL[1,a*] SALMIA BEDDU[2,b]
MUHD. FADHIL NURUDDIN[3,c], NASIR SHAFIQ[4,d]
and ZAKARIA CHE MUDA[5,e]

[1] N.L.Mohd Kamal, Lecturer. Department of Civil Engineering, Universiti Tenaga Nasional Malaysia

[2] Salmia Beddu, Senior Lecturer. Department of Civil Engineering, Universiti Tenaga Nasional Malaysia

[3] M.F. Nuruddin, Prof. Department of Civil Engineering, Universiti Teknologi PETRONAS Malaysia

[4] N.Shafiq, Assoc. Prof. Department of Civil Engineering, Universiti Teknologi PETRONAS Malaysia

[c]Yana_Kamal@uniten.edu.my, [b]Salmia@uniten.edu.my, [c]fadhilnuruddin@petronas.com.my, [d]nasirshafiq@petronas.com.my, [e]MZakaria@uniten.edu.my

Keywords: Microwave Incinerator, Rice Husk Ash, Used Engine Oil, Compressive Strength

Abstract. Rice is a primary source of food for billions of people and covers 1% of the earth's surface. On average 20% of the rice paddy is husk, giving an annual total production of 120 million tones. Nowadays, there are two common methods used to dispose the rice husk which is either it is being dump or burnt. Rice husk ash (RHA) which is produced by burning paddy husk led to the issue of ozone layer depletion. It also causes damage to the land and the surrounding area where it is being dumped. Previous studies have pointed out that RHA produced contains more than 80% pure silica and if properly prepared, it is in an active form which behaves very much like cement. Same goes with used engine oil (UEO). Many people are aware that UEO shouldn't be dumped, but recycled. It is incredibly toxic stuff and a gallon can contaminate one million gallons of water. Pouring it on land doesn't reduce the risk either as it can seep down into the water table.The objective of this research is to obtain an optimum percentage of inclusion of microwave incinerated rice husk ash (MIRHA) as a cement replacement and UEO in order to produce a better concrete in terms of compressive strength compared to normal OPC concrete. The test results showed MIRHA concrete performed better than normal OPC concrete and the incorporation of UEO and MIRHA in concrete showed the compressive strength give better performance.

Introduction

Rice husks are the hard protecting coverings of grains of rice. On average 20% of the rice paddy is husk, giving an annual total production of 120 million tones [1]. Lots of ways are being thought of for disposing of it by making commercial use of it. In the majority of rice producing countries much of the husk produced from the processing of rice is either burnt or dumped as waste. Many of the developing countries produce huge quantities of agro residues but they are used inefficiently and cause extensive pollution to the environment. Therefore burning procedure to obtain RHA that is highly reactive needs to be established so that it can be used as cement replacement. Burning the rice husk at high temperature will increase the SiO_2 content but it is not suggested to burn rice husk above 800°C longer than one hour, because it tends to cause a sintering effect (coalescing of fine particles) and is indicated by a dramatic reduction in the specific surface [2]. Current researches have shown that by certain burning method, the ash produced contains about 95% pure silica and if properly prepared, it is in an active form which behaves very much like cement [3]. Furthermore, at the optimum percentage replacement of RHA, it will improve the concrete performance, either its strength or durability [4].

This research was conducted to identify the optimum inclusion of MIRHA and its effect on compressive strength concrete. Burning the RHA with higher temperature will increase the SiO_2 content. But it is not suggested to burn rice husk above 800°C longer than one hour, because it tends to cause a sintering effect (coalescing of fine particles) and is indicated by a dramatic reduction in the specific surface [5]. In the literature, burning RHA with two stages with 550°C produce partially amorphous and partially crystalline. It is due to the actual temperature that can reach 950°C - 1000°C even when the incinerator has been automatically turned off and it will produced crystalline RHA.

In addition, the increase number of vehicles globally has cause an increased in the production of used engine oil. Approximately 1.35 billion gallons of used engine oil is generated yearly (Utah Department of Environment Quality)[6]. The study from El- Fadel [7] shows that more than 45% of used engine oil is being collected worldwide while the remaining 55% is thrown by the end user to the environment.

Mindess and Young (1981) [8] reported that the leakage of oil into the cement in older grinding units resulted in concrete with greater resistance to freezing and thawing. This implies that adding used engine oil to the fresh concrete mix could be similar to adding an air-entraining chemical admixture, thus enhancing durability properties of concrete while serving as another technique of disposing the oil waste.

The contribution of both MIRHA and UEO giving benifit to the concrete properties so far. Hence, potential of waste in concrete production will bring advantages towards green concrete for sustainable developement.

Materials and Experiment Details

Microwave Incinerator

The UTP Microwave Incinerator (UTPMI) used in the research adopted the Air Cooled Magnetron system with an overall dimension of 2.3(H)x4.0(W)x4.0(L) with a chamber capacity of 1 m^3. Ceramic filter is used in the emission and ash control system with PLC mode of operation. Flue Gas Filter attached to the microwave incinerator provides significant positive effect to the environment. It distils all the dust and ashes that are resulted from rice husk incineration, hence the air pollution from burning process can be reduced [9]. The temperature range is up to 1600°C with operating temperature of 800°C. Rice husks used in this research were taken from rice milling plant Bernas, Malaysia. Rice husks were dried under direct sunlight to reduce moisture content so that when burnt would not produce large amount of smoke. Fig. 1 shows the microwave incinerator used for in research.



Figure 1 Automatic UTP Microwave Incinerator

Specimen Preparing and Curing

The MIRHA was then ground by a Los Angeles abrasion machine until the particles were as small as those of CRM. The fine aggregate used was natural sand with the fineness modulus 2.7 and classified in Zone 3 while coarse aggregate used was crushed aggregate with the maximum size of 20 mm according to BS 812-103.2 1989. The regular tap water was used in the whole tests. The concretes were prepared in the laboratory using a mixer. The absolute volume method was used in calculating the mixture proportions. MIRHA was used as a replacement of cement on a weight basis. A number of mixes have been chosen so that the performance of concrete with different admixtures can be compared. MIRHA is then used to replace 5%, 10%, 15% and 20% of cement content in concrete with 0.45 w/c. The control concrete was designated NC (normal concrete) without any addition of MIRHA as a comparison. Superplasticizer was used in concrete containing MIRHA to increase its workability. Complete mixture proportion for 0.45 water cement ratio is showed in Table 1.

Compressive strength development of the concrete sample was measured according to BS EN 12390-3:2002 using Digital Compressive Testing Machine. The 150mm cubes were used for the determination of the compressive strength at 3, 7, 28 and 56 days of curing. During the test, concrete cube was loaded with 6.8 KN/s constant loads without any sudden shock loads. Compressive strength value was taken from ultimate load that can be sustained by the concrete cube divided by surface area of the cube.

Used engine oil was collected from workshop around Tronoh and Seri Iskandar, Perak. It was collected randomly at the service stations that have no proper dispose.

To study the potential of MIRHA and UEO in concrete, seven mixes has been cast with 20% of cement content has been replaced by MIRHA and conribution of various percentage of UEO. The mixture proportion of the concrete illustrated in Table 2. Concrete cubes of 100x100x100 mm were then water cured and the compressive strength monitored at ages 3, 7, and 28, 90 and 180 days.

Table 1 Mixture Proportions of MIRHA Concrete

Mix Code	MIRHA		SP	Cement
	(%)	(kg/m³)	(%)	(kg/m³)
NC	0	0	0	475
MIRHA5	5	23.75	0.4	451.25
MIRHA10	10	47.5	0.8	427.5
MIRHA15	15	71.25	1.5	403.75
MIRHA20	20	95	2	380

Table 2 Mixture Proportion of MIRHA Concrete with UEO

Mix	OPC	MIRHA	UEO
	(kg/m^3)	(kg/m^3)	(%)
OPC	325	-	-
MIRHA	260	65	-
MIRHA-UEO-0.15	260	65	0.15
MIRHA-UEO-0.3	260	65	0.3
MIRHA-UEO-0.5	260	65	0.5
MIRHA-UEO-0.8	260	65	0.8
MIRHA-UEO-1	260	65	1

Results and Discussion

MIRHA Concrete

The increase percentage of MIRHA added into the concrete directly led to the declining of Portland cement used in the mix proportion. Addition of MIRHA into concrete mixture significantly enhanced concrete strength performance. Higher compressive strength of MIRHA concrete samples compared to control concrete from early curing days also indicated that pozzolanic reaction started to occur during these ages. Figure 2 shows the compressive strength development of concrete with MIRHA at 800°C.

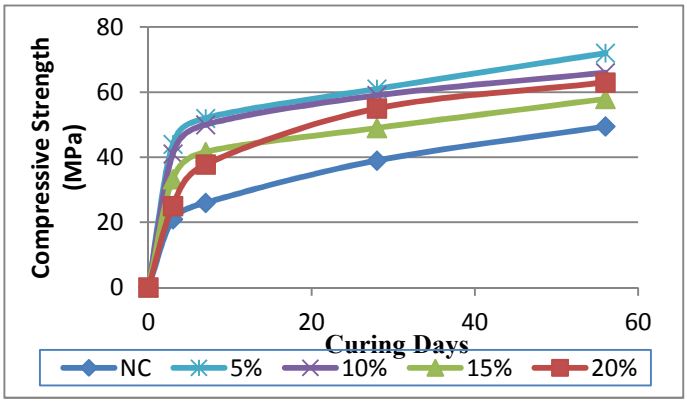


Figure 2 Compressive Strength Development of Concrete Sample With MIRHA at 800°C

Table 2 Compressive Strength (*Compared to control concrete with 0% of MIRHA)

Inclusion of MIRHA	Strength Increment at 28 days*	Strength Increment at 56 days*
5%	56%	44%
10%	51%	32%
15%	26%	16%
20%	41%	26%

The development of concrete strength obtained for different percentage inclusion of MIRHA in concrete is shown. From early curing days, MIRHA concrete samples showed early strength gain faster and 5% additions of MIRHA has the highest level of compressive strength. There is no significant difference of compressive strength between 5% and 10% MIRHA concrete in the short term (3, 7 and 28 days) but in the long term (56 days), the effect of absorptive character of MIRHA that caused lack of water in 10%, 15% and 20% MIRHA concrete slowed down the development of strength. It is believed that the adequate amount of water and high pozzolanic reactivity were the reasons why 5% MIRHA concrete has faster strength acceleration. Table 2 shows that at 28 days and 56 days 10%, 15% and 20% of MIRHA have lower compressive strength development of concrete. Compared to 5% inclusion, the low Portland cement content in the 10%, 15% 20% MIRHA mix proportion. It will reduce the production of (C-S-H) gels to fill up the pores structure inside the concrete and created water-filled space that affect the compressive strength of the concrete. Lower content of $Ca(OH)_2$ produced also affected the pozzolanic reaction with SiO_2 [10]. Perfect proportion between cement paste and water has made hydration process in this concrete sample accelerates faster than the other samples. However this acceleration can only be achieved with rich amount of cement content, correct proportion of aggregates and water content and also an optimum inclusion of MIRHA. It is shows the optimum mix proportion that was obtained from this research was based on the compressive strength of MIRHA concrete samples.

MIRHA Concrete with UEO

Figure 3 show that MIRHA concrete with incorporation of lower than 0.8% used engine oil significantly enhanced the strength performance. This was due to the effects of used engine oil and in deflocculating the agglomeration or lumps of cement grains. With adequate water, pozzolanic reaction was improved and hence increased the formation of C-S-H gel. Results of MIRHA concrete mixes at 28 days are shown in Figure 4. Compressive strength of MIRHA concrete containing 0.15, 0.3, 0.5, 0.8 and 1% of used engine oil were 45, 48, 49, 34 and 29 MPa respectively. Thus, it showed that the performance of used engine oil MIRHA concrete in terms of

compressive strength was comparable to the ones with superplasticizer. The compressive strength of MIRHA concrete containing 1% used engine oil is lower that MIRHA control concrete.

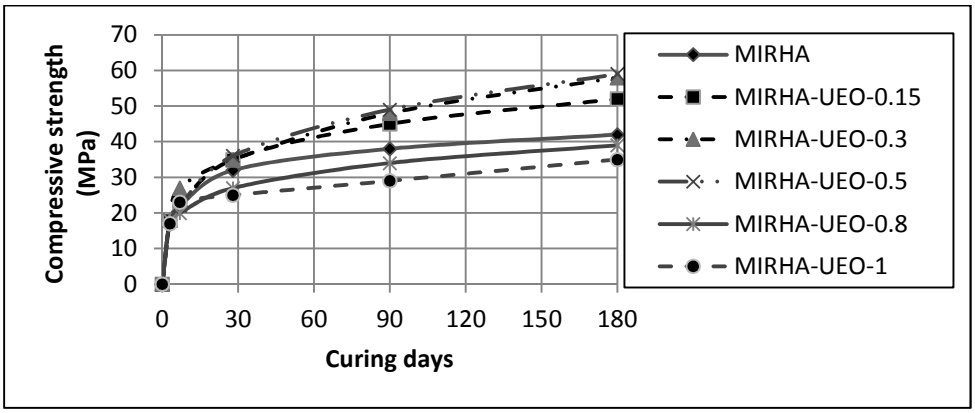


Figure 3: Strength development of MIRHA concrete with Used Engine Oil

Figure 3 also showed that at 28 days, 90 days and 180 days, compressive strength MIRHA concrete containing 0.15%-0.5% of used engine oil is higher as compared to MIRHA control mix. MIRHA concrete containing 0.8-1% used engine oil did not give significant effects to compressive strength development.

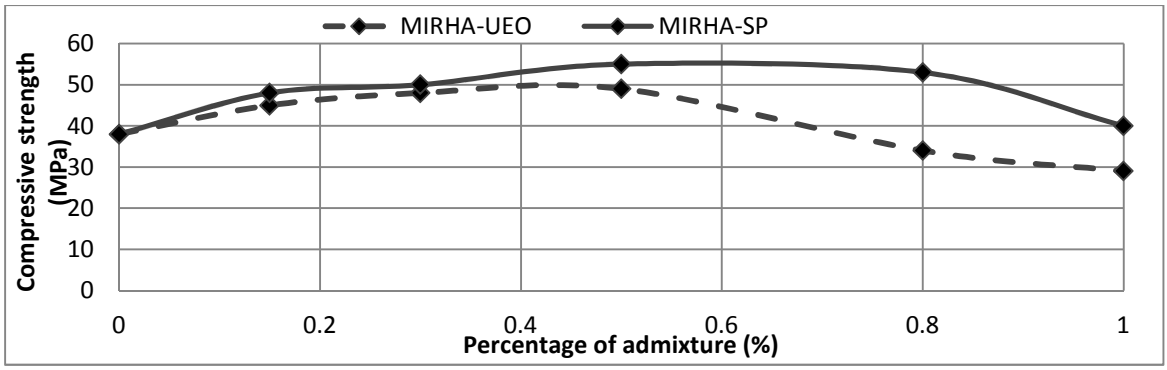


Figure 4: Compressive strength of MIRHA concrete at 28 days

The strength increment of MIRHA concrete was due to the amorphous silica and fineness of MIRHA used. The effective burning method of UTP microwave incinerator adopted to produce amorphous silica in the rice husk ashes was instrumental in creating good quality MIRHA concrete. The addition of MIRHA caused an increment in the compressive strength is due to the capacity of pozzolan, consumed the calcium hydroxide generated C-S-H gel.

Conclusion

From the tests that have been conducted, it can be concluded that:

1. Generally, 5% MIRHA replacement with cement and addition of superplasticizer to the mortar produced concrete with good performance at early age and gained higher strength.
2. Used engine oil can act as a chemical plasticizer similar to superplasticizer to improve workability, air content and strength of OPC and MIRHA concrete.
3. The results of 0.5% inclusion of chemical admixtures in both OPC and MIRHA concrete can be concluded that the compressive strength at 28 days of OPC concrete containing UEO and superplasticizer gave 19% and 14% lower than OPC control mix respectively. Compressive strength of MIRHA concrete containing UEO and superplasticizer showed increment of 26% and 45% respectively compared to MIRHA control mix.

References

[1] Contractor-Bronzeoak Ltd. Rice Husk Ash Market Study (2003).

[2] M.F. Nuruddin, N. Shafiq, N.L. Mohd Kamal, Microwave Incinerated Rice Husk Ash (MIRHA) Concrete: A New Material In The Construction Industry, UK Malaysia Engineering Conference (2008).

[3] United Nations Industrial Development Organization (with Govt. of Australia), Vienna, Rice-Husk Ash Cements (1984).

[4] Sensale, G.R. Strength Development of Concrete with Rice Husk Ash. Cement & Concrete Composites 28, pp 158-160 (2006).

[5] Hwang, Chao Lung and Chandra, Satish. The Use of Rice Husk Ash in Concrete. In S.Chandra, Waste Materials Used in Concrete Manufacturing (pp. 184-234). William Andrew Pub. (1996).

[6] M.F. Nuruddin, A. Kusbiantoro, N. Shafiq, Microwave incinerated rice husk ash (MIRHA) and its effects on concrete strength, International IMS Conference On Applications Of Traditional And High Performance Materials In Harsh Environments, American University of Sharjah, 23-24 Jan, 2008.

[7] M.F. Nuruddin, N.Shafiq, N.L.Mohd Kamal. Microwave Incinerated Rice Husk Ash (MIRHA) Concrete: A New Material In The Construction Industry. United Kingdom Malaysia Engineering Conference, 2008

[8] Utah Department of Environment Quality (2009)

[9] Bentech. Operation & Maintenance manual for Microwave Incinerator (2006)

[10] Andri Kusbiantoro, The Effects of Microwave Incinerated Rice Husk Ash (MIRHA) On Concrete Properties, Universiti Teknologi Petronas (2008).

Applied Mechanics and Materials Vol. 567 (2014) pp 440-445
© (2014) Trans Tech Publications, Switzerland
doi:10.4028/www.scientific.net/AMM.567.440

Numerical investigation of the response of protective barrier under blast loading

Kong Sih Ying[1,2, a], Alex M. Remennikov[2,b] and Brian Uy[3,c]

[1]Department of Civil Engineering, College of Engineering, Universiti Tenaga Nasional, Jalan IKRAM-UNITEN, 43009 Kajang, Selangor, Malaysia

[2]School of Civil, Mining and Environmental Engineering, University of Wollongong, Wollongong NSW 2522, Australia

[3]Centre for Infrastructure Engineering and Safety, University New South Wales, Sydney NSW 2052, Australia.

[a]ksy965@uowmail.edu.au, [b]alexrem@uow.edu.au, [c]b.uy@unsw.edu.au

Keywords: steel-concrete-steel, protective barrier, finite element, blast loading

Abstract. Non-composite steel-concrete-steel panels develop high load-carrying capacity through the tensile membrane resistance of the steel faceplates at large displacement. The response of a full-scale barrier structure composed of the non-composite SCS panels and steel posts under various blast loading scenarios was investigated using non-linear finite element software LS-Dyna. The simulation results showed that the barrier was able to withstand very large blast energy. It can be concluded that non-composite SCS panels can provide an attractive solution to expedite construction of high-performance protective barriers to resist extreme blast loadings.

Introduction

With the consideration of car bombings and accidental vehicle impacts on critical infrastructures, there is an increasing need to develop a cost-effective solution for protecting these facilities. Smith [1] presented extensive review on the design of different types of blast walls used in military and civilian applications. The blast barrier can be categorised into simple earth-filled walls, to more sophisticated reinforced concrete walls and composite walls. Earth-filled wall is easy to build, and is relatively cheap compared to other types of blast barriers. It relies on the inertial effect of the soil infill to resist the blast or impact loading. Therefore, enormous wall thickness is usually required (1-2 metres). Its application in the urban environment is limited due to its thickness and aesthetic aspect. The concrete in the reinforced concrete walls will shatter under strong impact or blast loading, producing high speed secondary fragments which are hazardous to the building and its occupants.

The composite walls can be divided into concrete-sand-concrete and steel-concrete-steel wall. The design of composite concrete-sand-concrete walls is provided in TM5-1300 [2]. The steel-concrete-steel (SCS) composite walls consist of a thick concrete core confined by two relatively thin steel faceplates. Crawford and Lan [3] presented the design concepts of axially restrained non-composite SCS panels for resisting blast loading and provided experimental verification for the full-scale blast wall. Remennikov et al. [4, 5] investigated experimentally the static and impact performance of non-composite SCS panels in which no shear connectors were utilised to connect the steel faceplates and the concrete core. Due to the specially designed connection details, the tested panels exhibited tensile membrane resistance at large deformation. The tensile membrane resistance achieved in the tests was significantly higher than the flexural resistance, and the panels were capable of resisting large support rotations without collapse. Kong et al. [6] presented FE simulation techniques for the SCS panels under static and impact loading and validated the simulation results against experimental results [4].

In this study, the response of protective barrier consists of non-composite SCS panels subjected to blast loading was investigated using the non-linear transient dynamic finite element software LS-Dyna.

Geometry of the protective barrier

The barrier consists of non composite steel-concrete-steel panels supported by the steel posts. No shear stud is used in the steel-concrete-steel panel, and the main load resistance for this type of panel is the tensile membrane action of steel plate at large displacement. The dimension of the full scale SCS panel is illustrated in Figure 1. The overall thickness of the SCS panel is 200 mm. The thickness of the concrete core and the steel faceplate is 180 mm and 10 mm, respectively. The length of the SCS panel between the flared ends is 3500 mm, and the height of the panel is 3500 mm. The angle of the flared ends is 30^o and the length of the flared ends is 172 mm.

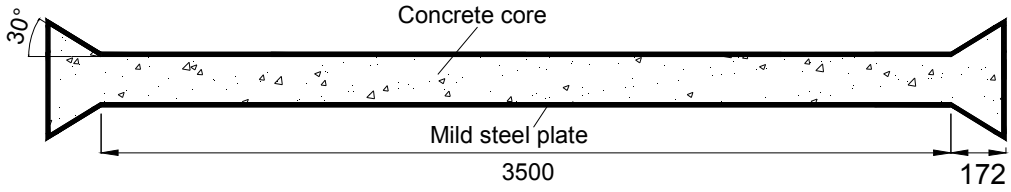


Figure 1: Geometry and dimension of the full scale non-composite SCS panel.

In the prototype barrier, non-composite SCS panels are connected to the steel posts, which are penetrated into the ground at one end in the reality. The design of the penetration depth and the soil-post interaction are ignored in this study and it is assumed that the posts act as cantilever beams. The post is composed of an I-beam with keyed connections, and bracings between the flanges and the web of the I-beam, as shown in Figure 2 (a). The depth between the flanges is 600 mm for the SCS panel with 200 mm thickness. The thickness of the flanges is 25 mm, the thickness of the web is 16 mm, and the thickness of the plate used to form the keyed connections and bracings is 10 mm. The details dimension of the post is illustrated in Figure 2 (b). The height of the post is 3500 mm and the void in the keyed connections is filled with 40 MPa concrete.

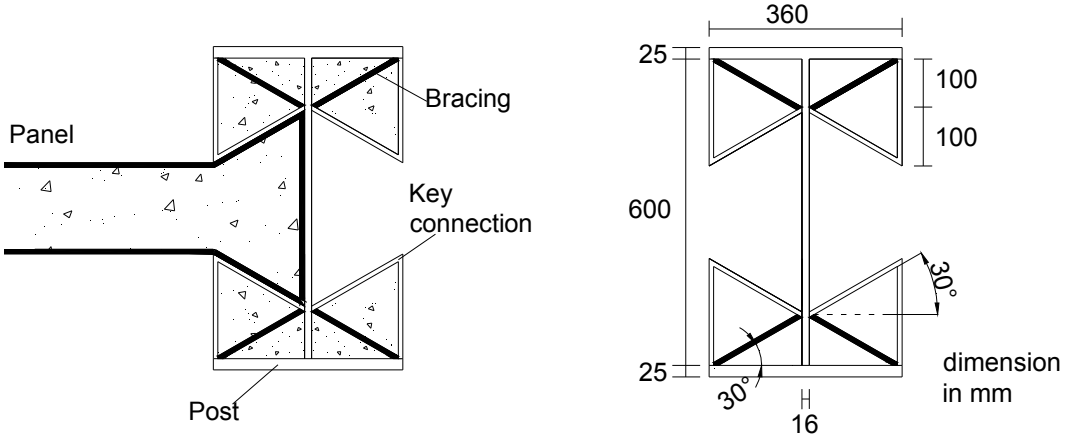


Figure 2: (a) Connection details between the non-composite SCS panel and the post, (b) geometry and dimension of the post.

FE model of the protective barrier subjected to blast loading

Figure 3 shows the FE model of the protective barrier supported by the steel posts. Three non-composite SCS panels were modelled, where the middle panel was modelled using a finer mesh size of about 25 mm. Two side panels were modelled using a mesh size of about 50 mm. The posts were

modelled in details where the steel plates in the post were modelled using Belytschko-Tsay shell elements [7], while the concrete infill was modelled using constant stress solid elements.

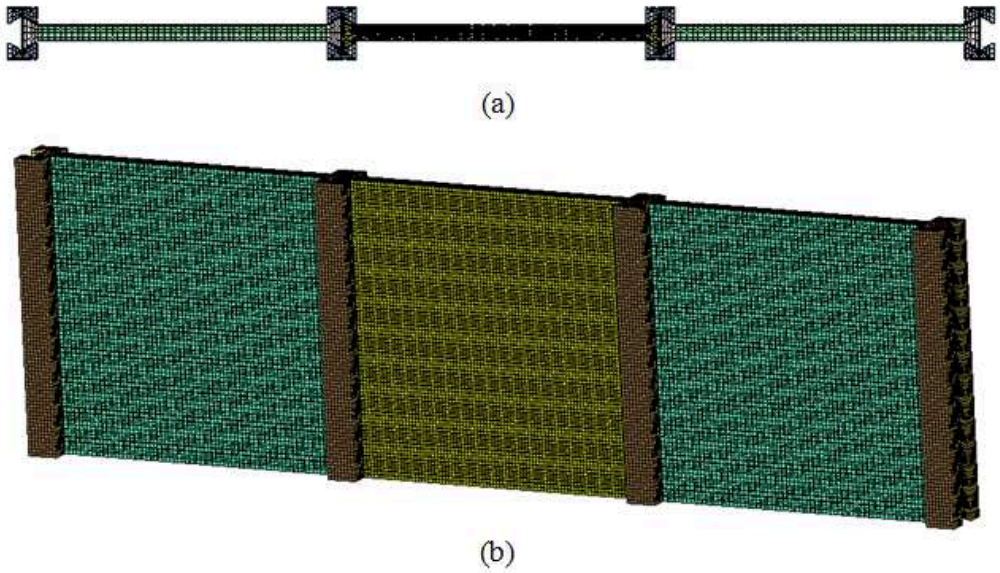


Figure 3: FE model of the barrier consists of non-composite SCS panels and posts (a) top view, (b) isometric view.

The Automatic-Surface-to-Surface contact algorithm was used to define the interaction between the SCS panels and the keyed connections with a dynamic coefficient of friction of 0.2. The mild steel was modelled using the Plastic Kinematic material model with the dynamic yield stress of 325 MPa and the plastic modulus of 230 MPa. The concrete core along the span of the SCS panel was modelled using the concrete material model damage release III (Mat 72 R3). The concrete infill in the posts and at the flared zones of the SCS panels was modelled using the CSCM 159 material model. The nodes at the bottom of the posts were restrained against translational and rotational degrees of freedom in x, y and z directions. Two posts at the far corner were restrained to move in the y direction (in-plane direction), to account for the continuity of the barrier structure beyond the three panels modelled in this study.

The loading of various blast scenarios was generated by using the Load_Blast_Enhanced command. In this study, the charge was positioned on the ground surface, and the standoff distance was 5 m or 10 m from the mid-span of the middle panel. The type of blast source was hemispherical surface burst with the initial shock wave of the detonation was reflected and reinforced by the ground. The blast loading was applied to the front faceplates of the SCS panels and the front flange of the steel posts using the Blast_Segment_Set algorithm.

For the barrier supported by the mild steel posts, four blast loading scenarios considered were (1) 500 kg TNT at 10 m standoff distance, (2) 250 kg TNT at 5 m standoff distance, (3) 500 kg TNT at 5 m standoff distance and (4) 750 kg TNT at 5 m standoff distance. The corresponding scaled distance (Z) for these blast loading conditions was (1) 1.26 $m/kg^{1/3}$, (2) 0.79 $m/kg^{1/3}$, (3) 0.63 $m/kg^{1/3}$ and (4) 0.55 $m/kg^{1/3}$. When the scaled distance decreased, the reflected pressure on the barrier increased and the reflected pressure became highly non-uniform when the scaled distance was less than 0.8 $m/kg^{1/3}$. The peak reflected pressure on the barrier when $Z < 0.8$ $m/kg^{1/3}$ was recorded near the bottom of the middle panel at the mid-span due to the position of the charge on the ground. The peak reflected pressure on the side panels was significantly lower than the peak reflected pressure on the middle panel.

Response of the protective barrier subjected to blast loading

The response of the barrier supported by the mild steel posts was similar when it was subjected to increased blast loading conditions. The response of the barrier is exemplified by the response of the middle panel and the mild steel posts of the barrier subjected to the blast loading of 500 kg TNT at 5 m standoff distance in Figure 4. The middle panel and the mild steel posts connecting to the middle panels showed most severe deformation as the charge was positioned at 5 m or 10 m from the centre of the middle panel.

When subjected to the blast loading, the panels and the mild steel posts started to deform simultaneously. At the early stage, the extensive damage of the concrete core near the posts (Figure 4) could be attributed to the shear failure of the unreinforced concrete core. Moderate damage was observed for the concrete infill in the posts and at the flared zone of the panels. As the displacement increased, the concrete core along the span of the middle panel was severely damaged and the front faceplate was separated from the concrete core. The rear faceplate was pushed in the direction of the blast loading by the concrete core and it started to yield at the flared zone and mid-span. At the maximum displacement, it was observed that no significant local bending deformation occurred at the rear flanges of the mild steel posts and the keyed connection was effective in restraining the in-plane displacement of the SCS panel. The in-plane displacement of the mild steel posts was less than 10 mm.

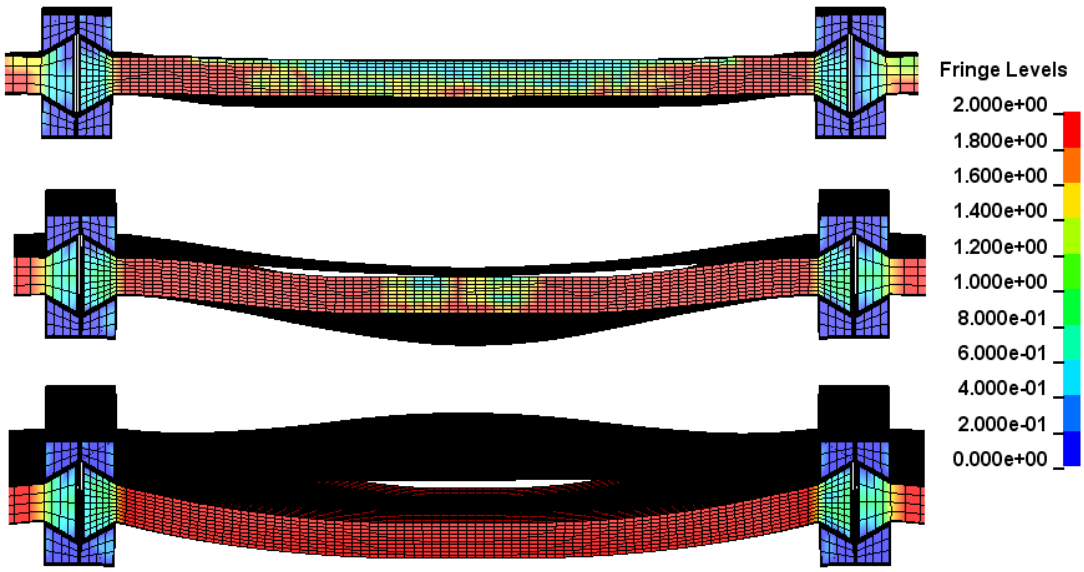


Figure 4: The response of the protective barrier with 200 mm thick non-composite SCS panels supported by the mild steel posts under the blast loading of 500 kg TNT at 5 m standoff distance.

Table 1 summarizes the peak displacement of the middle panel at mid-span and the maximum displacement of the mild steel post and the keyed connection. It shows that the peak displacement of the middle panel at mid-span was non-uniform, with the mid-height displacement showing lowest peak displacements. The peak displacement at the bottom of the middle panel was larger than the mid-height displacement due to the charge being positioned on the ground surface, and therefore generating higher blast pressure at the lower part of the panel. The middle panel showed highest peak displacement at the top (except the barrier subjected to the blast loading of 500 kg TNT at 5 m standoff distance) due to the deflection of the mild steel posts. The rear faceplate was yielded at the mid-span and the flared. When the blast loading increased, the plastic deformation of the rear faceplate was concentrated at the flared zone. The maximum support rotation of the middle panel was about 20^{o} when the barrier was subjected to the blast loading of 750 kg TNT at 5 m standoff distance.

Table 1: Deformation of the barrier with 200 mm thick SCS panels supported by mild steel posts under various blast loading conditions.

Blast threat Scenarios		Displacement of middle panel (mm)			Mild steel post		Keyed connection	
Standoff distance (m)	TNT mass (kg)	Bottom	Mid-height	Top	Displacement (mm)	Rotation (^{o})	Displacement (mm)	Rotation (^{o})
10	500	189	188	222	67	1.1	1.2	0.3
	250	265	239	269	89	1.5	2.8	0.65
	500	465	415	449	284	4.6	5.3	1.2
5	750	674	590	728	557	9.0	9.2	2.2

For all the blast loading scenarios considered, the mild steel posts supporting the middle panel were yielded at the base. When the barrier was subjected to the blast loading of 500 kg TNT at 10 m standoff distance, the maximum support rotation of the mild steel post was 1.1^o and the maximum strain of the shell elements adjacent to the base was about 0.06. The maximum support rotation of the mild steel post increased to 4.6^o and the maximum strain approached to the fracture strain of mild steel (0.25) when the blast loading was increased to 500 kg TNT at 5m standoff distance. As the blast loading further increased to 750 kg TNT at 5 m standoff distance, the shell elements of the rear flange and the keyed connection near the base reached the fracture strain and were eliminated from the simulation as shown in Figure 5. The maximum support rotation of the keyed connection was 2.2^o when the barrier was subjected to the blast loading of 750 kg TNT at 5 m standoff distance. These results showed that the design of keyed connection was sufficient in providing axial restraint to the panels. The flexural failure of the post was the critical design limit in the barrier supported by the posts.

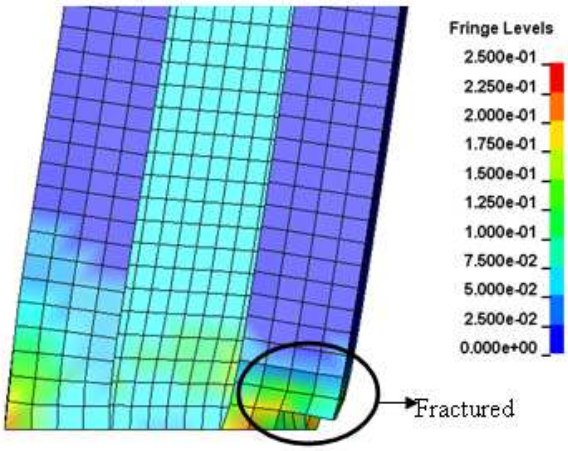


Figure 5: Fracture of the mild steel post at the base when the barrier was subjected to the blast loading of 750 kg TNT at a standoff distance of 5 m.

Summary

In this study, the response of non-composite SCS panel under post support conditions subjected to the blast loading was investigated. The prototype barrier with non-composite SCS panels is a viable alternative to the existing reinforced concrete blast wall. The prototype barrier have the potential lower construction cost and higher safety feature where not hazardous concrete fragments will be generated compared to the reinforced concrete blast wall.

References

[1] Smith, P.D. "Blast walls for structural protection against high explosive threats: A review." International Journal of Protective Structures 1 (2010), pp. 67-84.

[2] U.S. Department of the Army. Structures to Resist the Effects of Accidental Explosions, Technical Manual 5-1300, 1990.

[3] Crawford, J.E. and Lan, S.. "Blast barrier design and Testing", Structures Congress, St Louis, Missouri, USA (2006).

[4] Remennikov, A.M., Kong, S.Y. and Uy, B.. "Static and dynamic behaviour of non-composite steel-concrete-steel protective panels under large deformation", 4th International Conference on Steel & Composite Structures, 23-23 July 2010, Sydney, Australia.

[5] Remennikov, A.M., Kong, S.Y. and Uy, B.. "Impact resistance of non-composite axially restrained steel-concrete-steel sandwich panels", The 5th Civil Engineering Conference in the Asian Region and Australasian Structural Engineering Conference, 8-12 August 2010, Sydney, Australia.

[6] Kong, S.Y., Remennikov, A.M., Uy, B. "Numerical simulation of the response of non-composite steel-concrete-steel sandwich panels to impact loading". Australian Journal of Structural Engineering, Vol 12 (2012), No. 3.

[7] Hallquist, J.O. LS-DYNA keyword user's manual, Volume 1, Version 971. Livermore Software Technology Corporation (LSTC), 2010.

Applied Mechanics and Materials Vol. 567 (2014) pp 446-450
© (2014) Trans Tech Publications, Switzerland
doi:10.4028/www.scientific.net/AMM.567.446

POFA: A Potential Partial Cement Replacement Material in Oil Palm Shell Lightweight Aggregate Concrete

Khairunisa Muthusamy[1,a], Nur Azzimah Zamri[2,b]

[1,2] Faculty of Civil Engineering, Universiti Malaysia Pahang, 46300 Gambang, Pahang, Malaysia

[a]khairunisa@ump.edu.my,[b]nurazzimahzamri@yahoo.com

Keywords: Lightweight Aggregate Concrete, Palm Oil Fuel Ash, Oil Palm Shell, Partial Cement Replacement, Partial Coarse Aggregate Replacement

Abstract. Today, the necessity of environmental awareness and enforcement is more demanding and crucial than ever before. Environmental protection encompasses not only pollution but also sustainable development and conservation of natural resources and the eco-system. As a conclusion, protection and preservation of environment is still a pressing issue. This issue on environmental preservations and sustainability all over the world has lead to innovations of new material using by-products generated from various sectors such as palm oil industry. One of the potential recycle materials from palm oil industry is palm oil fuel ash which contains siliceous compositions and reacted as pozzolans to produce a stronger and denser concrete. Palm oil fuel ash (POFA) is by-product obtained by burning of fibers, shells and empty fruit bunches as fuel in palm oil mill boilers. Apart from POFA, oil palm shell (OPS), which also from oil palm waste has been used as lightweight aggregates resulting from never ending research conducted. In this investigation, these two types of waste were collected from the same palm oil mills in Kuantan, Malaysia and were both utilized inside lightweight aggregate concrete. By incorporating POFA and OPS as partial cement and coarse aggregate replacement, lightweight aggregate concrete with 35 MPa can be produced and is also significantly higher than control OPS concrete.

Introduction

In Malaysia, the generation of waste oil palm shell in increasing amount by local palm oil industry which disposed at landfill has lead the researchers to incorporate this material in lightweight concrete production. Palm oil fuel ash (POFA) is a recycle materials produced from palm oil industry which contains siliceous compositions and reacted as pozzolans to produce a stronger and denser concrete (Ahmad et al., 2008) [1]. The research had continued until the end of 20th century, where Salihuddin and Hussin (1993) have found this ash has high potential to be used as a cement replacement material but need to be grounded [2]. POFA need to be ground to increase its degree of fineness to improve its reactivity in concrete mixture that will improve the concrete properties.

So far OPS has been successfully incorporated as coarse aggregate replacement in lightweight concrete (Mannan and Ganapathy, 2001; Shafigh et al., 2012) and POFA being a pozzolanic material has been used as a partial cement substitute to produce various types of concrete (Abdul Awal, 1998; Sata et al., 2004; Megat Johari et al., 2012) [3-7]. However, the use of POFA as partial cement replacement in production of OPS lightweight aggregate concrete making yet to be explored. It is anticipated that formulation of OPS lightweight aggregate concrete integrating POFA to substitute the use of cement partially would produce a greener concrete and assist palm oil industry to be more environmental friendly.

Materials

The materials used in this study were consisted of ordinary Portland cement (OPC), palm oil fuel ash (POFA), oil palm shell (OPS), river sand, Type F superplasticizer and tap water. POFA and OPS was collected from single source palm oil mill in Gambang, Pahang, Malaysia. POFA was sieved passing 300 μm, oven-dried at 105 -110°C for 24 hours, and then ground using Los Angeles abrasion machine until they have reached the desired degree of fineness. The chemical compositions of OPC and POFA can be seen in Table 1.

Table 1: Chemical Composition of OPC and Palm Oil Fuel Ash

Chemical Constituents	OPC (%)	POFA (%)
Silicon dioxide (SiO_2)	16.05	51.55
Aluminium Oxide (AL_2O_3)	3.67	4.64
Ferric Oxide (Fe_2O_3)	3.41	8.64
Calcium Oxide (CaO)	62.28	5.91
Magnesium Oxide(MgO)	0.56	2.44
Sodium Oxide (Na_2O)	0.06	0.07
Pottasium Oxide (K_2O)	0.82	5.50
Sulphur Oxide (SO_3)	4.10	0.61

Ordinary Portland cement (OPC) which was conforming to Malaysian Standard MS 522: Part 1: 2007 for Portland cement specification from a single source was used throughout these experiments [8]. The cement used were stored away from damp floors and stacked close together in a well-aired, clean and dry place. The type of sand used throughout this study was river sand with a specific gravity of 2.68 and a fineness modulus of 2.62. The sand was air-dried before kept in container to protecting it from getting wet due to excessive moisture condition or rain from the surroundings.

Pozzolanic material used in this study was palm oil fuel ash (POFA) taken from Felda Lepar Hilir Gambang. The POFA was heated inside oven at 110±5° C for 24 hours to remove moisture before sieved and then grounded using grinding machine. In this study, oil palm shell (OPS) were used as lightweight coarse aggregate. The OPS were also taken from Felda Lepar Hilir Gambang. It was then sieved using 10 mm sieve and the OPS retained at 10 mm were taken. The OPS were then washed to removed oil and dirt. To preserve it, OPS were then air dried until the OPS turns into saturated surface dry (SSD) condition. After the drying process, the OPS were crushed using jaw crusher in order to obtain smaller particles.



Figure 1: Palm oil fuel ash (POFA)



Figure 2: Oil palm shell (OPS)

Mix Proportions and Test Methods. For 1 m^3 of concrete mix orders, 500 kg of cement, 870 kg river sand with fineness modulus of 2.62, 360 kg oil palm shell (OPS) and 4 litres of superplasticizer were used. The water/cement (w/c) ratio for this mix proportion was 0.45. For this

research experiment, the cement was replaced with 0%, 10%, 20%, 30%, 40% and 50% of palm oil fuel ash (POFA) by mass of cement. The concrete strength development was determined using compressive strength machine. 100 x 100 x 100 mm standard cubes were employed according to British Standard. The test was water cured and tested at the age of 7 and 28 days.

Results and Discussion

Physical and Chemical Properties of POFA. The raw POFA collected from palm oil mill is greyish in colour due to unburned carbon content in it. However, whitish ash is the best due to absence of unburnt carbon. The chemical analysis of palm oil fuel ash (POFA) and ordinary Portland Cement (OPC) used in this study are shown in Table 1. The chemical analysis reveals that POFA satisfies the requirement to be pozzolanic and may be classified into Class C. This justification is made base on the percentage of Calcium Oxide content in this POFA is 5.91 and silica, aluminium and ferric oxide is 64.83. Therefore, it is concluded that the POFA used in this study is from Class C.

Strength Investigation. As can be observed, the compressive strength developed for the 28-day samples is in the range of 21-35 N/mm² depending upon the percentage of cement replacement and it is quite above the requirement for structural lightweight agregate concrete with minimum compressive strength of 17 MPa [9]. The effect of POFA up to 30% replacement results in higher strength of concrete than control specimen.

This is due to the fact that fine POFA activates the pozzolanic property and improves the interfacial zone between the aggregates and the cement paste. The SiO_2 content in pozzolan reacts with free lime or calcium hydroxide ($Ca(OH)_2$) generated from the hydration process of cement to form calcium silicate hydrate gel (C-S-H) which fills up the voids between cement and aggregates thus increase the packing density. These reactions tend to improve concrete strength

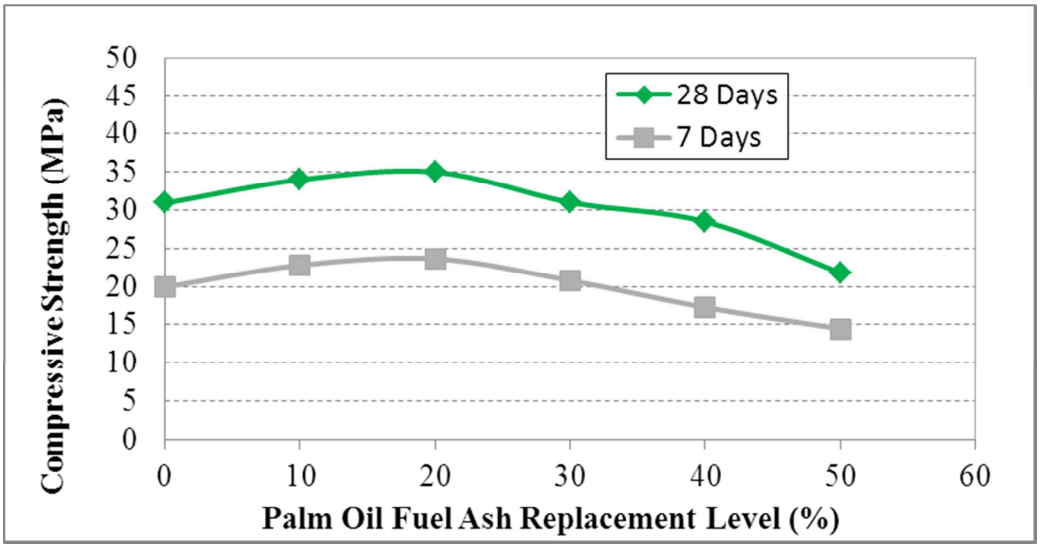


Figure 3: Effect of POFA Content on Compressive Strength of OPS Lightweight Aggregate Concrete at 7 and 28 days

Similar to the findings by Massazza (1993), the strength of specimen decreases when too much of POFA that function as partial cement replacement integrated in the concrete mix [10]. Evidently, replacement of 40 and 50% POFA causes the strength of concrete to decrease. This phenomenon shows that the negative effect resulting from the greatly amount of Portland cement that was been reduced. The concrete cube in Fig. 4 and 5 also shows abnormal failure when POFA added inside OPS lightweight aggregate concrete exceed 40%.



Figure 4: Concrete failure for OPS lightweight aggregate concrete containing 10% POFA



Figure 5: Concrete failure for OPS lightweight aggregate concrete containing 50% POFA

From the results, it is suggested that higher strength OPS lightweight aggregate concrete can be achieved by using a very high fineness palm oil fuel ash with appropriate amount of cement replacement. Moreover, the use of these two by-product materials as a substitution of coarse aggregate and partially replacement of cement type in concrete can reduce the quantity of coarse aggregate and cement in concrete making as well as reduce the quantity of waste material which results in more environmentally friendly.

Conclusion

Considering the results of the investigation mentioned in this paper, it can be concluded that higher strength of OPS lightweight aggregate concrete can be reached by utilizing fine POFA with appropriate amount of cement replacement. It is also possible to develop OPS lightweight aggregate concrete incorporating POFA as cement replacement for structural application that meets the requirement of BS and ASTM at 28-day of curing. It is also found that higher replacements of cement by POFA of more than 40% will results in significantly reduce the strength of OPS lightweight aggregate concrete incorporating POFA. OPS lightweight aggregate concrete incorporating POFA as cement replacement not only offers as a potential green construction material but also simultaneously reduces the solid waste dumped at the landfill.

Reference

[1] Ahmad, M.H., Omar, R.C., Malek, M.A., Md Noor, M. and Thiruselvam, S. 2008. Compressive strength of palm oil fuel ash concrete, ICCBT, 27 (2008) 297 – 306.

[2] Salihuddin, R. S. and Hussin, M. W., Palm oil fuel ash (POFA) as a future partial cement replacement material in housing construction. Proceedings of the International Symposium on Urban Housing: Issues on Environment and Technology, Bangkok, Thailand, (1993) 363-372.

[3] Mannan, M.A and C. Ganapathy, Mix design of oil palm shell concrete. Cement Concrete Research, 31 (2001) 1323-1329.

[4] Shafigh, P., M.Z Jumaat, H. Mahmud and N.A Abd Hamid, Lightweight concrete made from crushed oil palm shell : Tensile strength and effect of initial curing on compressive strength. Construction and Building Materials, 27 (2012) 252-258.

[5] Abdul Awal, A.S.M., A study on strength and durability performances of concrete containing palm oil fuel ash, University Teknologi Malaysia: PhD Thesis, (1998)

[6] Sata, V., C. Jaturapitakkul and K. Kiattikomol, Utilization of palm oil fuel ash in high-strength concrete. Journal of Materials In Civil Engineering, 16 (2004) 623-628.

[7] Megat Johari, M.A., A.M. Zeyad., N. Muhammad Bunnori and K.S. Ariffin. Engineering and transport properties of high-strength green concrete containing high volume of ultrafine palm oil fuel ash. Construction and Building Materials, 30 (2012) 281-288.

[8] Malaysian Standard. Portland cement (ordinary and rapid-hardening): Part 1: specification (second revision). Malaysia. MS 522: Part 1 (2003)

[9] Neville, A.M. Properties of concrete.4th Edition.Pearson Education Limited, (2005) 257, 689,698.

[10] Massazza, F., Pozzolanic cements. Cement and Concrete Composites, 15 (1993) 185 - 214.

Applied Mechanics and Materials Vol. 567 (2014) pp 451-456
© (2014) Trans Tech Publications, Switzerland
doi:10.4028/www.scientific.net/AMM.567.451

Precast Concrete Sheetpile For The Stabilization of Road Embankment on Soft Ground Adjacent to River

Nur Fadilah[1, a], Chong Yong Ong[2, b] and Kok Keong Choong[3,c]

[1]Rivo Precast Sdn Bhd, Lot 5127, Batu 6, Jalan Kenangan Off Jalan Meru, 41050 Klang, Selangor Darul Ehsan, MALAYSIA

[2,3]School of Civil Engineering, Universiti Sains Malaysia, Engineering Campus, 14300 Nibong Tebal, Seberang Perai Selatan, Pulau Pinang, MALAYSIA

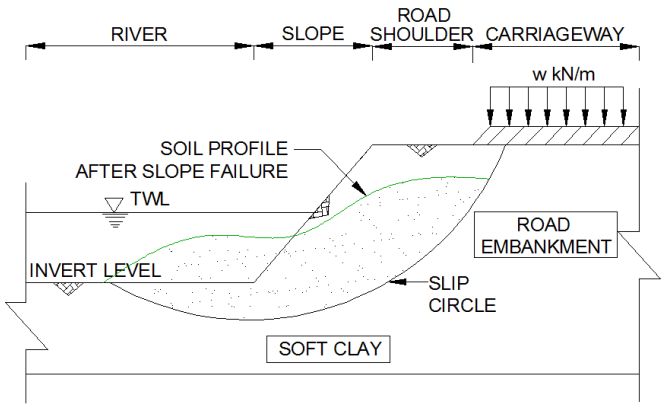
[a]rivoprecast@gmail.com, [b]cekkc@eng.usm.my

Keywords: road embankment; road settlement; soft ground; precast concrete sheet pile system

Abstract. Precast concrete sheetpile designed to restore and protect a road embankment, undergoing continuous settlement in soft ground condition in Jerlun and Kuala Sanglang in the state of Kedah, Malaysia is presented. The road built on soft ground has been in service for several years with some anticipated settlements. Major defects in the form of uneven settlements were spotted after few years of service. A survey was conducted and 5 spots along a 30m to 40m long stretch experiencing about 100mm settlements relative to the centerline of the road. Several attempts have been made to backfill and re-surface the affected areas but the road conditions did not last, posing danger to motorists. Investigations have revealed slip circles did occur at the affected areas with signs of lateral movements of earths towards the river. Precast concrete sheetpiles were designed to stabilize the road embankment to prevent further lateral movements of earth due to vehicular loads on the road. Analysis and design of the sheetpile system are presented. Construction aspects related to handling, installing and finishing works at site are highlighted.

Introduction

Today, due to the increasing number of vehicles used on roads, more roads are being constructed to cater for the massive traffic volume. They are now built across rivers, hills and mountains in order to link countries, cities or districts. For the roads built adjacent to river on soft ground, there is always problem caused by the road users. The major problem is the settlement of road embankment near to river. Fig. 1, shows the slip circle occurring at the affected area with the signs of lateral movements of earth towards the river.



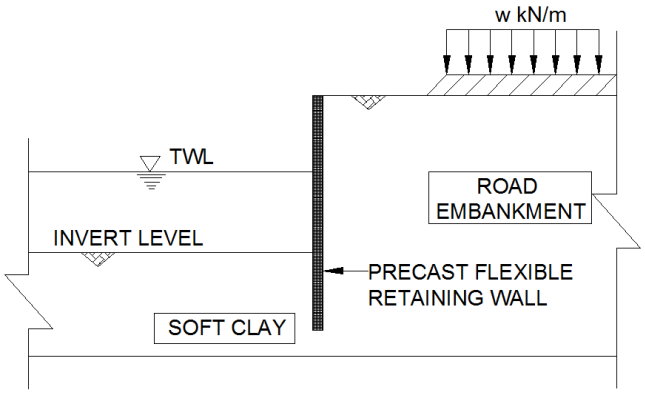
Figures 1. Slip circle in road embankment

Maintenance works such as backfilling and resurfacing the settled road have always been carried out. However, such measures are found to be not effective in the long run. In order to solve this problem, a new *Precast Concrete Sheetpile System* was developed.

Precast Concrete Sheetpile System

The development of reinforced concrete since late of 18th century by Francois Hennebique has brought the innovation to current concrete structures [1]. One of the current trend is to prefabricate components which is cost effective and short in construction period. Taking full advantage of the great features of precasting techniques, use of precast concrete sheetpile has been attempted as a solution to road embankment.

The basis of the above idea is that precast concrete flexible retaining wall in sheet pile form as shown in Fig.2, is able to provide protection to the road embankment effectively. The lateral earth pressure from road embankment and river bed has significant effect on the requirement of strength and stiffness of the precast concrete sheetpile. Therefore, adequate designed length of sheetpile is necessary in order to make the whole system functioning effectively.



Figures 2. Precast Concrete Sheetpile System as road embankment protection

Description of Projects

The above road embankment protection using precast concrete sheetpile has been implemented in two projects.

Project 1 (Jerlun, Kedah): The project site is located adjacent to the Korok River in the state of Kedah, Malaysia which supplies water to canal at northern part of Kedah paddy region. The road embankment is the only main road to the nearby town of Jitra. Below are some site constraints when carrying out the work:

(a) Limited space for stacking stock of precast concrete sheetpile
(b) The main road cannot be blocked during construction period
(b) Minimum disturbance and vibration by construction works due to village area nearby

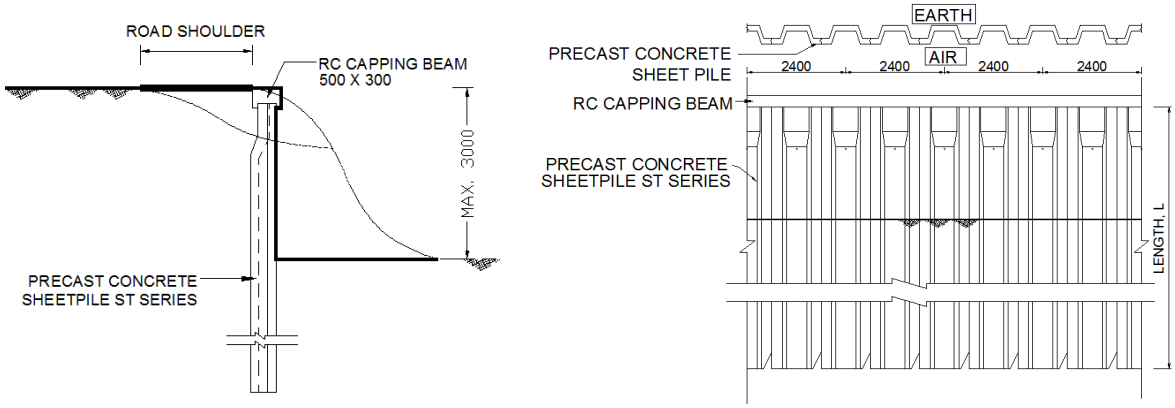
A total length on plan of 30 meters precast concrete sheetpile was built.

Project 2 (Kuala Sanglang, Kedah): The project site located adjacent to Fifth Sanglang Canal. The road embankment along the canal was finally decided to be blocked due to insufficiency of road width for traffic during construction. However, alternative road for the road users was provided. There are several site constraints when carrying out the work:

(a) Limited space for stacking stock of precast concrete sheetpile
(b) Minimum disturbance and vibration by construction works due to existence of electrical cables and village area nearby

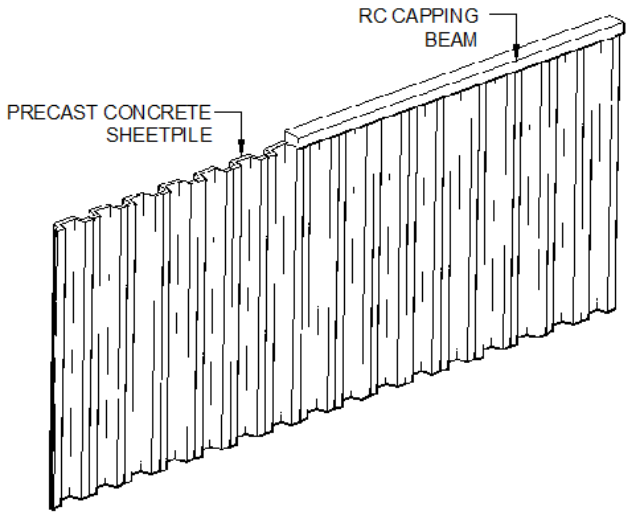
The total length on plan of precast concrete sheetpile constructed was 40 meters.

Fig.3a ,shows the typical section for both projects. The maximum exposed height is 3 meters. Precast sheetpile alignment was decided to be 2 meters from the road side. Elevation section for these two projects is shown in Fig.3b. Schematic diagram of precast concrete sheetpile is shown in Fig. 4.



(a) (b)

Figures 3. Precast concrete sheetpile: (a) Typical section, (b) Elevation section

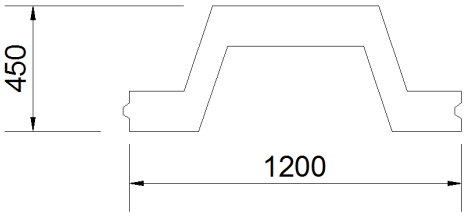


Figures 4. Schematic diagram of precast concrete sheetpile

Design and Development

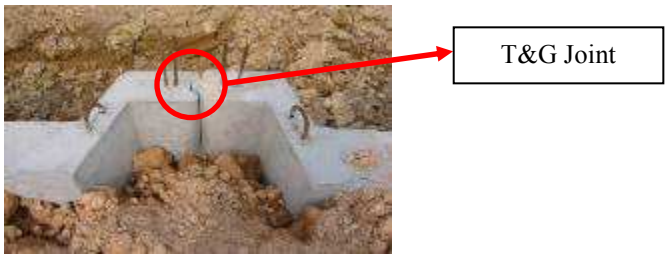
As mentioned earlier, proper design to ensure sufficiency of strength and stiffness of the precast concrete sheetpile has been carried out. This is important for the concrete sheetpile to function effectively as road embankment protection.

Sheetpile Section. Corrugated section as shown in Fig. 7, was chosen as it provides higher stiffness, section modulus and minimal self-weight [2]. Furthermore, rigid section with this corrugated profile may facilitate driving and handling process. Overall section of 450mm deep was selected with web and flange thickness (145 mm) containing reinforcing bars to provide adequate bending moment capacity as determined from structural analysis.



Figures 7. Corrugated section as precast concrete sheetpile section

Joint. Precast concrete sheetpile system consists of a series of precast concrete sections which were connected to each other by means of Tongue and Groove (T & G) joints to produce a continuous wall system [3]. The specially designed joint is shown in Fig. 8.



Figures 8. Tongue and groove joint of precast concrete sheetpile system

Sheetpile Length. Under different soil condition, the length of precast concrete sheet pile for Jerlun site and Kuala Sanglang site was determined to be 7.5 meters and 12.0 meters, respectively.

Design Data. Precast concrete sheetpile was designed considering all the following aspects: functionality, constructability from the point of view of precast technology – transportation, connection or joint, casting, de-moulding and stacking and site installation. To fulfill the above requirement, designed parameter values have been assigned practically. Table 1 shows the design data of precast concrete sheetpile.

Table 1. Design data of precast concrete sheetpile

Design Data	Unit	Value
Surcharge load	kN/m^2	10
Retained soil internal friction angle	degree	33
Retained soil density	kN/m^3	19
Soil active coefficient. K_a	-	0.29
Soil passive coefficient, K_p	-	3.39
Load factor for earth lateral pressure	-	1.4
Load factor for surcharge lateral pressure	-	1.5
Grade of concrete for Precast Concrete Sheetpile	N/mm^2	40

Design Code. Precast concrete sheetpile was designed based on BS 8110: Part 1:1997 and BS 8002: 1994 [4-5] using Retaining Wall Analysis Program.

Transporting. The overall dimension was designed not only to cater for functionality and structural requirement, but also transportability. Fig.9 shows a total of eight units concrete sheetpiles have been stacked on each other for the purpose of transportation.



Figures 9. Eight precast units on a trailer for transportation to site

Construction Sequence

Precast concrete sheetpile were cast in factory and delivered to site for installation by trailer and unloaded to the designated place using mobile crane as shown in Fig. 10.



Figures 10. Lifting of precast concrete sheetpile from trailer to storage area in site

The following sequence has followed during the construction of the precast concrete sheetpile wall.

Step 1: Setting out and preparation of working platform (Fig.11a). Wall alignment was set up by surveyor. Then, working platform and storage concrete sheetpile area were prepared.

Step 2: Pitching, aligning and inserting (Fig.11b and Fig. 11c). Precast concrete sheetpile were pitched and aligned at the designated points. Then, they were placed in a row with units butting each other.

Step 3: Driving (Fig.11d). Excavator Vibro PC400 with minimum noise due to vibration was used to drive the precast concrete sheetpiles to the required penetration depth.

Step 4: Constructing reinforced concrete capping beam. After steel reinforcement and timber formwork were placed in accurate position, capping beam was cast.

Step 5: Backfilling. The back of the wall was backfilled to the designated level with suitable material.



(a) (b) (c)

Figures 11. Installation sequence; (a) Pitching; (b) Aligning and placing in position; (c) Driving

The completed views of the two projects are shown in Fig. 12a and Fig. 12b.



(a) (b)

Figures 12. Completed view; (a) Jerlun, Kedah; (b) Kuala Sanglang, Kedah

Concluding Remarks

Development and construction of precast concrete sheetpile system in road embankment protection has been described. The effectiveness of the system as a solution in terms of functionality and structural capability has been illustrated via two projects in Jerlun and Kuala Sanglang in the state of Kedah, Malaysia. Site limitations were easily overcome with this innovative construction method. With the development of precast concrete sheetpile system, it can be further explore in new applications such as building platform or petrol tank pit earth retention. Hence, it is anticipated that this precast concrete sheetpile system will offer a better solution to sustainable earth retaining construction in the near future.

References

[1] D.G. Mcbeth, F. Hennebique and L.G. Mouchel, Francois Hennebique (1842-1921), Reinforced Concrete Pioneer, Proceeding of the ICE – Civil Engineering, Volume 126, Issue 2, 1998, pp. 86-95

[2] G.E. Tan, T.B. Ong, K.K Choong and C.Y. Ong, A New Form of Precast Closed Spandrel Arch Bridge System, Proceedings of the 7th International Conferences on Arch Bridges, 2013, pp. 195 – 202

[3] Product Brochure: Rivo Precast Concrete Sheetpile Wall by Rivo Precast Sdn Bhd, 2011.

[4] British Standard Institute. BS 8110:Part 1:1997, Structural use of concrete: Code of practice for design and construction, ISBN 0 580 26208 1, 1997.

[5] British Standard Institute. BS 8002:1994, Code of practice for earth retaining structures, ISBN 0 580 22826 6, 2001.

Applied Mechanics and Materials Vol. 567 (2014) pp 457-462
© (2014) Trans Tech Publications, Switzerland
doi:10.4028/www.scientific.net/AMM.567.457

Precast Concrete Soldier Pile System with Corrugated Section Post for Riverbank Protection

Nur Akmilah[1, a], Chong Yong Ong[2, b] and Kok Keong Choong[2,b]

[1]Rivo Precast Sdn Bhd, Lot 5127, Batu 6, Jalan Kenangan Off Jalan Meru, 41050 Klang, Selangor Darul Ehsan, MALAYSIA

[2]School of Civil Engineering, Universiti Sains Malaysia, Engineering Campus, 14300 Nibong Tebal, Seberang Perai Selatan, Pulau Pinang, MALAYSIA

[a]rivoprecast@gmail.com, [b]cekkc@eng.usm.my

Keywords: precast concrete soldier pile system, precast post, precast lagging, scouring, riverbank protection, corrugated section

Abstract. Gabions, rubble stone walls, L-shape concrete retaining wall and revetments are commonly used for riverbank protection against base scouring and soil slope erosion. These conventional solutions for low retaining wall structures are relatively cheap and easy to execute. However, they are proven not lasting with high maintenance costs. Although steel sheetpile walls are structures with better performance for slope stabilization purpose, they are very expensive to build and maintain against corrosion. To address the problem, a new precast concrete soldier pile wall system was developed to provide a permanent and relatively economical solution with several innovative features. The system is comprised of a series of precast posts driven to the predetermined depth and secondary precast lagging elements secured between posts to support the retained earths. The structural capacity that resists lateral load is derived from passive earth pressure mobilized in front the embedded body to toe of the posts. The lagging elements are installed at 0.5m to 1.0m below the river invert levels to provide protection against base scouring. The precast posts and laggings take the efficient structural shape of corrugated section. They are jointed with a specially designed tongue and groove (T&G) slots to facilitate installation. A pilot project where such innovative solution is presented.

Introduction

Malaysia is known to be one of the countries which is rich in natural resources. One of the natural resources is water from river. From statistic of Department of Irrigation and Drainage Malaysia 2006, Malaysia has a total length of 57 300 km river which is equivalent to 189 river systems [1]. The most common river channel pattern is meandering pattern. Figure 1 represents the plan view of meandering pattern. At the concave part of the river, bank erosion or scouring phenomenon happens; whereas at the convex part of the river, bank deposition phenomenon happens. Scour occurs when the hydrodynamic bottom stresses is more than sediment critical shear stress [2]. Figure 2 shows the formation of scour hole resulted from river wave and river current action. Immediate action need to be taken to protect the riverbank from being continuously scoured. Sheetpile retaining wall offers one solution. Steel sheetpile walls are widely used and pose better performance in terms of slope stabilization. However, they are not cost effective to build to be permanent structures as they are not corrosion resistance. In order to overcome this problem, a *Precast Concrete Soldier Pile System* was developed and introduced.

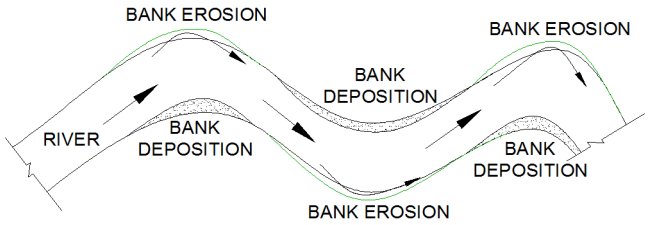


Figure 1: Plan view of meandering channel pattern

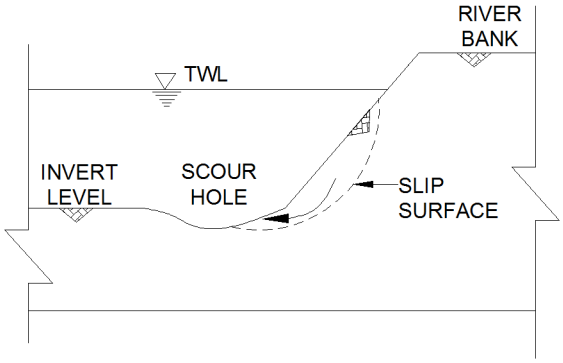


Figure 2: Formation of scour hole at the toe of riverbank

Precast Concrete Soldier Pile System

In order to achieve speedy construction for scouring prevention, solution using precasting technique was adopted. Precast concrete soldier pile system comprises of two major components; precast post and precast lagging (See Figure 3). Precast post acts as primary support to the retained soil and precast lagging or panel acts as secondary support to soil face. The mechanism of soil loads transfer in precast concrete soldier pile is that the soil loads transferred partially via the lagging and partially via the soil arching. When the soil between the precast posts is able to self support, the soil loads will be transmitted to adjacent precast post. Hence, passive earth pressure in front the embedded body to the toe of post may stabilize the system as well. Usually, the lagging element are installed at 0.5 meter to 1 meters below the river invert level to provide the protection against base scouring.

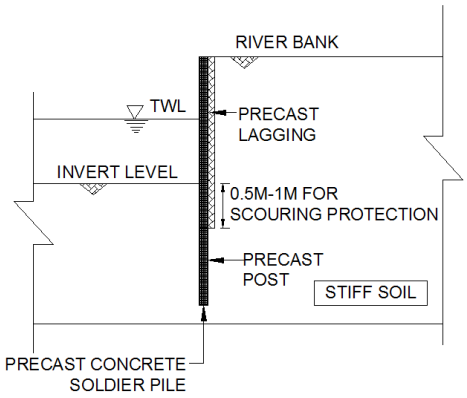


Figure 3: Precast soldier pile system for scouring protection

Description of the Project

The project site is located at riverbank of Langat River, Carey Island, Banting in the state of Selangor Darul Ehsan, Malaysia. Site location and channel pattern of Langat River are shown in Figure 4. As described earlier in Introduction, erosion always occurs at the concave part of the Langat River. Thus, the scouring protection location was decided to be at the concave part of Langat River (as shown in

red circle of Figure 4 and site photo in Figure 5). Figure 6 represents the typical section and elevation view of the project. The schematic diagram of precast concrete soldier pile system for this project is presented in Figure 7. Total length on plan of 220.30 meters precast concrete soldier pile system was built.

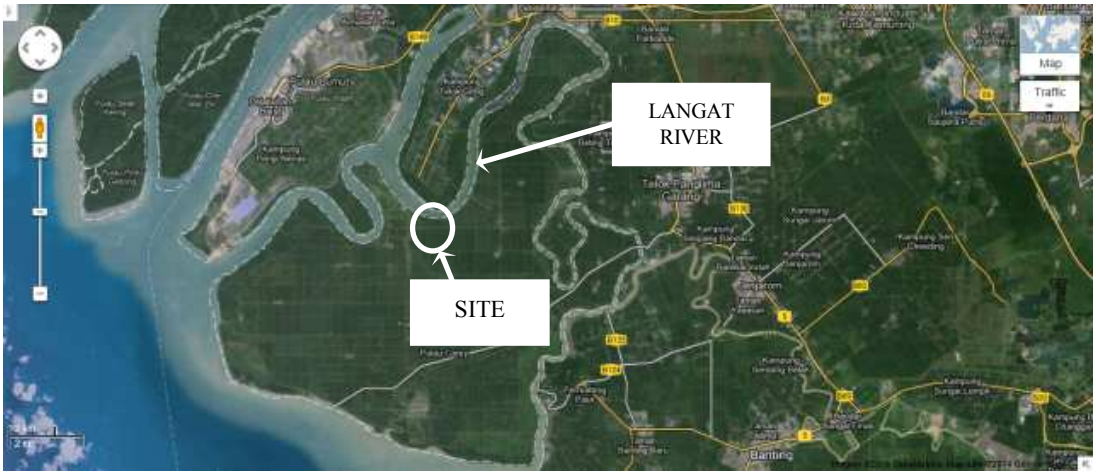
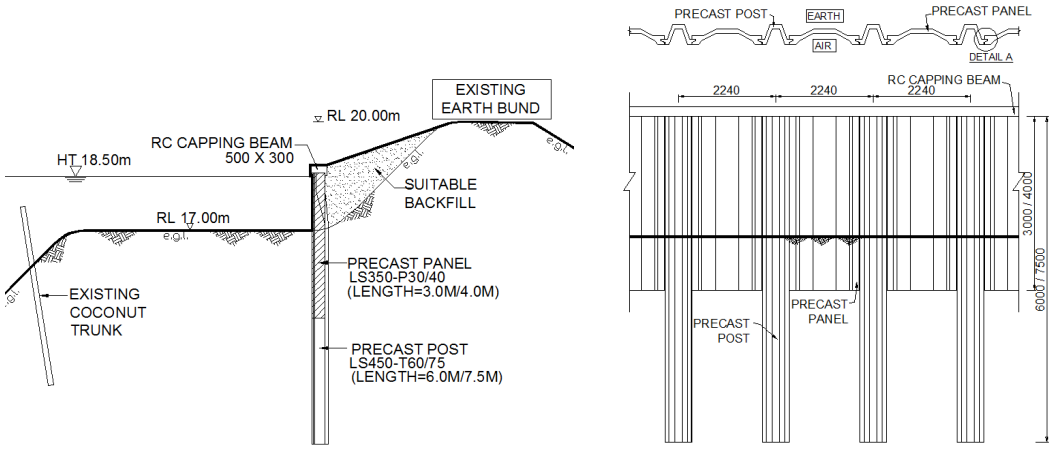


Figure 4: Channel pattern of Langat River and site location from Google Map



Figure 5: Erosion at riverbank of Langat River



(a) (b)

Figure 6: Precast concrete soldier pile system: (a) Typical section, (b) Elevation View

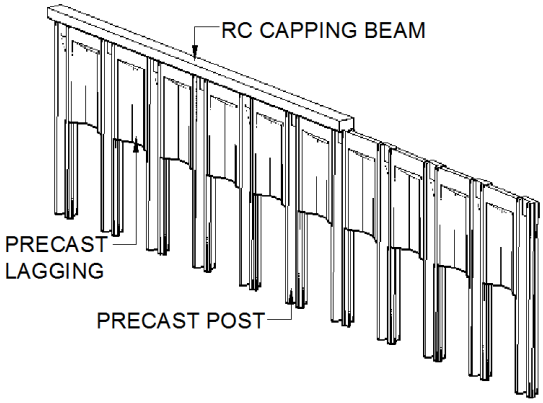
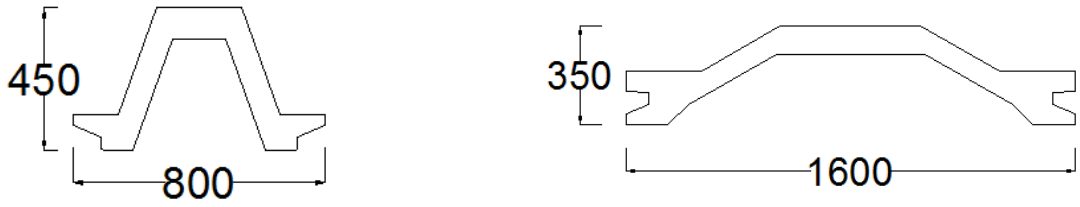


Figure 7: Schematic diagram of precast concrete soldier pile system

Design and Development

Precast Post and Precast Lagging Section. Corrugated section with high stiffness property was chosen as section for precast post and precast panel (see Figure 8). Furthermore, rigid section with this corrugated profile may facilitate driving and handling process. Overall section of 450 mm deep and 350 mm deep for precast post and precast panel, respectively were determined to resist the ultimate bending moment determined through structural analysis.



(a) (b)

Figure 8: Precast concrete soldier pile system; (a) Corrugated section of precast post; (b) Corrugated section of precast lagging

Joint. Tongue and Groove (T & G) slots are specially designed to facilitate the installation (see Figure 9). This joint will produce a continuous wall system.

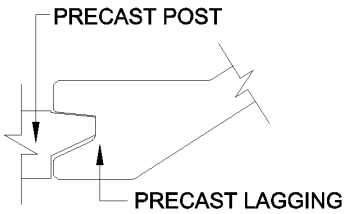


Figure 9: Tongue and groove joint of precast concrete sheetpile system

Length of Precast Post and Precast Lagging. From the result of Mackintosh Probe, 6 meters length of precast post was finally determined. As the height from top capping beam to river invert level is 1.5 meters, the precast lagging length was decided to be 3 m. However for the stretch with very serious eroded rivebank in front of the bund wall, longer post with 7.5m length and longer panel with 4m length are used in order to increase the service life span of these wall system.

Design Data. Precast concrete soldier pile system with concrete grade 40 MPa was designed considering all the following aspects: functionality, constructability from the point of view of precast technology – transportation, connection or joint, casting, de-moulding and stacking and site installation. Effective stress analysis was carried out for long term assessment. Table 1 shows the design data of precast concrete soldier pile system. Soil layer 1 indicates the depth from 0.00m to 2.5m from top of pile, whereas soil layer 2 indicates the depth from 2.5m to 7.5m from top of pile.

Table 1: Design data of precast concrete soldier pile system

Design Data	Unit	Soil Layer 1	Soil Layer 2
Retained soil internal friction angle	degree	28	29
Retained soil density	kN/m^3	18	19
Soil Cohesion	kN/m^2	10	12
Soil active coefficient. K_a	-	0.36	0.35
Soil passive coefficient, K_p	-	2.77	2.88
Surcharge load	kN/m^2	17	
Load factor for earth lateral pressure	-	1.4	
Load factor for surcharge lateral pressure	-	1.5	

Table 2: Effective stress analysis results

Conditions/ Results	6m length Precast Post and 3m length Precast Panel	7.5m length Precast Post and 4m length Precast Panel	7.5m length Precast Post and 3m length Precast Panel
FOS	4.01	2.34	2.80
Max BM, kNm	91.61	141.50	113.95
Max SF, kN	57.67	72.75	64.57

The maximum bending moment of 141.50 kNm and maximum shear force of 72.75 kN were used to carry out reinforced concrete design for reinforcement in the precast post and precast lagging.

Design Code. Precast concrete soldier pile system was designed based on BS 8110: Part 1:1997 and BS 8002: 1994 [3-4].

Transporting. The dimensions were designed considering functionality, required structural ability and also transportability.

Construction Sequence

After the casting of precast concrete soldier piles was completed in factory, they were delivered to site for installation by trailer in several trips. They were unloaded to the designated place using mobile crane. Before starting installation at site, wall alignment was set up. Then, precast solder pile units were pitched, aligned and inserted at the required position (see Figure 10).



Figure 10: Pitching of precast panel

Drop hammer was used to drive the precast concrete soldier pile to the required level in sequence. Then, the riverbank slope was backfilled. Lastly, insitu capping beam was cast. The completed installation views of Carey Island, Banting, Selangor project before and after capping beam casting are shown in Figure 11a and Figure 11b, respectively.



(a) (b)

Figure 11: Completed installation view at Carey Island, Banting, Selangor; (a); Before capping beam casting; (b) After capping beam casting

Concluding Remarks

Scouring protection using precast concrete soldier pile system in a project at Carey Island, Banting in the state of Selangor, Malaysia has been described. Use of the innovative section properties of the precast post and precast lagging was proven to be a practical solution in protecting the riverbank from scour. Further exploration on the usage in shore protection, bridge pile cap scouring protection and waterfront structures are currently underway. Besides, further research on precast post section in stiffer soil will be carried out in order to ensure easiness of driving in during installation.

References

[1] Department of Irrigation and Drainage. (2009). Manual and guidelines for water management.

[2] A.H. Steven, Scour and Scour Protection, The Coastal Infrastructure Design, Construction and Maintenance Training Workshop Course 4: Design of Maritime Structures, 2001.

[3] British Standard Institute. BS 8110:Part 1:1997, Structural use of concrete: Code of practice for design and construction, ISBN 0 580 26208 1, 1997.

[4] British Standard Institute. BS 8002:1994, Code of practice for earth retaining structures, ISBN 0 580 22826 6, 2001.

Applied Mechanics and Materials Vol. 567 (2014) pp 463-468
© (2014) Trans Tech Publications, Switzerland
doi:10.4028/www.scientific.net/AMM.567.463

Prediction of Failure Loads of RC Dapped-End Beams

Muhammad Aswin[1,a], Zubair Imam Syed[1,b], Teo Wee[1,c], M.S. Liew[1,d]

[1]Department of Civil Engineering, Faculty of Engineering, Universiti Teknologi PETRONAS, Bandar Seri Iskandar, 31750, Tronoh, Perak, Malaysia.

[a]aswin_tekniksipil@yahoo.com, [b]imam.syed@petronas.com.my, [c]teo_wee@petronas.com.my, [d]shahir_liew@petronas.com.my

Keywords: failure loads, reinforced concrete, dapped-end beams, Strut and Tie Model

Abstract. Shear failure remains the governing mode of failure for reinforced concrete (RC) dapped-end beams. Dapped-ends are commonly classified as disturbed regions (D-regions). Strut and tie model (STM) is a simple and rational way that can be applied to analyze D-regions. The current design codes such as ACI-318-08, Euro Code 2 and BS 8110 facilitate STM to predict the failure loads. In addition, the failure loads may be also predicted using the empirical method proposed in PCI Design Handbook. In this paper, the failure loads were predicted for 24 RC dapped-end beams following different codes. The significant parameters such as concrete compressive strength, dapped-end section size, shear span-depth ratio, type and effective range of stirrups, bent form of the longitudinal reinforcement, amount of dapped-end reinforcements and hanger reinforcements were varied to study their effects against the predicted failure load for RC dapped-end beams according to different codes. These predicted results were compared with the available experimental results to investigate the ability of various codes to predict the failure load reliably. In this study, the comparison shows that PCI Design Handbook and ACI-318-08 can predict the failure loads for RC dapped-end beams more accurately.

Introduction

The RC dapped-end beams are frequently used in concrete bridge girders and precast concrete constructions [1]. These beams enable the construction depth of a precast concrete floor or roof structure to be reduced, by recessing the corbels supporting into the depth of the beams supported. They are mainly used in drop-in beams between corbels (Fig.1a), as part of beam-to-beam connection (Fig.1b) and in suspended spans between cantilevers (Fig.1c). Mattock and Chan (1979) stated that the use of dapped-end beams facilitates the erection of a precast concrete structure, due to the greater lateral stability of an isolated dapped-end beam than that of an isolated beam supported at its bottom face [2].

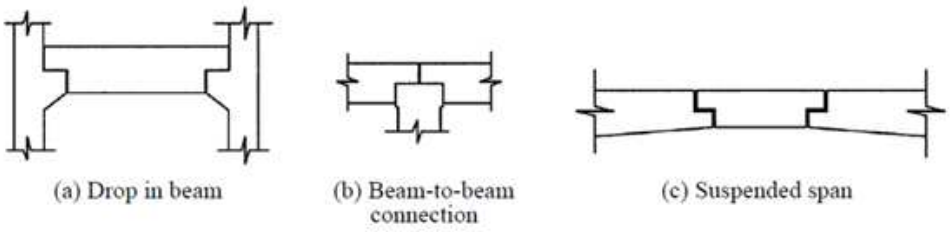


Figure1. Application of dapped-end beams [2]

Although dapped-end beams provide better lateral stability and reduce the construction height of precast concrete floors, very few studies on in-depth behavior of such members have been conducted in the past [3]. Some experimental investigations and development of analytical methods had been performed in order to predict the strength capacity of RC dapped-end beams. Lu et al.[2] indicated that shear strength of dapped-end beams increases with enhancement of concrete compressive strength, amount of main dapped-end reinforcements, and decrement of nominal shear

span-depth ratio. Whereas other study [4] proved that dapped-end beams exhibited the different shear capacity with variation of nib depth and shear span-depth ratio. Peng [5] demonstrated that RC dapped-end beams with proper anchorage and hanger reinforcement details have a higher strength capacity and some ductility even after yielding of hanger reinforcement. Experimental study on the shear resistance behavior of RC dapped-end beams was investigated on 24 test specimens until failure load [6]. In this study, to predict shear strength, the considered main parameters were dapped-end height, type and effective range of stirrups and bent form of the longitudinal reinforcement.

Dapped-end are commonly classified as discontinuity regions (D-regions) caused by abrupt change in beam depth and also due to presence of support point, consequently stress flow around the discontinuity is severely disturbed [7-10]. One way that can be applied to analyze the D-regions is the use of strut and tie model (STM), a simple and rational way. This method involves selection of an appropriate truss model on RC members to be analyzed, which is usually performed iteratively.

In this study, the failure load of RC dapped-end beams were predicted using STM model related to the current codes such as ACI 318-08 [11], Euro Code 2: BS EN 1992-1-1 [12], and British Standard: BS 8110-1 [13]. The failure loads were also calculated based on the empirical method specified in PCI Design Handbook [14]. The predicted failure load using different codes were compared to the available experimental results [6] to investigate the performance of current codes in estimating the failure loads of RC dapped-end beams.

Details of Specimens under Study

In this study, data of RC dapped-end beams tested by Wang et al. [6] were used to predict the failure loads according to different codes. The tests conducted on dapped-end beams by Wang et al. consist of three series, B1, B2 and B3. The overall dimensions of the used specimens in the tests are shown in Figure 2. All tested beams had the same length of 1500 mm. The reinforcement details and dimension of different series of beams are shown in Figure 2 (a-d). The test specimens were subjected to four-point-bending in a compression machine. The top steel spreader beam was used to divide the total applied load from machine head into two equal point loads as shown in Figure 2 (e). The load was applied until failure occurred.

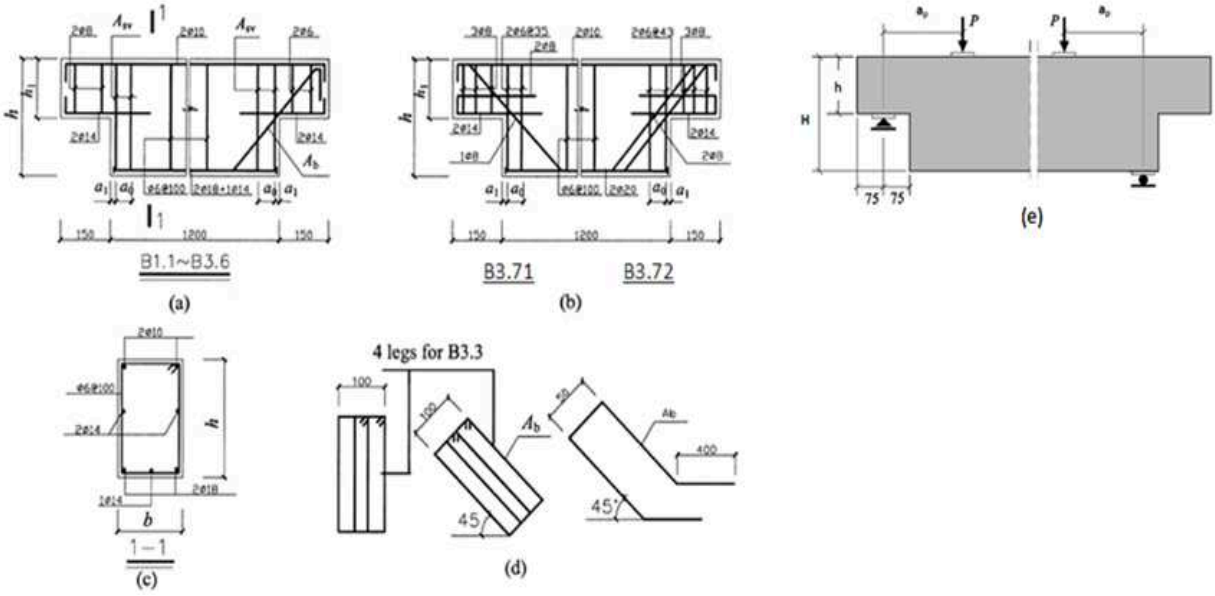


Figure 2. Test specimen details and experimental setup [6]

Strut and Tie Model (STM) and Potential Failure Modes

To obtain the final STM configuration as shown in Figure 3, a trial and error procedure was adopted in this study following the methods discussed previously by other researches [4,7,9,10,15,16]. To attain the position of struts and ties in the truss model, the potential failures modes discussed in PCI Design Handbook was also considered and steel reinforcement lay out of the test specimens [6] was taken into account.

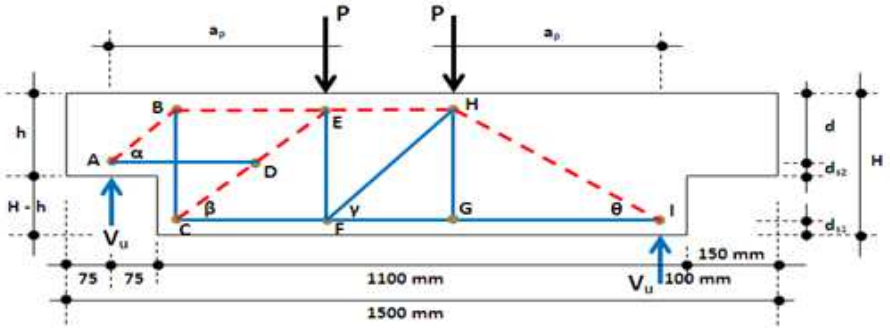


Figure3. STM configuration

ACI and EC do not provide specific guidance on STMs for different cases but their common provisions could be applied for the use of certain STM. In the other hand, the provisions of STM in BS are not clearly mentioned, but basically it can clarify that STM may be used for analysis. Based on STM configuration above, the internal force equilibrium yields: Strut AB = P/sinα, Strut BE = Pcotgα, Strut CD = P/sinβ, Strut DE = P/sinβ, Tie EF = 0, Tie AD = Pcotgα, Tie BC = P, and Tie CF = Pcotgβ. To determine the strength of tie members, [11-13] has the different values of strength reduction factor (φ) for steel reinforcement namely: 0.75; 0.87; 0.95, respectively. These conditions also can provide different values of the predicted failure load of RC dapped-end beams.

Five potential failure modes of RC dapped-end beam were established on PCI [14]. The considered failure modes are failures due to flexure and axial tension in extended end, direct shear at junction of dap and the component main body, diagonal tension emanating from reentrant corner, diagonal tension in extended end, and diagonal tension in un-dapped portion. According to the empirical method specified in PCI, the smallest value of strength capacity which calculated from following conditions is taken as the predicted failure load of RC dapped-end beams:

1. The flexure and axial tension in the nib.

   $A_s = [V_u * (a/d) + N_u * (h/d)]/ (\varphi * f_y)$ (1)

   Where $V_u = P$; φ = strength reduction factor = 0.75; and assumed that $N_u = 0$

2. Direct shear

   $A_s = (2*V_u)/(3*\varphi*f_y*\mu_e) + (N_u/ (\varphi*f_y)$ (2)

   $\mu_e = (1000*\varphi*\lambda*b*h*\mu)/ V_u$ (3)

   Where $\mu_e \leq 3.4$; λ = 1 for normal weight concrete; and μ = shear-friction coefficient = 1.4*λ

3. Hanger reinforcement for diagonal tension at reentrant corner

   $A_{sh} = T_{BC}/ (\varphi * f_{yp})$ (4)

   Where $T_{BC} = V_u = P$; and f_{yp} = the yield stress of hanger reinforcement

4. Diagonal tension in the nib

   $A_v = [(V_u/ \varphi) - 2*\lambda*b*d*\sqrt{f_c'}]/ (2*f_{yv})$ (5)

   f_{yv} = the yield stress of vertical reinforcement in the nib

Results and Discussion

The failure loads of RC dapped-end beams in this study were calculated using the mentioned codes and summarized together with the available experimental results as seen in Table 1. In Table 1, f_y represents yield stress of steel reinforcement, f_{cu}' is concrete compressive strength of standard cube, f_c' (f_{ck}) is cylinder concrete compressive strength, b and H are width and depth of beam, h and d are height and effective height of dapped-end, respectively. The shear span-depth ratio is denoted by λ_p, and a_p is shear span or distance from the applied load point to support, a_1 is the distance of the first stirrup to the end face of dapped-end beam, a_0 is the effective range of stirrups, and a is distance of support to center of hanger reinforcements. The considered parameters such as concrete compressive strength, dapped-end section size, shear span-depth ratio, type and effective range of stirrups, bent form of the longitudinal reinforcements, amount of dapped-end reinforcements and hanger reinforcements, it turns out provide effect against the predicted failure load of RC dapped-end beams.

Table 1.Test specimen details and analysis results

Series	No.	Concrete Strength		Dimensions													Hanger Reinforcement	Failure Load (kN)					Comparison of Failure Load			
										Range of Stirrups																
		f'_{cu}	$f'_c = f_{ck}$	b	H	h	d	D	L_{stb}	a_1	a_0	$a' = x_2$	a	a/d	$\lambda_p = a_p/d$	a_p	$A_{sh} = A_{sv,2}$	Test	ACI	BS	EC	PCI	ACI	BS	EC	PCI
		MPa	MPa	mm	mm	mm	mm	mm	mm	mm	mm	mm	mm	-	-	mm	mm	V_u^T	V_u^{ACI}	V_u^{BS}	V_u^{EC}	V_u^{PCI}	V_u^T/V_u^{ACI}	V_u^T/V_u^{BS}	V_u^T/V_u^{EC}	V_u^T/V_u^{PCI}
I	**B1.11**	16.90	11.32	214	370	170	145	345	150	50	50	75	150.00	1.03	3.38	490.10	1φ8 + 1φ14 (90^0)	58.77	76.31	96.90	88.47	76.89	0.7702	0.6065	0.6643	0.7643
	B1.12	16.90	11.32	214	370	164	139	345	150	60	60	75	165.00	1.19	3.23	448.97	1φ6	42.24	36.63	46.51	42.47	36.66	1.1532	0.9081	0.9946	1.1524
	B1.21	16.01	10.73	220	370	190	165	345	150	105	105	75	232.50	1.41	2.83	466.95	1φ8 + 1φ18 (45^0)	65.00	61.82	78.51	71.68	56.45	1.0514	0.8280	0.9068	1.1515
	B1.22	16.01	10.73	220	370	160	135	345	150	45	87	75	184.50	1.37	3.13	422.55	2φ8 @ 42	72.98	72.86	92.52	84.48	58.20	1.0016	0.7888	0.8639	1.2540
II	**B2.11**	19.53	13.09	150	300	150	125	275	150	30	30	75	120.00	0.96	2	250.00	1φ6	34.75	36.63	46.51	42.47	36.66	0.9487	0.7471	0.8182	0.9480
	B2.12	19.53	13.09	150	300	150	125	275	150	100	100	75	225.00	1.80	2	250.00	1φ6	31.75	36.63	46.51	42.47	36.66	0.8668	0.6826	0.7476	0.8662
	B2.21	19.53	13.09	150	300	150	125	275	150	30	100	75	190.00	1.52	2	250.00	2φ6 @ 70	55.22	73.26	93.03	84.94	52.33	0.7538	0.5936	0.6501	1.0552
	B2.22	19.53	13.09	150	300	150	125	275	150	40	104	75	199.00	1.59	1.9	237.50	2φ6 @ 64	65.83	69.12	87.77	80.14	49.96	0.9524	0.7500	0.8215	1.3177
	B2.31	19.53	13.09	150	300	150	125	275	150	40	40	75	135.00	1.08	1.87	233.75	1φ6 + 1φ14 (45^0)	75.73	69.12	87.77	80.14	73.65	1.0956	0.8628	0.9450	1.0283
	B2.32	19.53	13.09	150	300	150	125	275	150	75	75	75	187.50	1.50	2	250.00	1φ6 + 1φ14 (45^0)	65.00	52.99	67.29	61.44	53.03	1.2266	0.9660	1.0580	1.2258
III	**B3.11**	25.89	18.12	150	315	160	130	290	150	30	60	75	150.00	1.15	2.31	300.30	2φ6 @ 30	60.00	75.66	96.08	87.72	68.90	0.7930	0.6245	0.6840	0.8708
	B3.12	25.89	18.12	150	315	160	130	290	150	22	52	75	138.00	1.06	2.31	300.30	2φ6 @ 30	70.00	81.90	104.00	94.96	74.89	0.8547	0.6731	0.7372	0.9347
	B3.21	25.89	18.12	150	300	150	120	275	150	25	60	75	147.50	1.23	2.5	300.00	2φ6 @ 35	66.00	71.50	90.79	82.90	64.68	0.9231	0.7269	0.7962	1.0204
	B3.22	25.89	18.12	150	300	150	120	275	150	45	75	75	172.50	1.44	2.5	300.00	2φ6 @ 30	50.00	59.58	75.66	69.08	55.30	0.8392	0.6608	0.7238	0.9042
	B3.31	22.82	15.97	150	305	150	120	280	150	50	50	75	150.00	1.25	2.5	300.00	1φ6 + 4 legs	52.20	57.20	72.63	66.32	63.60	0.9126	0.7187	0.7871	0.8208
	B3.32	22.82	15.97	150	305	150	120	280	150	20	65	75	150.00	1.25	2.5	300.00	2φ6 @ 45 + 4 legs	63.00	75.26	95.57	87.26	63.60	0.8371	0.6592	0.7220	0.9906
	B3.41	22.82	15.97	150	310	100	75	285	150	30	30	75	120.00	1.60	4.07	305.25	1φ6	26.80	37.83	48.04	43.86	40.53	0.7084	0.5579	0.6110	0.6613
	B3.42	22.82	15.97	150	310	100	75	285	150	40	40	75	135.00	1.80	4	300.00	1φ6	26.40	34.54	43.86	40.05	40.53	0.7643	0.6019	0.6592	0.6514
	B3.51	22.82	15.97	150	305	155	125	280	150	30	30	75	120.00	0.96	2.4	300.00	1φ6 + 1φ14 (45^0)	79.10	71.88	91.27	83.34	82.81	1.1005	0.8666	0.9492	0.9552
	B3.52	22.82	15.97	150	305	150	120	280	150	30	30	75	120.00	1.00	2.5	300.00	1φ6 + 1φ14 (45^0)	75.00	68.10	86.47	78.95	79.50	1.1014	0.8674	0.9500	0.9434
	B3.61	22.67	15.19	150	300	150	128	275	150	38	68	75	147.00	1.15	2.34	299.52	2φ6 + 1φ14 (90^0)	63.20	74.52	94.63	86.40	69.22	0.8481	0.6678	0.7315	0.9130
	B3.62	22.67	15.19	150	300	150	128	275	150	23	58	75	127.00	0.99	2.42	309.76	2φ6 + 1φ8 (slope legs)	92.80	85.93	109.12	99.63	80.12	1.0800	0.8505	0.9315	1.1582
	B3.71	22.67	15.19	150	300	150	128	275	150	23	58	75	144.50	1.13	2.34	299.52	2φ6 @ 35 + 1φ8 (45^0)	90.00	116.55	148.00	135.13	116.63	0.7722	0.6081	0.6660	0.7717
	B3.72	22.67	15.19	150	300	150	128	275	150	13	56	75	137.50	1.07	2.38	304.64	2φ6 @ 43 + 2φ8 (45^0)	116.20	152.25	193.34	176.52	148.01	0.7632	0.6010	0.6583	0.7851
																						MEAN (M)	**0.9216**	**0.7257**	**0.7949**	**0.9643**
																						STANDARD DEVIATION (S)	**0.1448**	**0.1141**	**0.1249**	**0.1764**
																						COEFFICIENT oF VARIATION (CoV)	**0.1572**	**0.1572**	**0.1572**	**0.1830**

By comparing the failure load capacity of specimens with vertical stirrups (B3.11-B3.22) to specimens with inclined stirrups (B3.62, B3.71 and B3.72), it can be concluded that the inclined stirrups have more influence on the strength capacity than the vertical ones. It can also be seen that specimens which have the combined vertical stirrups and web bar bent along 90^0, B1.11 and B3.61, had a smaller failure load capacity than specimens with combined vertical stirrups and web bars bent along 45^0, B1.21 and B3.52. It clearly indicates that specimens with inclined stirrups and a bent reinforcement less than 90^0 provide a higher failure load capacity. This increase in capacity can be attributed to the fact that inclined reinforcements cross cracks subjected to shear displacements, hence a significant part of shear force can be transferred by the dowel action in these reinforcement bars.

Even though the reinforcement configuration is same, Table 1 shows that beam B1.12 has a higher load capacity compared to B2.11 and B2.12. This is caused by beam B1.12 has higher value of concrete compressive strength. The other case can be seen on comparison between B3.41 and B3.42 with B1.12 or B2.11. Beams B3.41 and B3.42 have a dapped-end height of 0.33*H and it showed smaller failure load compared to B1.12 or B2.11. The effect of dapped-end height on the failure load capacity is significant. Mattock et al. (1979) recommended that dapped-end height should not be less than 0.45*H [6]. By comparing B1.22 with B1.21 or B2.12 with B2.11 or B3.12 with B3.11, it can be seen that specimens whose closer stirrups distance had higher failure load.

According to the comparison between B2.2 and B2.1 group and also between B3.1-B3.2 and B2.1 group, it can be proved that specimens which have a higher numbers of stirrups had higher failure load capacity.

The comparisons among failure loads obtained from analytical methods with the available experimental results are presented in Figure 4. Whereas Table 1 exhibits the failure loads of available experimental results and from analytical results. It showed that the mean value of experimental-analytical ratio for the failure loads obtained from ACI-318-08, PCI Design Handbook, Euro Code 2 and BS 8110 as 0.9216; 0.9643; 0.7949; and 0.7257, respectively. It can be observed that PCI Design Handbook and ACI-318-08 provide better prediction of failure load capacity compared to Euro Code 2 and BS 8110.

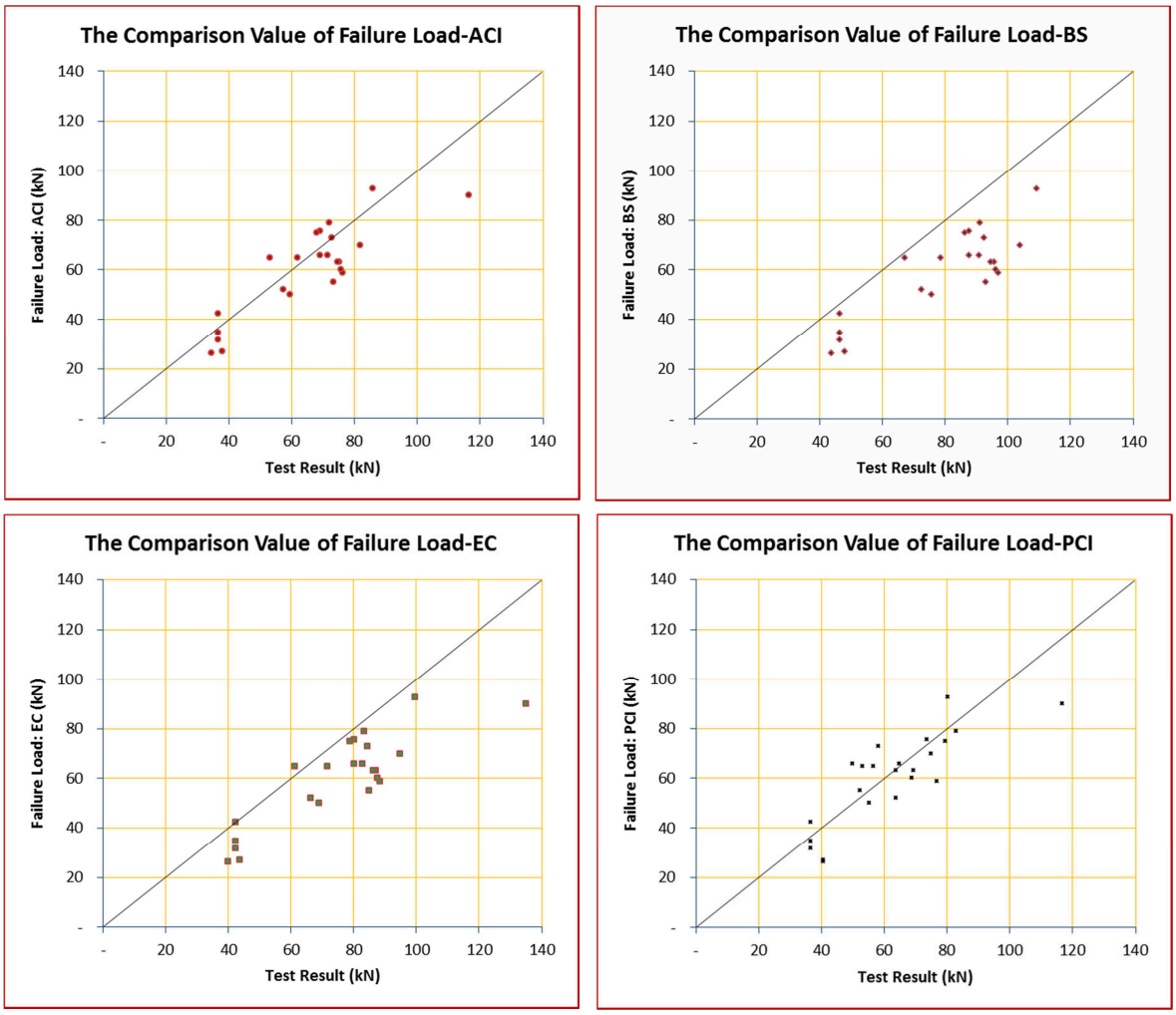


Figure4. Experimental-analysis results ratio for the predicted failure load

Conclusion

1. The influence of different important parameters on the failure loads was studied. The failure loads calculated using analytical and empirical methods were compared with the available experimental results. Parameters such as concrete compressive strength, dapped-end section size, shear span-depth ratio, type and effective range of stirrups, bent form of longitudinal reinforcements, amount of dapped-end reinforcements and hanger reinforcements were found to have significant effect on the predicted failure load capacity of RC dapped-end beams.
2. It was observed that RC dapped-end beam specimens with inclined stirrups, bent reinforcement less than 90^0, higher dapped-end height, closer stirrups distance and higher numbers of stirrups provide higher failure load capacity.

3. In this study, PCI Design Handbook and ACI-318-08 were found to provide better prediction of failure loads compared to Euro Code 2 and BS 8110.

Acknowledgment

The financial support was funded by Universiti Teknologi PETRONAS-Graduate Assistance (UTP-GA) Malaysia. The authors gratefully acknowledge the support provided by sponsor.

References

[1] Taher, S.E.-D.F, Strengthening of critically designed girders with dapped-ends, Structures and Buildings 158 Issue SB2, (2005), 141-152.

[2] Lu, W.Y., Lin, I.J., Hwang, S.J., Lin, Y.H., Shear strength of high-strength concrete dapped-end beams, Journal of the Chinese Institute of Engineers, Vol. 26, No. 5, (2003), 671-680.

[3] Yang, K.-H., Ashour, A.F., Lee, J.-K, Shear strength of RC dapped-end beams using mechanism analysis, Magazine of Concrete Research, Vol. 63 Issue 2, (2010), 81-97.

[4] Mattock, A.H., Strut-and-tie models for dapped-end beams, Concrete International, (2012).

[5] Peng, T., Influence of detailing on response of dapped-end beams, Thesis, McGill University-Montreal Canada, (2009).

[6] Wang, Q., Guo, Z., Hoogenboom, P.C.J., Experimental investigation on the shear capacity of RC dapped-ends beams and design recommendations, Structural Engineering and Mechanics, Vol. 21, No. 2, (2005), 221-235.

[7] Schlaich, J., Schafer, K., Design and detailing of structural concrete using strut-and-tie models, The Structural Engineer, Vol. 69, No. 6, (1991).

[8] Chen, B.S., Hagenberger, M.J., Breen, J.E., Evaluation of strut-and-tie modeling applied to dapped beam with opening, ACI Structural Journal, Vol. 99, No. 4, (2002).

[9] Shah, A., Haq, E., Khan, S., Analysis and design of disturbed regions in concrete structures, The12nd East Asia-Pacific Conference on Structural Engineering and Construction, Procedia Engineering, (2011).

[10] Mohamed, R.N., Elliott, K.S., Shear strength of short recess precast dapped end beams made of steel fibre self-compacting concrete, 33rd Conference on Our World in Concrete & Structures, Singapore Concrete Institute, (2008).

[11] ACI 318-08, Building code requirements for structural concrete and commentary, American Concrete Institute, USA, (2008).

[12] Euro Code 2, Design of concrete structures-Part 1-1: General rules and rules for buildings, BS EN 1992-1-1: 2004, British Standards (BSi), (2004).

[13] BS 8110, Structural use of concrete-Part 1: Code of practice for design and construction, British Standards (BSi), (1997).

[14] PCI Design Handbook, Precast and pre-stressed concrete, Precast/ pre-stressed concrete institute, USA, 7th Edition, (2010).

[15] Mitchell, D., Marchand, J., Croteau, P., Cook, W.D., Concorde over pass collapse: structural aspects, Journal of Performance of Constructed Facilities @ ASCE, Vol. 25, No. 6, (2011).

[16] Sanders, D.H., Example2: Dapped-end T-beam supported by an inverted T-beam, ACI, Farmington Hills, MI, (2002), 91-203.

Applied Mechanics and Materials Vol. 567 (2014) pp 469-475
© (2014) Trans Tech Publications, Switzerland
doi:10.4028/www.scientific.net/AMM.567.469

Prediction the Shear Strength for FRP Shear Strengthened RC Beams Based on Optimised Truss Models

YIN Hor[1,a] and TEO Wee[2,b]

[1,2]Civil Engineering Department, Universiti Teknologi PETRONAS, Malaysia

[a]horyin.itc@gmail.com, [b]teo_wee@petronas.com.my

Keywords: RC beams, FRP strengthening, Shear strength, Shear analysis, Optimised truss model

Abstract. This paper presents the analytical optimised truss model based on the principle of the minimum total strain energy theorem. The model was validated against 90 experimental data collected from the literature. The predicted shear strength in the analysis showed a very satisfactory correlation with the test results, with the average experimental/analytical failure load ratio of 1.09 and the coefficient of variation (C.O.V) of 14.1%. Furthermore, a comparison between the accuracy of the proposed model and the current design guidelines was also demonstrated in this study. It was observed that the optimised truss model led to be more viable than the standard 45-deg truss model in the design guidelines. A large dispersion of the results was found in ACI 440 with the C.O.V as far as 31.4%; whilst the TR 55 and fib 14 showed no significant difference with the C.O.V of 29.3% and 21.5%, respectively.

Introduction

Over the last two decades, fibre reinforced polymer (FRP) has been used for strengthening reinforced concrete (RC) structures as a common and popular technique. However, the shear behavior of externally bonded FRP in shear is still not well understood due to its complex nature of failure. The failures are characterised by brittle and catastrophic mechanisms that suddenly occur to fail without warning in advance.

Many researchers have attempted to quantify the extent of shear strength with numerous FRP shear strength models. The formulations of the shear strength have been mostly based on experimental studies and the use of the truss theory. In addition, the truss analogy used for the FRP shear contribution was taken similarly to the models for shear stirrups. To date, considerable research has been conducted on the FRP shear formulation based on the standard 45-deg truss model. Furthermore, the formulations utilised for the FRP contribution have been provided with similar variations, but mainly different methods for FRP effective strain (or stress) calculation. The effective strain formulations may have been derived from empirical regression and the concrete crack angle at 45-deg was also assumed. Current design guidelines for FRP strengthening RC members have adopted this assumption [1-3]. Nevertheless, variable concrete crack angles that may influence the FRP contribution have not been considered by a number of researchers.

In this study, the truss models that could be regarded as the most rational and unified design approaches for shear in RC structures as shown in evident sources [4], may be developed for the FRP shear strengthened RC beams. An optimisation truss model based on the minimum of the total strain energy theorem was employed in order to compute the FRP shear contribution. To truly capture the stress distribution of the strengthened beams, a variable concrete strut angle inside the truss model was performed rather than the traditional 45-deg of the strut within the truss model.

An effective strain formulation based on model calibration was proposed as a suitable strain for the optimised truss models. To verify the proposed truss models, the predicted shear strengths of 90 experimental data collected from published literature were compared against the actual testing results. Furthermore, the comparison accuracy between the prediction of the current design guidelines and the proposed truss models has also been presented in this paper.

Evaluation of FRP Contribution to the Shear Capacity

Current Design Guidelines. In current design guidelines for FRP shear strengthened RC beams, the nominal shear strength can be calculated as a sum of the contribution of the concrete, V_c, the transverse steel, V_s, and the FRP, V_{frp}, and written as follows:

$$V_n = V_c + V_s + V_{frp} \quad (1)$$

where the V_c, and V_s may be computed according to building design codes such as ACI 318-08 [5]. For the V_{frp}, the provisions were based on the 45-deg truss analogy as that used to calculate the transverse steel, V_s. Additionally, the design guidelines used the same analogy with different effective strain calculations. Table 1 summarises the current guidelines for the FRP contribution.

Table 1. The FRP shear contribution based on different design guidelines

<table>
<tr><td colspan="3">The expression of the FRP contribution, V_{frp}, based on different design guidelines</td></tr>
<tr><td>Concrete Society TR 55 (2012)</td><td>ACI 440.2R-08 (2008)</td><td>fib Bulletin 14 (2001)</td></tr>
<tr><td>$V_{frp} = \frac{A_f}{s_f}\left(d_f - \frac{n_s}{3} l_{t,\max}\cos\beta\right) E_{fu}\varepsilon_{fe}\left(\sin\beta + \cos\beta\right)$</td><td>$V_{frp} = \frac{A_f f_{fe}(\sin\beta + \cos\beta) d_f}{s_f}$</td><td>$V_{frp} = 0.9\varepsilon_{fe} E_{fu}\rho_f b_w d\left(\cot\theta + \cot\beta\right)\sin\beta$</td></tr>
<tr><td>$l_{t,\max} = 0.7\sqrt{E_{fu} t_f / f_{ctk}}$</td><td>$\varepsilon_{fe} = \kappa_v \varepsilon_{fu} \le 0.004$</td><td rowspan="3">$\varepsilon_{fe} = \min\left\{\begin{array}{l}\underbrace{\left(0.65\left(\frac{f_c'^{2/3}}{E_{fu}\rho_f}\right)\right)^{0.56} 10^{-3}}_{\text{CFRP peeling off failure}} \\ \underbrace{0.17\left(\frac{f_c'^{2/3}}{E_{fu}\rho_f}\right)^{0.30} \varepsilon_{fu}}_{\text{CFRP fracture failure}}\end{array}\right.$</td></tr>
<tr><td>$\varepsilon_{fe} = \min\left(\varepsilon_{fu}/2,\ 0.5\sqrt{f_{ctk}/E_{fu} t_f},\ 0.004\right)$</td><td>$\kappa_v = \frac{\kappa_1 . \kappa_2 . L_e}{11900 . \varepsilon_{fu}} \le 0.75$</td></tr>
<tr><td>Note: A_f is the FRP area; β is the inclination of FRP; s_f is the FRP spacing, d_f is the FRP effective depth; E_{fu} is in MPa; f_{ctk} is the characteristic concrete strength in MPa; and ε_{fe} is the effective strain in FRP. The anchorage coefficient, n_s, is taken as 0 for fully wrapped section, 1 for U-wrap, and 2 for Side-wrap. For more detail, they can be found in [1].</td><td>$L_e = \frac{23300}{\left(n_f . t_f . E_f\right)^{0.58}}$
$\kappa_1 = \left(\frac{f_c'}{27}\right)^{2/3}$, $\kappa_2 = \begin{cases}\left(d_f - 2L_e\right)/d_f ; \text{Side-wrap} \\ \left(d_f - L_e\right)/d_f ; \text{U-wrap}\end{cases}$
Note: f'_c and E_{fu} are in MPa. Further detail can be found in [2].</td><td>Note: E_{fu} is in GPa, and f'_c is in MPa. The concrete crack angle, θ, was assumed to be 45-deg. Further detail can be found in [3].</td></tr>
</table>

Truss Model Optimisation for the FRP Shear Contribution (V_{frp}). The truss model or strut-and-tie model (STM) has long been recognised as the rational conceptual tool for the design and detail of RC members [4]. In this study, an extensive STM to the case of FRP shear strengthened RC beams has been established [6]. An optimal truss model that could visualise the internal stress distribution of the FRP strengthened beams was proposed to compute the FRP contribution, V_{frp}.

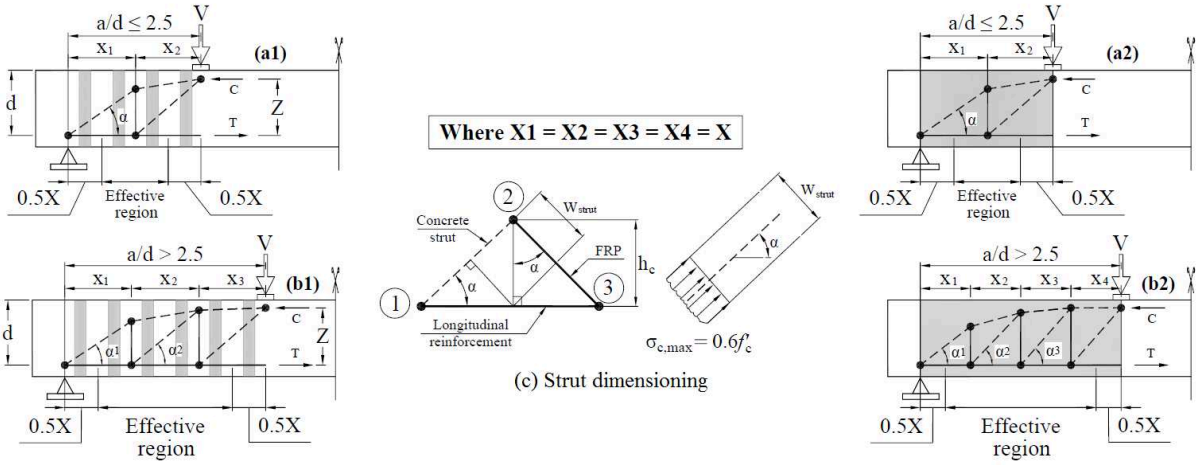


Figure 1. Proposed optimised truss layouts: (a1) a/d ≤ 2.5 with FRP strips, (a2) a/d ≤ 2.5 with continuous FRP sheets, (b1) a/d > 2.5 with FRP strips, (b2) a/d > 2.5 with the continuous FRP sheets, and (c) Proposed dimensioning of the concrete struts

To develop a suitable model representing the actual internal stress fields of an RC member is a tedious and iterative process. With many possible models, doubts could arise as to the efficient model being chosen. In a mechanical theory, it has long been recognised that loads are transmitted based on the principle of minimum strain energy. In this paper, the optimisation formulation suggested by [4] that was based on this principle was employed. The objective function for minimising the total strain energy may be expressed as follows:

$$\text{MINIMUM} \quad E_{pot}(\alpha_i) = \sum_{i=1}^{n} F_i l_i \varepsilon_i \tag{2}$$

where F_i is the tensile force in tie member i, l_i is the length of tie member i, ε_i is the strain of tie member i and α_i is the angle of the inclination of the concrete struts member i.

Fig. 1 depicts the proposed truss models. The models were developed corresponding to two a/d ratio criteria (a/d ≤ 2.5 and a/d > 2.5) and the type of strengthening schemes (laminate discrete strips and continuous sheets). It should be noted that the FRP continuous sheets may need to have three FRP ties to ensure better representation on the actual continuity; see Fig. 1(b2). Each panel of the truss model was arranged equally throughout the shear span. An effective region was defined by cutting off half of a panel (0.5X) at both end sides since the FRP at the nearby supports and applied loads might not have contributed to the shear capacity [7]. The FRP area in this region was incorporated in the optimised truss models.

From the illustration in Fig. 1, it can be seen that the proposed outlines more closely represented the actual stress distribution of the beams, whereby the compression struts was not imposed to be parallel at the standard 45-deg throughout; instead, it varied along the shear span. Once the optimised models were outlined, the next step was to assess the failure load of the FRP contribution. The failure loads were obtained as a minimum of a three limit criteria corresponding to the mechanism of the beams: (i) *concrete strut failure*, (ii) *flexural failure*, and (iii) *FRP debonding*. The summary of these failure criteria is shown in Table 2.

Table 2. Effective limiting strength of the optimised truss models

	Concrete strut failure	Flexural failure	FRP debonding failure
Limits	$\sigma_{c,\max} = 0.6 f'_c$	$F_{st} = A_s f_y \geq T_{st}$	$\varepsilon_{frp,e} = 0.016\left(\frac{f'^{2/3}_c}{E_f \rho_f}\right)^{0.42} \varepsilon_u$, (Eq. 5)

STM	$\sigma_{c,STM} = \frac{C_{strut}}{w_{strut} b}$	Note: f_y is the yield strength of longitudinal steel; A_s is the amount of longitudinal steel; and T_{st} represents the tensile force applied at the tension zone due to external couple moment. Flexural failure is considered to take place when T_{st} exceeded the allowable F_{st}.	$\varepsilon_{frp,STM} = \frac{f_{frp,STM}}{E_{frp}}$, $f_{frp,STM} = \frac{T_{frp}}{A_{frp}}$
	$w_{strut} = h_c \cos\alpha$ (see Fig. 1(c))		Note: Once $\varepsilon_{frp,STM}$ exceed $\varepsilon_{frp,e}$, then the FRP laminate was considered to debonded.

Effective Strain of the FRP Based on Model Calibration

According to the current code provisions, the FRP shear contribution may be calculated based on the 45-deg truss model as follows:

$$V_{frp} = \frac{A_f E_f \varepsilon_{fe} (\sin\beta + \cos\beta) d_f}{s_f} \tag{3}$$

In this equation, ε_{fe} is the effective strain in FRP which is the main factor concerned with by many researchers such as [8-11]. The study has shown that the effective strain, ε_{fe}, was greatly dependent on the stiffness of FRP, which was the product of the elastic modulus, E_f, and the ratio of FRP, ρ_f. This showed that as the FRP stiffness increased (stiffer), the effective strain in FRP decreased. Since the FRP contribution, V_{frp}, was obtainable directly from the experiment by subtracting the non-strengthened control specimen capacity, $V_{c,exp}$, from its respective strengthened specimen capacity, $V_{n,exp}$, then the effective strain in FRP, ε_{fe}, was determined as:

$$\varepsilon_{fe} = \frac{V_{frp} s_f}{A_f E_f (\sin\beta + \cos\beta) d_f} \tag{4}$$

Therefore, it can be plotted between the effective stain, ε_{fe}, and its rigidity ($E_f\rho_f$) throughout the experimental data. The curve fitting might be used to represent the dataset as the best fit.

Knowing that the effective strain, ε_{fe}, is the crucial effect for the FRP shear contribution, a similar procedure was employed to calibrate the effective strain model by the determination of the actual FRP shear contribution, $V_{frp,exp}$, from the collected database ($V_{frp,exp} = V_{n,exp} - V_{c,exp}$) within the proposed optimised truss models. Also, the variable compressive strut angle was accounted for as a main variable in the objective function (Eq. 2) for the realistic internal stress distribution of the beams in this study.

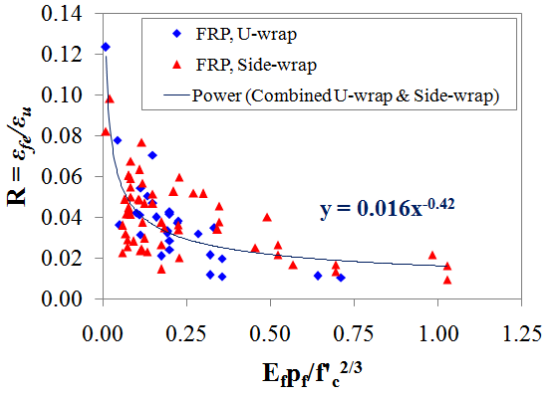


Figure 2. Proposed factor R versus the term of $E_f\rho_f / f'^{2/3}_c$

Due to the available data and time constraint, it was hard to identify the effect of different strengthening schemes (U-wrap and Side-wrap) since the data points of the U-wrap and Side-wrap in Fig. 2 seemed to be similar with not much dispersion from each other. Therefore, a single curve fitting was proposed in this study to represent all of the experimental data. The power regression line was used as the best fit to the data. The equation of this fit was given as:

$$R = \frac{\varepsilon_{frp,e}}{\varepsilon_u} = 0.016\left(\frac{f'^{2/3}_c}{E_f \rho_f}\right)^{0.42} \quad (5)$$

This equation was used to limit the calculating strain of FRP, $\varepsilon_{frp,STM}$, in the optimised model for determining the FRP debonding failure. Once $\varepsilon_{frp,STM}$ exceeded $\varepsilon_{frp,e}$, then the FRP laminate was considered to debonded.

Validation of the Optimised Truss Models

To validate the proposed optimised truss models, verification was carried out using the available experimental data in the literature. The database that was considered in the analysis consisted of 90 data beams. Out of the 90 beams, 57 beams were strengthened with Side-wrap whilst the remaining 33 beams were strengthened with U-wrap. All of the beams were strengthened with only external FRP and without any transverse steel in order to investigate purely the FRP shear contribution. The details of the geometrical and material properties of the experimental beams are summarised in Table 4, which can be downloaded through online via URL: https://drive.google.com/file/d/0B075-MWiPhDncW5wTnp2X0dvNUU/edit?usp=sharing.

The predicted shear strength is shown in Table 3 and graphically in Fig. 3 in term of $V_{n,exp}/V_{n,pre}$ ratio; whereby, the $V_{n,exp}$ represented the actual experimental result for the strengthened beams. Moreover, for $V_{n,pre}$, a similar approach in Eq. 1 was adopted and given as (no stirrups $V_s = 0$):

$$V_{n,pre} = V_{c,exp} + V_{frp,pre} \quad (6)$$

where $V_{c,exp}$ was the actual shear strength from the control specimen, and $V_{frp,pre}$ represented the predicted FRP shear contribution based on either the standard 45-deg or the optimised truss model. Table 3 shows the prediction of the optimised models in comparison with current design guidelines, and the effect of different wrapping schemes separately for Side-wrap and U-wrap.

As seen in Table 3, the prediction based on the proposed optimised truss model showed a very good correlation with the experimental data for both Side-wrap and U-wrap; whilst the design guidelines were very conservative. For the proposed model, the prediction showed that for Side-wrap and U-wrap, the average $V_{n,exp}/V_{n,pre}$ ratio was 1.08 and 1.06, respectively; whilst the coefficient of variation (C.O.V) was 14.5% and 13.6%, respectively. The comparison performance to the current design guidelines is depicted in Table 3. It is interesting to note that amongst the three design guidelines, the fib 14 gave a better prediction than the TR 55 and ACI 440.2R-08.

Table 3. Comparison of the prediction performances of the wrapping schemes

Wrapping Schemes	$V_{n,exp}/V_{n,pre}$ ratio based on the design guidelines and the optimised model			
Side-wrap	*(1)TR55*	*(2)ACI 440.2R-08*	*(3)fib Bulletin 14*	*(4) Optimised Truss*
Average	0.92	0.69	0.76	1.08
SD	0.25	0.23	0.16	0.16
C.O.V	27.2%	33.2%	21.1%	14.5%
U-wrap				
Average	0.72	0.67	0.71	1.06
SD	0.19	0.19	0.16	0.14
C.O.V	26.5%	27.9%	22.0%	13.6%

Note: For Table 3 and 4, the prediction $V_{n,pre}$ was given as $V_{c,exp} + V_{frp,pre}$, where the contributions $V_{frp,pre}$ were calculated based on: (1)Concrete Society TR 55 (2012), (2)ACI 440.2R-08 (2008), (3)*fib* Bulletin 14 (2001), and (4)Proposed optimised truss models

A graphical representation numerical analysis of the overall prediction was illustrated in Fig. 3. In the figure, two lines limiting to ±20% the deviation of the target bisector line from the experimental results were also provided. As can be observed for the proposed optimised models, almost all of the results fell within the ±20% bounds. This implies that the proposed model gave a

very good correlation between the prediction and the experimental data. For the overall prediction, the average $V_{n,exp}/V_{n,pre}$ ratio and C.O.V were 1.09 and 14.1%, respectively.

For the design guidelines, a large degree dispersion of the results was observed. In Fig. 3(b) for ACI 440, the average $V_{n,exp}/V_{n,pre}$ ratio and the C.O.V were as far as 0.68 and 31.4%, respectively.

Conclusion

In this paper, the proposed optimised truss model based on the principle of the minimum total strain energy for predicting the FRP shear contribution of the strengthened RC beams was presented. The effective strain based on model calibration was also demonstrated for the optimised truss models. The model was validated against the test results of the 90 beam data collected from the literature.

From the discussions, the optimised truss model can be a more viable than the standard 45-deg truss model. As in Fig. 3, the model showed a very good correlation between the prediction and the test results with the average $V_{n,exp}/V_{n,pre}$ ratio of 1.09 and an acceptable C.O.V of 14.1%.

As for the current design guidelines, it was observed that the assumption of the 45-deg truss model showed very conservative results and led to a large dispersion of the results. As for the ACI 440, the average $V_{n,exp}/V_{n,pre}$ ratio and the C.O.V were as far as 0.68 and 31.4%, respectively.

The model in this study has shown a capable prediction with sufficient accuracy and tends to be a more realistic model to represent the actual stress distribution in FRP strengthened RC beams. In addition, three main mechanism failures: concrete strut failure, flexural failure, and FRP debonding failure were also incorporated into the models. Hence, the proposed optimised truss models have ended up being an effective tool for design procedures on the FRP strengthened members.

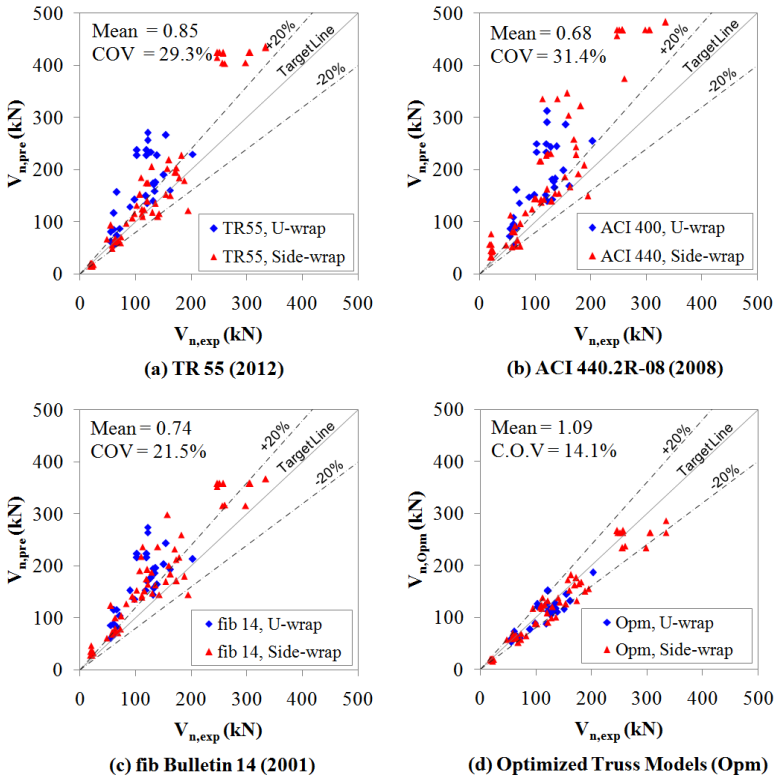


Figure 3. Comparison between the predicted shear strength and experimental results

References

[1] CNR-DT200/2004, Guide for the Design and Construction of Externally Bonded FRP Systems for Strengthening Existing Structures, Rome, (2004).

[2] ACI Committee 440 (ACI 440.2R-08), Guide for the Design and Construction of Externally Bonded FRP Systems for Strengthening Concrete Structures, Farmington Hills, (2008).

[3] fib Bulletin No. 14, Design and use of externally bonded fibre reinforced polymer reinforcement (FRP EBR) for reinforced concrete structures, Task Group 9.3, Switzerland, (2001).

[4] J. Schlaich, K. Schäfer, and M. Jennewein, Toward a consistent design of structural concrete, PCI J., 32 (1987) 74-150.

[5] ACI Committee 318 (ACI 318-08), Building Code Requirements for Structural Concrete and Commentary. Farmington Hills, (2008).

[6] W. Teo and Y. Hor, Analytical truss models for prediction the shear strength of FRP strengthened reinforced concrete members, FRPRCS11, UM, Guimarães, (2013).

[7] A. Bousselham and O. Chaallal, Mechanisms of shear resistance of concrete beams strengthened in shear with externally bonded FRP, J. Compos. Constr., 12 (2008) 499-512.

[8] T. C. Triantafillou, Shear strengthening of reinforced concrete beams using epoxy-bonded FRP composites, ACI Struct. J., 95, (1998).

[9] A. Khalifa, W. Gold, A. Nanni, and A. M.I., Contribution of Externally Bonded FRP to Shear Capacity of RC Flexural Members, J. Compos. Constr., 2 (1998) 195-202.

[10] Z. Zhang and C.-T. T. Hsu, Shear strengthening of reinforced concrete beams using carbon-fiber-reinforced polymer laminates, J. Compos. Constr., 9 (2005) 158-169.

[11] I. Bukhari, R. Vollum, S. Ahmad, and J. Sagaseta, Shear strengthening of reinforced concrete beams with CFRP, Magaz. Concr. Res., 62 (2010) 65-77.

Applied Mechanics and Materials Vol. 567 (2014) pp 476-481
© (2014) Trans Tech Publications, Switzerland
doi:10.4028/www.scientific.net/AMM.567.476

Predictive Stress-Strain Models for High Strength Concrete Subjected to Uniaxial Compression

Nasir Shafiq[1, a], Tehmina Ayub[1,b] and M. Fadhil Nuruddin[1,c]

[1]Civil Engineering Department, Universiti Teknologi PETRONAS, Bandar Seri Iskandar, 31750 Tronoh, Perak, Malaysia

[a]nasirshafiq@petronas.com.my, [b]tehmina@neduet.edu.pk, [c]fadhilnuruddin@petronas.com.my

Keywords: High strength concrete, Metakaolin, Compressive stress-strain, Predictive Models.

Abstract. To date, various predictive models for high strength concrete (HSC) have been proposed that are capable of generating complete stress-strain curves. These models were validated for HSC prepared with and without silica fume. In this paper, an investigation on these predictive models has been presented by applying them on two different series of HSC. The first series of HSC was prepared by utilizing 100% cement content, while second series was prepared by utilizing 90% cement and 10% Metakaolin. The compressive strength of the concrete was ranged from 71-87 MPa. For each series of HSC, total four cylinders of the size 100×200mm were cast to obtain the stress-strain curves at 28 days.It has been found that the pattern of the stress-strain curve of each cylinder among four cylinders of each series was different from other, in spite of preparing from the similar batch. When predictive models were applied to these cylinders using their test data then it was found that all models more or less deficient to accurately predict the stress-strain behavior.

Introduction

High strength concrete (HSC) is a well-known construction material forstructural application offering substantial benefits compared to traditional normal strength concrete. Generally, when a concrete is utilized or trialed for a construction purpose then compressive strength becomes the foremost property which a structural engineer considers for designing; especially, for the nonlinear analysis of a structural member, the knowledge of the complete compressive stress-strain curves is essential as it bases the derivation of the design curves[1].

History of modeling the stress-strain behavior of concrete can be traced back to 1943 when Jensen [2], for the very first time, proposed a predictive model for the concrete. After him, several predictive models for concrete were proposed including Hognestad,1951[3], Sargin & Handa,1969 [4], Popovics, 1973 [5], Wang et al., 1978 [6], Chu, 1985 [7], CEB-FIP Model code 1990 [8], Hsu & Hus, 1994 [9], Wee et al.,1996 [10], Van Gysel & Taerwe, 1996 [11] and Lu & Zhao, 2010 [1]. The description of these models is given in Table 1.

After review, these models have been grouped into three (Refer Table 1) as follows:

Type I. Single model capable of predicting stress-strain response from origin to the ultimate (i.e.$0 < \varepsilon \leq \varepsilon_u$).

Type II. Two models, one for predicting the behavior of rising branch up to the peak point (i.e.$0 < \varepsilon \leq \varepsilon_c'$), while second model for predicting the behavior of falling branch from peak point to the ultimate (i.e.$\varepsilon_c' < \varepsilon \leq \varepsilon_u$).

Type III. Two models, one for combine prediction of the behavior of rising branch and falling branch up to the limiting strain (i.e. $0 < \varepsilon \leq \varepsilon_{c,lim}$)., while second model predicts the behavior of the depressing branch from limiting strain up to ultimate strain(i.e.$\varepsilon_{c,lim} < \varepsilon \leq \varepsilon_u$).

In current investigation, all predictive models proposed to date for HSC have been applied to the test results of cylinders cast by HSC prepared with and without cement replacing material. The aim of this study was to assess the differencein the stress-strain curves obtained by using different predictive models available in the existing literature.

Table 1: Existing Stress-Strain Models for HSC

Authors (Year)	Model description	Parameter description	Valid compressive strength range	Authors Remarks
Single model capable of predicting stress-strain response from origin to ultimate (i.e. $0 < \varepsilon \leq \varepsilon_u$).				
Sargin & Handa (1969)	$\frac{f_c}{f_c'} = k_3 \frac{A\left(\frac{\varepsilon_c}{\varepsilon_c'}\right) + (D-1)\left(\frac{\varepsilon_c}{\varepsilon_c'}\right)^2}{1 + (A-2)\left(\frac{\varepsilon_c}{\varepsilon_c'}\right) + D\left(\frac{\varepsilon_c}{\varepsilon_c'}\right)^2}$	$A = \frac{E_{it}}{E_c}$; $D = 0.65 - 7.25 f_c' \times 10^{-3}$ $E_{it} = 5979\sqrt{f_c'}$; $\varepsilon_c' = 0.0021$		
Popovics (1973)	$\frac{f_c}{f_c'} = \frac{\beta\left(\frac{\varepsilon_c}{\varepsilon_c'}\right)}{\beta - 1 + \left(\frac{\varepsilon_c}{\varepsilon_c'}\right)^{\beta}}$	$\beta = .058 f_c' + 1$	Up to 51 MPa	
Wang et al. (1978)	$\frac{f_c}{f_c'} = \frac{A(\varepsilon_c/\varepsilon_c') + B(\varepsilon_c/\varepsilon_c')^2}{1 + C(\varepsilon_c/\varepsilon_c') + D(\varepsilon_c/\varepsilon_c')^2}$	A, B, C and D are constants which can be estimated by considering the condition A $\left\{\begin{matrix} \frac{f_c}{f_c'} = 0.45 \; for \; \varepsilon_c/\varepsilon_c' = \frac{0.45}{E_{it}/E_c} \\ \frac{f_c}{f_c'} = 1 \qquad for \qquad \varepsilon_c/\varepsilon_c' = 1 \end{matrix}\right\}$	Up to 76 MPa	
Carriera & Chu (1985)	$\frac{f_c}{f_c'} = \frac{\beta(\varepsilon_c/\varepsilon_c')}{\beta - 1 + (\varepsilon_c/\varepsilon_c')^{\beta}}$	$\beta = \frac{1}{1 - (\frac{f_c'}{\varepsilon_c' E_{it}})}$ $E_{it} = \frac{f_c'}{\varepsilon_c'}\left(\frac{24.82}{f_c'} + 0.92\right)$ $\varepsilon_c' = (1{,}680 + 7.1\, f_c') \times 10^{-6}$	23 to 80 MPa	Does not fit on current data due to negative value of β
Two models, one for combine prediction of the behavior of rising branch and falling branch up to the limiting strain (i.e. $0 < \varepsilon \leq \varepsilon_{c,lim}$)., while second model predicts the behavior of the depressing branch from limiting strain up to ultimate strain (i.e.$\varepsilon_{c,lim} < \varepsilon \leq \varepsilon_u$).				
CEB-FIP (1993)	For $0 \leq \varepsilon \leq \varepsilon_{c,lim}$ $f_c = f_c' \frac{\left(\frac{E_{it}}{E_c}\right)\left(\frac{\varepsilon_c}{\varepsilon_c'}\right) - \left(\frac{\varepsilon_c}{\varepsilon_c'}\right)^2}{1 + \left(\frac{E_{it}}{E_c} - 2\right)\left(\frac{\varepsilon_c}{\varepsilon_c'}\right)}$ For $\varepsilon > \varepsilon_{c,lim}$ $f_c = \frac{f_c'}{\left(\frac{\xi}{\eta_2} - \frac{2}{\eta_2^2}\right)\left(\frac{\varepsilon_c}{\varepsilon_c'}\right)^2 + \left(\frac{4}{\eta_2} - \xi\right)\left(\frac{\varepsilon_c}{\varepsilon_c'}\right)}$	$\frac{\varepsilon_{c,lim}}{\varepsilon_c'} = \frac{1}{2}\left[\left(\frac{E_{it}}{2E_c} + 1\right) + \sqrt{\left(\frac{E_{it}}{2E_c} + 1\right)^2 - 2}\right]$ $\eta_2 = \frac{\varepsilon_{c,lim}}{\varepsilon_c'}$ $\xi = 4\frac{\eta_2^2\left(\frac{E_{it}}{E_c} - 2\right) + 2\eta_2 - \frac{E_{it}}{2E_c}}{\left[\eta_2\left(\frac{E_{it}}{2E_c} - 2\right) + 1\right]^2}$		Modified form of Sargin and Handa (1969)
Hsu & Hsu (1994)	For $0 \leq \varepsilon \leq \varepsilon_{c,lim}$ $\frac{f_c}{f_c'} = \frac{n\beta(\varepsilon_c/\varepsilon_c')}{n\beta - 1 + (\varepsilon_c/\varepsilon_c')^{n\beta}}$ For $\varepsilon > \varepsilon_{c,lim}$ $f_c = 0.3 f_c' e^{-0.8\left(\frac{\varepsilon_c}{\varepsilon_c'} - \frac{\varepsilon_{c,lim}}{\varepsilon_c'}\right)^{0.5}}$	$\beta = \left(\frac{f_c'}{65.23}\right)^3 + 2.59$ Where, $E_{it} = 0.0736 w^{1.51} (f_c')^{0.3}$, $\varepsilon_o = (1680 + 7.1 f_c') \times 10^{-6}$ For $0 \leq \varepsilon \leq \varepsilon_c'$; n=1 For $\varepsilon_c' \leq \varepsilon \leq \varepsilon_d$; n=1 if $f_c' < 62\ MPa$ n=2 if $62\ MPa < f_c' < 76\ MPa$ n=3 if $76\ MPa < f_c' < 90\ MPa$ n=5 if $f_c' \geq 90\ MPa$ $\varepsilon_{c,lim}$is the strain at $0.3 f_c'$in the falling branch of stress-strain curve.	> 69 MPa	
Van Gysel & Taerwe (1996)	For $0 \leq \varepsilon \leq \varepsilon_{c,lim}$ $f_c = f_c' \frac{\left(\frac{E_{it}}{E_0}\right)\left(\frac{\varepsilon_c}{\varepsilon_0}\right) - \left(\frac{\varepsilon_c}{\varepsilon_0}\right)^2}{1 + \left(\frac{E_{it}}{E_0} - 2\right)\left(\frac{\varepsilon_c}{\varepsilon_0}\right)}$ For $\varepsilon > \varepsilon_{c,lim}$ $f_c = \frac{f_c'}{\left(\frac{\xi}{\eta_2} - \frac{2}{\eta_2^2}\right)\left(\frac{\varepsilon_c}{\varepsilon_0}\right)^2 + \left(\frac{4}{\eta_2} - \xi\right)\left(\frac{\varepsilon_c}{\varepsilon_0}\right)}$	$\frac{\varepsilon_{c,lim}}{\varepsilon_c'} = \frac{1}{2}\left[\left(\frac{E_{it}}{2E_c} + 1\right) + \sqrt{\left(\frac{E_{it}}{2E_c} + 1\right)^2 - 2}\right]$ $\eta_2 = \frac{\varepsilon_{c,lim}}{\varepsilon_c'}$ $\xi = 4\frac{\eta_2^2\left(\frac{E_{it}}{E_c} - 2\right) + 2\eta_2 - \frac{E_{it}}{2E_c}}{\left[\eta_2\left(\frac{E_{it}}{2E_c} - 2\right) + 1\right]^2}$		
Lu & Zhao (2010)	For $0 \leq \varepsilon \leq \varepsilon_L$ $\frac{f_c}{f_c'} = \left[\frac{(E_{it}/E_c)(\varepsilon_c/\varepsilon_c') - (\varepsilon_c/\varepsilon_c')^2}{1 + (E_{it}/E_c - 2)(\varepsilon_c/\varepsilon_c')}\right]$ For $\varepsilon > \varepsilon_d$ $\frac{f_c}{f_c'} = \frac{1}{1 + \lambda[(\varepsilon_c/\varepsilon_c') - 1/(\varepsilon_L/\varepsilon_c') - 1]^{2(1-\lambda)}}$	$\varepsilon_L = \varepsilon_c'\left[\left(\frac{1}{10}\frac{E_{it}}{E_c} + \frac{4}{5}\right) + \sqrt{\left(\frac{1}{10}\frac{E_{it}}{E_c} + \frac{4}{5}\right)^2 - \frac{4}{5}}\right]$	50-140 MPa	For $0 \leq \varepsilon \leq \varepsilon_L$), modified form of Sargin &Handa (1969)& for $\varepsilon > \varepsilon_L$, the model of Van Gysel & Taerwe (1996) are used
Two models, one for predicting the behavior of rising branch up to the peak point (i.e. $0 < \varepsilon \leq \varepsilon_c'$), while second model for predicting the behavior of falling branch from peak point to the ultimate (i.e.$\varepsilon_c' < \varepsilon \leq \varepsilon_u$).				
Wee et al. (1996)	For $f_c' \leq 50$ MPa $\frac{f_c}{f_c'} = \frac{\beta(\varepsilon_c/\varepsilon_c')}{\beta - 1 + (\varepsilon_c/\varepsilon_c')^{\beta}}$ For $50 < f_c' \leq 120$ MPa $\frac{f_c}{f_c'} = \frac{k_1\beta(\varepsilon_c/\varepsilon_c')}{k_1\beta - 1 + (\varepsilon_c/\varepsilon_c')^{k_2\beta}}$	$\beta = \frac{1}{1 - (\frac{f_c'}{\varepsilon_c' E_{it}})}$ Where, $E_{it} = 10{,}200\ (f_c')^{1/3}$ $k_1 = \left(\frac{50}{f_c'}\right)^{3.0}$; $k_2 = \left(\frac{50}{f_c'}\right)^{1.3}$	50- 120 MPa	

f_c' is the maximum compressive strength in MPa. ε_c' is the corresponding strains. β is the parameter that controls the descending branch. w is the unit weigh of the concrete in kg/m^3

Experimental Program

Series Mix Proportions, Materials and their Quantities. The details of the material utilized for the preparation of the HSC and their quantities are presented in Table 1.The physical and chemical properties of cement and mineral admixtures are given by the authors in [12].

Table 2: Series mix proportions and quantities for HSC

Series	Mix quantity (kg/m^3)						
	Cement	Metakaolin	Fine aggregate	Coarse aggregates		Water	Superplasticizer
				< 10mm	10-20mm		
"P"	450	-	670	600	500	180	Variable, target
"M"	405	45	670	600	500	180	slump 50 ± 10 mm

Specimens Sizes and Testing. For each series (as given in Table 2), 4 cylinders of size 100×200mm were cast and cured for 28 days. Slump of the concrete was determined conforming to specification C470/C470M, after mixing the concrete, as per ASTM C192/C192M-13. The slump of the concrete was found that slump is within the limit of 50 ± 10 mm.Concrete was then poured into the molds up to a cylinder height less than 3 to 6 mm from the top surface of the molds to provide mortar capping. The leftover space was capped with mortar plaster as recommended in BS 1881-110: 1983 standard to ensure the uniform distribution of the compressive load between cylinders and machine.Cylindrical specimens were then left to harden for 24 hours. After 24 hours, all cylinders were taken out from the molds and put into a water tank up to 28 days for wet curing.

After completion of the curing period of 28 days, all 8 cylinders (4 cylinders for each series) were air dried for few hours and tested using compression testing machine of 1000 kN capacity as perASTM Standard C39 (ASTM 2003).Strain measurements were recorded using linear variable differential transformer (LVDT). The compressive strength results of all cylinders along with the strain results are presented in the Table 3; however, stress-strain curves for all three series obtained from the testing of 100×200mm cylinders are presented in Fig. 1 and Fig. 2.

Table 3: Compression test results at 28 days

Series	Experimental Results				Average results (MPa)	Standard deviation (MPa)	Sample variance (%)
	Cylinder IDs	Compressive strength (MPa)	Strain (mm/mm)		Compressive strength		
			Peak	Ultimate			
"P"	Cylinder 1	71.56	0.002409	0.011739	72.88	1.75	3.048
	Cylinder 2	72.17	0.002377	0.018320	-	-	
	Cylinder 3	75.45	0.002362	0.012199	-	-	
	Cylinder 4	72.34	0.002204	0.011287	-	-	
"M"	Cylinder 1	85.23	0.002381	0.011832	85.75	1.087	1.182
	Cylinder 2	84.47	0.002416	0.017960	-	-	-
	Cylinder 3	86.67	0.002345	0.014493	-	-	-
	Cylinder 4	86.64	0.002233	0.013233	-	-	-

Note: Each number after hyphen i.e. 1 and 2 represent the batch number

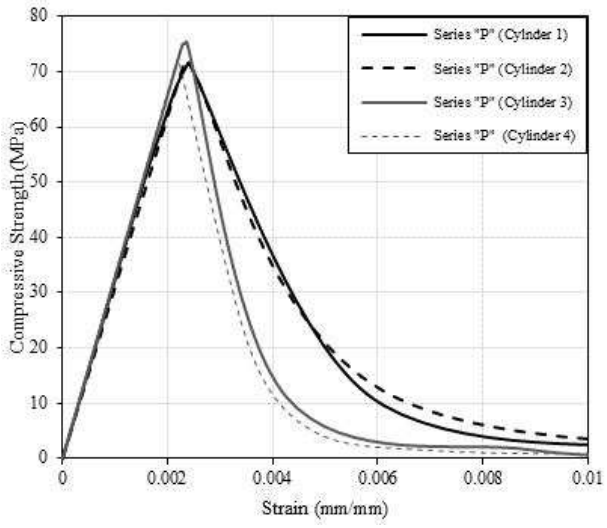


Fig. 1 Experimental stress-strain curves Series "P"

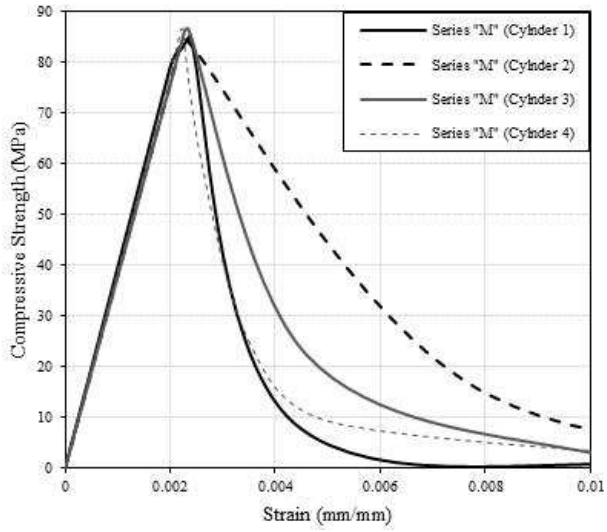


Fig. 2 Experimental stress-strain curves Series "M"

Analysis of the Experimental Result

The compressive strength results along with the average compressive strength, standard deviation and sample variance (or coefficient of variance) are presented in Table 3. The lower values of standard deviation and sample variance and the consistency of the stress-strain curves (in Fig. 1 and Fig. 2) show that all HSC series were well designed and highly cohesive. Higher average compressive strength was obtained in series "M" (Refer Table 3) which was 17.66% and 7.22% higher than series "P". This shows that the addition of Metakaolin as partial replacement of cement considerably enhanced the compressive strength.

Application of the Existing Predictive Stress-Strain Models on the Current Data

Existing models for the prediction of the stress-strain curves of HSC, as summarized in Table 1 were recently reviewed by Lu and Zhao (2010) who highlighted the deficiencies of these models and proposed a new empirical model. In current study, all models including the model of Lu and Zhao (2010) are applied on the current experimental data using the experimental results described in Table 3. The predicted and experimental stress-strain curves are presented in Fig. 3 and Fig. 4.With reference to [13], results of predicted compressive strength of series "P" and series "M" using the existing models were compared with the experimental stress strain by estimating the Root mean square error "*RMS*" and absolute fraction of variance "*V*". These parameters were calculated by selecting stress results of experimental and obtained through the predictive models which had the same strain values.

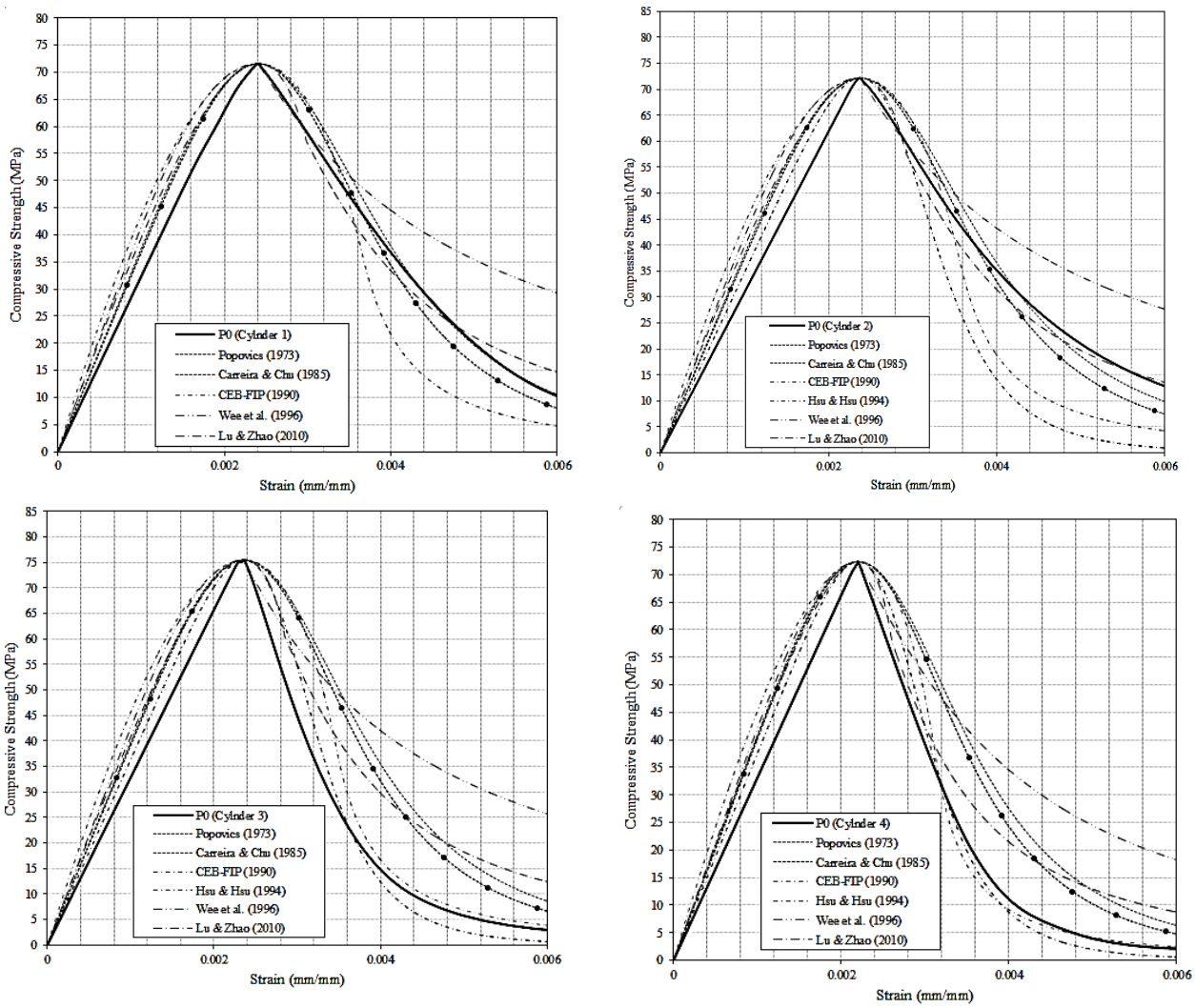


Fig. 3 Comparison of the Experimental and Predicted Stress-Strain Curves for Series "P"

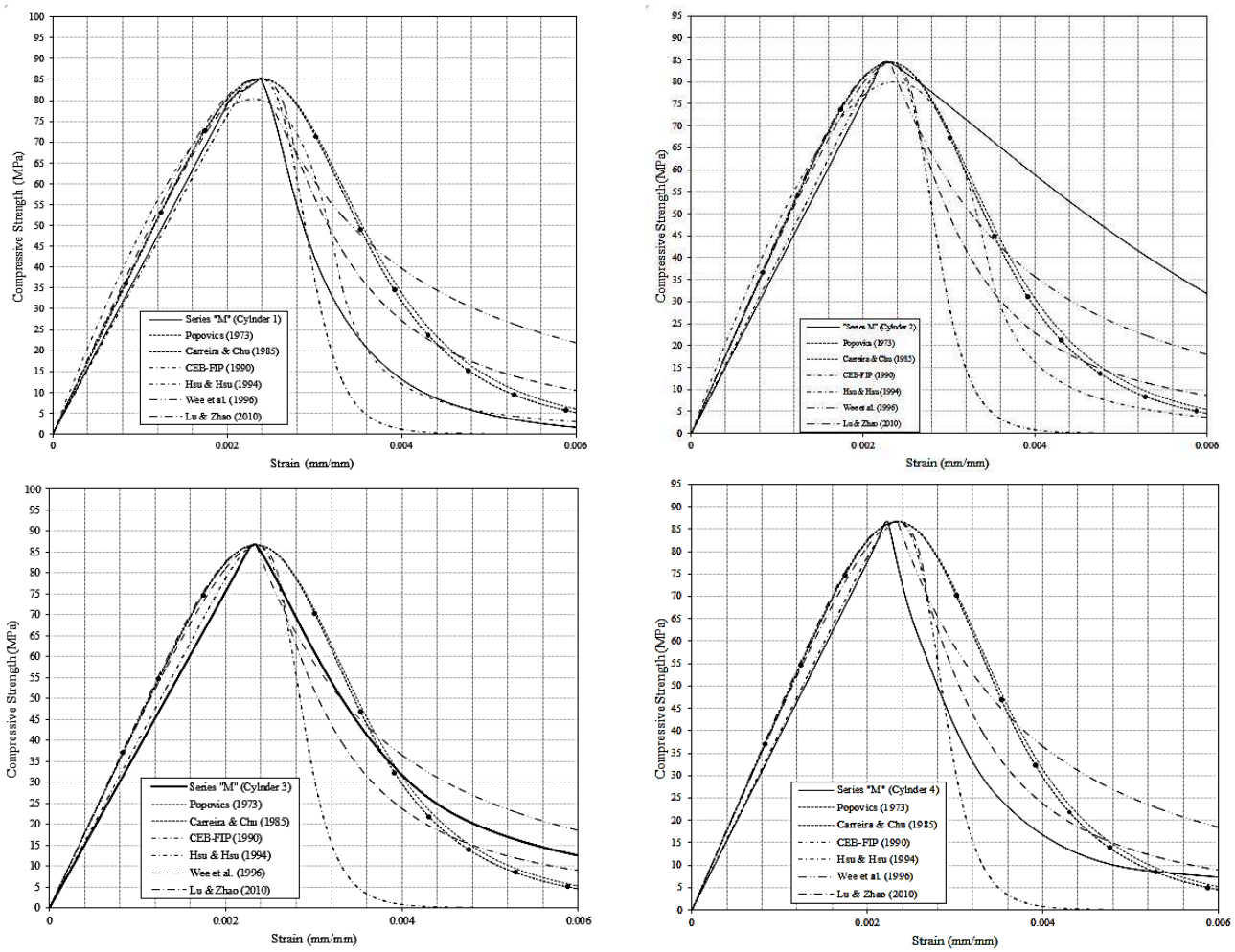


Fig. 4 Comparison of the Experimental and Predicted Stress-Strain Curves for Series "M"

Table 4: Root mean square error "RMS" and absolute fraction of variance "V"

Series	Cylinder		Popovics (1973)	Carreira & Chu (1985)	CEB-FIP (1993)	Hsu & Hsu (1994)	Wee et al. (1996)	Lu & Zhao (2010)
"P"	Cylinder 1	RMS	2.678	2.815	4.362	1.745	7.569	3.194
		Variance	0.998	0.998	0.995	0.999	0.985	0.997
	Cylinder 2	RMS	1.513	1.202	1.983	1.167	3.933	1.015
		Variance	0.999	1.000	0.999	1.000	0.996	1.000
	Cylinder 3	RMS	4.059	4.954	0.711	0.972	4.221	0.972
		Variance	0.996	0.994	1.000	1.000	0.996	1.000
	Cylinder 4	RMS	5.990	7.293	1.503	1.226	11.053	4.625
		Variance	0.986	0.979	0.999	0.999	0.953	0.991
"M"	Cylinder 1	RMS	2.701	3.049	1.462	2.156	5.228	2.558
		Variance	0.999	0.999	1.000	0.999	0.996	0.999
	Cylinder 2	RMS	3.646	3.684	4.049	2.461	3.253	2.723
		Variance	0.998	0.998	0.997	0.999	0.998	0.999
	Cylinder 3	RMS	3.146	2.917	5.554	7.243	3.462	2.510
		Variance	0.998	0.998	0.993	0.988	0.997	0.999
	Cylinder 4	RMS	9.132	9.526	8.171	22.058	5.268	1.764
		Variance	0.980	0.979	0.983	0.861	0.993	0.999

Root mean square error "RMS" and absolute fraction of variance "V" has been calculated manually using Eq. 1 and Eq. 2, which are described as follow:

$$RMS = \sqrt{\frac{\sum|t_i - o_i|^2}{n}} \tag{1}$$

$$V = 1 - \frac{\sum|t_i - o_i|^2}{\sum|o_i|^2} \tag{2}$$

Where, t_i and o_i are the experimental and predicted stress values at the same strain level and n is the number of observations. The estimated values of "RMS" and "V" are shown in Table 4, which shows that Lu & Zhao's model[1] is more efficient compared to the other predictive models based on the "RMS" and "V" values of all cylinders.

Summary

The published predictive models are evaluated in this study using the experimental results of two series of HSC as plain concrete (without replacing cement content) and the concrete in which 10% cement content was replaced with metakaolin. The experimental results of maximum compressive strength and its corresponding strain were used as input parameters of the proposed predictive models to generate the complete stress-strain curves. The predictive curves show good agreement with the experimental data indicating that the model equations are well derived; however all curves generated by these predictive models do not express the similar degree of agreement. In general, the stress-strain behavior of HSC can be well predicted by using the model proposed by Lu and Zhao (2010); however, further refinement can be done to fully utilize the engineering properties of HSC.

References

[1] Z.-H. Lu, Y.-G. Zhao, Empirical Stress-Strain Model for Unconfined High-Strength Concrete under Uniaxial Compression, Journal of Materials in Civil Engineering, 22 (2010) 1181-1186.

[2] V.P. Jensen, The Plasticity Ratio of Concrete and Its Effect on the Ultimate Strength of Beams, Journal of the American Concrete Institute, 14 (1943) 565-582.

[3] E. Hognestad, Study of combined bending and axial load in reinforced concrete members, Bull. Ser. No. 399, Univ. Illinois EngineeringExperimental Station, Champaign, IL. (1951).

[4] M. Sargin, V. Handa, A general formulation for the stress-strain properties of concrete, SM Report Solid Mechanics Division, University of Waterloo, Canada, (1969).

[5] S. Popovics, A numerical approach to the complete stress-strain curve of concrete, Cement and Concrete Research, 3 (1973) 583-599.

[6] P. Wang, S. Shah, A. Naaman, Stress-strain curves of normal and lightweight concrete in compression, in: ACI Journal Proceedings, ACI, 75 (1978) 603–611.

[7] D.J. Carreira, K.-H. Chu, Stress-strain relationship for plain concrete in compression, in: ACI Journal Proceedings, ACI, 1985.

[8] Comité Euro-International du Béton-Fédération Internationale de la Précontrainte, CEB-FIP model code 1990: design code, ThomasTelford, London, 1993.

[9] L. Hsu, C.-T. Hsu, Complete stress—strain behaviour of high-strength concrete under compression, Magazine of concrete research, 46 (1994) 301-312.

[10] T. Wee, M. Chin, M. Mansur, Stress-strain relationship of high-strength concrete in compression, Journal of Materials in Civil Engineering, 8 (1996) 70-76.

[11] A. Van Gysel, L. Taerwe, Analytical formulation of the complete stress-strain curve for high strength concrete, Materials and Structures, 29 (1996) 529-533.

[12] M.F.Nuruddin, S. U. Khan, T. Ayub and N. Shafiq, Effects of different mineral admixtures on the properties of fresh concrete, Accepted in "The Scientific World Journal" (2013).

[13] S. Khan, T. Ayub, S. Rafeeqi, Prediction of Compressive Strength of Plain Concrete Confined with Ferrocement using Artificial Neural Network (ANN) and Comparison with Existing Mathematical Models, American Journal of Civil Engineering and Architecture, 1 (2013) 7-14.

Applied Mechanics and Materials Vol. 567 (2014) pp 482-487
© (2014) Trans Tech Publications, Switzerland
doi:10.4028/www.scientific.net/AMM.567.482

Prospect of Adopting Kapok Fibre as Roof Insulation

MuhdFadhil Nuruddin[1,a], NadzhratulHusna Ahmad Puad[2,b], KhairunAziziMohdAzizli[3,c], Syed Ahmad Farhan[4,d], Azirul Zainal[5,e]

[1,2,4]Departmentof Civil Engineering, Faculty of Engineering,UniversitiTeknologi PETRONAS, Bandar Seri Iskandar,31750 Tronoh, Perak, Malaysia.

[3]Department of Chemical Engineering, Faculty of Engineering, UniversitiTeknologiPETRONAS, Bandar Seri Iskandar, 31750 Tronoh, Perak, Malaysia.

[5]Project Management and Delivery Department, Technology and Engineering Division, PETRONAS Holdings Berhad, Level 6, MenaraDayabumi, Jalan Sultan Hishamuddin, 50050 Kuala Lumpur, Malaysia.

[a]fadhilnuruddin@petronas.com.my,[b]nadzrahusnaz@gmail.com,[c]khairun_azizli@petronas.com.my,

[d]syfarisk@gmail.com, [e]azirul.zainalabidin@petronas.com.my

Keywords: kapok fibre, ceibapentandra,roof insulation, thermal comfort

Abstract. Interest on building insulation has started to develop among the research community in recent years. Kapok fibres have the potential to become a roof insulation material because of its low thermal conductivity. This paper reviews studies on kapok fibre as insulation material. It is revealed that there were no reported findings on the application of kapok fibre as roof insulation.Thorough study is highly recommended in this area since kapok fibre has good thermal and acoustic properties.

Introduction

Building occupants desire indoor thermal comfort for optimum productivity and contentment. Under hot climates, heat from direct sunlight flows into buildings through the roof and heats up the living space. As a result, indoor temperatures increase and occupants experience thermal discomfort. Consequently, occupants respond to the thermal discomfort by turning on fans or air-conditioners (AC). However, prolonged use of fans and AC leads to increased electricity consumption, which negatively affects the building owners economically and the whole country environmentally.

The roof is heavily exposed to direct sunlight throughout hot days. Therefore, improving the thermal performance of roofs is a vital strategy that should be adopted to make buildings energy-efficient. Roof insulation can block the flow of heat from direct sunlight into buildings through the roof structures. As a result, use of fans or AC to achieve thermal comfort is significantly reduced, leading to economic benefits for building owners and significant environmental benefits for the whole country if implemented at a large scale. Despite the benefits, factors such as lack of awareness and preparedness to make the initial investment to install roof insulation hinder its implementation [1, 2]. Figure 1 shows roofs that are exposed to direct sunlight.



Figures 1. Roofs that are exposed to direct sunlight, taken from [3]

Interest on building insulation has started to develop among the research community in recent years. However, the majority of research in this area focused on buildings under cold climates. Furthermore, research on wall insulation is more popular than roof insulation due to the location of the research institutes involved [1]. Wall insulation discussed in previous researches consists of installation of insulation materials in the wall structure and enhancement of the wall structure itself such as the adoption of new materials that reduces the thermal conductivity of cement paste used for the wall construction [4]. On the other hand, there are some researches carried out to develop new materials that can be adopted as roof insulation that consist of materials with high reflectivity [5] and low thermal conductivity. Interest in roof insulation is present in the research community and further developments in this area can produce significant benefits to many parties economically and environmentally.

Kapok Fibre

Kapok fibres have the potential to become a roof insulation material because of its low thermal conductivity. The kapok tree or also known as *Ceibapentandra (L.)*Gaertn. (Malvales: Malvaceae) can be found mostly in Southeast Asia, East Asia and Africa. Fruits obtained from kapok trees(Figure 2) are extracted to produce kapok fibres[6, 7]. Kapok fibres can be obtained directly from kapok trees since it is anatural cellulosic fibre [8]. Kapok trees can live up to 60 years. It becomes productive after four to five years and the yields will continue to grow within eight years. A kapok tree can produce 330 to 400 fruits per year [9]. Each fruit contains 200 seeds and each tree produces 1000 to 2000 pods yearly[10]. It has beenreported that kapok fibres consist of a hollow structure with a thin fibre wall with a diameter of 16.5 ± 2.4 µm, a large lumen with a diameter of 14.5 ± 2.4 µm and a structure that is cylindrical and non-twisted[11-13]. Even though it is made of unicellular fibres similar to cotton, its density is seven (7) times less than cotton [14].In addition, kapok fibres (Figure 3) are hydrophobic, resilient to fungi and bacterial attacks, and the texture is very soft owing to the presence of cuticle wax [12]. Due to its buoyancy, it has been used as a survival material such as safety jacket. Hollow structure of kapok fibre makes it the best insulation material among other natural fibres and competitive to synthetic fibres like polyester. Apart from that, the seeds are beneficial for human and livestock as a foodstuff[15]. Other properties of kapok fibre are shown in Table 1. Although it has many advantages, it is inflammable[12]. Currently, kapok fibres are mainly used in pillows, mattresses, quilts, soft toys, upholstery and thermal and acoustic insulation owing to its low density and insulation properties [16-19]. However, there is a lack of research on kapok fibre as insulation material. This paper reviews studies on kapok fibre as insulation material.

Table 1. Physical properties of Kapok fibre

Property	Kapok
Bulk density [8]	0.29 g/cm^3
Thermal conductivity [12]	0.03-0.04 W/mK
External wall diameter [13]	16.5 ± 2.4 µm
Internal wall diameter [13]	14.5 ± 2.4µm
Thickness of cell wall [20]	0.5 - 2.0 µm
Average length [20]	20.0 mm
Porosity [27]	84-99%
Specific surface area [28]	0.23 m^2/g
Hollowness [28]	73.08%



Figures 2. Kapok plant, taken from [21]



Figures 3. Kapok fibre, taken from [22]

Literature Search

All articles on kapok fibre published from 2009 to 2013 were retrieved from Scopus. Scopus is used because it is the largest online database of conference papers and peer-reviewed journals[23]. Articles in languages other than English are not included. “Kapok fibre”was used as the keyword. Documents other than articles such as reviews, letters, editorials and notes were excluded. The papers were categorized into five (5) groups according to different research areas, which are insulation, oil absorption, biodiesel, characterization and others. Articles grouped under the insulation research area were utilized in this review.

Review of Previous Research

Five (5) articles were found that reported findings on the application of kapok fibre as insulation. It is revealed that there were no reported findings on the application of kapok fibre as roof insulation. Research gaps are highlighted in Table 2.

Cui and Wang (2009) [8]studied the heat transfer through kapok to be used as an insulation material in fabric to minimize heat loss from the human body. Effect of different temperatures at different wind speeds onthe heat transfer through kapok was analysed and compared with cotton. The researcher designed a theoretical heat flow model that combines heat flow by conduction, convection and radiation and used an artificial climate chamber for testing. Experimental results were in line with the theoretical model. Findings also reveal that wind speed does not affect the transient heat loss from the human body because it takes time to penetrate into the fibrous insulation material. In addition, kapok has smaller transient maximum heat flow than cotton. This research proved that kapok can minimize heat losses from the human body better than cotton because it has better heat balance flow.

Yeoup Chung *et al.* (2009) [24] removed the combustible compounds of kapok to convert it into a flame-resistant fibre that can be used for insulation.Hydrophobic compounds were removed from kapok fibre through the exposure to gamma radiation and cleaved the methoxyl group in order to transform it into flame-resistant fibre.The researcher discovered no morphological change after radiation but the methoxyl group in lignin polymer like p-coumaryl alcohol, sinapyl alcohol and coniferyl alcohol was cleaved by irradiation.The chemical composition in kapok fibre was reduced remarkably with decreases of nitrobenzene oxidation products. Therefore, gamma ray treatment is an alternative method to convert kapok into a flame-resistant fibre.

Song and Yu (2011) [25] compared the heat transfer within kapok and other fibre assemblies, which are wool, cashmere, polyester and goose down to assess their potential as insulation materials.Radiative heat properties of assembled fibre and low bulk densities were characterized using Fourier transform infrared (FTIR) spectroscopy. Results showed that bulk density influenced the radiation heat transfer into the fibre assemblies. The radiative thermal conductivity of the fibres decreased as the bulk density was increased. Random was found to be the most suitable arrangement of fibre assemblies as it prevents radiative heat transfer more effectively compared to random ball and parallel arranged fibre assemblies. The increasing of temperature will increase the radiative heat conductivity, which shows that radiative heat conductivity is proportional to the cubic temperature. Experimental radiative heat conductivity result was compared to the theoretical model and some modifications have been done to the existing theoretical model in order to enhance it.

In 2013,Dieng*et al.*[26] conducted an experiment on kapok as thermal insulation material to analyse its heat retention. Results showed that there is an evolution of thermal impedanceas a function of heat capacity. The significant of pulse excitation and depth in the material was visualized in the evolution curves of temperature versus convective heat transfer coefficient. The optimum thermal insulation capacity depends on convective heat transfer coefficient and external pulse excitation.

The potential of kapok fibre as a sound insulating material was investigated by Xiang *et al.* (2013) [27].Based on the results analysed using impedance tube, kapok fibre showed an excellent acoustical performance. Bulk density, thickness and the orientation of assembled kapok fibre gave significant impact to sound absorption coefficient except for fibre length. Same thickness of kapok fibre assemblies with less bulk density were compared with other commercial sound insulating materials, which are glass wool and degreasing cotton fibre, and ended with the same sound absorption coefficient. Hollow structure of kapok fibre gives an advantage to its performance and the experimental acoustical damping performance agrees with the theoretical model. It is proven that kapok fibre can be a good candidate in the future as sound insulating material.

Table 2.Research gap

Reference	Heat Transfer	Flame-resistant	Heat Retention	Acoustic	*Roof*
Cui and Wang (2009) [8]	✓				
Yeoup Chung *et al.* (2009) [24]		✓			
Song and Yu (2011) [25]	✓				
Dieng*et al.*(2013) [26]			✓		
Xiang *et al.* (2013) [27]				✓	

Conclusion

It has been found that there is a lack of study done on kapok fibre as an insulation material. Moreover, the review also revealed that there is no research that explores the adoption of kapok fibre as a roof insulation material. Thorough study is highly recommended in this area since kapok fibre has good thermal and acoustic properties. Its application as an insulation material may be extended to the building industry especially in countries that produce kapok fibre.

References

[1] S. A. Farhan, M. F. Khamidi, A. M. A. Yacouby, A. Idrus, and M. F. Nuruddin, Critical Review of Published Research on Building Insulation: Focus on Building Components and Climate, presented at the IEEE Business, Engineering & Industrial Application Colloqium, Kuala Lumpur, Malaysia (2012).

[2] A. M. A. Yacouby, M. F. Khamidi, Y. W. Teo, M. F. Nuruddin, S. A. Farhan, S. A. Sulaiman, A. E. Razali, Housing Developers and Home Owners Awareness on Implementation of Building Insulation in Malaysia, WIT Transactions on Ecology and the Environment, 148 (2011) 219-230.

[3] Information on http://www.freeimageslive.co.uk/free_stock_image/calvi-rooftops-jpg

[4] S. A. Farhan, M. F. Khamidi, M. H. Murni, M. F. Nuruddin, A. Idrus, and A. M. A. Yacouby, Effect of Silica Fume and MIRHA on Thermal Conductivity of Cement Paste, WIT Transactions on the Build Environment, 124 (2012) 331-339.

[5]S. A. Farhan, M. F. Khamidi, D. F. Ziela, A. M. A. Yacouby, A. Idrus, M. F. Nuruddin, A. E. Razali, Performance of Reflective Insulation in Gable Roofs: Small-Scale Experimental Investigation, presented at the International Conference on Civil, Offshore & Environmental Engineering, Kuala Lumpur, Malaysia (2012).

[6] A. –M. Tang, Z. –H. Sun, X. Fu, M. Zi, H. –W. Zhang, G. Chen, Y. Lin, Chemical and structural characteristics of kapok fibres, ZhongguoZaozhiXuebao/ Translations of China Pulp and Paper, 23 (3) (2008) 1-5.

[7] C. Qiuling, W. Lin, Structure and property contrast of kapok fibre and cotton fibre, Cotton textile Technology, vol. 37 (11) (2009) 668-670.

[8] P. Cui and F. Wang, An investigation of heat flow through kapok insulating material, Tekstilvekonfeksiyon, 2 (2009) 88–92.

[9] D. Louppe, A.A. Oteng-Amoako, and M. Brink, (eds.), Plant Resources of Tropical Africa 7: timbers 1. PROTA Foundation, Backhuys Publishers, Leiden, the Netherlands.

[10] D. Narahari and R. AshaRajini, Chemical composition and nutritive value of kapok seed meal for broiler chickens. British Poultry Science, 44(3) (2003) 5005-509.

[11] H., Y., W. –D. Xiao and M. –W. Shi, Structure and performances of the kapok fibre, Journal of textile research, 26 (4) (2005) 4-6.

[12] M.L. Voumbo, A. Wereme, S. Gaye, M. Adj and G. Sissoko, Characterization of the thermophysical properties of kapok, Journal of Applied Sciences, Engineering and Technology, 2(2) (2010) 143-148.

[13] X. F. Huang and T.T. Lim, Performance and mechanism of hydrophobic-oleophilic kapok filter for oil/water separation, Desalination, 190 (1-3) (2006) 295-307.

[14] K. Manohar, D. Ramlakhan, G. Kochhar and S. Haldar, Biodegradable fibrous thermal insulation, J. Braz. Soc. Mech. Sci. Eng., 28(1) (2006) 45-47.

[15] A.A. Danso, State of Forest Genetic. (2001). Information on http://www.fao.org/DOCREP/004/AB391E /ab391e03.htm#TopOfpage

[16] K. Hori, M. E. Flavier, S. Kuga, T. B. T. Lam, K. Iiyama, Excellent oil absorbent kapok (Ceibapentandra (L.) Gaertn.)fibre: fibre structure, chemical characteristics, and application, Journal of Wood Sci, 46 (2000) 401-404.

[17] D.M. Bates, Malvales. Encyclopaedia Britannica (2004), CD version.

[18] C. Orwa, A. Mutua, R. Kindt, R. Jamnadassand S. Anthony, Agroforestree Database: a Tree Reference and Selection Guide Version 4.0. World Agroforestry Centre, Kenya (2009).

[19] S. Chaiarrekij, A. Apirakchaiskul, K. Suvarnakich and S. Kiatkamjornwong, Kapok 1: Characteristics of kapok fibre as a potential pulp source for paper making,Bioresources, 7(1) (2011) 475-488.

[20] P. Cui, F. Wang, A. Wei, K. Zhao, The Performance of Kapok/Down Blended Wadding, Textile Research Journal, 80(6) (2010) 516-523.

[21] Information on http://www.hoppie.nl/miami/blog/2012/mattfair24.jpg

[22]Information on http://www.wildfibres.co.uk/assets/images/autogen/a_natural-fibres-kapok-0375.jpg

[23] Information on http://www.elsevier.com/__data/assets/pdf_file/0007/148714/scopus_facts_and_figures.pdf

[24] B. Yeoup Chung, M. HoHyeong, B. Chull An, E. Mi Lee, S. Sik Lee, K. Jin-Hong, K. Jae-Sung, K. Tae-Hoon, C. Jae-Young, Flame-resistant kapok fibre manufactured using gamma ray. Radiation Physics and Chemistry, 78(7-8) (2009).513–515.

[25] W.F. Song and W.D. Yu, Study on radiative heat transfer property of fibre assemblies using FTIR. J Therm Anal Calorim, 103 (2011) 785–790.

[26] M. Dieng, I. Diagne, B. Fleur, A. Kane, M.L. Sow and G. Sissoko, Study of Heat Transfer in a Kapok Material from the Convective Heat Transfer Coefficient and the Excitation Pulse of Solicitations External Climatic. Journal of Applied Sciences, Engineering and Technology, (2013) 1–4.

[27] X. Hai-fan, D. Wang, L. Hui-chao, N. Zhao and J. Xu, Investigation on sound absorption properties of kapok fibres. Chinese Journal of Polymer Science, 31(3) (2013) 521–529.

[28] T. Rijavec, Influence of Kapok Hollowness on Its Liquid Retention Capacity, Tekstilec, 52 (10-12) (2009) 270-283.

Applied Mechanics and Materials Vol. 567 (2014) pp 488-493
© (2014) Trans Tech Publications, Switzerland
doi:10.4028/www.scientific.net/AMM.567.488

Rehabilitation of RC Structures Exposed to Salinity and Moisture Using CFRP

H. Fazli[1, a], W.Teo[1, b]

[1]Civil Engineering Department, Universiti Teknologi PETRONAS, Bandar Seri Iskandar, 31750 Tronoh, Perak, Malaysia

[a]hamed.fazli62@gmail.com, [b]teo_wee@petronas.com.my

Keywords: Concrete reinforced structures, Marine environment, Carbon fiber reinforced polymer (CFRP), Composite materials

Abstract. Marine concrete structures such as harbors, ports and bridges are exposed simultaneously to the action of physical and chemical deterioration processes. Deterioration of marine concrete structures and its rehabilitation are challenges of the world of today. Recently, the increasing usage of carbon fiber reinforced polymer (CFRP) composite appears to be a solution for rehabilitation and strengthening of the concrete structures because of its physical and mechanical properties, such as high strength-to-weight ratio, high corrosion /environmental degradation resistance, and easy to handle during construction. In general, rehabilitation of concrete structures is usually done by two types of materials, it is either using cementitious or advanced composite materials. The aim of this paper is to address the issues and challenges of concrete structures in marine environments and strengthening these structures. In the initial part of this paper, an overview of the problems associated with marine environment on concrete structure will be discussed.

Introduction

Because of reinforced concrete low cost, ease of construction and durability, it is an extensively used structural material. The concrete cover usually provides adequate corrosion protection from ingression of moisture and chlorides into the concrete then corrode the steel reinforcement. However, the embedded steel may corrode and lead to crack and spall the concrete cover because of expansive corrosion occurrence at the steel concrete interface. This allows more chlorides to ingress easily and eventually, the structure may be unable to safely perform the service for which it was designed because the load bearing capacity of the steel is reduced. Due to the harsh environment such as sea water, the deterioration of concrete structures in the marine environment has been a great issue for many years. Currently, civil engineers find out the potential of fiber reinforced polymer (FRP) composites as strengthening material for concrete structures damages in the marine environment for extending the service life of marine structures. CFRP has exceptional properties such as light weight, high tensile strength and stiffness and resistance to both chemicals and corrosion, make them particularly suitable for rehabilitation. Carbon fiber reinforced polymer (CFRP) as strengthening system materials have a huge resistance to aggressive environmental conditions. CFRP*'s* are normally used in the form of sheets and plates as externally bonded repair materials. Reduction in the strength and serviceability of the concrete structures due to corrosion of moisture and chloride-induced may lead to shear and flexural failure.

This paper summarizes the concept of problems associated with salinity and moisture on concrete structure, due to environmental condition and also the CFRP strengthened systems with different schemes.

Effect of Marine Environment on Strengthened RC Structures

Investigation on concrete structures expose to environmental condition has been started more than two decades ago. Practically, moisture and salinity are the factors that have a great influence on the CFRP strengthening system. Normally in the natural environment, the combination of

moisture and salinity creates more damages for the concrete structures. The influence of salinity and moisture on the strength of concrete structures will be discussed in details in the next subtitle.

Effect of Salinity on RC Structures Strength. High alkalinity (pH 12.5–13.5) property of the concrete and also protective film on the surface of the embedded steel protected the steel rebars against corrosion. While the concrete structure member exposed to harsh environment such as chlorides, the chloride concentration will increase and consequently decrease the alkalinity of the concrete, then the protective film is destroyed and corrosion on the surface of the steel started. The de-icing salt exposure reduces the serviceability of concrete structure. Ports, harbours or bridges are the offshore structures which are used in the coastal applications. Due to the deicing salts, these offshore structures are subjected to salt water. Environment chlorides can arise from seawater or salt spray particles. Chlorides also may originate from de-icing salts where these are used on road bridges.

Medeiros, Gobbi, Réus and Helene [1] investigated on the effect of the wetting and drying cycles on reinforced concrete structures in the marine environment, they verified that wetting and drying cycles have a strong effect on the chloride-ion content, which structures were exposed to wetting and drying chloride contents 3 to 8 of about times higher than structures where do not expose (P2 and P5). Fig. 1 illustrates that the pillars which subjected to the wet and dry cycle (P1, P8 and P11), shows highest chloride contents compared to the pillars which not subjected to wet and dry cycle (P2 and P5). These results specify that ion penetration in a reinforced concrete structures highly subjected to wet and dry cycle. The results also shows that, height and the distance from the sea are the factors which influence in the intensity of attack by chloride ions.

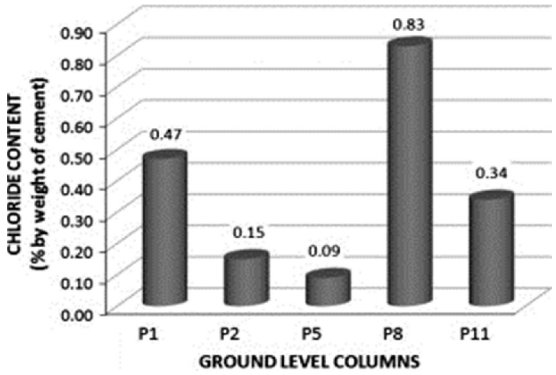


Figure 1: Chloride content (by weight of cement) at ground level pillars [1].

Castel et al. [2, 3] based on 17 years experimental works on reinforced concrete beams which exposed to a saline fog environment reported that between chloride content and long-term corrosion has no related. Even though the chloride content was well above the thresholds, and little corrosion of reinforcement found as evidence. Also they reported that corrosion occurred when between reinforcement and the surrounding concrete was a lack of intimate contact. Also Melchers and Li [4] concluded that the corrosion time to initiate for reinforcement of concrete structures expose to de-icing salts or marine environments, does not depend strongly on the reported concentration of chlorides at the reinforcement and this period was less than 5 years for many structures. However, corrosion time to initiate was at least 10 years and in most cases greater than 15 years for reinforced concrete structures constructed from limestone or (non-reactive) dolomite aggregates or with blast furnace cement.

Effect of Moisture on RC Structures Strength. Concrete is heterogeneous and porous material. Ingress of air and moisture is one of the major drawbacks which reach to the reinforcement of RC structure and it corrodes the reinforcement. Generally, the presence of air voids at the concrete-steel interface has been found to strongly influence the resistance to corrosion. If concrete is expose to long-term wetting, the water will ultimately reach the level of the reinforcement; either diffusion

through the porous structure of the concrete or by traveling along cracks in the concrete will corrodes the reinforcement. Bond strength between the steel and concrete due to the corrosion on reinforcement will reduced. The transport and fixation of moisture, ions and gases related to the corrosion process is thus strongly dependent on the permeability. Also another effect of the moisture conditions on concrete is by the interaction of chloride with the cement paste the rate of chloride ingress in concrete affected.

The main redox reaction can be describe the corrosion is Eq. 1 and Eq. 2 which respectively representing the anodic oxidation of iron and the cathodic reduction of oxygen.

$$Fe \longrightarrow Fe^{2+} + 2e^{-} \quad (1)$$

$$H_2O + \tfrac{1}{2} O_2 + 2e^{-} \longrightarrow 2OH^{-} \quad (2)$$

The overall reaction is represented by Eq. 3 where produced $Fe(OH)_2$.

$$Fe + H_2O + \tfrac{1}{2} O_2 \longrightarrow Fe(OH)_2 \quad (3)$$

Depending on the surrounding environment such as moisture, chloride, oxygen, pH and temperature, $Fe(OH)_2$ is just one of the several possible corrosion where can be produced [5].

Strengthening of RC Beams with Externally Bonded CFRP Composite

General. Rehabilitation is based on three main concepts: repair, strengthening, and retrofit [6]. Restoring a damaged structure member to its original capacity is defined as repair [7]. While strengthening defined as increasing the capacity of structural member further than its designed performance level and retrofit is used to seismic upgrade of a structure [8]. FRP material can be used for all three applications; In this paper, the focus is only on strengthening of concrete structures.

FRP strengthening externally bonding is done by sheets or plates to a concrete structural member. Sheets will be attached to the specimens by the hand-layup method as per the instructions provided by the manufacturer [7].

CFRP Fabric, CFRP plate and GFRP are kind of composites which mostly used for strengthening and rehabilitation the concrete structures. A lower ductility, higher Young's modulus and tensile strength of CFRP, makes it to become one of the composites mostly used for strengthening the concrete structures [9]. Over the past decades, considerable research has been done in performance of strengthening concrete structures with externally bonded CFRP composites. Previous studies found that, CFRP composites are increasing the strength of reinforced concrete (RC). Common effective methods of beams strengthening are using CFRP.

Different Strengthening Wrapping Schemes. To increase the shear resistance of RC beams several CFRP bonding schemes have been used. These schemes include bonding CFRP to the side of the beam only (two sides wrap), bonding CFRP to three sides, two side and tension face (U-wrap), and wrapping CFRP around the section (full wrap). CFRP sheets can be installed continuously or discrete strips for all wrapping scheme. The fibers in the CFRP two sides bonded may be oriented at different angles and also the FRP contribution to shear strength can be strip or continues [10] (Fig. 2). For design requirements based on factors such as the accessibility of the site, project budget and the amount of increase required in the shear capacity the strengthening scheme needs to be selected.

The wrapping scheme for shear strength is two sides wrap, and for both shear and flexural are U-wrap and full wrap. The recommended wrapping scheme is fully wrap the member whenever it is possible. However, in most situations, a U-wrap is the only economical and practical wrapping scheme.

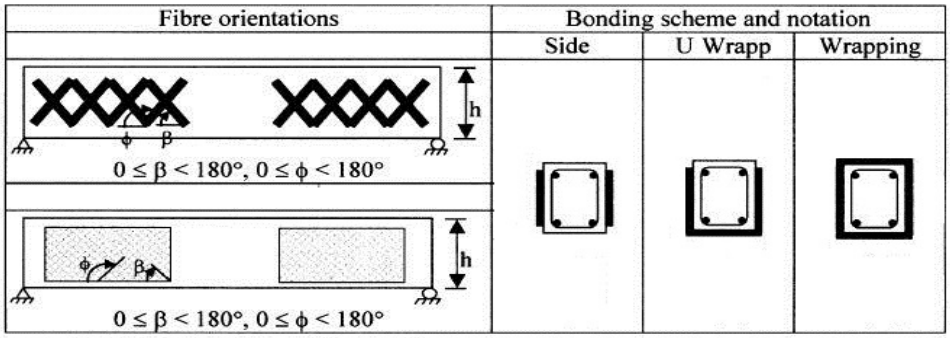


Figure 2: Recommended effectiveness CFRP wrapping scheme [10]

CFRP Strengthened Concrete under Environmental Exposure. The CFRP composites produced in two types which are fabric and plate. Many researchers have studied on the differences of these two types of CFRP's in different environmental condition. Grace N. F and Singh S. B [11] research results on durability of the externally bonded RC beams with CFRP plates and fabrics under harsh environmental conditions showed that RC beams strengthened with CFRP plates and expose to aggressive environmental exhibit increased load carrying capacity with respect to the base line beams under short term exposure. They found that between RC beams and CFRP plates and fabrics the most detrimental factor to the bond strength is long-term exposure to humidity. As well as, after long term exposure to 100% humidity, thermal expansion, freezing-and-thawing and dry heat the strengthened beams with CFRP plates load carrying capacity is reduced.

Cromwell, Harries and Shahrooz [12] studied on externally bonded CFRP to concrete and various environmental conditioning regimes. They concluded that CFRP plate performed very well than CFRP fabric in all conditions. Generally hand laid-up CFRP fabric material performed well under the environmental conditioning, although the effects of raised up temperature conditioning increased the absorption due to matrix damage. They reported that, salt water and alkaline exposures produced the greatest deterioration. Also, these processes are certainly most simulative of harsh environmental conditions to which civil infrastructure is exposed. As well as, simplest methods to conduct at room temperature and elevated temperatures.

Tuakta and Buyukozturk [13] studied for moisture effects on concrete/epoxy/FRP bond system. By means of the tri-layer fracture toughness they characterized the bond system, which can be experimentally achieved from peel and shear fracture tests. The bond strength draws on a certain value after a certain period of time. No more significant degradation may occur afterwards. After a very long moisture exposure, this asymptotic fracture toughness is the minimum bond strength a concrete-concrete/FRP bonded system that can retain. Also, moisture cyclic and moisture reversal conditioning tests showed that after consecutive wet–dry cycles the adhesive bond cannot recapture its original bond strength. Likewise, they reported that when the intermediate conditioning duration and the number of wet–dry cycles increases the residual bond strength decreases.

Costa and Appleton [14] study describes several case studies of different types of concrete structures, subject to the marine environment, which cause deterioration due to chloride-induced corrosion. The evaluation of the structures of this paper shows that, when damaged structures are exposed to harsh environments, such as the moisture and salinity, deterioration can be developed fast and leading to severe damage conditions in very short time periods. The concrete surface has higher deterioration in zones due to wetting and drying cycles of salt water. Corrosion rates in excess of 500 μm/year were measured in these very aggressive exposure conditions.

Shear and flexural behavior of RC beams strengthened by CFRP. Shear and flexural failures are very common. However, due to brittle characteristic and probability of sudden occurrence, any failure potential due to shear cracking will be disastrous. Reed and Peterman [15] studied on 30 years old damaged pre-stressed concrete girders and found out that capacity of flexural and shear improved with externally bonded CFRP composite sheets. Over 50% of the original design strength by using two layers of longitudinal carbon fiber reinforcement, and over 25% of the base strength

the specimens flexural capacity was increased. The shear capacity of the specimens also increased with CFRP U-stirrups strengthening. However, the mode of failure didn't change by using CFRP stirrups. The shear capacity of the specimen increases 30% in the specimen with U-stirrups.

Khalifa and Nanni [16] investigated on the modes of failure and shear behavior of T-section RC beams. They studied on CFRP amount, CFRP end anchorage, wrapping schemes and 90°/ 0° ply combination. They found that external bonded CFRP, increased the shear capacity of the beam significantly and U-wrap with end anchorage is the most effective configuration. Also, using CFRP on the beam sides compared to U-wrap only gives less shear contribution. They recommended to use continues wrap scheme due to the damage of strip would have more of an impact on the overall shear capacity, although maybe CFRP strips as capable as continuous CFRP sheets in the research laboratory.

Furthermore, Bousselham and Chaallal [17] studied on the understanding of the shear resistance mechanisms involved in RC beams strengthened in shear with externally bonded CFRP. They studied on 17 tests, which performed on full size T beams. They found that after yielding of the stirrups and resulting major cracking, the residual shear capacity of the RC beams becomes minimal if not negligible. Transverse steel in unstrengthened concrete beam contribute greater than corresponding FRP strengthened concrete beam. Also the use of truss analogy with angle of 45° is minimize the transverse steel contribute in shear resistance. The contribution of CFRP to the shear resistance, which is activated after the formation of the first diagonal cracks, does not vary linearly with the loading.

Experimental study on external FRP bonded RC beams with flexural and flexural-shear strengthening consisting of carbon FRP (CFRP) and glass FRP (GFRP) conducted by Dong, Wang and Guan [18]. They evaluate the different scheme wrapping of CFRP and GFRP to find out how it has affected the behaviour of the RC beams strengthened. All the beams tested under four-point bending with simply supported over a clear span of 1500 mm. They found out that using externally bonded of CFRP or GFRP sheets on tension face and/or lateral faces can significantly increase the flexural and shear capacity of the beams strengthened. The overall flexural capacity of the CFRP strengthened beams increase between 41% and 125% compared to the control beam. And between 31% and 74% the shear capacity increase on the CFRP or GFRP strengthened beams.

Summary

This paper has provided a review of research on RC structures exposed to harsh environmental condition and also application of externally bonded CFRPCs in civil construction in strengthening. Following general concluding remarks are made:

- Structures were exposed to wetting and drying chloride contents 3 to 8 of about times higher than structures where do not expose.
- In the moisture condition by the interaction of chloride with the cement paste the rate of chloride ingress in concrete affected.
- U-wrap strengthening is the only economical and practical wrapping scheme.
- CFRP plate performed very well than CFRP fabric and GFRP in all conditions.
- Between RC beams and CFRP plates and fabrics the most detrimental factor to the bond strength is long-term exposure to humidity.
- Externally bonded CFRP composite reinforcement is a viable solution towards enhancing strength exposed to salinity and moisture. It also enhances shear capacity.
- Salt water and alkaline exposures produced the greatest deterioration.
- Residual bond strength decreases by increases the intermediate conditioning duration and the number of wet–dry cycles the.
- Transverse steel in unstrengthened concrete beam contribute greater than corresponding FRP strengthened concrete beam.
- Using externally bonded of CFRP or GFRP sheets on tension face and/or lateral faces can significantly increase the flexural and shear capacity of the beams strengthened.

References

[1] M.H.F. Medeiros, A. Gobbi, G.C. Réus, P. Helene, Reinforced concrete in marine environment: effect of wetting and drying cycles, height and positioning in relation to the sea shore, J. Constr. Build. Mater. 44 (2013) 452-457.

[2] A. Castel, T. Vidal, R. Zhang, R. Francois, V. Sirivivananon, Initiation and propagation phase in reinforced concrete corrosion due to long term exposure in saline environment, in: F.T.E.e. al. (Ed.) CONSEC'07, Concrete under Severe Conditions,, Laborataire Central des Ponts et Chaussees, Paris 2007, pp. 307–314

[3] A. Castel, T. Vidal, R. François, G. Arliguie, Influence of steel - Concrete interface quality on reinforcement corrosion induced by chlorides, J. Mag. Concr. Res. 55 (2003) 151-159.

[4] R.E. Melchers, C.Q. Li, Reinforcement corrosion initiation and activation times in concrete structures exposed to severe marine environments, J. Cem. Concr. Res. 39 (2009) 1068-1076.

[5] T. Marcotte, Characterization of chloride-induced corrosion products that form in steel-reinforced cementitious materials, vol PhD, University of Waterloo, Waterloo, Canada, 2001.

[6] V.M. Karbhari, L. Zhao, Use of composites for 21st century civil infrastructure, J. Comput. Meth. Appl. Mech. Eng. 185 (2000) 433-454.

[7] M. Bergström, Life cycle behaviour of concrete bridges: Laboratory tests and probabilistic evaluation, Department of Civil and Environmental Engineering, vol PhD, Luleå University of Technology, , Luleå Sweden, 2006.

[8] F.i.d.b. fib, Retrofitting of Concrete Structures by Externally Bonded FRPs: With Emphasis on Seismic Applications, International Federation for Structural Concrete, 2006.

[9] M. Arockiasamy, S. Chidambaram, A. Amer, M. Shahawy, Time-dependent deformations of concrete beams reinforced with CFRP bars, J. Compos. Eng. 31 (2000) 577-592.

[10] J.F. Chen, J.G. Teng, Shear capacity of FRP-strengthened RC beams: FRP debonding, J. Construction and Building Materials 17 (2003) 27-41.

[11] Grace N. F, Singh S. B, Durability evaluation of carbon fiber-reinforced polymer strengthened concrete beams: experimental study and design, J. ACI STRUCT J 102 (2005) 40-53.

[12] J.R. Cromwell, K.A. Harries, B.M. Shahrooz, Environmental durability of externally bonded FRP materials intended for repair of concrete structures, J. Constr. Build. Mater. 25 (2011) 2528-2539.

[13] C. Tuakta, O. Büyüköztürk, Deterioration of FRP/concrete bond system under variable moisture conditions quantified by fracture mechanics, J. Compos. Constr. 42 (2011) 145–154.

[14] A. Costa, J.Appleton, Case studies of concrete deterioration in a marine environment in Portugal, J. Cem Concr Compos. 24 (2002) 169–179.

[15] C. Reed, R. Peterman, Evaluation of Prestressed Concrete Girders Strengthened with Carbon Fiber Reinforced Polymer Sheets, J. Bridge Eng 9 (2004) 185-192.

[16] A. Khalifa, A. Nanni, Improving shear capacity of existing RC T-section beams using CFRP composites, J. Cem. Concr. Compos. 22 (2000) 165-174.

[17] A. Bousselham, O. Chaallal, Mechanisms of shear resistance of concrete beams strengthened in shear with externally bonded FRP, J. Compos. Constr. 12 (2008) 499-512.

[18] J. Dong, Q. Wang, Z. Guan, Structural behaviour of RC beams with external flexural and flexural-shear, J.compositesb. 44 (2013) 604–612.

Applied Mechanics and Materials Vol. 567 (2014) pp 494-498
© (2014) Trans Tech Publications, Switzerland
doi:10.4028/www.scientific.net/AMM.567.494

Shear capacity of RC Beams with Web Openings Strengthened with Multi layers of CFRP

Bashar S. Mohammed[1,a] and Omar Alanni[2]

[1]Department of Civil Engineering Universiti Teknologi PETRONAS,

Bandar Seri Iskandar, 31750 Tronoh, Perak, Malaysia.

[2]Department of Civil Engineering, Universiti Tenaga National, Malaysia.

[a]bashar.mohammed@petronas.com.my

Keywords: RC beams, CFRP, shear force, beam with web opening.

Abstract. In some cases a cut-out web opening in a reinforced concrete (RC) beam is required to facilitate the passage of electrical and mechanical pipes and ducting from one side to another. The presence of cut-out web openings will lead to decreasing in the load carrying capacity of these RC beams. Therefore, strengthening the vicinity of these openings by using Carbon Fiber Reinforced Polymer (CFRP) will represent the best practical solution. In this study, thirteen RC beams with different sizes of cut-out web openings and with different layers of CFRP strengthening and also one solid RC beam (control) were prepared and tested to failure. The outcome of this experimental and analytical study showed that the modified Eurocode 2 model can reasonably be used in computing the shear forces of RC beams having the vicinity of their cut-out web openings strengthened with single/multi layers of CFRP. In addition, for safe design purposes, a reduction factor has been suggested as well.

Introduction

To facilitate the passage of pipes and ducts from one side to another, cut-out web openings in the existing reinforced concrete (RC) beams could be inevitable. These openings lead to reduction in load carrying capacity of the RC beams. This is due to the fact that creating an opening in an existing structural member (such as RC beams) will promote stresses concentration at the corners of the opening which initiate inclined and vertical cracks [1,2]. The best practical solution to restore the load carrying capacity of these beams is to strengthening the vicinity of cut-out web openings using Carbone Fiber Reinforced Polymer (CFRP). The advantages of using CFRP including their high strength-to-weight ratio, good corrosion resistance, good fatigue properties, electro-magnetic resistance, efficiency, reliability, cost effectiveness in rehabilitation and versatility in coping with different sectional shapes and corners [3-9]. Many studies on strengthening RC beams in shear area by using CFRP composites have been carried out. The effectiveness of CFRP in strengthening of RC beams depends on several parameters, including the stiffness of CFRP sheet, quantity of the thermosetting resin, compressive strength of the concrete, number of piles of CFRP sheet, wrapping scheme, and fibre orientation angle of the FRP. Abdalla et al. [10] have evaluated the effectiveness of using CFRP sheets to control local cracks around openings and to resist excessive shear stress in the opening cords. They concluded that the use of FRP sheet to strengthen the area around openings in the RC beams may retrieve the full capacity of the beam for relatively small opening. Therefore, the main aim of the research reported in this paper is to investigate the shear capacity of RC beams with cut-out web openings strengthened with single/multiple CFRP layers.

Experimental program

Experimental details and test setup. As shown in Table 1, fourteen RC beams with different sizes of cut-out web openings and different strengthening of CFRP layers were prepared, cast and tested to failure. The test set-up is shown in Fig. 1.

Table 1: Test Variables in Experimental Program

Beam number	Dimensions of opening (mm)		Description of beam
	Length	Depth	
B1	Solid		Control(solid) beam without opening
B2	100	120	Beam with small opening without CFRP
B3	240	120	without CFRP strengthening
B4	360	120	without CFRP strengthening
B5	360	150	without CFRP strengthening
B6	240	120	Strengthened by single layer of CFRP around the opening
B7	360	120	Strengthened by single layer of CFRP around the opening
B8	360	150	Strengthened by single layer of CFRP around the opening
B9	240	120	Strengthened by double layers of CFRP around the opening
B10	360	120	Strengthened by double layers of CFRP around the opening
B11	360	150	Strengthened by double layers of CFRP around the opening
B12	240	120	Strengthened by triple layers of CFRP around the opening
B13	360	120	Strengthened by triple layers of CFRP around the opening
B14	360	150	Strengthened by triple layers of CFRP around the opening



Figure 1: Test Setup

Experimental results. Table 2 shows the experimental results of the tested RC beams.

Table 2: Summary of experimental results

Beam	Ultimate load P_u (kN)	Ultimate shear (kN)	Shear capacity (%)	Reduction in shear capacity (%)	Mode of failure
B1	95.5	47.7	100	-	Flexural at mid span
B2	93.7	46.8	98	2	Flexural at mid span
B3	54.3	27.2	57	43	Shear at opening
B4	49.3	24.6	51.5	48.5	Shear at opening
B5	42.6	21.3	44.6	55.4	Shear at opening
B6	84.6	42.3	88.6	11.4	Shear (CFRP sheet rupture)
B7	76.3	38.1	79.8	20.2	Shear (CFRP sheet rupture)
B8	64.5	32.2	67.5	32.5	Shear (CFRP sheet rupture)
B9	94.2	47.1	98.7	1.3	Flexural at mid span
B10	93.9	47	98.5	1.5	Flexural at mid span
B11	82.4	41.2	86.3	13.7	Shear (CFRP sheet rupture)
B12	96.4	48.2	101	-1	Flexural at mid span
B13	94.1	47.5	99.5	0.5	Flexural at mid span
B14	93.7	47	98.5	1.5	Flexural at mid span

Results and Discussions

Effect of using CFRP on the shear capacity of the beam. As shown in Table 2, by comparing the shear capacity of the tested beams with the solid beam (B1), beam B2 showed only 2% reduction in the shear capacity. This indicates that small cut-out web opening has insignificant effects on the shear capacity of the RC beams. On the other hand, as the size of the cut-out web opening increases (B3-B5), the reduction in the shear capacity of the beams has reached up to 55.4% as for B5. However, a significant recovery was achieved in the shear capacities of the RC beams with their cut-out web openings have been strengthened with CFRP (one, two and three layers). For beams with one layer of CFRP, the recovery was in the range of 22.9% to 31.6%. While, higher shear capacity recovery for beams with more than one layer of CFRP have been observed. For beams with three CFRP layers, the failure mode has been changed to flexural with almost full recovery of the shear capacity (Table 2). It is worthy of note that the beams with their cut-out web opening strengthened with single layer of CFRP (B6 - B8), the failure mode was shear in the opening due to the rupture of the CFRP. Therefore, the authors suggest that wedge anchors are required to prevent such failure mode in future investigation.

To predict the shear capacity (V_c) of beam with cut-out web opening, Mansur [11] has recommended Equation (1).

$$V_c = \frac{1}{6}\sqrt{fc'} \times b_w \times (d - do) \quad (1)$$

where; d is the effective depth of the RC beam, d_o is the height of the web opening, b_w is the width of the RC beam and f_c' is the characteristic concrete compressive strength.

For concrete beams with strengthened opening, the shear force carried by each chord (V_r) should be resisted by concrete (V_c)and the CFRP sheets (V_f) as can be seen in Eq. 2.

$$V_r = V_c + V_f \quad (2)$$

Based on Eurocode 2, Triantafillou [12] has suggested Eq. 3 for predicting the shear capacity of RC beams with their cut-out web opening strengthened with CFRP layers:

$$V_f = 0.9\frac{\varepsilon_{fke}}{\gamma_f} E_f \rho_f b_w d_t (Sin\beta + Cos\beta) \quad (3)$$

where; γ_f is the partial safety factor for CFRP = 1.2, E_f is the elastic modulus of CFRP in the principle fibre orientation = 230 Gpa, β is the angle between the principal fibre orientation and longitudinal axis of the opening chord, ρ_f is the FRP reinforcement ratio, d_t is the effective depth of the top cord and ε_{fke} is the characteristic value of the effective FRP strain.

As shown in Table 3, the shear forces obtained from the Eurocode 2 are in good agreement with the experimental results. However, for safe design, the authors suggested that 0.8 reduction factor (R_f) should be included in Eq. 2 so that it can be rewritten as can be seen in Eq. 4.

$$V_r = (V_c + V_f) R_f \quad (4)$$

Therefore, for example, the shear force for beam B13 = 53.73 x 0.8 = 43 KN, which is less than the experimental value (47.5 KN).

Table 3: The comparison between the experimental results and theoretical analysis

Beam	V_c (KN)	Eurocode 2 models		V_{exp} (KN)
		V_f (KN)	V_r (KN)	
B6	19.31	21.31	40.62	42.3
B7	19.31	18.03	37.34	38.1
B8	16.09	17.76	33.82	32.2
B9	19.31	29.68	48.99	47.1
B10	19.31	29.68	48.99	47
B11	16.09	24.59	40.68	41.2
B12	19.31	34.42	53.73	48.2
B13	19.31	34.42	53.73	47.5
B14	16.09	28.69	44.78	47

Conclusions

The shear capacity of the reinforced concrete (RC) beam decreases as the size of the cut-out web opening increasing. However, using Carbon Fiber Reinforced Polymer (CFRP) in strengthening the vicinity of the opening would lead to recovery in the lost shear capacity. These recoveries depend on the layers of the CFRP used. Whereas, using three layers of CFRP will lead to full recovery of the shear capacity of the RC beam. It also has been found that using the modified theoretical model of Eurocode 2 will lead to reasonable prediction of the shear capacity of RC beams with cut-out web openings strengthened with single or multiple layers of CFRP. for safe design purposes, a reduction factor has been suggested as well.

References

[1] B.S. Mohammed, H. A. B. Badorul and K.K. Chong, Behavior of axially loaded fired-clay masonry panels with openings, The Indian Concrete Journal. 83 (2009) 9-16.

[2] B.S. Mohammed, L.W. Ean, M.A. Malek, One way RC wall panels with openings strengthened with CFRP, Construction and Building Materials Journal. 40 (2013) 575–583.

[3] H.T. Cheng, B.S. Mohammed, K.N. Mustapha, Interaction diagram and response surface plot of pretensioned inverted T-beam with web openings, International Journal of Modeling, Identification and Control. 7 (2009) 209-218.

[4] H.T. Cheng, B.S. Mohammed, K.N. Mustapha, Experimental and analytical analysis of pretensioned Inverted T-beam with web openings, International Journal of Mechanics and Materials in Design. 5 (2009) 203-215.

[5] H.T. Cheng, B.S. Mohammed, K.N. Mustapha, Finite element analysis and structural design pretensioned inverted T-beam with web openings, Frontier of Architectural and Civil Engineering. 3 (2009) 148-157.

[6] H.T. Cheng, B.S. Mohammed, K.N. Mustapha, Application of response surface methodology in finite element analysis of deflection of pretensioned inverted T-beam with web openings strengthened with GFRP laminates, 2nd International Conference on Information and Computing Science, ICIC (2009) 7 – 10.

[7] H.T. Cheng, B.S. Mohammed, K.N. Mustapha, Interaction diagram in finite element analysis of deflection of pretensioned inverted T-beam with web openings strengthened with GFRP laminates, 2nd International Conference on Information and Computing Science, ICIC (2009) 335 – 338.

[8] H.T. Cheng, B.S. Mohammed, K.N. Mustapha, Ultimate load analysis of pretensioned inverted T-beams with circular web openings, Frontiers of Architecture and Civil Engineering in China. 3 (2009) 262 – 271.

[9] B.S. Mohammed, H.T. Cheng, Immediate deflection of pretensioned inverted t-beam with circular web openings strengthened with GFRP using response surface methodology, Key Engineering Materials. 594-595 (2014) PP. 516 – 520.

[10] H.A. Abdalla, A.M. Torkey, H.A. Haggag, A.F Abu-Amira, Design against cracking at openings in reinforced concrete beams strengthened with composite sheet, Composite Structures Journal. 60 (2003) 197–204.

[11] M.A. Mansur, Effect of openings on the behavior and strength of R/C beams in shear, Cement and Concrete Composites. 20 (1998) 477-487.

[12] T.C. Triantafillou, Shear strengthening of reinforced concrete beams using epoxy-bonded FRP composites, ACI Struct. Journal. 95 (1998) 107-115.

Applied Mechanics and Materials Vol. 567 (2014) pp 499-504
© (2014) Trans Tech Publications, Switzerland
doi:10.4028/www.scientific.net/AMM.567.499

Single-Degree-of-Freedom based Pressure-Impulse Diagrams for Blast Damage Assessment

Zubair Imam Syed[1, a], Mohd Shahir Liew[2,b], Muhammad Hasibul Hasan[3,c] and Srikanth Venkatesan[4,d]

[1,2]Civil Engineering Department, Universiti Teknologi PETRONAS, 31750 Perak, Malaysia

[3]Department of Manufacturing and Materials Engineering, International Islamic University Malaysia, 53100 Kuala Lumpur, Malaysia

[4]School of Engineering and Science, Victoria University, Footscray campus, Vic 3011, Australia

[a]imam.syed@petronas.com.my, [b]shahir_liew@petronas.com.my, [c]hasibulhasan@iium.edu.my [d]srikanth.venkatesan@vu.edu.au

Keywords: Pressure-impulse diagrams; single degree of freedom models; blast loading

Abstract. Pressure-impulse (P-I) diagrams, which relates damage with both impulse and pressure, are widely used in the design and damage assessment of structural elements under blast loading. Among many methods of deriving P-I diagrams, single degree of freedom (SDOF) models are widely used to develop P-I diagrams for damage assessment of structural members exposed to blast loading. The popularity of the SDOF method in structural response calculation in its simplicity and cost-effective approach that requires limited input data and less computational effort. The SDOF model gives reasonably good results if the response mode shape is representative of the real behaviour. Pressure-impulse diagrams based on SDOF models are derived based on idealised structural resistance functions and the effect of few of the parameters related to structural response and blast loading are ignored. Effects of idealisation of resistance function, inclusion of damping and load rise time on P-I diagrams constructed from SDOF models have been investigated in this study. In idealisation of load, the negative phase of the blast pressure pulse is ignored in SDOF analysis. The effect of this simplification has also been explored. Matrix Laboratory (MATLAB) codes were developed for response calculation of the SDOF system and for repeated analyses of the SDOF models to construct the P-I diagrams. Resistance functions were found to have significant effect on the P-I diagrams were observed. Inclusion of negative phase was found to have notable impact of the shape of P-I diagrams in the dynamic zone.

Introduction

Pressure-impulse (P-I) diagrams are often defined as iso-damage curves derived for a given damage criteria and represented in the space of pressure and impulse of the pulse loading. P-I diagrams relate damage with both impulse and pressure, hence are widely used in damage assessment of structural elements under blast loading. P-I curves are also used for defining the level of protection and determining safe stand-off distance for an explosion. In assessing the behaviour of a blast-loaded structure, often the calculation of the final state is the principal requirement for a designer rather than a detailed knowledge of its displacement-time history. Due to the high degree of uncertainty involved in blast load prediction, complex time consuming detailed structural analysis is often not justified. SDOF analysis has the potential of giving a good prediction of final response of the critical point of a structure.

P-I curves are generated by applying different approaches and calculation techniques. Analytical methods are mainly used for theoretical development of P-I diagrams for elastic structures. Two main approaches used in analytical methods are the methods based on closed-form solutions and on energy balance. The energy balanced approach is based on the conservation of mechanical energy and has been widely used to obtain P-I diagram [1, 2]. Empirical methods to generate P-I diagrams

generally require a large number of tests, which requires significant amounts of resources and time. Moreover, experimentally generated P-I curves are more specific to a special situation. Researchers also used numerical analysis to construct and quantify damage by P-I curve. Based on two loosely coupled SDOF models, Ng and Krauthammer [3] generated P-I diagrams using a numerical approach. Non-linear finite element analysis has also been used in generating P-I diagrams. In this approach, repeated finite element analysis is performed with different combinations of pressure and impulse to construct P-I diagrams. Explosive loading shape has significant influence over the dynamic response of structures. Past attempts were taken to omit the load shape effect on rigid-plastic materials and on SDOF models to eliminate pulse load shape effect in both the elastic and elastic-plastic structures [1].

Significant advances have been achieved in the use of SDOF models in calculation of structural response under calculation [4]. Most of the available design tools for blast damage assessment exclusively use SDOF approach [5]. Accuracy of the dynamic response calculations significantly depend on whether the adopted resistance function resembles the actual hysteretic behaviour of the structure. The resistance of structural elements under blast load is highly non-linear and is significantly influenced by material, sectional properties, strain rate and loading duration. In practice, an idealised resistance function (R-Δ) is used, which is a prediction of the resistance that the element would offer in a quasi-static test. Effects of using idealisation of resistance function on P-I diagrams constructed from SDOF models have been investigated in this study. Some of the other aspects related to SDOF model response and also to the idealisation blast loading are often been neglected in SDOF analysis. The effects of damping and load rise time on P-I diagrams have also been investigated. In a SDOF model, simplified blast pressure profiles with positive phase is commonly used to obtain P-I diagrams for structural elements disregarding the contribution of negative phase. This simplified assumption of the insignificant contribution of the negative phase on the P-I diagrams obtained from SDOF model with non-linear resistance function has never been investigated before. In this research, the effect of inclusion of the pulse negative phase on the P-I diagrams has also been investigated.

Blast Load Idealisation

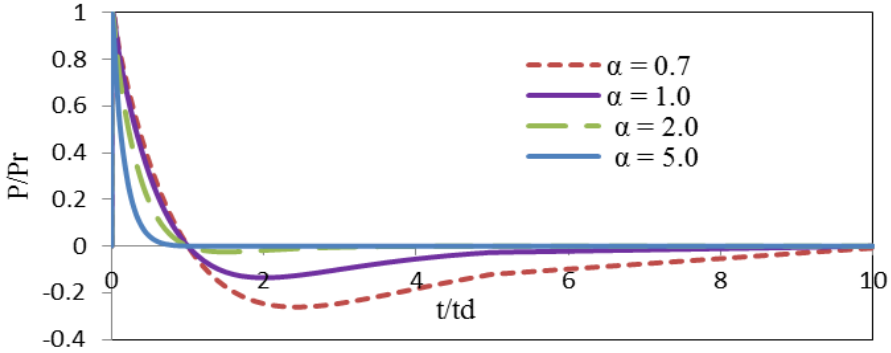
The shape and magnitude of a blast wave depends on the type of explosive and the distance from the detonation point to the target. While the source and physical nature of the explosion causing the shock wave can vary greatly, the pressure-time profile of a typical blast wave can be accurately represented [6]. Researchers often suggested that the overpressure-time curves could be represented by triangular equivalents. The usual simple way to simulate a blast load for structural analysis and design purposes is with a triangular distribution of pressure with respect to time, which has a start peak pressure, P_{so}, and decreases linearly with time to zero within a time period t_d. These equivalent triangles have the same initial peak overpressure but have a different duration, depending on the expected time of maximum structural response. However, chemical investigations and experimental data have shown that the evolution of blast load pressure (P) with time (t) can be simulated more accurately by a quasi-exponential distribution [7] as a modified Friedlander equation as given below in Eq. 1.

$$p(t) = p_{so}\left(1 - \frac{t}{t_d}\right) exp\left\{-\frac{\alpha t}{t_d}\right\} \tag{1}$$

where α is the dimensionless waveform parameter.

Available methods for damage assessment, especially with P-I diagrams have used idealised blast waves without the negative phase for damage assessment. The parameter α determines the extent of negative phase in the exponential distribution of Eq. 1. If α is smaller than unity, there is an important negative phase, while if α is larger than one, the negative phase becomes less significant. The value of α mainly depends on the type of explosion (chemical or nuclear) and scale distance.

The blast pulse profile for different values of waveform parameter α in Friedlander equation is shown in Fig. 1. In the figure the ratio between pressure at a given time (P) and the peak pressure (P_r) has been plotted against the ratio of corresponding time (t) to the positive duration value (t_d).



Figures 1. Blast load profile obtained using Friedlander equation with different values of waveform parameter (α)

The blast pulse profile presented by the Friedlander equation with an α value of unity has been found to match well with some experimental results [8]. However, depending on various factors such as change weight, scaled distance, type of blast and other factors, the blast pressure can have a negative phase much higher than the phase represented by the α value of one. In the investigation of the effect of a negative phase on structural response, Friedlander equation with different values of α was used in in this study.

MATLAB Code for SDOF Analysis and P-I Diagrams

An exact solution for the equation of motion of a SDOF system is usually not possible for blast loading, as the loading varies arbitrarily with time and mostly the response of the system under blast becomes non-linear. Hence, numerical time integration procedures are implemented in MATLAB code for obtaining solutions for SDOF models. For an inelastic system, the equation of motion to be solved numerically subjected to a set of initial conditions is given in Eq. 2.

$$m\ddot{u} + c\dot{u} + f_s(u,\dot{u}) = p(t) \tag{2}$$

The well-known numerical approximation method by Newmark was used for simulation of structural dynamics transient response calculation. The linear acceleration method has been used for the response calculation. Modified Newton-Raphson iteration was used in the numerical approximation procedure to minimise the errors and to obtain better stability and convergence. The results obtained from the MATLAB code developed for SDOF response calculation were compared with the available SDOF response calculation program NONLIN [9] to verify the reliability of the results obtained from the decloped code.

The numerical derivation of P-I curves for flexural failure using the SDOF model for an element subjected to blast load was established based on numerous discrete points determined by repeated analysis of the equivalent SDOF system. Each point represents the limit state of the structure with respect to the specified damage criterion. At each point, the positive phase time duration (t_d) of a blast pressure is firstly determined, then the peak blast pressure is increased from zero to the ultimate value P, until the maximum response of the equivalent SDOF system reaches the given deflection value according to the specified damage criterion. Impulse was calculated as the area under the pressure-time curve in the blast positive phase.

Effect of Resistance Functions on Response

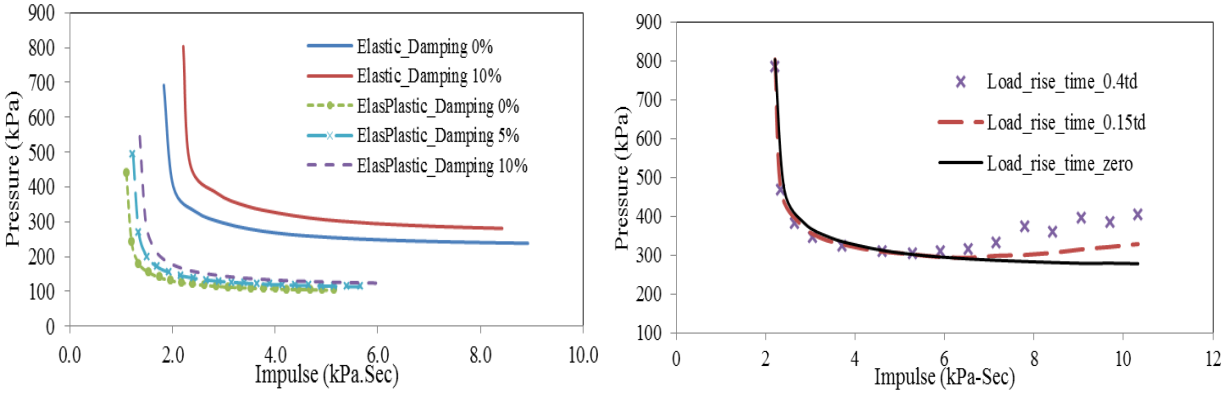
For the present study, one normal strength concrete beam (B40-D4) was selected from the beams tested under blast loading by Magnusson and Hallgren [10]. The SDOF response calculation was carried out for three reinforcement ratios (ρ). Selected reinforcement ratios were chosen to cover a wide range of reinforcement amounts in the beam. One of the ratios was selected well below the balanced reinforcement ratio, one was close to the balanced reinforcement ratio and the third one was over the balanced ratio; thereby representing under, balanced and over reinforced beams under blast load**.** The reinforcement ratios produced three different R-Δ relations to be employed in the SDOF model of the beam. The other SDOF parameters of the beam were obtained using the equivalent SDOF approach. Three different blast peak pressure values have been applied on the models, and for these three peak pressure values, two different positive phase durations (30 ms and 10 ms) were used to obtain responses under a wide range of different loading conditions. The bilinear and the non-linear resistance function models represent the same amount of strain energy; this is achieved by performing the bilinear idealisation whilst keeping the area under the bilinear curve equal to the area under the non-linear curve. Development of nonlinear resistance functions based on moment-curvature relationship was previously presented in Syed et al. [11].

The variation in peak response significantly depends on the shape of the idealised bilinear resistance function. Increased value of the reinforcement ratio reduces the variation in shape of the bilinear and non-linear functions thus reducing the variation of the peak response of the structural member. Generally, in all the cases, the responses are fairly close in terms of response time. Post-yield behaviour was greatly influenced by the shape of the resistance function under different blast loadings. The peak deflection from the non-linear R-Δ model appears to be smaller than that from the elastic-perfectly plastic R-Δ model. When the R-Δ relations are relatively matched, the analysis responses obtained from the two models are quite close, independent from the applied blast load. The variation between the non-linear and bilinear response is most significant in this study for a reinforcement ratio of 0.89%, hence, this reinforcement ratio was selected to explore the variation in response due to different positive phase durations.

Effect of Damping and Load Rise Time

Blast loads produce large plastic deformations of concrete elements before failure in a very short time; hence, it is assumed that the structural damping has little effect on peak displacement. Based on this consideration available design manuals and guidelines for protective design suggest ignoring the structural damping for blast response calculations. P-I curves were constructed for the SDOF model obtained from converting the same beam as used in the previous section with a reinforcement ratio (2.11%) close to the balanced reinforcement ratio for the selected beam. Fig. 2, demonstrates the P-I curves obtained with and without damping for a medium damage level that corresponds to a hinge rotation of 1.5°. For elastic analysis, an equivalent stiffness was calculated from the method discussed in the previous section, and for the elastic-plastic hardening part the secant stiffness was taken as 10% of the initial stiffness. The P-I curves were obtained for blast loading idealised as a descendent pressure pulse with zero rise time. It was found from this study that excluding damping from the response calculation provided a conservative estimate of damage assessment.

In reality, after reaching an object, blast pressure rises to the peak value almost instantly. Fig. 3, shows the effect of rise time of blast loading on P-I diagrams calculated from the same SDOF model used for the damping part. The load curve used is the same as before, only that a different time to reach the peak value has been used to investigate the effect of rise time on the P-I diagram. Fig. 3, clearly shows that the P-I points in the quasi-static region are highly sensitive to the blast rise time.

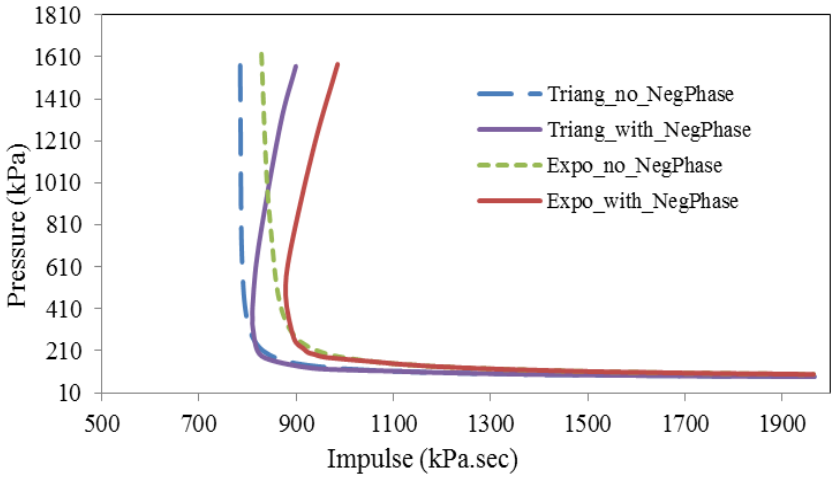


(a) (b)

Figures 3. P-I diagram for different (a) damping values for a SDOF model with elastic and elasto-plastic resistance, (b) rise time

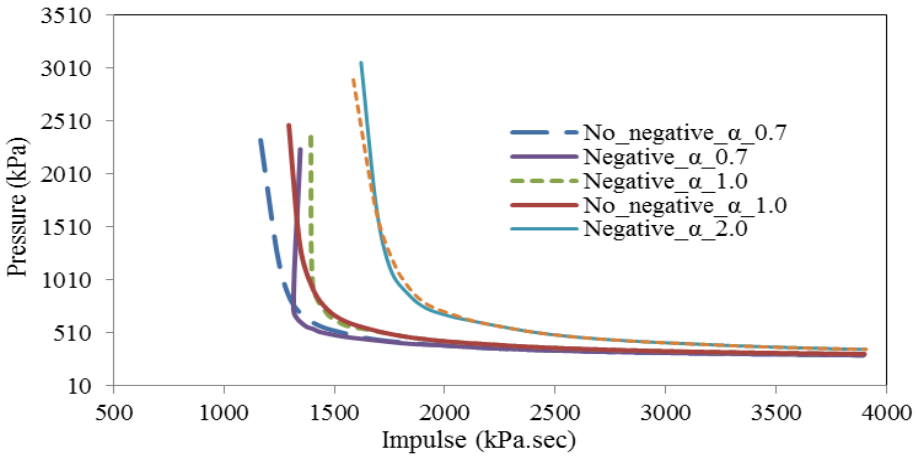
Effect of Negative phase on P-I diagrams

Pressure-time histories of experimental blast loads often demonstrate that the negative phase can be significantly high depending on various factors. P-I diagrams were constructed for both triangular and exponential loads, with and without the inclusion of negative phase in the blast loading. Idealised blast load with different peak and duration of the negative phase is used. The exponential load with different values of load shape parameter (α) has been used to construct the P-I diagrams. Figure 4 shows P-I diagrams for blast pressure with the same positive phase duration for triangular and exponential shape with and without the negative phase for a damage criteria of 1° support rotation.



Figures 4. P-I diagrams for blast pressure with and without negative phase for triangular and exponential loads

Four values of α were employed in the study to represent a wide range of possible negative phase in the blast load pulse. Figure 4 presents the effects of negative phase on P-I diagrams obtained for a 1.5° support rotation. The P-I curves are obtained using the first peak response of the SDOF models. Figure 5 clearly shows that the effect of negative phase is significant for α values of one and below one. The P-I diagrams presented in the figure is for 2° support rotation as damage criteria. But the effect starts diminishing from α value reaching two. It was observed that there is no effect of negative phase for the α values of 3 or above, as exponential blast load with wave form parameter (α) value of 3 or higher will virtually have no negative phase.



Figures 5. P-I diagrams for blast pressure with and without negative phase for different values of waveform parameter (α)

Conclusion

Different aspects of SDOF models used for the construction of P-I diagrams were discussed. The effects of idealised resistance functions on the response calculation have been investigated.The effect of damping and load rise time on P-I diagrams have been explored. The negative phase part of the pressure pulse of blast loading is often ignored in design and damage assessment of concrete elements under blast loading. The contribution of negative phase on the SDOF model response has also been investigated. It has been observed that the effect of negative phase could be significant depending on timing of the rebound of the structural system.

References

[1] Q.M. Li and H. Meng. Pressure-impulse diagram for blast loads based on dimensional analysis and single-degree-of-freedom model. J. of Engg Mech 128 (2002) 87-92.

[2] A.S. Fallah, E. Nwankwo and L.A. Louca. Pressure-impulse diagrams for blast loaded continuous beams based on dimensional analysis. J of Applied Mech 80 (2013) 051011-10.

[3] P.H. Ng and T. Krauthammer. Pressure–impulse diagrams for reinforced concrete slabs: Protective Technology Center, The Pennsylvania State University, 2004.

[4] T. Krauthammer, Modern Protective Structures, CRC Press, London, 2008

[5] PDC-TR 06-08, Single degree of freedom structural response limits for antiterrorism design, U.S. Army Corps of Engineers, 2008.

[6] M.S. Agbabian. Design of structures to resist nuclear weapon effects. ASCE Manual on Engineering Practice, 42 (1985).

[7] G.F. Kinney and K.J. Graham. Explosive Shocks in Air, Springer, New York, 1985

[8] Jacinto, A. C., Ambrosini, R. D., & Danesi, R. F. (2001). Experimental and Computational Analysis of Plates under Air Blast.

[9] NONLIN, Ver 6.0. US Federal Emergency Management Agency (FEMA) Training Centre 2007

[10] J. Magnusson and M. Hallgren. Reinforced high strength concrete beams subjected to air blast loading. *Structures and Materials 15(2004)* 53-62.

[11] Z.I. Syed, P.A. Mendis, N. Lam and T. Ngo. Curvature ductility of concrete element under high strain-rates. Applied Mechanics and Materials 166 (2012) 2910-2917.

Applied Mechanics and Materials Vol. 567 (2014) pp 505-510
© (2014) Trans Tech Publications, Switzerland
doi:10.4028/www.scientific.net/AMM.567.505

Strength Development of Concrete incorporating Metakaolin and PVA fibres

S.U.Khan[1, a], M.F. Nuruddin[2, b] and N. Shafiq[3, c]

[1,2,3]Civil Engineering Department, Universiti Teknologi PETRONAS,

31750 Tronoh, Perak Darul Rizuan, Malaysia

[a]sadaquat78@hotmail.com, [b]fadhilnuruddin@petronas.com.my,

[c] nasirshafiq@petronas.com.my

Keywords: PVA Fibres, Metakaolin, Compressive strength, Splitting tensile strength, Flexural Strength

Abstract. Study has been conducted to investigate the effect of aspect ratio and volume fraction of PVA fibres on the mechanical properties of concrete. Total eighteen (18) mixes of concrete have been examined using metakaolin up to 5% and PVA fibres of aspect ratio 45, 60, 90 and 120 with volume fraction 1 to 2%. Compressive strength, splitting tensile strength and flexural strength at 7 days and 28 days have been determined to check the effect of volume fraction and the aspect ratio of PVA fibres. It has been found that 2% volume fraction is better than 1% and there is increasing trend up to a certain value of aspect ratio in the strengths of concrete.

Introduction

During the last decade, the use of fibres other than steel fibres has been widely studied. Several studies have been conducted to evaluate the response of fibres such as polypropylene (PP) [1], Polyvinyl Alcohol **(**PVA) [2] and basalt fibres [3]. Cement composite has been developed called "Engineered Cementitious Composites" (ECC) in the last ten years. Cement, fly ash, fine silica sand, water, PVA fibres and chemical admixture are the constituent of ECC. ECC typically contains 2% of PVA fibres. The binder content is often above 1000 kg/m^3 [4]. ECC can achieve compressive strength ranges from 30-90 MPa and modulus of elasticity is 20-25 GPa, lower than normal concrete due to absence of coarse aggregates [5]. Due to higher binder content, the cost of ECC is 4 to 5 times of normal concrete [4].

The current study focuses the use of PVA fibres of different aspect ratio in concrete with cement content much lesser than ECC to develop sustainable concrete. Moreover, the effect of aspect ratio and volume fraction of PVA fibres on the strength of concrete has not been established. On the other hand, steel fibres have been widely studied and it has been reported that increase in aspect ratio of steel fibres and fibre volume fraction is favourable to flexural strength and splitting tensile strength of steel fibre reinforced concrete (SFRC), but this is not true for the compressive strength and optimum increase in compressive strength depends on the certain volume fraction of particular aspect ratio of steel fibre [6]. Hence, there is need to study the use of PVA fibres in concrete to study the strength development of concrete. Cube compressive strength, splitting tensile strength and flexural strength of concrete has been observed to investigate the effect of PVA fibres and to compare with SFRC. Also, locally produced Metakaolin (MK) as cement replacing material has been considered with PVA fibres which have not been studied so far.

Experimental Program

Eighteen (18) mix of concrete has been prepared, two (02) out of Eighteen (18) are control mixes without PVA fibres. Nomenclature and mix proportion detail of the concrete has been mentioned in Table 1. Three specimens for all concrete mix have been prepared to determine each mechanical property i.e. compressive strength, splitting tensile strength, and flexural strength. The effect of volume fraction of PVA fibres and the aspect ratio of PVA fibres on the compressive strength,

splitting tensile strength and flexural strength of concrete at 7 days and 28 days has been investigated. Ordinary Portland cement (OPC) has been used. Sand passing through a 3.125 mm (1/8") opening sieve and retained on sieve # 200 has been used as fine aggregates in all concrete mix; however 20 mm (3/4") opening sieve passing and 10 mm (3/8") opening sieve passing has been used as coarse aggregates.

Table 1: Mix Design for Experimental Program and Mix Proportion

MIX	MK	OPC	Fine Aggregates	Coarse Aggregates		PVA Fibre				
				<10mm	10-20mm	Volume fraction	Weight	Aspect ratio	Length	Diameter
	[kg/m^3]	[kg/m^3]	[kg/m^3]	[kg/m^3]	[kg/m^3]	%	[kg/m^3]	length/diameter	[mm]	[mm]
00-0	0	450	670	600	500	-	0	-	-	-
A1-0	0	450	670	600	500	1	13	45	30	0.667
A2-0	0	450	670	600	500	2	26			
B1-0	0	450	670	600	500	1	13	60	12	0.2
B2-0	0	450	670	600	500	2	26			
C1-0	0	450	670	600	500	1	13	90	18	0.2
C2-0	0	450	670	600	500	2	26			
D1-0	0	450	670	600	500	1	13	120	24	0.2
D2-0	0	450	670	600	500	2	26			
00-5	22.5	427.5	670	600	500	-	0	-	-	-
A1-5	22.5	427.5	670	600	500	1	13	45	30	0.667
A2-5	22.5	427.5	670	600	500	2	26			
B1-5	22.5	427.5	670	600	500	1	13	60	12	0.2
B2-5	22.5	427.5	670	600	500	2	26			
C1-5	22.5	427.5	670	600	500	1	13	90	18	0.2
C2-5	22.5	427.5	670	600	500	2	26			
D1-5	22.5	427.5	670	600	500	1	13	120	24	0.2
D2-5	22.5	427.5	670	600	500	2	26			

Polyvinyl Alcohol (PVA) fibres have been selected due to their reinforcing properties. Aspect ratio is one of the parameters of the current study, which has been varied from 45 to 120, and fibre volume fraction has been varied from 1 to 2% by volume of concrete with a variation of 1% in concrete mixes. Mineral admixture is the essential part of high strength concrete and in this study locally available kaolin has been calcined to form metakaolin (MK) and it has been used as mineral admixture. 5% MK by weight of cement has been used in concrete mixes. Superplasticizer of Type F or G of ASTM C 494 with a dosage 0.25 to 2% by weight of cement with a variation of 0.25% has been added in concrete mixes to achieve the slump of 50±10 mm in all concrete mix and water cement ratio has been taken as 0.4 in all concrete mix.

Results and Discussion

Compressive strength. Compressive strength of concrete having 1% fibres (A1-0) is slightly higher than control (00-0) and with increase in volume fraction, compressive strength is gradually increasing as compared with control (00-0) as shown in Figure 1. This enhancement in compressive strength is due to lateral confinement provided by fibres that enable the sample to withstand under higher compression and even after failure, cube having fibres retain their shape and very little disintegration observed in the cubes. From Figure 1, it is also evident that increase in aspect ratio positively affects the compressive strength at age of 7 and 28 days with 1% and 2% fibre volume fraction; however this trend is evident from B1-0 to C1-0 and from B2-0 to C2-0. Concrete with fibres having aspect ratio 45 (A1-0 and A2-0) are not comparable with other fibres as the diameter of this fibre is different as mentioned in Table 1. Therefore, with respect to aspect ratio, there is a trend of increase in compressive strength up to aspect ratio 90 and further increase in aspect ratio causes decrease in compressive strength. This response is similar to SFRC as reported by Yazıcı et al. [6]. Hence, it may comprehend that aspect ratio 90 is the optimum value for PVA fibres to be used in concrete without compromising the compressive strength. Also, it may infer that coarser fibre having long length and large diameter (Aspect ratio 45) is better for the compressive strength

as maximum strength has been observed with fibres having longest length (30 mm) and largest diameter (0.667 mm) as shown in Figure 1.

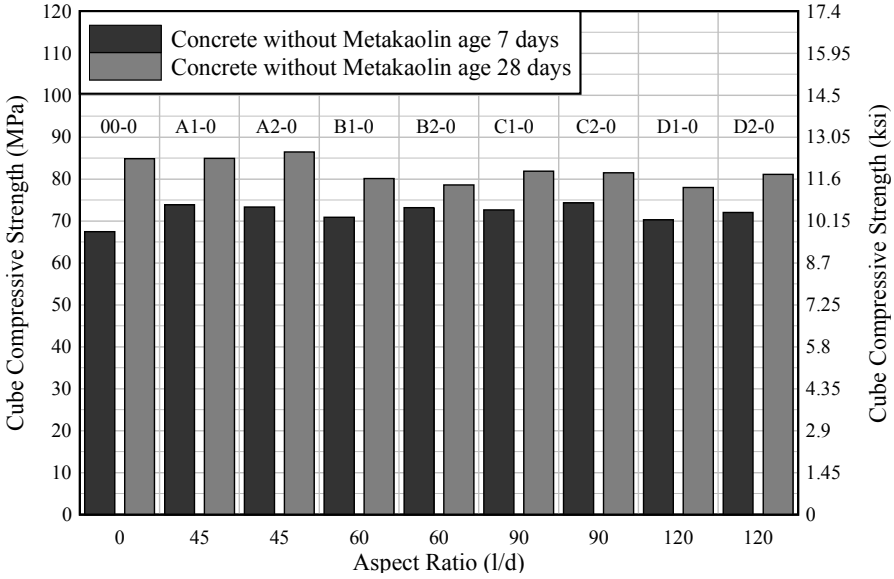


Figure 1: Cube Compressive Strength of Concrete without metakaolin

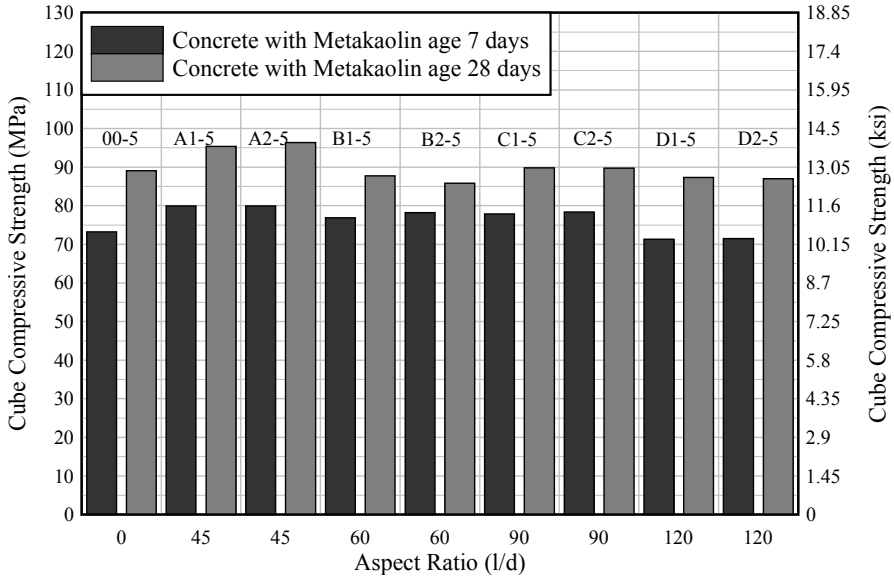


Figure 2: Cube Compressive Strength of Concrete with metakaolin

Addition of 5% MK (00-5) gives compressive strength almost 5% higher than control (00-0) as shown in Figure 1 and Figure 2. The higher reactivity of MK is the reason behind. MK increases the binder and ultimately increases the compressive strength. MK together with PVA fibres of aspect ratio 45, 60 and 90 with 1% and 2% fibre volume fraction, increased compressive strength, however, only PVA fibres of aspect ratio 45 is giving higher strength than control (00-5). PVA fibres of aspect ratio 120 and 5% MK has a similar trend as without MK as shown in Figure 2. The compressive strength is getting lesser with these fibres even in the presence of MK.

Splitting Tensile strength. In comparison with control (00-0), splitting tensile strength of concrete with fibres has been increased with fibre volume fraction 2% having aspect ratio 45, 60 and 90 (A2-0, B2-0, C2-0) as shown in Figure 3. The fibre of aspect ratio 120 (D2-0) is giving almost the same strength as control (00-0). There is an increasing trend in splitting tensile strength with respect to the aspect ratio, however, maximum splitting tensile strength has been observed with fibre having aspect ratio 45 and 60 with fibre volume fraction 2% (A2-0, B2-0).

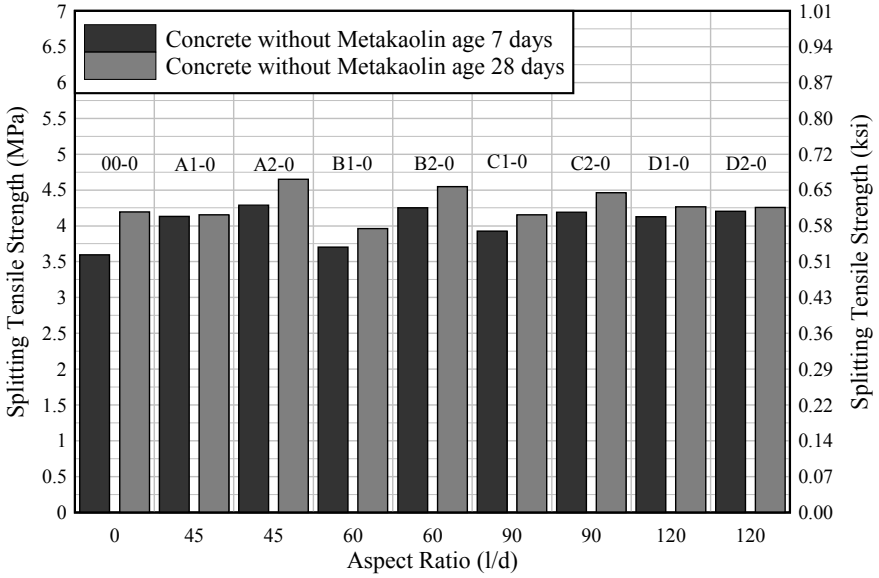


Figure 3: Splitting Tensile Strength of Concrete without metakaolin

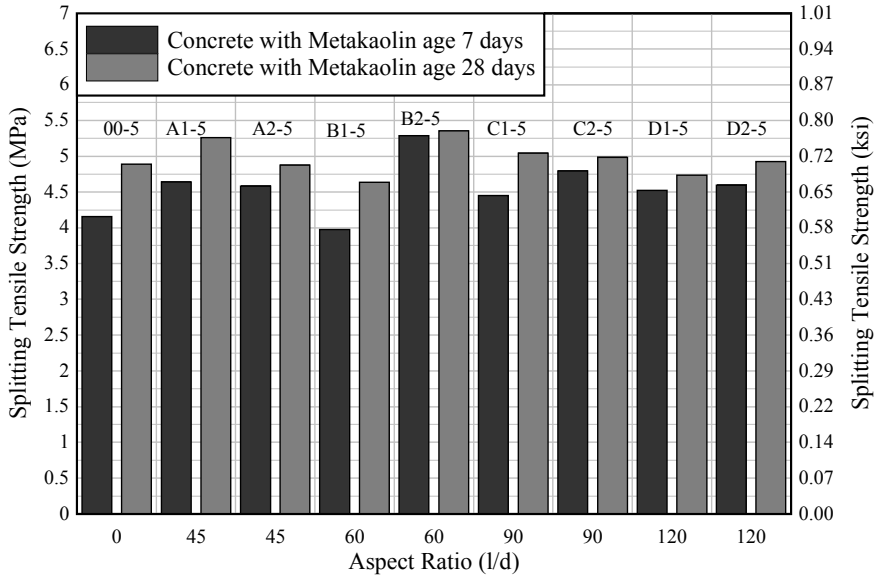


Figure 4: Splitting Tensile Strength of Concrete with metakaolin

With 5% MK (00-5), splitting tensile strength is increasing about 16.4% as shown in Figure 3 and Figure 4. And also MK with PVA fibres increase the splitting tensile strength with 1% fibre volume fraction of aspect ratio 45 and 2% fibre volume fraction of aspect ratio 60 (A1-5, B2-5) in comparison with control (00-0) as shown in Figure 3 and Figure 4. In other words, cement replacement with MK increase the fibre performance [7,8] and give further strength. It is also inferred that fibre performance depends on the cement paste and bonding gel available in concrete and for MK replace 5% cement increase the binding paste [9] and enhance the fibre performance. A similar trend has been observed in splitting tensile strength as increase in aspect ratio form 90 to 120, decrease the strength.

Flexural strength. In comparison with control (00-0) flexural strength of concrete with increase in fibre volume is increasing and maximum flexural strength has been observed in concrete A2-0 as shown in Figure 5, however, increase in strength is small. Large deformation has been observed before failure of beams with fibres indicating that mode of failure is shifting from brittle to ductile. Addition of MK (00-5) caused 6% increase in flexural strength as shown in Figure 5 and Figure 6. MK together with fibres causes small increase in flexural strength as shown in Figure 6. The

maximum strength has been observed with fibres having volume fraction 2% and aspect ratio 60. Further increase in aspect ratio has descending trend in flexural strength as shown in Figure 6. Note that the flexural strength is calculated by considering full cross section effective even though the formation of cracks has been observed prior to failure. Hence, the flexural strength would be much higher by considering the effective section remaining after cracking.

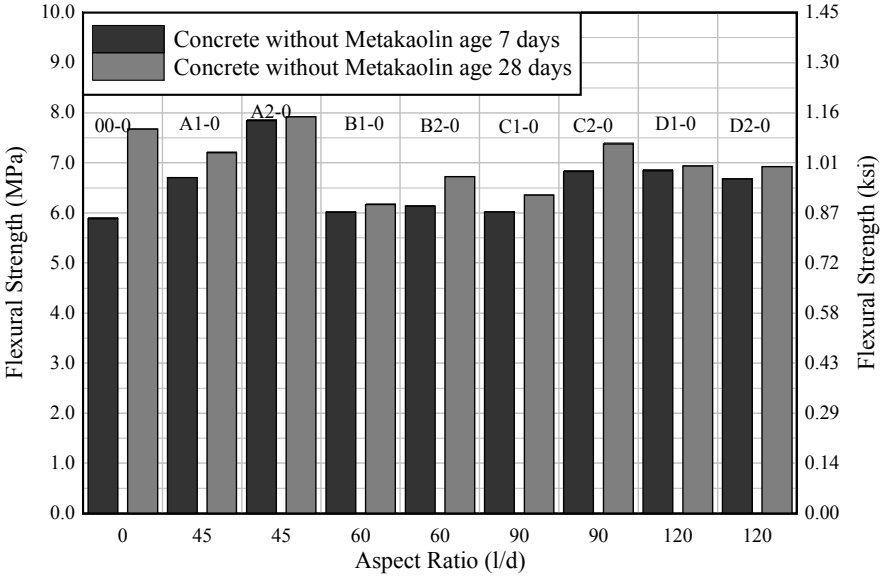


Figure 5: Flexural Strength of Concrete without metakaolin

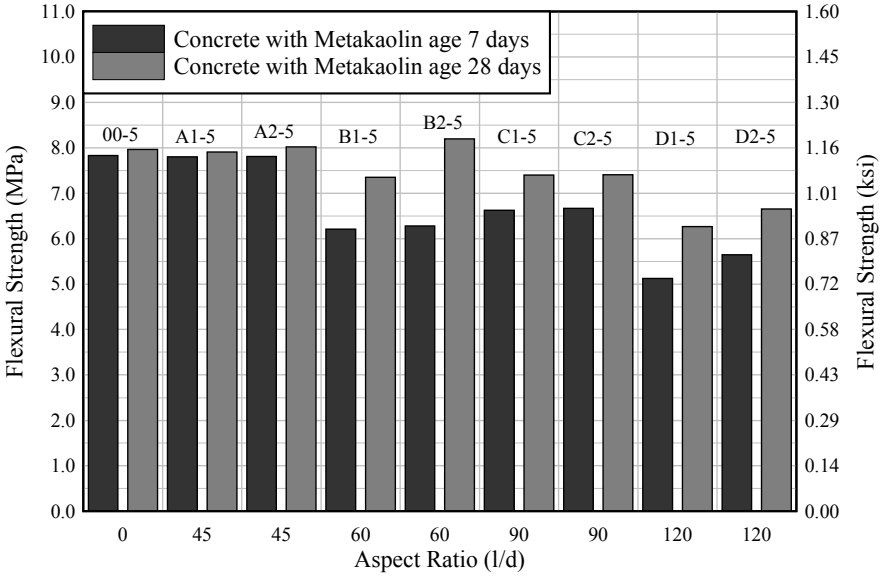


Figure 6: Flexural Strength of Concrete with metakaolin

Conclusions and Recommendations

1. Increase in compressive strength is due to lateral confinement provided by fibres that enable the sample to withstand under higher compression and even after failure, cube having fibres retain their shape and very little disintegration observed in the cubes.
2. Increase in aspect ratio positively affects the compressive strength at age of 7 and 28 days with 1% and 2% fibre volume fraction.
3. Increase in compressive strength has been observed up to aspect ratio 90 and further increase in aspect ratio causes decrease in compressive strength.

4. It may infer that coarser fibres having long length and large diameter are better for the compressive strength as maximum strength has been observed with fibres having longest length (30 mm) and largest diameter (0.667 mm).
5. Increasing trend with respect to the aspect ratio in splitting tensile strength has been observed, however, maximum splitting tensile strength has been observed with fibre having aspect ratio 45 and 60 with fibre volume fraction 2%.
6. Flexural strength of concrete with increase in fibre volume is increasing. Large deformation has been observed before failure of beams with fibres indicating that mode of failure is shifting from brittle to ductile. The maximum strength has been observed with fibres having volume fraction 2% and aspect ratio 60. Further increase in aspect ration has descending trend in flexural strength.

Acknowledgment

Authors wish to acknowledge the financial support provided by the Universiti Teknologi PETRONAS, Malaysia and the assistance from the lab technicians for their help during testing of the specimens and data acquisition.

References

[1] A. M. Alhozaimy, P. Soroushian and F. Mirza, Mechanical properties of polypropylene fiber reinforced concrete and the effects of pozzolanic materials, Cem. Conc. Comp. 18 (1996) 85-92.

[2] V. C. Li, Engineered Cementitious Composites (ECC) Material, Structural, and Durability Performance, (2008).

[3] L. J. Y. Y. Y. Meng, and Z. Yan, Experimental Research On The Mechanical Behavior Of Chopped Basalt Fiber Reinforced Concrete [J], Indust. Constr. 6 (2007) 002.

[4] S. M. Kazem and K. Mohammad, Improving the mechanical properties of concrete elements by bendable concretes. The 3rd ACF International Conference-ACF/VCA 2008, (2008) 571-577.

[5] V. C. Li and M. Li, Durability performance of ductile concrete structures, Proceedings of the 8th International Conference on Creep, Shrinkage and Durability of Concrete and Concrete Structures, (2009) 761-768.

[6] Ş. Yazıcı, G. İnan and V. Tabak, "Effect of aspect ratio and volume fraction of steel fiber on the mechanical properties of SFRC," Constr. Build. Mater. 21 (2007) 1250-1253.

[7] M. F. Nuruddin, S. U. Khan, N. Shafiq and T. Ayub, Strength development of high-strength ductile concrete incorporating Metakaolin and PVA fibers. The Scientific World Journal 2014 (2014) 11.

[8] A. Dubey and N. Banthia, Influence of high-reactivity metakaolin and silica fume on the flexural toughness of high-performance steel fiber reinforced concrete. ACI Mater J 95 (1998) 284-292.

[9] S. U. Khan, M. F. Nuruddin, T. Ayub and N. Shafiq, Effect of Different Mineral Admixtures on the properties of Fresh Concrete. The Scientific World Journal 2014 (2014) 11.

Applied Mechanics and Materials Vol. 567 (2014) pp 511-516
© (2014) Trans Tech Publications, Switzerland
doi:10.4028/www.scientific.net/AMM.567.511

Strengthening Schemes for Flexure and Torsion using FRP Laminates: A State of Art Review

Muhammad Imran[1, a], Nasir Shafiq[1, b] and Ibrisam Akbar[1, c]

[1]Departmnet of Civil Engineering Universiti Teknologi PETRONAS, Tronoh 31750, Perak, Malaysia

[a]engrimran_ce@hotmail.com, [b]nasirshafiq@petronas.com.my, [c] ibrisam_akbar@petronas.com.my

Keywords: CFRP, deficiency, eccentricity, flexure, reinforced concrete and torsion.

Abstract. RC beams as a structural member contain a variety of non-uniform loads. These non-uniform loads caused combined effects of flexure and torsion. There are numerous studies available, that suggests different strengthening schemes using FRP laminates, as a solution for flexure and torsion deficient beams. Most of the experimental studies suggested individual strengthening schemes for flexure or torsional deficiency RC beams. However, the combined effects were not studied due to difference in experimental setup, testing procedure and specimen detailing. Therefore, the outcome of previous studies was needed to combine together to facilitate the strengthening process as a guideline case of such deficiency. Therefore, a combined review is presented by suggesting different configuration for flexure and torsion deficient RC beams. Most of the studies suggested that the application of FRP laminates at the soffit of beam is suitable for flexural strengthening. The application of U-shape or full wrap are suitable for strengthen torsion deficient beams. Similarly, 45° wraps are more effective than 90°wraps for improving ductility of torsion deficient beams.

Introduction

In 90s steel plating was considered as a highly effective material for strengthening RC beam. However, from 1980's the availability of FRP at compatible prices and ease in application discovered as an alternative to steel plate [1]. The problems in steel plating are high cost, easily corrode, difficult to apply, less fatigue resistance, and increasing dead weight of the structure, and required continuous maintenance [2]. FRP is highly versatile that they can be mould into any shape, and the properties can be varied widely with differing fibre and orientations [3]. The commonly available of FRPs are aramid fibre reinforced polymers (AFRP), glass fibre reinforced polymers (GFRP) and carbon fibre reinforced polymers (CFRP).

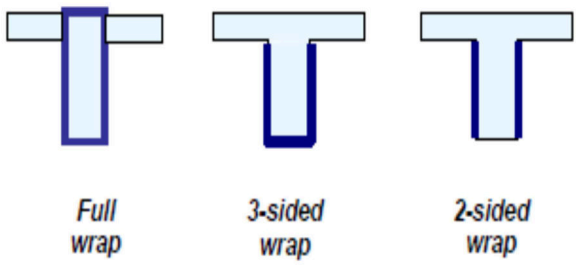


Figure 1: Common wrapping configuration [4].

Generally, there are two forms of FRP laminates available in markets, high strength fibre (flexible wrap) and high modulus fibre (sheet or rigid wrap). Both enhance the ultimate and the cracking strength of the RC beam tremendously. The application of both flexible and rigid wraps either separately or individually on RC beam is very common depending upon the deficiency required to handle. For example shear, three types of configurations are used a) full wraps, b) U-shape or three sided wraps and c) two sided wraps. Whereas, full wraps and three sided or U-shape wraps are also used for the torsion deficient beams to enhance torsional capacity of RC beam as shown in Figure 1[4].

Flexure Configuration

The most common failure mode of RC beams is the flexure failure under bending stresses. Most of the beams lost its design strength and durability, as the load exceeds to its design capacity. In

previous experimental studies different schemes have been proposed using FRP for strengthening RC beam, to prevent beam deficiency under bending stresses.

Experimental Studies (1991~2000). Ritchie *et al.* (1991) applied various plates at the soffit of beam for flexure strengthening such as carbon fibre, glass fibre, aramid fibre, steel plate and mixed carbon-glass fibre. The load carrying capacity reported is higher, when plate was extended up to the support or anchorage extended up to the full height of the web of beam. Steel plate revealed the highest strength; but due to several disadvantages and short service life due to that drawback it was not recommended. FRP on the other hand, found to be the most economical and feasible solution for installation and maintenance. The results reported that the externally bonded steel plates exhibited the several wide spaced cracks and closed spaced narrow cracks that gave alarming sign prior to failure. However, FRP exhibited brittle failure; but the behaviour can be modified by providing end anchorage [3]. Sharif *et al.* (1994) studied the effect of number of layers, bolted plate, additional side plates using FRP and I-shape plate to enhance flexural capacity of the beam. Results revealed that number of FRP layers caused premature failure and steel plate anchored with bolts delayed plate separation. No additional strength was reported, when applying plates at the side of the beam together with the bottom plate. FRP I-shape plate gives highest strength and ductility due to continuous FRP plate compared to other strengthening schemes [5]. Kachlakev and McCurry (2000) conducted an experiment on full scale beam by applying CFRP & GFRP strengthening schemes to upgrade RC beam under flexure, shear and combined flexure-shear. The beams strengthened only for flexure increased load capacity up to 31% and, for shear strengthening the deflection increased up to 200% compared to control beam. However, the combined use of CFRP at bottom and GFRP for shear on the web of beam achieved the required strength [1].

Experimental Studies (2001~2010). Lamanna *et al.* (2001) used fasteners during experimental study to prevent debonding and improving ultimate strength of RC beam using FRP composite material. Mechanical fastener improved ductility, but fastening process developed pre-cracks on the RC beams due to mechanical strikes. Therefore, it was suggested to apply adhesive bond to attain high strength than mechanical fasteners [6]. David *et al.* (2003) compared the effect of pre-cracked and un-cracked CFRP laminated beams. It was found that the strength was low when RC beam strengthened after crack appeared due to loading, than un-cracked beams. Debonding was not observed in between the two CFRP joined layers, but brittle failure was reported due to number of layers [7]. Pham and Al-Mahaidi (2004) listed the various failure modes which occurred due to debonding, when RC beam strengthened using CFRP laminates with different layers. The study reported brittle failure as the thickness of layer increased. Steel clamps were used to prevent delamination at the end and to increase the ductility. The study has also found that concrete cover and shear reinforcement have insignificant influence on the delamination of FRP strip [8]. Aram *et al.* (2008) studied the effect of RC beam strengthened using CFRP plates; and reported that all beams failed due to debonding, by upgrading stiffness and enhancing ultimate strength up to 100% compared to the control beam [9]. Al Saidy *et al.* (2010) conducted an experimental study on flexure strength of corroded RC beam with different levels of corrosion. Experimental study found that CFRP was more effective in harsh environment to restore the strength of RC beam. Flexurally strengthened RC beams failed prematurely in shear due to lowest shearing strength compared to flexure and elastic properties of CFRP laminates. Therefore, it was suggested to provide intermediate anchorage (CFRP laminates in L-shape, U-shape wrap) to maintain ductility [10].

Experimental Studies (2011~2013) Obaidat *et al*. (2011) investigated the preloaded or cracked RC beams with different strengthening configurations for flexure. The experimental study reported that the CFRP can restore the strength of preloaded RC beams efficiently. Similarly, as the length of CFRP increased the beam strength increased due to attainment of proper anchorage. Strength increased but brittle failure was reported by delaminating bottom strip [11]. The performance of high strength fibre (Flexible wraps) U-shape wrap was studied by El-Ghandour. (2011). U-shape wraps convert the brittle flexure failure and high shear damages to ductile failure [12]. Dong *et al.* (2011) also reported that the flexure efficiency of RC enhanced by applying side or U-shaped sheet

together with CFRP sheet at the soffit of beam at four point loading. In this study a number of CFRP sheets were applied, but the strength enhancement was not proportional with the number of layers, and as the thickness of the layer increased beam exhibited brittle failure [13, 14]. A recent study by Shannag *et al.* (2013) involved the experimental study for flexure strengthening under four point loading and covered various parameters such as CFRP length, width, reinforcement ratio, failure mode etc. It was reported that the CFRP strip was applied at the soffit to enhance the load carrying capacity and stiffness by reducing deflection. Debonding occurred, when applied strip covered half width, whereas delamination with concrete cover reported by applying full strip at the bottom [15]. Numerous studies suggested best strengthening scheme for flexure is the application of bottom strip; however additional strength can be enhanced by applying side wraps of U-shape wrap, but the influence of side wrap observed insignificant [14, 16-21].

Torsion Configuration

Torsion is among the most critical action of the structure besides axial, bending moment and shear stresses. Torsion stresses developed when shear force does not passed from shear centre. Numerous studies have been conducted to investigate the efficiency of FRP laminated beams. The studies were conducted under pure torsion [22, 23]. Some of the important experimental studies are as follows.

Experimental Studies (2000~2010) Ghobarah *et al.* (2002) investigated the torsional resistance of RC beam wrapped using FRP. The beams were strengthened using GFRP and CFRP fabrics to upgrade torsional resistance with different configurations. The results have shown that the application of full wraps enhanced the performance of RC beam than any other wrapping schemes. However, 45° wrapped beam was more effective than vertically wrapped beam under pure torsion because vertical fibres were subjected to the stresses, which were against fibre direction. On the other hand, inclined fibres were along the force direction. In this study the need of combined effects of flexure and torsion was highlighted for future work due to in practical perspectives that is hard to find pure torsion in any structure [24]. Panchacharam and Belarbi (2002) investigated the effects of GFRP sheets subjected to pure torsion. The experimental study focused on effect of anchorage on U-shape wrap and fibre orientation and effects of side wraps (web & bottom). The study concluded that 90° degree fibre over all give high strength whereas 0° degree fibre orientation gave ductility and continuous wraps were more suitable than wraps in form of strip because continuous provide excellent confinement than strip; similarly 3 side wraps and 4 side wrap exhibited almost similar behaviour. U-shape wrapped beam exhibited less strength due to shear flow was less controlled; however, anchorage at the end of wrap improved the strength of beam [23]. Ronagh *et al.* (2004) conducted an experimental study by using both CFRP and GFRP laminates for torsion strengthening. The configuration used U-shape wrap on full length & U-shape wrap in form of strips and full wrap on full length & full wrap in form of strips. The reported results revealed that the maximum torsional strength was achieved by applying CFRP up to 143%. Whereas, GFRP strengthened beams increased up to 110%. Full wrapped beams exhibited highest strength than U-shaped wrapped beams. Two common failure modes, FRP rupture and FRP debonding were observed by applying FRP fabric [2]. Hi and Al-Mahaidi (2006) conducted an experiment on hollow and solid beam tested under pure torsion; to observe the effect of torsion on beam. Photogrammetry was use to observed the crack pattern and deformation in beam. The study concluded that solid beam had high crack load; whereas ultimate load was almost same. Similarly, CFRP spaced strip and number of layers have closes strength and CFRP uniformly distribute the stresses throughout the beam [25]. Reza Mohammadizadeh *et al.* (2009) an experimental study was conducted on 16 RC beams tested under pure torsion to enhancing ultimate torsion strength using FRP laminates. The specimens were tested under pure torsion and CFRP wraps were used for strengthening with single and double layers. The result exhibited that the strength increased by applying double layer was significant. However, U-shape wrap was less effective than full wrapped to enhance torsional capacity of RC beam [26]. Deifalla and Ghobarah (2010) conducted an experimental study on torsional and shear strength on T-beams strengthened using CFRP laminates

with different arrangement of steel anchorage. The use of anchor contributed in delaying premature failure of CFRP laminated beams. The most effective anchorage system was steel angle attached with bold which prevent RC beams from premature failure [27].

Experimental Studies (2011~2013). Mahmood and Mahmood (2011) investigated the effect of CFRP laminated prestressed beams with and without conventional reinforcement. The testing was conducted under the application of pure torsional load; configuration used was strips (spaced with d/2), U-warp and full wrap. Results concluded conventional reinforcement have shown more torsional capacity than unreinforced specimen; full wrap, U-wrap and wrap inform of strip exhibited 79%, 74% and 68% increment in ultimate torsion strength of beam respectively [28]. Tudu (2012) conducted an experimental study to observe the effect of GFRP strengthened RC beam under combined effect of torsion and bending. Study concluded the same results as previous studies revealed that full wrap is more effective strengthening scheme for torsion strengthening whereas 45° wrap are more suitable than 90° wraps [29]. Jariwala *et al.* (2013) carried out an experimental study on GFRP laminate beams. The beams were tested under combined torsion and bending. The results summarized that the full transverse wraps give high torsional moment resistance than other wrapping schemes. On the other hand, vertical wraps were less effective than diagonal strip wrapping, which exhibited better performance in torsion resistance. However, additional corner strip with wrapping improve the ductility of beam [30]. More or less almost every study conducted on torsion strengthening have shown same verdict for full wrap and then 45° wrap as a suitable solution for torsion strengthening [31, 32]. Almost all strengthening scheme for torsion and shear are the same and suggested configuration and results after applying full wrap, U-shape wraps, 45° & 90° wraps are same in behaviour and failure mode [22, 31-36].

Conclusion

Based on comprehensive review of past experimental studies the suitable configuration for flexure and torsion are as follows: (a) Flexure deficient beam can be strengthened at the soffit of the beam to enhance flexure capacity of RC beam. Bottom laminates not only enhance flexural strength of RC beam but also highly contribute to enhance shear strength of RC beam by increasing load carrying capacity. Whereas, beams wrapped on web has shown less contribution in enhancing flexural strength of RC beam. Highest stiffness achieved by applying FRP wraps, but ductility reduced enormously compared to control beam. Ductility can be improved by applying end anchorage system. (b) RC beam having torsion deficiency can be improved by applying full FRP wraps on beams. Full wraps confined the beam by interlocking aggregates. However, practically application of full wrap is difficult; therefore U-shape wraps are more suitable. Similarly, 45° wraps are more effective in enhancing ductility and stiffness of torsion deficient beam compared to 90° wrap. Diagonally or 45° wrapped RC beam give high strength because the FRP fibre is perpendicular to stress compared to vertical wraps. Application of bottom wrap together with full or diagonal wrap applied on the web of beam found to be suitable for combined effects of flexure and torsion deficient beams, however experimental study is needed to validate proposed strengthening scheme.

Acknowledgement

The author would like to thank Universiti Teknologi PETRONAS for the graduate assistantship.

References

[1] D. Kachlakev and D. D. McCurry, "Behavior of full-scale reinforced concrete beams retrofitted for shear and flexural with FRP laminates," *Composites Part B: Engineering,* vol. 31, pp. 445-452, 2000.

[2] H. Ronagh, M. Ameli, and P. Dux, "Experimental investigations on FRP strengthening of beams in torsion," in *FRP Composites in Civil Engineering - CICE 2004*, ed: Taylor & Francis, 2004, pp. 587-592.

[3] P. A. Ritchie, D. A. Thomas, L. W. Lu, and G. M. Conelly, "External reinforcement of concrete beams using fiber reinforced plastics," *ACI Structural Journal,* vol. 88, 1991.

[4] R. Irwin and A. Rahman, "FRP strengthening of concrete structures–design constraints and practical effects on construction detailing," *Available: Science Direct, www. sciencedirect. com.[Accessed September, 2009],* 2002.

[5] A. Sharif, G. J. Al-Sulaimani, I. A. Basunbul, M. H. Baluch, and B. N. Ghaleb, "Strengthening of initially loaded reinforced concrete beams using FRP plates," *ACI Structural Journal,* vol. 91, 1994.

[6] A. J. Lamanna, L. C. Bank, and D. W. Scott, "Flexural strengthening of reinforced concrete beams using fasteners and fiber-reinforced polymer strips," *ACI Structural Journal,* vol. 98, pp. 368-376, 2001.

[7] E. David, E. Ragneau, and F. Buyle-Bodin, "Experimental Analysis of Flexural Behaviour of Externally Bonded CFRP Reinforced Concrete Structures," *Materials and Structures,* vol. 36, pp. 238-241, 2003.

[8] H. Pham and R. Al-Mahaidi, "Experimental investigation into flexural retrofitting of reinforced concrete bridge beams using FRP composites," *Composite Structures,* vol. 66, pp. 617-625, 2004.

[9] M. R. Aram, C. Czaderski, and M. Motavalli, "Debonding failure modes of flexural FRP-strengthened RC beams," *Composites Part B: Engineering,* vol. 39, pp. 826-841, 2008.

[10] A. H. Al-Saidy, A. S. Al-Harthy, K. S. Al-Jabri, M. Abdul-Halim, and N. M. Al-Shidi, "Structural performance of corroded RC beams repaired with CFRP sheets," *Composite Structures,* vol. 92, pp. 1931-1938, 2010.

[11] Y. T. Obaidat, S. Heyden, O. Dahlblom, G. Abu-Farsakh, and Y. Abdel-Jawad, "Retrofitting of reinforced concrete beams using composite laminates," *Construction and Building Materials,* vol. 25, pp. 591-597, 2011.

[12] A. A. El-Ghandour, "Experimental and analytical investigation of CFRP flexural and shear strengthening efficiencies of RC beams," *Construction and Building Materials,* vol. 25, pp. 1419-1429, 2011.

[13] J. Dong, Q. Wang, D. He, and Z. Guan, "CFRP sheets for flexural strengthening of RC beams," 2011, pp. 1000-1003.

[14] E. Ahmed, H. R. Sobuz, and N. M. Sutan, "Flexural performance of CFRP strengthened RC beams with different degrees of strengthening schemes," 2011.

[15] M. J. Shannag, N. M. Al-Akhras, and S. F. Mahdawi, "Flexure strengthening of lightweight reinforced concrete beams using carbon fibre-reinforced polymers," *Structure and Infrastructure Engineering,* pp. 1-10, 2013.

[16] H. Saadatmanesh and M. Ehsani, "RC Beams Strengthened with GFRP Plates. I: Experimental Study," *Journal of Structural Engineering,* vol. 117, pp. 3417-3433, 1991.

[17] e. a. Tom Norris, "Shear and Flexural Strengthening of R/C Beams with Carbon Fibre Sheets," *Journal of Structural Engineering,* vol. 123, 1997.

[18] M. El-Mihilmy and J. Tedesco, "Analysis of Reinforced Concrete Beams Strengthened with FRP Laminates," *Journal of Structural Engineering,* vol. 126, pp. 684-691, 2000/06/01 2000.

[19] A. M. Okeil, S. El-Tawil, and M. Shahawy, "Flexural Reliability of Reinforced Concrete Bridge Girders Strengthened with Carbon Fiber-Reinforced Polymer Laminates," *Journal of Bridge Engineering,* vol. 7, pp. 290-299, 2002.

[20] A. F. Ashour, S. A. El-Refaie, and S. W. Garrity, "Flexural strengthening of RC continuous beams using CFRP laminates," *Cement and Concrete Composites,* vol. 26, pp. 765-775, 2004.

[21] M. Z. Jumaat, M. A. Rahman, and M. A. Alam, "Premature Failures in Plate Bonded Strengthened RC Beams with an Emphasis on Premature Shear: A Review," *International Journal of the Physical Sciences,* vol. Vol. 6(2), pp. 156-168, 2011.

[22] C. Constantin E, "Analytical model for the torsional behaviour of reinforced concrete beams retrofitted with FRP materials," *Engineering Structures,* vol. 29, pp. 3263-3276, 2007.

[23] S. Panchacharam and A. Belarbi, "Torsional behavior of reinforced concrete beams strengthened with FRP Composites," 2002, pp. 1-11.

[24] A. Ghobarah, M. N. Ghorbel, and S. E. Chidiac, "Upgrading Torsional Resistance of Reinforced Concrete Beams Using Fiber-Reinforced Polymer," *Journal of Composites for Construction,* vol. 6, pp. 257-263, 2002.

[25] A. K. Y. Hii and R. Al-Mahaidi, "Experimental Investigation on Torsional Behavior of Solid and Box-Section RC Beams Strengthened with CFRP Using Photogrammetry," *Journal of Composites for Construction,* vol. 10, pp. 321-329, 2006.

[26] M. Reza Mohammadizadeh, M. Javad Fadaee, and Hamid Reza Ronagh, "Improving Torsional Behaviour of Reinforced Concrete Beams Strengthened with Carbon Fibre Reinforced Polymer Composite," ed, 2009.

[27] A. Deifalla and A. Ghobarah, "Strengthening RC T-Beams Subjected to Combined Torsion and Shear Using FRP Fabrics: Experimental Study," *Journal of Composites for Construction,* vol. 14, pp. 301-311, 2010.

[28] A. S. Mahmood and M. N. Mahmood, "Torsional Behavior of Prestressed Concrete Beams Strengthened with CFRP Sheets," in *16th International Conference on Composite Structures (ICCS 16)*, 2011.

[29] C. Tudu, "Study of torsional behaviour of rectangular reinforced concrete beams wrapped with GFRP," 2012.

[30] V. H. Jariwala, P. V. Patel, and S. P. Purohit, "Strengthening of RC Beams Subjected to Combined Torsion and Bending with GFRP Composites," *Procedia Engineering,* vol. 51, pp. 282-289, 2013.

[31] C. Constantin E, "Torsional strengthening of rectangular and flanged beams using carbon fibre-reinforced-polymers – Experimental study," *Construction and Building Materials,* vol. 22, pp. 21-29, 2008.

[32] Mohammadizadeh, M. R.Fadaee, and M. J., "Torsional Behaviour of High-Strength Concrete Beams Strengthened Using CFRP Sheets; an Experimental and Analytical Study," *Scientia Iranica Transaction a-Civil Engineering,* vol. 16, pp. 321-330, Jul-Aug 2009.

[33] M. Ameli, H. R. Ronagh, and P. F. Dux, "Behavior of FRP strengthened reinforced concrete beams under torsion," *Journal of Composites for Construction,* vol. 11, pp. 192-200, 2007.

[34] A. Hii and R. Al-Mahaidi, "Torsional Capacity of CFRP Strengthened Reinforced Concrete Beams," *Journal of Composites for Construction,* vol. 11, pp. 71-80, 2007.

[35] S. B. Talaeitaba and D. Mostofinejad, "A New Test Setup for Experimental Test of RC Beams under Combined Shear and Torsion," *Advanced Materials Research,* vol. 335, pp. 355-358, 2011.

[36] A. R. Zojaji and M. Z. Kabir, "Analytical approach for predicting full torsional behavior of reinforced concrete beams strengthened with FRP materials," *Scientia Iranica,* vol. 19, pp. 51-63, 2012.

Applied Mechanics and Materials Vol. 567 (2014) pp 517-521
© (2014) Trans Tech Publications, Switzerland
doi:10.4028/www.scientific.net/AMM.567.517

Tension Stiffening Analysis for Cyclically Loaded RC Beams

Ahmad Azim Bin Shukri[1, a], Mohd Zamin Jumaat [1,b] ,

[1] Department of Civil Engineering, University of Malaya, 50603 Kuala Lumpur, Malaysia

[a] ahmadazimshukri@siswa.um.edu.my, [b] zamin@um.edu.my.

Keywords: cyclic loading; hinge; ductility; partial interaction; shear friction

Abstract. Ductility is an important aspect of cyclically loaded reinforced concrete (RC) structures. One of the method that can be used to measure the ductility of an RC structure is the moment-curvature approach. However, due to it being a strain-based approach it cannot be used to directly simulate behaviour associated with interface displacement that occur when an RC member is cracked. This leads to dependency on empirical values, which imposes limitations on how the moment-curvature approach can be used. In recent years a new displacement based method for measuring ductility has been developed, and can simulate the interface displacement behaviours through the use of partial-interaction theory and shear friction theory. This paper aims to extend the general tension stiffening analysis of the displacement-based approach to allow for cyclic loading. The tension-stiffening analysis was then validated against experimental results and the results were found to agree fairly.

Introduction

A reinforced concrete structure may be subjected to various sources of cyclic loads, which may be something severe such as earthquakes and also regular sources of load such load from passing traffic on bridges. One of the way to ensure a structural member can withstand cyclic load is by measuring the maximum ductility using the strain-based moment-curvature approach to simulate the behaviour of the member during cyclic load.

There are however several things that have to be taken into consideration when using the moment-curvature approach. One of the limitations of moment-curvature approach is that due to the fact that it is strain based, it cannot be used to directly simulate the behaviour associated with interface displacement that takes place when an RC member is cracked. The interface displacement in RC takes the form of slip between steel reinforcement and adjacent concrete, which causes tension stiffening mechanism and also sliding of concrete-concrete interface during the formation of concrete wedges in the concrete softening mechanism. Normally the solution to this is by using empirically derived hinge lengths, and also assume full-interaction between the steel-reinforcement and surrounding concrete. The empirical nature of the assumptions used in the moment-curvature approach means that it cannot be used in situations outside the bound of tests that form them. This means the moment-curvature approach cannot be used for special concretes such as fibre reinforced concrete and strengthened structures such as by using fibre reinforced polymer (FRP).

Recently a new displacement-based method had been developed [1-6], which utilizes partial-interaction theory and shear friction theory to simulate the behaviour of interface displacement. In recent years several improvements were made to the approach, one of which is to allow the simulation of the behaviour of beam with multiple cracks. This paper intends to extend the tension stiffening model which is crucial to the moment-rotation approach to allow for multiple cracking in a cyclically loaded beam.

Mechanisms in Cracked RC Beams

As mentioned before there are two main mechanisms caused by interface displacement: tension stiffening and concrete softening. Concrete softening mechanism is caused by the formation of concrete wedges under high compressive stress. The strain caused by the wedge is governed by shear-friction properties. It is also size dependent because if the specimen will always have its natural angle as its wedge angle, provided that the specimen is large enough to accommodate the resulting wedge. The other mechanism is the tension stiffening mechanism, which refers to the increase in axial rigidity of reinforced concrete when crack occur when compared to bare steel reinforcement.

Tension Stiffening Model

The tension stiffening mechanism allows the transfer of stress from the reinforcement to the surrounding concrete through the interface bond stress-slip relationship. The concrete stress gradually increases the further away from the crack due to this process, and in the same way stress in the reinforcement gradually decreases. This stress transfer process continues until the tensile capacity of the concrete is reached after which another flexural crack will occur.

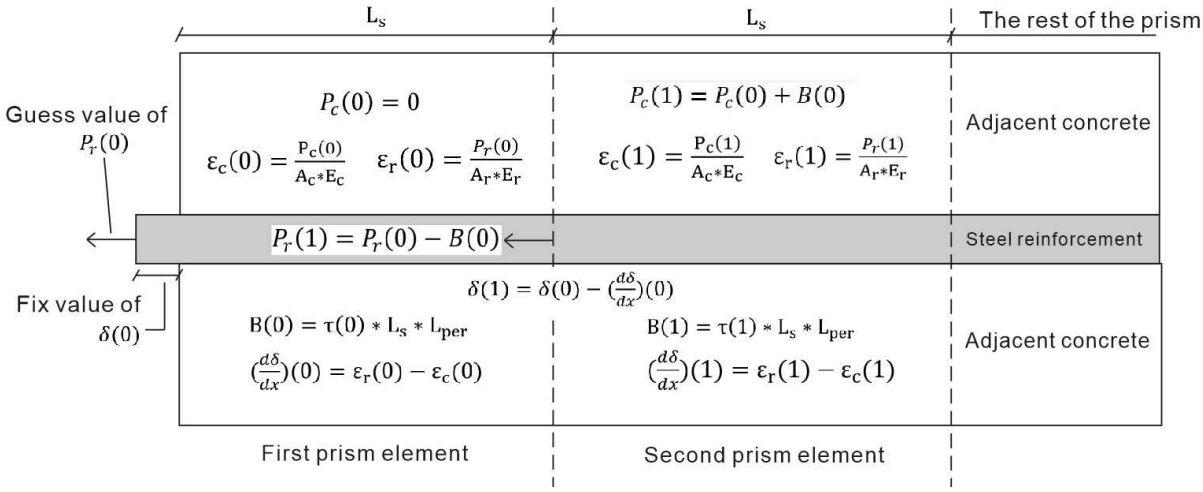


Figure 1 Partial-interaction Algorithm.

The algorithm of the tension stiffening analysis is presented briefly in Figure 1. At the crack face, the slip and force in reinforcement is at maximum values, while force in concrete is zero. The purpose of the analysis is to determine the amount of force that needs to be applied for a certain slip value to occur at the crack face, and in the beginning of the analysis the amount of slip that occur at the crack face is fixed to a certain value and the force in reinforcement is assumed. As the analysis moves to the prism, bond force at the reinforcement-concrete interface acts against the force pulling out the reinforcement. The amount of force exerted by the bond can be determined using any appropriate bond-slip model, such as the cyclic bond-slip model by Eligehausen et al. [7]. The bond force is thus calculated as:

$$B(n) = \tau(n) * L_s * L_{per}. \quad (1)$$

Where,

n= slice number.

$\tau(n)$= bond stress corresponding to slip $\delta(n)$.

L_s= length of one slice

L_{per}= perimeter of one steel reinforcement.

During cyclic loading, the bond stress in each prism slice is determined from its own unique bond-slip curve, which is due to the different amount of slip experienced by each slice. The bond stress would also act in the opposite direction during the reversal of load during cyclic loading, as the bond stress act against the applied force attempting to push the slipped reinforcement back into concrete.

Knowing the bond force, the force in the reinforcement and concrete at the next slice can also be determined:

$$P_r(\mathrm{n}+1) = P_r(\mathrm{n}) - B. \quad (2)$$

$$P_c(\mathrm{n}+1) = P_c(\mathrm{n}) + B. \quad (3)$$

The concrete strain can then be determined by assuming a linear tensile stress–strain relationship where it can be assumed that the concrete remains elastic because it is subjected only to tensile stresses:

$$\varepsilon_r(\mathrm{n}) = \frac{P_r(\mathrm{n})}{A_r * E_r}. \quad (4)$$

Determining the strain in steel require the use of a cyclic stress-strain model for steel, such as the one by Filippou et al. [8]. During monotonic loading or the initial loading of cyclic loading, strain is steel is determined as:

$$\varepsilon_c(\mathrm{n}) = \frac{P_c(\mathrm{n})}{A_c * E_c}. \quad (5)$$

Where,

A_r= Area of one steel reinforcement.

E_r= Modulus of elasticity of strain hardening modulus.

Beyond the initial loading, the strain in steel at each slice must be determined from its own unique stress-strain curve. The reason is the same as in the case of bond stress, where the different amount of slip experienced by each slice causes each slice to have its own strain value and thus follows its own stress-strain curve during cyclic loading.

Since the stress and strain of concrete in this model is dependent on the size of prism, the prism size is critical to the analysis. In this paper the prism size will be based on the recommended prism size as given by Muhamad et al. [6] which stated that the prism depth should be as deep as the bar plus the cover on both sides and the width of the prism is assumed to be the width of the entire beam evenly divided between adjacent bars. The difference in the steel strain and concrete strain is the change in slip, or slip-strain, which is experienced by the steel reinforcement as we progress to the next slice:

$$\left(\frac{d\delta}{dx}\right)(n) = \varepsilon_r(n) - \varepsilon_c(n). \quad (6)$$

It is the difference in slip that causes slip to occur, with the change in slip across the element simply being the integration of the slip strain across the element length. The new slip at the next slice is thus determined as:

$$\delta(n+1) = \delta(n) - \left(\frac{d\delta}{dx}\right)(n). \quad (7)$$

The analysis is continued until the final prism slice, and if the assumed force in the reinforcement at the crack face causes the slip and slip-strain to be reduced to a certain tolerance value, the analysis is ended. Otherwise another value of force is assumes and the whole procedure is repeated.

Validation of Tension Stiffening Model

It is difficult to compare the simulated tension stiffening analysis result with a set of experimental values. Therefore the partial-interaction model described in the previous section is applied in a moment-rotation model, and will be compared with experimental results of Ma et al. [9].

The moment-rotation model considers a single crack face of beam, where the force in tension region is governed by tension stiffening mechanism and the compression region is governed by concrete softening mechanism. Force in the tension region is thus determined from the tension stiffening model presented before, while force in the compression region is determined from any size-dependent cyclic stress-strain model for concrete, such as the one presented by Martinez-Rueda et al. [10]. For a given value of rotation, the forces acting at the crack face is determined and depth of neutral axis is adjusted until the summation of force is zero.

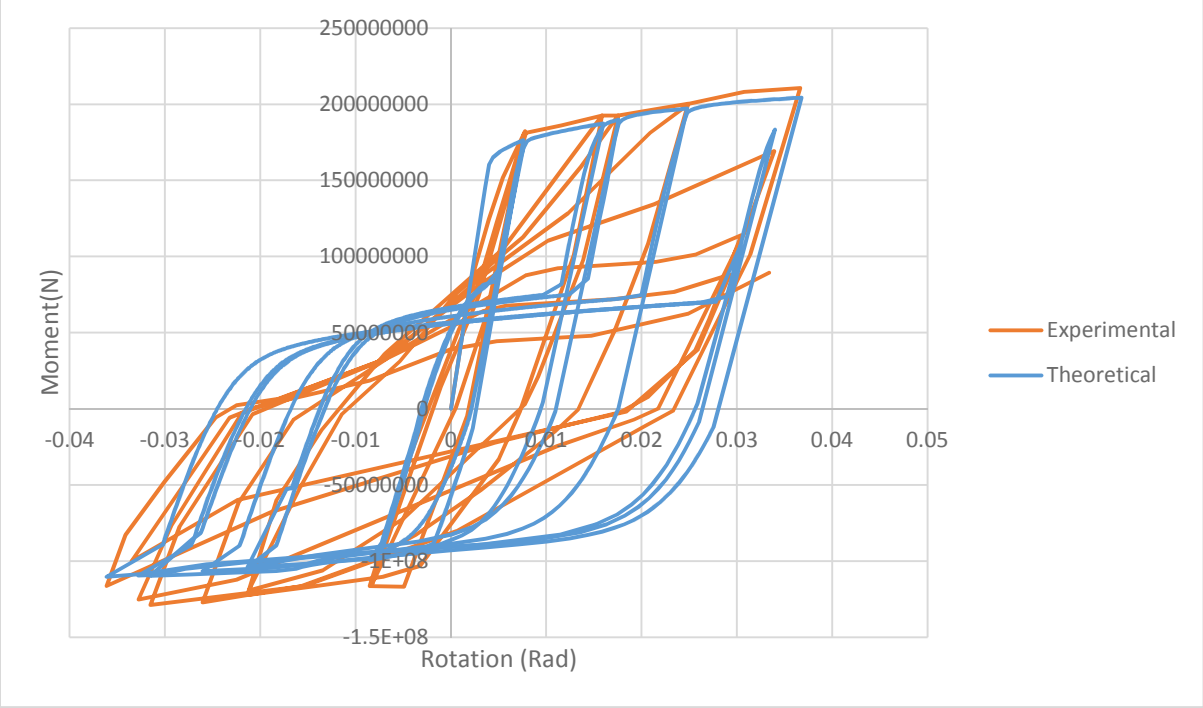


Figure 2 Comparison of simulated and experimental result.

Comparison between the simulated and experimental moment-rotation is given in Figure 2, where it can be seen that the model is able to simulate the maximum and minimum moments of the beam with high degree of accuracy. As it was proven [5] that reinforcement strain hardening have a great effect on the moment-rotation curve, deviations between simulated and experimental peak values is assumed to be caused by some differences between the strain hardening modulus used and actual beam strain hardening modulus. The use of multiple crack analysis was found to reduce the stiffness of the simulated curve, as the total rotation is taken as the sum of the local rotations at each crack, leading to smaller local crack widths and hence smaller slip of reinforcement.

Conclusion

The generic tension stiffening model of the moment-rotation approach was extended to allow for cyclic loading and multiple cracks. The moment-rotation curve generated using the model agree fairly with experimental results. The use of multiple crack analysis was found to reduce the stiffness of the simulated curve, which gives the curve a better agreement with experimental results.

Reference

[1] Visintin, P., Oehlers, D., Haskett, M., and Wu, C. (2013). Mechanics-based hinge analysis for reinforced concrete columns. J. Struct. Eng., 139(11), 1973–1980.

[2] Haskett, M., Oehlers, D. J., & Ali, M. S. M. (2008). Local and global bond characteristics of steel reinforcing bars. Engineering Structures, 30(2), 376-383.

[3] Ali, M. S. M., Oehlers, D. J., Griffith, M. C., & Seracino, R. (2008). Interfacial stress transfer of near surface-mounted FRP-to-concrete joints. Engineering Structures, 30(7), 1861-1868.

[4] Visintin, P., Oehlers, D. J., Wu, C., & Haskett, M. (2012). A mechanics solution for hinges in RC beams with multiple cracks. Engineering Structures, 36, 61-69.

[5] Visintin, P., Oehlers, D. J., Wu, C. W., & Griffith, M. C. (2012). The reinforcement contribution to the cyclic behaviour of reinforced concrete beam hinges. Earthquake Engineering & Structural Dynamics, 41(12), 1591-1608.

[6] Muhamad, R., Oehlers, D., & Ali, M. M. (2011). Discrete rotation deflection of RC beams at serviceability. Proc ICE Struct Buildings, 164, 1–14.

[7] Eligehausen R., Popov E.P., Bertero V.V. (1992). Local bond stress-slip relationship of deformed bars under generalized excitations. Earthquake Engineering Research Centre, UCB/EERC83/23.

[8] Filippou F.C., Popov E.P., Bertero V.V. (1983). Effects of bond deterioration on hysteretic behavior of reinforced concrete joints. Earthquake Engineering Research Centre, UCB/EERC-83/19.

[9] Ma S.M., Bertero V.V., Popov E.P. (1976). Experimental and analytical studies on the hysteretic behavior of reinforced concrete rectangular and T-beams. Earthquake Engineering Research Centre, UCB/EERC76/2

[10] Martinez-Rueda, J. E., & Elnashai, A. S. (1997). Confined concrete model under cyclic load. Materials and Structures, 30(197), 139-147.

Applied Mechanics and Materials Vol. 567 (2014) pp 522-528
© (2014) Trans Tech Publications, Switzerland
doi:10.4028/www.scientific.net/AMM.567.522

The Effect of MIRHA and Fly Ash on Mechanical Strength and Chloride Penetration Depth of DSCC

Muhd. Fadhil Nuruddin[1, a] Kok Yung Chang [1, b]

and Norzaireen Mohd. Azmee[1, c]

[1,2] Department Of Civil Engineering, Universiti Teknologi PETRONAS, Perak, Malaysia.

[a]fadhilnuruddin@petronas.com.my, [b]kyung1987@gmail.com, [c]norzaireen@gmail.com

Keywords: Ductile Self Compacting Concrete, MIRHA, Fly Ash, Chloride Penetration Depth

Abstract. Ductile self compacting concrete (DSCC) is one of the advanced materials which combines self compacting abilities and ductility to address the current industry problems. As the fly ash and microwave incinerated rice husk ash (MIRHA) are beneficial to the properties of concrete, it has led to a research on the effects of ternary blends of MIRHA, fly ash and cement in DSCC. Up to 20% of cement in DSCC was replaced with MIRHA and fly ash with 10% by weight respectively whilst maintaining satisfactory self compacting abilities. The effects of MIRHA and fly ash on mechanical strength and chloride penetration depth of DSCC were determined. The control DSCC mix was compared with the DSCC mix with MIRHA and fly ash. The results shown that substitution of MIRHA and fly ash into DSCC gave positive effects, it improved the mechanical properties and chloride permeability.

Introduction

Concrete is one of the most important materials needed to cater for the increasing number of construction project as it has been widely used as the major elements of building structures. Thus, concrete and its development are crucial for the construction industry. Traditionally, concrete is a strong matrix made by the mixture of cement, sand, aggregate and water. Nowadays, concrete is not only a mixture of binders and natural aggregates but with addition of cement replacement materials, chemical admixtures and others in order to improve and achieve specific properties [1]. Ductile self compacting concrete (DSCC) is one of the advanced concrete materials which combines both self compacting properties and ductility.

DSCC has been made possible by incorporating short discontinuous steel fiber in self compacting concrete; it improves ductility properties such as increase in tensile and flexural strength, strain hardening and toughness [2]. Discrete and discontinuous hybrid steel fibers were added randomly into the concrete in order to obtain the characteristics of DSCC [3]. The development of DSCC is beneficial to the industry as it can address several current construction issues such as the brittleness of the normal concrete and the dependent on the workmanship and compaction problems. It can be used in several structural applications with technical and economic advantages compared to the conventional reinforcement concrete [4-7].

As DSCC is made with relatively high content of fine particles, a stiff and strong fiber matrix interface can be achieved, resulting in a material of high post-cracking resistance and ductility. The compactness of self compacting concrete matrix due to the high amount of fine and extra-fine particles has improved the interface zone properties [8]. Furthermore, it improves the bonding between fibers and concrete matrix which can lead to post-cracking toughness and energy absorption capacity enhancement [9]. Previous researchers found that the fiber reinforced self compacting concrete improved the mechanical properties compared with other concretes such as normal vibrated concrete, self compacting concrete and fiber reinforced concrete [10-13]. Thus, combination of self compacting abilities and fiber reinforcement in concrete brought remarkable advantages [14].

On the other hand, partial replacement of cement by the mineral additives is necessary in order to achieve an economical and durable concrete as DSCC consists of high cement content. According to previous researches, ternary blends concrete indicates better performance than binary blends concrete as ternary blends of binder synergy the effects of the cement replacement materials and compensate the disadvantages of the materials itself [15,16]. This has led to the research on the possibilities of ternary blends of cement, MIRHA and fly ash in DSCC. Fly ash is a common mineral additive in concrete as its spherical shape provides ball bearing effects, the rheology properties have been improved which resulted excellent workability and flowability in self compacting concrete [17]. On the other hand, MIRHA is a new cement replacement material produced under controlled burning method using microwave system. The addition of MIRHA in concrete gives better strength and reduced the porosity due to the pozzolanic reaction between MIRHA and calcium hydroxide [18-20].

Durability is the resistance to physical and chemical deterioration of concrete resulting from interaction with external environment. Transportation of ion through a hydrated cement system becomes a primal factor to degrade concrete in an aggressive environment [21]. Although concrete is a fundamental component of modern infrastructure, its durability can be a major problem affecting the lifespan of structures and involving significant repair cost [22]. In the coastal area, the resistance to chloride of concrete is important as salt penetration from seawater spray may be responsible for the corrosion [23]. In such case, it is the chloride ion which destroys the protective environment for the steel reinforcement and results in the corrosion of the steel reinforcement and eventual concrete distress [24]. Hence, chloride ion diffusion has become a center for research on ion transport in concrete as chloride ingress causing the most detrimental effects on the degradation of concrete [25].

Experimental Work

The mechanical properties and chloride penetration depth of DSCC were studied. In order to determine the effects of MIRHA and fly ash in DSCC, one control mix and one optimum mix were adopted. The control mix (CM) consists of 1000kg/m^3 cement without any substitution and optimum mix (OM) was replaced 20% cement with MIRHA and fly ash in an equal percentage. The DSCC mixes were added with two different type of steel fibers which is straight fiber (SF) and end-hooked fiber (EH). The volume fraction of steel fiber was maintained at 2%. Both mixes were compared in terms of compressive and flexural strength as well as chloride penetration depth.

Material Properties. Type I Ordinary Portland Cement (OPC) which manufactured in accordance to BS EN 197-1:2000 [26] was used in DSCC mixes while MIRHA and fly ash are categorized as Type II in accordance to BS EN 206-1:2000 [27] were adopted. The chemical composition of OPC, MIRHA and fly ash was shown in Table 1. MIRHA is a new cement replacement material which produced by UTP. MIRHA is rich in SiO_2 as the rice husk was incinerated under controlled temperature by microwave incinerator. Unlike the open burning method, MIHRA has a better consistency of properties as the process of burning was controlled. After the incineration process, MIRHA was then ground using Los Angeles (LA) machine for 2000 cycles in order to increase its fineness. Fly ash was obtained from Manjung Coal-Based Thermal Power Plant which particle size is 1μm to 100μm. Besides that, river sand with fineness modulus of 2.8 was adopted as the aggregate in DSCC and polycarboxylate ether (PCE) based superplasticizer was used as the superplasticizer (SP) in DSCC. The steel fibers used are straight fiber (SF) with diameter of 0.2 mm and fiber length 20 mm and end-hooked (EH) with diameter of 0.3 mm and fiber length 25 mm. The properties of steel fibers adopted in this study are shown in Table 2.

Table 1. Chemical Oxide Composition of OPC, Fly Ash, MIRHA and Silica Fume

Constituent	Percentage [%]		
	OPC	Fly Ash	MIRHA
Na_2O	0.20	-	0.12
MgO	2.42	-	0.49
Al_2O_3	4.45	29.1	0.45
SiO_2	21.45	51.7	89.34
P_2O_5	0.11	1.7	2.58
K_2O	0.83	1.6	4.98
CaO	63.81	8.84	0.76
TiO_2	0.22	0.7	0.02
Fe_2O_3	3.07	4.76	0.40
SO_3	2.46	1.5	0.90
MnO	0.20	-	0.08

Table 2. Physical Properties of Steel Fiber

Fiber Properties	SF	EH
Average fiber length [mm]	20	25
Average fiber diameter [mm]	0.2	0.3
Aspect ratio [I/d)	100	83.33
Tensile strength [MPa]	> 2300	> 2300

Concrete Mix Proportion. The mix proportion of both DSCC mixes was selected based on the trial mixes and the criteria of self compacting abilities. Mix CM is made with 100% of cement without any replacement while mix OM is replaced with MIRHA and fly ash (FA) which consists of 10% each by weight. For the mixing of DSCC, pan mixer was adopted in mixing DSCC, the binders and sand are mixed for 2 minutes and followed up by pouring in 50% of the total mixing water and mix for 3 minutes. Next, 40% of water and 70% of SP were poured then mixed for 5 minutes and the remaining water and SP were added and mixed until form. Finally, the steel fibers are dispersed naturally and evenly to prevent fiber balling and mixed for 2 minutes. Slump flow and V-funnel tests were conducted in order to ensure the self compacting abilities of DSCC. The procedures were according to the European Guidelines and both DSCC mixes were complied with the requirements [28]. The final DSCC mix proportion is shown in Table 3.

Table 3. DSCC Mix Proportion

Mix	Description	OPC	MIRHA	FA	Sand	Steel Fibers	SP	Water
CM	OPC	1.0	-	-	1.0	0.152	0.025	0.17
OM	OPC&MIRHA,FA	0.8	0.1	0.1	1.0	0.152	0.025	0.18

Mechanical and Chloride Penetration Tests. There are 2 mechanical tests for comparing the control DSCC mixture (CM) and optimum mix (OM). Compressive strength tests of 1, 7, 14, 28 and 90 days were conducted while flexural strength tests of 7, 14 and 28 days were conducted. The testing procedures of both compressive and flexural strength tests are in accordance to BS EN 12390:2000 Part 3 & 5 [29,30]. The procedures of chloride penetration test were referred to the previous research [31]. Both specimens were water cured for 28 days before immersed into 4% sodium chloride solution. The specimens were tested at 7, 14, 28, 56 and 90 days after the immersion of 4% sodium chloride solution. Until the testing age, the specimens were splitted into two by concrete cutting machine. The splitted surface was sipred surface dry and sprayed with silver nitrate solution. Silver nitrate solution was used as the indicator for chloride attack because it is the most widely used method that is simpler and faster than other methods [32]. 0.1 mol/L $AgNO_3$ solution was applied as it gave the most clear colour of boundary [32]. The colour change

of the specimens was observed as the chloride affected area was white precipitated by silver chloride after the chemical reaction of silver nitrate and sodium chloride. Brown precipitate was shown on the surface which was not affected by chloride. The depth of the chloride penetration at every direction was measured and the average result was obtained.

Results and Discussions

Mechanical Strength. Based on Table 4, it shows the compressive and flexural strength of both DSCC mixes. In terms of compressive strength, the strength development of OM is slower than CM at early age. The compressive strength of OM was 50 MPa at 1 day which is 23% lower than the CM. This is due to the substitution of MIRHA and fly ash in OM as it regulated the cement content and led to heat of hydration reduced [33]. Hence, the strength development at early age was reduced. However, the strength development increased over the duration and OM possessed a higher rate than CM from 7 days to 90 days. The inclusion of MIRHA and fly ash has generated pozzolanic reaction in the mix after the hydraulic reaction of cement completed. This is because the SiO_2 content of MIRHA and fly ash reacts with calcium hydroxide which produced during the cement hydration process [32].

Table 4. Compressive and Flexural Strength of DSCC

	Compressive Strength [MPa]					Flexural Strength [MPa]		
Mix	1 day	7 days	14 days	28 days	90 days	7 days	14 days	28 days
CM	62	107	124	131	142	16	19	20
OM	42	94	115	134	153	17	21	22

Based on Table 4, it shows the compressive and flexural strength of both DSCC mixes. In terms of compressive strength, the strength development of OM is slower than CM at early age. The compressive strength of OM was 50 MPa at 1 day which is 23% lower than the CM. This is due to the substitution of MIRHA and fly ash in OM as it regulated the cement content and led to heat of hydration reduced [33]. Hence, the strength development at early age was reduced. However, the strength development increased over the duration and OM possessed a higher rate than CM from 7 days to 90 days. The inclusion of MIRHA and fly ash has generated pozzolanic reaction in the mix after the hydraulic reaction of cement completed. This is because the SiO_2 content of MIRHA and fly ash reacts with calcium hydroxide which produced during the cement hydration process [32].

Besides that, the rate of pozzolanic reaction is greatly influenced by the chemical composition as well as particle specific area of MIRHA and fly ash. As the mechanism of pozzolanic reaction is dissolution and diffusion controlled process [34], particle size and surface area plays an important role in the rate of reactivity. Due to the fineness of MIRHA and fly ash, it contributed to the high rate of hydration and the high content of SiO_2 of MIRHA makes it highly reactive [35]. Hence, the ternary blends of MIRHA and fly ash with cement in DSCC (OM) improved the compressive strength at the later ages compared to CM. Based on the results, OM has higher compressive strength than CM at 90 days which was 153 MPa and 8% higher than CM.

In terms of flexural strength, both mixes were improved by the addition of steel fibers [36]. However, there is difference in terms of flexural strength between the DSCC mixtures which due to the bond strength of DSCC matrix and steel fibers. OM recorded the highest flexural strength, 22 MPa at 28 days compared to CM which was 20 MPa at 28 days. This is due the pozzolanic reaction between cement, fly ash and MIRHA has reduced the porosity and increased the compactness and strength of DSCC [18].

Chloride Penetration Test. From the results as shown in Table 5, the chloride penetration depth of DSCC was increased over the duration of chloride immersion. In overall, OM had a better resistance to chloride penetration as the average depth of chloride penetrated was the lowest, which was 2.36 mm after 90 days of immersion. On the other hand, CM has a higher penetration depth which was 3.73 mm at 90days which was 58% higher than OM. The substitution of MIRHA and fly ash in OM gave pozzolanic reaction to the mixture and reacted with calcium hydroxide and formed calcium silicate hydrates. The formation of calcium silicate hydrates enhanced the concrete structure and enhanced its overall durability performance. In contrast, calcium hydroxide in the mixture was consumed by the pozzolanic reaction is beneficial as it was a byproduct of cement hydration which susceptible to environment attacks. Besides that, it conforms with other researches whereby the inclusion of high pozzolan materials in ternary blend of binder improved the impermeability of concrete to chloride attack [37].

Table 5. Chloride Penetration Depth of DSCC

Age of Chloride Immersion [days]	Average Chloride Penetration Depth [mm]	
	CM	OM
7	1.00	1.00
14	1.25	1.25
28	1.75	1.50
56	2.00	1.50
90	3.73	2.36

Conclusion

Based on the overview of studies, the properties of DSCC have been outlined. Several conclusions can be drawn:

1- DSCC with replacement of 10% MIRHA and 10% of fly ash (OM) has a better compressive and flexural strength compared to control DSCC mix (CM) without sacrifices the self compacting abilities.
2- The ternary blends of binder with MIRHA and fly ash synergize the effects on the chloride resistance due to refinement of porosity and permeability of DSCC.
3- The usage of MIRHA and fly ash are able to improve the properties of concrete due to pozzolanic reaction with the cement.

References

[1] E.G. Nawy, Concrete Construction Engineering Handbook, 2nd ed. Boca Raton: CRC Press, (2008).

[2] J. Ambroise, S. Rols, J. Pera, Properties of Self-leveling Concrete Reinforced by Steel Fibers. *43rd Brazilian Congress of the Concrete (IBRACON)*, August 2001, Brazil, 2001.

[3] M.F. Nururddin, N. Mohd. Azmee, K.Y. Chang, Effect of Fire Flame Exposure on Ductile Self-Compacting Concrete (DSCC) Blended with MIRHA and Fly Ash. *Construction and Building Materials.* Vol. 50, (2014), pp. 388-393.

[4] S. Goel, S.P. Singh, P. Singh, Flexural Fatigue Strength and Failure Probability of Self Compacting Fibre Reinforced Concrete Beams. *Engineering Structures*. Vol. 40, (2012), pp. 131-140.

[5] P. Groth, D. Nemegeer, The Use of Steel Fibres in Self-Compacting Concrete. *1st International RILEM Symposium on Self-Compacting Concrete*, September 1999, Stockholm, Sweden, 1999, pp. 497-507.

[6] C. Carlsward, M. Emborg, Shrinkage Cracking of Steel Fibre Reinforced Self Compacting Concrete Overlays – Test Methods and Theoretical Modeling. 5th *International RILEM Symposium on Self Compacting Concrete*, 3-5 September 2007, Gent, Belgium, 2007, pp. 793-798.

[7] L. Ferrara, A. Meda, Relationships between Fibre Distribution, Workability and the Mechanical Properties of SFRC Applied to Precast Roof Elements. *Material and Struc*tures. Vol. 39, (2006), pp. 411-420.

[8] V. Corinaldesi, G. Moriconi, Durable Fiber Reinforced Self-Compacting Concrete. *Cement and Concrete Research*. Vol. 34, (2004), pp. 249-254.

[9] L. Ferrara, Y.D. Park, S.P. Shah, A Method for Mix-Design of Fiber Reinforced Self-Compacting Concrete. *Cement and Concrete Research*. Vol. 37, (2007), pp. 957-971.

[10] M. Sahmaran, I. Ozgur Yaman, Hybrid Fiber Reinforced Self-Compacting Concrete with a High-Volume Coarse Fly Ash. *Construction and Building Materials*. Vol. 21, (2007), pp. 150-156.

[11] V.M.C.F. Cunha, J.A.O. Barros, J.M. Sena-Cruz, Pullout Behavior of Steel Fibers in Self Compacting Concrete. *Journal Material and Civil Engineering*. Vol. 22, (2010), pp. 1-9.

[12] M.C. Torrijos, B.E. Barragan, R.L. Zerbino, Physical-mechanical Properties and Mesostructure of Plain and Fiber Reinforced Self-Compacting Concrete. *Construction and Building Materials*. Vol. 22, (2008), pp. 1780-1788.

[13] T. Greengough, M. Nehdi, Shear Behaviour of Fiber Reinforced Self Consolidating Concrete Slender Beams. *ACI Materials Journal*. Vol. 105, (2008), pp. 468-477.

[14] A.P. Fantilli, P. Vallini, B. Chiaia, Ductility of Fiber-Reinforced Self-Consolidating Concrete under Multi-axial Compression. *Cement and Concrete Composites*. Vol. 33, (2011), pp. 520-527.

[15] A.M. Sharfuddin, O. Kavali, W. Anderson, Chloride Penetration in Binary and Ternary Blended Cement Concretes as Measured by Two Different Rapid Methods. Cement and Concrete Composites. Vol. 30, (2008), pp. 576-582.

[16] M. Gesoğlu, E. Güneyisi, E. Özbay, Properties of Self-Compacting Concretes Made with Binary, Ternary, and Quarternary Cementitious Blends of Fly Ash, Blast Furnace Slag, and Silica Fume. *Construction and Building Materials.* Vol. 23, (2009), pp. 1847-1854.

[17] N. Miura, N. Takeda, R. Chikamatsu, S. Rogo, Application of Super Workable Concrete to Reinforced Concrete Structures with Difficult Construction Conditions. *Proceedings of Concrete Institute.* 140, pp. 163-186.

[18] M.F. Nuruddin, N. Shafiq, N.L.M. Kamal, Microwave Incinerated Rice Husk Ask (MIRHA) Concrete: A new material in the construction industry. *UK Malaysia Engineering Conference 2008, 14-15 July 2008, University College London, London.*

[19] N.L.M. Kamal, M.F. Nuruddin, N. Shafiq, The Influence of Burning Temperature and Percentage Inclusion of Microwave Incinerated Rice Husk Ash (MIRHA) on Normal Strength Concrete. *ICCBT*, 2008.

[20] M.F. Nuruddin, N. Shafiq, N.L.M. Kamal, The Effect of Types of Rice Hush Ash on the Porosity of Concrete. *Joint Conferences of APSEC-EACEF*, 2009.

[21] T. Sugiyama, W. Ritthichauy, T. Tsuji, Experimental Investigation and Numerical Modeling of Chloride Penetration and Calcium Dissolution in Saturated Concrete. *Cement and Concrete Research.* Vol. 38, (2008), pp. 49-67.

[22] S. Donatello, A. Palomo, A. Fernández-Jiménez, Durability of very High Volume Fly Ash Cement Pastes and Mortars in Aggressive Solutions. *Cement and Concrete Composites.* Vol. 38, (2013), pp. 12-20.

[23] D.D. Tsay, A Study of the Influence of Sea Salt on the Corrosion of Reinforcement in Concrete. *Proceedings of Asian-Pacific Corrosion Control Conf.*, Beijing, China, vol. 2, pp. 1213-1223, 1991.

[24] N. Buenfield, Chlorides in Concrete Repair. *Concrete Repairs*. Vol. 2, (1986), pp. 24-27.

[25] C. Andrade, J. Kropp, Testing and Modelling the Chloride Ingress into Concrete. *Proceedings of the 2nd International RILEM Workshop*, 2000.

[26] BS EN 197-1: 2011. *Cement Composition, Specifications and Conformity Criteria for Common Cements.* BSI Standard Publications 2011.

[27] BS EN 206-1: 2000. *Specification, Performance, production and conformity.* BSI Standard Publications 2000.
[28] EFNARC. *The European Guidelines for Self Compacting Concrete.* 2005.
[29] BS EN 12390-3: 2002. *Testing Harderned Concrete Part 3 – Compressive Strength of Test Specimens.* BSI Standard Publications 2010.
[30] BS EN 12390-5: 2002. *Testing Harderned Concrete Part 5 – Flexural Strength of Test Specimens.* BSI Standard Publications 2010.
[31] E. Güneyisi, T. Özturan, M. Gesoğlu, Effect of Initial Curing on Chloride Ingress and Corrosion Resistance Characteristics of Concretes made with Plain and Blended Cements. *Building and Environments*. Vol. 42, (2007), pp. 2676-2685.
[32] F. He, C. Shi, Q. Yuan, C. Chen, K. Zhen, $AgNO_3$-Based Colorimetric Methods for Measurement of Chloride Penetration in Concrete. *Construction and Building Materials.* Vol. 26, (2012), pp. 1-8.
[33] The European Project Group (2005). The European Guidelines for Self Compacting Concrete. SCC European Project Group.
[34] R.P. Khatri, V. Sirivivatnanon, Effect of Different Supplementary Cementitious Materials on Mechanical Properties of High Performance Concrete. *Cement and Concrete Research*. Vol. 25, (1995), pp. 209-220.
[35] G. Sivakumar, R. Ravibaskar, Investigation on the Hydration Properties of the Rice Husk Ash Cement using FTIR and SEM. *Applied Physics Research.* Vol. 1, (2009), pp. 71-77.
[36] Y. Wang, S. Backer, Toughness Determination for Fibre Reinforced Concrete. *The International Journal of Cement and Lightweight Concrete.* Vol. 11, (1989).
[37] H. Yazici, The Effect of Silica Fume and High-Volume Class C Fly Ash on Mechanical Properties, Chloride Penetration and Freeze-Thaw Resistance of Self-Compacting Concrete. *Construction and Building Materials.* Vol. 22, (2008), pp. 456-462.

Applied Mechanics and Materials Vol. 567 (2014) pp 529-534
© (2014) Trans Tech Publications, Switzerland
doi:10.4028/www.scientific.net/AMM.567.529

The effect of palm oil fuel ash as a cementreplacement material on self-compacting concrete

BelalAlsubari[1, a],PayamShafigh[2, b],MohdZaminJumaat[3,c],
U. Johnson Alengaram[4,d]

[1,2,3,4]Department of Civil Engineering, University of Malaya, 50603 Kuala Lumpur, Malaysia

[a]belalalsubari@gmail.com, [b]pshafigh@um.edu.my, [c]zamin@um.edu.my, [d]johnson@um.edu.my

Keywords:self- compacting concrete; palm oil fuel ash; fresh properties; compressive strength; drying shrinkage; cement replacement materials.

Abstract. In this study ground palm oil fuel ash (POFA) has been used as cement replacement in percentages of 0%, 10%, and 20% in a self-compacting concrete (SCC). Fresh properties such as slump flow, T_{50}, V-funnel, J-ring, L-box and segregation index; concrete properties such as drying shrinkage strain, initial surface absorption test (ISAT) as well as compressive strength were investigated. Test results showed that substitution of cement with POFA up to 20%, the fresh properties of the concrete fulfilled the requirements of a self-compacting concrete. The results revealed that concrete has higher compressive strength, lower drying shrinkage, and lower initial surface absorption than control mix. The results indicated that POFA can be used up to 20% as a cement replacement material for producing self- compacting concrete.

Introduction

Self-compacting concrete (SCC) is highly flowable concrete, which can be placed in the formworks and also can flow through obstructions by its own weight and without the need of vibration. In addition, segregation resistance and the ability of SCC to remain homogeneous and stable must be fulfilled [1, 2]. Palm oil fuel ash (POFA), which is a waste from palm oil industry, is a type of SCM. Many researches have been carried out to examine the feasibility of using this ash as supplementary cementious materials (SCMs)[3-6].

The objective of this study is to investigate the use of POFA as cement replacement to produce SCC. The performance of concrete was investigated in terms of drying shrinkage strain, initial surface absorption. Besides that, fresh properties and compressive strength were examined to check the homogeneity, physical and mechanical properties of the concrete. If the findings of this research prove that POFA can be used as cement replacement material in producing SCC with improvement in its characteristics, it will lead to reduction in cement consumption and the cost of making concrete. Moreover, it will be helpful for the environment by reducing the emission of CO_2 and the volume of waste dumped of in landfills.

Experimental programme

Materials

Ordinary Portland cement (OPC) and POFA were used as binder. POFA used in this study was collected from palm oil mill located in Selangor Malaysia. The dry POFA was sieved through a 300 μm sieve to remove bigger size ash particles and foreign materials. A Los Angeles machine was used to grind the POFA to reduce the particle size and to improve its reactivity. The silica dioxide (SiO_2) content was 59.13%.

Local mining sand with a fineness modulus of 2.88, specific gravity of 2.56, and water absorption of 1.13% was used as a fine aggregate. Crushed limestone with a maximum size of 12.5 mm, specific gravity of 2.62, water absorption of 0.44%, and fineness modulus of 6.30 was used as coarse aggregate.

Mix proportions

Ground POFA was used to partially replace OPC at proportions of 10%, and 20% (SCC0, SCC10, and SCC20) by weight of binder as shown in Table 1. The targeted compressive strength of concrete incorporating ground POFA was at least 60 MPa at 28 days moist curing. All mixes had the same binder content of 480 kg/m^3, and the water to binder (W/B) ratio was kept at 0.35. A superplasticizer used in the concrete mixtures in order to obtain the fresh properties of SCC.

Table 1. Mix proportions of concretes

Mix No.	W/C ratio	Cement (Kg/m^3)	POFA (Kg/m^3)	F.A (Kg/m^3)	C.A (Kg/m^3)	Water (Kg/m^3)	S.P (% B)
SCC0	0.35	480	0 (0%)	925	758.2	168	1.3
SCC10	0.35	432	48 (10%)	923	752	168	1.4
SCC20	0.35	384	96 (20%)	944	772	168	1.8

Specimen preparation and testing methods

Fresh properties of mixes were determined for filling, passing abilities, and segregation resistance after mixing. All fresh properties were conducted according to EFNARC 2002 [1].

To conduct compressive strength test, 100 mm cube sizes were prepared. 3 specimens were used for each test.

To determine the drying shrinkage strain of concrete, prismatic concrete specimens 100×100 mm^2 in cross-section and 500 mm in length were used.

To conduct initial surface absorption test (ISAT), 100 mm cube sizes were also prepared. The concrete specimens were water cured for 28, and 56 days before subjected to the test.

Results and discussion

Fresh properties

Fresh properties of SCC concrete were determined by conducting the filling ability tests (slump flow, T_{50}cm spread time, and V-funnel flow time), passing ability tests (J-ring flow and L-box), and segregation resistance test (segregation index) of different SCC mixtures are given in Table 4. It can be seen that mixtures including POFA in concrete does not cause any severe adverse effect on filling ability, passing ability and segregation resistance.

Table 2. Fresh properties of SCC concrete.

Mix No.	filling ability			Passing ability		Segregation resistance
	Slump Flow (mm)	T_{50} spread time (s)	V-funnel time (S)	J-ring (mm)	L-box	Segregation Index
SCC0	700	3.5	6.5	690	94	6.8
SCC10	690	3.7	6.8	670	93	8.7
SCC20	660	4.6	8.8	630	84	13.0

Compressive strength

Development of compressive strength of all mixes is shown Table 5. The 28-day compressive strength of SCC0, SCC10, and SCC20 mixes were 67.0, 69.5, and 60.0 MPa respectively. Thus, all the concrete mixtures could be categorized as self-compacting concrete.
The compressive strength of mixtures containing ground POFA show lower strength at the early ages of 3 and 7 days. Compare to mix SCC0, the SCC10, and SCC20 mixes showed a reduction on the compressive strength of about 4% and 20% at 3 days and 3% and 24% at 7 days, respectively. For both early ages, the reduction of the compressive strength at 10% cement replacement level was negligible while at 20% cement replacement levels the reduction was significant. The reduction in the early age compressive strength can be attributed to the reduction in the cement content in the mix design [7].
The development of compressive strength of ground POFA is due to pozzolanic activity of this

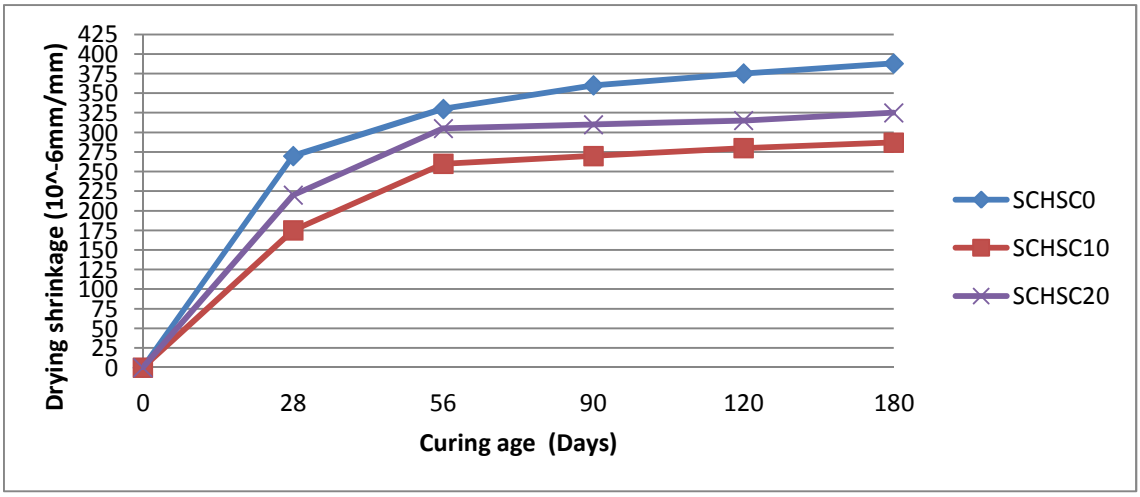
pozzolan which reacts with the Ca $(OH)_2$ liberated from cement hydration in the presence of water. This forms secondary calcium silicate hydrate (C–S–H). The pozzolanic reaction mainly contributes to increase the compressive strength of concrete at the later ages by improving the interfacial bond between paste and aggregate [8].

Table 3. Development of compressive strength of all mixes.

POFA %	Compressive Strength (MPa)					
	3 days	7 days	28 days	56 days	90 days	180 days
SCC0	51.0	57.5	67	70.5	72.0	73.3
SCC10	49.0	55.6	69.0	72.0	74.0	75.2
SCC20	40.9	43.8	60.8	65.9	69.0	70.4

Drying shrinkage strain

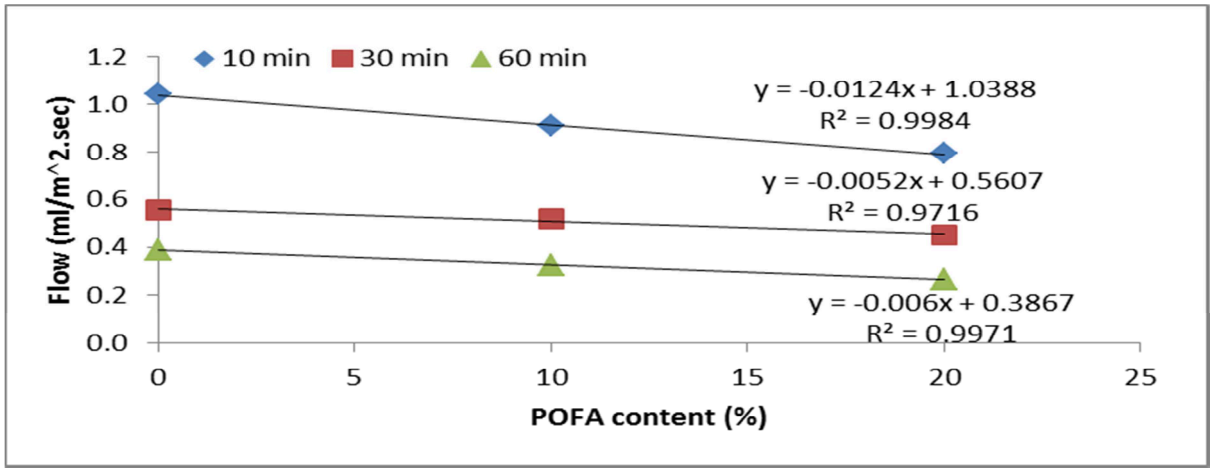
The results of drying shrinkage strain of all mixes up to six months are shown in Fig. 2. Drying shrinkage strain occurs when concrete hardens and dries out at the early age. It induces potential flow channels in the form of microcracks. These cracks initiate the access to harmful agents, and thus affect the durability of concrete. Test results of this study show that the incorporation of palm oil fuel ash reduce the drying shrinkage strain at any percentage of replacement (up to 20%). At age 180 days of drying, the drying shrinkage strain of control sample was 388 microstrain while those of concretes with 10%, and 20% POFA were 287, and 325 microstrain, respectively. These results agreed with observations reported by Tangchirapat et al. [9] for vibrated high strength concrete. In addition, this results agreed with findings for another type of cementitious material namely rice husk ash (RHA) reported by Mahmud et al. [10].



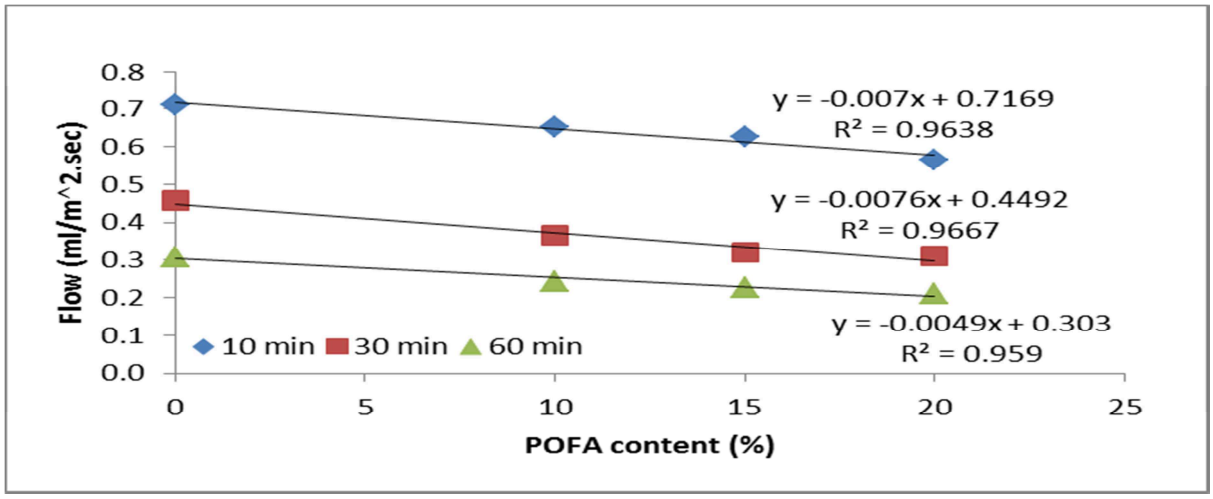
Figures 1. Development of drying shrinkage strain with time

Initial surface water absorption test (ISAT)

The initial surface absorption test was performed to obtain the flow within the concrete surface at intervals of 10, 30 and 60 minutes. Test results show that by incorporating POFA in SCC the ISAT value decreases. The lowest flow rate was at 20% cement replacement level at all ages. The initial surface absorption of SCC10 and SCC20 for 10 min interval was 16% and 32% lower than control mix (SCC0) at 28 days. Although, SCC20 had slightly lower compressive strength than that of SCC0 and SCC10 mixes, but SCC20 had lower concrete surface absorption. Consequently, it may be concluded that the SCC20 has better durability than that of SCC0 and SCC10 mixes. The observed reduction in initial surface absorption could be attributed to the more refined microstructure of the concrete containing POFA due to the formations of C-S-H gel by the pozzolanic reaction that gradually fill the original water filled space. Therefore, the pozzolanic effect of POFA reduced the pore diameters and improved strength and permeation characteristics of the concrete. Another possible reason is the high fineness of POFA that would become as filler between cement particles [11].



Figures 2. Effect of POFA content on initial surface absorption of concrete at the age of 28 days (2(a)).



Figures 2. Effect of POFA content on initial surface absorption of concrete at the age of 56 days (2(b)).

Conclusions

Based on the findings of this research, the following conclusions could be drawn:

1) Ground POFA can be used as a pozzolanic cement replacement material (up to 20%) to produce self-compacting concrete.
2) Incorporating ground POFA caused reduction in drying shrinkage strain of all the mixes containing POFA compared to concrete made just OPC.
3) Self-compacting concrete containing ground POFA showed significant reduction in the initial surface water absorption. POFA content at the 20% cement replacement level exhibited the lowest initial surface water absorption compared to all mixes.

Acknoweldgement

The authors gratefully acknowledge the financial support from University of Malaya under science fund project (13-02-03-3092).

References

[1] EFNARC, S., Guidelines for self-compacting concrete. February 2002, 2002.
[2] Sabet, F.A., N.A. Libre, and M. Shekarchi, Mechanical and durability properties of self consolidating high performance concrete incorporating natural zeolite, silica fume and fly ash. Construction and Building Materials, 2013. 44: p. 175-184.
[3] Sata, V., C. Jaturapitakkul, and K. Kiattikomol, Utilization of palm oil fuel ash in high-strength concrete. Journal of Materials in Civil Engineering, 2004. **16**(6): p. 623-628.
[4] Abdullah, K., et al., POFA: A potential partial cement replacement material in aerated concrete. 2006.
[5] Safiuddin, M., M.A. Salam, and M.Z. Jumaat, Key Fresh Properties of Self-Consolidating High-Strength POFA Concrete. Journal of Materials in Civil Engineering, 2013.
[6] Tangchirapat, W., et al., Use of waste ash from palm oil industry in concrete. Waste Management, 2007. 27(1): p. 81-88.
[7] Hussin, M.W. and A. Awal. Influence of palm oil fuel ash on strength and durability of concrete. in Proc., 7th Int. Conf. on Durability of Building Materials and Components. 1996. E & FN Spon London.
[8] Ismail, M.A., et al., Effect of POFA fineness on durability of high strength concrete. 2010.

[9] Cheerarot, R. and C. Jaturapitakkul, A study of disposed fly ash from landfill to replace Portland cement. Waste Management, 2004. 24(7): p. 701-709.
[10] Mahmud, H.B., et al., Mechanical properties and durability of normal and water reduced high strength grade 60 concrete containing rice husk ash. Journal of advanced concrete technology, 2009. **7**(1): p. 21-30.
[11] Kartini, K., H. Mahmud, and M. Hamidah, Absorption and permeability performance of Selangor rice husk ash blended grade 30 concrete. Journal of engineering science and technology, 2010. **5**(1): p. 1-16.

Applied Mechanics and Materials Vol. 567 (2014) pp 535-538
© (2014) Trans Tech Publications, Switzerland
doi:10.4028/www.scientific.net/AMM.567.535

The Laminated Composite Thermosetting Pipe

Thar M. Badri Albarody[1,a], and Zahiraniza Bt Mustaffa [1,b]

[1]Civil Engineering Department, Universiti Teknologi PETRONAS, Bandar Seri Iskandar, 31750 Tronoh, Perak, Malaysia

[a]t.albarody@ymail.com, [b]zahiraniza@petronas.com.my

Keywords: Thermosetting Pipe, Flexible pipeline, Laminated Composite, Shell Theories,

Abstract. The thermosetting pipes are eligible to be used in oil transportation where resistance to crude oil, paraffin build-up as well as ability to withstand relatively high pressures is required. Lamination design of such system could provide better strength and stability for internal and external loadings in both the circumferential and longitudinal directions. To this aim, a straightforward design and modeling of thermosetting pipe is developed via using first order shell theories. Apart from possessing an accurate operational condition, on account of its simplicity the proposed simulation seems also very suitable for further developing and prototyping purposes. Finally, it has been shown that the proposed thermosetting pipe, which partially attains some classical characteristic of both offshore and onshore pipeline by a different line of reasoning, is may serve as a reference in designing thermosetting pipe.

Introduction

Laminated Composite Thermosetting Pipe (LCTP), Fig. 1, is a system offers complete solution for offshore environment against highly corrosive fluids at various pressures, temperatures, adverse soil and weather conditions (especially in oil exploration, desalination, chemical plants, fire mains, dredging, portable water etc.)[1-3]. The chemical resistance, service temperature and the weight of such system helps reduce heavy and expensive construction cost[4, 5]. In this work, a pipe comprise an internal thermoplastic layer play as liner and a fluid-tight cover, and one or more dual-helical wounding tape stacks applied to the internal liner for absorbing axial and bending loads. The composite tape stacks are formed from a plurality of thin tape strips. All the layers are composed together to form on singular surface of the said thermosetting pipe.

Theoretical Model

Based on the laminated composite thick cylindrical shell theories [6, 7] the equations of motion could be drawn as:

$$\frac{\partial}{\partial\alpha}\mathrm{N}_{\alpha} + \frac{\partial}{\partial\beta}\mathrm{N}_{\beta\alpha} + \mathcal{F}_{\alpha} = \left(\bar{\mathrm{I}}_1\frac{\partial^2\mathrm{u_o}}{\partial\mathrm{t}^2} + \bar{\mathrm{I}}_2\frac{\partial^2\psi_{\alpha}}{\partial\mathrm{t}^2}\right),\ \frac{\partial}{\partial\beta}\mathrm{N}_{\beta} + \frac{\partial}{\partial\alpha}\mathrm{N}_{\alpha\beta} + \frac{\mathrm{Q}_{\beta}}{\mathrm{R}_{\beta}} + \mathcal{F}_{\beta} = \left(\bar{\mathrm{I}}_1\frac{\partial^2\mathrm{v_o}}{\partial\mathrm{t}^2} + \bar{\mathrm{I}}_2\frac{\partial^2\psi_{\beta}}{\partial\mathrm{t}^2}\right)$$

$$-\frac{\mathrm{N}^{\delta}_{\beta}}{\mathrm{R}_{\beta}} + \frac{\partial}{\partial\alpha}\mathrm{Q}_{\alpha} + \frac{\partial}{\partial\beta}\mathrm{Q}_{\beta} + \mathcal{F}_{\mathrm{n}} = \left(\bar{\mathrm{I}}_1\frac{\partial^2\mathrm{w_o}}{\partial\mathrm{t}^2}\right)$$

$$\frac{\partial}{\partial\alpha}\mathrm{M}_{\alpha} + \frac{\partial}{\partial\beta}\mathrm{M}_{\beta\alpha} - \mathrm{Q}_{\alpha} + \mathcal{C}_{\alpha} = \left(\bar{\mathrm{I}}_2\frac{\partial^2\mathrm{u_o}}{\partial\mathrm{t}^2} + \bar{\mathrm{I}}_3\frac{\partial^2\psi_{\alpha}}{\partial\mathrm{t}^2}\right),\ \frac{\partial}{\partial\beta}\mathrm{M}_{\beta} + \frac{\partial}{\partial\alpha}\mathrm{M}_{\alpha\beta} - \mathrm{Q}_{\beta} + \mathcal{C}_{\beta} = \left(\bar{\mathrm{I}}_2\frac{\partial^2\mathrm{u_o}}{\partial\mathrm{t}^2} + \bar{\mathrm{I}}_3\frac{\partial^2\psi_{\beta}}{\partial\mathrm{t}^2}\right). \quad (1)$$

Having applied the Navier' solution [8-10], the equations of motion can be written in terms of displacements as $\left(\mathcal{K}_{\mathrm{ij}} + \lambda^2\mathcal{M}_{\mathrm{ij}}\right)\{\Delta\} = \{\mathcal{F}\}$. Where $\mathcal{K}_{\mathrm{ij}}$ is the stiffness matrix and $\mathcal{M}_{\mathrm{ij}}$ is the mas matrix, $\{\mathcal{F}\}$ is the applied force, $\{\Delta\}^t = \left\{U_{mn}, V_{mn}, W_{mn}, \Psi^{\alpha}_{mn}, \Psi^{\beta}_{mn}\right\}$, and λ^2 is the eigenvalue of the problem[11, 12]. The configuration of the $\overline{\mathcal{K}}_{\mathrm{ij}}$ terms for the SS, cross-ply and rectangular plane form is listed below

$$\mathcal{K}_{11} = -\bar{\varsigma}^1_{11}\alpha^2_{\mathrm{m}} - \tilde{\varsigma}^1_{66}\beta^2_{\mathrm{n}},\ \mathcal{K}_{12} = -(\varsigma^1_{12} + \varsigma^1_{66})\alpha_{\mathrm{m}}\beta_{\mathrm{n}},\ \mathcal{K}_{22} = -\tilde{\varsigma}^1_{22}\beta^2_{\mathrm{n}} - \bar{\varsigma}^1_{66}\alpha^2_{\mathrm{m}} - \frac{\tilde{\varsigma}^1_{44}}{\mathrm{R}_{\beta}},$$

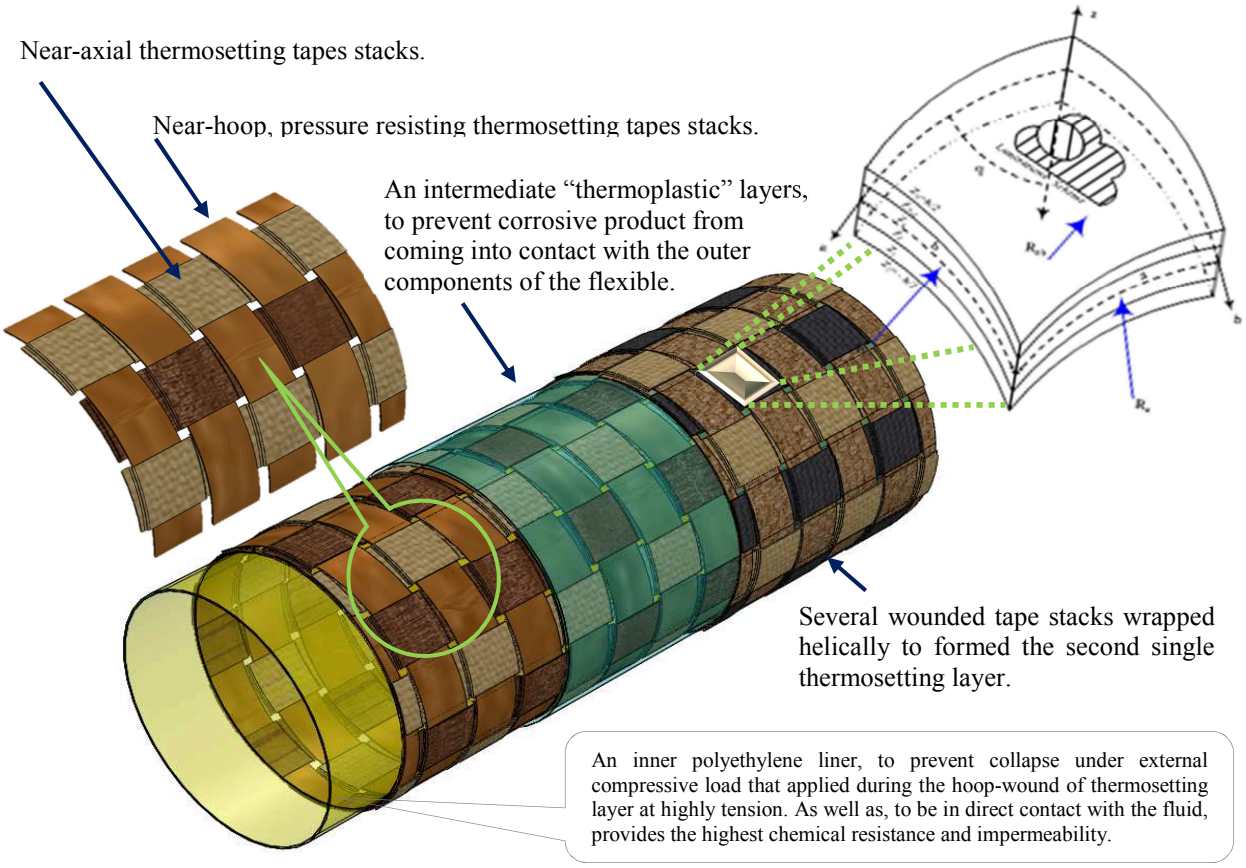


Fig. 1. Thermosetting pipe.

$$\mathcal{K}_{13} = \left(\frac{\varsigma_{12}^{1}}{R_\beta}\right)\alpha_m, \mathcal{K}_{23} = \left(\frac{\tilde{\varsigma}_{22}^{1}+\tilde{\varsigma}_{44}^{1}}{R_\beta}\right)\beta_n, \quad \mathcal{K}_{33} = -\tilde{\varsigma}_{44}^{1}\beta_n^2 - \bar{\varsigma}_{55}^{1}\alpha_m^2 - \left(\frac{\tilde{\varsigma}_{22}^{1}}{R_\beta}\right), \mathcal{K}_{14} = -\bar{\varsigma}_{11}^{2}\alpha_m^2 - \tilde{\varsigma}_{66}^{2}\beta_n^2,$$

$$\mathcal{K}_{24} = -(\varsigma_{12}^{2}+\varsigma_{66}^{2})\alpha_m\beta_n, \mathcal{K}_{34} = \left(-\bar{\varsigma}_{55}^{1}+\frac{\varsigma_{12}^{2}}{R_\beta}\right)\alpha_m, \mathcal{K}_{44} = -\bar{\varsigma}_{55}^{1} - \bar{\varsigma}_{11}^{3}\alpha_m^2 - \tilde{\varsigma}_{66}^{3}\beta_n^2,$$

$$\mathcal{K}_{15} = -(\varsigma_{12}^{2}+\varsigma_{66}^{2})\alpha_m\beta_n, \mathcal{K}_{25} = -\tilde{\varsigma}_{22}^{2}\beta_n^2 - \bar{\varsigma}_{66}^{2}\alpha_m^2 + \frac{\tilde{\varsigma}_{44}^{1}}{R_\beta}$$

$$\mathcal{K}_{35} = \left(-\tilde{\varsigma}_{44}^{1}+\frac{\tilde{\varsigma}_{22}^{2}}{R_\beta}\right)\beta_n, \quad \mathcal{K}_{45} = -(\varsigma_{12}^{3}+\varsigma_{66}^{3})\alpha_m\beta_n, \quad \mathcal{K}_{55} = -\tilde{\varsigma}_{44}^{1} - \bar{\varsigma}_{66}^{3}\alpha_m^2 - \tilde{\varsigma}_{22}^{3}\beta_n^2. \tag{2}$$

The mass matrix is diagonally by $\bar{I}_1$, $\bar{I}_2$, and $\bar{I}_3$ which are the inertia terms and could defined as:

$$\bar{I}_j = \left[I_j + \frac{I_{j+1}}{R_\beta}\right], \text{ for } j = 1,2,3, \quad \text{and } [I_1, I_2, I_3, I_4] = \sum_{k=1}^{N}\int_{h_{k-1}}^{h_k} I^k\,(1, \zeta, \zeta^2, \zeta^3, \zeta^4)d\zeta,$$

where Ik is the mass density of the kth layer of the shell per unit mid-surface area, and $\varsigma_{ij}^{p} \rightarrow p = 1,2,3,4$; is the stiffness properties and the superscript indicate to understand the differences between the extensional, extensional-bending and bending stiffness coefficients, which are defined as follows:

$$\underbrace{(\varsigma_{ij}^{1}, \varsigma_{ij}^{2}, \varsigma_{ij}^{3}, \varsigma_{ij}^{4})}_{(i,j=1,2,6)} = \sum_{k=1}^{N}\int_{h_{k-1}}^{h_k} \hat{\varsigma}_{ij}^{k}\,(1, \zeta, \zeta^2, \zeta^3)\,d\zeta, \quad \underbrace{(\varsigma_{ij}^{1}, \varsigma_{ij}^{2}, \varsigma_{ij}^{3}, \varsigma_{ij}^{4})}_{(i,j=4,5)} =$$

$$K_i^2 \sum_{k=1}^{N}\int_{h_{k-1}}^{h_k} \hat{\varsigma}_{ij}^{k}\,(1, \zeta, \zeta^2, \zeta^3)\,d\zeta, \text{ and all other } \varsigma \equiv 0 \tag{3}$$

where $[\bar{*}]_{ij}^{n} = [*]_{ij}^{n} - C_o[*]_{ij}^{n+1}$ and $[\tilde{*}]_{ij}^{n} = [*]_{ij}^{n} + C_o[*]_{ij}^{n+1}$and $\hat{\varsigma}_{ij}^{k}$ is the transformed properties of orthotropic materials. This method gives a solution for the same choice of deep shell stiffness coefficient, also K_i and K_j are shear correction coefficients, typically taken at 5/6 (Timoshenko 1921)[13, 14]. In addition, h_k is the distance from the mid-surface to the surface of the k^{th} layer having the farthest ζ-coordinate.

Parametric Analysis

Based on the thick laminated composite cylindrical shell theory, the transvers stress is simulated a cross the thickness of the pipe segment examining various orthotropy ratio. Fig. 2, displays that the transvers stress of laminated composite with weak orthotropy ratio could expand the pipe life. That's obvious, because the pipe properties in the hope direction almost equal to those in longitudinal direction [15-24]. Results reveal that constructing the pipe segment by composing more layers at cross ply scheme could give similar behavior to those of weak orthotropy ratio.

Conclusions

Although, the proposed flexible pipe is lighter in weight than prior art pipes it expect maintaining correct performances,particularly mechanical performances. It has been shown that the proposed formulation, which partially attains some classical expressions by a different line of reasoning, is may serve as a reference in designing the composite ball joint pipe and improve the standards and specifications on the flexible pipes. Apart from possessing a clear physical meaning, on account of its simplicity the presented treatment seems also very suitable for developing and prototyping purposes.

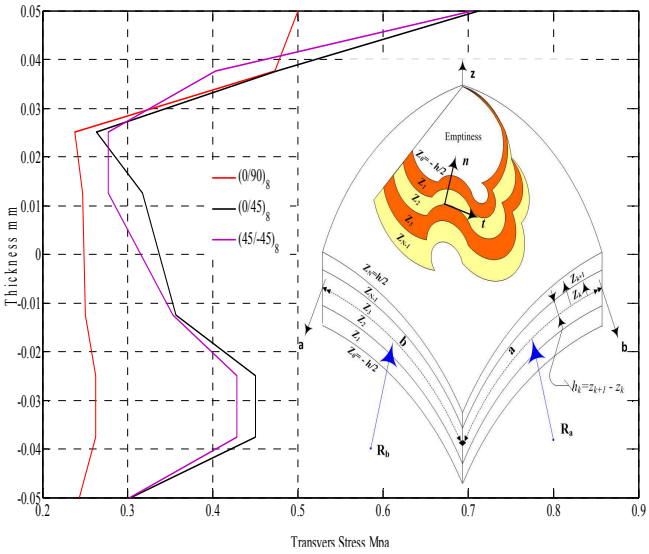


Fig. 2. The inter-laminar stresses that induced into the pipe at diffrent laminations scheme.

Acknowledgments

The authors would like to acknowledge Universiti Teknologi PETRONAS, Malaysia for sponsoring this research work.

References

[1] Mustaffa, Z., M.B. Taufiq, and B.M. Thar, *Wounding Composite Pipeline with Internally Pressurized Conditions.* Applied Mechanics and Materials, 2013. **353**: p. 3280-3283.
[2] Mustaffa, Z., M.B. Taufiq, and B.M. Thar, *Bending and Moment Stability in Reel Mechanisms.* Applied Mechanics and Materials, 2013. **353**: p. 3316-3319.
[3] Thar, B.M., M. Zahiraniza, and M. Badri Taufiq, *Pipeline Reeling.* Applied Mechanics and Materials, 2013. **376**: p. 185-189.
[4] Albarody, T.M.B., Z. Bt Mustaffa, and M.B. Taufiq, *Design and Modeling of Flexible Ball Joint Pipe*, in *Offshore Technology Conference*. 2013, SPE, My OnePetro, Doi:10.4043/24296-MS: Rio de Janeiro, Brazil.
[5] Bt Mustaffa, Z., M. Taufiq, and T. Albarody, *On the Specifications of Flexible Composite Ball Socket Joint Pipe Characterized by Barrel Shell Model*, in *Offshore Technology Conference*. 2013, SPE, My OnePetro, Doi:10.4043/24306-MS: Rio de Janeiro, Brazil.
[6] Qatu M.S., *Vibration of Laminated Shells and Plates*. 2004, London: Elsevier.
[7] Thar, B.M., M. Zahiraniza, and M.B. Taufiq, *Stress Analysis of Reeled Composite Pipelines Based on Shallow Shell Theories.* Applied Mechanics and Materials, 2013. **376**: p. 181-184.
[8] Reddy J.N., *Mechanics of Laminated Composite Plates and Shells*. 2004, New York: CRC Press.

[9] Albarody, T.M.B., H.H. Al-Kayiem, and M.B. Taufiq, *The Theory of Functional and Adaptive Shell Structures*, ed. Mschmoeltz. 2013, Saarbrücken, Germany.: LAP LAMBERT Academic Publishing GmbH & Co., ISBN: 978-3-8465-2175-5. 212 Pages.

[10] Albarody, T.M.B. and H.H. Al-Kayiem, *Laminated Smart Shell Structures; Theory and Analysis*, in *Shell Structures: Theory and Application*. 2013, CRC Press, Taylor & Francis, ISBN: 978-1-138-00082-7: London. p. 49.

[11] Al-Kayiem, H.H. and T.M. Badri, *Transient Analysis of Structronics Shell*, in *Trends in Intelligent Robotics, Automation, and Manufacturing*. 2012, Springer. p. 313-321.

[12] Badri, T.M. and H.H. Al-Kayiem, *Free vibration analysis of structronics shell*, in *Trends in Intelligent Robotics, Automation, and Manufacturing*. 2012, Springer. p. 322-330.

[13] Badri, T.M. and H.H. Al-Kayiem, *Dynamic Response of Magneto-Thermo-Electro-elastic shell structure closed-circuit surface condition.* Journal of Applied Sciences, 2012. **12**(24): p. 2541-2547.

[14] Badri, T.M. and H.H. Al-Kayiem, *Analytical Solution for Simply Supported and Multilayered Magneto-Thermo-Electro-Elastic Plates.* Asian Journal of Scientific Research, 2013. **6**(2): p. 236-244.

[15] Badri, T.M. and H.H. Al-Kayiem. *Analysis of electro/mgneto-mechanical coupling factor: In laminated composite plate construct fromrotated Y-cut crystals*. in *National Postgraduate Conference (NPC), 2011*. 2011: IEEE.

[16] Badri, T.M. and H.H. Al-Kayiem. *Reducing the magneto-electro-elastic*. in *Humanities, Science and Engineering (CHUSER), 2011 IEEE Colloquium on*. 2011. Penang: IEEE.

[17] Al-Kayiem, H.H. and T.M. Badri. *Transient Analysis of Structronics Shell*. in *The First International Conference on Intelligent Robotics, Automation and Manufacturing (IRAM 2012)*. 2012. Monash University, Malaysia: Springer series on Computer and Information Science (CCIS) © Springer-Verlag Berlin Heidelberg.

[18] Badri, T.M. and H.H. Al-Kayiem. *Numerical Analysis of Thermal and Elastic Stresses in Thick Pressure Vessels for Cryogenic Hydrogen Storage Apparatus*. in *2ed International Conference on Production, Energy and Reliability (ICPER 2012)*. 2010. A Conference of ESTCON, World Engineering, Science & Technology Congress.

[19] Badri, T.M. and H.H. Al-Kayiem. *Frequancy analysis of piezo-laminated shell structures*. in *3ed International Conference on Process Engineering and Advanced Materials, (ICPEAM 2012)* 2012. Malaysia: IEEE.

[20] Badri, T.M. and H.H. Al-Kayiem. *A static analysis of piezo-laminated shell structures*. in *3ed International Conference on Production, Energy and Reliability (ICPER 2012)*. 2012. Malaysia: IEEE.

[21] Badri, T.M. and H.H. Al-Kayiem. *Free vibration analysis of piezo-laminated shell structures*. in *3ed International Conference on Production, Energy and Reliability (ICPER 2012)*. 2012. Malaysia: IEEE.

[22] Badri, T.M. and H.H. Al-Kayiem. *Free Vibration Analysis of Structronics Shell*. in *The First International Conference on Intelligent Robotics, Automation and Manufacturing (IRAM 2012)*. 2012. Monash University, Malaysia: Springer series on Computer and Information Science (CCIS) © Springer-Verlag Berlin Heidelberg.

[23] Abdullah, A.P.M.Q. and T.M. Badri, *numerical investigation of static and dynamic stresses in spur gear made of composite material.* Journal of Engineering, 2011. **17**(4).

[24] Badri, T. and H. Al-Kayiem, *Numerical analysis of thermal and elastic stresses in thick pressure vessels for cryogenic hydrogen storage apparatus. J.* Applied Sci, 2011. **11**: p. 1756-1762.

Applied Mechanics and Materials Vol. 567 (2014) pp 539-544
© (2014) Trans Tech Publications, Switzerland
doi:10.4028/www.scientific.net/AMM.567.539

The Utilization of Rice Husks powder as an Antioxidant in Asphalt Binder

Mohammed Hadi Nahi[1, a], Ibrahim Kamaruddin[1,b] and Madzlan Napiah[1,c]

[1]Civil Engineering Department, Universiti Teknologi PETRONAS, Bandar Seri Iskandar, 31750 Tronoh, Perak, Malaysia

[a]eng_19mhq83@yahoo.com, [b]ibrakam@petronas.com.my, [c]madzlan_napiah@petronas.com.my

Keywords: Oxidation; antioxidant materials; asphalt bitumen; lignin; rice husks.

Abstract. Aging is one of the main contributors for asphalt failure. Oxidation aging is the main cause of long-term deterioration in asphalt pavements as a pavement ages, oxidation stiffens a pavement, making it more susceptible to failure from load and thermal stresses. Slowing a pavement's oxidative aging would maintain its elastic properties and delay aging problems. There is no performance enhancer in widespread use, acting as an antioxidant that slows the oxidative aging of asphalt binder. The main objective of this research is to investigate the feasibility of using biomass powder derived from rice husks as an antioxidant additive to control the asphalt age hardening. The waste of rice husks was dried at 40°C for 9–11 days. The dried materials was grounded, and sieved to get fine powder. To evaluate the performance of the antioxidant, samples have to be aged according to SUPERPAVE standards (RTFOT and PAV) and physical, chemical, and rheological properties have to be analyzed. The preliminary results of penetration test softening point test shows that adding 4% of rice husks' powder to 80/100 binder didn't change the grade of the binder.

Introduction

All Permanent deformation in asphalt pavement is one of the most commonly observed pavement distresses and is a major safety concern to transportation agencies. Millions of dollars annually spends on asphalt pavement maintenance. Researches into improvements of hot-mix asphalt materials mix designs, methods of pavement evaluation and design can provide extended pavement life and significant cost savings in pavement maintenance and rehabilitation.

The use of performance enhancers in asphalt binder is not a new concept. Many materials exist and are in wide use which improves the properties of asphalt binder. Thermoplastic copolymers improve asphalt binder by increasing high and low temperature rheological properties [1]. Chemicals such as hydrated lime and polyphosphoric acid also improve various properties of asphalt binder [2]. However, there are no performance enhancers in widespread use which slow the oxidative aging of asphalt binder by acting as an antioxidant. Slowing oxidative aging of asphalt binder would have great potential benefit for hot-mix asphalt pavements. As a pavement ages, it stiffens and becomes more susceptible to failure from load and thermal stresses [3].

Slowing oxidative aging would increase the service life of a pavement. The public could benefit by saving money and having less construction inconveniences. However, an antioxidant for use in asphalt pavements would need to be available in large amounts and be cost effective.

Antioxidants have been studied in asphalt pavements, but none have proven to be practical for incorporation into the asphalt industry. Lignin, a known antioxidant, is the second most available biological polymer on earth [4].

The Purpose of this Study is use the waste of Palm oil, coconut and rice husks to produce antioxidant (AOX) materials. The wastes of Palm oil, coconut and rice husks have been chosen due to the high content of lignin 33%, 31% and 28% respectively.

Background

Asphalt Oxidation. Asphalt oxidation is the main cause of long-term deterioration in asphalt pavements [5]. The complex reaction of the various chemicals present in asphalt with atmospheric oxygen cause aging throughout the life of the pavement. Oxidative aging causes the asphalt to harden and become brittle, which can eventually lead to pavement failure [6].

The rate of oxidative aging is primarily controlled by temperature. The oxidation rate of asphalt approximately doubles for every 10°C rise in temperature [7]. The asphalt binder in the mixture continues to age while the mix is being stored, transported, and eventually paved during construction (Roberts et al. 1996). Long-term oxidative aging begins immediately after a pavement has been constructed [3]. Long-term oxidation occurs at a much slower rate than the initial oxidation of asphalt during mixing and construction. However, many experts believe longterm oxidative aging to be the cause for many pavement failures in the field [5]. Long-term aging causes a further large increase in stiffness and loss of ductility. Eventually, thermal and/or load stresses cause the pavement structure to crack. Oxidative aging of asphalt is controlled by the chemical properties of the asphalt (Liu et al. 1998). Asphalt binders vary widely in chemical composition [3]. Their composition is determined by place of origin and the refining techniques used to produce the asphalt.

Asphalt binder is mainly composed of carbon and hydrogen, with nitrogen and sulfur filling in the lower percentages [8]. Trace amounts of heavy metals, such as vanadium and nickel, are also present. These elements combine to form the main fractions of asphalt cement: asphaltenes, saturates, naphthalene aromatics and polar aromatics (light and heavy resins, respectively). This separation method is known as Corbett's method and is the most widely used method to fractionate asphalt [6]. These four fractions chemically and physically interact with each other, forming a complex colloidal system. Asphaltenes and saturates are normally incompatible compounds, but they are brought together by the presence of aromatics. Each fraction provides different properties of asphalt. Asphaltenes are the main contributors of viscosity (hardening effects) while an abundance of aromatics and saturate decrease the ductility (elastic effects) [6]. There are many polymers available for use in asphalt pavements. Many polymers have the similar effects of decreasing asphalt's temperature susceptibility. However, none of them truly act as an antioxidant by preventing aging from oxygen radicals [1].

Chemical antioxidants have been studied in asphalt pavements. Chemicals such as lead diamyldithiocarbamate (LDADC), zinc kailkyldiathiophashate (ZDDP), zinc diabutyl dithiocarbamate (ZDBC), and napthenoid oil have been tested and proven to act as antioxidants in asphalt [9]. The chemicals reduce the ability of free radicals to rapidly oxidize asphalt. However, these chemicals have not been incorporated into the asphalt paving industry. LDADC contains lead and is therefore an environmental concern. ZDDP is used as an antioxidant to prevent wear in extreme pressure additives in gear oil formulations, while ZDBC is commonly used as an accelerator in rubber formulation [9]. ZDDP and ZDBC are not cost effective and therefore are not likely to be used at the wide scale needed for asphalt pavement construction. Wood lignin has also been researched as an antioxidant in asphalt. Wood lignin proved to be a very promising performance enhancer. At four and seven percent by weight, wood lignin provided benefit to the asphalt. The temperature performance grade significantly increased. An increased high temperature performance grade has a direct relationship to less rutting potential [3]. The low temperature performance grade of the binders was either not affected, or showed a limited variation from the control value. Therefore, the lignin had an overall effect of widening the temperature range of the binders.

Lignin As An Antioxidant. Lignin can be described as amorphous three-dimensional network polymers comprised of phenylpropane unites that link together in different ways [4]. The phenylpropane unit is a benzene ring with a tail of three carbons. The figure below illustrates one of the possible structures of lignin.

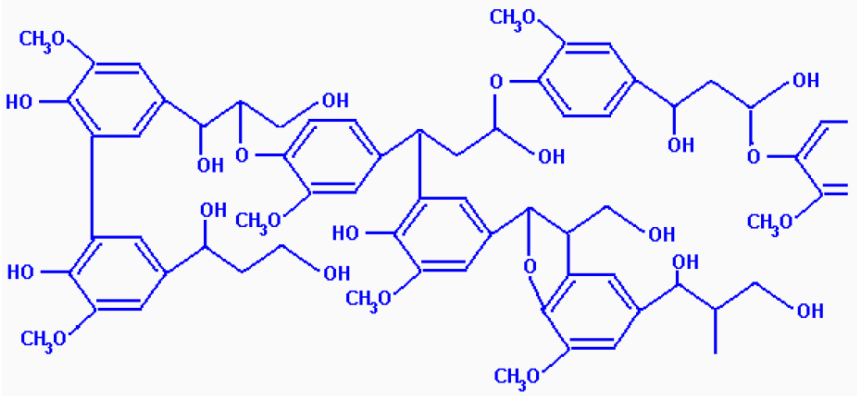


Figure 1. Chemical structure of lignin adopted by Mc Cready and Knee 2007 [10]

Lignin contains several functional chemical groups, such as phenolic, methoxyl, carbonyl and carboxyl. Most antioxidant effects of lignin are provided by the phenolic group capturing and reacting with the free radicals which contain oxygen. Free radicals are known to attack stable molecule structures of a substance by stealing an electron. Once the attacked molecule loses its electron, the substance's chemical structure then is changed. When the chemical reaction occurs, new materials are formed and the asphalt starts aging with asphaltenes generated. Instead of letting the free radicals, which contain the oxygen, oxidant the aromatics and convert aromatic molecules to asphaltenes, the lignin first reacts with those free radicals as a reducing agent. This radical scavenging property of lignin makes it recognized as an efficient antioxidant additive.

In the plant kingdom, lignin is present in large amounts in the cell wall of plants, especially in woody tissues. It is known that lignin can have different chemical composition and properties from trees, plants and agricultural crops. Even by operating different extraction methods, the physical and chemical properties are diverse [4].

The lignin used for this study was derived from three feed stocks including: corn stover, oak wood, and switch grass. Since the scavenging ability of lignin depends on the structural features of the lignin, the same amount of lignin with different structures may react with different amounts of free radicals [4]. That is to say, the bio-oil with higher amounts of lignin does not have to display better antioxidant effects.

Bio-Products as Antioxidant. Many previous studies have used bio-products derived from agricultural wastes as an antioxidant in asphalt binder. R. Christopher Williams in 2008 have used Four co-products were mixed with four asphalt binders in percentage of 3%, 6%, 9% and 12% by weight, to assess their oxidative effects. Three co-products contained lignin processed from corn. The fourth co-product had its lignin removed. The testing of the co-product without lignin supported the idea that there was beneficial antioxidant activity because samples without lignin aged significantly more than the samples with lignin. The optimum amount of co-products added was 6%.

Sheng tang in 2010 have blended bio-oil derived from corn Stover, oak wood, and switch grass. bio-oil added: 3%, 6% and 9% by weight. The bio-oil modified binders are stiffer than the initial binders when subjected to the aging process, and this shows benefits for rutting resistance. The stiffer bio-oil modified asphalt usually sacrifices some ability to prevent thermal cracking. Alejandra C. and Guillermo T. in 2012 produced Byproducts from red wine industry which is grape pomace. The dried grape pomace was grounded to obtain fine powder to apply as an antioxidant Modifier. powder added: 5%, 10% and 20% by weight. 10% addition of grape pomace is a suitable alternative to reduce the age hardening; it is economically feasible and environmental friendly. Even though 20% of pomace antioxidant addition showed the best behavior related to reduction of age hardening, it was observed a relaxation effect after short-term aging at low temperature [11].

Methodology

Antioxidant Preparation. The very first step for this research is to prepare the antioxidant material first. As stated earlier, the antioxidants (AOX) are biomass, rise husk, coconut shell, and palm shell. The proposed steps towards antioxidant material preparation are as below:

1) The biomass dried in the drying oven to get rid of any moisture content in it.

2) The biomass has grinded by using grinding machine until it gets to powder form.

3) The powdered biomass sieved using 75 micron sieve machine. Only the fine particles that passed the 75 micron sieve has been collected for the next step.

4) Step 1 to step 3 will be repeated again, this time for rise husk, coconut shell, and palm shell preparation.

5) The total four (4) powder samples labeled on separate tray/confinement. The materials which now possess the same size of normal bitumen filler can be used for further mixing and blending with virgin bitumen.

Preparation of the modified Asphalt Binders. A high speed shear mixer will be used to prepare the bio-oil modified asphalt binder. The bio-oil and asphalt binder mixing will be conducted at 155°Cat 5000 rotations per minute shearing speed for one hour. A high speed shear mill will be used to blend asphalt binder and biomass powder at 90°C for 15 minutes and then mixed for 5–10 minutes to obtain a homogeneous mixture. Three percentages of AOX were chosen: 5%, 10% and 12% by volume.

To calculate the percentages of the rice husks powder by volume, density test has been conducted for the small sample of the powder by using Helium pycnometer. The test was conducted at temperature 33.9 deg C.



Figures 2. Helium Pycnometer

Laboratory tests of the modified Asphalt Binders. Two tests have been conducted in this semester, penetration test and softening point test.

Penetration test

Softening point test

Results & Discussion. The results of the density test which conducted by using Helium Pycnometer shows that the density of rice husks is 1.67g/cc while the density of the 80/100 virgin bitumen is 1.02 g/cc. The calculated rice husks powder to be added to the binder as 4% by volume is 65.7 g. The result of the penetration test of the virgin bitumen 80/100 shows that the penetration value is between 80 to 85 which is at the lower limit as shown in Table 1.

Table 1. Penetration Value of the Virgin Bitumen 80/100

Sample	Penetration 1	Penetration 2	Penetration 3
1	83	84	85
2	82	85	81
3	80	84	81

The results of the softening point test of the virgin bitumen 80/100 shows that the softening value is between 43 and 43.5 which are at the lower limit as shown in Table 2.

Table 2. Softening Point Value of the Virgin Bitumen 80/100

Set No.	R	L
Virgin bitumen		
1	43	43.5
2	43.5	43
3	43	43
4	43.5	43

The result of the penetration test of the rice husks modified bitumen shows that adding 4% of rice husks powder have changed the penetration value but didn't change grade of the bitumen. As the penetration value is between 80 and 82 the modified bitumen still at the grade of 80/100and it is at the lower limit as shown in Table 3.

Table 3. Penetration Value of the Rice Husks Modified Bitumen

Sample	Penetration 1	Penetration 2	Penetration 3
1	80	82	80
2	82	81	80
3	80	81	82

The result of the softening point test of the rice husks modified bitumen shows that adding 4% of rice husks powder have changed the softening point value but didn't change grade of the bitumen. As the softening point value is between 47.2 and 48.2 the modified bitumen still at the grade of 80/100 as shown in Table 4.

Table 4. Softening Point Value of the Rice Husks Modified Bitumen

Set No.	R	L
Modified bitumen		
1	47.4	47.2
2	48.0	48.2
3	47.3	47.5
4	47.8	48.0

Conclusion & Future Directions

From the preliminary results it can be concluded that rice husks powder can use as cheap and environmentally friendly additive to the virgin bitumen without changing the grade of the bitumen. The next step of this research is to produce Palm shell powder and coconut shell powder and

conduct the density test for both of them using Helium Pycnometer. Penetration and softening point results are not sufficient to claim that rice husk is playing its role, if any, to reduce the oxidation. To study the effect of the of the produced antioxidant material the researcher going to age the virgin and the modified bitumen by conducting the short term aging using Rolling Thin-Film Oven (RTFO) test and the long term aging by using Pressure Aging Vessel (PAV). Penetration test, softening point test, DSR test and chemicals tests must be conducted for the bitumen before and after aging to study the effects of the proposed antioxidant materials.

References

[1] Lucena, Maria da Conceição Cavalcante, Sandra de Aguiar Soares, and Jorge Barbosa Soares. "Characterization and thermal behavior of polymer-modified asphalt." Materials Research 7.4 (2004): 529-534.

[2] Huang, Shin-Che, et al. "Rheological and Chemical Properties of Hydrated Lime and Polyphosphoric Acid–Modified Asphalts with Long-Term Aging." Journal of Materials in Civil Engineering 23.5 (2010): 628-637.

[3] Roberts, Freddy L., et al. "Hot mix asphalt materials, mixture design and construction." (1996).

[4] Dizhbite, Tatiana, et al. "Characterization of the radical scavenging activity of lignins—natural antioxidants." Bioresource Technology 95.3 (2004): 309-317.

[5] Domke, Christopher H., Richard R. Davison, and Charles J. Glover. "Effect of oxygen pressure on asphalt oxidation kinetics." Industrial & engineering chemistry research 39.3 (2000): 592-598.

[6] Ruan, Yonghong, Richard R. Davison, and Charles J. Glover. "Oxidation and viscosity hardening of polymer-modified asphalts." Energy & fuels 17.4 (2003): 991-998.

[7] Gawel, I., and K. Baginska. "Effect of chemical nature on the susceptibility of asphalt to aging." Petroleum science and technology 22.9-10 (2004): 1261-1271.

[8] Petersen, J. Claine. "Chemical composition of asphalt as related to asphalt durability: state of the art." Transportation research record 999 (1984).

[9] Ouyang, Chunfa, et al. "Improving the aging resistance of styrene–butadiene–styrene tri-block copolymer modified asphalt by addition of antioxidants." Polymer degradation and stability 91.4 (2006): 795-804.

[10] McCready, Nicolaus Straub. The Utilization of Agriculturally Derived Lignin as an Antioxidant in Asphalt Binder. ProQuest, 2007.

[11] Calabi-Floody, Alejandra, and Guillermo Thenoux. "Controlling asphalt aging by inclusion of byproducts from red wine industry." Construction and Building Materials 28.1 (2012): 616-623.

Applied Mechanics and Materials Vol. 567 (2014) pp 545-550
© (2014) Trans Tech Publications, Switzerland
doi:10.4028/www.scientific.net/AMM.567.545

Unconfined compressive strength performance of cement stabilized peat with rice husk ash as a pozzolan

Leong Sing Wong[1, a, *]

[1]Civil Engineering Department, College of Engineering, Jalan IKRAM-UNITEN, 43000 Kajang, Selangor, Malaysia

[a]wongls@uniten.edu.my

Keywords: Peat; binding action; rice husk ash; pozzolanic material; cement

Abstract. Peat is known to be highly compressible in nature due to its extremely high content of organic matter. As such, it is never a suitable foundation soil for construction purpose. Under such condition, it is compelling to investigate the underlying binding action of suitable materials that can be sustainably applied to stabilize the soil. The primary focus of this research article is to evaluate the effectiveness of rice husk ash as partial cement replacement in peat stabilization. Rice husk ash is basically a pozzolanic material which is produced by burning rice husk from the milling of paddy. Other than rice husk ash, Portland composite cement, calcium chloride, and silica sand were used as the materials for stabilizing the peat. An experimental based program was developed to gage the pertinent aspects that influenced the strength behavior of the stabilized peat. The strength behavior of the stabilized peat was evaluated on the basis of the results from unconfined compression tests. It was found from the test results that by partially replacing 10% of the cement with rice husk ash at an initial pressure of 50 kPa, binder dosage of 300 kg m^{-3}, silica sand dosage of 596 kg m^{-3} and a curing time of 28 days, the required unconfined compressive strength of 345 kPa could be exceeded. The positive result confirmed the role of rice husk ash at imparting filler and pozzolanic effects that enhanced the strength of the stabilized peat.

Introduction

In normal practice, rice husk is burnt in order to produce fuel for the milling of rice paddy. The byproduct of such burning process is known as rice husk ash. Generation of fuel from the rice paddy milling process has yielded a large amount of rice husk ash, which is normally dumped into landfills, thus contaminating soil and groundwater. Due to the environmental concern, it is beneficial to fully utilize rice husk ash for the making of cement-based materials. Nair et al. [1] have reported that an optimal amount of amorphous silica can be produced when the rice husk is incinerated at a temperature ranging from 500 to 700°C. Rice husk ash with high amorphous silica content can be applied as a pozzolanic additive of cement-based material such as concrete as evident in several studies [2-7]. High amounts (up to 30%) of rice husk ash could be blended with cement without adversely affecting the strength and permeability of concrete [3].

Despite the established trend of using rice husk ash as partial cement replacement in concrete, there was little focus in research on its usage as a pozzolanic additive in stabilized peat for geotechnical application. The reason for the lacking of such research in the area of geotechnical engineering is probably due to the extremely poor condition of peat which is known to contain high organic matter. Advancement of cement chemistry in recent years has seen the possibility of using a variety of additives to stabilize peat [8]. Wong et al. [9] found that a binder mixture of cement, superplasticizer, calcium chloride, silica sand and kaolin can impart a positive effect on peat stabilization. It is worth noting that unlike rice husk ash, kaolin is not considered as a waste material as the clay evolves due to weathering and decomposition of rock.

Therefore, it is a novel approach to research on the pozzolanic effect of rice husk ash in stabilized peat as there is a fundamental gap between the long term binding reactivity of rice husk ash with cement and the strength performance of the stabilized peat enhanced with rice husk ash.

This article aims to present experimental research findings on the strength behavior of stabilized peat with a special emphasis on the implication of rice husk ash as partial cement substitute. The ability of the stabilized peat to sustain compressive stress was gaged with respect to several factors that influenced its strength behavior.

Materials and methods

Peat under investigation. Samples of peat were obtained from a tropical peat swamp forest near Sri Nadi village in the area of Johan Setia of Klang district within the Selangor state of Malaysia (Fig. 1). Wong et al. [8] reported that the depth of the peat at site varies from point to point ranging from 1 to 3 m. The average phreatic level of the soil was found to be 0.5 m, which is close to the ground surface. Results on the basic characterization of the soil are shown in Table 1. The high natural water content of the soil implies that it has the ability to retain high amount of water at full saturation. Also, the soil was observed to be highly organic and fibrous as reflected by its high organic and fiber contents in Table 1. The soil specific gravity was discovered to be about 49% lower than that of soft clay from the study of Pakbaz & Alipour [10]. Due to its high acidity in natural condition, special attention must be paid on the selection of materials to stabilize the soil.



Fig. 1: Tropical peat swamp forest under study

Table 1: Basic characteristics of the peat

Soil property	Average value
Natural water content [%]	655
Fiber content [%]	91
Organic content [%]	93
Ash content [%]	7
Specific gravity	1.37
pH	3.46

Materials for the binder mixture. Portland composite cement (PCC), calcium chloride, silica sand and rice husk ash were identified as the materials to form the binder mixture for the peat stabilization. The PCC was formulated by mixing Portland cement with 2% polycarboxylate based superplasticizer per unit weight of cement for the purpose of workability enhancement. Basically, 4% calcium chloride by weight of the cement was included in the binder mixture to fasten the cement hydration process. Silica sand acted as the solid particles so that the cementation products

could bind the peat effectively. It is necessary to note that the rice husk was obtained from a rice mill in Kuala Selangor. A ferrocement furnace was used to incinerate the rice husk into rice husk ash. Evaluation on the optimal effect of rice husk ash in the peat stabilization was done by varying the quantity of rice husk ash from 5 to 35% as partial cement replacement.

Methods of testing in laboratory. Unconfined compression tests in accordance to US ASTM standard (ASTM D2166-06) were performed on specimens of stabilized and undisturbed peats. For the tests, test specimen was produced at a standard size of 50 mm diameter × 100 mm height. A specimen cutter was utilized to cut the peat specimen from a block sampler of undisturbed peat. The block sampler was previously used to sample undisturbed peat in a trial pit which was excavated to a depth of 0.5 m below the phreatic level of the soil. Mixing of the peat with the binder mixture for the preparation of the stabilized peat admixture was done in accordance to the procedure suggested by Hebib and Farrell [11]. In preparing a specimen of stabilized peat, the stabilized soil admixture was filled and tamped in 4 layers of equal thickness in a plastic tube of 50 mm internal diameter × 250 mm height. The plastic tube is made of polyvinyl chloride (PVC) and is split table into halves. In this way, each test specimen was able to be removed from the plastic tube after curing without the need for extrusion. The plastic tube was then allowed to stand vertically in a rack, submerged under water in a water tank and placed with a steel load that could impose an initial pressure of 50 kPa. Each stabilized peat specimen was later cured in water for the required duration of time before it was trimmed to the standard size for testing purpose. Note that each rack has the capacity of supporting 6 plastic tubes.

Results and Discussion

Influence of partial replacement of PCC with rice husk ash. Fig. 2 shows the implication of adding rice husk ash as partial replacement of PCC on unconfined compressive strength of stabilized peat after 28 days of curing time in water. It is observable from the figure that test specimen with 10% partial replacement of cement with rice husk ash has the highest unconfined compressive strength of 513 kPa. Such a strength value is about 30 times higher than that of untreated peat and exceeds the required unconfined compressive strength of 345 kPa as stipulated in ASTM D4609. It is mentioned in ASTM D4609 (Standard guide for evaluating effectiveness of admixture for soil stabilization) that an unconfined compressive strength of 345 kPa is required to ensure that a soil is stabilized [12]. The high strength of the test specimen at the optimal mix design is attributable to the hydration of cement and filler effects of both silica sand and rice husk ash. Silica sand strengthened the matrix of the test specimen due to solidity of its particles. Inclusion of rice husk ash further reduced the pore spaces of the test specimen, which eventually led to its robustness. The result confirmed that the test specimen is linear elastic and brittle. Brittle materials are characterized by a steep linear elastic curve, followed almost immediately by the breaking point, i.e. brittle failure [13].

Influence of dosage of the binder. It is evident from Fig. 3 that the unconfined compressive strength of the stabilized peat specimens increased nonlinearly with increasing binder dosage. The required unconfined compressive strength of 345 kPa was only exceeded after testing the specimen with 300 kg m^{-3} binder dosage. The threshold binder dosage is observed to be in between 250 to 300 kg m^{-3}. The finding implies that sufficient binder dosage was necessary to provide calcium source for the cementation of the stabilized soil to take place. Chen & Wang [14] reported that under a low binder dosage, the black humic acid in peat can retard the strength accumulation of stabilized peat.

Influence of curing time in water. Specimens prepared at the optimal mix designs were examined for its unconfined compressive strength with respect to curing time in water. Obviously, it can be seen in Fig. 4 that there was a slow increase in unconfined compressive strength of the stabilized peat after 7 days of curing time in water. This is due to the effect of calcium chloride that accelerated the cement hydration process in the stabilized soil. After hydration, pozzolanic action took place and it can be stated that the progressive increase in unconfined compressive strength is attributable to the function of rice husk ash as filler and pozzolanic additive at inducing the

formation of secondary cementation crystals (Calcium silicate and calcium aluminate crystals) in the stabilized soil. These cementing crystals refined the pores of the stabilized soil, which eventually increased its density and hardness. The slow pattern of increase in compressive strength with increasing curing time of cement-based material can also be noticed from the findings of Naji Givi et al. [15], Ferraro and Nanni [16], Sua-iam and Makul [17], and Gastaldini et al. [18].

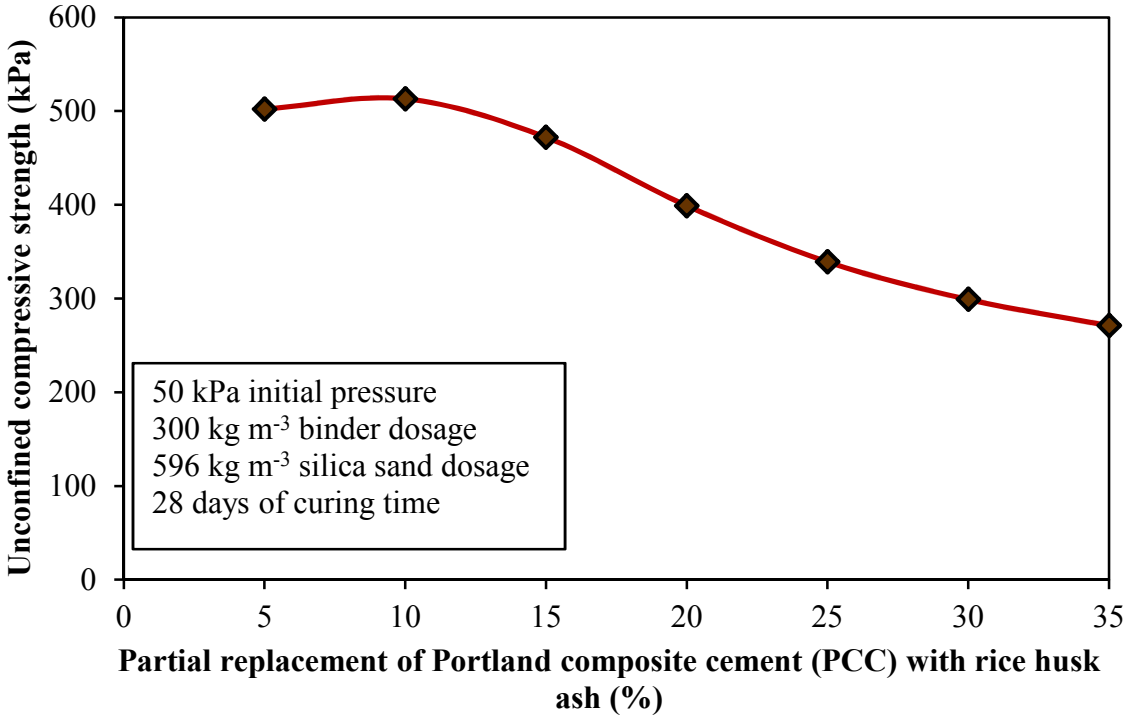


Fig. 2: Unconfined compressive strength influence of rice husk ash at partially replacing Portland composite cement (PCC) in stabilized peat

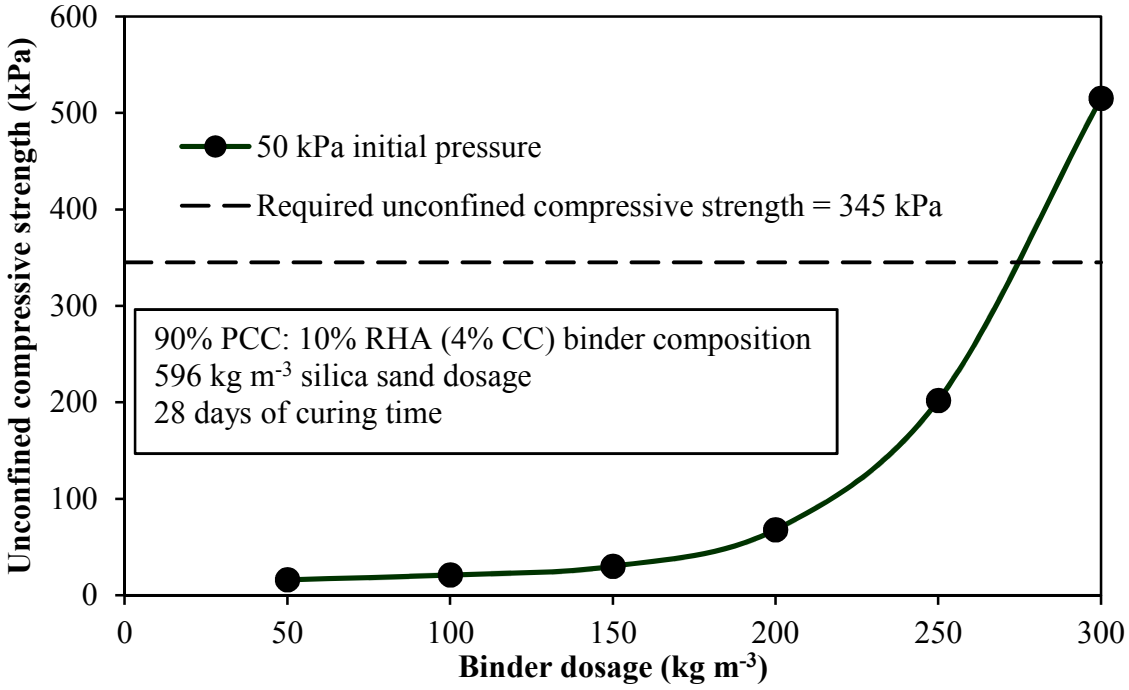


Fig. 3: Influence of binder dosage on unconfined compressive strength of stabilized peat (Notes: PCC = Portland composite cement, RHA = Rice husk ash and CC = Calcium chloride)

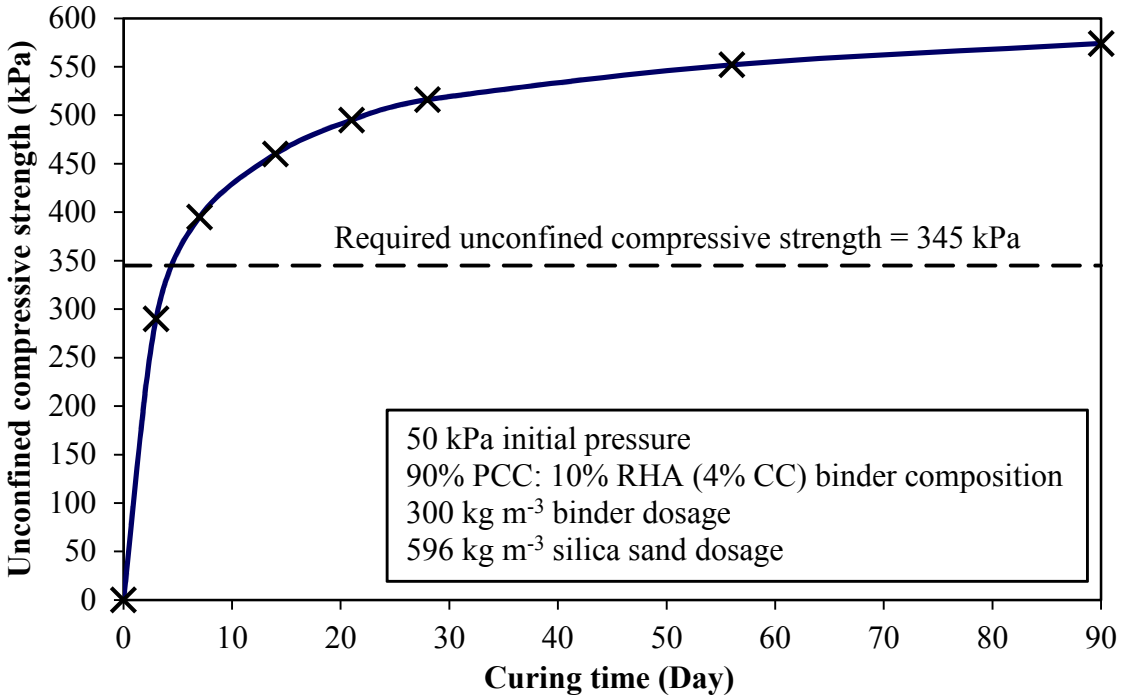


Fig. 4: Influence of curing time on unconfined compressive strength of stabilized peat (Notes: PCC = Portland composite cement, RHA = Rice husk ash and CC = Calcium chloride)

Conclusion

The unconfined compressive strength performance of stabilized peat with rice husk ash as a pozzolan has been evaluated. It can be concluded from the results of the study that the optimal mix design of the stabilized peat can be formulated with 50 kPa initial pressure, 300 kg m^{-3} binder dosage, 596 kg m^{-3} silica sand dosage and 90% PCC: 10% RHA (4% CC) binder composition. In long term, rice husk ash continued to play a significant role at promoting the filler and pozzolanic impacts on the stabilized peat.

Acknowledgement

The funding of this research was sourced from UNITEN Internal Research Grant under the J Code of J510050451.

References

[1] D.G. Nair, A. Fraaij, A. Klaassen, A. Kentgens, A structural investigation relating to the pozzolanic activity of rice husk ashes, Cement Concrete Res. 38 (2008) 861-869.

[2] H. Chao-Lung, B.L. Anh-Tuan, C. Chun-Tsun, Effect of rice husk ash on the strength and durability characteristics of concrete, Constr Build Mater. 25 (2011) 3768-3772.

[3] B. Chatveera, P. Lertwattanaruk, Durability of conventional concretes containing black rice husk ash, J Environ Manage. 92 (2011) 59-66.

[4] K. Ganesan, K. Rajagopal, K. Thangavel, Rice husk ash blended cement: Assessment of optimal level of replacement for strength and permeability properties of concrete, Constr Build Mater. 22 (2008) 1675-1683.

[5] R. Khan, A. Jabbar, I. Ahmad, W. Khan, A.N. Khan, J. Mirza, Reduction in environmental problems using rice-husk ash in concrete, Constr Build Mater. 30 (2012) 360-365.

[6] S.N. Raman, T. Ngo, P. Mendis, H.B. Mahmud, High-strength rice husk ash concrete incorporating quarry dust as a partial substitute for sand, Constr Build Mater. 25 (2011) 3123-3130.

[7] M.F.M. Zain, M.N. Islam, F. Mahmud, M. Jamil, Production of rice husk ash for use in concrete as a supplementary cementitious material, Constr Build Mater. 25 (2011) 798-805.

[8] L.S. Wong, R. Hashim, F. Ali, Utilization of sodium bentonite to maximize the filler and pozzolanic effects of stabilized peat, Eng Geol. 152 (2013) 56-66.

[9] L.S. Wong, R. Hashim, F. Ali, Improved strength and reduced permeability of stabilized peat: Focus on application of kaolin as a pozzolanic additive, Constr Build Mater. 40 (2013) 783-792.

[10] M.S. Pakbaz, R. Alipour, Influence on cement addition on the geotechnical properties of an Iranian clay, Appl Clay Sci. 67-68 (2012) 1-4.

[11] S. Hebib, E.R. Farrell, Some experiences on the stabilization of Irish peats, Can Geotech J. 40 (2003) 107-120.

[12] F. Sariosseiri, B. Muhunthan, Effect of cement treatment on geotechnical properties of some Washington State soils, Eng Geol. 104 (2009) 119-125.

[13] R. Whitlow, Basic soil mechanics, fourth ed., Pearson Education, London, 2001.

[14] H. Chen, Q. Wang, The behavior of organic matter in the process of soft soil stabilization using cement, Bull Eng Geol Environ. 65 (2006) 445-448.

[15] A. Naji Givi, S. Abdul Rashid, F.N.A. Aziz, M.A. Mohd Salleh, Assessment of the effects of rice husk ash particle size on strength, water permeability and workability of binary blended concrete, Constr Build Mater. 24 (2010) 2145-2150.

[16] R.M. Ferraro, A. Nanni, Effect of off-white rice husk ash on strength, porosity, conductivity and corrosion resistance of white concrete, Constr Build Mater. 31 (2012) 220-225.

[17] G. Sua-iam, N. Makul, Utilization of limestone powder to improve the properties of self-compacting concrete incorporating high volumes of untreated rice husk ash as fine aggregate, Constr Build Mater. 38 (2013) 455-464.

[18] A.L.G. Gastaldini, M.P. da Silva, F.B. Zamberlan, C.Z. Mostardeiro, Total shrinkage, chloride penetration, and compressive strength of concretes that contain clear-colored rice husk ash, Constr Build Mater. 54 (2014) 369-377.

CHAPTER 4:

Construction and Project Management

Applied Mechanics and Materials Vol. 567 (2014) pp 553-558
© (2014) Trans Tech Publications, Switzerland
doi:10.4028/www.scientific.net/AMM.567.553

A Field Study Of Mould Growth for Institute Higher Education Library Buildings in Malaysia

Suriani Ngah Abdul Wahab[1,a], Nurul Izma Mohammed [2,b], Mohd Faris Khamidi [3,c] and Nazhatulzalkis Jamaludin[4,d]

[1,2,4]Department of Civil Engineering, Faculty of Engineering, Universiti Teknologi PETRONAS, Bandar Seri Iskandar, 31750 Tronoh, Perak, Malaysia.
[3]School of the Built Environment, Heriot-Watt University Malaysia, Level 2, Menara PjH, 2 Jalan Tun Abdul Razak, Precinct 2, 62100 Putrajaya, Malaysia.
[a]suria275@perak.uitm.edu.my, [b]izma.mohammed@petronas.com.my, [c]m.khamidi@hw.ac.uk, [d]nazha150@perak.uitm.edu.my

Keywords: Mould growth; temperature; relative humidity; library

Abstract. This paper is part of a PhD field study that focuses on the importance of conducting a visual inspection and evaluation of the indoor climates in libraries. Libraries contain a large amount of stored books that require a stable relative humidity to guarantee its preservation. Mould can survive and grow when indoor relative humidity is high and fungus is present all the time in the air that we breathe. Recording data through visual inspection and field studies. Its recorded the indoor relative humidity, temperature and lighting to assess mould growth problems. The assessment technique for this paper is based on guidelines survey and literature review. Visual inspection found few symptoms of mould growth that related to the amount of moisture appeared when the relative humidity in the library increases. Finally, the recording data for temperature and relative humidity demonstrate the result show that the stable indoor climate in the library building.

Introduction

The library is an important place of knowledge. The purpose of libraries, archives and museums is to preserve the items collected. However, health factors as well as material preservation in the library must be taken serious consideration. Various health problems and damage to materials can be caused by several things. Usually the library requires features sound resistance and stringent control over indoor air conditions to provide comfort to the user and indirectly to keep books from being damaged. Therefore the adequate temperature is required to maintain and preserve sensitive materials and at the same time comfort the users. As such, research has shown that the materials which are kept in libraries probably be the source of allergens and may also be a nutrient for microorganisms reproduction, especially fungi[1]. The storage of books and documents preserved has created new man made environments for microbial species such as mould[2], [3]. The growth of fungi and some bacteria on stored materials contributes to biodeterioration and this can be a major concern, especially where water damage occurs. The situation becomes worsen when the library must has characteristics of sound resistance with the use of carpet and other materials.

According to Douglas (1993) the composite material used in libraries varies. For an instance libraries are made from many types of material and these becomes favourable environments for mould to grow[4]. The biological reason is related to the attack of materials by living organisms, such as bacteria, fungi or insect infestation (American Society for Testing and Material E632, 1996). In these circumstances, measurements of mould growth assessment are needed for efficiency and user satisfaction of library environments. The National Library of Australia (2004) mentioned in their report that a major crisis in the library throughout the world when deterioration happens to the materials in the library. The presence of mould in the library should be taken seriously as it is one of the significant causes of Sick Building Syndrome (SBS).

Sick Building Syndrome is a combination of weakness associated with an individual's place of work or house. Mould damage not only can cause a serious threat to library collections but it also can harm peoples' health. Small amount of mould growth at the workplaces are not a major concern but mould should not be allowed to give problems for some people[5]. Specific types and concentrations of mould in damp indoor environment can cause respiratory irritation to human health[6]. The rate of deterioration of the book in tropical countries is high because the factors cause deterioration is at optima. Mwiyeriwa (1988) proved that physical (acid, heat, humidity, and light), biological (moulds, insects, rodents) and careless handling methods are the factors causing the paper become deteriorate. Africa is one of the country that marked in this problem.[7]. There is a need for research on biological agent's deterioration of library materials for tropical countries to produce an effective way of controlling and to prevent deterioration of paper-based materials as well as possible strategies against biotic agents. Not much has been published yet on the evaluation of the indoor climate in libraries. This paper focuses on the importance of conducting visual inspection and evaluation of indoor climate by using humidity data logger that measures relative humidity, temperature and lighting in libraries.

Description of Mould Growth

Mould is part of the natural environment and microscopic subset of the fungi kingdom. It grows indoor and outdoor of buildings. Moulds reproduced by the spores, which are tiny and invisible to the naked eye and float through outdoor and indoor air. According to Occupational Safety and Health Administration (OSHA), more than 1000 species of mould found in the United States with more than 100,000 recognised species worldwide. Mould germinated with necessary conditions such moisture; temperatures condition; relative humidity and the sources of nutrients. However, according to Singh (1993)[8] the parameters of UV light; dust; pollution; pests; handling; visitors; fire and water; air movement; cultural/organisational/management are also considered as most risky factors to mould growth.

Moisture or water is the key factor of mould growth. Water can occur in different form and it originates from different sources. Moisture can be performed from seepage of plumbing[9][10], rainwater or groundwater leaking into the area, condensation[11][12], structural damage and high humidity levels. The temperature could be 10-35°C with optima of 20°C and above[13]. According to Wessel (1970) and Storey (2004) [14][15] mould also favour with temperature between 15-30°C and there are variety of mould will grow outside of these limit. While temperature below 10°C reduce spore germination and above 50°C will dehydrate and execute fungi within a few hours [13]. As stated by the Environmental Protection Agency maintaining humidity level below 60% and ideally between 30-50%, considerably can reduce the chance of mould growth. Consecutively for mould to grow and spread, there must be a food source and moisture. It has a greater chance of developing problems with Indoor Air Quality in the building when humidity is greater than 50%[16]. The reality in this situation, it is difficult to maintain a stable temperature or relative humidity level.

Methods For Evaluation Of Indoor Mould Growth

1) Visual Inspection

As stated in the American Industrial Hygiene Association (2008), the purpose of mould assessment is to (1) determine the presence, location and extent of past and current mould growth in buildings; 2) identify the source, cause and extent of water ingress, condensation or dampness indoors; 3) determine if there are plausible and significant indoor mould exposure pathways for occupants and; 4) use this information to make a mould exposure risk management decision [2]. New York City Department of Health and Mental Hygiene highlight the extent of any water damage

and mould should be visually assessed. A visual inspection is the most important initial step in identifying a possible contamination problem. Remediation of visually identified fungal contamination should proceed without further evaluation. In Malaysia, the Building Surveying Division, Royal Institution of Surveyor Malaysia (RISM) has developed guidelines for a practitioner to carry out visual inspection and introduced Building Assessment Rating System (BARIS) (RISM, 2012). According to Palaty (2010) [1] outcomes of visual inspections can lead to three possible outcomes as stated in table 1 below.

Table 1. Outcome of Visual Inspections

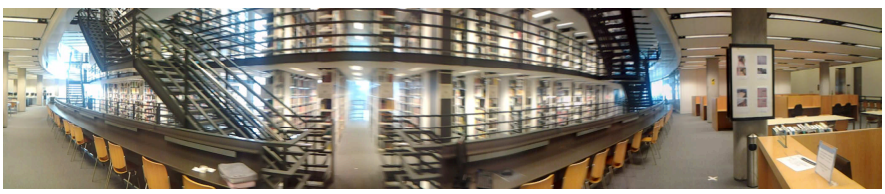
No	Possible Outcomes	Interpretation
1	No evidence of mould growth or moisture damage	No remediation action and further inspection required
2	Evidence of mould growth or moisture damage	Remediation actions need to be initiated to remove the mould and address the underlying cause of the moisture
3	Unclear mould or moisture is present	Proceed for mould sampling and further analysis

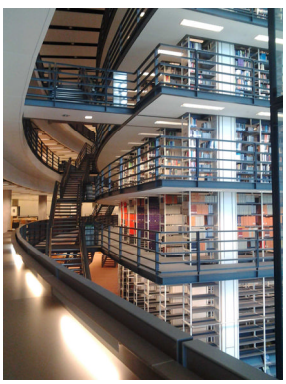
2) Field Measurement

The objectives can be fulfilled by conducting field measurement in the library of Universiti Teknologi Petronas or known as Information Resource Centre (IRC). To obtain the measurement of temperatures, relative humidity and light parameter and thereby to identify if they including the favour parameter of mould growth. There are varieties equipment to diagnose on water damage and potential condition of mould growth. There is Moisture meter (Protimeter Surveymaster SM), Hygro-Thermometer Humidity Alert (Extech), Temperature and Humidity Data logger, Infrared thermography, and Microclimate Data logger. As described in the literature review the presence of mould depends on several conditions. Temperature, relative humidity and the presence of light parameters are needed to find out the presence of fungi in the library. Thus, the researchers used a device which is Kimo Dataloger to measure the parameter found in the building.

Description of the library building

Information Resource Centre (IRC) was launched officially on 2004. Its built up area is 137,620 square feet with 4 levels. It has 213,067 volumes of books over 500,000 of bookshelves capacities as data on August 2013.The space in IRC consists of several areas such as 99 seating capacity Auditorium at level Basement, Reading area, Special collections rooms, Postgraduate Room, Closed Carrel, Discussion rooms, Platinum room, AV media room, IT Zone and others.



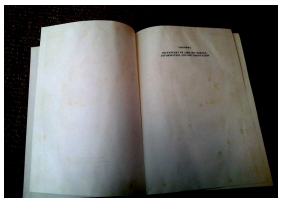
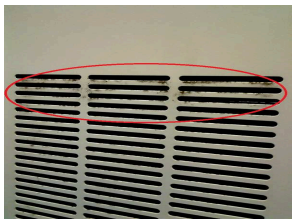


Figures 1. Information Resource Centre

Results and Discussion

In order to investigate the mould growth in the IRC, the researcher conducted visual inspection on the 22nd and 23rd November 2013 to identify visible mould. The result of the visual inspection is as Table 2 below.

Table 2. Visual inspection of IRC building

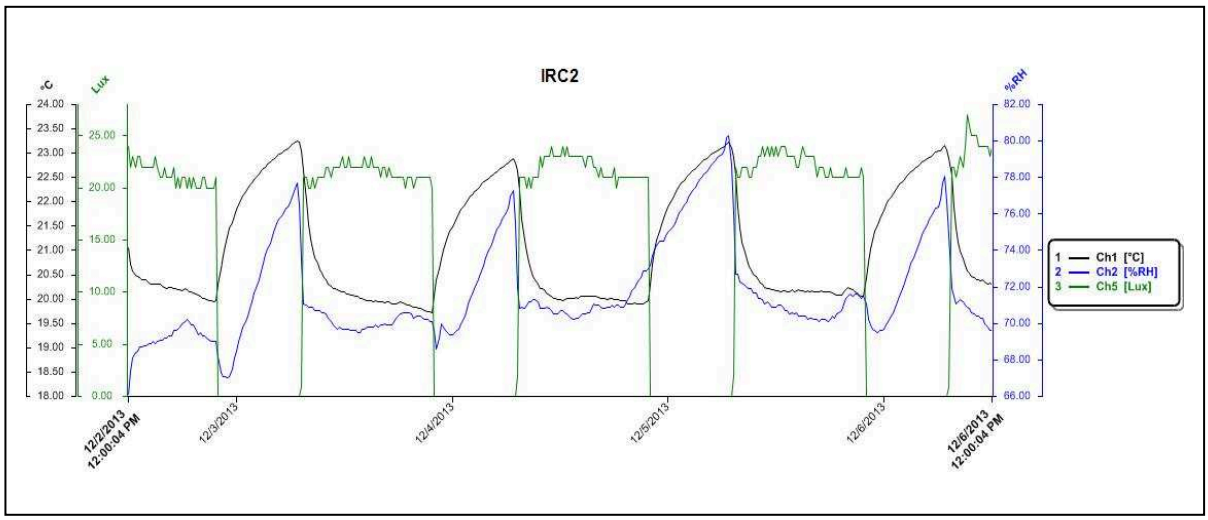
No	Location	Item/Material	Presence of Mould	Possible Causes	Photo
1	Ground Floor Open Collection	Books	Damp Stain	Moisture – relative humidity increase	
2	Level 1 IT Section Area	Carpet Carpet	Wet Stain Black Mould Green/ yellow mould	Dampness on carpet surface	
		Books	Mould	Moisture – relative humidity increase	
3	Ground Floor, Level 1, Level 2 and Level 3	Air condition outlet	Mould Stain	Moisture on surfaces	

Measurement in the library was carried out from 2nd December 2013 to 6th December 2013 for the ground floor and level 1 and from 7th December 2013 to 11th December 2013 for level 2 and 3. Temperature, relative humidity of the supply air and lighting were measured as well as temperature and relative humidity in the library at different locations such as central book shelves on every level. The measurement was conducted using humidity data logger at 15 minute intervals, 24 hours a day for four days. No measurement was carried in the library office, postgraduate room, special collection room, discussion room and other room. This is because the measurements focus on the open area which all the books are located. Figure 3 below shows the measured relative humidity, temperature and lighting reading on different locations in the IRC building.

Table 3. Measurement of relative, temperature and lighting for IRC building for 4 Days

Level	Temperature	Time	Relative Humidity	Time	Lighting	Time
GROUND FLOOR	**°C**	**24 hours**	**%**	**24 hours**	**Lux**	**24hours**
MIN T	19.72	21.45	66.1	12.00	0	12.00
MAX T	23.25	6.45	80.3	6.45	27	9.15
AVG T	21.06		71.7		13.26	
LEVEL 1						
MIN T	21.84	22.00	61.8	12.00	0	12.00
MAX T	23.42	6.45	77.8	6.30	19	00.15
AVG T	22.53		67.55		4.16	
LEVEL 2						
MIN T	22.4	18.00	58.7	19.00	0	12.00
MAX T	24.81	6.30	77.3	7.00	10	16.45
AVG T	23.49		67.59		2.59	
LEVEL 3						
MIN T	21.46	12.00	62.8	18.45	0	12.00
MAX T	24.86	24.00	77.3	7.15	79	8.30
AVG T	23.17		69.2		21.9	

The indoor air temperatures vary from 19.7°C to 24.8°C. The measured temperature in the book rack on ground floor varies from 19.7°C to 23.2°C, and is about 1 -2 °C lower than the temperature measured at the book rack on the level 1, level 2 and level 3. Measured temperature at the book rack on level 1, level 2 and level 3 are equally similar with temperature varies from 21°C to 24.8°C. The average temperature for the ground floor is recorded at 21°C and becomes the lowest average temperature compared to other level in the IRC building. The relative humidity in the library varies from 58.7% to 80.3%. The ground floor has been recorded as the place that has a high relative humidity with an average of 71.7% and the maximum RH recorded early in the morning as high as 80.3%. Figure 4 shows the details of the measured relative humidity for four days. Based on visual inspection it was found that some of books on the book rack located on the ground floor are identified with dust on the book cover. The books were also swelling and shrinking. The relative humidity increases consistently in the early morning from 6.30 am to 7.15 am. Overall relative humidity has been recorded at every level where it reached more than 60%. Mould can survive and grow when relative humidity reaches 60% and germination require higher relative humidity as well as time[16]. Measured lighting varies from 0 to 79 lux. Average lux was recorded from 2.59 to 21.9 lux with Level 3 recorded the maximum of 79 lux.



Figures 2. Relative humidity and temperature at Ground Floor

Conclusions

Results obtained in the field study revealed two things. First, even though the IRC building is a new building that was constructed with new materials and equipped with good air handling units that provide fresh air for the library, possibility of mould to grow became challenges to the books preservations. The Secondly, the measurement showed that there is an increased of relative humidity, especially early in the morning. The employees and maintenance department of library should be concern not only about visible mould but also about indoor relative humidity level. It would be careful for employees pay similar attention to the issue of indoor relative humidity level to that which they might pay to their health. Therefore, in the future to preserve valuable books in the library, the indoor climates require improvement. Furthermore, the researcher plans to continue research into other library buildings to formulate a strong correlation of mould growth and indoor climate measurement and reveal the species of mould and its character.

References

[1] W. K. Jan, *Aerobiological Engineering Handbook A Guide to Airborne Disease and Control Technologies*. McGraw-HILL New York: McGraw-Hill Companies, 2006, p. 846.

[2] M. Montanari, V. Melloni, F. Pinzari, and G. Innocenti, "International Biodeterioration & Biodegradation Fungal biodeterioration of historical library materials stored in Compactus movable shelves," vol. 75, pp. 83–88, 2012.

[3] B. Zyska, "Fungi isolated from library materials: A review of the literature," *Int. Biodeterior. Biodegradation*, vol. 40, no. 1, pp. 43–51, Jan. 1997.

[4] D. R. Harvey, *Preservation in libraries: principles, strategies and practices for librarians*. Bowker, 1993, p. 265.

[5] J. Myers, "Facts about Mold," no. December, pp. 1–11, 2011.

[6] C. Palaty, "Mould Assessment in Indoor Environments - Review of Guidelines & Evidence," 2010.

[7] O. M. Bankole, "A review of biological deterioration of library materials and possible control strategies in the tropics," *Libr. Rev.*, vol. 59, no. 6, pp. 414–429, 2010.

[8] J. Singh, "Building Pathology & Environmental Monitoring," pp. 1–25.

[9] Adan Olaf CG and S. A. Robert, "Introduction Of Fundamentals of Mold Growth in Indoor Environments and Strategies for Healthy Living," in in *Fundamentals of Mold growth in Indoor Environments and Strategies for Healthy Living*, Netherlands: Wageningen Academic Publishers, 2011, p. 302.

[10] Bornehag C.G, Blomquist.G, Gyntelberg.F, Jarvholm.B, Malmberg.P, Nordvall.L, Nielsen.A, Pershagen.G, and Sundell.J, "Dampness in Buildings and Health between Exposure to "' Dampness "' in Buildings and Health Effects," *Indoor Air*, vol. 11, pp. 72–86, 2001.

[11] WHO, *WHO Guidelines for Indoor Air Quality (Dampness and Mould)*. Copenhagen: World Health Organization Regional Office, 2009, p. 228.

[12] D. Haas, J. Habib, H. Galler, W. Buzina, R. Schlacher, E. Marth, and F. F. Reinthaler, "Assessment of indoor air in Austrian apartments with and without visible mold growth," *Atmos. Environ.*, vol. 41, no. 25, pp. 5192–5201, Aug. 2007.

[13] R. E. Child, "Mould Outbreaks in Library and Archive Collections," *Br. Libr. (Preservation Advis. Centre)*, no. 2004, p. 7, 2011.

[14] C. J. Wessel, "Environmental Factors Affecting The Permanence of Libary Materials," *Libr. Q.*, vol. 40, pp. 39–84, 1970.

[15] E. Storey, K. Dangman H, P. Schenck, R. DeBernardo L, C. Yang S, A. Bracker, and M. Hodgson J, *Guidance for Clinicians on the Recognition and Management of Health Effects related to Mold Exposure and moisture Indoors*. Farmington: U.S Environmental Protection Agency (EPA), 2004, p. 70.

[16] H. Viitanen, "Improved Model to Predict Mold Growth in," *VTT Tech. Res.*, 2007.

Applied Mechanics and Materials Vol. 567 (2014) pp 559-564
© (2014) Trans Tech Publications, Switzerland
doi:10.4028/www.scientific.net/AMM.567.559

Challenges for Implementation of Building Information Modeling (BIM) in Malaysian Construction Industry

Syed Shujaa Safdar Gardezi[1,a], Nasir Shafiq[1,b], Muhd Fadhil Nurudinn[1,c], Syed Ahmad Farhan[1,d] and Usman Aminu Umar[1,e]

[1]Department of Civil Engineering, Universiti Teknologi Petronas, Bandar Seri Iskandar, 31750 Tronoh, Perak, Malaysia.

[a]engineershujaa@gmail.com, [b]nasirshafiq@petronas.com.my, [c]fadhilnuruddin@petronas.com.my, [d]syfarisk@gmail.com, [e]usmanaumar@yahoo.com

Keywords: Building information modeling, challenges, Malaysian construction industry

Abstract. The construction industry of Malaysia is very dynamic in nature and the adoption of new technological advancements and construction methods has been a prime concerns for its key players and stakeholders. However, the adoption of BIM in such a dynamic industry is observed to be limited and its implementation has not been as successful as it should have been. The study focuses on the identification and prioritization the factors challenging the implementation of BIM in Malaysian construction industry. The data has been administrated through designed questionnaire by identifying the factors / barriers, by literature review, for implementation of BIM in construction industry. The prioritization of such factors is expected to help the major stake holders to address the issues according to their priority which will save lot of previous time and financial with smooth implementation of BIM in Architecture, Engineering and Construction (AEC) industry in future project.

Introduction

A model defining the physical and the functional characteristics of a facility in a digital representation form is known as Building information model. [1]. The concept of Building Information Modeling is to build a building in a virtual environment before its actual physical construction so that problems along with their potential impacts expected to be encountered during actual construction stage can be worked out and analyzed in advance[2].The potential utilization of BIM by the construction industry stake holders can result in greater benefits in terms of reducing cost, increase productivity, reduce errors and improve the quality of our work products ultimately in improvement of the built environment. BIM is the future in Construction Industry. BIM is setting new standards in AEC industry by encouraging the integrated roles of all stakeholders in a project has the potential to bring about great efficiency as well as create healthy harmony among them who all too often in the past saw themselves as adversaries[1]. As in most paradigm shifts there will undoubtedly be risks associated with this change. BIM also supports the concept of Integrated Project Delivery (IPD) to reduce waste and optimize efficiency through all phases of the project life cycle [3].

The construction industry of Malaysia is very dynamic in nature. The country is progressing with a vision on 2020 and the construction industry in a vital element of this vision. The adoption of new technological advancements and construction methods has been a prime concerns for its key players and stakeholders. However, the adoption of BIM in such a dynamic industry is observed to be limited and its implementation has not been as successful as it should have been. Although, there is now a serious concern about this technology and the industry professional are realizing the potential benefits of BIM. There is still long way to cover for its full implementation as no. of issues, challenges and barriers still required to be managed. This study is being conducted to highlight some of the factors that are, specifically, affecting the implementation of BIM in Malaysian Construction Industry.

Literature Review

Benefits of Implementing BIM in AEC:

Many researchers and industry professional have highlighted the potential benefits of BIM implementation. From AEC main stake holder's point of view, these potential benefits can be broadly classified into the three categories of Owners, Designers and Contractors:
Eastman et al. [4] and Reddy (2011) summarized the following benefits of BIM for project owners:

1 Early design assessments ensuring that the project requirements are met
2 Evaluation of building performance and maintainability by operations simulation
3 Reliability in cost estimates and reduction in quantity of variation orders thus enabling low financial risks.
4 Generation of 3D renderings and walk-though animations enables better marketing strategies.
5 Complete information about building and its systems in a single file[5].

Following are some of the main benefits of BIM for project designers:

1 Better design by rigorously analyzing digital models and visual simulations and receiving more valuable input from project owners;
2 Advance predictions of environmental performance of building designs by early incorporation of sustainability features.
3 Visual and analytical checks enable better code compliance.
4 Early forensic analysis to graphically assess potential failures, leaks, evacuation plans.
5 Quick production of shop or fabrication drawings [6]

The contractors and subcontractors can use BIM for the following applications [7]:

1 High profitability;
2 Better customer service;
3 Cost and schedule compression;
4 Better production quality;
5 More informed decision making;
6 Better safety planning and management.

Challenges for Implementing BIM in AEC:

Despite of the benefits of BIM mentioned above, the implementation of BIM in AEC is very challenging task and requires managing certain barriers before its successful implementation in AEC industry of any country. These barriers or challenges vary from country to country and are largely dependent upon the industry environments. Research contributions of few researchers are given in Table 1 below.

Table 1: Challenges and risks identified by previous researchers

Researchers	Findings/ Conclusions
Salman Azhar, Michael Hein and Blake Sketo [2]	Has identified the following risks for BIM implementations : • Ownership of BIM data • Control over entry of data and responsibilities for inaccurate data. • The issue regarding responsibility for proper technological interface among various programs. • The management issues regarding the implementation and use of BIM. • Lack of clear consensus regarding methodology to implement or use BIM. • Requirement of standardized BIM process and guidelines for its implementation.

Thompson and Miner[8].	The BIM related risks can be divided into two broad categories: (1) Technology-related risks; and (2) Process-related risks. The first technology-related risk is • Lack of BIM standards for model integration and management by multidisciplinary teams. • The interoperability issues pose considerable risk. • Licensing issues when team members are other than owner and architect/engineer. The process-related risks include legal, contractual and organizational risks. • Legal risk includes the lack of determination of ownership of the BIM data and the need to protect it through copyright laws and other legal channels. • Contractual issue includes controlling authority of the data entry into the model and responsibility for any inaccuracies.
Ku and Taiebat [5]	Their identified the following barriers to BIM implementation: • Learning curve and lack of skilled personnel • High cost to implementation • Reluctance of other stakeholders (e.g. architect, engineer, contractor) • Lack of collaborative work processes and modeling standards • Interoperability • Lack of legal/contractual agreements
Fischer and Kunz[9]	Highlighted two main reasons for slower adoption of BIM. • Technical • Managerial
Bernstein and Pittman[10]	Classified the technical reasons broadly classified into three categories: • The need for well-defined transactional construction process models to eliminate data interoperability issues, • The requirements that digital design data be computable, and • The need for well-developed practical strategies for the purpose • The management issues cluster around the implementation and use of BIM. • Absence of clear consensus as how to implement or use BIM. • Unavailability of single document or treatise on BIM that instructs on its application or usage (AGC, 2005). • Inability of several software firms to treat the process as a whole. • Requirement to standardize the BIM process and the guidelines for its implementation. • Issue regarding the development and operation of BIM models among the AEC industry stakeholders (i.e. owners, designers and constructors). • Unclear methodology for distribution of cost for development and operations of BIM technology

Research Methodology

The research work has been carried out by studying literature on issues, challenges and barriers faced for implementation of BIM in construction industry. The literature review includes following book, newsletter, journal/conference papers, government reports and websites. A total of 17 factors were highlighted by assigning nominal scale 0 to 5 to represent ‘very weak’ to ‘very strong’ effects to study their impact in BIM implementation in AEC industry of Malaysia. Data collection administered by designed questionnaire. The feedback was tabulated and analyzed by using computer software. Based upon the data collection and analysis, the factor affecting the construction industry the most were identified and probable solutions were suggested accordingly.

Analysis of Results and Discussions

A total no. of 287 survey questionnaires was distributed among the industry professionals through online submissions and personal interactions during various seminars, conferences and scholarly sessions. However, researchers were able to receive a response rate of 38% for the study.

Demographic Results:

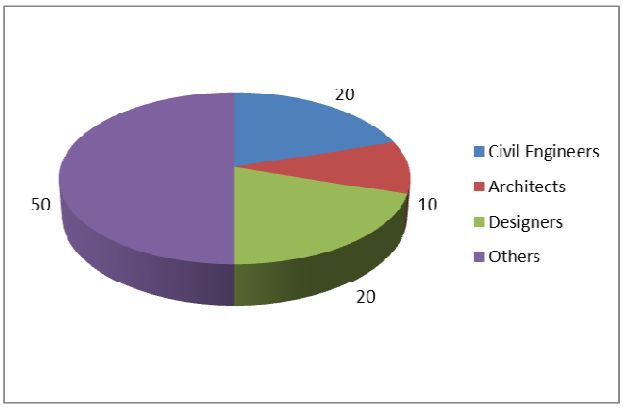


Figure1: Professional participation

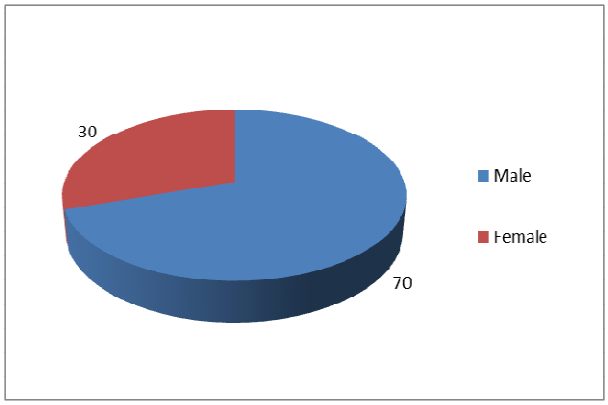


Figure 2: Gender participation

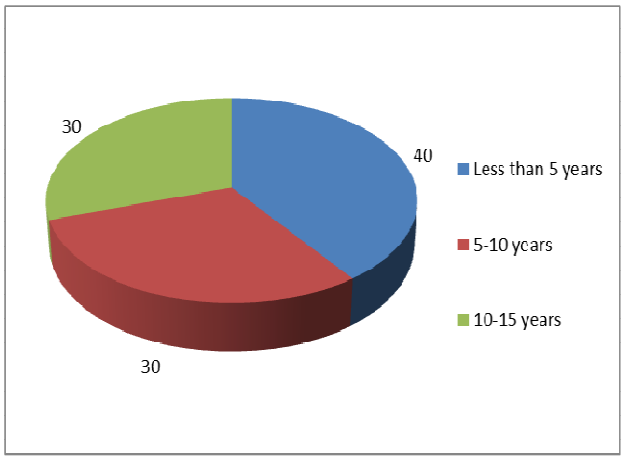


Figure 3: Professional experience

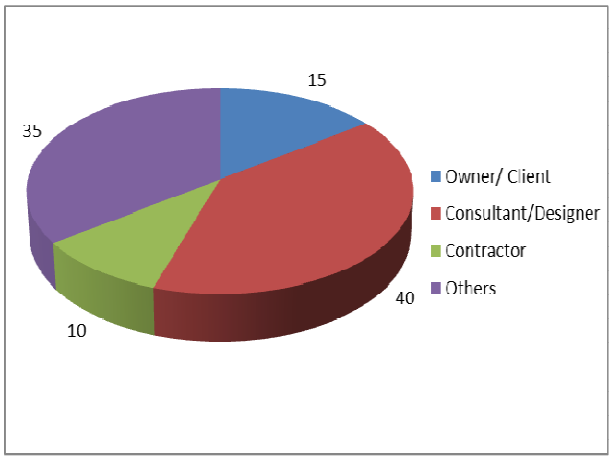


Figure 4: Professional roles

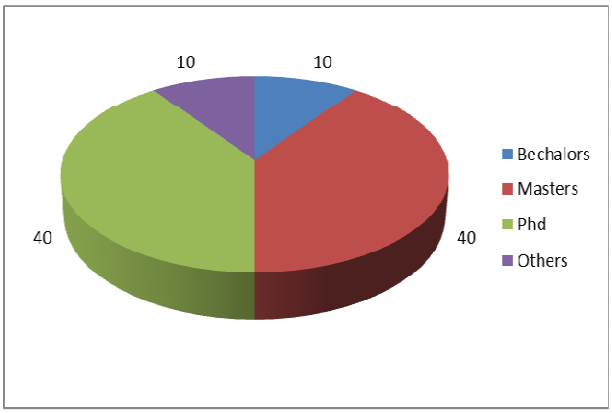


Figure 5: Qualifications

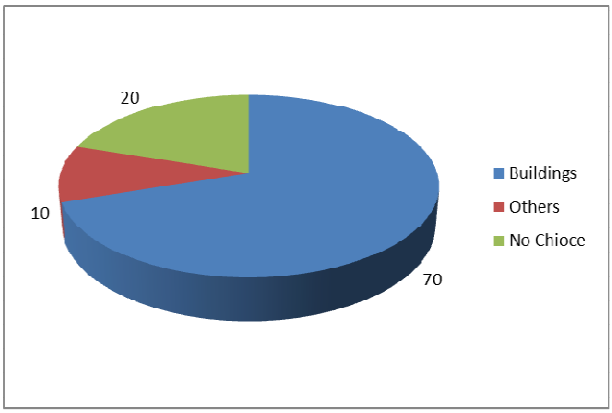


Figure 6: Industry / sectorial distributions

Factors Results:

The frequency analysis has been performed on the data and the following results have been achieved:

Statistical and practical significance result 17 factors challenging the implementation of BIM

Item No.	Factor		Frequency %age				
			1	2	3	4	5
1	High initial cost of softw are and hardw are	HICSH	1	5	12	66	16
2	High Cost of training	HCT	0.5	4.5	29	45	21
3	High cost of implementing the process and technology.	HCIPT	4	8	33	29	26
4	Behavior of professionals to change from drafting to modeling i.e. change from current practices	BOP	1	11	12	44	32
5	Weak Support from Organization environment and culture in implementation of BIM.	WSO	3	2	40	10	45
6	Non-availability of support from top management in organizations for implementation of BIM	NASTM	6	2	37	34	21
7	Non-availability of skilled professionals	NASP	2	1	19	67	11
8	Lack of BIM object libraries and standard modeling protocols	LBOLS	4	8	32	34	22
9	Industry resistance to process change	IRPC	1	5	50	10	34
10	Lack of standardized process and guidelines for implementation of BIM in the construction industry.	LSPG	1	4	23	54	18
11	Compatibility issue betw een softw are platforms	CIBST	3	1	40	22	34
12	Absence of interoperable environment in the construction industry	AIECI	2	2	39	35	22
13	Limited use of BIM in construction industry	LBCI	4	1	50	31	14
14	Non-availability of market support/trends for BIM implementation	NAMSB	1	12	22	65	0
15	Lack of comparative analysis betw een traditional project delivery methods and BIM based project delivery methods	LCADM	0	11	78	0	11
16	Lack of comparative analysis betw een the existing methods and BIM technology in terms of cost utilized by organizations	LCACU	0	14	15	0	71
17	Non-availability of opportunities to apply the technology	NAOAT	0	10	25	20	45

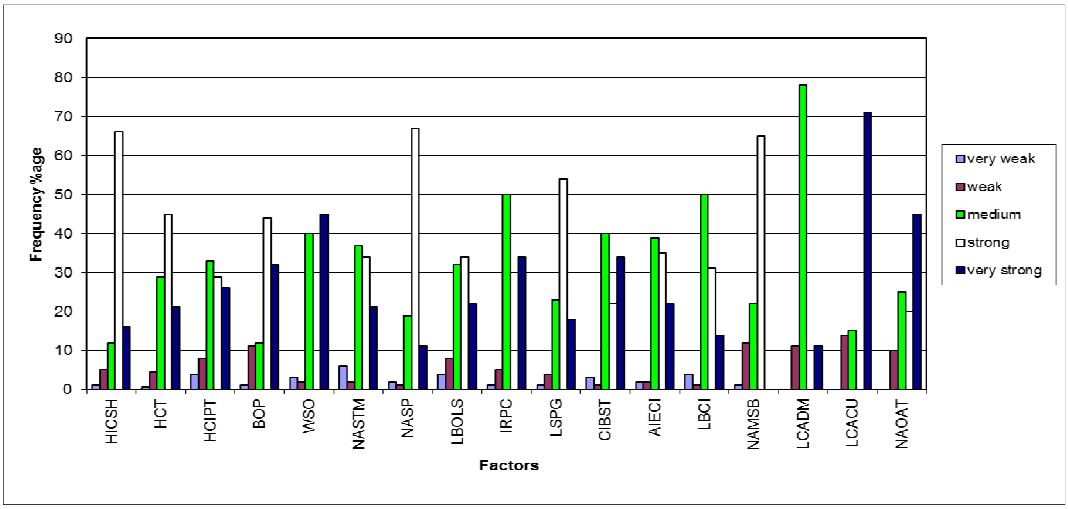


Figure 7: Frequency Analysis Graph

Discussions

The frequency analysis yielded that the High initial cost of software and hardware (HICSH), Non-availability of skilled professionals (NSAP), Non-availability of market support/trends for BIM implementation(NAMSB), Lack of comparative analysis between the existing methods and BIM technology in terms of cost utilized by organizations (LCACU) and Weak Support from Organization environment and culture in implementation of BIM (WSO) are the top five prominent barriers to the implementation of BIM in Malaysian construction industry.

Conclusions

The challenges for implementation of BIM faced by the construction industry of Malaysia have been focused in this study and top five influential factors have been identified. Most of the top ranked challenges are caused due to the factors which are driven by cost, market trends and organizational behaviors. The implementation of BIM will allow major stake holders to analyze space and understand the complexity of the project in AEC industry of Malaysia and provide them opportunities of doing more value-added activities. A close coordination among the industry stake holders with a specific vision and environment needs to be developed in AEC industry to enjoy the fruitful benefits of BIM implementation. The support by the concerned authorities, extensive consultation between the professional and industry practitioners is the only key to success.

References

[1] S. Azhar, M. Hein, and B. Sketo, "Building information modeling (BIM): Benefits, risks and challenges," in *Proceedings of the 44th ASC National Conference*, 2008.
[2] S. Azhar, "Building information modeling (BIM): Trends, benefits, risks, and challenges for the AEC industry," *Leadership and Management in Engineering,* vol. 11, pp. 241-252, 2011.
[3] S. Glick and A. Guggemos, "IPD and BIM: benefits and opportunities for regulatory agencies," in *Proceesings of the 45th Associated Schools of Construction (ASC?) Annual Conference, Gainesville, FL, 1-4 April*, 2009.
[4] C. Eastman, P. Teicholz, R. Sacks, and K. Liston, *BIM handbook: A guide to building information modeling for owners, managers, designers, engineers and contractors*: Wiley. com, 2011.
[5] K. Ku and M. Taiebat, "BIM experiences and expectations: The constructors' perspective," *International Journal of Construction Education and Research,* vol. 7, pp. 175-197, 2011.
[6] W. Kymmell, *Building information modeling: planning and managing construction projects with 4D CAD and simulations*: McGraw Hill Professional, 2008.
[7] B. Hardin, "BIM and Construction Management: Proven Tools, Methods, and Workflows," 2009.
[8] D. Thompson and R. G. Miner, "Building information modeling-BIM: Contractual risks are changing with technology," *WWW document] URL http://www. aepronet. org/ge/no35. html,* 2007.
[9] M. Fischer and J. Kunz, "The scope and role of information technology in construction," in *Proceedings-Japan Society of Civil Engineers*, 2004, pp. 1-32.
[10] P. G. Bernstein and J. H. Pittman, "Barriers to the adoption of building information modeling in the building industry," *Autodesk Building Solutions,* 2004.

Applied Mechanics and Materials Vol. 567 (2014) pp 565-570
© (2014) Trans Tech Publications, Switzerland
doi:10.4028/www.scientific.net/AMM.567.565

Embodied Carbon of Buildings: Tools, Methods and Strategies

Syed Ahmad Farhan[1,a], Nasir Shafiq[1,b], Khairun Azizi Mohd Azizli[2,c], Usman Aminu Umar[1,d], Syed Shujaa Safdar Gardezi[1,e]

[1]Department of Civil Engineering, Faculty of Engineering, Universiti Teknologi PETRONAS, Bandar Seri Iskandar, 31750 Tronoh, Perak, Malaysia.

[2]Department of Chemical Engineering, Faculty of Engineering, Universiti Teknologi PETRONAS, Bandar Seri Iskandar, 31750 Tronoh, Perak, Malaysia.

[a]syfarisk@gmail.com, [b]nasirshafiq@petronas.com.my, [c]khairun_azizli@petronas.com.my, [d]usmanaumar@yahoo.com, [e]engineershujaa@gmail.com

Keywords: low-carbon building, embodied carbon, carbon emission, operational carbon, carbon footprint, life-cycle assessment

Abstract. Embodied carbon can be defined as the "CO_2 emissions produced during the extraction of resources, transportation, manufacture, assembly, disassembly and end-of-life disposal of a product". Calculation of the carbon footprint of buildings is important to promote the construction of low-carbon buildings that release significantly less CO_2 compared to conventional buildings. However, researchers and practitioners in this area tend to disregard the embodied carbon and pay more attention to the operational carbon when calculating the carbon footprint of buildings. This paper reviews the current state and trend of research on the embodied carbon of buildings with focus on the tools, methods and strategies employed and makes recommendations for future research direction.

Introduction

Embodied carbon can be defined as the "CO_2 emissions produced during the extraction of resources, transportation, manufacture, assembly, disassembly and end-of-life disposal of a product" [1]. It is expressed in kg or tonnes of CO_2 and also referred to as embedded carbon [2]. In the case of buildings, the products, as mentioned in the definition, are the materials and components [3, 4] and the end-of-life disposal of these products includes demolition, reuse and recycling of them. The overall carbon footprint of buildings is the summation of embodied and operational carbons, which is the CO_2 emission that results from building operations [5].

Buildings consume large amounts of energy that leads to the release of CO_2 [6]. There is a lot of research conducted to address this issue, from developing novel strategies to enhance energy-efficiency of buildings [7–9] to generating awareness on the importance of making buildings energy-efficient [10, 11]. Therefore, calculation of the carbon footprint of buildings is important to promote the construction of low-carbon buildings that release significantly less CO_2 compared to conventional buildings. However, researchers and practitioners in this area tend to disregard the embodied carbon and pay more attention to the operational carbon when calculating the carbon footprint of buildings [12]. Nonetheless, interest in the embodied carbon of buildings has started to appear in recent research literature [6]. It has been reported that the embodied carbon contributes 21% of the total CO_2 emission of a building [13]. Therefore, future research literature should take into account both embodied and operational carbons when calculating the carbon footprint of buildings because the embodied carbon has a significant contribution to this value.

This paper reviews the current state and trend of research on the embodied carbon of buildings with focus on the tools, methods and strategies employed. Firstly, existing tools that have been adopted by previous researchers to estimate embodied carbon are reviewed. Then, developments of new tools and method are discussed. After that, previous studies on the strategies to reduce embodied carbon are reviewed.

Literature Search

Research articles on the embodied carbon of buildings were searched from the Scopus database. Scopus was chosen for this purpose because of the size of its database, which is currently the largest on the Internet [14]. Search results consisted of articles that contain keyword entries "embodied carbon" and "building*" in the "Title", "Abstract" and "Keywords" fields and were published from 2010 to 2013. However, the author does refer to several other articles found through citations but the majority of the articles reviewed in this paper are those that appeared in the search results.

Adoption of Existing Tools to Estimate Embodied Carbon

Previous researchers utilized several tools to determine embodied carbon of buildings. Bendewald and Olgyay (2010) [15] adopted the Green Footstep tool, which was developed by Rocky Mountain Institute [16], to estimate the embodied carbon of the Lodge and Learning Centre (LLC) located in the Archbold Biological Station (ABS) in Florida, USA. Valkhoff (2011) [17] used an assessment tool called Cocon [18] to calculate the embodied carbons of 20 types of walls used for timber-frame houses in France. Sansom and Pope (2012) [5] adopted a life-cycle assessment (LCA) model called CLEAR [19], which is based on BS EN ISO 14040:2006 [20] and 14044:2006 [21] and represented through a software called GaBi 4 [22]. Yuan and Qiu (2012) [6] and Basbagill *et al.* (2013) [23] employed Building Information Modelling (BIM) tools to complement their assessments of embodied carbon. Rossi *et al.* (2012) [24] utilized a software called Equer [25] to determine the embodied carbons of steel-framed and masonry houses located in Brussels, Belgium. Table 1 presents the existing tools adopted in previous research to estimate embodied carbon.

Table 1. Existing tools adopted in previous research to estimate embodied carbon

Existing Tools Adopted	References
Green Footstep	Bendewald and Olgyay (2010) [15] Rocky Mountain Institute [16]
Cocon	Valkhoff (2011) [17] Floissac (2009) [18]
CLEAR	Sansom and Pope (2012) [5] Griffin *et al.* (2011) [19]
BIM	Yuan and Qiu (2012) [6] Basbagill *et al.* (2013) [23]
Equer	Rossi *et al.* (2012) [24] Polster *et al.* (1996) [25]

Development of New Tools and Method to Estimate Embodied Carbon

Some researchers developed new tools to estimate the embodied carbon of buildings. Densley Tingley and Davison (2012) [26] developed a tool called Sakura that incorporates a new methodology for deconstruction design to promote reuse of building materials that can reduce embodied carbon. Sakura can calculate the embodied carbon based on, among others, parts of the building structure, life-span of building components, lives of reused building components and life-cycle stages of the building. Rossi *et al.* (2012) [24] developed a basic tool for LCA to determine the embodied carbons of steel-framed and masonry houses. Memarzadeh and Golparvar-Fard (2012) [13] presented a new tool to target, inspect and generate visuals of predicted and actual embodied carbon of buildings with n-dimensional augmented reality (DnAR) models. Moncaster and Symons (2013) [27] presented a design decision tool to calculate the whole-life embodied carbon and energy of buildings called the ECEB. This is to respond to the UK Government's recommendation in the Innovation and Growth Team (IGT) Final Report [28] for a development of

a method that could be used as a design decision tool at feasibility design stage while complying with the European TC350 standards [29–31]. Iddon and Firth (2013) [32] developed a BIM tool to simultaneously estimate embodied and operational carbons over a 60-year life-span for a typical four-bedroom detached house. Table 2 presents the new tools developed in previous research to estimate embodied carbon.

Basbagill *et al.* (2013) [23] proposed a decision support method that incorporates BIM, LCA, energy simulation, maintenance, repair and replacement (MRR) scheduling and sensitivity analysis softwares and can forecast decisions that crucially influences the embodied impact of the building. In this method, material quantities are recorded in the BIM and then the embodied carbon is determined. After that, sensitivity analysis is performed to find out the impact of each building component over numerous designs.

Table 2. New tools developed in previous research to estimate embodied carbon

New Tools Developed	References
Sakura	Densley Tingley and Davison (2012) [26]
Basic tool for LCA	Rossi *et al.* (2012) [24]
Tool to use with DnAR models	Memarzadeh and Golparvar-Fard (2012) [13]
ECEB	Moncaster and Symons (2013) [27]
BIM tool	Iddon and Firth (2013) [32]

Adoption of Strategies to Reduce Embodied Carbon

Several strategies were adopted in previous research to reduce the embodied carbon of buildings. Bendewald and Olgyay (2010) [15] employed the reuse of materials to reduce the embodied carbon of the LLC sited in the ABS in Florida, USA. Goggins (2010) [33] introduced ground granulated blast-furnace slag (GGBS) to replace 50% of cement in a concrete mix, which reduces the embodied carbon of a 3-storey office block located in Galway, Ireland from 412,792 to 285,931 kg CO_2. Monahan and Powell (2011) [1] reported that the adoption of timber frame instead of masonry construction for a house model based on a three-bedroom semi-detached low-energy house located in Norfolk, UK can reduce the embodied carbon by 51%. Valkhoff (2011) [17] and Čuláková *et al.* (2013) [34] reported that the use of plant-based materials in walls can generate negative embodied carbons due to their ability to store carbon. Crockford *et al.* (2011) [35] reported that the adoption of 40% cement replacement materials and 76% recycled aggregates in the concrete mix used to construct the Aquatics Centre in London resulted in a reduction of the embodied carbon by 4000 tons CO_2. Arnold *et al.* (2011) [36] discussed about the lightweight cable-net roof employed for the Velodrome in London that reduced the embodied carbon by 45% compared to the conventional steel structure due to the reduction in the roof steel weight from 1300 to 160 tons. Song and Peña-Mora (2012) [37] proposed the adoption of emissions liability insurance as a new insurance product to oversee the embodied carbon in the construction process. Nordby and Shea (2013) [38] reported that the adoption of wood-based exterior wall design concepts instead of concrete and rock wool can significantly reduce embodied carbon. Table 3 presents the strategies adopted in previous research to reduce the embodied carbon of buildings.

Table 3. Strategies adopted in previous research to reduce embodied carbon

Strategies	References
Reuse of materials	Bendewald and Olgyay (2010) [15]
Replacement of cement with GGBS in concrete mix	Goggins (2010) [33]
Adoption of timber frame instead of masonry construction	Monahan and Powell (2011) [1]
Use of plant-based materials in walls	Valkhoff (2011) [17] Čuláková *et al.* (2013) [34]
Adoption of cement replacement materials and recycled aggregates in concrete mix	Crockford *et al.* (2011) [35]

Adoption of lightweight cable-net instead of conventional steel structure for roof	Arnold *et al.* (2011) [36]
Adoption of emissions liability insurance	Song and Peña-Mora (2012) [37]
Adoption of wood-based exterior wall instead of concrete and rock wool	Nordby and Shea (2013) [38]

Conclusion and Recommendations

Tools and methods adopted to estimate the embodied carbon of buildings have been reviewed. Strategies to reduce embodied carbon have been discussed. At present, there is a lack of research on embodied carbon compared to operational carbon when calculating the carbon footprint of buildings. This paper highlights the current state and trend of research in this area for researchers to refer to when designing future research works. Recommendations for future research directions are listed as follows:

1) Development of new tools and methods to improve the efficiency and ease of conducting estimations, projections, assessments and monitoring of the embodied carbon of buildings
2) Investigation of novel strategies to reduce the embodied carbon of buildings
3) Assessment and monitoring of the embodied carbon of existing buildings
4) Calculation of the embodied carbons of alternative building materials

References

[1] J. Monahan and J. C. Powell, "An embodied carbon and energy analysis of modern methods of construction in housing: A case study using a lifecycle assessment framework," *Energy Build.*, vol. 43, no. 1, pp. 179–188, 2011.

[2] S. Sturgis and G. Roberts, "Redefining zero: carbon profiling as a solution to whole life carbon emission measurement in buildings," *RCIS Research Report*, 2010. [Online]. Available: http://www.isurv.com/site/. [Accessed: 28-Nov-2013].

[3] K. Symons and D. Symons, "Embodied energy and carbon - what engineers need to know," *Struct. Eng.*, vol. 87, no. 9, pp. 19–23, 2009.

[4] IStructE Sustainable Construction Panel, "What is embodied carbon?," *Struct. Eng.*, vol. 86, no. 16, p. 13, 2008.

[5] M. Sansom and R. J. Pope, "A comparative embodied carbon assessment of commercial buildings," *Struct. Eng.*, vol. 90, no. 10, pp. 38–49, 2012.

[6] L. Yuan and J. Qiu, "An analysis of embodied carbon of different types of residential buildings in China," *Adv. Mater. Res.*, vol. 450–451, pp. 1557–1561, Jan. 2012.

[7] S. A. Farhan, M. F. Khamidi, D. F. Ziela, A. M. Al Yacouby, A. Idrus, M. F. Nuruddin, and A. E. Razali, "Performance of reflective insulation in gable roofs: small-scale experimental investigation," in *Proceedings of ICCOEE2012: 2012 International Conference on Civil, Offshore & Environmental Engineering, Kuala Lumpur, Malaysia, June 12-14*, 2012.

[8] S. A. Farhan, M. F. Khamidi, M. H. Murni, M. F. Nuruddin, A. Idrus, and A. M. Al Yacouby, "Effect of silica fume and MIRHA on thermal conductivity of cement paste," in in *High Performance Structures and Materials VI. WIT Transactions on the Built Environment 124*, W. P. De Wilde, C. A. Brebbia, and S. Hernandez, Eds. Great Britain: WIT Press, 2012, pp. 331–339.

[9] A. M. Al Yacouby, M. F. Khamidi, M. F. Nuruddin, S. A. Farhan, and A. E. Razali, "Experimental study on the effects of roof colors on thermal performance of housing in Malaysia," in *Proceedings of ICCOEE2012: 2012 International Conference on Civil, Offshore & Environmental Engineering, Kuala Lumpur, Malaysia, June 12-14*, 2012.

[10] A. M. Al Yacouby, M. F. Khamidi, Y. W. Teo, M. F. Nuruddin, S. A. Farhan, S. A. Sulaiman, and A. E. Razali, "Housing developers and home owners' awareness on implementation of building insulation in Malaysia," in in *Management of Natural Resources, Sustainable Development and Ecological Hazards III. Ravage of the Planet VI 3*, C. A. Brebbia and S. S. Zubir, Eds. Great Britain: WIT Press, 2012, pp. 219–230.

[11] S. A. Farhan, M. F. Khamidi, A. M. Al Yacouby, A. Idrus, and M. F. Nuruddin, "Critical review of published research on building insulation: focus on building components and climate," in *Proceedings of BEIAC2012: 2012 IEEE Business, Engineering and Industrial Applications Colloquium, Kuala Lumpur, Malaysia, April 7-8*, 2012.

[12] D. H. Weight, "Embodied through-life carbon dioxide equivalent assessment for timber products," *Proc. Inst. Civ. Eng.*, vol. 164, no. EN4, pp. 167–182, 2011.

[13] M. Memarzadeh and M. Golparvar-Fard, "Monitoring and visualization of building construction embodied carbon footprint using DnAR - N-dimensional augmented reality models," in *Construction Research Congress 2012: Construction Challenges in a Flat World, Proceedings of the 2012 Construction Research Congress*, 2012, pp. 1330–1339.

[14] "Scopus Facts & Figures," 2013. [Online]. Available: http://cdn.elsevier.com/assets/pdf_file/0007/148714/scopus_facts_and_figures.pdf. [Accessed: 15-Jan-2014].

[15] M. Bendewald and V. Olgyay, "Carbon neutrality based on native-site carbon storage," *ASHRAE Trans.*, vol. 116, no. Part 2, pp. 16–24, 2010.

[16] Rocky Mountain Institute, "Green Footstep," 2009. [Online]. Available: http://greenfootstep.org. [Accessed: 14-Jan-2014].

[17] H. Valkhoff, "An environmental assessment of insulation materials and techniques for exterior period timber-frame walls," *PLEA 2011 - Archit. Sustain. Dev. Conf. Proc. 27th Int. Conf. Passiv. Low Energy Archit.*, pp. 333–338, 2011.

[18] L. Floissac, *COCON Comparaison de solutions Constructives de Confort et d'emissions de CO2 Version 2.3.0.3*. 2009.

[19] A. Griffin, I. Millar, N. Avery, N. Coleman, and P. Hodgson, "CLEAR - An LCA model for construction," in *LCM Conference 2011, Berlin, Germany*, 2011.

[20] International Organization for Standardization, "ISO 14040:2006, Environmental management - Life cycle assessment - Principles and framework," Geneva, 2006.

[21] International Organization for Standardization, "ISO 14044:2006, Environmental management - Life cycle assessment - Requirements and guidelines," Geneva, 2006.

[22] "GaBi LCA software developed by PE International," 2012. [Online]. Available: www.gabi-software.com. [Accessed: 15-Jan-2014].

[23] J. Basbagill, F. Flager, M. Lepech, and M. Fischer, "Application of life-cycle assessment to early stage building design for reduced embodied environmental impacts," *Build. Environ.*, vol. 60, pp. 81–92, Feb. 2013.

[24] B. Rossi, A.-F. Marique, M. Glaumann, and S. Reiter, "Life-cycle assessment of residential buildings in three different European locations, basic tool," *Build. Environ.*, vol. 51, pp. 395–401, May 2012.

[25] B. Polster, B. Peuportier, I. Blanc-Sommeureux, P. Diaz Pedregal, C. Gobin, and E. Durand, "Evaluation of the environmental quality of buildings towards a more environmentally conscious design," *Sol. Energy*, vol. 57, pp. 219–230, 1996.

[26] D. Densley Tingley and B. Davison, "Design for deconstruction and material reuse," *Proc. Inst. Civ. Eng.*, vol. 164, no. EN4, pp. 195–204, 2011.

[27] A. M. Moncaster and K. E. Symons, "A method and tool for 'cradle to grave' embodied carbon and energy impacts of UK buildings in compliance with the new TC350 standards," *Energy Build.*, vol. 66, pp. 514–523, 2013.

[28] HM Government, "Low Carbon Construction Innovation & Growth Team Final Report," 2010.

[29] British Standards Institution, "BS EN 15643 Sustainability of Construction Works - Assessment of Buildings in Part 2: Framework for the Assessment of Environmental Performance," London, 2011.
[30] British Standards Institution, "BS EN 15804 Sustainability of Construction Works in Environmental Product Declarations. Core Rules for the Product Category of Construction Products," London, 2012.
[31] British Standards Institution, "BS EN 15978 Sustainability of Construction Works – Assessment of Environmental Performance of Buildings – Calculation Method," London, 2011.
[32] C. R. Iddon and S. K. Firth, "Embodied and operational energy for new-build housing: A case study of construction methods in the UK," *Energy Build.*, vol. 67, pp. 479–488, 2013.
[33] J. Goggins, "Reducing the embodied energy and embodied carbon of reinforced concrete structures in Ireland," in *Structures and Architecture - Proceedings of the 1st International Conference on Structures and Architecture, ICSA 2010*, 2010, pp. 1680–1687.
[34] M. Čuláková, S. Vilčeková, J. Katunská, and E. K. Burdová, "Multi-criteria analysis of material selection in order to reduce environmental impacts," *Chem. Eng. Trans.*, vol. 35, pp. 379–384, 2013.
[35] I. Crockford, M. Nelson, S. Fraser, G. Mungal, and J. Nicholson, "Delivering London 2012 : The Aquatics Centre," *Proc. Inst. Civ. Eng.*, vol. 164, no. CE6, pp. 44–50, 2011.
[36] R. Arnold, C. Banister, A. Weir, D. Dabasia, and D. Goodliffe, "Delivering London 2012: the Velodrome," *Proc. Inst. Civ. Eng.*, vol. 164, no. CE6, pp. 51–58, 2011.
[37] X. Song and F. Peña-Mora, "Introducing the concept of emissions liability insurance in managing greenhouse gas (GHG) emissions and promoting sustainability in construction projects," in *Construction Research Congress 2012: Construction Challenges in a Flat World, Proceedings of the 2012 Construction Research Congress*, 2012, pp. 1850–1858.
[38] A. S. Nordby and A. D. Shea, "Building materials in the operational phase: Impacts of direct carbon exchanges and hygrothermal effects," *J. Ind. Ecol.*, vol. 17, no. 5, pp. 763–776, 2013.

Applied Mechanics and Materials Vol. 567 (2014) pp 571-576
© (2014) Trans Tech Publications, Switzerland
doi:10.4028/www.scientific.net/AMM.567.571

Evaluation Of Multi Storey Structures In Malaysia

Narayanan Sambu Potty[1, a] and Mohd Redzuan Abdul Hamid[1]

[1] Department of Civil Engineering, Universiti Teknologi PETRONAS, Bandar Seri Iskandar, 31750 Tronoh, Perak Darul Ridzuan, Malaysia

[a]narayanan_sambu@petronas.com.my

Keywords: Assessment, Wind loads, Earthquake, Serviceability.

Abstract. Malaysia has not traditionally considered earthquake and hurricane loading in design. Several tremors in neighboring countries necessitated a relook at the seismic reliability of structures in Kuala Lumpur and Penang with significant seismic risk. The study started with simple vertical load analysis (the current practice) and then the earthquake and the wind loading were imposed. The integrity of structures was evaluated for serviceability deflections using UBC 1997, IS 875-3-1987 and IS 1893. Permissible deflections were exceeded at 40 m/s for 87 m height buildings; at 45m/s for above 70 m height buildings; at 50 m/s for buildings above 59.5 m height. Higher value of ground accelerations (>0.1 g) results in exceeding the serviceability deflections

Introduction

Recent earthquakes in Sumatra in 2002 (Mw = 7.4), early 2003 (Mw = 5.8) and Aceh 2004 (Mw = 9.1- 9.3) caused vibrations and panic in in Penang and Kuala Lumpur, though Malaysia is about 350 km away from significant earthquakes. Cracks were reported in buildings in Penang due earthquake on 2nd November 2002 [1].

Literature Review

Though buildings vibrate during an earthquake, not all of them respond equally. If the ground frequency of oscillation is close to the natural frequency of the building, resonance and continued oscillation may cause severe damage. Small building are affected more by high frequency earthquake waves (short and frequent). Large structures or high rise buildings are affected more by low-frequency. A skyscraper will sustain greater shaking by long-period earthquake waves than by the shorter waves. The behavior of a building during earthquakes depends critically on its overall shape, size and geometry, in addition to how the earthquake forces are carried to the ground [2]. Hence, at the planning stage, unfavorable features are to be avoided and a good building configuration chosen. The choice of shapes and structure has significant bearing on the performance of the building. The wide range of structural damages observed during past earthquakes across the world is very educative in identifying structural configurations that are desirable versus those which must be avoided [3]. Codes also give recommendations on the EQ resistant features to be adopted in design [4][5][6][7].

When the provisions in the code are revised, re-assessment of structures safety becomes necessary under the new provisions. [8] recommended the seismic retrofit measures for Elevated Steel Water Tanks when the seismic zone of the location of the structure was changed from Zone 2 to Zone 3 in India. Assessments are also done on fleet of offshore structures to prioritize maintenance [9], [10],[11]. Seismic evaluation is also undertaken when seismic events cause public concern. Seismic assessment of structures based on questionnaire survey were carried out by Narayanan and Sirajuddin [12] and Potty and Sirajuddin [13] and by non –linear analysis of masonry structures by Potty and Sirajuddin [14] in Kollam, India. Wind speed provisions in IS 875-1987[15] and MS 1553: 2002[16] have been reported in Narayanan et al [17]. Design of structures in Malaysia follows BS 5400 [18], BS 8110 [19], BS 5950 [20]) and other standards. They lack

detailed and specific requirements on seismic load. Hence engineers use [21], [22] or [6]. However, the right ground acceleration for Malaysia has to be used. The choice is based on the importance of the structure and severity of failure. The design of Penang Bridge used higher value of ground acceleration compared to design of Bakun Hydroelectric Plant [23]. The 26 December 2004 earthquake caused IEM to come out with several short and long term recommendations on issues regarding earthquake [24]. Short term initiatives recommended include reviewing current Engineering Design and Construction Standards and Practices as well as suggesting that design of high rise buildings should cater for long period vibration. Sensitive and important structures are also recommended for seismic vulnerability assessment [24]. Seismic zone mapping carried out by SEER recommended for Peninsular Malaysia, the ground acceleration of 0.03g to 0.05g, while in East Malaysia, the level of acceleration recommended increases from Sarawak towards Sabah, due to existence of active fault in Sabah. Maximum ground acceleration for design in Sabah would be 0.15g [25]. Majority of the buildings in Kuala Lumpur have height between 12m to 99m [26]. This study involved the detailed analysis of buildings considering earthquake and wind loads. For low rise buildings, the effects of lateral load are considered minimum while for skyscrapers, it is assumed that lateral loads have been considered in design of the structural members and framing systems [27]. An important parameter is the type of framing system, which is kept constant so that the behaviour of structures towards the lateral loads can be fully associated with the height.

Methodology

The analysis considers structures up to 40 m height, considering the limit of applicability of framed structures. To avoid more complicated parameters and variables, the base areas of the structures are assumed to be square, chosen as 24m x 24m, 30m x 30m, and 36m x 36m to see the relationship between aspect ratio and structural displacement where column-to-column distance is assumed to be 6m. Beam size and slab thickness are assumed as 0.15m X 0.45m and 0.15m respectively. Column sizes are based on column sizing from real structures and vary with height. All columns are assumed square.

General types of loadings are considered are vertical loads (DL and LL) and horizontal loads (wind and earthquake loads). DL and LL for slabs (2 kN/m^2) are based on BS 6399 Part 1[28] and Part 2 [29]. Self-weight of structure and loading from brick walls are calculated based on density of concrete and bricks (24 kN/m^3 and 22 kN/m^3 respectively) [30]. Static approach of wind load analysis as per UBC 1997 [22] places Kuala Lumpur under Exposure B. Exposure B is terrain with buildings, forest or surface irregularities, covering at least 20 per cent of the ground level area extending 1 mile (1.61 km) or more from the site. Basic wind speed for Kuala Lumpur area is 35.1 m/s, peak 3-second gust at 10m above grade for a 50-year return period [31]; [16]. The modeled frame structure will be imposed to wind speeds from 20 m/s up to 50 m/s (20 m/s, 25 m/s, 30 m/s, 35 m/s, 40 m/s, 45 m/s, 50 m/s). Earthquake loading is also assessed based on UBC 1997 [22]. While wind loading is directly related with the height of the structure, earthquake loading is governed by the total mass of the structure. The total mass of the structure and mass for each floor is evaluated by sizing of structural members. Live load is excluded. Malaysia falls under zone 2A with seismic factor of 0.15. The importance factor is based on the function and occupancy of the structure. Importance factor of 1 is considered. R factor is based on framing system. For this analysis, ordinary moment resisting frame system is assumed with R factor of 3.5. The performance of structure toward earthquake loading is also dependent on the type of founding soil. Stronger soil will have lower coefficient with lower amplification of ground acceleration compared to softer soil. The soil is assumed to be type SA where Cv and Ca have values of 0.12 and 0.15 respectively.

Results and Discussion

For assessing the structure under wind loading, the critical parameter is the maximum displacement of the structure. Serviceability check consider H/100 to H/600 for maximum

deflection depending on building type and material used. The value assumed usually is H/400 and H/500 [32][33]. Cooney and King [34] recommend the limit for the sway of columns due to wind as h/500 and less than 4mm per storey. Lateral frame deflections have historically been based on a first order analysis. In this analysis, maximum allowable deflection for a structure is taken as H/500. In addition to this, structural members exceeding maximum stress and deflection are also considered to have failed. The maximum displacement of structures of different height, base area and imposed wind loads was evaluated. It is observed that theoretically all buildings studied are safe for wind speed of 20 m/s, 25 m/s, 30 m/s, and 35 m/s even though lateral loads had been excluded in the design. This is the reason for the negligible structural damage for buildings in Malaysia where maximum basic wind speed is around 32 m/s to 34 m/s [16]. For each plan size, the practical range of heights for moment resisting frames has been studied. So for plan sizes 18 x 18, 24 x 24, 30 x 30 and 36 x 36, heights of 24.5 m, 87.5 m, 87.5m, and 87.5 m respectively were considered. For 40 m/s wind speed the maximum deflection exceed the permissible values only for 24 x 24 plan size and height of 87.5m. For 45 m/s and 50 m/s wind speed, the cases for which maximum deflections exceed the permissible values were identified. Based on data taken from Malaysian Meteorological Department, highest maximum wind speed ever recorded was 41.7 m/s, at Kuching, Sarawak on 15 September 1992. This means wind speed beyond 40 m/s was only recorded during the last 20 years in a place very far from Kuala Lumpur. For wind speed of 45 m/s and 50 m/s, high rise buildings with more than 17 stories, will be severely affected by the lateral loads. Studies also show that low rise and medium rise buildings up to 15 stories performed very well in resisting lateral load without any additional bracing or lateral design. This means that for buildings up to 15 stories / 53m, the loadings are governed by gravity instead of lateral loads. However, for buildings more than 15 stories, the lateral loads gives more effect compared to gravity loads based on the gradient of the displacement curve. The relationship and trends between the base area and the displacement of the buildings are interpreted based on Figures 1, 2 and 3. Figure 4 shows the plot of vulnerability of structure vs. height of building. The resistance of structure contributed by the column is represented with the number of column given in a structure. The ratio between exposed surface area (to wind) and number of columns represent the resistance of structure towards lateral loadings. Higher ratio characterizes lower vulnerability of structure towards wind loads and vice versa. The difference of resistance given for different base area also increases with height. This answers the higher differences in deflections for high rise structure compared to medium and low rise structure with respect to different base areas.

The equivalent lateral seismic load is based on UBC 1997 for zone 2A with ground acceleration of 0.15g. The horizontal displacement of each building was evaluated. In UBC 1997[22] zoning categories Malaysia falls in Zone 2A. All coefficients and constants are pre-determined by zoning. Alternately, IS 1893 has simpler and direct method for determining the equivalent lateral loads. As most of the constants and coefficients in IS 1893 [7] is not determined by zoning criteria, the ground acceleration appropriate for Malaysia can be chosen. The study is done using ground acceleration of 0.1g, 0.15g and 0.2g. Using this code, Buildings with 3, 5, 15, and 25 storeys are analyzed, representing low, medium and high rise buildings. The results are plotted as in Figure 5 to observe the trends of the deflections with respect to the height of the structures. It is observed that very low rise and high rise structures tend to have more effect toward seismic loading compared to medium rise structure, having deflection more than permissible values.

To study the horizontal displacements of buildings due to different magnitude ground accelerations, IS 1893 [7] is used. Based on study, low rise and medium rise buildings seem to be able to survive in ground acceleration of 0.05g. SEER mapping shows that Peninsular Malaysia has so far only experienced ground acceleration between 0.03g to 0.05g. Kuala Lumpur and Penang have not experienced 0.05g ground acceleration and no structural damage is reported due to earthquake so far. However, the study suggests that structural improvement for existing high rise with more than 77 meter height is required when ground acceleration is considered. Ground acceleration beyond 0.1g will cause severe damages to all moment resisting frame structure

regardless their height. Having examined both UBC 1997 [22] and IS 1893 [7], it is seen that the behaviour of structures toward seismic load is independent of their base areas.

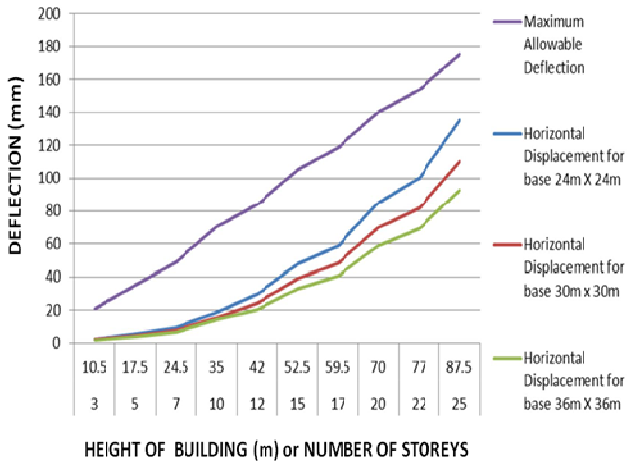


Figure 1 Deflection Vs. height of buildings for wind speed of 35 m/s

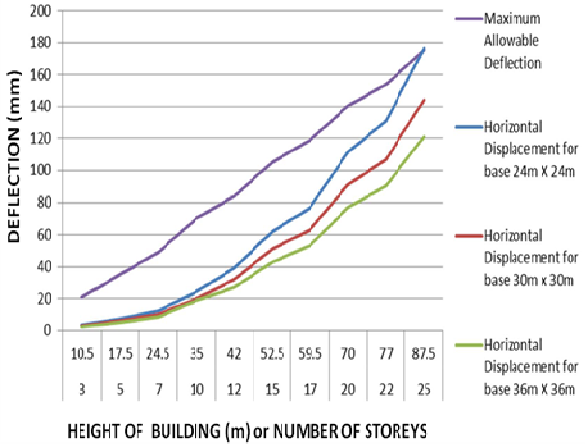


Figure 2 Deflection Vs. height of buildings for wind speed of 40 m/s

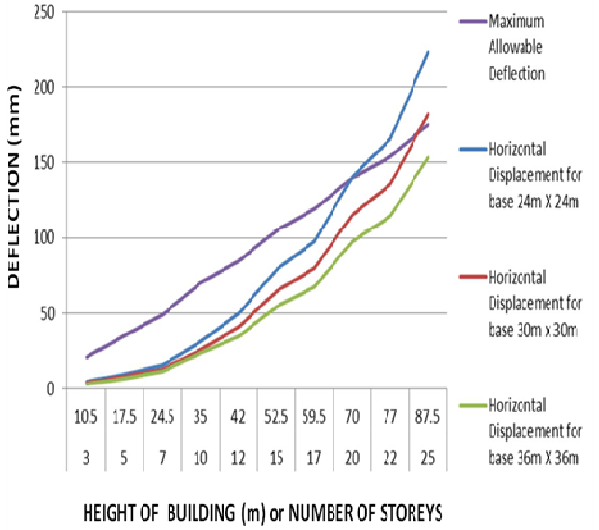


Figure 3 Deflection Vs. height of buildings for wind speed of 45 m/s

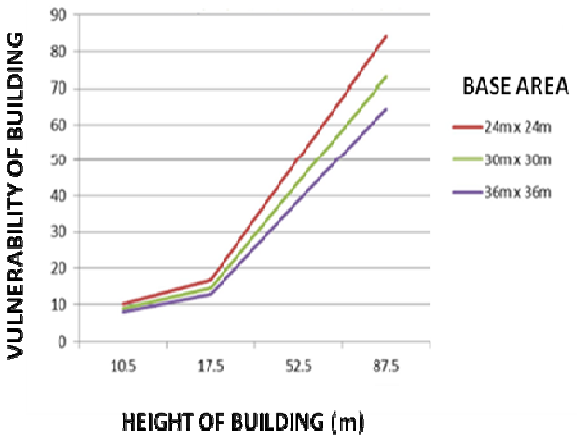


Figure 4 Relationship between height and resistance given by the column

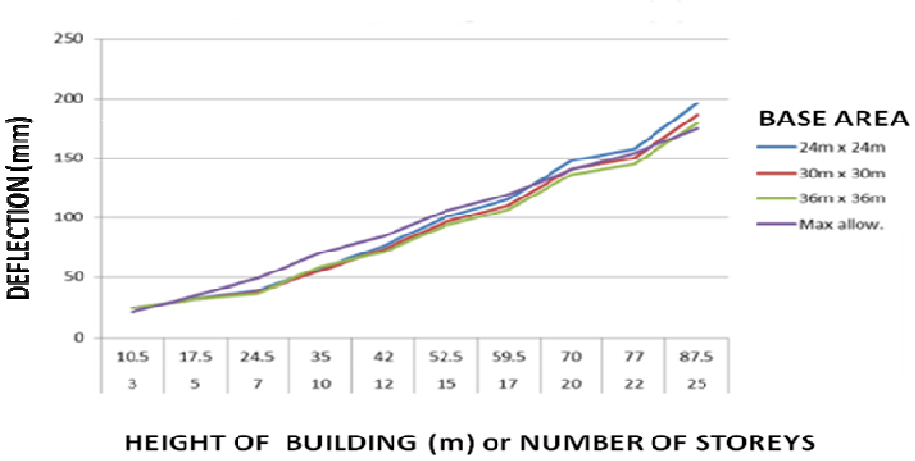


Figure 5 Maximum deflections vs. height of the structures due to EQ [22]

Unlike wind loading where lateral load is represented by imposed area, seismic load is characterized by the weight of the whole structure. Lighter structures with lower base shear usually

survive seismic load. As number of columns are usually proportionate to the weight of the building, proportional resistance is given by the column to resist seismic load. That explains the differences of deflection with respect to base areas are much lower compared to wind loading.

Conclusions

The practical height of moment resisting frame without lateral loads design is restricted at 25 storey (87.5m). Moment resisting frames are not recommended for structures beyond this height. For new structures, seismic loadings should be considered for the design of low rise shop-house or bungalows as they are theoretically more vulnerable to seismic forces compared to medium rise structures. As current condition in Malaysia, study shows that all structures are safe for 35 m/s wind load and medium rise structures are safe for ground acceleration of 0.05g. These explain the zero documented structural failure due to these loads in Malaysia. However, all structures theoretically will fail if the magnitude of wind loadings and ground accelerations are slightly increased beyond typical condition on Malaysia. Most of old structures without enhancement could fail if geological conditions in Malaysia get worse than the historical events.

Acknowledgements

This work was supported by the Universiti Teknologi PETRONAS, under the URIF PROJECT titled “Seismic vulnerability Assessment, Analysis and Retrofit of Special Structures”.

References

[1] A. Adnan, Hendriyawan and M. Irsyam, The Effect Of The Latest Sumatra Earthquake To Malaysian Peninsula, Journal Of Civil Engineering, 15, 2, 2002.

[2] H.J. Lagorio, Earthquakes: An Architect’s Guide to Non-Structural Seismic Hazard, John Wiley & Sons, Inc., USA, 1990.

[3] C.V.R. Murty, Learning Earthquake Design and Construction, IIT Kanpur – BMPTC Earthquake Tips. March, 2005.

[4] EC 2, Eurocode 2: Design of concrete structures: Part 1-1: General rules and rules for buildings.

[5] EC 3, Eurocode 1993-1-1:2005: Design of Steel Structures. Part 1-1. General Rules for and rules for buildings.

[6] EC 8, Eurocode 1998-1:2004 Design of Structures for Earthquake Resistance – Part 1: General Rules, Seismic Actions and Rules for Buildings.

[7] IS 1893 Criteria for EQ Resistant Design of Structures Part 1 General Provisions.

[8] N.S. Potty and S. Nambissan, Seismic Retrofit Of Elevated Steel Water Tanks, International Conference on Construction and Building Technology ICCBT 2008, 16-20 June, Kuala Lumpur, Malaysia, 2008.

[9] N.S. Potty N.S. and M.K.B. Mohd Akram, Structural Integrity Management For Fixed Offshore Platforms in Malaysia, World Academy of Science, Engineering and Technology, 58, 2009, pp. 1079 - 1087.

[10] N.S. Potty. and M.K.M. Akram, Development of a Risk Based Underwater Inspection (RBUI) Methodology for Malaysia Fixed Offshore Structure, 2011 National Postgraduate Conference – Energy and Sustainability: Exploring the Innovative Minds, art. 6136363.

[11] N.S. Potty, Ahmad Fawaz, Nur Ilyani Hasimy, N.J. Cossa and M.K.M Akram, Strength Assessment of Fixed Offshore Platforms for life extension, IJAER, xx, 2013, pp.

[12] S.P. Narayanan, and M. Sirajudin, Assessment of Building for Seismic Resistance , Malaysian Journal of Civil Engineering, 23, 1, 2011, 86-104.

[13] N.S. Potty and M. Sirajuddin, Seismic Risk Assessment Of Buildings In Kollam India, Bitech 2011 International Building And Infrastructure Technology Conference, 2011, June 7-8. ISBN 978-967-394-029-5.

[14] N.S. Potty and M.Sirajjudin, Non Linear Seismic Analysis of Masonry Structures, Journal of Design and Built environment, University Malaya, 9, 2011, 1-16, December.

[15] IS 875(3), COP for Design loads for buildings and structures: Wind Loads. 1987.

[16] MS 1553, Malaysian Standard, COP on Wind Loading for Building Structure. 2002.

[17] N.S. Potty, M.R.A. Hamid, M.A. Rosli, Seismic Evaluation of High Rise Structures in Malaysia, International Journal Applied Engineering Research, 8, 12, 2013, 1459 – 1477.

[18] BS 5400 – 2, British Standard. Steel, concrete and composite bridges, 1978.

[19] BS 8110-1, British Standard Structural use of concrete, 1997.

[20] BS 5950 – 1, Structural use of steelwork in building.

[21] AASHTO 2007, LRFD Bridge Design Specifications, 4th Ed., Washington, DC.

[22] UBC 1997, Uniform Building Code.

[23] N.K. Koong and K.W. Won, Earthquake Hazard and Basic Concepts of Seismic Resistant Design of Structures. Master Builders, 2005.

[24] IEM, 2005, Position Paper on Issues Related to Earthquake. Malaysia.

[25] Ngu, K., 2005, Earthquake Hazard and Basic Concept of Seismic Resistant Design of Structure. Master Builders 4th quarter, pp. 90-95.

[26] M.R.A. Hamid, Analysis of Existing High-Rise Reinforced Concrete Structures in Malaysia Subjected to Earthquake and Wind Loadings, UG Thesis, UTP, September 2012.

[27] Wikipedia, 2012, October 17, Skyscraper Design and Construction. Retrieved November 8, 2012, from Wikipedia : http://en.wikipedia.org/wiki/Skyscraper_design_and_construction.

[28] BS 6399: 1, British Standards. Loads for buildings: COP for dead and imposed loads, 1997.

[29] BS 6399: 2, British Standards. Wind loads for buildings, 1997.

[30] BS 648, British Standard. Schedule of weights of building materials, 1964.

[31] F. Shafii and M.Z. Othman, Country Report: Wind Loading for Structural Design in Malaysia. APEC-WW-21st Century Centre of Excellence Programme, 2004. UTM.

[32] L. Griffis, Serviceability Limit States under Wind Load. Engineering Journal/AISC, 2003.

[33] ASCE, Wind Drift Design of Steel-Framed Buildings: State-of-the-Art Report, Journal of Structural Engineering, 114 (1988), No. 9, September.

[34] R.C. Cooney and A.C King, The Branz Report: Serviceability Criteria for Buildings, Building Research Association of New Zealand, 1988.

Applied Mechanics and Materials Vol. 567 (2014) pp 577-582
© (2014) Trans Tech Publications, Switzerland
doi:10.4028/www.scientific.net/AMM.567.577

Evaluation of Roofing Systems in Malaysia Based on MS 1553, BS 6399, EC1-1-4 and IS 875 Wind Codes

Kang Seavhai[1,a] and Narayanan S. P.[1,b]

[1]Civil Engineering Department, Universiti Teknologi PETRONAS, Malaysia

[a]kangseavhai@gmail.com, [b]nsambupotty@yahoo.com

Keywords: averaging time, pressure, pullout, rectangular building, roofing sheet, wind speed.

Abstract. This paper evaluates the performance of different roofing sheet systems for different roof types using four different codes namely MS 1553, EC1-1-4, IS 875 and BS 6399. The maximum roof pressures using different codes (MS 1553, EC1-1-4, IS 875 and BS 6399) on critical and general area of the different roof types considering buildings with non-dominant opening, dominant opening and canopies have been evaluated. The maximum recommended wind speed in MS 1553 namely 33.5 m/s has been used as the reference for the numerical comparison. The major differences in the codes include averaging time for wind speed, terrain, reference height, and pressure coefficients. The study examines the conservativeness or not of the codes if used in the Malaysian context, even though they have been developed for a different wind climate and region. Further, the results of static test on different steel roofing sheets used in Malaysia using AS 1562.1 available as the limit state wind pressure capacities in the technical brochures are compared with design wind pressures for critical and interior regions of the roof for different wind zones. The suitability of a particular roofing sheet system for a particular wind zone is then assessed.

Introduction

The roofing is a very critical element for the safety of buildings and has historically suffered severely during strong wind events. Roof systems have performed well under normal conditions of load. Their performance under extreme wind loads has been disastrous, the predominant failure mode being uplift [1,2,3,4,5,6,7,8,9]. Lysaght Company provides steel roof cladding materials in Malaysia and static testing of wind pressure capacities were conducted in company laboratory in Australia using AS 1562.1 method [10]. Wind codes being used in Malaysia are MS 1553 [11] and BS 6399-2 [12]. The introduction of Eurocodes for structural design in Malaysia necessitates examination of EC1-1-4 [13]. IS 875-3 [14] is the Indian wind code in which zone 2 has tropical climate with cyclones. It is necessary to examine the conservativeness of the wind codes if used in the Malaysian context and to provide guidelines on the suitability of particular roofing sheet system for a particular wind zone. All of them have been studied and reported.

Literature Review

Type of Roof Cladding, Material Specifications and Limit State Wind Pressure Capacities. Lysaght provides several types of thin steel roofing sheets with different thickness namely trapezoidal, square fluted, pierce fastened, corrugated and concealed fix fluted pan profile. The first four are fixed using self-driven bolts whereas the last one is of concealed fixed nature. Table 1 provides the base metal thickness (BMT) and minimum roof pitch of different types of steel roofing sheet. The sheets are available in two types: (1) Zincalume steel – which is metallic coated steel product, composed of 55% Aluminium, 43.5% zinc and 1.5% Silicon. (2) Colorbond steel – which combines the superior strength of steel, corrosion resistance of zinc/aluminium alloy steel coating. The limit state wind pressure capacities were tested in NATA registered laboratories in Australia according to AS 1562.1 [10] and AS 4040.2 [15]. The pressure capacities for serviceability are based on a deflection limit of (span/120) + (maximum fastener pitch/30). The pressure capacities for

strength have been determined by testing the cladding to failure (ultimate capacity). The wind pressure capacities were tested with different types of steel roofing sheets of different thickness and types of connections for different spans (from 0.6m to 4.5m) for the single span, internal span and end span respectively. The results are given in the technical brochures [16,17,18,19,20].

Table 1: Different types of steel roofing sheets, BMT and Minimum roof pitch [16,17,18,19,20]

Type of sheet/ profile/cladding	BMT (mm)	Minimum roof pitch
Concealed fix, fluted pan	0.42, 0.48, 0.60	1 degree (1 in 57.3)
Trapezoidal steel	0.42, 0.48	3 degrees (1 in 20)
Subtle square fluted steel	0.35, 0.42, 0.48	2 degrees (1 in 30)
Pierce-fastened roofing	0.42, 0.55, 0.75	2 degrees (1 in 30)
corrugated	0.42, 0.48	5 degrees (1 in 12)

Types of Roof Cladding Connections and Method of Connection. Figure 1a, 1b and 1c shows details of the connections of steel roofing sheets to the purlins as recommended by [8,10,16,17,18,19,20,21]. Use of 5 fasteners per sheet per support is recommended (either rib fixed or pan fixed) (Fig. 1a; 1b). For concealed fixing, the clips are provided corresponding to each rib (Fig. 1c).

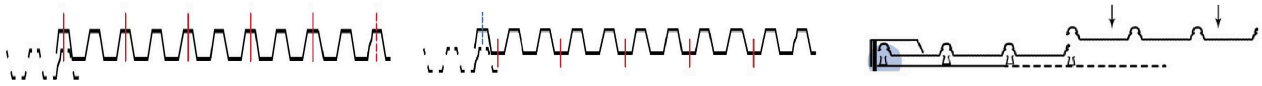


Fig. 1a: Screw Fix through Rib Fig. 1b: Screw Fix through Pan Fig. 1c: Concealed fix, fluted pan profile

Figure 1: Details of connecting the roofing sheets to purlins

Ultimate Pull-out Strength Capacities of Screws. The ultimate average pullout strength of screws connecting the roofing sheets to steel purlins are tested under the laboratory condition and the results are based on different thickness of the purlins, and available in technical brochure (Table 2)[22].

Table 2: Ultimate Average Pullout Data [22]

Base Thickness	G450 Steel	Base Thickness	G450 Steel
1.0mm	-	1.9mm	5500N
1.2mm	3100N	2.4mm	7300N
1.5mm	4200N	3.0mm	9800N

Wind Speeds. The wind speeds in MS 1553-2002, IS 875-3-1987, BS 6399-2-1997 and EC1-1-4-2005 are based on 3-second gusts, 3 second gusts, 10 minute mean and hourly means respectively.

Building Types. Rectangular plan buildings may have different roof types like mono-slope, pitched (gabled or hipped), canopy (pitched or troughed), saw tooth (single or multi span) and circular arch roofs. These building types are further classified based on percentage openings into non-dominant and dominant opening and open (canopy type). All of them have been considered in the study.

Reference Height. For calculation and comparison of wind pressures in different codes, MS 1553-2002 is used as the reference. The reference heights are calculated based on roof pitch of 10 degree and average roof height to width ratio of the building of 1.0. Buildings with average roof heights 3, 5, 10 and 15m are considered in this study. The different reference heights of the buildings with different wind codes have been discussed in [23,24,25,26].

Number of Terrain Categories (TCs). EC1-1-4-2005 specifies 5 TCs (0, I, II, III and IV) whereas MS 1553-2002 and IS 875-3-1987 specify only 4 (I, II, III and IV). BS 6399-2-1997 defines three categories of terrains namely sea, country and town.

External Pressure Coefficients, Internal Pressure Coefficients and Net Pressures Coefficient. Determination of external, internal and net pressures coefficients as per MS 1553-2002, IS 875-3-1987, EC1-1-4-2005 and BS 6399-2-1997 have been discussed in [23,24,25,26].

Wind pressure on the roofs. Determination of roof pressures as per MS 1553-2002, IS 875-3-1987, EC1-1-4-2005 and BS 6399-2-1997 have been discussed in [23,24,25,26].

Objectives of Study

The objectives of the study are: (a) To compare the maximum positive and negative pressures on the local and general area of the roof for rectangular plan buildings with average roof height not greater than 15m for different roof types and building with different permeability or opening condition using MS 1553-2002 Simplified procedure, EC1-1-4-2005, BS 6399-2-1997 Standard procedure, and IS 875-3-1987. (b) To evaluate the suitability of roofing systems for building with different roof heights, terrains and wind zones.

Methodology

A comparison of the codes requires the wind speed to be converted to the averaging time used in different codes (since 3 second winds speeds have been tabulated in MS 1553-2002 for Malaysia). The roof pressures for different roof types and building permeability or openings condition have been compared. Since the reference heights in EC1-1-4-2005, BS 6399-2-1997 and IS 875-3-1987 are different, those values corresponding to the average roof heights assumed for MS 1553-2002 have been evaluated for use in the respective codes. The wind speeds at the reference height are used to evaluate the pressures on the roof using the pressure coefficients. Using the basic wind speed of 33.5 m/s, and appropriate values for other parameters, the design wind pressures are calculated. Considering external pressure and internal pressure towards the roof as positive, three cases of total pressure can be evaluated (Fig. 2). The value of the terrain height multiplier varies with height (z) and the terrain category. The critical positive (case b) and negative pressures (case c) in Fig. 2 have been evaluated for different height and terrain categories for different roof types and building conditions. Using wind speed of 33.5 m/s converted to the corresponding averaging time, the values of roof pressures as per MS1553-2002; EC1-1-4-2005, BS 6399-2-1997 and IS 875-3-1987 are evaluated and compared. The design maximum pressures calculated using MS 1553-2002 are compared with the limit state wind pressures for local and general areas on roof and suitability of spans are decided. Two methods are used to evaluate the wind loading on the screws (1) To use the finite element model to find out the reaction of the screws on the middle purlin under maximum loading and (2) To use the simple method of dividing the total load on the middle purlin by the number of screw fasteners on the middle purlin to get the reaction. The values are compared with the average pull-out strength of screws from purlin obtained from the technical brochures.

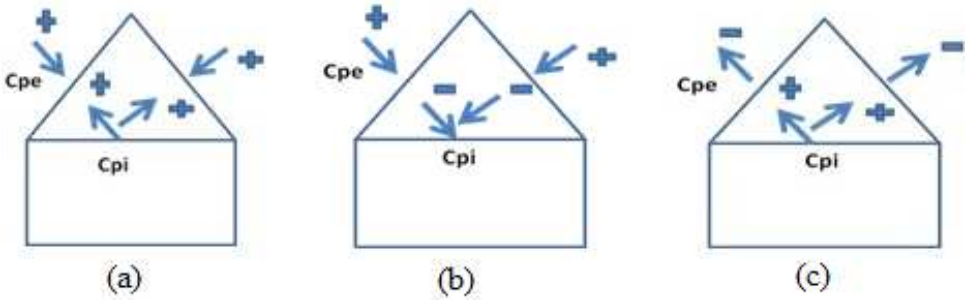


Figure 2: Cases of roof wind pressure on duopitch rectangular buildings

Results and discussion

General. The analysis has been done considering the maximum 3 second basic wind speed in Malaysia, which is 33.5m/s. The corresponding 10 minute mean wind and mean hourly wind speeds

are calculated with conversion factors (0.697 and 0.658) obtained from the Durst curves available in ASCE 7-10 [27] as 23.4 m/s and 22.0 m/s respectively.

Comparison of roof pressures. The maximum negative and positive pressures on general and local areas for all types of roofs with as per MS 1553, EC1-1-4, IS 875-3 and BS 6399-2 for different terrains indicate increasing trend of values with increasing height and decreasing trend from TC 1 to TC 4, as expected [23-26]. To determine conservativeness of the different codes if used in Malaysia, all pressures determined using different codes have divided by the corresponding pressures determined using MS 1553.

Roof pressure ratios for buildings with non-dominant opening. Ratios for all terrain categories for EC1-1-4-2005 are generally higher than 1.0 for all types of roofing considered except in TC4 for circular arch roof where the ratio of the maximum negative pressure on local and general areas are less than 1.0. For IS 875-3-1987 in the case of duopitch roofs, the ratios are generally less than 1.0 for TC1 and TC2. For monoslope and flat roofs all ratios are less than 1.0. For circular arch roofs, the ratios of the negative pressures are less than 1.0. For multi sawtooth and multi duopitch roofs, all ratios are generally less than 1.0 expect for the maximum positive pressure on general areas which are greater than 1.0. For BS 6399-3-1997, all ratios for duo-pitch, mono-pitch and multi duo-pitch roofs are generally greater than 1.0 except for local areas of TC1 where the ratios are less than 1.0. For flat roofs the ratios are generally less than 1.0 except for the ratios of maximum negative pressure on general areas in TC3 and TC4. For multi span sawtooth roofs, the ratios on local areas are generally less than 1.0 except for TC3 and TC4 where the maximum negative pressure ratios on local areas are higher than 1.0.

Roof pressure ratios for buildings with dominant openings. Ratios for all terrain categories for EC1-1-4-2005 are generally higher than 1.0 for all types of roofing considered except for circular arch roof where the maximum negative pressure ratios on local areas are less than 1. For IS 875-3-1987 in the case of flat roofs, multi span duo-pitch, multi span sawtooth, duo-pitch, monoslope roofs the ratios are generally less than 1.0. For circular arch roofs, except for maximum negative pressure ratios for local areas, all values are generally greater than 1.0. Ratios for all terrain categories for BS 6399-3-1997 are generally higher than 1.0 for all types of roofing considered except for the maximum negative pressure ratios for local areas in TC1 are less than 1, the minimum ratio is about 0.87.

Roof pressure ratios for canopies. Ratios for all terrain categories for EC1-1-4-2005 are generally higher than 1.0 for all types of canopies considered except for monoslope canopies where the maximum negative pressure ratios for block under are less than 1, the lowest ratio is about 0.58. Ratios for all terrain categories for IS 875-3-1987 are generally higher than 1.0 for all types of canopies considered except for monoslope canopies where the maximum negative pressure ratios for block and empty under are less than 1, the lowest ratio is about 0.61. Ratios for all terrain categories for BS 6399-3-1997 are generally higher than 1.0 for all types of canopies considered except for monoslope canopies where the maximum negative pressure ratios for block under are less than 1 for TC1, the lowest ratio is about 0.81.

Consideration of Bending Failure of the Roofing Sheets. The suitable spans for each type of roofing sheets have been determined for different terrains and height of the structures for all roof types and buildings with different permeability or opening condition. The overall results of the suitability of spans are summarized below.

Terrain Category I, height from 3m - 5m: It is suitable and economical to use Subtle square fluted with minimum BMT of 0.42mm with span below 1.2m. For Subtle Square fluted, Trapezoidal, HR-29 and Custom blue orb 17 with BMT of 0.48mm, 0.48mm, 0.42m and 0.8mm respectively are suitable to use with 1.5m span. HR-29 with BMT of 0.55mm can use up to 2.1m span. Custom orb 16 with minimum BMT of 0.42mm is recommended to use with span not greater than 0.9m. Klip Lok Optima is not recommended to use. From 10m-15m: It is suitable and economical to use Subtle square fluted with minimum BMT of 0.42mm with span below 0.9m. For Subtle Square fluted, Trapezoidal, HR-29 and Custom blue orb 17 with BMT of 0.48mm, 0.48mm, 0.42m and 0.8mm

respectively are suitable to use with 1.2m span. HR-29 with BMT of 0.55mm can use up to 1.8m span. Custom orb 16 with minimum BMT of 0.42mm is recommended to use with span not greater than 0.9m. Klip Lok Optima is not recommended to use.

Terrain Category II, height from 3m - 5m: It is suitable and economical to use profile Subtle square fluted with minimum BMT of 0.42mm for span below 1.5m. For trapezoidal and Subtle square fluted with BMT of 0.48mm can support the span up to 1.8m. Using HR-29 with minimum BMT of 0.42mm can use with 2.1m span. Custom orb 16 with minimum BMT of 0.42mm is recommended to use with span not greater than 1.2m. Klip Lok Optima is not recommended to use. From 10m-15m: It is suitable and economical to use Subtle square fluted with minimum BMT of 0.42mm with span below 1.2m. For trapezoidal, Subtle square fluted and custom blue orb 17 with BMT of 0.48mm, 0.48mm and 0.80mm respectively can use with 1.5m span. HR-29 with BMT of 0.42mm can use with 1.8m span. Custom orb 16 with minimum BMT of 0.42mm is recommended to use with span not greater than 1.2m. Klip Lok Optima is not recommended to use.

Terrain Category III, height from 3m - 5m: It is suitable and economical to use Subtle square fluted with minimum BMT of 0.42mm with spans below 1.8m. For trapezoidal, Subtle square fluted and Klip Lok Optima with BMT of 0.48mm, 0.48mm and 0.6mm respectively can support span up to 2.1m. HR-29 and Trapezoidal with BMT of 0.42mm and 0.48mm respectively can use up to 2.4m span. Custom orb 16 and custom blue orb 17 with minimum BMT of 0.42mm and 0.6mm respectively are recommended to use with spans not greater than 1.5m. Klip Lok Optima without edge stiffener is not recommended to use. From 10m – 15m: It is suitable and economical to use Subtle square fluted with minimum BMT of 0.42mm for the spans below 1.5m. For trapezoidal and Subtle square fluted with BMT of 0.48mm can support the span up to 1.8m. Using HR-29 with BMT of 0.55mm can use with 2.4m span. Custom orb 16 with minimum BMT of 0.42mm is recommended to use with span not greater than 1.2m. For Custom blue orb 17 and Klip Lok Optima with BMT of with 0.60mm can use with spans not greater than 1.5m. Klip Lok Optima without edge stiffener is not recommended to use.

Terrain Category IV, height from 3m - 5m: It is suitable and economical to use Subtle square fluted with minimum BMT of 0.42mm for the span below 1.8m. For trapezoidal, Subtle square fluted and Klip Lok Optima with BMT of 0.42mm, 0.48mm and 0.6mm respectively can support the span up to 2.1m. Using HR-29 and Trapezoidal with BMT of 0.42mm and 0.48mm respectively can use with 2.4m span. Custom orb 16 and custom blue orb 17 with minimum BMT of 0.42mm and 0.6mm respectively are recommended to use with span not greater than 1.5m. Klip Lok Optima without edge stiffener and Custom blue orb 17 with BMT of 0.6mm and 0.48mm respectively can use with 1.8m span. From 10m – 15m: It is suitable and economical to use Subtle square fluted with minimum BMT of 0.42mm for the span below 1.8m. For trapezoidal and Subtle square fluted with BMT of 0.42mm, 0.48mm respectively can support the span up to 2.1m. Custom orb 16 and custom blue orb 17 with minimum BMT of 0.42mm and 0.6mm respectively are recommended to use with span not greater than 1.5m. Klip Lok Optima with and without edge stiffener and Custom blue orb 17 with BMT of 0.6mm, 0.6mm and 0.8mm respectively can use with 1.8m span.

Consideration of Pull-out Failure of the Screws. All design pull out loads on the screws (5 screw fasteners per sheet) for all terrain categories with all roof types and different buildings conditions are lower than 3100N which is the minimum ultimate average pull out strength of the screws from purlin of 1.2 mm section thickness (Table 2). It is indicated using 5 screw fasteners per sheet for all type of roofing sheets connected to the purlin are safe under static loading.

References

[1] J. E. Minor, K. C. Mehta, and J. R. McDonald, Failures of structures due to extreme winds, ASCE J. of structural division, 98(11), 1972, 2459-2473.
[2] Narayanan.S and Mathews,M.S , 1996, Behaviour of Roofs of Industrial Structures to cyclonic Wind Loads, INCODIM, Chennai, January.
[3] Narayanan.S and Mathews,M.S, 2002, Cyclone Resistant Industrial Buildings Through Planning Design and Construction, 2nd World Engineering Congress, Kuching , Malaysia
[4] Narayanan.S and Mathews,M.S, 2002, Improving Cyclone Resistant Characteristics of Roof Cladding of Industrial Sheds In India, 2nd World Engineering Congress, Kuching , Malaysia
[5] Narayanan, S and Mathews, M.S,2003, Engineering Roofing Systems for Cyclone Resistance, International Seminar on Industrial Structures, Coimbatore, India, Proceedings, pp46.
[6] Narayanan, S and Mathews, M.S,2003, Wind Loads on Roof Claddings of Industrial Sheds in India, International Seminar on Industrial Structures, Coimbatore, India, Proceedings, pp47.
[7] S. Narayanan, Improving Cyclone Resistant Characteristics of Roof Cladding of Industrial Sheds, doctoral diss., IIT Madras, India, 1999.
[8] S. Narayanan and M. S. Mathews, Behaviour of Roofing Sheet Systems under Static Uplift Loads, IE, India, Civil, 2003, 216 – 222.
[9] M. Mahendran, Wind Resistant Low Rise Buildings in the Tropics, ASCE J. of Performance of Constructed facilities, 9(4), 1995 330-346.
[10] AS 1562.1-1992, Design and Installation of Sheet Roof and Wall Cladding.
[11] MS 1553-2002, Code of Practice on Wind Loading for Building Structure.
[12] BS 6399-2:1997, Loading for buildings. Wind loads (Technical Committee B/525, 1997)
[13] EC1-1-4:2005, Eurocode 1: Actions on Structures – General Actions – Wind Actions
[14] IS 875-3-1987, Design Loads for Buildings and structures (Bureau of Indian Standards).
[15] AS 4040.2-1992, Methods of Testing Sheet roof and Wall Cladding.
[16] Lysaght HR-29, Steel Roofing & Walling Profile. Technical Brochure.
[17] Custom Orb Custom Blue Orb, Traditional Corrugated Steel Cladding. Technical Brochure.
[18] Lysaght Klip-Lok Optima, The Widest Concealed-Fixed Cladding. Technical Brochure.
[19] Lysaght Spandek Optima, Trapezoidal Steel Cladding with Longer Spanning Capability. Technical Brochure.
[20] Lysaght Trimdek Optima, Subtle Square Fluted Steel Cladding with Extra-wide Span, Technical Brochure.
[21] AISC 325, Steel Construction Manual (American Institute of Steel Construction, 2011).
[22] Lysaght Spandek, Roofing and Walling Solutions. Technical Brochure.
[23] K. Seavhai and S. Narayanan, Roof Wind Pressures for Rectangular Low Rise Buildings Using MS 1553, EC1-1-4, BS 6399-2 and IS875-3, RASE 2013, December 13-15, India.
[24] S. Narayanan, and K. Seavhai, Comparative Study of Roof Wind Pressures for Permeable Buildings, CHUSER 2014, 7-9 April, Penang, Malaysia.
[25] S. Narayanan, K. Seavhai and T. Wee, Building roofing sheets systems for different wind zones in Malaysia, ICMSC 2013, December 12-14, Kollam, India.
[26] K. Seavhai and S. Narayanan, Roof Wind Pressures For Duopitch Roof Permeable Buildings, CHUSER 2014, 7-9 April, Penang, Malaysia.
[27] ASCE 7-10, Minimum Design Loads for Buildings and Other Structures.

Applied Mechanics and Materials Vol. 567 (2014) pp 583-588
© (2014) Trans Tech Publications, Switzerland
doi:10.4028/www.scientific.net/AMM.567.583

Implementation of Dam Safety Management Program in Malaysia: From Theory to Practice

LARIYAH Mohd Sidek[1,a], HIDAYAH Basri[1,b], SIVADASS Thiruchelvam[1,c]
RAHSIDI Sabri Muda[2,d], AZWIN ZAILTI Abdul Razad[2,e], and ZURAIDAH Ali[1,f]

[1]Centre for Sustainable Technology and Environment, College of Engineering, Universiti Tenaga Nasional, Jalan IKRAM – UNITEN, 43000 Kajang, Selangor, Malaysia

[2]TNB Research Sdn. Bhd. No. 1, Lorong Ayer Itam, Kawasan Institusi Penyelidikan, Kajang, 43000, Kajang, Selangor, Malaysia

[a]lariyah@uniten.edu.my, [b]BHidayah@uniten.edu.my, [c]sivadass@uniten.edu.my, [d]rashidi@tnbr.com.my, [e]azwin@tnbr.com.my, [f]zue@uniten.edu.my

Keywords: dam safety, emergency response plan, water security, risk

Abstract. Dam plays vital roles to mankind since the beginning of civilization. It serves the purpose for water supply, irrigation, hydropower and flood control. Despite the benefits of dam served over a decade, dams also poses high risk especially to the people downstream, as it may fail due to several failure modes, such as flood loading, earthquake and piping failure. History proved that dam failure has caused catastrophic impact to the people and environment. The dam owner is responsible to ensure that their dam is safe to the public and environment. In Malaysia, the key utility company, Tenaga Nasional Berhad has proactively played its role as the owner of the largest hydropower scheme by spearheading the effort of developing its own dam safety program. This paper revolves around the journey of TNB in developing an Emergency Response Plan (ERP) as part of their dam safety program.

Introduction

Dams are often referred to as monolithic hydraulic structures. Made of adequately impermeable materials, dams are built to create a storage compartment known as reservoir at the upstream to store water for various purposes. These hydraulic structures supply raw water to water treatment plants. In some parts of the world, dams are built as a control measure for flood mitigation. In Malaysia, dams contribute to irrigation and flood control mechanisms, on top of its predominant role in generating/ producing hydroelectric energy power source for local consumption.

Despite the aforementioned benefits, dams can also impose risks to the public. Once a dam is built, it requires constant maintenance and monitoring, regular safety inspections as well as scheduled rehabilitation in order to ensure its capability to function well. In line with current global awareness of water security, the aspect of dam safety has drawn increasing attention from the public as it constitutes the element of a country's national security. The consequences of dam failure may involve substantial downstream injury and property damage as well as catastrophic and long-lasting environmental effects [1].

This type of disaster can be devastating for people, community structures, environment, the country's economy, also the owner's business. Loss of human life is generally accepted as the most important consequence, therefore it often dominates dam safety decisions [2]. Previous disasters have exhibited that the repercussions of dam failures are directly related to the evacuation time available should failures occur. Thus, dam safety programs are vital to minimize the impacts of dam failure. Also, it is important to ensure that the dam owner and related agencies are ready, and equipped with the necessary knowledge and action plans in the event of dam failure.

In Malaysia, there are almost 51 recorded dams (60% of the dams are of earthfill type) under different ownerships [3]. To-date we have not experienced any failures with the dams. Nevertheless,

as dams in Malaysia continue to age, it is timely that we take notice of the conditions of these dams from the safety perspective. We could not afford to wait until failure occurs, which may jeopardize public safety.

Causes of Dam Failure

Dam failure disasters usually cause huge loss of lives, also destruction of properties and environment. For example, the failure of Vajont dam in Italy back in 1963 caused 2600 deaths. Similarly, the failure of Teton dam in America in 1976 led to hundreds of deaths and an estimated economic loss of approximately 1 billion dollars. Adding to the grim statistics would be the failure of Gouhou dam in China in 1993 which claimed 300 lives. Based on statistical analysis of 534 dam failures from 43 countries before 1974, it was reported that earth-rock dam failure accounted for the largest proportion of all failures which related to 49% overtopping, 28% seepage in dam body and 29% seepage in foundation [4]. Since dam failures may cause tremendous loss of lives and property, professionals who are experienced in the field of dam engineering have paid continuing efforts on design, construction, operation, and maintenance of dams to improve the safety of dams.

As commonly known, dams could provide many potential benefits such as supplying water for drinking, irrigation and industrial purposes. Other than that, dams are built to control floods, for generating hydroelectricity, recreation and navigation purposes. At the same time, dams can result in risks to the public. Once a dam is built, it requires constant maintenance and monitoring, regular safety inspections as well as rehabilitation when necessary to ensure its capability to function well. Dam failure can occur in several forms such a collapse or breach of the structure. Dams built with small storage capacity can contain enough volumes of water that could hold few or no reverberation. Large dams; however, can cause catastrophic disasters that could result in significant flooding downstream.

There are two reasons for dam failure: natural causes and human attributes. The former includes external causes such as heavy rains, hurricanes, earthquakes, while the latter are referred to as internal causes which are due to aging of materials, dam body defects, foundation defects, etc.. Human attributes include global climate warming which enhances atmospheric circulation which leads to extreme rainfall. Besides, internal causes include terrorist attacks or wars. Also, major construction projects can increase the potential threats causing dams to break. For instance, in the flood control system of 7 biggest rivers in China by 2009 [3], there were about 85 thousand reservoirs and 30 thousand more that are endangered, as well as various embankments measuring about 2500 thousand kilometers long.

In the event of a dam failure, the flow of water energy in the reservoir has a capability of causing rapid and unforeseen flood downstream. This could result in loss of lives, property damages as well as a devastating effect on the surroundings.

Emergency Response Plan

As being outlined by the Chief Government Security Office (CGSO) Malaysia which is an important arm under Prime Minister's Office of Malaysia, dams are considered as one of the 15 national strategic targets [5]. Therefore, it is essential to strengthen national strategy, timely response, and rapid recovery of this critical infrastructure in the event of an attack, natural disaster, or other types of emergency. Potential risks associated with the failure or disruption of these assets could result in significant destruction including loss of life (LOL), massive property damage, and severe long-term consequences.

Emergency Response Plan (ERP) is defined as the detailed contingency program that includes actions that have to be taken in order to control and/or minimize the impact of an emergency situation. This plan requires prompt corrective measures beyond the normal procedures in order to protect human lives, optimize damage and/or loss, minimize injuries, and to reduce the consequences of the

disaster towards physical assets as well as the environment. This plan is put into effect whenever a disaster that could threaten lives and the environment occurs. Disasters, either man-made or a natural calamity, can result in major damage within the surrounding area of the dams.

Establishing an ERP is a crucial requirement in order to prepare for a dam failure that extends beyond normal operating procedures. The purposes of an ERP are as follows:

- To reduce the risk of losing human lives and injuries
- To minimize damage to the properties
- To provide a plan of action in order to carry out repairs and reduce the impact of any such event where ever possible.
- To prevent escalation of losses.
- To assure fast response and quick recovery.

Development of Emergency Response Plan for TNB's Hydro Scheme

Many existing dams still pose increasing hazards to the downstream areas due to structural deterioration, inadequate design, faulty construction, and poor operation and maintenance. These dams are referred to as distressed dams. Looking from the stand-point of Malaysia, 20% of its dams are in the range which problems often begin to manifest [2]. Othman [2] also highlighted that It is also worth noting that the safety review of the oldest dam, Bukit Merah Dam (1906) was conducted in 1998 and the review for Sungai Perak Hydroelectric Scheme comprising the Temengor (1978) and Chenderoh (1930) dams was carried out in May 2003. Tenaga Nasional Berhad (TNB) is the owner of most of the larger dams in Malaysia. In fulfilling its corporate responsibility, TNB has initiated a programme to conduct dam break studies for all their hydropower dams. The first dam break study was conducted in year 2003 to 2005 for the Sg. Perak Hydro Scheme by Tenaga Nasional Berhad Research (TNBR) in collaboration with several specialists. In 2008, TNBR accomplished another dam break analysis which was for the Kenyir Power Station. Under both studies, the Emergency Action Plan (EAP) for Sg. Perak Hydro Scheme and Dam Safety Emergency Plan (DSEP) for Kenyir Power Station were developed.

The EAP and DSEP developed for both dams are an internal document of TNB designed to assist the dam personnel in identifying, monitor ing, responding to and mitigating dam safety emergencies. However, EAP does not cover warning dissemination to public and evacuation of populations at risk as these are the responsibilities of the local authorities. In view of this, TNB has decided to combine and integrate the two developed EAP and DSEP of Sg. Perak Hydro Scheme and Kenyir Power Station to a standardised format, termed the Emergency Response Plan (ERP). The ERP developed will be expanded to suit the local agencies as a local emergency response plan (LERP) and internal station personnel as a Internal Emergency Response Plan (IERP) under the Dam Safety Programme for its hydroelectric schemes.

Drill Exercise for a Typical Main Hydroelectric Dam

Drill exercise means a type of emergency action plan exercise that tests, develops, or maintains skills in an emergency response procedure [6]. It is usually conducted in house to ensure all personnel involved are able to perform their responsibilities during emergency. Apart from that, drill exercise also meant to verify other means of communication along with the owner's response.

As part of the requirements in the development and implementation of the Dam Safety Emergency Response Plan (ERP) for a major hydropower power station (HPS) located in Peninsular Malaysia, TNB Research Sdn. Bhd. (TNBR) in collaboration with Universiti Tenaga Nasional (UNITEN) had organized a drill exercise for personnel at HPS. A briefing on the drill exercise and was conducted on the 31st October 2012 and the drill exercise was conducted on the 1st November 2012 at the Control Centre of, HPS. The drill exercise was conducted based on the Internal Emergency Response Plan (IERP) recently developed and it involved only the TNB personnel.

The drill exercise was conducted to ensure all HPS personnel are fully cognizant of the procedures and actions required during a dam emergency. The drill exercise also intended to ensure that emergency procedures and equipment work properly. The objectives of the drill exercise were:

i. To promote emergency preparedness.
ii. To evaluate emergency operations.
iii. To evaluate emergency policies, plans, procedures & facilities.
iv. To train personnel in emergency management duties.
v. To demonstrate operational capability.

The drill exercise was conducted based on the "flood loading dam safety event" at selected dam. Three levels of scenarios, Dam Safety Event, Dam Safety Emergency and End of Event had been carefully planned to ensure that all actions to handle the flood loading event as described in the IERP would be executed.

A group of observer were appointed to evaluate the drill exercise. The evaluation results were presented to all the participants followed by active discussions for future improvement. The observation during the drill exercise includes timeliness of drill exercise, accuracy of actions and flow process, format and content of the Notification Forms, communication facilities and organisation of ERP team. Figure 1 shows situation at Emergency Command Centre during the drill exercise.



Figure 1 : Situation at Emergency Command Centre (ECC) during Drill Exercise

SOP Development Workshop with Local Agencies

During emergency situation, it is important to coordinate communication between dam owner and local agencies, in order to ensure smooth actions. During any dam safety event, the role of local agencies is to evacuate people living at the downstream of the dam to safe location.

Certain conditions may develop that will require warning and evacuation of the population at risk located downstream. The HPS ERP has been expanded to cover warning dissemination to local agencies and termed as Local Emergency Response Plan (LERP). The LERP describes the mechanism of notification and information dissemination between the dam personnel and the local agencies. The LERP shall comprise Standard Operating Procedure (SOP) of agencies for the warning and evacuation of the population at risk at the downstream.

A tabletop exercise is also planned under this program to coordinate dam personnel with local agencies. The purpose of a tabletop exercise is to facilitate a learning environment where response agencies can come together, face to face, to understand and talk through an integrated response to a specific emergency situation. Tabletops provide an ideal environment for learning, discussing, and identifying issues that may not be as obvious when players are physically separated as they are during drills and other exercises [7].

Prior to tabletop exercise for HPS, a workshop between all relevant local agencies was conducted to build specific products such as a draft plan or policy. The three-day workshop on the development of the agencies SOP, jointly organised by Majlis Keselamatan Negara (MKN) and TNB, was conducted on 18th to 20th June 2013 at a venue located near to the studied HPS. The workshop was attended by representatives from various government agencies (state and federal level) and TNB who have significant roles during occurrence of dam emergency at HPS. The main objective of the

workshop is to develop the SOP for the agencies at state level, which shall form part of the content in the LERP for HPS.



Figure 2 : SOP Development Workshop for a Typical Main Hydroelectric Scheme

Workshop Outcome

The workshop had been conducted successfully with positive responses and high commitments given by the agencies representatives. All of the agencies recognized the importance of LERP to reduce loss of lives and properties due to dam failure incident. The agencies also agreed with their role in the development of the SOP for warning dissemination, evacuation of population at risk as well as emergency actions to be executed. One of the key points was addressed by the participants was the importance of tabletop exercise to assess the efficiency of the SOP that has been developed for each agency.

Conclusion

The intention of the country to be a heavily industrialized nation depends on the ability to meet the required electricity demand. Therefore, hydropower plants play an important role to support the national grid which creates the confidence in the investors. However, it has been acknowledged that hydropower related structures mainly the dam can be seen as potential hazard to the community living nearby and also to the socio-economic status of the affected region. In relation to that, dam owners have to take greater responsibility to ensure the possible risks being mitigated or minimized. This also shows that the dam owner operates their business with greater sense of a good corporate citizen. Having an appropriate dam safety program in place will not only increases the public safety should any untoward incidence occur but also able to reduce the impact on economic strength and environment. Dam owners with the help of local authorities are instrumental in the formulation of an intended dam safety program. Learning from experience from this paper, we can construe that it is essential for conducting drill and tabletop exercise as preparation for the worst case scenario occurring from a dam failure. These two exercises evaluate and assess the readiness of the dam owner and local authorities in facing dam related disaster. The outcome of this dam safety program would be setting-up a better line of communication between agencies in order to save more lives during dam related emergency. Along the line of conducting this program, we anticipate the SOPs related to the drill and tabletop exercise could be further refined whenever any glitch is detected, which in turn improves any search and rescue mission. To enhance this dam safety program, the dam owner should consider to conduct community and stakeholders awareness program which will further reduce the risk to people living at the downstream of the dam. Life saving missions could only be successful if the relevant SOPs have been tested and refined with proper sense of coordination between the dam owner and all other critical agencies.

Reference

[1] McClelland, D.M., and Bowles D.S. (2002). Estimating life loss for dam safety risk assessment: A review and new approach, IWR report 02-R-3, Institute for Dam Safety Risk Management Utah State University, Logan.
[2] Othman, Z.I. (2006). Overview of dam safety in Malaysia. Jurutera. Institution of Engineers Malaysia.
[3] *ICOLD Bulletin* 111, Dam-break flood analysis, 1998.
[4] Lio, Y., Chen, L, Xu, M., Tong, X. Review of Dam-break Research of earth-rock Dam. 2012 International Conference on Modern Hydraulic Engineering. Procedia Engineering, 28(2012), 282-383.
[5] Chief Government Security Office (CGSO). (2013). Background. Retrieved 30 January 2013, from http://www.cgso.gov.my/~cgso/portal/index.php/en/faq.html
[6] Robert, J. V. Liability Emergency Action Plans and the Dam Safety Regulations. Dam Safety and Floodplain Management, Virginia Deparyment of Comservation & Reacreation http://www.handp.com/wp-content/uploads/Why-Your-EAP-Is-So-Important-Presentor-Rob-VanLier-PE-VADCR.pdf
[7]Information on http://www.damsafetyaction.org/TX/dam_owner/law.php

Applied Mechanics and Materials Vol. 567 (2014) pp 589-594
© (2014) Trans Tech Publications, Switzerland
doi:10.4028/www.scientific.net/AMM.567.589

Major Challenges to the Sustainable Operations of Construction Equipment in Malaysia

M. Waris[1,a *], M. Shahir Liew[2,b], M. Faris[3,c] and I. Arazi[4,d]

[1,2]Department of Civil Engineering, Universiti Teknologi PETRONAS, Tronoh, Malaysia

[3]School of Built and Environment, Heriot-Watt University, Putrajaya, Malaysia

[4]Department of Civil Engineering, National Defence University of Malaysia, Kuala Lumpur

[a]alwaris2002@yahoo.com, [b]shahir_liew@petronas.com.my, [c]M.Khamidi@hw.ac.uk

Keywords: Sustainable construction; onsite mechanization; non-road construction vehicles

Abstract. The growing considerations of people, profit and planet have emphasized the integration of sustainable concepts in the construction processes. The previous research in sustainable construction has underlined the issues pertaining to raw material and its manufacturing; design aspects along with the occupancy phase of a building life cycle. However, concerned over GHG emissions from the operation of non-road diesel equipment are still being ignored in the established literature. These non-road construction equipment consume fossil fuel and a serious threat for green environment. In addition to this, health and safety issues are also important concerns for the human well-being. Thus, mitigating these impacts are the important aspects of sustainable planning for onsite construction activities. A questionnaire survey was carried out to explore the contractors views towards potential challenges that are relevant with the growing attention of sustainability in construction sector. A group of large civil contractors of Malaysian construction industry were solicited through online survey to prioritize the potential barriers. The research findings presents a broader view and a number of challenges that inhibits the contractors for acquiring, adopting and implementing sustainable practices for onsite mechanized construction activities.

Introduction

The word 'sustainability' is demanding and an area under discussion by the fellow researchers and scientist of 21st century. Its realization is constantly being spreading and well accepted around the globe. There are many definitions and understandings of sustainability in the available literature. But it still circles around the three basic elements i.e. people, profit and planet [1]. The most popular and widely been accepted definition of sustainable development is given by United Nations (U.N.) Bruntland Commission which is stated as, *"satisfaction of present needs without compromising the ability of future generations to meet their own needs*" [2]. It is envisaged that the adoption of sustainable measures will improve the human civilization in the coming decades. In this new regime, scientist and engineers from all the disciplines are striving to meet the constraints of triple bottom line of sustainability. As a fact, sustainable development is considered as an important issue for the construction industry. Because construction activities are related to environmental hazards and pollution [3]. According to International Council for Building (CIB), the whole life cycle of building construction in European Union countries consumes a high proportion of energy consumption which is 40% of the total energy. Secondly, a large amount of waste, remnants are also produced which is equal to the 40% of all man-made waste [4]. Construction industry is also utilizing raw materials and thus depleting non-renewable resources.

The notion of 'sustainability' in construction is a focal point of many researchers. It has been reviewed from different perspective of a building life cycle. In a broader view, sustainable issues in construction are directly related to extraction and manufacturing of building materials, design, engineering methods, onsite construction, operation, demolition and recycling [5]. It is also known as "cradle to grave" life cycle. During all these construction phases, large quantities of natural

resources are consumed and pollutants are emitted to the environment. Therefore, it could not be possible to implement sustainable agenda without addressing all the major causes and sources of environmental pollutants. In this context, the previous research studies have more discussed about sustainable issues related to raw material and its manufacturing; design aspects along with the occupancy phase of a building life cycle. The aim of this research paper is to present important challenges which are being faced by the construction organizations in implementing the agenda of sustainability with reference to the onsite mechanized construction activities.

Sustainable Practices and its Associated Challenges

The need of GHG emissions control from the mechanized construction activities are gradually increasing in developed and industrialized countries. U.S. government has passed environmental regulations that mount pressure on construction companies to measure and reduce their carbon emissions from their construction equipment and vehicles. In this context, U.S. Environmental Protection Agency (EPA) has established procedures for non-road construction equipment (diesel engine) to comply with 'Tier System". This "Tier System" stipulates permissible emission rates for off-road diesel engines based on its manufacturing year and corresponding engine power [6]. Other initiatives are Voluntary Diesel Retrofit Program, Carl Moyer Program and Texas Emissions Reduction Plan. These are incentive based program that facilitates the contractors to adopt new technology and retrofit their equipment to cut down current level of emissions. These incentives were offered for those operators who promote the use of exhaust treatment devices, upgrade their engines, use ultra low sulphur, bio-degradable fuel and keep their equipments in good working condition [7].

According to previous research, fuel type, equipment idling, maintenance and its proper selection are highly related to GHG emissions. A similar study has proven that appropriate selection and planning of construction equipment can led to the decrease in GHG emissions. As the emissions produced by a diesel engine is a product of engine horse power, operating hours, its emission and load factor. Due to which, emissions from non-road equipment are directly linked with the equipment operating hours. Thus, if the equipment is running for a longer duration. It will consume more amount of fossil fuel and the corresponding rate of GHG is high [8].

The precedent research shows that the proper selection of construction equipment and machineries can also be helpful to reduce GHG emissions. As, GHG emissions are directly related to the operation of equipment. The more the operating hour of machinery, the higher the energy consumption and hence more will be the rate of emissions [8]. The Dutch government has announced sustainable measures for acquiring off-road construction equipment and vehicles. This standard has established actions and plans for confirming environmental sustainability in acquisition, operation, maintenance of construction equipment [9].

Mechanized equipment are also responsible for health and safety issues of workers. They may cause serious accidents, fatalities and injuries, if adequate safety precautions were not taken place [10, 11]. In United States, construction industry is also responsible for fatal accidents. A report has mentioned that it accounts 20% of on-duty fatalities and 12% disabling injuries [12]. Onsite health hazards and accidents are also been reported in UK construction industry. A report published by Health and Safety Executive (UK) showed concern over the high mortality rates due to construction accidents. The census showed these accidents accounts for more than 2800 deaths in the last 25 years [13]. Apart from this, safety and environmental priorities in under developed countries are also not up to the mark [14]. So, careful safety procedures and programs are vitals aspects of sustainable agenda in construction.

Methodology

This research is based on the qualitative and quantitative data analysis. First literature review was carried out to find the relevant information and secondary data. This includes refereed journal,

books, conference proceedings and online reports. This phase ended-up with a list of potential challenges that are considered important for sustainable operation of onsite construction equipment. The aim of quantitative data analysis was to explore the understanding of respondents towards onsite sustainability issues during mechanized construction practices. It also determined the ranking of potential barriers that inhibit the adoption of sustainable practices. For achieving this endeavor, a structured closed ended questionnaire was sent to the civil contractors of Malaysia. The survey questionnaire is a proven data collection methodology and it is highly effective option for gathering significant information. It is also considered as economical approach when the respondents are geographically distributed. The targeted respondents were selected by random sampling of Construction Industry Development Board (CIDB) G7 contractors. The Master Builder Association of Malaysia reported that despite a large number of registered civil contractors, only 12% are actually doing construction business [15]. In this view, the list of respondents were developed from the directory of CIDB Malaysia and it was dully been confirmed that respondents must engaged in construction activities. The class G7 comprises of large scale contractors in Malaysia and involve in complex construction projects including Mass Rapid Transit (MRT) projects, highways, bridges, railways tracks and etc. It is thereof, assumed that this group of contractors are well organized and concerned towards sustainable practices in construction. An online survey was initiated for collecting feedbacks and a total of 400 questionnaires were sent to the targeted respondents. The next section will discuss about the results and analysis of this survey.

Results and Analysis

The targeted respondents were rigorously follow-up for their feedbacks via emails and telephonic reminders. A total number of 86 feedbacks received which were completed satisfactorily. Hence, the makes a total response rate of 21.5%. This response rate is well acceptable in view of past researchers. This low rate of returned questionnaire is normally attributed to construction industry. According to precedent researchers, an average response rate in the construction management surveys are in the range of 20 to 30% [16, 17]. Hence, the current percentages of feedbacks are good enough for a meaningful analysis.

Background and Experience of the Respondents. There were responses from the diversified professionals of Malaysian construction industry. Among them were, project managers, construction managers, engineers, quantity surveyor and equipment managers. However, project managers accounted 35% of the total feedbacks. It has been observed from the feedbacks that majority of the respondents i.e. 61.3% are participating in roads and highways projects.

The demographic information of the respondents reveals that questionnaire was filled up by the well educated professionals. As the majority of them (88%) have their bachelor's degree in engineering. There were some other respondents who are more qualified and have postgraduate qualifications as well. The respondents who have acquired Master of Science and Master of Engineering degrees are 3.25% and 4.8% respectively. Beside educational background, the field experience of respondents is also considered as a benchmark for their eligibility to answer the questionnaire. The survey results show that respondents have ample professionals experience. This includes 43% respondents who have more than 20 years of experience while 36% have working experience between 11 – 20 years. This statistics is very much satisfactory in terms of contextual information of respondents. The data shows that participation level of respondents were mainly from the senior management level with sufficient academic qualification and experience.

Acceptance and Understanding of Sustainable Construction. The acceptance of sustainability importance in construction practices are fundamental steps towards a green environment. It's not been considered as individual efforts to achieve the goals. In fact, its importance emerges from the government and subsequently stimulates the private sector to show their responsibilities and commitments. In Malaysia, government has already taking initiatives to promote the agenda of sustainability. The tenth Malaysian Plan has emphasized for achieving socio-economic and

environmental sustainability in many industrial sectors including construction. The government is also initiating "MyCarbon" programme to encourage companies to measure their carbon emissions. So, achieving the agenda of sustainability is a two pronged strategy in which government and private sector are two faces of a coin. The respondents believed that it is an equal responsibility of both the stakeholders to go ahead with rational measures. Some of them have their opinion that the government must start some incentive and rebate programs that will motivate construction firms for adopting sustainable practices.

The survey has also determined the level of understanding of sustainable knowledge among the professionals of Malaysian construction industry. As these professionals are involved in key decision making process. So, their understanding and acceptance is very much important for sustainable construction. The survey results show a good percentage of professionals who have knowledge of sustainable construction. A total of 86% of respondents claimed that they have satisfactory knowledge, where as 14% stated that they insufficient awareness about sustainability.

Major Challenges for Sustainable Operation of Non-road Construction Equipments. The relative importance index method was used for determining the significance level of various challenges derived from the literature review. Relative Importance Index (RII) is a non-parametric technique widely used by construction and facilities management researchers for analyzing structured questionnaire responses for data involving ordinal measurement of attitudes. For this part of the questionnaire, the five-point likert scale of 1 to 5 (with 1 = strongly disagree, 2 = disagree, 3 = neutral, 4 = agree and 5 = strong agree) was adopted and the relative importance indices (RII) for each of the enablers was calculated by using Eq. 1.

$$RII = \frac{\sum w}{A \times N} = \frac{5n_5 + 4n_4 + 3n_3 + 2n_2 + 1n_1}{5 \times N} \quad \text{(Equation 1)}$$

Whereas, $\sum W$ represents the assigned weight of each variable, A shows the maximum weight and N is the sum of all respondents. The value of RII ranges from 0 to 1 with 0 not inclusive. The significance level of challenging factors increases with the corresponding high value of RII and vice versa is the case for less important factors. Table 1 shows the relative importance index (RII) for the challenges that were ranked from the respondent's feedbacks.

Table 1. Overall Ranking of Challenges

Description	RII	Rank
C_1: Lack of incentives from clients/government for adopting sustainable practices	0.80	1
C_2: Perception of additional cost being incurred in procurement of sustainable technologies	0.78	2
C_3: Limited availability of local suppliers who deal in sustainable technologies	0.77	3
C_4: Limited knowledge on green/sustainable technologies	0.76	4
C_5: Lack of information and guidelines for sustainable use of equipments	0.76	4
C_6: Lack of criteria for the selection of sustainable equipments and machineries	0.76	4
C_7: Perception of extra time being incurred in meeting sustainable requirements	0.74	5
C_8: Limited support from senior management	0.72	6
C_9: Unwilling to change the traditional working styles	0.72	6
C_{10}: Perception that environment friendly technology/equipments are inefficient	0.67	7

The major challenges in the operation of non-road equipment and vehicles were ranked in Table 1. It shows the overall ranking assign to each factor were perceived by the respondents. Based on the ranking, the three most important challenges were: (1) lack of incentive from the government (RII = 0.80); (2) cost of procurement (RII = 0.78); (3) limited availability of local suppliers that deals in green technology (RII = 0.77).

The factors were also analyzed by using Spearman's correlation test. This correlation test is a measure of strength between two variables. It determines the non-parametric relationship of two associated variables on an ordinal scale. As shown in Table 2, all independent variables C_1 to C_{10}

(i.e. challenges for sustainable operation of onsite construction vehicles) were significantly related to each other and have high degree of correlations and agreements.

Table 2. Spearman's Rho Correlation for Challenges to Sustainable Operation

	C_1	C_2	C_3	C_4	C_5	C_6	C_7	C_8	C_9	C_{10}
C_1	1.000	.545**	.354**	.436**	.405**	.542**	.690**	.298**	.452**	.604**
C_2	.545**	1.000	.480**	.536**	.481**	.539**	.415**	.533**	.284**	.242*
C_3	.354**	.480**	1.000	.742**	.667**	.509**	.376**	.572**	.453**	.263*
C_4	.436**	.536**	.742**	1.000	.773**	.537**	.561**	.510**	.487**	.449**
C_5	.405**	.481**	.667**	.773**	1.000	.564**	.612**	.494**	.618**	.486**
C_6	.542**	.539**	.509**	.537**	.564**	1.000	.717**	.568**	.460**	.406**
C_7	.690**	.415**	.376**	.561**	.612**	.717**	1.000	.511**	.563**	.631**
C_8	.298**	.533**	.572**	.510**	.494**	.568**	.511**	1.000	.452**	.342**
C_9	.452**	.284**	.453**	.487**	.618**	.460**	.563**	.452**	1.000	.662**
C_{10}	.604**	.242**	.263*	.449**	.486**	.406**	.631**	.342**	.662**	1.000

**. Correlation is significant at the 0.01 level (2-tailed).
*. Correlation is significant at the 0.05 level (2-tailed).

Conclusion

The concept of sustainability in mechanized construction is an innovative idea. From the available research data, it has been established that no study was undertaken specifically for determining the sustainable issues of onsite mechanization. Therefore, this research paper has investigated major challenges that were perceived by the respondents for the sustainable operation of non-road construction equipments and vehicles. It was found out that Malaysian civil contractors have good understanding with the concept of sustainable construction. However, the implementations of sustainable practices are still at moderate level with in the local construction industry. Analysis of the data further shows that the major challenges facing for sustainable operation of construction vehicles and equipments include: (1) lack of incentive from the government, (2) cost of procurement, (3) limited availability of local suppliers that deals in green technology, (4) limited knowledge on green/sustainable technologies, (5) lack of information and guidelines for sustainable use of equipments, (6) lack of criteria for the selection of sustainable equipments and machineries, (7) perception of extra time being incurred in meeting sustainable requirements, (8) limited support from senior management, (9) unwilling to change the traditional working styles, and (10) perception that environment friendly technology/equipments are inefficient.

These results of the survey can be taken as guiding steps for devising strategies at government and industry level for promoting sustainability agenda in construction.

References

[1] Labuschagne, C., and Brent, A.C. 2005. Sustainable project life cycle management: the need to integrate life cycles in the manufacturing sector. International Journal of Project Management, 23(2): 159-168.

[2] World Commission on Environment and Development. 1987. Brundtland Report. Our common future. Oxford University Press. UK.

[3] Rees, W.E. 1999. The built environment and the ecosphere: a global perspective. Building Research and Information, 27(5): 206-220.

[4] International Council for Building. 1999. CIB Agenda 21 on sustainable construction. Rotterdam.

[5] Persson, U. 2009. Management of sustainability in construction works. Phd thesis, Division of Construction Management, Lund University, Sweden.

[6] Avetisyan et al. 2012. Decision models to support greenhouse gas emissions reduction from transportation construction projects. Journal of Construction Engineering and Management, 138(5): 631-641.

[7] Bailey, K. 2005. Emission reduction incentives for off-road diesel equipment used in the port and construction sectors. ICF Consulting, Virginia.

[8] Kim et al. 2012. Greenhouse gas emissions from onsite equipment usage in road construction. Journal of Construction Engineering and Management, 138(8): 982 – 990.

[9] Dutch Ministry of Infrastructure and the Environment. 2011. Criteria for the sustainable procurement of heavy-duty motor vehicles and mobile equipment including maintenance services, Netherlands.

[10] Idro, G.I. 2011. Effect of mechanization on occupational health and safety performance in the Nigerian construction industry. Journal of Construction in Developing Countries, 16 (2): 27-45.

[11] Kartam, N. 1997. Integrating safety and health performance into construction CPM, Journal of Construction Engineering and Management, 123(2): 121-126.

[12] Loushine et al. 2003. Safety and quality management systems in construction: some insight from contractors. In Proceedings of the IJIE Conference, Las Vegas, USA.

[13] Health and Safety Executive. 2009. The Health and Safety Executive Statistics, UK.

[14] Mbuya, E, and Lema, N. M. 1996. Towards development of a framework for integration of safety and quality management techniques in construction project delivery process. International Journal of Quality, 14(5), 1-15.

[15] Bahaman, A. T. S. 2011. The key issues in the Malaysian construction industry: public and private sector engagement, Master Builders Association Malaysia, Penang.

[16] Akintoye, A, 2000. Analysis of factors influencing project cost estimating practice. Construction Management and Economics, 18(1): 77 – 89.

[17] Dulami et al. 2003. Organizational motivation and inter-organizational interaction in construction innovation in Singapore. Construction Management and Economics, 21(3): 307 – 318.

Applied Mechanics and Materials Vol. 567 (2014) pp 595-600
© (2014) Trans Tech Publications, Switzerland
doi:10.4028/www.scientific.net/AMM.567.595

Number of Bidders in Small and Medium Public Construction Procurement in Malaysia

Mohd Azrai Azman[1, a]

[1]Department of Quantity Surveying, Faculty of Architecture, Planning and Surveying, Universiti Teknologi MARA (UiTM), Kampus Samarahan 1, Jalan Meranek, 94300 Kota Samarahan, Sarawak, Malaysia.

[a]mohdazrai@sarawak.uitm.edu.my

Keywords: construction; procurement; public; bidding; auction; Malaysia; small; medium; contractor; microeconomics

Abstract: A competitive bidding price depends on a number of bidders who enter the auction. It increases the intensity of competition and it reduces the purchasing cost. The number of bidders is important because the cost of bidding may become a sunk cost. The probability to win an auction depends on the expected number of bidders. This affects bidders' decisions on whether to bid or not to bid. The research uses several statistical analyses to examine the 195 bidding data collected from Public Works Department of Malaysia. It finds that the project value, the distance from the project site to supply source and state region affect the number of bidders.

Introduction

The objective of this paper is to explore the factors that affect number of bidders in small and medium public procurement auction in Malaysia through empirical analysis on Public Works Department's bidding data.

Background

Public construction accounts almost 17% of total construction Gross Development Product (GDP) in Malaysia [1]. Since 2001, public construction contracted in huge percentage because of the economic liberalization agenda, as more investments for business facilities are made through private finances [2]. Although the public finance construction has been reduced, the value of public construction is at RM13, 881 million. In Malaysia, there are too many contractors. The country has the highest builders' licenses ownerships in the world [3]. All procurement of works more than RM 500,000.00 must be contracted through private sources using open bidding to encourage competitive prices [4]. In terms of numbers, small and medium contractors account 93% or 56,904 from 61,292 of the total registered contractors [5]. Table 1 shows *Pusat Khidmat Kontraktor* (PKK) registration of contractors according to bid values allowed and their paid-up capital. PKK is a public agency which facilitates the registration of indigenous contractors.

Table 1: Class of registration [5]

Class of registration	Bid value [RM]	Paid-up capital [RM]
A	> 10 million	600,001
B	5,000,001 – 10 million	400,001
C	2,000,001 – 5 million	100,001
D	500,001 – 2 million	35,001
E	200,001 – 500,000	17,501
F	Below 200,000	10,000

Competitive price in bidding

There is a connection between a large number of bidders and competitiveness of price. A large number of bidders implies a price reduction [6, 7]. In theory, if bidding process is according to merit, it improves price competitiveness [8]. These merits are firm capacity, experiences on similar projects and types of expertise. Skitmore [9] explains that selective bidding is also acceptable when reasonable number of bidders enters the bidding. Dell'Isola [10] says that bid price is 15% more expensive if only two bidders enter the bid. There will be a 10% bid price reduction when a large number of bidders are involved. A study made in the United States on 84 projects shows that a reduced number of bidders increase the bid prices. When only one bidder enters the bid, the price is roughly 15% more expensive. There will be a 4% reduction if one new bidder enters the bid. It reduces to 27% when eight bidders enter the bid. The reduction becomes stagnant when more than eight bidders enter the bid [6]. According to this study, the competitiveness of the bid could be maximised if at least eight bidders enter the bid. After that, the competitiveness may not improve.

Economic conditions and project value

Number of bidders depends on economic conditions. In good times, when there are plenty of works, fewer bidders would be interested to bid [9]. A study in Hong Kong shows that economic conditions measured by Tender Price Index (TPI) affect the number of bidders to bid [11]. It also depends on the nature of works. Bigger contractors are more competitive on large contracts. The small and medium bidders are obligated to small and medium contracts respectively [12]. Because of the competitive nature of bidding, one must know their competitors. It is known that they know their competitors through suppliers and subcontractors [13]. In Malaysia, a few public departments publicise the list of bidders during bid opening.

Location factor and technology

Brockmann [14] mentioned that it is unlikely for a construction contractor to place bid in an area which is far away from its operational office as this would increase its marginal cost e.g. transportation and logistics cost. In fact, a study shows that when it comes to supply-chains of construction products and methods, most contractors from rural areas need to find suitable suppliers in the urban area [15]. However, this brings to expensive cost of transportation for materials and machineries. Recent study shows that contractors from the Malaysian State of Kelantan have to bid projects outside the state when few number of projects available [16]. It has been a government procedure for small projects (Class F) to be awarded to local district contractors [4]. Small contractors prefer to use local labour that lives near the area because they are cheaper than foreign labour. However, they are less productive and difficult to adapt new technology [15]. In terms of cost estimating bias, it shows that variations in prices are greatly affected by the local market even though Peninsular Malaysia is small. Location plays an important role in deciding the cost estimation accuracy [17].

Arguments on competitive bidding

Large part of a bidding cost is un-coverable because it depends on the bidders' initiative to bid and it could be recovered if they won the contract [18]. Efficient bidders submit their bid aggressively because they have a higher probability to win but not inefficient firms [11]. In certain types of procurement i.e. traditional contract work in Commonwealth Countries, a public agency has to provide the costs of tender documents and consultations. Few costs are involved if the public agency chooses to use design and build construction. The public agency could only recover the documentation cost if more bidders submit bids. Based on neo-classical microeconomics, there is no certainty to say that when more bidders submit bids, the prices will be more competitive [11].

This is because the price reduction could also happen because of bidders' desperation to win the bidding. The probability of winning is less when more bidders enter the bidding and the chance to win is greater for First Price Auction if they bid at cost or they could bid higher when they know most bidders will place the bid higher for Average Bid Method [19]. This means that competitive bidding may not reflect back to bidder's competitiveness because it also depends on type of auctions.

Empirical analysis on bidding data

The analysis uses 195 data collected from PWD of Malaysia. The data is restricted to additional public school buildings because they are the highest number of data available. The data are limited to class contractors from B to E class which are considered small and medium class contractors according to PKK registration. All projects were restricted to the first half of 2007 and located in Peninsular Malaysia. Only three (3) variables are selected for the analysis i.e. state (of Kedah, Penang, Perak, Negeri Sembilan, Melaka, Johor, Pahang, Terengganu and Kelantan), project estimation in Ringgit Malaysia [RM] and the distance from project site to Central Business District (CBD) in Kilometre [km]. Natural logarithm transformation improves the linearity of the data (denoted as ln or LN).

Analysis shows that 165 or 89.67% out of 184 bidders had won the contracts to carry out construction businesses in their respective states. The following Table 2 is the descriptive statistics of data collected for selected states in Peninsular Malaysia. It shows that Terengganu and Kelantan have the highest number of bidders in terms of mean with 25 bidders per auction and Johor has the lowest with 11 numbers of bidders per auction. Pearson's coefficient shows that the correlation between project estimation and distance from site to CBD is not significant according to 2-tailed test ($p>0.05$). However, it finds that the relationship between distance from site to CBD and state is significant ($p<0.05$). The point-biserial correlation coefficient is $r_{pb} = 0.325$ and $R^2 = 0.106$. It means that distance from site to CBD accounts for 10.1% of the variability in the state.

Table 2: Number of bidders enters PWD bidding

State	Kedah	Penang	Perak	N9	Melaka	Pahang	Johor	Terengganu & Kelantan
Mean	18.28	19.17	15.40	13.50	13.69	14.80	11.02	25.82
Minimum	6.00	6.00	3.00	4.00	7.00	8.00	4.00	8.00
Maximum	33.00	26.00	28.00	28.00	21.00	27.00	26.00	50.00
Std. Deviation	6.11	6.99	6.60	6.89	4.44	5.24	4.74	12.08

One-way ANOVA examines the mean difference between states in terms of number of bidders which enter the bidding. Shapiro–Wilk test shows that a few states are not equally distributed ($p<0.05$). These states are Penang and Terengganu & Kelantan. This test is more applicable when examining the normality of data for a small sample size [20]. Levene test shows that ($p>0.05$) the data variances are equal, thus meeting the model assumption. This test also shows that statistic = 1.194, df1 = 7 and df2 = 187. ANOVA test shows that there is a significant difference between the mean number of bidders (F statistic = 7.99, $p<0.05$). According to post-hoc Turkey test, it shows that there are significance mean differences between the states ($p<0.05$). The states are Kedah vs. N9 and Johor, Penang vs. Johor, Terengganu and Kelantan vs. N9 and Johor. This goes to show that the number of bidders differ significantly according to states.

Figure 1 and Figure 2 displays the curve estimation based on linear and logarithmic functions. The observed points are number of bidders against project value and also distance from CBD. Figure 1 shows that when the value of project increases, the number of bidders increases. Statistical

analysis shows that (F=3.995, df1=1, df2=165, p<0.05) and (F=4.548, df1=1, df2=165, p<0.05) according to linear and logarithm function respectively. In addition, ANOVA result from Linear Multiple Regression (LMR) shows that there is a significant relation (p<0.05) between the project estimation and number of bidders (refer to Table 3).

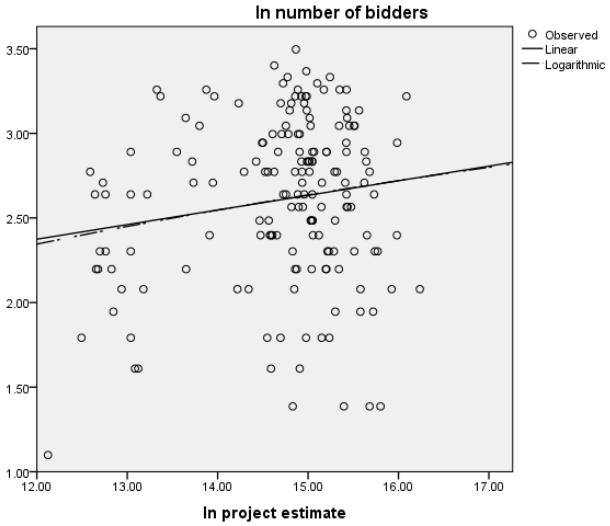


Figure 1: Natural logarithm number of bidders versus project estimate [RM]

Table 3: ANOVA result on number of bidders versus project estimate [RM]

Model		Sum of Squares	df	Mean Square	F	Sig.
1	Regression	0.957	1	0.957	3.995	0.047[a]
	Residual	39.535	165	0.240		
	Total	40.492	166			

a. Predictors: (Constant), ln project estimate
b. Dependent Variable: ln number of bidders

Figure 2 shows that if the site moves away from the Central Business District (CBD), the number of bidders decrease. Statistical analysis shows that (F=21.821, df1=1, df2=193, p<0.05) according to linear function. To further support this statement, the ANOVA result from LMR shows that there is a significant relation (p<0.05) between project estimation and number of bidders (refer to Table 4).

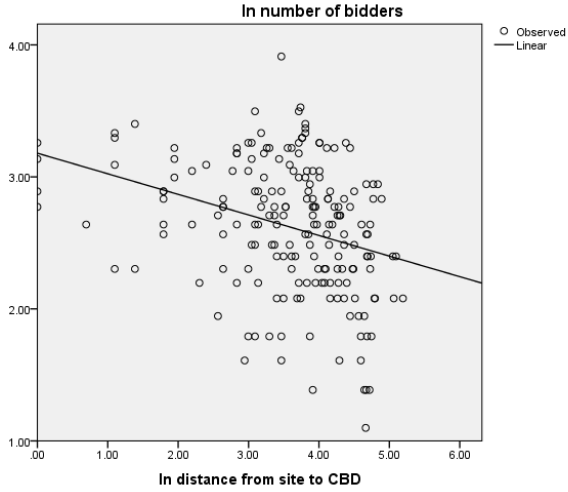


Figure 2: Natural logarithm number of bidders versus distance from site to CBD [km]

Table 4: ANOVA result on number of bidders versus distance from site to CBD [km]

Model		Sum of Squares	df	Mean Square	F	Sig.
1	Regression	4.977	1	4.977	21.821	0.000[a]
	Residual	44.021	193	0.228		
	Total	48.998	194			

a. Predictors: (Constant), ln distance from site to CBD
b. Dependent Variable: ln number of bidders

Results and discussion

It appears that regional factor (state), project value and distance from site to CBD are significant factors that affect the number of bidders entering a bidding. Some states in Malaysia have large potential bidders to bid particularly in the states of Terengganu and Kelantan. These two (2) states have a large number of registered contractors [21]. The state of Johor is the second highest state with registered contractors but has the lowest number of bidders entering bidding with the average of 11 per bid. This happens because the allocation of projects amongst the states in Malaysia is varied. Bidders in the State of Johor did not submit bids aggressively because there were a plenty of jobs. According to CIDB in the year 2007, public project value and number of projects in Johor is the highest among the selected states [1]. In addition, only a few bidders won the contracts outside the state where they operate. Proposed projects become more attractive to bidders when the project value increases. It suggests that it is more profitable to bid a larger project than a smaller one. Bidders are also very sensitive to costs which are related to distance. Result shows that less number of bidders when the distance from site to supply source is further from CBD. This affects bidders' profit margin when they have to incur more operational cost from travelling and transportation.

Conclusion

Small and medium class contractors appear to be more regionalist as they are more often to bid on projects located at the state where they operate. They are also concerned with the marginal cost in which operational cost increase as the result of the increase in distance from the project site to CBD. Bidders are also more willing to bid on more expensive projects even if the probability to win reduces when more bidders enter the bidding because bidders are attracted to its high pay-off of winning. Further research is necessary to quantify the effect of number of bidders on competitive prices.

Acknowledgments

The author acknowledges the support of the PWD of Malaysia, which contributed the data needed and Universiti Teknologi MARA for providing the funding. Ref. no: 600-RMU/DANA 5/3 (4/2013).

References

[1] CIDB, Construction Quarterly Statistical Buletin, in: CIDB (Ed.) CIDB, Kuala Lumpur, 2012.
[2] Italian Trade Agency, Overview of Malaysian construction sector, in: Italian Trade Agency (Ed.) Italian Trade Agency,, Rome, 2012.
[3] H. Adnan, C. Heap-Yih, M.H. Idris, N. Ahmad, African Journal of Business Management 5 (2011) 13364-13372.

[4] Ministry of Finance, Tatacara perolehan secara sebut harga, in: Ministry of Finance (Ed.) Ministry of Finance,, Putrajaya, 2009.
[5] Ministry of Works, Maklumat asas Kementerian Kerja Raya, in: Ministry of Works (Ed.) Ministry of Works,, Kuala Lumpur, 2012.
[6] P.G. Carr, Journal of Construction Engineering and Management 131 (2005) 1165-1172.
[7] I. Pegg, The effect of location and other measureable parameters on tender levels, Cost Study F33, BCIS 1983-4-219, BCIS, RICS, London, 1984, pp. 5-17.
[8] D.S. Drew, M. Skitmore, Construction Management and Economics 10 (1992) 227-247.
[9] M. Skitmore, Fundamental research in bidding and estimating, British/Israeli Seminar on Building Economics: The International Council for Building Research Studies and Documentation CIB W-55, Haifa, Israel, 1988.
[10] M.D. Dell'Isola, Architect's essentials of cost management, John Wiley & Sons, Inc., New York, 2002.
[11] S.C. Ngai, D.S. Drew, H.P. Lo, M. Skitmore, Construction Management & Economics 20 (2002) 473-482.
[12] D.S. Drew, M. Skitmore, Construction Management & Economics 15 (1997) 469-489.
[13] B.-L. Oo, D.S. Drew, G. Runeson, Construction Management & Economics December 2010 (2010) 1321-1329.
[14] C. Brockmann, Collusion and corruption in the construction sector, in: G.d. Valence (Ed.) Modern construction economics: theory and application, Spon press, Oxford, 2011, pp. 29-62.
[15] E.M. Kamal, R. Flanagan, Journal of Engineering, Design and Technology 10 (2012) 180-198.
[16] A. Omran, A.H.K. Pakir, M. Rmali, A. Termizi, University of Bucharest (2011) 159.
[17] M.A. Azman, Z. Abdul-Samad, S. Ismail, International Journal of Project Management (2012).
[18] J. Budde, R.F. Göx, Review of Accounting Studies 4 (2000) 5-13.
[19] P.G. Ioannou, R.E. Awwad, Journal of Construction Engineering and Management 136 (2010) 936-946.
[20] Hun Myoung Park, Univariate analysis and normality test using SAS, Stata, and SPSS, The University Information Technology Services (UITS) Center for Statistical and Mathematical Computing, Indiana University, Indiana, 2008.
[21] PKK, Direktori kontraktor - pertanyaan kontraktor (kepala dan subkepala), PKK, Putrajaya, 2013.

Applied Mechanics and Materials Vol. 567 (2014) pp 601-606
© (2014) Trans Tech Publications, Switzerland
doi:10.4028/www.scientific.net/AMM.567.601

Private Finance Initiatives (PFI): *Getting it right*

Abdullahi A. Umar[1, a], Noor Amila W. A. Zawawi[1,b], Abdul-Ganiyu Otairu[2,c], Idris Othman[1,d]

[1]Universiti Teknologi PETRONAS Bandar Seri Iskandar 31750 Tronoh Perak, Malaysia

[2] Insitu-Holmes Ltd, Suite C-59, 2nd floor, IDE Plaza Utako, Abuja, Nigeria

[a]abdulproject@yahoo.com, [b]amilawa@petronas.com.my, [c]rigatab@yahoo.com, [d]idris_othman@petronas.com.my

Keywords: PF2, PFI Skills, public sector capacity, infrastructures

Abstract: Recently, the UK government reformed the popular PFI into what is now referred to as PF2 after years of denying that the PFI was not delivering value for money. The reform is the result of many factors, principal of which was public sector PFI capacity deficiencies which has compromised the success of many projects. Therefore, this study set out to determine the most important PFI skills from the perspectives of public and private sector PFI practitioners and if there exists differences in opinion between the sectors. A survey of the most important PFI skills was conducted among practitioners during the course of 2 infrastructure conferences held in Kuala Lumpur, Malaysia. Factor analysis of 17 PFI skills produced 3 factor groupings that broadly explain the PFI skills requirements. These skills include Contract design skills, Contract Management skills, and Risk identification and Management skills. There was however no statistically significant difference in opinion between the public and private sector respondents.

1. Introduction

Governments' effectiveness has come to be assessed based on the performance of public infrastructure and services [1]. Infrastructure contributes to economic growth and development [2]. Infrastructure provision continues to be a problem despite the recognition of their importance to economic growth globally. Governments are increasingly finding it difficult to finance new infrastructure or renew existing ones due to paucity of funds. However, over the last two decades, there has been a shift private provision of infrastructure under the concept known as private finance initiative (PFI) [3]. But private provision has become bedeviled with increased renegotiations [4], failures and cancellations [5]. The problems among other things seems to reflect some form of weak PFI capacity within the client organisation; since the superior expertise of the private sector is not in doubt [6]. Several reports have pointed to this problem [7]; and consequently, governments have invested in training their procurement staff. But in a recent survey in the UK, only 48% of those who received training in 2010 agreed the training was useful to them. An effective capacity building strategy can only be successful when the exact skills requirements have been identified. Therefore, there is an urgent need to identify the specific types of skills required for the efficient implementation of the PFI. The objectives of the study are to determine and rank the most important PFI skills and also determine if differences in opinion exists between the public and private sectors on these skills.

2. PFI performance

The tales and experiences on PFI have not gone the way the proponents have espoused. Although there have been marginal improvements in services, these have been overshadowed by large scale failures. These failures include poor financial performance and benefits shortfall resulting from wrong demand forecasts [8]; service cuts, poor designs, and excessive profiteering by the private providers [9]. Basically, the high cost of PFI projects can be attributed to the high costs of capital given their high leveraged financing of 10%-90% equity-to-Debt ratio. For example, it was reported

that a 1% reduction in interest rates will generate an annual savings of £400 million pounds for the £40 billion PFI debts the UK [11]. HM Treasury (2012, p.6) in outlining the rationale for its current Private Finance 2 (PF2) argued that the PFI as currently practiced is bedevilled by many problems limiting value for money. In order to overcome these problems, the UK government has made structural changes to the PFI and now terms it Private finance 2 (PF2). One of the overarching missions intended to get the PF2 performing better than the PFI as stated by the document was the need to grow public sector PFI procurement capacity [7].

In an early National Audit Office report, the declining levels of skills among construction related disciplines, resulting from a declining enrolment into construction courses has been highlighted [12]. According to the report, this has had the effect of forcing both the public and private sector to rely on a declining skills pool. And the private sector always has an upper hand in securing the needed skills due to remuneration differentials between both sectors [13]. However, governments, aware of the need for expertise spend huge sums annually in training their staff. Despite these training efforts, in the UK for instance, about 80% of public sector staff admitted to having very significant skills gap in their departments, with 84% of these agreeing it was difficult recruiting and retaining skilled personnel, and a further 40% admitted that their departments were ineffective in maintaining information on their staff skills [14]. But what is even more disturbing is the fact that only 48% of those surveyed in the 2010 civil service people survey cited above agreed that the training they had was useful. This seem to suggests that the training do not match the skill requirements of their responsibilities, hence, there needs to be a focused attempt to identify the desired skills relevant to those in charge of PFI within the public sector.

2.1.Public sector Skills requirement under private provision

The change in duties which has befallen the public sector procurement staff under the PFI has been challenging, rather than specify inputs, they are now made to specify output requirements. This is a difficult task for public procurement staff and requires a diverse array of skills to achieve, unlike the private sector who are used to these types of forecasting 'games'. Skills are the knowledge and experiences required by an individual to carry out a task effectively [14]. It has been argued that public sector contracting skills has been very much discussed by researchers and the skills required to efficiently negotiate and manage long term PFI contracts are seriously lacking [10]. But, in order to properly determine the public sector skills requirements, it is pertinent to understand the roles of the public sector through a 'thematic analysis'. The PFI is a contract for service and using this as our basis for analysis, the public sector has the following duties under the PFI:

1. Identifying projects (sometimes, unsolicited private sector proposals are welcomed)
2. Specifying output requirements
3. Selection of preferred bidder
4. Negotiations with the preferred bidder
5. Financial structuring & financial close
6. Contract governance (regulating provisions through the life of the contract)

These seemingly simple tasks involve an array of professionals working together and contributing different skills. The public sector in particular has often been criticised for a lack of skills in key areas, heightened by staff 'churn', lack of transparency and consistency in practice, as well as a lack of best practice models [15]. The RICS faculty went further to list major skills that the public sector client requires for effective PFI procurement. They include skills in client understanding, process understanding, politics, negotiations, management, whole life-cycle costing, facilities management, construction, financial modelling, stakeholder management, Project management, Strategic planning, Contract management and people skills. In another study, contract management, commissioning and managing advisers, risk identification and management, and commercial skills were argued as lacking in the public sector [16]. The importance of stakeholder management skills has also been growing over the years [18]. This is because, even after successfully contracting with the private sector, failure to recognise and take into cognisance the many stakeholders has led to

protests which turned violent in some cases resulting in the failures of water projects in Buenos Aires (Argentina), Cochabamba (Bolivia); buy-back of the Skye toll Bridge (UK). The failure of Enron also led to the loss of billions of dollars by shareholders, billions in employees' retirement benefits and jobs. All these failures have had serious adverse effects for society and governments at large. While society lost money, investors lost confidence in the government regulatory oversight.
Furthermore, inadequate capacity results in over reliance on consultants whose advice may not be binding irrespective of the outcome of their purported expert opinions. They are also a drain on public budget. For example, in the years 2009-2010, the UK government spent £789 million on consultants, and an additional £215million on interims [19]. Contract design is at the heart of effective risk management and transfer. Effective contract design was responsible for saving the Portland General Electric (PGE) of the state of Oregon (US) from going down with its parent company-Enron-due to proper ring-fencing mechanism introduced into the contract. However, other Enron projects in India (Dabhol power project) and Africa (Cameroun's SONEL) which were not ring-fenced could not be continued.
Even the World Bank, which is seen as the most prominent advocate for PFI has acknowledged that government still needs to retain sufficient expertise to monitor the performance of the private sector and enforce its obligations [20]. It has been argued that the public sector has poor expertise in negotiations and contract governance [21]. While on the other hand contract management and monitoring has been argued as a very crucial part of achieving the goals of PFI projects (Grimsey & Lewis, 2004). In order to achieve success in PFI procurement, Staff with experience in complex procurement having a strong mix of commercial, financial, technical and sector specific experience are required [22].

3. RESEARCH METHODOLOGY

Published literatures on PFI were reviewed from which PFI related skills were identified and a 5 point Likert scale-based questionnaire developed. The respondents were requested to tick the degree to which they agreed that a particular skill was important on a scale of 1-5. 1 represents strongly disagree while 5 denotes strongly agree and 3 the mid-point signifies neutral. The questionnaires were distributed to delegates who attended 2 infrastructure-based conferences at different times within the span of 3 months (April - June). Out of the 165 questionnaires distributed, about 43 respondents completed and returned their questionnaires. Although the response rates seem low (26.06%), it is however comparable with the 21% (31 responses) [23]; and 9% [24]. The resulting data were then analysed using IBM SPSS statistical software version 20. The results are presented below and inferences drawn.

4. RESULTS AND DISCUSSION

It is pertinent to assess the reliability of any scale to be interpreted and the greater the consistency in responses among items the higher coefficient alpha will be. The reliability test returned an alpha =.961 which according to the classification by George & Mallery [25] is considered excellent. The validity of a scale is simply the square root of its reliability coefficient [26]. Consequently the validity for this scale is .98 which is also considered excellent. The respondent profiles shows that there were 27 public sector respondents and 16 private sector respondents. The regional profile also shows that only 1 respondent originated from Europe, 2 from North America, 5 from the Middle East, 7 from Africa, 28 from Australasia (Asia & Pacific) while no respondent from Latin America filled the questionnaire.
A normality test was conducted to determine the nature of the distribution, the *Kolmogorov-Smirnov* and *Shapiro-Wilk* tests both returned a statistically significant result (sig=.001) indicating the distribution is different from a normal distribution [27]. This means non-parametric tests would be employed for the analysis. There was also no significant difference between the mean and the 5% trimmed mean (mean=4.11, 5% trimmed mean= 4.20), indicating that extreme scores did not

have any influence on the mean (Pallant, 2005). The mean score of the variables was used to rank them as shown on table 1 below:

Table 1: Ranking of PFI procurement skills

	PFI procurement skills	Mean score
1	Stakeholder management skills	4.35
2	Contract management skills	4.28
3	Risk identification & management	4.23
4	Bid evaluation skills	4.23
5	Regulatory governance skills	4.21
6	Output specification skills	4.21
7	Negotiation skills	4.16
8	Business analysis skills	4.16
9	Sector-specific skills	4.16
10	Demand forecasting skills	4.09
11	life-cycle costing skills	4.07
12	Environmental/sustainability skills	4.05
13	Financial engineering/modelling	4.02
14	Human Capital /organisation audit skills	4.00
15	Contract design skills	3.98
16	Managing advisers	3.95
17	Design/Technical skills	3.77

Stakeholder management (Mean Score= 4.35) ranked as the most important skill from table 1 above and since there was no significant difference across sectors, this means that the importance of stakeholders is increasingly being recognised across both sectors. This is consistent with the arguments advanced by [17] & [18]. Contract Management skill (Mean Score= 4.28) was ranked in second place showing that post implementation monitoring is important to the success of PFI projects. Risk Identification & Management, and Bid Evaluation Skills (Mean Score= 4.23) tied in third place, these two skills are complimentary because the whole essence of evaluating bids is to ensure value for money and appropriate risk sharing and transfer. Risk management runs throughout the duration of the contract and the risk profile of the project changes according to the stage of the project. However, environmental/sustainability skills (Mean score=4.05) and financial engineering skills (Mean score=4.02) did not rank very well, being in the bottom half of the table. Given the importance climate change is gaining across the globe, it is surprising that sustainability skills ranked so low. Financial engineering on the other hand has attained significant importance under the PFI given the impact of issues such as the use of derivatives in financing operations, refinancing, and excess profitability. But both skills, despite their perceived importance were ranked in the bottom half of the table. However, a critical look at the values shows that despite the rankings, the mean score values for both skills were very close to the mean of the entire distribution. Perhaps, the most disappointing performance came from Contract design skills (Mean score=3.98), contract design is at the heart of PFI and most projects which have ran into problems did so because the contract was not properly designed to shift the right risks to those capable of managing them. The importance of good contract design came to the fore during the Enron collapse, while Enron's PGE contract in Oregon (U.S.A) was ring-fenced protecting it from the problems of Enron, their Dabhol (India) & AES-SONEL (Cameroon) could not go on because ring-fencing was not built into the contract.

A final procedure performed on the data was the *factor analysis*. Factors are a more efficient way of representing outcomes in certain studies than individual variables [26]. But factorability had to be determined using the *Kaiser-Meyer-Olkin's* (KMO) measure of sampling adequacy and *Bartlett's test of sphericity* to ensure the factorability of the variables. The KMO value must be greater than 0.6 and *Bartlett's test of sphericity* must be significant to qualify for factor analysis [27]. For our

data, the KMO was 0.844 while the *Bartlett's test of Sphericity* was significant (sig=.001) suggesting that the data was factorable. The 3 factors that summarise all the individual variables using the identified 'thematic' relationships are:

1) Contract design
2) Contract management
3) Risk Identification & Management

Consistent with [6]; [16]; and [21] contract management; can be seen as a very important factor in the success of PFI projects. Contract design, which is used to allocate and share risks, rewards and responsibilities also plays a vital role in achieving better outcomes for both parties in a PFI contract. Finally, risk management, which is a continuous process occurring throughout the life of the contract has also been shown to be critical. Expertise in the above skills is very essential for the success of the proposed PF2 as the PFI would now be called.

The Mann-Whitney U non-parametric test for two independent samples was used to test differences across sectors, and it returned a non-significant result (sig=.230). This suggests there was no statistically significant difference between both sectors on their ranking of the most important PFI skills. While it may be surprising that both sector that have different goals and objectives within the framework of the partnership do not differ regarding the desired skills, it should be noted that professional perspectives often remain the same irrespective of sector affiliations.

5. CONCLUSION

Contracting the private sector to provide public infrastructure and services would continue for a long time to come. This situation is made even more certain given the present global economic outlook which is not showing signs of strong improvements. Both developing and developed countries are all facing similar economic troubles creating a stiff competition for the available private sector capital for infrastructure investments. The good news is that private capital is environment-conscious; therefore, if developing countries can develop the requisite capacity, they can be strong contenders for the limited private capital for infrastructure investments. For the 'new' PF2 to succeed, it is pertinent that issues of PFI capacity in the public sector be urgently resolved.

REFERENCES

[1] Renee Kuriyan and Isha Ray, "Outsourcing the State? Public-Private Partnerships and Information Technologies in India," *World Development, 37 (10)*, pp. 1663-1673, 2009.

[2] Louis P. Cain, "Historical perspective on infrastructure and US economic development ," *Regional Science and Urban Economics, 27 (2)*, pp. 117–138, 1997.

[3] Peter Fewings, *Construction Project Management: An Integrated Approach*. Abingdon: Taylor & Francis, 2005.

[4] J.Luis Guasch, Jean-Jacques Laffont, and Stephane Straub, "Renegotiation of concession contracts in Latin America: Evidence from the water and transport sectors," *International Journal of Industrial Organization, 26*, pp. 421-442, 2008.

[5] Antonio Estache, "PPI partnerships versus PPI divorces in LDCs: (or are we switching from PPPI to PPDI?)," Washington D.C, 2005.

[6] Darrin Grimsey and Mervyn K. Lewis, *Public-Private Partnerships: The Worldwide Revolution in Infrastructure Provision and Project Finance*. UK: Edward Elgar Publishing Ltd, 2004.

[7] HM Treasury, "A New Approach To Public Private Partnerships ," London, 2012.

[8] Bent Flyvbjerg, "Survival of the unfittest: why the worst infrastructure gets built—and what we can do about it," *Oxford Review of Economic Policy,25(3)*, pp. 344–367, 2009.

[9] Veronica Vecchi, Mark Hellowell, and Stefano Gatti, "Does the private sector receive an excessive return from investments in health care infrastructure projects? Evidence from the UK," *Health Policy,110* , pp. 243-270., 2013.

[10] House of Commons Treasury Committee, "Private Finance Initiative, Seventeenth Report of Session 2010–12, HC 1146 ," London, 2011.

[11] NAO, "Modernising Construction," London, 2001.

[12] Cesar Cordova-Novion and Stéphane Jacobzone, "Strengthening the Institutional Setting for Regulatory Reform: The Experience from OECD Countries, Working Papers on Public Governance, No. 19 ," Paris, 2011.

[13] NAO, "Identifying and meeting central Government's skills requirements," UK, 2011.

[14] RICS Project Management Faculty, "Project Management and the PFI," UK, 2003.

[15] NAO, "Commercial skills for complex government projects," London, 2009.

[16] Terry H.Y. Li, S. Thomas Ng, and Martin Skitmore, "Conflict or consensus: An investigation of stakeholder concerns during the participation process of major infrastructure and construction projects in Hong Kong," *Habitat International, 36*, pp. 333-342, 2012.

[17] NAO, "Central Government's use of Consultants and Interims," London, 2010.

[18] World Bank. (2011) World Bank PPP. [Online]. http://ppp.worldbank.org/public-private-partnership/overview/ppp-objectives

[19] Julie De Brux, "The Dark and Bright Sides of Renegotiation: An Application to Transport Concession Contracts," *Utilities Policy*, pp. 77-85, 2010.

[20] NAO, "From Private Finance Units to Commercial Champions: Managing complex capital investment programmes utilising private finance- A current best practice model for Departments," UK, 2010.

[21] D.G. Proverbs, G.D. Holt, and P.O. Olomoaiye, "The management of labour on high rise construction projects: an international investigation," *International Journal of Project Management, 17 (3)* , pp. 195–204, 1999.

[22] J. R. Graham and C. R. Harvey, "The theory and practice of corporate finance: Evidence from the field," *Journal of Financial Economics, 60 (3)*, pp. 187–243., 2001.

[23] D. George and P. Mallery, *SPSS for Windows step by step: A simple guide and reference. 11.0 update (4th ed.).* Boston: Allyn & Bacon., 2003.

[24] Neil J. Salkind, *Statistics for People who (think they) Hate Statistics, 2nd Edition*. United States of America: Sage Publications Inc., 2004.

[25] Julie Pallant, *SPSS Survival Manual: A Step by Step Guide to Data Analysis Using SPSS*. Australia: Allen & Unwin, 2005.

Applied Mechanics and Materials Vol. 567 (2014) pp 607-612
© (2014) Trans Tech Publications, Switzerland
doi:10.4028/www.scientific.net/AMM.567.607

Resource Management in Construction Project

Idris Othman[1], Madzlan Napiah[1], Narayanan Sambu Potty[1]

[1,] Civil Engineering Department, Universiti Teknologi PETRONAS, Malaysia

[1]idris_othman@petronas.com.my

Keywords: Construction Project Management, Resource Management, Manpower, Machineries, Materials

Abstract: Construction projects experience various problems and complex factors such as cost, duration, quality and safety. Construction sector is diverse as it contains sub-contractors, contractors, consultants, architects, owners, and others. The aim of this paper is to identify and analyze resource management issues in construction project. Other than that is to ascertain the significance of the resource management as one of the key element in construction project success. A literature review and a questionnaire survey were done for data collection and analyzed using Relative Importance Index and Cronbach's alpha. The questionnaires were distributed to the team members of KLIA 2 – New Low Cost Terminal Project: Client, Architects, Main Contractor, and Sub-Contractor. The findings revealed that dependent on foreign workers to respond to the high demand of skilled workers, weather condition affecting machineries/equipment-work-related performance and weaknesses in quality assurance for the supply of construction materials should be given serious attention in order to ensure the productivity and financial performance of the projects.

Introduction

Project management involves managing the resources – workers, machines, money, materials and methods used. Resources are the means of production needed to complete a project. In light of the increasingly challenging construction environment, companies are taking a closer look at their operations, searching for untapped profit-boosting opportunities and new sources of competitive differentiation. Stakeholders are discovering that their process for managing tools / machines / equipment, materials, labor, methods, costs and consumables – a process often referred to as "Construction Resources Management" – is broken.

One of a must criterion to have a good project management in construction is the resources management must enthusiastically pursue to achieve the efficient utilization of equipment, material, labor and method. The use of new and advance equipment and innovative methods has made possible wholesale changes in construction technologies nowadays. Material handling including procurement, inventory, shop fabrication and field servicing requires specific attention to reduce cost. As for those who are responsible for cost control of constructed facilities, improvement of labor productivity would be their major and persistent concern[1].

Problem Statement

Construction is one of the industries that use large scale equipment, materials and labor compared to other industries. Stakeholders that involved in managing the resource management in construction project all differ in terms of education, experience and view. According to the studies previously done by other researchers on various construction projects worldwide, it shows that problems and issues regarding the resource management in construction project influenced the performance and success of the project. Applicable methods of improvement on these issues are needed in order to improve the performance of the project.

Objectives of the Study

The objectives of the study as below:-

- To identify resource management issues in construction project.

-To analyze the most important factors contributing to resource management in construction project.

Scope of the Study

The scope of this study is on resource management in the construction site. It covers three (3) components of resources: manpower/labor, machineries/equipment, and material. The study will focus on construction project and a case study will be done at "Kuala Lumpur International Airport 2 – New Low Cost Terminal Project" (Package TB001).

Literature Review

Manpower

Manpower is one of the most constrain challenge facing by Malaysian construction industry as it rely too heavy on large number of foreign labor workforce. Economic Report 2011/2012 stated that total employment of foreign labor force was about 12,645,700 while 768,800 were involved in construction sector. There is a heavy dependency of foreign workers in local construction industry as it has not successful in attracting potential local youth to involve in this sector. This is mainly because of the 'Dirty, Dangerous, Difficult' image of construction industry given to the public[1]. Therefore, the gap has to be filled by foreign workers. High rising in standards of living and economic growth in Malaysian society created a high demand on construction activities. At the end, huge amount of foreign workers were imported into our country as unskilled or semi-skilled labor which doing some manually jobs. Meanwhile, adoption of modern technology and training for the laborer would increase productivity. Shehata and El-Gohary[2] conducted a case study in construction project in Egypt to provide a guide for necessary steps required to improve construction labor productivity and consequently, the project performance.

Machineries / Equipment

In order to increase job-site productivity, it is beneficial to select equipment with proper characteristics and a size most suitable for the work conditions at a construction site [3]. Alinaitwi et al.[4] found that among the top ten factors affecting construction productivity in Uganda are lack of tools/ equipment, tools/ equipment breakdown and harsh weather conditions. Unavailability of equipment is a procurement problem that can affect the project completion [5]. Occasionally the lack of equipment may cause major design variations or adjustments to project scheduling to accommodate the replacement.

Materials

Decisions about material procurement may also be required during the initial planning and scheduling stages. The availability of materials may greatly influence the schedule in projects with a fast track or very tight time schedule: sufficient time for obtaining the necessary materials must be allowed. In some case, more expensive suppliers or shippers may be employed to save time [3]. Material procurement and storage on construction sites need to be properly planned and executed to avoid the negative impacts of material shortage or excessive material inventory on-site." Deficiencies in the supply and flow of construction material were often cited as major causes of productivity degradation and financial losses. Efficient planning of materials procurement and storage on construction sites can lead to significant improvements in construction productivity and project profitability. Overlooking these critical interdependencies between material procurement

and site-space availability can lead to serious project problems including material shortages, improper storage, poor and unsafe site layout, and productivity losses [6]. Koskela and Howell [7] recognize that maintaining a comprehensive up-to-date plan is difficult. Therefore, being based on an out-of-date plan, the tasks pushed to execution often cannot be performed, as they lack either predecessor tasks or other inputs.

Methodology of the Study

Literature Review

The literature review is the first phase of research in order to obtain the information and knowledge of the resource management in construction project. It was done based on the past researches and case studies conducted by the previous researchers. At this first phase, research was carried out based on documentation research such as books, conference tests, bulletin, project papers and mostly journals.

Data Collection

Data collection was done using qualitative research which concerned with testing the theory as per stated in the objective. The aim of data collection was to gather the information regarding the topic, resources management and the resources itself in construction projects. The data collection was carried out by two ways as following:-

1. Questionnaire
2. Case Study

Data Analysis

Relative Importance Index (RII)

The Relative Importance Index (RII) was used to decide various professionals' opinions of the RII in construction projects. RII is calculated as stated below [8]:

Relative Importance Index Formula:

$$\mathrm{RII} = \frac{\sum W}{(A * N)}$$

Where,

W = weights given to each factor by the respondents and will ranges from 1 to 5

A = highest weight

N = total number of respondents

Cronbach's Alpha using SPSS Software

Cronbach's alpha is a coefficient that describes how well a group of items focuses on a single idea or constructs. It is calculated among the set of variables used in the factor analysis to determine the reliability of those questions for measuring a single construct. For this study, Cronbach's alpha analysis was done using Statistical Package for the Social Sciences (SPSS) software.

Result and Discussion

Twenty organizations that involved in construction of Kuala Lumpur International Airport 2 – New Low Cost Terminal Project were contacted out of which twenty eight individual respondents responded. Only respondents with minimum qualification of Diploma were approached for answering the questionnaire. This was done to preserve the quality of the opinion gathered in the survey. The results of all the manpower/ labor issues in construction project as ranked per relative importance index analysis have been gathered in Table 1 below:-

Table 1: Resource Management Issues in Construction Project for Manpower/Labor

Rank	Resource Management Issues in Construction Project	RII
1	Construction has to depend on foreign workers to respond to the high demand of skilled workers.	0.771
2	The construction industry lacks appeal to young, potentially skilled workers.	0.714
3	Shortage of skilled workers.	0.700
4	Occupational stress/Workplace stress – influence in labor performance. (Example of stressful events: firings, altered responsibilities, trouble with bosses, variation of working hours or conditions, retirement and vacations).	0.686
5	Communication between labors – different spoken language causes misinterpretation of information.	0.643
6	Lack of skill and low level of initiative - labor-related factors causing low productivity.	0.629

Based on the result in Table 1, most of the respondents agreed that construction has to depend on foreign workers to respond to the high demand of skilled workers while least agreed that lack of skill and low level of initiative - labor-related factors causing low productivity.

Table 2: Ranking of Resource Management Issues in Construction Project for Machineries/ Equipment

Rank	Resource Management Issues in Construction Project	RII
1	Weather factor – effecting machineries/equipment-work-related performance and efficiency.	0.714
2	Type and size of machineries/equipment – appropriate selection in accordance to works to be executed.	0.700
3	Financial burden in the acquisition phase - contractors are invariably plagued with huge capital investment.	0.671
4	Procurement of major construction machineries/equipments - causes high delivery time uncertainty, which disrupt the construction schedule.	0.657
5	Equipment mobility - machineries/equipments are not available at the correct location and time.	0.629
6	Poor machine maintenance practices – causes cost and time exceeds the designated budget or schedule on projects.	0.614

Table 2 shows machineries/ equipment issues in construction project as ranked per relative importance index analysis. Most of the respondents shared the same opinion that weather factor can be affecting machineries/equipment-work-related performance and efficiency, and financial burden happened in the acquisition phase where contractors are invariably plagued with huge capital investment. Least agreed that poor machine maintenance practices cause cost and time exceeds the designated budget or schedule on projects.

Table 3: Ranking of Resource Management Issues in Construction Project for Materials

Rank	Resource Management Issues in Construction Project	RII
1	Quality assurance - deficiencies in the supply and flow of construction material causes productivity degradation and financial loss.	0.771
2	On site managing - improper handling and managing materials on site during a construction process influence the total project cost, time and the quality.	0.700
3	Material supply - required materials are not available at the correct location and time.	0.686
4	Incompetence suppliers – affect materials delivery and quality.	0.671
5	Material shortages – due to being based on an out of date plan, including last minute improvisation. (material ordered very late – buffer at supplier, material ordered very early – buffer at site)	0.643
6	The size of construction site and material storage location - labors require extra time to move materials.	0.629

Table 3 shows materials issues in construction project as ranked per relative importance index analysis. Most of the respondents agreed that weaknesses in quality assurance where deficiencies in the supply and flow of construction material causes productivity degradation and financial loss. Slightest agreed that material shortages – due to being based on an out of date plan, including last minute improvisation is a serious issue.

Cronbach's Alpha Analysis

Cronbach's alpha is commonly used as a measurement of reliability of a set of questions in a survey instrument. Generally a questionnaire with value of 0.8 is considered reliable. The closer the value to '1', the more reliable the questionnaire is. If it is above 0.7, it is adequate and anything above 0.8 is considered optimal. Using the Statistical Package for the Social Science (SPSS) software, the value of Cronbach's alpha for questionnaire is obtained as shown in Table 7.

Table 7: Cronbach's Alpha

Cronbach's Alpha	Cronbach's Alpha Based on Standardized Items	N of Items
0.885	0.887	36

This questionnaire attained 0.885 which is considered acceptable and reasonably high level of reliability. To prove the reliability or Cronbach's alpha score for particular set of item from the questionnaire, the Inter-Item Correlation Matrix is referred from the SPSS analysis. The correlation above 0.3 or 0.4 between these items can be considered as an appropriate level. If the correlation value is below 0.3 or nearly zero or negative, it is considered unacceptable as the item is not correlating well with the others.

Conclusion

It can be concluded that resource management in construction project need to be further improved and monitored frequently for its effectiveness. Members in the project team had the awareness

about resource management in construction project. However, improvements in many aspects need to be considered in order to ensure the effectiveness. Responses from the respondents shows various opinion and views towards the subject matter. It helps to rank the most common issues pertaining resource management specifically manpower/ labor, machineries/ equipment and materials management in the construction project. This rank can help future construction project with expected issues that might be faced during the construction work. Given that the feedbacks of the survey came from the construction team, all members are aware that the issues of dependent on foreign workers to respond to the high demand of skilled workers, weather condition affecting machineries/equipment-work-related performance and weaknesses in quality assurance for the supply of construction materials should be given serious attention in order not to jeopardize productivity and financial performance of the projects.

References

[1] I.Othman, A.Idrus & M.Napiah, "Human Resource Management in The Construction of a Sustainable Project: Towards Successful Completion"WIT Transactions on Ecology and The Environment, Vol.162,© 2012 WIT Press,

[2] Shehata, M. and El-Gohary, K. (2011). "Towards improving construction labor productivity and project's performance." Alexandria Engineering Journal, 50(4), 321-330.

[3] Hendrickson, C. (1998). Department of Civil and Environmental Engineering, Carnegie Mellon University, Pittsburgh, PA l52l3. Version 2.2 (Summer, 2008). "Chapter 4: Labor, Material, and Equipment Utilization." Project Management for Construction, Fundamental Concepts for Owners, Engineers, Architects and Builders.

[4] Alinatwi, H., Mwakali, J., and Hansson, B. (2007). "Factors affecting the productivity of building craftsmen – studies of Uganda." Journal of Construction Engineering and Management, 13(3), 169-176.

[5] O'Brien, J. J. (1998) Construction Change Orders. McGraw Hill, New York.

[6] Jang, H. , Lee, S. , and Choi, S. (2007). "Optimization of floor-level construction material layout using genetic algorithms." Automation. Construction. , 16 (4), 531–545.

[7] Koskela, L., and Howell, G., (2001), "Reforming project management: the role of planning, execution and controlling", Proceedings of the 9th International Group for Lean Construction conference, Kent Ridge Crescent, Singapore, 6-8 August, 2001.

[8] Assaf, S. A., Al-Khalil, M. & Al-Hazmi, M. (1995) Causes of delays in large building construction projects. Journal of Construction Engineering and Management, ASCE, 11(2), pp. 45-50.

Applied Mechanics and Materials Vol. 567 (2014) pp 613-618
© (2014) Trans Tech Publications, Switzerland
doi:10.4028/www.scientific.net/AMM.567.613

Risk Ranking of Malaysian Public Private Partnership Projects

Hadi Sarvari[1,a], Alireza Valipuor[1,b], Nordin Yahaya[1,c]
and Norhazilan Md Noor[1,d]

[1]Faculty of Civil Engineering, UTM, Skudai, 81310, Johor, Malaysia

[a]shadi7@live.utm.my, [b]valireza2@live.utm.my, [c]nordiny@utm.my, [d]norhazilan@utm.my

Keywords: Risk identification, Risk assessment, Risk ranking, PPP, Malaysia.

Abstract. In the past two decades, public private partnership (PPP) has been one of the prevailing ways for the development of infrastructure in Malaysia. However, it involves many risks and uncertainties due to large investments and a long concession period. It is very important to recognize and find out ways to cope with the critical risks that are related to the investments made in PPP projects by foreign investors. The aim of this article is to risk ranking associated with PPP projects using a risk matrix. The papers carries out literature review, consultation and questionnaire survey (among a panel of experts) to identify common risks in PPP projects. The risks identified from the literature were classified according to the type of risk. Finally, the results show that third party tort liability, interest rate volatility, construction cost overruns, and changes in law are critical risks.

Introduction

During the past two decades, PPPs have become a government's favored approach to public infrastructure procurement [1]. Generally, PPPs are used to cover all the contractual relationships among the public and the private sectors to provide an asset or deliver a service. Also, there are similar definitions of a public–private partnership; for example, according to the European Commission, the PPP is cooperation between the public and the private sectors to ensure the funding, renovation, construction, management, and maintenance of the infrastructure projects [2].

PPPs can be referred to as an efficient way of providing the funds to the private sector for the development of public infrastructure, and they play an important role in reducing the financial burden on the government [3]. The advantages of PPPs consist of the addition of the financial resources of the private sector, technical and managerial skills, innovation, the low cost of the life cycle, proper risk distribution, better quality of service and performance, and improved public management [4]. From another point of view, PPP projects usually consist of a long bussiness period and heavy investments, therefore causing a high rate of risks associated with them.

The list of prominent failed PPP Projects includes the Malaysian privatized national sewerage project, the Betuwe Railway in Netherlands [5], the Sydney Cross City Tunnel, the 9th Shen Yang Water Plant, the 4th Min Jiang River Bridge in Fuzhou City, and the Hou Shi power plant in Zhang Zhou City. The list of reasons for the failure of these PPP projects includes the lack of precise evaluation of the risk factors and management [6]. It is necessary to take all the risk factors expected during the duration of the project into consideration by the public clients and the private bidders. It is very difficult to cope with the associated risks, and a proper management framework is required on a theoretical and practical basis [7]. The process of the valuation of risk is quite complicated due to the complication of the modeling requirements and because of the subjective nature of the available data used to conduct the evaluation of the PPP projects. Developing countries lack the presence of a mature PPP organizational system; therefore, proper research is needed for the precise assessment of risks and management.

This study emphasizes on the Malaysian's PPP projects. Many previous studies have focused on risk assessment and management in PPP projects. However, only a little effort has been committed

to the systematic identification and assessment of risk in Malaysian PPP projects as reported by international construction management journals in recent years. Therefore, it is valuable and necessary to conduct a more up-to-date evaluation of the potential risks in Malaysian PPP projects. The research findings will contribute to both practice and research in risk management for Malaysian PPP projects and also provide valuable information for those international companies that are interested in or intend to invest in the Malaysian infrastructure construction sector.

The quantitative methods currently used in the risk assessment include a ranking method which uses scales of 1 to 5 to measure its likelihood of occurrence (probability) and its consequences (impact) [7]. To make a holistic assessment and ranking of the risks, we have used this method as an assessment technique in this research paper. Also, risks have been identified and classified through the literature review in the PPP projects, distribution of the questionnaires and interviews with the different PPP experts.

Research Methodology

The research methodology is adapted and demonstrated according to the research framework of Yelin [8] based on a comprehensive literature review and face-to-face interviews as qualitative tools. Quantitative tools for data analysis include a questionnaire survey for data collection and risk analysis matrix. The questionnaire survey and interviews were conducted as secondary resources to identify the important risks in Malaysian PPP Projects.

Result and Discussion

Risk identification is the first step in managing project risks. In order to identify risk factors in a PPP project, previous studies were assessed in this field. As a result, this step provides a list of vital risks. Data were collected through proper mechanisms, such as a literature review of previous studies of PPP projects [9, 3, 10, 11, 12, 13, 14, 15, 16, 17, and 18], a comprehensive questionnaire, interviews with different PPP experts, and a review of documents. The risk breakdown structure (RBS) was adopted to analyze the risks on the basis of their origins and their adverse effects on the project. More than 120 risks were found through this method. The risks were not considered to have low probabilities of occurrence and lower relative impacts. The research identified 51 important risks and then grouped them into ten different categories. A panel of experts was formed to identify the risks that have a strong influence on the objective of the project such as time, price and quality, and high probabilities of occurrence. All risks observed in the questionnaire can occur in any PPP project.

This research was not only carried out to point out the risks but to identify the proper risk map that can significantly affect the completion of PPP projects. Based on the survey results, the risk relative importance index was calculated for each risk based on probability and impact. According to the risk relative importance values, those ranked one, or extreme risk levels (out of 51 risk items), are assumed to be appropriate to represent the key risks. After calculation, the results showed that there are 10 risk items with values equal to an extreme risk level category (20%), 18 risk items with values equal to a high risk level category (35%), and 13 risk items with values equal to a medium risk level category (25%). We can focus on the extreme risk level category for more control. The score and rank of each risk is shown in Table 1.

To properly evaluate PPP power station project risks, one must consider both the probability of occurrence and the impact of consequences on project objectives once the risk event occurs. Some authors contend that multiplying the probability and severity values might be misleading [19]. The best way to determine this is to plot the probability of a risk–impact matrix (Figure 1). In the matrix, the *x*-axis represents the impact value while the *y*-axis represents the probability value. Both scales are 1–5 (1 being very low to 5 being very high), and the baseline risk level is compared with RRI to generate the best risk map. The risk analysis matrix and the proper risk map (risk matrix) are

presented in Figures 1 and 2 respectively. They show the converted numerical values and the calculation of the relative importance (RI).

Table 1. Risk ranking associated with Malaysian PPP projects

Risks associated with PPP Projects	Probability	Impact	P * I	Rank
Political:				
Changes in law	4.60	3.68	16.95	4
Delay in project approvals and permits	3.28	3.08	10.12	14
Poor public decision making process	2.80	2.39	6.69	24
Expropriation/nationalization of assets	2.32	2.05	4.76	38
Strong political opposition/hostility	1.75	2.04	3.57	44
Inconsistencies in government policies	1.70	1.50	3.06	46
Unstable government	1.42	2.21	1.72	50
Legal:				
Legislation change/inconsistencies	1.95	2.85	5.56	32
Corruption and lack of respect for law	2.30	2.36	5.20	34
Change in tax regulation	3.77	4.29	16.20	5
Industrial regulatory change	3.50	2.83	9.93	15
Economic:				
Interest rate volatility	4.35	4.22	18.36	2
Inflation rate volatility	2.09	2.87	5.99	30
Foreign exchange and convertibility	3.32	1.95	6.47	27
Poor financial market	3.74	4.24	15.87	6
Market:				
Market demand	3.05	3.75	12.07	10
Tariff change	2.97	3.65	10.86	12
Projects finance:				
Financial attraction of project to investors	3.30	2.95	9.74	16
High finance cost	2.85	1.25	8.12	19
Lack of creditworthiness	1.22	1.30	1.62	51
Project selection:				
Public opposition to projects	2.74	1.69	4.63	39
Uncompetitive tender	2.99	1.71	5.13	35
Level of demand for the project	2.25	1.45	3.26	45
Relationship:				
Different working methods/know-how	2.53	2.88	7.29	21
Inadequate experience in PPP	2.55	1.59	4.82	37
Lack of commitment from public/private partner	1.72	2.46	4.23	41
Organization and coordination risk	1.57	1.45	2.28	49
Third party tort liability	4.26	4.45	18.97	1
Inadequate distribution of responsibility and risk	1.55	1.8	2.79	47
Construction:				
Excessive contract variation/contractual risk	3.72	2.58	7.018	22
Construction time delay	3.23	2.02	6.53	26
Availability of finance	3.09	1.86	5.75	31
Construction cost overruns	4.05	4.30	17.45	3
Land acquisition	2.75	3.05	8.39	18
Availability of appropriate labor/material	2.22	2.91	6.46	28
Design deficiency	2.83	2.67	7.57	20
Geotechnical conditions/ground condition	2.65	3.2	8.48	17
Late design changes	1.81	2.32	4.20	42
Contractor failure/capability of SPV	1.52	3.27	4.97	36
Project delay	2.45	2.83	6.93	23
Consortium inability	2.1	1.79	3.76	43
Completion risk	1.4	1.65	2.31	48
Operation:				
Operation cost overrun	3.71	3.95	14.69	7
Residual value (after concession period)	3.57	3.39	12.12	9
Operation financial risk	1.92	2.79	5.36	33
Maintenance cost higher than expected	3.50	3.82	13.37	8
Low operating productivity	3.47	3.05	10.59	13
Risk regarding pricing of product/service	2.23	1.94	4.37	40
Natural:				

Force majeure	3.56	3.10	11.05	11
Environment	3.25	2.05	6.66	25
Weather	2.86	2.19	6.26	29

The risk matrix includes a legend of risk level that would be of assistance to project participants when the risk is unknown, and it would also provide the framework to rank risk elements by order of severity for subsequent mitigation: Extreme risk (E)—occurrence would prevent achievement of objectives, causing unacceptable cost overruns, schedule slippage, or project failure; High risk (H)—could substantially cause a delay in the project schedule or considerably affect the technical performance or costs; requires a strategy to handle; Medium risk (M)—requires identification and control of all the responsible factors by monitoring conditions and reevaluation of the project milestones; Low risk (L)—normal control and monitoring procedures are adequate.

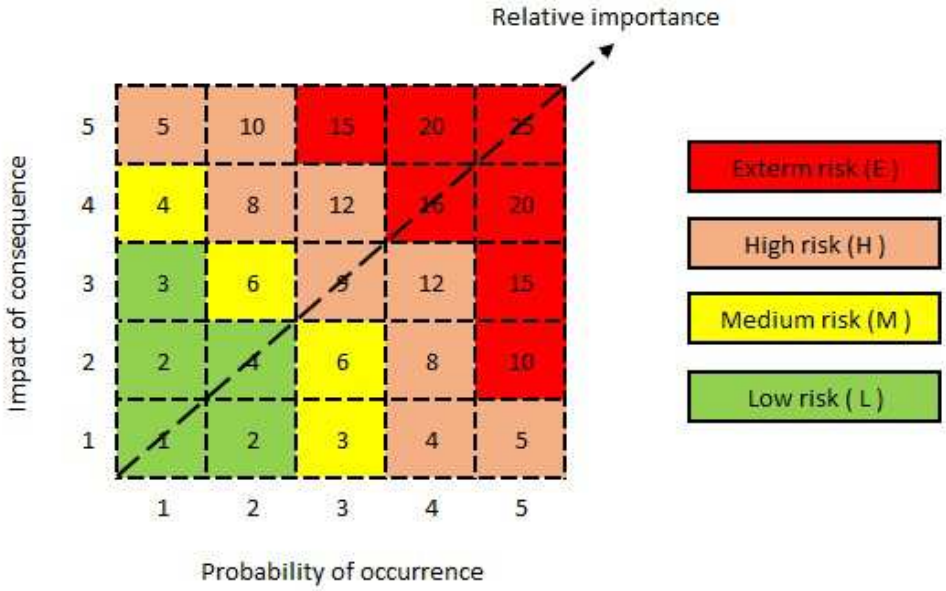


Fig. 1. Risk analysis matrix

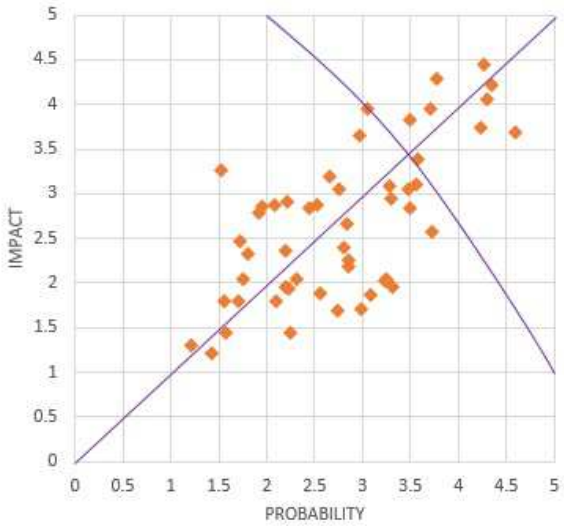


Fig. 2. Risk matrix

Summary

This paper has studied the probability and consequences of risks in Malaysian PPP projects. The findings from this paper are that the risk factors are clustered into ten groups, namely political, construction, legal, economic, operation, market, project selection, project finance, relationship, and natural factor. Risk factors are assessed based on two criteria: probability and impact. The top risks, according to their risk significance index score, were as follows: third-party tort liability (18.97), interest rate volatility (18.36), construction cost overrun (17.45), changes in law (16.95), changes in tax regulation (16.20), poor financial market (15.87), operation cost overrun (14.69), maintenance cost higher than expected (13.37), residual value (12.12), and market demand (12.07). Another conclusion that can be drawn from the mean calculation is that three of the risks are related to the operation group and two of them are associated with the economic group. Also, it could be asserted that most of the main risk items in Malaysian PPP projects are at a national or industry level, which is associated with operational, economic, and legal conditions.

Acknowledgement

The work described in this paper was fully supported by a joint grant from the research grants MOSTI (Malaysia, UTM& Vote No.(4S084).

References

[1] M. Handley-Schachler, and S. Gao, "Can the private finance initiative be used in emerging economies? Lessons from the UK's successes and failures." Managerial Finance, 29 (2003) 36–51.

[2] European Commission. "Green paper on public-private partner- ships and community law on public contracts and concessions." 327 Final, European Commission, Brussels, Belgium (2004).

[3] B. Li, A. Akintoye, P.J. Edwards, and C. Hardcastle, "The Allocation of Risk in PPP/PFI Construction Projects in the UK". International Journal of Project Management, 23 (2005) 25–35.

[4] The World Bank. Toolkits for Private Participation in Water and Sanitation, Washington, D.C. (1997).

[5] D. Y. Chang, and L. L. Zhang, "Fuzzy set approaches in economic management", Beijing Economics Institution Press, Beijing, 190, (1995).

[6] J. Li, Zou, H. Cheng, and Z.H. Dai, "Contract conditions of BOT projects in China." Proc. of CRIOCM 2007 International Re- search Symp. On Advancement of Construction Management and Real Estate, Sydney, Australia, (2007) 966–979.

[7] D. Grimsey, and M. K. Lewis, "Evaluation the risks of public private partnership for infrastructure", Int. J. Proj. Manage, 20 (2002) 107-118.

[8] Y. Xu, A.P. Chan, J.F. Yeung, "Developing a fuzzy risk allocation model for PPP projects in China", Journal of Construction Engineering and Management, 136 (2010) 894-903.

[9] K. Yongjian, W. ShouQing, A. P. Chan, "Proffered Risk Allocation in China's Public Private Partnership (PPP) Projects", Journal of Project Management, 28 (2009) 482-492.

[10] L.Y. Shen, A. Platten, X. Dang, "Role of public private partnership to manage risk in public sector project in Hong Kong", International Journal of Project Management, 24 (2006) 587-594.

[11] A.D. Ibrahim, A.D.F. Price, A.R.J. Dainty, "The analysis and allocation of risks in public private partnerships in infrastructure projects in Nigeria", Journal of Financial Management of Property and Construction, 11 (2006) 149 – 163.

[12] Yuan, J.F., Peng, X., Li, D.M., "Critical risks identification of Public Private Partnerships in China and the analysis on questionnaire survey", IEEE, (2008).

[13] X. Yelin, H. Cheng, P.C. Chan, "Risk Factors for Running Public Private Partnerships (PPP) – An Empirical", IEEE, (2009).

[14] R. Aspin, "Public-private partnerships and effective risk management for local government", paper presented to the 19th EAROPH World Planning and Housing Congress and Australian National Housing Conference, Melbourne, (2004) 19-22.

[15] H.J. Xiao, G. Zhang, "Modelling optimal risk allocation in PPP projects using artificial neural networks", International Journal of Project Management, 29 (2001), 591–603.

[16] X. Zhang, "Paving the Way for Public–Private Partnerships in Infrastructure Development", Journal of Construction Engineering and Management, (2005).

[17] L.B. Singh, S.N. Kalidindi, "Traffic revenue risk management through Annuity Model of PPP road projects in India", International Journal of Project Management, 24 (20006) 605–613.

[18] A. Ng, M. Loosemore "Risk Allocation in the private provision of public infrastructure", International Journal of Project Management, 25 (2007) 66-76.

[19] B. Kangari, "Risk perception and tendering in construction project", Journal of Construction Engineering and Management, 121(1995) 422–429.

Applied Mechanics and Materials Vol. 567 (2014) pp 619-624
© (2014) Trans Tech Publications, Switzerland
doi:10.4028/www.scientific.net/AMM.567.619

Service and Construction Sector of Malaysia: Causality Link (1991-2013)

Raza Ali Khan[1, a], Mohd. Shahir Liew[1,b] Zulkipli Bin Ghazali[1,c]

[1] Universiti Teknologi PETRONAS Malaysia

[a]alikhan.raza@gmail.com, [b]shahir_liew@petronas.com.my [c]zulkipli_g@petronas.com.my

Keywords: Causality, Linkage, co-integration

Abstract. The number of research studies has been conducted over the importance of service and construction sector in an economy and confirmed that these two sectors are always being closely associated to the aggregate economy and play crucial role in the socio economic development of a country. The objective of this study is to examine the link between the construction and service sector of Malaysia during the last two decades by using time series econometric analysis. The Granger causality approach is used to obtain the objective of the study. The results of the study suggest that there is a uni-directional (one way) association between the service and construction sector in Malaysia i.e. construction sector to service sector. The construction sector plays a significant role to motivate the economic activities of the service sector in Malaysia and the service sector take 6 months (two quarters) to absorb the impact of a shock coming from the construction sector. The results of the study are important and useful for developing future policies for the construction and services sectors of Malaysia. The results are also important and informative for interested parties of the sectors.

Introduction

The service and construction are two important sectors of developing and developed economies, playing an efficient role in generating new economic activities and business opportunities. They have a significant proportion of GDP and engaged number of skilled, semi-skilled and unskilled people. It is estimated that an approximately 70% of value added and employment generated by the service sector in developed economies [1]. A cross- country comparison in Asia shows the contribution of the services sector in gross domestic product (GDP) is about 65% in Singapore, 54% in Sri Lanka, 53% in Pakistan, 52% India and 42% in Indonesia. The socio-economic development of high income economies is captured by large services sectors and its contribution to GDP has reached to more than 70 % because of strong backward and forward linkage with the rest of the major sectors of the economy, construction sector is one of them [2]. In case of Malaysia the contribution of the service sector is rapidly growing in all other sectors of the economy as well as in overall GDP. The growth rate of the sector is continuously rising and reached to 58% of total GDP, which is higher than all other major sectors of Malaysian economy such as agriculture, manufacturing, mining and construction. It has a strong association with all major sectors of the economy and provides significant amounts of inputs to them. This study is conducted over the association of services and construction sectors of Malaysia.

The construction sector activities also play a major role in stimulating economic activities and developing infrastructure for other sectors of the economy. It has also a strong association with other sectors of the economy and generates significant economic opportunities through linkages with other industries. Organization for economic cooperation and development (OECD) conducted a study over linkages of sectors in selected OECD member countries; find out that the construction sector has one of the highest backward linkages with the rest of the economy [3]. The objective of

this study is to develop understanding about the service and construction sector of the Malaysia, and empirically examine the role and the causality link between the two sectors, construction and services of Malaysia during 1991-2013.

Literature Review

The modern world has widely recognized the role and contribution of the service sector in the economy, which is rapidly growing in the national economy of the developed and developing countries. It is the largest and fastest growing sector in the competitive modern economy. The proportion of services sector in total GDP is 47% percent for developing economies like Indonesia, 53% in newly industrialized countries like Malaysia and 73 % in high income countries like USA [2]. The growing importance of the service sector is not a current phenomenon; it has been recognized for several decades such as studies conducted by [4, 5] have already identified the long run trend between service sector and the national economy. A comprehensive study conducted over 123 countries for the period 1970-1980, concluded that the services increase the GDP per capita of these economies [6]. Similarly an Indian study also concluded that the services sector plays leading role in Indian economy, higher growth rate in services sector leads to economic growth of India [7]. The frontiers between services sector and industry are changing rapidly. Approximately 50% of all services in the modern world are traded while setting in the form of goods. Designing, planning, marketing, and logistics, transportation, communication consultancy and financial services have a substantial contribution of value added to goods [2].

There is a significant contribution of the services sector in a construction project. The success of any construction project depends on the expertise and services of construction professionals such as architect, consultant, and contractors. They work as a manager or an organizer and make sure that the project should be completed successfully without exceeding the estimated budget and allocated time [8].

The construction sector also plays a significant role in stimulating the services sector by providing infrastructure such as educational institutes for education services, hospitals for health services, office buildings for banking and other financial institutes, roads and highways for transport services. The construction sector produces one of the highest multiplier effects through its strong association with other sectors of the economy [9].

In short the link between services and construction sector play a pivotal role in the economic development of a country. There is a need to understand the relationship and the nature of the linkage between the two sectors for maintaining the momentum of economic growth and development in the country. The focus of this study is to measure the linkage between services and construction sector of Malaysia through Granger causality approach.

Methodology

The quantitative paradigm of research is used to satisfy the objective of the study. The descriptive statistical analysis is conducted to compare the basic parameters of the two studied sectors. The Pearson correlation test is conducted to measure the strength of the relationship between the variables and econometric Granger causality model used to examine the causality and direction of the link between the concerned sectors services and construction.

Data and Sample Size: The quarterly time series (1991-2013) data for services and construction sector output in value term is obtained from the Department of Statistics Malaysia. The two data series are transformed in the natural logarithm form for maintaining the uniformity and controlling the variation in the data series i.e. LSERV and LCONS.

Granger Causality Approach: Granger causality is standard econometric model to measure the causal link and direction of the link between the variables. Following two equations are developed on the basis of General Granger Causality Model for testing the causality between LSERV and LCONS.

$$LSERV_t = \alpha_1 + \sum_{i=1}^{n} \beta_i \, LSERV_{t-i} + \sum_{j=1}^{j} \gamma_1 \, LCONS_{t-j} + \mu_{1t} \quad (1)$$

$$LCONS_t = \alpha_2 + \sum_{k=1}^{k} \beta_2 \, LCONS_{t-k} + \sum_{l=1}^{l} \gamma_2 \, LSERV_{t-l} + \mu_{2t} \quad (2)$$

Where $LSERV_t$ and $LCONS_t$ are two stationary series of the concerned sectors i.e. log services sector output and log construction sector output with zero mean and constant variance: μ_{1t} and μ_{2t} are two uncorrelated white noise error term series. The causality between the concerned variables can be determined by testing the following null and alternate hypothesis:

Research Hypothesis:

Null hypothesis for Equation1: $LSERV_t$ does not Granger cause $LCONS_t$
Alternate hypothesis: $LSERV_t$ Granger cause $LCONS_t$
Null hypothesis for Equation 2: $LCONS_t$ does not Granger cause $LSERV_t$
Alternate hypothesis: $LCONS_t$ Granger cause $LSERV_t$

As a result of this test, three situations can be occurred, unidirectional causality, bi-directional causality or the variables may be independent. The unidirectional causality from $LSERV_t$ to $LCONS_t$ exists if the null hypothesis of Equation 1 ($LSERV_t$ does not Granger cause $LCONS_t$) is rejected, means statistically estimated coefficient on the lagged LCONS in Equation 1 is different from zero i.e. $\sum_{j=1}^{j} \gamma_{1j} \neq 0$. Similarly unidirectional causality from $LCONS_t$ to $LSERV_t$ exists if the null hypothesis for Equation 2 is rejected i.e. $LCONS_t$ does not Granger cause $LSERV_t$, statistically $\sum_{l=1}^{l} \gamma_{2l} \neq 0$ means estimated coefficient on the lagged $LSERV_t$ is different from zero. The bi-directional causality occurs if the null hypotheses for both equations 1 and 2 are rejected i.e. $\sum_{j=1}^{j} \gamma_{1j} \neq 0$ for equation 1 and $\sum_{l=1}^{l} \gamma_{2l} \neq 0$ for equation 2. The variables will be considered independent if the test is failed to reject the null hypothesis for both Equation 1 and Equation 2 and the coefficient of LCONSt in Equation 1 and coefficient of $LSERV_t$ in Equation 2 are equal to zero.

Unit Root Test: The basic condition for using a Granger causality test is the variable data series should be stationary and free from unit root. The Augmented Dickey Fuller (ADF) and Phillips Perron (PP) tests are normally used to identify this problem with the null hypothesis that the series has unit root problem versus alternate hypothesis the series is stationary. The Equation 3 and Equation 4 are developed on the basis of Dickey Fuller Model Equation for testing unit root problem in the series. If the null hypothesis H_0: $a_2 = 0$, is accepted for Equation 3, this implies that services sector series has a unit root problem otherwise series will be considered free from unit root and can be used for Granger causal analysis. Similarly if the null hypothesis H_0: $c_2 = 0$, is accepted for Equation 4 against the alternative H_1: $c_2 \neq 0$, implies that construction output series has a unit root and stationary problem, in reverse case it will be considered stationary series, free from unit root [10].

$$\Delta LSERV_t = a_0 + a_1 T + a_2 LSERV_{t-1} + \sum_{t=1}^{n} b_i \, \Delta LSERV_{t-1} + \varepsilon_t \quad (3)$$

$$\Delta LCONS_t = c_0 + c_1 T + c_2 LCONS_{t-1} + \sum_{t=1}^{n} d_i \, \Delta LCONS_{t-1} + \varepsilon_t \quad (4)$$

Where $\Delta LSERV_t = LSERV_t - LSERV_1$ and $\Delta LCONS_t = LCONS_t - LCONS_1$, a_0 and c_0 are drift term and T represent to time trend. ε_t = Error term

Results and Discussion

Comparison of Basic Facts: The performance of the two sector services and construction in term of average output, growth, contribution to GDP and average employment during the study period (1991-2010) are reported in Table 1. The size of services sector in term of average output is 13 times greater than the construction sector. The average contribution of the services sector to GDP is also 12.25 times higher than construction sector i.e. 49% and 4% respectively. The average growth rate of the services sector is approximately double as compared to the construction sector. The average employment contribution 6.5 times of the construction sector i.e. 51% and 8 % respectively. In last two decades approximately 50% of the Malaysian economy captured by the services sector.

Table 1: Output, Growth, GDP contribution and Employment contribution comparison

Description	Services Sector	Construction Sector
Average output (RM 000, million)	186378	14416
Average growth (%)	8	4.2
Average contribution to GDP (%)	49	4
Average employment (%)	51	8

Data Source: Department of Statistics Malaysia

Correlation Test: The Pearson correlation test conducted to measure the strength of association between the concerned variables. Table 2 shows that there is a strong correlation between the services and construction sectors. But this test does not inform about causal association between the sectors.

Table 2: Correlation Matrix

Sectors	Services	Construction
Services	1	
Construction	0.95	1

Source; Author's Calculation

Series Unit Root Test: In order to satisfy the stationary requirement and to know the order of integration in each variable series ADF and PP tests are conducted. Table 3 depicts the unit root test results. The null hypothesis in both series LSERV and LCONS is rejected at the 1% level of significance after first differencing the series. This implies that the series are stationary and do not have a unit root problem at first difference. Both ADF and PP tests suggest that there is chances of the long run equilibrium relationship between the two sectors (Services and Construction) as the series are integrated order one I(1). Therefore the first differenced series can be used for Granger causality analysis, which satisfies the stationary assumption.

Table 3: Unit Root Test Results

Series	DF Test (Level)	ADF (First Difference)	PP (First Difference)
LSERV	-1.3323	-12.1716***	-73.9593***
LCONS	-1.6068	-3.1452**	-10.7521***

***, (**) denotes rejection null hypothesis at 1% and 5% sig. Level

Granger Causality Test: The unit root test confirms that the both series are stationary at first difference and integrated order one; hence the series can be used for Granger causality analysis. The Granger causality test results achieved by estimating causality Equations 1 and 2. Table 6 reports the causality test results. The test results confirm that the services sector does not play significant role in motivating construction sector of Malaysia, because the null hypothesis LSERV does not cause LCONS statistically cannot be rejected. However the construction sector significantly supports to services sector activities as the null hypothesis, LCONS does not Granger cause LSERV, is rejected at the 5% significance level in testing the Equation 2. There is a uni-directional (one way) relationship between the services and construction sector i.e. construction to services sector.

Table 6: Granger Causality Results

NULL Hypothesis	Lag order	F-statistics	P-value
LSERV does not Granger cause LCONS	2	1.2719	0.2856
LCONS does not Granger cause LSERV	2	4.2509	0.0174**

***, (**) denotes rejection the hypothesis at 1% and (5%) level of significance respectively

Conclusion

The services and construction sector of Malaysia are the two important sectors of the Malaysian economy. The average output and contribution in GDP of the services sector are approximately 12.5 times higher than construction during the study period. There is a strong correlation between the quarterly outputs of the two sectors. The important finding of this study is uni-directional causal relationship between the sectors. The construction sector has backward and forward linkage with the services sector in Malaysia and causes to promote the output activities of the sector. However the services sector has not significant effect over the construction sector in the short run. Another important finding of the study is that the two sectors have long run equilibrium relationship as the data series of concerned variables are integrated order one. These results of the study are important and valuable for developing the relative policies for the two sectors such as allocation of resources, investment and tax policies.

Acknowledgement

The authors would like to acknowledge the Department of Civil Engineering Universiti Technologi PETRONAS (UTP) for providing facilities and research environment to conduct this study.

References

[1] A.Wolfl, "Productivity Growth in Service Industries: An Assessment of Recent Patterns and the Role of Measurement," in *OECD Science, Technology and Industry Working Papers, 2003/7*, ed. OECD Publishing. , 2003.

[2] A. Ahmed and H. Ahsan, "Contribution of Services Sector in the Economy of Pakistan " in *PIDE Working Papers 2011: 79* ed. Pakistan: Pakistan Institute of Development Economics, 2011.

[3] R. Pietroforte and T. Gregori, "An input-output analysis of the construction sector in highly developed economies," *Construction Management and Economics,* vol. 21, pp. 319-327, 2003.

[4] V. Fuchs, "The Service Economy," National Bureau of Economic Research Columbia University Press, New York1968.

[5] C. Clark, "The Conditions of Economic Progress," Macmillan, London1941.

[6] P. Kongsamut, S. Rebelo, and D. Xie, "Beyond Balanced Growth," in *IMF Working Paper, WP/01/85*, ed, 2001.

[7] D. P. Rath and R. Rajesh, "Analytics and Implications of Services Sector Growth in Indian Economy," *The Journal of Income and Wealth* vol. 28, 2006.

[8] A. A. Hussain and A. Omran, "Roles of Professionals in Construction Industry " presented at the The International Conference on Economics and Administration, Romania, 2009.

[9] Park and Se-Hark, "Linkages between industry and services and their implications for urban employment generation in developing countries," *Journal of Development Economics,* vol. 30, pp. 359-379, 1989.

[10] D. Dickey and W. Fuller, "Distributions of the estimators for autoregressive time series with a unit root," *Journal of the American Statistical Association,* vol. 74 pp. 427- 31, 1979.

Applied Mechanics and Materials Vol. 567 (2014) pp 625-630
© (2014) Trans Tech Publications, Switzerland
doi:10.4028/www.scientific.net/AMM.567.625

The Development of Building Information Modeling (BIM) Definition

Aryani Ahmad Latiffi[1,a], Juliana Brahim[1,b] and Mohamad Syazli Fathi[2,c]

[1]Faculty of Technology Management and Business, Universiti Tun Hussein Onn Malaysia (UTHM), Parit Raja, Batu Pahat, Johor, 86400, Malaysia.

[2]UTM Razak School of Engineering and Advanced Technology, Universiti Teknologi Malaysia, Kuala Lumpur, 54100, Malaysia

[a]aryani@uthm.edu.my, [b]gp130036@siswa.uthm.edu.my, [c]syazli@utm.my

Keywords: Building Information Modeling (BIM), Building Description System (BDS), Building Product Data (BPM), History, Definition

Abstract. Conventional practice on managing information in construction has sometimes created a miscommunication and errors among construction players. Therefore, Information Communication Technology (ICT) has introduced Building Information Modeling (BIM) for managing construction projects effectively and efficiently. Different terms on definition of BIM have been used and expanded widely with different perspectives. The aim of this paper is to explore the notion of BIM development from the year of 1975 to 2013. The methodology of this paper is based on literature review on BIM definitions. The findings reveal that there are six perspectives in BIM development which are design, estimation, construction process, building life cycle, performance and technology. From the development of BIM, it can be concluded that BIM is a new methodology that involves the use of technologies in order to improve collaboration and communication of construction players as well as the management of documentation.

Introduction

Construction projects involve complex sets of relationships between parties under different professional background in order to achieve complex goal [1]. The complexities of construction projects are resulting from a thousand of documents and drawings that being used manually. In conventional practice, construction parties still use 2-Dimensional (2D) information which is sometimes resulting in miscommunication among them and not appropriate for complex projects [1,2,3,4,5,6]. Miscommunication in construction could lead to mistakes in construction process such as fumble of design; drawings are not updated, delay, cost overrun, poor quality of works, as well as design clashes. Therefore, Information Communication Technology (ICT) is required for managing a bundle of information and documents, decision making tasks and to deliver the level of consistency and reliability of information in construction [7]. As a result, Building Information Modeling (BIM) has been introduced in construction projects in effective and efficient way by computerized and integrated information management systems [8]. The purpose of this paper is to review the development of BIM starting from 1975 to 2013 in terms of the definition. A literature review and timeline development of BIM from 1975 to 2013 was established to view on how BIM is being developed.

The Building Information Modeling (BIM) Methodology

BIM concept is originated from Professor Charles Eastman at the Georgia Tech School of Architecture in late 1970 [6,9]. Since its development, it has broadened up in wide perspectives. The perspectives are design, estimation, construction process, building life cycle, performance and technology. The purpose of BIM implementation in construction projects are vary throughout construction projects phases, which are pre-construction phase, construction phase and post-construction phase [9,10].

The Architecture, Engineering and Construction (AEC) industry had started practically using BIM in construction projects from the mid-2000s [9, 10]. The example of BIM projects are Sutter

Medical Centre, Castro Valley, California USA; Crussel Bridge, Helsinki, Finland; One Island East Office Tower, Hong Kong (HK); National Cancer Institute (NCI), Putrajaya, Malaysia and Sultan Ibrahim Hall formerly known as Multi-Purpose Hall of Universiti Tun Hussein Onn, Johor, Malaysia [9,11]. During the late 1970s, Eastman claimed that drawings for construction were inefficient due to its limitation to visualize the buildings as well as the drawings were not updated [1,12]. Therefore, there are several organizations in the USA and Finland which had developed a computer programs using ICT in order to solve those problems. Figure 1 shows development of BIM definition which was developed based on the computer programs from 1975 to 2013.

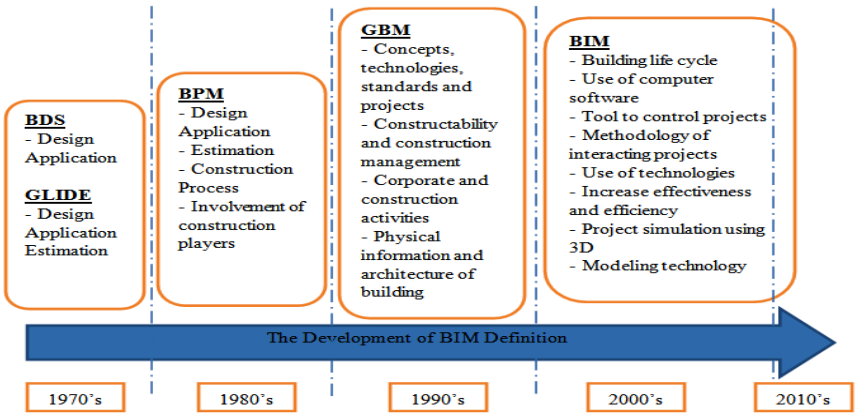


Figure 1: The Development of BIM Definition from 1975 to 2013

Based on Figure 1, it shows how the development of BIM definition has been expanded. In 1975, Building Description Systems (BDS) had been introduced by Professor Charles Eastman for easier coordination during design development [12]. BDS is defined as database that capable for describing buildings at allowing design and construction [13]. BDS has been used to construct model of complex physical systems that consists of specification of elements. The benefits of BDS are to define, modify and arrange a large number of elements as well as for design clashes detection [12]. BDS operates with individual library elements from the database [14,15]. In addition, BDS enhances in representing custom-designed and building systems where the attention is given to the features distinguishing general from special purpose building description systems, data structures, access scheme and the method of interaction between database and analysis programs [13,14,15] BDS could reduce cost of design, through drafting and analysis efficiency [12,15,16]. However, BDS did not get wide popularity because not many architects had a chance to grip on it [14]. Due to the limitation of technology in late 1970s, BDS had been limited to individual library and to potential design choices such as architectural, structural or energy aspect. Therefore, in 1977, Graphical Language for Interactive Design (GLIDE) had been introduced where it incorporated with many part of BDS [16]. Figure 2 shows the example of GLIDE project.

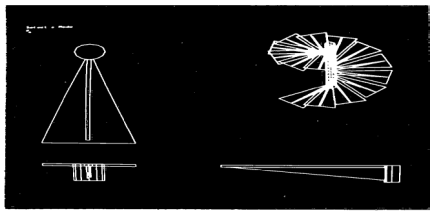


Figure 2: Example of GLIDE Project in Demonstrates the Spiral Staircase. [16]

Based on Figure 2, GLIDE demonstrates the spiral staircase as an image, shape and a model. GLIDE has been expanded to cover certain elements of building and used as a tool in checking the accuracy of data cost estimating and evaluation of structural design. From the improvement of GLIDE, the 2D drawings produced are more consistent and accurate. However, BDS and GLIDE are limited to the involvement of construction players at design stage only. In order to achieve more comprehensive improvement of the programs, construction players need to get involved and

collaborate more in construction phase. After the GLIDE was first introduced, it had been used until 1988. Then a new program called Building Product Model (BPM) had come up in 1989. BPM had covered design application, estimation, construction process and involvement of construction players [17,18]. In Finland, BPM known as RATAS which is acronym for Finland words for 'Computer Aided Building Design' [17]. It was used to conduct a study in computer integrated in construction process. RATAS was a national framework program for IT in construction which consists of a series of Research and Development (R&D) projects [17]. It was a conceptual model that using objects attributes and different types relation of objects. The model was able to describe data in particular buildings by using different types of application software but under the same conceptual information structure.

Contrast with BDS and GLIDE, BPM acted as a project library that consists of information of projects from planning to the completion of construction. It is a high level computer interpretable communication for Computer Aided Design (CAD) in construction [19]. As such, it can be used as a compilation and discussion of concepts, technologies, standards as well as projects [20, 21]. However, the communication under BPM only focused on product information while the AEC industry requires the integration of information and knowledge that used for design and construction management [19]. Then in 1995, Generic Building Model (GBM) had been introduced using the concept of BPM [20]. GBM had been expanded to integrate information from current and future design that could be used throughout the life cycle in construction process. As the results, GBM had been able to improve projects information that enhanced incorporation of the construction activities. However, the construction industry had become more complex and challenging. It required the adoption of ICT widely for the purpose of better performance and expectation of projects.

Therefore, Building Information Modeling (BIM) had been used to fulfill the AEC industry requirements. It had been implemented in many countries such as the USA, Finland, HK, Australia including Malaysia. In 2000, BIM was defined as a structured model that representing building elements [22]. The use of BIM had been expanded from the pre-construction phase to post construction phase. Until 2005, it had been defined as a development and use of computer software to simulate the construction and operational of a facility [23]. BIM is used as a tool to control the information as well as organization, duties and processes that need from the stage of planning, design, construction, maintenance and lastly demolition.

In 2006, BIM was defined as a new methodology to manage and increase the AEC performance in completing and managing the projects [24, 25]. In 2008, BIM was adapted as a project simulation that consisted of 3-Dimensional (3D) model of a project component. It was linked and integrated with the information required throughout the project phases. After 2008 till 2013, BIM had been enlarged as a technology revolution that helped to transform the way buildings were conceived, designed, constructed as well as operated [10,26,27,28]. The adoption of BIM concept was said as paradigm shift for AEC industry that helped to achieve efficiency and effectiveness in construction projects [29]. It was a set of digital tools that helped AEC industry to manage construction projects by improving the planning process, design, construction as well as the operation of the facility [9]. BIM was also known as a new way approaching design and documentation by helping the collaboration of construction players to insert, extract, update or modify the information of facility [30, 31, 32]. The technology revolution was said due to the use of 3D CAD software programs. As per to date, BIM is regarded as a set of design management tools that gives advantages through the construction project phases.

Discussion

This paper reviews and analyzes the definitions and developments of BIM from six important perspectives. There are design, estimation, construction process, building life cycle, performance as well as technology.

Table 1: Analysis of BIM development from 1975 to 2013.

Development	Construction Phases			Category
	Pre-Construction	Construction	Post-Construction	
BDS	√			Design
GLIDE	√	√		Design and Estimation
BPM	√	√		Design , Estimation and Construction Process
GBM	√	√		Design , Estimation and Construction Process
BIM	√	√	√	Design , Estimation, Construction Process, Building Life Cycle, Performance and Technology

Table 1 presents the analysis of BIM development from the year 1975 to 2013. In 1975, BDS was focused more on design application and limited to certain elements in building. However, due to the limitation of BDS, GLIDE had been introduced in 1977. GLIDE was able to visualize and make estimation from the design. The accuracy of the design produced by GLIDE was more accurate and reliable. However, the application of BDS and GLIDE was only limited to design stage in pre-construction phase. Therefore in 1989, BPM had been introduced to replace BDS and GLIDE. It had expanded to construction phase where it focused more on design, estimation and construction process perspective. BPM was used to translate the information regarding the projects and make relationship between the activities in construction life cycle such as earthworks, structural works, architectural works and infrastructures. The data in BPM was used in making significant changes in the project delivery process. However, BPM was only concentrated on the communication on the product information. Therefore, GBM had been introduced to improve the integration of information with construction activities.

Until 2000, BIM had been introduced to overcome the complexity of construction projects until 2000. It involved the collaboration of construction players throughout the construction projects phases. BIM was implemented in order to achieve smooth communication and progress of work. The use of BIM was focused on design and process in construction project, performance and technology perspective. Until 2013, BIM was regarded as a methodology to effective and efficient performance in projects and it was recognized as a technology due to the use of 3D model in construction projects.

As the conclusion, the development of BIM from 1975 to 2013 had introduced a new methodology using software technology in construction. The technology had helped the construction players in improving collaboration and communication among them. It had also improved the management of documentation in order to achieve more effective and efficient performance in construction projects.

Conclusion

The revolutionary of BIM enhanced to overcome the complexities in construction projects. BIM is a set of digital tools that helps AEC industry to manage projects effectively by improving the planning process, design and others activities in construction. Since its development, it has expanded into six perspectives which are design, estimation, construction process, building life cycle, performance and technology. Ever since that, BIM is used as a design management tools by the AEC industry in order to improve collaboration and communication among construction players as well as the management of documentation in the construction projects.

Acknowledgement

The authors would like to thank to *Ministry of Education of Malaysia (MOE)*, and *Office of Research, Innovation, Commercialization and Consultancy (ORRIC), UTHM* for supporting this research under the *Exploratory Research Grant Scheme (ERGS), (Vote No. E029).*

References

[1] Crotty, R. The Impact of Building Information Modeling. Spoon Press. London. 2012

[2] Barati, R., Charehzehi, A., and Preece, C.N. Enhancing Planning and Scheduling Program Using Benefits of BIM-Based Applications. Civil and Environmental Research. Vol.3 (2013) 41-39.

[3] Zakaria, Z., Ali, N.M., Haron, A.T., Ponting, A.M., and Hamid, Z.H., (2013). Exploring the Adoption of Building Information Modeling (BIM) In the Malaysian Construction Industry: A Qualitative Approach. International Journal of Research in Engineering and Technology Vol.2 (2013) 384-394.

[4] Ham, N.H., Min, K.M., Kim, J.H., Lee, Y.S., and Kim, J.J. A Study on Application of BIM (Building Information Modeling) to Pre-Design in Construction Project. Third 2008 International Conference on Convergence and Hybrid Information Technology. Vol.1 (2008) 42-49.

[5] Arayici, Y. Towards Building Information Modeling for Existing Structures. Structural Survey Vol.26(3) (2008) 210-222

[6] Reddy, K.P. BIM for Building Owners and Developers: Making a Business Case for Using BIM on Projects. John Wiley and Sons, Inc. United State of America, 2012.

[7] Ahuja, V., Yang, J., and Shankar, R. Benefits of Collaborative ICT adoption for Building Project Management. Construction Innovation Vol. 9(3) (2009) 323-340.

[8] Sebastian, R. Changing Roles of the Clients, Architects and Contractors Trough BIM. Engineering Construction and Architectural Management Vol.18(2) (2011) 176-187

[9] Ahmad-Latiffi A., Mohd, S., Kasim, N., and Fathi, M. S. Building information Modeling (BIM) Application in Malaysia Construction Industry. International Journal of Construction Engineering and Management, Vol. 2(4A) (2013) 1-6

[10] Azhar, A., Hein, M., and Sketo, B. Building Information Modeling (BIM): Benefits, Risks and Challenges. Proc., 44th Associated Schools of Construction National Conference, Auburn, AL. (2008)

[11] Eastman, C. BIM Handbook: A Guide to Building Information Modeling for Owners, Managers, Designers, Engineers and Construction. Second Edition. New Jersey. John Wiley & Son Inc. (2011)

[12] Eastman, C., Lividini, J., and Stoker, D. A Database for Designing Large Physical Systems. , National Computer Conference and Exposition (1975) 603-611.

[13] Eastman, C. General Purpose Building Description Systems. Computer Aided Design. Vol. 8(1) (1976) 17-26.

[14] Dobelis, M. Drawback of BIM Concept Adoption. The 12th International Conference on Engineering Graphics (2013) 57-67.

[15] Architectural Research Lab ARL, (2012). History of BIM. Information on http://www.architecturalresearchlab.com/arl/2011/08/bim-history

[16] Eastman, C., and Henrion, M. GLIDE: A Language for Design Information systems. ACM SIGGRAPH Computer Graphics. Vol.11 (2) (1977) 24-33.

[17] Hatti, M. What is Ratas. (1996). Information on http://cic.vtt.fi/projects/ratas/whatis.html

[18] Bjork, B.C. Basic Structure of a Proposed Building Product Model. Computer Aided Design. Vol.21(2) (1989) 71-78.

[19] Luiten, G.T., Tolman, F.P., and Fischer, M.A. Project-Modelling in AEC to Integrate Design and Construction. Computers in Industry Vol.35 (1) (1998) 13-29.

[20] Eastman, C. M., and Siabiris, A. A Generic Building Product Model Incorporating Building Type Information. Automation in Construction. Vol.3 (4) (1995) 283-304.

[21] Khemlani, L. Building Product Models: Computer Environments Supporting Design and Construction: Charles M. Eastman, 1999, CRC Press. Automation in Construction Vol.11 (2002) 495-496

[22] Ameziane, F. An Information Systems for Building Production Management. International Journal of Production Economics. Vol.64 (1) (2000) 345-358.

[23] Associated General Contractors of America. The Contractor's Guide to BIM 1st Edition. AGC Research Foundation, Las Vegas, NV. (2005)

[24] Penttila, H. Describing the Changes in Architectural Information Technology to Understand Design Complexity and Free Form Architectural Expression. ITCON 11 (Special Issue the Effects of CAD on Building Form and Design Quality). (2006) 395-408

[25] Love, P. E. D., Simson, I. Hill, A. and Standing, C. From Justification to Evaluation : Building Information Modelling for Asset Owners. Automation in Construction. Vol.35 (2013) 208-216

[26] Kymmell, W. Building Information Modelling : Planning and Managing Construction Project with 4D CAD and simulation. United State of America. Mc Graw Hill. (2008)

[27] Hardin, B. BIM and Construction Management. Indianapolis: Wiley Publishing, IN. (2009)

[28] JKR, Laporan Tahunan JKR. (2011), pp.28-29. Information on https://www.jkr.gov.my/var/files/File/dokumen/laporan_tahunan_jkr_2011.pdf

[29] Wong, K.D.A., Wong, K.W.F., and Nadeem, A. Government Roles in implementing Building Information Modelling Systems Comparison between Hong Kong and The United States. Construction innovation Vol.11 (1) (2009) 61-76

[30] NBIMS. National Building Information Modelling Standard. (2010). Information on http://www.wbdg.org.pdfs/NBIMSv1 p1.pdf

[31] Haron, A.T., Marshall-Ponting, A.J., Abd Hamid, Z., MohamadKamar, K.A., Hashim, S., and AbdWahab, N.. Building Information Modelling (BIM): The Core Concept and The Benefits. (2012). Information on http://ibsresearch.blogspot.com/2012/08/building-information-modelling-bim-cor.html

[32] Ahmad, A.H. Building Information Modelling (2012). Information on http://1bina.my/blog/2012/03/06/building-information-modeling

Applied Mechanics and Materials Vol. 567 (2014) pp 631-636
© (2014) Trans Tech Publications, Switzerland
doi:10.4028/www.scientific.net/AMM.567.631

The Effects of Orientations on the Room's Thermal Performance in the Tropics

Leng Pau Chung[1, a], Mohd Hamdan Ahmad[2,b] Dilshan Remaz Ossen[1,c] Malsiah Binti Hamid[1,d] Mohammad Baharvand[1,e]

[1]Department of Architecture, Faculty of Built Environment, Universiti Teknologi Malaysia, Johor Bahru, Johor Malaysia

[2]Institute Sultan Iskandar of Urban Habitat and Highrise, Level 4, Dewan Sultan Iskandar, Universiti Teknologi Malaysia, Johor Bahru, Johor Malaysia

[a] pcleng2@live.utm.my , [b] b-hamdan@utm.my , [c] b-dilshan@utm.my , [d] malsiah@utm.my,

[e] baharvand12@gmail.com

Keywords: orientation, natural ventilation, thermal performance, windows

Abstract. Thermal performance of terrace house in Malaysia very much depends on the spatial design due to limited responsive environment factors. Building orientation is one of the important responsive factors under design consideration. The main concerns of the opening's orientation are solar radiation and wind. In Malaysia, the maximum amount of solar radiation directly affects the thermal performance and thus the orientation of the window should be designed in the way to minimize solar gain and maximize natural ventilation. This paper investigates the effect of building orientation on the thermal performance of the residential room with solar chimney. The case study house facing north was located at Kuching, Sarawak, Malaysia. The field measurement was conducted in the case study house compound on 16 may 2012 to obtain the boundaries condition for CFD (Computational Fluid Dynamic) simulation. Four cardinal orientations were selected to investigate the thermal performance via CFD in DesignBuilder. The results show that the south facing window could maintain the lowest air temperature in the indoor environment with mean air temperature of 31.78°C and air mean velocity 0.023m/s with 35°C extreme outdoor temperature and zero wind velocity.

Introduction. Sustainability becomes the trend of the building industry development over the concerns of global warming in recent years. As one of the main contributors of the carbon footprint in global context, building industry has the great responsibility to reduce the emission of the greenhouse gases [1]. In Malaysia, housing considered as the major contributor of carbon emission and energy user, which contribute 30% of the total due to the critical dependents of mechanical ventilation system [2] Thus, rethinking the design for the sustainable residential building with natural ventilation system is critically important in order to ensure the sustainability no longer a myth. There are dozens of way to go sustainability; however, the best way to achieve sustainability in housing design is adapting the passive architecture development concept as strategies to improve the indoor thermal environment and reducing the dependents on mechanical cooling system [3].The orientation of building is a significant consideration in early design process for architects. Thus, in this paper the effects of four cardinal orientations on the thermal performance of the residential room in single storey terrace house that attached with solar chimney were investigated.

Hot and humid climate in Malaysia considered as the most challenges climate to moderate or handle through architecture design, due to its long hour and high intensity solar radiation throughout day time, the heavily rains and prevailing winds caused by Monsoon seasons [4]. The terminology of "passive architecture" can be defined as the 'ecological building', 'green building', and 'energy efficient' building that shield the occupants from local climate elements which form the protective skin that create thermal comfort to occupants. Thus, from the definition of the passive architecture, other than huge roof that could protect occupants from direct solar radiation, the orientation of the

building façade should be one of the considerations in design. According to Zhu and Lin (2004), the orientation is the passive strategies that should be considered by designer [5]. Other than that, Thomas and Granham (2007) stated that building orientation is the first action and priority in the decision making in passive building design [6]. Building orientation in tropical region should be seriously considered since it has direct effect and interaction with solar radiation and wind direction [6]. Givoni (1994) supports the fact that the orientation of the building would be influenced by the local wind directions which alleviate the effective cross ventilation [7] According to Al-Tamimi *et al*. (2011), room located at east orientation has higher temperature compared to west direction unless with window-wall ratio of 25% both rooms have the similar air temperature [4]. In a study by Joseph (2003) stated that the north side has the lowest solar intensity from 43.6 W/m² to 65.5W/m² while west and east sides have similar solar intensity ranged from 86.1 W/m² to 89.6 W/m² [8]. In this study, the optimum thermal performance of the case study residential room would be studied in order to obtain the absolute comfortable environment in air temperature and air velocity aspects.

Research Flow & Method

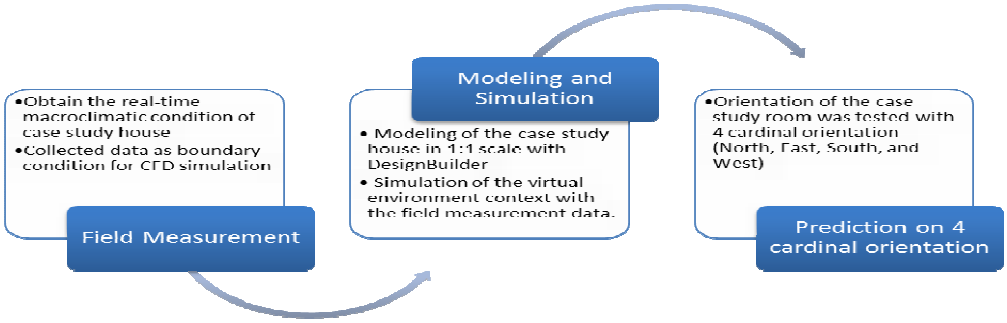


Figure 1: Research flow for the study initated with field measurement and the collected data to be input as the boundary condition for CFD simulation

In this study, field measurement will be carried out at the case study house compound in order to obtain the real time weather data for the CFD simulation. The collected data was utilized as the boundary condition for the CFD simulation for further prediction of the model. The results of the simulations were compared with the real time outdoor weather data as the benchmark of thermal performance of the indoor environment.



Figure 2: Location of the case study house

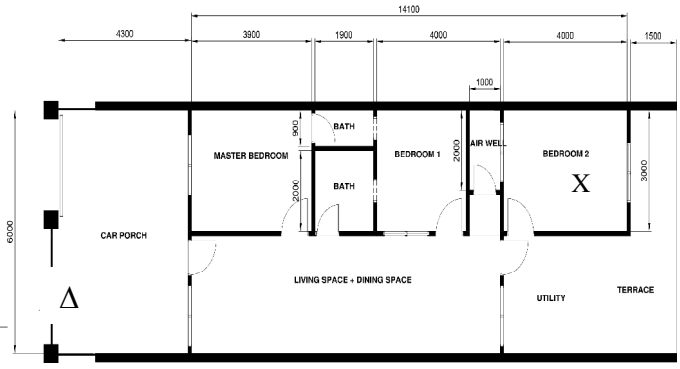


Figure 3: The positions of HOBO U30 Weather station (Δ) and location of the case study room (x)

Field Measurement. The field measurement was carried out in a single storey terrace house in Kuching, Sarawak, Malaysia from 8:00am to 7:00pm of 16 May 2012. The north facing case study house partitioned with two party walls with thickness 230mm and the internal partitions with thickness 150mm are made up with single brick wall plastered on both side. The external wall with cement and lime plaster is 200mm and the total U value for the walls is about 0.5 W/m²K. The

house comprised of 3 bedrooms, a living cum dining space and a utility room. All the windows are single clear glazed sliding windows (1.5m x 1.2m, and 0.9m above the floor) except bedroom 3 which attached to the solar chimney, which is fitted with glass panes louvers window (1.5m x 1.2m, 0.9 above the floor). The single layer clear glass pane window with U value 1.22 W/m²K which installed in case study room (3m x 4m with ceiling height 3m) is facing south and the solar chimney (0.5m x 2m x 8m height) is attached on the north wall of the room. Clay tiles are selected for the roofing material with U value 6.16 W/m²K and no insulation material occupied for both walls and roofs for heat transmission. In order to obtain the real time weather data, HOBO U30 weather station was set up at the case study house compound. The measured parameters included solar radiation, wind direction, wind velocity, air temperature and relative humidity. The measurement only carried out from 8am to 7pm since the study is focus on the effect of the solar radiation to the solar chimney which incorporated with the orientation of room.

Table 1: Field Measurement Input Data for CFD simulation

Time	Air Temperature [°C]	Humidity [%]	Wind Speed [m/s]	Solar radiation [W/m²]	Wind Direction [°]
8am	24.2	100	0	31	0
9am	25.6	97	0.03	765	160
10am	26.6	91	0	732	0
11am	31.9	79	0.09	881	120
12pm	31.8	72	0.18	992	140
1pm	32	63	0.1	1000	120
2pm	33.4	63	0.09	760	130
3pm	33.5	44.5	0	852	0
4pm	35	32.3	0	509	0
5pm	33.2	30	0.02	310	200
6pm	30	89	0	112	0
7pm	30	96	0	25	0

CFD Simulation. The field measurement weather data as shown in Table 1 was input as the boundary condition for the CFD simulation. The CFD simulation was carried out using DesignBuilder simulation program. The modeling info is as stated in the section 3.1 for the construction template The activity set as domestic bedroom and the occupancy set as 0.0229. The metabolic activity set as bedroom with factor 0.9. The HVAC template set as 'natural ventilation-

Table 2: Coordinate of monitoring point for modeled case study room

Monitoring Point	X (m)	Y (m)	Z (m)
A	1.712	-3.65	1.3
B	1.712	-2.17	1.3
C	1.712	-0.65	1.3
D	1.712	0.44	1.3
E	1.712	0.44	4.0
F	1.712	0.44	6.5

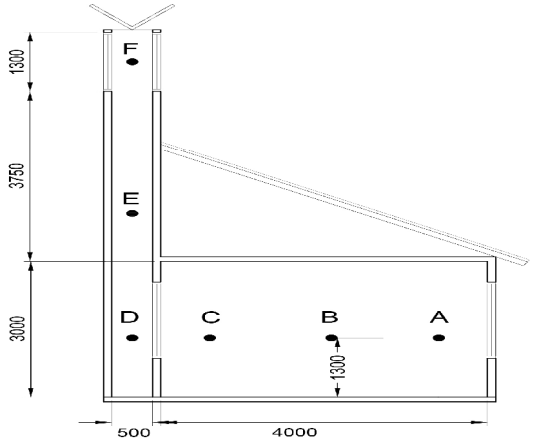


Figure 4: The position of monitoring points in the case study room.

no heating or cooling' and the outside air set as 3 Ac/h. The CFD calculation used the standard K-ε epsilon turbulent model with 5000 iteration. In this study, only the case study room and solar chimney will be modeled in order to reduce the complexity of the simulation and time consumed for simulation. A layer of adiabatic component was modeled means no heat transfer. The simulation used the Cartesian type-grid system with total number of cell produced is 12 numbers (x-direction) x 22 numbers (y-direction) x 31 numbers (z-direction). The max aspect ratio is 6.614. The monitoring points for the CFD slices are listed as in table 2 and figure 4 below. After the CFD simulation has converged, the CFD slices were exported as csv. file in Microsoft Excel and the air velocity and air temperature on the specific points were extracted for analysis purpose. In the simulation, the highest value of the air temperature, which is 35°C with zero wind velocity at 4pm of 16 May 2012 has been selected in order to find out the thermal performance of the room under extreme climatic condition.

Designbuilder is reliable software developed by EnergyPlus, which is established by U.S.DOE building energy simulation program for building simulation, heating and cooling, energy analysis and so forth [9]. Validation of the software with field measurement has been recognized and carried out by researchers as a method to verify the simulation software [10-12] DesignBuilder has been validated by researchers and this software is considered as useful and reliable [12, 13].

Result and Discussions

Field Measurement: Outdoor Climate Condition. Daily climatic patterns in tropical climate region require effective design strategies to achieve thermal comfort. Understanding of outdoor climatic condition is important before carrying out simulation. The purpose to carry out the field measurement is to obtain the real-time condition of the outdoor environment for the input of simulation. Out of the measured data, the hottest hour was chosen to input as the boundary condition as only the great temperature differences between indoor and outdoor will promote the ventilation rate for indoor room. According to Table 1, the variance range of the air temperature is 24.2°C at 8am to 35°C at 4pm while the relative humidity range from 30% at 5pm to 100% at 8am. 35°C is the maximum air temperature of year 2012 according to Malaysia meteorological department data. [14] The air temperature is inversely proportional to the humidity. The wind speed in Malaysia is considered low, where most of the times are 0 m/s and the highest value recorded as 0.18 m/s at 12pm. The peak of the solar radiation value is at 12pm with 1000 W/m² at 1pm. During the day time the South-East wind is dominant with less diversity. However the direction of air flows no longer significant during the evening due to radiation of the land and environment has caused the air flow direction to divert.

CFD Simulation: Effects of Thermal Performance in Varied Orientation. From the analysis of the results from simulation, the air temperature at point A,B,C and D for four cardinal orientations considered as static. This means that the temperature for the indoor environment is stable. However, point E and F for four orientations increase drastically due to the stack effect. The heat is moving upwards and increase. Out of four orientations, East and North facing window have the highest air temperature for both space, which are test room (point A, B and C) and solar chimney (point D,E, and F). The East facing window posses the highest temperature in five points (A,B,C,D and E) compared to other orientation which ranged from 34.65°C to 42.09°C while South facing windows posses the lowest from 31.77°C to 37.86°C. This fact is supported by Al-Tamimi (2011). [4]. Point E and F should have higher temperature compared to A, B,C and D due to its function as solar chimney. The discussion would taken point B as example since it is the habitable zone. With no ventilation and extreme outdoor temperature, the differences for in/outdoor temperature for four orientations were +0.74 (north), +0.36 (east), +3.21 (south) and +0.84 (west). This shows that the south facing window is the best orientation at May 2012 since it shaded from the evening sun. For

the air velocity stated in figure 6, the east facing window has the greatest differences from point A to E, which is 86.11% difference. This is caused by the west facing solar chimney absorbed direct radiation from sun and create the great temperature differences. However, air convection happens in solar chimney and indirectly increase the room air temperature since both are connected.

In this case, the south facing window posses the ideal condition. The air flow slowly increase in the room, started from 0.008m/s at point A up to 0.037m/s at point C. Although it is low compared to west facing window, with deviation -0.007m/s (point A and C) and -0.09m/s (point B), the acceptable comfort is still complementary with the lower indoor air temperature. In Figure 7, the temperature reduction that compared to outdoor temperature occurred at point D, E and F which is located at solar chimney are ranged from -0.238°C for North facing window, -2.836°C for South Facing Window, -5.242°C for West window and -7.018°C for East window. The results showing that the solar chimney is functioning as vertical solar updraft tunnel. The air pressure created by warm air due to the solar radiation updrafted via solar chimney and replaced by cold air in lower room via outdoor wind from window. The higher the air temperature differences between point D, E, F and point A, B, C, the higher the speed of air velocity updrafted via the indoor room. Figure 9 shows that the solar chimney (red colour) has higher air temperature compared to the room (green) and the countour outline showing that the air is updrafted by the solar chimney. The findings show that the south orientation facing window are most suitable since it could reduce the heat transfer from glazing and induce buoyancy of the air without influenced by radiation effect.

In addition, according to figure 8, the average air temperature for the outdoor is 30.6°C and indoor is 30.078°C while the average wind velocity is 0.0425m/s and 0.0219m/s respectively. Obviously, the outdoor air temperature and air velocity is higher than the indoor environment, with differences of 1.71% for air temperature and 48.47% for air velocity. This shows that the solar chimney has the ability to reduce the air temperature and maintain the indoor air speed. The diurnal air temperature of outdoor environment fluctuated between 24.2°C to 35°C while air velocity between 0m/s to 0.18m/s. The comparison between outdoor and indoor thermal performance is important since the trend of air temperature and air velocity in the indoor could be compared with the outdoor.

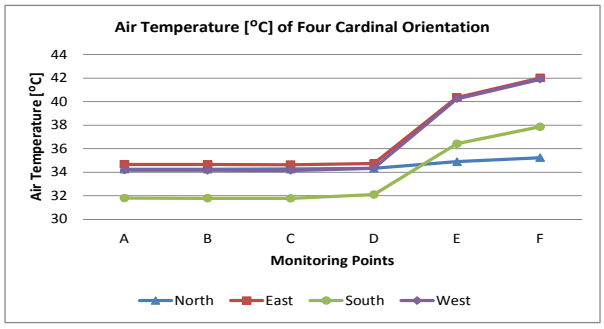


Figure 5: Diurnal pattern of air temperature for case study model at 16 May 2012.

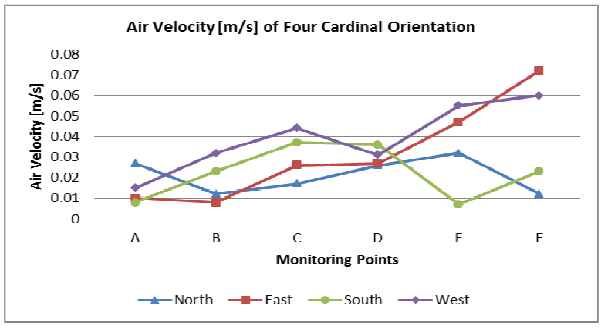


Figure 6: The diurnal pattern of air velocity for case study model at 16 May 2012

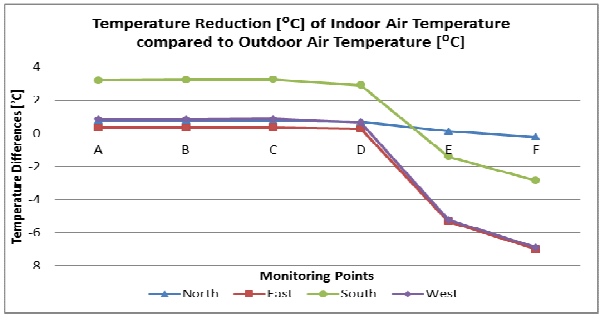


Figure 7: The temperature reduction of indoor air temperature compared to outdoor environment

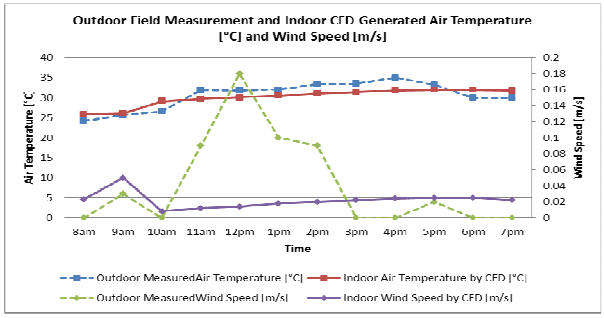


Figure 8: Comparison of the measured outdoor and CFD generated indoor average room air temperature and air velocity.

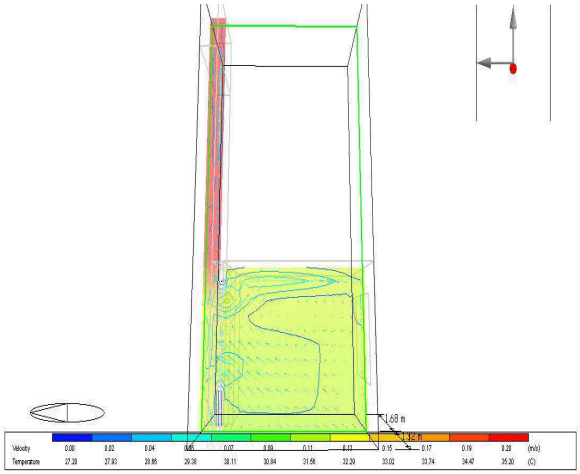


Figure 9: The air magnitude has been updrafted shows that stack ventilation happened in solar chimney.

Conclusion. Appropriate selection of window orientation could reduce the heat transmission and thus increase the thermal comfort of indoor environment. Among the scenarios, the east window are always hottest compared to window in other orientations. The south facing window is the best orientations out of four since it could maintain the lower air temperature and induced steady air buoyancy effect in the indoor environment. In order to improve the thermal performance, the selection of glazing with low U value and shading device to minimize the solar radiation should be considered. In summary, although the air flow and air temperature do not achieve the standard thermal comfort condition, however, the significant improvement could enhance the thermal performance comparable to outdoor temperature.

Acknowledgment. The authors would like to thank Institute Sultan Iskandar of Urban Habitat & Highrise for the financial support and assistance from research grant

References

[1] Z.M. Gill, M.J. Tierney, I.M. Pegg, N.Allan. Measured energy and water performance of an aspiring low energy/ carbon affordable housing site in the UK. Energy and Buildings. 2011;43(1):117-25.
[2] K. King, J. Goodwin, N.Passant, N.Brophy, I. Tsagatakis. Local and Regional CO2 Emissions Estimates for 2005-2006 for the UK. UK: AEA Report to DEFRA, 2008.
[3] A.M. Abdul Rahman, N.S.A.Rahim, K.Al-Obaidi, M.Ismail, L.Y.Mui. Rethinking the Malaysian Affordable Housing Design typology in View of Global Warming Considerations. Journal of Sustainable Development. 2013;6(7):134-46.
[4] N.Al-Tamimi, S.F.S.Fadzil, W.M.W.Harun. The Effects of Orientation, Ventilation and Varied WWR on the Thermal Performance of Residential Rooms in the Tropics. Journal of Sustainable Development. 2011;4(2):142-9.
[5] Y.X.Zhu, B.R. Lin. Sustainable housing and urban construction in China. Energy and Buildings. 2004;36(12):1287-97.
[6] R.Thomas, T. Granham. The environments of architecture: Environmental design in context. Great Britain: Taylor and Francis; 2007.
[7] B.Givoni. Passive and Low Energy Cooling of Buildings. New York: International Thomson Publishing ITP; 1994.
[8] J.C.Lam, D.H.W.Li. An analysis of daylighting and solar heat for cooling-dominated office buildings. Solar Energy. 1999;65(4):251-62.
[9] DesignBuilder. Energyplus: U.S. Department of Energy; 2013 [cited 2013 28 November 2013]. Available from: http://www.designbuilder.co.uk/content/view/29/44/.
[10] M.Z.I.Bangalee, J.J.Miau, S.Y.Lin. Computational techniques and a numerical study of a buoyancy-driven ventilation system. International Journal of Heat and Mass Transfer. 2013;65(0):572-83.
[11] G.Evola, V.Popov. Computational analysis of wind driven natural ventilation in buildings. Energy and Buildings. 2006;38(5):491-501.
[12] M.Baharvand, M.H.Ahmad, T.Safikhani, R.B.A.Majid. DesignBuilder Verification and Validation for Indoor Natural Ventilation. JBasic Appl Sci Res. 2013;3(4):182-9.
[13] DesignBuilder. An Inter-program Analysis of Computational Fluid Dynamics Based on PHOENICS and DesignBuilder Software. Newcastle: Northumbria University, 2012 Contract No.: NE18ST.
[14] Meterological Department, Malaysia. Records of Meterological Data, Kuching. Kuching Station. Kuching, Sarawak 2012

Applied Mechanics and Materials Vol. 567 (2014) pp 637-641
© (2014) Trans Tech Publications, Switzerland
doi:10.4028/www.scientific.net/AMM.567.637

The Importance of Lightweight Concrete Technology Development for IBS Industry in Malaysia Based on Cost Comparison between Concrete Slab and Hollow Core Slab: A Case Study of LRT Car Park Project

Mohd Zakwan Ramli[1,a], Harlina Mohd Mahayudin[2], G. Hayder[1], Z. M. Hafiz[1], M. Daud[1] and A. M. Salleh[1]

[1]Civil Engineering Department, College of Engineering, Universiti Tenaga Nasional, Jalan IKRAM-UNITEN, 43000 Kajang, Selangor, MALAYSIA

[2]Planning Unit, Gabungan Strategik Sdn Bhd, 73-I-G, Jalan Teknologi 3/9, Bistari De Kota, Kota Damansara, PJU 5, 47810 Petaling Jaya, Selangor, MALAYSIA

[a]Zakwan@uniten.edu.my

Keywords: Industrialised Building System, cost comparison, cast-in-situ, hollow core slab, lightweight IBS.

Abstract. There are several issues related to the implementation of new Industrialised Building System (IBS) technology in Malaysia which some of them are the awareness among industry players, and lack of development on the new technology in the industry. The main constraint that has always been discussed by the IBS players is time and cost. To have more reliable product or technology in terms of cost and time, it is important to craft and develop new idea as well as technology in our own country. The objective of this study was to highlight the cost comparison between cast in-situ concrete slab and hollow core slab (lightweight) which it can be a starting point for future research on the development of new lightweight IBS technology in Malaysia to get the most reliable cost with latest technology by using local resources. Informations on costs and work durations are collected and analysed between two floors using two different construction methods (hollow core slab and conventional concrete slab). Hollow core slab (lightweight IBS) has similar or less cost with shorter construction period (30% shorter) for the project.

Introduction

There are several issues that connected to the implementation of new Industrialised Building System (IBS) technology or system in Malaysia which some of them are the awareness among industry players, and lack of exposure on the new technology in the industry [1]. Stated under Action Plan R32 which is based on IBS Roadmap 2011-2015, Government of Malaysia encouraged private sector by assisting in technical and financial part to support R&D in IBS technology [2]. To have more reliable product or technology in terms of cost and time, it is important to craft and develop new idea as well as technology in the country. An affordable new and innovative approaches and technology are needed in the design and construction [3].

The most used IBS technology for construction in Malaysia is precast concrete. Precast concrete is the most IBS technology that construction companies claimed as reliable to be used in terms of cost and time. Even though it is the most current and popular IBS product for structure, it still needs to be upgraded to be more reliable technology for IBS.

Other lightweight IBS technology especially for slab such as Expanded Polystyrene (EPS) lightweight concrete slab and bubble slab requires high investment costs if it has to be manufactured locally because they are patented overseas. These will give extra costs for manufacturer to manufacture the technology as it can only be set up by their agent or representatives and as a result, the costs will be incurred by clients and contractors. It is very important to innovate and develop local technology for lightweight concrete which uses local resources as it always has the market demands in our construction industry. Based on a case study done by Hazem [4], the lightweight

concrete technology used saves 40% of overall construction period, 30% on construction costs and 30-40% on energy costs. It is recommended to replace the traditional building practices by IBS, which will save on labour, cost and time of construction, and the durability and quality [3]. The adoption of IBS promises to ensure efficient, clean, safe, skilled workers, proper coordination and management, precision, innovative and new attributes [1].

In this study, the objective is to highlight the cost comparison between cast in-situ concrete slab and hollow core slab (lightweight) which can be a starting point for future research on the development of new lightweight IBS technology in Malaysia to have advance IBS technology and cost with latest technology by using local resources.

Methodology

This study was done on a car park project for Light Rail Transit (LRT). Public transport development project was planned under the National Key Results Area (NKRA) which is a program by Government under the Government Transformation Program (GTP). Time is very important in the NKRA project which that explained why it is important to develop new technology for lightweight concrete slab with a reliable cost.

During this study, this project has been started and still in progress. All drawings, specifications and other information regarding the cost and value of project items are collected from construction site, managers, contract personnel, and mostly are from contractor.

This study focused on slab structures which are 1B Floor (in-situ slab) and 2B Floor (hollow core slab). Design load for the structure is 2.5 kN/m^2. The estimated costs are including labour costs. The elements chose for the analysis are depending on relation for work procedure between hollow core slab and in-situ slab. To ensure that all analysed costs are comparable, the costs are converted to per area measurement using metrical measurement (m^2). Fig. 1 shows the side layout drawing for the car park project which also shows the two floors for the two slabs in this study.

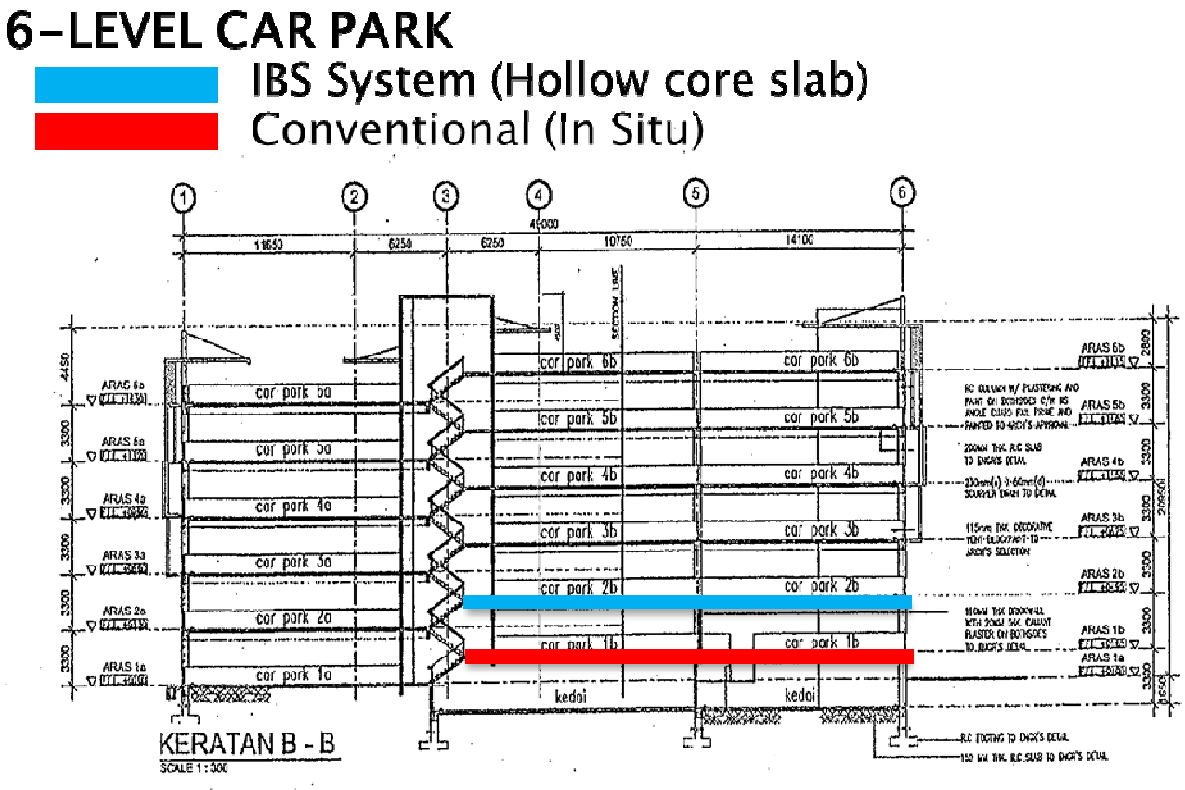


Fig. 1: Side layout drawing of LRT car park project

Result and Discussion

In-situ Slab (conventional). Total net area for the 1B Floor is 3139.82 m^2. Table 1 shows the results for in-situ slab cost analysis. Based on the work process of in-situ slab, there are four elements which are concrete, reinforcement bar, formwork and propping/scaffolding. The total cost for in-situ slab is RM 197.63 per square meter while the duration is 9 days. Based on a study by Chan [5], the cost for conventional method mostly contributed by labour to fabricate and install formwork and props to support the fresh concrete.

Table 1: In-situ slab cost analysis with its duration

COST	
Elements	*Total [RM]*
Concrete	288,549.46
Rebar (Various sizes)	229,623.26
Formwork (Sides & Soffit)	89,78.85
Propping/Scaffolding	12,559.28
Total Cost [RM/m^2]	197.63
DURATION	
Elements	*Duration [Days]*
Erection of Scaffolding	2
Formwork	3
Rebar	3
Concrete	1
Total [Days]	9

Hollow Core Slab (IBS). Total net area for the 2B Floor is also 3139.82 m^2. There are few additional elements in Table 2 which shows the results for the hollow core slab cost analysis. These elements are based on work process for the hollow core slab which related to the work process of in-situ slab. Labour cost is also included in each element. The total cost per square meter for this lightweight IBS is RM 192.00 and it only took 6 days for the hollow core slab.

Table 2: Hollow core slab cost analysis with its duration

COST	
Elements	*Total [RM]*
Hollow Core Slab (HCS) Items	468,430.03
Installation Cost	13,501.20
Concrete Topping	54,162.70
Grouting	28,830.55
Formwork (Undersides of HCS at perimeter beam end)	5,577.86
Fabric Reinforcement (BRC A7)	32,340.09
Total Cost [RM/m^2]	192.00
DURATION	
Elements	*Duration [Days]*
Hollow Core Slab	3
BRC Mesh	1
Floor Topping	1
Grouting	1
Total [Days]	6

The result shows that hollow core (lightweight) slab saves about 30% of duration and uses almost 3% less cost than in-situ slab in the project. As a result, there will be cost saving in the overall cost and the project cost will be noticeably reduced. By taking the deduction between RM 197.63 and RM 192, it will give a total of RM 5.63 saving costs and after multiplied by 3139.82 m^2 following with 7 floors total for this car park project, it will gives a total amount of RM 123,740.30 cost savings. By referring to Lai [6] which stated that lightweight precast product can saves more time and costs as less material used, less labours used as the element is lightweight, and also less machinery to lift the elements for installing purposes. It has been proved in the construction industry on other countries that lightweight structure elements can save money and time. The lightweight concrete technology can be further developed to get more less costs in the IBS construction industry as the hollow core slab is the platform for researchers to get notice the importance of lightweight concrete in the industry.

There are also some developed lightweight concrete technologies in other countries which use the concept of reducing costs by reducing the concrete weight. In developing the lightweight concrete technology, there are two basic concepts that can be applied which are based on material development or can be based on its physical design. This lightweight technology has been well developed in other countries and one of the best technologies on material based is expanded polystyrene concrete slab which based on study by Hazem [4]. While for the physical design, the best example extracted by author is the lightweight biaxial slab which uses "bubble-lattice" in their design. The concept of this technology is based on creating voids to have a lighter slab which uses less concrete and less steel. The lightweight bubble concrete slab can save the costs ranging from 16% to 30% and it can also save the construction period up to 35% [7].

These technologies which were developed on the international level will help IBS industry players in Malaysia to develop more on its lightweight concrete technology. The lightweight concrete will help builders to reduce not only on their time and direct costs, but it can also decrease the cost of the foundation and column or support arrangements for their structure because of the decreasing of the elements' self-loads.

Conclusion

In this study, the costs for using conventional and IBS in construction are compared with their period in the construction. It shows that hollow core slab (lightweight element) can ease Malaysia construction industry in terms of cost and time. This study can be a starting point to encourage researchers to innovate and develop new local IBS technology especially the one that uses local resources to get more reliable IBS product in future.

References

[1] A. B. A. Rahman, & W. Omar, Issues and Challenges In The Implementation of Industrialised Building Systems In Malaysia, Proceedings of the 6th Asia-Pacific Structural Engineering and Construction Conference (2006)

[2] I. Din, IBS Roadmap – Status Towards 2015, The International Constructional Steel Conference (2012)

[3] W.E. Alaghbari, A.K. Razali, S. Azizah, Ernawati, The significant factors causing delay of building construction projects in Malaysia, Engineering, Construction and Architectural Management, Vol. 14(2), pp.192 – 206 (2007)

[4] M.N.A. Hazem, Plastbau®, Better Way for Build in View of Sustainable Construction, King Abdulaziz City for Science and Technology (2005)

[5] T.K. Chan, Comparison of Precast Construction Costs: Case Studies in Australia and Malaysia, In: C. Egbu, E.C.W. Lou (Eds), Proceedings 27th Annual ARCOM Conference (2011)

[6] T. Lai, Structural Behaviour of BubbleDeck® Slabs and Their Application to Lightweight Bridge Decks, PhD Dissertation, Massachusetts Institute of Technology (2010)

[7] C. Sergiu, G. Roxana, D. Gabriela, Summary of Tests and Studies Done Abroad On The Bubble Deck System, Buletinul Institutului Politehnic Din Iasi, Universitatea Tehnică Gheorghe Asachi din Iaşi (2009)

Applied Mechanics and Materials Vol. 567 (2014) pp 642-647
© (2014) Trans Tech Publications, Switzerland
doi:10.4028/www.scientific.net/AMM.567.642

The Performance Measurement of Supply Chain Management (SCM) in Malaysian Infrastructure Project

Mohamad Razali Abd Wahab[1,a], Hayroman Ahmad[1,b,]

[1]Faculty of Architecture, Planning and Surveying, Universiti Teknologi Mara (UiTM) Perak, 32610 Seri Iskandar, Perak, Malaysia

[a]razaliwhb@gmail.com, [b]hayro724@perak.uitm.edu.my

Keywords: Supply Chain Management, Infrastructure, Performance Measurement, Dimension.

Abstract. The infrastructure project is a great challenge to the key player due it volume and complexity. The problem facing by most of infrastructure project in term of management aspect, such as management conflict and unsatisfied output becomes an obstacle to fulfill the government strategy mainly Malaysia. Supply Chain Management (SCM) is viewed as a strategic tool to tackle that issue but there is a lack of comprehensive view of SCM concept and lack of reliable measure which contribute to improper guideline to the practice of SCM. Due to that this paper aims to identify reliable performance measure of SCM through perception of key player in infrastructure project. The indicator for performance measure of SCM is based on survey that *carried out on 116 key players of Malaysian Infrastructure Project*. Statistical techniques were used to form, verify and test the reliability of the questionnaire. The conceptual classification of the previous literature review and justification of experts during the pilot study proposed six (6) indicators for measuring performance of supply chain management (SCM). However, in this study five (5) indicators have been identified, namely *Information Dissemination, Management, Leadership, Relationship Development, Customer Management and Activities Sequences*. Hence this measure could be used to evaluating and control the performance of supply chain and as a guidance for a new initiatives to improve and develop supply chain.

Introduction

Infrastructure contributes major roles in the development of the country. Realizing the importance of infrastructure to the economic growth, the Malaysian Government under Ten Malaysian Plans, RMK-10 (2011 – 2015) aims to provide world class infrastructure and improve the quality of infrastructure [24]. According to Sambasivam & Soon [23] in Malaysia the construction sector can be divided into four categories: office, retail, residential and infrastructure.

However, there are obstacles in the real scenario of the construction industry, including infrastructure. The problem facing by most of infrastructure project in term of management aspect, such as management conflict and unsatisfied output becomes an obstacle to fulfill the government strategy mainly Malaysia [7].

Hence, to tackle those issues a comprehensive management tool is required. Supply Chain Management (SCM) is viewed as a strategic tool as it is functioning as an overall management process to monitor and control all such logistic activities [12]. Implementation of SCM could benefit of organization in term of improving efficiency and productivity, improve collaboration among supply chain partner, reducing construction cost, reducing delay and other [12, 19]

Based on the various definitions, SCM in construction can be divided into three key elements: functions, entities and benefit/target. The first element, function, can be described as integrated management of all processes and individual that involved in managing the flow of resources in construction within an integrated network [10]. The second element entities resulting from the upstream level (client, planner, consultant and etc.) and downstream level (builders, manufacturer, supplier and etc.) [10,11] and the third element, benefit/target gives a value chain that will improve customers satisfaction, delivery and quality of the product, reducing cost and maximize margin in the supportive environment [3,10].

Although the benefit of SCM has been realized, the implementation of SCM practice is still an issue cause by improper guideline to the practice of SCM due to lack of comprehensive view of SCM concept and lack of reliable measure [2]. The previous research among Malaysian construction industry also found that problem to implement SCM practice cause by lack of management tool and practice [8]. Due to this issue, this paper aims to identify reliable performance measure of SCM through perception of key player in infrastructure project.

The performance of supply chain needs to be control according to its structural which is a part of main element for SCM and an important part of the control is the installation of a monitoring mechanism to continuously assess how supply chain operates [26]. Neely et al. [5] explained that performance measurement is defined as "the process of quantifying the efficiency and effectiveness of the past actions" and performance measure was defined as "a parameter used to quantify the efficiency or effectiveness of the past actions". Yeung et al. [21] supported this by their explanation that performance measurement determined by the metric number of indicators which include both financial and non-financial indicators. Performance measurement and performance measure play an important role in setting objective, evaluating performance and determining future courses of actions [4]. The important thing is, without deep understanding of how to measure performance/excellent, those entities will manage the process and resource by their own way [15].

This research sets the findings covering five infrastructures sub-sector that stated by the Economic Planning Unit of Malaysia (EPU) [14]: Energy Supply, Water Management, Transportation, Communication and Waste Management.

In order to achieve the objective, the relevant indicators in the construction industry has been identified from the previous literature review. Indicators from eight previous literatures in the construction industry has been grouped according to the same conceptual meaning and produce 15 combination of indicators for performance measure of SCM (Table 1). This step has been explained by Amponsah [13] as the criteria that have similar nature logically should be grouped into one category for easier pairwise comparison during the survey. Taking into consideration of conceptual classification during the literature review and justification by five experts (through questionnaires and pilot survey) in various disciplines of Infrastructure project environment the selected indicators were: *management leadership, relationship development, information dissemination, customer management, activities sequences and green supply chain*. This step has been applied by Ahmad et al. [17] that justified five success criteria of conceptual classification during the literature review and justification by nine experts (through a questionnaire as well as a pilot survey) in various disciplines of Hospital project environment.

Research Methodology

This study is to identify reliable performance measure of SCM through perception of key player in infrastructure project. In order to achieve the target, this research focused on exploratory study with combination of literature review and questionnaire survey.

The information that is gathered from literature review adopted from various sources comprising of relevant books, journals articles, thesis and dissertation, conference proceeding, research paper and report. The information from these various sources is used to improved understanding of SCM in infrastructure and produce a combination of indicators for performance measure of SCM practice as discuss in the introduction.

For questionnaire survey, the exploratory research method was used for the study, which involved quantitative data gathering stage. A set of questionnaire consist of 50 questions, complete with a simple briefing about the research was sent to the relevant client, implementer, consultant, contractor (Registered Class A/G7 Contractor) and supplier in Infrastructure project. A total of 500 questionnaires were distributed to the several key player of the Malaysian Infrastructure project, which was randomly selected through email, online questionnaire, by post and by hand. Out of 500 questionnaires distributed, 116 were completed and returned representing 23% response rate.

Table 1: Summary of measurement item based on literature review
Source: Researcher Analysis

AUTHOR	INDICATORS OF PERFORMANCE MEASURE														
	1	2	3	4	5	6	7	8	9	10	11	12	13	14	15
Akintoye et al. [1]		√				√		√	√	√	√		√	√	
Wickramatillake, et al. [9]		√			√		√	√							
Albaloushi & Skitmore [19]		√					√	√	√	√	√				
Abd. Shukor et al. [6]		√			√	√		√		√	√	√			
Meng, et al [27]			√	√		√	√	√				√			
Markard [22]			√				√		√	√	√	√			√
Emuze & Smallwood [16]	√	√	√	√		√			√		√			√	
Adetunji et al. [20]						√		√		√	√	√			
FREQUENCY FACTOR	**0.1**	**0.6**	**0.4**	**0.3**	**0.3**	**0.6**	**0.5**	**0.8**	**0.5**	**0.6**	**0.8**	**0.5**	**0.1**	**0.3**	**0.1**

Legend:-

1 = Education
2 = Management Leadership
3 = Objective
4 = Problem Solving
5 = Technology Utilization
6 = Relationship Development
7 = Supply Chain Technical
8 = Information Dissemination
9 = Resource Planning
10 = Customer Management
11 = Activities Sequences
12 = Continuous Improvement
13 = Supplier Management
14 = Other
15 = Green Supply Chain

Result and Discussion

Demographics. The respondent involved in this research were the key players of infrastructure project such as implementer and client, consultant and contractor/supplier.

Total respondent involve in this survey were 116, which could be divided into Implementer (28%), Client (9%), Consultant (26%) and Contractor (37%). From Table 2, the majority of respondents are Mid-Level Manager (48%) which involve in the management of the companies. Besides that, the majority of the respondents were involved in Transportation (56%) while the second majority is Water Management (28%). From respondent's experience, the majority of the respondents have more than 10 years' experience (48%), which show that respondent have enough experience in the project as stated by Ahmad [18] that respondent which have degree and master with more than 7 years experience can be considered as senior position in organization. Beside that experience give high impact in term of knowledge and competencies of the works [18].

Table 2: Summary of Demographics From The Study

Title	Item	Statistics		Title	Item	Statistics	
		N	%			N	%
Job title/Position	Senior Level Manager	24	21	Specialization	Energy Supply	10	9
	Mid-Level Manager	56	48		Water Management	32	28
	Junior Level Manager	32	28		Transportation	65	56
	Other	4	3		Communication	6	5
Type of Organization	Implementer	33	28		Waste Management	3	3
	Client's Department	10	9	Experience in Infrastructure project	< 1 years	3	3
	Consultant	30	26		1 – 5 years	37	32
	Contractor/Supplier	43	37		5 – 10 years	20	17
					More than 10 years	56	48

Data Analysis and Discussion. The data from the questionnaire was analyzed by using SPSS software to form the new indicator and quality measure of this indicator. In this research, the principal component analysis (PCA) was applied as the first step to all question of each indicator to form the new component/factor for each indicator. This step is justified by Sousa Jabbour [2] where the principal component analysis divided the questions into groups (factors) in order to summarize their relationship pattern. As the result, five indicators consist more than two components, except indicator 'Green Supply Chain' that only consist of one component which not been considered for further analysis

Then each of these indicator was analyzed for quality measure using factor analysis and reliability test as below:-

Factor Analysis.

1. Measuring sampling adequacy (MSA) for each item in indicator by the Kaiser-Meyer-Olkin (KMO) test (Ahmad [18]: Cut off point 0.5, Sousa Jabbour [2]: Cut off point 0.5)
2. The Eigenvalue of each component in indicator > 1 (Ahmad [18] : > 1, Sousa Jabbour [2] : > 1)
3. Data reduction of each item in the indicator by using Varimax Rotation Method

Reliability

1. The alpha value as minimum as 0.7 (Ahmad [18], Sousa Jabbour [2])

The first step for quality measure was to calculate the global Cronbach's Alpha of the indicators for performance measure. The value of 0.786 – 0.847 was obtained could be considered as acceptable and the scale has a good internal consistency. The combination of PCA method and Varimax Rotation Method with KMO test was used for data reduction of all variable under each indicator. In order to justify the result, the variable with the value of MSA more than 0.5, Eigenvalue more than 1, communalities more than 0.5 and coefficient of anti-image matrices more than 0.6 was considered to form the component [2]. As the result, the global KMO test that verifies the adequacy of the sample of five indicators was 0.731 – 0.842 and is considered adequate.

Besides that, the data reduction of the variable which below the required limit gives a higher accumulated variance value (%) which is 58.581 – 69.419. Table 3 presents the indicators which satisfies the quality measure limit with the list of components which been named based on the group of question.

Conclusion

This research was to identify the performance measure of SCM through perception of key player in Malaysian infrastructure project. In order to achieve that, six indicators listed by conceptual classification during the literature review and justification of expertise in an infrastructure environment where test to several key player such as implementer, client, consultant and contractor/supplier.

The analysis of the qualitative data from SPSS instrument identifies five indicators that satisfy the quality measure limit. Overall the questionnaire's reliability can be acceptable and have a good internal consistency with reliability value 0.786 – 0.847 for the five indicators. This five indicators which representing the real feedback from infrastructure project environment namely *information dissemination, management leadership, relationship development, customer management and activities sequences*. Eventhough there were many research identify indicator in construction industry in term of performance measure of supply chain but characteristics of practice that explained by Chia & MacKay [25] as 'practices influence and are influenced by individuals, by organizations, by the environment and by the concept that development' shown that difference measure are required for difference categories of construction industry. So hopefully this effort in identifying performance measurement of supply chain in infrastructure could be used to evaluating and control the performance of supply chain and as a guidance for a new initiatives to improve and develop supply chain.

Table 3: Quality Measures Result for the Proposed Indicators

	Indicators				
	1	**2**	**3**	**4**	**5**
Label	**Information Dissemination**	**Management Leadership**	**Relationship Development**	**Customer Management**	**Activities Sequences**
Component	Sharing of SCM Information Implementation of SCM Information	Top Management Commitment Human Capital Development	Management of information system Team-building Management Comprehensive management of project and delivery process	Comprehensive delivery services and system Strategic cooperation with customer	System for planning and monitoring activities in project System and procedure to handle the unseen situation for construction resources
Cronbach's Alpha	0.835	0.835	0.786	0.842	0.847
KMO	0.828	0.829	0.731	0.842	0.829
Communality	Min : 0.521 Max : 0.801	Min : 0.565 Max : 0.691	Min : 0.588 Max : 0.847	Min : 0.519 Max : 0.728	Min : 0.544 Max : 0.668
Eigenvalue	Min : 1.251 Max : 3.608	Min : 1.277 Max : 3.996	Min : 1.113 Max : 3.439	Min : 1.093 Max : 3.841	Min : 1.320 Max : 4.117
Accumulated explained variance (%)	69.419	58.581	65.704	61.673	60.416

References

[1] A. Akintoye, G. McIntosh & E. Fitzgerald, A Survey of Supply Chain Collaboration and Management in the UK Construction Industry, *European Journal of Purchasing and Supply Management*. 6 (2000) 159-168

[2] A.B. Sousa Jabbour, A.G. Alves Filho, A.B. Noronha Viana & C.J. Chiappetta Jabbour, Measuring Supply Chain Management Practices, *Journal of Measuring Business Excellence*. 15 (2011) 18-31.

[3] A. Cox, & M. Townsend, Strategic Procurement in Construction: Towards Better Practice in the Management of Construction Supply Chain. London: Thomas Telford Publishing. (1998)

[4] A. Gunasekaran, C. Patel & R.E. McGaughey, A framework for Supply Chain Performance Measurement, *International Journal of Production Economics*. 87 (2004) 333-347

[5] A. Neely, C. Adams & M. Kenerly, The Performance Prism : The Scorecard for Measuring and Managing Business Success, Financial Time, Prentice-Hall, London (2002)

[6] A.S. Abd Shukor, M.F. Mohamad, R. Mahbub & F.M. Halil, Supply Chain Management : A review of the concepts and success factor, *International Sysposium on Construction in Developing Economics : Commonalities Among Diversities*. Penang (5-7 October 2009) 74-89

[7] B. Flyvbjerg, Design by Deception, *Harvard Design Magazine*. (2005) 50-59

[8] C.C. Chee, Supply Chain Management Through Partnering in Malaysian Construction Industry, *Unpublished Master Thesis*. Universiti Teknologi Malaysia, (2003).

[9] C.D. Wickramatillake, S.C. Lenny Koh, A. Gunasekaran & S. Arunachalam, Measuring Performance Within the Supply Chain of a Large Scale Project, *Supply Chain Management : An International Journal*. 12 (2007) 52-59

[10] CIDB-UUM, Draft Final Report of Supply Chain in the Malaysian Construction Industry, *Contruction Industry Development Board of Malaysia (CIDB)*, Kuala Lumpur, 2010.

[11] C.M. Harland, Supply Chain Management:Relationships, Chain and Networks. *British Journal of Management , 7* (Special Issue), (1996) 863-880.

[12] C.S. Abdullah, A.A. Othman & F. Zulhumadi, Construction Supply Chain Management (CSCM): Practices in the Malaysian Construction Industry, *2nd International Conference on Logistics and Transportation. Rydges Lakeland Resort Queenstown, Queenstown*, (16-18 December 2010).

[13] C.T. Amponsah, Using Multi-Criteria Decision Making to Determine the Critical Success Factor for Procurement of Capital Project Under Public-Private Partnerships, *Proceeding of International Symposium on the Analytic Hierarchy Process*. (2011).

[14] Economy Planning Unit of Malaysia, Dasar-dasar Utama : Infrastruktur dan Kemudahan Awam, *Official Portal : http://www.epu.gov.my/web/guest/infrastructureutilities*. (10/01/2013).

[15] E. Westerveld, The project excellent model : Linking Success Criteria and Critical Success Factors, International Journal of Project Management. 21(2003) 411-418

[16] F. Emuze & J. Smallwood, Conceptual Framework for Improving the Construction Supply Chain, 6th Nordic Conference on Construction Economics and Organization – Shaping the Construction/Society Nexus, (13-15 April 2011)

[17] H. Ahmad, A.R. Abdul Aziz, M. Jaafar & A. Alias, Differences Between Client and D&B Contractors Perceptual Emphasis Towards Success Criteria's for Public Hospital Project, in *proceeding of Modern Methods and Advances in Structural Engineering and Construction*. (2011) 363-369.

[18] H. Ahmad, Kriteria Kejayaan Projek Pembinaan Hospital Awam di Malaysia, *Unpublished PHD Thesis*. Universiti Sains Malaysia, (2009).

[19] H. Albaloushi & M. Skitmore, Supply Chain Management in UAE Construction Industry, *International Journal of Construction Management*. 8 (2008) 53-71.

[20] I. Adetunji, A.D.F. Price & P. Fleming, Achieving Sustainability in the Construction Supply Chain, *Proceeding of the Institution of Civil Engineers*. (2008) 161-172

[21] J.F.Y. Yeung, A.P.C. Chan, Y.H. Chiang & D.W.M. Chan, A Critical Review of Performance Measurement in Construction, Journal of Facilities Management. 8 (2010) 269-284

[22] J. Markard, Tranformation of Infrastructures : Sector Characteristics and Implications for Fundamental Change, Journal of Infrastructure System. 17 (2011) 107-117

[23] M. Sambasivam & Y.W. Soon, Cause and Effects of Delays in Malaysian Construction Industry, *International Journal of Project Management*. 25 (2007) 517-526.

[24] Rancangan Malaysia Kesepuluh, *Ringkasan Eksekutif*, Unit Perancang Ekonomi Jabatan Perdana Menteri Malaysia. (2010).

[25] R. Chia & B. MacKay, Post-processual Challenges for the Emerging Strategy-as-practice Perspective : Discovering Strategy in the Logic of Practice, Human Relation. 60 (2007) 217-242

[26] R. Vrijhoef & L. Koskela, Role of Supply Chain Management in Construction, Proceeding IGLC-7. Universiti of California, Berkeley, USA (26-28 July 1999)

[27] X. Meng, M. Sun & M. Jones, Maturity Model for Supply Chain Relationships in Construction, Journal of Management Engineering. 27(2011) 97-105

Applied Mechanics and Materials Vol. 567 (2014) pp 648-653
© (2014) Trans Tech Publications, Switzerland
doi:10.4028/www.scientific.net/AMM.567.648

Research on HGV Collisions with Concrete Bridge Piers

WEE Teo[1, a], HOR Yin[1], MUI'NUDDIN Maharun[2], SARAVANAN Karuppanan[2], M. SHAHIR Liew[1], A. RAHMAN Salleh[3, b] and T. C. Wong[3]

[1]Civil Engineering Department, Universiti Teknologi PETRONAS, Malaysia

[2]Mechanical Engineering Department, Universiti Teknologi PETRONAS, Malaysia

[3]Bridge Division, Public Works Department, JKR, Malaysia

[a]teo_wee@petronas.com.my, [b]arahmans@jkr.gov.my

Keywords: Bridge piers, Heavy truck, HGV, Vehicle collision, Finite element analysis, LS-DYNA.

Abstract. Bridge piers are highly vulnerable to accidental collision with heavy truck vehicles. Current design and assessment codes account the effect of vehicle collision by means of an equivalent static load. This methodology although is simple but have raised many concerns on their suitability to reflect the exact collision condition, which is highly dynamic. Therefore many existing bridge piers are in great danger of malicious impact. Recently, a research collaboration is initiated between JKR and UTP to investigate the impact vulnerability of RC bridge piers when subjected to HGV truck collisions. The work involves using nonlinear finite element (FE) simulation to conduct complex vehicle-pier impact scenarios. This paper is intended to present the general outlook plan of this project with emphasis focused on the consideration of FE models used for HGV trucks and concrete bridge piers.

Introduction and Background

Bridges are essential public transportation assets that facilitate the transport of people and goods. They form parts of a structure in the road networks, which are vital in the support of the growth of a nation economy. There are currently more than ten thousand bridges in Malaysia [1]. Out of these, some 8000 bridges in the country are under the custodian of Public Works Department (or locally known as "JKR"), with eighty percent of these bridges are made of concrete. It is therefore the sole responsibility of JKR to ensure that their entire bridge inventory is well maintained and in a safe condition for use. Any structural deficiency or damage on the bridge may pose a significant danger to the general public, cause traffic disruption and increase the maintenance cost. Due to potentially severe socioeconomic impacts, any bridge's vulnerability should be avoided or minimized to as much as possible at all time.

Bridge piers adjacent to the carriageway of roads are highly vulnerable to impact due to Heavy Goods Vehicle (HGV). Although this kind of impact event is rare in occurrence for most bridge structures but their consequences can be disastrous. Therefore, consideration of the piers subject to HGV impact scenarios should not be overlooked in both during the design of new bridges or the assessment of existing bridge structures. Current design and assessment codes [2-5] addressed the effect of vehicle impacts on bridge supporting structures (which cover piers and walls of bridge) by characterizing the transverse dynamic impact load as an equivalent static load. Although the approach is relatively simple, but it neglected many important factors that characterize and influence the actual demand of the bridge piers due to HGV collision. For instance, the design collision loads are taken as constant values with the effects of the vehicle speed and vehicle characteristics, such as their mass and relevant stiffness, are all ignored. Furthermore, the dynamic interactions between the colliding vehicle and pier are also completely ignored.

Recently, the basis of the above method has been questioned by some researchers [6-8], in particular by El-Tawil et al. [6]. In their study, it has been found that the peak dynamic forces generated from the vehicle/pier collision process were higher than the design collision loads specified by AASHTO-LRFD. At the end, they concluded that current bridge design provisions on vehicle impact could be unsafe and that many of the existing bridge piers are in danger of malicious disaster. Therefore on the basis of the above findings, it is clear that a proper and accurate analysis technique is really needed in the design and assessment of bridge piers for vehicle collision loads.

Because full-scale vehicle crash tests are extremely expensive and time-consuming to perform, it has become customary to use computer modelling to simulate vehicle impact scenarios. Over the decades, the improvement of nonlinear finite element modelling and ever increasing computational power of high-performance computers have made it possible to conduct complex and detailed computer simulation on vehicle impact scenarios with ease. As evidences clearly showed, some researchers [6, 8] have successfully employed computer simulation to study the behaviour and performance of bridge piers on vehicle impact.

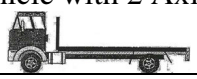
In 2012, a research project was initiated between JKR and UTP to investigate the vulnerability of reinforced concrete (RC) bridge piers subjected to HGV collision. Numerical simulation using nonlinear finite element (FE) program LS-DYNA [9] will be employed in this study. The primary intention is to assess the dynamic shear capacity of the concrete piers subjected to various vehicle impact scenarios. This is because previous studies have shown RC members that are designed to fail in flexure under static load may fail in shear when subjected to impact. The concrete material under impact loads behaves differently from that under static loads, more brittleness and increased strength due to high strain rate effect. Furthermore, shear is found to be the main governing failure mechanism and play a vital role in the overall impact behaviour of RC structures.

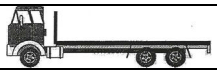
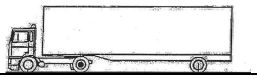
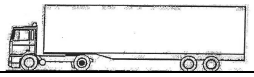
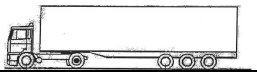
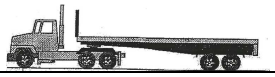
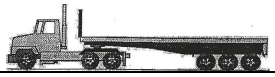
This paper is intended to present the general outlook plan of this project with the emphasis focused on the consideration of FE models for HGV trucks and concrete bridge piers. As a start, the overall vehicle classifications in Malaysia are discussed and then the corresponding FE models of HGV trucks with respect to axle configurations and Gross Vehicle Weight (GVW) ratings are outlined. Next, details of the concrete bridge pier models are featured with explanation on the type of material models and elements used in LS-DYNA for modelling of concrete and steel rebars. And finally, a brief outline of the proposed experimental impact test setup for validation process will be explained.

Heavy Vehicle Classifications in Malaysia

In Malaysia, any road vehicles that exceed the unladen weight (also known as BTM) of 7,500 kg are classified as heavy vehicles. According to the Road Transport Department Malaysia (RTD or locally known as JPJ), the maximum allowable GVW (also known as BDM) in the country is 51,000 kg. The GVW ratings are categorized based on the type of vehicle axle configurations and also the regions in the country. Table 1 shows the maximum allowable GVW rating for various vehicle axle configurations in Malaysia obtained from RTD [10].

Table 1: Maximum Allowable GVW Ratings in Malaysia (Amendment 2003) [10]

Vehicle Axle Configurations	Maximum Allowable Gross Vehicle Weight (GVW) [kg]	
	Peninsular M'sia	Sabah / Sarawak
Rigid Vehicle with 2 Axles (1 + 1) 	18,000	16,000
Rigid Vehicle with 3 Axles (1 + 2)	25,000	21,000

		
Articulated Vehicle with 3 Axles (1 + 1 + 1) 	30,000	26,000
Articulated Vehicle with 4 Axles (1 + 1 + 2) 	37,000	32,000
Articulated Vehicle with 5 Axles (1 + 1 + 3) 	39,000	34,000
Articulated Vehicle with 5 Axles (1 + 2 + 2) 	40,000	34,000
Articulated Vehicle with 6 Axles (1 + 2 + 3) 	44,000	38,000
Articulated Vehicle with 7 Axles (1 + 2 + 4) 	51,000	44,000

FE Models of HGV Truck Vehicles

After obtaining the information regarding the maximum allowable GVW rating (Table 1), it is then used as a reference to decide the type of vehicle models to be used in the computer simulation. This is because the objective of this work is not intended to develop a new vehicle model (because currently no vehicle models are available in Malaysia), but to study the effect of HGV collision on a concrete pier. Therefore several publicly available validated vehicle models provided by the NCAC [11] and Politecnico di Milano [12] are chosen for the simulation.

The three models chosen in this study are:

1. Ford Single Unit Truck F800. This vehicle model, as shown in Fig. 1, is an 8-tons single unit truck obtained from NCAC [11], which represents a typical medium duty truck specification. The model has been validated by NCAC and was used extensively by several other researchers on their studies of vehicle collision on bridge piers [6, 8] and building columns [13].



Figure 1: Ford Single Unit Truck F800 Model [10]

2. 16-tonnes HGV Truck. A 16-tons HGV truck that complies with the requirements of the European Standard CEN-EN 1317 was obtained from the NCAC website [12], as shown in Fig. 2. The development of this model was done in Politecnico di Milano and their reliability was validated with series of impact simulations against roadside safety barriers [14], although no simulation was done before on concrete bridge pier. This model is chosen because it matched with the axle configuration and GVW rating of Malaysia vehicle classification for rigid vehicle with 2 axles (1 + 1), refer to Table 1.

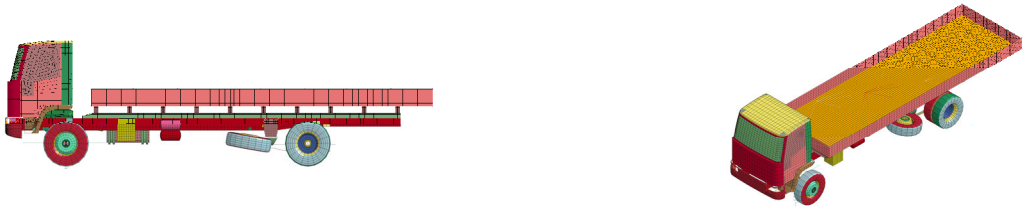


Figure 2: 16-tons HGV Truck Model [12]

3. 38-tonnes HGV Truck. The third model used in this study is a 38-tons tractor-trailer HGV, which represents a typical heavy duty truck specification, as shown in Fig. 3. This is the only articulated HGV model used in the study, whereas the others are all rigid frames. Similar to 16-tons HGV model, this is a European test vehicle model that complies with the requirements of the European Standard CEN-EN 1317 and is originally developed in Politecnico di Milano. This model is chosen because it matches to the axle configuration and GVW rating of an articulated vehicle with 5 axles (1 + 1 + 3) specified in the Malaysia vehicle classification, as listed in Table 1.

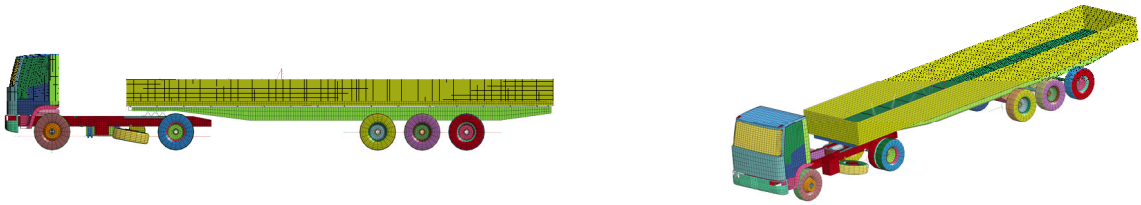
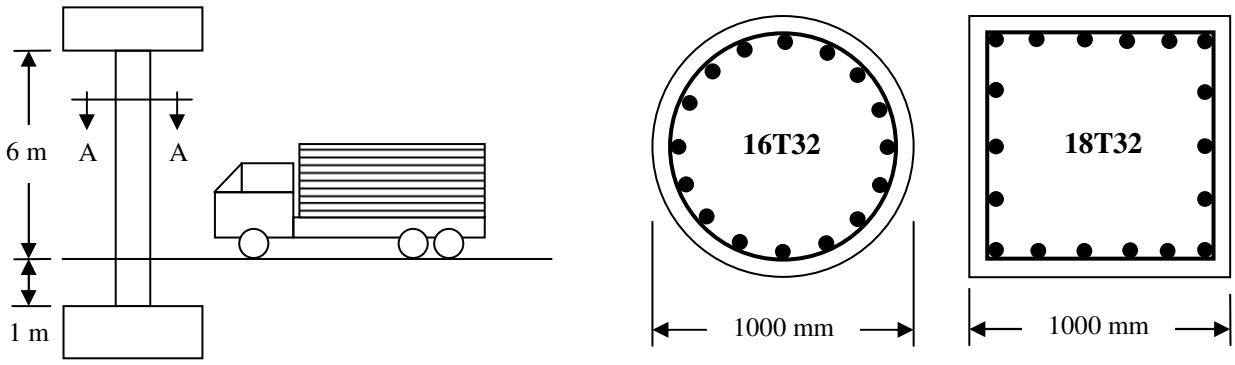


Figure 3: 38-tons Tractor-Trailer HGV Model [12]

All HGV models are simulated with direct head-on collision on bridge pier. Three impact velocities studied in this research are 8.33 m/s (30 km/h), 16.67 m/s (60 km/h) and 25 m/s (90 km/h). The last impact velocity of 25 m/s (90 km/h) corresponds to the maximum national speed limits applied for heavy vehicles in Malaysia expressway.

FE Model of Concrete Bridge Piers

In practice, bridge piers come with various section sizes depending on the design consideration. Two pier cross-sections are considered in this study, namely circular and square sections. The cross-sectional dimensions of the circular and square pier sections are 1000 mm diameter and 1000 x 1000 mm respectively, as illustrated in Fig. 4(b). Both piers are reinforced with 32 mm diameter high tensile steel rebar as the longitudinal reinforcement. The longitudinal reinforcement ratio constitute of 1.45%. So in circular section 16 Nos. of T32 bars are provided, whereas in square section 18 Nos. of T32 bars are provided. Both pier sections provide similar amount of transverse shear reinforcement of T16 at spacing of 150 mm, which translates to shear reinforcement ratio of 0.25%. The total pier height is assumed as 7.0 m, measured from the top of the pile cap to the tip of the pier; see Fig. 4(a). The pier is modelled as fixed at the bottom end and pinned support at the tip of the pier. So it may simply be idealized as a propped cantilever structure.



(a) Elevation View of the Bridge Pier (b) Cross-section Detail A-A

Figure 4: Details of the Bridge Piers

The concrete is modelled using eight-node hexahedron solid elements with a single integration point. In LS-DYNA material library, there are several material models available that can be used to simulate the behaviour of concrete structures subjected to impulsive loading [9]. Material model type *MAT_072R3 (*MAT_CONCRETE_DAMAGE_REL3) is used in this study for the concrete. As for the reinforcement rebar, it is modelled using two-node beam elements. The formulation of truss elements are defined for transverse shear reinforcement, whereas Hughes-Liu beam elements with 2 x 2 Gauss integration are specified for longitudinal reinforcement. Material type *MAT_003 (*MAT_PLASTIC_KINEMATIC) is used for the reinforcement rebar in this study. In vehicle-pier crash simulation, the contact interface between the colliding vehicle and pier structure must be defined. The contact algorithm CONTACT_AUTOMATIC_SINGLE_SURFACE in LS-DYNA is used in this study. This type of contact is the most common and convenient for application in the vehicle crash simulation [15].

Finally, to ensure the confidence of the created FE pier models, experimental data is needed for the validation process. In this study, several series of drop impact tests will be carried out on scaled-down reinforced concrete pier members. The pier members have cross-sectional dimensions of 200 mm diameter for circular section and 200 x 200 mm for square section, which correspond to a geometrical scale factor of 5.0 on the prototype cross-sections shown in Fig. 4(b). To represent as closely as possible to the actual layout of a bridge pier, the pier members are manufactured in T-shape with fixed condition at one end and allow to test horizontally with drop weight fall freely onto the top surface of the pier member. The proposed free drop impact test setup is shown in Fig. 5. The main parameters of this study comprise: (1) pier span length, (2) pier cross-sections, (3) impact load intensity (different drop heights and weights), (4) shear reinforcement ratios, and (5) longitudinal reinforcement ratios.

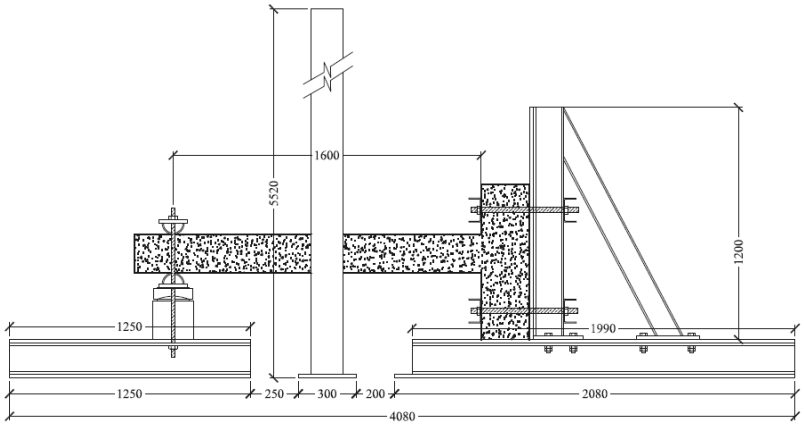


Figure 5: Details of the Free Drop Impact Test Setup (Elevation View)

Closing Remarks

This research project is considered the first of its kind in Malaysia whereby it aimed to investigate numerically the impact vulnerability of concrete bridge piers when subjected to HGV collision. FE vehicle models obtained from NCAC are used in this study and found to match considerably well with the actual vehicle axle configurations and GVW ratings specified in Malaysia heavy vehicle classification. The modelling of concrete pier is considered the biggest challenge in the FE analysis. Validation process is a must and time-consuming, and considered to be imperative in order to verify the FEA accuracy. The outcome from this research study will confirm the viability of the FE models (both vehicle and pier models) used in this study and provide a good basis of analysis technique for future design and assessment of concrete bridge piers in the condition of heavy vehicle collision. Ongoing research is currently being pursued in UTP and the results obtained will be presented in the forthcoming publications.

Acknowledgements

This research was financially supported by a grant (JAR12 04: Design of Bridge Pier Structures Subjected to Impact Loading) funded by the Public Works Department (or locally known as JKR) of Malaysia.

References

[1] S. M. Idris, Z. Ismail, Appraisal of Concrete Bridges: Some Local Examples, Jurutera, July 2007, pp. 36-41.

[2] BS EN 1991-1-7: 2006, Eurocode 1: Actions on structures – Part 1-7: General actions – Accidental actions, European Committee for Standardization, July 2006.

[3] BS EN 1991-2: 2003, Eurocode 1: Actions on structures – Part 2: Traffic loads on bridges, European Committee for Standardization, Sept 2003.

[4] BD 60/04, The Design of Highway Bridges for Vehicle Collision Loads, Design Manual for Roads and Bridges, Vol. 1, Sec. 3, Part 5, 2004.

[5] BD 48/93, The Assessment and Strengthening of Highway Bridge Supports, Design Manual for Roads and Bridges, Vol. 3, Sec. 4, Part 7, 1993.

[6] S. El-Tawil, E. Severino and P. Fonseca, Vehicle Collision with Bridge Piers, Journal of Bridge Engineering, ASCE, Vol. 10, No. 3, May-June 2005.

[7] A. Ghose, Strategies for the Management of Bridges for Vehicular Impacts, Structures and Buildings, Proceedings of the Institution of Civil Engineers, 162, Feb. 2009, pp. 3-10.

[8] H. Sharma, S. Hurlebaus, P. Gardoni, Performance-based Response Evaluation of Reinforced Concrete Columns Subject to Vehicle Impact, International Journal of impact Engineering, 43, 2012, pp. 52-62.

[9] LS-DYNA, Keyword User's Manual, Vol. 1 & 2, Version 971, Livermore Software Technology Corporation (LSTC), May 2007.

[10] Road Transport Department (RTD) Malaysia, Last time visit on 8th February 2013.

[11] National Crash Analysis Center (NCAC), Available in: http://www.ncac.gwu.edu/.

[12] European Standard EN-1317 Test Vehicle Models, CM/E Group - Politecnico di Milano, Italy. Available in: http://www.ncac.gwu.edu/vml/models.html

[13] H. Kang, J. Shin, J. Kim, Analysis of Steel Moment Frames Subjected to Vehicle Impact, 5th Asia Pacific Congress on Computational Mechanics & 4th International Symposium on Computational Mechanics (APCOM & ISCM 2013), Singapore, 11-14th December 2013.

[14] E. Oldani, L. Castelletti, M. Anghileri, M. Mongiardini, Impact Analysis of a 16t Truck Against Different Road Safety Restraint Systems, 5th European LS-DYNA Users Conference, Birmingham, UK, 25-26th May 2005.

[15] B. Ferrer, S. Ivorra, E. Segovia, R. Irles, Tridimensional modelization of the impact of a vehicle against a metallic parking column at a low speed, Engineering Structures, 32, 2010, pp. 1986-1992.

Applied Mechanics and Materials Vol. 567 (2014) pp 654-659
© (2014) Trans Tech Publications, Switzerland
doi:10.4028/www.scientific.net/AMM.567.654

Analytic Network Process Approach to Risk Allocation of EPC Projects Case Study: Gas Refinery EPC Projects in Iran

Alireza Valipour[1, a], Hadi sarvari[1.b], Nordin Yahaya[1.c], Norhazilan Md Noor[1.d], Seyed Meysam Khoshnava[1.e]

[1]RESA group Faculty of Civil Engineering, Universiti Teknologi Malaysia,

Skudai, Johor 81310, Malaysia,

[a]valireza2@live.utm.my, [b]shadi7@live.utm.my, [c]nordiny@utm.my, [d]norhazilan@utm.my, [e]kmseyed4@live.utm.my

Keywords: Risk allocation, ANP method, Criteria, EPC project

Abstract. Risk allocation is the most significant factor in risk management. Earlier research has shown that risk allocation is essential to achieve success in construction projects. Risk allocation may fail to be achieved due to lack of a mechanism for joint risk management. Successful optimal risk allocation requires one to identify and evaluate the risk allocation criteria, which interact and overlap with each other and can lead to significant variation in the decision outcome in risk allocation. This study aims to allocate the risks in EPC projects using the analytic network process (ANP) method. The ANP approach is preferable in identifying the problems of interdependence and feedback among various criteria factors. The method utilizes data that are collected through a literature review, interviews, and a questionnaire distributed to EPC project experts. The results have shown that 12 risks are allocated to the developer, 9 risks are shared between developer and contractor, and 12 risks are allocated to the contractor. In conclusion, ANP is found to be suitable in analyzing the feedback and interdependencies among risk allocation criteria.

Introduction

Recently, the engineering, procurement, and construction (EPC) method has been implemented by governments in infrastructure projects such as power plants, gas refineries, and transportation [1]. The Iranian government is that of another developing country interested in finding private investment to develop and maintain associated gas and oil industrial, power plant, and road networks via EPC contracts [2]. There have been many unsuccessful EPC projects in Iran due to cost overruns, delays, poor quality, arbitration, and increasing litigation, such as the Bed Boland 2 gas refinery.

Risk is one of the key factors that could directly influence the failure of an EPC project. There are some risks in the operation of EPC projects due to their complexity, such as interdependencies associated with activities, phase overlap, operation fragmentation, and contractual concession terms and large investment [3]. Risk management is a key approach to project management that includes four main parts: risk identification, risk assessment, risk allocation between sectors, and responses to reduce risk [4]. In fact, risks in projects cannot be removed. However, they need to be managed [5]. In this regard, risk allocation is a vital component of EPC risk management. Appropriate risk allocation is a flexible and complex process that leads to frequent conflict among project partners. There are various elements for implementing equitable risk allocation such as the ability to manage risk and the attitude of stakeholders towards risk [6, 7]. It is essential to consider allocating criteria and influencing factors to obtain appropriate risk allocation. Consequently, accurate risk management and allocation for completion of any EPC and construction project requires proper research and study for management of a lot of risks [8]. Risk allocation is based on conceptual principles. Factors that influence risk allocation can be classified into two approaches: qualitative and quantitative [9]. The qualitative approach identifies which risk is allocated to the sector, and the qualitative approach determines the percentage allocated to each risk among sectors [9]. In this regard, various studies have been done with different approaches. Medda in 2007 used the game theory approach for developing the risk allocation process [10]. Lam et al. considered risk

allocation based on qualitative expert knowledge and linguistic principles that preceded fuzzy set theory in a quantitative model [7]. Jin made a model of risk allocation using artificial neural networks [11]. Xu et al. developed a fuzzy synthetic evaluation method to obtain an appropriate risk allocation [13]. Khazaieni et al. provided a fuzzy AHP method to balance risk allocation [14]. Also, previous researchers have used a case study for risk allocation, including Abednego and Ogunlana, who studied equitable risk allocation in a PPP toll way project in Indonesia [12]. Ng and Loosemore studied risk allocation in a railway project in Sydney [5]. These studies focused on the ability to handle risk allocation among partners based on influence and principle risk allocation criteria. Accordingly, researcher Thomas found that risk allocation is often influenced by agents [18] , risk attitudes, and management capabilities [11]. However, there has been a lack of attention to dependencies, relationships, and feedback among risk allocation criteria in previous studies of risk allocation methods. The influence of criteria can lead to variations in the decision outcome of risk allocation based on attitude, manageability, and acceptability of risk among partners. This study provides a quantitative equitable risk allocation model through the ANP approach to overcome the problems of feedback and interdependencies among risk allocation criteria. This study focuses allocation of risk in an EPC gas refinery project in Iran.

Methodology

Description of ANP Method:

ANP suggests explaining decision-making problems [16]. Saaty (2006) appreciated that many decision problems could not be solved in a linear structure due to the actual independence and feedback relating to the different factors [16]. Saaty (2006) extended ANP by reflecting the interaction and feedback with the decision problems. This method is divided into two elements [16]. The first step is a linear structure that contains a network connection between goal, criteria, and subcriteria. The next step is the feedback network that contains the network connection involving elements and clusters. The network connection associated with the ANP method can create interdependencies among criteria and calculate the respective weights of each criterion. The results of these calculations are a type of supermatrix. They can be used to determine the weight among criteria and alternatives since the calculations are of the relationships among evaluations and the supermatrix [16].

Risk Identification and Determining the Important Risks:

Identification of risk is the first stage of risk management. In order to identify risk in the gas refinery EPC project in Iran, a decision team consisting of a project designer, manager, contractor, and project stakeholder was established. Data were collected through a mechanism such as literature review of previous research related to EPC projects, a questionnaire survey, and interviews with experts involved in Iranian EPC projects [17]. This study identified 33 significant risks and then categorized them into six groups.

Identify and Evaluate Significant Risk Allocation Criteria

After conducting a comprehensive literature review on risk allocation of construction projects and risk allocation criteria, a total of 20 criteria for optimal risk allocation of construction projects were identified. After summarizing the opinions of experts from face-to-face interviews, a total of 15 risk allocation criteria were identified and categorized into three groups that formed the basis for developing the subsequent questionnaire survey form. The significant risk allocation criteria for the Iranian EPC project are shown in Table 1.

Table1. Significant risk allocation criteria

Group of criteria	Criteria	Thomas	Lam	Loosemore	khazaieni	Xu
B1: Risk management competency	C11: Identification of risk					*
	C12: Foreseen of risk	*	*	*	*	*
	C13: Evaluation of risk	*	*		*	*
	C14: Bear the risk at the lowest price					
	C15: Capability of control risk				*	*
	C16: Resources of control risk				*	*
	C17: Control the chance of risk	*	*	*	*	
	C18: Minimize the loss if risk occurs	*		*		
	C19: Sustain the consequence	*	*		*	*
	C110: Expertise of control risk					*
B2: Incentive mechanism	C21: Obtain reasonable					
	C22: Obtain intangible assess					
	C23: Level of governmental support	*				
B3: Risk preference	C31: Assume the direct					
	C32: Risk attitude			*	*	*

Application ANP to Equitable Allocation Model

Step 1: Determine clusters, elements, and sub-elements to be initially used in the recommended model. The key selection elements and sub-elements are determined in this step by EPC experts. In the model network decision, one set of elements is involved: one element and so one sub-cluster are determined for the criteria. These elements are identified as optimal risk allocation criteria. In total, 15 sub-elements have been identified in sub-clusters from which to choose the best to bear the risk of the above factors.

Step 2: Build an ANP network structure including clusters, elements, sub-elements, and alternatives utilizing Super Decisions software as shown in Fig 1. The model produced by elements and sub-elements established in the first step can be seen in Fig 2.

Step 3: The next step is to obtain pairwise comparison matrices between various criteria groups and the various criteria factors within the same group. These comparisons were collected in comparison matrices. The following question was asked of the expert team to compare each criteria group and criteria factors with attention to their impact on the optimal risk allocation of each risk in gas refinery projects. The experts were asked to perform a pairwise comparison using an ANP scale (1–9). To reflect the interdependencies of this simple network, pairwise comparisons among all the group of criteria and criteria factors were performed, and these relationships were evaluated. The averages of the answers were inserted into the Super Decision software to calculate consistency of pairwise comparison matrices. CR was used to check consistency according to the pairwise comparison. If the consistency value of CR was less than 0.1, it indicated that such a pairwise comparison matrix contained satisfactory consistency (Saaty, 2005).

Step 4: The next step is to create un-weighted, weighted, and limit super-matrices of all the elements within a network structure. The un-weighted super-matrix includes the local priorities insulated from the pairwise comparisons. Influence priority is assigned as zero when an element has no influence on another element [16]. Multiplying the cluster weights to their relative blocks in the un-weighted super-matrix yields the weighted matrix. In this method, the component is weighted with its corresponding cluster matrix weight. Then, the weighted super-matrix must be converted to a limited matrix by raising the weighted super-matrix to powers [16]. The results of the priorities are extracted and obtained from the limit matrix. The above computing process is accomplished using Super Decision software ANP version 2.2.4.

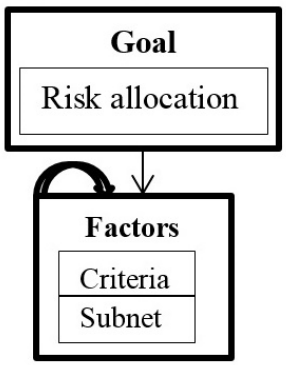


Figure1. ANP Network structure

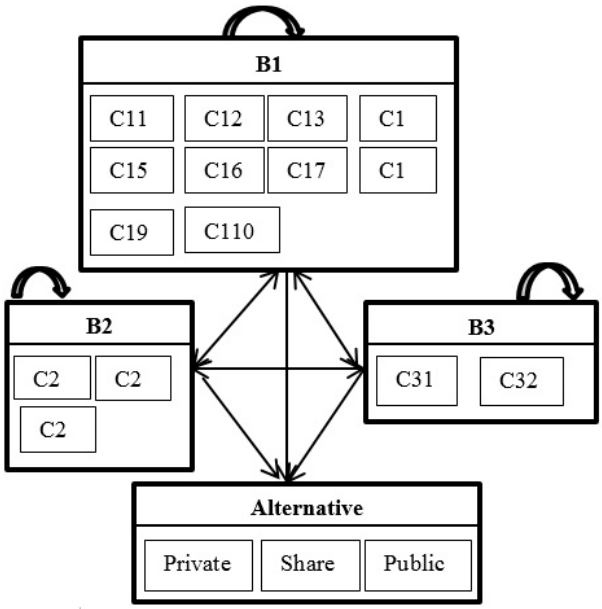


Figure2. Network subnet criteria

Step 5: Choose best part for risk allocation of inflation risk using alternative scores. Raw values are summed up, and each row in the raw column can be divided through the sum in order to get normal values. To obtain ideal values, each value in the raw values column is separated by the greatest value of the column. The results are 0.225, 0.601, and 0.173 for alternatives (private, shared, and public), respectively (as shown in Fig 3). The minimum response rate of 55% is adopted based on previous studies in UAE [19] to the allocated risk for each partner. The actual numeric outcomes of the application of the recommended model for allocation of risk in Iranian gas refinery EPC projects are shown in Table 2.

Name	Graphic	Ideals	Normal	Raw
Private		0.374	0.225	0.374
Public		0.287	0.173	0.287
Shared		1	0.601	1

Figre3: Risk allocation for inflation risk

Conclusion

Stakeholders of PPP projects accept that equitable risk allocation is vital to reducing disputes and to successfully implementing these projects. The applicability of a multi-attribute decision-making approach for equitable risk allocation among partners in Iranian EPC projects using an analytic network process (ANP) was investigated in this study. This study provides a systematic quantitative approach based on relationships and feedback among criteria and barriers to optimal risk allocation. The structure of network criteria and network barriers involves the tendency of the parties to bear risk based on attitude, benefit criteria, and contingency barriers. First, 84 risks were identified through a literature review, questionnaire, and interviews, of which 43 of these were recognized as significant risks in Iran. In addition, 15 criteria for optimal risk allocation were identified through a literature review and interviews. Finally, applying this model, nine shared risks were identified in Iranian EPC projects. The presented method provides a beneficial tool for EPC project decision makers that compensates for a shortage of adequate experience in selecting the best appropriate allocation of risk positions from a number of possible alternatives.

Table2: Final risk allocation for Iranian EPC project

No	Risk factor	Respondent			Final allocated	No	Risk factor	Respondent			Final allocated
		D	S	C				D	S	C	
1	Political sanctions	61	13	26	D	18	Lake of resources	15	21	64	C
2	Social instability	59	21	20	D	19	Technology matching	26	16	58	C
3	Change in law	63	22	15	D	20	Delayed in design	59	31	10	D
4	Limitation of laws	58	24	18	D	21	force majeure	14	73	13	S
5	Political corruption	64	12	24	D	22	Poor weather conditions	14	68	18	S
6	Inflation risk	14	74	12	S	23	Disaster-prone areas	16	71	13	S
7	Exchange rate fluctuations	17	61	12	S	24	Harsh environmental conditions	14	59	27	S
8	Periodic fluctuations in the economy	14	65	21	S	25	Schedule of construction delayed	25	14	61	C
9	Large change in interest rates	9	73	12	S	26	Material price fluctuations	6	21	73	C
10	Delay in payments	68	13	19	D	27	Limited funding	72	6	22	D
11	Building materials production ability	13	6	81	C	28	Disorderly vicious competition	25	12	63	C
12	Delayed opening LC	59	22	19	D	29	Inadequate QA/QC inspections	58	4	38	D
13	Delay in equipment delivery to the site	57	31	12	D	30	Procurement progress delayed	10	23	67	C
14	Bad Local market order	63	15	25	D	31	Inadequate design quality	25	13	62	C
15	Design failures	25	64	11	S	32	Technology maturity	20	23	57	C
16	Used improper construction method	18	24	58	C	33	Subcontractor nonperformance of the contract	23	10	67	C
17	Poor quality	32	11	57	C		C: contractor S: share D: Developer				

Acknowledgement

The work described in this paper was fully supported by a joint grant from the research grants MOSTI (Malaysia, UTM& Vote No.(4S084).

References

[1] Liu.J ., Wu, Song-yan., Zhao., Xiao. Y., Liu, Bing-wu, Application of Fuzzy Theory in Contractor Risk Assessment under EPC Model. ICIECS International Conference on (2009).

[2] Rezaee Nik. E., A. Nazari., F. Honari Choobar, Power Plant Project Risk Assessment Using Fuzzy-ANP and Fuzzy- Topsis Method. Int. J. Eng.Trans. 25(2) (2012) 107.

[3] Yeo. K.T., J.H. Ning, Integration supply chain and critical chain concepts in engineer-procure construct (EPC) projects. Int. J. Proj. Manage. 20 (2002) 253.

[4] Shen. L.Y., Platten. A., Deng. X.P, Role of public private partnerships to manage risks in public sector projects in Hong Kong. Int. J. Proj. Manage. 24(7) (2006) 587-594.

[5] Ng. A., M. Loosemore, Risk allocation in the private provision of public infrastructure. Int. J. Proj. Manage. 25(1) (2007) 66-76.

[6] Zhang.X. Q., Kumaraswamy. M. M., Zheng. W., Palaneeswaran. E, Concessionaire selection for build-operate-transfer tunnel projects in Hong Kong. J. Constr. Eng. Manage. 128(2) (2002) 155-163.

[7] Lam. K., Wang. D., Lee. P. T., Tsang.Y, Modeling risk allocation decision in construction contracts. Int. J. Proj. Manage. 25(5) (2007) 485-493.

[8] Tang. L., Q. Shen., E.W. Cheng, A review of studies on Public–Private Partnership projects in the construction industry. Int. J. Proj. Manage. 28(7) (2010) 683-694.

[9] Yamaguchi. H., T.E. Uher., G. Runeson, Risk Allocation in PFI Projects. 17th Annual ARCOM Conf (2001).

[10] Medda. F, A game theory approach for the allocation of risks in transport public private partnerships. Int. J. Proj. Manage. 25(3) (2007) 213-218.

[11] Jin. X.H, Neuro fuzzy decision support system for efficient risk allocation in public-private partnership infrastructure projects. J. Comput. Civ. Eng. 24(6) (2010)525-538.

[12] Abednego. M.P., S.O. Ogunlana, Good project governance for proper risk allocation in public–private partnerships in Indonesia. Int. J. Proj. Manage. 24(7) (2006) 622-634.

[13] Xu. Y., A.P. Chan., J.F. Yeung, Developing a fuzzy risk allocation model for PPP projects in China. J. Constr. Eng. Manage. 136(8) (2010) 894-903.

[14] Khazaeni. G., M. Khanzadi., A. Afshar, Fuzzy adaptive decision making model for selection balanced risk allocation. Int. J. Proj. Manage. 30(4) (2012) 511-522.

[15] Wang. M.T. H., Y. Chou, Risk allocation and risk handling of highway projects in Taiwan. J. Manage. Eng. 19(2) (2003) 60-68.

[16] Saaty. Thomas L., Vargas. Luis G, Decision making with the analytic network process: Economic, political, social and technological applications with benefits, opportunities, costs and risks (Vol. 95): Springer, 2006.

[17] RezaValipour. A., Hadi .S., Nordin. Y., Noorhazilan. N. M., Rashid, A. S. A, Analytic Network Process (ANP) to Risk Assessment of Gas Refinery EPC Projects in Iran. J. Appl. Sci. Res. 9(3) (2013)1359-1365.

[18] Thomas. A, S.N. Kalidindi, K. Ananthanarayanan, Risk perception analysis of BOT road project participants in India. Constr.Manage. Econom. 21(4) (2003) 393-407.

[19] El-Sayegh, S.M, Risk assessment and allocation in the UAE construction industry. Int. J. Proj. Manage. 26(4) (2008) 431-438.

CHAPTER 5:

Building, Highway, Geotechnical, Transportation Engineering and Geoinformatics

Applied Mechanics and Materials Vol. 567 (2014) pp 663-668
© (2014) Trans Tech Publications, Switzerland
doi:10.4028/www.scientific.net/AMM.567.663

A Review on the Factors Influencing the Park-and-Ride Traffic Management Method

Irfan Ahmed Memon[1,a], Madzlan Napiah[2,b], Mir Aftab Hussain Talpur[3,c], M. Rehan Hakro[4,d], and Imtiaz Ahmed Chandio[5,e]

[1,2,3,4,5] Department of Civil Engineering, Universiti Teknologi PETRONAS, Malaysia

[a]irfanahmed04crp26@hotmail.com, [b]madzlan_napiah@petronas.com.my, [c]aftab_g01903@utp.edu.my, [d]rehanhakro@yahoo.com, [e]imtiazutp@gmail.com,

Key words: Park-and-Ride, Model Shift, Mode Choice, Factors influencing, Travel behavior

Abstract. Park-and-ride is a traffic management method of traffic congestion problem in urban areas. As an extent of total demand management, park-and-ride service (P&R service) has broadly implemented in many countries. P&R service has proven to be progressive in alleviating traffic congestion despite of complication in finding parking spaces in the city centers. The objective of this research is to discuss a model to shift car travelers' to park-and-ride service (P&R service) and to investigate the factors which influence car travelers' behavior. This study can support policy makers' with useful information for future planning and development of park-and-ride service. Research outcomes will support policy-making and provide base for future study on modal choice behavior model for park-and-ride service.

Introduction

Transportation planning plays a significant role in environmentally sustainable and balanced transportation system [1]. In the developed countries, it is pragmatic that highway development supported cars and dominated on the public transport [2]. The increasing cars are growing the environmental effects, for instance noise and exhaust emissions. Other effects of these developments are physical interruption, hindrance and jamming [3]. The transportation sector is one of the major contributors of air pollution, and it significantly consumed non-renewable resources, such as petroleum [4]. The rapid increase of cars in cities not only makes worst environmental conditions, but also creates social issues such as poor health conditions and traffic jams [5]. Meanwhile, car travel is attractive and pleasing as compare to other modes of transportation [6]. Car travelling is usually more relaxed, flexible and quicker for demanding lifestyles; it is more personal, and it may have further influence as a status of symbol or replication of personality [6]. Land-use aspects such as urban sprawl and low-density in suburban zones also have encouraged the demand of private mode as comparatively suitable mode of mobility [7].

Consequently, one mutual motivating conclusion from several land-use researches was summarized that existence of rail transport system is a positive sign in terms of enhanced accessibility to the downtown area [3]. Actually, actions on the way to reduce long term traffic congestion cannot depend on the establishment of public transportation alone as the light rail but also setting up the park-and-ride and other travel demand management methods [8]. When executed consequently and efficiently, the park- and-ride service (P&R service) can be one of the several alternative policies that would be the answer to resolving the issue of urban congestion and convenience for long term [9]. Park-and-ride comprises of parking services at commute stations, bus stops and highway onramps, mostly at the fringes of the city, to facilitate the use of transit and rideshare, parking is usually free or relatively cheaper than in city centers [10].

The use of park-and-ride service is influenced by several factors, such as facility of public transport, time, cost, convenience, circumstance of the parking and parking area quality, etc. [11]. Other depending factors such as; choice or time and price saving are associated with traveling by

car for entire trip. Therefore, it is proved by previous researches that the willingness of car travelers to use park-and-ride service increases when the travel time of using P&R service is minimum [12]. To provide minimum travel time by P&R service, dedicated bus lane in the city center needs to be introduced allowing efficient shift at the P&R service, which probably would consumes little time in travel. Furthermore, it is essential to save the money and also time to use park-and-ride service in comparison of another mode of transport [3].

The purpose of this study is to identify the factors affecting travelers' choice of the P&R use. In this study, a logistic model structure will be proposed and the use of the model will be explained using a case study.

Literature Review

Why park-and-ride? Park-and-ride service can enhance commute and rideshare travel. Turnbull et al. [11] discussed the effects of park-and-ride services on transport systems. Morrall and Bolger [13, 14] concluded that the provision of park-and-ride service has a main impact on the area of city center transit trips made by travelers. The travel impact summary of park-and-ride service shows the impacts of park-and-ride on different transportation aspects such as, traffic, alternative modes, accessibility and few more aspects are shown in Table 1.

Table 1: Summary of travel impact [10]

Objective	Rating	Comments
Reduce total traffic	1	Reduce a portion of car trips
Reduce peak period traffic	2	Tends to reduce trips during peak periods.
Shift peak to off-peak periods.	0	
Shifts automobile travel to alternative modes	3	Supports transit and ridesharing
Improve access, reduce the need for travel.	0	
Increased ridesharing	3	Supports ridesharing
Increased public transit	3	Supports transit use.
Increased cycling	1	Supports cycling when bike parking is provided.
Increased walking, telework, reduce freight traffic	0	

Rating from 3 (very beneficial) to -3 (very harmful). 0 indicates no impact or mixed impacts.

Parkhurst [15] discovered that while park-and-ride services decreases urban congestion, it can increase the peripheral urban vehicular traffic as motorists ignored to reach the facilities or additional trips, and in some cases, moving from non-motorized trips to motorized trips [15]. Real influences depend on the quality of commute and ride-and-share facilities, the availability of incentives such as high occupancy vehicle (HOV) priority, travelers' financial reasons, and physical features such as distribution of employment and jobs. Various transportation organizations are using advanced parking management systems to point out the vacant parking spaces [16].

Traffic congestion and usage of private car is widely concerned with each other. To reduce traffic congestion, mainly there are two approaches. One is to discourage the usage of private car and another is encouraging the usage of alternative mode of transport. As illustrated in Figure 1 that how these objectives are connected with more widely accepted measures for car travel reduction [17]. Park-and-ride has important consequences for the success of a transit system [18]. These two objectives are divided into two categories; discouragement of using a car and encouragement alternatives modes as shown in Figure 1. The discouragement objective is further divided into two phases; travel and car ownership. In detail, the travel is also split into two aspects; "by other modes" and "by car". "By other modes" aspect is connected with tele-working measure only, whereas "by car" aspect is the part of traffic management which is linked with road pricing, fuel taxes, car sharing, parking control, tele-working, de-marketing, vehicle taxes and park-and-ride measures. Similarly, car ownership phase is directly linked with de-marketing of car and vehicle taxes.

In contrast with the discouragement objective, the encouragement objective depends on use of alternative modes, which is divided into two aspects; public transport and walking and cycling. The two aspects have associated with traffic management. The public transport aspect deals with service

perfection and information system, park-and-ride, marketing, pedestrian and cycling facilities measures. While the walking and cycling aspect is only linked with pedestrian and cycling facilities measure. However, these two objectives along with their aspects and measures are associated with land use planning. Precisely, as described in Figure 1, there are measures which encourage the use of alternatives modes and discourage the car travel. Specially, park-and-ride is the only measure which lies in both encouragement of public transport and discouragement of trip by the car.



Figure 1: The role of park-and-ride in car travel reduction [17]

Factors that influence choice of travel mode. Various factors are used in numerous types of transport models and attitude models. Magelund [19] studied various factors affecting travelers' choice between car and public transport. In her model, Magelund did not include car ownership as a descriptive factor. Thus, it is measured to be based on the other factors. Her study indicates that gender does not explain behavior but strongly correlate with income and work-related factors. Income and work, on the other hand, have a direct influence on the choice of travel mode. The result shows that attitudes have a strong point of clarification. Travelers' choose public transport is characterized by low income and parking conditions at their work place. For people who select car, their choice is clarified by work-related factors [19, 20].

Discrete Choice Models

Discrete-choice models have been developed to investigate factors influencing travel behavior. The common theoretical base is random utility theory [21, 22], where, it is expected that individuals always choose substitute with the highest utility. Thus, there is a random part that cannot be perceived by the analyst. These models forecast probability made by an individual as a utility of various factors that express the alternatives. These models compromise of sophisticated analysis of different factors influencing the mode choice and trade-offs between the factors. Although, discrete choice models can be established on either observed behavior (Revealed Preferences data) or on hypothetical choice surveys (Stated Preference data). An important motive for emerging discrete choice models to determine the consequences of policy measures. It is imperative to recognize and comprise characteristics, and their values may be different than practical policy judgments. In a

travel mode choice model, these factors include measures of service (travel time, frequency, reliability of service, *etc*.) and travel cost.

Several researchers' have used this model in their studies, like Himanen & Kulmala, 1988 [23], Lindstrom Olsson, 2003 [20], R. Hole, 2004 [24], D.M. Bos et al., 2004 [25], Ghani et al., 2006 [26], LIU, 2007 [27], Bajracharya, 2008 [28], Hamid et al., 2008 [3], Hui, He, 2009 [29], Baohong et al., 2012 [30], Ettema et al., 2012 [31], Duncan et al., 2013 [18], Elias et al., 2013 [32], and Ceder et al., 2013 [33].

Travel choice model. The model is based on the reality that all travelers select the alternative with the maximum utility, whereas, the utility rely on the characteristics of the alternative and the travelers' measured factors. The utility of an alternative *i* to person *n* can be written as:

$$\mathrm{U_{in}} = V_{in} + \varepsilon_{\mathrm{in}} \tag{1}$$

Ui represents the total utility for alternative i. ε is unobserved part, the unobserved part is due to; missing factors, unobserved differences in the preference of individuals, measurement errors and use of substitute variables. The observable utility part V_{in} is a weighted sum of observable characteristics of the considered alternatives, for example travel time components X_k[34].

$$V_i = \sum_k \beta_k X_k \tag{2}$$

Whereas; the parameters β_k represent the relative weight of each of the influencing factors X_k [34]. These include measures of travel time, travel cost, transfers require, crowding, seat availability, and others. For instance; total travel time, in-vehicle travel time, out-of-vehicle travel time, travel cost, number of transfers (transit modes), walk distance and reliability of on time arrival [35]. These factors can be shown in equation 3;

$$V(X_{in}) = \beta 1 * Xi_1 + \beta 1 * Xi_2 + \ldots\ldots \tag{3}$$

The unobservable part is supposed to be stochastic and equally distributed with a standardized difference. Suppose that the unobservable part is freely identically Gumbel distributed. The probability of selecting a particular alternative ***i*** (multinomial logistic model) as shown in equation 4 and the proof of this equation can be found at "Discrete choice analysis: theory and application to predict travel demand" book [36].

$$\mathrm{Pi} = \frac{\exp(\mu V(\mathrm{Xi}))}{\sum_{\mathrm{j}} \exp(\mu V(\mathrm{Xi}))} \tag{4}$$

Pi is the probability of choosing alternative i, V(Xi) represents observable part of the utility. j is equals to all the alternative the individual chooses between, μ is scale parameter. The scale parameter cannot be estimated separately. Instead the estimated parameter (β) is a product of β and μ.

There are two types of choice models; disaggregated model and aggregate model. Disaggregated (microscopic) model is applied at individual travelers to find out the factors which have significant influence in individual trip making. Therefore, this model allows the estimation of parameters values connected with factors which effects in values for relative importance respectively of these factors. Finally, this model can be used in what-if predictions. A sample of travelers is taken for the choice alternatives and their individualities are strong-minded. For each traveler the probabilities of choosing each of his/her alternatives are estimated. Conclusion of these probabilities provides the percentage of users that will use specific alternative. In contrast aggregate (macroscopic) models the behavior of bigger groups of users whose behavior is expected to be identical. Aggregate models work with normal standards for these groups. These are flexible in usage but provide less awareness about travel choice behavior and are not much accurate in their results.

Conclusion

This paper has discussed the use of public transportation through park-and-ride service; it is a well-known approach in initiating sustainable transportation agenda. Similarly it elaborates the factors which are influencing the usage of park-and-ride service as transportation demand management strategy. The discrete choice models have discussed which investigates the factors influencing travel behavior. This model is based on utility theory of travel behavior in which travel choice model has adapted. There are also aggregate and disaggregated models discussed. Discrete choice model is best approach to investigate the factors which influencing travel behavior of travelers. Different factors influence such as; environment, trip, transport, individual, quality, and measures affecting specific factors have been known by discrete choice model. It is observed that this model also can help to know the influence of many other factors which were rarely considered before. Such as, uncertainty specific factors in this current uncertain environment of developing countries cities. It will support policy makers' for future planning and development of park-and-ride service. Research outcomes will support policy-making and provide base for future study on modal choice behavior model for park-and-ride service.

References

[1] T. P. C. B. Program, *The transportation planning process: key issues : a briefing book for transportation decisionmakers, officials, and staff*: Transportation Planning Capacity Building Program, 2007.
[2] T. W. Sanchez*, et al.*, *Moving to equity: addressing inequitable effects of transportation policies on minorities*: Civil Rights Project at Harvard University, 2003.
[3] N. A. Hamid*, et al.*, "Travel Behaviour of the Park And Ride Users and the Factors Influencing The Demand for the Use of the Park and Ride Facility," presented at the EASTS International Symposium on Sustainable Transportation incorporating Malaysian Universities Transport Research Forum Conference 2008 (MUTRFC08). . , 2008.
[4] L. Redman*, et al.*, "Quality attributes of public transport that attract car users: A research review," *Transport Policy,* vol. 25, pp. 119-127, 2013.
[5] D. L. Greene and M. Wegener, "Sustainable transport," *Journal of Transport Geography,* vol. 5, pp. 177-190, 1997.
[6] C. J. Bergstad*, et al.*, "Affective–symbolic and instrumental–independence psychological motives mediating effects of socio-demographic variables on daily car use," *Journal of Transport Geography,* vol. 19, pp. 33-38, 2011.
[7] A. Kerr*, et al.*, "The call of the road: factors predicting students' car travelling intentions and behaviour," *Transportation,* vol. 37, pp. 1-13, 2010/01/01 2010.
[8] R. D. Knowles, "What future for light rail in the UK after Ten Year Transport Plan targets are scrapped?," *Transport Policy,* vol. 14, pp. 81-93, 2007.
[9] V. T. P. Institute, "Park &Ride – Convenient Parking For Transit Users," in *TDM Encyclopedia*, ed, 2010.
[10] V. T. P. Institute, "Park & Ride Convenient Parking For Transit Users," in *Online TDM Encyclopedia*, ed. Victoria, BC, Canada: Victoria Transport Policy Institute, 2010.
[11] K. F. Turnbull and N. R. C. T. R. Board, *Effective use of park-and-ride facilities*: National Academy Press, 1995.
[12] M. de Jong and H. Geerlings, *Roadmap for Infrastructure Appraisal*: DUP Science, 2004.
[13] J. Morrall and D. Bolger, "The Relationship Between Downtown Parking supply and Transit Use," *ITE Journal,* pp. 32-36, Feburary 1996.
[14] J. Morrall and D. Bolger, "Park-and-Ride: Canada's Most Effective TDM Strategy " in *Cost effectiveness through innovation: proceedings of the 1996 TAC annual conference*, Charlottetown, Prince Edward Island, Canada, 1997.
[15] G. Parkhurst, "Influence of bus-based park and ride facilities on users' car traffic," *Transport Policy,* vol. 7, pp. 159-172, 2000.

[16] SAIC, "Evaluation of Transit Applications of Advanced Parking Management Systems Final Evaluation Report," Research and Innovative Technology Administration (RITA) 2008.
[17] C. Wright and J. Egan, "De-marketing the car," *Transport Policy,* vol. 7, pp. 287-294, 2000.
[18] M. Duncan and R. K. Christensen, "An analysis of park-and-ride provision at light rail stations across the US," *Transport Policy,* vol. 25, pp. 148-157, 2013.
[19] L. Magelund, "Valg af transportmiddel i storbyen – bil og kollektiv transport i bolig-arbejdsrejsan," presented at the Transportrådet, Köpenhamn, 1997.
[20] A.-L. Lindstrom Olsson, "Factors that influence choice of Travel mode in major Urban areas," Ph.D, Department of Infrastructure, Royal Institute of Technology, Stockholm, 2003.
[21] T. A. Domencich and D. McFadden, *URBAN TRAVEL DEMAND - A BEHAVIORAL ANALYSIS*. Oxford England: North-Holland Publishing Company Limited, 1975.
[22] J. d. D. Ortuzar and G. Willumsen, Luis, *Modelling Transport, 4th Edition* vol. 4th: Wiley Press, 2011.
[23] V. Himanen and R. Kulmala, "An application of logit models in analysing the behaviour of pedestrians and car drivers on pedestrian crossings," *Accident Analysis & Prevention,* vol. 20, pp. 187-197, 1988.
[24] A. Risa Hole, "Forecasting the demand for an employee Park and Ride service using commuters' stated choices," *Transport Policy,* vol. 11, pp. 355-362, 2004.
[25] I. D. M. Bos*, et al.*, "The choice of park and ride facilities: an analysis using a context-dependent hierarchical choice experiment," *Environment and Planning A,* vol. 36, pp. 1673-1686, 2004.
[26] Nor Ghani Md. Nor and A. R. M. Nor, "Predicting the Impact of Demand- and Supply-Side Measures on Bus Ridership in Putrajaya, Malaysia," *Journal of Public Transportation,* vol. Vol. 9, 2006.
[27] G. Liu, "A behavioral model of work-trip mode choice in Shanghai," *China Economic Review,* vol. 18, pp. 456-476, 2007.
[28] A. R. Bajracharya, "The impact of modal shift on the transport ecological footprint, A case study of the proposed Bus Rapid Transit System in Ahmedabad, India," Masters of Science International Institute for Geo-information Science and Earth Observation Enschede, 2008.
[29] Y. Hui and X. He, "Study on Influence Factors and Demand Willingness of Park and Ride," in *Intelligent Computation Technology and Automation, 2009. ICICTA '09. Second International Conference on*, 2009, pp. 664-667.
[30] B. He*, et al.*, "The Attitude and Preference of Traveler to the Park & Ride Facilities: a Case Study in Nanjing, China," *Procedia - Social and Behavioral Sciences,* vol. 43, pp. 294-301, 2012.
[31] D. Ettema*, et al.*, "How in-vehicle activities affect work commuters' satisfaction with public transport," *Journal of Transport Geography,* vol. 24, pp. 215-222, 2012.
[32] W. Elias*, et al.*, "Travel behavior in the face of surface transportation terror threats," *Transport Policy,* vol. 28, pp. 114-122, 2013
[33] A. Ceder*, et al.*, "Modelling public-transport users' behaviour at connection point," *Transport Policy,* vol. 27, pp. 112-122, 2013.
[34] P.H.L. Bovy*, et al.* (2006). *Course CT4801: Transportation Modeling*
[35] Frank S. Koppelman and C. Bhat. (2006). *A Self Instructing Course in Mode Choice Modeling: Multinomial and Nested Logit Models*
[36] M. E. B. Akiva and S. R. Lerman, *Discrete choice analysis: theory and application to predict travel demand* vol. 9: The MIT press, 1985.

Applied Mechanics and Materials Vol. 567 (2014) pp 669-674
© (2014) Trans Tech Publications, Switzerland
doi:10.4028/www.scientific.net/AMM.567.669

Assessing UAV Landslide Mapping Using Unmanned Aerial Vehicle (UAV) for Landslide Mapping Activity

Munirah Radin Mohd Mokhtar [1, a], Abdul Nasir Matori[1,b]
Khamaruzaman Wan Yusof [1,c] Abdul Mutalib Embong[1,d]
and Muhammad Ikhwan Jamaludin[1,e]

[1] UniversitiTeknologi PETRONAS (UTP), Bandar Seri Iskandar, 31750 Tronoh,
Perak Darul Ridzuan, Malaysia

[a]munirah_g01254@utp.edu.my,[b]nasrat@petronas.com.my,
[c]Khamaruzaman.yusof@petronas.com.my, [d] mutalib_embong@petronas.com.my,
[e]ikhwan.jamaludin@gmail.com

Keywords: Unmanned Aerial Vehicle (UAV),Real Time Kinematic(RTK), orthophoto, digital Elevation Model (DEM),landslide.

Abstract. The purpose of this research is to improve the landslide mapping using unmanned aerial vehicle (UAV) for the area of slope displacement. It further presents the UAV namely multi-motor that being used to capture images at the research area located in Parit, Perak. The objective of this research paper is to develop a three dimensional of landslide area produced from the UAV images. For the whole process of image processing, thirty six control points are established using global positioning system (GPS) staic mehtod using Agisoft Photoscan. The results show that the digital elevation model (DEM), aspect Model, slope model, and digital orthophoto can be obtained using the procedure and method used in the study. The information is obtained through accurate assessment results and used to create a 3D model which is then used to monitor technique applications. The restitution stereo model is also by three dimensional rotations or transformation in 3D surface. From here, the landslide can be detected by calculation of three difference epoch data achieved from Digital Elevation Model (DEM) generation. Prior to that, this paper focuses on the monitoring of that area based on DEM area and volume generated from 3D surface analysis. To conclude this study shows that UAV can be used for producing digital map.

Introduction

A new method for landslide monitoring by using unmanned aerial vehicle or also known as multi- rotor hexacopter to reduce the cost of data acquisition at site and has become the notion and new approach of this research. The result obtained is a three dimensional model of the research area produced by UAV images acquired.

Generally UAV aerial photography is enables to capture a small area compared to the satellite images. This paper presents that the height of UAV is at 150m altitude from the ground. In this research, the digital camera with high resolution 16.1 megapixels is attached at the UAV to capture the images. The UAV that being used in this research is known as hexacopter, which has six blades and been installed with GPS onboard.From the previous literature review, a study does mention about the application of UAV in aerial photography that provides a new approach for high resolution images in monitoring and mapping our real world [2].According to [1] UAV performance depends on the criteria of the weight, endurance and range, maximum altitude, engine type, thrust loading and wing loading.

UAVs are progressively more seen as an attractive low cost alternative or supplement to aerial and terrestrial photogrammetry due to their low cost, flexibility, availability and readiness for task. In addition, UAV can be operated in dangerous or for the moment inaccessible locations.UAV can also provide both a quick overview of a situation, as well as detailed area records. However, past to a successful UAV operation, broad mission planning is necessary. This mission planning of course is dependent on the kind of application and in particular on the specifics of the location at the flight area. In many occasions, no detailed field information is available, only elementary maps or restricted graphical information [1]

UAV platforms are currently become an important source of data for assessment, observation, mapping and 3D modeling issues. New applications in the short- and close-range domain are introduced, being the UAVs a low-cost alternative to the classical manned aerial photogrammetry. Besides, the rotary or fixed wing UAVs, accomplished of performing the photogrammetric data achievement with amateur or SLR digital cameras, can take off in manual, semi-automated and independent modes [4].

Research Methodology

This study was conducted in Parit, Seri Iskandar, which is located approximately at 4°23'04.03"N in latitude and100°56'34.89"E in longitude.There are two different study sites represented in this research. These sites are being selected as research area due to its slope appropriate degree for the study site. Before the capture of data is carried out, flight planning should be considered in advance.In order to obtain high quality images in flight, planning certain requirements like the coordinate of study area, the flying high, and coverage photo overlapped should be taken into consideration.

This research study used close range photogrammetry and the data were used in the approach of unmanned aerial vehicle (UAV), that of consecutive stereo pairs in a flight line. Achievement of data was done by capturing the photographs of the object. The photographs were taken by aerial standards, those from high oblique kind. This technique is far lower in cost compared to aerial airborne or satellite images, moderately because it requires only an ordinary digital camera. The camera used metric camera in this research was SONY NEX5, a digital camera that acquire model images. Fig.1 and Fig.2 indicate the equipment of the data acquistion, multi-rotor UAV and the location of study area for this research.



Fig1. Multi-Rotor UAV



Fig 2.Study Area in Parit, Perak. Malaysia
[Source: http://earth.google.com]

Flight planning is the main task needs to be considered int this study. It involves calculation of the study area, number of strips required, pixel size, photo scale, flying height and percentage of end lap and side lap. Google earth can be fully utilised as a route planning and showed the point consists of waypoints for the starting and ending point of each coordinate for flight map. The altitude (flying height) of UAV actually depends on the coverage research study area. For the purpose of this

research the flying height was about 150m from the ground. All images from aerial photographs were stored in JPEG file format. To start fly the UAV Hexacopter, the UAV team on the ground will set the gimball controller for flight plan.Fig.3 shows the flow how the UAV data acquistion during the capturing data images.

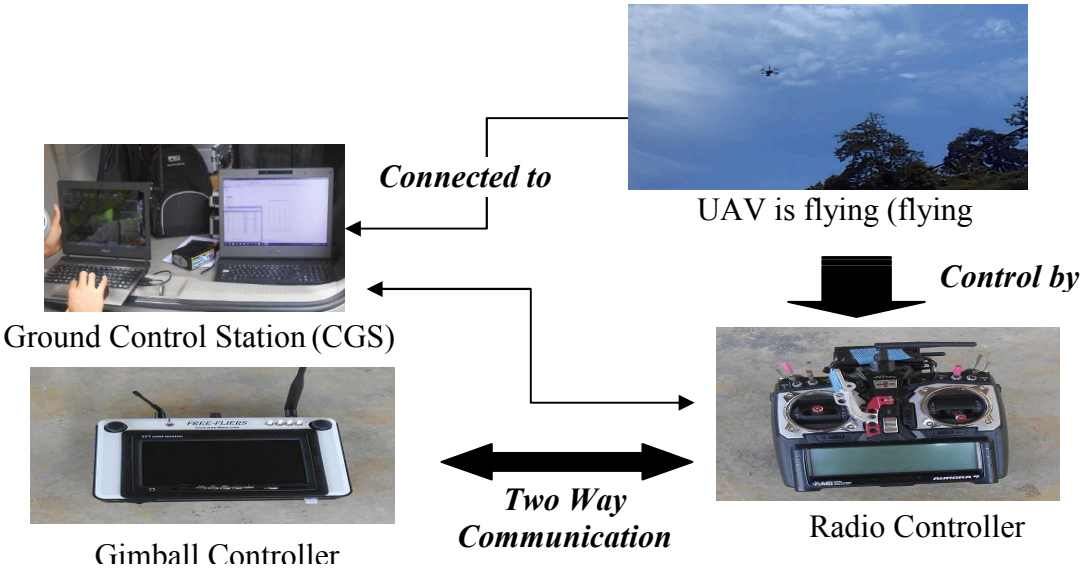


Fig 3. UAV Data Acquisition

Instrumentation and Facilities

This research involved data collection survey and analyzing data. The most important step to be carried out in this part of research work is to establish the ground control points (GCPs) at the study area located in Seri Iskandar, Perak. The equipments that used in this research study were a digital camera, a reflectorless Electronic Total Station (ETS), GPS (Hyper II) and UAV (Hexacopter). Besides, the data were processed using software Agisoft Photoscan Profesional, and Global Mapper. The camera calibration was conducted before data acquisition.A set of instruments was required to fulfill the objectives of this research. List of instruments and facilities involved in this research are as the follows in Fig.4:

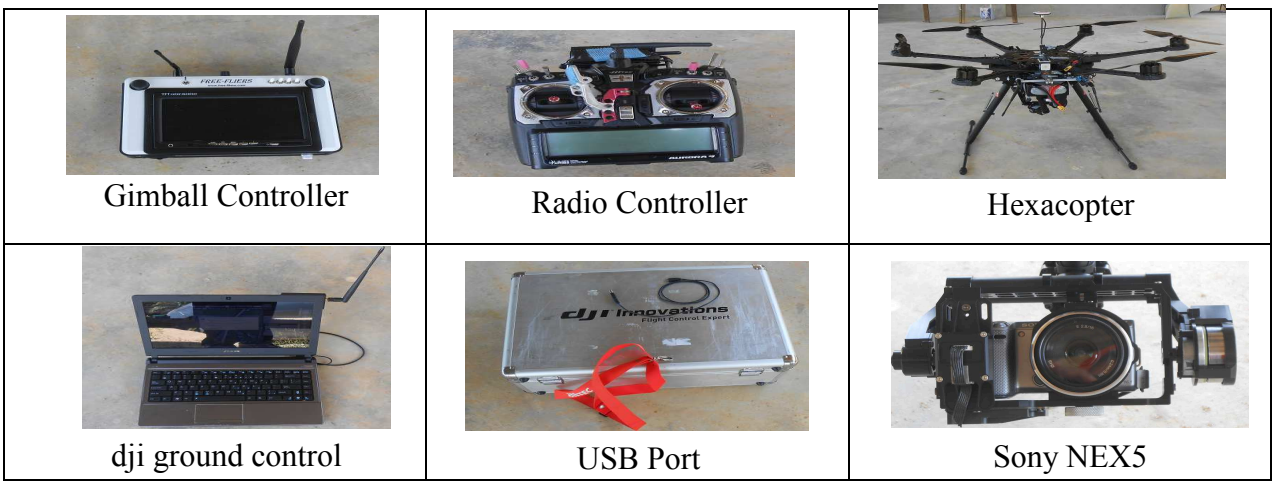


Fig 4. Instrumentation and Fasilities

UAV at the research study was mounted with digital camera and GPS receiver. The data acquisition were acquired in small format images with attached digital camera known as Sony NEX 5N with

16.1 megapixels resolution, at the bottom of unmanned aerial vehicle (UAV), Hexacopter. Once this was achieved, the UAV images were able to be processed in photogrammetric software.

Image Processing

The results and analysis of the field data demonstrate that unmanned aerial vehicle (UAV) application which can be adopted in showing an integrated monitoring technique in surface measurement involved in landslide. The flowchart in Fig.5 describes the phases of activities in surface monitoring measurement process involved for this research study and steps for data image processing. This flow chart shows data acquisition on site investigation and image processing using photogrammetric software. The projection coordinates for the establishment in Malaysia_RSO2000 projection. In this research, Agisoft PhotoScan was used to process all images acquired. After the data were collected, then next task which is processing data can start. Data processing was done using Agisoft Photoscan , providing the 3D model which would then be georeferenced using the measured control points. From here, Digital Elevation Model (DEM) would be generated.

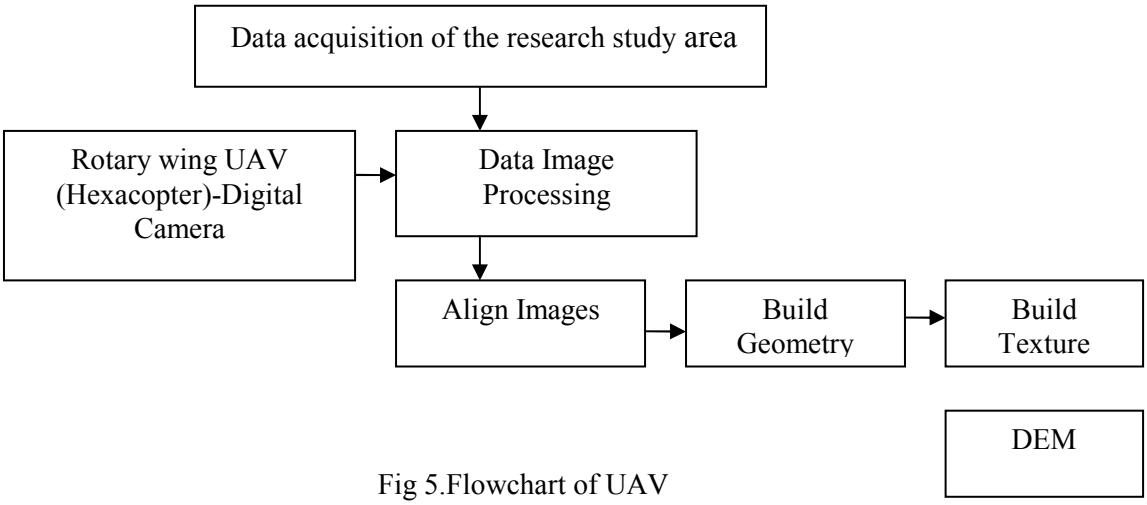


Fig 5.Flowchart of UAV

.The Unmanned Aerial Vehicle (UAV) needs a professional expertise handle from the ground, in this research UAV images are processed using photogrammetry technique that is important to use ground control points before captured UAV images [3] The processing of the images is done by matching well defined colour levels and shape in corresponding area of the images [4]. The three sets of data epoch were analyzed for slopes volume changes. The three sets of data were compared by differentiate the coordinates of the fixed point from control point.

Results and Discussion

The images from digital camera have the potential to be used in aerial photogrammetry and from here, an analysis can be carried out for the product of aerial photogrammetry such as orthophoto and DEM.To study the capabilities of close range photogrammetry method using unmanned aerial vehicle or (UAV). Next, it enables the investigation of the mass movement on the case study, where three observations data are conducted to determine the change of physical surfaces of land. In this method, the problem of finding the physical movement of landslide is solved by generating 3D model. Fig.6 is the orthphoto images or digital map. From the 3D model we can determine the changes of surface and comparison of different observation data.

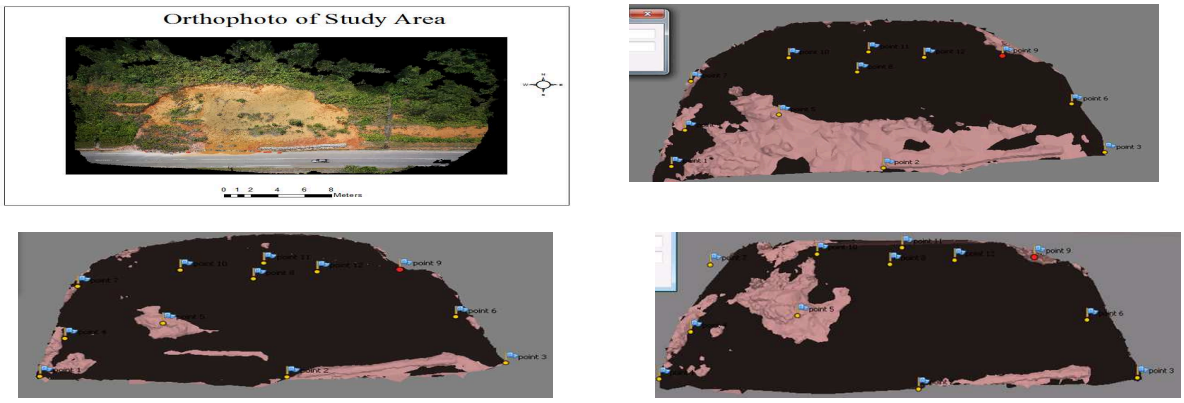
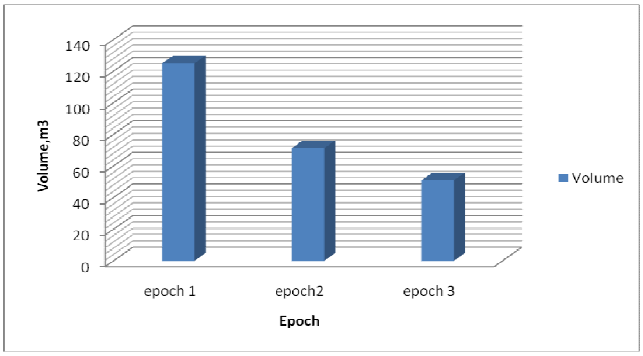


Fig 6.Digital Orthophoto and the Slope Changes



Epoch	Volume
epoch 1	124.921
epoch2	71.2677
epoch 3	50.9087

Fig7.The distribution of Slope

In this study the results of analysis for the graph in Fig.7 it was verified that the change of the volume for slopes increase from 50.9087 m^3 to 124.921m^3 differences of the soil between three data epochs. The elevation is detected with mass movement from top view of the slope moving downward. This study applied ground based control point (static GPS) to obtain accurate 3D coordinates of the sufrace of the slope. The difference of the terrain changes together with volume changes variations between the three sets of data can be calculated during the measurement. This research proves that application of UAV on landslide validate for checkout for the stability of slope. The results shows that the volume moved so it proved that the soil have mass movement.

From the slope analysis it is identified in mass movement is also referred to slope movement, surface area and volume of soil. The difference is calculated from three epoch data. From the digital orthophoto area three images analysis shown in Fig.6, it is evident that all information is given by the Agisoft database design in Agisoft lens software. Using this software as a tool in making decision and development in the future is easy for the users to update their data in the future planning and activities for that area. The software may allow the users to produce and report information in ways that they could not do before, and this information needs to be produced at the right time in the decision process.Besides, it is also proven that the rotary-wing UAV was successfully used to capture the images at the site study. From these field observations, it shows that this UAV system is easy to handle, can cover small areas, can fly closer to the object and thus the resolution can be increased dramatically.

Conclusion

The obtained results show in this study, the method of applying close range photogrammetry technique using UAV in performing 3D object measurement is proven valid to obtain Digital

Elevation Model (DEM) for landslide monitoring. The results and findings show the digital orthophoto images of study can be provided by UAV approach. This approach can solve problems arose in risky places and at the same time can reduces cost, simpler more. Besides that actual time of observation in field data collected takes only one hour to accomplish the observation. From the combination of control points in ground control UAV images can generate Digital Elevation Model (DEM).

Acknowledgement

The authors would like to thank Universiti Teknologi Petronas, Malaysia for the technical and financial support received.

References

[1] H. Eisenbei, *UAV Photogrammetry*. 2009.

[2] Arko Lucieer, Sharon Robinson, and Darren Turner ,Sept 2010 ."Using an Unmanned Aerial Vehicle (UAV) for Ultra-High Resolution Mapping of Antarctic Moss Beds".15th Australian Remote Sensing & Photogrammetry Conference.

[3] S.Suganthi,K.Srinivasan (2010):Digital Elevation Model Generation And Its Application In Landslide Studies Using Cartosat-1,International Journal of Geomatics and Geosciences,Volume 1.

[4] Daaam, I., Conference, B., & Engineering, I. (2010). APPLICATION OF CLOSE-RANGE PHOTOGRAMMETRY IN REVERSE ENGINEERING, (April).

Applied Mechanics and Materials Vol. 567 (2014) pp 675-680
© (2014) Trans Tech Publications, Switzerland
doi:10.4028/www.scientific.net/AMM.567.675

Assessment on Bearing Capacity of Two Clay Layers Soil Using COMSOL

Masyitah Md Nujid[1,a] and Mohd Raihan Taha[2,b]

[1] Faculty of Civil Engineering, Universiti Teknologi MARA (Pulau Pinang),
13500 Permatang Pauh, Pulau Pinang, Malaysia
[2] Department of Civil and Structural Engineering, Universiti Kebangsaan Malaysia,
43650 Bangi Selangor, Malaysia
[a]masyitahnujid@gmail.com, [b]profraihan@gmail.com

Keywords: Layered soil, ultimate bearing capacity, COMSOL Multiphysics

Abstract. Natural soils are often deposited in layers and homogeneous soils which are very rarely found in nature. Thus, bearing capacity of layered soil cannot be treated anymore as single soil since the soil strength and stiffness parameters are different and increase their linearly with depth. There are two cases which can be consider as inhomogeneous layer soil where strong clay overlaying weak clay layers or weak clay overlaying strong clay layers. A parametric study was conducted to assess the ultimate bearing capacity of a smooth strip footing subjected to vertical load resting on two undrained clays layered soil. A two dimensional (2D) plane strain model incorporated in COMSOL Multiphysics (version 4.3a) which a finite element software was adopted with two physical branches that have been chosen. Two clays layered soil were assumed as linear elastic incompressible material which failed in the Mohr-Coulomb criterion. The finite element results were presented in terms of a modified bearing capacity factor for different ratios of top layer thickness, strength and stiffness ratio of two clay layers. The computation results were then compared to published studies. The numerical analysis showed that strong clay overlaying weak clay layers with c1/c2 >1 resulted in increase of Nc* as h/B ratio increase. In contrast, for a case where weak clay overlaying strong clay layers with c1/c2 <1 showed decrease of Nc* as h/B ratio increase. In comparing results of bearing capacity factor, Nc* indicated a similar trend from previous studies. Stiffness parameters did not affect the solutions as long as remain constant for all cases within suitable ranges of parameters.

Introduction

The ultimate bearing capacity calculation is based on the assumption that the soil is perfectly rigid plastic with the strength characterized by an angle of friction and cohesion. This approach is highly applicable and successful for homogeneous soils, however in practice the soil properties vary with depth [3] and natural soils are often deposited in layers and homogeneous soils are very rarely found in nature. Thus, bearing capacity of layered soils cannot be treated anymore as single soil since the soil strength and stiffness parameters are increasing linearly with depth [5,6]. There are two cases considered as inhomogeneous layer soil [2,11,12]. First case when the top layer weaker than the bottom layer and the second case is a top layer stronger than the bottom layer. It is generally assumed that general bearing capacity failure occurs in the upper layer which calculated based on soil strength parameters of the top layer of strong soil with the thickness of the layer which is larger in comparison to the width of footing [2,12]. For nonhomogeneous clay layers, strength soil has an important influence in the calculation of bearing failure.

Advanced computer technology with finite element package allows analysis being done easily. A few studies have been conducted to estimate bearing capacity failure of a rough strip footing resting on two clay layers with a parametric study on the effect of the thickness ratio of the top layer to the width of the footing and the cohesion ratio of the top to bottom soil layer [2,8,12]. Therefore the study focuses on the application of finite element method involving multiphysics element and a parametric study which conducts to assess the ultimate bearing capacity of a smooth strip footing subjected to vertical load resting on two clays layered soil. A two dimensional (2D) plane strain model incorporated in COMSOL Multiphysics (version 4.3a) which a finite element software was adopted with two physical branches (Solid Mechanics and Mathematics) had been chosen. Two clays layered soil were assumed as linear elastic incompressible material which failed in the Mohr-Coulomb criterion.

Modelling in COMSOL Multiphysics

Figure 1 shows a two dimensional (2D) plane strain of smooth strip footing geometry using the Geomechanis (Solid Mechanics branch) the Ordinary Differential Equation (ODE) and Differential Algebraic Equation (DAE) interfaces (Mathematics branch) [4]. The geometry footing of width B = 2m lying on the surface of a finite soil layer with thickness h is having a shear strength parameters c1 overlying another soil stratum having shear strength parameters c2. Soil was assumed to be weightless and the water table was well below from footing base. Clay was homogeneous in each layer with undrained shear strength c1 and c2 respectively. Due to symmetry only right side of geometry will be modelled. The depth of soil layered H was based on [1] with h varies on top layer and width of footing B was kept constant to have some effect of ratio layer thickness (h/B). The ultimate bearing capacity was calculated by the function strength ratio (c1/c2) and stiffness ratio (E1/E2). Only soil strength and stiffness parameters were varied according to cases. The material properties, boundary conditions and loads were specified. The mesh was initialized, refined and a parametric solver was used to calculate the solution for applying pressure until the model reaches the desired displacement increments.

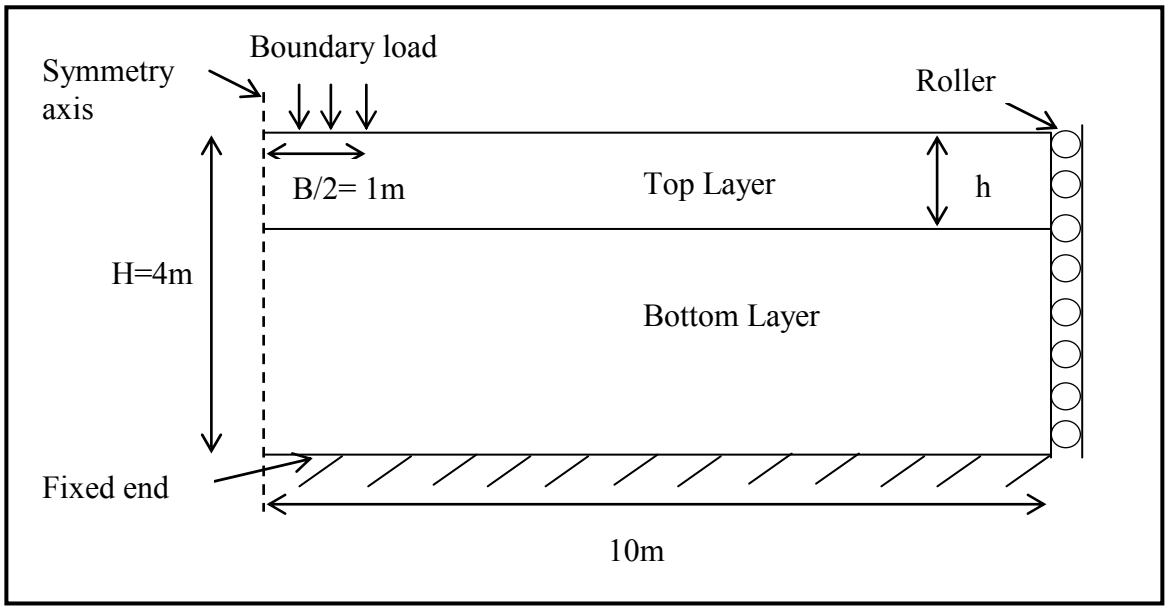


Figure 1: Geometry and Boundary Condition of Problem Model

Result and Discussion

A similar approach was used in this study by [12] to model a strip footing under vertical load up to ultimate bearing capacity. The modified bearing capacity factor, N_c* can be calculated using the following formula (Eq. 1) :

$$Nc^* = qu / c1 \quad (1)$$

Where N_c* was modified bearing capacity factor, q_u is ultimate bearing capacity and c1 was the undrained cohesion of clay at the top layer. A parametric study was performed for a modified bearing capacity factor N_c* as a function of h/B (0.125, 0.25, 0.5, 0.75, 1), c1/c2 (0.5, 0.8, 1, 2, 4) and E1/E2 (0.5, 1, 2). Note that this study focused on thickness of layered soil rather than footing width.

The Nc* value calculated from finite element results for footing on surface in two clay layers that were given in Figure 2. It is shown that strong clay overlaying weak clay layers with c1/c2 >1 resulted in increase of Nc* as h/B ratio increase. In contrast, for a case where weak clay overlaying strong clay layers with c1/c2 <1 showed decrease of Nc* as h/B ratio increase. For a homogeneous soil where c1/c2 equal to one showed that the modified bearing capacity factor was in the range 5.215 to 5.220 for all cases of h/B ratio. It was larger than theoretical value 5.14 with a difference of 1.5%. The result consistent with the finding from [7,10] which is bearing capacity factor for strip footing was 5.282 and 5.24 respectively. The error occurred due to smooth footing being analysed in this study while previous studies considered as rough surface footing. Another reason was not implemented finer mesh element near the edge of footing base [12]. Not more than 10% error allowed for a case like this [1]. Similarly, as shown in Figure 2 that the present calculated value of Nc* compared to [12] were underestimated.

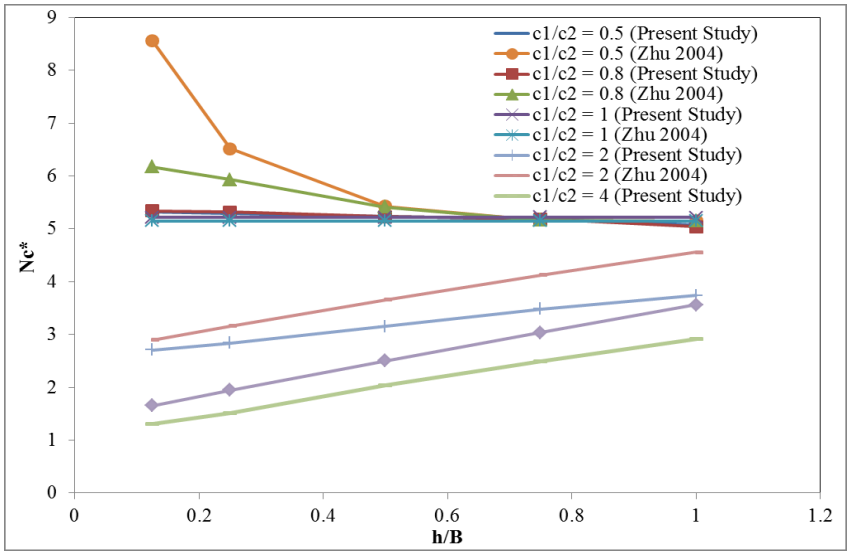


Figure 2: Modified Bearing Capacity factor Nc*

Figure 3-7 show comparison of the modified bearing capacity factor for h/B the ratio from 0.125 to 1.0 for different cases of strength, function ratio c1/c2 > 1, c1/c2 = 1 and c1/c2 < 1. For all cases indicate a similar trend between previous studies [12] using finite element method and [9] from upper, average and lower bound limit analysis. However, as can be seen from these figures the present calculated value of modified bearing capacity factor Nc* for h/B ratio 0.75 and 1.0 depict

that lowest values from comparative studies. This results were showing the same trend for a case c1/c2 < 1, where the Nc* affected by the thickness of top layer when h/B < 1 [2,12].

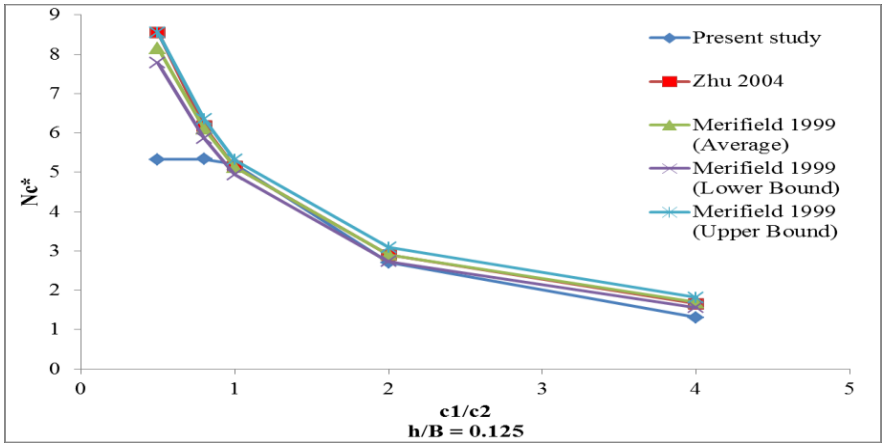


Figure 3: Comparison of Modified Bearing Capacity factor Nc* for h/B = 0.125

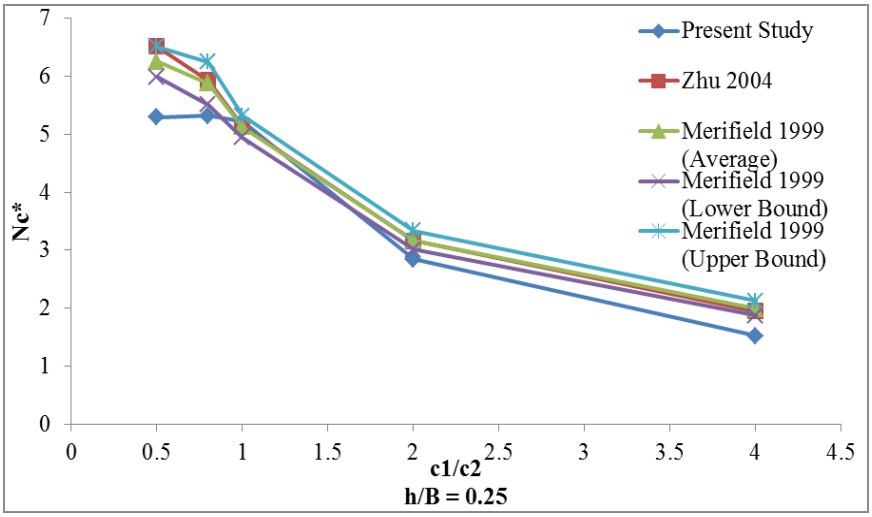


Figure 4: Comparison of Modified Bearing Capacity factor Nc* for h/B = 0.25

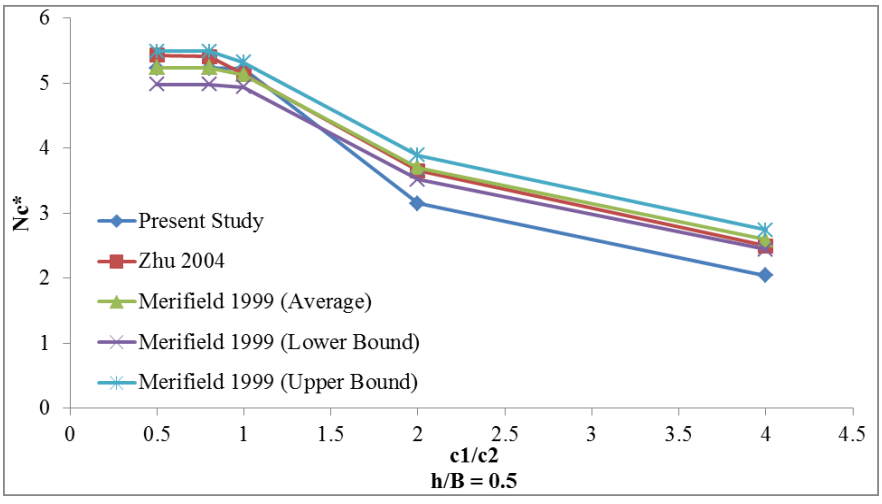


Figure 5: Comparison of Modified Bearing Capacity factor Nc* for h/B = 0.50

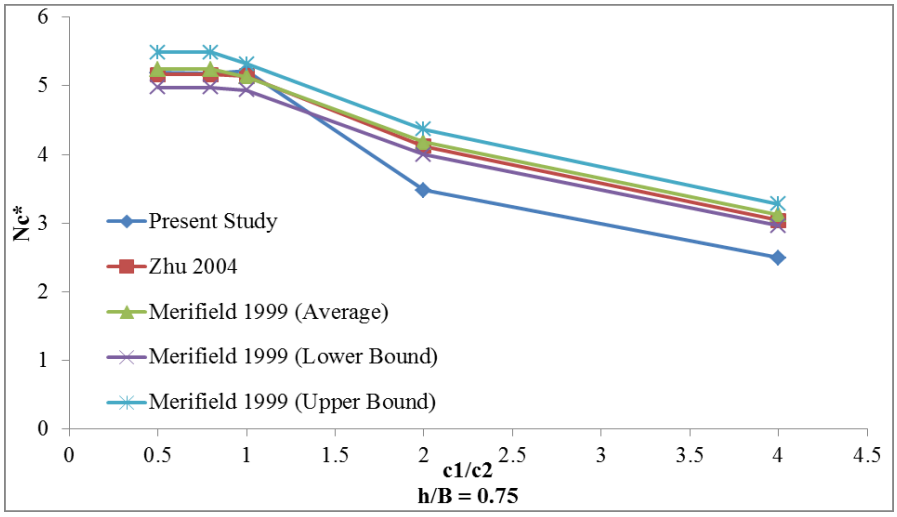


Figure 6: Comparison of Modified Bearing Capacity factor Nc* for h/B = 0.75

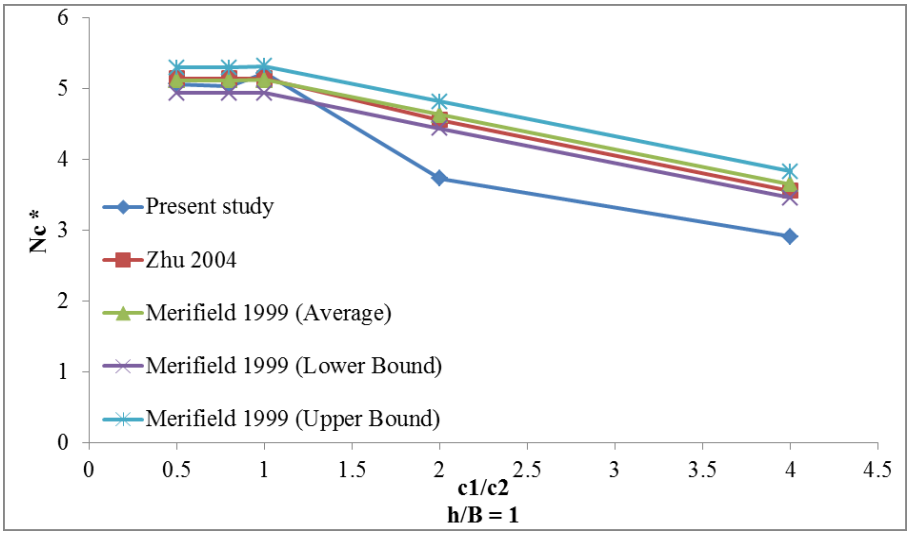


Figure 7: Comparison of Modified Bearing Capacity factor Nc* for h/B = 1.00

The present study adopted a stiffness ratio function in the analysis. The stiffness ratio was varied according to cases. Even though the stiffness ratio changed to upper and lower of layered soils in each case, it found that the ratio did not give significant results in bearing capacity analysis. The study supported from a previous result [2,8,12] where elasticity parameters which were Young's modulus and Poisson ratio did not affect so much in results.

Summary

This parametric study was done to assess the bearing capacity of a smooth strip footing on two clays layered soil as function of strength ratio (c1/c2), relative layer thickness (h/B) and stiffness ratio (E1/E2). A COMSOL Multiphysics (version 4.3a) a finite element package was used in the analysis and the results were presented in graphical forms. The numerical analysis showed that strong clay overlaying weak clay layers with c1/c2 >1 resulted in increase of Nc* as h/B ratio increase. In contrast, for a case where weak clay overlaying strong clay layers with c1/c2 <1 showed decrease of Nc* as h/B ratio increase. For comparison results of bearing capacity factor, Nc* indicated a similar trend from previous studies. Stiffness parameters did not affect the solutions as long as remain constant for all cases within suitable ranges of parameters.

References

[1] Bowles, J. E. Foundation Analysis and Design. Third Ed. McGraw-Hill (1982).

[2] Bandini, P. M. & Pham, S. M. Bearing Capacity of Embedded Strip Footings in Two-Layered Clay Soil. Geo-Frontiers ASCE, 332–341 (2011).

[3] Burd, H. J. & Frydman, S. Bearing capacity of plane-strain footings on layered soils. Canadian Geotechnical Journal, 34(2), 241–253 (1997).

[4] COMSOL Multiphysics. Introduction To COMSOL Multiphysics User Guides (2012).

[5] Davis, E. H. & Booker, J. R. The effect of increasing strength with depth on the bearing capacity of clays. Géotechnique, 23(4), 551–563 (1973).

[6] Gibson, R. E. Some Results Concerning Displacement And Stresses In A Non-Homoheneous Geotechnique, 2(1), 58–67 (1967).

[7] Griffiths, D. V, M., Fenton, G. A., Manoharan, N, A. Bearing Capacity of Rough Rigid Strip Footing on Cohesive Soil : Probabilistic Study (2002), 743–755.

[8] Han, J and Jiang, G. Influence of Inclined Bedrock on Undrained Bearing Capacity of Shallow Strip Foundations. Geo-Frontiers ASCE, 322-331 (2011).

[9] Merifield, R. S., Sloan, S. W. and Yu, H. S. Rigorous Plasticity Solutions For the Bearing Capacity of Two-Layered Clays. Geotechnique, 49(4), 471 - 490 (1999).

[10] Merifield, R. S. & Nguyen, V. Q. Two- and three-dimensional bearing-capacity solutions for footings on two-layered clays. Geomechanics and Geoengineering: An International Journal, 1(2), 151–162 (2006).

[11] Szypcio, Z. & D. K. The bearing capacity of layered subsoil. Studia Geotechnica et Mechanica, XXVIII(1), 45–60 (2006).

[12] Zhu, M. Bearing Capacity of Strip Footings on Two-layer Clay Soil by Finite Element Method" Proceedings of ABAQUS Users' Conference, 777–787 (2004).

Applied Mechanics and Materials Vol. 567 (2014) pp 681-686
© (2014) Trans Tech Publications, Switzerland
doi:10.4028/www.scientific.net/AMM.567.681

Bearing Capacity of Shallow Foundation's Prediction through Hybrid Artificial Neural Networks

Aminaton Marto[1,a], Mohsen Hajihassani[2,b] and Ehsan Momeni[1,c]

[1]Faculty of Civil Engineering, Dept. of Geotechnics and Transportation, Universiti Teknologi Malaysia, 81310 UTM Johor Bahru, Johor, Malaysia

[2] Construction Research Alliance, Universiti Teknologi Malaysia, 81310 UTM Johor Bahru, Johor, Malaysia

[a]aminaton@utm.my, [b]mohsen_hajihassani@yahoo.com, [c] mehsan23@live.utm.my

Keywords: Shallow Foundations; Bearing Capacity; Artificial Neural Networks; Particle Swarm Optimization.

Abstract. The utilization of Artificial Neural Network (ANN) for bearing capacity estimation has some disadvantages such as getting trapped in local minima and slow rate of learning. Recent developments of optimization algorithms such as Particle Swarm Optimization (PSO) have made it possible to overcome ANN drawbacks and improve its efficiency. This paper presents a unified approach of ANN based on PSO algorithm to predict bearing capacity of shallow foundations in granular soils. To generate the network, numbers of 40 datasets including the recorded cases of full-scale axial compression load test on shallow foundations in granular soils were collected from literatures. Each dataset refers to a set of 6 inputs consisted of footing length and width, embedded depth of the footing, average vertical effective stress of the soil, friction angle of the soil, and ground water level as well as one output consisted of the ultimate axial bearing capacity. Several sensitivity analyses were conducted to determine the optimum parameters of PSO algorithm and the network architecture was determined following the trial and error method. The results demonstrate that the presented model predicts the bearing capacity of shallow foundations with high degree of accuracy.

Introduction

In designing shallow foundations, satisfying two major criteria is of prime importance: allowable settlement and ultimate bearing capacity. The latter can be defined as the maximum axial load which the soil can tolerate before failure occurred. Among many researchers, Terzaghi's [1] theory of bearing capacity was the first comprehensive theory for estimating the bearing capacity of shallow foundations. His contribution was later extended by some other scholars [2,3]. However, various bearing capacity formulas show wide degree of variability; in addition, the developed bearing capacity theories incorporate several assumptions to simplify the problems [4].

Apart from analytical methods on estimation of bearing capacity, numerous researchers have reported semi-empirical solutions for determining the bearing capacity of foundations e.g. [5]. Nevertheless, difficulty in collecting undisturbed samples as well as uncertainty associated with soil behaviour and stress-strain history of the soil, are the major impeding factors in applying these methods for bearing capacity estimation [6]. Although direct determination of the axial bearing capacity of foundations at the site, by loading the foundation, is the most reliable way for determining the bearing capacity, due to economic reasons and some other factors such as time, in practice, conducting the footing load tests is not of interests.

During the last decade, several researchers have established Artificial Neural Network (ANN) models for predicting the ultimate bearing capacity. Table 1 shows some recent studies on the application of ANN in foundation engineering. This table also highlights the reliability of the proposed ANN-based predictive models, the dataset number and major inputs of each predictive model.

Table 1. ANN application in shallow foundation

Reference	Database	Major Inputs*	Desired outputs	Reliability (R^2*)
Shahin et al. [6]	189	N,q, G	Settlement	0.82
Soleimanbeigi and Hataf [7]	351	G,ϕ,γ	Bearing Capacity	0.94
Soleimanbeigi and Hataf [8]	123	G,S,R	Settlement	0.77
Padmini et al. [9]	97	γ, G, ϕ	Bearing Capacity	098
Ornek et al. [10]	28	G,S	Bearing Capacity	0.95
Nazir and Momeni [11]	75	G,ϕ,σ'	Bearing Capacity	0.99

*N: standard penetration test N value; G: footing geometrical properties; q: footing net applied pressure; ϕ: Friction angle of soil; γ: Unit weight of soil; σ' effective stress of the soil; S: settlement of the footing; R^2: coefficient of determination

Though many studies suggest the utilization of ANN for bearing capacity estimation but the use of conventional ANN has some disadvantages such as getting trapped in local minima and slow rate of learning [12]. Recent developments of optimization algorithms such as Particle Swarm Optimization (PSO) have made it possible to overcome ANN drawbacks and improve its efficiency [13,14]. This paper suggests the applicability of Hybrid PSO-based ANN model, as a more reliable, fast and practical tool, in predicting the bearing capacity of shallow foundations in granular soils.

Develop a Predictive PSO-based ANN Model

The search process of conventional ANNs might fail and return unsatisfied solution [15]. Hence, many attempts have been made to increase the accuracy and performance on ANNs using optimization algorithms. Several studies have been conducted to determine the ability of PSO algorithm to train ANNs and proved that the PSO is an applicable tool to increase the ability of ANNs. In a PSO-based ANN model, in each iteration, PSO searches to find a set of weights and biases to minimize an objective function such as Mean Square Error (MSE) or Root Mean Square Error (RMSE). This progress is continued to find the best weights and biases for an ANN to minimize the error function.

Artificial Neural Network. An artificial neural network (ANN) is a soft computation technique that is able to find a complex nonlinear relationship between its feeding data and desired outputs. Basically, an ANN consists of three components: network architecture, transfer function and learning law. The network architecture deals with determination of model inputs and outputs, number of hidden layers and nodes in each hidden layer, as well as division of the available data for training and testing purposes. A transfer function is a non-linear function that, when applied to the net inputs of a neuron in a hidden layer, determines its output. Sigmoidal functions are among the most widely used transfer functions in ANNs mainly because they are continuous, real valued functions whose domains and derivative is real and positive respectively. Nevertheless, after selecting the best network structure and before interpreting the net information, ANN needs to be trained. One of the common training algorithms is Back-Propagation (BP). BP employs supervised learning, through iterative adjusting the connection weights, to minimize the Mean Square Error (MSE) between the network outputs and the desired outputs. For more details about BP-ANN, readers are referred to studies conducted by other researchers e.g. [11,16].

Particle Swarm Optimization (PSO) Algorithm. PSO algorithm, invented by Kennedy and Eberhart [17], is an optimization technique inspired from the social behavior of particles in a swarm like bird flocks. This technique can be utilized to solve global optimization problems within a nonlinear procedure. The particles in PSO which characterize potential solution are scattered in the multidimensional search space and move throughout this space. The position of each particle is altered based on its experience and that of neighboring particles and consequently, takes advantage of its own experience and their neighbors.

The solving an optimization problem using PSO is activated with initialization of random particles which are assigned with random positions and velocities. Subsequently, each particle saves

its best position, known as personal best (P_{best}) and also the overall best value obtained by other particles, known as global best (G_{best}). The pbest and gbest of each particle is updated by computing a new velocity in each iteration. The PSO procedure is conducted on the foundation of two simple equations (Eq. 1 and Eq. 2):

$$V_{new}=V+r_1C_1*(P_{best}-P)+r_2C_2*(G_{best}-P) \quad \text{Equation 1.}$$

$$P_{new}=P+V_{new} \quad \text{Equation 2.}$$

in which, V_{new}, V, P_{new}, and P are new velocity, current velocity, new position and current position of particles, respectively. C_1 and C_2 are acceleration constants, P_{best} is personal best position of particle and G_{best} is global best position among all particles. r_1 and r_2 are random values in the range (0,1) sampled from a uniform distribution.

Input Variables. One of the most important steps in establishing the ANN-based predictive models is identifying the effective input parameters. Recent studies (Table 1) show that footing geometry and some soil properties such as internal friction angle and unit weight of the soil are the most widely used inputs to ANN-based predictive models. In addition, some other studies suggest the importance of other factors such as ground water level below the footing, in designing the shallow foundations [18,19]. Hence, in this study, the effective parameters to the single output (bearing capacity) of the PSO-based ANN models are set to be the ground water level, GW, footing geometry including length, L and width, W, embedded depth, D_f, as well as some important soil properties such as internal friction angle of the soil, ϕ, and effective stress of the soil at W/2 below footing, σ'. The compiled dataset used for developing the predictive model includes a total of 40 recorded cases of axially footing load tests in both granular and sandy soils reported by Akbas and Kulhawi [20]. Table 2 shows the range of data used for developing the predictive model of bearing capacity.

Table 2. The range of data used for model development

Parameter	Category	Minimum	Maximum	Unit
W	Input	0.25	3.02	m
L	Input	0.25	3.02	m
D_f	Input	0	3.02	m
GWL	Input	1	10.7	m
ϕ	Input	30	53	-
σ'	Input	2.7	124.1	kPa
Q	Output	25	10300	kN

Modelling Procedure. In order to develop a PSO-based ANN model to simulate the axial bearing capacity of shallow foundations in granular soils a MATLAB code was written and subsequently, PSO parameters consisting of number of particles and acceleration constants of C_1 and C_2 were determined using the sensitivity analyses. A model with one hidden layer was chosen to be used in simulation as an initial model and the number of nodes in the hidden layer was determined following the trial-error method. To assess the performance of each model, the data were divided into two sections; 75 percent (including 30 datasets) to train the model and 25 percent (including 10 datasets) to test. The performance of each model was evaluated using the coefficient of determination (R^2) and Root Mean Square Error (RMSE) for testing datasets.

As previously mentioned, a series of sensitivity analyses was conducted to obtain the optimum number of particles. While a small swarm may fail to converge to a global solution, choosing a large swarm may lead to delay in the convergence and decrease efficiency. These sensitivity analyses were completed by setting fixed iteration number of 1000 repetitions for each model with various numbers of particles. Fig. 1 shows the values of R^2 and RMSE for different models with various swarm size. As it can be seen in this figure, the values of R^2 increased and values of RMSE decreased by increasing in the number of particles between 5 and 75. Afterwards, no significant increase in the values of R^2 can be seen as well as any significant decrease in the values of RMSE. Therefore, swarm size of 75 was selected to be used in the modelling.

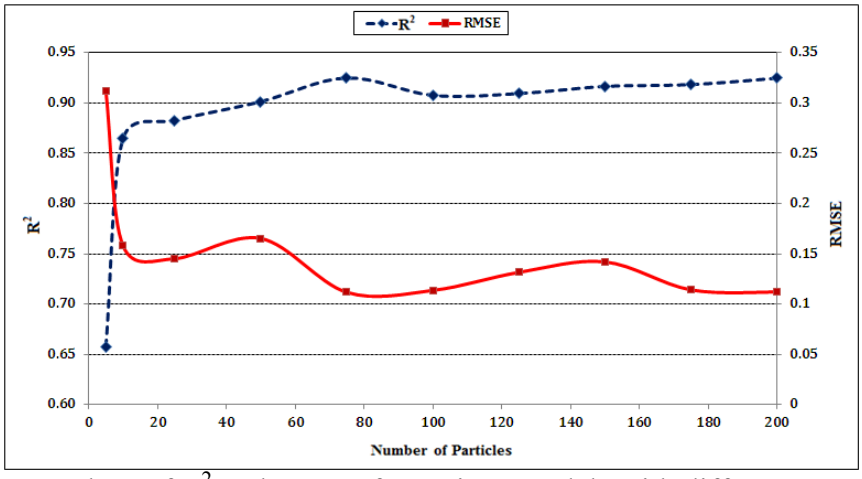


Figure 1. Values of R^2 and RMSE for various models with different swarm size

Determining the optimum acceleration constants (C_1 and C_2) were conducted in the next step. Based on literature studies, different values of C_1/C_2 were used in the sensitivity analyses, as displayed in Fig. 2. As it can be seen in this figure, the best results (highest value of R^2 and lowest value of RMSE) were obtained when C_1=C_2. Therefore, value of 2 was selected for C_1 and C_2 to be used in simulation.

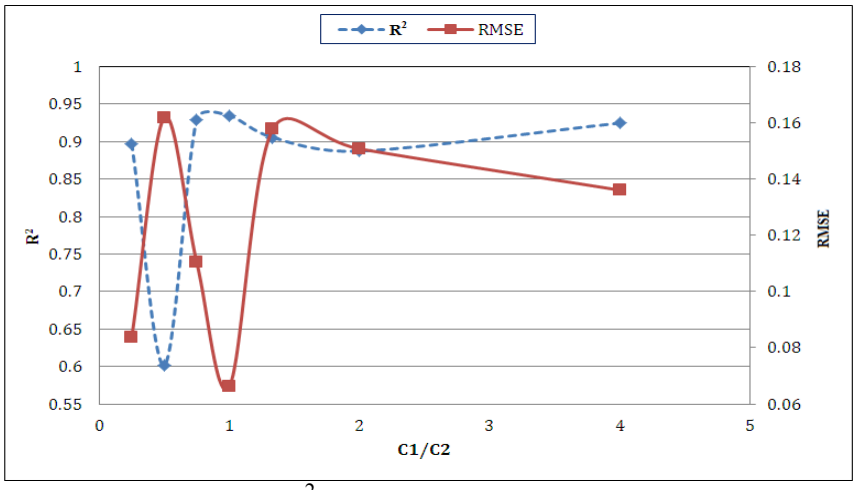


Figure 2. Values of R^2 and RMSE for different values of C_1/C_2

After determining the optimum values of PSO parameters, the number of nodes in hidden layer was determined following the trial-error method. Therefore, 7 models with different number of nodes of 3, 6, 9, 12, 15, 18 and 21 were considered. All models were trained with optimized PSO parameters obtained in previous analyses. The results of the analyses are shown in Table 3.

Table 3. Values of R^2 and RMSE for training and testing datasets in different models

Model	Nodes in hidden layer(s)	Training		Testing	
		R^2	RMSE	R^2	RMSE
1	3	0.974	0.086	0.658	0.156
2	6	0.988	0.049	0.970	0.100
3	9	0.997	0.043	0.991	0.033
4	12	0.971	0.061	0.968	0.062
5	15	0.970	0.072	0.927	0.076
6	18	0.948	0.081	0.917	0.094
7	21	0.953	0.082	0.934	0.086

According to the table, model 3 with 9 nodes in the hidden layer presents the best performance among all models in terms of values of R^2 and RMSE for training and testing datasets. Therefore, this model was selected to predict axial bearing capacity of shallow foundations in granular soils.

Analysis of the Results. In order to develop a PSO-based ANN model to axial bearing capacity of shallow foundations in granular soils, 40 datasets were collected. Each dataset includes six inputs and one output. 75 percent of datasets were randomly selected to train the models and the rest of datasets were used to assess the performance of each models. It is worth mentioning that the testing datasets have no role in learning procedure. The optimum PSO parameters were determined by means of sensitivity analyses and the numbers of nodes in hidden layer were determined following the trial-error method. Finally, an optimized model with 9 nodes in the hidden layer was obtained to be used in prediction. Figs. 3 and 4 show a graphical comparison between measured and predicted values of bearing capacity of shallow foundations for different training and testing datasets. According to these figures, the predicted values are in very close agreement with the measured values.

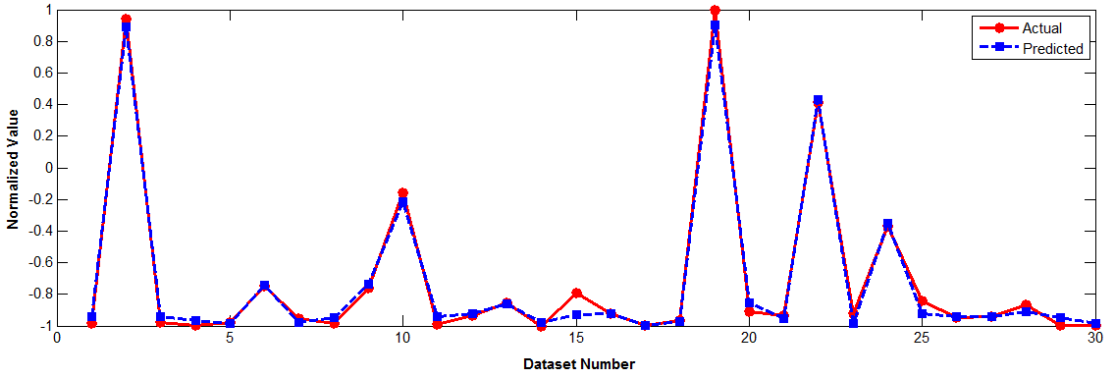


Figure 3. Comparison between measured and predicted values for different training datasets

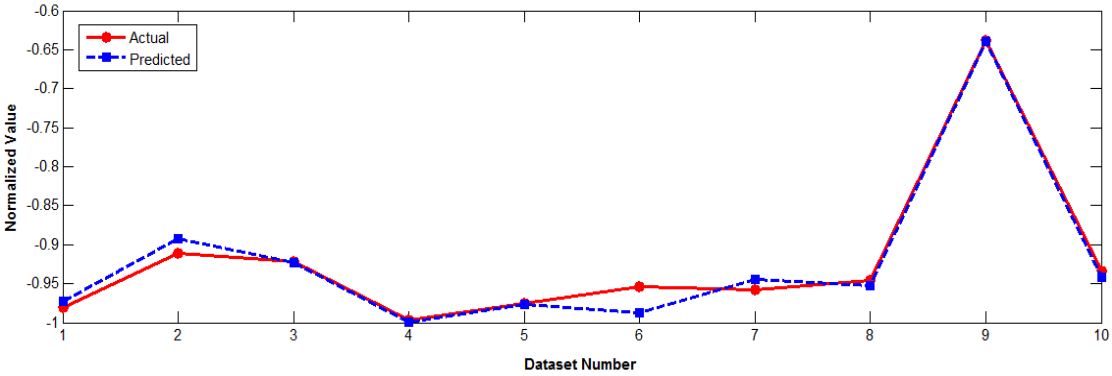


Figure 4. Comparison between measured and predicted values for different testing datasets

Summary and Conclusion

The study highlighted the application of Particle Swarm Optimization-based Artificial Neural Network (PSO-based ANN) in predicting the bearing capacity of shallow foundations in granular soils. The dataset used in developing the PSO-based ANN predictive model included 40 recorded cases of footing load tests in cohesionless soils. 75 percent of dataset were used for training the predictive model while the last 25 percent were used for testing purpose. Effective parameters including ground water level, footing geometry (length, width and embedded depth), and friction angle of soil as well as effective stress of soil were inputs to the predictive model of bearing capacity. The model performance was assessed based on the coefficient of determination (R^2) value. The R^2 values equal to 0.997 and 0.991 for training and testing datasets indicate the predicted bearing capacities using PSO-based ANN model is in close agreement with the measured bearing

capacities. From the results, it can be concluded that PSO-based ANN predictive model, as a feasible and accurate tool, can be implemented for predicting the bearing capacity of shallow foundations.

References

[1] K. Terzaghi, Theoretical soil mechanics, John Wiley & Sons, New York, 1943.
[2] G.G. Meyerhof, Some recent research on the bearing capacity of foundations, Can Geotech J 1 (1963) 16-26.
[3] A.S.Vesic, Analysis of ultimate loads of shallow foundations, JSMFD ASCE 99 (1973) 45-73.
[4] B.M. Das, Principles of Foundation Engineering, 6th ed, USA: Brooks/Cole, 2004.
[5] G.G. Meyerhof, Bearing Capacity and settlement of pile foundation, Journal of the Geotechnical Engineering Division 102 (1976) 197-228.
[6] M.A. Shahin, H.R. Maier, M.B. Jaksa, Predicting settlements of shallow foundations using artificial neural networks, J. Geotech. Geoenviron. Eng 128 (2002) 785-793.
[7] A. Soleimanbeigi, N. Hataf, Predicting ultimate bearing capacity of shallow foundations on reinforced cohesionless soils using artificial neural networks, Geosynthetics International 12 (2005) 321-332.
[8] A. Soleimanbeigi, N. Hataf, Prediction of settlement of shallow foundations on reinforced soils using neural networks, Geosynthetics International 13 (2006) 161-170.
[9] D. Padmini, K. Ilamparuthi, K.P. Sudheer, Ultimate bearing capacity prediction of shallow foundations on cohesionless soils using neurofuzzy models, Computers and Geotechnics 35 (2008) 33-46.
[10] M. Ornek, M. Laman, A. Demir, A. Yildiz, Prediction of bearing capacity of circular footings on soft clay stabilized with granular soil, Soils and Foundations 52 (2012) 69-80.
[11] R. Nazir, E. Momeni, Prediction of axial bearing capacity of spread foundations in cohesionless soils using artificial neural network, 9th international conference of geotechnical & transportation engineering, Johore Bahru, Malaysia, 2013.
[12] Y. Lee, S.H. Oh, M.W. Kim, The effect of initial weights on premature saturation in back-propagation learning, Proceedings of the International Joint Conference on Neural Networks, 1991, pp. 765-770.
[13] R. Eberhart, J. Kennedy, A new optimizer using particle swarm theory, Proceedings of the International Symposium on Micro Machine and Human Science, IEEE, 1995, pp. 39-43.
[14] R. Mendes, P. Cortez, M. Rocha, J. Neves, Particle swarms for feedforward neural network training, Proceedings of the International Joint Conference on Neural Networks, IEEE, 2002, pp. 1895-1899.
[15] S.W. Liou, C.M. Wang, Y.F. Huang, Integrative discovery of multifaceted sequence patterns by frame-relayed search and hybrid PSO-ANN, Journal of Universal Computer Science 15 (2009) 742-764.
[16] A. Marto, M. Hajihassani, R. Kalatehjari, E. Namazi, H. Sohaei, Simulation of Longitudinal Surface Settlement Due to Tunnelling Using Artificial Neural Network, International Review on Modelling and Simulations 5 (2012) 1024-1031.
[17] J. Kennedy, R.C. Eberhart, Particle swarm optimization, Proceedings of IEEE International Conference on Neural Networks, Piscataway, 1995, pp. 1942-1948.
[18] J.B. Burland, M.C. Burbidge, Settlement of foundations on sand and gravel, Proceedings of the Institution of Civil Engineering, Part I, Vol. 78, pp. 1325-1381, 1985.
[19] K.C. Foye, R. Salgado, B. Scott, Assessment of variable uncertainties for reliability-based design of foundations, ASCE J Geotech Geoenviron Eng. 132 (2006) 1197-1207.
[20] S.O. Akbas, F.H. Kulhawy, Axial Compression of Footings in Cohesionless Soils, II: Bearing Capacity, J. Geotech. Geoenviron. Eng. 135 (2009) 1575-1582.

Applied Mechanics and Materials Vol. 567 (2014) pp 687-692
© (2014) Trans Tech Publications, Switzerland
doi:10.4028/www.scientific.net/AMM.567.687

Comparison of Seismic Performance between Single and Double Unit Tunnel Form Building Under In-plane Lateral Cyclic Loading

Shamilah Anudai@Anuar[1a] & Nor Hayati Abdul Hamid[2b]

Faculty of Civil Engineering,

Universiti Teknologi MARA, 40450 Shah Alam, Selangor, Malaysia.

[a]shamilahanuar@yahoo.com, [b]abdulhamid_nrhyt@yahoo.com

Keywords. Tunnel form building, Lateral strength, Stiffness, Crack, Equivalent viscous damping

Abstract. This paper summarizes the comparison of seismic performance between single and double unit tunnel form building (TFB) under in-plane lateral cyclic loading. Experimental work was carried out to determine the lateral strength capacity, stiffness, ductility, and equivalent viscous damping (EVD) for both specimens. The comparisons of these parameters for both specimens were made to determine its percentage difference. The maximum lateral strength capacity obtained from single unit TFB with 8.68% higher than double unit TFB. As for stiffness behaviour, single unit was found to be much more stiffened compared to double unit. The EVD value showed that single unit absorbed much more energy compared to double unit of TFB. However, double unit TFB indicated a significant percentage of increment compared to the single unit TFB. Therefore, double unit TFB is safer to be built compared to single unit especially for seismic regions.

Introduction

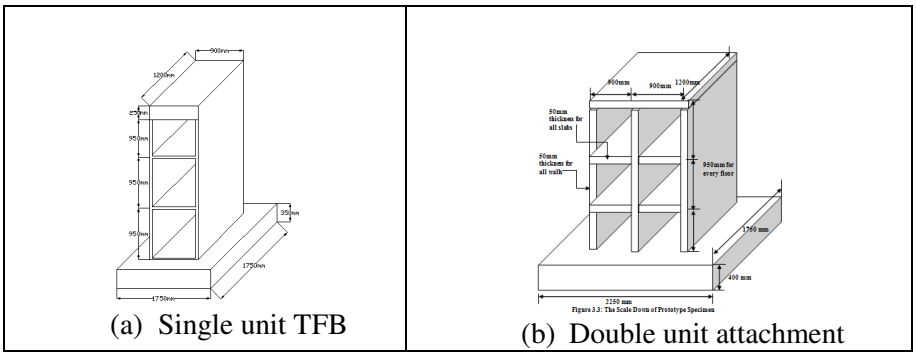
Tunnel form building (TFB) is an Industrialized Building System (IBS) that comprises walls and slabs as main components using cast in-situ method and steel formwork approaches. Shear walls (main component) can provide higher lateral stiffness and strength in order to cater the larger amount of seismic energy and minimize the damage to the structure [1].This system has become popular and it is widely used for construction of high rise RC building such as apartments, hotels, offices, and low cost flats. The advantages of using IBS are; this technique simplifies the whole construction process by enabling a smooth and fast operation that can result in cost effective for long term usage, productivity and high quality finishing.

Many countries have used TFB for their high rise building such as Turkey, Japan, California, and including Malaysia. Some of these countries are actually located in the high seismic regions that may cause significant damages to the TFB system. However, the TFB system has survived in several earthquake events (Kocaeli earthquake with 7.4 magnitude, Duzce earthquake with 7.2 magnitude, and Bingol earthquake with 6.5 magnitude) in Turkey from 1999 to 2004 [3]. This indicates that this type of building is vulnerable to earthquake excitation due to the location of lateral load resisting walls along the transverse and the longitudinal direction of the building [4].

Even though Malaysia is located in low seismic zones, it is surrounded by Indonesia and Philippines which are located in the Pacific Ring of Fire. Due to this reason, Malaysia has become susceptible to their seismic wave that can be felt in high rise buildings in this country. The effect of ground motion to our existing buildings depends on the distance from the epicentre and the magnitude of the earthquake. The areas that could feel earthquake tremor is mostly in the Klang valley, Johor, Selangor, and Kuala Lumpur due to long-distance earthquake. Therefore, the aim of this paper is to make the comparison between single and double unit TFB under in-plane lateral cyclic loading. Both TFBs were designed, constructed, and tested under in-plane lateral cyclic loading to examine its seismic performance. Both specimens were constructed using BS8110, which have no provision for seismic load. The seismic parameters that were compared are; lateral strength, stiffness, ductility, and equivalent viscous damping (EVD). Furthermore, the crack initiation and propagation observed through this experimental work will be discussed in this paper.

Methodology

Design and construction of the specimen. In this study, two specimens of TFB were designed, constructed, and tested under in-plane lateral cyclic loading. The first one is the single unit TFB and the second one is a double unit TFB as shown in Fig. 1 (a) and (b), respectively.



(a) Single unit TFB (b) Double unit attachment

Figure 1. Prototype of (a) single unit and (b) double unit attachment

The reinforcement bars for the foundations were 16mm for both specimens but they differed in spacing; 150mm (single unit) and 200mm (double unit) for both longitudinal and transverse reinforcements. The reinforcement used for overlapping, from the foundation to the wall, is T-10 with 400 mm length. The BRC wire mesh used in this specimen was a single layer BRC-8 for the wall, and BRC-6 for slab with spacing of 80 mm and 100 mm, respectively. The dimension size of the specimen was one-third scale due to the laboratory capacity limitations. The concrete grade for the shear wall and foundation were 35 N/mm2 and 40 N/mm2, respectively. The dimensions and material properties for both prototype specimens are tabulated in Table 1.

Table 1. The dimensions and material properties used for construction of single unit and double unit TFBs.

Structural Element	Structural dimension	Single Unit TFB		Double Unit TFB		Material description	Properties
		Actual size	Scale Down	Actual size	Scale Down		
Foundation	Length	5250	1750	6750	2250	Concrete strength	
	Width	3900	1300	5250	1750	a) Foundation	40 N/mm^2
	Depth	1050	350	1200	400	b) shear wall and slab	35 N/mm^2
Shear wall	Height	2850	950	2850	950	steel reinforcement strength	
	Width	3900	1200	3900	1200	a) Foundation	460 N/mm^2
	Thickness	150	50	150	50	b) shear wall and slab	250 N/mm^2
Slab	Length	2400	800	4800	1600	Aggregate size	
	Width	3600	1200	3600	1200	a) Foundation	20 mm
	Thickness	150	50	150	50	b) shear wall and slab	10 mm

Instrumentation and experimental set-up. Five LVDTs were installed to the single unit TFB and the systematic location of LVDT is shown in Fig. 2(a). Meanwhile, as for double unit TFB, six LVDTs were placed on the opposite of the double actuator, as shown in Fig. 2 (b). The main function of LVDTs is to measure the lateral displacement when subjected to in-plane cyclic loading. Both of the specimens were tested under in-plane direction using 500kN capacity of the double actuator located at the top of the TFB.

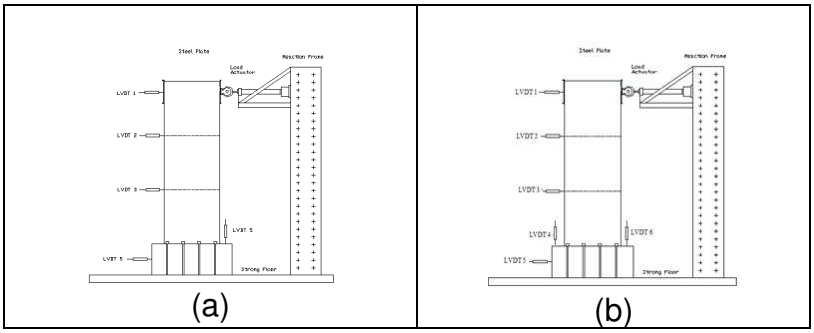


Figure 2. Experimental set up for testing (a) single unit and (b) double unit TFB

In total, ten successive cycles were applied to the both single and double unit TFBs, as shown in Fig. 3. Initially, ±0.01% drift was applied and increased by 0.25%, starting at ±0.1% drift until ±0.75% drift. Each drift comprised of two cycles (push and pull) approaches. In this method, the displacement was controlled in order to obtain the lateral load capacity for both specimens.

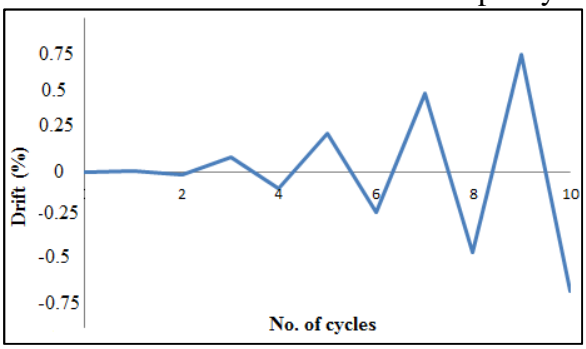


Figure 3. Loading regime applied to both single and double unit TFBs

Experimental results and analysis

Visual observation. The specimens were tested to determine the damage and crack patterns under minor to moderate earthquakes. The first specimen (single unit) started to crack at 0.1% drift, while the crack for the double unit specimen started at 0.25% drift. Fig. 4 (a) shows the occurrence of hairline crack obtained from 0.25% drift on the wall-slab joint on the first floor (inner wall). At the end of this drift, the crack occurred on the edge of the wall and propagated along the wall. Meanwhile, Fig. 4 (b) shows the hairline crack that occurred at the wall-slab joint on the first floor and the second crack occurred on the wall surface on the outer part.

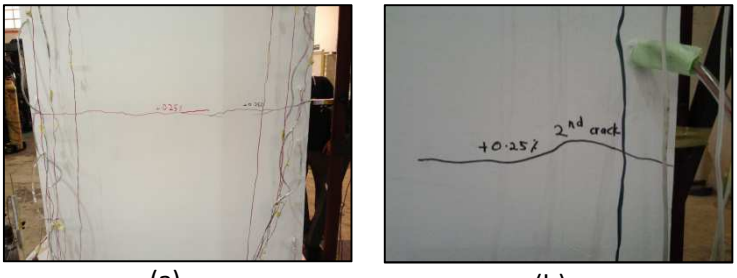
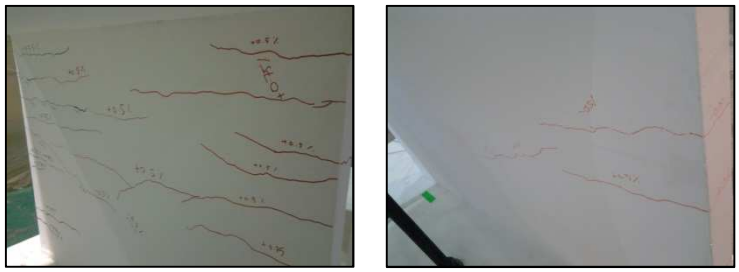


Figure 4. Initial cracks observed at 0.25% drift for (a) single unit and (b) double unit TFB

At 0.5% drift, the single unit TFB experienced many cracks starting at the edge of the wall on the second floor. Most of the cracks started to propagate from the right to the left wall on the inner first and second floor level, as shown in Fig. 5 (a). The double unit TFB started to crack on the outer wall on the second floor, as shown in Fig. 5 (b). In addition, during the second cycle, the crack

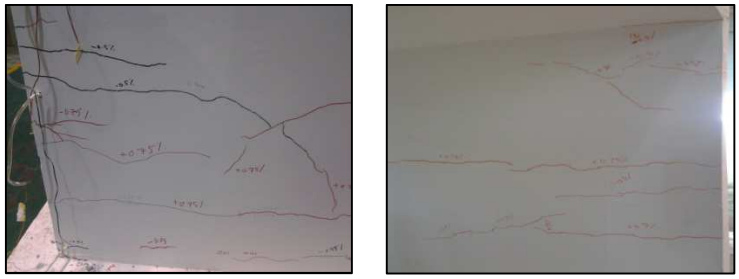
started to propagate along the same wall. Many cracks appeared at the edge and the centre of the inner wall the first and second floors.



(a) (b)

Figure 5. Crack patterns observed at 0.5% drift for (a) single unit and (b) double unit TFB

At the final drift (0.75%), the extension of the cracks started to take over on the inner and outer wall for both specimens for both single and double unit TFBs. Many cracks started to occur on the outer part of both walls and were connected to the previous cracks along the wall. Furthermore, at the end of this drift, a diagonal crack started to form at the middle of the first floor wall (outer) for the single unit TFB, as demonstrated in Fig. 6 (a). Meanwhile, the crack obtained from 0.5% drift started to propagate and connect with new cracks at 0.75% drift for double unit TFB, as illustrated in Fig. 6 (b).



(a) (b)

Figure 6. Crack patterns observed at 0.75% drift for (a) single unit and (b) double unit TFBs

Experimental results and discussions

Fig. 3 shows the comparison of hysteresis loop obtained from the single and double unit TFBs under in-plane lateral cyclic loading. Hysteresis loops that were obtained from the double unit TFB showed the small enclosed pattern compared to the single unit. This indicates that during testing, double unit specimen dissipated less energy dissipation as compared to the single unit specimen. This is because the connection at the foundation beam was not fully tied to cater for lateral loading. The strength capacity of the single unit was higher than double unit specimen starting at 0.10% drift to 0.75% drift.

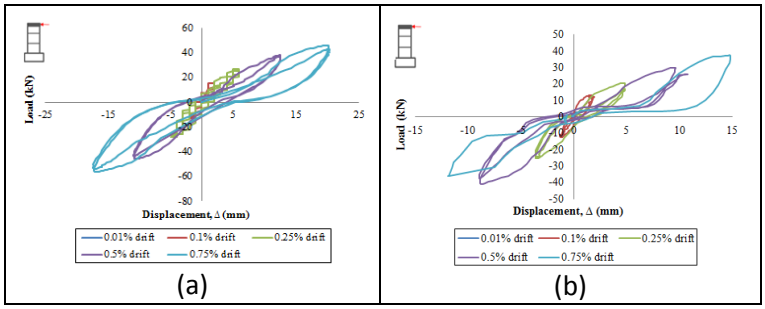


Figure 7. Comparison of hysteresis loops between single and double unit TFB, (a) single unit TFB and (b) double unit TFB

The maximum stiffness obtained from the single unit TFB was 84.9% in difference to the double unit TFB, as shown in Table 2. This indicates that the single unit TFB becomes stiffener than the double unit TFB. However, the displacement ductility for the double unit TFB was bigger than the single unit TFB with 70.07% difference. This is due to the connection at the foundation beam which was not strong enough to cater lateral load. Energy absorption for the single unit TFB gave greater value compared to the double unit, which resulted in 93.11 % difference from the first cycle. This indicates that the single unit absorbed more energy during the first strike of the earthquake, as compared to the double unit TFB.

Lateral strength is the strength capacity of the structure to resist the lateral load. Lateral strength can be obtained by plotting a graph of displacement versus load. This graph is known as hysteresis loop, the maximum lateral load of each drift can be seen through peak point of each loop. Equivalent viscous damping (EVD) is defined as the lost amount of energy per cycle when the structure is imposed to the seismic loading. EVD can be obtained by determining the area under hysteresis loops for each drift. Stiffness is the ability to resist the in-plane lateral cyclic loading under its elastic deformation range. It can be obtained by dividing the force over deflection. Meanwhile, ductility can be defined as the ability of the structure to dissipate the energy released by the earthquake event without decreasing the strength of the structure. Ductility can be acquired by dividing the lateral and yield displacements.

Table 2. The comparison of seismic behaviour between single and double unit TFBs

Description	Single Unit		Double Unit	
Lateral Strength capacity	0.10%	13.08	0.10%	13.08
	0.25%	16	0.25%	20.49
	0.50%	38.09	0.50%	29.89
	0.75%	46.05	0.75%	37.37
Stiffness	0.10%	5.69	0.10%	5.69
	0.25%	8.00	0.25%	3.23
	0.50%	3.03	0.50%	2.18
	0.75%	2.31	0.75%	1.74
Ductility	0.10%	0.07	0.10%	0.31
	0.25%	0.14	0.25%	0.85
	0.50%	0.87	0.50%	1.82
	0.75%	1.38	0.75%	2.86
EVD	1st cycle	12.97	1st cycle	4.73
	2nd cycle	10.28	2nd cycle	6.44

Conclusion and recommendations

The aim of this paper is to compare the performance of two types of 3-storey TFB subjected to in-plane cyclic loading. Comparisons were made in term of lateral strength, stiffness, ductility, and EVD for both specimens. Moreover, visual observations of the crack patterns were also recorded during this experimental study. It can be concluded that, single unit TFB performed well under minor to moderate earthquakes compared to double unit TFB in terms of discussing the parameters above. It is possible to use higher drift for double unit TFB in order to determine its capacity due to its double size compared to single unit TFB. It is recommended that the lateral strength capacity for double unit TFB can be determined by pushing higher drift and exceeding the yield point of TFB limit. The orientation of double unit also plays an important role where the back-to-back attachment of TFB gives higher lateral strength compared to attach unit.

Acknowledgement

The authors would like to thank the e-Science Fund, Ministry of Science and Innovation (MOSTI), Putrajaya, Malaysia, and RMI (Research Management Institute), for funding this research work. Nevertheless, the authors also would like to express their gratitude to the technicians in Heavy Structures Laboratory, Faculty of Civil Engineering, UiTM in helping to conduct this research work successfully.

References

[1] A. K. H. Kwan and J. Q. Xia, Shake-Table Tests of Large Scale Shear Wall and Infilled Frame Models, Proc. Instn. Civ. Engrs. Structs. & Bldgs., Feb 1995, 66-77

[2] Balkaya C., and Kalkan E. (2004). Seismic Vulnerability, Behavior and Design of Tunnel Form Buildings. Engineering Structures 26(2004), 2081-2099

[3] British Standard, BS8110-1, 1997, Structural use of concrete-Part 1: Code of practice for design and construction, BS8110-1:1997.(1997), London, UK, 172

[4] Kalkan, E., and Bahadir Yuksel, S., Pros and Cons of Multistory RC Tunnel-Form (Box-Type) Buildings, The Structural Design of Tall and Special Buildings, 2007

[5] Tae-Won Park, Lan Chung and Jinkoo Kim, Seismic Performance Evaluation of Tall and Non-Seismic Designed Wall-Type Structures by Shaking Table Tests, the structural design of tall and special buildings, 20, 314-326 (2011)

Applied Mechanics and Materials Vol. 567 (2014) pp 693-698
© (2014) Trans Tech Publications, Switzerland
doi:10.4028/www.scientific.net/AMM.567.693

Development Spectral Library of Vegetation Stress for Hydrocarbon Seepage

Muhammad Ikhwan Jamaludin[1, a], Abdul Nasir Matori[2, b], Mohammad Faize Kholik[3, c] and Munirah Mohd Mokhtar[4, d]

[1,2,3,4]Universiti Teknologi PETRONAS (UTP), Bandar Seri Iskandar, 31750 Tronoh, Perak Darul Ridzuan, Malaysia

[a]ikhwan.jamaludin@gmail.com, [b]nasrat@petronas.com.my, [c]faizelepmiri@gmail.com, [d]munirah_g01252@utp.edu.my

Keywords: Hyperspectral remote sensing, seepage hydrocarbon, oil and gas exploration, vegetation stress, spectral library

Abstract. Spectral Library is data archive of spectral signatures of various natural and man-made materials. In oil and gas industry, spectral library might not be heard often, but these tools can pose a great help for future oil and gas exploration. A developing spectral library for hydrocarbon is basically a new advancement in this field, and this project may implement the spectral library on global hydrocarbon seeps in the future. In this paper, the procedure in the developing spectral library from vegetation stress was demonstrated. In order to obtain these spectral signatures of hydrocarbon, the usage of hyperspectral remote sensing analysis and spectroradiometer is required. But for the early stage of development, spectrophotometer with the range up to 740 ηm was used to extract the spectral signature of the plants in term of green percentage. Nine samples of palm oil trees represent the stressed vegetation was planted with 10% and 40% porosity of crude oil and control samples having three palm oil trees for each of those. The vegetation has been left in an open environment with enough sunlight and watered daily. The significance result of changes in green percentage in the spectral signature of the trees with different porosity level was compared to the control samples. It shows that the existence of crude oil influences the health of the vegetation which has been notified through the spectral signature of the plant. This paper signifies a first step towards the development of spectral signature of hydrocarbon for oil and gas exploration.

Introduction

Spectral Libraries are data archives that consist of spectral signatures measured on selected natural and/or man-made materials [1]. The data in these libraries should also include the meta-information on the records. The two main purposes of having these spectral library data is for: the use of the data in remote sensing as in-situ radiance/reflectance measurements for the calibration and/or end-members selection further data processing [2]; or the use of the measurements for rapid laboratory assessment by diffuse reflectance spectroscopy (DRS), for example soil properties [3]. There exist a lot of spectral libraries such as the Jet Propulsion Laboratory (JPL) spectral library, John Hopkins University (JHU) spectral library where its compilation is available in NASA's ASTER spectral library collection. The ASTER library collection includes spectra of rocks, minerals, lunar soils, vegetation, and many more, covering the visible through the thermal infrared wavelength region (0.4-15.4μm) of the electromagnetic spectrum [1]. In terms of hydrocarbon spectral library, there is mostly data about the rocks and minerals, but almost none spectral data for the hydrocarbon itself on different kind of soils. For soils, there exists the Global Soil Spectral Library which is an on-going development by Viscarra Rossel, under soil spectrometry group.

Due to the reservoir seeps to the surface, a hypothesis arises that there will be effects on the vegetation of the soil. It was assumed that natural gases displaces the soil air and that oxygen shortage is the cause of changes in vegetation growth and reflectance, where this effect can be seen within 2 weeks of hydrocarbon microseepage on the surface [4].

Hydrocarbon microseepage is a phenomenon where the hydrocarbon from a certain reservoir flows out of its settlement, up to the surface. Unlike macroseepage, this seepage cannot be seen physically, thus the term is known as microseepage. Due to the energy contained in the reservoir fluid itself, some of its energy is being dispersed to the surrounding soil during its travel upwards to the surface, inducing stress on the soil. In addition, the surface vegetation is also affected by this phenomenon, due to the oxygen depletion and many other factors caused by the hydrocarbon seepage.

A pre-assumption can be made that the spectral reflectance data of soil and vegetation under the influence of hydrocarbon seepage from the reservoir will be much different if compared to those not affected by this phenomenon. To make a better analysis, a high spectral resolution data are needed, thus the usage of hyperspectral data is deemed very suitable for this case to get the best data possible for analysis.

After all of the data gained from the experimental procedure has been analyzed and trimmed for the best reflectance data, then the next procedure is to create a spectral library of vegetation under the influence of hydrocarbon seepage effect. These data would be a benchmark for future researches on similar topics of hydrocarbon seepage. The objective of the study is therefore to develop a hydrocarbon spectral library of vegetation stress.

Methods and Materials

Three units of palm oil plants will be used as sample A: control sample. While sample B and C (contains three units of each) represent 10% and 40% porosity filled with crude oil. Each sample of palm oil will have at least 3-4 palm oil trees. The preparation of vase to contain this set up and the calculation of the volume of the container were using formula (1),

$$V=\pi r^2 h \quad (1)$$

Where V = Volume (cm3), r = radius of the container (cm), h = height of the container (cm). The volume of each container is important to determine the volume of crude oil needed to fill in the void porosity of the soil later on.

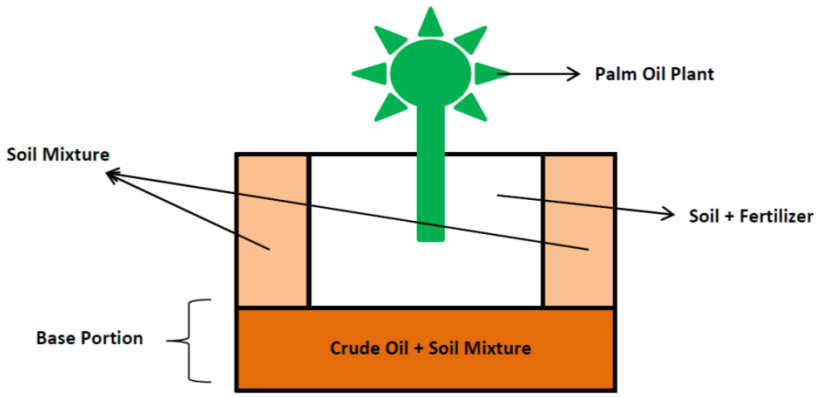


Figure1. Experimental setup

Later, weigh the dry weight of the soil, wet the soil with water and measure in the new weight of the soil. Then calculate the porosity of the mixture using the formula (2) to get the porosity percentage in the soil mixture,

$$\frac{Wet\ Mixture\ Weight - Dry\ Mixture\ Weight}{Dry\ Mixture\ Weight} \times 100\% \quad (2)$$

The porosity result was multiplied by the volume of the base portion, to get the volume of oil needed to fill in the 100% porosity of the mixture. Based on the percentage of the each sample, both crude oil and soil will mix together in the mixture. Next, place in the palm oil plant in the center of the container, and then fill in the void spaces surrounding the plant with the soil. Lastly, the set up was placed in a safe outside environment with enough sunlight to resemble the same condition of the study area and being watered daily. All the set up was conducted in the Environmental Laboratory of Civil Engineering Dept. Universiti Teknologi PETRONAS (UTP) (Fig. 2).

The spectral data being extracted from the leaves of each sample using spectrophotometer (Fig. 3) range up to 740 ηm to obtain the spectral signature result of the trees. Also the height and leaves anomalies are been observed weekly as to monitor the plant's growth rate.



Figure 2. Experiment Set Up Area



Figure 3. Spectral Extraction using Spectrophotometer

Result and Interpretation

The results presented in this paper only illustrate the changes of green percentage through spectral analysis and also the physical observations of the palm oil trees. The spectral signature of each tree was taken using a spectrophotometer with a spectral range up to 740 ηm.

Physical Observation and Interpretation. Each of the samples were watered daily, and observation were made weekly on any changes happening to the samples. The next tables show the sample conditions from week one, week three, week five and its observation:

Table 1. Week 1 observation

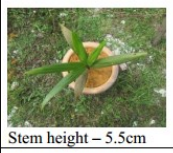
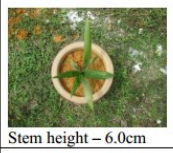
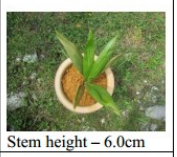
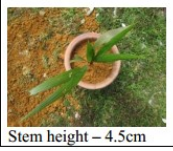
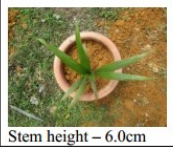
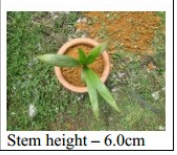
Sample	Observation		
	A	B	C
Control	 Stem height – 4.5cm	 Stem height – 4.5cm	 Stem height – 5.0cm
10% Crude	 Stem height – 5.5cm	 Stem height – 6.0cm	 Stem height – 6.0cm
40% Crude	 Stem height – 4.5cm	 Stem height – 6.0cm	 Stem height – 6.0cm

Table 2. Week 3 observation

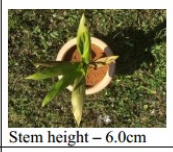
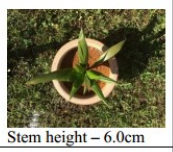
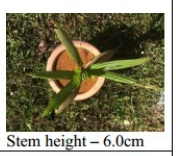
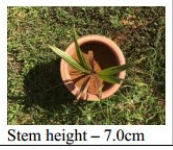
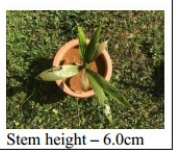
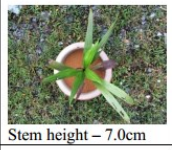
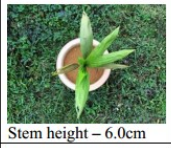
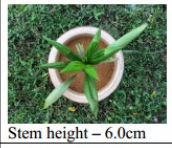
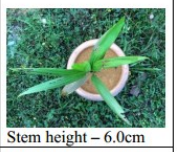
Sample	Observation		
	A	B	C
Control	 *(Destroyed)*	 Stem height – 6.0cm	 Stem height – 6.0cm
10% Crude	 Stem height – 6.0cm	 Stem height – 6.0cm	 Stem height – 6.0cm
40% Crude	 *(Destroyed)*	 Stem height – 7.0cm	 Stem height – 6.0cm

Table 3. Week 5 observation

Sample	Observation		
	A	B	C
Control	 *(Destroyed)*	 Stem height – 7.0cm	 Stem height – 6.5cm
10% Crude	 Stem height – 6.0cm	 Stem height – 6.0cm	 Stem height – 6.0cm
40% Crude	 *(Destroyed)*	 Stem height – 7.0cm	 Stem height – 6.0cm

It is observed that the samples mixed with 10% crude oil (B sample) are getting greener is compared to other samples. The samples mixed with 40% crude oil are not showing any growth and the leaf colors are also turning yellowish green, and slowly dying. This is scenario agreed by [4] stated that at the small amount of hydrocarbon seepage to surface, the vegetation appears to be greener than usual. While in high amount of hydrocarbon concentration, the vegetation is dying.

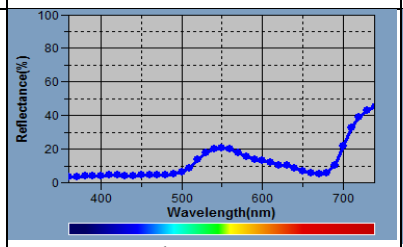
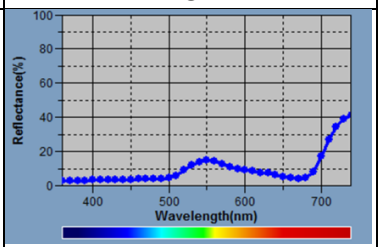
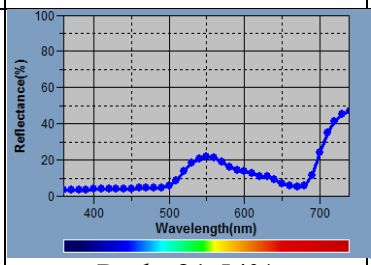
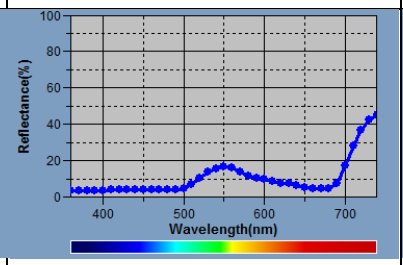
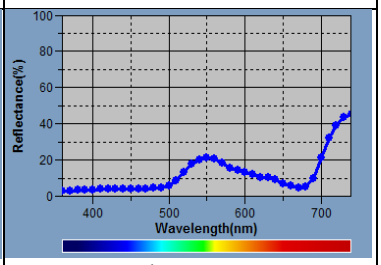
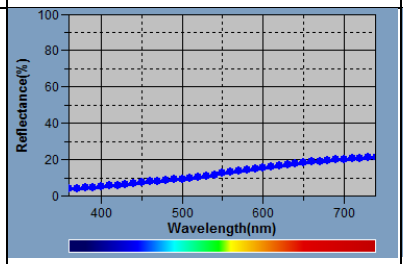
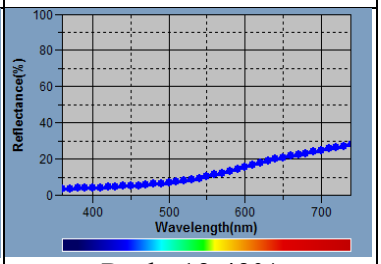
Almost all of the samples leaves are turning to yellowish green, which are expected. Due to the existence of hydrocarbon in the soil, it reduces the oxygen in the soil, thus interrupting the growth of the palm oil tree. As shown in the Table 3, the palm oil with 40% of crude oil are in fact dying, where sample B, does not have any green leaf at all, while sample C are about to die.

Spectral Data and Interpretation. The spectral data extraction was taken using a spectrophotometer with a spectral range up to 740 ηm. This result can only show the spectra of the green percentage of young leaves. At the range up to 740 ηm, the RGB wavelength (red, green and blue spectra) could signify the greenness of the leaves of the all the samples undergoing hydrocarbon seepage. Spectral data for all samples were taken at Centre of Intelligent Signal and Imaging Research (CISIR), Electrical & Electronic Department (UTP).

The spectrophotometer needs to be calibrated at zero and white light condition prior to use, and we have selected the spectral graph as the output. The spectral data were taken two times per each sample, where first spectral data were taken at an older leaf, and the second one at a younger leaf of the palm oil tree samples. The output from the spectrophotometer was then transferred to the computer through LAN cable and all data was extracted using SpectraMagic NX software.

From the spectral plot below, we are looking at the green spectra wavelength, where the peak percentage at the 550 ηm spectral wavelength shows the greenness of the sample leaf. Shown below are the spectral plot (Table 4) and its peak percentage at 550 ηm (represent greenness) for all samples:

Table 4. Spectral plot of RGB

Sample	Observation		
	A	B	C
Control	Destroyed	 Peak: 20.75%	 Peak: 14.65%
10% Crude	 Peak: 21.54%	 Peak: 16.32%	 Peak: 21.13%
40% Crude	Destroyed	 Peak: 12.31%	 Peak: 13.43%

From the spectral plot obtained on Table 4, the greenness of each sample that shows in RGB spectra. The two destroyed samples spectral data were not taken in the measurement. Based on these data, the difference crude oil saturation induced on the palm oil tree has different physical effects on the greenness of the plants. With 10% crude oil saturation, the highest peak show by sample A and C each at 21.54% and 21.13%. While from 40% crude oil saturation samples, the less green percentage show from the spectra with maximum peak at approximately 10%, means there is almost no green in the leaf.

Based from 10% and 40% crude oil saturation result and compare it with the control samples it is agreed that the hydrocarbon seepage pose physical effects towards the spectral changes of the plants. Moreover, the analysis has to take into account on parameters, the spectral changes and its physical effects. Therefore, comparing the physical effects and the spectral changes on the samples, it is enough to say that the hydrocarbon seepage at different concentration will generate an effect towards the spectral signature of the vegetation, and it is expecting to see the hydrocarbon signature if we further increase the spectra wavelength.

Summary

In short, this paper has shown the required result in the early stage of the development of spectral library of hydrocarbon, although the full reading for the hydrocarbon spectral library of vegetation stress could not be shown here. Based on the result presented through the changes of green percentage of spectral data and also the physical observation, it is safely said that this research is going on track and will be getting a positive result once the spectroradiometer is available.

As a full procedure already been discussed here, next paper will come out with the spectral library of hydrocarbon through vegetation stress. It can be further continued by using the developed spectral library to find hydrocarbon signatures in the real field through remote sensing analysis.

This can play a major milestone for oil and gas exploration activities since this method requires less cost, and more rapid analysis. Moreover, it can also be used to detect hydrocarbon gas leakage for pipelines buried under the ground.

Acknowledgement

The authors would like to thank Miss Nadira Binti Nordin, Research Scientist, CISIR, Electrical & Electronic Department, UTP for the much help in operating the spectrophotometer throughout the research conducted.

References

[1] Lukas, B., Ales, K., Vit, P., Radka, K., Lubos, B., Building Soil Spectral Library for Czech Soils for Quantitative Digital Soil Mapping, Soil & Water Res., 6 (2011) pp.165-172.

[2] Selige, T., Bohner, J., Schmidhalter, U., High Resolution Topsoil Mapping Using Hyperspectral Image and Field Data in Multivariate Regression Modelling Procedures, Geoderma, 136, (2006) pp. 235-144.

[3] Viscarra Rossel, R.A., Walvoort, D.J.J., McBratney, A.B., Janik, L.J., Skjemstad, J.O., Viscible, Near, Infrared, Mid Infrared, or Combined Diffuse Reflectance Spectroscopy for Simultaneous Assessment of Various Soil Properties, Geoderma, 135 (2006) pp. 59-75.

[4] Noomen, M. F., Hyperspectral Reflectance of Vegetation Affected By Underground Gas Seepage, (2007) pp. 1-167.

Applied Mechanics and Materials Vol. 567 (2014) pp 699-704
© (2014) Trans Tech Publications, Switzerland
doi:10.4028/www.scientific.net/AMM.567.699

Distribution of Stress on Stone Column-Reinforced Soft Soil under Cylindrical Storage Tank

Kousik Deb[1, a] and Amit Kumar Das[2, b]

[1]Associate Professor, Department of Civil Engineering, Indian Institute of Technology Kharagpur, Kharagpur 721302, India

[2] Research Scholar, Department of Civil Engineering, Indian Institute of Technology Kharagpur, Kharagpur 721302, India

[a]kousik@civil.iitkgp.ernet.in, [b] amitkdas.iitkgp@gmail.com

Keywords: Axi-symmetric analysis; soft soil; stone column; storage tank; stress distribution

Abstract. Structures with circular foundation (chimney, silo, oil tank) constructed on compressible soft soil, often have to opt for ground improvement like stone columns before construction. In this paper, the stress distribution on stone column-reinforced ground under cylindrical storage tank has been presented. Actual foundation soil reinforced with stone column is assumed as composite ground of soil and hollow cylindrical stone rings keeping the area ratio constant to carry the analysis in axi-symmetric condition. The soft soil, stone columns and granular fill are idealized using mechanical elements. The floor slab of the storage tank is assumed to be flexible enough to satisfy the theory of thin plate. Governing differential equations are derived to determine the vertical settlement and solved with finite difference technique. Contact stress at ground level is calculated from vertical settlement. It is observed that soft soil experiences heavy settlement and contact stress when the tank is full despite of low spacing to diameter ratio ($S/d_c = 3$) and reasonable modular ratio ($E_c/E_s = 20$). It is also observed that stress acting on edge stone column is lower as compared to the stress acting on center stone column even under uniformly loaded condition.

Introduction

In the present scenario, it has become necessary to use the land with poor soil quality after proper ground improvement measurements. Stone column is one of the popular ground improvement techniques to improve the soft soil. Circular/cylindrical storage tank, a common structure for industries like oil refineries is constructed on stone column-improved ground. Distribution of stress on stone column-improved ground due to the stiffness difference between the soft soil and stone column is very important for the design of the improved ground below the circular storage tank.

Studies have been carried out to analyze the interaction between soil and circular plate or raft. Selvadurai [1] studied the behavior of uniformly loaded circular plate resting on isotropic elastic halfspace using energy theorem. Zaman et al. [2] used energy approach to study the interaction between uniformly loaded thin circular plate and isotropic elastic halfspace. Mastrojannis et al. [3] assumed the circular raft as thin circular plate and analyzed the problem of adhesive contact between an axi-symmetrically loaded circular raft and foundation soil. Faruque and Zaman [4] investigated the interaction between a thin circular plate and isotropic elastic halfspace using variational approach. Vallabhan and Das [5] assessed the ground settlement below a circular tank foundation assuming bottom slab as thin circular plate. Rad and Alibeigloo [6] studied the annular circular plate resting on elastic foundation to obtain stress and displacement.

Studies also available which investigated the behavior of stone column-improved ground. Balaam and Booker [7] used unit cell method to carry out analysis of uniformly loaded rigid rafts resting on stone column-reinforced ground. Mitchell and Huber [8] converted stone columns in concentric stone rings keeping the area ratio constant to execute axi-symmetric approach for the analysis of stone column-reinforced ground. Lee and Pande [9] used an axi-symmetric model to

study the interaction between circular footing and stone column-reinforced ground. Experimental investigation along with numerical analysis was also performed to investigate the stone column-reinforced ground behavior considering single and group of stone columns [10]. Indraratna et al. [11] adopted method of stone column conversion in concentric stone rings to analyze the vertical drain-improved soft soil under circular embankment. Studies carried out with mechanical model as well to predict settlement of axi-symmetrically loaded geosynthetic-reinforced granular fill resting on stone column-reinforced ground [12]. Dey et al. [13] studied the flexural response of aqueduct resting on reinforced elastic foundation beds.

Thus, despite the availability of studies on stone column-improved ground or unreinforced ground under circular raft or storage tank, research work on the behavior of stone column-reinforced soil under circular storage tank is very limited. It is also observed that unit cell method is accurate near the embankment centerline where lateral displacement is zero [14] and this method may predict erroneous settlement for foundation with limited extent [15]. Therefore, in the present work, a study has been carried out in axi-symmetric condition incorporating the effect of all stone columns to investigate the vertical settlement and contact stress at the ground level of the stone column-reinforced soft soil in contact with cylindrical storage tank.

Mathematical Formulation

Modeling. Present study is carried out with an idealized model replacing actual model with mechanical elements. Fig. 1 (a) shows the sectional elevation of ground soil reinforced with stone columns converted to stone rings and bottom slab of the tank assumed as circular thin plate with loading. Granular fill and soft soil are idealized with Pasternak shear layer and spring-dashpot system, respectively. Stone columns are represented with stiff springs. Conversion of stone columns to equivalent stone ring is showed in Fig. 1(b).

Stone columns are converted into equivalent stone rings keeping the ratio of stone column to total improved area are constant [8]. Thickness (t_c) of equivalent stone ring and spacing (S_e) between them can be expressed as: $t_c = \beta d_c^2/(4S_e)$ and $S_e = 0.909S$ (triangular arrangement) or $1.128S$ (Square arrangement), where S is spacing between stone columns, d_c is diameter of stone column and β is equal to 3 and 4 for triangular and square arrangement, respectively. One can write radius of i^{th} equivalent stone ring as: $r_i = iS_e$.

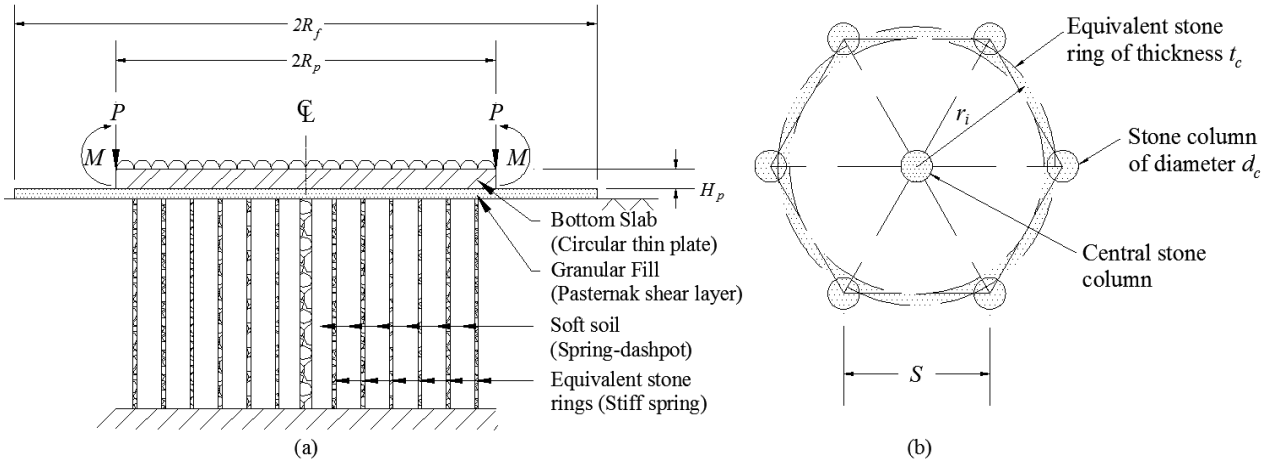


Figure 1. Cylindrical storage tank on stone column-reinforced ground (a) typical view floor slab of storage tank resting on stone column reinforced ground; (b) conversion of stone columns in equivalent stone ring (not to scale)

Formulation. A cylindrical tank of radius R_p is resting on granular fill of radius R_f. Considering the bottom slab to be flexible enough to satisfy the assumptions of thin circular plate theory. For axially symmetric deformations, the governing differential equation can be written as:

$$D\left(\frac{\partial^4 w}{\partial r^4}+\frac{2}{r}\frac{\partial^3 w}{dr^3}+\frac{1}{r^2}\frac{\partial^2 w}{\partial r^2}-\frac{1}{r^3}\frac{\partial w}{\partial r}\right)-H_f\left(\frac{G_{f1}}{r}\frac{\partial w}{\partial r}+G_{f2}\frac{\partial^2 w}{\partial r^2}\right)+kw=q \tag{1}$$

where

$$G_{f1}=\frac{G_{f0}}{1+\dfrac{G_{f0}\left|\partial w/\partial r\right|}{\tau_{fu}}} \tag{2}$$

$$G_{f2}=\frac{G_{f0}}{\left(1+\dfrac{G_{f0}\left|\partial w/\partial r\right|}{\tau_{fu}}\right)^2} \tag{3}$$

and D is flexural rigidity of the bottom slab or plate, q is uniformly distributed load on the bottom slab, G_{f0} is shear modulus of granular fill, H_f is thickness of granular fill and w is vertical settlement.

In the non-dimensional form, the governing differential equation at any time t, can be written as:

$$q^*=D^*\frac{\partial^4 W_p}{\partial R^4}+2\frac{D^*}{R}\frac{\partial^3 W_p}{\partial R^3}+\left(\frac{D^*}{R^2}-G_{f2}^*\right)\frac{\partial^2 W_p}{\partial R^2}-\left(\frac{D^*}{R^3}+\frac{G_{f1}^*}{R}\right)\frac{\partial W_p}{\partial R}+KW_p \qquad \text{for } R\le 1 \tag{4}$$

$$KW_f-G_{f2}^*\frac{\partial^2 W_f}{\partial R^2}-\frac{G_{f1}^*}{R}\frac{\partial W_f}{\partial R}=0 \qquad \text{for } R>1 \tag{5}$$

Where W_p and W_f are non-dimensional vertical settlement of the plate and that of granular layer beyond the plate, respectively.

In the non-dimensional form k can be written as:

$$K=\frac{k}{k_{s0}}=\frac{1}{U_{axi}\left[1+(W_p/q_{su}^*)\right]} \qquad \text{within soft soil region for } R\le 1$$

$$=\frac{\alpha}{1+(\alpha W_p/q_{cu}^*)} \qquad \text{within stone column region for } R\le 1$$

$$=\frac{1}{\left[1+(W_f/q_{su}^*)\right]} \qquad \text{for } R>1$$

Where U_{axi} is degree of consolidation at any time t, q_{su}^* and q_{cu}^* are non-dimensional ultimate bearing capacity of soft soil and stone column material, respectively.

Following Deb et al. [12], subgrade modulus or spring constant ratio, α can be expressed as:

$$\alpha=\frac{(1+\nu_s)(1-2\nu_s)E_c}{(1+\nu_c)(1-2\nu_c)E_s} \tag{6}$$

The non-dimensional parameters are written as follows:

$$q^* = \frac{q}{k_{s0}R_p},\ W_p = \frac{w_p}{R_p},\ W_f = \frac{w_f}{R_p},\ R = \frac{r}{R_p},\ D^* = \frac{D}{k_{s0}R_p^4},\ G_{f1}^* = \frac{G_{f1}H_f}{k_{s0}R_p^2},\ G_{f2}^* = \frac{G_{f2}H_f}{k_{s0}R_p^2},$$

$$q_{su}^* = \frac{q_{su}}{k_{s0}R_p},\ q_{cu}^* = \frac{q_{cu}}{k_{s0}R_p},\ \alpha = \frac{k_{co}}{k_{s0}}$$

Where E_c and E_s are elastic modulus of stone column and soft soil, respectively, v_c and v_s are the Poisson ratios of stone column and soft soil, respectively, k_{c0} and k_{s0} are initial modulus of subgrade reaction of stone column and soft soil, respectively.

Boundary Condition. To solve the governing differential equation of the bottom slab, following boundary conditions have been used as:

At $R = 0$, $\partial W_p/\partial R = 0$ and $Q^* = 0$

At $R = 1$, $M_r^* = M^*$, $Q^* = \dfrac{G_{f0}^*}{1+\dfrac{G_{f0}^*\left|\partial W_f/\partial R\right|}{\tau_{fu}^*}}\ \partial W_f/\partial R - \dfrac{G_{f0}^*}{1+\dfrac{G_{f0}^*\left|\partial W_p/\partial R\right|}{\tau_{fu}^*}}\ \partial W_p/\partial R + P^*$ and $W_p = W_f$

Where M^* and P^* are the non-dimensional moment and line load acting at the edge of the slab. Due to symmetry, only half of the tank foundation is considered. Finite difference technique has been used to solve the governing differential equations.

Results and Discussion

In the present study, two distinct cases of a cylindrical storage tank have been taken up to study the settlement and contact stress at the ground level. In first case, the storage tank is assumed to be almost empty, which means there is no distributed load on the floor slab of the tank except self weight. Since, the tank is empty, there is no lateral pressure on the tank wall, hence no moment (or negligible moment) at the edge of the floor slab of the tank is considered. However, a line load along the edge is present due to the self weight of tank wall. In the second case, tank is assumed to be full. Therefore, in this case distributed load on the bottom slab and moment at the edge both are very high. The line load in this case is same as earlier. All the quantities are presented in non-dimensional form. Fig. 2 shows the vertical settlement profile of the ground as well as bottom slab. It is observed that when the tank is full, vertical settlement at the centre is 26 times the settlement when the tank is almost empty.

Fig. 3 shows how contact pressure or stress distribution changes with change in the filling condition of the storage tank. The stress acting on stone column is more as compared to the soft soil due to the higher stiffness of the stone column with respect to soft soil. It is observed that contact pressure at the center for filled up tank is 21 times the contact pressure for empty tank. It is also observed that in empty condition, intensity of the contact pressure is almost same in every stone column, but in full condition contact pressure is more towards the center stone column as compared to the edge stone columns of the tank. The contact pressure on stone column reduces by 18% from center stone column to the stone column near the edge of the tank floor slab in full condition of the tank. The stress concentration ratio (ratio between the stress on stone column and the stress on soft soil) at centre is 4.9, whereas the same is 5.3 at the edge of the bottom slab when the tank is in full condition.

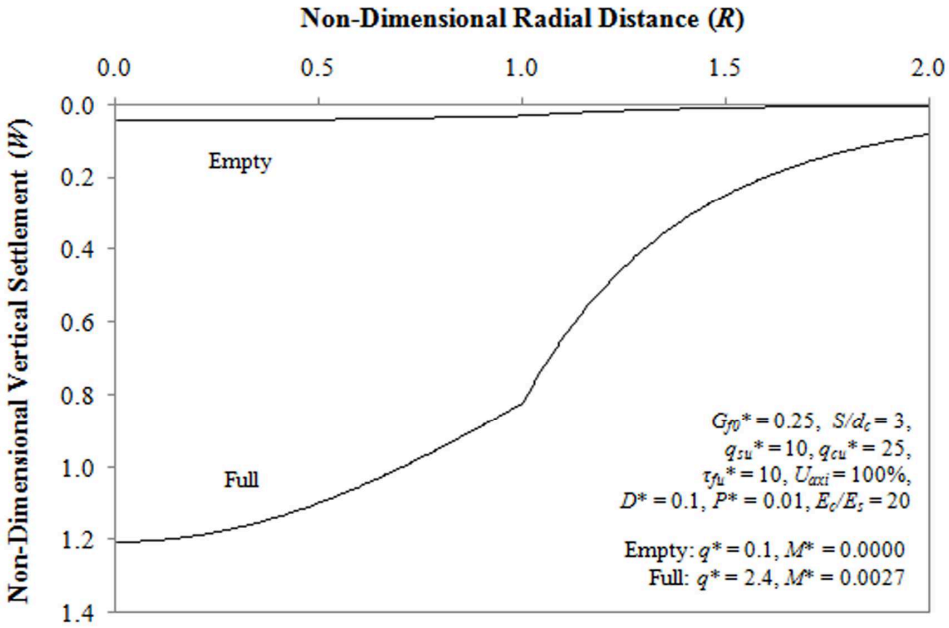


Figure 2. Effect of liquid height in tank on vertical settlement

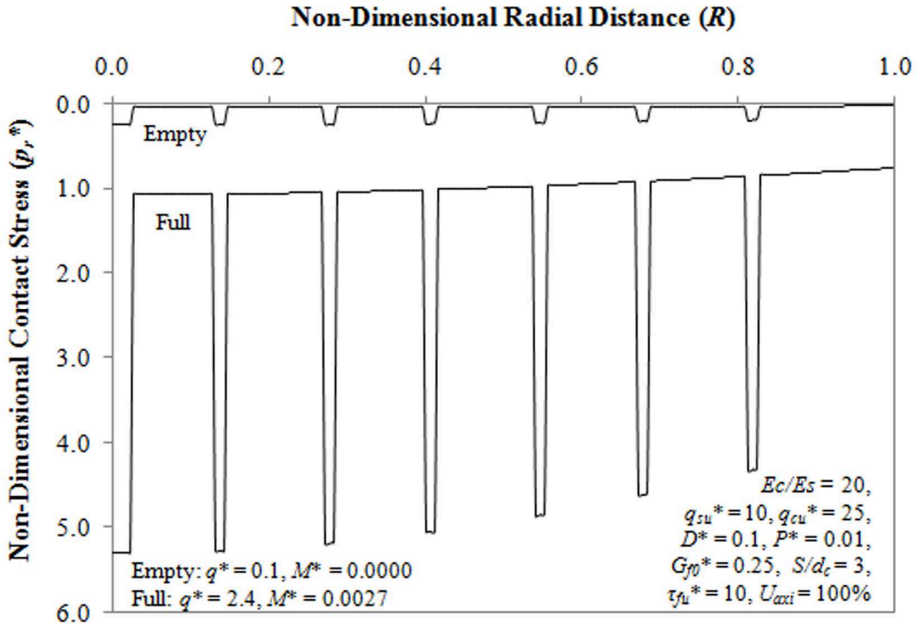


Figure 3. Effect of liquid height in tank on contact stress

Conclusions

The analytical method developed in the present work can be used to study the stresses acting on stone column-reinforced soft soil under cylindrical storage tank. Observations show that the soft ground experiences heavy displacement and development of contact stress when tank is full, whereas in the empty condition, only self weight of the tank does not cause reasonable displacement. It is also observed that stress acting on edge stone columns is less as compared to the stress acting on center stone columns when the tank is full. Under the chosen design parameters, the pressure acting on edge stone column is lower as compared to the pressure acting on center stone column. Thus, during design of the stone columns, different stresses have to be considered for central and edge stone columns. The stress on the centre stone column is 4.9 times more than the stress action on surrounding soil, whereas the same is 5.3 times more at the edge stone column when the tank is in full condition.

Acknowledgement

The authors sincerely acknowledge the financial support provided by SERB, Department of Science and Technology, India for this research work.

References

[1] Selvadurai A.P.S., The Interaction between a Uniformly Loaded Circular Plate and an Isotropic Elastic Halfspace: A Variational Approach, J. Structural Mech. 7 (1979) 231-246.

[2] Zaman, M.M., Kukreti, A.R., Issa, A., Analysis of circular plate-elastic half-space interaction using an energy approach, Appl. Math. Modelling. 12 (1988) 285-292.

[3] Mastrojannis, E.N., Keer, L.M., Mura, T., Axisymmetrically loaded thin circular plate in adhesive contact with an elastic half-space, Computational Mechanics. 3 (1988) 283-298.

[4] Faruque, M.O., Zaman, M., A mixed-variational approach for the analysis of circular plate-elastic halfspace interaction, Computer Methods in Applied Mechanics and Engineering. 92 (1991) 75-86.

[5] Vallabhan, C.V.G., Das, Y.C., Analysis of circular tank foundations, J. Eng. Mech. 117 (1991) 789-797.

[6] Rad, A.B., Alibeigloo, A., Semi-Analytical Solution for the Static Analysis of 2D Functionally Graded Solid and Annular Circular Plates Resting on Elastic Foundation, Mechanics of Advanced Materials and Structures. 20 (2013) 515-528.

[7] Balaam, N.P., Booker, J.R., Analysis of rigid rafts supported by granular piles, Int. J. Numer. Analyt. Meth. Geomech. 5 (1981) 379–403.

[8] Mitchell, J.K., Huber, T.R., Performance of a stone column foundation, J. Geotech. Engrg. 111 (1985) 205–223.

[9] Lee, J.S., Pande, G.N., Analysis of stone-column reinforced foundations, Int. J. Numer. Anal. Meth. Geomech. 22 (1998) 1001-1020.

[10] Ambily, A.P., Gandhi, S.R., Behavior of stone column based on experimental and FEM analysis, J. Geotech. Geoenviron. Eng. 133 (2007) 405–415.

[11] Indraratna, B., Aljorany, A., Rujikiatkamjorn, C., Analytical and numerical modeling of consolidation by vertical drain beneath a circular embankment, Int. J. Geomech. 8 (2008) 199-206.

[12] Deb, K., Basudhar, P.K., Chandra, S., Axi-symmetric analysis of geosynthetic-reinforced granular fill-soft soil system with group of stone columns, Geotech. Geol. Engrg. 28 (2010) 177-186.

[13] Dey, A., Chandra, S., Basudhar, P.K., Flexural response of aqueduct resting on reinforced elastic foundation beds, National Conference on Recent Advances in Ground Improvement Techniques, 24-25 February, CBRI Roorkee, India (2011).

[14] Indraratna, B., Balasubramaniam, A.S., Balachandran, S., Performance of test embankment constructed to failure on soft marine clay, J. Geotech. Engrg. 118 (1992) 12-33.

[15] Elshazly, H.A., Hafez, D.H., Mossaad, M.E., Reliabilty of conventional settlement evaluation for circular foundation on stone column, Geotech. Geol. Engrg. 26 (2008) 323-334.

Applied Mechanics and Materials Vol. 567 (2014) pp 705-710
© (2014) Trans Tech Publications, Switzerland
doi:10.4028/www.scientific.net/AMM.567.705

Effect of soil depth on the quantification of soil moisture content value estimated from NOAA satellite images

Abdalhaleem A. Hassaballa[1,a], Abdul Nasir B. Matori[1,b] and Helmi Z. M. Shafri[3,c]

[1]Geoinformatics and Highway Cluster, Department of Civil Engineering, Universiti Teknologi PETRONAS, Bandar Seri Iskandar, 31750 Tronoh, Perak Darulridzuan, Malaysia.

[3]Department of Civil Engineering, Faculty of Engineering, University Putra Malaysia, 43400, Serdang, Selangor Darul Ehsan, Malaysia.

[a]halimhasbo@hotmail.com, [b]nasrat@petronas.com.my, [c]helmi@eng.upm.edu.my

Keywords: Soil Moisture Content, NOAA Applications, Moisture Depth, Perak State.

Abstract. Soil moisture (MC) is considered as the most significant boundary conditions controlling most of the hydrological cycle's processes especially over humid areas. However, MC is very critical parameter to measure because of its variability in both space and time. The fluctuation of MC along the soil depth in turn, makes it so difficult to assess from optical satellite techniques. The study aims to produce a rectified satellite's surface temperature (Ts) in order to enhance the spatial estimation of MC. The study also aims to produce MC estimates from three variable depths of the soil using optical images from NOAA 17 in order to examine the potential of satellite techniques in assessing the MC along the soil depths. The universal triangle (UT) algorithm was used for MC assessment based on Ts, vegetation Indices (VI) and field measurements of MC; which were conducted at variable depths. The study area was divided into three classes according to the nature of surface cover. The resultant MC extracted from the UT method with rectified Ts, produced accuracies of MC ranging from 0.65 to 0.89 when validated with in-situ measured MC at depths 5cm and 10 cm respectively.

Introduction

Surface Soil moisture plays a very important role in land surface hydrology as it controls the portioning of rainfall into run off and infiltration [1, 2]. Along with surface temperature, it affects the depth of planetary boundary layer, circulation/ wind patterns [1, 3] and regional water energy budgets. Soil moisture tracks the perceptible evaporative water over period of weeks and provides a historical record of atmospheric-land interaction. Moreover, it integrates the land surface hydrology and also acts as an interface between the land surface and the atmosphere. [4]. On a regional scale, the importance of soil moisture appears in agricultural assessment (crops yield management, irrigation management, etc.), flood and draught control [5]. The important structural properties as another example are highly influenced by soil water because it makes soil heavier and softer to hold them. So, it is important to know and address the moisture amount and variation of the soil water over the years. This can assist in maintaining the engineering structures like dams, bridges, roads, etc. that are adequately suitable for the soil conditions. Among the wide range of MC applications in urban areas, the flood prediction is also an example which based on the spatial distribution of the saturation of ground soil [6, 7].

There have been considerable advances in the monitoring and retrieval of MC from Optical/IR remote sensing sensors. These advances are found in sensors with a high temporal resolution to meet the dynamic nature of MC [8-10]. In spite of the all spatial advantages, there still some critical challenges that reduce the spatial estimation accuracies of MC such as the MC observation depth, which remains a challenging issue for the optical/IR sensors since they have passive spectral properties, the optical signal's capability limitation which represented in clouds and atmospheric attenuation is also considered as one of the most troublesome problems in assessing the surface

parameters. This study intends to raise the accuracy of spatial MC assessment by producing a rectified satellite's surface temperature (Ts) through a correlation process with in-situ measurements of Ts at satellites overpass times, so as to diminish the attenuation caused by the clouds. In addition, it aims to produce MC estimates from three variable depths of the soil using optical images from NOAA 17 in order to examine the potential of NOAA satellite techniques in assessing the MC along the soil strata.

The study area

The study area covers two distinctive districts of Perak state (Malaysia), which are Perak Tengah & Manjung with an area of 2,400 square kilometers [11]. The two neighbor districts lay between latitude 4°00` – 4°30` N and longitude 100°30` – 101°00` E (Fig. 1) and separated by Sungai Perak (Perak River) which runs along the study area from the north to the south and surrounds Manjung district from the southern side to the coast downstream.

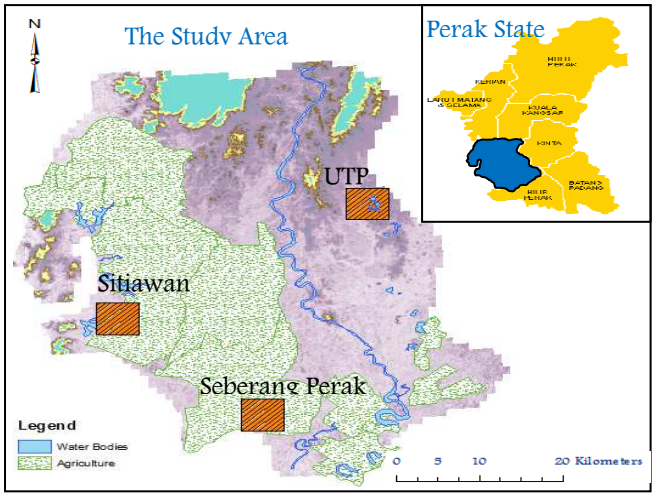


Figure 1: The study area with classified map for surface cover representation

Three stations were selected throughout the study area in terms of their variety in environmental and vegetation cover explained as Sitiawan to represent urban area with impervious surfaces, UTP represent a mixed surface cover type and Seberang Perak represents agricultural land.

Methodology

Data Collection. Two sets of data were used along the study, Terrestrial and Spatial data. The terrestrial set represented in field measurements of Ts and MC, which was conducted during the satellite's overpassing time using mini thermometer and a NETRON 740 soil moisture probe respectively. The spatial dataset, which is optical/IR images was acquired from NOAA 17 satellites. In order to process the acquired satellite's images for Ts and emissivity extraction, subset area has been delineated surrounding each weather station and any spatial computation performed within each subset area was assumed to represent the average value of the sub area pixels.

Soil Moisture Estimation. A simple regression between MC, Ts and the normalized difference vegetation index (NDVI) is normally achieved; in order to predict the MC through different soil depths according to the Universal Triangle theorem. Carlson [12] and Gillies [13] found that, the relationship between MC, NDVI*, and Ts* can be expressed through a regression formula such as:

$$\theta = \sum_{i=0}^{i=n} \sum_{j=0}^{j=n} a_{ij} NDVI^{*(i)} Ts^{*(j)} \quad (1)$$

In terms of a second order polynomial, the above equation can be expanded as:

$$MC = a_{00} + a_{10}NDVI^{*} + a_{20}NDVI^{*^2} + a_{01}T^{*} + a_{02}T^{*^2} + a_{11}NDVI^{*}T^{*} + a_{22}NDVI^{*^2}T^{*^2} + a_{12}NDVI^{*}T^{*^2} + a_{21}NDVI^{*^2}T^{*} \quad (2)$$

$$T^{*} = \frac{T - T_o}{T_s - T_o} \quad (3)$$

$$NDVI^{*} = \frac{NDVI - NDVI_o}{NDVI_s - NDVI_o} \quad (4)$$

Ts and NDVI are observed land surface temperature and normalize difference vegetation index, respectively, and the subscripts o and s stand for minimum and maximum values.

Split-window Algorithm for Ts Estimation. The general form that is intensively used for Ts extraction from satellite images is the split-window technique, which could be written as:

$$Ts = T_4 + A(T_4 - T_5) + B \quad (5)$$

Where Ts represents the land surface temperature, T_4 and T_5 represent the brightness temperature for channel 4 and 5 respectively, A and B are the coefficients determined by the impact of atmospheric conditions and other related factors on the thermal spectral radiance and its transmission in channels 4 and 5. Using the parameters A_0, P and M given by Becker [14, 15] proposed a simplified algorithm with the two coefficients A and B as:

$$A = (M - P)/2 \quad (6)$$

$$B = A_0 + T_4(P - 1) \quad (7)$$

Where the parameters A_0, P and M have been calculated by Becker [14] as:

$$A_0 = 1.274$$

$$P = 1 + 0.15616\frac{(1-\varepsilon)}{\varepsilon} - 0.482\frac{\Delta\varepsilon}{\varepsilon} \quad (8)$$

$$M = 6.26 + 3.98\frac{(1-\varepsilon)}{\varepsilon} + 38.33\frac{\Delta\varepsilon}{\varepsilon} \quad (9)$$

NDVI. The NDVI measurements were made with a combined red and near-infrared radiometer, developed at the NASA/Goddard Space Flight Center, which measures the reflected radiation in the bands (0.58-0.68 µm) and (0.73-1.1 µm).

Surface emissivity. Emissivity (ε) was estimated via an empirical algorithm based on the relationship between ε and the logarithm of NDVI [16, 17] in the range [0.955, 0.985].

Results and Discussion

Satellite's corrected Ts. Satellite Ts and NDVI were used in conjunction with in-situ measured Ts and MC which were achieved at two depths at surface 5 cm and 10 cm. The values of satellite Ts extracted from the images were rectified through applying a linear regression sketch with measured Ts taken in-situ in the same time of images acquisition. Figure 2 shows the satellite's-in-situ Ts relationships along 3 different depths of measured Ts taking Seberang Perak field as an example.

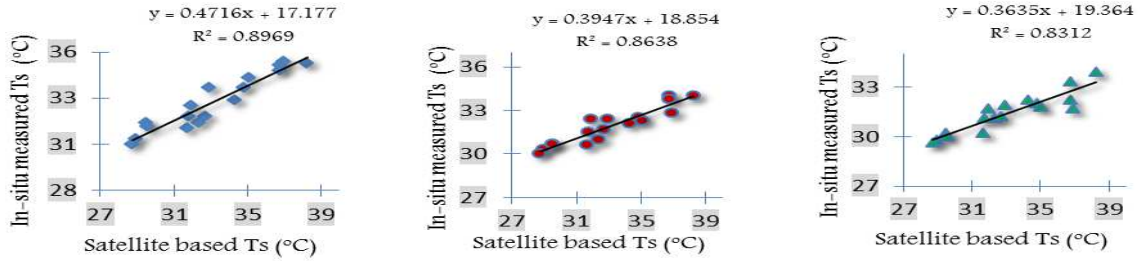


Figure 2: Correlation of Ts measured in-situ and satellite Ts for Ts correction at depths (a) 5cm, (b) 10 cm, (c) 15 cm of NOAA 17 over Seberang Perak paddy field

Moisture estimation from satellite's-corrected Ts. The MC parameters were generated according to the Universal Triangle (eq. 2) over each of the 3 locations. In which, the resultant corrected Ts was used beside NDVI and field measured MC that conducted as daily-base in concurrent time with the satellite's overpassing times. Figure 3 below shows the MC maps generated from parameters of daily MC measured in-situ at 5 cm, 10 cm and 15 cm depths. These maps are sort of raster images produced by ArcGIS software in which each pixel represents a unique value of MC.

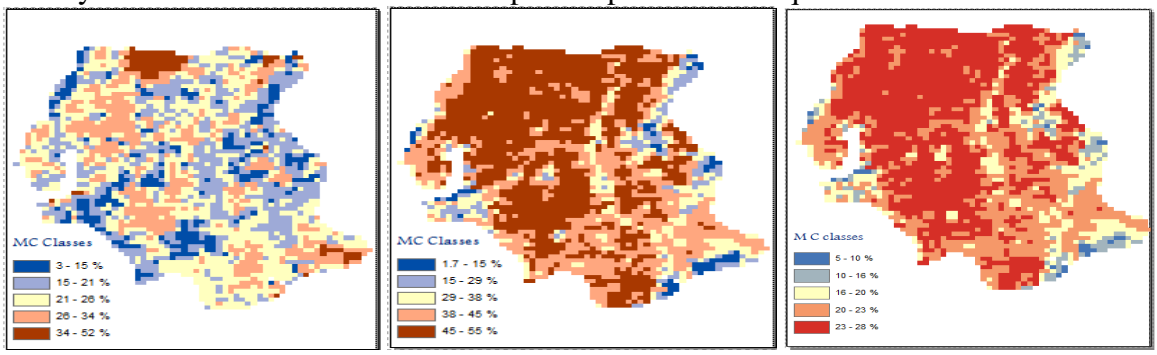


Figure 3: MC maps using corrected-Ts parameters at depths (a) 5 cm, (b) 10 cm and (c) 15 cm Seberang Perak field using NOAA 17 images

It could be distinguished from the produced MC maps that, the surface MC is mainly dependent on the Ts quantum; so it decreases with the increase of Ts. For instance, in the MC maps that are generated according to the urban area parameters, the higher the surface temperature, the lower are the MC values. This could be justified as that: In the study of surface MC-Ts relationship, it is agreed that, the built up areas always have a higher Ts than vegetative ones, due to the up-willing emission from the asphalted surfaces roofing machines etc. which causes reduction in MC values, while in the vegetative areas, Ts is relatively low which allow high MC as in [16]. Although the correction of Ts is a simple method to enhance the MC extraction from space, it involved a better extraction of the surface (5cm) and sub-surface (10 cm) MC. Soil MC variation and distribution over the area showed good compatibilities in terms of the LULC distribution when corrected-Ts was applied. Thus, these maps (fig. 3) availed concise representations of surface MC distribution.

Moisture content validation

An experimental validation was applied to the reserved dataset of NOAA 17 images. Images were manipulated in order to sufficiently validate the Universal Triangle algorithm used in the study. The reserved MC values which were collected in-situ from the 3 locations were used in the validation as well. Figure 4 below represents only the validation of UTP measurements as an example, where the field MC values were correlated against the satellites MC with the corrected Ts.

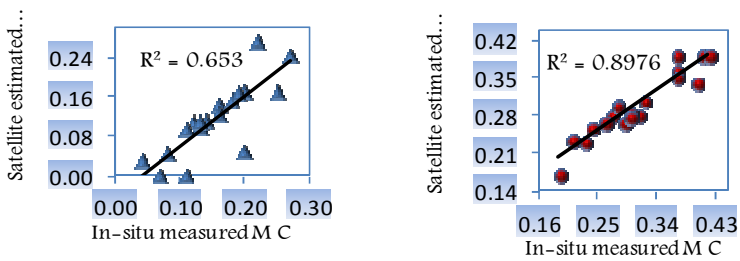


Figure 4: Graphical representations of UTP MC Validation using UT method from NOAA 17 at depths (left) 5cm and (right) 10cm

It is evident from all of the generated MC maps that, the vegetated areas within the study area are most likely to carry much MC than the buildup areas as well as the bare soils. This could be seen most obviously in the agricultural fields whose area is covered with vegetation that is uniformly growing. Mainly, the highest MC values are located to the agricultural areas which cover specifically Seberang Perak beside some other distributed locations covered by vegetation.

Moisture depth correlation

Moisture connection along the soil strata is a very significant parameter which assists in the study and evaluation of the ground water and water table recharges as well as the assessment of the root zone MC for agricultural crops. The study examined the correlation between the acquired MC values along the upper soil zone (5cm), the sub-surface zone (10 cm) and the root zone (15 cm -) as an attempt to avail a threshold study of deep MC, ground water, water table from optical/IR remote sensing. This attempt could be quite beneficial for the study of pore water pressure, which is considered as a basic influencing factor in soil stability in the sloppy areas[7]. Moreover, MC depths correlation can assist in modelling the hydrological cycle and share in monitoring the infiltration, seepage and even the water deep percolation. Fig. 5 below shows a typical correlation between the satellites' MC at the depths 5 cm, 10 cm and 15 cm for Seberang Perak paddy field.

The MC depth's correlation showed a quite close similarity in the attitude between MC status, particularly between depths 10 cm and 15 cm as seen in (fig. 5). This similarity implies that, the steadiness in MC manner of fluctuation within the deeper strata of soil can give a quantitative indication of the water availability in the zones that are not detectable by the passive remote sensors.

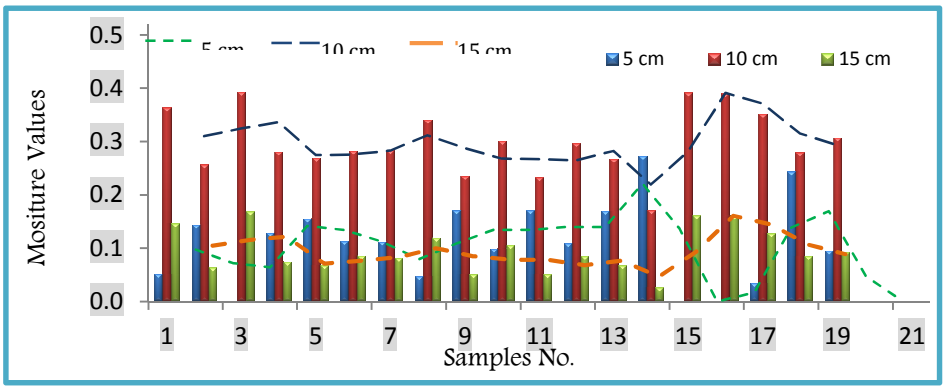


Figure 5: Correlation among the values of satellite MC at different depths for Seberang Perak

On the other hand, the status of MC at the top layer of the surface (5 cm) didn't show abrupt connection to MC at 10 cm depth. This could be justified as that, the MC at surface is always exposed to the weather conditions which could cause either a rapid dryness or wetness to soil according to the weather, while the MC status beneath the surface is always pending to the dynamics of soil saturation.

Conclusion

Optical/thermal infrared images from AVHRR 17 satellite were acquired in order to generate enhanced MC maps. The study has succeeded in rectifying the extracted Ts from satellites with in-situ measurements towards the removal of attenuation caused by clouds and other aerosols. The correlation between the satellite and in-situ measurements of Ts values resulted in coefficients of 89%, 86%, 83 % for Ts at depths 5 cm, 10 cm and 15 cm respectively from NOAA 17 over Seberang Perak paddy field. The MC validation produced a reasonable connection with a high significance between MC estimated over the agricultural land of Seberang Perak and its in-situ measurements. That is attributed to the uniformity of the vegetation cover which tends to reduce the Ts values producing a relatively high MC over the entire area. On the other hand, a moderate relationship was found between the two sets of MC over Sitiawan area (built up area). This is

certainly because soils at the urban areas get impervious due to compaction beside other activities. Moreover, the third part which is occupied by partial vegetation cover shared with scattered patches of agricultural fields beside some residential areas producing a significant correlation along the distributed surface covers. Finally, the correlation of MC along the soil depths found to be a very strong along the depths (10 -15 cm) underneath the soil surface.

Results from MC depth's investigations give the potential of future use of the satellite's surface MC in the assessment of the subsurface and ground water due to the tied correlation between the subsurface and root MC zones.

References

[1] J. Zhang and T. J. Crowley, "Historical climate records in China and reconstruction of past climates," *Journal of Climate,* vol. 2, pp. 833-849 %@ 0894-8755, 1989.
[2] A. A. Hassaballa and A. B. Matori, "Study on surface moisture content, vegetation cover and air temperature based on NOAA/AVHRR surface temperatures and field measurements," in *National Post Graduate Conference NPC*, Malaysia, 2011, pp. 1-5
[3] J. M. Lanicci*, et al.*, "Sensitivity of the Great Plains severe-storm environment to soil-moisture distribution," *Monthly Weather Review,* vol. 115, pp. 2660-2673, 1987.
[4] R. Bindlish and A. P. Barros, "Parameterization of vegetation backscatter in radar-based, soil moisture estimation," *Remote Sens Environ,* vol. 76, pp. 130-137 2001.
[5] J. D. Hanson*, et al.*, "Calibrating the root zone water quality model," *Agronomy Journal,* vol. 91, pp. 171-177 %@ 0002-1962, 1999.
[6] Z. Su*, et al.*, "Preliminary Results of Soil Moisture Retrieval From ESAR (EMAC 94) and ERS-1/SAR, Part II: Soil Moisture Retrieval," 1995, pp. 7-19.
[7] A. A. Hassaballa*, et al.*, "Extraction of soil moisture from RADARSAT-1 and its role in the formation of the 6 December 2008 landslide at Bukit Antarabangsa, Kuala Lumpur," *Arabian Journal of Geosciences,* pp. 1-10 %@ 1866-7511, 2013.
[8] H. L. Penman, "Natural evaporation from open water, bare soil and grass," *Proceedings of the Royal Society of London. Series A. Mathematical and Physical Sciences,* vol. 193, pp. 120-145 %@ 1364-5021, 1948.
[9] J. E. Christiansen, "Pan evaporation and evapotranspiration from climatic data," *Proc Amer Soc Civil Eng, J Irrig Drainage Div,* vol. 94, pp. 243-265, 1968.
[10] K. P. Georgakakos and O. W. Baumer, "Measurement and utilization of on-site soil moisture data," *Journal of hydrology,* vol. 184, pp. 131-152 %@ 0022-1694, 1996.
[11] JPM, "Basic Population Characteristics By Administrative Districts," Kuala Lumpur2010.
[12] T. N. Carlson*, et al.*, "A method to make use of thermal infrared temperature and NDVI measurements to infer surface soil water content and fractional vegetation cover," *Remote Sensing Reviews,* vol. 9, pp. 161-173 %@ 0275-7257, 1994.
[13] R. R. Gillies and T. N. Carlson, "Thermal remote sensing of surface soil water content with partial vegetation cover for incorporation into climate models," *J. Appl. Meteorol. ,* vol. 34, pp. 745-756 1995.
[14] F. Becker and Z.-L. Li, "Temperature-independent spectral indices in thermal infrared bands," *Remote sensing of environment,* vol. 32, pp. 17-33 %@ 0034-4257, 1990.
[15] A. A. Hassaballa and A. B. Matori, "The estimation of air temperature from NOAA/AVHRR images and the study of NDVI-Ts impact: Case study: The application of split-window algorithms over (Perak Tengah & Manjong) area, Malaysia," in *International Conference on Space Science and Communication (IconSpace)*, Malaysia, 2011, pp. 20-24
[16] M. S. Moran*, et al.*, "Estimating crop water deficit using the relation between surface-air temperature and spectral vegetation index," *Remote sensing of environment,* vol. 49, pp. 246-263 %@ 0034-4257, 1994.
[17] A. A. Van de Griend and M. Owe, "On the relationship between thermal emissivity and the normalized difference vegetation index for natural surfaces," *Int J Remote Sens* vol. 14, pp. 1119-1131 1993.

Applied Mechanics and Materials Vol. 567 (2014) pp 711-716
© (2014) Trans Tech Publications, Switzerland
doi:10.4028/www.scientific.net/AMM.567.711

Erosion Assessment of Slope Failure Tragedies; A Case Study in Malaysia

Mohd Fozi Ali[1, a], Mohd Adzreel Makatar[1,b] , Khairi Khalid[1,c] and Nor Faiza Abd Rahman[1,d]

[1] Faculty of Civil Engineering
Universiti Teknologi MARA,Malaysia

[a] mohdfozi@salam.uitm.edu.my, [b] adzreel.makatar@gmail.com, [c]khairikh@pahang.uitm.edu.my
[d]norfaiza128@gmail.com

Keywords: Erosion induced slope failure, slope characteristics, erosion and rainfall characteristics, structures characteristics.

Abstract. Slope Failure is a serious geologic hazard in many countries in the world including Malaysia. In this country, most cases of the tragedies involved a hillside areas and cause of deaths, injuries and property damages. There are many factors of slope failure which is related to erosion such as slope characteristics, erosion and rainfall characteristics, and structure characteristics. The paper was focused on producing a slope hazard category at Sg. Ruil, Cameron Highland and Hidayah Madrasah Al-Taqwa Orphanage, Hulu Langat since both locations were experiencing the slope failures in 2011. The task involved with the collection of the historical data, soil sampling and laboratory testing. The ROM Scale was calculated of 15.62 and 8.23 at Sg. Ruil, Cameron Highland and Hulu Langat, respectively. While, in that order the ROSE Index was calculating to be 329.6 and 317.8 ton.m/ha.hr. The study found that about 54% and 39% of the slope hazard parameters at Sg Ruil, Cameron Highland and Hulu Langat, respectively were categorized under critical condition. This finding is very useful and recommended to be one of a management tools to be considered for future development at the study area.

Introduction

In August 2011, a huge tragedy on the slope failure in Cameron Highland was spread in Malaysian media and reported about seven peoples were found dead and two were in seriously injured in this tragedy [1]. Similar tragedy also happened at Hidayah Madrasah At-Taqwa Orphanage, Hulu Langat on May 2011 and in this tragedy 19 people were found dead, while nine others survive [2].

Based on these tragedies, slope failure seems to be one a huge disaster in this country. One of the main factor triggers this failure involving erosion induced slope failure. Reference [3] stated in their internal report in 2005, one of the factors that reduced the factor of safety which are affected on the stability of slope is geomorphological process which are involving geological movement, erosion a nd deposition. Other researcher pointed out, landscape instability always happened together with gully erosion presence [4]. The affecting of soil erosion usually involved with rainfall erosivity, soil erodibility, topography, vegetative cover, management and conservation practices [5]. While other researcher was strongly recommended the correlation between rainfall intensity and soil strength is tremendous which can affecting to slope stability [6].

Considering all the above issues, this study utilizes erosion induced slope failure to categorize a slope hazard at Sg. Ruil, Cameron Highland and Hidayah Madrasah Al-Taqwa Orphanage, Hulu Langat. The first section of the paper gives some details on the methodology been applied in the study including the study area, a data collection, fieldworks study and laboratory testing. It followed by a discussion on ROM Scale and ROSE Index. The third section shows the results of slope characteristics, erosion and rainfall characteristics, structure characteristics and details parameters slope hazard

category for both of the study area. The paper concludes with identifying key issues and gives some directions for future research.

Materials and Method

Study Area and Methods. This study is focused on the parameters that involving erosion induced slope failure as in Figure 1. Therefore, historical data is important in this study together with soil sampling and rainfall data collection. The study areas are located in the state of Pahang and Selangor as in Figure 2(a) and 2(b). Laboratory testing such as sieves analysis and hydrometer testing are conducted to indentify physical properties of soil which are related to factors triggering erosion induced slope failure. ROM Scale [7] and ROSE index [8] are utilized in order to measure the level risk of particular soil and rainfall condition before the level risk of slope is finalized.

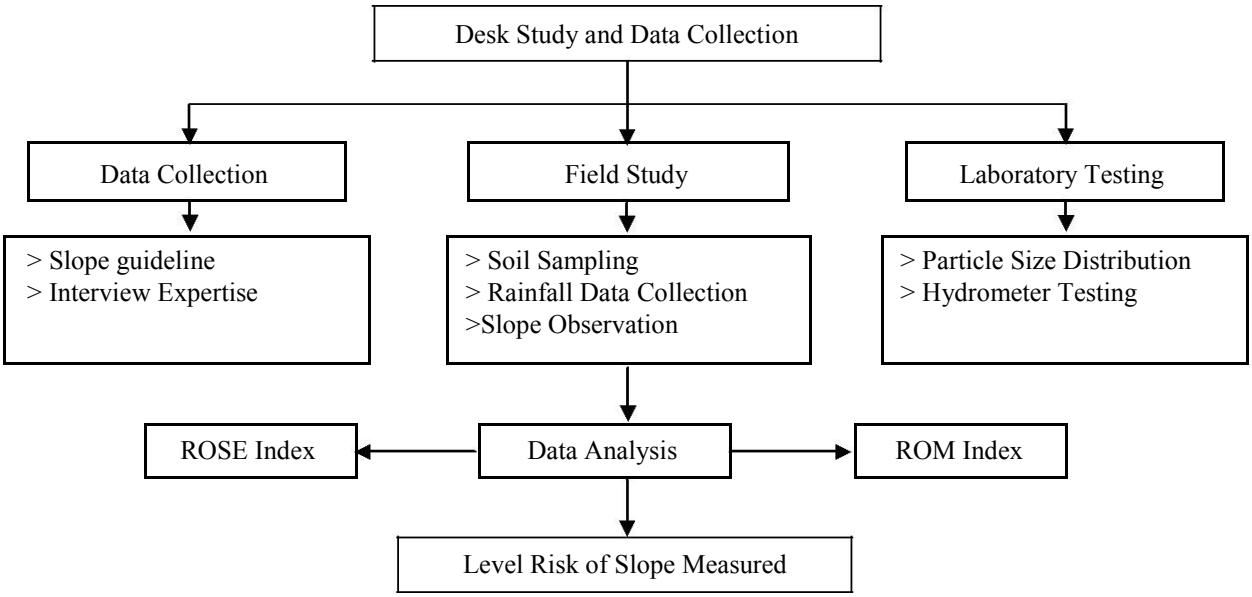


Fig. 1. A flowchart of the methodology





(a) (b)

Fig. 2(a). A study area, Cameron Highlands
Fig. 2(b). A study area, Hulu Langat

Data Collection. In order to determine the parameters involving erosion induced slope failure, data were obtained from a few agencies in Malaysia such as Slope Engineering Branch, Public Works Department Malaysia (PWD), Department of Irrigation and Drainage Malaysia (DID)

and International Research Centre on Disaster Prevention (IRCDIP), UiTM. All of the guidelines or regulations information about slope failure which is related to erosion were collected and to be measured as factors governing erosion induced slope failure.

ROM Scale and ROSE Index. The ROM scale is used to obtain the degree of soil erodibility was created based on EI_{ROM} equation as shown in Equation 1.

$$Degree\ of\ erodibility\ index = \frac{\%\ Sand + \%\ Silt}{2\ (\%\ Clay)}$$

Besides that, a rainfall erosivity with respect to ROSE Index is used to categorize rainfall erosivity. The ROSE Index can be used generally as the rainfall erosivity which is theoretically estimated since the automatically rain gauge stations are located in the study areas [9]. These methods will increase the understanding of risk level of erosion based on landslide nomograph and useful as a pre-warning landslide risk level information to relevant authorities.

Results and Discussion

Slope Characteristics. In the study, all the parameters which are related to erosion were collected and level risk of slope were determined. Table 1 shows slope characteristics at a different level of slope hazard category. It observed that the critical condition of the slope hazard category only happened if the slope steepness more than 35^{o} and a slope height exceeding 5 meter.

Table 1. Slope Characteristics

Slope Characteristics					
Hazard Category	Type of Slope	Slope Shape	Plan Profile	Slope Steepness (^{o})	Slope Height (m)
Low	Cut	Simple	Concave	<15	< 3
Moderate	Natural	Planar	Straight	15 – 25	3 - 4
High	Embankment	Asymmetrical	Convex	25 – 35	4 - 5
Critical		Compound		>35	> 5

Table 2 summaries the slope characteristics of the study area. The measurement and analysis proved that both of the study area having a critical slope characteristics. Slope steepness and slope height at both of the study area were observed in critical condition. A critical factor in terms of slope characterictics at Sg Ruil, Cameron Highlands was a slope height, which is 162.0m. While at Hulu Langat, a critical factor in terms of slope characterictics is slope steepness.

Table 2. Slope Characteristics at the study area

Slope Characteristics					
Location	Type of Slope	Slope Shape	Plan Profile	Slope Steepness (^{o})	Slope Height (m)
Kg. Sg. Ruil, Cameron Highland	Natural	Compound	Convex	32.0	162.0
Hidayah Madrasah At-Taqwa Orphanage Hulu Langat	Cut	Planar	Concave	37.2	23.8

Erosion and Rainfall Characteristics. The erosion and rainfall characteristics are summaries in Table 3 at a different level of slope hazard category. It observed that the critical condition of the slope hazard category only happened if the ROM Scale more than value of eight(8), ROSE Index exceeding 2000 ton.m/ha.hr and a rainfall intensity above 6.0 cm/hr.

Table 3. Erosion & Rainfall Characteristics

Erosion and Rainfall Characteristics					
Hazard Category	Vegetation Cover	ROM Index	Erosion Features	ROSE Index(ton.m/ha.hr)	Rainfall Intensity (cm/hr)
Low	Good	<1.5	Sheet	<500	<1
Moderate	Average	1.4 - 4.0	Sheet & Gully	500 – 1000	1.1-3.0
High	Poor	4.0 – 8.0	Rill & Gully	1000 – 2000	3.1 – 6.0
Critical		>8.0	Major & Gully	>2000	> 6.0

Table 4 summaries the erosion and rainfall characteristics of the study area. The measurement and analysis proved that both of the study area having a critical erosion characteristic. ROM Scale for both location were calculated to be more than value of eight(8). ROSE Index in both areas was considered in low slope hazard category but the calculated rainfall intensity was in critical condition. Both of slopes were also indicated low category of hazard for vegetation cover.

Table 4. Erosion & rainfall characteristics at the study area

Erosion and Rainfall Characteristics					
Location	Vegetation Cover	ROM Index	Erosion Features	ROSE Index (ton.m/ha.hr)	Rainfall Intensity (cm/hr)
Kg. Sg. Ruil, Cameron Highland	Good	15.62	Major Gully	329.6	10.00
Hidayah Madrasah At-Taqwa Orphanage, Hulu Langat	Good	8.23	Major Gully	317.8	19.53

Structures Characteristics. The structures characteristics of the study area are summaries in Table 5. It observed that the land use of residential, impervious area, commercial zone and construction sites contributed more towards critical slope hazard category compared to other land used type.

Table 5. Structures Characteristics

Structures Characteristics			
Hazard Category	Structures Present	Main Cover	Landuse
Low	None	Grass	Water Body/Bareland
Moderate	Crib Wall/Pilled Wall/ Surface Netting	Shrub/Fern	Horticultural/Permanent Cropland/Cropland
High	Soil Nailing/Gabion Wall/Rock Bolts/Stitching	Jungle	Rangeland/Grassland/ Forest/Swamps
Critical	Concrete Wall/Masonry Retaining Wall	Plantation/Agriculture	Residential/Impervious/ Commercial/Construction

In Table 6, both of slopes indicates a same condition which having no structures for both of slopes, shrub is a main ground cover and forest is the dominant land used. All of these parameters were indicated as low, moderate and high level of hazard category, respectively of each parameters.

Table 6. Structures Characteristics of the study area

Structures Characteristics			
Location	Structures Present	Main Cover	Landuse
Kg. Sg. Ruil, Cameron Highland	None	Shrub	Forest
Hidayah Madrasah At-Taqwa Orphanage, Hulu Langat	None	Shrub	Forest

Percentage of Slope Hazard Parameters. All the slope hazard parameters as the previous sections were accumulated and summarized in Table 7. The slope at Kg. Sg. Ruil, Cameron Highland is tremendously triggered by the erosion induced slope failure. 54% of parameters show as critical level, 8% is at a high level of hazard, while 15% and 23% were in moderate and low hazard category. The similar trend is also observed at Hulu Langat.

Table 7. Percentage of slope hazard category

Hazard Category	Sg Ruil, Cameron Highland	Hulu Langat
Low	23%	38%
Moderate	15%	15%
High	8%	8%
Critical	54%	39%

Conclusion

In this study three main characteristic were included to represent as a factor involving in erosion induced slope failure. The combination of these main parameters was produce a level of slope risk which is critical, high, moderate and low. It can be concluded that erosion induced slope failure can be categorized as important factors triggering to slope failure in these two incidents. It shows that many parameters are in critical level of risk.

Acknowledgement

This project was funded by Research Management Institute (RMI) of Universiti Teknologi MARA (UiTM), Malaysia.

References

[1] H. M. Online, "Tanah runtuh gegar Brinchang, 7 maut", from http://www.harian-metro-online.com/tanah-runtuh-gegar-brinchang-7-maut, 2011, Accessed on 18 July, 2012.

[2] B. H. Online, "Terkini tragedi tanah runtuh rumah anak yatim di Batu 14, Hulu Langat", from http://harian-hullahup.blogspot.com/2011/05/hulla-tragedi-terkini-tragedi-tanah.html, 2011, Accessed on 18 July, 2012.

[3] Software Technical Report, "Slope management and risk tracking system", Slope Engineering Branch, Public Works Department. 2005.

[4] R.P.C. Morgan, "Soil erosion, processes and mechanics of erosion", National College of Agricultural Engineering Silsoe, Bedfordshire. pp.11, 1980.

[5] T. Bhattacharyya, R. Babu, D. Sakar, C. Mandal, B. L. Dhayani and A. P. Nagar", Soil loss and crop productivity model In humid sub-tropical India", Current Science. Volume 93, No.10, 2007.

[6] J. C. Fan and M. F. Wu, "Effects of soil strength, texture, slope steepness and rainfall intensity on interill erosion of some soils in Taiwan", 10th Intenational Conservation Organization Meeting. Purdue University and the USDA-ARS National Soil Erosion Research Laboratory, 1999.

[7] Z.A. Roslan and M. Mazidah, "Establishment of soil erosion scale with regards to soil grading characteristic", 2nd World Engineering Congress, Sarawak, Malaysia, pp.235 – 239, 2002.
[8] Z.A. Roslan and H. Shafee, "The risk of rainfall erosivity based on ROSE index", International Research Centre on Disaster Prevention (IRCDIP),Universiti Teknologi MARA, 2005.
[9] Z. A. Roslan, "Forecasting erosion induced landslide", University Publication Centre (UPENA), UniversitiTeknologi MARA, Shah Alam, 2009.

Applied Mechanics and Materials Vol. 567 (2014) pp 717-723
© (2014) Trans Tech Publications, Switzerland
doi:10.4028/www.scientific.net/AMM.567.717

Flood Disaster Forecasting: A GIS-based Group Analytic Hierarchy Process Approach

Abd Nasir Matori [1] , Dano Umar Lawal [2]

[1, 2] Civil Engineering Department, Universiti Teknologi PETRONAS, Malaysia

[a]nasrat@petronas.com.my [b]bblawaldano@gmail.com

Keywords: Geospatial Technology-based Group Analytic Hierarchy Process, Spatial flood simulation

Abstract: Geographic Information System (GIS) was integrated with Group Analytic Hierarchy Process (GAHP) to facilitate the simulation of flood likely areas based on a total number of five set of criteria/factors believed to be triggering flood generation in the study area. Two categories of experts namely hydrologists and geologists were considered. Saaty's 1-9 scale of preference was employed in rating each factor's influence in flood generation and the ratings from the experts were aggregated using a Geometric Mean method. Having done with the aggregation, priory weights of the factors were calculated; weights were further normalized through the Analytic Hierarchy Process (AHP). The result was further integrated into GIS system for spatial simulation of the likely flood areas. The result forecasted 39.1% of the total area to be very highly susceptible to flooding. Validation was carried out by superimposing the known flood extent map from radar satellite data over the flood forecasting model developed herein.

Introduction

Flood is the most devastating of all geological events. Factually, floods have been part and parcel of the human lives. They are regular phenomena that made a basic and persistent feature of all river basin and lowland coastal systems [1]. In the most developed nations, severe floods can be seen as the most frequent and costliest natural catastrophes in terms of human and economic damages. Likewise they are the key cause of hazard-related deaths in the less developed nations. Since ancient times, the natural disasters troubled human development with distressing consequences. Therefore, a group decision making can be an efficient means of minimizing the flood disastrous effects. A group decision making is a vital part of the modern emergency planning and management [2]. The view of one expert may vary from others, but this will often be to the advantage of the planning authorities since it offers a useful medium for all expectations to be questioned and refined. The end result is therefore more realistic. [3] described how the civil defense and emergency management group decisions shared numerous exclusive characteristics. First of all, the group must frequently make several sophisticated and multi-faceted decisions in a short period, thereby contributing to a great "decision load". Secondly, these decisions may have possibly serious significances. [4] uses the terminology "decision quality" in describing the point to which a wrong decision could lead to disastrous outcomes. Thirdly, the group decision must frequently be prepared with incomplete information (equally in terms of quality and quantity), mainly in the initial phases of a disaster because of emergency management problems.

The Group Analytic Hierarchy Process (GAHP) [5-7] has great potential for use in the group emergency decision making. The Analytic Hierarchy Process (AHP) is a mathematical modeling technique for multi-criteria decision making [5] ; [8][9, 9] ;[10][10]; and [11]. It was developed by Saaty, a mathematician in early 70s. The AHP method helps to specify numerical weights representing the relative importance of factors, elements, criteria for flood susceptibility models (see also [12];[13, 13]; [14]; [11]. AHP allows both qualitative and quantitative approaches to solve complex decision problems. Therefore, vast majority of the work and literature available on the application of AHP in geo-engineering are dedicated to the generation of relative weights of influential factors based on a group decision making and integration of the weights into GIS environment for spatial modeling. For instance, [15] generated relative weights of influential factors

affecting urban (Lanzhou city, China) geo-environment using AHP, where the suitability potentials of urban land use were evaluated using GIS.

In this study, the principles of Multi-Criteria Decision Making (MCDM) in the context of group analytic hierarchy process (GAHP) have been integrated with GIS to simulate and forecast the flood susceptible zones. The objectives are to develop a flood susceptibility map based on the views of two category of experts (hydrologists and geologists) using some hydrogeological indexes. The data preparation and integration were carried out in GIS environment.

Study Area

The State of Perlis is bounded by Thailand in the north, Kedah in the south, while its western coastline borders the Straits of Malacca as illustrated in Fig. 1. It is bounded by longitudes 100 º 07' 02"E/ 100 º 22' 33"E and latitudes 6 º 43' 19"N/6 º 15' 13"N respectively. Perlis has history of flooding in 2005, 2009, 2010 and 2011.



Figure 1: Map of Peninsular Malaysia showing the study area

Methodology of the Study

Flood Influencing Criteria/Factors Selection

Certain natural flood influencing factors were considered in this study in order to forecast the flood susceptible zones in the study area. The factors considered herein are: rainfall, geology, slope gradient, land use, and the soil type. [16] and [17] used the same factors in their flood studies. Therefore, these factors are believed to be influencing flood generation in the area. However each factor has difference weightage to the flood occurrences. The weightage derivation will be explained in the following section.

Weighting the Flood Influencing Criteria/Factors

Based on the method of the MCDM, each factor's weight was computed and assigned to the factors discussed previously in GIS environment. [18] and [19] described MCDM as a method that permits each criterion to be weighted with respect to its relative importance/influence. Experts' judgments were used in assigning the weight of each criterion. The experts' ratings were aggregated using a Geometric Mean method as follows: Geometric Means = $((X_1)(X_2)(X_3)....(X_N))^{1/N}$; where X = Individual score and N = Sample size (Number of scores). Therefore, the experts' preferences helped in carrying out the pairwise comparison matrix. As mentioned earlier, AHP technique developed by [5] was used in coming up with the relative weights based on the Saaty's scale of influence 1 to 9 as shown in Table 1. The weights of the factors were generated based on the steps described by [20].

Integration of GAHP into GIS system

In this stage, the GAHP results were integration into GIS system to simulate the flood vulnerable areas. Combining all the thematic layers (the factors) using the Weighted Linear Combination (WLC) method in accordance with the computed weights was carried out in GIS. The Weighted Linear Combination, or simple additive weighting, relies on the concept of a weighted average where continuous criterions are standardized to a collective numeric range, and then combined by means of a weighted average [21][21]. The overlay of the thematic layers was to obtain the final simulation of the flood forecasted zones. The results of the final analysis managed to indicate the potential flood areas in the study area.

GAHP Results

Pairwise Comparisons of the Factors

It is normally presumed that Multi-Criteria Decision Analysis (MCDA) started at the beginning of 60s. A good number of experts of MCDA considered that their discipline stems mainly from the early work on goal programming as well as study of [22] [21][21]. Simon proposes a framework for analyzing human decision-making processes by differentiating between the intelligence, design, along with choice phases Hence, MCDA techniques are numerical algorithms that define suitability of a particular solution on the basis of the input criteria and weight together with some mathematical or logical means of determining trade-offs when conflict arise. By this technique, a weight value ranges from 1 to 9 was assigned to each factor by the experts to reflect their relative significance. Using the WLC method, all the map layers (the factors) were overlaid in the final GIS spatial analysis for flood susceptible zones simulation.

WLC technique can be carried out using any type of GIS system possessing the overlay. This permits the evaluation criterion map layers to be overlaid in order to obtain the composite map layer which is output. Therefore, the output of this WLC method gave a map which simulated the most potential flood susceptible zones of Perlis. Fig. 2 shows the flood forecasting model. The responses of the experts were computed in Table 1 and 2 below:
Where, C1 = Rainfall; C2 = Geology; C3 = Soil type; C4 = Slope gradient; C5 = Land use.

Table 1: A matrix of pair-wise comparisons of five criteria for the AHP process

	C1	C2	C3	C4	C5
C1	1.00	1.15	2.73	1.22	1.57
C2	0.87	1.00	0.48	0.47	0.60
C3	0.37	2.09	1.00	0.78	0.80
C4	0.82	2.13	1.28	1.00	0.84
C5	0.64	1.66	1.25	1.18	1.00
SUM	3.70	8.03	6.74	4.65	4.81

Table 2: Determining the relative criterion weights

	C1	C2	C3	C4	C5	Weights
C1	0.27	0.14	0.41	0.26	0.33	0.28
C2	0.24	0.12	0.07	0.10	0.12	0.13
C3	0.10	0.26	0.15	0.17	0.17	0.17
C4	0.22	0.27	0.19	0.22	0.17	0.21
C5	0.17	0.21	0.19	0.25	0.21	0.21
SUM	1.00	1.00	1.00	1.00	1.00	1.00

Table 3: Determining Consistency Ratio (CR)

STEP I :											
C1	1.00	1.15	2.73	1.22	1.57						
C2	0.87	1.00	0.48	0.47	0.60						
C3	0.37	2.09	1.00	0.78	0.80						
C4	0.82	2.13	1.28	1.00	0.84						
C5	0.64	1.66	1.25	1.18	1.00						
			*				STEP II : SUM1/WEIGTH				
	0.28	0.13	0.17	0.21	0.21						
			=			SUM1					
C1	0.28	0.15	0.46	0.26	0.32	1.48		0.28			5.24
C2	0.24	0.13	0.08	0.10	0.12	0.68	/	0.13	=		5.18
C3	0.10	0.27	0.17	0.17	0.16	0.88		0.17			5.21
C4	0.23	0.28	0.22	0.21	0.17	1.11		0.21			5.21
C5	0.18	0.22	0.21	0.25	0.21	1.07		0.21			5.19
									SUM2		26.04

Table 4: Random Inconsistency Indices

n		3.00	4.00	5.00	6.00		7.00	8.00	9.00	10.00
RI		0.58	0.90	1.12	1.24		1.32	1.41	1.45	1.49

The Consistency Index (CI), which is a measure of departure from consistency, was calculated using the formula:

$$CI=\frac{\lambda-n}{n-1} \qquad (1)$$

Where, n = number of factors (i.e. 5) and λ = average value of the consistency vector determined in step ii above.

λ = 5.24 + 5.18 + 5.21 + 5.21 + 5.19 = 26.04/5 = 5.21

Based on equation (3), CI = 5.21-5/5-1 = 0.05

Step IV: Calculating the Consistency Ratio (CR). The Consistency Ratio is defined as:

$$CR=\frac{CI}{RI} \qquad (2)$$

Where, RI is the random inconsistency index whose value depends on the number (n) of factors being compared; for n = 5, RI = 1.12 as illustrated in Table 4 [5]. The value of the CR is shown in Table 3.

Using Equation (4),

$$CR = \frac{0.05}{1.12} = 0.04$$

Therefore, since 0.04 < 0.1, it indicates that there is a realistic degree of consistency in the pairwise comparison and as a result, the weights 0.28, 0.13, 0.17, 0.21 and 0.21 (i.e. 28.15%, 13.13%, 16.85%, 21.33% and 20.54% respectively) can be assigned to rainfall, geology, soil type, slope gradient and land use respectively.

GAHP Spatial Flood Forecasting Model

The combination of all parameters was carried out in GIS using the WLC method. This is based on the weights generated from the GAHP. The WLC formula is shown below:

$$FSZ = \sum_{wixi} \quad (3)$$

Where, *FSZ* is the Flood Susceptible Zones; w_i is the factors weights which must sum up to 1, and x_i is the criterion score i. All these relevant data were uploaded into the GIS system before analysis was carried out using a total of five thematic maps: land use, geology, rainfall distribution, soil type and slope gradient. Fig. 2 presents the result of the GIS spatial simulation model for flood susceptible zones. In Fig. 2, the white, lemon green, orange, light blue and red colors represent very highly, high, moderate, little as well as hardly susceptible zones to flooding. These are basically based on the ratings of the flood influencing factors given by the experts.

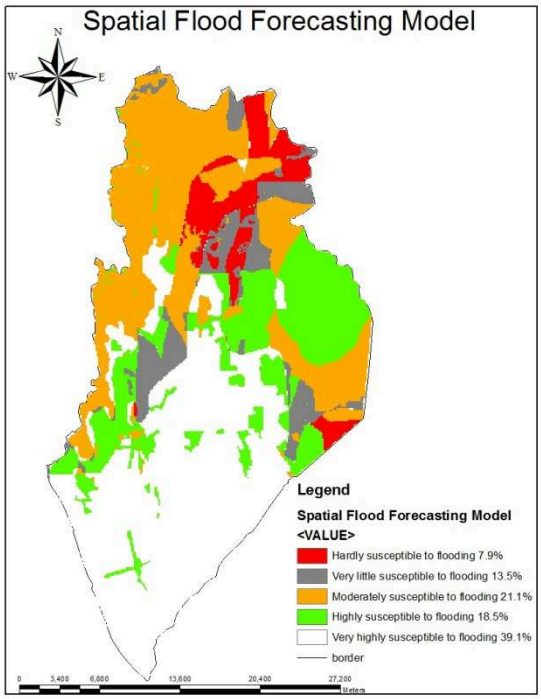


Figure 2: Map of Forecasted Flood Susceptible Zones of Perlis

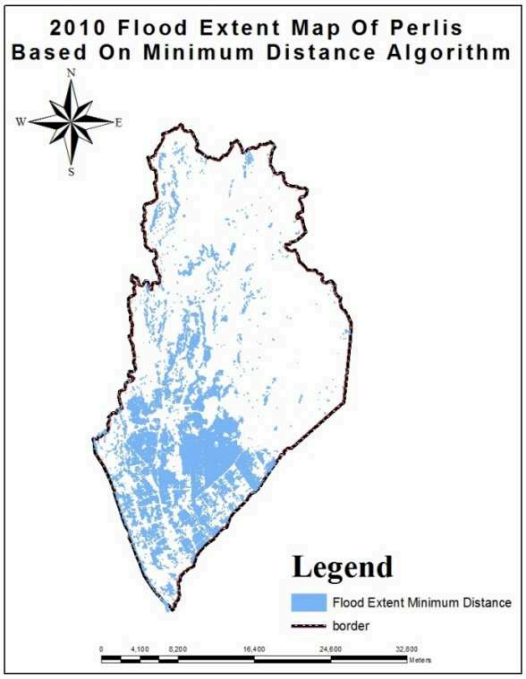


Figure 3: Flood Extent Map of the Study Area

Validating the GAHP Spatial Flood Forecasting Model

In validating the GAHP spatial flood forecasting models, the flood extent map (Fig. 3) developed based on a Minimum Distance classification technique embedded in ENVI 4.8 software was used. Radar satellite during-flood image dated November, 2010 of Perlis, Malaysia was used. In determining the reliability of GAHP spatial flood forecasting model, the model (Fig. 2) was overlaid with the flood extent map (Fig. 3). Fig. 4 was obtained by the overlay operation. An analysis of the Fig. 2 revealed that the majority of the flooded areas to be scattered over areas identified as very high susceptible, high susceptible, and moderately susceptible to flooding. Hence, this shows a very high correlation of the two (Fig. 2 and 3).

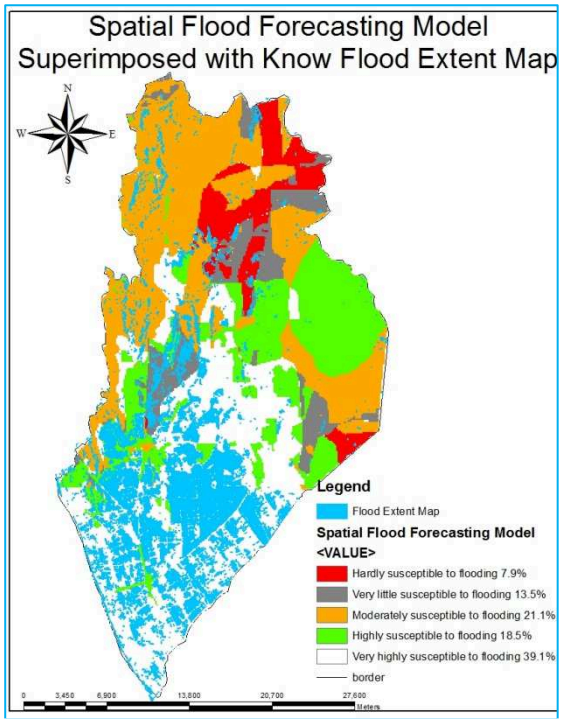


Figure 4: Superimposed of Spatial Flood Forecasting Map and Flood Extent Map

Conclusion

In this study, GIS-based group analytic hierarchy process was successfully applied in simulating the flood susceptible zones for Perlis State. In recent years, GIS proved profound potentials in combating flood catastrophes. The social and economic losses as a result of flood disasters, technologic crises, as well as global epidemics are growing; needing more effective group decision making under uncertainty. In this study, the efficiency of GIS-based GAHP as spatial multi-criteria forecasting tool was discovered. Hence, this system will help civil authorities such as planners and emergency agency in taking positive and in-time steps during the pre-disaster situations. It will similarly help them during post-disaster activities to assess damages and losses caused as a result of flood.

References

[1] D. M. Necsoiu, *A Data Fusion Framework for Floodplain Analysis using GIS and Remotely Sensed Data.* 2000.

[2] J. Cosgrave, "Decision making in emergencies," *Disaster Prev. Manage.,* vol. 5, pp. 28-35, 1996.

[3] J. K. Levy and K. Taji, "Group decision support for hazards planning and emergency management: A Group Analytic Network Process (GANP) approach," *Math. Comput. Model.,* vol. 46, pp. 906-917, 2007.

[4] N. R. F. Maier, *Problem-Solving Discussions and Conferences: Leadership Methods and Skills.* McGraw-Hill New York, 1963.

[5] T. L. Saaty , "The Analytic Hierarchy Process: Planning, Priority Setting, Resource Allocation. McGraw-Hill, New York." 1980.

[6] T. L. Saaty, *Fundamentals of Decision Making and Priority Theory with the Analytic Hierarchy Process.* RWS publications Pittsburgh, 1994.

[7] T. L. Saaty and G. Hu, "Ranking by eigenvector versus other methods in the analytic hierarchy process," *Applied Mathematics Letters,* vol. 11, pp. 121-125, 1998.

[8] E. W. L. Cheng and H. Li, "Analytic hierarchy process: an approach to determine measures for business performance," *Measuring Business Excellence,* vol. 5, pp. 30-37, 2001.
[9] G. Coyle, "The Analytic Hierarchy Process, Practical Strategy. Open Access Material, AHP," 2004.
[10] M. Modarres, S. Sadi-Nezhad and F. Arabi, "Fuzzy analytical hierarchy process using preference ratio: A case study for selecting management short course in a business school," *International Journal of Industrial Engineering Computations,* vol. 1, pp. 173-184, 2010.
[11] D. C Chen,., P. C Chen,., Y. C Lee,., S. U You,. and H. C Jao,., "Using an analytic hierarchy process to develop competencies on mould product creativity for vocational college students. *World Transactions on Engineering and Technology Education* (WIETE) ," vol. 9, pp. 54-59, 2011.
[12] D Emmanouloudis, D Myronidis, K Ioannou, "Assessment of flood risk in Thasos Islandwith the combined use of multicriteria analysis AHP and Geographical Information System.Innovative Applications of Informatics in Agriculture and Environment ," vol. 2, pp. 103-115 ESRI, 2008.
[13] R Sinha, G Bapalu, L Singh, B Rath, "Flood risk analysis in the Kosi river basin, northBihar using multi-parametric approach of analytical hierarchy process (AHP). Journal of IndianSociety of Remote Sensing," vol. 36, pp. 335-349, 2008.
[14] V Meyer, S Scheuer, D Haase, "A multicriteria approach for flood risk mapping exemplifiedat the Mulde river, Germany. Natural Hazards ," vol. 48, pp. 17-39, 2009.
[15] F.C Dai,., C.F Lee,., X.H Zhang,., "Assessment of landslide susceptibility on the natural terrain of Lantau Island, Hong Kong. Environmental Geology ," vol. 61, pp. 257-271, 2001b.
[16] B. Pradhan, "Flood susceptible mapping and risk area delineation using logistic regression, GIS and remote sensing," *Journal of Spatial Hydrology,* vol. 9, 2010.
[17] S. Yahaya, N. Ahmad and R. Abdalla, "Multicriteria analysis for flood vulnerable areas in Hadejia-Jama'are River basin, Nigeria," *European Journal of Scientific Research,* vol. 42, pp. 71-83, 2010.
[18] J. R. Eastman, "Multi-criteria Evaluation and Geographical Information Systems Eds. Longley PA, Goodchild MF, Magurie DJ and Rhind DW, Second ed. John Wiley and sons, New York," vol. 1, pp. 493-502., 1996.
[19] R. R. Navalgund, "Revised Development plan of Ahmedabad Urban Development Authority Area – 2011. Ahmedabad Urban Development Authority and Space applications Centre, Ahmedabad, India, Technical, Report 1 SAC/RSAG/TR/12/AUG/1997," pp. 142, 1997.
[20] J. Malczewski , " GIS and Multicriteria decision analysis. John Wiley and Sons, Inc. United States of America, ," pp. pp. 177-192., 1999.
[21] S. Drobne and A. Lisec, "Multi-attribute decision analysis in GIS: weighted linear combination and ordered weighted averaging," *Nature,* vol. 4, pp. 28, 2009.
[22] H. Simon, "The new science of management decisionPrentice-Hall," *Englewood Cliffs, NJ,* 1977.

Applied Mechanics and Materials Vol. 567 (2014) pp 724-729
© (2014) Trans Tech Publications, Switzerland
doi:10.4028/www.scientific.net/AMM.567.724

Generation, propagation, run-up and impact of landslide triggered tsunami: a literature review

Indra Sati H. Harahap[1, a] and Vo Nguyen Phu Huan[1,b]

[1]Civil Department, Universiti Teknologi Petronas, Perak, Malaysia

[a]indrasati@petronas.com.my, [b]phuhuan129@yahoo.com

Keywords: Tsunami, landslide, propagation, run-up, impact

Abstract. Submarine landslide is the most serious threat on both local and regional scales. Tsunami phenomenon induced by submarine slide has put us on the challenge in understanding from generation mechanism to propagation and coastal inundation and mitigating the risk from it. Submarine slides can trigger tsunamis with high run-up affecting offshore structures, subsea facilities and human lives along the shoreline. Unfortunately, there are no effective numerical models that could simulate simultaneously all stages of generation, propagation and run-up of tsunamis phenomena. This paper presents a comprehensive review on the landslide tsunami phenomenon.

Introduction

Geohazards represent a world-wide concern in deep water and have potentiality in leading to damage or uncontrolled risk. They are always associated with geological or geotechnical features and processes in the vicinity of a planned offshore structure. Important offshore geohazards include i) slope instability (consisting of submarine slides, debris-flows, turbidity currents); ii) pore pressure phenomena (e.g. shallow gas accumulations, gas hydrates, surface erosion by shallow water flows, mud volcanism) and iii) seismicity. Geohazards need to be carefully evaluated before field development can start, as they present threat to human life, environment, seabed installation and drilling operation. Figure 1 illustrates schematically different geohazards. However, the geohazard natures and their impact are not well known.

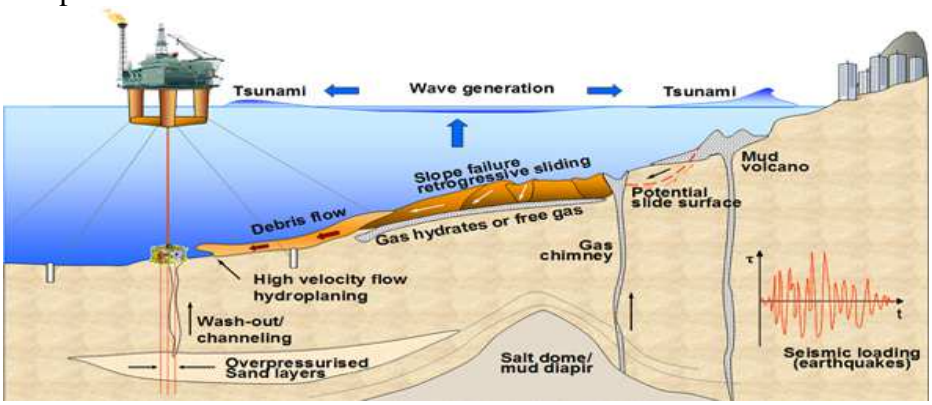


Figure1: Schematic diagram of different geohazards [1]

The submarine landslide is now accepted as an important source of tsunami wave generation. It is the second in frequent tsunami source for about 10% of all tsunami waves [1].

Submarine mass failure (SMF) or submarine landslide is the most serious threat on both local and regional scales. In addition to damaging directly offshore installations, slope failures may also cause devastating tsunami. Thus, tsunamis become a serious natural hazard for the environment and populations in exposed areas.

Tsunami waves due to submarine slide are sophisticated phenomena that may be divided into three parts: i) triggering mechanism, ii) tsunami generation, iii) propagation and run-up at the beach or offshore structure.

Literature review

a) Initiation of tsunami wave by submarine landslide

Only part of all submarine landslides cause of generating tsunamis [2]. There have many papers that deal with the efficiency of submarine landslides to cause tsunami waves.
Murty cites basic physics to scrutinize the validity of hydrodynamic simulations as applied to landslide tsunamis [3]. He assumes that tsunami generation from submarine landslides depends on some factors including: the weight of the slide material, density and speed of the slide material, duration of the slide, angle of the slide, water depth, etc.
Ruff compares energy of generating tsunami by earthquakes with submarine landslides by experiment [4]. He concludes that large tsunami wave can be generated by some submarine landslide.
Okak and Synolakis [5] present a simpler physical model than Ruff [4]. They used two source mechanisms: seismic dislocation and underwater slumps. They assess amplitude of energy generated into a tsunami wave using two source above. They concludes that both source can generate tsunamis of energy.

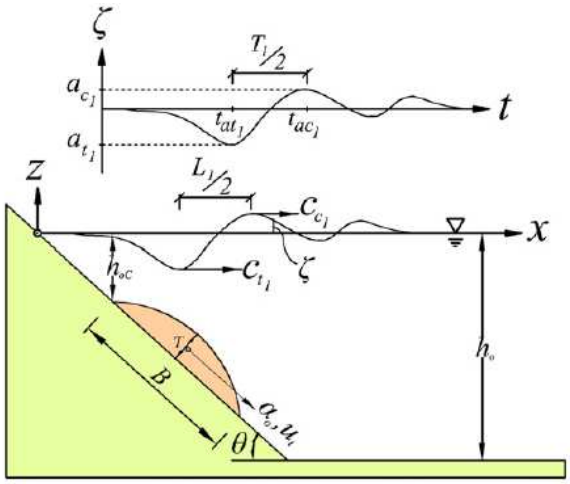


Figure 2: General feature of tsunami generation by solid block motion [6]

S. T. Grilli and P. Watts introduced the first simple model to emulate a landslide is solid block sliding down a slope [6]. The volume and speed of sliding mass are the main factors to generate tsunami wave. All forms of submarine slides can have the potential to generate tsunami [7].
In addition the application of these models to wave generation is also important. The first application for tsunami wave simulation was based on conventional nonlinear shallow water (NSW) wave equations due to its simplicity. But it is known that the NSW equations do not correctly capture the interaction between slides and wave generation [8]. P. J. Lynett, J. C. Borrero have derived and used a fully nonlinear BM rather than an NSW model to simulate SMF tsunami generation [9].

b) Propagation of tsunami wave

Generated tsunami by submarine landslide are basically linear and have long waves. The amplitude of the soil motion does not effect to linear waves. And we have the formula to describe concern between wave speed and wave length.

$$C = \sqrt{gH} \tag{5}$$

Where g is the acceleration of gravity, and H is the local water depth.

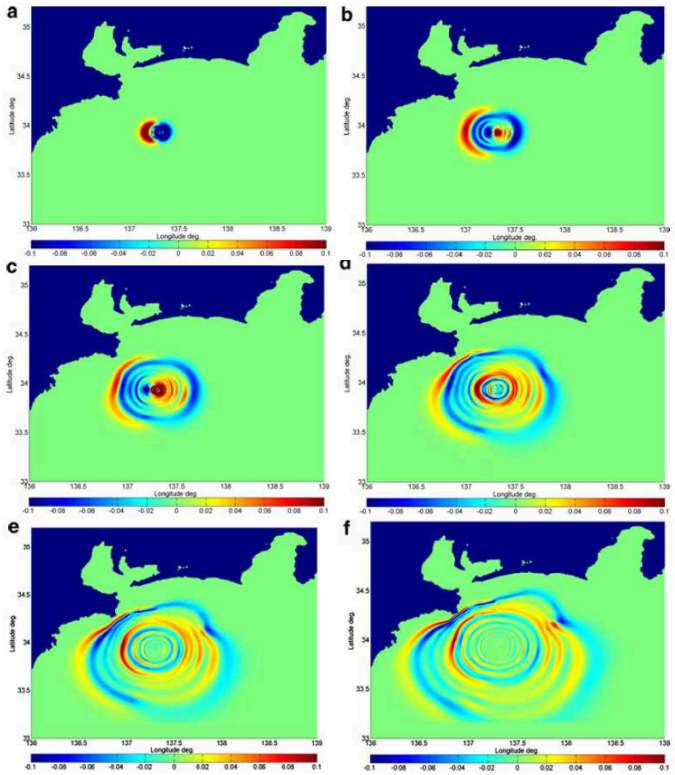


Figure 3: Simulated water surface elevation [9]

Nature of tsunami waves can be characterized as nonlinearity effects and frequency dispersion which causes shorter waves to propagate at a slower speed and thus causes an initial packet of waves to disperse as it propagates. Regarding this, the Boussinesq-type models (BM) are more efficient and accuracy than models developed based on Nonlinear Shallow Water (NSW) equations which can lead to errors in the wave shape and arrival time [10]. The BM relaxes the restriction on nonlinearity of NSW and originally includes the effect of frequency dispersion.

Clearly, the inclusion of the dispersive effects is important for the determination of the time history of the wave motion at a point. The wave profiles are in good agreement with experiment. The BM model has shown a significant improvement over previous simulation made with an earlier tsunami source and shallow water wave tsunami propagation models by reproducing correctly times of tsunami arrival relative to strong after shock that occurred roughly 20min after the main shock [10]. Reynolds averaged Navier-Stokes (RANS) equations with the k - ε turbulence model could provide capacity and accuracy in predicting the breaking of wave in generation and propagation [11].

c) Run up of tsunami wave

The modeling of tsunami flows at most types of shorelines remains a difficult but important problem. For coastal communities within the wave run-up region, the tsunami flows around, through, and over buildings. This turbulent, fast-moving flow results in building damage, collapse, or floating away. People are drowned, due to the high water, the difficulty of withstanding the fluid forces, coping with the large turbulent eddies, or impact with debris. In order to simulate the inundation on shoreline by a tsunami, a numerical model must be capable of allowing the shoreline to move in time. However, the accurate prediction of run-up onto real coastlines with structures and human habitation still remains incomplete. Especially, tsunami wave were generated by submarine landslide; they have long wave and large run-up heights [12]. Pedersen generalized from the progress of wave run-up modeling into two directions: one is the integration of run-up facilities in general wave propagation models with high order inherent dispersion and another is the involvement of the representation of accurate shoreline in models.

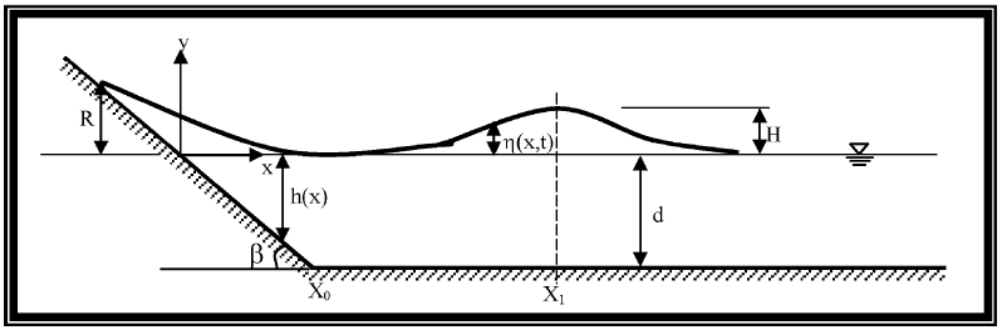


Fig. 3 Solitary wave run-up [12]

The NSW and BM models can provide good prediction with laboratory results of run-up height and inundation over coastal terrain. Figure 3 shows the run-up of a tsunami, represented by a solitary wave, on uniform slope [13]. The principal limitation to their accuracy in predicting shoreline inundation in tsunami applications stems from factors not covered by the basic theory: frequency dispersion and the interaction with fixed obstacles and the interaction the mass of transported debris resulting from destruction of structures. In addition, it is clear that, for the case of breaking tsunami wave, the Boussinesq's model is superior to NSW due to the exclusion of accumulation of dispersion effects in the NSW model [13]. However, this more advanced method has been unable to capture fully flow of tsunami when it breaks onto a beach, and very computationally expensive. RANS model [14,15] was proposed to predict breaking wave in deep and shallow water, including wave pre-breaking, overturning and post-breaking processes. However, this more advanced method has been unable to capture fully flow of tsunami when it breaks onto a beach, and very computationally expensive.

Table 2: Summary of governing equation

	Navier Stoke equation	**NSW model**	**BM model**	**RANS model**
Propagation Stage	- Simplicity	-	- Taking into account the nonlinearity & frequency dispersion. - Reproducing correctly arrival time	- Predicting well the breaking wave
	-	-	-	-
Run-up Stage	-	- Predicting well run-up height on a uniform slope	- Predicting well run-up height on a uniform slope	- Treating well the breaking wave and interaction with structures
	- Leading errors in wave shape and arrival time	- Excluding the frequency dispersion and nonlinearity	- Inaccurately predict the full structure of flow	- Very computationally expensive
All stages	NOT GOOD -	NOT GOOD -	GOOD ✓	GOOD ✓

d) Impact of tsunami wave

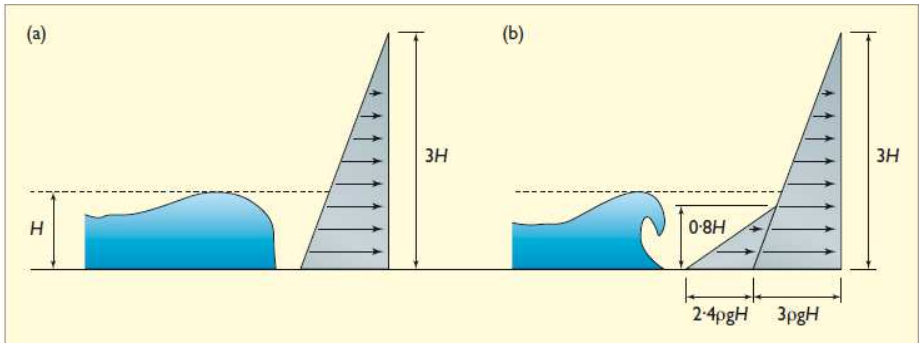


Figure 4: The Japanese design method assumes tsunami wave pressure [16]

Okada et al. proposed a Japanese design method for tsunami loading on structures [17]. Figure 4 (a) showed that the impact force is equivalent hydrostatic load. The pressure distribution will be truncated at the height of the building if the height of the building is less than 3H.

There have three type of tsunami impact force: i) Overflow; ii) Bore; iii) Breaking. The power of the tsunami is greatly different depending on the place and the condition [18]. But type 3: breaking is the type of tsunami that causes the most serious damage. Figure 5 shows the impulsive bore force in type 3 is so higher than two remain type.

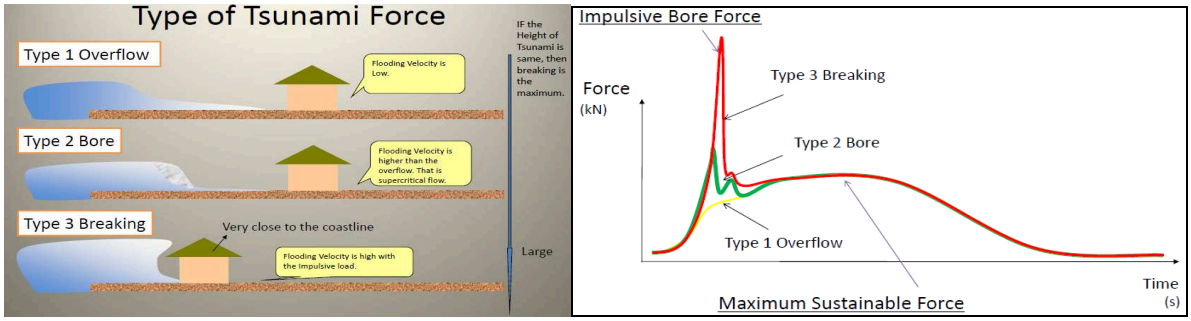


Figure 5: Type of tsunami force [18]

There is very little guidance provided by structural design codes for the forces induced by tsunami effects on coastal construction. A set of generalized equations were created from currently available building codes and published literatures, which contain information and recommended equations on flooding, breaking waves and tsunamis (Pacheco and Robertson, 2005). The existing design codes investigated are the City and County of Honolulu Building Code (CCH 2000); the 1997 Uniform Building Code (UBC 1997), the 2003 International Building Code (IBC 2003); the SEI/ASCE 7-02 (ASCE 7, 2002); and the Federal Emergency Management Agency Coastal Construction Manual (FEMA 2000).

Conclusion

Now, physical understanding of slide tsunami hazards is poor. How to understand substance of tsunami clearly and how to find methods to reduce damage from tsunami wave. This is not simple task because of the complexity and multi scale of process.

Understanding tsunami wave loading on coastal houses is important to improve the design of coastal structures. It is very dangerous with these structures close to coastline because they may be damaged by tsunami force.

Therefore, the need for comprehensive model base on mesh free method that could cover all aspects of tsunami phenomena and provide real-time modeling of the event would be one of good future research direction.

References

[1] V. K Gusiakov, Tsunami history: recorded in The Sea, Harvard University Press, Cambridge, 15 (2009) 23–54.

[2] P. Watt, Tsunami features of solid block underwater landslide, Journal of Waterway, Port, Coastal and Ocean Engineering (2000).

[3] T.S. Murty, Tsunami wave height dependence on landslide volume, Pure and Applied Geophysics 160 (2003) 1-7.

[4] L. J. Ruff, Some Aspects of Energy Balance and Tsunami Generation by Earthquakes and Landslides, Pure Appl. Geophys. 160 (2003) 2155–2176.

[5] E. A. Okal, C. E. Synolakis, Theoretical Comparison of Tsunamis from Dislocations and Landslides, Pure Appl. Geophys. 160 (2003) 2177–2188.

[6] S. T. Grilli and P. Watts, Modeling of waves generated by a moving submerged body: Applications to underwater landslides, Engrg. Analysis with Boundary Elements (1999) 645-656.

[7] D. R Tappin, Digital elevation models in the marine domain: investigating the offshore tsunami hazard from submarine landslide, Geol. Soc. London (2010) 81-101.

[8] D.R. Tappin, Submarine Mass Failures as tsunami sources – their climate control, Phil. Trans. R. Soc. A 368 (2010) 2417–2434.

[9] P. J. Lynett and P. L.-F. Liu, A numerical study of submarine-landslide-generated waves and run-up, Proc. R. Soc. Lond. A 458, vol. 458 (2002) 2885-2910.

[10] P. J. Lynett, J. C. Borrero, P. L.-F. Liu, and C. E. Synolakis, Field Survey and NumericalSimulations: A Review of the 1998 Papua New Guinea Tsunami, Pure Appl. Geophys, vol. 160 (2003) 2119-2146.

[11] D. Yuk, S. C. Yim, and P. L.-F. Liu, Numerical modeling of submarine mass-movement generated waves using RANS model, Computers & Geosciences, vol. 32, no. 7 (2006) 927-935.

[12] E. A. Okal and C. E. Synolakis, Source discriminants for near-field tsunamis, Geophys. J. Int., 158 (2004) 899 – 912.

[13] S. T. Grilli, M. Ioualalen, J. Asavanant, F. Shi, J. T. Kirby, and P. Watts, Source constraintsand model simulation of the December26, 2004 Indian Ocean Tsunami, Journal of Waterway, Port, Ocean and Coastal Engineering, vol. 133, no. 6 (2007) 414-428.

[14] D. Yuk, S. C. Yim, and P. L.-F. Liu, Numerical modeling of submarine mass-movement generated waves using RANS model, Computers & Geosciences, vol. 32, no. 7 (2006) 927-935.

[15] T. Capone, A. Panizzo, and J. J. Monaghan, SPH modelling of water waves generated by submarine landslides, Journal of Hydraulic Research, vol. 48, no. 1 (2010) 80-84.

[16] N. I. Thusyanthan, S. P. Gopal, Tsunami wave loading on coastal houses: a model approach, Civil Engineering 16 (2008) 77–86.

[17] T. Okada et al, Tsunami Loads and Structural Design of Tsunami Refuge Buildings, (2005).

[18] T. Arikawa, Tsunami and Damage to Coastal Facilities of the March 11, 2011, Tohoku, Japan Earthquake, 15th World Conference on Earthquake Engineering (2012).

Applied Mechanics and Materials Vol. 567 (2014) pp 730-735
© (2014) Trans Tech Publications, Switzerland
doi:10.4028/www.scientific.net/AMM.567.730

Human Error Causes in Slope Engineering Practices

Sadaf Qasim[1,a], Indra Harahap[1,b] , Syed Baharom[1,c] and Muhammad Imran[1,d]

[1]Universiti Teknologi PETRONAS, Bandar Seri Iskandar, Perak, Malaysia

[a]nuzhaterm@gmail.com,[b]indrasati@petronas.com.my,[c]sybaharom@petronas.com.my,
[d]engrimran_ce@hotmail.com

Keywords: Slope engineering practices; uncertainty; human error; human error causes

Abstract. Landslide/slope failures have been accounted, as the second natural disaster for Malaysia after flood.From the landslides investigations reports, it is shown that landslides in Malaysia were caused mainly by factors like lack of maintenance, less coordination during construction stage and design problem apart from rainfall. The slant of this study facilitated multidisciplinary perceptions regarding human error causes in existing practices to be captured. This approach has the worth to offer the usefulness of progressive actions that are taken to strengthen the slopes. Conducting the surveys with focussed group respondents, could provide benchmarking to gauge any change in influences and resource use as efforts are made to advance the consideration of slope stability in hill site developments.

Introduction

A natural disaster, by its nature is always multifaceted and unpredictable. Landslide is one of the major geo-hazard accompanied by uncertainties that give rise to hundreds of deaths every year. From the landslides investigations reports, it is shown that landslides in Malaysia were caused mainly by failures of the retaining wall and other factors like lack of maintenance, less coordination during construction stage and design problem apart from rainfall [1,2.3,4,5,6,7,8].

Human uncertainty is not new, the calamitous failure of Kwun Lung Lau landslide in Hong Kong is the participation of human uncertainty [9]. Human errors can be abusing of the prescriptive method [6], construction errors like over excavation or wrong side excavation and in case of maintenance errors, broken drainage facilities [10,11,12,13,14] as tabulated in Table. 1. According to Madelsohn [15], 75% of the problems on the construction sites are generated in the design phase. Landslide came into prominence in Malaysia in 1993, when an apartment block near Kuala Lumpur collapsed due to a landslide as shown in Fig.1. In one of the very latest reports of "The Penang Safety Guideline for Hillsite Development 2012" the major causes of slope failures have been accounted. It can be summarized as design, construction maintenance and communication errors [16].

Table 1. Engineering Classification of Human Errors [14]

Human Errors	Description of Human Errors
Design Errors	A. Improper Drainage Facility B. Inappropriate Gradient C. Unread ground water conditions D. Inaccurate soil parameters used
Construction Errors	A. Wrong/Over excavation B. Poor Compaction/Improper Topsoil/Filled material
Maintenance Errors	A. Clogged Drains B. Gulley Formation C. Internal Erosion D. Lateral Movements/Settling of ground

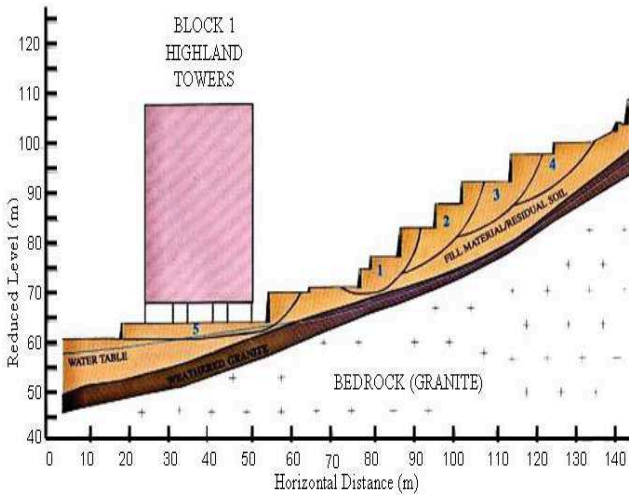


Figure 1. Highland Towers Collapse [6]

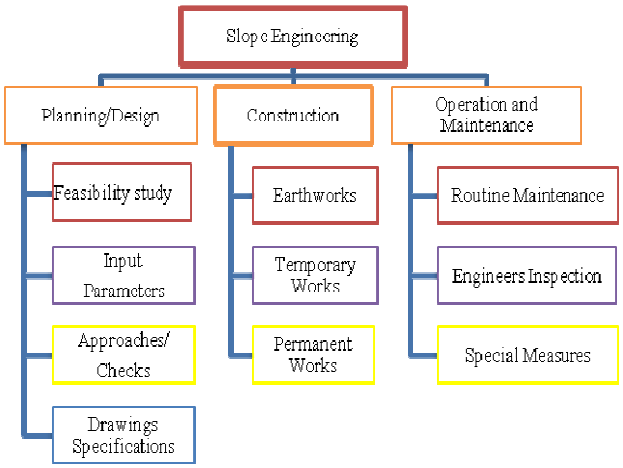


Figure 2. Slope Engineering Tasks

In this paper author has taken three main objectives:

i. To classify the stages which are responsible for slope instability/slope failures.
ii. To identify the human error causes of the identified stages by utilizing absolute probability judgement criteria.
iii. To verify the human error causes in relation with other studies.

Human Error Causes Responsible for Slope Failures

A general survey was conducted in response of literature review findings, a total of 155 Malaysian based civil engineering industry practitioners (including architects, engineers, quantity surveyors, academicians and contractors) were enquired about the factors responsible for slope failures. The survey questions are prepared on the bases of the available literature and the records of slope failure reports prepared by various governmental and nongovernmental agencies involved with slope failure mitigation and management measures. The designed questionnaire, tries to catch up those factors (apart from rainfall) due to which slope failures are increasing. For the choice of respondents, snowball sampling technique is used. The snowball sampling technique is much like asking your subjects to nominate another person with the same trait as your next subject. The researcher then observes the nominated subjects and continues in the same way until the obtaining sufficient number ofsubjects. Snowball sampling technique works like a chain referral. Respondents were encouraged to furnish further causes that they measured imperative, and in reply there was some suggestion related with the individuals virtues (like communication ability and decisive power) and to “practices” were significant as tabulated in Table 2. This paper deliberates on the identification of the human error causes in different stages (from planning until maintenance), but with reference to the interview study as shown in Fig. 2.

Results and Discussion

Regarding different stages involved to confirm slope stability, from planning until maintenance numbers of human error causes (HECs) are governing, and the affect of the governing causes are further used to overcome the chances of slope instabilities or slope failures. Under the category of feasibility study, development plans, planning for drainage facility, site reassessment and counter checking of survey data has been considered. All the subtask items of feasibility study show more or less same HECs. Most of them are reflecting individual’s attitude /organizational trends (namely poor feedback, time constraints, inexperienced, etc.). This is in real the validation of the findings put forwarded by Too and associates [17]. According to Too and associates [17]many of the

problems linked with hillside are due to human errors, in the early phase with the development. This is also propped up by Corrie [18] who found that the reasons of project failures going on during implementation or after completion can often be sketched back to deficiencies in the planning stages. Likewise, Frimpong and associates [19] reported that most of hillside failures can be overcome if located at the initial stage during the development project. Hence, good practice and successful project planning, controlling and monitoring should be fixed early in order to develop project performance. Gue and Wong [10] also admitted and emphasized to cover these flaws through desk study, site reconnaissance and sub surface investigations [10]. All the failures can be avoided, if proper care has been given during planning, sub surface investigation, analyses, design and construction. The need of specialist input is usually neglected due to over confidence. Therefore, many projects suffer due to inexperienced professionals [20]. According to Oakes [21], the benefits of a good project development plans must include earlier identification of risks and issues; adoption of good practice; availability of skills and experience; improved communication; improved ability to allocate resources; improved predictability of project delivery; and greater confidence to take risks.

Table 2. Human Error Causes at Different Stages of Slopes Engineering Practices

Stages	Sub-Stages	Human Error Causes
Planning and Design	Feasibility study Input Parameters Approaches and Checks Technical drawings/specifications	inadequacy of the available data
		Inexperience
		ambiguous/ outdated standards
		Absolute judgement required
		Inaccurate soil parameters
		Deficient thumb rules
		Improper experimental setup
Construction	Earthworks Temporary works Permanent works	Improper sequencing
		Lacking in supervision
		Inexperience
		Over excavation/improper method of excavation
		Inadequate temporary support
		Excessive construction loads
		Material deficiencies
		ambiguous/ outdated standards
Operation and Maintenance	Routine monitoring/maintenance Engineers inspection Special measures	communication power
		No independent check
		Mismatch between perceived and real risk
		Application of unsuitable maintenance criteria
		Following outdated strategies
		Weak decisive power
		Inexperience

In category of "selection of input parameters" the two most important parameters required for analyzing and design cut slopes in residual soils are effective stress strength parameters and ground water table. As Taha and associates reported [22], that information about the shear strength of soil and its behaviour is essential for safe and economic design of geotechnical structures. Gue and Cheah [23] also confirmed that sub surface investigations and laboratory tests are not carried out to determine representative soil parameters, subsoil and ground water profile for analysis and design of slopes. A lack of good understanding of soil behaviour is usually a significant cause to slope failures [23].One of the facts discovered through experts that improper experimental setup has also been observed in many of the projects. According to Tan and Gue [24], selection of appropriate shear strength parameters is very crucial in design of cut slopes. It is significant to admit that stiff

materials like residual soils have discontinuities which the small scale tests may sometimes unable to detect, and over-estimate soil shear strength. On the other hand, if large-sized particles, of the residual soil mass cannot be quantitatively assessed and the small-scale laboratory tests carried out on the matrix material of the residual soils will usually under-estimate the shear strength parameters of the in-situ material mass. Hence special care has to be taken, in the selection of representative soil strength for slope stability analysis [24].

Water management is an essential factor in controlling slope stability. Surface drainage and protection are necessary to reduce infiltration and erosion caused by heavy rainfall especially during monsoon. When designing surface drainage on steep slopes, it is important to make sure that drains have sufficient capacity to take run off. General guidelines for design of permanent drainage are based upon a 100-year return -period of rainfall and temporary drainage is based upon a 10-year return periods [25, 26]. Deep underdrains can be utilized to lower groundwater levels in slopes and intercept seepage before it can reach the slope face. In drainage facility planning and design, the major basic event is non conformance/inadequacy of the available data like groundwater conditions (resulting from 10 years return-period from rainfall or representative groundwater level (through observation and estimation), peak runoff, discharge capacity, etc. This basic event can be assessed easily by keeping in view the findings of Gue and Wong [10]. Irrespective of the expansion pattern, because of urbanization in the hilly area, imperviousness of the surface increases and this leads to high runoff generation. Safe drainage of such high runoff to the ultimate outlet (river or water bodies in the form of lake) always remains a challenging task [27]. The design discharge must have the provision to adjust the future possible development of the area. Discharge may increase with time primarily due to three factors: 1) increase in building density and paved area, 2) increase in rainfall intensity because of impact climate change, and 3) increase of per capita water utilization because of improved life style and better water supply [27]. Considering these factors, it is advisable to go for an appropriate design of the drainage system, so that the system remains sufficient to meet the increasing future demand at least for the next 50 years [27].The construction of the structures such as soil nailing, contiguous bored piles and retaining walls needs full expertise.As pouring of concrete/spraying of concrete, twisting and placing of steel as the structures requires proper sequence and experienced supervision in the tasks. It is also supported by the investigation results indicated that the collapsed of the segmental retaining wall wasmainly due to the internal instability. Due to the space constraints and the existing reservoiron top of the slope, the excavation into the toe of the slope was limited. The anchorage lengthfor the segmental retaining wall was also limited resulting insufficient resistance [28]. The bad construction practices can be prevented if proper supervision by design consultants collectively with reliable experienced contractors having clear methods/statements for construction is followed [6]. According to Gue and Tan [2] the personnel supervising hill-site developments must have enough familiarity and experience in geotechnical engineering and geology to spot any irregularities that might be dissimilar from those predict and advocate in design [2].

Undoubtedly, in maintenance issues, most of the time abrupt but wise/proper judgements and decisions have to be made by the analyst. Of course in tropical countries like Malaysia where an average rainfall is 2550mm, which is above the global average, drainage is the major concern from every aspect (from planning till maintenance) [10]. Malaysian practice on slope maintenance has always consulted the guidelines published by Hong Kong GEO for both routine maintenance and layman and Engineer's inspection. Detailed recommendations for the necessary maintenance regime are stated in Geoguide 5 (2003). However, such a scheme has only become popular after it has been identified as one of the root causes of landslide incidents. These are damaged/clogged drains, inadequate surface erosion control, etc [29]. Landslide cases like Bukit Antarabangsa (2008), Bukit Antarabangsa (1999), and Highland Towers (1993) are the examples of the above mentioned root causes [11, 13, 30, 31]. In concern with slope maintenance factors, it is suggested that awareness alone is not enough, it is the authorities involved must know how to take up the work and must have in hand proper set of standards of good practice for slope maintenance [2].

Conclusion

Through conducting surveys and concerning materials, it is apparent that the causes of slope failures are related to poor and/or flawed design and construction and non-preferential maintenance criteria. It is also pertinent to note that at every related tasks/subtasks involved in slope engineering practices, human errors are observed. The quantification or the significant level of these human errors can be overcome by countering the causes responsible for its generations.This research aims to reduce cases of slope failures and construction collapses due to unintended human errors in structural design and construction in the country. Although it is not so straightforward, but by identifying human error causes, it can be minimized with some extent.

Reerences

[1] Gue, S.S. and T.Y. Chin, Mitigating the Risk of Landslide on Hill -site Development in Malaysia. 2nd World Engineering Congress, Srawak Malaysia, 2002.

[2] Gue, S.S. and Y.C. Tan, Landslides: Cases histories, lessen learned and mitigation measures. Paper presented at the Landslide, sinkhole, structure failure: Myth or science? Ipoh, Malaysia. 2006.

[3] Samah, F.A., Landslide in hillside development in the Hulu Kelang, Klang Valley. presented at the Post-Graduate Seminar Universiti Teknologi Malaysia, 2007.

[4] Jamaluddin, T.A., Human Factors and Slope Failures in Malaysia, . Bulletin of the Geological Society of Malaysia, 2006(52): p. 75-84.

[5] Rasip, M.K., Isu pembangunan di kawasan tanah tinggi dan berbukit (kes kajian: Majlis Perbandaran Ampang Jaya) Universiti Teknologi Malaysia, Johor Bahru. 2006.

[6] Gue, S.S. and Y.C. Tan, Landslides: Abuses of The Prescriptive Method. International Conference on Slope 2006 Kuala Lumpur, 2007.

[7] IEM, .Official statement of Bukit Antarabangsa lanslide accident on 6 December 2008, Jurutera. Selangor, Malaysia: The Institution of Engineers, Malaysia. 2009.

[8] Too, E., N. Adnan, and B. Trigunarsyah. Project Governance in Malaysia Hillside Developments. in Proceedings of the Sixth International Conference on Construction in the 21st Century: Construction Challenges in the New Decade, Kuala Lumpur. 2011. Quensland University of Technology Australia.

[9] Morgenstern, N.R. Managing risk in geotechnical engineering. in $10t_h$ Pan American Conference on Soil Mechanics and Foundation Engineering. 1995.

[10] Gue, S.S. and S.Y. Wong, How to Improve Slope Management and Slope Engineering Practices in Malaysia.www.gnpgeo.com.my, 2008.

[11] JKR, Jabatan Kerja Raya Final Investigation Report Investigation of Slope Failure at Taman Bukit Mewah, Bukit Antarabangsa Hulu Klang Salengor, in Cawangan Kejuruteraan Cerun, Jabatan Kerja Raya Malaysia. 2009.

[12] Raya, J.K., National Slope Master Plan Sectoral Report Research and Development, 2009. Jabatan Kerja Raya Malaysia.

[13] Aun, O.T., Mitigation And Rehabilitation of Natural Disasters In Malaysia. The Ingenieur, 2008. 39.

[14] Qasim, S. and I.S.H. Harahap, Human Error related Risks of Malaysian Landslides, in Geotechnical Engineering For Disaster Mitigation And Rehabilitation And Highway Engineering 2011. 2011. p. 527-533.

[15] Madelsohn, R., The Constructability Review Process: A Contractor's Perspective,". Journal of Management in Engineering ASCE, 1997. 13(3): p. 17-19.

[16] Ahamad, H.Z., Safety Guidelines for Hillsite Development. Penang Town and Country Planning Department, 2012.

[17] Too, E., N. Adnan, and B. Trigunarsyah. Project Governance in Malaysia Hillside Developments. in Sixth International Conference on Construction in the 21st Century (CITC-VI) "Construction Challenges in the New Decade". 2011. Kuala Lumpur, Malaysia.

[18] Corrie, R.K., Project Evaluation. London: Thomas Telford LTD. 1991.

[19] Frimpong, Y., J. Oluwoye, and L. Crawford, Causes of Delay and Cost Overruns in Construction of Groundwater Projects in Developing Countries; Ghana as a case study. . International Journal of Project Management, 2003. 21(5): p. 321-326.

[20] Gue, S.S., S.S. Liew, and Y.C. Tan. Lessons Learned from Some Failures of Housing Projects. in Seminar on Failures Related to Geotechnical Works. 2000. IEM 23-24 October.

[21] Oakes, G., Project Reviews, Assurance and Governance Aldershot, England ; Burlington, VT: Gower, 2008.

[22] Taha, M.R., et al., Geotechnical behaviour of a Malaysian residual granite soil. Pertanika Journal of Science & Technology, 1999. 7(2): p. 151-169.

[23] Gue, S.S. and S.W. Cheah, Geotechnical Challenges in Slope Engineering of Infrastructures. International Conference on Infrastructure Development, Putrajaya 2008.

[24] Chin, T.Y. and G.S. Sew, The Determination of Shear Strength in Residual Soils for Slope Stability Analysis, in Seminar Cerun Kebangsaan. 2001: Cameron Highlands p. 1-18.

[25] Gue, S.S. and Y.C. Tan, Guidelines for development on hill-sites. Tropical Residual Soils Engineering, 2004: p. 121.

[26] Mohamad, A.b., et al., Guidelines for Slope Design. Slope Engineering Branch, Jabatan Kerja Raya MALAYSIA, 2010.

[27] Sarma, A.K., Planning and Design of Drainage in Hilly Area: A Conceptual Guideline Integrated Landuse Planning and Water Resources Management (ILPWRM), 2012: p. 1-27.

[28] Siong, L.C. and T.S. Meng. Collapse 0f A Reinforced Soil Segmental Retaining Wall. in IEM-GSM Oktoberforum2005: "Case Histories in Engineering Geology and Geotechnical Engineering". 2005. Petaling Jaya.

[29] Gue, S.S. and S.Y. Wong, Slope Engineering Design and Construction Practice in Malaysia. CIE-IEM Joint Seminar on Geotechnical Engineering, Yilan, Taiwan, 2009.

[30] Jaapar, A.R.B., A framework of a national slope safety system for Malaysia. 2006, University of Hong Kong.

[31] Aiun, O.T. and O.H. Miin, Geotechnical Failures/Issues,Dispute Resolution and Mitigation. The Journal of the Institute of Engineers Malaysia, 2010. 71(1).

Applied Mechanics and Materials Vol. 567 (2014) pp 736-741
© (2014) Trans Tech Publications, Switzerland
doi:10.4028/www.scientific.net/AMM.567.736

Measuring Driver's Percent-Time-Spent-Following Using a Moving Video Recording Technique

Muttaka Na'iya Ibrahim[1,a] and Othman Che Puan[2,b]

[1,2]Faculty of Civil Engineering, Universiti Teknologi Malaysia, 81310, Skudai, Johor, Malaysia

[a]email: mnibrahim3@live.utm.my
[b]email: othmancp@utm.my (Corresponding author)

Keywords: Two-lane highways, Video recording technique, Test vehicle, Following time, PTSF

Abstract

The percent time spent following (PTSF) or proportion of following time (PFT) relative to total travel time taken by vehicles to traverse a particular segment of two-lane highways has been used as key performance index for evaluating the level-of-service of the road. From the context of travel time, this implies that PTSF is a space related indicator and thus supposed to be measured over a road segment. However, this indicator is measured in the field based on specific point observation; as equivalent to the percent of vehicles traveling with time headways shorter than 3 s. The accuracy of PTSF estimates based on this approach has been questioned and criticized by many; as spot measured values may not to be real representative of segment estimates. This paper presents an exploration into the application of moving video recording technique for PTSF measurement. PTSF was estimated based on test vehicle following time on two-lane highways using moving car observer method as an alternative approach for field measurement of the indicator along road segment as opposed the existing practice of spot measurement and assumed representative of long segment. Findings from this work demonstrate that the approach used in this study is promising for field measurement of PTSF; as estimates obtained relate well with the major vehicle's following cause factors.

Introduction

Vehicles following time (FT) on two-lane highways is the average amount of travel time spent by fast moving vehicles behind slow moving ones due to inability to pass. The proportion of vehicles following time in relation to the total travel time taken to traverse a road segment (in percent) is an essential phenomenon on two-lane highways that has considerable implications on the overall traffic operations. Particularly, the level of service (LOS) of two-lane highways is evaluated based on the *proportion of time spent in following* and is estimated using a surrogate measure; the percent-time-spent-following (PTSF) as the spot proportion of vehicles traveling with headways less than 3 s [1].

Time headway has been the key variable used for field estimation of PTSF; of which the percent of vehicles passing a specific point with headways shorter than 3 s out of the total number of observed vehicles is regarded as the average percent of travel time spent in following or PTSF. This implies that PTSF is a space related and not point specific measure. Thus, the use of the spot observation criterion and assumed applicable for road segment could be misleading. For the fact that the indicator is segment related, its measurement ought to have been based on space observation and not specific point. A few previous studies [2-8] utilized the spot approach for field measurement of PTSF, comparison between 3 s surrogate measure and analytical methods, and development of performance evaluation models for two-lane highways. It is doubtful that the spot observed values be real representative of segment estimates; especially, for conditions where operational performance and geometry vary along the road. Similarly, the percent of traffic with headways less than 3 s at a particular point could be the same for two different traffic streams and thus increases worry over the accuracy of the surrogate measure [9].

On the basis of the ambiguity associated with the accuracy of estimating time spent in following on two-lane roads based on spot observation coupled with the fact that PTSF is a space related

measure (and not specific point based), it is indeed desirable to develop other techniques for field measurement of PTSF based on segment observation. This could produce results based on actual time spent in following as opposed the current practice of spot measurement and assumed as representative of road section estimates.

This paper presents an exploration into the application of moving video recording technique for PTSF measurement on two-lane highways based on test vehicle following time using moving car observer (MCO) method as an alternative approach for field evaluation of the indicator along road segment as opposed the current practice of spot measurement and assumed representative of long segment.

Method

This study was carried out to explore on the application of moving video recording technique using MCO method for measuring drivers' PTSF on two-lane highways based on test vehicle following time as an alternative approach for field evaluation of the measure along road segment. The choice of MCO method for the study is based on the fact that PTSF is both space and travel time related parameter; as such for it to be measured along road section, the required variables need to be observed within the traffic stream under study. Data for the work were collected on four segments of rural two-lane highways on routes 5 (Pekan Nanas – Pontian road) and 23 (Tangkak – Jementah road) respectively, in Johor, Malaysia.

Data Collection

Data for the study were collected using MCO method in accordance with procedures in the Manual of Transportation Engineering Studies [10] based on floating-car driving technique. In this technique, the driver of the test car drives into the traffic stream under study and overtakes as many vehicles as overtake the test car along the road segment as passing opportunities permit. In this way, the test vehicle approximates the behaviour of an average vehicle in the traffic stream and is generally applied only on two-lane highways [11]. Consequently, the time spent in following by the test vehicle is considered as the average following time or PTSF over the segment evaluated.

A segment length of 3.5 km was used for the data collection by performing six test runs in each traffic direction which was demonstrated as adequate for reliable and unbiased estimates of travel times and traffic volumes [12]. A passenger car was used as the test vehicle; also referred to as *test car* in this study. The test car was equipped with a Video Velocity Box (VBox). VBox is an on-board data acquisition system used for real time event recording which comprised of video recorder, GPS data-logger, camera, and a memory card. To collect the required information, the VBox is connected to the test car and powered by cigar plug. On connecting the VBox to the test car, the system detects and records the speed of the car at every moment; either at stationary or moving state. The camera attached to the system and fixed on the test car's front windscreen records the traffic event of the road under study. The system automatically stores the recorded traffic events onto the memory card inserted into the VBox and later uploaded for processing.

The video records of the traffic events were later uploaded and played back in a computer to extract the required information. During the playback of the video records, speed of the test car at any point along the road segment is displayed on the computer screen. A typical video scene during the playback is shown in Fig. 1. Also, from the video records, travel times and hourly traffic volumes (using appropriate relationships) for each direction were determined. Likewise, the test car following times for each run were estimated from the video display based on the time spent by the test car behind its immediate lead vehicle. Subsequent sections described the details of the procedures. Included are, criterion used for defining the test vehicle as a follower, determination of spacing, time headway, following time as well as the proportion of following time (PFT).

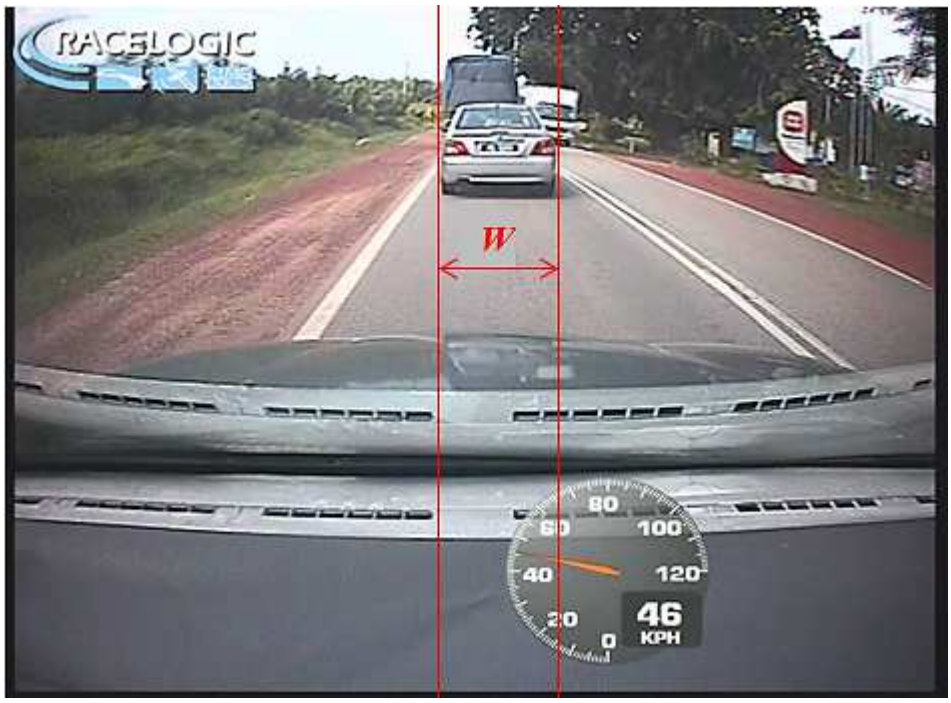


Figure 1. Typical Video Scene during Playback

Criteria for Defining Test Vehicle as a Follower

The 3 s headway criterion based on space measurement was used to define the test car as either a follower or a leader. At any particular time, the test car is only considered in following condition if its time headway relative to its immediate lead vehicle is shorter than 3 s, otherwise, it is a leader (or free moving).

Determination of Headway between Test Car and Lead Vehicle

The headway between the test car and its immediate lead vehicle while moving in the traffic stream was estimated as the ratio of the distance headway (spacing) between the two vehicles and speed of the test car. The speed of the test car at any moment is usually obtained from the video scene in the course of playback. To estimate the spacing between the vehicles, the camera used for the traffic events recording was calibrated prior to the data collection. The calibration was aimed at developing a relationship between the actual spacing (between the test car and lead vehicle) and rear width of lead vehicle at various spacings.

The calibration was carried out using two vehicles; one as test car and the other as lead vehicle. Four (4) classes of vehicles were used as the lead vehicles respectively in accordance with classification in the Malaysian Highway Capacity Manual [5] in order cover the various categories of vehicles expected to be encountered in the field. The test car equipped with VBox for continuous events recording was stationed at one point while the lead vehicle positioned ahead of it at an initial spacing of 7.5 m rear to rear; and then varied in increment of 5 m. All events were recorded into the VBox after which video record was uploaded and played back in computer for data extraction. During the playback, the rear width of the lead vehicle, W (mm), was measured for each position and recorded against the actual ground spacing, L (m) between the vehicles. From pairs of recorded variables, a relationship was developed for estimating spacing from the video display based on the rear width of lead vehicle.

Results and Discussions

Calibration Models for Estimating Spacing and Time Headway

Table 1 presents the relationships developed between spacing (L) and rear width of lead vehicle (W) for the four classes of vehicles considered.

Table 1. Calibration Models for Estimating Spacing between Test Car and Lead Vehicle

Vehicles Classes	Models	R^2
Class 1: Cars/Small Vans	$L = 237.71W^{-0.920}$	0.9994
Class 2: Lorries (with 2 axles)/Large Vans	$L = 326.80W^{-0.923}$	0.9998
Class 3: Large Lorries/Trailers (≥ 3 axles)	$L = 365.01W^{-0.920}$	0.9996
Class 4: Buses	$L = 358.42W^{-0.919}$	0.9997

From the relationships in Table 1, for any measured value of *W* for a particular class of lead vehicle, a corresponding value of *L* is estimated. The time headway is then estimated as the ratio between *L* and the speed of the test car corresponding to the measured *W*. The estimated headway is then checked against 3 s; if it is less than the 3 s, time spent behind the lead vehicle at that headway is recorded and then taken as the *following time* until the displayed speed value changes. When the displayed speed of the test car changes; the width of the lead vehicle is measured again to estimate the corresponding spacing and headway. From the results of the calibrated models, there exists a strong correlation between the variables used in developing the models. This is evidently confirmed by the high values of the coefficient of correlation (R^2).

Determination of Following Time

As mentioned in the preceding section, the following time is considered as the travel time spent by the test car behind the lead vehicle at headways shorter than 3 s. Therefore, the proportion (percent) of the test vehicle following time (PFT) is determined as the ratio between the travel time spent behind the lead vehicle at headways less than 3 s and the total travel taken to traverse the road section. On the basis of floating-car driving technique, the PFT of the test car represents the PTSF for the segment evaluated, as estimates based on this approach is considered an approximate for the traffic stream [12]. In a simple relationship, the percent of test vehicle following time or PTSF can be expressed as in Eq. 1.

$$PFT = PTSF = 100\frac{\sum_{i=1}^{n} t_i}{T}. \qquad \text{(Equation 1.)}$$

t_i = individual test car following time at headways shorter than 3 s (minutes)
T = total travel time taken to traverse the segment under study (minutes)

Using Eq. 1, the proportion of the following times over the studied segments were determined as presented in Table 2.

Table 2. Values of Proportion of Following Time for the Roads Studied

Routes No.	Segment No.	Test No.	T [mins]	FT [mins]	PFT [%]	q [pcu/h]	PHV [%]	q_o [pcu/h]
5	1	1	2.95	1.75	59.32	586	19.41	554
		2	2.98	1.88	63.09	854	7.60	777
	2	1	2.96	1.80	60.81	554	21.80	586
		2	2.72	1.16	42.65	777	9.18	854
23	1	1	3.51	2.39	68.09	212	29.62	192
		2	3.67	3.06	83.34	226	36.13	297
	2	1	3.39	2.72	80.24	238	33.53	283
		2	2.97	1.07	36.03	297	19.89	226

T = Total travel time, FT = Following time, PFT = Proportion of following time, q = flow rate in the analysis direction, PHV = Proportion of heavy vehicles, q_o = Opposing flow rate

The results presented in Table 2 showed the estimated values of PFT based on the proportion of travel time spent in following (at headways less than 3 s). Furthermore, factors considered as the major causes (flow rates in the analysis and opposing directions, and proportion of heavy vehicles in the traffic stream) for vehicles' following on two-lane highways were equally presented. A cross examination of the estimates revealed that in most cases, PFT values increase with increase in the values of variables upon which vehicles' following on two-lane highways depends on. This is more pronounced with respect to increase in the proportion of heavy vehicles in the traffic stream; and is associated with the the fact that heavy vehicles usually travel at much lower speeds relative to those of passenger cars. As such, they cause formation of platoon with a resulting effect of forcing fast moving vehicles to be in following. On comparing the PFT values for route 5 and route 23, it could be seen that in most cases, route 23 recorded more PFT than route 5, even though route 5 experienced higher flow rate. The higher proportion of heavy vehicles on route 23 compared to route 5 was responsible for this. Equally, in terms of road geometry, route 23 has far more percent of no-passing zone than route 5. This also has an increasing effect on vehicles following because it limits overtaking opportunities along segment. The effect of the factors affecting vehicles following time exhibited in this study are well consistent with the findings reported in the existing literature using other approaches.

Conclusions

This study was carried out to explore on the application of moving video recording technique using moving car observer method for field evaluation of test vehicle following time on two-lane highways based on travel time and time spent by the test vehicle behind its immediate lead vehicle at time headway shorter than 3 s over a particular road section. The investigation was aimed at utilizing the technique as an alternative approach for field measurement of PTSF along road segment in contrast to the current practice of specific point measurement and deemed applicable for long section. Findings from the study revealed that the approach used demonstrated that PTSF can be measured along road segment based on the proportion of test vehicle following time relative to the total travel time taken by the vehicle to traverse a particular segment of two-lane highway. This is supported by the fact that the proportion of the test vehicle following times estimated for the four segments used in this study relates well with the major factors affecting following time on two-lane highways.

Acknowledgement

The authors would like to express deep appreciations to the Ministry of Higher Education, Malaysia, through Research Management Centre (RMC), Universiti Teknologi Malaysia (UTM) and UTM for providing a research grant (Q.J130000.7801.4L100), opportunity and necessary facilities to support this research work.

References

[1] TRB. Highway Capacity Manual, 5th Ed. 2010: National Research Council, Washington, D.C.

[2] Al-Kaisy, A. and C. Durbin. Estimating Percent Time Spent Following on Two-Lane Highways: Field Evaluation of New Methodologies,, in Presented at the Transportation Research Board 86th Annual Meeting, January 21-25,2007, Transportation Research Board, Washington, D.C.

[3] Dixon, M.P., S.S.K. Sarepali, and K.A. Young. Field Evaluation of Highway Capacity Manual 2000 Analysis Procedures for Two-Lane Highways. Transportation Research Record: Transportation Research Board, National Research Council, Washington, D.C., 2002. 1802(2002): p. 125-132.

[4] Luttinen, R.T. Capacity and Level of Service on Finnish Two-Lane Highways, in Helsinki 2001, Finnish Road Administration, Traffic and Road Engineering, Finnra Reports 18/20012001: Helsinki, Finland.

[5] HPU. Malaysian Highway Capacity Manual 2011: Highway Planning Unit, Ministry of Works, Malaysia.

[6] Polus, A. and M. Cohen. Theoretical and Empirical Relationships for the Quality of Flow and for a New Level of Service on Two-Lane Highways. Journal of Transportation Engineering, ASCE, 2009. 135(6): p. 380-385.

[7] Polus, A. and M. Cohen. Estimating percent-time-spent-following on two-lane rural highways. Transportation Research Part C: Emerging Technologies, 2011. 19(6): p. 1319-1325.

[8] Van As, C. and A. Van Niekerk. South African Highway Capacity Research, in TRB Workshop 153,2007, South African National Roads Agency, Limited.

[9] Al-Kaisy, A. and C. Durbin. Evaluating new methodologies for estimating performance on two-lane highways. Canadian Journal of Civil Engineering, NRC Research Press, 2008. 35(8): p. 777-785.

[10] Robbertson, H.D. and D.J. Findley. Manual of Transportation Engineering Studies. 2nd ed. 2010: Institute of Transportation Engineers.

[11] Roger, P.R., S.P. Elena, and R.S. William. Traffic Engineering, 3rd Ed.2004, New Jersey: Pearson Prentice Hall.

[12] Mortimer, W. Moving Vehicle Method for Estimating Traffic Volumes and Speeds. Highway Research Board Bulletin 156, Highway Research Board, Washington DC, 1957.

Applied Mechanics and Materials Vol. 567 (2014) pp 742-748
© (2014) Trans Tech Publications, Switzerland
doi:10.4028/www.scientific.net/AMM.567.742

Modeling Pedestrian Behavior in Rail Transit Terminal

Zanariah Abd Rahman[1,a] ,Masria Mustafa[2,b] ,Yasmin Ashaari[3,c] and Ahmad Farhan Mohd Sadullah[4,d]

[1]Post Graduate Student, Faculty of Civil Engineering, Universiti Teknologi MARA, 40450 Shah Alam, Selangor, MALAYSIA

[2,3]Lecturer, Faculty of Civil Engineering, Universiti Teknologi MARA, 40450 Shah Alam, Selangor, MALAYSIA

[4]Lecturer, School of Civil Engineering, Universiti Sains Malaysia, 14300 Nibong Tebal, Pulau Pinang, MALAYSIA

[a]zanariah@salam.uitm.edu.my, [b]masria@salam.uitm.edu.my, [c]yasmin8766@salam.uitm.edu.my, [d]cefrhn@eng.usm.my

Keywords: Pedestrians Flow, Route Choice, Social Force Model, Rail Transit, Microscopic Simulation.

Abstract. This paper concerns a review of the existing research in pedestrian behavior in rail transit terminal. A comprehensive review of the existing method and model are looking at the parameters of the pedestrian behavior and flow in relation to the pedestrian interaction and evacuation planning in rail transit terminal. It is shown in the review that a lack of an overall and detailed consideration of pedestrian behavior studies along the area of rail transit terminal in Malaysia. The necessity to integrate transportation engineering and pedestrian model is important where it will be a start to an upcoming research related to a development of safety management system of pedestrian in term of evacuation strategies and performances in rail transit. This can be a reference point for the traffic engineer to design walking infrastructures for many other public transit areas in Malaysia.

Introduction

Up until the mid-1900s, pedestrian behavior was practically overlooked in the transportation and planning literatures and therefore this topic had become suddenly popular where many papers related to pedestrian behavior had been published [1]. It is vital to embark into the knowledge of pedestrian flow for more efficient planning and safer design in accordance to the observation of the pedestrian behavior rather than relying on the rules that set to accommodate people's travel and lifestyle [2]. Rail transit terminal has the advantage of low pollution, high speed and easy traffic, low energy consumption and comfort. That is why there will be more projects involving rail transportation that has been constructed, planned and will be constructed in the near future. There has been considerable progress over the topic of pedestrian movement analysis and their behavior. This topic has attracted more interest mainly due to the increasing technology and development of new simulation models. In order for sustainability development that meets the needs of the present without compromising the ability of future generations to meet their own needs, pedestrian simulation software can contribute to this aim in the field of building design and engineering [3]. With the use of pedestrian simulation technology, the problems that related with pedestrian comfort and safety can be identified and discussed by engineers or other concerned party and solution of the problem can be determined.

Theories on pedestrian flow are referred to several fields such as walking behavior, route choice, boarding and alighting or interaction between public transport vehicle and walking as and access mode and also activity behavior for example decision making and waiting [4]. The increasing number of pedestrians in the infrastructures creates problems of interaction. The pedestrians are influence by each other in their walking behavior either with mutual or reciprocal

action. They need to avoid or overtake each other in order to maintain the speed but it is hard to do especially in narrow lane or bottleneck area [5]. Other than that, emergency doors also can be one of the elements of bottlenecks in the evacuation process of the pedestrian where when assessing a pedestrian model, this should be accurately predict the behavior of pedestrians around emergency doors. [6]. Modeling a wide range of walking behaviors is not simple and some model developed from discrete choice and social force can describe how pedestrians deviate from their free flow behaviors due to the presence of other pedestrians [7].

Most pedestrian theories are based on the fundamental of vehicle traffic flow and there has been very limited research works use pedestrian flow characteristic to calibrate parameters of simulation model [8]. A better understanding of human behavior is the key to planning and management of pedestrian flows. In order to determine the pedestrian behavior, some parameters should be measures such as walking speed, spatial use and person counts [9]. There are different factors affecting the walking speeds of pedestrians, such as the personal characteristics of pedestrians like age, gender, weight, height and breadth. Besides that are also the characteristics of the trip like walking purpose, route familiarity and luggage, properties of the infrastructure and environmental characteristics [10].

The need of pedestrian behavior model

Providing a quality transit service is not simple where it must be design as attractive as possible, providing a user-friendly signage and information for the pedestrian to move around in the terminal before reaching their final destination. In order to achieve that, it must be from the supportive effort between transit properties, local government and private developers [11]. In the case of an emergency, the movement of a pedestrian usually is more straightforward than in the normal cases [12]. The movement of commuters in a railway station however is more complicated because they choose the route to reach their destination which is usually helped by signboard or map. A well-developed skill in measuring a complex traffic situation and being able to select and accomplish an appropriate response is a crucial key for a safe pedestrian behavior [13].

The success in commercializing the evacuation simulation software was contributed from the application of microscopic simulations. Each individual simulated as an independent agent with various traits where these virtual agent have properties such as age, size and gender [14]. With the simulation technology also, the pedestrian's behavior in fire evacuation can be predicted as well as the overall behavior where the pedestrian interact with one another in a complicated way. This model will therefore leading to an optimal pedestrian traffic control providing the description of pedestrian behavior in bottlenecks and emergencies situation such as in evacuation process or in the course of large public events like concert and sports events. Planner and managers can use the model and simulations to gain insight into the efficiencies of evacuation in the existing facilities and later improve and optimize the plans toward better design and plan. Apart from that, rail terminal in Malaysia has been popularly known by the Malaysian to be poor in comfort and convenience level of service. Therefore, the contribution from the research outcomes will hopefully able to overcome the existing problem and also avoid the repetition or replication of the existing problem embedded in the future design rail transit terminal.

Current status in Malaysia

The existing studies largely focusing into the design of the rail transit terminal. Therefore, for a deeper understanding of the pedestrian behaviour, it is necessary to analyse the effect of terminal facilities in the design and operation of the rail transit terminal. In the developing country as Malaysia, the Ministry of Transportation (MOT) provides the main transit services through a highly integrated system that includes cars, buses, and new technology transit such as LRT and Monorail.

An overcrowding scenario especially at the platform of rail terminal can be created from the train passenger who arrived at the station and also the passenger waiting to board the train. Most of

the research has been identified focusing on walking behavior of pedestrian at the platform where little attention has been paid to the influence of waiting pedestrian or idling pedestrian to the crowd.

The Malaysian governments in the Malaysia's Economic Transformation Programme from Suruhanjaya Pengangkutan Awam Darat (SPAD) aims on a transform of Kuala Lumpur into one of the world's most liveable cities through the strategies of reducing congestion, pollution and increase the incidence of cycling and walking. Therefore, improving the user-friendliness of rail terminal will indirectly increase the likehood of the Malaysian to use public transport mainly rail services [15]. Having the research to be carried out based from this will give a simple understanding on the theoretical aspect where the modeling and equation of the pedestrian traffic flow will gives proper planning in Malaysian pedestrian route choice.

Simulation model for pedestrian behavior

A study on pedestrians' behavior during emergency evacuation at Shuangjing station in Beijing shows the result that from the evacuation capacity model, 8942 people can be evacuated from Shuangjing station within 6 minutes under emergency. It was found that the elements that were critically affected the emergency evacuation process were the characteristic of the evacuees, the evacuation facilities and the evacuation organization and management [16].

On the evacuation of pedestrian's crowd in a transit terminal subway station, an agent-based model was used for the evacuation process and the effective evacuation time was considering the effect from the density of the occupant and the width of the exit door and automatic fare gates. Simulated using FDS + Evac, it was found that the evacuation time becomes longer with the increasing of the occupants densities and different occupant densities correspond to a different critical exit width. The automatic gates however played the roles of making the evacuation process more orderly [17].

A study related on pedestrian dynamics focusing on bonding effects in Mass Rapid Transit (MRT) stations in Singapore, bonding rate was evaluated by recognizing and counting bonded groups inside walking crowds. The bonding between pedestrians was considered occurred when there was a physical contact, talking, gathering or leaning back toward to wait. Using simulation, the result demonstrated that bonding force redistributes walking speed thus causing a delay effects and overtaking phenomenon. Bonding forces also generate negative effects in pedestrian evacuation dynamics [14].

The functional relation between the density of pedestrian and walking speed has been measured by many and a clear indication has been found where a major number of parameters such as cultural differences are captured for example the speed of Indian test persons is seemingly less dependent on density than the speed of German test persons. A major railway was observed and almost immediately, the type of travelers hence the walking behavior was strongly varies within the time of the day where changes occur within minutes and rush hour passengers were very different from sight seers or football fans [18].

Table 1: Classification of Behavior According to Pedestrian Complexity [19]

Stimulus	Simple or standard situations	Complex or new situations
Reaction	Automatic reaction, reflex	Result of evaluation, decision process
Characterization	Well predictable	Probabilistic
Modeling concept	Social force model, etc	Decision theoretical model, etc
Example	Pedestrian motion	Destination choice by pedestrians

When human behavior is "chaotic" and unpredictable, a gas kinetic pedestrian model can be followed and behavioral changes can be guided by a so-called social fields or social forces. Table 1 suggested that since pedestrian is used to the situation they normally confronted, the reaction will

usually be automatic and determined by their experience of which reaction will be the best. Therefore, it is possible to put the rules of pedestrian behavior into equation of motion. [19].

Pedestrian simulation can be categorized into three which are macroscopic models, microscopic models and mesoscopic models. In microscopic models, each pedestrian is modeled as a separate entity where the crowd density rather than the individual pedestrians is the main object of the modeling in macroscopic models. In mesoscopic models, pedestrians are assigned to one of a number of predefined regions. The main drawback of this model is the discrete nature of regions and pedestrians where each pedestrian can only occupy one region at a time [20].

There are several types of Microscopic Pedestrian Simulation Model (MPSM) which are Benefit Cost Cellular Model, Magnetic Force Model, Queuing Network Model, Cellular Automata Model and Social Force Model. These pedestrian simulations nowadays have been used widely as tools in managing the operational and strategies of pedestrian movement. Each simulation package has its characteristics and advantages. Cellular automata demand fewer computations than social force or utility based model but the simulation of 10.000 pedestrians using cellular automata approach cannot be performed faster than in real time [20]. Social force is one of the typical continuous model where the model work by describing the motions of the pedestrian as if they were subjected to social force (acceleration, reflecting and attractive effects). The critical problem is the description of interactions among pedestrian. Social force model provides and effective approach to describe interactions while in cellular automata, the interactions are limited to the area of an immediate neighborhood [21].

The Social Force Model (SFM) is a physical model based on social field theory where the dynamics of each pedestrian is determined by driving forces that direct the pedestrian towards their destination, social or pedestrian forces that avoid collision between two pedestrians through repulsive forces and granular forces that existed when two pedestrian touch each other and start pushing each other in a panic situation. Despite its simplicity, SFM has been successfully reproducing several collective pedestrian flow phenomena and the strength of SFM lies in dealing with panic situations and several simulation case studies on escape panic from a room [22].

The greatest advantage for the SFM which differentiates it from other MPSM model is the ability in representing the communication between pedestrians in a more realistic way. As for this distinction, most researchers considered SFM as the representative model for the environmental phenomena that are triggered by the interaction among pedestrian such as congestion.

SFM has been widely used recently in a form of pedestrian model in computer simulation software where SimWalk uses SFM as its fundamental equation to determine the path of the pedestrian [23]. This software can also design the pedestrian walking areas and simulating the movement of pedestrian through finding the shortest route for the pedestrian to reach destination after evading all the obstacles.

Experimental approach

Generally, pedestrian modeling consists of microscopic and macroscopic models. In microscopic models, each pedestrian is represented separately as an individual agent and his/her behaviors are explored independently. While in macroscopic models, pedestrians are analyzed in groups where it is generally described by mass densities, flow and average velocity [24].

An approach to extract individual pedestrian data from digital video footage were conducted in a large scale walking experiment at Delft University of Technolgy where a group of 80 pedestrians were observed at the area of approximately 14m by 12m using a video camera mounted 10m height at the ceiling. This includes pedestrian detection and tracking whereby this approach was found suitable to detect all pedestrians in the detection zone and track them with a high accuracy. In other hand, an interesting observation technique was found used to study pedestrian flow in Mekka where using a ‘probes’ (instrumented pedestrians) that walk along with the pedestrian stream will allow the trajectories of a number of pedestrian to be determine and also to interfere the average speed of the pedestrian flow from that [25].

Video recording has become common and suitable equipment for empirical pedestrian study recently. Automatic evaluation of pedestrian trajectories could be the advantage, but video recording also has its limitations. The pedestrian could be hidden in the video in a huge crowd [26]. It is definitely that an automated procedure has enormous advantages over the labour-intensive manual data collection. This is true especially for the pedestrian experiments where many hours of high density pedestrian traffic operation have been monitored [25]. However, there are some significant benefits from being able to develop method of automatically collecting data using an image processing techniques applied to video sequences provided that if a specially designed and located cameras and other electronic equipment can be installed in all the experiments sites and the data collected will be much better [27].

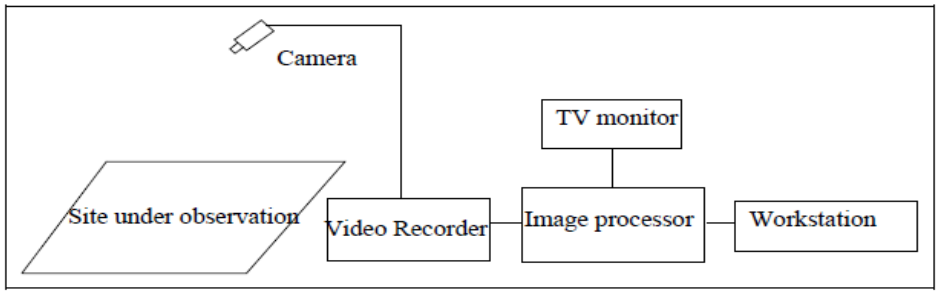


Figure 1. On-Site Recording (VCR and a camera) and an Image Processor Hosted by a Workstation [27].

An experimental set up was carried out using two camera positions typical of conventional surveillance CCTV equipment at peak hour recording at Liverpool St. railway station, a major commuter station in London, UK. It consists of equipment for on-site recording (VCR and a camera) and an image processor hosted by a workstation. Figure 1 shows the development environment where a standard domestic camera is used to record scenes at the interest area. The recording are digitized and processed by a transputer-based image processor under the control of a standard workstation [27].

A study on pedestrian speed and flow relationships for walking facilities in Hong Kong and the data was collected at each survey site encompassed pedestrian travel times, pedestrian flows/densities and physical dimension of the surveyed areas. The study adapted an approach to collect data of walking speed and flow using a time-lapse photography technique. The time-lapse photography techniques have been successfully used for many traffic studies, mostly when detailed investigation is needed. Several significant advantages when using the time-lapse photography techniques such as [28]:

- Provide a permanent record that can be referred repeatedly in order to obtain additional data.
- Supply a variety of supplementary data such as pedestrian flow, pedestrian walking speed and pedestrian walking behavior.
- The emotion of pedestrian can be investigated frame by frame with a high-speed camera.
- Reduce survey personnel which subsequently reduce the cost.

Application and impact to the society

Modeling and visualizing the dynamic behavior of pedestrians, especially in railway stations is relatively new. In rail transit terminal, people behave differently compared to normal circumstances because they may be in a hurry to catch their train or they are wandering about because they have missed the train. Moreover, walking conditions in rail transit terminal differ substantially from those outside because of the higher densities of people, wider range of walking purposes and speeds. As a consequent, specific behavior of passengers in rail transit terminal needs to be studied as this will be the reference point for the traffic engineer in designing walking infrastructures for other places such as shopping mall, stadium and many other public transit areas in Malaysia. It will

also enhance the fundamental theory in modeling and equation of the pedestrian flow that will gives a proper planning in pedestrian route choice. This research is focusing on the fundamental theory of pedestrian traffic flow related in the rail transit terminal.

A deeper exploration on this issue will give a positive impact to some important implications for the theory and modeling of transit use and the factor that influence the use of it. Furthermore, it can be used as a basic guideline for planner, designers and policy maker in strategizing the design of a sustainable transit–pedestrian oriented development and also improve the built environment for pedestrian in the rail transit terminal. Pedestrian simulation will help railway operator, planner and architect shape the best station design in the future. The simulation also will calculate the capacity, identify the best routes for pedestrian, assess queuing patterns at the ticket window and work out evacuation procedures.

Malaysia as for now is a highly motorized country and educating the society into changing travel mode from auto trips to walking trips can help the country to defeat some important objective such as obesities and reducing the air pollution and dependencies towards oil from auto use. The main scientific contribution of the research will be the integration of pedestrian choice models describing various dimensions of pedestrian behavior including walking, route choice, performance of activities, and interaction of passengers in rail transit terminal into a consistent framework. With the development of the pedestrian simulation modeling, it will provides an analytical evaluation of the quality of urban space for both pedestrian and rail terminal as to improve the operation of public transport terminals in Malaysia. Other than that, the simulation will give an overview on the effect of the interaction between pedestrian and rail terminal for safety prevention and accident analysis in enhancing the safety level of the pedestrians. With this, it will put back the public interest towards public transport in Malaysia especially into rail transit system.

Acknowledgment

This study is funded by Research Management Institute (RMI), Universiti Teknologi MARA (UiTM) under the Research Acculturation Grant Scheme (RAGS)

References

[1] Agrawal. A. W., Schlossberg. M. and Irvin. K. (2008). *How Far, by Which Route and Why? A Spatial Analysis of Pedestrian Preference.* Journal of Urban Design, Vol 13. No 1

[2] Tipakornkiat C., Limanond T. and Kim H. (2012). *Determining and Influencing Area Affecting Walking Speed on Footpath: A Case Study of a Footpath in CBD Bangkok, Thailand*. Physica A 391 (2012) 5453-5464.

[3] IISD. (2012). "What is Sustainable Development?" Retrieved 29/11/12 from http://www.iisd.org/sd/

[4] Campanella, M. C., Hoogendoorn, S. P. and Daamen, W. (2011). *A methodology to Calibrate Pedestrian Walker Models Using Multiple-Objectives*. New York: Springer (pp. 755-759).

[5] Teknomo, K. (2002). Microscopic *Pedestrian Flow Characteristics:Development of an Image Processing Data Collection and Simulation Model*. Graduate School of Information Sciences, Tohoku University, Japan.

[6] Daamen, W. and Hoogendoorn, S.P. (2012). *Calibration of Pedestrian Simulation Model for Emergency Doors for Different Pedestrian Types.* TRB Annual Meeting Technical Papers (pp 1-12). Washington DC Transportation Research Board.

[7] Campanella, M. C., Hoogendoorn, S. P. and Dameen, W. (2011). *Calibrating Walker Models: Variations of Parameter Due to Traffic Regimes*. European Conference on Mathematical and Theoretical Biology.

[8] Hongfei, J., Lili, Y. and Ming, T. (2009). *Pedestrian Flow Characteristic Analysis and Model Parameter Calibration in Comprehensive Transport Terminal*. J Transpn Sys Eng & IT, 9(5), 117-123.

[9] PED. (2012). 6th International Conference on Pedestrian and Evacuation Dynamics Retrieved 30/11/12, from http://www.ped2012.org/

[10] Daamen, W. and Hoogendoorn, S.P. (2003). *Research on PedestrianTraffic Flows in Netherlands*. Procceding Walk 21 IV (pp.101-117). Portland, Oregon, United States.

[11] O'Sullivan. S. and Morral. J. (1996). *Walking Distance to and from Light Rail Transit System.* Transportation Research Recod (TRR) Journal-1538.

[12] Schadschneider, A., Klingsch, W., Klüpfel, H., Kretz, T., Rogsch, C., & Seyfried, A. (2008). Evacuation Dynamics: Empirical Results, Modeling and Applications.

[13] Oxley J., Fildes B., Ihsen E., Charlton J., and Day R., (1997). *Differences in Traffic Judgements Between Young and Old Adult Pedestrians. Accident Analysis and Prevention*, Volume 29, No.6, pp 839 – 847.

[14] Xu, S. and Duh, H. B. L. (2010). *A Simulation of Bonding Effect and Their Impacts on Pedestrian Dynamics*. IEEE Transaction on Intelligent Transportation Systems. Vol 11. No 1.

[15] National Land Public Transport Masterplan Final Draft (2012). Suruhanjaya Pengangkutan Awam Darat (SPAD) Malaysia.

[16] Cheng H. and Yang X., (2012). *Emergency Evacuation Capacity of Subways Station*. Social and Behavioral Sciences 43 (2012) 339 – 348.

[17] Lei W., Li A., Gao R., Hao X. and Deng B., (2012). *Simulation of Pedestrian Crowds' Evacuation in a Huge Transit Terminal Subway Station*. Physica A 391 (2012) 5355 – 5365.

[18] Davidich, M and Koster, G. (2012). *Towards Automatic and Robust Adjustment of Human Behavioral Parameters in a Pedestrian Stream Model to Measured Data*. Safety Science. Volume 50 (2012). Pp 1253-1260.

[19] Helbing, D. and Molnar, P. (1995). *Social Force Model for Pedestrian Dynamics*. Physical Review E. Volume 51, No.5, pp 4282 – 4286.

[20] Bauer, D., Seer, S. and Brandle, N. (2007). *Macroscopic Pedestrian Flow Simulation for Designing Crowd Control Measures in Public Transport After Special Events*. Summer Computer Simulation Conference (SCSC). ISBN 1-56555-316-0.

[21] Qi, Z. and Baoming, H. (2011). *Simulation Model of Pedestrian Interactive Behavior*. Physica A 390 (2011) 636 – 646.

[22] Shiwakoti, N., Sarvi, M. and Rose, G. (2008). *Modeling Pedestrian Behavior Under Emergency Conditions – State of the Art and Future Directions*. 31st Australasian Transport Research Forum. Pp 457-473.

[23] Zainuddin, Z., Thinakaran, K., & Abu-Sulyman, I. M. (2009). *Simulating the Circumambulation of the Ka'aba using SimWalk*. © EuroJournals Publishing, Inc. 2009, Vol.38 No.3 (2009), pp.454-464.

[24] Sahaleh, A.S., Bierlaire, M., Farooq, B., Danalet, A., Hänseler, F.S. (2012). *Scenario Analysis of Pedestrian Flow in Public*. *STRC 2012*.

[25] Hoogendoorn, S. P., Daamen, W. and Bovy, P. H. L. (2003). *Extracting Microscopic Pedestrian Characteristic from Video Data.* TRB Annual Meeting.

[26] Johansson, A., Helbing, D., Al-Abideen, H. Z., and Al-Bosta, S. (2008). *From Crowd Dynamics to Crowd Safety*. World Scientific Publishing Company (WPSC)

[27] Davies, A. C., Yin, J. H. and Velastin, S. A. (1995). *Crowd Monitoring Using Image Processing*. IEE Electronic and Communications Engineering Journal. Vol 7. No 1. pp 37-47.

[28] Lam, W. H. K. and Cheung, C. Y. (2000). *Pedestrian Speed/Flow Relationships for Walking Facilities in Hong Kong*. Journal Transportation Engineering. 126: 343-349.

Applied Mechanics and Materials Vol. 567 (2014) pp 749-754
© (2014) Trans Tech Publications, Switzerland
doi:10.4028/www.scientific.net/AMM.567.749

Statistical Analysis of Dynamic Bearing Capacity of Driven Pile

Ardy Arsyad[1, a], Suyadi[1,b] and Lawalenna Samang[1,c]

[1]Department of Civil Engineering, Faculty of Engineering, Hasanuddin University, P. Kemerdekaan Km. 10 Makassar 90254 Indonesia

[a]ardy.arsyad@unhas.ac.id, [b]suyadimerauke@yahoo.co.id, [b]lawalenna_samang@yahoo.com

Keywords: Dynamic Formulas, Pile Bearing Capacity, Normal Distribution, Probabilistics.

Abstract. This paper presents the use of statistical-probabilistic method in determining pile bearing capacities over a number of driven piles. Four dynamic formulas were employed to estimate pile bearing capacity including modified ENR, Hiley, Navy – McKay and Danish. We investigated the final setting data of 47 concrete piles with 600 mm diameter in the construction projects of New Naval Engineering Building Hasanuddin University. Based on the data, pile bearing capacity were computed and then analyzed statistically. Goodness of fit with Kolmogorov-Smirnov and Shapiro-Wilk were used to fit the probability distribution function (PDF) of the pile bearing capacity data to the PDF model. It was found that the pile bearing capacity estimated using ENR is more uniform with 506 tons average pile capacity and 6.4% COV, while that with Hiley and Danish are less various with 252 tons and 346 tons average pile capacity, and 14.7% and 16.6% COV respectively. Navy-McKay was found to have 465.8 tons average pile capacity with higher variability of 44.08%. A 90% Probability of pile bearing capacity estimated by ENR is 535 tons, or 1.17 times the upper bound, and 1.4 times the lower bound of pile capacity measured by pile driving analyzer (PDA). In comparison, 90% probability estimated by Danish is 420 tons or 0.93 times and 0.92 of the upper and lower bound of pile capacity measured by PDA, respectively. The Navy-McKay seeems to be overestimated whereas Hiley is underestimated.

Introduction

In recent years, there is a new approach in structural and geotechnical building inh relation to deal with uncertainties facts in designing process. This approach is the use of reliability based design by using statistics and probabilistic analysis. Most of pile foundation design formulas take account factors of safety, as empirical value, in order to prevent failure of design and to anticipate unexpected condition of design in the process of construction. Griffith et al. [1] suggested that factors of safety in specifically geotechnical engineering could be approached in two ways. the factor of safety obtained from allowable load for design (Terzaghi's load capacity), as estimated ultimate load. This approach is for pile load capacity cases. Phoon et al. [2] stated that, in general, 3the application of factor of safety is most uncertain element. Factor of safety is determined by the experience and the judgement of the geotechnical engineer. Therefore, it is commonly that engineers use different safety factor for different location or even for the same location [3]. Due to uncertainty of safety factor, the determination of pile bearing capacity is also uncertain. Different methods used in determing pile bearing capacity will lead to different results and generally engineers consider the lowest result indicating preference of conservative design rather than optimum design . This will be a part of engineering judgement driven by limited data obtained in geotechnical survey. To overcome uncertainty in pile design, statistic-probabilistic could be used. Therefore, this study aims to investigate the pile bearing capacity which is determined based on dynamic formula with statistic-probabilistical approach.

Case Study

The project of Engineering Faculty New Campus, Hasanuddin University is located about 19 km southeast of Makassar, the capital of South of Sulawesi. The project has been constructing several buildings over the area of 630×330 m^2, including Faculty, Center of Technology, Civil Engineering,

Architecture, Electrical Engineering, Mechanical Engineering, Geology Engineering, and Naval Engineering Buildings. The object of the study is Naval Engineering Building A with 2364.48 m^2. During the construction, 109 pre-cast concrete piles were driven for foundations of the building, in which 47 piles with 0.6 m and 62 piles with 0.5 m diameters. The concrete compressive strength of the pile is 52 Mpa. Hammer used in the driving is diesel hammer with 6.3 ton weight. To determine pile bearing capacity, dynamic methods were employed including Hiley (Eq. 1), ENR (Eq. 2), Navy-McKay (Eq. 3) and Danish (Eq. 4).

Formula Hiley.

$$Q_u = \frac{e_h \,.\, W_r \,.\, \mathrm{h}}{s+1/2(k_1+k_2+k_3)} x \frac{W_r + n^2 \,.\, W_p}{W_r + W_p} \quad (1)$$

Modified New ENR.

$$Q_u = \frac{e_h \,.\, E_h}{s+c} x \frac{W_r + n^2 \,.\, W_p}{W_r + W_p} \quad (2)$$

Navy-Mc.Kay.

$$Q_u = \frac{e_h \,.\, w_r \,.\, h}{s(1+0.3C_1)} \quad (3)$$

$$c_1 = \frac{w_r}{W_p}$$

Danish.

$$Q_u = \frac{e_h \,.\, E_h}{s + C_2} \quad (4)$$

$$c_2 = \sqrt{\frac{e_h \,.E_h \,.\, L}{2 \,.\, A \,.\, E}}$$

where

e_h is hammer efficiency
E_h is hammer energy
s is average penetration in the last 20 blows
n is restitution coefficient
w_r is weight of hammer
w_p is weight of pile
c is empirical coefficient of energy loss during driving
K_1 is elastic compression of capbox and pilecap, K_2 for elastic compression for pile and K_3 for elastic compression of soil
A is Area of pile section
Ep is elastic modulus of pile
h is drop height of ram
L is length of pile
Q_u is ultimate bearing capacity

Determination of bearing capacity using Dynamic Formula

During construction from November 2011 – February 2012, the contractor collected driving data of the piles, including final setting of pile. Final setting data over 47 piles with 600 diameter is shown in Table 1. The depth peneration of the pile for the final blow of hammer during driving and rebound were also obtained. The length of pile driven into the ground varies from 6 m to 10 m. The pile bearing capacity was determined by using the dynamic methods. Hammer energy can be obtained from multiplication of hammer weight and drop its height, whereas hammer efficiency is

0.85 based on the type of hammer as diesel hammer. Restitution coefficient was selected as 0.5 due to the pile is concrete pile with wooden cushion [4]. Ultimate bearing capacity (Q_u) was estimated by using dynamic formulas. The safety factor of ENR formula is 6, while that of Danish, Hiley and Navy-McKay are 3. It can be seen in Fig. 1, the bearing capacity of pile estimated by dynamic formulae varies. For example, Navy-McKay has fluctuated pile bearing capacity, while ENR seems to be more uniform. Danish and Hiley perform little variability, but not as uniform as ENR does.

Statistic-Probabilistic Method

Pile bearing capacities were analyzed statistically by generating their histogram and quantifying their probabilities. Once the histogram was obtained, the probability distribution function (PDF) can be generated and a goodness of fit with Kolmogrov-smirnov and Shapiro-Wilk test was used to examine the fitnes of the PDF of the data to PDF model. It was found that the pile bearing capacity data with Danish, ENR, and Hiley show a normal distribution, while that with Navy-McKay is less significant to match with normal distribution (Fig. 2). The statistical parameters can be determined, shown in Table 2. Average pile bearing capacity estimated with Danish is accounted for 345.9 tons with the COV of 16.6%, while ENR is accounted for 506 tons with a 6.4% COV. Navy-McKay based estimation is 465 tons average pile bearing capacity with very wide values with a 44.08% COV. Hiley estimation resulted in the lowest value, 252 tons with 14.7% COV

Cumulative probability of those dynamic methods are presented by Fig. 3. Fifty percent and 90% of cumulative probability (P_{50} and P_{90}) for Danish are 320 and 420 tons. On the other hand, P_{50} and P_{90} of the pile bearing capacity estimated by ENR are 490 and 535 tons. the Navy-McKay and Hiley were found to be 280 and 780 tons, and 280 and 290 tons. To examine reliability of the statistical results, their results were compared to the bearing capacities which is obtained from Pile Driving Analyzer (PDA) test. Two PDA tests were commenced by contractors during pile driving, with two ranges of bearing capacity. They are 343 tons - 455 tons, and 353 tons - 449 tons. It can be seen that average bearing capacity with Danish formula is very close to PDA result, while that with ENR over estimate the lower bound of PDA result. Navy-McKay and Hiley results are out of range of PDA test results. However, these findings require more data of PDA tests and static load tests to confirm the reliability of statistical results of pile bearing capacity and this will become future research.

Summary

1. ENR formula generates a uniform pile beearing capacity with a 506 tons average and 6.4% COV.
2. Hiley and Danish generate 252 tons and 346 tons average pile capacity with 14.7% and 16.6% COV, respectively.
3. Navy-McKay yields a 465 tons average pile capacity with higher variability, 44.08%.
4. Compared to the PDA results, 90% Probability of pile bearing capacity estimated by Danish is very close, 0.93 times and 0.92 of the upper and lower bound of pile capacity measured by PDA, respectively. In comparison, 90% probability estimated by ENR is 1.17 times and 1.4 times the upper and lower bound of pile capacity measured by PDA, respectively.

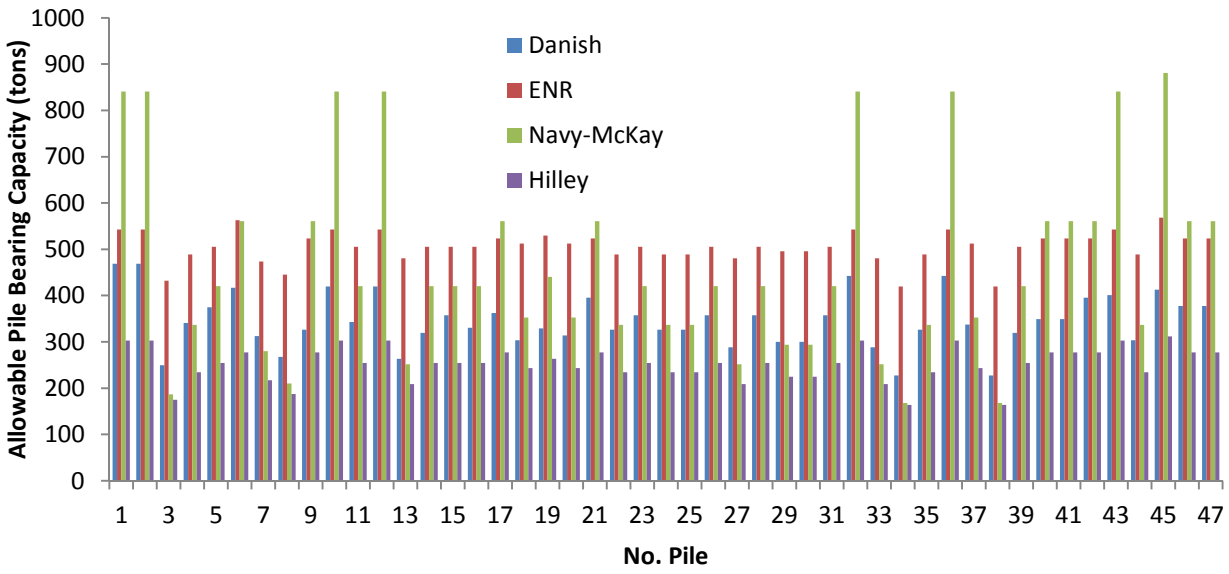


Figure 1. Pile bearing capacity estimated by Danish, ENR, Navy-McKay, Hiley.

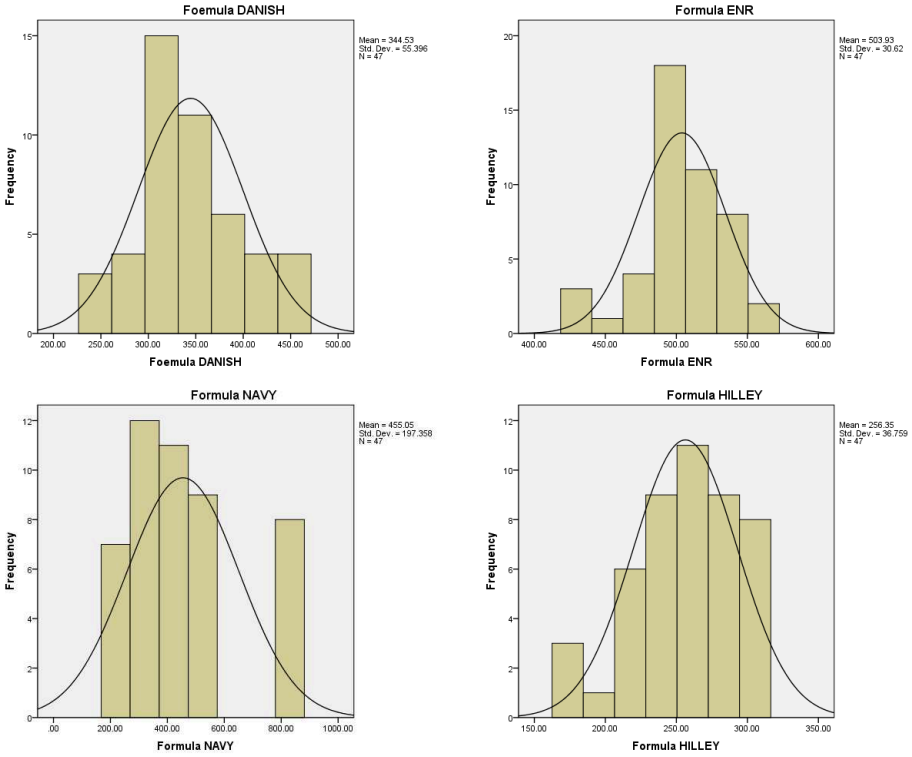
Table 1. Data of final setting of piles during construction.

No.	date	No. Pile	Diameter (m)	Blows	data					
					Wr (ton)	Wp (ton)	h (m)	S, (m)	k (m)	l (m)
1	2	3	4	5	6	7	8	9	10	11
1	11-Nov-11	1	0.6	316	6.3	2.40	2.10	0.00200	0.012	6.00
2	11-Nov-11	40	0.6	513	6.3	2.40	2.10	0.00200	0.012	6.00
3	12-Nov-11	42	0.6	460	6.3	2.40	2.10	0.00900	0.014	6.00
4	12-Nov-11	5	0.6	215	6.3	2.40	2.10	0.00500	0.012	6.00
5	12-Nov-11	9	0.6	901	6.3	2.40	2.10	0.00400	0.014	6.00
6	16-Jan-12	9A	0.6	396	6.3	2.40	2.10	0.00300	0.013	6.00
7	12-Nov-11	20	0.6	284	6.3	2.40	2.10	0.00600	0.012	6.00
8	12-Nov-11	45	0.6	349	6.3	2.40	2.10	0.00800	0.016	6.00
9	4-Jan-12	26	0.6	583	6.3	2.40	2.10	0.00300	0.010	12.00
10	16-Jan-12	53	0.6	273	6.3	2.40	2.10	0.00200	0.012	8.00
11	16-Jan-12	43	0.6	330	6.3	2.40	2.10	0.00400	0.013	8.00
12	16-Jan-12	52	0.6	251	6.3	2.40	2.10	0.00200	0.011	8.00
13	16-Jan-12	17	0.6	659	6.3	2.40	2.20	0.00700	0.016	10.00
14	16-Jan-12	27	0.6	509	6.3	2.40	2.10	0.00400	0.011	10.00
15	31-Jan-12	11	0.6	168	6.3	2.40	2.10	0.00400	0.012	7.00
16	1-Feb-12	46	0.6	328	6.3	2.40	2.10	0.00400	0.013	9.00
17	1-Feb-12	35	0.6	290	6.3	2.40	2.10	0.00300	0.017	9.00
18	1-Feb-12	14	0.6	541	6.3	2.40	2.20	0.00500	0.021	10.00
19	1-Feb-12	24	0.6	439	6.3	2.40	2.20	0.00400	0.021	10.00
20	1-Feb-12	50	0.6	740	6.3	2.40	2.20	0.00500	0.020	9.00
21	2-Feb-12	29	0.6	306	6.3	2.40	2.10	0.00300	0.024	7.00
22	2-Feb-12	19	0.6	318	6.3	2.40	2.10	0.00500	0.019	7.00
23	2-Feb-12	30	0.6	342	6.3	2.40	2.10	0.00400	0.016	7.00
24	2-Feb-12	31	0.6	417	6.3	2.40	2.10	0.00500	0.015	7.00
25	2-Feb-12	6	0.6	477	6.3	2.40	2.10	0.00500	0.016	7.00
26	2-Feb-12	8	0.6	325	6.3	2.40	2.10	0.00400	0.012	7.00
27	2-Feb-12	7	0.6	530	6.3	2.40	2.20	0.00700	0.018	7.00
28	2-Feb-12	12	0.6	411	6.3	2.40	2.10	0.00400	0.013	7.00
29	2-Feb-12	54	0.6	214	6.3	2.40	2.20	0.00600	0.020	8.00
30	3-Feb-12	44	0.6	275	6.3	2.40	2.20	0.00600	0.013	8.00
31	3-Feb-12	55	0.6	359	6.3	2.40	2.10	0.00400	0.014	7.00
32	3-Feb-12	49	0.6	114	6.3	2.40	2.10	0.00200	0.014	7.00
33	3-Feb-12	38	0.6	288	6.3	2.40	2.20	0.00700	0.020	7.00
34	3-Feb-12	32	0.6	727	6.3	2.40	2.10	0.01000	0.010	7.00
35	4-Feb-12	21	0.6	240	6.3	2.40	2.10	0.00500	0.020	7.00
36	4-Feb-12	33	0.6	302	6.3	2.40	2.10	0.00200	0.010	7.00
37	6-Feb-12	2	0.6	223	6.3	2.40	2.20	0.00500	0.022	7.00
38	6-Feb-12	3	0.6	196	6.3	2.40	2.10	0.01000	0.010	7.00
39	6-Feb-12	16	0.6	512	6.3	2.40	2.10	0.00400	0.010	10.00
40	6-Feb-12	15	0.6	396	6.3	2.40	2.10	0.00300	0.024	10.00
41	6-Feb-12	25	0.6	382	6.3	2.40	2.10	0.00300	0.016	10.00
42	6-Feb-12	4	0.6	230	6.3	2.40	2.10	0.00300	0.012	7.00
43	6-Feb-12	18	0.6	436	6.3	2.40	2.10	0.00200	0.016	9.00
44	6-Feb-12	28	0.6	333	6.3	2.40	2.10	0.00500	0.020	9.00
45	8-Feb-12	47	0.6	526	6.3	2.40	2.20	0.00200	0.022	9.00
46	11-Feb-12	51	0.6	397	6.3	2.40	2.10	0.00300	0.016	8.00
47	11-Feb-12	41	0.6	361	6.3	2.40	2.10	0.00300	0.017	8.00

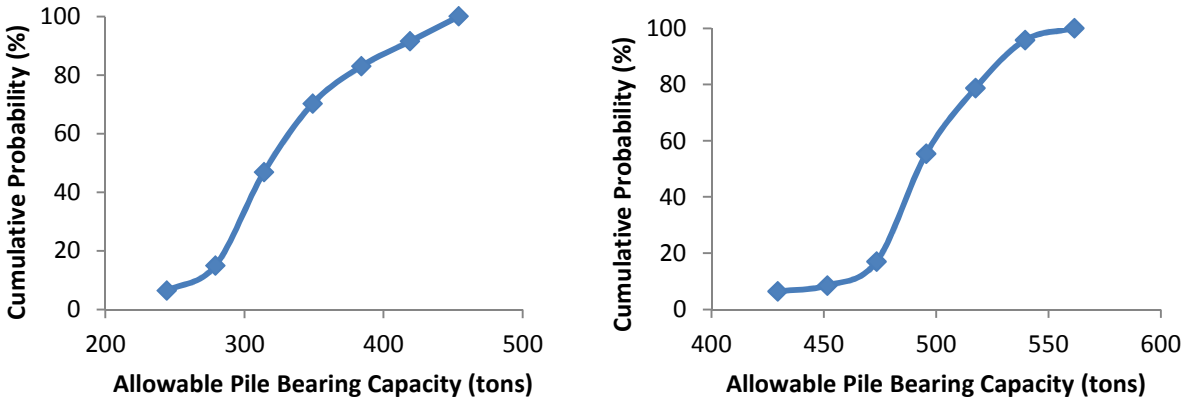
Table 2. Statistical parameters of dynamic methods.

Descriptive Statistics

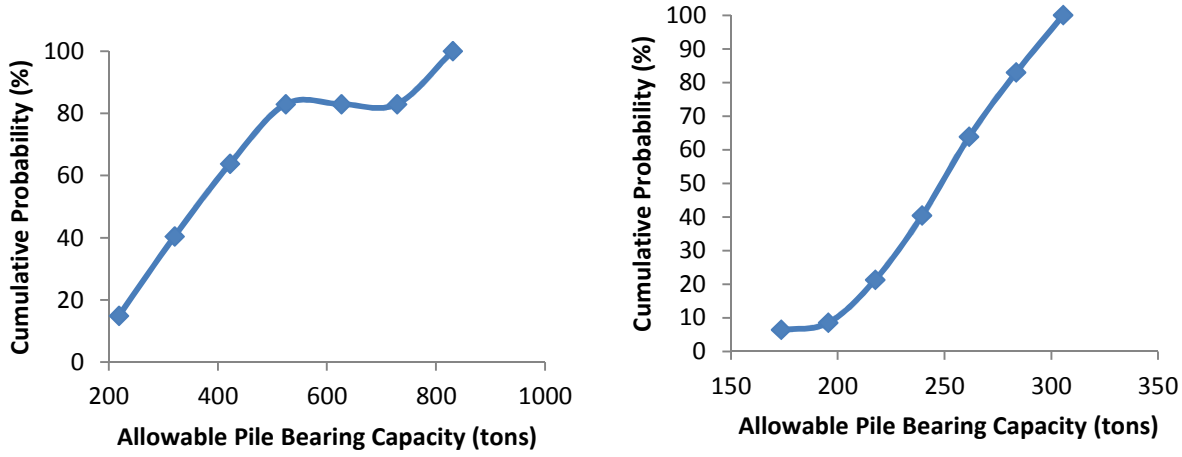
Formula	N	Range	Minimum	Maximum	Sum	Mean		Std. Deviation	COV (%)
	Statistic	Statistic	Statistic	Statistic	Statistic	Statistic	Std. Error	Statistic	Statistic
Danish	47	241.26	227.50	468.76	16261.88	345.9974	8.37647	57.42616	16.58
ENR	47	148.43	419.91	568.34	23796.70	506.3128	4.73653	32.47201	6.4
Navy - McKay	47	712.86	168.20	881.06	21891.90	465.7851	30.03579	205.91500	44.08
Hiley	47	147.91	163.98	311.89	11855.65	252.2478	5.40682	37.06731	14.7



`Figure 2. Normal distribution of pile bearing capacities based on dynamic methods.



(a) (b)



(c) (d)

Figure 3. Cumulative probability of pile bearing capacity estimated by (a) Danish, (b) ENR, (c) Navy-McKay, (d) Hiley

Table 3. Evaluation of the performance of dynamic methods

Formula	Statistics			Cumulative probability				
	Mean	Sd	Rank	P_{50}	P_{90}	P_{90}/ lower PDA	P_{90}/upper PDA	Rank
ENR	506.3	6.4	1	490	535	1.42	1.17	2
Hiley	252.4	14.7	2	280	290	0.81	0.63	3
Danish	345.9	16.6	3	320	420	0.93	0.92	1
Navy-McKay	465.8	44.08	4	280	780	0.81	1.71	4

References

[1] Griffiths, D.V., Fenton, G.A. and Manoharan, N., (2002). "Bearing capacity of a rough rigid strip footing on cohesive soil: A probabilistic study," ASCE J. Geotech. Geoenv. Eng., 128(9), 743--755.

[2] Phoon, K. K., and Kulhawy, F. H. (1999). "Evaluation of geotechnical property variability." Can. Geotech. J., 36(4), 625-639.

[3] Gobel, G.G. (1999): Geotechnical related development and implementation of load and resistance factor design (LRFD) methods, Synthesis of Highway Practice, NCHR syntesis276, TRB, NRC

[4] Chellis, R.D., (1951). Pile foundation, McGraw Hill Book Company, 704p.

[5] Hiley, A., (1925). A rational pile driving formula and its application in piling practice explained. Engineering(London), 119, Pp. 657-721.

Applied Mechanics and Materials Vol. 567 (2014) pp 755-762
© (2014) Trans Tech Publications, Switzerland
doi:10.4028/www.scientific.net/AMM.567.755

The use of Bitumen Linear Viscoelastic Properties to Assess Rutting Sensitivity

Salah E. Zoorob, Ibrahim B Kamaruddin, Madzlan B Napiah
UniversitiTeknologiPetronas, Bandar Seri Iskanadar, 31750 Tronoh, Perak DarulRidzuan, Malaysia.
salah.zoorob@petronas.com.my,ibrakam@petronas.com.my, madzlan_napiah@petronas.com.my

Keywords: Bitumen, Viscoelasticity, SHRP specifications, Energy Equation, Rutting, DSR Frequency Sweeps.

Abstract. The use of viscosity temperature relationships to predict creep performance of road bitumens have been shown to be inadequate in particular with respect to the analysis of polymer modified binders. In this paper we explore the origins of the US Strategic Highway Research Programmebinder performance grading system and detail two examples of more recent developments towards improved creep characterisation.Starting from first principles, an equation to analyse the ratio of dissipated to stored energy during sinusoidal loading of viscoelastic bitumen was derived. The energy equation was contrasted with an empirical relationship proposed by Anderson D.A., and with a second more theoretical derivation proposed by Shenoy A.Using frequency sweep data from a conventional 40/50 pen grade bitumen and a proprietary SBS modified binder, the applicability of the energy equation was subsequently compared to the two aforementioned post-SHRP creep relations. Recommendations are made regarding the suitability of the proposed relations in ranking bitumen creep performance.

Introduction

In the US binder grading system bitumen is classified by two numbers, (e.g. “64-28”, “58-22”, etc.)indicating the high and low temperature performance designations respectively. The system was intended to be applicable to both unmodified and polymer modified bitumens.The specifications were designed to address three main failure mechanisms for asphalt mixtures, i.e. 1- Permanent deformation at high service temperatures, 2- Fatigue cracking at intermediate temperatures, 3- Brittle fracture at low temperatures.

Both fatigue failure and brittle fracture at low temperatures tend to occur in older pavements. Therefore the specification includes measurements on binders in three states: unaged, after ageing in the Rolling Thin Film Oven Test (RTFOT) to simulate short term ageing that occurs during mixing and compaction processes, and after both RTFOT and ageing in the Pressure Ageing Vessel (PAV) to simulate long term ageing (5-10 years) in the field. As an example PG 64-22 grade bitumen implies the following:

- 64°C is the average 7-day maximum pavement ‘design’ temperature. G*/sinδ at 10 rad/s (measured using a DSR) must have a minimum value of 1 kPaunaged and 2.2kPa after RTFOT. To perform well in terms of resisting rutting, a binder should either be stiff (high G*), or elastic (low sinδ), or both. The 40/50 pen bitumen described in earlier parts of this paper satisfies these two requirements.
- -22°C is the minimum pavement design temperature. At -12°C (10°C is added to speed up laboratory testing), the binder must have a maximum stiffness of 300 MPa and a minimum m-value (slope of creep stiffness v.s. loading time) of 0.3 after RTFOT & PAV, when measured using the Bending Beam Rheometer. Binders that fulfil both criteria are better able to relax thermal stress build-up at low temperatures.

Further DSR measurements are required to calculate the fatigue parameter (G*sinδ at 10rad/s) at an intermediate temperature, e.g. for a PG 64-22 grade, fatigue testing is conducted at 25°C. A maximum value is specified as more compliant, elastic binders help to address the problem of fatigue cracking.

Revisiting the Origins of the SHRP Linear Viscoelastic Binder Properties

The starting point in the development of the US Strategic Highway Research Program (SHRP)binder specifications,which were conducted from 1988 through 1994, was the followingequation describing the energy dissipated per cycle (W_d):

$$W_d = \pi \times \sigma_0 \times \varepsilon \times \sin\delta \quad (1)$$

Based on Eq. 1, parameters for rutting and cracking were then determined in the SHRP specification as follows.At temperatures in the range 40 to 60°C(i.e. the highest pavement temperatures), the main distress mechanism is rutting. In the specification, bitumen rutting was assumed to be stress-controlled (σ) cyclic loading phenomenon. It was considered that part of W_d is recovered in elastic rebound, whilst the remaining work is dissipated in permanent deformation and heat. For a σ-controlled repetitive phenomenon, $\sigma = \sigma_0$ and$\varepsilon = \sigma_0/G^*$, $W_d$can thus be shown as [4]:

$$W_d = \pi \times \sigma_0 \times \varepsilon \times \sin\delta = \pi \times \sigma_0 \times \frac{\sigma_0}{G^*} \times \sin\delta = \pi \times \frac{\sigma_0^2}{\left(G^*/\sin\delta\right)} \quad (2)$$

Thus in order to control rutting, W_d should be minimized by maximizing the value of $G^*/\sin\delta$. The basic consideration behind the SHRP parameter ($G^*/\sin\delta$)was that the contribution of the binder to rutting resistance can be increased by increasing its total resistance (G^*) and/or increasing its elasticity (i.e. lower $\sin\delta$). SHRP thus used the parameter ($G^*/\sin\delta$) to rank rutting susceptibility of pavements. DSR measurements were conducted on the original binders at the average 7 day maximum pavement temperature at a frequency of 10 rad/s. 10 rad/s was assumed to simulate the average frequency of a stress wave in the surface layer of a typical pavement as caused by a vehicle moving at 80-100 km/h.

Within the intermediate temperature, 10 to 30°C, bitumens are relatively harder and more elastic than at higher temperatures. The prevailing failure mode at these temperatures is fatigue cracking. For viscoelatic materials, both G^* and δ play a role in damage induced by fatigue. The SHRP specifications stipulate that fatigue cracking is primarily due to repeated loading on the pavement surface, and a strain-controlled (ε) phenomenon is assumed. For a strain-controlled repetitive phenomenon, $\varepsilon = \varepsilon_0$, and $\sigma = \varepsilon_0 \times G^*$, W_d can be expressed as [4]:

$$W_d = \pi \times \sigma \times \varepsilon_0 \times \sin\delta = \pi \times (\varepsilon_0 \times G^*) \times \varepsilon_0 \times \sin\delta = \pi \times \varepsilon_0^2 \times (G^* \times \sin\delta) \quad (3)$$

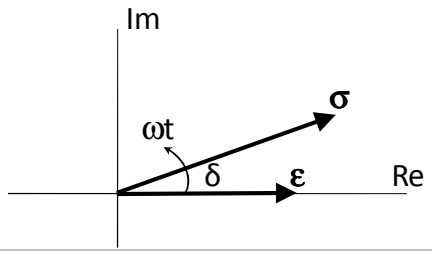
By accepting that the amount of work dissipated (W_d) is directly proportional to ($G^*\sin\delta$), it can be inferred that to prevent fatigue cracking($G^*\sin\delta$) shouldbe minimized.

Background to the Energy Equation

Unfortunately, no derivation can be readily found in the SHRP documentation as to the origins of Eq. 1. Since the origins of energy Eq. 1 were unclear, it was decided to derive it from first principles as described next. When a viscoelastic material is subjected to a sinusoidally varying stress, a steady state will eventually be reached in which the resulting strain is also sinusoidal, having the same angular frequency but retarded in phase by an angle δ. The strain lags the stress by the phase angle δ. If the origin along the time axis is selected to coincide with a time at which the strain passes through its maximum, the strain and stress function can be written as:

$$\varepsilon = \varepsilon_0 \cos(\omega t) \qquad \sigma = \sigma_0 \cos(\omega t + \delta) \qquad \sigma^* = \sigma_0' \cos(\omega t) + i\sigma_0'' \sin(\omega t)$$

It can be useful to visualise the observable stress and strain as the projection on the real axis of vectors rotating in the complex plane at a frequency ω. If we capture their positions just as the strain vector passes the real axis, the stress vector will be ahead of it by the phase angle δ as seen in Fig.1.



$$\tan\delta = \frac{\sigma_0''}{\sigma_0'}$$

$$\left|\sigma^*\right| = \sigma_0 = \sqrt{(\sigma_0')^2 + (\sigma_0'')^2}$$

$$\sigma_0' = \sigma_0 \cos\delta$$

$$\sigma_0'' = \sigma_0 \sin\delta$$

Figure 1: The "rotating-vector" representation of harmonic stress and strain

This complex form of the stress function can be used to define the two different dynamic moduli, both being ratios of stress to strain as usual but having very different molecular interpretations and macroscopic consequences. The first of these is the "real", or "storage" modulus, defined as the ratio of the in-phase stress to the strain: $E' = \sigma_0' / \varepsilon_0$. The other is the "imaginary" or "loss" modulus, defined as the ratio of the out-of-phase stress to the strain: $E'' = \sigma_0'' / \varepsilon_0$.

Mechanical Work Done Per Loading Cycle

The quantity ($\int\sigma\ d\varepsilon$) is the strain energy per unit volume (since σ = force/area and ε = distance/length). Integrating the in-phase and out-of-phase components separately:

$$W = \oint \sigma\ d\varepsilon = \oint \sigma\ \frac{d\varepsilon}{dt}\ dt$$

$$= \int_0^{2\pi/\omega} (\sigma_0' \cos\omega t)(-\varepsilon_0 \omega \cdot \sin\omega t)dt + \int_0^{2\pi/\omega} (\sigma_0'' \sin\omega t)(-\varepsilon_0 \omega \cdot \sin\omega t)dt = 0 - \pi\sigma_0''\varepsilon_0 \qquad (4)$$

note that the in-phase components produce no net work when integrated over a cycle, while the out-of-phase components result in a net dissipation per cycle equal to: $W_{dis} = \pi\sigma_0''\varepsilon_0 = \pi\sigma_0\varepsilon_0 \sin\delta$

This should be interpreted to illustrate that the strain energy associated with the in-phase stress and strain is reversible, i.e. that energy which is stored in the material during a loading cycle can be recovered without loss during unloading. Conversely, energy supplied to the material by the out-of-phase components is converted irreversibly to heat. The maximum energy stored by the in-phase components occurs at the quarter-cycle point, and is equivalent to:

$$W_{st.1/4} = \int_0^{\pi/2\omega} (\sigma_0' \cos\omega t)(-\varepsilon_0 \omega \cdot \sin\omega t)dt = -\frac{1}{2}\sigma_0'\varepsilon_0 = -\frac{1}{2}\sigma_0\varepsilon_0 \cos\delta$$

Integrating the total energy Eq. 4 for a ¼ cycle results in the following term; $(-0.5\varepsilon_0\sigma'_0 - 0.25\pi\varepsilon_0\sigma''_0)$. The relative dissipated to stored energyat the ¼ cycle point is then related to the phase angle by the following relationship:

$$\frac{W_{dis.1/4}}{W_{st.1/4}} = \frac{-(0.5\varepsilon_0\sigma_0\cos\delta) - (0.25\pi\varepsilon_0\sigma_0\sin\delta) + (0.5\sigma_0\varepsilon_0\cos\delta)}{(-0.5\sigma_0\varepsilon_0\cos\delta)} = 0.5\pi\tan\delta \qquad (5)$$

In this paper, it is proposed that the ratio of dissipated to stored energy (Eq. 5) may thus be used as a criterion for assessing bitumen viscoelastic performance, a lower ratio indicating greater elasticity and hence lower creep. As described earlier in the SHRP rutting criteria, rutting is assumed to be a stress-controlled repetitive phenomenon ($\sigma = \sigma_0$) which has been debatable. On the other hand using a generalised energy relation as in Eq. 5 to rank binder performance eliminates the requirement for pre-defining a stress or strain-controlled loading regime.

Refinement of the SHRP Binder Specifications

The parameter $|G^*|/\sin\delta$ for high temperature performance grading of bitumenshas not been found to be adequate in rating various binders, especially some polymer-modified ones, for their rutting resistance. This has led researchers to seek other possible parameters that may better relate to rutting resistance and also to search for ways to improve the existing parameter $|G^*|/\sin\delta$ so that it

is more sensitive to pavement performance.An excellent contribution to this subject has been made by Shenoy A. [6] as described next.

During repeated creep recovery tests, on applying a stress of σ_0kPa for a duration of "t" seconds, the total deformation (or the maximum strain γ_{max}) that the material undergoes must be the sum of the elastic and viscous deformations. The deformation behaviour has to be mapped by the following equation relating the applied constant stress with the maximum strain:

$$\%\gamma_{max} = 100\sigma_0 \div |G^*| \quad (6)$$

where;σ_0 = applied stress (kPa) in a creep experiment and $|G^*|$ = the complex modulus (kPa) obtained from oscillatory shear. To obtain a relationship between $\%\gamma_{max}$ and stiffness $|G^*|$, comparisons must be made on a common platform, thereby requiring the time scales to be matched. For example, if the loading in a creep experiment is 1 second, then a $|G^*|$ value at oscillation frequency ω = 1 rad/s must be used, whereas if the loading time is 10 seconds, then a $|G^*|$ value at ω = 0.1 radians/s must be used to match the time scale [6].

In the linear range of response, under constant stress, the strain per unit stress is a unique function of time (t) referred to as the shear creep compliance function, which can be described by the following equation:

$$J(t) = J_e + J_d\psi(t) + \frac{t}{\eta} = \frac{\%\gamma(t)}{100\sigma_0} \quad (7)$$

where; J(t) = shear creep compliance, J_e = elastic recoverable shear compliance, J_d = delayed recoverable shear compliance, $\psi(t)$ = the normalized retardation function which ranges from zero at t = 0 to one when steady-state deformation is achieved, η = steady state viscosity, and (t/η) = contribution of the viscous deformation at time t that is unrecoverable.

The recoverable shear compliance $J_r(t)$, which can be measured directly from the recoverable deformation following the cessation of creep loading, is given by: $J_r(t) = J_e + J_d\psi(t)$ (8)

If it is assumed that sufficient time has elapsed for asymptotic conditions to be reached, then the steady-state recoverable creep compliance J_{rec} can be written as: $J_{rec} = J_e + J_d$ (9)

It has been shown that the steady-state recoverable creep compliance is related to the steady shear flow property as follows [6]:

$$J_{rec} = \lim_{\dot{\gamma}\to 0} J(\dot{\gamma}) = \frac{\tau_{11} - \tau_{22}}{2\tau_{12}^2} \quad (10)$$

where;τ_{11} - τ_{22} = the normal stress difference, τ_{12} = shear stress. The following relationships have also been shown to be true:

$$[\tau_{11} - \tau_{22} = 2C^{-2}G'] \text{ for } [\omega = C\dot{\gamma}], \text{ and } [\tau_{12} = C^{-1}G''] \text{ for } [\omega = C\dot{\gamma}], \quad (11)$$

where; G' = storage modulus, G" = loss modulus, and C = arbitrary adjustable constant. When C = 1, the model suggests an association between steady and dynamic shear data at an equivalent shear rate and frequency. It may be noted that the value of C truly does not matter as it cancels out in the ratio when Eq. (10& 11) are combined [6]. During creep recovery after the removal of the applied stress, the strain rates are very low and hence, the comparison is made in the low shear rate / low frequency regimes. In the limit of shear rates tending to zero, or in other words, in the low shear rate / low frequency regions, the relationship given by Eq.10 can be rewritten as follows:

$$J_{rec} = G'/(G'')^2 \quad (12)$$

Or from the definition of J_{rec}, can be written as:

$$\frac{\%\gamma_{rec}}{100\sigma_0} = \frac{G'}{(G'')^2} \quad (13)$$

If sufficient time is given for creep recovery, all elastic strain is recovered and viscous strain is left unrecovered. The delayed elastic portion of strain leaves remnants of elastic strain, which then adds to the viscous strain if sufficient time for recovery has not elapsed.If elastic recovery is not complete, then every subsequent cycle would have its peak value decreasing and its unrecoverable strain value decreasing, thereby showing nonlinear behaviour. Since the line joining the unrecoverable strain after every cycle is nearly a straight line in almost all cases, there is good

evidence to suggest that the delayed elastic strain effect is minimal.The % recoverable strain can be defined as: $\%\gamma_{rec} = \%\gamma_{max} - \%\gamma_{unr}$ (14)

Combining Eq.6, 13& 14, the following equation is written with a rearrangement of the terms as [6]:

$$\frac{\%\gamma_{unr}}{\%\gamma_{max}} = 1 - \frac{|G^*|G'}{G''^2} \quad (15)$$

Using the fact that G' = $|G^*|\cos\delta$ and G''= $|G^*|\sin\delta$, Eq. 15 can be simplified as:

$$\frac{\%\gamma_{unr}}{\%\gamma_{max}} = 1 - \frac{1}{\tan\delta\sin\delta} \quad (16)$$

Eq.16 provides a refinement of the Superpave specification parameter, by providing a value of $(\%\gamma_{unr} \div \%\gamma_{max}) = 1$ when $\delta = 90°$. However, the form of the equation does not allow its use for values below $\delta = 52°$, because it would then predict unrealistic negative values of $(\%\gamma_{unr} \div \%\gamma_{max})$. Substituting Eq. 6 into Eq. 16 gives the expression for % unrecovered strain asfollows [6]:

$$\%\gamma_{unr} = \frac{100\sigma_0}{|G^*|}\left(1 - \frac{1}{\tan\delta\sin\delta}\right) \quad (17)$$

To minimize the unrecovered (or permanent) strain, the following term needs to be maximized:

$$|G^*| / \left(1 - \frac{1}{\tan\delta\sin\delta}\right) \quad (18)$$

Eq. 18could then be the new specification parameter, replacing $|G^*|/\sin\delta$. The high specification temperature can now be specified as the temperature at which the term given by Eq. 18 takes a value of 1 kPa for the original unaged binder and a value of 2.2 kPa for the RTFOT aged binder.

It can also be seen that Eq. 17 predicts that the $\%\gamma_{unr} = 0$ at conditions when the following equality holds:

$$(\tan\delta \times \sin\delta = 1) \quad \text{or} \quad \delta(\omega_{spec}, T_{hi.spec}) \approx 52° \quad (19)$$

Eq. 19 implies that the temperature at which $\delta = 52°$ for a particular predetermined frequency could be used as the new high temperature specification parameter ($T_{hi,spec}$). This would ensure that the unrecovered strain is minimal or close to zero at conditions of temperature $<(T_{hi,spec})$ and frequency of loading $>(\omega_{spec})$.

Introconversion of Dynamic Data and Flexural Creep Data

An equation for the approximate introconversion of dynamic mechanical data to creep compliance was proposed more than 30 years ago by polymer scientists as follows [5]:

$$J(t) \approx J'(\omega) + 0.4\,J''(0.4) - 0.014\,J''(10\omega) \qquad t \rightarrow 1/\omega \quad (20)$$

where; J(t) = creep compliance at time t (1/Pa), J'(ω) = storage compliance at frequency ω (1/Pa), J''(0.40) = loss compliance at frequency 0.40 (1/Pa), J''(10ω) = loss compliance at frequency 10ω (1/Pa).Eq. 24 isquite accurate but requires data at 3 specific frequencies (ω, 0.4ω, and 10ω) for the computation of creep compliance. As an alternative, an empirical equation was developed by Anderson A., which agrees with the approximation of Eq. 20to within 3% for paving grade bitumens at low to intermediate temperatures, with the following form[1]:

$$S(t) = \frac{1}{J(t)} \approx \frac{3G^*(\omega)}{[1 + 0.2\sin(2\delta)]} \qquad t \rightarrow 1/\omega \quad (21)$$

where; S(t) = creep stiffness at time t (Pa), J(t) = extensional creep compliance at time t (1/Pa), G*(ω) = complex modulus at frequency ω (Pa), and δ = phase angle at frequency ω (degrees).Eq. 21 is in terms of creep stiffness, which is the inverse of the extensional creep compliance and hence, the factor of 3 in converting from shear to extensional modulus. Because of the empirical nature of Eq. 21, it is not recommended for use when G* is < 10^5 Pa [1], especially for modified binders, without further verification.

Comparison of Binder Characterisation Relations

Fig. 2 shows a comparison between three binder characterisation equations having different origins, all relating unrecovered to recovered compliance. The 1st relation, based on first principles, is the (dissipated : stored energy) ratio as described earlier in Eq. 5. The 2nd relation is the unrecovered to recovered compliance (J_{unr}/J_{rec}) in accordance with the [6]treatment, which is obtained by dividing Eq. 17 by Eq. 12. The 3rd empirical relation is based on the analysis ofAnderson A. [1], (relation obtained by dividing the creep compliance J(t) as shown earlier in Eq. 21 by the storage compliance J' = cosδ/G*).

The data shown in Figs.2&3 were obtained from DSR frequency sweeps (0.01 to 80 Hz) conducted at 20°C and 40°C, respectively, on a 40/50 pen grade unmodified bitumen. Bearing in mind that the empirical nature of Anderson's Eq. 21 was not verified for use when G* is less than (≈ 10^5 Pa), it is interesting to note from Fig. 2 that at 20°C (where almost all the G* values are > 10^5 Pa) there is progressively close agreement between Anderson's equation and the fundamental dissipated/stored energy relation as frequency (and hence G*) values increase. As discussed earlier, the Shenoy[6] equation only allows treatment of data when the phase angle exceeds 52° and hence the truncated set of data points shown (red symbols) in Fig. 2. At 40°C, where creep is expected to become more problematic, there appears to be much better agreement between the Shenoy and Anderson's relations at frequency values less than 1 Hz (G* < 40 kPa).

Fig. 4 compares the three relationships using 40/50 pen bitumen against an SBS modified binder at 40°C. The effect of polymer modification on dramatically reducing the ratio of creep to elastic response is most strikingly demonstrated by the SBS lines (lower 3 lines in Fig.4). Using any of the three aforementioned relationships, a clear improvement in creep performance is readily predicted. Ranking the three analysis methods, it appears that with enhanced elasticity due to polymer modification, the Shenoy equations are the most sensitive at high temperature / low G* conditions.

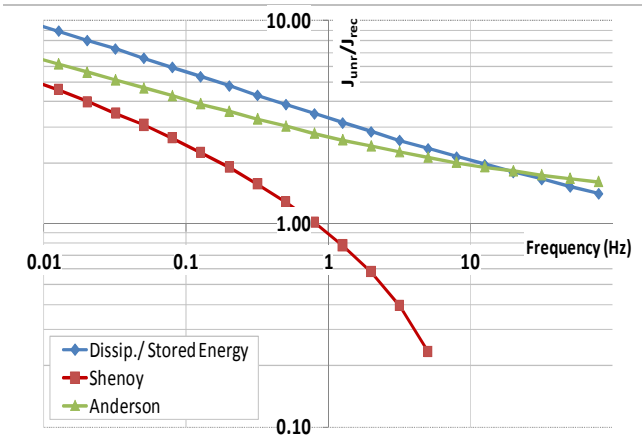


Figure 2: Comparison of the 3 binder characterisation relations on a 40/50 pen at 20°C

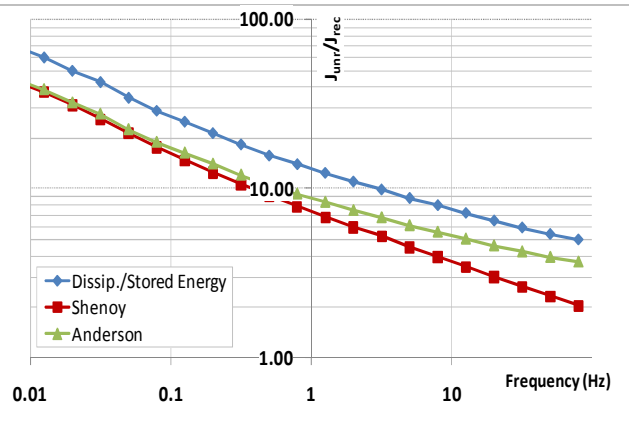


Figure 3: Comparison of the 3 binder characterisation relations on a 40/50 pen at 40°C

Overall, for unmodified bitumens, the Anderson's empirical (J(t)/J') relation fits very well with the fundamental (dissipated/stored) energy relation in particular at lower temperatures (e.g. G* values in excess of about 5 MPa), and fits very well with the Shenoy relation at higher temperatures (G* < 10^5) values. The use of the relation (creep/elastic response) [6] is restricted to phase angles in excess of 52°, but has proved itself to be most sensitive to the effect of elastomer modification at high temperatures (low G* values). By combining the Shenoy [6] & Anderson's [1] treatments it is possible to adequately assess the creep response of a binder (including polymer modified bitumens) over a wide range of G* and temperature regimes.

Adopting any of the 3 relationships described above for characterising bitumen performance in creep mode can be considered an improvement on the SHRP criteria of simply maximising G*/sinδ (see Eq. 2). As a crude illustration, Fig. 5 compares the G*/sinδ criteria to the (dissipated/stored

energy) criteria by assessing the sensitivity to variation in loading frequency at 40°C. The inverse of the G*/sinδ (which at a particular stress level, is defined by SHRP as the energy dissipated per cycle) was multiplied by a constant to allow direct visual comparison with the (dissipated/stored energy) equation. The slopes of the lines clearly demonstrate that the G*/sinδ criteria is far too sensitive to frequency and is incapable of significantly differentiating between the pen. grade and the polymer modified bitumens, in particular at the lower frequency end where creep becomes more critical.

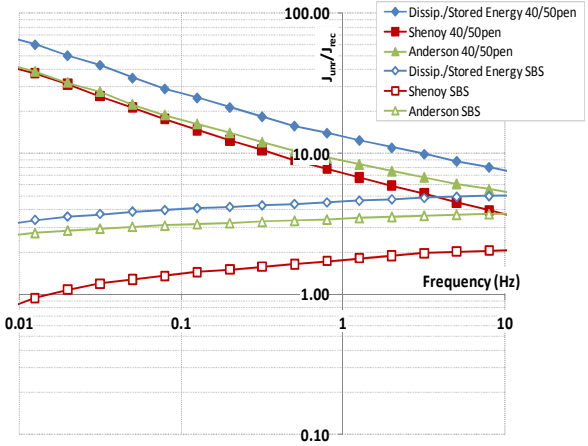


Figure 4: Comparison of the 3 binder characterisation relations at 40°C. Upper 3 data sets = 40-50 pen bitumen, lower 3 data sets = SBS modified binder.

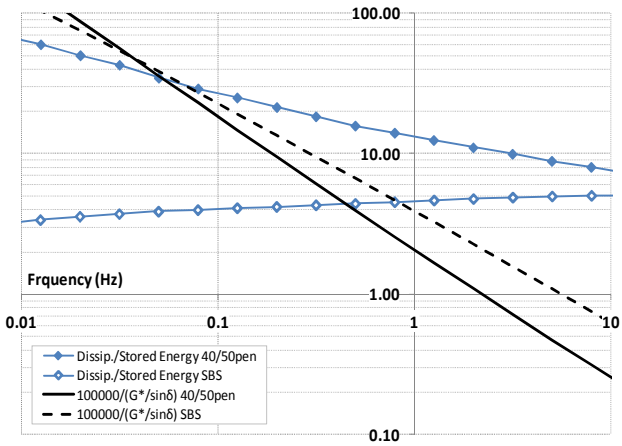


Figure 5: Comparison the frequency sensitivity of the (G*/sinδ) SHRP relationship to a more fundamental (dissipated/stored energy) ratio at 40°C.

Summary

The specification parameter $|G^*|/\sin\delta$ for high temperature performance grading of paving bitumens has not been found to be adequate in rating various binders, especially some polymer-modified ones (PMBs), for their rutting resistance. In the SHRP specifications, bitumen rutting is assumed to be stress-controlled cyclic loading phenomenon and in order to control rutting, the energy dissipated per cycle should be minimized by maximizing the value of G*/sinδ. Unfortunately G*/sinδ cannot distinguish between total energy dissipated and energy dissipated in permanent flow and hence cannot capture the recovery component.

Starting from the equation of energy dissipated per cycle, i.e. $(W_d = \pi \times \sigma_0 \times \varepsilon \times \sin\delta)$, it was shown that the maximum energy stored by the in-phase component occurs at the quarter-cycle point. Tobypass the SHRP requirement for pre-defining a stress or strain-controlled loading regime, the relative dissipated to stored energy at the quarter-cycle point was then related to the phase angle as follows; $(0.5\pi \tan\delta)$.This fundamental ratio was subsequently compared to two otherpublished bitumen performance characterisation equationsalso relating unrecovered to recovered compliance(J_{unr}/J_{rec}) but having different origins.

The firstempirical relation (obtained by dividing the creep compliance $J(t) = [1 + 0.2\sin(2\delta)]/3G^*$ by the storage compliance J'was based on the analysis of Anderson [1]. The second relation, published by Shenoy[6] (obtained by dividing $(\sigma_0/G^*) \times (1 - 1/(\tan\delta \sin\delta))$ by G'/G''^2 .In comparison with the SHRP G*/sinδ rutting criteria, all the alternative relationships proposed in this paper gave greatly improved bitumen creep characterisation capabilities, in particular their ability to differentiate between penetration grade and PMBs.

References

[1] Anderson D.A., Christensen D.W., Bahia H.U., Dongre R., Sharma M.G., Antle C.E.(1994), Strategic Highway Research Program, SHRP-A-369, "Binder Characterization and Evaluation, Volume 3: Physical Characterization, Chapter 1: Linear Viscoelastic Model", ISBN 0-309-05767-1.

[2] Ballie M., Chailleux E., Dumas P., Eckmann B., Leroux C., Lombardi B., Planche J-P., Such C., Vaniscote J-C(2008), "Characteristics of bituminous binders and their consequences on the mechanical performance of asphalts", 4thEurasphalt&Eurobitume Congress, Copenhagen, paper no. 402-108.

[3] Carswell J., Claxton M.J., Green P.J. (2000), "The classification of bitumens and polymer modified bitumens within the SHRP performance grading system", 2ndEurasphalt&Eurobitume Congress, Barcelona, Book 1, pp. 100-110.

[4] Chen J.S. and Tsai C.J. (1999), "How good are linear viscoelastic properties of asphalt binder to predict rutting and fatigue cracking?", Journal of Materials Engineering and Performance, Vol. 8 (4), pp. 443-449.

[5] Nielsen L.E., "Mechanical Properties of Polymers and Composites, Vol. 1"(1974), ISBN 0 8247 6183 9.

[6] Shenoy A. (2001), "Refinement of the Superpave specification parameter for performance grading of asphalt", Journal of Transportation Engineering, Vol. 127, pp. 357-362.

Applied Mechanics and Materials Vol. 567 (2014) pp 763-768
© (2014) Trans Tech Publications, Switzerland
doi:10.4028/www.scientific.net/AMM.567.763

Time-Space Geography: A Creditable Transport Accessibility Measure for Rural Dwellers

Mir Aftab Hussain Talpur[1,a], Madzlan Napiah[2,b], Irfan Ahmed[3,c], Imtiaz Ahmed[4,d] and Shabir Hussain[5,e]

[1,2,3,4,5]Departmment of Civil Engineering, Universiti Teknologi PETRONAS, Malaysia

[a]aftab_g01903@utp.edu.my, [b]madzlan_napiah@petronas.com.my, [c]irfan.am_g02556@utp.edu.my, [d]imtiazutp@gmail.com, [e]shkhahro@gmail.com

Keywords: Time, Rural inhabitants, Time-space prism, Inaccessibility, Rural population, Travel patterns, Policy makers

Abstract. Time is considered as an important element for rural inhabitants to access different essential activities efficiently. A time-space prism is a tool through which inaccessibility problems of the rural population can be resolved. Hence, the motive of this research is to examine the travel patterns, and to develop a time-space prism for the local population of the study area. The time-space prism was developed from the data, which were collected from the sampled households with the help of a questionnaire survey. This research found that transportation facilities in rural sub-regions could reduce the travel time of people, which could enhance their capability of accessing routine activities within the available time. The accessibility standards can be improved in this way, which can put the positive impacts on the sub-regional economy.

Introduction

In terms of transportation planning, accessibility is defined as, *"people's ability to access divergent destinations with ease and comfort"* [1-3]. There are various approaches available to measure the accessibility, like Handy and Niemeier [4]; Halden et al. [5]; Baradaran and Ramjerdi [6]; Geurs and van Eck [7]; Geurs and van Wee [8] and Vandenbulcke et al. [9], but the orthodox accessibility measure includes Hansen [10] and the time-space geography of Hägerstrand [11]. Considering the person-based approach, Hägerstrand introduced the time-geography and time-space based on persons travel scenarios and routine works, which was further discussed by Neutens et al. [12]; Winter and Yin [13] and Sui [14]. The time and space constraints graphically symbolize the time-space autonomy of that person as shown in the shaded region of Fig. 1.

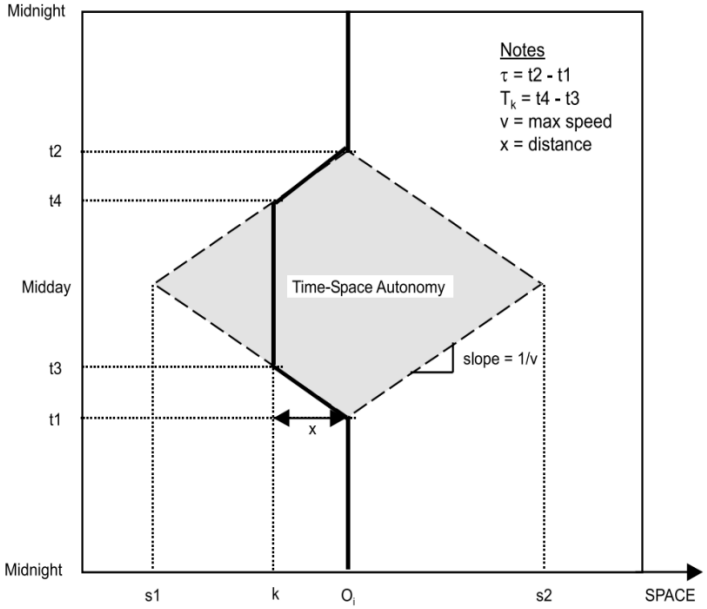


Figure 1. Time-space prism of rural inhabitants [15]

Fig. 1 shows a time-space diagram of a person, who works at location (k) together with time constraints of (t1) and (t2) [15]. The ability of a person to participate in different activities is concerned with the time-space prism, and depended on the spatial and temporal distribution of activities. Like, if an individual chooses to work at location (k) from time (t3) to (t4), the space trajectory can be seen in the dark black solid line (see Fig. 1). A time-space prism is defined as, *"a geographic area in which an individual can perform different activities"*. Time-space geography calculates the individual's possibilities in terms of performing various activities despite constraints. This method is helpful and much useful in solving the accessibility-related problems of the sparsely located rural population. Therefore, this method was selected to solve the accessibility problems of the rural population. The purpose of this study is to analyze travel patterns and different activities of rural households with constraints and develop a time-space prism. This step would help in understanding the different temporal accessibility constraints of the rural population of the study area. The different accessibility constraints then can be resolved by implementing transportation policy proposals accordingly.

Material and Methods

The sub-region of Badin was chosen for this study, which is considered as one of the most deprived sub-region of Pakistan [16, 17]. This sub-region is positioned between 24° 13' and 25° 12' north latitudes, and 68° 21' and 69° 20' east longitudes. To satisfy the objectives of the study, the data were collected through a questionnaire survey, interviews from household heads, field visits and personal observations [18]. The total number of 100 sampled household heads with the help of 100 questionnaires was interviewed. This sample size was selected to satisfy with the standard sampling procedures, i.e. 10% of the total population [19]. Then, cluster-sampling methodologies were devised to choose the lower-income group, which was the target of the study. The basic time-space prism was drawn based on real-time data (see Fig. 2), which were collected from the study area. Whereas, the improved time-space prism was also delineated, this was based on a high average commuting speed of rural households. To develop basic and improved prisms for the study area, the values of their angles (θ_1) and (θ_2) were determined with the help of following trigonometric expression:

$$\theta = \tan^{-1} [\text{time/distance}] \quad (1)$$

Where,
θ = Prism's Angles or Slopes
time = Average Travel Time of Rural Households to their Workplaces
distance = Average Travel Distance of Rural Households to their Workplaces

Analysis of Regional Trip Data. This analysis was carried out to examine the ability of rural households in relation to their daily routine trips. The two aspects were highlighted during the data collection, i.e. the household and trip characteristics. The household aspect included household income, household size and vehicle ownership. While, the trip information included the number of trips, duration, distance, purpose and travel mode. The variables examined from the household data are regional household income (hhi) in Pakistan Rupees (PRs); regional household size (hs); regional trip purpose (tp) and regional travel mode (tm).

These two aspects, which were considered during the data collection process, actually helped in understanding the travel behavior of the study area's population with constraints. Consequently, the collected data highlighted household trip characteristics together with trip distance and time. Afterwards, the prism angles were determined with the help of a trigonometric formula (see Equation 1) by using trip distance and time data.

Results and Discussion

The regional trip purposes were divided into eleven clauses, i.e. *Market/Shopping, Market/Shopping/Health, Market/Health, Education, Market, Health, Office, Recreation, Market/Recreation, Shopping* and *Work*. The regional travel mode was categorized into seven different groups, i.e. *Walk, Bicycle, Tractor-Trolley, Motorcycle, Private Car/Jeep, Rent Car/Jeep* and *Bus*.

The legends as used in Tables 1 and 2 are described *as (0 for Walk; 1 for Animal Cart; 2 for Cycle; 3 for Tractor-Trolley; 4 for Motorcycle; 5 for Private Car/Jeep; 6 for Rental Car/Jeep and 7 for Bus)*. Tables 1 shows information about the sub-regional trip distribution of the rural population; whereas, Table 2 highlights the average distance to workplaces.

Table 1. Rural Regional Trips Distribution

Regional Travel Mode	CLASSIFICATION OF REGIONAL TRIPS						Total Trips with Different Modes
	Regional Household Vehicle Ownership						
	0	1	2	3	4	5	
0	25	3	--	--	15	5	48
2	--	--	2	--	--	--	2
3	--	--	--	3	--	--	03
4	10	--	--	--	2	--	12
5	03	--	--	--	--	2	5
6	03	--	--	--	--	--	3
7	20	--	2	--	03	02	27
Total	61	3	4	3	20	09	100

It is palpable from Table 1 that 61% population has no vehicle ownership, and they have used different travel modes to reach their destinations. Approximately, 48% of the population used to walk to reach their relevant workplaces and left over 52% used other modes of travel.

The average distance was also calculated for regional household's trips using different travel modes as described in the Table 1. The average distance to reach workplaces is given in the Table 2.

Table 2. Average Distance to Workplaces

Regional Travel Mode	AVERAGE DISTANCE TO WORK (kms)						Average Distance with Different Modes
	Regional Household Vehicle Ownership						
	0	1	2	3	4	5	
0	0.85	0.76	--	--	0.78	0.34	0.68
2	--	--	2	--	--	--	2
3	--	--	--	8.3	--	--	8.3
4	13.50	--	--	--	11	--	12.25
5	216.66	--	--	--	--	250	233.33
6	55	--	--	--	--	--	55
7	13.05	--	15	--	22.33	9	14.84
All Modes	59.81	0.76	8.5	8.3	11.37	86.44	29.19

From Table 2, it is further illustrated that people used to walk around 0.85 km to perform their routine works, who also do not have any vehicle ownership. Households, who have no vehicle ownership traveled up to average 59.81 km to reach their respective workplaces using different transport modes. Average 0.68 km rural people of study area walked to reach their destinations, who have vehicle ownership as well.

Table 3 bestows information about an average travel time to workplaces using the modes and distances as described in Tables 1 and 2 respectively.

Table 3. Average Travel Time to Workplaces

Regional Travel Mode	AVERAGE TRAVEL TIME TO WORK (mins)						Average Time with Different Modes
	Regional Household Vehicle Ownership						
	0	1	2	3	4	5	
0	41.36	38.33	--	--	42.33	22	36
2	--	--	27.5	--	--	--	27.5
3	--	--	--	63.33	--	--	63.33
4	33	--	--	--	35	--	34
5	140	--	--	--	--	165	152.5
6	55	--	--	--	--	--	55
7	44.5	--	50	--	60	55	52.37
All Modes	62.77	38.33	38.75	63.33	45.77	80.66	54.93

Regional households without personal vehicles and by using mode *'Walk'* took time of about 41.36 minutes to reach their workplaces (see Table 3). Nevertheless, same when uses other transport modes, the average time is about 62.77 minutes depending on the traveling distance. Households with the vehicle ownership (e.g. car/jeep) used to walk for 22 minutes to reach their destinations. These households drove their personal vehicles for long-distance and took one hour sixty-five minutes. For a short distance, rural households took fifty-five minutes through *'Bus'* to reach their respective workplaces.

Improving Time-space Prism (TSP). Rural households can improve their TSP, if they would be able to reach their respective destinations in minimum time. The angles of TSP were identified based on the maximum speed of journeys, which were traveled by rural households. The basic and improved TSPs of the rural inhabitants were delineated as shown in Fig. 2.

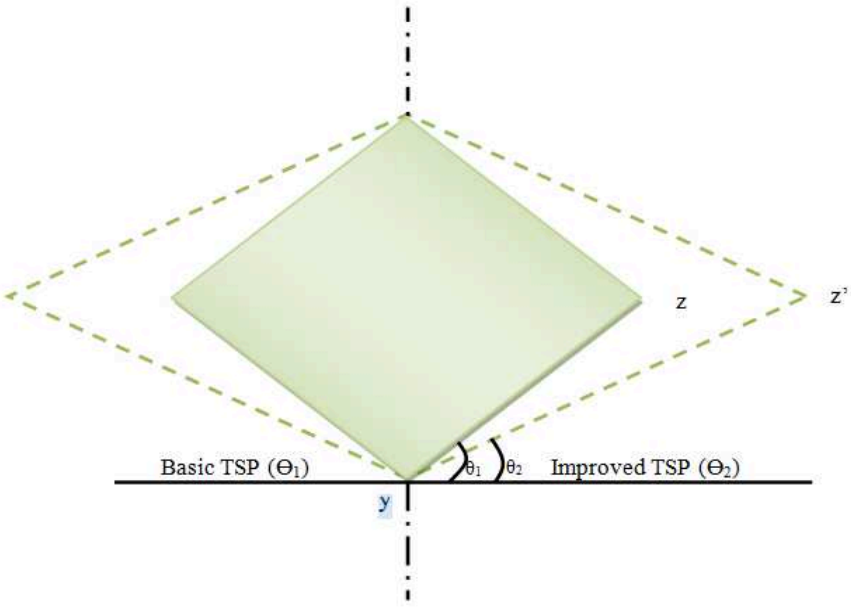


Figure 2. Basic and improved TSPs

The angle (θ_1) was drawn by keeping in view regional household vehicle ownership, who used the same travel mode for their destinations. This angle can be further explained by the travel speed, which rural households traveled according to their vehicle ownership. This TSP of rural households is called a basic TSP.

Table 4 depicts the computed angles of basic and improved TSPs, which were found out with the help of pre-defined trigonometric function (see Equation 1).

Table 4. TSP's Basic and Improved Values

Regional Travel Mode	BASIC AND IMPROVED ANGLES (DEGREES) Regional Household Vehicle Ownership						Average Degrees with Different Modes
	0	1	2	3	4	5	
0	**88.82**	--	--	--	--	--	88.82
2	--	--	**85.84**	--	--	--	85.84
3	--	--	--	**82.53**	--	--	82.53
4	67.75	--	--	--	**72.55**	--	70.15
5	32.86	--	--	--	--	**33.42**	33.14
6	45.00	--	--	--	--	--	45.00
7	73.65	--	73.30	--	69.58	--	72.17
All Modes	*61.61*	--	*79.57*	*82.53*	*71.06*	*33.42*	65.63

Table 4 confirms the results of (θ) by taking the values of Tables 2 and 3, i.e. the average household distances and time. The bold diagonal values are actually the values of a basic TSP; whereas, the shaded values represent the improved values of the TSP in a row *"All Modes"*. This table also depicts that rural individuals can improve their accessibility criterion by using the different transport modes available to them. Persons, who used to walk to their workplaces and have no vehicle ownership, possessed the highest degree of 88.82. Further, by using available transport modes, they can improve it to 61.61 degrees. At the same time, the rural individuals, who have bicycles, can improve their TSP up to 79.57 degrees. However, it should be noted that rural individuals traveling through transport modes (e.g. car or tractor-trolley) could not improve their TSP. This is a result of the maximum use of their TSP. This is further elaborated that rural individuals, who have some sort of vehicle ownership, either would improve their TSP or would remain at their basic level.

Conclusion

Time is too important to perform daily routine activities in a rural environment, where essential work sites and markets are sparsely located. This is a basic element, which hindered the rural population in performing their jobs in time. The rural people faced difficulties to perform their routine activities, and become stagnant because of the shortage of time and unavailability of transport services. TSP technique was implemented in this study as the rural population of the study area could manage their time schedule and perform their activities in a satisfactory manner. The goal of the study was achieved, and TSP was developed together with the analysis of rural regional travel patterns. The results and scrutiny of this research can assist decision-makers to incorporate policies accordingly, to curb the accessibility and related issues of rural inhabitants. On one hand, this study could help the deprived population of the study area to stand on their feet. On the other, this research could remarkably upgrade the living standards of rural citizens of the developing countries.

Acknowledgements

The authors are grateful to the Department of Civil Engineering, Universiti Teknologi PETRONAS, Malaysia for its support and for the provision of suitable research environment and facilities.

References

[1] C. Curtis, "Planning for sustainable accessibility: The implementation challenge," *Transport Policy,* vol. 15, pp. 104-112, 2008.

[2] R. Vickerman, "Location, accessibility and regional development: the appraisal of trans-European networks," *Transport Policy,* vol. 2, pp. 225-234, 1995.

[3] M. A. H. Talpur, M. Napiah, I. A. Chandio, and S. H. Khahro, "Research Framework Focusing Transportation Accessibility Planning, Computer Based Modeling and Transportation Policy Outlines for Remote Regions of Developing World," *Research Journal of Environmental and Earth Sciences,* vol. 5, pp. 32-40, 2013.

[4] S. L. Handy and D. A. Niemeier, "Measuring accessibility: an exploration of issues and alternatives," *Environment and Planning A,* vol. 29, pp. 1175-1194, 1997.

[5] D. Halden, "Using accessibility measures to integrate land use and transport policy in Edinburgh and the Lothians," *Transport Policy,* vol. 9, pp. 313-324, 2002.

[6] S. Baradaran and F. Ramjerdi, "Performance of accessibility measures in Europe," *Journal of Transportation Statistics,* vol. 4 (2/3), 2001.

[7] K. Geurs and V. E. Ritsema, "Accessibility measures: review and applications. Evaluation of accessibility impacts of land-use transportation scenarios, and related social and economic impact," National Institute of Public Health and the Environment, 2001.

[8] K. T. Geurs and B. Van Wee, "Accessibility evaluation of land-use and transport strategies: review and research directions," *Journal of Transport Geography,* vol. 12, pp. 127-140, 2004.

[9] G. Vandenbulcke, T. Steenberghen, and I. Thomas, "Mapping accessibility in Belgium: a tool for land-use and transport planning?," *Journal of Transport Geography,* vol. 17, pp. 39-53, 2009.

[10] W. G. Hansen, "How Accessibility Shapes Land Use," *Journal of the American Institute of Planners,* vol. 35, pp. 73-76, 1959.

[11] T. Hägerstrand, "What about people in Regional Science?," *Papers in Regional Science,* vol. 24, pp. 6-21, 1970.

[12] T. Neutens, F. Witlox, and P. Demaeyer, "Individual accessibility and travel possibilities: A literature review on time geography," *European Journal of Transport and Infrastructure Research (EJTIR),* vol. 7 (4), pp. 335-352, 2007.

[13] S. Winter and Z.-C. Yin, "The elements of probabilistic time geography," *GeoInformatica,* vol. 15, pp. 417-434, 2011.

[14] D. Sui, "Looking through Hägerstrand's dual vistas: towards a unifying framework for time geography," *Journal of Transport Geography,* vol. 23, pp. 5-16, 2012.

[15] J. B. Odoki, H. R. Kerali, and F. Santorini, "An integrated model for quantifying accessibility-benefits in developing countries," *Transportation Research Part A: Policy and Practice,* vol. 35, pp. 601-623, 2001.

[16] "Badin " Bureau of Statistics, Government of Pakistan, Islamabad, 1998.

[17] "District Vision Badin (A Framework for Sustainable Development)," ed: International Union for Conservation of Nature and Natural Resources. The World Conservation Union (IUCN), Pakistan, Sindh Programme Office,1-Bath Island Road,Karachi-75530, 2006, p. 134.

[18] D. Akerele, S. Momoh, S. A. Adewuyi, B. B. Phillip, and O. F. Ashaolu, "Socioeconomic determinants of poverty among urban households in South-West Nigeria," *International Journal of Social Economics,* vol. 39 (3), pp. 68-181, 2012.

[19] A. Turner, I. Yansaneh, M. Jambwa, J. Banda, C. Menozzi, B. Kassa, and P. Benjamin, "Designing Household Survey Samples: Practical Guidelines," United Nations, Newyork, 2008.

Applied Mechanics and Materials Vol. 567 (2014) pp 769-774
© (2014) Trans Tech Publications, Switzerland
doi:10.4028/www.scientific.net/AMM.567.769

Application of Geographic Information System (GIS) and Analytic Network Process (ANP) for sustainable tourism planning in Cameron Highlands, Malaysia

Mansir Aminu[1,a], Abdul-Nassir Matori[1,b], Khamaruzaman Wan Yusof[1,c] and Rosilawati Binti Zainol[2,d]

[1]Civil Engineering Department, Universiti Teknologi PETRONAS, Seri Iskandar, 31750 Tronoh, Perak Darul Ridzuan, Malaysia.

[2]Department of Urban and Regional Planning, University of Malaya, 50603 Kuala Lumpur, Malaysia.

[a]mansiraminu@yahoo.com, [b]nasrat@petronas.com.my, [c]khamaruzaman.yusof@petronas.com.my, [d]rosilawatizai@um.edu.my

Keywords: Conservation; tourism, sustainable development, Analytic Network Process, Geographic Information System.

Abstract. This paper discusses an approach based on an integrated use of GIS and ANP for sustainable tourism planning of Cameron Highlands, Malaysia. ANP was utilized to evaluate the relative priorities for the sustainable tourism development of the highland based on chosen criteria and indicators (elements). Pair wise comparison technique was used in order to evaluate possible alternatives from different perspectives. Having derived the weights from the pairwise comparison method, unweighted supermatrix, weighted supermatrix and the limit supermatrix were then computed. The limit supermatrix was normalized to derive the priorities; the result was then transferred into GIS framework. Elements evaluated and ranked are represented by criterion maps. The criterion maps were evaluated by reclassifying the data layers, to represent different needs for the sustainable tourism development of the highland. Spatial models reflecting the views of experts involved were aggregated using the weighted sum method of GIS. Subsequently sustainable tourism development model was generated, which will ensure that future generations benefit from the natural endowments of Cameron Highlands.

1. Introduction

Tourism is a sector that has increasingly identified the natural environment as a crucial attraction of many destinations and one that can be utilized as important resource product [1]; [2]. Increased environmental awareness in the 1980s resulted in the reassessment of the role of tourism and an increased recognition of its adverse effects [3]; [4]; [5]. Even though it is acknowledged that tourism contributes to environmental deterioration of natural areas and can be self-destructive [6]; [7], there is also acknowledgement of tourism's potential to lead to significant improvement of the environment as well as economic benefits [8]; [9].

Sustainable tourism can be a major tool for the conservation of natural areas and for raising the environmental awareness of residents and visitors. Such form of tourism conserves both natural and cultural assets; it guarantees the protection of nature and indigenous cultures. Sustainable tourism provides mechanisms to preserve threatened areas that could protect wildlife [10]. Sustainable tourism planning is enhanced by applying a tool like Geographic Information System (GIS). GIS is a useful instrument to environmental managers in identifying localities that need immediate attention, and allow the experimentation of these areas with various management approaches, without risking them in experimentation. GIS data can be used to identify conflicts, examine impacts and support a decision-making process.

GIS is further strengthened by its capability of working along with Analytic Network Process (ANP) of Multi Criteria Evaluation (MCE). ANP of MCE can help the decision makers to translate environmental, economic and social issues into manageable units of information. ANP has the

capability to evaluate physical processes such as biodiversity conservation and development using expert opinion to make the best selection among the variables under consideration. All this could further facilitate and offer more tools to sustainable tourism planning and decision-making.

An early application of GIS in tourism planning is provided by [11] in Virgin Islands, United states of America (USA). He used three models to define conservation areas, ecological research areas, and areas of residential and recreational development while, he then used a fourth model for the resolution of conflict among competing uses. Reference [12] used multi-criteria evaluation method and GIS as a practical instrument to evaluate the suitability of Guilan Province coast of Iran for sustainable tourism destinations using Analytical Hierarchy Process (AHP) and GIS. Similarly, [13] discussed the use of GIS in identifying ecotourism suitable areas in Northern Ontario, Canada. Reference [14] utilized GIS to determine suitable areas for tourism development at Lombok Island of Indonesia. Reference [15] came up with a GIS based decision support system for sound spatial planning for tourism in Mauritius. Reference [16] used GIS and AHP to identify and prioritize potential ecotourism sites in SuratThani Province, Thailand.

Reference [17] used a GIS-based spatial decision support system (SDSS) to help visitors of Great Smoky Mountains National Park of the United States of America choose and plan their activities more effectively to match their personal preferences and constraints. Reference [18] used a Regional Tourism Planning Spatial Decision Support System in order to analyze, evaluate, predict and optimize tourism planning of Anhui Province, China.

Looking at the previous studies in the area of research a number of them only centered on identifying potentials of tourism destinationswith regard to tourism development, without focus on the protection of such destinations from tourism and other forms of developmental activities. Furthermore, some of the previous researches have only used GIS without any decision support system like Multi Criteria Evaluation (MCE); however, some studies have made an attempt to close this gap by utilizing an aspect of MCE which is Analytic Hierarchy Process (AHP) in dealing with tourism issues. Though, AHP has been condemned to be inadequate for complex decisions like sustainable tourism. AHP regards elements as independent of other elements, which rarely occurs in real life situation. Therefore the technique has been widely criticized [19].The aim of this study therefore is to plan for sustainable tourism development in Cameron Highlands, Malaysia using spatial modeling techniques of GIS and ANP.

2. Material and methods

2.1 Study area

Cameron Highlands is a hill station situated on the main mountain range of Peninsular Malaysia. It is located at Pahang state. Its geographical coordinates are 4° 19' 16"-4° 37' 6" North, 101° 19' 59"-101° 36' 35" East. The highland lies at an altitude of 1,829 meters. Its land area is 712 square kilometers. During the day, the temperature of the highland rarely rises above 25 °C; at night, the temperature can sometimes drop to as low as 9 °C.

2.2Material

The study involves field visit of the study site with regard to spatial data capture as well as questionnaire administration and interview. It also involved the use of satellite image and conventional maps. Data extraction was performed on the satellite image in order to generate part of the vector data. Conventional maps were digitized into a GIS compatible format. Global Positioning System (GPS) was used to capture points of interest. Another set of digital data was sourced from various government departments such as the department of surveying and mapping Malaysia, Malaysia center for remote sensing, department of wildlife and national parks and other relevant agencies. The data collected was processed using GIS.

For the relative priorities from expert opinion; it was obtained using a questionnaire survey. In this study, the questionnaires were distributed to experts and follow up interviews were conducted in some instances, to make sure the respondents understood the contents of the questionnaire, due to the complex nature of the method under consideration. The priorities were computed using ANP.

2.3Methods

2.3.1. Analytic Network Process (ANP) and priority weighting

ANP is a generalized form of AHP in multi-criteria evaluation. The model is represented by a network structure; which indicates all dependences among varying clusters and determining the direction of influences. ANP model can set connections among elements within a cluster. Connection can also be set between elements in different clusters (i.e., outer dependence). The modeling process is divided into four steps as follows;

2.3.1.1.Pairwise comparison and relative weight estimation

ANP uses pair-wise comparison in the determination of relative weights as in the standard AHP. Here pairwise comparisons of the elements in each level are conducted with respect to their control criterion. Reference [20] recommended a scale of 1–9 when comparing two elements.

2.3.1.2. Formation of unweighted super-matrix

The unweighted supermatrix contains all the pairwise comparisons made throughout the network.

2.3.1.3 .Formation of weighted super-matrix

The weighted supermatrix is derived by using cluster weight in multiplying all the corresponding elements in a component of the unweighted supermatrix.

2.3.1.4 .Calculation of global priority vectors and weights

The limit super-matrix is obtained by raising the weighted super-matrix to powers by multiplying it times itself. The limit matrix is reached when the column of numbers is the same for every column; the matrix multiplication process is stopped in order to obtain the priorities.

2.3.2 GIS based evaluation and analysis of sustainable tourism development criteria

Criterion maps were evaluated and analyzed using spatial analyst tools, such as distance operators, view-shed, interpolation, conversion and reclassification functions. Other spatial analyst tools used in the study includes times function, extract by mask, and mosaic functions. Finally, weighted sum overlay was used to compute the priorities derived from ANP.

3. Results and discussion

The unweighted super-matrix was computed by using the results of all pairwise comparisons made throughout the network(Table 1). Afterwards the weighted super matrix was obtained by multiplying all the elements in a component of the unweighted supermatrix by the corresponding cluster weight. (Table 2) and the limit super-matrix was generated by raising the weighted super-matrix to powers until it converges (Table 3); and limit matrix was normalized to obtain the priorities (Table 4).The relative weights obtained from ANP analysis were assigned to the factor raster layers created. The ANP computations were developed in the super decisions software version 2.0.8 and results transferred into GIS environment, with the aid of ArcGIS software version 9.3.

Table 1: Unweighted supermatrix

		Accessibility		Cultural heritage		Eco-system diversity						Wildlife		
Cluster (Criteria)	**Nodes (Sub-criteria)**	PM	PE	AS	CG	EL	VS	WQ	SL	OS	FR	SH	RF	EF
Accessibility	1. Proximity from main road (PM)	0.0000	0.0000	0.1667	0.0000	0.2500	0.2500	0.1667	0.0000	0.2500	0.1667	0.1667	0.1667	0.2500
	2. Proximity to eco-trail (PE)	0.0000	0.0000	0.8333	0.0000	0.7500	0.7500	0.8333	0.0000	0.7500	0.8333	0.8333	0.8333	0.7500
Cultural heritage	1. Aboriginal settlement (AS)	0.9000	0.9000	0.0000	0.0000	0.9000	0.9000	0.9000	0.0000	0.9000	0.9000	0.9000	0.9000	0.9000
	2. Cultural ground (CG)	0.1000	0.1000	0.0000	0.0000	0.1000	0.1000	0.1000	0.0000	0.1000	0.1000	0.1000	0.1000	0.1000
Eco-system diversity	1. Elevation (EL)	0.5415	0.0000	0.0000	0.0000	0.0000	0.0000	0.0000	0.0000	0.0000	0.1000	0.1167	0.0825	0.1003
	2. Viewshed (VS)	0.2899	0.0000	0.0000	0.0000	0.0000	0.0000	0.0000	0.0000	0.0000	0.0000	0.0000	0.0583	0.0706
	3. Water quality (river) (WQ)	0.1050	0.7500	0.0000	0.0000	0.0000	0.7500	0.0000	0.0000	0.5000	0.0000	0.0685	0.1167	0.0829
	4. Slope (SL)	0.0000	0.0000	0.2911	0.0000	0.0000	0.0000	0.0000	0.0000	0.0000	0.9000	0.7462	0.7425	0.7462
	5. Open space (OS)	0.0636	0.2500	0.1522	0.0000	0.7500	0.2500	0.7500	0.0000	0.0000	0.0000	0.0000	0.0000	0.0000
	6. Forest reserve (FR)	0.0000	0.0000	0.5567	0.0000	0.2500	0.0000	0.2500	0.0000	0.5000	0.0000	0.0685	0.0000	0.0000
Wildlife	1. Species habitat (SH)	0.0000	0.0000	0.0000	0.0000	0.0000	0.1047	0.0000	0.0000	0.0000	0.0000	0.0000	0.2500	0.1667
	2. Rare flora (RF)	0.5000	0.7500	0.2500	0.0000	0.5000	0.2583	0.5000	0.0000	0.1250	0.5000	0.5000	0.0000	0.8333
	3. Endangered fauna (EF)	0.5000	0.2500	0.7500	0.0000	0.5000	0.6370	0.5000	0.0000	0.8750	0.5000	0.5000	0.7500	0.0000

Table 2: Weighted supermatrix

		Accessibility		Cultural heritage		Eco-system diversity						Wildlife		
Cluster (Criteria)	**Nodes (Sub-criteria)**	PM	PE	AS	CG	EL	VS	WQ	SL	OS	FR	SH	RF	EF
Accessibility	1. Proximity from main road (PM)	0.0000	0.0000	0.0556	0.0000	0.0625	0.0625	0.0417	0.0000	0.0625	0.0417	0.0417	0.0417	0.0625
	2. Proximity to eco-trail (PE)	0.0000	0.0000	0.2778	0.0000	0.1875	0.1875	0.2083	0.0000	0.1875	0.2083	0.2083	0.2083	0.1875
Cultural heritage	1. Aboriginal settlement (AS)	0.3000	0.3000	0.0000	0.0000	0.2250	0.2250	0.2250	0.0000	0.2250	0.2250	0.2250	0.2250	0.2250
	2. Cultural ground (CG)	0.0333	0.0333	0.0000	0.0000	0.0250	0.0250	0.0250	0.0000	0.0250	0.0250	0.0250	0.0250	0.0250
Eco-system diversity	1. Elevation (EL)	0.1805	0.0000	0.0000	0.0000	0.0000	0.0000	0.0000	0.0000	0.0000	0.0250	0.0292	0.0206	0.0251
	2. Viewshed (VS)	0.0966	0.0000	0.0000	0.0000	0.0000	0.0000	0.0000	0.0000	0.0000	0.0000	0.0000	0.0146	0.0176
	3. Water quality (river) (WQ)	0.0350	0.2500	0.0000	0.0000	0.0000	0.1875	0.0000	0.0000	0.1250	0.0000	0.0171	0.0292	0.0207
	4. Slope (SL)	0.0000	0.0000	0.0970	0.0000	0.0000	0.0000	0.0000	0.0000	0.0000	0.2250	0.1866	0.1856	0.1866
	5. Open space (OS)	0.0212	0.0833	0.0507	0.0000	0.1875	0.0625	0.1875	0.0000	0.0000	0.0000	0.0000	0.0000	0.0000
	6. Forest reserve (FR)	0.0000	0.0000	0.1856	0.0000	0.0625	0.0000	0.0625	0.0000	0.1250	0.0000	0.0171	0.0000	0.0000
Wildlife	1. Species habitat (SH)	0.0000	0.0000	0.0000	0.0000	0.0000	0.0262	0.0000	0.0000	0.0000	0.0000	0.0000	0.0625	0.0417
	2. Rare flora (RF)	0.1667	0.2500	0.0833	0.0000	0.1250	0.0646	0.1250	0.0000	0.0313	0.1250	0.1250	0.0000	0.2083
	3. Endangered fauna (EF)	0.1667	0.0833	0.2500	0.0000	0.1250	0.1592	0.1250	0.0000	0.2187	0.1250	0.1250	0.1875	0.0000

Table 3: Limit matrix

		Accessibility		Cultural heritage		Eco-system diversity						Wildlife		
Cluster (Criteria)	**Nodes (Sub-criteria)**	PM	PE	AS	CG	EL	VS	WQ	SL	OS	FR	SH	RF	EF
Accessibility	1. Proximity from main road (PM)	0.0399	0.0399	0.0399	0.0000	0.0399	0.0399	0.0399	0.0000	0.0399	0.0399	0.0399	0.0399	0.0399
	2. Proximity to eco-trail (PE)	0.1692	0.1692	0.1692	0.0000	0.1692	0.1692	0.1692	0.0000	0.1692	0.1692	0.1692	0.1692	0.1692
Cultural heritage	1. Aboriginal settlement (AS)	0.1935	0.1935	0.1935	0.0000	0.1935	0.1935	0.1935	0.0000	0.1935	0.1935	0.1935	0.1935	0.1935
	2. Cultural ground (CG)	0.0215	0.0215	0.0215	0.0000	0.0215	0.0215	0.0215	0.0000	0.0215	0.0215	0.0215	0.0215	0.0215
Eco-system diversity	1. Elevation (EL)	0.0173	0.0173	0.0173	0.0000	0.0173	0.0173	0.0173	0.0000	0.0173	0.0173	0.0173	0.0173	0.0173
	2. Viewshed (VS)	0.0093	0.0093	0.0093	0.0000	0.0093	0.0093	0.0093	0.0000	0.0093	0.0093	0.0093	0.0093	0.0093
	3. Water quality (river) (WQ)	0.0660	0.0660	0.0660	0.0000	0.0660	0.0660	0.0660	0.0000	0.0660	0.0660	0.0660	0.0660	0.0660
	4. Slope (SL)	0.0956	0.0956	0.0956	0.0000	0.0956	0.0956	0.0956	0.0000	0.0956	0.0956	0.0956	0.0956	0.0956
	5. Open space (OS)	0.0464	0.0464	0.0464	0.0000	0.0464	0.0464	0.0464	0.0000	0.0464	0.0464	0.0464	0.0464	0.0464
	6. Forest reserve (FR)	0.0534	0.0534	0.0534	0.0000	0.0534	0.0534	0.0534	0.0000	0.0534	0.0534	0.0534	0.0534	0.0534
Wildlife	1. Species habitat (SH)	0.0162	0.0162	0.0162	0.0000	0.0162	0.0162	0.0162	0.0000	0.0162	0.0162	0.0162	0.0162	0.0162
	2. Rare flora (RF)	0.1309	0.1309	0.1309	0.0000	0.1309	0.1309	0.1309	0.0000	0.1309	0.1309	0.1309	0.1309	0.1309
	3. Endangered fauna (EF)	0.1409	0.1409	0.1409	0.0000	0.1409	0.1409	0.1409	0.0000	0.1409	0.1409	0.1409	0.1409	0.1409

Table 4: Priorities

Clusters (Criteria)	Nodes (Sub -criteria)	Limiting
Accessibility	1. Proximity from main road (PM)	0.0399
	2. Proximity to eco-trail (PE)	0.1692
Cultural heritage	1. Aboriginal settlement (AS)	0.1935
	2. Cultural ground (CG)	0.0215
Eco-system diversity	1. Elevation (EL)	0.0173
	2. Viewshed (VS)	0.0093
	3. Water quality (river) (WQ)	0.0660
	4. Slope (SL)	0.0956
	5. Open space (OS)	0.0464
	6. Forest reserve (FR)	0.0534
Wildlife	1. Species habitat (SH)	0.0162
	2. Rare flora (RF)	0.1309
	3. Endangered fauna (EF)	0.1409

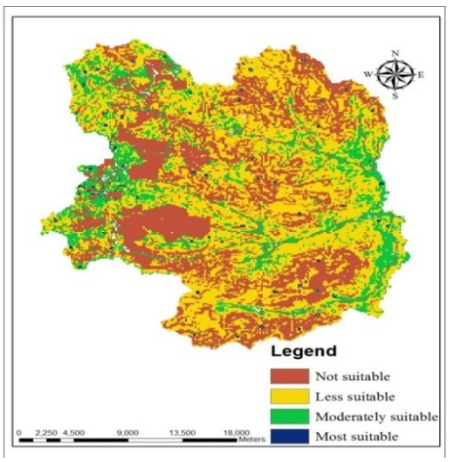


Figure 1: Sustainable tourism map

3.1. Spatial analysis

Table 4 shows the priorities of factors for sustainable tourism development derived from expert opinion. As seen from the table, the most important factors are Aboriginal settlements (0.1935). The second being proximity to eco-trail (0.1692) and the least being view-shed (0.0093). The priorities are based on equal importance of the cluster weights. The weights derived from ANP analysis were assigned to the raster data layers. The weighted sum function was then applied via the model builder tool in order to obtain the sustainable tourism map.

As shown in Figure 1, the not suitable category occupies the most significant area of the highland. The not suitable category are areas of Cameron Highlands that are highly sensitive to human disturbance such as forest reserve, habitat area, water body, steep slopes, high elevations,rare flora and endangered fauna. Therefore, these areas cannot be used for tourism activities; they can only be used for research and educational activities under certain guidelines. Less suitable category are areas of the highlands next in hierarchy to the not suitable category that can be used by the tourists to observe the natural endowment of the highlands underthe control of a tour guide. Moderately suitable areas are localities of the highlands that are more distant from the high biodiversity areas. These localities can allow for camping and be provided with lookout areas for the tourist. Lastly, the most suitable areas are parts of the highlands with the least amount of biodiversity. Therefore they can accommodate low density chalets. All the above mentioned activities will be carried outunder laid down rules and regulations to be abided by the tourists.

Conclusion

The study demonstrates the possibility of using ANP model with expert views to make the best selection among the factors for sustainable tourism. An important aspect of the approach proposed here is its hybrid nature, which combines spatial data with expert evaluations. In order to run the model, the spatial data were compiled from various sources thus represent objective data. Other aspects of the information used by the model were collected from the expert's opinion and introduced into the model.

Another point worth highlighting is the network structure of ANP. This can be regarded as one of the strength of the method, since it offers the possibility of simulating complex physical processes through expert opinion. The major drawback of the network structure is the large number of pairwise comparisons needed for its implementation. Thus, even with a simple network structure of this case study, there were a large number of pairwise comparisons. Greater potential of ANP over analytic hierarchy process (AHP) must also be discussed, in that it allowed for interaction and feedback among factors responsible for sustainable tourism development. The model could be replicated in highlands with similar characteristics to the one in focus; due to its flexible nature of accommodating changes in the decision maker's preference. These can be achieved by modifying the factors and interdependences for sustainable tourism development based on the local condition.

References

[1] B. Farrell,D. Runyan, Ecology and tourism, Annals of Tourism Research, 18(1) (1991).
[2] I. Haig,N. McIntyre, Viewing nature: The role of the guide and the advantages of participating in commercial ecotourism,The Journal of Tourism Studies, 13(1)(2002) 39-48.
[3] B. Archer,C. Cooper, The positive and negative impacts of tourism, In W. F. Theobald (Ed.), Global Tourism 1998 (2nd ed., pp. 63-81). Oxford: Butterworth-Heinemann.
[4] H. Coccossis,P. Nijkamp (Eds.),Sustainable tourism development,Aldershot, England: Avebury 1995.
[5] C. Cooper, J. Fletcher, D. Gilbert, S. Wanhill, Tourism principles and practice. London: Pitman Publishing 1993.

[6] P. F. J.Eagles,S. McCool,Tourism in national parks and protected areas, Planning and management. Wallingford, UK: CABI Publishing 2000.
[7] L. Twining-Ward,Towards sustainable tourism development:observations from a distance. *Tourism Management, 20 (1999)* 187-188.
[8] G. Herath, Research methodologies for planning ecotourism and nature conservation,*Tourism Economics, 8*(1), (2002) 77-101.
[9] J. Pigram, Alternative tourism: Tourism and sustainable resource. In V. I. Smith & W. T. C. Eadington (Eds.), *Tourism alternatives, potentials and problems in the development of tourism 1992* (pp. 76-87), Philadelphia: Pennsylvania Press.
[10] M. Aminu,*A Geographic Information System for Sustainable Tourism Planning: An integrated approach*, VDM Verlag Dr. Muller Aktiengesellschaft& Co. KG, 2009.
[11] J.K. Berry, GIS in island resource planning: A case study in map analysis. In D Maguire *et al*. (eds) *Geographical Information Systems: Volume 2 Applications.* Harlow: Longman (1991).
[12] M.H.Abed, M. Monavari, A. Karbasi, P. Farshchi,Z. Abedi,Site Selection Using Analytical Hierarchy Process by Geographical Information System for Sustainable Coastal Tourism*2011 International Conference on Environmental and Agriculture Engineering IPCBEE vol.15(2011) © (2011) IACSIT Press, Singapore*
[13] R.W.Butler, *Tourism-an evolutionary perspective*. In J.G. Nelson, R.W. Butler, and G. Wall (Eds.) Tourism and Sustainable Development Monitoring, Planning, Managing, Waterloo, Ontario: Department of Geography, University of Waterloo (1993).
[14] Y. Minagawa,N. Tanaka,*Application of Geographic Information Systems to Tourism Development Planning*: A Case Study of Lombok, Indonesia. Nagoya, Japan: UNCRD Research report Series No. 27 (1998).
[15] J. Beedasy,D. Whyatt, "Diverting the tourists: A spatial decision-support system for tourism planning on a developing island", *International Journal of Applied Earth Observation and Geo-information*Volume 1, Issues 3–4, 1999, Pages 163–174
[16] K. Bunruamkaew,Y. Murayama, Site Suitability Evaluation for Ecotourism Using GIS & AHP: A Case Study of SuratThani Province, Thailand. *International Conference: Spatial Thinking and Geographic Information Sciences2011.*
[17] A.S. Dye, S. Shaw, A GIS-based spatial decision support system for tourists of Great Smoky Mountains National Park: J Retailing ConsumServ 14(2007):269–278
[18] L. Zha, Y. Wang, Research on Regional Tourism Planning Spatial Decision Supporting System: 2010 Sixth International Conference on Natural Computation (ICNC 2010).
[19] O. Nekhay, M. Arriaza, L. Boerboom,Evaluation of soil erosion risk using Analytic Network Process and GIS: A case study from Spanish mountain olive plantations: Journal of Environmental ManagementVolume 90, Issue 10 (2009).
[20] T.L. Saaty,*The Analytic Hierarchy Process: Planning, Priority Setting, Resource Allocation*. McGraw-Hill, New York 1980.

A

Abrasion Resistance 393
Activated Sludge 44, 98
Adsorption 20
Aero-Packer 167
Aggregate Packing 422
Air Pollution 3
Alkali Silica Reaction 405
Alum 116
Alum Sludge 62
Anaerobic Digestion 172
Analytic Network Process 769
Analytical Prediction 345
Anchor Piles 191
Anodes 241
ANP Method 654
ANSYS 253
Antioxidant Materials 539
ArcSWAT 86
Artificial Dissipation Method 265
Artificial Neural Network (ANN) 681
Artificial Recharge Pond 38
Asphalt Bitumen 539
Assessment 571
Attached-Growth 104, 167
Auction 595
Averaging Time 577
Axi-Symmetric Analysis 699

B

Beach Profile Change 32
Beam with Web Opening 494
Bearing Capacity 681
Bends 253
Biaxial Bending 339
Bidding 595
Binding Action 545
Bio-Balls 167
Biodegradation 104
Biodiesel Blend (B5) 139
Biomass 172
Bioremediation 139
Bioretention 155
Bitumen 755
Black Paint 56
Blast Loading 440, 499
Bond Loss 369
Bonding Matrix 387
Brackish Water 161
Bridge Piers 648
Brittleness 381
Building Description System (BDS) 625
Building Information Modeling (BIM) 559, 625
Building Product Data (BPM) 625

C

Calcined Kaolin 375
Carbon Emission (CE) 565
Carbon Fiber Reinforced Polymer (CFRP) 488
Carbon Footprint 565
Cast-*In Situ* 637
Cathodic Protection 241
Causality 619
Ceibapentandra 482
Cement 333, 545
Cement Replacement Materials 529
CFRP 494, 511
Challenges 559
Chloride Penetration Depth 369, 522
Chopped Basalt Fiber Stands 381
Classic Spar 235
Co-Integration 619
Collapse 191
Column Study 155
Compaction Energy 422
Composite 411
Composite Material 488
Compressive Strength 345, 428, 434, 505, 529
Compressive Strength Loss 369
Compressive Stress-Strain 476
COMSOL Multiphysics 675
Concrete Armor Unit 313
Concrete Beam 411
Concrete Reinforced Structures 488
Configuration 197
Connectors 399
Conservation 769

Consolidation 110
Construction 595
Construction Project Management 607
Contaminant 92
Contaminated Sediments 50
Contractor 595
Conventional Riser-Guard 210
Corrugated Section 457
Cost Comparison 637
Courtyard 14
Crack 687
Crest Height 313
Crest Width 313
Criteria 222, 654
Cyclic Loading 517

D

Dam Safety 583
Damaged 191
Damaged Beam 399
Dapped-End Beams 463
Debonding 399
Decision Making Tool 222
Decommissioning 222
Deficiency 511
Definition 625
Deformation 325
Degradation 80
Design Variants 14
Dielectric 333
Digital Elevation Model (DEM) 669
Dimension 642
Displacement 295
Distillation 161
Distribution Characteristics 26
Drag Coefficient 241, 247
Dredging 50
Drying Shrinkage 362, 529
DSCC 393
DSR Frequency Sweeps 755
Ductile Self-Compacting Concrete 522
Ductility 351, 517
Duffing Model 228
Durability 369
Dynamic Creep 422
Dynamic Formulas 749

E

Earthquake 571
Eccentricity 339, 511
Ecological Risk Assessment 50
Electrochemical 44, 80
Electrokinetic 110
Electromagnetic 183
Electroosmotic Stabilization 110
Elemental Composition 150
Embodied Carbon 565
Emergency Response Plan 583
Emission 3
Empty Fruit Bunches 150
Energy Equation 755
Engineered Cementitious Composites 428
Engineering Properties 422
Environmental Loads 295
Environmental Screening 50
EPC Project 654
Equivalent Impulse Load 210
Equivalent Viscous Damping 687
Erosion Characteristics 711
Erosion Induced Slope Failure 711
Ex-Mining Lakes 177
Ex-Mining Site 38
Expansion 405
Experimental Study 14

F

Factors Influencing 663
Failure Loads 463
Failure Mechanism 191
Failure Paths 307
Fatty Acid 74
Field Experiment 32
Finite Element (FE) 440
Finite Element Analysis (FEA) 648
Finite Element Method (FEM) 253
Flexible Pipeline 535
Flexural Performance 411
Flexural Strength 345, 428, 505
Flexure 339, 511
Floating Wetland 68
Fly Ash 356, 362, 393, 417, 522
Following Time 736
Force Coefficients 259
Free Span Pipelines 228
Frequency Domain 289
Fresh Properties 529

FRP Strengthening 469
Functionality 150

G

Gas Exploration 693
Geographic Information System (GIS) 769
Geographic Information System Software 144
Geopolymer 417
Geopolymer Concrete 362
Geospatial Technology-Based Group Analytic Hierarchy Process 717
GFRP Grating Types 387
Ground Water 32, 92
Groundwater Interaction 38
Groundwater Modeling 38
Guying System 191

H

Heavy Metals 177
Heavy Truck 648
HGV 648
Hierarchy Process 144
High Performance Fiber Reinforced Concrete 345
High Strength Concrete 476
Hinge 517
History 625
Hollow Core Slab 637
Human Error 730
Human Error Causes 730
Humid Tropical Soils 8
Hydration 333
Hydraulic Retention Time 68
Hydrodynamic Forces 241, 247
Hydrologic Modeling 86
Hyperspectral Remote Sensing 693

I

ICU-V 313
Impact 724
Impact Resistance 393
In-Line Spacing 259
In Place 191
Inaccessibility 763
Industrial Discharge 116
Industrialised Building System 637
Inertia Coefficient 241, 247
Infrastructure 601, 642
Intact 191
Integrated 167
Irrigation Uniformity 26
Isotherm 20

K

Kaolin 375
Kapok Fibre 482
Kenaf Fibres 351
Kerosene 183
Kinetic 20, 80

L

Laboratory Experiment 277
Laminated Composite 535
Landfill 92, 144
Landslide 216, 669, 724
Langat River 86
Lateral Strength 687
Layered Soil 675
Leachate 92
Library 553
Life-Cycle Assessment 565
Lightweight Aggregate Concrete 446
Lightweight IBS 637
Lignin 539
Linear Array 259
Linkage 619
Load Carrying Capacity 351
Long-Crested Waves 235
Low-Carbon Building 565
LS-DYNA 648

M

Machineries 607
Magnetic Field 98
Malaysian Construction Industry 559
Malaysian Offshore Locations 241
Mangrove 277
Mangrove Bark 74
Manpower 607
Marine Environment 488
Marine Growth 247
Marshall Test 422
Material Size 104
Materials 607
Mechanical Property 375, 381

Medium 595
Metakaolin 476, 505
Microclimate Performance 14
Microeconomics 595
Microscopic Simulation 742
Microwave Incinerator 434
MIRHA 356, 393, 522
Mode Choice 663
Model Shift 663
Modflow 92
Moisture Depth 705
Monopod Platform 295
Monsoon 161
Mooring Line 197, 204
Morison Equation 241, 247, 259
Mould Growth 553
Moulded 387
Mulch Materials 155
Multi Body Interaction 289
Multi-Criteria Decision Analysis/Aid or Multi-Criteria Decision Makers 144

N

Natural Ventilation 631
Navier-Stokes Equations 265
Neural Network 122
Ni (II) 20
Nitrogen Dioxide 3
NOAA Applications 705
Non-Road Construction Vehicles 589
Normal Distribution 749
Nutrient Pollutants 155

O

Offshore 387
Offshore Pipelines 265
Offshore Platform 325
Oil Exploration 693
Oil Palm Shell 446
Oil Palm Shell Reinforced Concrete 351
Oil Spill 74
Onsite Mechanization 589
Operational Carbon 565
Optimised Truss Model 469
Optimum Cement Replacement 375
Orientation 631
Orthophoto 669
Oxidation 539

P

P. putida 139
PAHs 80
Palm Oil Fuel Ash 446, 529
Parallelization 216
Park-and-Ride 663
Partial Cement Replacement 446
Partial Coarse Aggregate Replacement 446
Partial Interaction 517
Particle Swarm Optimization (PSO) 681
Pearson Correlation 417
Peat 545
Pechini's Method 44
Pedestrians Flow 742
Penang Port 301
Perak 177
Perak State 705
Performance Measurement 642
PETRONAS 191
PF2 601
PFI Skills 601
Phenolic 387
Phosphate 62
Phosphorus Removal 62
Physical Properties 98
Physico-Chemical Properties 177
Physico-Chemical Treatment 116
Pile Bearing Capacity 749
Pipeline 253
Planning 144
Plasticity 191
Platform 191
Policy Makers 763
Polyester 387
Pond-Aquifer Interaction 38
Porosity 319
Potable Water 56
Pozzolanic Material 545
PPP 613
Precast Concrete Sheet Pile System 451
Precast Concrete Soldier Pile System 457
Precast Lagging 457
Precast Post 457

Prediction 122
Predictive Models 476
Pressure 577
Pressure-Impulse Diagrams 499
Pretension 204
Probabilistics 749
Probability of Failure 283
Procurement 595
Produce Water 80
Propagation 724
Protective Barrier 440
PSI Technique 325
PTSF 736
Public 595
Public Sector Capacity 601
Pullout 577
Pultruded 387
PV-DC Heater 56
PVA Fiber 345, 428, 505

Q

Quasi-Static Analysis 197, 204

R

Radial Basis Function (RBF) 122
Rail Transit 742
Rainfall 32
Rainfall Characteristics 711
RAO 235
RC Beam 469, 494
Reactive Silica 405
Real Time Kinematic (RTK) 669
Rectangular Building 577
Regression 271
Regression Analysis 375
Rehabilitation of Low Level Outlet 128
Reinforced Concrete 339, 463, 511
Relative Humidity 553
Relative Importance Index 222
Reliability 271
Reliability Assessment Model 283, 307
Reliability Index 283
Removal Efficiency 68
Removal Performance 104
Repair for Shear 399
Reserve Strength Ratio (RSR) 191, 271, 283
Reservoir Drawdown 128
Reservoir Sedimentation 128
Resonant Motion 289
Resource Management 607
Response 295
Rice Husk 150, 539
Rice Husk Ash 434, 545
Rice Husk Carbon 20
Risk 583
Risk Allocation 654
Risk Assessment 613
Risk Identification 613
Risk Management 50
Risk Ranking 613
River 122
Riverbank Protection 457
Rivers 177
Road Embankment 133, 451
Road Settlement 451
Roof Insulation 482
Roofing Sheet 577
Route Choice 742
RSM 98
Run-Up 724
Rural Inhabitants 763
Rural Population 763
Rutting 755

S

SACS v5.3 191
Sand 56
Scouring 457
Seabed Condition 301
Seawater 161
Sediment 122
Seepage Hydrocarbon 693
Self-Compacting Concrete 356, 428, 529
Self-Compacting Geopolymer Concrete 362
Serviceability 571
Setting Time 417
Shallow Foundations 681
Shear Analysis 469
Shear Force 494
Shear Friction 517
Shear Strength 469
Shell Theories 535
Short-Crested Waves 235
SHRP Specifications 755
Simulation 216
Single Beam Echo Sounder 301
Single Degree of Freedom Models 499

Single Sludge 167
Slope Characteristics 711
Slope Engineering Practices 730
Small 595
Social Force Model 742
Soft Ground 451
Soft Soil 699
Soil Moisture Content 705
Soil Pollution 183
Soil Water Retention Curve 8
Soil Water Retention Functions 8
Solar Distillation System 56
Solar Energy 161
Solar Intensity 161
Solar Still 161
Sorption 150
Sorption Capacity 74
Spatial Flood Simulation 717
Spectral Library 693
Splitting Tensile Strength 345, 505
Sprinkler Irrigation 26
Stand Chopped Basalt Fiber 356
Station-Keeping Systems 197, 204
Steel-Concrete-Steel 440
Steel Plate 399
Stiffness 687
Stone Column 699
Storage Tank 699
Stormwater Runoff 155
Stream Flow 86
Strength 417
Stress Distribution 699
Structural Response 253
Structures Characteristics 711
Strut Model 463
Submerged Breakwater 319
Sugar Cane Bagasse Ash 369
Sulphur Dioxide 3
Supply Chain Management 642
Surface Area 150
Surface Cover 133
Surface Water Interaction 38
Sustainable Construction 589
Sustainable Development 769
Swash Zone 32
System Probability of Failure 307
System Reliability Index 307

T

Tarpon Monopod 191
Temperature 553
Tensile Strength 428
Test Vehicle 736
Thermal Comfort 482
Thermal Performance 631
Thermosetting Pipe 535
Ti/RuO_2 Anode 44
Tie Model 463
Time 763
Time-Space Prism 763
Torsion 339, 511
Total Suspended Solids 133
Toughness 381
Tourism 769
Transverse Spacing 259
Travel Behavior 663
Travel Patterns 763
Treatment Efficiency 155
Tropical 161
Tropical Rainfall 133
Tsunami 216, 724
Tubular Cylinders 241, 247
Tunnel Form Building 687
Turbidity 133
Two Dimensional Array 259
Two-Lane Highways 736

U

Ultimate Bearing Capacity 675
Ultimate Strength 191
Uncertainty 730
Underground Water Sludge 110
Uniformity Coefficients 26
Unmanned Aerial Vehicle (UAV) 669
Unpiggable 253
Used Engine Oil 434

V

Van Der Pol Model 228
Vegetation Stress 693
Vehicle Collision 648
Vessel Collision 210
Video Recording Technique 736
Vinyl Ester 387
Viscoelasticity 755

Visual MODFLOW 38
Volatile Fatty Acids 172
Vortex-Induced Vibration (VIV) 228, 265

W

Wastewater Treatment 62, 98, 104
Water Quality 68, 177
Water Security 583
Wave Dissipation 277
Wave Forces 259
Wave Profile within the Gap 289
Wave Tank Test 235
Wave Transmission 313, 319
Weight Loss 369
Welded Wire Mesh 411
Wind Loads 571
Wind Speed 577
Windows 631
Workability 381

A

Ab Latip, A.S. 325
Abdulbasit, A. 14
Abdulla, A.I. 411
Abdullah, S.N.H. 313
Ahmad, H. 642
Ahmad, M.H. 631
Ahmad, S.S. 14
Ahmed, M.O. 197, 204
Ajab, H. 80
Akbar, I. 339, 387, 511
Akmilah, N. 457
Al-Mattarneh, H. 183, 333
Al-Yacouby, A.M. 241, 247, 259
Alam, M.A. 399
Alanni, O. 494
Albarody, T.M.B. 253, 535
Alengaram, U.J. 411, 529
Ali, M.F. 86, 711
Alsubari, B. 529
Alwadie, A. 333
Aminu, M. 769
Aminuddin, A.G. 155
Anuar, S.A. 687
Arazi, I. 589
Arsyad, A. 92, 749
Aryani, A.L. 625
Ashaari, Y. 742
Askari, M. 8
Aswin, M. 463
Ayub, T. 345, 476
Azimi, S.J. 351
Aziz, H.A. 144
Aziz, R. 301
Azizli, K.A.M. 144, 482, 565
Azman, M.A. 595
Azmee, N.M. 393, 522
Azwin Zailti, A.R. 583

B

Babangida, N.M. 8
Baharom, S. 730
Baharuddin, K.B. 3
Baharun, M.H. 428
Baharvand, M. 631
Bakar, A.S.A. 122
Beddu, S. 434
Bin Chepuan, O. 736
Bin Ghazali, Z. 619
Bin Hassan, S. 26
Bin Shukri, A.A. 517
Brahim, J. 625

C

Chandio, I.A. 663, 763
Chang, K.Y. 393, 522
Charanvarma, S. 228
Chaudhuri, M. 20
Choong, K.K. 451
Chuan, S.Y. 116
Chung, L.P. 631

D

Dahim, M. 183
Das, A.K. 699
Daud, M. 637
Deb, K. 699
Demie, S. 362

E

Eik, L.H. 191
Eisakhani, M. 116
Elhsameed, A.A. 369
Elshekh, A.E.A. 356, 381
Embong, A.M. 669
Emparan, Q.A. 139
Erikol, O.P.D. 428
Ezechi, E.H. 167, 172

F

Fadilah, N. 451
Farhan, S.A. 482, 559, 565
Faris, M.K. 553, 589
Fathi, M.S. 625
Fazli, H. 488

G

Gardezi, S.S.S. 559, 565
Goh, S.S. 283

H

Hafiz, Z.M. 637
Hajihassani, M. 681
Hajrah, 92
Hakro, M.R. 663
Hamid, M.B. 631
Hamid, M.R.A. 571
Hamid, N.H.A. 687
Harahap, I.S.H. 216, 325, 724, 730
Hasan, M.H. 499
Hashim, A.M. 133, 277, 313
Hassaballa, A.A. 705
Hayder, G. 637
Heng, G.C. 44
Hidayah, B. 68, 583
Hua, C.K. 62
Huan, V.N.P. 216, 724
Humaira, H.S. 68
Husna, T. 155
Hussain, S. 763

I

Ibrahim, Z. 411
Idichandy, V.G. 241, 247, 259
Imran, M. 339, 511, 730
Iqbal, F. 110
Irfan, A. 763
Isa, M.H. 20, 44, 56, 74, 80, 122, 167
Iskandar, N.A. 271
Ismail, R. 183
Izzuddin, A. 387

J

Jabbar, A.S.A. 399
Jamal, M.H. 32
Jamaluddin, M.A.B. 295
Jamaludin, M.I. 669, 693
Jamaludin, N. 553
Jansen, L. 128
Julien, P.Y. 128
Jumaat, M.Z. 399, 411, 517, 529

K

Kamaruddin, I. 422
Kamaruddin, I.B. 539, 755
Karim, A.T.A. 139
Karuppanan, S. 210
Kassim, M.A. 104
Keong, C.K. 457
Khairuddin, N. 277
Khalid, K. 86, 711
Khan, R.A. 619
Khan, S.U. 375, 505
Khan, T. 20
Kheang, T.S. 307
Kholik, M.F. 693
Khoshnava, S.M. 654
Kok, K.H. 68
Kurian, J.V. 197, 204, 235, 241, 247, 259, 265, 271, 283, 295, 307
Kusbiantoro, A. 417
Kutty, S.R.b.M. 80, 167
Kutty, S.R.M. 172

L

Lai, K.Y. 104
Lam, W.H. 301
Lariyah, M.S. 68, 583
Lawal, D.U. 717
Liem, N.D. 86
Liew, M.S. 191, 210, 222, 235, 241, 247, 259, 271, 283, 295, 307, 463, 499, 589, 619, 648
Liew, W.L. 104
Loh, S.K. 104
Lun, N.K. 222

M

Madzlan, N. 422, 539, 663, 755, 763
Maharun, M. 648
Mahayudin, H.M. 637
Makatar, M.A. 711
Malakahmad, A. 56, 116, 150
Malkawi, A. 333
Manap, N. 50
Marto, A. 681
Maslan, M. 139
Matori, A.N. 325, 669, 693, 705, 717, 769
May, R. 38

Md Nujid, M. 675
Memon, F.A. 362
Memon, I.A. 663
Mohammed, B.S. 428, 494
Mohammed, N.I. 3, 553
Mohd Ahmadan, N.A. 161
Mohd Kamal, N.L. 434
Mokhtar, M.M. 693
Mokhtar, M.R.M. 669
Momeni, E. 681
Muda, K. 98, 104
Muda, Z.C. 434
Muhammad, R.U.M. 8, 20, 122
Murshed, N.A. 428
Mustafa, M. 742
Mustaffa, Z. 253
Mustapha, K.N. 399
Muthusamy, K. 446
Muttaka, N.I. 736

N

Nahi, M.H. 539
Namazi-Saleh, F. 265
Namdar, A. 351
Napiah, M. 607
Narayanan, S.P. 577
Nasma Noor, N.V. 289
Nazirul, M.Z. 62
Ng, C.Y. 235
Noor, N.D.M. 313
Noor, S.F.M. 139
Nor Azazi, Z. 155
Norhati, I. 14
Norhazilan, M.N. 613, 654
Nur Asmaliza, M.N. 68
Nur Azzimah, Z. 446
Nur Syamimi, Z. 98
Nuruddin, M.F. 356, 362, 381, 393
Nurudinn, M.F. 183, 333, 345, 369, 375, 405, 428, 434, 476, 482, 505, 522, 559

O

Olisa, E. 177
Olufemi, J.A. 422
Ong, C.Y. 451, 457
Orji, K.U. 74, 161, 177
Osman, M. 26
Osman, S.B.S. 110
Ossen, D.R. 631
Otairu, A.G. 601
Othman, I. 601, 607
Othman, N. 3, 32

P

Palaniandy, D.K. 210
Perissin, D. 325
Potty, N.S. 571, 607
Puad, N.H.A. 482

Q

Qasim, S. 730
Qeshta, I.M.I. 411

R

Rahim, A.F.A. 167, 172
Rahman, N. 417
Rahman, N.F.A. 86, 711
Rahsidi, S.M. 583
Ramli, M.Z. 637
Remennikov, A.M. 440
Riahi, A. 56, 161
Robabeh, A. 74, 177
Roshdi, A.M. 253

S

Sadullah, A.F.M. 742
Saeed, M.O. 20, 144
Salih, A.F.M. 356, 381
Salleh, A.M. 637
Salleh, A.R. 648
Salleh, W.M.N.W. 14
Samang, L. 749
Samat, S.R. 32
Sapari, N.B. 56, 74, 150, 161, 177
Saravanan, K. 648
Sarvari, H. 613, 654
Seavhai, K. 577
Sebastian, A.A. 241, 247, 259
Shafigh, P. 411, 529
Shafiq, N. 339, 345, 356, 362, 369, 375, 381, 434, 476, 505, 511, 559, 565

Shafri, H.Z.M. 705
Shah, S.M.H. 133
Shahedan, N.F. 417
Shashikala, A.P. 228, 289
Si, Z.Y. 104
Sidek, L.M. 62, 128
Sillanpää, M. 98
Singh, B.S.M. 56
Siti Nooriza, A.R. 405
Sohaili, J. 98
Soon, C. 301
Suliman, Y.G. 422
Sunar, N.M. 139
Suriani, N.A.W. 553
Suyadi, 749
Syed Mohsin, S.M. 351
Syed, Z.I. 210, 463, 499

T

Taha, M.R. 675
Tahir, W. 38
Talpur, M.A.H. 663, 763
Teh, H.M. 319
Thiruchelvam, S. 583
Thong, Y.H. 104

U

Umar, A.A. 601
Umar, U.A. 559, 565
Uy, B. 440

V

Valipour, A. 613, 654
Venkatesan, S. 499
Voon, M.C. 271
Voulvoulis, N. 50

W

Wahab, A.K.A. 32
Wahab, M.M.A. 271, 283, 307
Wahab, M.R.A. 642
Waris, M. 589
Wee, T. 463, 469, 488, 648
Wong, L.S. 545
Wong, T.C. 648

Y

Yahaya, N. 613, 654
Yaqub, A. 80
Yavari, S. 150
Yenduri, A. 197, 204
Yew, W.T. 301
Yin, H. 469, 648
Ying, K.S. 440
Yusof, K.W. 8, 26, 56, 122, 133, 177, 669, 769
Yusoff, I. 38

Z

Zahiraniza, M.B. 133, 265, 535
Zainal, A. 482
Zainol, R.B. 769
Zanariah, A.R. 742
Zawawi, N.A.W.A. 222, 601
Zoorob, S.E. 755
Zubair, A. 92
Zuraidah, A. 583